THE JOURNAL
OF
CHEMICAL PHYSICS

VOLUME 35, NUMBER 1 JULY, 1961

Vibrational Relaxation in Carbon Dioxide*

W. J. WITTEMAN†

University of Maryland, Institute for Fluid Dynamics and Applied Mathematics, College Park, Maryland

(Received November 21, 1960)

The vibrational excitation of a CO_2 molecule in collision with another CO_2 molecule is investigated. A derivation of the cross section by means of the method of the distorted waves and the rate of total energy transfer are presented. There are two relaxation processes with different relaxation times related to direct excitation of the bending mode and excitation in series of the valence mode. Experimental results obtained by the author, to be published separately, confirm this conclusion. The experimental relaxation time for the bending vibration was about one-half of the calculated value, which may be considered a fair agreement in view of the uncertainty involved in the interaction potential and of other approximations which had to be introduced into the calculations.

1. INTRODUCTION

THE problem of vibrational excitation by means of inelastic molecular collisions has been studied by some authors[1–3] in connection with the temperature and density dependence of the vibrational relaxation. This relaxation process can be complicated when more different degrees of freedom, which can be also degenerated, are available for the vibrational energy. Each degree of freedom can be excited directly, which means a direct transfer from translation to vibration, and also in series, when the transfer of energy is between the vibrational degrees.

In this field the calculations for the linear CO_2 molecule are especially interesting because it happens that the energy quanta of the bending modes are approximately half the quanta of the valence mode. Therefore it is possible that during elastic collisions two quanta of the bending modes will be transferred into the valence mode. This case of exact resonance has been indicated in the work cited in reference 2. But the authors, however, did not consider the various possibilities in which the energy can be exchanged. There is the possibility that one quantum of the valence mode may be transferred not only as two quanta to one of the degenerated bending modes, but also as one quantum to each of the two independent bending modes by the collision. Moreover it may happen that the energy is exchanged between the valence mode of one molecule and the binding modes of the other.

We will treat the problem by assuming that the interaction potential is small and may be approximated as an exponential as was first done by Jackson and Mott[4] for mathematical reasons. It has been suggested by Landau and Teller[1] that the probability of exciting a vibration depends on the linear momentum that can be transmitted to it. Therefore only the components of short-range forces in the directions of the normal coordinates of the vibrations are important in the calculation of the transition probabilities. Consequently as an extension to what is done in the work cited in reference 3, we substitute for the interaction potential

$$V=V_0\exp\{-\alpha(r+A_1s_1\cos\theta+A_2s_{2,1}\sin\theta\sin\phi+A_2s_{2,2}\sin\theta\cos\phi)\},\qquad(1)$$

where the projections of the normal coordinates of the vibrations are taken in the direction of r. Here s_1, $s_{2,1}$, and $s_{2,2}$ are the normal coordinates of the valence mode and degenerated bending modes, respectively; A_1 and A_2 are internal motion coefficients corresponding

* This research was supported by the U. S. Air Force through the Air Force Office of Scientific Research of the Air Research and Development Command.

† Present address: Philips Research Laboratories, Eindhoven, Netherlands.

[1] L. Landau and E. Teller, Physik. Z. Sowjetunion **10,** 34 (1936).

[2] Z. Slawsky, R. N. Schwartz, and K. F. Herzfeld, J. Chem. Phys. **20,** 1591 (1952).

[3] R. N. Schwartz and K. F. Herzfeld, J. Chem. Phys. **22,** 767 (1954).

[4] J. M. Jackson and N. F. Mott, Proc. Roy. Soc. (London) **A137,** 703 (1932).

Copyright © 1961 by the American Institute of Physics

to the ratios of atomic vibrational amplitudes to their respectively normal coordinates.

It is well known that in thermal collisions the distance of closest approach is much larger than the interatomic distances inside the molecule. Therefore we consider for simplicity the interaction potential as spherical symmetric and average the final results over the angles θ and ϕ.

In our calculations we will make some more simplifying assumptions, which are:

(a) Vibrational energy may be transferred between vibrational and translational degrees of freedom, or between different vibrational modes, only during collisions.

(b) The rotations of the molecules play no role in the energy exchange. This can be justified by knowing that the duration of a collision is short compared with the rotation time.

(c) Triple collisions may be ignored.

The linear CO_2 molecule has 4 vibrational degrees of freedom, associated with two longitudinal vibrations, one symmetric, one asymmetric, and two modes of vibration perpendicular to its axis, which are degenerated. So these are three different wave numbers which can be obtained from spectroscopic data. The corresponding frequencies are:

vibration a:

$\nu_3=7134\times10^{10}$ sec^{-1} (longitudinal and asymmetric),

vibration b:

$\nu_1=3855\times10^{10}$ sec^{-1} (longitudinal and symmetric, or valence mode),

vibration c:

$\nu_2=2000\times10^{10}$ sec^{-1} (perpendicular to its axis, or bending mode).

The energy associated with vibration a is very small and for temperatures below 1000 K it is less than 8% of the vibrational energy of the bending modes. Therefore this vibration may be ignored and we consider only vibrations b and c.

2. METHOD OF DISTORTED WAVES

We shall use the method of distorted waves[4,5] in the discussion of molecular-collision phenomena, involving the excitation of vibrations by the impact of other molecules and the transfer of excitation between two molecules on collision.

The motion of two colliding molecules may be described in terms of that of the motion of the molecules relative to each other or to their center of mass, the free motion of the center of mass of the complete system, and the motion of the individual atoms of each molecule relative to the center of mass of each. The motion of the center of mass of the complete system is like a free particle and may be separated out.

Let Ψ be the wave function which describes the collision of two molecules in space. Here Ψ depends on s_1, $s_{2,1}$, $s_{2,2}$, and the distance r between the two centers of mass of the colliding molecules, and satisfies the Schrödinger equation

$$H\Psi=E\Psi, \tag{2}$$

where E is the total energy;

$$E=(\hbar^2k^2/2\mu)+\epsilon_1+\epsilon_{2,1}+\epsilon_{2,2}, \tag{3}$$

the sum of kinetic energy of the relative motion and of the energy of the vibrations b and c, respectively. The Hamiltonian H is given by

$$H=(-\hbar^2/2\mu_1)\nabla_{s_1}{}^2-(\hbar^2/2\mu_2)\nabla_{s_{2,1}}{}^2-(\hbar^2/2\mu_2)\nabla_{s_{2,2}}{}^2$$

$$+2\pi^2\mu_1\nu_1{}^2s_1{}^2+2\pi^2\mu_2\nu_2{}^2s_{2,1}{}^2+2\pi^2\mu_2\nu_2{}^2s_{2,2}{}^2-(\hbar^2/2\mu)\nabla_r{}^2+V,$$

where μ_1 and μ_2 are the reduced masses associated with the vibrations b and c, respectively, and μ the reduced mass of the total system:

$$\mu_1=14.60\times10^{-24}g$$

$$\mu_2=13.38\times10^{-24}g$$

$$\mu=36.80\times10^{-24}g.$$

We may expand the function Ψ in the form

$$\Psi=\sum_{nm_1m_2}R_k\psi_n(s_1)\psi_{m_1}(s_{2,1})\psi_{m_2}(s_{2,2}). \tag{4}$$

The functions R_k depend only on the relative motion of the centers of mass of the two molecules and the kinetic energy for this motion at infinity is obtained by using Eq. (3) as the difference between the total energy and the vibrational energy. Therefore the summation in Eq. (4) is only taken over the vibrational states. The ψ_n, ψ_{m_1}, and ψ_{m_2} represent the proper wave functions of the vibrations b and c, respectively. Substitution of Eq. (4) in Eq. (2) gives

$$\sum_{nm_1m_2}\psi_n\psi_{m_1}\psi_{m_2}\{(\hbar^2/2\mu)\nabla_r{}^2+(\hbar^2k^2/2\mu)\}R_k$$

$$=\sum_{nm_1m_2}V\psi_n\psi_{m_1}\psi_{m_2}R_k. \tag{5}$$

Next we introduce for the function R_k an expansion in partial waves with spherical harmonics. This can be done, for the potential is assumed to be spherically symmetric;

$$R_k=\sum_l P_l(\cos\theta')\,(f_{lk}/r). \tag{6}$$

[5] N. F. Mott and H. S. Massey, *The Theory of Atomic Collisions* (University Press, Cambridge, England, 1952).

Substitution of Eq. (6) in Eq. (5) gives for a partial wave

$$\sum_{nm_1m_2}\psi_n\psi_{m_1}\psi_{m_2}\{(d^2/dr^2)+k^2-[l(l+1)/r^2]\}f_{lk} = (2\mu/\hbar^2)\sum_{nm_1m_2}V\psi_n\psi_{m_1}\psi_{m_2}f_{lk}.$$

Multiplying both sides of this equation by $\psi_n^*\psi_{m_1}^*\psi_{m_2}^*$, integrating over s_1, $s_{2,1}$, and $s_{2,2}$ and making use of the orthogonality of the functions, we obtain

$$\{(d^2/dr^2)+k^2-[l(l+1)/r^2]\}f_{lk}=(2\mu/\hbar^2)V_0 \times\exp(-\alpha r)\sum_{nm_1'm_2'}B_{n'n}C_{m'm_1}C_{m_2'm_2}f_{lk'}, \quad (7)$$

where the following abbreviations have been used:

$$B_{n'n}=\int_{-\infty}^{\infty}\psi_n^*\psi_{n'}\exp(-\alpha A_1 s_1\cos\theta)\,ds_1 \quad (8)$$

$$C_{m_1'm_1}=\int_{-\infty}^{\infty}\psi_{m_1}^*\psi_{m_1'}\exp(-\alpha A_2 s_{2,1}\sin\theta\sin\phi)\,ds_{2,1} \quad (9)$$

$$C_{m_2'm_2}=\int_{-\infty}^{\infty}\psi_{m_2}^*\psi_{m_2'}\exp(-\alpha A_2 s_{2,2}\sin\theta\cos\phi)\,ds_{2,2}. \quad (10)$$

Since the conditions of the problem require one collision to be incident on the other, we define the function $R_{k_0}=\sum_l P_l(\cos\theta')(f_{lk_0}/r)$ representing the incident and elastic scattered wave. Therefore this function must have the asymptotic form

$$R_{k_0}\xrightarrow[r\to\infty]{}\exp(ik_0z)+g_0(\theta')\exp(ik_0r)/r. \quad (11)$$

The first term represents a particle moving along the polar axis $\theta'=0$. The second term represents the elastic scattered particle that is moving radially outward. With the aid of Eq. (11) we find the asymptotic form for f_{lk_0}. We therefore require an expansion of $\exp(ik_0z)=\exp(ik_0r\cos\theta')$ in Legendre polynomials;

$$\exp(ik_0r\cos\theta')=\sum_{l=0}^{\infty}(2l+1)i^l(\pi/2k_0r)^{\frac{1}{2}}J_{l+\frac{1}{2}}(k_0r)\times P_l(\cos\theta'). \quad (12)$$

The Bessel function has the asymptotic form

$$J_{l+\frac{1}{2}}(k_0r)\xrightarrow[r\to\infty]{}(2/\pi k_0r)^{\frac{1}{2}}\sin(k_0r-\tfrac{1}{2}l\pi).$$

The asymptotic form of the left side of Eq. (11) should be

$$R_{k_0}\xrightarrow[r\to\infty]{}\sum_l D_l\sin(k_0r-\tfrac{1}{2}l\pi+\delta_{lk_0})P_l(\cos\theta')/r, \quad (13)$$

where D_l is a constant and δ_{lk_0} is a phase shift. Substitution of Eqs. (12) and (13) into Eq. (11) gives finally,

$$f_{lk_0}\xrightarrow[r\to\infty]{}(2l+1)i^l\exp(i\delta_{lk_0})\sin(k_0r-\tfrac{1}{2}l\pi+\delta_{lk0})/k_0. \quad (14)$$

The function $R_k=\sum_l P_l(\cos\theta')f_{lk}/r$ represents the inelastic scattered wave and therefore has the asymptotic form

$$R_k\to g_k(\theta')\exp(ikr)/r. \quad (15)$$

The nondiagonal matrix elements $B_{n'n}$, $C_{m_1'm_1}$, $C_{m_2'm_2}$ in Eq. (7) are very small compared with the diagonal terms B_{nn}, $C_{m_1m_1}$, and $C_{m_2m_2}$. Therefore, we may neglect all products on the right-hand side, except $f_{lk}B_{nn}C_{m_1m_1}C_{m_2m_2}$ and $f_{lk_0}B_{n_0n}C_{m_10m_1}C_{m_20m_2}$. We solve Eq. (7) by the method of successive approximations. We set for the waves representing the incident and elastically reflected particles,

$$f_{lk_0}=f_{lk_0}^{(0)}+f_{lk_0}^{(1)}$$

and for the inelastic scattered waves,

$$f_{lk}=f_{lk}^{(1)}.$$

We obtain thus two equations,

$$\{(d^2/dr^2)+k_0^2-[l(l+1)/r^2]-(2\mu/\hbar^2)V_0\exp(-\alpha r)\}f_{lk_0}=0 \quad (16)$$

$$\{(d^2/dr^2)+k^2-[l(l+1)/r^2]-(2\mu/\hbar^2)V_0\exp(-\alpha r)\}f_{lk} =(2\mu/\hbar^2)V_0\exp(-\alpha r)f_{lk_0}B_{n_0n}C_{m_10m_1}C_{m_20m_2}. \quad (17)$$

From these two equations we have to find a solution for f_{lk}. We will first consider an auxiliary function F satisfying the equation

$$\{(d^2/dr^2)+k^2-[l(l+1)/r^2]-(2\mu/\hbar^2)V_0\exp(-\alpha r)\}F_{lk}=0, \quad (18)$$

with boundary conditions $F=0$ for $r=0$ and with the asymptotic value

$$F=\sin(kr-\tfrac{1}{2}1+\delta_{lk}).$$

By comparing Eq. (14) it is easy to see that

$$f_{lk_0}=(2l+1)i^l\exp(i\delta_{lk_0})F_{lk_0}/k_0.$$

We substitute $f_{lk}=yF_{lk}$ in Eq. (17) and obtain

$$2(dF_{lk}/dr)(dy/dr)+F_{lk}(d^2y/dr^2) =(2\mu/\hbar^2)V_0\exp(-\alpha r)[(2l+1)/k_0]i^l \times\exp(i\delta_{lk_0})F_{lk_0}B_{n_0n}C_{m_10m_1}C_{m_20m_2}.$$

Multiply both sides by F_{lk} and integrate with respect to r between the limits 0 and r. The resulting equation can be integrated for large r, for we know the asymptotic value of F_{1k}. We obtain

$$y=k^{-1}\{-\cot(kr-\tfrac{1}{2}l\pi+\delta_{lk})+\text{const}\} \times(2\mu/\hbar^2)[(2l+1)/k_0]i^l\exp(i\delta_{lk_0})A_{lk}B_{n_0n}C_{m_10m_1}C_{m_20m_2},$$

where we have introduced the abbreviation

$$A_{lk}=\int_0^{\infty}V_0\exp(-\alpha r)F_{lk_0}F_{lk}dr. \quad (19)$$

Comparing this result with the asymptotic expression (15) we get

$$f_{lk}=-\exp\{i(kr+\delta_{lk})\}(2\mu/\hbar^2)[(2l+1)/k_0k]$$
$$\times\exp(i\delta_{lk_0})A_{lk}B_{n_0n}C_{m_{10}m_1}C_{m_{20}m_1}. \quad (20)$$

From expression (15) we deduce that $|g_k(\theta')|^2 1/r^2$ is the number of molecules per unit volume at distance r, which have undergone a transition in their vibrational states during the collision. Of these, the number crossing unit area per unit time is proportional to $|g_k(\theta')|^2 k/r^2$ where, as in the incident beam, the number crossing unit area per unit time is proportional to k_0. Hence we have for the particle flux per unit angle and per unit incident flux,

$$\sigma(\theta')=|g_k(\theta')|^2 k/k_0, \quad (21)$$

which we call the differential cross section. By using Eq. (20) we get

$$\sigma(\theta')=(k_0^3k)^{-1}\left(\frac{2\mu}{\hbar^2}\right)^2 B_{n_0n}{}^2C_{m_{10}m_1}{}^2C_{m_{20}m_2}{}^2$$
$$\times\Big|\sum_{l=0}^{\infty}\exp\{i(\delta_{lk}+\delta_{lk_0})\}(2l+1)P_lA_{lk}\Big|^2. \quad (22)$$

The total inelastic cross section σ_i is the total particle flux per unit incident flux and therefore the integral of Eq. (21) over the sphere with unit radius. Because of the orthogonality of the Legendre polynomials, it contains no products of factors involving different values of l;

$$\sigma_i=(4\pi/kk_0^3)(2\mu/\hbar^2)^2B_{n_0n}{}^2C_{m_{10}m_1}{}^2C_{m_{20}m_2}{}^2$$
$$\times\sum_{l=0}^{\infty}(2l+1)A_{lk}{}^2. \quad (23)$$

The problem is to find the terms A_{lk}, defined by Eq. (19). It should be noted that this is a difficult question and so far only the exact value of A_{0k} has been obtained. Therefore, we shall introduce some approximate calculations for the series in Eq. (23). We make first some general remarks. The first term in Eq. (23) is the most important one. It can be shown that for small values of r, in the region $r<1/\alpha$ the ratio of the functions F_{lk} and F_{0k} is small and increases about as r^l. Thus the product of F_{lk_0} and F_{lk} will be very small where $V_0e^{-\alpha r}$ is appreciable; then the higher terms A_{lk} will be very small and consequently the terms A_{lk} become less important as l increases.

If we omit the potential in Eq. (18), the solutions of it, which we call $F_{lk'}$, are related to Bessel functions. So we have

$$F_{lk}'=(\pi kr/2)^{\frac{1}{2}}J_{l+\frac{1}{2}}(kr). \quad (24)$$

Next we define A_{lk}' in analogy with Eq. (19) as

$$A_{lk}'=\int_0^{\infty}V_0\exp(-\alpha r)F_{lk_0}'F_{lk}'dr. \quad (25)$$

It is also possible to show that the terms $A_{lk'}$ decrease very fast as l increases. On account of the smallness of A_{lk} and A_{lk}' for larger values of l, we approximate Eq. (23) by substituting for the second and following terms $A_{lk}=\text{const}\ A_{lk}'$ or

$$A_{lk}/A_{lk}'=A_{0k}/A_{0k}'. \quad (26)$$

With this approximation we shall obtain an easier expression for the cross section.

3. CALCULATION OF THE QUANTITIES A_{0k} AND A_{0k}'

The calculation of A_{0k} is similar to the one-dimensional problem and has been carried out by Jackson and Mott.[4] Substitute

$$z=(2/\alpha)\{(2\mu/\hbar^2)V_0\}^{\frac{1}{2}}\exp(-\tfrac{1}{2}\alpha r)$$

in Eq. (18) and take $l=0$. We obtain the equation

$$(d^2F/dz^2)+z^{-1}(dF/dz)+[(q^2/z^2)-1]F=0, \quad (27)$$

where $q=2k/\alpha$.

According to their calculations the final result becomes

$$A_{0k}=(\pi\alpha/8)(\hbar^2/2\mu)\frac{(q_0q\sinh\pi q_0\sinh\pi q)^{\frac{1}{2}}}{\cosh\pi q-\cosh\pi q_0}(q^2-q_0^2). \quad (28)$$

The calculations of the function $A_{0k'}$ can be easily carried out. We notice $F_{0k'}=\sin kr$. Consequently we obtain

$$A_{0k}'=\frac{2\alpha k_0kV_0}{\{\alpha^2+(k_0+k)^2\}\{\alpha^2+(k_0-k)^2\}}. \quad (29)$$

4. EXPRESSION FOR THE CROSS SECTION

We have seen in Eqs. (22) and (23), that the phase shifts δ_{lk} and δ_{lk_0} are of no significance in the calculation of the total cross section. Therefore, we take both values equal to zero. We substitute $F_{lk'}$ from Eq. (24) into Eq. (22) and obtain

$$\sigma'(\theta')=\frac{1}{k_0^3k}\left(\frac{2\mu}{\hbar^2}\right)^2 B_{n_0n}{}^2C_{m_{10}m_1}{}^2C_{m_{20}m_2}{}^2$$
$$\times\left|\sum_{l=0}^{\infty}(2l+1)P_l\int_0^{\infty}V_0e^{-\alpha r}(\pi kr/2)^{\frac{1}{2}}J_{l+\frac{1}{2}}(kr)(\pi k_0r/2)^{\frac{1}{2}}\right.$$
$$\left.\times J_{l+\frac{1}{2}}(k_0r)dr\right|^2. \quad (30)$$

In this expression we substitute the following formula[6]

$$\frac{\sin\omega r}{wr}=(\pi/2)\sum_l(2l+1)\frac{J_{l+\frac{1}{2}}}{(kr)^{\frac{1}{2}}}(kr)\frac{J_{l+\frac{1}{2}}}{(k_0r)^{\frac{1}{2}}}(k_0r)P_l(\cos\theta),$$

where w is the vector difference between k and k_0 and

[6] G. N. Watson, *Theory of Bessel Functions*, (University Press, Cambridge, England, 1944), p. 363, Eq. (3).

θ the angle between k and k_0. We obtain

$$\sigma'(\theta') = (k/k_0)(2\mu/\hbar^2)^2 B_{n_0n}{}^2 C_{m_1 0 m_1}{}^2 C_{m_2 0 m_2}{}^2 \times\left\{\int_0^\infty V_0 e^{-\alpha r} r^2 \frac{\sin\omega r}{\omega r} dr\right\}^2.$$

The integral on the right side can be evaluated by taking the direction of w as the polar axis. We find finally for the total cross section

$$\sigma_i' = 4\pi(k/k_0)(2\mu/\hbar^2)^2 B_{n_0n}{}^2 C_{m_1 0 m_1}{}^2 C_{m_2 0 m_2}{}^2 \alpha^2 V_0{}^2 \times\frac{\{2\alpha^2+2k_0^2+2k^2\}^2+\frac{16}{3}k_0^2k^2}{\{\alpha^2+(k_0+k)^2\}^3\{\alpha^2+(k_0-k)^2\}^3}. \quad (31)$$

On applying Eq. (26) we notice that

$$\sigma_i = (A_{0k}/A_{0k}')^2 \sigma_i'. \quad (32)$$

The substitution of Eqs. (28), (29), and (31) into Eq. (32) gives

$$\sigma_i = (\pi^3/\alpha^4) B_{n_0n}{}^2 C_{m_1 0 m_1}{}^2 C_{m_2 0 m_2}{}^2 \frac{\sinh\pi q_0 \sinh\pi q}{(\cosh\pi q_0 - \cosh\pi q)^2} \times\frac{(k^2-k_0^2)^2}{k_0^2} \frac{\{2\alpha^2+2k_0^2+2k^2\}^2+\frac{16}{3}k_0^2k^2}{\{\alpha^2+(k_0+k)^2\}\{\alpha^2+(k_0-k)^2\}}. \quad (33)$$

The total energy in the collision is conserved and therefore we have the following relation for k and k_0:

$$k_0^2 - k^2 = \pm\Delta E 2\mu/\hbar^2,$$

where ΔE is the energy exchanged between vibration and translation during a collision.

In the event of an elastic collision, $|k_0| = |k|$, or $\Delta\epsilon_1+\Delta\epsilon_{21}+\Delta\epsilon_{22}=0$ there may be an energy exchange between the two modes during the collision. This process is described by the elastic cross section, which can be obtained by taking $k_0=k$ in Eq. (33).

$$\sigma_e = (\pi/\alpha^4) B_{n_0n}{}^2 C_{m_1 0 m_1}{}^2 C_{m_2 0 m_2}{}^2 \frac{\{2\alpha^2+4k_0^2\}^2+\frac{16}{3}k_0^4}{\{\alpha^2+4k_0^2\}}. \quad (34)$$

5. TOTAL EFFECTIVE COLLISIONS PER UNIT TIME

We notice that translation for our purpose can be considered as an exterior degree of freedom and therefore we assume that the velocities of the molecules are distributed according to the Maxwell distribution law. The total number of effective collisions per unit time and per unit volume is then equal to

$$Q = (\pi/2) N_0^2 (2\mu/\pi kT)^{\frac{1}{2}} \int_0^\infty \exp(-\mu v'^2/2kT)\sigma v'^3 dv', \quad (35)$$

where σ is given by Eqs. (33) or (34). Notice all collisions are counted twice. This is necessary because during the collision the energy can be transferred to each of the two molecules.

We consider first the collisions which activate the vibration. We substitute $v_v' = k_0\hbar/\mu$ and integrate with respect to k between the limits zero and infinity and use the condition: $k_0^2 - k^2 = 2\mu E/\hbar^2$. We obtain:

$$Q_a = 4\pi^2(2\pi)^{\frac{1}{2}} N_0{}^2 B_{n_0n}{}^2 C_{m_1 0 m_1}{}^2 C_{m_2 0 m_2}{}^2 \alpha^{-6}\mu^{\frac{1}{2}}(kT)^{\frac{1}{2}}\hbar^{-4}(\Delta E)^2 \exp(-\Delta E/kT) \times\int_0^\infty \exp(-x^2)\frac{\sinh\pi q_0 \sinh\pi q}{(\cosh\pi q_0 - \cosh\pi q)^2} \frac{\frac{64}{3}x^4+(8\hbar^2\alpha^2/\mu kT+\frac{64}{3}\Delta E/kT)x^2+4(\hbar^2\alpha^2/2\mu kT+\Delta E/kT)^2}{x^2+d^2} x dx, \quad (36)$$

where

$$d^2 = \frac{2\mu kT}{4\alpha^2\hbar^2}\left(\frac{\hbar^2\alpha^2}{2\mu kT}+\frac{\Delta E}{kT}\right)^2; \qquad x^2 = \frac{\hbar^2k^2}{2\mu kT}.$$

We notice that $(\hbar^2\alpha^2/2\mu kT)$ is only 2% of $\Delta E/kT$; therefore, it can be neglected. We consider first the integral on the right side of Eq. (36). The integrand has its maximum for πq about 50. Therefore, we may simplify the first part of it by

$$\frac{\sinh 2\pi k/\alpha \sinh 2\pi k_0/\alpha}{(\cosh 2\pi k/\alpha - \cosh 2\pi k_0/\alpha)^2} = \exp[-(k_0-k)2\pi/\alpha]. \quad (37)$$

So far the integral is still too complicated. However, an approximate evaluation can be obtained by developing the exponent into a power series around the maximum as was done in reference 1. We finally obtain

$$Q_a = 256/9\pi^3(6)^{\frac{1}{2}} N_0{}^2\alpha^{-6}\mu^{\frac{1}{2}}(kT)^{\frac{1}{2}}\hbar^{-4}(\Delta E)^2 \exp(-\Delta E/kT)(d^2+b^2)^{-1}\exp(-3b^2) \times(\{\tfrac{5}{12}+\tfrac{1}{2}\Delta E/kT+\tfrac{3}{16}(\Delta E/kT)^2\}b+(\tfrac{5}{8}+\Delta E/kT)b^3+b^5) B_{n_0n}{}^2 C_{m_1 0 m_1}{}^2 C_{m_2 0 m_2}{}^2,$$

where $b = [\pi\mu\Delta E/\alpha\hbar(2\mu kT)^{\frac{1}{2}}]^{1/3}$.

Next we consider the collisions which deactivate the vibrations. The integration is now with respect to k_0 between the limits zero and infinity and we use the condition $k^2 - k_0^2 = (2\mu/\hbar^2)\Delta E$. We obtain similarly,

$$Q_d = Q_a \exp(\Delta E/kT).$$

If ΔE is large compared to kT, Q_a is much smaller than Q_d; physically this is so because collisions which activate the vibration need more energy than those which deactivate the vibration, and are consequently rarer.

The quantity Q is evaluated as a product of four factors. The last three $B_{n_0n}^2$, $C_{m_{10}m_1}^2$, and $C_{m_{20}m_2}^2$ can be considered as the transition probability of the three oscillators from the states n_0, m_{10}, and m_{20} to n, m_1, and m_2, respectively. The remaining factor depends only on the translational motion and the energy of the quantum jumps involved. For the elastic collisions we obtain by using Eq. (34)

$$Q_e=\tfrac{4}{3}(\pi^2/\alpha^4)N_0^2(2\mu/\pi kT)^{\frac{1}{2}}(\hbar/\mu)^4(2\mu kT/\hbar^2)^3B_{n_0n}^2C_{m_{10}m_1}^2C_{m_{20}m_{20}}^2\int_0^\infty e^{-y}\frac{y^3+3py^2+3p^2y}{y+p}dy,$$

where $y=\hbar^2k_0^2/2\mu kT$ and $p=(\alpha^2\hbar^2/8\mu kT)$ $(p<1)$. We get for the integral

$$(p+1)^2-p^3e^p(-\gamma-\log p+p/1!-p^2/2.2!+\cdots),$$

where $\gamma=0.5772$. We obtain for Q_e

$$Q=\tfrac{64}{3}(2\pi)^{\frac{1}{2}}N_0^2\alpha^{-4}\mu^{\frac{1}{2}}(kT)^{\frac{1}{2}}\hbar^{-2}\{(p+1)^2-p^3e^p(-\gamma-\log p+p\cdots)\}B_{n_0n}^2C_{m_{10}m_1}^2C_{m_{20}m_2}^2.$$

We write, for convenience,

$$Q_{a,d,e}=N_0^2P_{a,d,e}B_{n_0n}^2C_{m_{10}m_1}^2C_{m_{20}m_2}^2. \tag{38}$$

6. INTERACTION POTENTIAL

It is usual to represent the interaction potential for molecular collisions by the Lennard-Jones expression

$$V'=-4\epsilon[(r_0/r)^6-(r_0/r)^{12}].$$

The sixth power in the first term represents the attraction and the twelfth power the short range repulsive energy. It has been worked out by Herzfeld, that the regions where the force of interaction $-dV'/dx$ is strongest are the ones which contribute most to the energy transfer. Therefore, we are interested in the region for small r. It is mentioned in the introduction, that the interaction potential can be approximated as an exponential

$$V=V_0\exp(-\alpha d),$$

where d is the sum of the distance of separation of the centers of gravity of the two molecules r and the projections of the normal co-ordinates of the vibrations s_1, $s_{2,1}$, and $s_{2,2}$.

The factor α of the potential function can be obtained by fitting the exponential curve to the Lennard-Jones potential at the point where collisions are most favorable (see Table I).[2]

The internal motion coefficients A_1 and A_2, corresponding to the ratios of atomic vibrational amplitudes to their respective normal co-ordinates, can be obtained as follows. Let us assume first that the molecular orientation prior to collision is most favorable for the excitation of the bending mode, e.g., an approach perpendicular to the line direction of the molecule. So we have $d=r-(x_c-x_g)$, where x_c and x_g are the co-ordinates of the C atom and center of gravity in the direction of motion, respectively. We find

$$d=r-(m_{0_2}/m_{c0_2}) \qquad s_2=r-\tfrac{8}{11}s_2. \tag{39}$$

Second, we assume that the molecular orientation prior to collision is such as to be most favorable for the excitation of the valence mode, e.g., an approach along the line direction of the CO_2 molecule. We find similarly

$$d=r-\tfrac{1}{2}s_1.$$

Therefore,

$$A_1=\tfrac{1}{2} \quad \text{and} \quad A_2=\tfrac{8}{11}. \tag{40}$$

7. TRANSITION PROBABILITIES OF THE OSCILLATORS

The expressions B_{n_0n}, $C_{m_{10}m_1}$, and $C_{m_{20}m_2}$ can be evaluated for any quantum jump by using the harmonic oscillator wave functions and expressing the potential function as power series in s_1, $s_{2,1}$, or $s_{2,2}$. So we get

$$B_{n_0n}=\int_0^\infty\psi_{n_0}^*\{1-\alpha A_1s_1\cos\theta+2!^{-1}(\alpha A_1s_1\cos\theta)^2-\cdots\}\times\psi_n ds_1.$$

For $n=n_0$ (no energy transfer) we get practically $B_{n_0n}=1$. When there is only one quantum jump involved we find by neglecting very small terms:

$$B_{n,n+1}=-\alpha A_1\cos\theta[\hbar(n+1)/4\pi\mu_1\nu_1]^{\frac{1}{2}} \quad \text{(activation)} \tag{41}$$

$$B_{n,n-1}=-\alpha A_1\cos\theta[\hbar n/4\pi\mu_1\nu_1]^{\frac{1}{2}}, \quad \text{(deactivation)}. \tag{42}$$

We obtain, for the C_{m_1}'s,

$$C_{m_1m_1+1}=-\alpha A_2\sin\theta\sin\phi[\hbar(n+1)/4\pi\mu_2\nu_2]^{\frac{1}{2}} \quad \text{(activation)} \tag{43}$$

$$C_{m_1m_1-1}=-\alpha A_2\sin\theta\sin\phi[\hbar n/4\pi\mu_2\nu_2]^{\frac{1}{2}} \quad \text{(deactivation)}. \tag{44}$$

When there are two quantum jumps involved we find

$$C_{m_1m_1+2}=\tfrac{1}{2}(\alpha\sin\theta\sin\phi A_2)^2[\hbar(n+2)(n+1)/16\pi^2\mu_2^2\nu_2^2]^{\frac{1}{2}}$$

(activation) (45)

$$C_{m_1m_1-2}=\tfrac{1}{2}(\alpha\sin\theta\sin\phi A_2)^2[\hbar n(n-1)/16\pi^2\mu_2^2\nu_2^2]^{\frac{1}{2}}$$

(deactivation). (46)

Similar expressions can be obtained for the C_{m_2}'s by substituting $\cos\phi$ instead of $\sin\phi$.

Although there is no restriction that only one or two quantum jumps are possible, we find that a change of more quanta in either mode during a collision is so improbable as to be negligible.

8. RELAXATION TIMES

The amount of energy fed per unit time into a particular mode of vibration can be obtained by multiplying $(Q_a - Q_d)$ with the energy quantum associated with this mode. There are, however, for the molecules many initial states of vibration and each state has an occupation density q. We define $q_{nm_1m_2}$ as the amount of molecules per unit volume with the vibration b in state n and the vibrations c in state m_1 and m_2, respectively. q_{m_1} means the amount of molecules per unit volume with the vibrational state m_1. Each vibration is partly excited by direct excitation and partly in series with the other vibration.

The quantum jumps for b are about twice as large as those for the c mode. One may expect therefore that a direct excitation is less probable for the b mode.

Let us first calculate the energy transferred per unit time in the c mode. It is sufficient to consider only one degenerated c mode and to multiply the result with 2, so that we obtain the total energy of the c modes. During these collisions there is neither energy fed into the b mode nor in the other c mode. Their quantum numbers do not change and we substitute $B_{n0n}=1$ and $C_{m_20m_2}=1$. By using Eq. (38) we obtain the following series

$$dE_2/dt=2h\nu_2N_0P_a(\sum_{m_1=0}^{\infty}q_{m_1}C_{m_1m_1+1}^2)$$

$$-2h\nu_2N_0P_d(\sum_{m_1=0}^{\infty}q_{m_1}C_{m_1m_1-1}^2)-dE_1/dt, \quad (47)$$

where we have neglected double or multiple quantum jumps, which probabilities are many orders of magnitude smaller. The first term expresses activation and the second term deactivation. The last term on the right side represents the exchange between the b and c mode. This series can be simplified by using the probability relations, between the transitions $C_{m_1m_1+1}$, $C_{m_1m_1-1}$ and $C_{0,1}$, which are obtained from Eq. (43) and Eq. (44) (see reference 2).

By using Eq. (38) we obtain the relation

$$P_d(h\nu_2)=P_a(h\nu_2)\exp(h\nu_2/kT).$$

Equation (47) becomes

$$dE_2/dt=2h\nu_2N_0P_aC_{0,1}^2$$

$$\times\{\sum_{m_1=0}^{\infty}(m_1+1)q_{m_1}-\exp(h\nu_2/kT)\sum_{m_1=0}^{\infty}m_1q_{m_1}\}-dE_1/dt.$$

Next we use the relations for

$$E_2=2\sum_{m_1=0}^{\infty}m_1h\nu_2q_{m_1}:\sum_{m_1=0}^{\infty}q_{m_1}=N_0.$$

The quantity $C_{0,1}$ depends on the angles θ and ϕ. There are, however, all possible orientations and therefore we have to average the factor $\langle\sin^2\theta\sin^2\phi\rangle$ over all possible values for θ and ϕ. We substitute $C_{0,1}^2=\frac{1}{3}C_{0,1}^{*2}$, where $C_{0,1}^*$ means the maximum value of $C_{0,1}$. This is for $\sin\theta=\sin\phi=1$. We obtain

$$dE_2/dt=\tfrac{1}{3}N_0P_aC_{0,1}^{*2}[\exp(h\nu_2/kT)-1]\{E_2(T)-E_2\}$$

$$-dE_1/dt, \quad (48)$$

where $E_2(T)=2N_0h\nu_2/[\exp(h\nu_2/kT)-1]$, the energy for the translation temperature.

Next we consider the more complicated excitation process for the b mode in which we will neglect again the probabilities for double or multiple quantum jumps. In this process the energy can be transferred in four different ways:

(a) First, we have the possibility that a quantum is transferred by direct excitation. We obtain for this part of the energy transfer an equation similar to Eq. (48). However, it turns out that this direct energy exchange is negligible slow.

(b) Second, there is a possibility that the transferred quantum $h\nu_1$ is obtained partly from one quantum $h\nu_2$ of one of the c modes and the rest from the translation. But also in this combined direct and indirect excitation process are the calculated transition probabilities small compared with the cases c and d.

(c) Third, we consider the case that the energy is only exchanged between b and c mode during elastic collisions. The b mode is activated by gaining one quantum, while the c modes are deactivated by losing two quanta. There are different ways in which the various quantum numbers can change. Therefore, we consider now only the collisions in which the quantum numbers of one c mode change by two. The corresponding energy which is fed per unit time in the b mode is

$$dE_1^1/dt=h\nu_1N_0P_e\{\sum_{n=0}^{\infty}\sum_{m_1=0}^{\infty}(B_{n,n+1}{}^2C_{m_1m_1-2}{}^2$$

$$-B_{n,n-1}{}^2C_{m_1m_1+2}{}^2)q_{nm_1}\}. \quad (49)$$

In this type of collisions there is a possibility that the b mode of one molecule is activated while the c mode of the other molecule is deactivated, or the entire energy exchange is within the same molecule. In order to obtain the average values for the B's and C's we multiply in the first case the average value of $\langle\cos^4\theta'\rangle$ with the average value of $\langle\cos^2\theta\rangle$. We obtain the factor 1/15. In the second case the two normal coordinates are always perpendicular and we average over $\langle\cos^2\theta\sin^4\theta\sin^4\phi\rangle=1/35$. Further, on account of the degeneracy we have to multiply the sum of these average values with 2 and we obtain finally the factor 100/525.

$$dE_1^1/dt=\tfrac{100}{525}h\nu_1N_0P_e$$

$$\times\{\sum_{n=0}^{\infty}\sum_{m_1=0}^{\infty}(B_{n,n+1}{}^{*2}C_{m_1m_1-2}{}^{*2}-B_{n,n-1}{}^{*2}C_{m_1m_1+2}{}^{*2})q_{nm_1}\},$$

where we have substituted the maximum values for the B's and C's. We use the probability relations obtained from Eqs. (41), (42), (45), and (46) (see reference 2).

We obtain

$$dE_1^1/dt=\tfrac{100}{525}h\nu_1N_0P_eB_{0,1}{}^{*2}C_{0,2}{}^{*2}$$

$$\times\{\sum_{n=0}^{\infty}\sum_{m_1=0}^{\infty}(m^2-4nm-2n-m)q_{nm_1}\}. \quad (50)$$

We will use a Maxwellian distribution for all $q_{nm_1m_2}$ and derive the following expressions:

$$\left.\begin{aligned}
&\sum_{n=0}^{\infty}\sum_{m_1=0}^{\infty}m^2q_{nm_1}=\frac{1+\exp(h\nu_2/kT_2)}{\{\exp(h\nu_2/kT_2)-1\}^2}N_0\\
&\sum_{n=0}^{\infty}\sum_{m_1=0}^{\infty}-2nq_{nm_1}=\frac{-2N_0}{\{\exp(h\nu_1/kT_1)-1\}}\\
&\sum_{n=0}^{\infty}\sum_{m_1=0}^{\infty}-4nm_1q_{nm_1}\\
&\qquad=\frac{-4N_0}{\{\exp(h\nu_2/kT_2)-1\}\{\exp(h\nu_1/kT_1)-1\}}\\
&\sum_{n=0}^{\infty}\sum_{m_1=0}^{\infty}=-\dot{m}_1q_{nm_1}=\frac{-N_0}{\{\exp(h\nu_2/kT_2)-1\}}.
\end{aligned}\right\} \quad (51)$$

Eq. (50) becomes with these expressions:

$$dE_1^1/dt=\tfrac{200}{525}h\nu_1N_0{}^2P_eB_{0,1}{}^{*2}C_{0,2}{}^{*2}$$

$$\times\left[\frac{1}{\{\exp(h\nu_2/kT_2)-1\}^2}-\frac{1+\exp(h\nu_2/kT_2)}{\{\exp(h\nu_2/kT_2)-1\}\{\exp(h\nu_1/kT_1)-1\}}\right]. \quad (52)$$

TABLE I. The factor α of the repulsive force field as a function of temperature is obtained by fitting the exponential curve to the Lennard-Jones potential at the point where collisions are most favorable.*

T	$E_2/k=975°$ $\alpha(\text{cm}^{-1})$	$E_1/k=1820°$ $\alpha(\text{cm}^{-1})$
300	4.43×10^8	4.38×10^8
400	4.43×10^8	4.38×10^8
500	4.42×10^8	4.37×10^8
600	4.41×10^8	4.37×10^8
700	4.40×10^8	4.36×10^8
800	4.39×10^8	4.36×10^8
900	4.38×10^8	4.35×10^8
1000	4.37×10^8	4.35×10^8

* See reference 2.

We use the relations $2\nu_2=\nu_1$ and $C_{0,2}{}^2=\frac{1}{2}C_{0,1}{}^4$.

$$dE_1^1/dt=\tfrac{100}{525}N_0P_eB_{0,1}{}^{*2}C_{0,1}{}^{*4}\left\{\frac{\exp(h\nu_2/kT_2)+1}{\exp(h\nu_2/kT_2)-1}\right\}$$

$$\times\{E_1(T_2)-E_1\}, \quad (53)$$

where

$$E_1(T_2)=\frac{h\nu_1N_0}{\exp(h\nu_1/kT_2)-1}$$

and

$$E_1=\frac{h\nu_1N_0}{\exp(h\nu_1/kT_1)-1}.$$

(d) Fourth, we consider the transferred energy of the elastic collisions in which the quantum $h\nu_1$ of the b mode is obtained from two c modes, each giving one quantum. During such collisions there are two transition probabilities, each of two arbitrary c modes may transfer one quantum, or it may be done by the remaining two c modes. There are, however, six combinations for the c modes. The mutual orientation of the respective normal co-ordinates in each combination is not the same. In the combination, in which the transfer is entirely within the molecule, the normal co-ordinates of the vibrations are always perpendicular and consequently we average over $\langle\cos^2\theta\sin^4\theta\sin^2\phi\cos^2\phi\rangle=1/105$. In the other five combinations we obtain the product of the average values $\langle\cos^2\theta\sin^2\theta\sin^2\phi\rangle$ and $\langle\cos^2\theta'\rangle$ equal to 1/45. We calculate the transferred energy in this process by substituting the maximum values for the B's and C's and multiply the result with

$$\tfrac{1}{3}(5\times\tfrac{1}{45}+\tfrac{1}{105})=\tfrac{38}{945}.$$

$$dE_1''/dt=\tfrac{38}{945}h\nu_1N_0P_e\{\sum_{n=0}^{\infty}\sum_{m_1=0}^{\infty}\sum_{m_2=0}^{\infty}(B_{n,n+1}{}^{*2}C_{m_1m_1-1}{}^{*2}C_{m_2m_2-1}{}^{*2}-B_{n,n-1}{}^{*2}C_{m_1m_1+1}{}^{*2}C_{m_2m_2+1}{}^{*2})q_{nm_1m_2}\}, \quad (54)$$

which reduces to

$$dE_1''/dt=\tfrac{38}{945}h\nu_1 N_0 P_e B_{0,1}^{*2} C_{0,1}^{*4}\{\sum_{n=0}^{\infty}\sum_{m_1=0}^{\infty}\sum_{m_2=0}^{\infty}(m_1m_2-nm_2-nm_1-n)q_{nm_1m_2}\} \tag{55}$$

where we have used Eqs. (41), (42), (43), and (44). By using the Maxwell distribution we obtain:

$$\sum_{n=0}^{\infty}\sum_{m_1=0}^{\infty}\sum_{m_2=0}^{\infty}m_1m_2q_{nm_1m_2}=\frac{N_0}{\{\exp(h\nu_2/kT_2)-1\}^2}$$

$$\sum_{n=0}^{\infty}\sum_{m_1=0}^{\infty}\sum_{m_2=0}^{\infty}-2nm_1q_{nm_1m_2}=\frac{-2N_0}{\{\exp(h\nu_2/kT_2)-1\}\{\exp(h\nu_1/kT_1)-1\}}$$

$$\sum_{n=0}^{\infty}\sum_{m_1=0}^{\infty}\sum_{m_2=0}^{\infty}-nq_{nm_1m_2}=\frac{-N_0}{\{\exp(h\nu_1/kT_1)-1\}}.$$

Eq. (55) becomes, with these expressions,

$$dE_1''/dt=\tfrac{38}{945}h\nu_1 N_0^2 P_e B_{0,1}^{*2} C_{0,1}^{*4}\left[\frac{1}{\{\exp(h\nu_2/kT_2)-1\}^2}-\frac{1+\exp(h\nu_2/kT_2)}{\{\exp(h\nu_2/kT_2)-1\}\{\exp(h\nu_1/kT_1)-1\}}\right].$$

Comparing this requlting with Eq. (52) we obtain at once

$$dE_1''/dt=\tfrac{38}{945}P_e N_0 B_{0,1}^{*2} C_{0,1}^{*4}\left\{\frac{\exp(h\nu_2/kT_2)+1}{\exp(h\nu_2/kT_2)-1}\right\}\{E_1(T_2)-E_1\}. \tag{56}$$

Now we set $E_1=E_1'+E_1''$ and obtain for the total energy rate transferred in the b mode the following equation

$$dE_1/dt=0.22N_0P_eB_{0,1}^{*2}C_{0,1}^{*4}\left\{\frac{\exp(h\nu_2/kT_2)+1}{\exp(h\nu_2/kT_2)-1}\right\}\{E_1(T_2)-E_1\} \tag{57}$$

Eqs. (48) and (57) are the relaxation equations. We conclude therefore that there is for the b mode an excitation in series and for the c mode a direct excitation. The relaxation times are

$$\tau_2=[0.33N_0P_aC_{0,1}^{*2}\{\exp(h\nu_2/kT_2)-1\}]^{-1}$$

$$\tau_{1,2}=\left[0.22N_0P_eB_{0,1}^{*2}C_{0,1}^{*4}\left\{\frac{\exp(h\nu_2/kT_2)+1}{\exp(h\nu_2/kT_2)-1}\right\}\right]^{-1}.$$

This conclusion has been verified by our experiments. However, the experimental values for $\tau_{1,2}$ could not be obtained accurately; they are at least one order of magnitude smaller. We find at 1000°K $\tau_{1,2}=1.45\times10^{-6}$ and $\tau_2=6.15\times10^{-6}$ sec. The theoretical values of τ_2 are for temperatures around 1000°K in fairly good agreement with our experimental results. For lower temperatures the values of τ_2 are too large compared with experimental data. The reason is that by lower energies we are not allowed to make such rough approximations in the calculation of the integral in Eq. (36).

ACKNOWLEDGMENTS

The author wishes to thank Professor J. M. Burgers for many helpful suggestions and discussions concerning this work. He also gratefully acknowledges a stimulating discussion with Professor K. F. Herzfeld.

Diffusion and Heterogeneous Reaction. IV. Effects of Gas-Phase Reaction and Convective Flow*

HENRY WISE AND CLARENCE M. ABLOW

Department of Chemical Physics, Stanford Research Institute, Menlo Park, California

(Received April 18, 1960)

The kinetics of atom recombination by homogeneous and heterogeneous reaction are examined. The analysis includes the combined effects of first-order surface reaction and third-order gas-phase reaction in a system undergoing diffusive and convective flow. On the basis of this model the rate constants for the homogeneous rate of recombination of oxygen atoms and of hydrogen atoms are derived from published experimental measurements.

INTRODUCTION

IN a preceding publication[1] the flow equations governing recombination of atoms by heterogeneous reaction in the absence of gas-phase interaction have been established. The equations were applied to a system consisting of a cylindrical tube into which the atoms were allowed to diffuse in a radial and longitudinal direction toward the wall of the tube and an end plate[2] of specified catalytic activities. In such a system the atom concentration at any point in the cylinder is governed by the balance between diffusion and atom removal by the heterogeneous reaction, provided that the total gas pressure is kept sufficiently low so that the gas-phase reaction may be neglected. Such a model, with both radial and longitudinal diffusion gradients considered, is adequate to interpret those experimental measurements in which the efficiency of various solid surfaces for atom recombination is under investigation.[3–6] Once these surface activities are determined, the measurement of the kinetics of homogeneous, gas-phase atom recombination may be carried out. Such a procedure requires an increase in the total gas pressure of the system containing atoms and molecules and determination of the atom concentration gradient resulting from the presence of the two "atom sinks," the catalytic surface reaction, and the three-body gas-phase interaction.

In the analysis to be presented the influence of homogeneous atom recombination on heterogeneous reaction is examined in some detail. Subsequently, convective flow of the gas is added to diffusive flow of the atoms in the cylinder. This effect is of special interest since flow systems have been employed for the study of gas-phase kinetics of atoms with some speculation as to the relative contributions of convective and diffusive flow. Also, various problems related to propulsion in the upper atmosphee require a detailed analysis of the interaction of the fluid-dynamic and reaction-kinetic parameters.

MATHEMATICAL MODEL

In this analysis we consider a single reactive species (atoms) which disappears by simultaneous first-order heterogeneous reaction and third-order homogeneous reaction with another atom or a molecule acting as the third body. If n particles per unit volume of an active species diffuse through an inert gas of concentration M, the diffusion being superposed on a bulk flow at velocity v in the axial direction down a cylindrical tube, then a steady-state balance of the number of active particles entering and leaving an arbitrary volume results in

$$D\Delta n - v(\partial n/\partial x) - n^2(2k_1M + 3k_2n) = 0, \qquad (1)$$

where D is the interdiffusion coefficient for the active species, k_1 and k_2 the rate constants for the homogeneous reaction with molecules and atoms, respectively, as third bodies, and Δ is the Laplacian operator taking in the present case of cylindrical symmetry the form

$$\Delta n = (\partial^2 n/\partial r^2) + (1/r)(\partial n/\partial r) + \partial^2 n/\partial x^2 \qquad (2)$$

with r the radial and x the axial coordinates.

It is assumed that the concentration of product molecules relative to the total concentration M is small so that the variation in M down the length of the tube may be neglected. Similarly, the variations in gas temperature due to the heat released in the atom recombination are assumed to have negligible effect on the diffusion coefficient and the rate constants. Thus all coefficients appearing in Eq. (1) are constants.

The catalytic activities of the cylinder wall at $r = R$ and of the probe surface located at a distance $x = L$ from the atom source are expressed by the boundary conditions[1]

$$(\partial n/\partial r)(R, x) = -n(R, x)/\delta R \qquad (3)$$

$$(\partial n/\partial x)(r, L) = -n(r, L)/\delta' R, \qquad (4)$$

* This work was sponsored by Project Squid, which is supported by the Office of Naval Research, Department of the Navy.

[1] H. Wise and C. M. Ablow, J. Chem. Phys. **29,** 634 (1958).

[2] In the experimental apparatus the end plate is simulated by a catalytic probe surface which removes at a given cross section of the cylinder a fraction of those atoms which have survived the collisions with the walls during their journey through the tube.

[3] W. V. Smith, J. Chem. Phys. **11,** 110 (1943).

[4] J. W. Linnett and D. G. H. Marsden, Proc. Roy. Soc. (London), **A234,** 489, 504 (1956).

[5] J. C. Greaves and J. W. Linnett, Trans. Faraday Soc. **54,** 1323 (1958).

[6] B. J. Wood and H. Wise, J. Chem. Phys. **29,** 1416 (1958).

where δ and δ' are the dimensionless numbers[7]

$$\delta=4D[1-(\gamma/2)]/\gamma cR, \qquad \delta'=4D[1-(\gamma'/2)]/\gamma' cR.$$

Here γ is the recombination coefficient for the cylinder wall, γ' that for the probe, and c the mean velocity of the reacting species. Furthermore, the density of active species has a uniform value at the source, $x=0$

$$n(r, 0)=n_0, \tag{5}$$

and because of symmetry no radial density gradient exists at the axis of the cylinder,

$$(\partial n/\partial r)(0, x)=0. \tag{6}$$

Conditions (3)–(6) are sufficient to ensure a unique non-negative solution to the partial differential equation (1). Because of the nonlinear nature of the equation, numerical approximate solutions valid for particular values of the parameters were obtained.

In preparation for numerical solution it is useful to identify the dimensionless variables and parameters, as these provide a description of the solution in fewest terms. By using n_0 as a unit for atom density one may define

$$u=n/n_0, \qquad C=3k_2n_0/2k_1M.$$

A length associated with the kinetic parameters is

$$b=(3D/4k_1Mn_0)^{\frac{1}{3}}.$$

By using b as a unit of length, one may define

$$y=x/b, \qquad L_1=L/b, \qquad F=\delta R/b,$$

$$s=r/b, \qquad R_1=R/b, \qquad F'=\delta' R/b.$$

Finally a dimensionless convective velocity may be defined as

$$V=vb/D.$$

In these terms the differential equation and boundary conditions determining u as a function of y and s read

$$\partial^2u/\partial s^2+(1/s)(\partial u/\partial s)+(\partial^2u/\partial y^2)$$
$$=V(\partial u/\partial y)+\tfrac{3}{2}u^2(1+Cu), \tag{7}$$

$$u+F(\partial u/\partial s)=0 \quad \text{at} \quad s=R_1, \tag{8}$$

$$u+F'(\partial u/\partial y)=0 \quad \text{at} \quad y=L_1, \tag{9}$$

$$u=1 \quad \text{at} \quad y=0, \tag{10}$$

$$\partial u/\partial s=0 \quad \text{at} \quad s=0. \tag{11}$$

The problem of solving Eq. (7)–(11) is greatly simplified in the absence of a radial concentration gradient. Such a condition is a satisfactory approximation at elevated pressures of inert gas in cylinders of large radius, since the atoms suffer many collisions in the gas phase before reaching the wall[8] (see Table I).

TABLE I. Parameters used in calculations for homogeneous hydrogen atom recombination in the presence of molecular hydrogen.

Homogeneous rate constant k_1	10^{16} (mole/cc)$^{-2}$ sec^{-1}
Interdiffusion coefficient[a] D	$(1.4\times10^3)/P$ cm^2/sec
Gas temperature T	300°K
Atom velocity c	2.5×10^5 cm/sec
Cylinder radius R	2.5 cm
Recombination coefficient of glass walls γ	10^{-4}
Recombination coefficient of end plate γ'	10^{-2}

[a] I. Amdur, J. Chem. Phys. **4**, 339 (1936); pressure P in mm Hg.

[7] H. Motz and H. Wise, J. Chem. Phys. **32**, 1893 (1960).

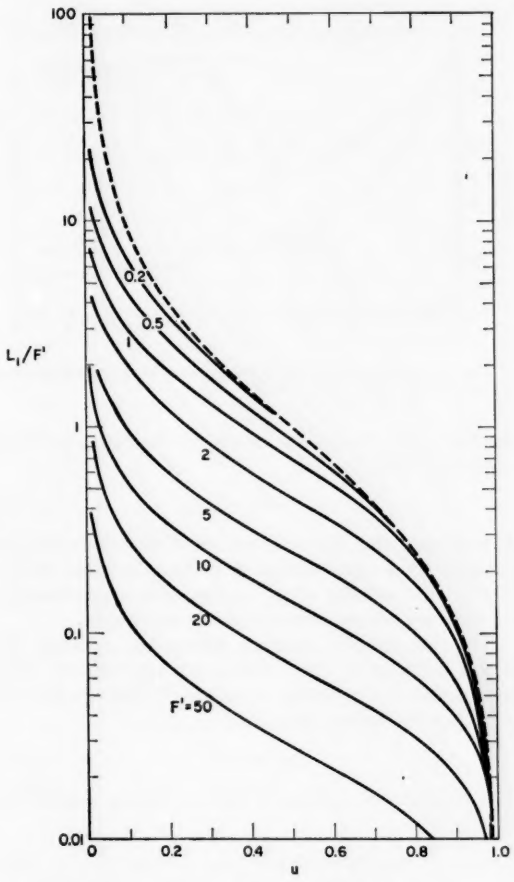

FIG. 1. Gas-phase and surface recombination in the absence of convective flow ($V=0$). — — —: $F'=0$.

[8] In the case of hydrogen in a glass cylinder ($R=2.5$ cm) at a total pressure of 1 mm and an atom pressure of 0.2 mm, $F=\delta R/b\leq25$ (cf. Table I).

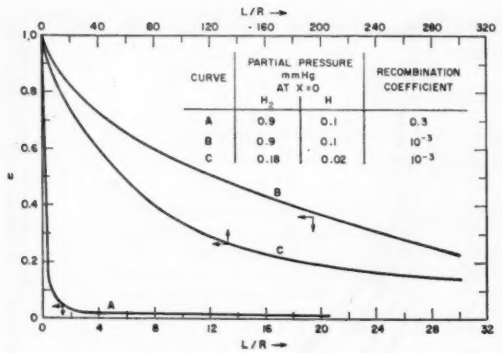

FIG. 2. Homogeneous and heterogeneous atom recombination in the absence of convective flow.

In this case, boundary condition Eq. (8), becomes approximately

$$\partial u/\partial s=0.$$

It is evident that the complete set of equations may be satisfied by u as a function of y alone. In other words, if $F\gg 1$ the density of active species is approximately uniform on planes normal to the cylinder axis.

The second-order ordinary differential equation for u as a function of y thus obtained is conveniently split into a pair of first-order equations by introduction of auxiliary variable w defined by

$$du/dy=w. \tag{12}$$

The differential equations and boundary conditions then read

$$dw/du=V+(3u^2/2w)(1+Cu); \tag{13}$$

$$u=1 \quad \text{at} \quad y=0; \tag{14}$$

and

$$u+F'w=0 \quad \text{at} \quad y=L_1. \tag{15}$$

These equations may now be solved for specified flow and reaction conditions imposed on the system.

GAS-PHASE RECOMBINATION WITHOUT CONVECTIVE FLOW

In the absence of convective flow, $V=0$, Eq. (13) may be readily integrated to give

$$w^2=u^3+\tfrac{3}{4}Cu^4+K_1, \tag{16}$$

where K_1 is a constant of integration. By a combination of analytic and numerical methods of approximation, the explicit relations between the variables u, L_1, and F' were obtained (cf. Appendix). The results of these computations for the condition $C\ll 1$, i.e., $k_1M\gg k_2n_0$, are shown as a family of curves in Fig. 1.

In the absence of gas-phase recombination ($b=\infty$, i.e., $F'=0$) the atom concentration at the probe is related to the catalytic activity of the surface material[1] by the equation $u_L=1/[1+(L/\delta' R)]$. The curve appropriate to this condition has been added to Fig. 1 in order to indicate the contribution of the gas-phase reaction.

It is apparent that on the basis of these theoretical calculations the measurement of the rate constant for the recombination of atoms by three-body gas-phase collisions may be carried out in a steady-state experiment. From the experimentally observed atom concentration profile as a function of probe location for surfaces of known catalytic activities, the kinetic parameter may be evaluated. An indication of the relative efficiency of the two atom sinks, i.e., gas-phase reaction[9] and surface reaction, may be obtained from the data presented in Fig. 2. At a total gas pressure of 1 mm Hg in the presence of a very active probe (curve A) the relative atom concentration decreases rapidly within a short distance from the atom source. As a matter of fact the heterogeneous reaction completely overshadows the gas-phase recombination under these conditions

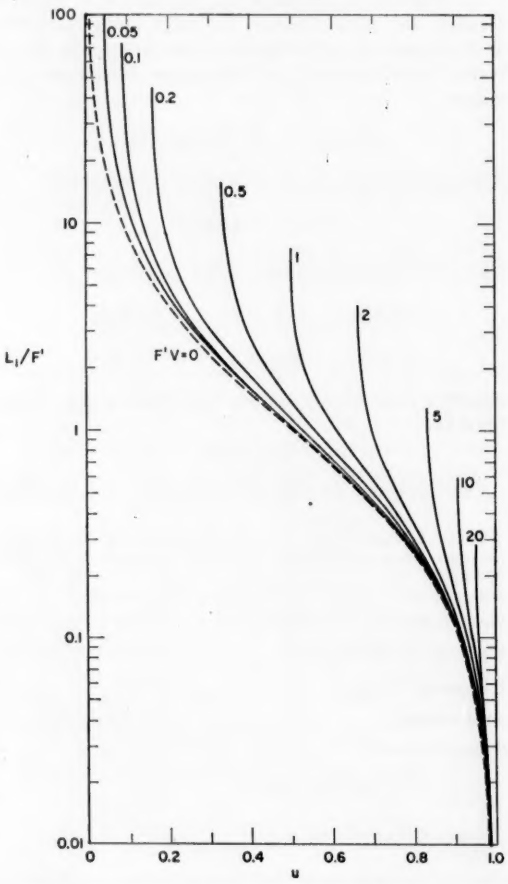

FIG. 3. Heterogeneous atom recombination in the presence of convective flow.

[9] The data used in these calculations are summarized in Table I.

and curve A is identical to that calculated in the absence of homogeneous reaction. A decrease in the catalytic activity of the probe surface by a factor of 300 manifests the contribution of the three-body recombination process. As shown by curve B, the atom concentration is reduced to $\frac{1}{2}$ of its value at the source when the probe is located at a distance of 12 cylinder radii from the source. For a probe of identical activity but at a total gas pressure of 0.2 mm Hg, a similar reduction in relative atom concentration spreads the reaction zone to 60 radii. Such considerations offer a useful guide in the design of experiments on the measurement of the homogeneous atom-recombination rate.[10]

HETEROGENEOUS ATOM RECOMBINATION IN THE PRESENCE OF CONVECTIVE FLOW

In the course of our numerical calculations it was found desirable to integrate Eq. (1) for the condition

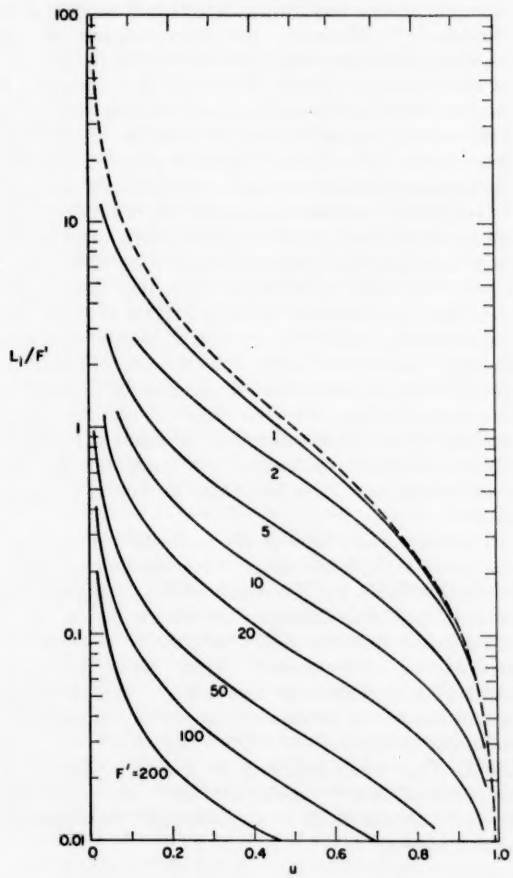

FIG. 4. Gas-phase and surface recombination in presence of convective flow ($V=1$). — — —: $F'=0$.

[10] Preliminary experimental measurements have demonstrated the feasibility of this steady-state technique for the measurement of gas-phase reaction rates.

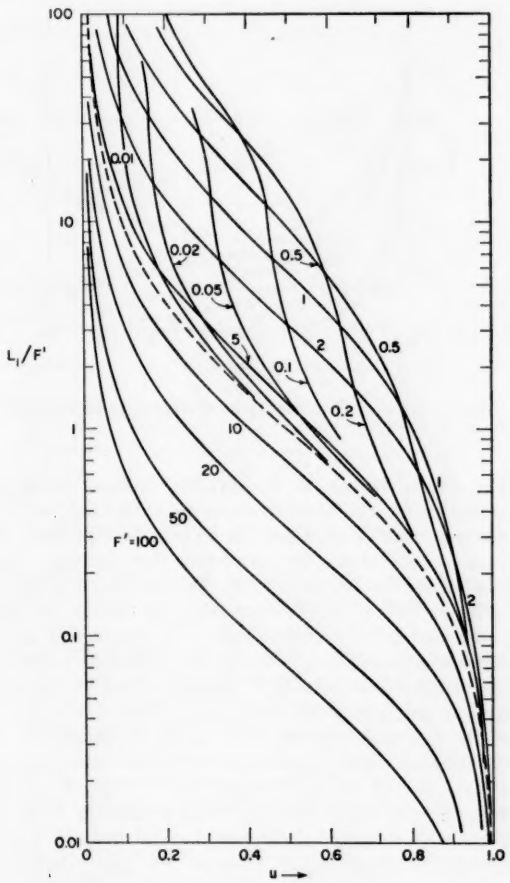

FIG. 5. Gas-phase and surface recombination in presence of convective flow ($V=10$). — — —: $F'=0$.

of surface reaction with convective flow in the absence of gas-phase recombination, i.e., $k_1=k_2=0$ for various catalytic activities and flow velocities. The contribution of forced convection to the diffusive transport of atoms is clearly demonstrated in Fig. 3. The product $F'V$ is proportional to the convective flow velocity and inversely proportional to the surface activity of the probe. For a surface material of specified catalytic efficiency the contribution of convective flow to the mass transport becomes pronounced particularly at large distance from the atom source. The curves shown (Fig. 3) are a suitable reference in the subsequent analysis in which homogeneous reaction is taken into account.

GAS-PHASE AND SURFACE RECOMBINATION IN THE PRESENCE OF CONVECTIVE FLOW

The solution of Eq. (12) for finite values of the flow-velocity parameter V requires numerical integration. A series of such machine computations were carried out

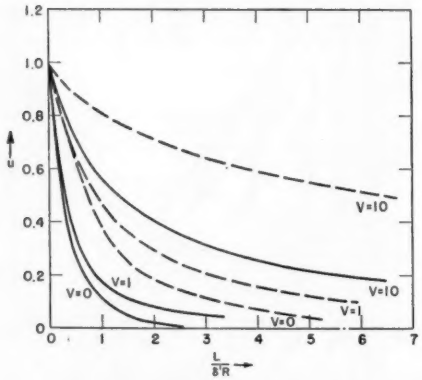

FIG. 6. Effect of flow velocity on relative atom concentration. — — —: $F'=1$; —: $F'=5$.

for several values of V including various catalytic activities for the heterogeneous recombination on the probe surface (Figs. 4 and 5). As is to be expected, the transport of atoms by convective flow increases the local atom concentration over that calculated for pure diffusive flow at a given position and activity of the probe and for a specified rate of homogeneous atom recombination (Fig 6.) On the other hand, at constant gas velocity a decrease in F' brought about by increasing the strength of the probe as an atom sink relative to the gas-phase reaction rate causes a diminution in the distance required to reduce the atom concentration by a specified amount. Inspection of Figs. 4 and 5 indicates that small changes in the parameter F' have a more pronounced influence on the atom density gradient at high rather than at low gas velocities.

An interesting result of this theoretical analysis is to be found in a detailed examination of the curves presented in Fig. 5. It is noted that at low values of F' the curves cross over each other. This phenomenon can be understood by considering a system in which the values of δ', L, R, and V are fixed. Under these conditions a plot of the relative atom concentration u versus the reaction-kinetics parameter b yields the curve shown in Fig. 7. From the definitions of the dimensionless parameters it is apparent that for a constant value of V, the velocity v is inversely proportional to b and the homogeneous rate constant k_1 is inversely proportional to b^2. Therefore, an increase in b causes the gas-phase reaction rate to decrease more rapidly than the velocity and, as a result, the relative atom concentration rises at a fixed point within the cylinder. Further increase in b causes the gas-phase reaction to cease. Also, the flow velocity becomes sufficiently reduced so that the atom concentration at the references cross section approaches a value determined by diffusive flow and heterogeneous reaction on the solid surface. Consequently, a maximum is observed in the plot of u vs b (Fig. 7).

This result of the theoretical analysis points to certain basic requirements in the design of experiments for the measurement of homogeneous atom-recombination rates in a dynamic system with bulk flow. At low convective flow velocities the probe surface of the calorimeter employed for the determination of residual atom concentration at a given distance from the source should be of low catalytic activity in order to obtain sufficient spatial resolution. On the other hand, at high gas velocities a more catalytic surface is needed (small F'); otherwise, a very long cylinder is required to observe changes in atom concentration with distance from the atom source.

DISCUSSION

Several measurements of the rate of atom recombination by three-body, gas-phase collisions have been carried out in a dynamic system with a catalytic surface as a calorimetric tool for the detection of residual atom densities.[11–13] However, the interpretation of the experimental results was made difficult by the presence of diffusion terms in the differential flow equation. It may be of interest to examine some of these data in the light of the present theoretical analysis which takes into account diffusive and convective flow in a system undergoing homogenous and heterogeneous reaction. In particular, we have considered the results reported by Amdur[11] in order to derive from them a value for the rate constant of gas-phase recombination of hydrogen atoms. In these experiments molecular and atomic hydrogen were pumped through a glass cylinder, the recombination tube. The fraction of atomic hydrogen at any cross section within this tube was obtained by means of a platinum-catalyst calorimeter exposed to the stream of gas. On the basis of the theoretical analysis presented in this paper the fractional concentration of atomic hydrogen was computed for the experimental condition prevalent in Amdur's experiments.

The parameters used in the evaluation of the rate constant for hydrogen-atom recombination are summarized in Table II. The results of the theoretical and experimental determinations are shown in Fig. 8. It can be seen that the theory adequately predicts the experimental observations.[11] From these data one obtains an average rate constant for the gas-phase recombination of atomic hydrogen by three-body collisions, $k=(1.6\pm0.1)\times10^{16}$ $(\text{mole/cc})^{-2}$ sec^{-1} at 300°K. This value compares to a rate coefficient of $k=(0.9\pm0.7)\times10^{16}$ $(\text{mole/cc})^{2}$ sec^{-1} computed by Carreri[14] on the basis of various other experimental measurements.

[11] I. Amdur, J. Am. Chem. Soc. **60,** 2347 (1938). In this work the results obtained by other authors are reviewed.
[12] W. Steiner, Trans. Faraday Soc. **31,** 623 (1935).
[13] L. Farkas and H. Sachse, Z. physik. Chem. (Leipzig) **B27,** 111 (1934).
[14] G. Carreri, J. Chem. Phys. **21,** 749 (1953).

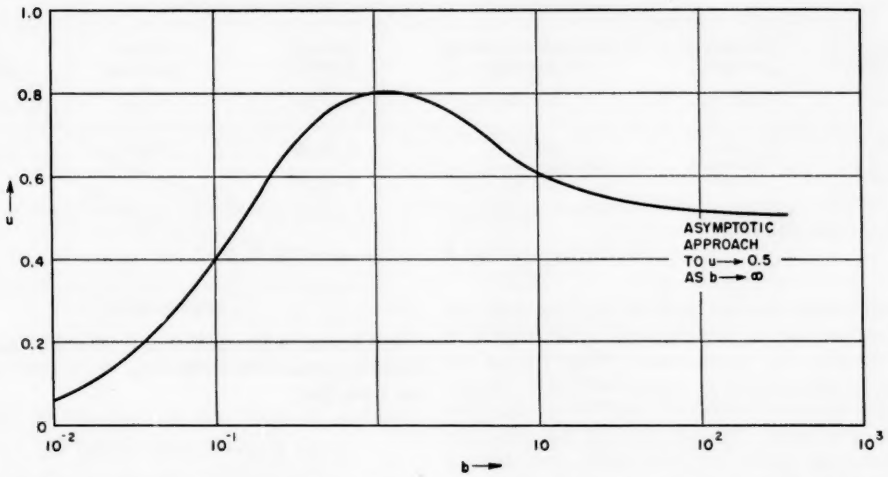

FIG. 7. Variation in relative atom concentration with flow velocity and reaction kinetics ($\delta' = L = R = 1$; $V = 10$).

It should be noted that the surface recombination coefficient of the calorimeter deduced from Amdur's measurements is somewhat lower than would be expected on the basis of more recent determination[15] of the catalytic activity of platinum. However, the experimental measurements of the gas-phase atom recombination[11] were carried out in glass tubes whose walls were coated with phosphoric acid. Under these conditions we have observed reduced catalytic activity of platinum, possibly due to poisoning of the surface.

More recently, Krongelb and Strandberg[16] reported a very interesting study of oxygen-atom recombination in which paramagnetic resonance techniques were employed for the quantitative analysis of oxygen atoms in the gas phase. Since these measurements included both diffusive and convective flow of the reactant species, we have examined the results in some detail. In the experiments with diffusive flow (side-arm method) the authors make the assumption that the loss of atoms by volume recombination can be neglected although the total gas pressure ranged from 0.7 to 2.1 mm Hg. At these pressures such an assumption cannot be supported since the rate of atom removal by homogeneous reaction[17] is of the same magnitude as that by heterogeneous reaction. Our interpretation of their results[16] in terms of a mechanism involving gas-phase and surface reaction in a diffusion tube (without convective flow) yields a recombination coefficient of oxygen atoms on glass and an estimate of the rate constant for the three-body, gas-phase recombination involving two atoms and an oxygen molecule as summarized in Table III. A measure of the applicability of the present theoretical analysis to the experimental measurements[16] is found in Fig. 9. The construction of the theoretical curve is based on the diagram shown in Fig. 10, which represents the profile of the relative atom concentration between the atom source and the probe located at y (rather than merely the atom concentration at one point, namely the probe surface, as shown in Fig. 1). The decrease in atom concentration with distance has been computed for a range of surface-recombination efficiencies, gas-phase reaction rates, and probe locations. At a point where the F' curve (dashed line) intersects the u curve (solid line), the relative atom concentration u is that to be expected at the probe of activity F' and position $L_1 = y$, as shown in Fig. 1. However, the solid curve connecting this point with the atom source ($y = 0$) represents the intervening concentration profile in the presence of homogeneous reaction in the gas and heterogeneous reaction on the solid surface.

In our intrepretation of the experimental measurements in a flow system[16] we have included the contribution of diffusive flow to the convective mass transfer of the gas (Table III). The rate constants so obtained are somewhat higher than those found in the absence of convective flow. However, the results compare favorably with other values for the rate constant recently obtained.[17–19]

In a recent publication[20] Schiff and co-workers measured the gas-phase recombination of oxygen atoms in a flow system containing a catalytic probe as an atom detector. Their interpretation of the results sug-

[15] B. J. Wood and H. Wise (to be published).
[16] S. Krongelb and M. W. P. Strandberg, J. Chem. Phys. **31,** 1196 (1959).
[17] R. R. Reeves, J. Manella, and P. Harteck, J. Chem. Phys. **32,** 632 (1960).
[18] J. A. Golden and A. L. Myerson, J. Chem. Phys. **28,** 978 (1958).
[19] C. B. Kretschmer, Aerojet-General Corp., Azusa, California (private communication).
[20] L. Elias, E. A. Ogryzlo, and H. I. Schiff, Can. J. Chem. **37,** 1680 (1959).

TABLE II. Parameters for hydrogen atom recombination in gas phase.

Average linear gas velicity v cm/sec	Total average pressure mm Hg	Recombination coefficient of calorimeter γ'	Diffusion coefficient[a] D cm²/sec	Kinetic parameter b (cm)	Rate constant k (mole/cc)$^{-2}$ sec^{-1}
410	0.58	10^{-3}	2.3×10^{3}	9.5	$1.7_8\times10^{16}$
245	1.00	10^{-3}	1.4×10^{3}	5.7	$1.4_6\times10^{16}$

[a] I. Amdur, J. Chem. Phys. **4**, 339 (1936).

gests a mechanism in which the kinetics of the slow step in the reaction are to be first-order with respect to atomic oxygen and second-order with respect to molecular oxygen, with O_3 as an intermediate. However, the analysis presented does not take into account the contribution of atom diffusion towards the probe nor the perturbation in the steady-state atom concentration profiles brought about by moving the catalytic surface to different positions within the reaction chamber. For a reaction of first-order in oxygen atoms (cf. Appendix B) we have computed the theoretical atom concentrations to be expected in a cylinder on the basis of the experimental results given in Table IV and compared them with those observed by the authors as shown in Fig. 11. The slope of the curve computed on the basis of the experimental results given in footnote 20($VR/2D=0.25$) is much steeper than that observed experimentally. In order to bring the data into coincidence, the value of the gas velocity would have to be increased by a factor of 20 to 30, or the rate constant decreased by a factor of 10^3. Such a rate constant would no longer agree with published data for ozone formation. On the other hand, the data[20] can be fitted to a third-order reaction involving the square of the oxygen atom concentration (Fig. 11). The rate constant so obtained is about 5×10^{13}. It is apparent from this analysis that a logarithmic decay in atom concentration with distance is not necessarily an indication of a first-order reaction in a system in which fluid-dynamic and reaction-kinetic parameters interplay.

APPENDIX A

A solution to Eq. (12) for $V=0$ is obtained by the following procedure. From Eqs. (12), (14), and (16), one finds that

$$y=\int_u^1 [z^3+(3C/4)z^4+K_1]^{-\frac{1}{2}}dz, \tag{17}$$

where z is a variable of integration.

If u_1 is the value of the nondimensional concentration u at the end of the tube $y=L_1$, constant K_1 may be evaluated by Eqs. (15) and (16) to be

$$K_1=(u_1/F')^2-u_1^3-(3C/4)u_1^4,$$

so that

$$L_1=\int_{u_1}^1 [(z^3-u_1^3)+(3C/4)(z^4-u_1^4)+(u_1/F')^2]^{-\frac{1}{2}}dz. \tag{18}$$

Equation (18) shows L_1 to be given by an elliptic integral. The explicit relations among L_1, u_1, C, and F' may be obtained by use of tables of elliptic functions. It was considered more convenient, however, to determine these relations by a combination of analytic and numerical methods of approximation. The family of curves in Fig. 1 exhibit the results for the condition that C is negligibly small, i.e., $C=0$ in these computations.

For small finite values of C, one may obtain the concentration as a function of distance without further

TABLE III. Recombination of oxygen atoms.[a]

Pressure mm Hg	Convective flow velocity cm/sec	Tube radius cm	Rate constant [(mole/cc)$^{-2}$ sec^{-1}]$\times10^{-15}$	Recombination coefficient of glass $\times10^3$
0.7	0	0.5	5.6	2
1.9	0	0.25	3.4	8
2.1	0	0.5	3.6	4
5.0	280	0.5	10.0	...
5.0	362	0.5	8.3	...

[a] Calculated from the experimental data reported in footnote 16.

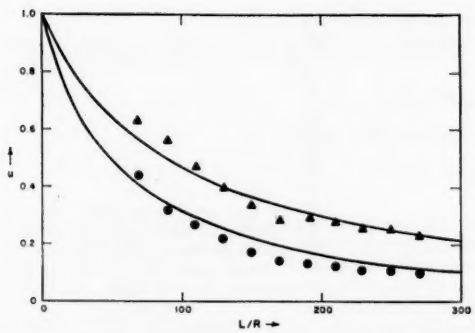

FIG. 8. Gas-phase recombination of hydrogen atoms in a flow system. —: theoretical; ●, ▲: experimental.[11]

computation as follows. In the range of interest, $0<u_1<z<1$,

$$0.75(z^3-u_1^3)\leq z^4-u_1^4\leq 1.25(z^3-u_1^3).$$

Thus, one may put approximately

$$(3C/4)(z^4-u_1^4)=(3C/4)(z^3-u_1^3)$$

with an error relative to $(z^3-u_1^3)$ of $(3C/16)$. With this approximation Eq. (18) may be written

$$L_1=(1+3C/4)^{-\frac{1}{2}}\int_{u1}^{1}[z^3-u_1^3+u_1^2/F'^2(1+3C/4)]^{-\frac{1}{2}}dz. \tag{19}$$

If the relation of Eq. (18) is expressed by

$$L_1=f(u_1, F', C),$$

then Eq. (19) shows that, for small C,

$$f(u_1, F', C)=(1+3C/4)^{-\frac{1}{2}}f(u_1, F'', 0),$$

where

$$F''=F'(1+3C/4)^{\frac{1}{2}}. \tag{20}$$

It follows that

$$(L_1/F')\,(\text{for } C\neq 0)=(L_1/F'')\,(\text{for } C=0).$$

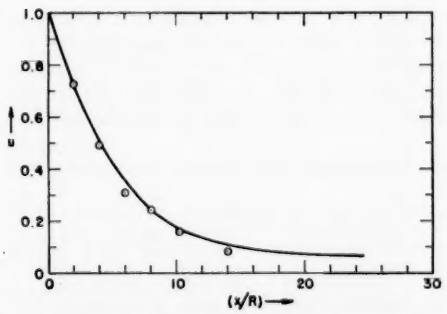

FIG. 9. Comparison of experimental measurements with theoretical analysis of oxygen atom recombination (total pressure 2.1 mm Hg cylinder diam=1.0 cm). —: theoretical; ⊙: experimental.[16]

TABLE IV. Data employed in calculations of homogeneous recombination of oxygen atoms.[a]

Rate constant	$k=10^{14}(\text{mole/cc})^{-2}\,\text{sec}^{-1}$
Total pressure	$p=5$ mm Hg
Gas velocity	$v=30$ cm/sec
Diffusion coefficient at $P=5$ mm Hg	$D=48$ cm²/sec
Tube radius	$R=0.875$ cm
Recombination coefficient	
quartz	$\gamma=2\times10^{-4}$
Ag_2O[b]	$\gamma'=2\times10^{-4}$
Computed parameters:	
$\delta=\delta'=18$	
$VR/2D=0.27$	
$kM^2R^2/D=0.12$	

[a] The data are based on results presented in the work cited in footnote 20.
[b] Based on measurements in our Laboratory.

Thus the curves of Figs. 1 or 10 may be used for any small value of C by entering the graph with the F'' of Eq. (20) in place of F'.

APPENDIX B

Homogeneous atom removal by an over-all third-order reaction whose rate depends on the atom concentration to the first power leads under steady-state

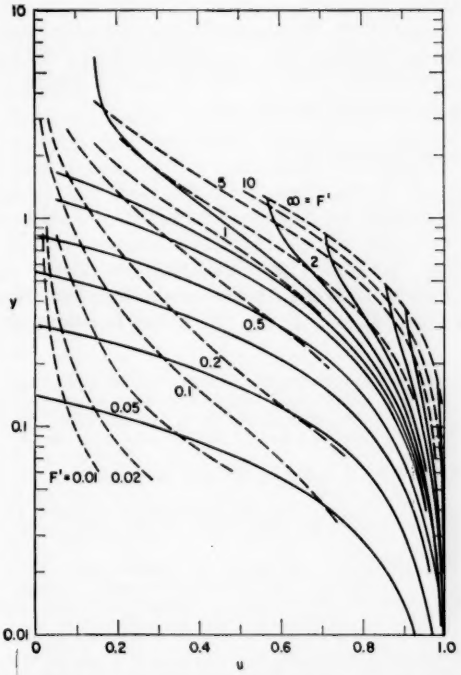

FIG. 10. Relative atom concentration as a function of gas-phase kinetics, probe location, and probe activity ($V=0$). —, concentration profile; — — —, probe location.

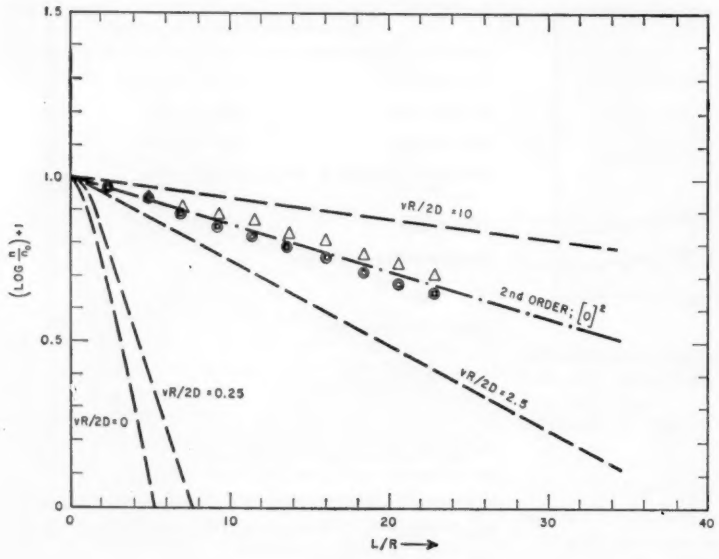

FIG. 11. Comparison of experimental measurements with theoretical analysis based on kinetics of first and second order with respect to oxygen atoms. ⊙, △: experimental data[20]; — — —: theoretical, rate $\propto [O][M]^{\frac{1}{2}}$ (cf. Table IV); —•—: theoretical, rate $\propto [O]^2[M]$.

conditions to the following equation in the presence of convection flow and diffusion,

$$D\Delta n - v(\partial n/\partial x) - k_3 n M^2 = 0 \qquad (21)$$

with the boundary conditions identical to those given by Eqs. (3)–(6). Equation (21) may be solved analytically to yield the atom concentration n at a distance x from the source in a cylinder of length L and at a distance r from the cylinder axis,

$$n/n_0 = 2\exp[\nu(\lambda-\xi)]$$

$$\cdot \sum_{i=1}^{\infty} [f_i(\xi)\, J_0(\alpha_i r/R)]/[\alpha_i(1+\delta^2\alpha_i^2) f_i(\lambda)\, J_1(\alpha_i)], \quad (22)$$

where $\xi=(L-x)/R$, $\lambda=L/R$, $\nu=vR/2D$, $K=k_3M^2R^2/D$, α_i is the ith root of the equation $J_0(\alpha)=\alpha\delta J_1(\alpha)$, J_0 and J_1 are the Bessel functions of the first kind,[1]

$$\beta_i=[\nu^2+K^2+\alpha_i^2]^{\frac{1}{2}},$$

and

$$f_i(\xi)=\sinh\beta_i\xi+\delta'(\beta_i+\nu)\cosh\beta_i\xi-\delta'\nu\exp(-\beta_i\xi).$$

In the absence of forced convection ($v=0$) and homogeneous gas-phase reaction ($k_3=0$), Eq. (22) reduces to the one derived in the work cited in footnote 1. The atom concentration averaged over the tube cross section at a distance x from the atom source is found from

$$\bar{n}/n_0 = 4\exp[\nu(\lambda-\xi)]$$

$$\times \sum_{i=1}^{\infty} [f_i(\xi)]/[\alpha_i^2(1+\delta^2\alpha_i^2) f_i(\lambda)]. \quad (23)$$

At $x=L$, the average concentration of active species is

$$(\bar{n}/n_0)_L = 4\exp(\nu\lambda) \sum_{i=1}^{\infty} \delta'/[\alpha_i(1+\delta^2\alpha_i^2) f_i(\lambda)]. \quad (24)$$

Some Deductions from a Formal Statistical Mechanical Theory of Chemical Kinetics*

JOHN ROSS† AND PETER MAZUR

Lorentz Institute for Theoretical Physics, Leiden, Netherlands

(Received December 27, 1960)

A perturbation solution of an assumed Boltzmann-type equation for bimolecular chemical reactions in a homogeneous gas phase consisting of molecules with or without internal degrees of freedom, leads to the conclusion that the law of mass action as well as the usually assumed phenomenological rate expressions for chemical reactions, is strictly valid only in lowest order of the perturbation. Higher order perturbations introduce an affinity and time dependence in the rate coefficient and the law of mass action becomes inadequate to the extent of the contribution of the effects of the perturbations.

A transition state formulation of rate coefficients for bimolecular gas-phase reactions is presented under less restrictive sufficient conditions than reported previously.

1. INTRODUCTION

THE purpose of this communication is the formulation of some deductions from a formal theory of chemical kinetics for homogeneous, bimolecular gas-phase reactions. The model adopted consists of an isothermal ideal gas phase in which a chemical reaction as well as its reverse reaction proceeds. A Boltzmann equation is assumed for the description of the irreversible process of the chemical reaction. The equation is solved formally first for a system of particles without internal degrees of freedom by a perturbation scheme which, in analogy to the Enskog perturbation method of solution of the Boltzmann equation for transport processes, is based on the supposition that the momentum relaxation time of all gaseous species is short compared to the chemical relaxation time. This type of perturbation solution has been considered by a number of authors,[1–5] with the primary aim of calculating the magnitude of the first-order perturbation of the Maxwellian distribution of speeds. We show that the zeroth-order solution leads, as expected, to the usual phenomenological rate expression with a rate coefficient independent of time or affinity, and hence to the law of mass action. Higher order solutions, however, introduce an affinity and time dependence in the rate coefficient and the law of mass action becomes inadequate to the extent of the contribution of the effects of the perturbations. Similar results are obtained for reacting systems with internal degrees of freedom.

The conclusions, derived here from illustrations of the coupling of the chemical reaction rate to the relaxation of translational and internal degrees of freedom, can be extended to other cases of interest,[6] for instance ionic reactions where a coupling exists between the reaction rate and the relaxation of the distribution of ions.[7]

Eliason and Hirschfelder[8] have presented a collision theory treatment for the rate of bimolecular gas-phase reactions, but have not taken into account the possibility of an affinity dependence of the rate coefficient. E. E. Nikitin and N. D. Sokolov [J. Chem. Phys. **31,** 1371 (1959)] have pointed out the inadequacy of the usually assumed phenomenological rate expression for gaseous dissociation reactions retarded by vibrational relaxation.

Next, we derive in a simple manner the entropy production for chemically reacting systems to the various orders of the perturbation solution. This problem has been considered previously by Prigogine[9] and Reik.[10]

Finally we derive a "transition state" formulation of rate coefficients for bimolecular gas-phase reactions under less restrictive sufficient conditions than those reported previously.[8,11–13]

* This research was supported in part by the European Division of the U. S. Air Research and Development Command.

† Fellow of the John Simon Guggenheim Memorial Foundation, 1959–1960, on leave of absence from Department of Chemistry, Brown University, Providence, Rhode Island.

[1] C. F. Curtiss, Ph.D. thesis, University of Wisconsin, Madison, Wisconsin, 1948.

[2] I. Prigogine and E. Xhrouet, Physica **15,** 913 (1949).

[3] I. Prigogine and M. Mahieu, Physica **16,** 51 (1950).

[4] K. Takayanagi, Progr. Theoret. Phys. (Kyoto) **6,** 486 (1951).

[5] R. D. Present, J. Chem. Phys. **31,** 747 (1959).

[6] Waite has discussed the time dependence of rate coefficients for reactions in solids and liquids; T. R. Waite, J. Chem. Phys. **32,** 21 (1960); **28,** 103 (1958); Phys. Rev. **107,** 463 (1957).

[7] We are indebted to Dr. M. Eigen for an instructive discussion on this point.

[8] M. A. Eliason and J. O. Hirschfelder, J. Chem. Phys. **30,** 1426 (1959).

[9] I. Prigogine, Physica **15,** 272 (1949).

[10] H. G. Reik, (a) Z. Physik **148,** 156 (1957); (b) **148,** 223 (1957).

[11] J. O. Hirschfelder, C. F. Curtiss, and R. B. Bird, *The Molecular Theory of Gases and Liquids* (John Wiley & Sons, Inc., New York, 1954); S. Chapman and T. G. Cowling, *The Mathematical Theory of Non-Uniform Gases* (Cambridge University Press, New York, 1952).

[12] H. Eyring, J. Walter, and G. E. Kimball, *Quantum Chemistry* (John Wiley & Sons, Inc., New York, 1944).

[13] S. Glasstone, K. J. Laidler, and H. Eyring, *The Theory of Rate Processes* (McGraw-Hill Book Company, Inc., New York, 1941).

2. CHEMICAL REACTIONS IN SYSTEMS WITHOUT INTERNAL DEGREES OF FREEDOM

Consider an isothermal, spatially uniform ideal gas phase of four chemical species, $S=A, B, C, D$. In this section, we restrict the analysis to particles without internal degrees of freedom which may react according to the reversible one-step mechanism

$$A+B\rightleftarrows C+D. \tag{1}$$

The statistical mechanics of the irreversible process of the chemical reaction is assumed to be described by the time dependence of singlet distribution functions according to Boltzmann-type equations[1-3,10,11] For species A we have

$$[\partial(n_A f_A)]/\partial t=\sum_S E_{AS}+R_A, \tag{2}$$

$$E_{AS}\equiv n_A n_S\int\cdots\int(p/\mu)\sigma_{AS}(p,\Omega)[f_A(\mathbf{p}_A')f_S(\mathbf{p}_S')-f_A(\mathbf{p}_A)f_S(\mathbf{p}_S)]d\mathbf{p}_S d\Omega, \tag{3}$$

$$R_A\equiv\int\cdots\int(p/\mu)\sigma_{AB}^*(p,\Omega)[n_C n_D f_C(\mathbf{p}_C')f_D(\mathbf{p}_D')-n_A n_B f_A(\mathbf{p}_A)f_B(\mathbf{p}_B)]d\Omega d\mathbf{p}_B, \tag{4}$$

and similar equations hold for the other species.[14]

Here E_{AS} is the collision integral for elastic collisions and R_A the collision integral for chemical reaction collisions. The other symbols denote the following: $n_S(t)$ = time-dependent number density of species S; $f_S(\mathbf{p}_S;\ t)$ = singlet momentum distribution function, normalized to unity; $\sigma_{AS}(p,\ \Omega)$ = differential elastic scattering cross section; $p=|\mathbf{p}_A-\mathbf{p}_S|=|\mathbf{p}_A'-\mathbf{p}_S'|$ is the invariant absolute value of the relative momentum; $\sigma_{AB}^*(p,\ \Omega)$ = differential chemical reaction cross section, a function of the absolute value of the relative momentum, $p=|\mathbf{p}_A-\mathbf{p}_B|$, of the colliding particles A and B and the solid scattering angle Ω; μ = the reduced mass of the colliding system in the respective collision integral. If two particles with unprimed (primed) momenta collide, there result two particles with primed (unprimed) momenta.

The rate of the chemical reaction follows from integration of Eq. (2) over momentum $\mathbf{p}_A$. Since the integral of E_{AS} over momentum $\mathbf{p}_A$ vanishes[11] we obtain

$$-(dn_A/dt)=k_f n_A n_B-k_r n_C n_D, \tag{5}$$

with the definitions

$$k_f\equiv\int\cdots\int(p/\mu)\sigma_{AB}^* f_A f_B d\Omega d\mathbf{p}_A d\mathbf{p}_B, \tag{6}$$

$$k_r\equiv\int\cdots\int(p/\mu)\sigma_{AB}^* f_C' f_D' d\Omega d\mathbf{p}_A d\mathbf{p}_B. \tag{7}$$

Equation (5) coincides with the usual phenomenological rate expression assumed on the basis of the law of mass action for the reaction Eq. (1) only if k_f and k_r are independent of affinites, concentrations or time. In that case these quantities may be identified with the rate coefficients defined by the phenomenological rate expression and assumed to be functions of temperature only.

At equilibrium the collision integrals E_{AS} and R_A equal zero and the equilibrium solution of Eq. (2) must be of the form

$$n_S^{eq}f_S^{eq}=n_S^{eq}\exp-\beta[(p_S^2/2m_S)+\epsilon_S-\mu_S^0], \tag{8}$$

where ϵ_S is the one-level internal energy of species S referred to a common origin for all species and β^{-1} is kT. The total energy is a summational invariant for collisions leading to chemical reaction

$$\frac{p_A^2}{2m_A}+\epsilon_A+\frac{p_B^2}{2m_B}+\epsilon_B=\frac{p_C^2}{2m_C}+\epsilon_C+\frac{p_D^2}{2m_D}+\epsilon_D; \tag{9}$$

the kinetic energy is a summational invariant of elastic collisions. The equilibrium densities satisfy the relation for the equilibrium constant,

$$n_C^{eq}n_D^{eq}/n_A^{eq}n_B^{eq}=\exp(-\beta\Delta\mu^0)\equiv K \tag{10}$$

$$\Delta\mu^0\equiv(\mu_C^0+\mu_D^0)-(\mu_A^0+\mu_B^0), \tag{11}$$

and the quantities μ_S^0 are the standard chemical potentials of the species.

A perturbation solution analogous to the Enskog solution of the Boltzmann equation for transport phenomena (reference 11, Chap. 7) may be attempted. If ϵ is a perturbation parameter, we seek a formal solution of the equation

$$\epsilon\{[\partial(n_A f_A)/\partial t]-R_A\}=\sum_S E_{AS}, \tag{12}$$

with the expansion for the time derivative

$$\frac{\partial}{\partial t}=\frac{\partial}{\partial t}\Big)_0+\epsilon\frac{\partial}{\partial t}\Big)_1+\epsilon^2\frac{\partial}{\partial t}\Big)_2+\cdots, \tag{13}$$

and the proposed expansion for the momentum dis-

[14] Strictly, this set of assumed Boltzmann-type equations describes an isolated rather than an isothermal system. In an adiabatic system the temperature is a function of time through the progress variable for reactions with finite enthalpy changes. The maintenance of constant temperature is accomplished by thermal conduction to the walls. For the sake of simplicity it is assumed that this process does not interfere significantly with the progress of the chemical reaction.

tribution function

$$f_A = f_A^0[1+\epsilon\phi_A^{(1)}+\epsilon^2\phi_A^{(2)}+\cdots] \tag{14}$$

$$f_A^0 = \exp-\beta[(p_A^2/2m_A)+\epsilon_A-\mu_A^0]. \tag{15}$$

A chemical reaction perturbs the Maxwellian distribution of speeds, for instance by removal of fast reactant molecules with kinetic energy larger than some activation energy; elastic collisions tend to restore this distribution. The perturbation method is based on the assumption that the rate of depletion of the molecular distribution of speeds by the chemical reaction is slow compared to the rate of replenishment by elastic collisions. For many chemical reactions at arbitrary concentrations of reactants and products the chemical relaxation time is far longer than the momentum relaxation time, that is, the characteristic time associated with the attainment of the Maxwellian distribution.[15]

The zeroth order of the perturbation treatment obtained by the substitution of Eq. (14) in Eq. (12) is

$$E_{AS}^{(0)}(n_A n_S f_A^{(0)} f_S^{(0)}) = 0, \tag{16}$$

with solution $n_S f_S^{(0)}$, namely, a Maxwellian distribution of speeds multiplied by an arbitrary density n_S corresponding to the arbitrary chemical potential

$$\mu_S = RT \ln n_S + \mu_S^0. \tag{17}$$

No relation exists among the quantities μ_S; the affinity $\mathfrak{A}$ is defined as the difference between the sums of the chemical potentials of the reactants and that of the products

$$\mathfrak{A} = -[(\mu_C+\mu_D)-(\mu_A+\mu_B)], \tag{18}$$

and hence vanishes only at equilibrium. For the special condition of absence of products, attainable only at some initial instant, in a closed system, the affinity is $\mathfrak{A}=\infty$. The rate of the chemical reaction Eq. (5), becomes in this order

$$-\frac{dn_A}{dt}\Big)_0 = k_f^{(0)} n_A n_B - k_r^{(0)} n_C n_D \tag{19}$$

$$k_f^{(0)}(T) = \int\cdots\int (p/\mu)\sigma_{AB}^* f_A^{(0)} f_B^{(0)} d\Omega d\mathbf{p}_A d\mathbf{p}_B \tag{20}$$

$$k_r^{(0)}(T) = \int\cdots\int (p/\mu)\sigma_{AB}^* f_C'^{(0)} f_D'^{(0)} d\Omega d\mathbf{p}_A d\mathbf{p}_B, \tag{21}$$

where the subscript on the half-bracket in Eq. (19) indicates the rate of disappearance of species A in the lowest order of the perturbation [see Eq. (13)].

The quantities $k_f^{(0)}$ and $k_r^{(0)}$ are independent of affinity, concentrations or time and therefore, as expected, the law of mass action holds in lowest order of the perturbation analysis. The ratio $k_f^{(0)}/k_r^{(0)}$ can easily be shown to be equal to the equilibrium constant K, Eq. (10); this is a corollary of the law of mass action.

We proceed to the next order of perturbation and obtain from Eqs. (12)–(14) the relations

$$f_A^{(0)}\frac{dn_A}{dt}\Big)_0 - R_A^{(0)} = \sum_S E_{AS}^{(1)} \tag{22}$$

$$E_{AS}^{(1)} = n_A n_S \int\cdots\int (p/\mu)\sigma_{AS} f_A^{(0)} f_S^{(0)}[\phi_A^{(1)}(p_A')+\phi_S^{(1)}(p_S')-\phi_A^{(1)}(p_A)-\phi_S^{(1)}(p_S)]d\Omega d\mathbf{p}_S \tag{23}$$

$$R_A^{(0)} = \int\cdots\int (p/\mu)\sigma_{AB}^*[n_C n_D f_C'^{(0)} f_D'^{(0)} - n_A n_B f_A^{(0)} f_B^{(0)}]d\Omega d\mathbf{p}_B. \tag{24}$$

With the aid of Eq. (19) we can rewrite Eq. (22) to read

$$f_A^{(0)}[k_r^{(0)} n_C n_D - k_f^{(0)} n_A n_B] - R_A^{(0)} = \sum_S E_{AS}^{(1)}, \tag{25}$$

or

$$\{-f_A^{(0)} k_f^{(0)} + \int\cdots\int (p/\mu)\sigma_{AB}^* f_A^{(0)} f_B^{(0)} d\Omega d\mathbf{p}_B\} n_A n_B [1-\exp(-\beta\mathfrak{A})]$$

$$= \sum_S n_A n_S \int\cdots\int (p/\mu)\sigma_{AS} f_A^{(0)} f_S^{(0)}[\phi_A^{(1)}(p_A')+\phi_S^{(1)}(p_S')-\phi_A^{(1)}(p_A)-\phi_S^{(1)}(p_S)]d\Omega d\mathbf{p}_S. \tag{26}$$

[15] A transport process, like thermal conduction, also perturbs the Maxwellian distribution of speeds. There, the Enskog perturbation method is based on the assumption that the momentum relaxation time is much shorter than the hydrodynamic relaxation time associated with the attainment of equilibrium in configuration space.

Similar first-order equations exist for the other species and the resultant set of four coupled integral equations determines the perturbation functions $\phi_S^{(1)}$.

All the densities n_S are related to given initial conditions $n_S(0)$ and the progress variable of the chemical reaction ξ. Equation (26) shows that the perturbation $\phi_A^{(1)}$, for species A for instance, is a function of the affinity and vanishes at equilibrium. We write for $\phi_A^{(1)}$ therefore

$$\phi_A^{(1)} \equiv [1-\exp(-\beta\mathcal{A})]D_A[p_A;\beta,\xi,n_S(0)], \quad (27)$$

which defines the quantity D_A, in general, a function of the progress variable ξ and the initial conditions $n_S(0)$ for all species. The factor $[1-\exp(-\beta\mathcal{A})]$ represents the driving force of the chemical reaction and is the analog of temperature gradients, etc., in the theory of transport phenomena. A finite chemical reaction rate, i.e., a finite affinity, gives rise to a perturbation of the Maxwellian distribution of speeds. The analytic form of the perturbation function $\phi_S^{(1)}$ expresses the coupling between the macroscopic process of the reaction and the microscopic process of the attendent continuous momentum redistribution.[16] The details of the dynamics are represented by the function D_S which depends in particular on the relative magnitude of the elastic and chemical reaction cross sections in pertinent ranges of relative energy. For many reactions the magnitude of the function D_S alone will assure a small and frequently negligible perturbation $\phi_S^{(1)}$ for arbitrary affinity $\mathcal{A}$, since we have

$$0 \leq |1-\exp(-\beta\mathcal{A})| \leq 1. \quad (28)$$

There is no need for the perturbation to be a monotonic function of the progress variable ξ; the behavior depends entirely on the relative concentrations and cross sections of the reactants and products and no general rules are apparent (see Sec. 5). However, $\phi_S^{(1)}$ can always be made as small as desired for sufficiently small affinity.

The contribution of the first-order perturbation to the rate of the chemical reaction may be written

$$-\frac{dn_A}{dt}\Big)_1 = k_f^{(1)} n_A n_B - k_r^{(1)} n_C n_D \quad (29)$$

$$k_f^{(1)} = [1-\exp(-\beta\mathcal{A})]\int\cdots\int (p/\mu)\sigma_{AB}^* f_A^{(0)} f_B^{(0)}\{D_A[p_A;\beta,\xi,n_S(0)]+D_B\}d\Omega d\mathbf{p}_A d\mathbf{p}_B \quad (30)$$

$$k_r^{(1)} = [1-\exp(-\beta\mathcal{A})]\int\cdots\int (p/\mu)\sigma_{AB}^* f_C'^{(0)} f_D'^{(0)}\{D_C[p_C';\beta,\xi,n_S(0)]+D_D\}d\Omega d\mathbf{p}_A d\mathbf{p}_B. \quad (31)$$

The quantities $k_f^{(1)}$ and $k_r^{(1)}$ are seen to be dependent on affinity, and implicitly, on time through the progress variable of the reaction; furthermore, the ratio $k_f^{(1)}/k_r^{(1)}$ is also a function of time. We conclude that the law of mass action, and therefore the usually assumed phenomenological rate expression, holds strictly only in lowest order of the perturbation analysis. The law of mass action is sufficient only to the extent that the effect of the perturbed momentum distribution function on the rate of the reaction is negligible.

Another observation follows: knowledge of chemical reaction cross sections as a function of relative energy, as determined by *a priori* calculations or molecular beam experiments, is not always sufficient for the *a priori* evaluation of chemical rates. This information permits only the calculation of the lowest order rate coefficients $k_f^{(0)}$ and $k_r^{(0)}$. The computation of higher order contributions, $k_f^{(1)}$, etc., if of importance, also requires the solution of the statistical equations for the perturbed distribution functions. At times this additional analysis may be necessary even if only as a justification for the adequacy of the lowest order rate coefficients.

[16] Hence we disagree with Reik[10] who states that a chemical reaction, in contradistinction to ordinary transport phenomena, can proceed in the absence of a perturbed Maxwellian distribution of speeds.

3. ENTROPY PRODUCTION

The entropy production in a chemical reaction to various orders in the perturbation has been discussed by Reik,[10] but we return to this problem briefly for a simple derivation. Let ρ be the total number density and s the specific entropy; we define the entropy by the equation

$$\rho s = -k\sum_j \int\cdots\int n_j f_j[\ln(n_j f_j)-1]d\mathbf{p}_j, \quad (32)$$

in which the summation extends over the species of the system. The entropy production

$$\dot{S} \equiv d(\rho s)/dt \quad (33)$$

then becomes

$$\dot{S} = -k\sum_{j,k} \int\cdots\int [(1/\epsilon)E_{jk}+R_j]\ln(n_j f_j)d\mathbf{p}_j \quad (34)$$

on substitution of Eq. (12). We note the equation

$$\int\cdots\int E_{jk}\ln(n_j f_j^{(0)})d\mathbf{p}_j = 0, \quad (35)$$

which is valid because $\ln(n_j f_j^{(0)})$ is a linear combination of summational invariants for elastic collisions and because the averages of such invariants formed with the

collision integrals E_{jk} vanish. Furthermore, we have seen before that $E_{jk}^{(0)}=0$ [Eq. (16)], so that the entropy production can be rewritten

$$\dot{S}=-k\sum_{j,k}\int\cdots\int[(1/\epsilon)(E_{jk}-E_{jk}^{(0)})\ln(f_j/f_j^{(0)}) + R_j\ln(n_j f_j)]d\mathbf{p}_j. \quad (36)$$

The distribution functions are again expanded in a power series in ϵ as in Eq. (14) and there corresponds a similar development for the entropy production

$$\dot{S}=\dot{S}^{(0)}+\epsilon\dot{S}^{(1)}+\epsilon^2\dot{S}^{(2)}+\cdots. \quad (37)$$

The entropy production in lowest order is

$$\dot{S}^{(0)}=-k\sum_j\int R_j^{(0)}(\ln n_j+\beta\mu_j^0)d\mathbf{p}_j + \beta k\sum_j\int R_j^{(0)}[(p_j^2/2m_j)+\epsilon_j]d\mathbf{p}_j, \quad (38)$$

where the explicit form of $f_j^{(0)}$ [Eq. (15)] has been introduced. The second sum of integrals on the right-hand side of Eq. (38) is identically zero because the total energy is conserved in a chemical reaction. The remaining first sum can be rewritten

$$\dot{S}^{(0)}=-k\sum_j\beta\mu_j\int R_j^{(0)}d\mathbf{p}_j. \quad (39)$$

The relation between the rates of disappearance of the species is simply

$$-\frac{dn_A}{dt}\Big)_0=-\frac{dn_B}{dt}\Big)_0=\frac{dn_C}{dt}\Big)_0=\frac{dn_D}{dt}\Big)_0\equiv J^{(0)}, \quad (40)$$

so that finally the entropy production in lowest order becomes

$$\dot{S}^{(0)}=-(\mathfrak{A}J^{(0)}/T). \quad (41)$$

This is of the expected bilinear form, a product of the "flux" $J^{(0)}$ and the thermodynamic affinity $\mathfrak{A}$. The next higher order equation for the entropy production is

$$\dot{S}^{(1)}=-k\sum_{j,k}\int\cdots\int\{E_{jk}^{(1)}\phi_j^{(1)}+R_j^{(0)}\phi_j^{(1)} + R_j^{(1)}\ln(n_j f_j^{(0)})\}d\mathbf{p}_j. \quad (42)$$

From the relation Eq. (22) we obtain

$$\int\cdots\int(\sum_k E_{jk}^{(1)}+R_j^{(0)})\phi_j^{(1)}d\mathbf{p}_j = \int\cdots\int\frac{\partial(n_j f_j^{(0)})}{\partial t}\phi_j^{(1)}d\mathbf{p}_j=0, \quad (43)$$

because the momentum distribution function is normalized to unity in all orders. The reduction of the remaining terms in Eq. (43) follows the above procedure, Eqs. (38)–(41), and the first-order entropy production is therefore again of the bilinear form

$$\dot{S}^{(1)}=-\frac{\mathfrak{A}J^{(1)}}{T};\qquad J^{(1)}\equiv-\frac{dn_A}{dt}\Big)_1. \quad (44)$$

Beyond the first order, however, the simple bilinear form is not retained.

4. CHEMICAL REACTIONS IN SYSTEMS WITH INTERNAL DEGREES OF FREEDOM

We consider next an isothermal multicomponent ideal gas phase in which the molecules may have internal structure. A molecule of species $S=A, B, C, D$ may exist in a spectrum of internal states due to the possibility of electronic, vibrational, rotational, etc., degrees of freedom. The set of quantum numbers specifying completely the state of an isolated molecule is denoted by a single lower case letter. Each quantum state i of each species S is viewed as a component of the system and the postulated Boltzmann equation for the time rate of change of each such component and its associated momentum distribution function reads[11,8]

$$\frac{\partial(n_{iA}f_{iA})}{\partial t}=\sum_{j,S}E_{AS}(ij)+\sum_{jkl,S}I_{AS}(kl|ij)+\sum_{jkl}R_A(kl|ij) \quad (45)$$

$$E_{AS}(ij)\equiv n_{iA}n_{jS}\int\cdots\int(p/\mu)\sigma_{AS}(ij;p,\Omega)[f_{iA}'f_{jS}'-f_{iA}f_{jS}]d\Omega d\mathbf{p}_S \quad (46)$$

$$I_{AS}(kl|ij)\equiv\int\cdots\int(p/\mu)\sigma_{AS}(kl|ij;p,\Omega)[n_{kA}n_{lS}f_{kA}'f_{lS}'-n_{iA}n_{jS}f_{iA}f_{jS}]d\Omega d\mathbf{p}_S \quad (47)$$

$$R_A(kl|ij)\equiv\int\cdots\int(p/\mu)\sigma^*(kl|ij;p,\Omega)[n_{kC}n_{lD}f_{kC}'f_{lD}'-n_{iA}n_{jB}f_{iA}f_{jB}]d\Omega d\mathbf{p}_B. \quad (48)$$

The collision integrals are labeled $E_{AS}(ij)$ for elastic collisions between two molecules of species A in quantum state i and species S in quantum state j; $I_{AS}(kl|ij)$ for inelastic collisions between two molecules of species A and S in transition between the internal states (ij) and (kl); and $R_A(kl|ij)$ for chemical reaction collisions of the reaction

$$A(i)+B(j)\rightleftarrows C(k)+D(l), \quad (49)$$

where the letters in parentheses again indicate the quantum state of the reactants and products. The cross sections appearing in the collision integrals are

therefore defined. The density of species S in quantum state i is n_{iS} and the associated momentum distribution function, normalized to unity, is f_{iS}.

The rate of disappearance of each component, say $A(i)$, is obtained by integration over momentum of Eq. (45),

$$-(dn_{iA}/dt)=\sum_{jkl}[k_f(kl|ij)n_{iA}n_{jB}-k_r(kl|ij)n_{kC}n_{lD}]+\sum_{jkl,S}\int I_{AS}(kl|ij)d\mathbf{p}_A \tag{50}$$

$$k_f(kl|ij)=\int\cdots\int(p/\mu)\sigma^*(kl|ij;\,p,\,\Omega)f_{iA}f_{jB}d\Omega d\mathbf{p}_A d\mathbf{p}_B \tag{51}$$

$$k_r(kl|ij)=\int\cdots\int(p/\mu)\sigma^*(kl|ij;\,p,\,\Omega)f_{kC}'f_{lD}'d\Omega d\mathbf{p}_A d\mathbf{p}_B, \tag{52}$$

and the over-all rate of the chemical reaction by summation over-all quantum states of Eq. (50).

$$-\frac{dn_A}{dt}=\sum_{ijkl}[k_f(kl|ij)n_{iA}n_{jB}-k_r(kl|ij)n_{kC}n_{lD}]. \tag{53}$$

At equilibrium all collision integrals in Eq. (45) equal zero and the equilibrium solution for non-degenerate quantum states is

$$n_{iS}^{eq}f_{iS}^{eq}=\exp-\beta\{(p_S^2/2m_S)+\epsilon_{iS}-\mu_{iS}^{eq}\}. \tag{54}$$

The equilibrium chemical potentials of all quantum states of a given species are equal to each other

$$\mu_{iS}^{eq}=\mu_{jS}^{eq}=\cdots, \tag{55}$$

and equal to the chemical potential of species S, μ_S^{eq}.[17]

We seek a formal perturbation solution of Eq. (45) with the restriction that the distribution of internal states is other than an equilibrium solution only because of the occurrence of the chemical reaction. More involved situations are possible in that a non-equilibrium internal distribution may be attained by the passage of a sound or shock wave. These additional complications are omitted. Now the hypothesis basic to the perturbation method is the requirement that a chemical relaxation time be slow compared to all other relaxation times, namely, of momentum and of the internal degrees of freedom. If ϵ is a perturbation parameter, the postulated solution of the equation

$$\epsilon\left[\frac{\partial(n_{iA}f_{iA})}{\partial t}-\sum_{jkl}R_A(kl|ij)\right]=\sum_{j,S}E_{AS}(ij)+\sum_{jkl,S}I_{AS}(kl|ij), \tag{56}$$

is

$$n_{iA}f_{iA}=n_{iA}^{(0)}f_{iA}^{(0)}[1+\epsilon\phi_{iA}^{(1)}+\epsilon^2\phi_{iA}^{(2)}+\cdots], \tag{57}$$

where $f_{iA}^{(0)}$ is the Maxwellian distribution of momentum,

$$n_{iA}^{(0)}f_{iA}^{(0)}=\exp\left[-\beta\left(\frac{p_A^2}{2m_A}+\epsilon_{iA}-\mu_{iA}^{(0)}\right)\right] \tag{58}$$

$$f_{iA}^{(0)}=f_A^{(0)}=\frac{1}{(2\pi m_A kT)^{\frac{3}{2}}}\exp\left[-\frac{\beta p_A^2}{2m_A}\right], \tag{59}$$

and $n_{iS}^{(0)}$ is the number density of species S distributed canonically among the internal states. For a given species the corresponding chemical potentials are again all equal to each other

$$\mu_{iS}^{(0)}=\mu_{jS}^{(0)}=\cdots, \tag{60}$$

and equal to the chemical potential of species S, μ_S. No relation exists among the chemical potentials of the various species; the affinity is again defined as

$$\mathfrak{A}=-[(\mu_C+\mu_D)-(\mu_A+\mu_B)]. \tag{61}$$

The lowest order equation of the perturbation analysis obtained by substitution of Eq. (57) in Eq. (56) is

$$E_{AS}^{(0)}(i,j)=0$$
$$I_{AS}^{(0)}(kl|ij)=0, \tag{62}$$

with $n_{iS}^{(0)}f_{iS}^{(0)}$ as solution. Hence the rate of disappearance of species A in this order can be derived from Eq. (53) by substitution of Eq. (59) for $n_{iS}^{(0)}f_{iS}^{(0)}$ and recognition that in lowest order the affinity of each possible reaction [Eq. (49)] is given by Eq. (61). We obtain the expected equations

$$-\left(\frac{dn_A}{dt}\right)_0=\sum_{ijkl}[k_f^{(0)}(kl|ij)n_{iA}^{(0)}n_{jB}^{(0)}-k_r^{(0)}(kl|ij)n_{kC}^{(0)}n_{lD}^{(0)}], \tag{63}$$

or

$$-\left(\frac{dn_A}{dt}\right)_0=k_f n_A n_B[1-\exp(-\beta\mathfrak{A})], \tag{64}$$

with

$$k_f=\sum_{ijkl}\frac{n_{iA}^{(0)}}{n_A}\frac{n_{jB}^{(0)}}{n_B}k_f^{(0)}(kl|ij)$$

$$k_f^{(0)}(kl|ij)=\int\cdots\int(p/\mu)\sigma^*(kl|ij;\,p,\,\Omega)\times f_A^{(0)}f_B^{(0)}d\Omega d\mathbf{p}_A d\mathbf{p}_B. \tag{65}$$

[17] For ideal gases the density of species S, n_{is}, and the chemical potential μ_s obey the equation

$$n_s=\exp[\beta(\mu_s-\mu_s^0)].$$

The standard chemical potential μ_s^0 is related to the translational Z_{tr} and internal Z_{int} partition functions,

$$\exp(\beta\mu_s^0)=Z_{tr}Z_{int}.$$

Integration of Eq. (54) over momentum and summation over the quantum states of species S leads at once to the cited equalities among the chemical potentials.

As before, the subscript zero on the half-bracket $-dn_A/dt)_0$ indicates the rate of disappearance of a chemical species in lowest order of the perturbation, in this case species A distributed canonically among its internal states. The rate expression Eq. (64) is in concordance with the law of mass action.

The next higher approximation in the perturbation scheme brings along a number of complexities. The equation to be solved for the perturbation function $\phi_{iA}^{(1)}$ is

$$f_{iA}^{(0)}\frac{dn_{iA}^{(0)}}{dt}\Big)_0-\sum_{jkl}R_A^{(0)}(kl\,|\,ij)=\sum_{j,S}E_{AS}^{(1)}(i,j)+\sum_{jkl,S}I_{AS}^{(1)}(kl\,|\,ij) \tag{66}$$

$$E_{AS}^{(1)}(ij)=n_{iA}^{(0)}n_{jS}^{(0)}\int\cdots\int(p/\mu)\sigma_{AS}f_{iA}^{(0)}f_{jS}^{(0)}[\phi_{iA}^{(1)}(p_A')+\phi_{jS}^{(1)}(p_S')-\phi_{iA}^{(1)}(p_A)-\phi_{jS}^{(1)}(p_S)]d\Omega d\mathbf{p}_S \tag{67}$$

$$I_{AS}^{(1)}(kl\,|\,ij)$$

$$=n_{iA}^{(0)}n_{jB}^{(0)}\int\cdots\int(p/\mu)\sigma_{AS}(kl\,|\,ij;\,p,\Omega)f_{iA}^{(0)}f_{jS}^{(0)}[\phi_{kA}^{(1)}(p_A')+\phi_{lS}^{(1)}(p_S')-\phi_{iA}^{(1)}(p_A)-\phi_{jS}^{(1)}(p_S)]d\Omega d\mathbf{p}_S, \tag{68}$$

which may be rewritten

$$[1-\exp(-\beta\alpha)]\sum_{jkl}[-f_{iA}^{(0)}k_f^{(0)}(kl\,|\,ij)+\int\cdots\int(p/\mu)\sigma^*(kl\,|\,ij;\,p,\Omega)f_{iA}^{(0)}f_{jB}^{(0)}d\Omega d\mathbf{p}_B]n_{iA}^{(0)}n_{jB}^{(0)}$$
$$=\sum_{j,S}E_{AS}^{(1)}(i,j)+\sum_{jkl,S}I_{AS}^{(1)}(kl\,|\,ij). \tag{69}$$

To the first-order perturbation we have

$$n_{iA}f_{iA}=n_{iA}^{(0)}f_{iA}^{(0)}(1+\phi_{iA}^{(1)}) \tag{70}$$

with the normalization conditions

$$\int f_{iA}d\mathbf{p}_A=\int f_{iA}^{(0)}d\mathbf{p}_A=1. \tag{71}$$

$$n_{iA}^{(1)}/n_{iA}^{(0)}\equiv\int f_{iA}^{(0)}\phi_{iA}^{(1)}d\mathbf{p}_A \tag{72}$$

$$n_{iA}=n_{iA}^{(0)}+n_{iA}^{(1)}. \tag{73}$$

The form of the perturbation function $\phi_{iA}^{(1)}$ is suggested by the structure of Eq. (69) and (72), namely,

$$\phi_{iA}^{(1)}\equiv[1-\exp(-\beta\alpha)]D_{iA}[p_A,\epsilon_{iA};\beta,\xi_i,n_S(0)], \tag{74}$$

where the defined function D_{iA} depends on momentum, the energy of the quantum state i of species A, the temperature, the set of progress variables ξ_i of all reactions in which component $A(i)$ participates, and the initial densities $n_S(0)$. The elastic collision integrals $E_{AS}^{(1)}$ contribute to the perturbation of the distribution of momenta, whereas the inelastic collision integrals $I_{AS}^{(1)}$ give rise to deviations from the canonical distribution of densities in internal states $n_{iS}^{(0)}$. Both perturbations are included in the function $\phi_{iA}^{(1)}$; the proportion of each depends on the relative magnitude of the corresponding cross sections. The contributions of the first-order perturbation to the rate of the chemical reaction appear not only in the distribution functions but also in the densities of the internal states of all species. If we denote the first-order perturbation contribution to the rate by $dn_A/dt)_1$, we have

$$-\frac{dn_A}{dt}\Big)_1=\sum_{ijkl}\{\kappa_f^{(1)}(kl\,|\,ij)n_{iA}^{(0)}n_{jB}^{(0)}-\kappa_r^{(1)}(kl\,|\,ij)n_{kC}^{(0)}n_{lD}^{(0)}\}$$
$$+\sum_{ijkl}\left\{k_f^{(0)}(kl\,|\,ij)n_{iA}^{(0)}n_{jB}^{(0)}\left[\frac{n_{jB}^{(1)}}{n_{jB}^{(0)}}+\frac{n_{iA}^{(1)}}{n_{iA}^{(0)}}\right]-k_r^{(0)}(kl\,|\,ij)n_{kC}^{(0)}n_{lD}^{(0)}\left[\frac{n_{kC}^{(1)}}{n_{kC}^{(0)}}+\frac{n_{lD}^{(1)}}{n_{lD}^{(0)}}\right]\right\} \tag{75}$$

$$\kappa_f^{(1)}(kl\,|\,ij)=[1-\exp(-\beta\alpha)]\int\cdots\int(p/\mu)\sigma^*f_A^{(0)}f_B^{(0)}\{D_{iA}[p_A,\epsilon_{iA};\beta,\xi_i,n_S(0)]+D_{jB}\}d\Omega d\mathbf{p}_A d\mathbf{p}_B. \tag{76}$$

Thus, if we let $k_f^{(1)}$ and $k_r^{(1)}$ be defined by the relation

$$-\frac{dn_A}{dt}\Big)_1=k_f^{(1)}n_An_B-k_r^{(1)}n_Cn_D, \tag{77}$$

these quantities are

$$k_f^{(1)}=\sum_{ij}\frac{n_{iA}^{(0)}}{n_A}\frac{n_{jB}^{(0)}}{n_B}[\sum_{kl}\kappa_f^{(1)}(kl|ij)]+\sum_{ijkl}k_f^{(0)}(kl|ij)\frac{n_{iA}^{(0)}}{n_A}\frac{n_{jB}^{(0)}}{n_B}\left(\frac{n_{jB}^{(1)}}{n_{jB}^{(0)}}+\frac{n_{iA}^{(1)}}{n_{iA}^{(0)}}\right) \tag{78}$$

$$n_{iA}^{(1)}/n_{iA}^{(0)}=[1-\exp(-\beta\mathcal{A})]\int f_{iA}^{(0)}D_{iA}[p_A,\epsilon_{iA};\beta,\xi_i,n_S(0)]d\mathbf{p}_A,$$

with an analagous equation for $k_r^{(1)}$. As defined, the deviations from the canonical densities $n_{iA}^{(1)}$ are also proportional to the driving force of the chemical reaction.

The conclusions which followed Eqs. (29)–(31) may also be drawn here: The quantities $k_f^{(1)}$ and $k_r^{(1)}$ are functions of the affinity and implicity of the time through the progress variables of the possible reactions. The ratio $k_f^{(1)}/k_r^{(1)}$ is also a function of time and hence the law of mass action, as well as the usually assumed phenomenological rate expression, holds strictly only in lowest order of perturbation. In that lowest order all distributions which are relevant for the evaluation of the chemical reaction rate are given by their equilibrium values.

5. DISCUSSION

The magnitude of the deviation from the Maxwellian distribution of speeds or internal distribution functions induced by chemical reactions depends on the details of specific molecular models. The problem of the disturbance of the momentum distribution function has been approached by a number of authors.[1–5] Prigogine and Xhrouet assumed the following forms for the chemical reaction cross section σ^*

$$\sigma^*=0 \quad \text{if} \quad E<\epsilon^*$$

$$\sigma^*/\sigma=1 \quad \text{if} \quad E>\epsilon^* \tag{79a}$$

$$\sigma^*/\sigma=1-\exp(-E/2\epsilon^*), \tag{79b}$$

and described the elastic scattering cross section σ by hard-sphere interactions.[18] They solved an assumed Boltzmann equation for the case of total absence of products by a Sonine polynomial expansion and found the perturbation function ($\phi^{(1)}$ in our notation) to be proportional to kT/ϵ^*. For $\epsilon^*>10kT$ the effect of the perturbation on the rate was negligible. Present[5] repeated this procedure for the chemical reaction cross section given by

$$\sigma^*=0 \quad \text{if} \quad E<\epsilon^*$$

$$\sigma^*/\sigma=[1-(\epsilon^*/E)] \quad \text{if} \quad E>\epsilon^*, \tag{80}$$

a model in which only the initial relative energy along the line of centers on collision may contribute to the activation energy. His results are substantially the same as those of Prigogine and Xhrouet. There remain a number of difficulties in these calculations. Takayanagi has objected to the expansion of the solution of the Boltzmann equation for chemical reactions in Sonine polynomials because such solutions diverge. Furthermore, Takayanagi has pointed out the importance of the mass ratio of the reactants and has shown that a light molecule as a participant in a chemical reaction can have a strongly perturbed momentum distribution which may then influence the rate considerably.

Although a hard-sphere model may be a reasonable approximation to the chemical reaction cross section, it is rather poor for the elastic cross section. The differential elastic cross section for realistic models of interactions increases rapidly for small scattering angle and small relative energies whereas the hard-sphere model yields a differential scattering cross section independent of angle or energy. Small angle scattering may contribute significantly to the attainment of the Maxwellian distribution of speeds, hence estimates of the magnitude of the perturbation in the momentum distribution function by a chemical reaction based on such a model may for this reason be too large.

The influence of a perturbed internal distribution induced by a chemical reaction on the rate of the reaction has been considered by Eyring and Zwolinski[19] and Montroll and Shuler.[20]

The model used by Montroll and Shuler (a generalization of the model used by Eyring and Zwolinski) consists of a dilute gaseous solution of harmonic oscillators at a given internal temperature in a rare gas at a different temperature. The momentum distributions are assumed to be Maxwellian. A chemical reaction is said to occur if a given level of the oscillator is excited and the chemical products are not considered. Excitation to the critical energy level leading to chemical reaction can only be attained by a stepwise activation process because of the selection rules for harmonic oscillator transitions. Montroll and Shuler find that the rate of the chemical reaction is essentially unaffected by the deviation from an internal canonical distribution if the activation energy ϵ^* of the reaction is larger than about $10kT$. Nikitin and Sokolov, estimate a considerable retardation of the rate of decomposition reactions induced by nonequilibrium vibrational distributions in anharmonic oscillators. No conclusions should be drawn from the similarity of the results obtained by Montroll

[18] The initial relative kinetic energy is denoted by E and the threshold or activation energy by ϵ^*.

[19] B. J. Zwolinski and H. Eyring, J. Am. Chem. Soc. **69**, 2702 (1947).

[20] E. W. Montroll and K. E. Shuler, Advances in Chem. Phys. **1**, 361 (1958).

and Shuler and Prigogine *et al.* There is no *a priori* reason for expecting a connection between the deviation of the Maxwellian distribution and the deviations from internal distributions, as their origins are, and their magnitudes may be, quite different.

6. "TRANSITION STATE" METHOD OF CHEMICAL KINETICS

The rate coefficient may under certain circumstances be expressed as a ratio of partition functions or proportional to $\exp[-\Delta F^{\ddagger}/RT]$, where $\Delta F^{\ddagger}$ is a free-energy difference related to these partition functions according to the formulas of statistical thermodynamics. This subject is referred to as the "transition state" or "activated complex" method and the Eyring theory.[11–13] In this section we derive such a formulation for the rate coefficient of a bimolecular gas-phase reaction under less restrictive sufficient conditions than presented previously. The analysis has some similarity with the derivations given in references 8 and 12. One difference is the confinement here to the use of operationally defined concepts.

We suppose from the start that the statistical mechanical expression for the rate coefficient in the transition state approach is strictly time independent. As we have seen, this implies the lowest order rate coefficient, one calculated with a Maxwellian distribution of speeds and canonical internal distributions. Since the derivation of a time-dependent rate coefficient is quite outside the domain of the transition state approach, these conditions on the distribution functions need not be viewed as additional assumptions. We begin, therefore, with the equation for the lowest order rate coefficient in the forward direction of Eq. (49), i.e., Eq. (65);

$$k_f(kl\,|\,ij) = \int\cdots\int (p/\mu)\sigma^*(kl\,|\,ij;\, p,\Omega) f_{iA}^{(0)} f_{jB}^{(0)} d\Omega d\mathbf{p}_A d\mathbf{p}_B. \quad (81)$$

The momentum distribution functions $f_{iA}^{(0)} = f_A^{(0)}$ are Maxwellian and the internal distribution densities for nondegenerate states are canonical,

$$n_{iA}^{(0)}/n_A = [\exp(-\beta\epsilon_{iA})]/Z_A, \quad (82)$$

where Z_A is the internal partition function of species A. The total cross section $C_{ij}^{kl}(E)$ a function of the relative energy E is

$$C_{ij}^{kl}(E) = \int \sigma^*(kl\,|\,ij;\, p,\Omega)\, d\Omega. \quad (83)$$

The basic and only assumption of the derivation is the supposition that each of the total cross sections $C_{ij}^{kl}(E)$ has an energy threshold below which it is negligible. Hence, we write for the total cross section

$$C_{ij}^{kl}(E) = 0 \qquad \text{if} \quad E < \epsilon_{ij}^{kl}$$
$$C_{ij}^{kl}(E) = [1 - (\epsilon_{ij}^{kl}/E)]\alpha_{ij}^{kl}(E) \quad \text{if} \quad E > \epsilon_{ij}^{kl}; \quad (84)$$

the second equation [Eq. (84)] defines the function $\alpha_{ij}^{kl}(E)$ and its variation with energy from some constant value represents the deviation from a classical hard-sphere model.

The rate coefficient for the disappearance of species A is

$$k_f = \sum_{ij} \frac{n_{iA}^0}{n_A} \frac{n_{jB}^0}{n_B} \{\sum_{kl} k_f(kl\,|\,ij)\} \quad (85)$$

$$k_f = \sum_{ijkl} \frac{\exp\{-\beta[\epsilon_{iA}+\epsilon_{jB}]\}}{Z_A Z_B} \int\cdots\int (p/\mu)\left(1 - \frac{\epsilon_{ij}^{kl}}{E}\right)\alpha_{ij}^{kl}(E) f_A^{(0)} f_B^{(0)} d\Omega d\mathbf{p}_A d\mathbf{p}_B \quad (86)$$

obtained with the use of the above relations. The momentum distribution functions are

$$f_A^{(0)} = \left(\frac{1}{2\pi m_A kT}\right)^{\frac{3}{2}} \exp\left[-\frac{\beta p_A^2}{2m_A}\right], \quad (87)$$

and a transformation to relative and center-of-mass coordinates leads to

$$k_f = \frac{8\pi\mu}{(2\pi\mu kT)^{\frac{1}{2}}} \sum_{ijkl} \frac{\exp\{-\beta[\epsilon_{iA}+\epsilon_{jB}]\}}{Z_A Z_B} \int_{\epsilon_{ij}^{kl}} (E - \epsilon_{ij}^{kl})\alpha_{ij}^{kl}(E) \exp(-E/kT) dE. \quad (88)$$

If we introduce the variable $\xi \equiv (E - \epsilon_{ij}^{kl})$, then k_f can be written

$$k_f = 2\left(\frac{2kT}{\pi\mu}\right)^{\frac{1}{2}} \frac{1}{Z_A Z_B} \sum_{ijkl} \exp\{-(1/kT)[\epsilon_{iA}+\epsilon_{jB}+\epsilon_{ij}^{kl}]\}\kappa_{ij}^{kl} \quad (89)$$

$$\kappa_{ij}^{kl} \equiv \frac{1}{(kT)^2} \int_0^\infty \xi\alpha_{ij}^{kl}(\xi+\epsilon_{ij}^{lk}) \exp(-\xi/kT) d\xi. \quad (90)$$

For classical hard spheres κ_{ij}^{kl}, as defined, is independent of temperature, and equals the total cross section $\pi\sigma_{ij}^2$, a constant for this case. The hard-sphere diameter for the reactants in quantum states (i, j) is denoted by σ_{ij} (See Appendix).

Next we denote the sum $(\epsilon_{iA}+\epsilon_{jB}+\epsilon_{ij}^{kl})$ by ϵ_{ij}^{*kl} and observe that the summation of $\exp[-\epsilon_{ij}^{*kl}/kT]$ over the indexes may be viewed formally as a partition function,[21]

$$k_f=2(2kT/\pi\mu)^{\frac{1}{2}}\exp(-\Delta F^{\ddagger}/kT)\kappa(T) \quad (91)$$

$$\exp(-\Delta F^{\ddagger}/kT)\equiv\sum_{ijkl}\frac{\exp[-(\epsilon_{ij}^{kl}/kT)]}{Z_AZ_B} \quad (92)$$

$$\kappa(T)\equiv\sum_{ijkl}\exp[-(\epsilon_{ij}^{*kl}/kT)]\kappa_{ij}^{kl}\cdot/\sum_{ijkl}\exp[-(\epsilon_{ij}^{*kl}/kT)]. \quad (93)$$

To obtain the rate coefficient in the form [Eq. (91)] no reference has been necessary to the nature, or existence of potential energy surfaces for the reacting system; to the Born-Oppenheimer approximation; the influence of rotation; and in particular, there has been no need to postulate the physical existence of an activated complex or transition state.[8,22]

The expression for the rate coefficient [Eq. (91)] has the expected exponential temperature dependence and a pre-exponential temperature factor of $T^{\frac{1}{2}}$ which arises from the proper consideration of the three-dimensional relative translational motion. The terms κ_{ij}^{kl} may have a slowly varying temperature dependence arising from deviations from classical hard-sphere interactions. It is interesting to note that such deviations enter only in the pre-exponential temperature factor. (This clearly indicates how difficult it is to deduce information about the details of chemical interactions, say the energy dependence of chemical reaction cross sections, from measurements of the temperature dependence of rate coefficients.)

All the quantities necessary for the computation of the rate coefficient [Eq. (91)] that is ϵ_{iA}, ϵ_{jB}, ϵ_{ij}^{kl}, Z_A, Z_B, and κ_{ij}^{kl} are defined operationally. Their *a priori* calculation from the Schrödinger equation for the reacting system may well require various approximations.[8] The sum of energies $(\epsilon_{iA}+\epsilon_{jB}+\epsilon_{ij}^{kl})=\epsilon_{ij}^{*kl}$ may be identified with a potential energy barrier only in a limiting classical mechanical interpretation. The height of the barrier is just equal to this sum if the reacting system at the top of the barrier has zero kinetic energy.[23,24]

[21] The summation over the final states k, l has been retained for the sake of generality. If the chemical reaction scattering follows the laws of classical mechanics, then each threshold energy ϵ_{ij}^{kl} is uniquely determined by the initial states only.

[22] The assumption of chemical equilibrium between reactants and activated complex[18] is untenable and unnecessary.[8,12]

[23] E. Wigner, Trans. Faraday Soc. **34**, 29 (1938).

[24] J. Hirschfelder and E. Wigner, J. Chem. Phys. **7**, 616 (1939).

ACKNOWLEDGMENT

We thank Professor J. O. Hirschfelder for a critical reading of the manuscript.

APPENDIX

The reduction of the expression for the rate coefficient in the transition-state formulation [Eqs. (91)–(93)], is straightforward if all chemical reaction scattering cross sections can be described by a classical hard-sphere model. In that case the total reaction cross section Eqs. (83), (84), is

$$C_{ij}^{kl}(E)=0 \quad \text{if} \quad E<\epsilon_{ij}^{kl} \quad (A1)$$

$$C_{ij}^{kl}(E)=[1-(\epsilon_{ij}^{kl}/E)]\pi\sigma_{ij}^2 \quad \text{if} \quad E>\epsilon_{ij}^{kl}, \quad (A2)$$

where σ_{ij} is the arithmetic mean of the hard-sphere diameters of the reactants in initial internal states (i, j), and ϵ_{ij}^{kl} is the threshold energy. If, as assumed, the scattering process follows the laws of classical mechanics, then the notation for the final state (k, l) is redundant and therefore omitted from now on. The quantity κ_{ij} [Eq. (90)] becomes simply

$$\kappa_{ij}=\pi\sigma_{ij}^2, \quad (A3)$$

and the coefficient $\kappa(T)$, [Eq. (93)], is

$$\kappa(T)=\frac{\sum_{ij}\pi\sigma_{ij}^2\exp(-\epsilon_{ij}^*/kT)}{\sum_{ij}\exp(-\epsilon_{ij}^*/kT)} \quad (A4)$$

$$\epsilon_{ij}^*=\epsilon_{ij}+\epsilon_{iA}+\epsilon_{jB}. \quad (A5)$$

The rate coefficient

$$k_f=2(2kT/\pi\mu)^{\frac{1}{2}}\kappa(T)\exp(-\Delta F^{\ddagger}/kT) \quad (A6)$$

$$\exp(-\Delta F^{\ddagger}/kT)=(1/Z_AZ_B)\sum_{ij}\exp(-\epsilon_{ij}^*/kT), \quad (A7)$$

with $\kappa(T)$ given by Eq. (A4) is a natural extension of the collision theory to the case where the reactants may exist in more than one initial state. If only one initial state is allowed to the reactants, then we have for the internal partition functions of the reactants

$$Z_A=Z_B=1. \quad (A8)$$

for the coefficient $\kappa(T)$

$$\kappa(T)=\pi\sigma^2, \quad (A9)$$

and for the factor $\exp(-\Delta F^{\ddagger}/kT)$

$$\exp(-\Delta F^{\ddagger}/kT)=\exp(-\Delta E^{\ddagger}/kT) \quad (A10)$$

$$\Delta E^{\ddagger}=\epsilon_{11}^*, \quad (A11)$$

where $\epsilon_{11}^*=\epsilon_{11}+\epsilon_{1A}+\epsilon_{1B}$, ϵ_{11} is the threshold energy, and ϵ_{1A}, ϵ_{1B} the one-level energies of the reactants. Now the rate coefficient has the well-known form of the collision theory,

$$k_f(T)=2(2kT/\pi\mu)^{\frac{1}{2}}\pi\sigma^2\exp(-\Delta E^{\ddagger}/kT). \quad (A12)$$

Remarks on the Electronic Spectra and Structures of Compounds of Chromium and Benzene*

R. STEPHEN BERRY

Sterling Chemistry Laboratory, Yale University, New Haven, Connecticut

(Received December 19, 1960)

An orbital level diagram and assignments of electronic spectra are given for the benzene-chromium compounds. These are based principally on symmetry arguments, atomic spectra and dichroism measurements. The problem of the energy involved in distorting benzene rings is also discussed.

I. INTRODUCTION

THIS note is written in an attempt to interpret the electronic spectra[1,2] and skeletal structure[3] of the benzene-chromium compounds and to relate these to a set of orbitals based on molecular symmetry and spectral assignments. We shall discuss the assignments particularly in terms of polarization, and also of intensity; we shall then consider aspects of the energetics of the distortion of the benzene ring. No attempt is made to carry out extensive orbital calculations; rather, we can compare our empirically deduced orbital diagram with those calculated for the cyclopentadienyl-metal compounds like ferrocene.[4-6]

Crystalline dibenzene chromium itself is composed of two distorted benzene rings which can be pictured easily as lying on opposite threefold faces of an octahedron about the chromium atom. The observed C—C bond distances,[3] 1.353 and 1.439 A, correspond closely to a hypothetical cyclohexatriene molecule. The short C—C bonds of one ring lie opposite the long bonds of the other, giving the molecule D_{3d} symmetry. It is perhaps easiest to interpret the behavior of this molecule and the other arene-chromium compounds by starting with the picture of two benzene rings in D_{6h} symmetry (one directly above the other), lying on opposite faces of a chromium atom in a d^6 configuration, or more specifically, in a pseudo-octahedral field. Then the six electrons of chromium fill the t_{2g} orbitals. These orbitals point toward alternate C—C bonds in just the way necessary to force the ring π electrons into the D_{3d} structure. (This approach has the convenience that D_{3d} is a subgroup of both D_{6h} and O_h although neither of these two is contained in the other.) The now-trigonal structure of the two benzene rings lowers the symmetry of the ligand field about the chromium, causing the t_{2g} level to split into a_{1g} and e_g orbitals. The $3d$ a_{1g}, in a natural coordinate system for the trigonal field, looks like $2z^2-x^2-y^2$, with a density maximum pointing toward the center of the rings. This a_{1g} orbital can mix with the $4s$ a_{1g} orbital which looks like $x^2+y^2+z^2$, to produce a low-energy a_{1g} level with high density midway between the rings, and a high-energy orbital pointing its density very strongly toward the benzene rings. The e_g orbitals from the octahedral t_{2g} set, and the higher $3d$ e_g' orbitals can also mix, so that the low-energy e_g pair have nodal surfaces principally cutting the octahedral faces where the rings lie, while the other, high-energy e_g' orbitals have their nodal surfaces mainly out of the way of the benzene rings. We shall also have to consider the $4p$ a_{2u} and $4p$ e_u orbitals in the trigonal field. Figure 1 indicates the relation of the D_{3d} cyclohexatriene structure to the octahedral ligand field.

In the benzene-chromium compounds, the empty $3de_g'$ orbitals have particularly high amplitudes close to the short C—C bonds. It is reasonable to expect that a large fraction of the binding energy involving the π electrons occurs as a result of mixing the πe_g orbitals with these $3d$ e_g' orbitals. The only other orbital mixing which will be particularly important to us is that of the $4p$ e_u' chromium orbitals and the excited ring $\pi e_u'$ orbitals.

II. SPECTRA AND ORBITAL LEVELS

With the foregoing introduction as a basis, we can use the observed spectra of the complexes,[1,2] the ionization potentials of benzene[7] and chromium,[8] and the atomic spectrum of chromium[8] to infer the orbital structure of the benzene-chromium compounds, and to assign their spectral band systems. In their discussion of spectra, Yamada *et al.*[1,2] report six bands, as indicated in Table I. They suggest that Band IV is due to a $\pi \rightarrow \pi^*$ transition within the rings, on the basis of in-

* Contribution Number 1649 from the Sterling Chemistry Laboratory, Yale University.

[1] S. Yamada, H. Nakamura, and R. Tsuchida, Bull. Chem. Soc. Japan **30**, 647 (1957).

[2] S. Yamada, H. Yamazaki, H. Nishikawa, and R. Tsuchida, Bull. Chem. Soc. Japan **33**, 481 (1960).

[3] F. Jellinek, Nature **187**, 871 (1960).

[4] These calculations have been reviewed in detail by (a) G. Wilkinson and F. A. Cotton, Prog. Inorg. Chem. **1**, 1 (1959). See especially (b) J. D. Dunitz and L. E. Orgel, J. Chem. Phys. **23**, 954 (1955) and references 5 and 6.

[5] M. Yamazaki, J. Chem. Phys. **24**, 1260 (1956).

[6] A. D. Liehr and C. J. Ballhausen, Acta Chem. Scand. **11**, 207 (1957).

[7] W. C. Price and R. W. Wood, J. Chem. Phys. **3**, 439 (1935); K. Watanabe, *ibid.* **22**, 1564 (1954).

[8] Charlotte E. Moore, *Atomic Energy Levels*, National Bureau of Standards, Circular No. 467 (U. S. Government Printing Office, Washington, D. C., 1952), Vol. II.

TABLE I. Representative spectral information.[a]

Compound	Form	Band I′	"Spin-forbidden" band	Band I	Band II	Band III	Band IV
bz_2CrI	H_2O soln. frequency (ev)	1.07	2.15	3.14	3.72	4.57	5.51
	$\log\epsilon_{max}$	0.95	1.8	approx 2.75	3.76	3.75	4.14
	Ethanol soln. frequency			approx 3.14	3.71	4.54	5.75
	$\log\epsilon_{max}$			approx 2.75	3.80	3.78	4.28
	Crystal frequency			2.77	3.55–3.72	4.36	>4.96
	$\log\alpha_{max}$ (stronger component)			1.85	1.75	1.7	"marked"
	Polarization (stronger component boldface)			*x*, *y*; **z**	*x*, *y*; **z**	**z**	**x**, **y**
$bzCr(CO)_3$	Methanol soln. frequency	(absent)	2.19–2.23	3.30	3.98	4.89	
	$\log\epsilon_{max}$		1.8	3.3	3.86	3.74	
	Ethanol soln. frequency	(absent)	2.27–2.31	3.30	3.97	4.88	
	$\log\epsilon_{max}$		1.8	3.4	3.54	3.64	
	Crystal frequency			3.26	4.01		
	$\log\alpha$ (stronger component)			1.85	1.9		
	Polarization			*x*, *y*; **z**	*x*, *y*; **z**		

[a] See references 1 and 2.

etnsity, polarization and solvent shift. They also point out that the frequency of this band is not characteristic of a benzenoid transition and suggest that when the benzene-chromium compounds form, considerable change in the aromatic system takes place. We accept their assignment of Band IV, and can add a little theoretical evidence which perhaps helps to support their identification. The two extreme models which one can choose for the π electrons of the benzene rings are (a) the usual molecular orbital model in which the six π electrons are completely delocalized and move in an uncorrelated way over the entire ring, and (b) a localized double-bond model in which the π electrons are restricted to staying in their own electron-pair bonds. The former can be improved in the usual way with the help of configuration interaction. The latter can be improved in two steps; ultimately, we might include many valence bond structures and obtain the same result that we would get from the MO picture; along the way, however, we might keep the double bonds localized and yet permit them to interact via dispersion forces. These do seem to be the major source of interaction between π electron pairs in the polyenes.[9,10] In either an MO or interacting-double-bond model, the first allowed transition of benzene is $^1E_{1u}\leftarrow{}^1A_{1g}$, which appears at about 7.3 ev in benzene. The interacting-double-bond model places this transition at considerably lower energy; we can see this as follows. We construct wave functions based on the two-electron functions for three individual double bonds, A, B, and C, so that the ground-state Ψ_0 may be written as a product ABC. Then the first excited state is one in which all three electron pairs share excited character (the exciton model). This can be written as

$$\Psi_\pm\sim ABC^*+\exp(\pm 2\pi i/3)AB^*C+\exp(\pm 4\pi i/3)A^*BC.$$

The excitation energy can be expressed as

$$\Delta E=(A/\mathfrak{IC}/A^*)-(AB^*/\mathfrak{IC}/A^*B).$$

The parameters $(A/\mathfrak{IC}/A^*)$ and $(AB^*/\mathfrak{IC}/A^*B)$ might be found empirically from the spectra of ethylene and *cis*-butadiene, respectively. The former is known to be 7.6 ev. The *cis*-butadiene spectrum has not been reported; we take the value of 1.8 ev on the basis of a calculation carried out for both *cis*- and *trans*-butadiene[11] which gives good agreement for the uv spectrum of the *trans*-molecule. Hence the model predicts the $\pi\rightarrow\pi^*$ transition to fall at 5.8 ev, which may be compared with the observed value of 5.51 and 5.75 ev for dibenzene chromium iodide in water and ethanol solutions, respectively. (We might point out that the observed benzene levels $^1B_{2u}<(^1B_{1u}?)<{}^1E_{1u}$ are quite different in the exciton model, which gives $^1E_{1u}<{}^1B_{2u}<{}^1B_{1u}$.) We take this "agreement" to indicate that the assignment of Band IV as a $\pi\rightarrow\pi^*$ transition is reasonable, and that the interaction between the ring and chromium electrons may introduce some localization of the π electrons which in turn causes the frequency of the benzene $^1E_{1u}\leftarrow{}^1A_{1g}$ transition to drop. With this assignment made, we may proceed to the other bands.

[9] W. T. Simpson, J. Am. Chem. Soc. **73**, 5363 (1951); **77**, 6164 (1955).

[10] R. S. Berry, J. Chem. Phys. **30**, 936 (1959).

[11] R. S. Berry, J. Chem. Phys. **26**, 1660 (1957).

We can start to place orbitals on an energy scale and to assign transitions. Figure 2 shows the levels and transitions as we shall now derive them. The $\pi \rightarrow \pi^*$ transition is presumably that involving the πe_u filled and $\pi e_g'$ unfilled levels, neither of which is appreciably shifted from its hypothetical unperturbed origin by any nearby metal orbital. The πa_{1g}, πa_{2u}, $\pi a_{1u}'$, and $\pi a_{2g}'$ orbitals can be placed approximately if we do a straightforward semiempirical molecular orbital calculation, using the observed 5.75-ev energy difference as the characteristic parameter $(\beta'+\beta'')$. (There are two interaction integrals rather than β alone, but the form of the energy levels is the same as that of benzene, if one replaces 2β with $\beta'+\beta''$.)

Band III is the only band whose dichroism shows a minimum in its less intense component at the same frequency its stronger z-polarized component has a maximum.[1] This we take to indicate that there is little or no x, y-polarized contribution to Band III. It must therefore be an $a_{1g} \rightarrow a_{2u}$ transition, and can be either $\pi a_{2u} \rightarrow d a_{1g}'$ or $d a_{1g} \rightarrow p a_{2u}'$. The excited a_g' metal orbital is necessarily higher after interacting with the lower-energy filled a_{1g} chromium orbital, and must therefore be more than 5 ev above the πa_{2u} level. It is probably higher still. The assignment of Band III is therefore made as $a_{1g} \rightarrow a_{2u}'$, involving orbitals principally associated with the metal atom.

The next band we assign is I′, a band appearing only in the Cr^+ compounds. It seems very probable that this involves a transition to a hole in the e_g or a_{1g} orbital, whichever is higher. On the basis of intensity, the transition seems to be forbidden, and, therefore, Yamada *et al.* have suggested that it involves metal orbitals alone. Guided by atomic energy levels, the orbital calculations for ferrocene,[4–6] and the assignment of Band I as described below, we choose to place a_{1g} below e_g, and to assign I′ as a transition $a_{1g}^2 e_g^3 \rightarrow a_{1g} e_g^4$, which does involve metal orbitals principally, and is symmetry forbidden. No possibility exists for any intraconfigurational transitions involving $a_{1g}^2 e_g^3$ or $a_{1g} e_g^4$. The chromium (I) compounds do have the possibility of exhibiting an allowed $\pi e_u \leftrightarrow e_g$ transition.

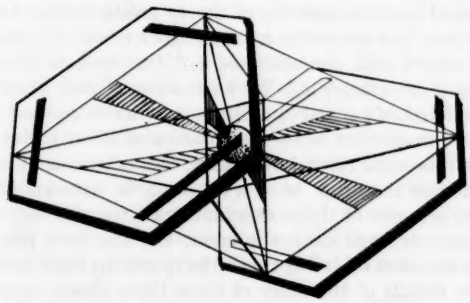

FIG. 1. Benzene rings on threefold-symmetric faces of an octahedron. The directions of six of the electron-density maxima for t_{2g} orbitals are shaded, to indicate how the repulsion of π and d electrons might introduce a distortion of the benzene rings.

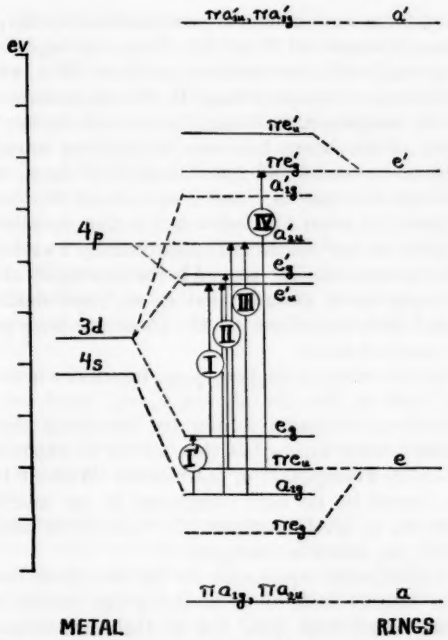

FIG. 2. Orbital diagram and spectral assignments. Energies are chosen to fit dibenzene chromium iodide in ethanol, according to the data of reference 1, but the other compounds are essentially the same.

Presumably this falls at still lower energy than the weak Band I′. We therefore place the e_g orbitals approximately 1 ev above the a_{1g}, to agree with our assignment of Band I′, and put the πe_u level midway between these two, to account for the nonobservance of the long wavelength allowed electronic transition.

To help us place the other orbitals and assign the other bands, we examine the orbital energy levels of the separated rings and chromium atom. Let us assume that the ionization potential of a "cyclohexatriene" ring is the same as tha tof benzene, namely, 9.24 ev.[7] The ionization potential of Cr^0 is 6.763 ev[8] so that we can place the unsplit $3d$ orbitals of Cr approximately 2.5 ev above the πe_u orbitals of the ring system. From observed atomic energies,[8] we can estimate that the chromium $4s$ level lies 0.65 ev below the $3d$, and the $4p$ level, 2.5 ev above the $4s$. Then in formation of dibenzene chromium, the $4s$ and $3d$ levels split into upper and lower groups, each containing an a_{1g} and an e_g set, as shown in Fig. 2.

The $4p$ a_{2u} level finds no nearby orbital of similar symmetry and therefore is not shifted, in first order. This fits well (within 0.3 ev) with the placement and assignment of Band III. The other $4p$ orbitals of symmetry e_u, can mix with the empty $\pi e_u'$ orbitals to give one doubly degenerate set below the $4p$ atomic limit and another pushed above the $\pi e_g'$ level. With this qualitative arrangement, we find that four allowed transitions should appear with energies between 3 and 4 ev.

One of these transitions is in principle fixed by the previous assignments of I′ and III. These two imply that the $e_g \rightarrow a_{2u}'$ transition should fall at about 3.5 ev, which suggests that it is part of Band II. We can probably reject its assignment to Band I because of the low intensity of the latter, but even without the intensity problem, we would find this difficulty: If the $e_g \rightarrow a_{2u}'$ transition were part of I, and if a_{1g} is about 1 ev below e_g, then e_u' is about 1 ev below a_{2u}', so that the allowed transition $e_g \rightarrow e_u'$ should fall approximately 1 ev below I. But no transition is observed in the 2-ev region of the spectrum, so we presume that $e_g \rightarrow a_{2u}'$ and similarly $a_{1g} \rightarrow e_u'$ both contribute to II. These are both pure x, y-polarized bands.

The placement of the two $a_g \rightarrow e_u$ transitions immediately tells us that the allowed $e_g \rightarrow e_u'$ band can be assigned as transition I, and the remaining charge transfer process $\pi e_u \rightarrow e_g'$ as that part of II which contributes its **z** component of polarization. Without this, there would be no such component in our analysis. Hence the e_g' level lies about 1.2 ev above the unsplit $3d$ level, as drawn in the figure.

An alternative explanation for the first three bands might identify Band I as involving the excited a_{1g}' orbital, which falls quite low in the calculations of Yamazaki[5] for ferrocene. This would require, however, that the e_g' orbitals also lie at low energies and that a_{1g} and e_g be nearly degenerate, in order to account for the x, y-polarized component of the transition. This, in turn, would require that either $\pi e_u \rightarrow e_g'$ allowed transition be found at comparable energy, or that the a_{1g} and e_g chromium be somewhat above the πe_u level. This, in turn, would imply the existence of a strong band for Cr (I) at about 1 ev, which is not observed. Regarding the position of the a_{1g}' orbital, it is very possible that it lies higher than shown in the diagram, to maintain the center of gravity of the levels.

Regarding the "spin-forbidden" transition, it is tempting to assign this as arising from the same configuration as one of those produced by transition I or II since these would make the transition allowed on all grounds except spin. On the basis of our orbital diagram, there is no singlet-singlet Laporte-forbidden transition within the $4s$–$3d$ shell which could fit. Furthermore, an oscillator strength of no more than 10^{-5}, estimated from the data of reference 2, is consistent with this assignment.

We might briefly consider intensities in the other bands. For Band I′, f seems to be of the order of 10^{-3}, consistent with its assignment as a symmetry-forbidden spin-allowed transition. In solution, Bands I, II and III have estimated oscillator strengths of about 0.01, 0.1 and 0.1, respectively. The solution spectra give an intensity for Band I which seems quite low for the assignment we have made. The crystal spectra intensities are somewhat higher, consistent with our assignment. It is quite possible that the rings become regular hexagons in solution, according to the infrared and Raman spectra.[12,13] Then the molecule goes into D_{6h} symmetry. In the D_{3d} symmetry of the crystal, the transition of Band I gives excited states of A_{1u}, A_{2u} and E_u symmetry; the A_{2u} is achieved by an allowed z-polarized transition and the E_u, by allowed x, y-polarized transition. In D_{6h} symmetry, the upper states can be B_{1u}, B_{2u} and E_{1u}; only the latter is allowed, and that by x, y-polarized radiation only. The dichroism measurements show that the x, y component of Band I is indeed weaker than the z component in the crystal spectrum, as one would expect if the e_u' orbitals contain a large contribution from the $\pi e_u'$ ring orbitals. In effect, the stronger component has considerable charge-transfer character. This component becomes forbidden if the symmetry becomes D_{6h}, and will decrease markedly in intensity if the rings approach hexagonal symmetry closely. By contrast, when D_{6h} symmetry is achieved, Band II loses the x, y-polarized part of the $\pi e_u \rightarrow e_g'$ transition and the entire (x, y-polarized) $e_g \rightarrow a_{2u}'$ transition, but keeps the $a_{1g} \rightarrow e_u'$ x, y-polarized transition and especially the z-polarized component of the $\pi e_u \rightarrow e_g'$ transition, which is probably the strongest part of Band II. Band III retains its allowed character also, if the rings become regular.

With regard to solvent shifts, we can say relatively little except to speculate that perhaps solvents interact as follows. Interaction is negligible with the "protected" $4p$ a_{2u} orbital, and slight with the a_{1g} occupied chromium orbital, so that III shows a blue shift. Interaction energies between solvent and orbitals e_g and e_u' may be about the same, so that there is no blue shift observed for I. This suggests that the blue shift of II is due at least in part to its $e_g \rightarrow a_{2u}'$ contribution. One might expect that the e_g' orbitals would be protected and suffer little interaction with solvent, so that the $\pi e_u \rightarrow e_g'$ component could also contribute to the blue shift of II.

Comparing our orbital diagram with those derived from various approaches for ferrocene,[4–6] we find a rough similarity to all that these results, (which almost necessarily arises from the order of the levels of the separated systems). Our diagram is particularly close to the results of Dunitz and Orgel.[4] They have not inquired into the splitting of the $4p$ levels, so that their $4p$ level lies above the e_{1g}', analogous to our e_g'; this is in accord with our unshifted a_{2u}', but we have placed the e_u' level below e_g'. We have reversed their order of the filled $3d$ a_{1g} and e_g orbitals, in order to account for the z component of the polarization of Band I. But in the dibenzene chromium system, this orbital can interact with the other $3d$ e_g level, while in ferrocene, the two sets are of different symmetries (e_{2g} and e_{1g}, respectively) and cannot interact. We also have placed the πe_1 filled orbital between the e_g and a_{1g} filled levels. The details of the order of these three closely spaced

[12] H. P. Fritz, W. Lüttke, H. Stammreich, and R. Forneris, Chem. Ber. **92**, 3246 (1959).

[13] R. G. Snyder, Spectrochim. Acta **15**, 807 (1959).

levels might be verified by a study of the dichroism of Band I′. The calculations of Dunitz and Orgel place the unfilled a_{1g}' level rather high, at about the same energy as the unfilled e'_{1g} level of ferrocene. As we pointed out previously, the a_{1g}' chromium level might perfectly well be placed at about the same energy as the e_g'. The level scheme of Yamazaki[5] is essentially similar, so far as the filled levels go, except that it places the ring e_u level above the metal e_g level. The unfilled orbitals of this calculation, which are apparently consistent with the first two observed bands of ferrocene, are much more closely spaced, than those of Fig. 2, especially because Yamazaki places the $3d$ a_{1g} and $4p$ a_{1u} levels below the unfilled e levels. If this were the case of the benzene-chromium compounds, then these would be pure x, y-polarized bands in the region below 3 ev, and no such bands have been observed. Liehr and Ballhausen[6] have placed the metal a_{1g} and e_g filled orbitals together for bicyclopentadienyl chromium. Such a degeneracy fits nicely with our notion that the t_{2g}^6 configuration is a good starting approximation in the benzene-chromium compounds. Nonetheless our assignment of Band I′ implies that there should be some separation of these two levels when benzene is a ligand. Their electrostatic model places the unfilled a_{1g}' orbital below the e_{1g} pair, in contrast to Fig. 2; it also places the $4p$ e_u level below the $4p$ a_u, as our interpretation does, in contrast to the results of Yamazaki.

A recent treatment by Robertson and McConnell[14] of magnetic resonance properties of sandwich compounds suggests that perhaps the e_g metal orbital lies below the a_{1g}. This suggestion is based on the fact that the observed g value of dibenzene chromium (I) is close to the free electron value. It is quite possible that this might be the case. This would require the assignment of Band I as a $\pi e_u \rightarrow e_g'$ process with considerable charge-transfer character, implying that it should be rather intense. This would also require that the $4p$ e_u level be raised about 1 ev so that the $a_{1g} \rightarrow e_u'$ transition fall with II, rather than I. But this leaves no $e_g \leftrightarrow e_u$ transition to provide the z polarized component of Band II, and would also shift the $4p$ level higher and the $3d$ level considerably lower. We therefore prefer to assume for the time being that the e_g level is higher than the a_{1g}, and that the orbital angular momentum is nearly quenched, making the g value near 2. This might be connected either with the large spin density appearing on the rings[15] or with the detailed way in which the two sets of e_g orbitals derive from atomic d orbitals, or both.

We may conclude with a few miscellaneous comments about the spectra of the benzene-chromium compounds. The fact that benzene chromium tricarbonyl[2] shows no z-polarized Band III is in no way a difficulty. The lowest $\pi - \pi^*$ x, y-polarized transition of the three carbonyl groups could easily be responsible for the rising x, y component of the crystal spectrum around 2700 A, where the data end. The spectrum of dibenzene chromium (0) itself has not been reported. We can predict rather easily that it should have a spectrum much like dibenzene chromium iodide, except that Band I′ will be missing. Furthermore, someplace beyond Band IV, there should be more bands of the metal-to-ring type, and probably at quite high energies, another $\pi \rightarrow \pi^*$ transition like the allowed transition of Band IV, but involving πe_g and $\pi e_u'$. It is possible that this band may lie in the 1700–1800 A region; as our diagram is drawn, however, we would place it closer to 1400 A.

III. RING DISTORTION

The next matter we wish to discuss is the problem of the energy involved in distorting the benzene rings into the structures observed in the dibenzene chromium crystal.

One model which we can use is based on the stable benzene ring as a starting point. We can use the appropriate force constant data taken from the infrared spectrum of benzene to estimate the increase in total ring energy when alternate C—C bonds are stretched and compressed to give the distorted structure. We can also estimate how much of this is pure π electron energy from a semi-empirical molecular orbital model. The appropriate motion of the carbon atoms is almost exactly (to within about 0.001 A) a motion along the C—C stretching symmetry coordinate of symmetry type B_{2u},

$$S_{14} = (1/6^{\frac{1}{2}})(r_1 - r_2 + r_3 - r_4 + r_5 - r_6),$$

where r_1 through r_6 represent the six bond lengths. The frequencies of the B_{2u} vibrations were found by Mair and Hornig[16] to be 1311 and 1147 cm^{-1} and the carbon-carbon force constant for S_{14} was obtained by Hornig[17] as either 4.361 or 3.926×10^5/cm. From these values, we find that the ring structure observed in dibenzene chromium lies only 3.48 or 3.13 kcal away from the potential minimum. The zero-point energy of the B_{2u} higher-frequency vibration is 1.87 kcal. Therefore a benzene ring needs only 1.61 or 1.26 kcal to arrive at the distorted form adiabatically. Alternatively, since the first overtone of the 1311 cm^{-1} B_{2u} vibration shows that the potential curve is very harmonic,[17] we can use the harmonic oscillator function to find that the observed distorted structure lies 1.36 or 1.29 classical amplitudes from the potential minimum, and therefore, if other motions are neglected, an ordinary free benzene ring in its ground vibrational state spends between 33.4 and 36% of its time at least as distorted as the rings found in dibenzene chromium crystal. In order for the rings to show stable vibrations in the crystal, at frequencies comparable to the free benzene frequencies[12,13]

[14] R. E. Robertson and H. M. McConnell, J. Phys. Chem. **64**, 70 (1960).
[15] R. O. Feltham, P. Sogo, and M. Calvin, J. Chem. Phys. **26**, 1354 (1957).
[16] R. D. Mair and D. F. Hornig, J. Chem. Phys. **17**, 1236 (1949).
[17] D. F. Hornig, J. Am. Chem. Soc. **72**, 5772 (1950).

the potential minimum of the distorted configuration (in the presence of a chromium atom, of course) must be at least as far below the energy of the regular form as the energy of the free distorted molecule lies above that of the free regular hexagon. If we assume that the undetected B_{2u} mode (ν_{14}) of the rings in dibenzene chromium has its frequency shifted as little as the observed modes,[12,13] then we can infer that the distorted structure needs about 6.5 kcal or more, per benzene, to stabilize it. It would be very helpful if this mode could be detected somehow. Conceivably, ν_{14} might be at considerably lower energy in dibenzene chromium than in benzene itself.

Before we continue this line of reasoning, let us try to estimate the change in energy of the π electrons alone in our delocalized-electron model, when the benzene skeleton is distorted. We use two values, β' and β'', for the interactions across long and short double bonds, respectively.[18] The orbital level scheme is the same as for benzene except that β must be replaced by the average of β' and β''. We can examine $(\beta'+\beta'')/2\beta$ with the help of the formula given by Mulliken[19] for variation of β under small displacements,

$$\beta/\beta' = [S/(1+S)]\cdot[(1+S')/S'].$$

The $p\pi$ overlap integrals are 0.242 for the benzene distance, and 0.278 and 0.233 for the observed ring distances (with $Z=3.18$ in the $2p\pi$ functions). Then the ratio $(\beta'+\beta'')/2\beta$ is 1.046. Therefore, according to the "magic formula," we would conclude that the π electron system of benzene is more stable with a three-fold-symmetric skeleton than with a regular hexagon. This is perhaps an example of the limitation of the formula. In any case, it would appear from this calculation, just as with a conjugated polyene, like butadiene, that the change of π electron energy associated with small distortions of the skeleton is itself small. By "small," we mean only that the energy is small compared with the total π electron interaction energy, or with the energy necessary to establish a harmonic potential well supporting, say three or more levels. The energy is not small compared with the zero-point energy and can definitely influence the force constants of bonds. The B_{2u} benzene skeletal vibration frequency, for example, has a zero-point energy very close to our estimate of the π electron energy change.

In view of the rather low energy necessary to displace the potential minimum, and of the direction which the π electron energy change might have, we are led to suggest that perhaps the rings of dibenzene chromium are distorted in the crystal and are regular hexagons in fluid phases. The frequency of the B_{2u} vibration of dibenzene chromium becomes a very important quantity, since it is a measure of the ease with which this distortion can be made. Crystalline benzene itself shows anisotropic motion of the carbon atoms,[20] in which the amplitudes are particularly large along the circumscribed circle about the regular hexagon. This motion has been attributed to libration. The distorted structure of benzene in dibenzene chromium leaves the carbon atoms on this circle circumscribed about the regular hexagon. Perhaps part of the apparent anisotropic motion of benzene is due to the β_{2u} (ν_{14}) normal mode, with its rather large amplitudes.

Up to this point we have not discussed the difference in the energy associated with localizing the π electrons of benzene. We have only showed that in benzene itself, the distortion involves a rather small total energy change which might be opposite in direction to the change in pure π electron energy. The phenomenon we may ask about now is this: when a benzene ring is distorted, to what extent do electron correlations lead to increased contributions from pairwise-localized canonical structures in the exact wave function? We must specify "pairwise-localized" structures rather than just Kekule's structures because it is important to include dipole-dipole correlations in assessing the behavior of neighboring double bonds.[9,10] Then, we can ask what effect the presence of perturbing charges like the d electrons of chromium will have on the π electron wave function of benzene. We shall not try to answer these questions at this time, except to make a cursory comparison on the basis of the observed spectra. For benzene, the center of gravity of the three lowest singlet states lies at 6.0 ev, which we may take as twice the separation of the lowest unfilled and highest filled orbitals. The spectrum of butadiene and the estimate made in Part II of this paper suggest that the energy difference between highest filled and lowest unfilled orbitals of "cyclohexatriene" is about the same as for ethylene. (The spectral shift is attributed to the splitting of terms within a configuration.) This value is 7.6 ev. A cyclohexatriene orbital model in its crudest form makes all three filled orbitals degenerate; this is the form on which our dispersion interaction is based. Then the energy of the cyclohexatriene π electron system is of the order of $6\times7.6/2$ or 22.8 ev. The benzene π electron energy is $2\times2\times3+4\times3$ or 24 ev, and the net difference in energy of the two π electron systems is 1.2 ev.

A last inference which one might draw from the suggestions presented here is that the two benzene rings of dibenzene chromium are perhaps not free to rotate in the way the cyclopentadienyl rings can rotate in ferrocene-like compounds. The five-membered cyclopentadiene ring has no distortion available to it permitting all the ring electron pairs to avoid the metal d electrons and at the same time to carry the attractive

[18] In this sense, our placement of the perturbed a_{1g}, a_{2u}, a'_{1u} and a'_{2g} π orbitals in Fig. 2 is not entirely consistent; we used the exciton model to help justify the assignment of Band IV as a $\pi\rightarrow\pi^*$ transition, yet placed the perturbed orbital levels as they would be in free benzene, in their unperturbed positions, except for the revised value of β.

[19] R. S. Mulliken, J. Phys. Chem. **56**, 295 (1952).

[20] E. G. Cox, Revs. Modern Phys. **30**, 159 (1958).

ring nuclei with them. The benzenes of dibenzene chromium, on the other hand, can move into a single structure which lowers the π d interaction, and introduces a barrier to rotation. Substitution experiments based on isomer formation might come to mind which would show whether this barrier is larger than, say, kT at room temperature.

Note added in proof. Two articles have appeared recently concerning dibenzene chromium which prompt some comment here. In the first of these [D. A. Levy and L. E. Orgel, Mol. Phys. **4**, 93 (1961)], the authors place the a_{1g} orbitals above the e_g, on the basis of the magnetic measurements of reference 14. We would like to add to our discussion that this orbital sequence would be acceptable according to the foregoing spectral analysis as follows. As we mentioned in Sec. II, the $3de_g'$ orbital must be placed below $4pe_g'$; then we must disallow our strong-field approximation enough to keep the $3de_g \rightarrow 4pe_u'$ transition as part of Band II, using the term-splitting of the configurations as our rationale. Band II still contains $3da_{1g} \rightarrow 4pe_u'$, but $3de_g \rightarrow 4pa_{2u}'$ must lie at very high energy. This assignment has one slightly unattractive feature not previously mentioned. The $\pi e_u \rightarrow 3de_g'$ transition attributed to Band I has a z component allowed in both threefold and sixfold symmetry. Rather, its x, y component disappears in D_{6h} symmetry. One therefore loses the simple interpretation of the apparent structural and spectral changes associated with the change of state.

The second reference [R. D. Feltham, J. Inorg. Chem. **16**, 197 (1961)] contains spectral information similar to that of references 1 and 2, further electron spin measurements and a spectrum of dibenzene chromium itself in cyclohexane solution. No Band I′ is reported; a very weak band is found, corresponding to the spin-forbidden transition, a very broad band is formed with λ_{max} at about 3150 A, and the absorption rises at short wavelengths, as Band IV appears. Our assignment suggests that Band I would be very weak and possibly undetectable. The breadth of the observed band is not inconsistent with the possibility that it contains both Bands II and III.

THE JOURNAL OF CHEMICAL PHYSICS VOLUME 35, NUMBER 1 JULY, 1961

Quantum Statistical Mechanics of Isotope Effects*

I. OPPENHEIM

National Bureau of Standards and Physics Section, Convair, San Diego

AND

A. S. FRIEDMAN

National Bureau of Standards and United States Atomic Energy Commission

(Received December 27, 1960)

Expansions in powers of Planck's constant are utilized in a discussion of isotope effects on the thermodynamic properties of fluid systems. Theoretical calculations of the differences in the equations of state of the hydrogen isotopes and of the helium isotopes are presented and comparison with experimental results are made. Agreement between theory and experiment is excellent.

1. INTRODUCTION

SOME considerations for demonstrating the necessity for a quantum statistical treatment of isotope effects are discussed. In statistical mechanics, one obtains expressions for thermodynamic properties of a system in terms of the phase space distribution functions. The distribution functions are derivable, in theory, from a knowledge of intermolecular interactions. For the simple systems being considered in the density range pertinent for our calculations, the potential energy of the system of N particles U^N is considered to be a sum of pair potentials U_{ij},

$$U^N(\mathbf{R}^N) = \sum_{i<j}^{N} U_{ij}(\mathbf{R}_i, \mathbf{R}_j), \tag{1}$$

where $\mathbf{R}^N$ is the $3N$-dimensional position vector of the N particles. This discussion will be restricted to spatially uniform fluid systems and it is assumed that the structureless particles are spherically symmetric and that U_{ij} depends only on the scalar distance R between particles i and j; i.e.,

$$U_{ij} = U_{ij}(R). \tag{2}$$

* Supported in part by the U. S. Atomic Energy Commission, Division of Research. A portion of this work is contained in a thesis presented by one of us (I.O.) in partial fulfillment of the requirements for the degree of Doctor of Philosophy at Yale University.

The potentials considered will have the general form

$$U(R)=\epsilon\gamma(R/a), \tag{3}$$

where a and ϵ are a characteristic length and energy, respectively. For many purposes, the various isotopic species of a substance may be considered to be characterized by the same values of a and ϵ.[1] Thus, classical statistical mechanics would predict the same thermodynamic properties for the various isotopes of a substance.

In quantum mechanics, however, there is another parameter which is important in describing the molecular dynamics of the system. This parameter, the mean de Broglie wavelength Λ, is given by

$$\Lambda=(\hbar^2/2mkT)^{\frac{1}{2}}, \tag{4}$$

and is a measure of the importance of wave character of the particle. If the de Broglie wavelength is of the order of a, quantum mechanics must be used to describe the dynamics of the system. Since Λ is a function of the mass of the particles, quantum statistical mechanics provides a rationale for the difference in behavior of the isotopic species of a substance.

2. GENERAL THEORY

Expansions of various thermodynamic quantities in powers of Λ^2 have been obtained by many investigators.[2–14] Explicit expressions for the coefficients of Λ^2 in these expansions are presented. The conditions under which these terms are important are indicated.

We may write an expression for quantum corrections to the Helmholtz free energy A in the form

$$A=A_{cl}+(\Lambda^2V/12)I_1+0(\Lambda^4), \tag{5}$$

where A_{cl} is the classical Helmholtz free energy, V is the volume of the system, and I_1 is given by

$$I_1=I_1(V,T)=\int\rho_{cl}^{(2)}(R)\nabla^2U(R)d\mathbf{R}. \tag{6}$$

The quantity $\rho_{cl}^{(2)}$ is the classical pair distribution function.

Expressions for other thermodynamic variables can be easily obtained from Eq. (5). In particular, an expression for the pressure of the system may be written as

$$p=-(\partial A/\partial V)_T=p_{cl}-(\Lambda^2V/12)[I_1/V+(\partial I_1/\partial V)_T]+0(\Lambda^4), \tag{7}$$

where p_{cl} is the classical pressure and $(\partial I_1/\partial V)_T$ is given by

$$(\partial I_1/\partial V)_T=\int(\partial\rho_{cl}^{(2)}/\partial V)_T\nabla^2U(R)d\mathbf{R}. \tag{8}$$

The expression for the internal energy is given by

$$E=E_{cl}+(\Lambda^2V/12)[2I_1-T(\partial I_1/\partial T)_V]+0(\Lambda^4), \tag{9}$$

where E_{cl} is the classical expression for the internal energy.

The above equations can be readily formulated in terms of the radial distribution function

$$g_{cl}(R)=[\rho_{cl}^{(2)}(R)/(\rho)^2]=(V^2/N^2)\rho_{cl}^{(2)}(R), \tag{10}$$

where $\rho=N/V$ is the number density of the system. In terms of $g_{cl}(R)$, Eqs. (6) and (8) become

$$I_1=(N^2/V^2)\int g_{cl}(R)\nabla^2Ud\mathbf{R} \tag{11}$$

and

$$(\partial I_1/\partial V)_T=-(2/V)I_1+N^2/V^2\int(\partial g_{cl}/\partial V)_T\nabla^2Ud\mathbf{R}. \tag{12}$$

It is easy to see that if quantum effects are to be important, then Λ^2VI_1/A_{cl} or Λ^2VI_1/E_{cl} cannot be too small compared to 1. Since A_{cl} or E_{cl} will be of the order of NkT, we have the condition

$$\Lambda^2VI_1/NkT<1 \tag{13}$$

TABLE I. Values of ϵ, a, and λ^{*2} for the hydrogen and helium isotopes.

	$\epsilon\times10^{+16}$ ergs	ϵ/k	$a(A)$	λ^{*2}
H_2	51.1	37.0	2.93	2.988
HD	51.1	37.0	2.93	1.992
D_2; HT	51.1	37.0	2.93	1.495
DT	51.1	37.0	2.93	1.195
T_2	51.1	37.0	2.93	0.996
He^3	14.4	10.22	2.56	9.527
He^4	14.4	10.22	2.56	7.145
He^6	14.4	10.22	2.56	4.763

[1] For those processes which depend on the detailed behavior of the intermolecular potential, e.g., high energy scattering, it is no longer possible to assign the same a and ϵ to different isotopes. Furthermore, when the symmetry of the molecule is changed by isotopic substitution, as, e.g., in H_2 and HD, attention must be paid to the effect on the intermolecular potential. An article by J. Bigeleisen discussing the latter point has appeared in J. Chem. Phys. **34,** 1485 (1961).

[2] G. V. Chester, Phys. Rev. **93,** 606 (1954).

[3] J. E. Mayer and W. Band, J. Chem. Phys. **15,** 141 (1947).

[4] J. G. Kirkwood, Phys. Rev. **44,** 31 (1933).

[5] J. G. Kirkwood, Phys. Rev. **45,** 116 (1934).

[6] G. E. Uhlenbeck and E. Beth, Physica **3,** 729 (1936).

[7] K. Husimi, Proc. Phys. Math. Soc. Japan **22,** 264 (1940).

[8] H. S. Green, J. Chem. Phys. **19,** 955 (1951); **20,** 1274 (1952). See references therein to previous work.

[9] M. L. Goldberger and E. N. Adams II, J. Chem. Phys. **20,** 240 (1952).

[10] A. J. F. Siegert, J. Chem. Phys. **20,** 572 (1952).

[11] I. Oppenheim, N. B. S. Report 3756, October 31, 1954.

[12] A. W. Saenz and R. C. O'Rourke, Revs. Modern Phys. **27,** 381 (1955).

[13] E. Wigner, Phys. Rev. **40,** 749 (1932).

[14] I. Oppenheim and J. Ross, Phys. Rev. **107,** 28 (1957).

TABLE II. Values of $(\lambda^*\beta\epsilon/4\pi)^2$.

$\beta\epsilon$	He^3	He^6	H_2	D_2
0.4	0.99065 $T=25.6°K$	0.00483	0.00303 $T=92.6°K$	0.00151
0.6	0.0217 $T=17.0°K$	0.0109	0.00681 $T=61.7°K$	0.00341
0.8	0.0386 $T=12.8°K$	0.0193	0.0121 $T=46.3°K$	0.00606
1.0	0.0603 $T=10.2°K$	0.0302	0.0189 $T=37.0°K$	0.00946
1.2	0.0869 $T=8.52°K$	0.0434	0.0272 $T=30.8°K$	0.0136

for convergence of the power series expansions, but

$$\Lambda^2 V I_1/NkT \quad \text{not} \quad \ll 1, \tag{14}$$

if quantum effects are to be of any importance.

By comparing I_1 with the integrals arising in the classical theory of liquids, statements can be made on the order of magnitude of Λ when quantum effects become important. In the classical theory:

$$E_{cl} = (3N/2\beta) + 2\pi N^2/V^2 \int_0^\infty R^2 U(R) g_{cl}(R)\, dR$$

$$= (3N/2\beta) + (2\pi/v^2)\epsilon a^3 \int_0^\infty x^2 \gamma(x) g_{cl}(x)\, dx, \tag{15}$$

where

$$v = V/N \quad \text{and} \quad \beta = 1/kT,$$

and x and $\gamma(x)$ are dimensionless quantities which are

TABLE III. Values of the parameter $(-\lambda^3\beta v/12) I_1(R)$.

$T°K$	$\beta\epsilon$ \ v^*	3.644	2.262	1.483	1.220	Species
25.6	0.4	0.396	0.721	1.35	1.83	
17.0	0.6	0.754	1.306			He^3
12.8	0.8	1.22				
10.2	1.0					$\epsilon/k=10.22$
8.52	1.2					
25.6	0.4	0.198	0.360	0.673	0.914	
17.0	0.6	0.377	0.653	1.17		
12.8	0.8	0.611	1.00			He^6
10.2	1.0	0.922				$\epsilon/k=10.22$
8.52	1.2	1.33				
92.6	0.4	0.124	0.226	0.422	0.573	
61.7	0.6	0.236	0.409	0.736	0.921	H_2
46.3	0.8	0.383	0.628	1.08		
37.02	1.0	0.579	0.895	1.47		$\epsilon/k=37.02$
30.8	1.2	0.837	1.22			
92.6	0.4	0.062	0.113	0.211	0.286	
61.7	0.6	0.118	0.204	0.368	0.460	D_2
46.3	0.8	0.191	0.314	0.540	0.725	
37.0	1.0	0.289	0.447	0.735	0.978	$\epsilon/k=37.02$
30.8	1.2	0.419	0.610	0.954		

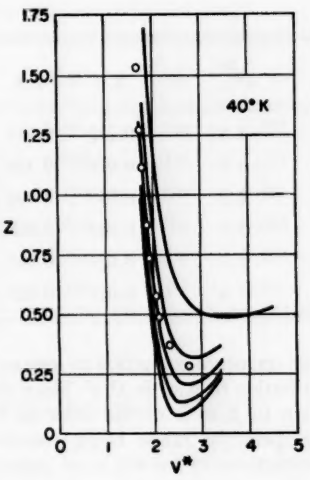

FIG. 1. Compressibility factor vs reduced volume for the hydrogen isotopes at 40°K. The curves, from the upper one down, are for H_2 (experimental), and HD, D_2 (~HT), DT, and T_2 (theoretical). The circles are D_2 (experimental).

defined by the relations

$$x = R/a \tag{16}$$

and

$$\gamma(x) = U(R)/\epsilon. \tag{17}$$

The characteristic length a will be chosen to be the point at which $U(R)$ is zero, i.e., $U(a)=0$. The characteristic energy ϵ will be chosen to be the depth of the potential well. The classical expression for the pressure can be written

$$p_{cl} v\beta = 1 - 2\pi(\beta\epsilon) a^3/v \int_0^\infty x^3 \gamma'(x) g_{cl}(x)\, dx. \tag{18}$$

The order of magnitude of the Λ^2 correction term for $pv\beta$ is

$$\Lambda^2 I_1 v\beta = 4\pi(\beta\epsilon)\Lambda^2 a/v \int_0^\infty \nabla_x^2 \gamma(x) g_{cl}(x) x^2 dx. \tag{19}$$

If it is assumed that the integrals in Eqs. (18) and (19) are of the same order of magnitude, then the ratio of

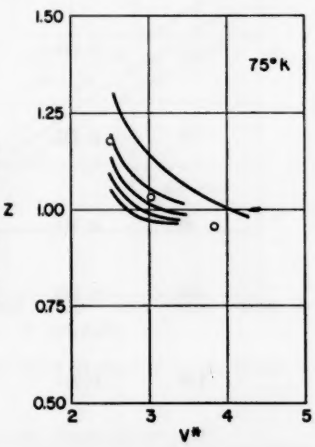

FIG. 2. Compressibility factor vs reduced volume for the hydrogen isotopes at 75°K. The curves, from the upper one down, are for H_2 (experimental), and HD, D_2 (~HT), DT, and T_2 (theoretical). The circles are D_2 (experimental).

TABLE IV. $(Z-Z_{cl})/\Lambda^{*2}$.

v^* \ $\beta\epsilon$	0.2	0.3	0.4	0.5	0.6	0.7	0.8	0.9	1.0	1.1	1.2
1.4	0.112	0.182	0.260	0.342	0.424	0.506	0.588	0.670	0.752	0.835	0.917
1.8	0.078	0.123	0.165	0.216	0.270	0.320	0.378	0.432	0.484	0.538	0.590
2.2	0.056	0.090	0.127	0.167	0.207	0.247	0.294	0.334	0.375	0.408	0.458
2.6	0.040	0.068	0.093	0.127	0.158	0.188	0.218	0.249	0.279	0.309	0.339
3.0	0.029	0.047	0.066	0.090	0.116	0.138	0.160	0.183	0.206	0.228	0.250
3.4	0.021	0.029	0.041	0.055	0.070	0.088	0.109	0.124	0.139	0.155	0.170

the quantum correction to $p v\beta$ to the nonideality contribution to $p_{cl}v\beta$ is Λ^2/a^2. Since the nonideality correction to $p_{cl}v\beta$ is of the order of 1 in the density and temperature range being considered here, quantum corrections to $p v\beta$ will be of importance when $\Lambda \sim a$.

In principle, the theory developed above may be used to predict the thermodynamic properties of the various isotopic species of a substance. In practice, however, this theory does not result in good theoretical predictions for the absolute values of thermodynamic properties in the intermediate density range Therefore, the theory developed here will be used to predict differences in the thermodynamic properties of systems consisting of pure isotopes with the same temperature, number of particles, and total volume. If we use α and β as subscripts to denote two isotopes of a given substance, we can write, by using Eqs. (5), (7), and (9)

$$A_\alpha - A_\beta = (\Lambda_\alpha^2 - \Lambda_\beta^2)(V/12) I_1 + 0(\Lambda^4) \tag{20}$$

$$E_\alpha - E_\beta = (\Lambda_\alpha^2 - \Lambda_\beta^2)(V/12)(\beta\partial I_1/\partial\beta + 2I_1) + 0(\Lambda^4) \tag{21}$$

and

$$p_\alpha - p_\beta = (\Lambda_\beta^2 - \Lambda_\alpha^2)(V/12)(I_1/V + \partial I_1/\partial V) + 0(\Lambda^4). \tag{22}$$

3. COMPRESSIBILITY DIFFERENCES FOR ISOTOPES OF HYDROGEN AND HELIUM

The results of some numerical computations carried out in the framework of the theory just developed are

TABLE V. Compressibility differences between the hydrogen isotopes.

T, °K	$\beta\epsilon$	v^*	$Z_{H_2}-Z_{HD}$	$Z_{H_2}-Z_{D_2}$	$Z_{H_2}-Z_{DT}$	$Z_{H_2}-Z_{T_2}$
40	0.925	1.8	0.443	0.664	0.797	0.885
		2.2	0.342	0.514	0.616	0.684
		2.6	0.255	0.382	0.458	0.509
		3.0	0.188	0.282	0.338	0.376
		3.4	0.127	0.191	0.229	0.255
50	0.740	1.8	0.341	0.512	0.614	0.682
		2.2	0.265	0.397	0.476	0.529
		2.6	0.199	0.299	0.358	0.398
		3.0	0.146	0.219	0.263	0.292
		3.4	0.096	0.143	0.172	0.191
64	0.578	2.2	0.197	0.296	0.354	0.394
		2.6	0.150	0.225	0.270	0.300
		3.0	0.109	0.164	0.197	0.219
		3.4	0.067	0.100	0.120	0.133
75	0.493	2.2	0.163	0.245	0.294	0.326
		2.6	0.124	0.187	0.224	0.249
		3.0	0.088	0.131	0.158	0.175
		3.4	0.054	0.081	0.097	0.107
90	0.411	2.6	0.096	0.144	0.173	0.192
		3.0	0.068	0.102	0.123	0.136
		3.4	0.042	0.063	0.076	0.085
100	0.370	2.6	0.085	0.128	0.153	0.170
		2.8	0.072	0.109	0.130	0.145
		3.0	0.060	0.090	0.108	0.120
		3.4	0.037	0.056	0.067	0.074
150	0.247	2.6	0.053	0.079	0.095	0.106
		3.0	0.037	0.056	0.067	0.075
		3.4	0.025	0.037	0.044	0.049

TABLE VI. $Z_{He^3}-Z_{He^4}=Z_{He^4}-Z_{He^6}$.

v^* \ $\beta\epsilon$	0.2	0.3	0.4	0.5	0.6	0.7	0.8	0.9	1.0
1.4	0.267	0.434	0.619	0.815	1.010	1.205	1.401	1.596	1.791
1.8	0.186	0.293	0.393	0.515	0.643	0.762	0.900	1.029	1.153
2.2	0.133	0.214	0.303	0.398	0.493	0.588	0.700	0.796	0.893
2.6	0.095	0.162	0.222	0.303	0.376	0.448	0.519	0.593	0.665
3.0	0.069	0.112	0.157	0.214	0.276	0.329	0.381	0.436	0.491
3.4	0.050	0.069	0.098	0.131	0.167	0.210	0.260	0.295	0.331

presented here. The differences in the compressibility factors,

$$Z=pV/NkT=p^*v^*/T^*, \tag{23}$$

where

$$v^*=V/Na^3$$

$$T^*=kT/\epsilon$$

and

$$p^*=pa^3/\epsilon \tag{24}$$

of the hydrogen isotopes in the temperature range $40°K\leq T\leq 150°K$, and the reduced volume range, $1.8\leq v^*\leq 3.4$ have been computed. Comparison with experimental data on H_2 and D_2 is made. The differences in the compressibility factors for the helium isotopes in the temperature range, $10.2°K\leq T\leq 50°K$, and the reduced volume range $1.4\leq v^*\leq 2.4$ have also been computed. The calculations have been made with only the terms of order $\hbar^2$ in the expansions described in Sec. 2. It has been assumed that the Lennard-Jones 6–12 potential

$$\gamma(x)=4(1/x^{12}-1/x^6) \tag{25}$$

gives an adequate representation for the force fields of the molecules considered.

It is convenient to express the expansions in terms of reduced variables. Equation (7) becomes:

$$p^*=p_{cl}^*-[\lambda^{*2}/24(2\pi)^2](\partial/\partial v^*)[(4\pi\beta\epsilon/v^*)I^*]+0(\lambda^{*4}), \tag{26}$$

where

$$\lambda^*=[h/a(m\epsilon)^{\frac{1}{2}}] \tag{27}$$

and

$$I^*=\int g_{cl}(x)\{\gamma''(x)+[2\gamma'(x)/x]\}x^2dx. \tag{28}$$

The quantum corrected values of a and ϵ as determined from second virial coefficient data[15] as well as values of λ^{*2} for the hydrogen and helium isotopes are presented in Table I.

Multiplication of Eq. (26) by $v^*\beta\epsilon$ results in

$$Z=Z_{cl}-(\lambda^*\beta\epsilon/4\pi)^2(2\pi/3)v^*(\partial/\partial v^*)(I^*/v^*)+0(\lambda^{*4}) \tag{29}$$

and a parameter of interest determining convergence of the expansion is $(\lambda^*\beta\epsilon/4\pi)^2$. This parameter is tabulated in Table II for He^3, He^6, H_2, and D_2 for a number of temperatures.

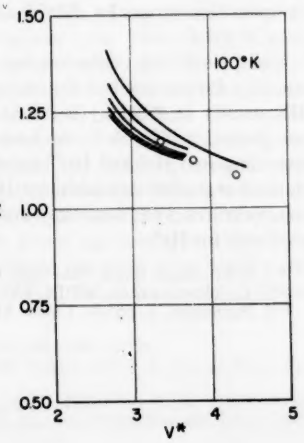

FIG. 3. Compressibility factor vs reduced volume for the hydrogen isotopes at 100°K. The curves, from the upper one down, are for H_2 (experimental), and HD, D_2 (~HT), DT, and T_2 (theoretical). The circles are D_2 (experimental).

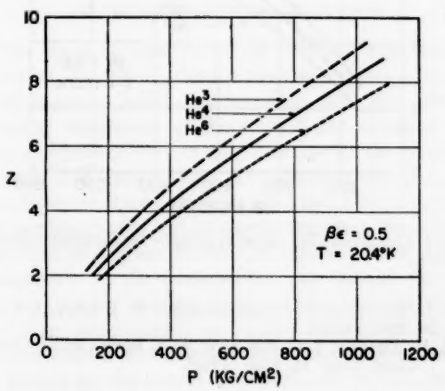

FIG. 4. Compressibility factor vs pressure for the helium isotopes at 20.4°K.

[15] J. deBoer and A. Michels, Physica **5**, 945 (1938).

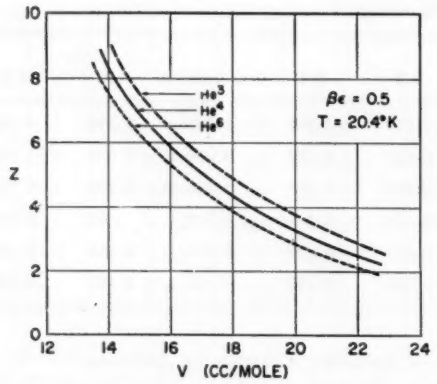

FIG. 5. Compressibility factor vs volume for the helium isotopes at 20.4°K.

I^* was computed using the values of $g(x)$ tabulated by Kirkwood, Lewinson, and Alder,[16] for the cut off Lennard-Jones potential as modified by Zwanzig, Kirkwood, Stripp, and Oppenheim.[17] The method of numerical integration and the intervals used were those described in reference 16 for equation-of-state calculations. It was found convenient to tabulate values of $(4\pi\beta\epsilon/v^*)I^*$ since smooth curves as functions of v^* were obtained for this function. The values of the derivative with respect to v^* of this function were computed numerically and graphically; the results are probably accurate to a few percent in the reduced volume range from 3 to 1.4.

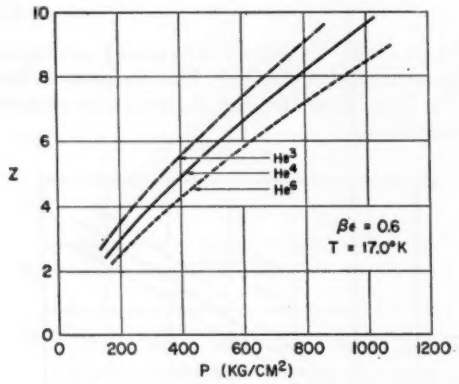

FIG. 6. Compressibility factor vs pressure for the helium isotopes at 17.0°K.

[16] J. G. Kirkwood, V. A. Lewinson, and B. J. Alder, J. Chem. Phys. **20,** 929 (1952).
[17] R. W. Zwanzig, J. G. Kirkwood, K. S. Stripp, and I. Oppenheim, J. Chem. Phys. **21,** 1268 (1953).

In Table III, some values of the parameter $(-\lambda^2\beta v/12)I_1(R)$ over a range of values of $\beta\epsilon$ and v^* for He^3, He^6, H_2, and D_2 are presented.

In Table IV, the main results of this computation are presented and values of $(Z-Z_{cl})/\lambda^{*2}$ for ranges of $\beta\epsilon$ and v^* are given.

In Table V, the compressibility factor differences between the hydrogen isotopes are tabulated for the temperature range 40–150°K and the volume range $v^*=1.8$ to 3.4.

The compressibility factor is plotted as a function of the reduced volume for the 40, 75, and 100°K isotherms in Figs. 1, 2, and 3, respectively. The H_2 isotherms in these figures are experimental values.[18] The circles

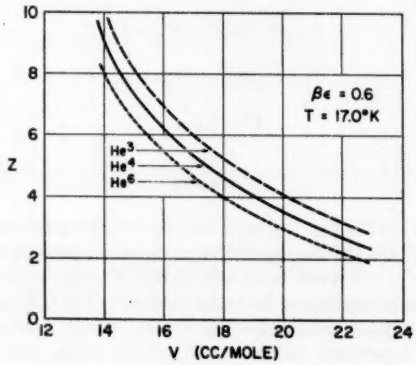

FIG. 7. Compressibility factor vs volume for the helium isotopes at 17.0°K.

represent experimental deuterium points,[19] and the agreement between the experimental and theoretical D_2 values seems to be very good. At lower temperatures, however, more terms in the expansion are necessary, and, at very low temperatures, account ought to be taken of statistics.

In Table VI, the compressibility factor differences between the helium isotopes are tabulated for the temperature range $1\leq T^*\leq 5$ and the volume range $1.4\leq v^*\leq 3.4$.

Compressibility isotherms for He^4 have been measured by Buchmann[20] at liquid-hydrogen temperatures. His results at 20.4°K ($\beta\epsilon=0.5$) and 17.0°K ($\beta\epsilon=0.6$) are plotted in Figs. 4–7; the broken lines correspond to the computed He^3 and He^6 isotherms. No experimental data of state are available for He^3 except at very low temperatures and densities, and of course, none are available for He^6.

[18] A. S. Friedman, thesis, Ohio State University, 1950.
[19] H. L. Johnston, *et al.*, MDDC-850.
[20] E. Buchmann, Z. physik. Chem. **A163,** 461 (1933).

Nuclear Transfer Effects in Nuclear Magnetic Resonance Pulse Experiments

D. E. WOESSNER

Socony Mobil Oil Company, Inc., Field Research Laboratory, Dallas, Texas

(Received December 16, 1960)

The Bloch equations for the nuclear magnetic resonance of a single nuclear species which is transferred between state environments having different relaxation times (T_1 or T_2) and different resonance frequencies have been solved for rf pulse experiments. Expressions have been obtained for the free precession signals in two-pulse experiments. A theoretical study of the signal envelopes has been made for several specific instances. In particular, the effect of the frequency difference between the two states on transverse (T_2) relaxation has been investigated; the predicted effect is large in some cases. The longitudinal (T_1) relaxation is independent of the frequency separation. A reduction of phase dispersion by the second pulse which is similar to that in molecular diffusion is also predicted.

I. INTRODUCTION

MOST characteristics of nuclear magnetic resonance free precession signals[1] are affected by the motions of the molecules, ions, or atoms either containing or in the vicinity of the observed nuclei. These effects provide methods of studying kinetic phenomena. The importance of lattice motions as mechanisms for narrowing resonance absorption and for spin-lattice relaxation was first analyzed theoretically and experimentally by Bloembergen, Purcell, and Pound[2]; a more general theoretical approach has been made by Kubo and Tomita.[3]

This paper is concerned with interpretation of free precession signals derived from nuclei in state environments possessing distinguishable time-averaged resonance line centers and relaxation characteristics. When the nuclei are constrained to particular state environments, the free precession signal is merely the sum of all the different signals. However, characteristics of the signal are changed if the nuclei are allowed to transfer between distinguishable states by some kinetic molecular process such as chemical exchange or internal rotation. Such physical processes transfer nuclear spin magnetization between the types of states. For very rapid transfer, the free precession signals will possess the weighted-average characteristics and be independent of the transfer rate. The effects of most interest are those associated with the "intermediate" rates, where the resonance frequency separation, the reciprocals of the relaxation times, and the nuclear state environmental transfer rates have values of the same order of magnitude. The damping by such state transitions on modulation of the spin-echo envelope for states in which nuclei experience indirect scalar spin-spin coupling between states has been treated by Hahn and Maxwell.[4] The effects on observable longitudinal (T_1) and transverse (T_2) relaxation times and fractional populations of the states have been analyzed with the use of a general stochastic theory by Zimmerman and Brittin[5] for the cases in which the resonance frequencies of all the sites are equal.

The purpose of this paper is to extend the cases covered by the previous analysis[5] to include unequal resonance frequencies but not indirect nuclear spin-spin coupling. When a given nucleus transfers from environmental state a to state b, its precessional phase angle is different from that of a nucleus already in b states. Because the transfer occurs randomly, this generally results in a destructive interference between the precessional signals of the two nuclei and, hence, leads to a damping of the envelope of the resultant signals. This effect should be greatest when the average lifetime τ_a in a state is sufficient to produce a 180° relative phase difference, i.e., when $\tau_a\Delta\omega=\pi$, where $\Delta\omega$ is the angular frequency separation. As part of a general consideration of the observable effects of the nuclear transfers, special emphasis is directed toward an investigation of the effect of the resonance frequency difference on relaxation times and state populations inferred from free precession data.

II. MATHEMATICAL METHODS

The starting point is the set of Bloch equations[6] in which U, V, and M_z denote the components of nuclear magnetization which are in phase with the effective rotating component of the rf field, out of phase with this component, and in the direction of the large stationary field, respectively. The simplest case is that of two different state environments a and b between which the nucleus makes instantaneous transfers. The average lifetimes of a given nucleus in states a and b are the reciprocals of the probabilities per second, or rates, C_a and C_b for leaving these states. The fractions of nuclei in states a and b are P_a and P_b, respectively. The magnetization which is lost by one state environment is gained by the other. This involves the assumption

[1] E. L. Hahn, Phys. Rev. **80**, 580 (1950).
[2] N. Bloembergen, E. M. Purcell, and R. V. Pound, Phys. Rev. **73**, 679 (1948).
[3] R. Kubo and K. Tomita, J. Phys. Soc. Japan **9**, 888 (1954).
[4] E. L. Hahn and D. E. Maxwell, Phys. Rev. **88**, 1070 (1952).
[5] J. R. Zimmerman and W. E. Brittin, J. Phys. Chem. **61**, 1328 (1957).
[6] F. Bloch, Phys. Rev. **70**, 460 (1946).

that the nuclear environmental state transitions are not effective in either spin-spin or spin-lattice relaxation. The Bloch equations modified to include the transfer effects are[7]:

$$\dot{U}_a=-(\omega_a-\omega)V_a-U_a/T_{2a}-C_aU_a+C_bU_b \quad (1)$$

$$\dot{U}_b=-(\omega_b-\omega)V_b-U_b/T_{2b}-C_bU_b+C_aU_a \quad (2)$$

$$\dot{V}_a=(\omega_a-\omega)U_a-V_a/T_{2a}-C_aV_a+C_bV_b-\omega_1M_{za} \quad (3)$$

$$\dot{V}_b=(\omega_b-\omega)U_b-V_b/T_{2b}-C_bV_b+C_aV_a-\omega_1M_{zb} \quad (4)$$

$$\dot{M}_{za}=M_{0a}/T_{1a}-M_{za}/T_{1a}-C_aM_{za}+C_bM_{zb}+\omega_1V_a \quad (5)$$

$$\dot{M}_{zb}=M_{0b}/T_{1b}-M_{zb}/T_{1b}-C_bM_{zb}+C_aM_{za}+\omega_1V_b, \quad (6)$$

where $\omega_1=\gamma H_1$, ω_a is the precessional frequency, T_{1a} and T_{2a} are the longitudinal and transverse relaxation times for nuclei in state a, and M_{0a} is the equilibrium magnetization along the direction of the stationary field for nuclei in a. Similar definitions apply for b states.

Apply at time t_i to a system described by these equations a short, intense rf pulse of duration t_w and intensity H_1 such that ω_1, $1/t_w \gg 1/T_{2a}$, $1/T_{2b}$, $1/T_{1a}$, $1/T_{1b}$, C_a, C_b, $|(\omega_a-\omega)|$, $|(\omega_b-\omega)|$, and $|(\omega_a-\omega_b)|$. Immediately following this pulse the magnetization of each state is given by the equations

$$U(t_i+t_w)=U(t_i) \quad (7)$$

$$V(t_i+t_w)=V(t_i)\cos\theta-M_z(t_i)\sin\theta \quad (8)$$

$$M_z(t_i+t_w)=V(t_i)\sin\theta+M_z(t_i)\cos\theta, \quad (9)$$

where $\theta=\omega_1 t_w$. In the absence of the rf field, $\omega_1=0$ and Eqs. (1) through (6) may be written as

$$\dot{F}_a=-\alpha_{2a}F_a+C_bF_a \quad (10)$$

$$\dot{F}_b=-\alpha_{2b}F_b+C_aF_b \quad (11)$$

$$\dot{M}_{0a}-\dot{M}_{za}=-\alpha_{1a}(M_{0a}-M_{za})+C_b(M_{0b}-M_{zb}) \quad (12)$$

$$\dot{M}_{0b}-\dot{M}_{zb}=-\alpha_{1b}(M_{0b}-M_{zb})+C_a(M_{0a}-M_{za}), \quad (13)$$

where $F_a=U_a+iV_a$ and

$$\alpha_{1a}=1/T_{1a}+C_a, \quad (14)$$

$$\alpha_{2a}=1/T_{2a}+C_a-i(\omega_a-\omega). \quad (15)$$

Similar definitions apply for α_{1b} and α_{2b}. In Eqs. (12) and (13) use is made of the facts that $\dot{M}_{0a}=\dot{M}_{0b}=0$ and $C_aM_{0a}=C_bM_{0b}$.

Equations (10) through (13) represent two sets of two simultaneous equations of the form

$$\dot{m}=-\alpha m+bn \quad (16)$$

$$\dot{n}=am-\beta n. \quad (17)$$

[7] H. M. McConnell, J. Chem. Phys. **28**, 430 (1958).

The solutions of these equations are

$$m(t)=A_+\exp(-\phi_+t)+A_-\exp(-\phi_-t) \quad (18)$$

$$n(t)=B_+\exp(-\phi_+t)+B_-\exp(-\phi_-t), \quad (19)$$

where

$$2\phi_\pm=(\alpha+\beta)\pm[(\alpha-\beta)^2+4ab]^{\frac{1}{2}}, \quad (20)$$

and $A_\pm$ and $B_\pm$ are related by

$$B_\pm=-(\phi_\pm-\alpha)A_\pm/b. \quad (21)$$

The integrating constants, $A_\pm$ and $B_\pm$, are determined by the values of m and n at $t=0$, with the aid of Eq. (21).

These solutions fail when $(\alpha-\beta)^2+4ab=0$. The appropriate solutions are then

$$m(t)=\{A'[1-\tfrac{1}{2}(\alpha-\beta)t]+bB't\}\exp[-\tfrac{1}{2}(\alpha+\beta)t] \quad (22)$$

$$n(t)=\{B'[1+\tfrac{1}{2}(\alpha-\beta)t]+aA't\}\exp[-\tfrac{1}{2}(\alpha+\beta)t]. \quad (23)$$

The integrating constants, A' and B', are also determined from the initial boundary conditions. The failure of solutions (18) and (19) is purely mathematical and

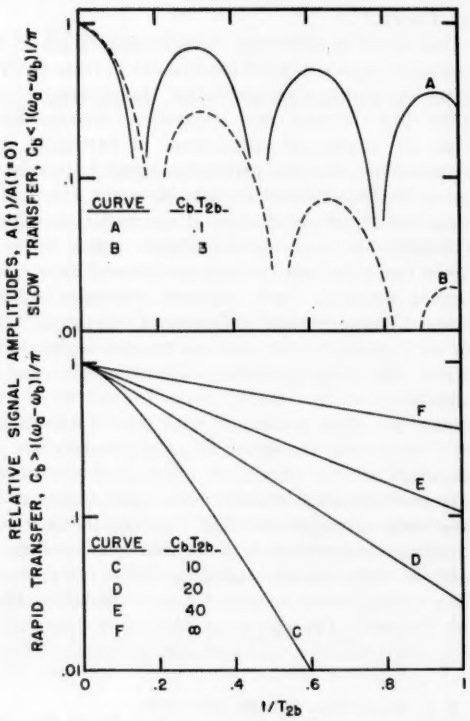

FIG. 1. Theoretical relative free decay signal amplitude versus reduced time after a 90° pulse for several values of reduced transfer rate when $P_a=P_b$, $C_a=C_b$, $T_{2a}=T_{2b}$, and $\omega_a-\omega_b=20/T_{2b}$.

has no special physical significance. This is elaborated in the following section.

III. CALCULATED FREE PRECESSION SIGNALS

The free precession signals may be calculated in the following manner. Add the solutions of Eqs. (10) and (11) after supplying the proper boundary conditions with the aid of Eqs. (7) through (13). Then separate the real and imaginary parts of the motion of the total nuclear magnetization and transform to the laboratory coordinate system.

A. Free Decay Following a Single Pulse

If the nuclear spin system was at thermal equilibrium at the beginning of the pulse, the in-phase component of nuclear magnetization, $U=U_a+U_b$, and the out-of-phase component, $V=V_a+V_b$, for $\omega=\frac{1}{2}(\omega_a+\omega_b)$ are

$$U=-M_0\sin\theta_1\{F_{2-}[dt]\exp(-ct)+F_{2+}[dt]\exp(ct)\}\exp(-\phi_2 t), \quad (24)$$

and

$$V=-M_0\sin\theta_1\{F_{2-}[dt+\tfrac{1}{2}\pi]\exp(-ct)+F_{2+}[dt-\tfrac{1}{2}\pi]\exp(ct)\}\exp(-\phi_2 t), \quad (25)$$

respectively, where

$$F_{2-}[T]=f\cos T+g\sin T, \quad (26)$$

$$F_{2+}[T]=-f\cos T-(1-g)\sin T, \quad (27)$$

$$\phi_2=\tfrac{1}{2}(1/T_{2a}+1/T_{2b}+C_a+C_b), \quad (28)$$

$$f=-\tfrac{1}{4}\{c(P_b-P_a)(\omega_a-\omega_b)+d(P_b-P_a)(1/T_{2a}-1/T_{2b})+C_a+C_b]\}/(c^2+d^2), \quad (29)$$

$$g=\tfrac{1}{2}-\tfrac{1}{4}\{c[(P_b-P_a)(1/T_{2a}-1/T_{2b})+C_a+C_b]-d(P_b-P_a)(\omega_a-\omega_b)\}/(c^2+d^2), \quad (30)$$

and

$$M_0=M_{0a}+M_{0b}. \quad (31)$$

The symbol T represents the argument of the $F_{2\pm}$ functions in Eqs. (24) and (25). In Eqs. (24), (25), (29), and (30), c and d are half the real and imaginary parts, respectively, of the quantity $[(\alpha_{2a}-\alpha_{2b})^2+4C_aC_b]^{\frac{1}{2}}$. The respective magnitudes of c and d are

$$|c|=[(X^2+Y^2)^{\frac{1}{2}}+X]^{\frac{1}{2}}/\sqrt{8} \quad (32)$$

$$|d|=[(X^2+Y^2)^{\frac{1}{2}}-X]^{\frac{1}{2}}/\sqrt{8}, \quad (33)$$

where

$$X=(1/T_{2a}-1/T_{2b}+C_a-C_b)^2-(\omega_a-\omega_b)^2+4C_aC_b \quad (34)$$

$$Y=-2(\omega_a-\omega_b)(1/T_{2a}-1/T_{2b}+C_a-C_b). \quad (35)$$

The algebraic sign of d is always positive, but the sign of c is positive except for negative Y values.

The observed nuclear induction signals are found by transforming back to the stationary laboratory coordinate system. For a single-coil spin-echo system, where the excitation coil also picks up the free precession signal,

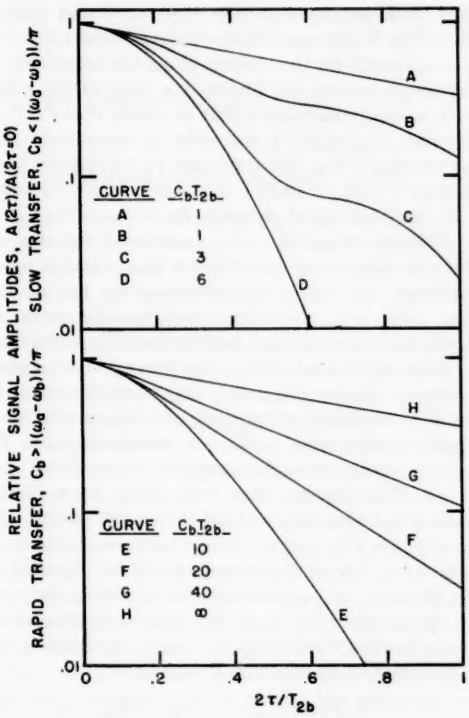

FIG. 2. Theoretical spin-echo amplitudes at time $t=2\tau$ versus reduced 2τ in 90°–180° pulse sequences for several values of reduced transfer rate when $P_a=P_b$, $C_a=C_b$, $T_{2a}=T_{2b}$, and $\omega_a-\omega_b=20/T_{2b}$.

the observed magnetization is

$$M_X=U\cos\omega t-V\sin\omega t, \quad (36)$$

where $\omega=\frac{1}{2}(\omega_a+\omega_b)$, the value chosen above. Ordinarily, the phase of the signal is not sensed. In this case, the rectified signal envelope is

$$A=[U^2+V^2]^{\frac{1}{2}}. \quad (37)$$

Equation (25) shows that the V component is composed of two parts; one part leads the rotating coordinate system as time passes; the other lags it. This is easily seen by considering the case of extremely small nuclear rates, i.e., when C_a, $C_b\approx 0$. In this case $d=\frac{1}{2}|(\omega_a-\omega_b)|$, $f=0$, and $c=\mp\frac{1}{2}(1/T_{2a}-1/T_{2b})$. The upper sign applies when $\omega_a>\omega_b$, and the lower applies when $\omega_a<\omega_b$. With these relations in mind, examination of Eqs. (25) through (30) shows that the term containing $F_{2-}[T]$ describes the lagging part of the magnetization and $F_{2+}[T]$ describes the leading part. In this limit, M_X is given by the relation

$$M_X=M_0\sin\theta_1\{P_a\sin\omega_a t\exp(-t/T_{2a})+P_b\sin\omega_b t\exp(-t/T_{2b})\}, \quad (38)$$

which is found by applying Eqs. (24) and (25) to (36). This is the sum of two damped sine waves, the expected result for the absence of nuclear transfers.

A simple system for illustrating some of the effects of the nuclear transfers is that in which $P_a=P_b$, $T_{2a}=T_{2b}$, and $|(\omega_a-\omega_b)|$ is an order of magnitude or so greater than $1/T_{2b}$. The condition $P_a=P_b$ results in the equality $C_a=C_b$. Figure 1 contains a family of curves of the rectified signal envelope for $\omega_a-\omega_b=20/T_{2b}$ and for different values of C_bT_{2b}, the reduced transfer rate which is defined as the transfer rate relative to the relaxation rate $1/T_{2b}$, as calculated by use of Eqs. (24), (25), and (37). For small transfer rates, the curves show the expected modulation. The envelope of the peaks of the modulations has the expected exponential decay, $\exp(-t/T_{2b})$. For larger transfer rates, the period of modulation increases, and the over-all decay becomes much more rapid but nonexponential. The curve is most strongly damped when $C_b\approx|(\omega_a-\omega_b)|/\pi$. This transfer rate corresponds to a lifetime equal to the time required for the nucleus to get 180° out-of-phase with respect to nuclear precession in the other state. Greatest damping would be expected for this lifetime. As C_b increases, the damping decreases and the shape of the curve approaches an exponential decay. Finally, when $C_b^2\gg(\omega_a-\omega_b)^2$, the damping may be described by an effective T_2 as follows:

$$1/T_2=1/T_{2b}+(\omega_a-\omega_b)^2/8C_b. \tag{39}$$

This contribution of $(\omega_a-\omega_b)$ to $1/T_2$ for $P_a=P_b$ is the same as that calculated by Anderson[8] for a Markoffian transfer process. When $(C_a+C_b)^2\gtrsim(\omega_a-\omega_b)^2$, $d=0$ and hence no modulation occurs on the rectified envelope. Also, the fact that $d=0$ means that the observable precessional frequency is that of the rotating coordinate system, which is the weighted-average frequency for this case of equal populations.

A more general treatment for large transfer rates elucidates the above points. When the conditions C_a, $C_b\gg1/T_{2a}$, $1/T_{2b}$, $|(\omega_a-\omega_b)|$ and $(\omega_a-\omega_b)^2\gg(1/T_{2a}-1/T_{2b})^2$ prevail, it can be shown that

$$|c|=\tfrac{1}{2}\{C_a+C_b+(P_b-P_a)(1/T_{2a}-1/T_{2b}) -\tfrac{1}{2}[1-(P_b-P_a)^2](\omega_a-\omega_b)^2/(C_a+C_b)\}, \tag{40}$$

$$d=\tfrac{1}{2}|(P_b-P_a)(\omega_a-\omega_b)|. \tag{41}$$

Then, M_X is given by the relation

$$M_X=M_0\sin\theta_1\sin\omega_{av}t\exp(-t/T_2), \tag{42}$$

where

$$\omega_{av}=P_a\omega_a+P_b\omega_b, \tag{43}$$

$$1/T_2=P_a/T_{2a}+P_b/T_{2b}+\tfrac{1}{4}[1-(P_b-P_a)^2] \times(\omega_a-\omega_b)^2/(C_a+C_b). \tag{44}$$

The result that the observed frequency is the weighted average of the different frequencies agrees exactly with theory and observation for steady-state experiments.[9] As the transfer rate increases to extremely large values, the observed relaxation rate approaches the weighted-average rate.

B. Signals Following the Second Pulse

As in the usual spin-echo case, several signals follow a second pulse. The calculations of these signals are tedious. It is helpful to leave ω unspecified until the end of the derivation. This enables one to separate the echo signal from the free decay signals immediately following the second pulse. The ultimate choice of $\omega=\frac{1}{2}(\omega_a+\omega_b)$ greatly minimizes the number of terms. The final results are independent of the choice of ω, of course. Three types of U and V components result. One type results from the M_z component which existed at the time of the application of the pulse:

$$U_1=-M_0\sin\theta_2[1-(1-\cos\theta_1)F(T_1)] \times\exp[-\phi_2(t-\tau)]\times\{F_{2-}[d(t-\tau)]\exp[-c(t-\tau)] +F_{2+}[d(t-\tau)]\exp[c(t-\tau)]\} \tag{45}$$

$$V_1=-M_0\sin\theta_2[1-(1-\cos\theta_1)F(T_1)] \times\exp[-\phi_2(t-\tau)]\times\{F_{2-}[d(t-\tau)+\tfrac{1}{2}\pi] \times\exp[-c(t-\tau)]+F_{2+}[d(t-\tau)-\tfrac{1}{2}\pi] \times\exp[c(t-\tau)]\}. \tag{46}$$

Here $F(T_1)$ is the sum of the solutions of Eqs. (12) and (13) evaluated at time τ. Also, τ is the time of application of the second pulse, and θ_1 and θ_2 are the ω_1t_w products for the first and second pulses, respectively. This function describes the time dependence of M_z under the influence of spin-lattice relaxation and the environmental state transitions:

$$F(T_1)=[g'\exp(-c'\tau)+(1-g')\exp(c'\tau)] \times\exp(-\phi_1\tau), \tag{47}$$

where

$$\phi_1=\tfrac{1}{2}(1/T_{1a}+1/T_{1b}+C_a+C_b) \tag{48}$$

and

$$g'=\tfrac{1}{2}-\tfrac{1}{4}[(P_b-P_a)(1/T_{1a}-1/T_{1b})+C_a+C_b]/c', \tag{49}$$

in which

$$c'=\tfrac{1}{2}[(1/T_{1a}-1/T_{1b}+C_a-C_b)^2+4C_aC_b]^{\frac{1}{2}}. \tag{50}$$

Since Eqs. (5) and (6) do not contain the precessional frequency, $F(T_1)$ is independent of $(\omega_a-\omega_b)$ and is also the result previously derived.[5]

The other two types of components result from the magnetization which existed in the XY plane at the beginning of the pulse. One of these is the reduced continuation of the free decay following the first pulse

[8] P. W. Anderson, J. Phys. Soc. Japan **9**, 316 (1954).

[9] H. S. Gutowsky and A. Saika, J. Chem. Phys. **21**, 1688 (1953).

as follows:

$$U_2=-\tfrac{1}{2}M_0\sin\theta_1(1+\cos\theta_2)\exp(-\phi_2 t)\times\{F_{2-}[dt]\exp(-ct)+F_{2+}[dt]\exp(ct)\} \quad (51)$$

$$V_2=-\tfrac{1}{2}M_0\sin\theta_1(1+\cos\theta_2)\exp(-\phi_2 t)\times\{F_{2-}[dt+\tfrac{1}{2}\pi]\exp(-ct)+F_{2+}[dt-\tfrac{1}{2}\pi]\exp(ct)\}. \quad (52)$$

The third type is the spin-echo signal:

$$U_E=-\tfrac{1}{2}M_0\sin\theta_1(1-\cos\theta_2)\exp(-\phi_2 t)\times\{j\sin[d(t-2\tau)]\exp(-ct)+2[f\cos(dt)+(g+j)\times\sin(dt)]\sinh[c(t-2\tau)]-2(g+j-1)\times\sin[d(t-2\tau)]\exp(ct)\} \quad (53)$$

$$V_E=-\tfrac{1}{2}M_0\sin\theta_1(1-\cos\theta_2)\exp(-\phi_2 t)\times\{j\cos[d(t-2\tau)]\exp(-ct)+2[f\sin(dt)-(g+j)\cos(dt)]\cosh[c(t-2\tau)]+(2g+j-1)\cos[d(t-2\tau)]\exp(ct)\}, \quad (54)$$

where

$$j=\tfrac{1}{2}-g-\tfrac{1}{2}[c^2+\tfrac{1}{4}(\omega_a-\omega_b)^2]/(c^2+d^2). \quad (55)$$

The magnetizations of these three types in the stationary coordinate system are given by the following transformations:

$$M_{X1}=U_1\cos[\omega(t-\tau)]-V_1\sin[\omega(t-\tau)], \quad (56)$$

$$M_{X2}=U_2\cos\omega t-V_2\sin\omega t, \quad (57)$$

$$M_{XE}=U_E\cos[\omega(t-2\tau)]-V_E\sin[\omega(t-2\tau)], \quad (58)$$

where $\omega=\frac{1}{2}(\omega_a+\omega_b)$, as usual. Phase shifts between these signals have been omitted.

Ordinarily a distribution of applied magnetic field values exists over the volume containing the sample. Hence, Eqs. (56) through (58) must be integrated over the distribution of ω values. The result of this is that the observed rectified envelopes have their maximum values at $t=\tau$, $t=0$, and $t=2\tau$, respectively. This distribution also causes the free precession following the first pulse to be damped so as to have its maximum at $t=0$. The free decay envelopes in Fig. 1 were calculated for a uniform applied field. The different types of precession do not mutually interfere when any of the following conditions are met: (1) the distribution of ω causes the free precession following the first pulse to be damped out at $t=\tau$, (2) the applied pulses obey the conditions $\theta_1=\frac{1}{2}\pi$ and $\theta_2=\pi$, or (3) the pulses obey the conditions $\theta_1=\pi$, $\theta_2=\frac{1}{2}\pi$. The amplitudes of the observed envelopes at their maximum values are independent of the width of the distribution of ω values.

The refocusing action of the second pulse causes the expected result that at $t=2\tau$, the time of maximum of the echo amplitude, $U_E=0$ so that the echo amplitude is given by Eq. (54). The usual application of the echo involves measurement of the echo amplitude at time 2τ as a function of 2τ. By setting $\tau=\frac{1}{2}t$, Eq. (54) becomes

$$V_E=-\tfrac{1}{2}M_0\sin\theta_1(1-\cos\theta_2)\exp(-\phi_2 t)\times\{j\exp(-ct)+2f\sin(dt)-2(g+j)\cos(dt)+(2g+j-1)\exp(ct)\}. \quad (59)$$

This equation shows that the echo envelope would not be merely a sum of two exponential decay functions but would be modulated in addition. This results from the fact that the nucleus alternately experiences two different precession frequencies. Hence, this bears some qualitative similarity to the echo-envelope modulation produced by the mixing of states by indirect spin-spin coupling[4] in magnetic resonance or by the Zeeman effect in nuclear electric quadrupole resonance.[10] However, this situation differs in that the modulation results from the random nuclear transfers while such motions cause indirect spin-spin coupling modulations to decrease in amplitude.[4] The special case plotted in Fig. 2 shows echo envelopes which exhibit a monotonic decrease of amplitude with increase of time. The transfer is simultaneously a creator and destroyer of modulation. For zero transfer rate, $f=0$ and $(g+j)=0$; the magnitudes of these quantities increase with increasing transfer rate, become greatest when $\frac{1}{2}(C_a+C_b)\approx|(\omega_a-\omega_b)|/\pi$, and decrease to very low values at very large transfer rates, approaching zero as the rates approach infinity. For small transfer rates, an increase of rate increases the damping rate represented by c and ϕ_2; this tends to counteract the effects of the simultaneous increase of the magnitudes of f and $(g+j)$.

Consider the simple case used for illustrating the theoretical free decay, i.e., $P_a=P_b$, $C_a=C_b$, $T_{2a}=T_{2b}$, and $|(\omega_a-\omega_b)|=20/T_{2b}$. Figure 2 shows a family of curves for different reduced transfer rates as calculated by use of Eq. (59). For small rates, the curves show little or no modulation and have the exponential decay like the free decay, $\exp(-t/T_{2b})$. For greater rates, modulation becomes appreciable and the curve becomes increasingly damped. As for the free decay, the damping is strongest when $C_b\approx|(\omega_a-\omega_b)|/\pi$. As before, with increase of C_b, the damping decreases; and when $C_b^2\gg(\omega_a-\omega_b)^2$, the damping is given by Eq. (39). The damping is described by Eq. (44) for the more general case for which (44) was derived.

However, the damping is of a different character, compared to that for the free decay, when C_b is of the same order of magnitude as $|(\omega_a-\omega_b)|$. This can be shown quantitatively in a convenient mathematical form when Eqs. (18) and (19) are not solutions of Eqs. (10) and (11). For Eqs. (12) and (13) which describe M_z, this situation arises only for the trivial case of no transfers. But nontrivial cases arise for the U

[10] M. Bloom, E. L. Hahn, and B. Herzog, Phys. Rev. **97**, 1699 (1955).

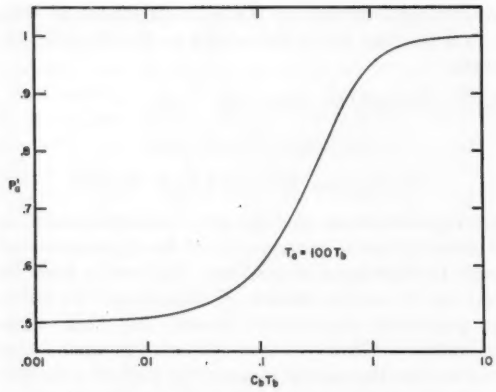

FIG. 3. Theoretical values of the apparent fractional population of the long relaxation time state as a function of reduced transfer rate when $P_a=P_b$, $C_a=C_b$, $T_a=100T_b$, and $\omega_a=\omega_b$.

and V magnetizations when the conditions $(1/T_{2a}-1/T_{2b}+C_a-C_b)=0$ and $(\omega_a-\omega_b)^2=4C_aC_b$ occur simultaneously.

Application of boundary conditions to Eqs. (22) and (23) yields the following U and V components. The magnetization following a single rf pulse is then given by the relations

$$U'=-\tfrac{1}{2}M_0\sin\theta_1(P_b-P_a)(\omega_a-\omega_b)t\exp(-\phi_2 t) \quad (60)$$

$$V'=-M_0\sin\theta_1[1+\tfrac{1}{2}(P_b-P_a)(1/T_{2a}-1/T_{2b})t + \tfrac{1}{2}(C_a+C_b)t]\exp(-\phi_2 t). \quad (61)$$

The components for the spin-echo are

$$U'_E=\tfrac{1}{4}M_0\sin\theta_1(1-\cos\theta_2)(P_b-P_a)(\omega_a-\omega_b) \times(t-2\tau)\exp(\phi_2 t) \quad (62)$$

$$V'_E=\tfrac{1}{2}M_0\sin\theta_1(1-\cos\theta_2)[1+\tfrac{1}{2}(P_b-P_a) \times(1/T_{2a}-1/T_{2b})t+\tfrac{1}{2}(C_b+C_a)t + \tfrac{1}{2}(\omega_a-\omega_b)^2\tau(t-\tau)]\exp(-\phi_2 t). \quad (63)$$

The transformations to laboratory coordinates are Eqs. (36) and (58).

Equations (60) through (63) do not yield any unique physical results. These equations apply when $c=d=0$, the situation when the more general results fail. The same results can be found by taking in proper fashion the limits of the more general results for $c=d=0$. This is accomplished by letting $d=0$ and $c\ll 1$, expanding the exponential functions as series, and retaining in the final results only those terms not containing c.

Comparison of Eqs. (61) and (63) when $P_a=P_b$, $C_a=C_b$, and $T_{2a}=T_{2b}$ illustrates the different damping character for the echo envelope compared to that for the free decay. The echo envelope for $\tau=\frac{1}{2}t$ is less strongly damped than the free decay because it contains the additional term $(\omega_a-\omega_b)^2t^2/8$ in this special case. This is illustrated by the theoretical curves: Curve E of Fig. 2 lies above curve C of Fig. 1. Hence, for "intermediate" transfer rates, the second pulse has a refocussing effect or reduction of phase dispersion, even in the absence of a distribution of applied magnetic field values. This phenomenon is qualitatively similar to that in diffusion of molecules into different values of magnetic field.[11] Aside from a different statistical problem, the main difference is that here the precession frequency is restricted to two particular values; while for molecular diffusion, a range of values is available to each nucleus.

IV. EFFECTS OF NUCLEAR TRANSFER RATE ON APPARENT RELAXATION TIMES[12]

There is no effect from a difference $(\omega_a-\omega_b)$ of resonance frequencies of the state on the observed (apparent) longitudinal relaxation times. An examination of Eqs. (47) through (50) shows that when $T_{1a}=T_{1b}$ the longitudinal relaxation curve is a simple exponential with a time constant T_{1a}. This behavior is independent of transfer rates. However, even when $T_{2a}=T_{2b}$, the transverse relaxation curve depends on both the transfer rate and frequency separation. These damping effects are most pronounced when the transfer rate is of the same order of magnitude as $|(\omega_a-$

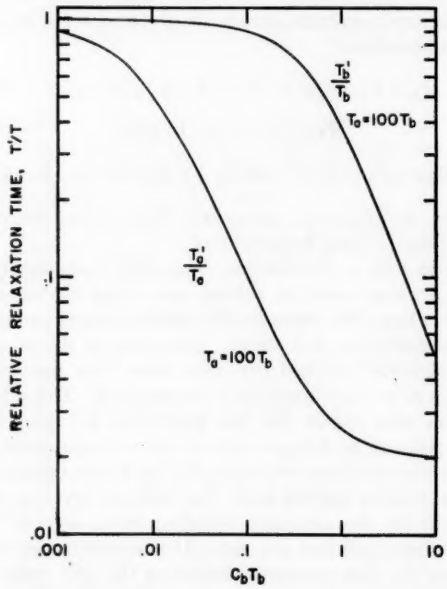

FIG. 4. Theoretical shortening of apparent relaxation times versus reduced transfer rate when $P_a=P_b$, $C_a=C_b$, $T_a=100T_b$, and $\omega_a=\omega_b$.

[11] H. Y. Carr and E. M. Purcell, Phys. Rev. **94**, 630 (1954).

[12] In these discussions it is assumed that T_2 (observed) is determined by measuring the echo amplitude at time 2τ as a function of 2τ, and that T_1 (observed) is determined by measuring the difference between the initial free precession amplitudes which follow the pulses in 90°–90° pulse sequences as a function of τ.

$\omega_b)|/\pi$; this behavior is observable when $|(\omega_a-\omega_b)|T_{2a}\gtrsim 2\pi$. It is of interest to note that Eqs. (12) and (13) also describe the spin-lattice relaxation when nonequivalent nuclei exchange energy by mutual spin flip-flops[13,14] if C_a and C_b are changed to flip-flop rates.[15] Hence, nuclear transfer and spin flip-flop processes have the same effect on observed T_1 values. This is not the case for T_2 because a spin flip-flop dephases the nuclei.

A. Apparent Relaxation When $\omega_a=\omega_b$

When $T_{1a}\neq T_{1b}$ and $T_{2a}\neq T_{2b}$ with the added condition $\omega_a=\omega_b$, both T_1 and T_2 relaxation curves are sums of two exponential functions whose coefficients and time constants are the apparent state populations and relaxation times, respectively. Both curves are described by Eq. (47) in the form

$$F(t)=P_a'\exp(-t/T_a')+P_b'\exp(-t/T_b'), \qquad (64)$$

where T' and P' signify the apparent relaxation times and population fractions, respectively. This reduced expression (64) is, of course, equivalent to that one obtained previously by stochastic processes.[5,16] Nevertheless, it is very informative to review a few pertinent facts described by Eq. (64) in order to illustrate later the damping effects on relaxation by the added condition of $(\omega_a-\omega_b)\neq 0$. For the illustrative discussions to follow, it is assumed that $P_a=P_b$ and $T_a=100T_b$.

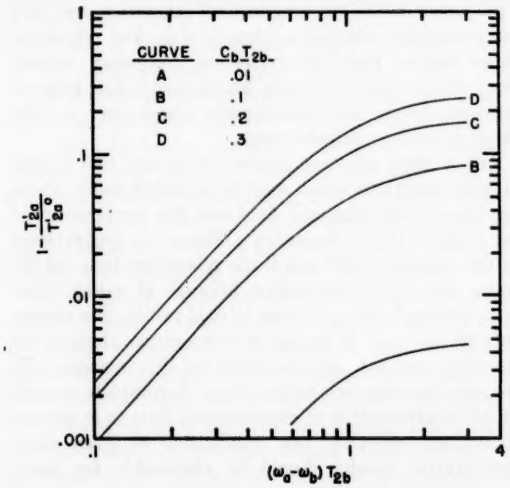

FIG. 5. Theoretical fractional decrease of the apparent long transverse relaxation time versus reduced frequency separation for several values of reduced transfer rate when $P_a=P_b$, $C_a=C_b$, and $T_{2a}=100T_{2b}$.

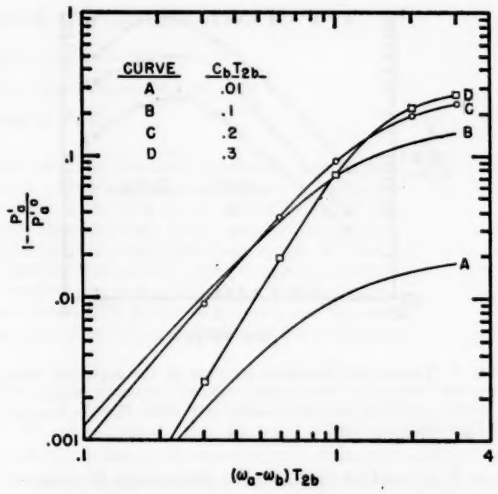

FIG. 6. Theoretical fractional decrease of the apparent fractional population of the long transverse relaxation time state versus reduced frequency separation for several values of reduced transfer rate when $P_a=P_b$, $C_a=C_b$, and $T_{2a}=100T_{2b}$.

Figure 3 shows a theoretical plot of P_a', the apparent population of the long relaxation time state, as a function of C_bT_b, the reduced transfer rate which is defined here as the transfer rate relative to the greater relaxation rate. When $C_bT_b=3$, P_a' is essentially unity; and since $P_a'+P_b'=1$, P_b' is essentially zero. A curve for infinite T_a (not shown) differs very little from the one for $T_a=100T_b$.[16] In experimental practice, the relaxation curve (spin echo or free decay amplitudes vs τ) cannot be resolved into two components if $C_bT_b\gtrsim 2$. For $C_bT_b=0.2$, two component relaxation resolution is possible even though the transfer rate C_a is 20 times its relaxation rate, $1/T_a$. Hence, two-state relaxation resolution is generally possible unless the shorter relaxation time site b has $C_b\gtrsim 1/T_b$.

Figure 4 shows a plot of relative relaxation times T'/T as functions of C_bT_b. The apparent relaxation times T' for both states decrease with an increase of nuclear transfer rate. The populations P' also change such that the over-all relaxation remains unchanged, i.e.,

$$P_a'/T_a'+P_b'/T_b'=\text{a constant}=P_a/T_a+P_b/T_b. \qquad (65)$$

For large C_bT_b values, $1/T_b'$ bedomes very large while $1/T_a'\rightarrow P_a/T_a+P_b/T_b$. Simultaneously, P_b' becomes small as $P_a'\rightarrow 1$. In general, for $C_bT_b\ll 1$ and $T_a/T_b\gg 1$, the apparent relaxation times are given by

$$1/T_a'\approx 1/T_a+C_a \qquad (66)$$

$$1/T_b'\approx 1/T_b+C_b. \qquad (67)$$

Within the range of two-component resolution for either

[13] D. E. Woessner and H. S. Gutowsky, J. Chem. Phys. **29**, 804 (1958).
[14] R. T. Schumacher, Phys. Rev. **112**, 837 (1958).
[15] The values of the mutual flip-flop rates depend, in general, on the value of $(\omega_a-\omega_b)$, but this does not affect the forms of the mathematical relations (12) and (13).
[16] D. E. Woessner and J. R. Zimmerman, J. Phys. Chem. (to be published).

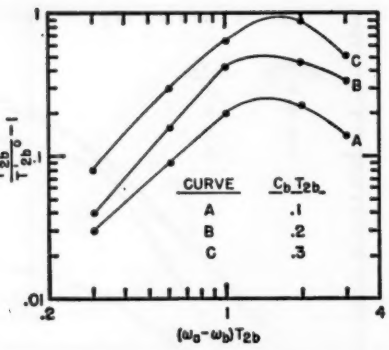

FIG. 7. Theoretical fractional increase of the apparent short transverse relaxation time versus reduced frequency separation for several values of reduced transfer rate when $P_a=P_b$, $C_a=C_b$, and $T_{2a}=100T_{2b}$.

T_1 or T_2 relaxation systems, the percentage decrease of T_a' with increase of C_bT_b is much greater than that of T_b'. From inspection of Figs. 3 and 4 with $T_a \gg T_b$, the observable T_a' may be many times smaller than its *true* value while T_b' may be near its *true* value; yet the observable population fractions, P_a' and P_b' may be approximately equal to their respective *true* values. The situation for $T_a=10T_b$ is qualitatively the same as presented above.

Suppose the T_1 values for the sites are much greater than the respective T_2 values. It is then possible to have simultaneously $C_bT_{1b} \gg 1$ for longitudinal relaxation and $C_bT_{2b} \ll 1$ for transverse relaxation. Then single-component longitudinal and two-component transverse relaxation behavior can be observed.[5,17] A different physical process can also yield this kind of observation.[18]

B. Apparent Transverse Relaxation When $\omega_a \neq \omega_b$

Transverse relaxation behavior under the condition $\omega_a \neq \omega_b$ is more complicated to discuss than the one described previously because of the additional frequency separation variable. The damping for $|(\omega_a-\omega_b)| \gg 1/T_2$ was discussed previously in Part III(B). It would be difficult to make general statements regarding smaller frequency separations. However, considerations of the effect of frequency separation on apparent relaxation times and populations compared to the values for no frequency difference is worthwhile.

For $T_{2a}=100T_{2b}$ and $P_a=P_b$ and a range of values of frequency separation, transverse relaxation curves have been computed from equation (59) for t values from $t=0$ to $t=20T_{2b}$ for several values of C_bT_{2b}. From $t=10T_{2b}$ to $20T_{2b}$, the semilogarithmic relaxation curve plot of amplitude versus time is a straight line; from the values at $t=15T_{2b}$ and $20T_{2b}$, the value of T_{2a}' was calculated from a simple exponential function containing these points: the value of P_a' is the coefficient of the exponential. These values (T_{2a}', P_a') compared to those ($T_{2a}'^0$, $P_a'^0$) for zero frequency separation are presented in Figs. 5 and 6, respectively, as functions of reduced frequency separation, $(\omega_a-\omega_b)T_{2b}$. The effect of frequency separation in both instances is to decrease T_{2a}' and P_a'. Values of the simple exponential function (described above) for small values of t were subtracted from the computed [Eq. (59)] relaxation curves; the logarithms of these differences were plotted vs time. For the larger values of frequency separation, the plots deviated seriously from straight lines. Straight lines which satisfy a reasonable fit through these points were drawn in the same fashion experimental curves would be treated. From the slopes, values of T_{2b}' were calculated; these values compared to $T_{2b}'^0$ are plotted as a function of reduced frequency separation in Fig. 7. The values of T_{2b}' are increased by frequency separation and pass through maxima

These specific cases illustrate qualitatively the damping effects on transverse relaxation. The most readily observable feature is the nonlinearity at small values of time for the semilogarithmic relaxation plots when the frequency separation is large (see Fig. 2). This never occurs for longitudinal relaxation and only for transverse relaxation when $\omega_a \neq \omega_b$. For relaxation times shorter than the reciprocal frequency separation, this nonlinearity may be obscured. For long relaxation times, such phenomena occur over a wide range of nuclear transfer rates.

For a given physical system there are two experimental conditions which may be adjusted easily. These are the applied magnetic field and the temperature of the sample. If the frequency difference is proportional to the magnetic field and if the relaxation times of the states are field independent because of rapid intrastate motion,[2] then a change in field results in a change only of $(\omega_a-\omega_b)$. A change of temperature changes the transfer rates but, unfortunately for this instance, also changes the state relaxation times. A complete quantitative interpretation of experimental data is in general exceedingly difficult, but qualitative or even semiquantitative results should be obtainable for many experimental situations.

ACKNOWLEDGMENTS

The author is very grateful to Dr. J. R. Zimmerman for his continued interest during the progress of this work and his many helpful comments in preparing the manuscript. He also wishes to thank Dr. D. Weiser for helpful discussions concerning some of the mathematical procedures.

[17] J. R. Zimmerman and J. A. Lasater, J. Phys. Chem. **62**, 1157 (1958).
[18] D. W. McCall, D. C. Douglass, and E. W. Anderson, J. Chem. Phys. **30**, 1272 (1959).

Trapped Radicals in Irradiated *n*-Propanol at 77°K

R. S. ALGER, T. H. ANDERSON, AND L. A. WEBB

U. S. Naval Radiological Defense Laboratory, San Francisco 24, California

(Received December 27, 1960)

The free radicals formed in solid *n*-propanol by radiolysis were examined by electron paramagnetic resonance (EPR) techniques and compared to radicals in photolyzed propanol-hydrogen peroxide mixtures. Identification of the radicals is based on modifications in the EPR hfs introduced by substituting deuterium for hydrogen at selected positions in the molecules. Radiolysis leads to radical formation by removing a hydrogen atom from the α carbon while photolysis apparently favors hydrogen abstraction from the β carbons. Mass spectrographic analysis of the gas liberated during irradiation gave corroborative evidence regarding the hydrogen atoms; however, the analysis also showed that some hydrogen escaped from other than the α and β carbon positions. The experimental EPR hf spectra are compared to a series of constructed spectra obtained by summing Gaussian absorption curves according to the interactions indicated by the proposed models of the radicals.

INTRODUCTION

ELECTRON paramagnetic resonance (EPR) has become one of the more powerful tools in the study of organic radicals. Scores of published spectra illustrate the use of this technique particularly for the detection and study of radicals generated by ionizing radiations.[1–5] In principle these spectra can divulge the immediate environment of the unpaired electron through the hyperfine structure produced by interacting magnetic nuclei. Unfortunately, theoretical and experimental limitations have restricted reliable identification to a few of the simplest radicals. The objectives of this study were first, to move the radical formed by irradiation of normal propanol toward this select group of "the identified species" and second, to clarify some of the similarities and differences between this radical and the radical generated by uv illumination of propanol containing hydrogen peroxide.[4,5] Interest in propanol arises primarily from past evidence indicating that the unpaired electron interacts with only part of the carbon atoms in the chain. Therefore, this is the simplest alcohol molecule in which the EPR hfs can be used to identify the interacting portion of the molecule.

In interpreting the spectra reported here, the unpaired electrons are assumed to interact equally with all of the hydrogen nuclei attached to a particular carbon atom. The spectra for methanol and ethanol, as well as other similar compounds, support this assumption leading to $n+1$ lines with a binomial relationship between amplitudes resulting from n equally interacting hydrogen nuclei. Such equivalence is not necessarily universal as has been demonstrated in β-succinic acid.[6]

In this study, the primary identification of the radicals is based on the method of isotope substitution using deuterium at selected positions in the molecules. Implicit in this labeling technique is the assumption that deuterium can be substituted for hydrogen without altering the radicals to be produced. Past evidence has demonstrated that, unfortunately, hydrogen and deuterium are not always equivalent in a molecule. In a study of the radiolysis of ethanol, Burr reported that in some positions, hydrogen atoms were abstracted more easily than deuterium atoms[7]; e.g., he reported a ration of $K_H/K_D=1.3$ where K=rate of C—H bond cleavage at room temperature. Obviously the rigor of this labeling method is compromised by such uncertainty of the hydrogen-deuterium equivalence in the particular reactions of interest.

Since much of the evidence regarding the identity of the radicals in propanol is of a circumstantial nature, the interpretation of experimental results acquires additional significance when the information for other members of the alcohol series is also considered. To assist in this comparison, the published characteristics of radicals in methanol and ethanol have been collected in Table I together with a summary of our results for propanol. Accordingly, the radical responsible for the five-line EPR spectrum in x-rayed propanol becomes the primary concern of this paper.

PROCEDURE

In general the approach centered on EPR measurements of the irradiation products in propanol samples labeled with deuterium. Propanols deuterated 98% in the labeled position were used both as received and in some cases after purification in a preparative vapor-phase chromatography column. In the cases examined purification did not alter the hf structure detectably.

The convention indicated in Table II was adopted in an attempt to minimize the confusion inherent in describing the effects of administering a variety of treat-

[1] C. P. Poole, Jr., and R. S. Anderson, ASTIA Document No. AD214504.
[2] B. Smaller and M. S. Matheson, J. Chem. Phys. **28**, 1169 (1958).
[3] W. Gordy, W. Ard, and H. Shields, Proc. Natl. Acad. Sci. U. S. **41**, 983 (1955).
[4] M. Fujimoto and D. J. E. Ingram, Trans. Faraday Soc. **54**, 1304 (1958).
[5] R. S. Alger, T. H. Anderson, and L. A. Webb, J. Chem. Phys. **30**, 695 (1959).
[6] C. Heller and H. M. McConnell, J. Chem. Phys. **32**, 1535 (1960).
[7] J. G. Burr, J. Chem. Phys. **61**, 1477 (1957).

TABLE I. Characteristics of radicals in alcohols at 77°K.

Property	Compound and method of generating radicals: Methanol x rays	Methanol uv	Ethanol x rays	Ethanol uv	Propanol x rays	Propanol uv
Number of species detected	2		2		2	probably 2
Number of lines						
species (a)	1		1		1	
species (b)	3	3	5	perhaps 6	5	6
Intensity ratios species (b)	1:2:1	1:2:1	1:4:6:4:1		1:2:2:2:1	
Suggested radical	CH_2OH	CH_2OH	CH_3CHOH		CH_3CH_2CHOH	CH_3CHCH_2OH
Thermal stability of species (b) Change in number of lines in boiling CH_4	3→0		5→0		5→0	approaches 1
Optical stability of species (a) bleaches with 5460 illumination	yes		yes		yes	
Change under illumination with short uv	3→2		center line grows		center line grows	center line accentuated

ments to eight slightly different types of samples. The Roman numeral indicating the position of the labeled carbon has been used throughout to designate the compound. A subscript (p) shows that the alcohol contained 5% hydrogen peroxide. In addition, the term "irradiation" has been limited to bombardment with x rays or electrons while "illumination" designates the use of visible or ultraviolet photons. "Short uv" means the region from 2000 to 2800 A, while uv wavelengths longer than 2800 A are called "long uv."

Two sample arrangements used for EPR measurements were: (a) solid alcohol balls about $\frac{1}{8}$ in. in diam and (b) sealed 4-mm-OD Pyrex vials containing purified alcohol. Balls formed by placing a drop of alcohol on the surface of liquid nitrogen were maintained at 77°K during exposure to 50-kv peak x rays and subsequent EPR measurement in a 9.5-kMc rectangular cavity.[5] After degassing by repeated freezing and thawing on a vacuum line, the purified alcohol was sealed in vials and exposed at 4°K to 2-Mv peak x rays from the Van de Graaff generator at a dose rate of about 5 megarep/hr. The liquid-helium Dewar system and cavity arrangement was similar to that described by Wall.[8]

Other propanol samples, admixed with 5% H_2O_2, were photolyzed with uv light from a filtered AH6 mercury-vapor lamp to obtain radicals by abstraction in the manner described by Fujimoto and Ingram.[4] Since the type of radicals formed depends on photon energy, the uv light was filtered to pass either short uv or long uv.

Secondary evidence was obtained from mass spectrographic analysis[9] of the off-gases. To minimize the gas contribution from reacting radicals, the analysis included only the gases escaping from solid samples at 77°K. Samples of the various deuterated alcohols were degassed and sealed in $1\frac{1}{2}$-cc vials. Two-mev electrons shot into the alcohol samples through a 0.020 in. thick Pyrex window produced about 0.2 cc of gas at standard temperature and pressure with total exposures of 5.4 to 6 μa min.

[8] L. A. Wall, D. W. Brown, and R. E. Florin, J. Phys. Chem. **63**, 1762 (1959).

[9] Mass Spectrographic analysis performed at Stanford Research Institute.

RESULTS

X-Ray Irradiation

Irradiated propanol shows optical and EPR characteristics typical of the alcohols already described. After exposure (IV) is colored purple and contains at least two paramagnetic species at 77°K, e.g., see the solid line in Fig. 1. Bleaching the color centers with light from the mercury green line (5460 A) reduces the central region of the hf structure as indicated by the dashed line. Subtracting the spectrum of the colorless radicals from the initial curves leaves a broad central peak as shown by the dotted line. During the bleaching process the side bands of the five-line spectrum grow slightly in a manner analogous to methanol and ethanol. However, the five lines do not match the intensity ratios of ethanol. The EPR spectrum follows the general pattern of the other alcohols reported, with a splitting between the lines of about 18 gauss and a g essentially equal to that of diphenylpicrylhydrazyl.

TABLE II. Designation of labeled samples.

$CH_3CH_2CD_2OH$ = (I)	$CH_3CH_2CD_2OH$ + 5% H_2O_2 = (I_p)
$CH_3CD_2CH_2OH$ = (II)	$CH_3CD_2CH_2OH$ + 5% H_2O_2 = (II_p)
$CD_3CH_2CH_2OH$ = (III)	$CD_3CH_2CH_2OH$ + 5% H_2O_2 = (III_p)
$CH_3CH_2CH_2OH$ = (IV)	$CH_3CH_2CH_2OH$ + 5% H_2O_2 = (IV_p)

The influence of the deuterium is readily apparent in the hf structure of irradiated (II) and (I), given in Fig. 2. When the deuterium is on C_β (II) the spectrum is ill resolved although the characteristics of two close-spaced lines are discernible. If the deuterium atoms are attached to C_α (I), a spectrum consisting of five main absorption peaks develops; however, the splitting, amplitude, and line shapes do not match the hf structure of the ordinary propanol (IV), shown at the top of Fig. 2. The over-all splitting of 100 gauss in combination with the very broad central peak suggests the presence of several species. Substituting the deuterium on the C_γ (III) leads to a hyperfine structure that matches ordinary propanol (IV) in all respects, indicating no detectable interaction between the unpaired electron and the deuterium atoms in this position. Other characteristics of these radicals are their thermal and optical stability. When heated to 111°K by submersion in boiling methane, all of the radicals in Fig. 2 disappeared promptly. When the radicals in (IV), (II), and (III) were illuminated with short uv, the five-line spectrum was reduced and a single center line developed, e.g., see the dotted curves of Fig. 2. Propanol (I) was not illuminated with the uv band.

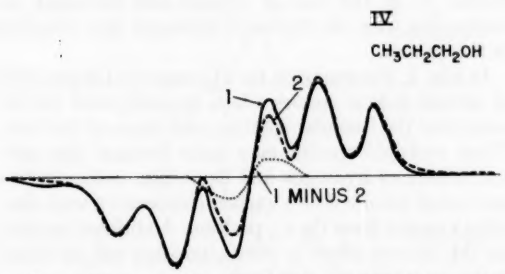

FIG. 1. Effect of 5460-A illumination on EPR hf structure of x rayed (IV). (1, after x ray and storage overnight; 2, after bleaching with 5460 A light.)

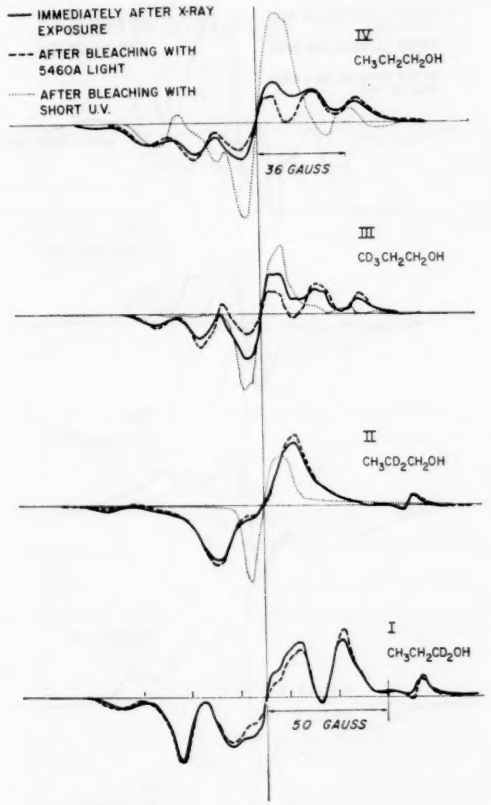

FIG. 2. EPR spectra of irradiated propanol labeled with deuterium.

Samples of (IV) and (I) sealed in Pyrex vials were exposed to x rays at both liquid-nitrogen and liquid-helium temperatures. Essentially the same hf structure was obtained at both temperatures, i.e., the spectra of Fig. 2. At 4°K a search for the hydrogen 502-gauss doublet and the 152-gauss triplet of deuterium indicated that hydrogen and deuterium atoms were not trapped in concentrations comparable to the radicals in Fig. 2.

Mass spectrographic analysis of the gas escaping from the various propanols gave the concentrations of H_2, HD, and D_2 listed in Table III. Apparently the loss of deuterium from C_α is favored over the other carbon positions.

Ultraviolet Illumination

The hf structure for the radicals produced by long uv activation of the various propanols containing hydrogen peroxide was generally poorly resolved, and the structure differed significantly from the spectra produced by x rays. When Fig. 3 containing the spectra produced by uv excitation is compared to Fig. 2, it is apparent that the uv species generally have a broader total width and a larger number of absorption bands. Only (I) and (I_p) exhibit compatible spectra. If the spectrum for (IV_p) is compared to the propanol curves (as in the work cited in reference 4), the structures appear to coincide somewhere between the curves at 90° and 110°K. The 90° curve is indicated in Fig. 3.

TABLE III. Hydrogen and deuterium content of gas escaping during irradiation from solid propanol labeled with deuterium.

	Relative volume percent			Relative total percent	
Compound	H_2	HD	D_2	H_2	D_2
(I)	57.8	38.8	3.9	77	23
	60	40	...		
(II)	78.4	20.2	1.4	90	10
	80.3	18.5	1.2		
(III)	85.9	13.0	1.1	92	8
	86	13	1		

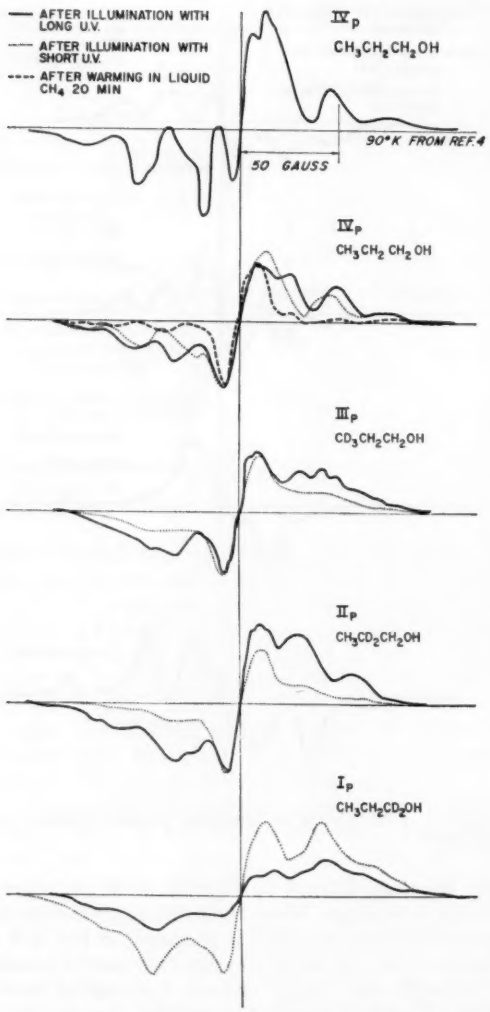

FIG. 3. EPR spectra of labeled propanols resulting from uv photolysis of 5% peroxide.

Although the curves display similar hf structures, the splittings between bands, as can be seen from the comparison scales, are larger for the 90° curve, and the central peak is more pronounced. Warming the radicals produced by the long uv to 111°K in boiling methane accentuated the central peak (as described in the work cited in reference 4) and reduced the side bands as indicated in Fig. 3. Both short uv illumination and heat accentuated the center line.

DISCUSSION AND CONCLUSIONS

X-Ray Irradiation

Under x-ray bombardment, normal propanol develops at least two paramagnetic species. As in the case of methanol and ethanol, the identity of the photosensitive radical responsible for the single EPR absorption line remains unknown.[10] The remaining comments are restricted to the more stable radicals which do not bleach under visible light and which exhibit an hf structure of five lines in ordinary propanol (IV).

According to the spectra in Fig. 2, the presence of deuterium was detected only in the radicals generated in (I) and (II). Within the validity of the following assumption, the spectra, supported by the admittedly meager mass spectrometer data, argue that the unpaired electron belongs to C_α. (a) In (III) the nonequivalence of deuterium and hydrogen did not affect the radical produced; (b) an unpaired electron on C_β could interact detectably with hydrogen nuclei on both C_α and C_β; and (c) the radical was formed by removing a hydrogen from the molecule. The suggested radical then is

$$CH_3\,\boxed{CH_2CH}\,OH$$

where only the enclosed portion of the molecule is detected. As in the case of ethanol and methanol, no interaction with the hydroxyl hydrogen was observed in the quintet.

In Fig. 2, the spectrum for (I) suggests the presence of several radical species whose superimposed hfs accounts for the irregular splitting and shape of the lines. These multiple species may arise because the nonequivalence of hydrogen and deuterium makes hydrogen escape from a β or γ carbon competitive with deuterium escape from the C_α position. Additional support for this isotope effect in the C_α position will be found in the uv results which follow.

uv Illumination

It is apparent that the electrons unpaired through the chemical attack of uv-excited hydrogen peroxide in propanol do not encounter the same environment as electrons unpaired by x rays. Both the thermal stability of the radicals and their hf structure support this difference. Although the poorly resolved spectra prevent close analysis, there appears to be some divergence between the results with deuterium substitution and our extrapolation from the results obtained in the work cited in reference 4. These differences may arise in part from any nonequivalence of hydrogen and deuterium, and partly from the dependence of the radical species on wavelength of exciting uv. Fujimoto and Ingram concluded that the peroxide abstracts hydrogen preferentially from the C_α or C_β position and suggests CH_3CHCH_2OH as the radical responsible for their published hf structure. In their analysis, the unpaired electron has the strongest interaction with the hydrogens on C_γ. Under these circumstances the substitution of deuterium on C_γ should alter considerably the hf structure observed. The spectra for (III_p) and (IV_p) in Fig. 3 show a difference in the resolved side bands

[10] H. Zeldes and R. J. Livingston, J. Chem. Phys. **30,** 40 (1959).

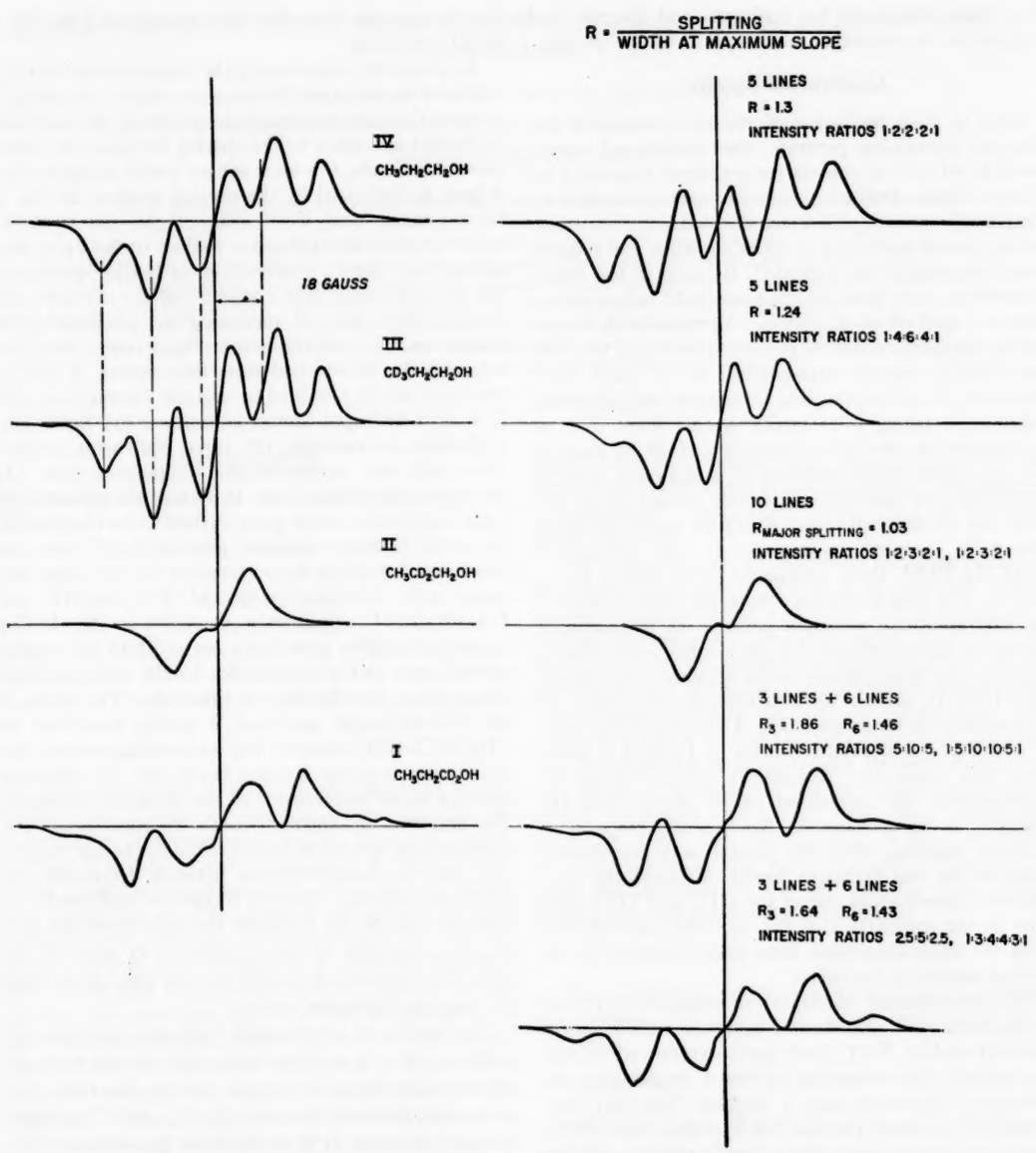

FIG. 4. Comparison of constructed Gaussian curves (right) to experimental determinations (left).

indicative of the smearing effect of deuterium. If the interaction between the unpaired electron and C_β were unresolvably small, as indicated by the interaction constants in the work cited in reference 4, (II_p) should exhibit the same hf structure as (IV_p) unless the deuterium in this position influences the chemical abstraction. The hf structures for (IV_p) and (II_p) in Fig. 3 show considerable resemblance in marked contrast to the large difference between (IV) and (II) in Fig. 2. Finally, if the peroxide abstracts hydrogen primarily from C_β a similarity should exist between the six-line portion of the spectrum produced in (I) by x rays and in (I_p) by long uv illumination if the structure CH_3CHCD_2OH is responsible for the sextet. Although poorly resolved, the splitting, total width, and general shape of the hyperfine structure of (I_p) in Fig. 3 bears a strong resemblance to the corresponding spectrum in Fig. 2. Although positive identification of the radicals in propanol-hydrogen peroxide mixtures suffers from poor resolution, all of the above predictions based on

the model suggested by Fujimoto and Ingram find support in the deuterium modifications of the spectra.

Constructed Spectra

Due to poor resolution of the hf structure in the samples containing peroxide, the constructed curves were fitted only to spectra from radicals generated by x rays. Figure 4 shows a series of curves generated by graphically summing Gaussian derivative curves whose width at half-maximum to splitting ratios and relative peak amplitudes are indicated. Because of the broad linewidths, very weak interactions could escape detection and such effects may in part be responsible for the better resolution obtained in the calculated curves. The two five-line spectra corresponding to (IV) and (III) represent all of the possible interaction arrangements capable of giving five equally spaced lines. The n-hydrogens can produce a maximum of 2^n hf lines in the case of no equal couplings or a minimum of $n+1$ lines when all couplings are equal; consequently, five lines can be obtained either with four equally or three unequally coupled hydrogens. If the radical is CD_3CH_2CHOH, three hydrogens are available on C_α and C_β. The four-hydrogen case would have to involve the OH to obtain sufficient protons, an arrangement foreign to the experience with the alcohol series. Consequently, the three-proton model appears most attractive. If the C_α protons interact twice as strongly as the C_β protons, the structure in Fig. 4 with intensity ratios of 1:2:2:2:1 is obtained. Ratios of 1:4:6:4:1 result from four equivalent protons. A comparison of the experimental and calculated curves shows that the behavior at the extreme side bands favors the unsymmetrical coupling, while the central peak corresponds more to the four-hydrogen model. Although our best resolved experimental curves for (III) and (IV) were used in the comparison of Fig. 4, some contributions from the single absorption band may be adding to the central portion of the curves.

The experimental spectrum for irradiated (II) can be matched with considerable accuracy with a poorly resolved doublet. If a C_α hydrogen was removed to form the radical, the remaining hydrogen would split the resonance absorption into a doublet. The two deuteriums on C_β would produce five hyperfine lines which, due to the weaker interaction at the C_β position and the smaller magnetic moment of deuterium, would have a splitting of about $2\frac{1}{4}$ gauss. The curve in Fig. 4 was constructed from 10 Gaussian derivatives with intensity ratios of 1:2:3:2:1, and 1:2:3:2:1 with a splitting between the centers of the quintets of $14\frac{3}{4}$ gauss. In view of the large number of lines available for the construction, the close resemblance in Fig. 4 is not surprising.

As previously mentioned, the irregularities near the center of the propanol (I) spectrum suggest the presence of more than one paramagnetic species. If the spectrum is divided according to the spacing between the outermost side bands, the total spread would accommodate 6 lines, as indicated by the vertical markers in Fig. 2. On the other hand, if (I) followed the pattern of the other alcohols and formed a radical by losing a deuterium from the C_α position, the—CH_2CD—portion of the molecule would give a triplet due to the two C_β hydrogens, with a general smearing of the spectrum by the deuterium. The construction in Fig. 4 results from the superposition of six- and three-line spectra. A six-line spectrum can be obtained by suitable interactions with 3, 4, or 5 hydrogen atoms, as follows: (1) three nonequivalent interactions; (2) three equivalent interactions and one nonequivalent interaction; and (3) five equivalent interactions. In view of the evidence for equal interactions on a given carbon atom observed in the other propanol samples, alternative (1) was not constructed. Spectra were generated for the other two cases with intensity ratios of 1:3:4:4:3:1 and 1:5:10:10:5:1, respectively, as shown in Fig. 4. The second alternative provides a better fit to the experimental curve at the extreme side bands, while the third arrangement matches best in the center. The origin of the four-hydrogen spectrum is easily visualized as CH_3CHCD_2OH, whereas five equivalent protons are not readily available without the benefit of a chemical reaction or an involvement of the hydroxyl hydrogen. The apparent agreement between the constructed and experimental spectrum lends credibility to the suggestion that the nonequivalence between deuterium and hydrogen influences radical formation sufficiently to shift the site of the unpaired electrons from the preferred C_α position to the C_β position in some of the molecules. Additional support for this view stems from the mass spectrometer results.

The release of considerable hydrogen gas from all samples indicates that no one position in the molecule is responsible for all of the gas. In fact, the total deuterium gas liberated from the C_α, C_β, and C_γ positions accounts for only 41% of the total gas released. The only unmarked position available for supplying the hydrogen gas is the OH termination which in Burr's measurements on ethanol was the prominent position for hydrogen abstraction following the initial radical production. Burr found that in ethanol approximately 82% of the abstracted gas came from this OH position.[7]

Crystal Structure of Vanadyl Bisacetylacetonate. Geometry of Vanadium in Fivefold Coordination*

RICHARD P. DODGE, DAVID H. TEMPLETON, AND ALLAN ZALKIN

Department of Chemistry and Lawrence Radiation Laboratory, University of California, Berkeley, California

(Received November 28, 1960)

The structure of vanadyl bisacetylacetonate has been determined from three-dimensional x-ray diffraction data. The crystals are triclinic, space group $P\bar{1}$, with $a=7.53\pm0.02$ A, $b=8.23\pm0.03$ A, $c=11.24\pm0.04$ A, $\alpha=73.0°$, $\beta=71.3°$, $\gamma=66.6°$, $Z=2$. The structure consists of discrete molecules of $VO(C_5H_7O_2)_2$. Each vanadium atom has five oxygen neighbors at the corners of a rectangular (nearly square) pyramid, with vanadium near its center of gravity. The vanadium-oxygen distances are 1.56 A to the apex atom (vanadyl oxygen) and 1.96, 1.96, 1.97, and 1.98 A to the others. Other bond distances average 1.28 A for C—O, 1.40 A for C—C (ring), and 1.52 A for C—C (methyl). Standard deviations are 0.01 A for V—O bonds and 0.02 A for C—O and C—C bonds. Each acetylacetone skeleton is planar, and this plane makes an angle of 163° with the plane of the other acetylacetone skeleton of the same molecule.

INTRODUCTION

THE crystal structure of vanadyl bisacetylacetonate,

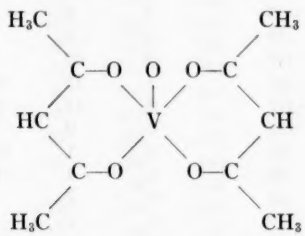

has been determined to establish the geometry of the bonds about five-coordinated vanadium (IV). In his discussion of this compound and its reactions, Jones[1] assumed a square planar arrangement of four oxygen atoms about the vanadium atom, with the bond of the fifth oxygen presumably perpendicular to the plane of the other four. From the chemical evidence, it was impossible to rule out the trigonal bipyramidal arrangement of the five bonds. The work of Feltham[2] on the electron spin-resonance spectra of the compound indicates that the bipyramidal structure is improbable. The geometry of these five bonds can be expected to be similar in such compounds as vanadyl tetraphenylporphine.[3] The present work shows that the five oxygen atoms are at the corners of an approximately square pyramid, but that vanadium is near the center of gravity of this pyramid rather than at the center of its base.

EXPERIMENTAL

Single crystals of vanadyl bisacetylacetonate were provided by Dr. Rue L. Belford. The crystals were blue-green in color, and those selected for study averaged 0.1 mm in thickness. Their shape corresponded to class $\bar{1}$ with only three forms appearing. These forms correspond to {100}, {010}, and {001} as we have chosen the axes.

The parameters of the reciprocal cell were obtained from quartz-calibrated[4] zero-level Weissenberg photographs (rotation about a and b) and zero-level precession photographs (precession about a, b, and c). Intensities were evaluated by visual comparison with a set of standard intensities for 1165 independent reflections on multiple-film Weissenberg photographs with rotation about a. About 230 reflections were recorded as too weak to be observed. About 190 other reflections too weak to be observed, but for which the observational sensitivity was not as great, were completely excluded from the calculations. Similar intensity observations made with rotation about b were used to scale the intensities of the first set. All these photographs were made with Cu$K\alpha$ radiation.

UNIT CELL AND SPACE GROUP

The diffraction symmetry confirms that the crystals are triclinic. The parameters found for the reciprocal cell are:

$a^*=0.1459$ A^{-1} $b^*=0.1349$ A^{-1} $c^*=0.0957$ A^{-1}

$\alpha^*=101.0°$ $\beta^*=103.5°$ $\gamma^*=109.5°$.

By the transformation formulas, the direct cell parameters are:

$a=7.53\pm0.02$ A $\alpha=73.0°$

$b=8.23\pm0.03$ A $\beta=71.3°$

$c=11.24\pm0.04$ A $\gamma=66.6°$.

The density found by suspension in a liquid of equal density is 1.49, which corresponds to 2.01 molecules in the unit cell. This value suggests that the space group is $P\bar{1}$, and the agreement with the intensity data which

* This work was supported by the United States Atomic Energy Commission.

[1] M. M. Jones, J. Am. Chem. Soc. **76**, 5995 (1954).

[2] R. D. Feltham, Ph.D. dissertation, University of California, Berkeley, 1957.

[3] K. Ueno and A. Martell, J. Phys. Chem. **60**, 934 (1956).

[4] A. Pabst, Am. Mineralogist **42**, 664 (1957).

TABLE I. Observed and calculated structure factors, F_O and F_C, each multiplied by 10. An asterisk (*) denotes that the reflection was too weak to be detected. Because of an error in card sorting which was not discovered until after the data were on magnetic tape, reflections with $l=9$ are listed out of their natural order, but this order had no effect on any of the crystallographic calculations. Excluded from the list are approximately 190 undetected and 3 very strong reflections which were omitted from the calculations as described in the text and reflection 248 which unintentionally was omitted from the calculations.

$h=0$

k	l	F_O	F_C	k	l	F_O	F_C	k	l	F_O	F_C
0	2	52	−41	2	−10	*	−54	5	2	212	196
0	3	93	90	2	11	114	92	5	−2	243	244
0	4	269	273	2	−11	99	73	5	3	215	192
0	5	200	205	2	−12	91	69	5	−3	*	67
0	6	161	−149	3	0	234	−135	5	4	145	−138
0	7	161	−151	3	1	111	118	5	−4	*	−2
0	−9	*	51	3	−1	237	−207	5	5	124	−123
0	8	70	78	3	2	128	144	5	−5	*	−38
0	10	120	−98	3	−2	335	−319	5	6	*	14
0	−11	*	−26	3	3	55	−97	5	−6	266	258
0	12	108	−93	3	−3	*	−16	5	7	133	158
0	13	86	72	3	4	*	1	5	−7	140	125
1	0	313	−329	3	−4	168	171	5	9	85	−62
1	−1	375	388	3	5	472	513	5	−9	75	−66
1	2	67	−54	3	−5	*	−35	5	8	*	42
1	−2	371	−387	3	6	*	58	5	−8	*	−53
1	3	468	515	3	−6	153	−147	5	10	*	−44
1	−3	168	−178	3	7	207	−221	5	11	105	101
1	4	109	118	3	−7	177	−177	5	12	79	58
1	−4	46	5	3	9	140	137	6	0	*	−48
1	5	417	−430	3	−9	109	96	6	1	140	145
1	−5	329	333	3	8	*	−56	6	−1	144	−141
1	6	159	−159	3	−8	*	44	6	2	*	11
1	−6	132	120	3	10	164	177	6	−2	*	−1
1	7	138	115	3	−10	117	−101	6	3	328	−350
1	−7	*	−14	3	−11	120	−109	6	−3	121	123
1	9	200	−198	3	12	153	−121	6	4	83	−67
1	−9	*	−45	4	0	93	175	6	−4	134	117
1	8	247	229	4	1	105	59	6	5	85	−76
1	−8	141	−138	4	−1	363	370	6	−5	73	−90
1	−10	110	100	4	2	194	−197	6	6	105	110
1	−11	120	92	4	−2	157	159	6	−6	149	−148
1	−12	*	−37	4	3	*	20	6	7	*	−70
1	−13	83	−73	4	−3	275	−285	6	−7	109	99
2	0	383	−370	4	4	315	328	6	9	*	−11
2	1	315	−266	4	−4	169	−181	6	8	132	−155
2	−1	251	−196	4	5	*	37	6	10	*	62
2	2	171	152	4	−5	106	89	6	11	*	22
2	−2	278	279	4	6	106	−118	7	0	*	45
2	3	62	39	4	−6	*	5	7	1	*	58
2	−3	167	164	4	7	*	−33	7	−1	*	−26
2	4	785	−808	4	−7	134	−112	7	2	164	−173
2	−4	228	−217	4	9	*	53	7	−2	156	−160
2	5	278	−280	4	−9	*	42	7	3	*	55
2	−5	*	−30	4	8	*	61	7	−3	121	−104
2	6	207	259	4	−8	130	−121	7	4	128	142
2	−6	*	−55	4	10	144	−146	7	−4	*	38
2	7	140	124	4	−10	108	104	7	5	*	49
2	−7	153	160	4	11	120	−114	7	−5	78	83
2	9	103	−104	4	−11	66	−63	7	6	*	−33
2	−9	*	−41	4	13	65	67	7	7	113	−105
2	8	153	−139	5	0	140	−136	7	9	132	119
2	−8	210	207	5	1	*	5	7	8	*	74
2	10	74	67	5	−1	75	−62	7	10	*	−13

TABLE I.—*Continued.*

h=0

k	*l*	F_o	F_c	*k*	*l*	F_o	F_c	*k*	*l*	F_o	F_c
7	11	111	−106	8	−2	71	73	8	7	75	85
8	0	*	−68	8	3	111	104	9	1	67	75
8	1	79	−86	8	4	67	67	9	2	*	54
8	−1	106	110	8	5	*	−36	9	3	*	−13
8	2	*	−21	8	6	*	−40	9	4	59	−70

h=1

k	*l*	F_o	F_c	*k*	*l*	F_o	F_c	*k*	*l*	F_o	F_c
0	2	516	−542	−1	7	233	−223	−2	−13	30	−32
0	3	553	529	−1	−7	130	−114	3	0	655	603
0	−3	371	−399	−1	−9	188	−176	3	1	137	107
0	4	168	145	−1	8	160	−162	3	−1	182	136
0	5	97	−63	−1	10	106	104	3	2	114	−56
0	−5	350	327	−1	−10	104	−90	3	−2	413	−373
0	6	123	−115	−1	−11	151	−127	3	3	*	12
0	7	77	−63	−1	12	72	−51	3	−3	227	−199
0	−7	212	−194	−1	−13	43	41	3	4	111	137
0	9	122	109	2	0	162	−119	3	−4	193	180
0	−9	92	81	2	1	425	371	3	5	287	257
0	8	153	157	2	−1	243	−283	3	−5	146	130
0	−8	115	100	2	2	215	−167	3	6	213	−215
0	10	223	−235	2	−2	92	27	3	−6	*	−14
0	−10	164	140	2	3	246	−220	3	7	127	−146
0	11	64	−49	2	−3	248	230	3	−7	186	−186
0	−12	114	−89	2	4	*	−75	3	9	104	111
0	13	78	72	2	−4	223	−171	3	−9	87	95
1	2	452	456	2	5	132	136	3	8	*	67
1	−2	663	593	2	−5	189	−180	3	−8	92	−90
1	3	380	332	2	6	473	497	3	−10	64	−57
1	−3	*	−27	2	−6	323	−263	3	11	132	−108
1	4	141	−164	2	7	186	−175	3	−11	77	−60
1	−4	43	10	2	−7	*	81	3	12	120	−102
1	5	348	−336	2	9	145	−130	−3	0	331	−315
1	−5	108	68	2	8	226	−224	−3	1	219	−210
1	6	*	−1	2	−8	212	211	−3	−1	123	−92
1	−6	242	234	2	−10	77	−61	−3	2	266	−263
1	7	224	240	2	12	101	−88	−3	−2	370	339
1	−7	218	205	2	−12	78	74	−3	3	180	184
1	−9	66	−59	2	13	110	−88	−3	−3	269	−235
1	8	184	188	−2	0	99	67	−3	4	216	199
1	−8	91	−82	−2	1	138	126	−3	−4	240	−229
1	11	233	215	−2	−1	350	−307	−3	5	119	−95
1	−11	109	93	−2	2	197	192	−3	6	141	−154
1	12	81	74	−2	−2	*	84	−3	−6	211	210
−1	0	257	225	−2	3	110	−86	−3	8	125	130
−1	1	763	827	−2	−3	405	368	−3	−8	167	−172
−1	−1	373	−291	−2	4	168	−146	−3	10	66	−58
−1	2	558	−476	−2	−4	476	−444	−3	−10	228	204
−1	−2	427	−398	−2	−5	263	−282	−3	−11	65	72
−1	3	71	−46	−2	7	135	115	−3	12	92	102
−1	−3	66	87	−2	−7	391	393	−3	−12	90	−64
−1	−4	563	519	−2	9	160	−167	4	0	433	−372
−1	5	87	82	−2	−9	107	−106	4	1	309	−283
−1	6	107	−94	−2	11	96	95	4	−1	374	349
−1	−6	419	−444	−2	−11	95	94				

TABLE I.—*Continued.*

h=1

k	*l*	F_O	F_C	*k*	*l*	F_O	F_C	*k*	*l*	F_O	F_C
4	2	150	−106	5	8	106	−115	7	0	99	77
4	−2	111	71	5	10	65	86	7	−1	76	74
4	3	149	150	5	−10	55	−57	7	2	140	−131
4	−3	197	−171	5	11	96	84	7	−2	*	−34
4	4	106	94	5	13	77	−57	7	3	76	−60
4	−4	184	−169	−5	0	114	−99	7	−3	137	−122
4	5	332	−341	−5	1	85	81	7	4	168	184
4	−5	*	52	−5	−1	152	−150	7	5	107	−93
4	6	*	−64	−5	−2	170	159	7	−5	65	81
4	7	143	136	−5	3	103	−89	7	9	76	65
4	9	106	−109	−5	−3	219	225	7	8	130	128
4	8	*	42	−5	4	205	−236	7	11	84	−80
4	−8	153	−133	−5	−4	160	153	−7	0	127	120
4	10	113	−100	−5	8	167	−158	−7	1	103	−102
4	−10	106	88	−5	−8	91	91	−7	−1	174	177
4	12	149	116	−5	10	56	62	−7	2	101	−113
4	13	106	74	6	0	*	0	−7	−2	118	−139
−4	0	228	216	6	1	167	153	−7	4	106	109
−4	1	134	103	6	−1	72	−71	−7	−5	72	94
−4	−1	134	126	6	2	*	42	−7	6	59	−57
−4	2	89	58	6	−2	98	−96	−7	−7	110	−115
−4	−2	115	−109	6	3	224	−225	−7	−9	48	63
−4	3	228	−227	6	−3	*	−29	8	0	87	−98
−4	−3	62	−46	6	4	254	252	8	−1	61	57
−4	4	138	124	6	−4	131	144	8	2	65	67
−4	−4	111	97	6	5	332	344	8	−2	57	62
−4	5	199	207	6	−5	116	−112	8	3	74	80
−4	−5	169	162	6	6	74	64	8	−3	62	79
−4	7	107	−121	6	−6	104	−95	8	−5	64	−66
−4	−7	91	−95	6	7	107	−85	8	9	175	−155
−4	9	127	113	6	9	133	136	−8	0	54	64
−4	−9	203	195	6	8	92	−93	−8	−1	109	−109
−4	11	86	−88	6	10	103	81	−8	−2	78	−84
−4	−11	176	−159	6	11	61	−60	−8	3	95	−115
5	0	222	−213	6	12	61	−46	−8	−3	55	57
5	1	116	103	−6	0	145	−145	−8	−4	80	91
5	−1	110	−100	−6	1	135	−130	−8	−7	67	62
5	2	300	299	−6	−1	111	115	−8	−8	78	84
5	−2	176	172	−6	2	107	131	9	1	95	82
5	3	*	−30	−6	−2	*	−26	9	−1	65	−80
5	4	443	−454	−6	3	125	130	9	3	107	−96
5	−4	73	61	−6	−3	205	−201	9	4	68	−61
5	5	92	−93	−6	4	65	−68	9	8	79	−79
5	−5	76	−85	−6	−4	181	−174	−9	−2	66	71
5	6	60	71	−6	−6	84	88	−9	−3	95	109
5	−6	150	129	−6	7	163	180	10	2	43	−59
5	7	103	93	−6	−9	87	−84	10	3	55	52
5	−7	123	98	−6	−8	77	−59	10	4	78	66
5	9	*	24	−6	−11	45	42				

h=2

k	*l*	F_O	F_C	*k*	*l*	F_O	F_C	*k*	*l*	F_O	F_C
0	0	617	−681	0	3	248	219	0	5	221	−236
0	1	424	−511	0	−3	182	−199	0	−5	*	45
0	−1	64	35	0	4	*	9	0	6	163	−154
0	−2	184	187	0	−4	275	−268	0	−6	211	203

TABLE I.—*Continued.*

$h=2$

k	l	F_O	F_C	k	l	F_O	F_C	k	l	F_O	F_C
0	7	80	69	−1	−11	126	−111	3	3	193	208
0	−7	*	−1	2	0	316	319	3	−3	224	−214
0	9	*	1	2	1	373	364	3	4	111	−71
0	−9	*	−42	2	−1	108	−144	3	−4	*	27
0	8	184	186	2	2	242	−258	3	5	318	−277
0	−8	48	−23	2	−2	286	−269	3	−5	272	294
0	10	171	−162	2	3	87	62	3	6	274	−285
0	−10	186	155	2	−3	*	−1	3	−6	132	147
0	11	*	55	2	4	322	318	3	7	124	−108
0	−11	*	20	2	−4	328	340	3	−7	136	−134
0	12	178	172	2	5	192	200	3	9	65	64
0	−12	73	−64	2	−5	*	6	3	−9	155	118
1	−1	161	−182	2	6	369	378	3	8	129	131
1	−2	101	107	2	−6	329	−330	3	−8	*	−18
1	3	53	70	2	7	84	−70	3	10	102	−105
1	−3	62	60	2	−7	134	−137	3	11	116	−121
1	4	77	−92	2	9	*	59	3	12	*	−31
1	−4	*	−23	2	−9	*	16	3	13	106	90
1	5	134	−124	2	8	157	−163	−3	0	239	−232
1	−5	323	−330	2	−8	113	113	−3	1	50	46
1	6	135	137	2	10	118	114	−3	−1	62	−69
1	−6	*	33	2	−10	76	−64	−3	2	219	222
1	7	309	335	2	11	*	−51	−3	−2	216	233
1	−7	239	235	2	−11	60	−42	−3	3	270	263
1	9	126	−117	2	12	122	−101	−3	−3	254	−225
1	−9	150	−133	2	13	*	−17	−3	4	*	13
1	8	116	−119	2	14	73	75	−3	−4	145	−147
1	−8	*	−7	−2	0	85	76	−3	5	184	−192
1	10	*	−4	−2	1	332	342	−3	−5	87	−84
1	−10	123	−85	−2	−1	157	−159	−3	6	*	27
1	11	200	205	−2	2	250	206	−3	−6	122	116
1	−11	80	63	−2	−2	236	226	−3	7	170	202
1	12	*	−43	−2	3	228	−207	−3	−7	118	115
1	−12	89	81	−2	−3	404	409	−3	9	*	−23
1	13	100	−85	−2	4	197	−203	−3	−9	146	−147
−1	0	141	130	−2	−4	214	215	−3	8	*	14
−1	1	457	422	−2	5	*	56	−3	−8	153	−162
−1	−1	60	62	−2	−5	161	−161	−3	−10	72	72
−1	2	135	−119	−2	6	253	274	−3	11	41	52
−1	−2	275	−264	−2	−6	124	−137	−3	−11	105	76
−1	3	247	−218	−2	7	102	−112	4	0	691	−652
−1	−3	183	−187	−2	−7	93	107	4	1	456	−395
−1	4	412	408	−2	9	*	−59	4	−1	109	97
−1	−4	145	242	−2	−9	*	−8	4	2	285	270
−1	5	42	16	−2	8	176	−162	4	−2	355	367
−1	−5	228	231	−2	−8	102	96	4	3	*	33
−1	6	173	−215	−2	10	*	−1	4	−3	75	74
−1	−6	225	−228	−2	−10	131	−104	4	4	205	−211
−1	7	262	−274	−2	11	*	9	4	−4	123	−118
−1	−7	*	−19	−2	−11	*	1	4	5	183	−195
−1	9	181	188	−2	12	63	−74	4	−5	*	−5
−1	−9	152	127	−2	−12	41	39	4	6	*	34
−1	8	*	34	3	0	399	379	4	−6	118	131
−1	−8	*	−76	3	1	433	−430	4	7	102	114
−1	10	*	19	3	−1	506	489	4	−7	67	66
−1	−10	*	22	3	2	254	124	4	9	94	−99
−1	11	147	−132	3	−2	132	−123				

TABLE I.—*Continued.*

h=2

k	*l*	F_O	F_C	*k*	*l*	F_O	F_C	*k*	*l*	F_O	F_C
4	−8	54	−69	−5	−4	102	103	7	5	223	−241
4	10	*	64	−5	5	95	101	7	−5	*	5
4	11	58	64	−5	−5	*	−17	7	6	119	−130
4	12	130	109	−5	6	*	−47	7	−6	83	70
4	14	75	−71	−5	−6	108	−115	7	7	96	105
−4	0	93	95	−5	7	139	−143	7	9	*	−77
−4	1	211	−202	−5	−7	73	−83	7	8	82	81
−4	−1	213	205	−5	−9	*	27	7	10	164	−142
−4	−2	141	−134	−5	8	125	−131	7	11	*	11
−4	3	70	−67	−5	−8	87	72	7	12	81	78
−4	−3	144	−176	−5	−10	87	−66	−7	0	*	50
−4	4	163	170	6	0	141	140	−7	1	125	−141
−4	−4	63	−63	6	1	75	67	−7	−1	*	61
−4	5	82	106	6	−1	*	14	−7	2	*	40
−4	−5	73	86	6	2	101	−110	−7	−2	*	−4
−4	6	*	−43	6	−2	156	−161	−7	3	130	152
−4	−6	95	105	6	3	74	−69	−7	−3	*	−78
−4	7	*	10	6	−3	59	−56	−7	−4	79	−82
−4	−7	76	−61	6	4	261	279	−7	−5	89	98
−4	9	70	59	6	−4	153	148	−7	−6	*	30
−4	−9	131	123	6	5	375	407	−7	−7	64	−64
−4	8	135	147	6	−5	*	10	−7	−8	63	−53
−4	−8	*	−47	6	6	178	−205	8	0	93	−86
−4	−10	114	98	6	−6	82	64	8	1	*	−4
−4	−11	72	−57	6	7	*	21	8	−1	72	−73
5	0	102	−81	6	−7	98	−96	8	2	122	129
5	1	274	282	6	9	132	139	8	−2	*	5
5	−1	231	−204	6	8	83	93	8	3	*	3
5	2	145	134	6	10	*	26	8	−3	149	137
5	−2	184	−165	6	11	95	−85	8	4	95	−100
5	3	329	−333	6	12	*	6	8	−4	51	51
5	−3	160	164	6	13	66	57	8	5	*	−48
5	4	264	−264	−6	0	119	−146	8	−5	54	−54
5	−4	192	−195	−6	1	*	14	8	6	*	24
5	5	241	253	−6	−1	67	84	8	7	*	30
5	−5	160	−159	−6	2	116	138	8	9	119	−117
5	6	184	198	−6	−2	108	120	8	8	61	−68
5	−6	*	−67	−6	3	*	3	8	10	73	70
5	7	141	−146	−6	−3	152	163	8	11	48	42
5	−7	*	−6	−6	4	150	−155	−8	0	109	130
5	9	*	2	−6	−4	*	−58	−8	−2	74	−92
5	8	93	−104	−6	−5	*	−31	−8	−3	51	−62
5	−8	96	79	−6	−6	*	42	−8	−4	48	58
5	10	90	90	−6	−7	93	89	9	2	106	−99
5	11	*	−21	−6	−9	58	−54	9	−2	89	−84
5	12	100	−67	−6	−8	*	33	9	3	112	−94
5	13	58	−53	7	0	96	96	9	−3	42	−40
−5	0	*	32	7	1	75	−83	9	4	*	36
−5	1	129	122	7	−1	128	122	9	5	87	70
−5	−1	203	−222	7	2	*	32	9	9	71	70
−5	2	*	−55	7	−2	108	103	10	2	49	−53
−5	−2	*	−49	7	3	66	53	10	3	62	63
−5	3	108	−103	7	−3	*	−16	10	6	55	−51
−5	−3	*	43	7	4	75	74				
−5	4	83	−96	7	−4	77	−77				

TABLE I.—*Continued.*

$h=3$

k	l	F_O	F_C	k	l	F_O	F_C	k	l	F_O	F_C
0	0	228	−271	−1	−10	118	98	3	4	245	−232
0	1	61	−83	−1	11	64	−65	3	−4	296	−296
0	2	147	−165	−1	12	67	52	3	5	150	−153
0	−2	126	106	−1	13	48	58	3	−5	126	134
0	3	326	331	2	0	206	218	3	6	*	−47
0	−3	73	74	2	1	138	−136	3	−6	266	272
0	4	86	30	2	−1	180	147	3	7	*	15
0	−4	163	−154	2	2	157	−179	3	−7	*	−33
0	5	435	−405	2	−2	65	19	3	9	84	−67
0	−5	138	−125	2	3	70	85	3	8	183	199
0	7	223	237	2	−3	173	−161	3	−8	*	17
0	9	171	−194	2	4	217	273	3	10	131	−133
0	11	96	92	2	−4	366	316	3	−10	66	58
0	−11	120	102	2	5	59	62	3	11	*	8
0	12	168	160	2	−5	275	281	3	12	106	87
0	13	89	−87	2	6	136	−147	3	13	72	62
1	−1	80	−89	2	−6	164	−173	−3	0	280	−308
1	−2	449	−417	2	7	178	−178	−3	1	246	261
1	−3	82	75	2	−7	190	−192	−3	−1	*	−14
1	4	232	−258	2	9	279	290	−3	2	355	398
1	−4	149	126	2	−9	101	77	−3	−2	185	194
1	5	69	51	2	8	109	−108	−3	3	*	9
1	−5	267	−267	2	−8	*	23	−3	−3	117	101
1	6	208	207	2	10	99	104	−3	4	121	−109
1	−6	185	−186	2	11	70	−57	−3	−4	80	−82
1	7	139	129	2	−11	67	−70	−3	5	63	−78
1	−7	46	38	2	12	*	2	−3	−5	102	−132
1	9	109	−118	2	13	100	96	−3	6	99	108
1	−9	49	−42	2	14	66	62	−3	−6	*	35
1	8	234	−226	−2	0	114	114	−3	7	85	90
1	−8	158	148	−2	1	227	234	−3	−7	113	105
1	10	60	55	−2	−1	241	−219	−3	8	69	−86
1	−10	116	−101	−2	2	117	−125	4	0	173	−158
1	11	53	−41	−2	−2	62	56	4	1	115	99
1	12	168	−181	−2	3	283	−307	4	−1	292	−267
1	13	109	−111	−2	−3	180	183	4	2	516	506
1	14	50	43	−2	4	*	15	4	−2	246	248
−1	0	194	178	−2	−4	211	232	4	3	107	−98
−1	1	129	−96	−2	5	268	313	4	−3	165	160
−1	−1	222	225	−2	−5	177	−174	4	4	180	−167
−1	2	238	−233	−2	6	*	−35	4	−4	61	−58
−1	−2	243	−231	−2	−6	79	−79	4	5	102	108
−1	3	333	−332	−2	7	169	−209	4	−5	109	−107
−1	−3	200	−210	−2	−7	120	−102	4	6	143	157
−1	4	516	537	−2	9	98	109	4	−6	*	45
−1	−4	62	73	−2	−9	83	77	4	7	124	129
−1	5	87	−80	−2	8	132	−143	4	−7	103	95
−1	−5	185	178	−2	−8	82	62	4	9	90	−85
−1	6	192	−206	−2	−10	80	−62	4	−9	66	−52
−1	−6	173	192	−2	−11	44	−48	4	8	133	−138
−1	7	65	66	3	0	114	−109	4	−8	*	−13
−1	−7	163	150	3	1	481	−478	4	10	92	97
−1	9	93	109	3	−1	382	347	4	11	130	131
−1	−9	163	148	3	2	64	−53	4	13	103	−70
−1	8	212	244	3	−2	207	217	4	14	73	−69
−1	−8	75	−73	3	3	190	188	−4	0	98	−101
−1	10	69	−64	3	−3	116	−115	−4	1	249	−260

TABLE I.—*Continued.*

h=3

k	*l*	F_o	F_c	*k*	*l*	F_o	F_c	*k*	*l*	F_o	F_c
−4	−1	197	200	−5	3	*	−24	7	3	138	154
−4	2	*	−20	−5	−3	133	−143	7	−3	*	35
−4	−2	*	45	−5	4	*	63	7	4	64	−72
−4	3	90	117	−5	−4	46	55	7	−4	84	−77
−4	−3	131	−141	−5	5	81	73	7	5	*	−41
−4	4	*	−33	−5	−5	109	123	7	−5	85	−84
−4	−4	102	−102	−5	−6	54	−56	7	6	*	50
−4	5	85	−71	−5	−7	45	−57	7	−6	52	47
−4	−5	*	20	−5	−9	60	63	7	7	161	160
−4	6	84	−87	−5	−8	55	46	7	9	97	−92
−4	−6	102	103	6	0	96	100	7	8	*	−15
−4	−7	98	−92	6	1	152	−137	7	11	82	78
−4	−8	109	−115	6	−1	181	188	7	12	69	60
−4	10	58	−70	6	2	74	−70	−7	1	88	−101
−4	−10	70	65	6	−2	65	−66	−7	−2	96	107
5	0	205	190	6	3	122	123	−7	3	55	87
5	1	153	169	6	−3	*	3	−7	−4	64	−68
5	−1	250	−242	6	4	47	38	−7	−6	49	59
5	2	181	−174	6	−4	*	37	8	0	*	12
5	−2	316	−308	6	5	59	−54	8	1	46	40
5	3	231	−234	6	−5	125	117	8	−1	127	−139
5	−3	*	57	6	6	370	−404	8	2	46	57
5	4	*	4	6	−6	90	73	8	−2	83	−79
5	−4	109	−81	6	7	90	−87	8	3	139	−157
5	5	267	279	6	−7	97	−81	8	−3	77	76
5	−5	*	−15	6	9	*	0	8	4	80	−80
5	6	210	204	6	8	131	134	8	−4	47	40
5	−6	142	−136	6	−8	76	−75	8	5	88	83
5	7	188	−199	6	10	*	−46	8	−5	26	−34
5	−7	82	−63	6	11	91	−81	8	6	70	72
5	9	*	21	6	13	81	74	8	10	126	109
5	−9	54	47	−6	1	88	88	8	11	83	69
5	8	63	62	−6	−3	179	169	9	0	76	74
5	−8	77	69	−6	−5	67	−61	9	−1	40	47
5	10	*	42	−6	6	60	82	9	2	119	−124
5	11	113	−110	−6	−7	76	78	9	−2	54	−48
5	14	66	57	−6	−8	57	63	9	−3	62	−70
−5	0	93	87	7	0	92	−92	9	4	139	137
−5	1	*	27	7	1	46	−51	9	5	75	81
−5	−1	*	−64	7	−1	*	22	10	3	76	78
−5	2	125	−137	7	2	82	90	10	5	137	−143
−5	−2	182	−223	7	−2	168	188				

h=4

k	*l*	F_o	F_c	*k*	*l*	F_o	F_c	*k*	*l*	F_o	F_c
0	0	104	−98	0	−5	102	−106	0	−10	56	−50
0	1	168	148	0	6	209	229	0	11	44	57
0	−1	120	−119	0	−6	142	−131	0	13	82	−98
0	2	503	577	0	7	98	104	1	0	64	75
0	−2	157	135	0	−7	119	99	1	1	59	46
0	3	231	262	0	9	109	−117	1	−1	40	36
0	−3	196	196	0	−9	91	−82	1	2	233	−319
0	4	151	129	0	8	118	−130	1	−2	237	−214
0	−4	83	−58	0	−8	*	−6	1	3	314	−375
0	5	113	−128	0	10	67	50	1	−3	120	103

TABLE I.—*Continued.*

$h=4$

k	l	F_O	F_C	k	l	F_O	F_C	k	l	F_O	F_C
1	4	186	−223	2	11	47	−45	−3	−7	118	101
1	−4	177	165	2	12	87	69	−3	−9	44	−23
1	5	224	251	2	13	81	78	−3	8	81	−84
1	−5	*	−34	−2	0	155	153	−3	10	60	71
1	6	30	−13	−2	1	33	−22	4	0	*	2
1	−6	107	−114	−2	−1	160	−151	4	1	297	307
1	7	171	−204	−2	2	259	−276	4	−1	265	−275
1	−7	58	−45	−2	−2	287	−310	4	2	311	333
1	9	*	5	−2	3	104	−120	4	−2	70	−79
1	−9	81	70	−2	−3	54	−26	4	3	57	12
1	8	88	−86	−2	4	130	133	4	−3	62	56
1	−8	165	137	−2	−4	104	100	4	4	152	−126
1	10	123	133	−2	5	178	212	4	−4	105	99
1	−10	77	−73	−2	−5	*	32	4	5	125	135
1	11	93	−86	−2	6	130	−152	4	−5	83	−77
1	12	66	−73	−2	−6	*	2	4	6	189	201
−1	0	71	55	−2	7	63	−81	4	−6	105	−92
−1	1	282	−273	−2	−7	126	−123	4	7	*	−2
−1	−1	272	269	−2	9	109	130	4	9	*	36
−1	2	*	16	−2	−9	74	59	4	8	158	−164
−1	−2	39	15	−2	8	*	31	4	−8	101	89
−1	3	54	51	−2	10	46	33	4	10	123	133
−1	−3	161	−148	3	0	178	−179	4	11	*	25
−1	4	103	97	3	1	166	−189	4	12	175	−173
−1	−4	*	9	3	2	48	−23	4	13	57	−51
−1	5	149	−150	3	−2	194	182	−4	0	108	−130
−1	−5	*	−44	3	3	244	310	−4	1	122	−132
−1	6	198	−199	3	−3	*	−4	−4	−1	*	55
−1	−6	186	185	3	4	232	−283	−4	2	146	186
−1	7	211	258	3	−4	261	−265	−4	−2	163	180
−1	−7	*	14	3	5	91	−99	−4	3	110	124
−1	9	48	−48	3	−5	91	−83	−4	−3	*	49
−1	8	122	170	3	6	215	249	−4	4	63	−57
−1	−8	102	−87	3	−6	93	65	−4	−4	140	−156
−1	10	91	−91	3	7	259	290	−4	5	*	−37
−1	−10	54	50	3	9	140	−153	−4	−5	64	−61
−1	12	60	52	3	−9	110	−96	−4	−6	100	90
2	0	91	98	3	8	119	127	−4	9	72	−88
2	1	120	−155	3	−8	35	−30	−4	−8	97	−92
2	−1	160	182	3	10	59	−61	5	0	283	289
2	−2	*	−4	3	11	144	135	5	1	95	−82
2	3	41	36	3	12	89	80	5	−1	*	26
2	−3	246	−245	3	13	47	−34	5	2	239	−219
2	4	183	259	−3	0	84	−90	5	−2	133	105
2	−4	*	16	−3	1	206	249	5	3	*	−13
2	5	167	−192	−3	−1	55	−55	5	−3	*	−19
2	−5	275	281	−3	2	81	79	5	4	123	116
2	6	289	−340	−3	−2	*	−5	5	−4	93	98
2	−6	63	54	−3	3	236	−278	5	5	137	131
2	7	69	−81	−3	−3	200	206	5	−5	195	165
2	−7	40	−38	−3	4	120	−132	5	6	*	9
2	9	92	96	−3	−4	*	−2	5	−6	76	−61
2	−9	36	32	−3	5	63	64	5	7	243	−270
2	8	60	35	−3	−5	107	−120	5	−7	105	−83
2	−8	84	−66	−3	6	68	70	5	9	154	180
2	10	96	−84	−3	−6	*	3	5	8	*	33
2	−10	76	71	−3	7	*	−22	5	10	41	−36

TABLE I.—*Continued.*

					$h=4$						
k	l	F_O	F_C	k	l	F_O	F_C	k	l	F_O	F_C
5	11	107	−82	6	11	*	−24	8	1	119	113
5	13	101	104	6	12	71	56	8	−1	95	−84
−5	0	65	45	−6	0	39	33	8	2	53	−53
−5	1	39	−25	−6	−1	83	−85	8	−2	162	−159
−5	−1	129	129	−6	−2	89	−92	8	3	92	−100
−5	2	56	−51	−6	3	59	−63	8	4	48	32
−5	−2	*	−31	−6	−4	65	82	8	−4	54	50
−5	3	54	51	−6	6	32	64	8	5	107	106
−5	−3	104	−110	−6	−6	67	−90	8	6	*	−9
−5	4	78	80	7	0	152	−159	8	7	74	−70
−5	−4	*	3	7	1	82	77	8	9	*	76
−5	−5	147	151	7	−1	170	−169	8	8	81	49
−5	−7	70	−70	7	2	40	−12	8	12	80	−73
6	0	112	−94	7	−2	81	85	9	1	54	−63
6	1	139	−137	7	3	57	−51	9	−1	119	117
6	−1	138	142	7	−3	106	89	9	2	60	−48
6	2	48	53	7	4	124	−134	9	3	99	92
6	−2	*	41	7	−4	*	−26	9	4	166	151
6	3	94	94	7	5	106	108	9	5	43	−45
6	−3	*	−34	7	−5	91	−88	9	6	133	−126
6	4	95	−68	7	6	147	145	9	9	72	−20
6	−4	222	−191	7	7	123	121	9	10	75	−62
6	5	196	−193	7	9	*	−39	10	2	68	73
6	6	161	−163	7	8	*	−48	10	3	59	68
6	−6	96	85	7	11	127	110	10	4	49	−47
6	7	141	−132	7	12	62	46	10	5	105	−103
6	9	123	−132	7	13	86	−80	10	6	42	43
6	8	154	148	−7	−2	42	60	10	7	70	77
6	10	108	−120	8	0	155	144				

TABLE II. Final parameters.

Atom	x	y	z	$\sigma(x)$	$\sigma(y)$	$\sigma(z)$	B, A²
Vanadium 1	0.1436	0.2902	0.2231	0.0004	0.0003	0.0002	2.4
Oxygen 2	0.9404	0.4142	0.3592	0.0014	0.0011	0.0008	3.0
Oxygen 3	0.9978	0.1214	0.2689	0.0014	0.0011	0.0008	2.8
Oxygen 4	0.1472	0.5359	0.1367	0.0014	0.0010	0.0007	2.6
Oxygen 5	0.2200	0.2302	0.0532	0.0014	0.0010	0.0007	2.6
Oxygen 6	0.3316	0.1887	0.2793	0.0016	0.0012	0.0009	3.8
Carbon 7	0.2753	0.5372	0.4396	0.0026	0.0020	0.0014	4.4
Carbon 8	0.8224	0.3521	0.4561	0.0022	0.0016	0.0012	2.8
Carbon 9	0.7836	0.1965	0.4661	0.0022	0.0017	0.0012	3.1
Carbon 10	0.8672	0.0924	0.3700	0.0022	0.0016	0.0011	2.8
Carbon 11	0.7900	0.9408	0.3825	0.0023	0.0017	0.0012	3.4
Carbon 12	0.7765	0.2166	0.0125	0.0024	0.0017	0.0013	3.5
Carbon 13	0.2215	0.5917	0.0195	0.0022	0.0016	0.0011	2.9
Carbon 14	0.7039	0.5090	0.0751	0.0022	0.0017	0.0012	3.1
Carbon 15	0.7070	0.6861	0.0565	0.0021	0.0015	0.0011	2.6
Carbon 16	0.6307	0.7855	0.1659	0.0024	0.0018	0.0013	3.8

was achieved confirms this choice. All atoms occur in the general twofold positions, $\pm(xyz)$.

DETERMINATION OF THE STRUCTURE

Preliminary attempts to solve the structure by projections failed because of lack of resolution and certain blunders. A three-dimensional Patterson function located the vanadium atom unambiguously. Starting with signs based on vanadium only, the [100] projection quickly refined to a point where six carbon atoms and one oxygen atom were shown as resolved peaks and the other carbon and oxygen atoms were shown as four unresolved double peaks. The [010] projection

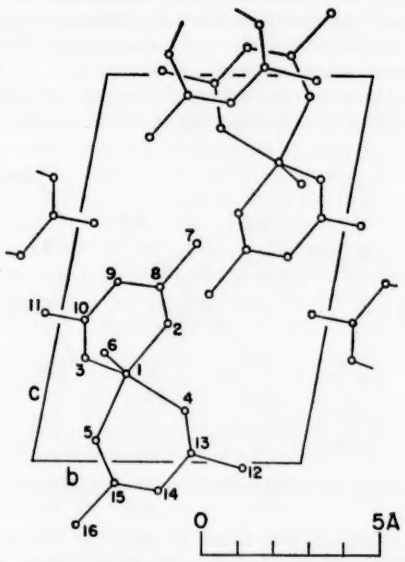

FIG. 1. The crystal structure of vanadyl bisacetylacetonate, projected along [100]. One unit cell is outlined. The numbering of the atoms corresponds to the identification in the text and tables.

still failed to resolve atoms, but indicated that the chelate rings were nearly coplanar and approximately parallel with b. This knowledge and assumptions of reasonable bond distances led to a trial structure in three dimensions. An electron density calculation in three dimensions then revealed all the carbon and oxygen atoms. In the meantime, about half of the oxygen and carbon atoms had been located independently by a study of the smaller peaks of the three-dimensional Patterson function. For this structure the "unreliability factor" $R=\Sigma \| F_o|-|F_c\| / \Sigma |F_o|$ was 0.207.

REFINEMENT OF THE STRUCTURE

The structure was refined by the method of least squares, neglecting hydrogen atoms. Atomic scattering factors were taken from Freeman[5] for V^{2+} and neutral C and from Berghuis, *et al.*,[6] for neutral O. Individual isotropic temperature factors were used throughout. First we used the IBM 650 computer and the largely

TABLE III. Bond distances in vanadyl bisacetylacetonate.

Atoms	Distance,[a] A	Atoms	Distance,[a] A
V—O_5	1.56	C_7—C_8	1.51
...	...	C_{10}—C_{11}	1.53
V—O_2	1.97	C_{12}—C_{13}	1.52
V—O_3	1.96	C_{15}—C_{16}	1.51
V—O_4	1.98	...	...
V—O_5	1.96	C_8—C_9	1.39
...	...	C_9—C_{10}	1.40
O_2—C_8	1.29	C_{13}—C_{14}	1.38
O_3—C_{10}	1.28	C_{15}—C_{16}	1.42
O_4—C_{13}	1.28	...	...
O_5—C_{15}	1.29	...	...

[a] Standard deviations are 0.01 A for V—O bonds and 0.02 A for C—O and C—C bonds. Chemically equivalent bonds are grouped together.

TABLE IV. Bond angles in vanadyl bisacetylacetonate.

Atoms	Angle[a]	Atoms	Angle[a]
O_2—V—O_3	87.2°	O_2—C_8—C_7	114.9°
O_4—V—O_5	87.9°	O_3—C_{10}—C_{11}	117.2°
...	...	O_4—C_{13}—C_{12}	115.4°
O_2—V—O_4	83.8°	O_5—C_{15}—C_{16}	115.9°
O_3—V—O_5	83.5°	...	...
...	...	O_2—C_8—C_9	123.6°
O_2—V—O_5	149.8°	O_3—C_{10}—C_9	124.2°
O_3—V—O_4	145.5°	O_4—C_{13}—C_{14}	124.6°
...	...	O_5—C_{15}—C_{14}	122.5°
O_2—V—O_6	104.5°	...	...
O_3—V—O_6	106.3°	C_7—C_8—C_9	121.5°
O_4—V—O_6	108.2°	C_9—C_{10}—C_{11}	118.5°
O_5—V—O_6	105.6°	C_{12}—C_{13}—C_{14}	119.9°
...	...	C_{14}—C_{15}—C_{16}	121.5°
V—O_2—C_8	128.6°	...	...
V—O_3—C_{10}	129.4°	C_8—C_9—C_{10}	123.3°
V—O_4—C_{13}	128.7°	C_{13}—C_{14}—C_{15}	124.4°
V—O_5—C_{15}	129.5°	...	...

[a] Standard deviations are about 1° or less. Chemically equivalent angles are grouped together.

[5] A. J. Freeman, Acta Cryst. **12**, 261 (1959).

[6] J. Berghuis, I.J. M. Haanappel, M. Potters, B. O. Loopstra, C. H. MacGillavry, and A. L. Veenendaal, Acta Cryst. **8**, 478 (1955).

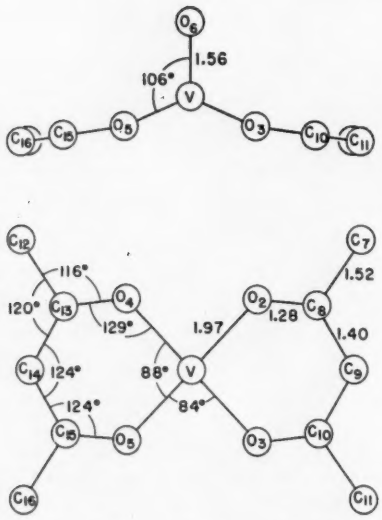

FIG. 2. Average bond distances and bond angles.

diagonal "LS-II" program of Senko and Templeton[7] modified for space group $P\bar{1}$. The weighting and treatment of undetected reflections was done as described elsewhere.[8] Five cycles of refinement reduced R to 0.114 (observed reflections only). The resulting structure is described by Dodge.[9]

Examination of the records of these refinement cycles suggested that the best fit had not been achieved. Four additional cycles of refinement were carried out with the IBM 704 computer and the full-matrix program of Busing and Levy.[10] Observed reflections were given unit weight. Unobserved reflections were given zero weight unless F_c exceeded 7.3, a value about 1.5 times the average limit of detection; in the latter case F_o was taken as zero and given unit weight. Before the final two cycles, six reflections with especially large discrepancies were removed from the data; these consisted of $15\bar{3}$, $1\bar{5}2$, and $2\bar{4}2$ which were erroneously recorded as absent when actually they fell off the films and 011, 202, and 212 which were observed very strong, but not as strong as calculated. After the last cycle, further checking revealed that 157, $22\bar{8}$, and $3\bar{4}\bar{4}$ had been recorded as absent by errors of transcription, that $22\bar{9}$ actually was absent but had been assigned the intensity of $22\bar{8}$, and that $36\bar{8}$ had been assigned an incorrect intensity. After correction, these five reflections were in excellent agreement with calculation. There remain eight absent reflections with structure factors calculated greater than 7.3, but none exceeding 8.4. This is considered to be satisfactory agreement, since hydrogen atoms are excluded from the calculation. The observed and calculated structure factors from the final cycle are listed in Table I (with the five corrections mentioned before); the corresponding R is 0.092 (observed reflections only).

The sharp eyes of a referee discovered one additional error. The observed intensity of reflection 248, a very weak reflection, was listed as reflection 246 and was included in all calculations with those indices. Reflection 246 was also correctly listed as too weak to be observed. The incorrect listing of F_o has been removed from Table I.

TABLE V. Oxygen-oxygen distances.

Atoms	Distance, A	Atoms	Distance, A
O_2—O_3	2.71	O_2—O_6	2.80
O_4—O_5	2.73	O_3—O_6	2.82
...	...	O_4—O_6	2.87
O_2—O_4	2.64	O_5—O_6	2.81
O_3—O_5	2.61	...	...

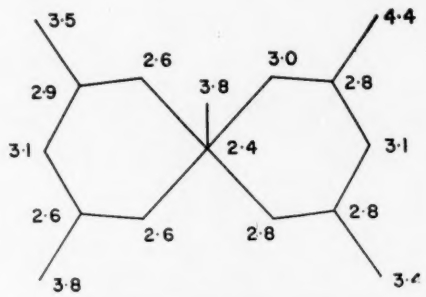

FIG. 3. Individual isotropic temperature parameters.

The final atomic parameters are listed in Table II. The results confirm that the earlier refinement[9] had not adequately converged and that one full-matrix cycle achieved results that would have required several diagonal cycles. Of 48 atomic coordinates, 29 changed by more than one standard deviation; two changed by more than 5 standard deviations. The largest change in a bond distance was that of the V—O_6 bond which was 1.59 A after the diagonal refinement and 1.56 A in the final structure. These differences are attributed more to lack of convergence than to the presence of the defective data in the earlier cycles.

DISCUSSION OF THE STRUCTURE

The structure consists of discrete molecules, arranged in the unit cell as indicated in Fig. 1. There are just two orientations of molecules, and one is the in-

[7] M. E. Senko, Acta Cryst. **10**, 385 (1957).
[8] G. L. Hardgrove and D. H. Templeton, Acta Cryst. **12**, 29 (1959).
[9] R. P. Dodge, Ph.D. dissertation, University of California, Berkeley, 1958.
[10] W. R. Busing and H. A. Levy, ORNL Central Files Memorandum 59-4-37 (April 1959).

verse of the other. This crystal may have application, because of this alignment, in the observation of directionally-dependent spectroscopic properties.

The bond distances and angles are listed in Tables III and IV. The molecule has no crystallographic symmetry, but chemically equivalent bond distances are equal to the experimental accuracy. Chemically equivalent angles are nearly equal. If these quantities were exactly equal, the molecule (with the possible exception of the hydrogen atoms) would have symmetry *mm*2 (C_{2v}). The molecular shape is shown in Fig. 2 with average values of equivalent distances and angles. The bond distance of the vanadyl ion, 1.56 A, is of special interest because we know of no other measurement of this bond. The C—C and C—O bond distances are in accord with values for analogous structures.[11–16]

The five neighbors of vanadium are at the corners of a rectangular (nearly square) pyramid, with vanadium approximately at its center of gravity. This geometry can be considered to be derived from the square planar configuration, discussed in the Introduction, by bending the two chelate rings away from the fifth oxygen. This bending lengthens four oxygen-oxygen distances, which otherwise would have been the shortest, and at the same time makes two others shorter. The distances in the actual structure are listed in Table V. It is plausible that the distances O_2—O_4 and O_3—O_5 would be shorter than the distances to O_6, but we find the difference unexpectedly large.

The structure of V_2O_5 also has vanadium in five-fold coordination, though in a different valence state.[17] In that case there is one close neighbor, at 1.54 A, and four others at 1.77, 1.88, 1.88, and 2.02 A. The coordination geometry is said to consist of "distorted trigonal bipyramids."[17] However, the distortion is so great that the coordination also can be described as a distortion of a square pyramid, with the close neighbor again at the apex. The fact that the distances are mostly slightly shorter than in our structure is consistent with the higher formal valence state.

Each acetylacetone skeleton is accurately planar as expected, but not quite coplanar with the other acetylacetone skeleton of the same molecule. The planes of these two parts of the molecule meet at an angle of 163°. It is interesting that these planes are a compromise between those that would contain the vanadium atom and those that would be coplanar, assuming no change in the oxygen and vanadium positions. We interpret this fact as evidence for conjugation effects between the two rings.

The individual temperature parameters of the atoms are superimposed on an outline of the molecule in Fig. 3. There is a definite trend for the terminal atoms of the skeleton to have greater thermal motion than the atoms of the rings.

ACKNOWLEDGMENTS

We thank Dr. R. L. Belford for providing the crystals and Mrs. Helena W. Ruben, Dr. M. E. Senko, and Dr. R. E. Jones for their help.

[11] H. Koyama, Y. Saito, and H. Kuroya, J. Inst. Polytech. Osaka City Univ., Ser. C. **4,** 43 (1953).
[12] R. B. Roof, Acta Cryst. **9,** 781 (1956).
[13] S. Shibata, Bull. Chem. Soc. Japan **30,** 753 (1957).
[14] V. M. Padmanabhan, Proc. Indian Acad. Sci. **47,** 329 (1958).
[15] L. M. Shkolnikova and E. A. Shugam, Kristallografiya **5,** 32 (1960).
[16] V. Amirthalingam, V. M. Padmanabhan, and J. Shankar, Acta Cryst. **13,** 201 (1960).
[17] A. Byström, K. A. Wilhelmi, and O. Brotzen, Acta Chem. Scand. **4,** 1119 (1950).

Vapor Pressures of the Neon Isotopes*

JACOB BIGELEISEN AND ETIENNE ROTH†

Chemistry Department, Brookhaven National Laboratory, Upton, New York

(Received December 6, 1960)

The ratio of the vapor pressures of Ne^{20} and Ne^{22} have been measured in the temperature range 16–30°K. An accuracy of about 1% in the logarithm of the vapor-pressure ratio has been achieved. The latter is checked by comparisons of (1) triple-point pressures, (2) equilibrium fractionation experiments, and (3) the entropy difference of the condensed phases with thermal measurements.

The Debye temperature for the solid derived from the ratio of the vapor pressures, 74.6°K, is in good agreement with values derived from the Debye-Waller temperature factor and theoretical calculations by Bernardes. The discrepancy between the characteristic temperatures derived from measurements of free energy with those from heat capacities is attributed to the role of the anharmonicity of the lattice.

It is shown that the difference in the thermodynamic properties of solid and liquid neon in the vicinity of the triple point can be attributed to the change in coordination number.

INTRODUCTION

IN a preliminary communication[1] we have called attention to the need for new data on the vapor pressures of the neon isotopes. A summary of the results obtained for solid neon in the temperature range 16.4–24.6°K was given in the form of either a Debye or an Einstein temperature. The Debye temperature for Ne^{20}, 74.6°K, found from vapor-pressure measurements, is in good agreement with Henshaw's[2] value, 73°K, obtained from the angular dependence of the intensity of neutron scattering. Theoretical calculations of the zero-point energy by Bernardes[3] also give 73°K for the Debye temperature, while heat capacity measurements[4] give 63°K. Recently the heat capacity of separated neon isotopes has been measured by Clusius and co-workers,[5] from which these authors obtain a Debye temperature of 66.7°K for Ne^{20} at 10°K. The discrepancy is real and will be discussed in terms of the anharmonic effects.

Measurements have also been made on the vapor pressures of the neon isotopes in the liquid range 24.6–30.1°K. Independent of our investigation, measurements in the liquid range have been made by Boato, Casanova, and Vallauri.[6] The latter workers determined the equilibrium distribution between liquid and vapor and calculated the vapor-pressure ratio by a correction to Raoult's law. Their calculated vapor-pressure ratios appeared to be in marked disagreement with our data (see note at end of reference 6). The discrepancy has been found to be the result of an error in sign and the results of both laboratories will be shown to be in excellent agreement.

The present paper presents a brief description of the experimental method[7] used in our measurements, the experimental results, and an interpretation of the experimental data.

EXPERIMENTAL METHOD

The vapor-pressure ratio of isotopic liquids can be determined either by differential manometry or the measurement of equilibrium liquid-vapor distribution equilibria. Each of the methods has inherent advantages and disadvantages. The method of differential manometry requires high chemical purity, enriched isotopes in quantities of the order of a tenth of a liter or more (NTP) of gas, good thermal equilibrium between two samples, constant temperature of the sample for periods of the order of an hour, and precise measurements of small pressure differences. The liquid-vapor equilibration method has modest requirements of chemical purity and temperature stability, and does not require significant quantities of enriched isotopes. Frequently the natural abundance is sufficient. The method depends entirely on isotope ratio determinations with a precision of the order 0.01–1.0%. In the liquid-vapor equilibration method it is essential to achieve equilibrium with respect to mass transport. Finally, if one desires the vapor-pressure ratio, then one must consider the problem of nonideal solution behavior. Mass transfer equilibrium is not easily established between a solid and a vapor because of the slow diffusion in the solid. Thus a conventional distribution experiment is not applicable to the solid. Since our experiments were designed to study the vapor-pressure ratio in both the liquid and solid range, we chose the method of differential manometry.

* Research carried out under the auspices of the U. S. Atomic Energy Commission.

† Visiting chemist at Brookhaven National Laboratory 1957–1958. Permanent address: Centre d'Etudes Nucleaires de Saclay, Gif-sur-Yvette, France.

[1] E. Roth and J. Bigeleisen, J. Chem. Phys. **32**, 612 (1960).

[2] D. G. Henshaw, Phys. Rev. **111**, 1470 (1958).

[3] N. Bernardes, Phys. Rev. **112**, 1534 (1958).

[4] K. Clusius, Z. physik. Chem. **B4**, 1 (1929).

[5] K. Clusius, P. Flubacher, U. Piesbergen, K. Schleich, and A. Sperandio, Z. Naturforsch. **15a**, 1 (1960).

[6] G. Boato, G. Casanova, and M. E. Vallauri, Nuovo cimento **16**, 505 (1960).

[7] A more detailed description is available in the D.Sc. thesis of E. Roth at the Faculty of Sciences, University of Paris (1960).

The basic design of the cryostat was similar to the Giauque-Johnston[8,9]-type apparatus for determination of heat capacity and vapor pressure of condensed gases. The usual calorimeter was replaced by a sample vessel designed to accommodate three different samples in good thermal contact with one another, ordinary neon, enriched Ne^{20}, and enriched Ne^{22}. The total pressure of the ordinary neon was measured and served as a thermometer. The pressure difference between the enriched neon samples was measured on one of three differential manometers.

A sample of ordinary or enriched neon is a three component mixture, Ne^{20}, Ne^{21}, and Ne^{22}. The Ne^{21} is generally a minor component, and to a sufficient approximation, the system can be represented as a two-component one by the approximation $P_{Ne^{21}}=\frac{1}{2}(P_{Ne^{20}}+P_{Ne^{22}})$. One defines effective mole fractions of Ne^{20} and Ne^{22} by the relations

$$X_{20}'=X_{20}+\tfrac{1}{2}X_{21} \tag{1a}$$

$$X_{22}'=X_{22}+\tfrac{1}{2}X_{21}. \tag{1b}$$

Under the assumption of Raoult's law, the total pressure of a solution of neon isotopes of natural isotopic abundance is

$$P_N=X_{20,N}'P_{20}+X_{22,N}'P_{22}. \tag{2}$$

The vapor pressure difference between a sample enriched in Ne^{20} and one enriched in Ne^{22} is

$$\Delta P=(X_{20,0}'-X_{20,2}')P_{20}+(X_{22,0}'-X_{22,2}')P_{22}, \tag{3}$$

where the symbol $X_{20,0}'$ is the effective mole fraction of Ne^{20} in a sample enriched in Ne^{20} and $X_{20,2}'$ is the similar quantity in a sample of enriched Ne^{22}. The vapor pressure ratio can be expressed in terms of P_N, ΔP and the effective mole fractions by combining Eqs. (2) and (3)

$$P_{20}/P_{22}=\left[1+\left(\frac{X_{22,N}'}{X_{22,2}'-X_{22,0}'}\right)\frac{\Delta P}{P_N}\right]\Big/\left[1-\left(\frac{X_{20,N}'}{X_{22,2}'-X_{22,0}'}\right)\frac{\Delta P}{P_N}\right]. \tag{4}$$

The solutions, in fact, should not obey Raoult's law. Deviations are to be expected from the gas imperfection, the fact that the difference between the Gibbs and Helmholtz free energies of the condensed phase $PV_{l,s}$ is not negligible with respect to RT, and a volume change will occur on mixing the pure isotopes.[10,11] The vapor pressure of such a solution in which one component 2, is present in small amount is

$$\ln P=\ln(X_1P_1^0/Y_1)+(P-P_1^0)(-B+\bar{V}_1/RT)+\tfrac{1}{2}[(V_1^0-V_2^0)^2X_2/\beta V_1^0RT], \tag{5}$$

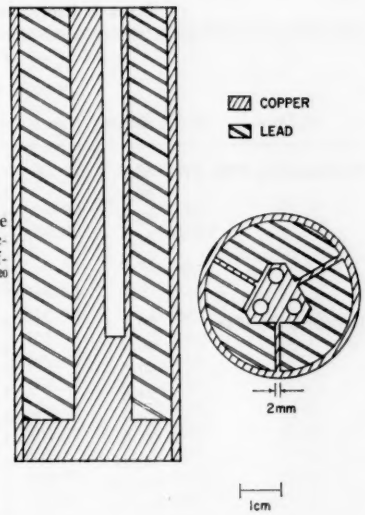

FIG. 1. Sample holder for measurement of pressure difference between Ne^{20} and Ne^{22}.

where P_1^0 is the vapor pressure of pure component 1; X_1 and Y_1 are the mole fractions of the major component in the condensed and gaseous phases, respectively; β is the compressibility of the condensed phase; and B is the second virial coefficient when the equation of state of the gas is written

$$PV/RT=1+BP. \tag{6}$$

From Eq. (5) and an analogous equation for component 2, one can show that a significant correction has to be applied to Raoult's relationship between the composition of the gaseous and condensed phases and the vapor pressures of the pure components. Detailed calculations for the solutions used in our experiments show that $\ln P_{Ne^{20}}/P_{Ne^{22}}$ can be calculated from (4) to within 0.1% of the value obtained from Eq. (5). This is consistent with the results of Keesom and Haantjes[12] who found no deviations from Raoult's law by the method of differential manometry with samples of various composition.

If the difference in effective mole fractions of Ne^{22} in the enriched Ne^{22} and Ne^{20} samples is in the range 0.5–1.0, mass spectrometer analyses of the composition can be made with sufficient precision such that the limitation in the precision in $\ln P_{Ne^{20}}/P_{Ne^{22}}$ is given by the precision in $\Delta P/P_N$. The present experiments were designed to give a precision of the order of 1% in $\ln P_{Ne^{20}}/P_{Ne^{22}}$. This requires that the samples of "Ne^{20}," "Ne^{22}," and ordinary neon be within 10^{-3} °K of one another. The absolute temperature need be kept and known to the order to 10^{-2} °K during the course of measurement of ΔP and P_N, a time of the order of one hour.

Another set of limitations on the design of the "calorimeter", differential manometers and the con-

[8] W. F. Giaque and C. J. Egan, J. Chem. Phys. **5**, 45 (1937).
[9] H. L. Johnston, J. T. Clarke, E. B. Rifkin, and E. C. Kerr, J. Am. Chem. Soc. **72**, 3933 (1950).
[10] J. S. Rowlinson, *Liquids and Liquid Mixtures* (Butterworths Scientific Publications, Ltd., London, 1959), p. 121.
[11] I. Prigogine, R. Bingen, and A. Bellemans, Physica **20**, 633 (1954).
[12] W. H. Keesom and J. Haantjes, Physica **2**, 986 (1935).

TABLE I. Experimental determination of the vapor pressures of the neon isotopes.

Date	Series	P_N in int. mm	$10^3\Delta P/P_N$	P_{20} in int. mm	P_{22} in int. mm	$\ln P_{20}/P_{22}$	$T°K$
December 19, 1958	88.3	1.53	8.48	1.55	1.37	0.123	16.42
	88.4	1.99	7.44	2.01	1.81	0.108	16.66
	88.5	2.03	7.87	2.05	1.83	0.113	16.67
	88.7	2.06	7.96	2.08	1.86	0.115	16.69
	88.6	2.07	7.82	2.09	1.87	0.113	16.70
	88.8	2.21	7.57	2.23	2.00	0.109	16.76
December 20, 1958	90.2	2.63	7.86	2.66	2.37	0.114	16.93
	90.3	2.70	7.66	2.73	2.44	0.111	16.96
	90.5	3.10	7.35	3.13	2.81	0.1059	17.10
	90.6	3.14	7.32	3.17	2.85	0.1059	17.11
	90.7	3.41	7.65	3.44	3.08	0.1076	17.20
	90.9	3.57	7.34	3.60	3.24	0.1059	17.25
	90.11	3.58	7.44	3.61	3.25	0.1063	17.26
	90.12	3.59	7.42	3.62	3.26	0.1068	17.26
	90.13	4.49	7.48	4.53	4.07	0.1080	17.50
	90.14	4.91	7.19	4.96	4.47	0.1034	17.60
	90.15	5.04	7.13	5.09	4.59	0.1026	17.63
	92.8	6.10	6.90	6.15	5.57	0.0993	17.86
	92.9	6.26	7.04	6.31	5.70	0.1013	17.89
	90.17	6.53	7.02	6.58	5.95	0.1009	17.94
	90.16	6.56	6.91	6.61	5.99	0.0993	17.95
	90.18	6.64	7.03	6.68	6.03	0.1014	17.96
	92.10	8.50	6.88	8.57	7.77	0.0989	18.28
	92.13	9.50	6.80	9.58	8.69	0.0978	18.43
	92.14	9.51	6.77	9.59	8.70	0.0972	18.44
	92.1	16.14	6.355	16.27	14.85	0.0912	19.12
	92.4	16.35	6.372	16.48	15.04	0.0876	19.14
December 21, 1958	94.1	16.43	6.424	16.56	15.10	0.0921	19.14
December 20, 1958	92.3	16.45	6.290	16.58	15.15	0.0901	19.15
	92.2	16.45	6.277	16.58	15.15	0.0899	19.15
December 21, 1958	94.2	16.79	6.283	16.92	15.46	0.0904	19.18
	94.3	17.04	6.299	17.17	15.69	0.0902	19.21
	94.4	17.31	6.320	17.45	15.94	0.0906	19.23
	94.5	17.72	6.235	17.86	16.33	0.0893	19.26
	94.6	29.18	5.886	29.39	27.02	0.0841	19.98
	94.7	29.36	5.857	29.58	27.20	0.0837	19.99
	94.8	29.43	5.848	29.64	27.27	0.0835	19.99
	94.9	29.52	5.851	29.74	27.35	0.0835	20.00
December 11, 1958	70.2	34.41	5.698	34.65	31.95	0.0814	20.24
December 17, 1958	82.16	39.64	5.576	39.91	36.86	0.0795	20.46
	82.17	39.84	5.573	40.11	37.05	0.0795	20.47
	82.18	40.05	5.521	40.33	37.28	0.0787	20.48
December 18, 1958	86.11	44.82	5.517	45.13	41.71	0.0787	20.65
December 11, 1958	70.3	51.19	5.428	51.53	47.70	0.0773	20.87
	70.4	51.43	5.424	51.77	47.92	0.0773	20.88
December 15, 1958	78.11	56.28	5.258	56.65	52.56	0.0748	21.03
	78.12	57.93	5.242	58.31	54.11	0.0746	21.07
	78.13	58.14	5.246	58.52	54.31	0.0747	21.08
December 11, 1958	70.6	79.42	5.096	79.92	74.33	0.0725	21.62
	70.7	79.86	5.051	80.36	74.79	0.0718	21.63

TABLE I.—Continued

Date	Series	P_N in int. mm	$10^3\Delta P/P_N$	P_{20} in int. mm	P_{22} in int. mm	$\ln P_{20}/P_{22}$	T°K
December 18, 1958	86.12	89.49	4.977	90.04	83.90	0.0707	21.83
December 17, 1958	84.3	90.11	4.973	90.66	84.48	0.0707	21.84
	84.2	90.32	4.944	90.87	84.71	0.0702	21.87
December 10, 1958	62.5	105.66	4.822	106.36	99.32	0.0684	22.14
	62.3	105.91	4.851	106.61	99.52	0.0688	22.14
	62.4	106.73	4.846	107.44	100.30	0.0688	22.16
	62.6	107.74	4.796	108.45	101.32	0.0680	22.18
	62.7	108.13	4.805	108.85	101.68	0.0682	22.18
	62.8	111.00	4.767	111.73	104.43	0.0675	22.24
	62.9	111.50	4.770	112.23	104.89	0.0676	22.25
	62.10	112.57	4.768	113.31	105.90	0.0676	22.27
	64.1	139.57	4.595	140.37	131.51	0.0651	22.75
	64.2	144.09	4.434	144.88	136.06	0.0629	22.82
	64.3	145.36	4.607	146.18	136.94	0.0646	22.83
	64.4	147.03	4.540	147.85	138.64	0.0643	22.86
	64.6	147.88	4.572	148.71	139.38	0.0648	22.87
	64.5	147.95	4.581	148.78	139.43	0.0649	22.88
December 12, 1958	72.2	159.28	4.528	160.18	150.22	0.0642	23.04
December 10, 1958	62.1	159.30	4.509	160.29	150.37	0.0639	23.04
December 12, 1958	72.1	159.39	4.532	160.28	150.30	0.0642	23.04
December 10, 1958	62.2	160.49	4.437	161.47	151.64	0.0628	23.06
	64.8	168.47	4.510	169.41	158.92	0.0639	23.16
	64.7	168.49	4.507	169.43	158.94	0.0639	23.16
	64.9	168.57	4.519	169.51	159.00	0.0640	23.17
	64.10	168.76	4.496	169.70	159.23	0.0637	23.17
	64.11	168.82	4.499	169.76	159.27	0.0638	23.17
December 17, 1958	84.4	207.29	4.345	208.41	195.98	0.0615	23.60
	84.5	208.93	4.329	210.04	197.56	0.0613	23.61
	84.6	209.59	4.330	210.71	198.19	0.0613	23.62
December 12, 1958	72.7	224.92	4.353	226.13	212.61	0.0616	23.77
	72.6	224.95	4.347	226.16	212.66	0.0615	23.77
December 13, 1958	74.4	249.92	4.220	251.22	236.67	0.0597	24.01
	74.5	250.40	4.187	251.70	237.23	0.0592	24.01
December 12, 1958	72.9	274.81	4.172	276.22	260.40	0.0590	24.22
	72.10	274.90	4.183	276.32	260.45	0.0592	24.22
	72.11	274.95	4.172	276.36	260.53	0.0590	24.22
December 13, 1958	74.7	294.32	4.112	295.82	279.12	0.0581	24.36
December 12, 1958	72.12	311.51	3.986	313.05	295.91	0.0563	24.49
	72.13	311.70	4.071	313.27	295.76	0.0575	24.50
	72.14	311.70	4.077	313.27	295.53	0.0576	24.50
	72.15	312.12	4.125	313.71	295.94	0.0583	24.50
December 21, 1958	94.10	327.90	3.820				24.61
	94.11	331.77	3.622				24.64
December 13, 1958	74.8	335.40	3.410				24.68
	74.9	336.36	3.388				24.69
	74.10	336.36	3.373				24.69
	74.11	336.43	3.362.				24.69
	74.12	336.79	3.356				24.69

TABLE I.—Continued

Date	Series	P_N in int. mm	$10^3\Delta P/P_N$	P_{20} in int. mm	P_{22} in int. mm	$\ln P_{20}/P_{22}$	T°K
December 21, 1958	94.14	343.59	3.319	345.00	329.26	0.0467	24.75
	94.12	344.02	3.315	344.43	329.69	0.0467	24.75
	94.13	344.41	3.315	345.82	330.07	0.0466	24.76
December 13, 1958	74.14	395.61	3.218	397.18	379.61	0.0453	25.17
	74.13	396.02	3.213	397.60	379.90	0.0456	25.17
December 16, 1958	80.3	449.27	3.354	451.13	430.33	0.0472	25.54
	80.4	449.83	3.351	451.69	430.88	0.0472	25.55
December 13, 1958	74.15	480.31	3.076	482.14	461.74	0.0432	25.75
	74.16	480.74	3.080	482.57	462.13	0.0433	25.76
	76.4	605.95	2.924	608.14	583.69	0.0411	26.43
	76.3	605.97	2.924	608.16	583.71	0.0412	26.43
December 22, 1958	96.1	623.74	2.900	625.98	601.01	0.0407	26.52
December 13, 1958	76.1	677.06	2.850	679.44	652.81	0.0401	26.80
	76.2	677.88	2.848	680.27	653.62	0.0398	26.81
	76.5	778.47	2.750	781.12	751.57	0.0386	27.25
	76.6	778.80	2.754	781.45	751.85	0.0385	27.25
December 22, 1958	96.2	1035	2.578	1038	1001	0.0361	28.20
December 13, 1958	76.7	1144	2.536	1148	1108	0.0355	28.57
	76.8	1175	2.521	1179	1138	0.0353	28.66
	76.9	1183	2.515	1187	1146	0.0353	28.69
	76.10	1185	2.502	1189	1148	0.0351	28.70
December 22, 1958	96.9	1292	2.497	1296	1251	0.0349	29.01
	96.8	1580	2.444	1584	1531	0.0342	29.74
	96.5	1600	2.421	1605	1552	0.0339	29.81
	96.4	1613	2.405	1618	1565	0.0337	29.83
	96.3	1619	2.393	1624	1571	0.0335	29.84
	96.7	1635	2.376	1640	1586	0.0332	29.90
	96.6	1721	2.345	1726	1670	0.0328	30.11

necting lines was set by the amounts and isotopic compositions of the enriched samples. The experiment was designed to be performed with about 500 cc (NTP) of enriched gases. The volumes of the sample holder, manometer, and connecting lines, must be kept to a minimum to avoid changes in isotopic composition by vaporization. The lines must be large enough to avoid appreciable corrections from the thermomolecular effect, which depends on the molecular weight. Careful attention to the various dead volumes and the selection of tubes 2 mm i.d. to connect the sample volumes at 10–30°K with room temperature, a distance of approximately 1.75 m, provided an experimental arrangement such that no corrections are necessary for isotope fractionation or the thermomolecular effect.[13]

The sample container, shown schematically in Fig. 1, was made from a cylindrical rod of copper. The cross section perpendicular to the cylinder axis was machined as shown in Fig. 1. Three holes 80 mm long×4.75 mm diam drilled in the central copper section served as sample vessels. Some shredded copper was inserted to aid in thermal conduction in the solid neon. The holes were closed by copper caps through which the 2 mm i.d.×0.13 mm wall thickness stainless-steel tubes joined the sample vessels. A copper tube enclosed the finned section. All joints were silver soldered. The space between the inner section and the copper cylinder was filled with lead to serve as a large thermal sink for the sample container. The outer surface was bifilar wound with a constantan resistance heater. A 12-cm copper wire 0.8 mm diam connected the sample holder with the outer container. It served as a heat leak from the sample holder. The temperature was maintained constant by balancing the heat input against the heat leaks. A copper-constantan thermocouple soldered to the inner copper section of the sample vessel served as a secondary thermometer. The sample vessel contained 84 cc of lead and 48 cc of copper. Through its design, it

[13] Detailed calculations are given in work cited in reference 7.

had both a high thermal diffusivity in the vicinity of the samples and a high heat capacity, which added to the thermal stability of the assembly.

The calorimeter was surrounded by a massive radiation shield of the Giauque-Johnston type. Above the radiation shield was an auxiliary shield as described by Johnston *et al.*[9] Each of the shields was supplied with a heater and thermocouple. The assembly was enclosed in a vacuum-tight jacket, which was suspended in a metal Dewar. Liquid hydrogen was used as the refrigerant. Its temperature was controlled by regulating the pressure to within the order of a millimeter by means of a Sommers-type regulator.[14] The liquid hydrogen Dewar was surrounded by a Dewar filled with liquid nitrogen.

The pressure above the sample of ordinary neon was measured up to one atmosphere with a mercury manometer, which was read to ± 0.01 mm with a Wild cathetometer. The usual meniscus corrections[15] were made. The readings were reduced to 0°C and the standard acceleration of gravity 980.665 cm sec^{-2}. The local acceleration was taken as 980.267 cm sec^{-2}. Above one atmosphere the pressure of the ordinary neon was measured to ± 5 mm with a precision calibrated Bourdon gauge. The pressure difference between the enriched Ne^{20} and Ne^{22} samples was measured on one or more of three parallel differential manometers, mercury manometer, oil manometer filled with degassed dibutyl sebacate, or a sylphon bellows manometer. Most of the measurements were made with the oil manometer, which was calibrated against mercury. The sylphon bellows manometer had a very small dead volume and was designed for operation at high pressure. It had a linear displacement of 8 μ/mm Hg pressure difference. The displacement of the sylphon bellows was measured by a transformer induction coil which surrounded a magnetic core mounted on top of the sylphon bellows. The transformer coil was moved by a precision micrometer until it gave a null signal. The sensitivity of the manometer was about 0.05 mm Hg pressure difference. In actual performance, the limitation was found to be the reproducibility of the sylphon extension, which set a limit of ± 1 mm on the pressure difference that could be measured reliably. This was barely adequate for the high pressure experiments, where the pressure differences were of the order of 30 mm Hg or higher. The sylphon bellows manometer was calibrated against both the oil and mercury manometers. The use of the sylphon bellows manometer was restricted to measurements made above 29°K.

A preliminary test of the apparatus was made by filling the three sample holders with ordinary neon. The pressure difference between samples of ordinary neon in the holes which were to be filled with enriched neon was measured as a function of pressure. A small asymmetry was found. The pressure difference between samples was found to be proportional to the absolute pressure and the value of $\Delta p/p$ found was 5×10^{-5}. Since the difference in vapor pressures of the neon isotopes is of the order of 5%, the asymmetry correction is 0.1% in $\ln P_{Ne^{20}}/P_{Ne^{22}}$. The correction, although negligible, was applied to the data on the neon isotopes.

During the measurement of the vapor pressures the radiation shields were maintained a few degrees warmer than the sample container. The stainless-steel tubes were heated to eliminate the possibility of condensation in them.

The samples of enriched neon isotopes were kindly placed at our disposal by Dr. G. R. Grove of the Mound Laboratory of the Monsanto Chemical Company. They were enriched in a thermal diffusion column. The sample of enriched Ne^{22} was known to have a small quantity of air in it. The enriched samples were therefore purified by passage over hot uranium (900°C) and then hot copper oxide (670°C), followed by a liquid-nitrogen trap. The uranium removed oxygen and nitrogen and converted water to hydrogen. The hydrogen was reduced back to water by the copper oxide and was subsequently removed by the liquid nitrogen trap. Mass spectrometric analysis showed no detectable impurities. During the transfer of the purified samples to the cryostat, one of them became slightly contaminated with helium. The helium was removed by cooling the sample in the sample vessel to 6°K and pumping. This operation removed the helium completely. At this temperature the ordinary neon showed a pressure of 0.00 ± 0.01 mm Hg.

The enriched neon samples were analyzed on a mass spectrometer, which was calibrated by a sample of ordinary neon. Several samples of spectroscopically pure ordinary neon obtained from the Air Reduction Company were used for the calibration and they all gave identical results. The absolute abundance of similar neon samples has been determined by Nier.[16] The correction factor applied to our measures 22/20 ratio was 0.9309 and for the 21/20 ratio 0.965. The isotopic composition of the samples used in the vapor pressure measurements was

	Ordinary Ne	Ne^{20} sample	Ne^{22} sample
Ne^{20}	90.92%	$99.8_8\pm0.02$%	27.1 ± 0.3%
Ne^{21}	0.26	0.04	0.63 ± 0.01
Ne^{22}	8.82	0.08	72.2 ± 0.2.

The analyses of the enriched neon samples is in substantial agreement with independent analyses by Dr. G. R. Grove.

EXPERIMENTAL RESULTS

Several series of measurements were made. In general the absolute temperature of the samples was constant to within 0.01°K during the course of the

[14] H. S. Sommers, Rev. Sci. Instr. **25**, 793 (1954).
[15] J. Kistemaker, Physica **11**, 277 (1944).
[16] A. O. C. Nier, Phys. Rev. **79**, 450 (1950).

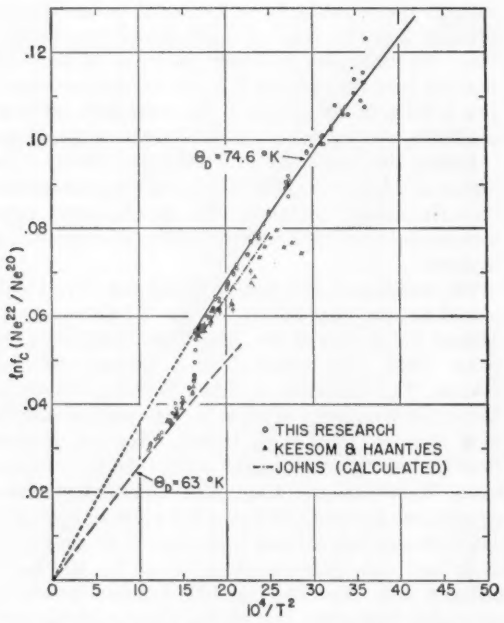

FIG. 2. Plot of $\ln f_c(Ne^{22}/Ne^{20})$ *vs* $1/T^2$. The sharp break in the curve comes at the triple point.

measurements. A few measurements where the temperature drifted by several hundredths of a degree during the course of measurement were rejected, even though they were in substantial agreement with the remainder of the data. The temperature scale on which the data are reported is the Crommelin and Gibson scale.[17] This scale was chosen since it shows the smallest deviations of measured vapor pressures of ordinary neon as a function of the temperature. The choice of a different temperature scale is of no consequence since $(d\ln P_{Ne^{20}}/P_{Ne^{22}})/dT$ is of the order -5×10^{-3}/°K. The Crommelin and Gibson vapor-pressure measurements show a scatter of the order of 10^{-2} °K. A shift in the absolute temperature scale is of even less importance for the present measurements. The vapor pressure ratios of Ne^{20}/Ne^{22} were calculated with the following constants in Eq. (4)

$$\frac{P_{20}}{P_{22}}=\frac{1+0.12343\Delta P/P_N}{1-1.2559\Delta P/P_N}, \tag{7}$$

where ΔP and P_N are, respectively, the measured pressure differences for the enriched samples described above and the pressure of ordinary neon. The results are given in Table I. The observed quantities tabulated are $\Delta P/P_N$ and P_N. The calculated quantities are P_{20}, P_{22}, and $\ln P_{20}/P_{22}$.

In the region between the triple points of Ne^{20} and Ne^{22}, Eq. (4) is not applicable unless one uses extrapolated values for the supercooled liquid or superheated crystal. Direct values of $\ln P_{20}/P_{22}$, P_{20}, and P_{22} are not tabulated for this temperature interval. They can be calculated by the method given in the next section.

A comparison of our experimental results with the data of Keesom and Haantjes[12] is given in terms of $\ln f_c$, the reduced partition function ratio of the two isotopes in the condensed phase. The results are shown graphically in Fig. 2. The present results are in substantial agreement with those of Keesom and Haantjes.[12] The scatter in the present data is an order of magnitude smaller than in the Leiden data at 20°K. Our results are systematically higher by about 6% in $\ln P_{Ne^{20}}/P_{Ne^{22}}$ than the data of Keesom and Haantjes. The reason for the discrepancy is not apparent. We attribute it tentatively to the possibility of systematic errors in the determinations of the isotopic abundances made by Keesom and Haantjes.

In Fig. 3 we give a comparison of the present results with the measurements of Boato, Casanova, and Vallauri.[6] These workers measured the equilibrium fractionation of the neon isotopes between liquid and vapor. From Eq. (5) and the following assumptions: (1) $B_{Ne^{20}}\cong B_{Ne^{22}}$; (2) $V_{Ne^{20}}\cong V_{Ne^{22}}$; and (3) $P_{Ne^{20}}-P_{Ne^{22}}\cong P\ln P_{Ne^{20}}/P_{Ne^{22}}$, we obtain the following relationship between the isotopic fractionation factor and the vapor-pressure ratio

$$\ln P_{Ne^{20}}/P_{Ne^{22}}=(\ln\alpha)(1-BP+PV_l/RT), \tag{8}$$

where

$$\alpha=(Ne^{20}/Ne^{22})_{\text{gas}}/(Ne^{20}/Ne^{22})_{\text{liquid}}. \tag{9}$$

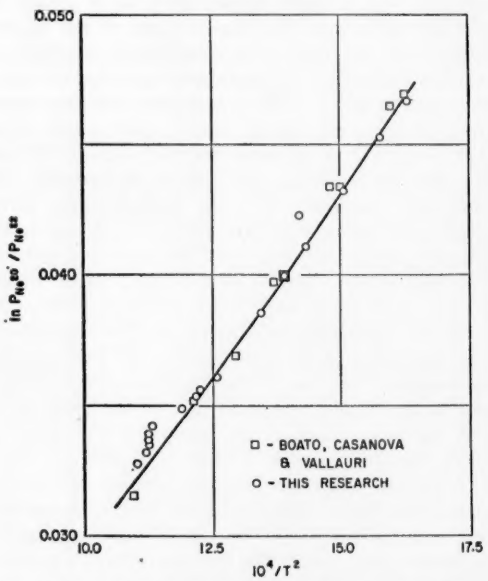

FIG. 3. Comparison of manometric and isotopic determinations of $\ln P_{Ne^{20}}/P_{Ne^{22}}$ in the liquid range.

[17] C. O. Crommelin and R. O. Gibson, Proc. Amst. Acad. **30**, 364 (1927).

The second virial coefficient B in Eq. (6) is related to the reduced virial coefficients by the relation

$$B=b_0B^*/RT. \tag{10}$$

It was calculated by the method given in Hirschfelder, Curtiss, and Bird.[18] The molal volumes of the liquid were taken from the compilation by de Boer and Lunbeck.[19] The agreement between the present measurements by differential manometry with enriched samples with the isotope fractionation experiments using precision isotope analysis is quantitative. It shows that the corrections for deviation from Raoult's law for solutions of the neon isotopes is adequately given by Eq. (5). The concentraton range involved is practically from pure Ne^{20} to pure Ne^{22}.

TRIPLE POINTS OF Ne^{20}, Ne^{22}, AND ORDINARY NEON

The triple-point pressures of the pure neon isotopes when combined with other thermodynamic data can serve as a useful check on the self-consistency of the solid and liquid vapor-pressure ratios. In addition, they are useful in the intercomparison of temperature scales.

The triple-point pressures of Ne^{20} and Ne^{22} have been measured directly by Clusius *et al.*[5] to be 325.10 mm and 327.73 mm Hg, respectively. These workers report triple-point temperatures of 24.66° and 24.84°K, respectively, based on the lead thermometer. Ne^{20} and Ne^{22} form nearly ideal solutions both in the liquid and solid phases. The triple-point temperatures and pressures of ordinary neon have been corrected by Henning and Otto[20] to the ice point 273.16°K. A summary is given in Table II. It is apparent that the 1960 lead scale of Clusius *et al.* is in disagreement with the 1927 Leiden scale and the Henning and Otto scale. At 7.2°K Clusius *et al.* report their scale to be 0.045°K higher than that of Pearson and Templeton.[21] The latter comparison is made on the basis of the superconducting transition in lead.

We shall utilize the triple-point pressure data to show the self-consistency of our vapor-pressure ratios. This comparison is practically independent of the temperature scale. We write

$$P_{T_{20}}{}^{20}-P_{T_{22}}{}^{22}=P_{T_{20}}{}^{20}[(R-1)/R]-[(dP_{(s)}{}^{22}/dT) +\tfrac{1}{2}(d^2P_{(s)}{}^{22}/dT^2)(T_{22}-T_{20})](T_{22}-T_{20}), \tag{11}$$

where $P_{T_{22}}{}^{22}$ = vapor pressure of Ne^{22} at its triple point; $P_{T_{20}}{}^{20}$ = vapor pressure of Ne^{20} at its triple point; and $R=P^{20}/P^{22}$ at T_{20} for pure solids. Assuming ideal solution, dP^{22}/dT and d^2P^{22}/dT^2 can be calculated from the relationship

$$P_{22}=P_N\left(\frac{R}{0.9105R+0.0895}-\frac{P_{20}-P_{22}}{P_N}\right), \tag{12}$$

and dP_N/dT and d^2P_N/dT^2, where P_N is the vapor pressure of ordinary neon. The data of both Crommelin and Gibson, and Henning and Otto give $dP_N(s)/dT=$ 139 mm/°K at $P_N(s)=325$ mm. Using the data of Clusius *et al.* for $P_{T_{20}}{}^{20}$, $P_{T_{22}}{}^{22}$, and our data for $R(s)$ we calculate $T_{22}-T_{20}$ to be 0.153°K. Assuming the T, x freezing-point diagram to be linear, we calculate the triple-point pressure of ordinary neon to be 325.21 mm from this value of $T_{22}-T_{20}$, our values of $R(s)$ and $R(l)$, and $dP_N(s)/dT$ and $dP_N(l)/dT$.

In a separate experiment we have determined the pressure of ordinary neon to be 336.63 mm at the "triple point" of 72.5$_5$% Ne^{22} and 325.06 mm at the "triple point" of ordinary neon. Extrapolating to pure Ne^{22} we obtain 341.65 mm for the pressure of ordinary neon at the triple point of Ne^{22}. The pressure of Ne^{22} at this temperature is calculated from Eq. (2) to be 327.33 mm in reasonable agreement with the measurements of Clusius *et al.* The temperature difference between the triple point of Ne^{22} and ordinary neon is

$$16.59\Big/\frac{dP_N(l)}{dT}\left\{1+\frac{[d^2P(l)/dT^2]\Delta T}{2[dP(l)/dT]}\right\}$$

or 0.137°K. The change of pressure with temperature for the liquid is calculated from the data on the solid and the heat of fusion. A linear extrapolation to pure Ne^{20} gives $T_{22}-T_{20}$ equal to 0.150°K in close agreement with the experiments of Clusius *et al.* The difference in $T_{22}-T_{20}$ calculated from Clusius *et al.* measurements and our measurements, 0.003°K, corresponds to 2% in $\ln R(s)$ if all other quantities are assumed to be exact.

We shall compare the triple-point data on a defined temperature scale, which is consistent with the Crommelin and Gibson scale, namely, 325.06 mm ordinary neon equals 24.590°K. The triple-point data on this scale are given in Table III. There appears to be a systematic difference in the triple-point pressure measurements of Clusius and co-workers and our

TABLE II. Triple-point temperatures and pressures of ordinary neon.

T°	P in mm	Reference
24.58	323.5	Crommelin and Gibson[a]
24.59		Clusius[b]
24.55		Clusius[c]
24.56	325	Henning and Otto[d]

[a] See reference 17.
[b] See reference 4.
[c] K. Clusius, Z. physik. Chem. **B31,** 459 (1936).
[d] See reference 20.

[18] J. O. Hirschfelder, C. F. Curtiss, and R. B. Bird, *Molecular Theory of Gases and Liquids* (John Wiley & Sons, Inc., New York, 1954), pp. 162–166.
[19] J. de Boer and R. J. Lunbeck, Physica **14,** 520 (1948).
[20] F. Henning and J. Otto, Physik Z. **37,** 633 (1936).
[21] W. B. Pearson and J. M. Templeton, Phys. Rev. **109,** 1094 (1958).

TABLE III. Triple-point data of Ne^{20}, Ne^{22}, and ordinary neon. (Defined scale 325.06 mm ordinary neon = 24.590°K.)

	Ne^{20} Clusius *et al.*	This research	Ne(N) Clusius *et al.*	This research	Ne^{22} Clusius *et al.*	This research
P in mm	325.10	(324.95±0.10)	(325.21)	325.06±0.1	327.73	327.33±0.1
T	24.578	(24.577)	(24.591)	24.59_0	24.730	24.72_7

measurements of the order of 0.2 mm Hg. This corresponds to a change of 1% in $\ln R$, which is just the estimated accuracy of our vapor-pressure ratio measurements in the temperature range between 16.1° and 28.2°K.

DISCUSSION

The quantity of direct theoretical significance is the reduced molecular partition function ratio of the condensed phase and not the vapor-pressure ratio. For a liquid or solid in equilibrium with a monatomic gas, the reduced partition function ratio is calculated from the vapor-pressure ratio by the equation[22]

$$\ln f_c = [1 + P(B - V/RT)] \ln P'/P, \tag{13}$$

where

$$f_c = \frac{\bar{Q}(T, V, m)/\bar{Q}'(T, V', m')}{(m/m')^{\frac{3}{2}}}. \tag{14}$$

The $\bar{Q}$ and $\bar{Q}'$ are, respectively, molecular quantum-mechanical partition functions for the heavy and light isotope in the condensed phase.

Figure 2 gives a plot of $\ln f_c$ for Ne^{22}/Ne^{20} calculated from the present vapor-pressure measurements and from the Leiden data. They are compared with theoretical calculations for the solid carried out by Johns[23] based on an anharmonic Einstein lattice using the method of Henkel.[24] Johns used a 14–6 potential with energy parameters evaluated by Zucker.[25] The lattice constant a_0 was used as a variable to minimize the free energy of the solid as a function of the temperature. The values of the lattice constant derived in this method ranged from 4.539–4.581 A between 0–24°K. This is in definite disagreement with the experimental value determined by Henshaw by neutron diffraction, 4.429 A at 4°K. The zero-point energy of the lattice changes from 71.7° to 95.4°K when a_0 changes from 4.564 to 4.429 A. A value of 95.4°K for the zero-point energy of the lattice would lead to values of $\ln f_c$ substantially larger than the experimental data. The vapor-pressure data suggest a revision in Zucker's constants.

For the purpose of comparison with heat capacity measurements on solid neon[4] and the heat capacities of the separated isotopes,[5] we shall consider the harmonic approximation to $\ln f_c$. In the harmonic approximation[22]

$$\ln f_c = \sum_{j=1}^{\infty} (-1)^{j+1} \frac{3B_{2j-1}(h/kT)^{2j}}{2j(2j)!} (\mu_{2j}' - \mu_{2j}) \qquad [h\nu_{\max}'/kT < 2\pi]. \tag{15}$$

The isotopic moments are related by

$$\mu_{2j}' - \mu_{2j} = \mu_{2j}'[1 - (m'/m)^j] \tag{16}$$

and

$$\ln f_c = \sum_{j=1}^{\infty} (-1)^{j+1} \frac{3B_{2j-1}(h/kT)^{2j}}{2j(2j)!} [1 - (m'/m)^j] \mu_{2j}' \qquad [h\nu_{\max}'/kT < 2\pi]. \tag{17}$$

For comparison with other data in the literature we shall consider the Debye frequency distribution. The moments are related to the Debye temperature by the equation

$$\mu_{2j}' = [3(k\theta_D'/h)^{2j}]/2j + 3. \tag{18}$$

Thus from the ratio of the vapor pressures of solid Ne^{20} and Ne^{22} we derive $\theta(Ne^{20}) = 74.6$°K. This is in good agreement with Henshaw's value[2] of 73°K from the Debye-Waller temperature factor for the neutron scattering intensity. Recently Bernardes[3] has calculated the zero-point energy of solid neon using a Lennard-Jones 6–12 potential. The potential parameters ϵ and σ are derived from the equation of state of the gas. The calculated zero-point energy corresponds to $\theta_D = 73$°K. On the other hand the heat capacity data give 66.7° and 65.2°K for the Debye temperatures of Ne^{20} and Ne^{22}, respectively. The discrepancy is not due to the assumption of a Debye frequency distribution.

The heat capacity of a harmonic lattice is[26]

$$(Cv/3R) - 1 = -\sum_{j=1}^{\infty} (-1)^j \frac{B_{2j-1}(1-2j)}{(2j!)} \mu_{2j} \qquad [(h\nu_{\max}/kT) < 2\pi]. \tag{19}$$

If we consider only the contribution from the second moment μ_2, then $\ln f_c/(1 - Cv/3R)$ is independent of the moment, or the frequency distribution. If one considers the μ_4 terms, then a discrepancy of about 1°K arises in θ_D calculated from Eqs. (17) and (19), if the lattice is face-centered cubic with nearest-neighbor interaction only. This is reduced somewhat by the contribution

[22] J. Bigeleisen, J. Chem. Phys. **34**, 1485 (1961). See Eqs. (2.10) and (2.17).
[23] T. F. Johns, Phil. Mag. **27**, 229 (1958).
[24] J. Henkel, J. Chem. Phys. **23**, 681 (1955).
[25] I. J. Zucker, J. Chem. Phys. **25**, 915 (1956).
[26] E. Montroll, in *Handbook of Physics*, edited by E. U. Condon and H. Odishaw (McGraw-Hill Book Company, Inc., New York, 1958).

from μ_6 and higher terms. It is clear that the discrepancy of the θ_D values derived from the energy and free energy on the one hand, and those derived from the heat capacity on the other, is due to the anharmonicity of the lattice. This is in agreement with the fact that the ratio $\theta(Ne^{20})/\theta(Ne^{22})$ from the heat capacity measurements is 1.023 instead of 1.049. The anharmonicity of the lattice will play a more significant role in the heat capacities than in the free energy.

Henshaw[2] has investigated the structure of liquid neon. The most probable separation of atoms in the liquid is 3.17 A compared with 3.13 A in the solid. The number of nearest neighbors is 8.8 in the liquid compared with 12 in the face-centered cube. If we use a lattice approximation to the liquid, then $(\theta_{solid}/\theta_{liquid})^2$ is approximately 12/8.8 in the vicinity of the triple point. Using $\theta_{solid}=74.6°K$ one calculates θ_{liquid} to be 63°K. This is compared with the experimental data for $\ln f_c$ in the liquid in Fig. 2. The agreement between the calculation and experiment is rather good over the temperature range studied, T^*, equal kT/ϵ, 0.72–0.86. At higher temperatures $\ln f_c$ must drop off sharply as the liquid expands and approach a value close to zero at the critical temperature.

ENTROPIES OF LIQUID AND SOLID Ne^{20} AND Ne^{22}

The vapor-pressure measurements can be compared with the heat capacities of the separated isotopes. A convenient quantity for comparison is the entropy difference of the condensed phase. This involves the vapor-pressure ratio and its temperature coefficient on the one hand and an integration of the heat capacity data. The entropy difference is given by the equation

$$S(Ne^{22})-S(Ne^{20})=R\ln\bar{Q}/\bar{Q}'+RT[(\partial\ln\bar{Q}/\bar{Q}')/\partial T]_V. \quad (20)$$

Instead of $\bar{Q}/\bar{Q}'$ we shall use the function f_c, defined by Eq. (14) and

$$S(Ne^{22})-S(Ne^{20})=\tfrac{3}{2}R\ln 22/20+R\ln f_c + RT[(\partial\ln f_c)/\partial T]. \quad (21)$$

TABLE IV. Comparison of entropies of Ne^{22} and Ne^{20} from vapor-pressure data and heat capacity measurements.

$T°$	$S(Ne^{22})-S(Ne^{20})$ Vapor pressure[a]	$S(Ne^{22})-S(Ne^{20})$ Heat capacity[b]	Δ
20.0	0.151 eu	0.160 eu	0.009
24.2	0.175	0.188	0.013
26.0	0.208	0.226	0.018

[a] This research.
[b] Data of Clusius *et al.*[5]

The reduced partition function ratio f_c is related to the vapor-pressure ratio by Eq. (13). The comparison with the entropy difference from calorimetric measurements thus implicitly assumes the validity of the Sackur-Tetrode equation for an ideal monatomic gas and the third law of thermodynamics. These need hardly be questioned. The entropy comparison is given in Table IV.

The entropy comparison in the last column shows a trend with the temperature. Nevertheless, the deviation of the entropy difference from vapor pressure measurements from those from thermal measurements is within the precision of the latter. The maximum discrepancy 0.02 eu would mean an error of 10% in $\partial\ln f_c/\partial T$. This corresponds to an accuracy of one per cent in the logarithm of the vapor-pressure ratio. The scatter in the third law comparison of the entropy difference given by Clusius *et al.* using the vapor-pressure data of Keesom and Haantjes is significantly reduced by the use of our vapor-pressure measurements.

ACKNOWLEDGMENTS

It is a pleasure to thank Dr. G. R. Grove of the Mound Laboratory for making the enriched samples of Ne^{20} and Ne^{22} available to us. We also thank R. Rohrbach and A. P. Schlafke for a generous supply of liquid hydrogen. Finally, Dr. Lewis Friedman kindly assisted with some of the experimental measurements for the period when one of us (J.B.) was called away from the Laboratory.

Note on the Separability Theorem for Electron Pairs*

PER-OLOV LÖWDIN

Quantum Chemistry Group for Research in Atomic, Molecular and Solid-State Theory, Uppsala University, Uppsala, Sweden

and

Quantum Theory Project, Departments of Physics and Chemistry, University of Florida, Gainesville, Florida

(Received December 12, 1960)

It is shown that, if two functions $\Lambda_A(1, 2, 3, \cdots p)$ and $\Lambda_B(1, 2', 3', \cdots q')$ describing two groups A and B of electrons are orthogonal with respect to electron 1 then there exists a complete orthonormal set of one-electron functions $\phi_k(1)$ such that the functions actually occurring with nonvanishing coefficients in the expansion of one of the functions cannot simultaneously occur in the expansion of the other function. This is a generalization of a separation theorem recently found by Arai.

I. INTRODUCTION

IN the independent-particle model, the properties of a molecular system are studied by means of a basis consisting of one-electron functions or spin orbitals. Since the covalent boad in chemistry is associated with an electron pair, one has also investigated the possibility of constructing the total wave functions by means of *two-electron functions*.[1] In this way, one obtains a picture of the total molecule corresponding to its actual chemical bonds, and this approach has also practically turned out to be very useful.[2] In other cases, it may seem more convenient to consider the molecule as built up of larger "groups" of electrons[3] and to introduce a basis consisting of functions of several electron coordinates. The method of "atoms in molecules" belongs ultimately to this type of theory.[4]

In the electron-pair theory, considerable simplifications are obtained in the calculations by assuming that the two-electron functions are not only orthogonal in the two-electron space but also with respect to each one of the electronic coordinates. Recently Arai[5] has shown that, if the two-electron functions are antisymmetric, the assumption of "strong orthogonality" leads to an important separation theorem. The purpose of the present little note is to show that by extending Arai's arguments, one can remove the symmetry conditions and further generalize the theorem to groups of electrons.

II. SEPARATION THEOREM FOR ONE-ELECTRON FUNCTIONS

For an orientation, let us start by considering two quadratically integrable and normalized functions $A(x)$ and $B(x)$ of one electron coordinate x which are orthogonal so that

$$\int A^*(x)B(x)dx=0.$$

Introducing a complete orthonormal set $\{\psi_k(x)\}$ we obtain in mean

$$A(x)\sim\sum_k \psi_k(x)A_k, \tag{1}$$

$$B(x)\sim\sum_k \psi_k(x)B_k, \tag{2}$$

where the Fourier coefficients A_k and B_k are given by the relations

$$A_k=\int \psi_k^*(x)A(x)dx$$

and

$$B_k=\int \psi_k^*(x)B(x)dx.$$

From the completeness of the set $\{\psi_k(x)\}$ follows according to Parseval's second relation that

$$\int A(x)B(x)dx=\sum_k A_k^*B_k. \tag{3}$$

Orthogonality between $A(x)$ and $B(x)$ implies hence in general that the total sum $\sum_k A_k^*B_k$ is vanishing, but we will now also prove that there exists at least one representation in which *every term* in this series is vanishing, so that the Fourier coefficients of A and B are never simultaneously nonvanishing.

For this purpose, we will introduce the two column vectors $\mathbf{A}=\{A_k\}$ and $\mathbf{B}=\{B_k\}$. The orthogonality

* Sponsored in part by the King Gustaf VI Adolf's 70-Years Fund for Swedish Culture, Knut and Alice Wallenberg's Foundation, The Swedish Natural Science Research Council, and in part by the Aeronautical Research Laboratories, Wright Air Development Division of the Air Research and Development Command, U. S. Air Force, through its European Office under a contract with Uppsala University.

[1] A. C. Hurley, J. Lennard-Jones, and J. A. Pople, Proc. Roy. Soc. (London) **A220,** 446 (1953).

[2] L. A. Schmid, Phys. Rev. **92,** 1373 (1953); R. G. Parr, F. O. Ellison, and P. G. Lykos, J. Chem. Phys. **24,** 1106 (1956); J. M. Parks and R. G. Parr, *ibid.* **28,** 335 (1958); R. McWeeny and K. A. Ohno, Proc. Roy. Soc. (London) **A225,** 367 (1960); and several other papers.

[3] R. McWeeny, Proc. Roy. Soc. (London) **A253,** 242 (1959); Revs. Modern Phys. **32,** 335 (1960).

[4] For references, see, e.g., T. Arai, Revs. Modern Phys. **32,** 370 (1960).

[5] T. Arai, Technical Report No. 43 from The Uppsala Quantum Chemistry Group; J. Chem. Phys. **33,** 95 (1960).

relation can then be written

$$\mathbf{A}^\dagger\mathbf{B}=\sum_k A_k^*B_k=0. \tag{4}$$

Let us further define a new representation $\{\phi_k\}$ obtained from the old representation $\{\psi_k\}$ by a unitary transformation $\mathbf{U}$, so that $\phi_k(x)=\sum_\alpha\psi_\alpha(x)U_{\alpha k}$ or $\boldsymbol{\phi}=\boldsymbol{\psi}\mathbf{U}$. The Fourier coefficients of $A(x)$ and $B(x)$ in the new representation are now given by the components α_k and β_k, respectively, in the column matrices

$$\boldsymbol{\alpha}=\mathbf{U}^\dagger\mathbf{A}, \qquad \boldsymbol{\beta}=\mathbf{U}^\dagger\mathbf{B}, \tag{5}$$

and, for the scalar product, one obtains $\mathbf{A}^\dagger\mathbf{B}=\boldsymbol{\alpha}^\dagger\boldsymbol{\beta}=\sum_k\alpha_k^*\beta_k=0$. One can now easily arrange so that every term in the last sum vanishes, for instance by choosing such a unitary transformation $\mathbf{U}$ that makes $\phi_1(x)=A(x)$, and the remaining functions of the set orthogonal. In this representation $\alpha_1=1$, $\alpha_2=\alpha_3=\cdots=0$, whereas $\beta_1=0$, which proves the theorem. This result is trivial, of course.

In order to generalize this result, we will consider the matrix $\mathbf{C}=\mathbf{A}\mathbf{A}^\dagger$ which is the projection matrix with respect to the axis along the vector $\mathbf{A}$ and which fulfills the relations $\mathbf{C}^\dagger=\mathbf{C}$, $\mathbf{C}^2=\mathbf{C}$, $\mathbf{C}\mathbf{A}=\mathbf{A}$, and $\mathbf{C}\mathbf{B}=0$. Now let $\mathbf{U}$ be a unitary transformation which brings the Hermitean matrix $\mathbf{C}$ to diagonal form

$$\mathbf{U}^\dagger\mathbf{C}\mathbf{U}=\mathbf{D}=\text{ diagonal matrix.} \tag{6}$$

Since $\mathbf{D}=\mathbf{U}^\dagger\mathbf{A}\mathbf{A}^\dagger\mathbf{U}=\boldsymbol{\alpha}\boldsymbol{\alpha}^\dagger$, one obtains particularly $D_{kk}=|\alpha_k|^2$. Multiplying the relation $\boldsymbol{\alpha}^\dagger\boldsymbol{\beta}=0$ to the left by $\boldsymbol{\alpha}$, we get $\mathbf{D}\boldsymbol{\beta}=0$ and for the kth component

$$(\mathbf{D}\boldsymbol{\beta})_k=D_{kk}\beta_k=|\alpha_k|^2\beta_k=0, \tag{7}$$

i.e.,

$$\alpha_k^*\beta_k=0. \tag{8}$$

The result is the same as before, but the formalism is such that it can be extended to many-electron functions too, and then the theorem is no longer trivial.

III. SEPARATION THEOREM FOR ELECTRON GROUPS

Let us consider two quadratically integrable p-electron functions $\Lambda_A=\Lambda_A(1, 2, 3, \cdots p)$ and $\Lambda_B=\Lambda_B(1, 2, 3, \cdots p)$ describing two groups of electrons A and B. Without imposing any symmetry conditions, we will assume that the two functions are orthogonal with respect to one of the electronic coordinates, say 1,

$$\int\Lambda_A^*(1, 2, 3, \cdots p)\Lambda_B(1, 2', 3', \cdots p')dx_1=0. \tag{9}$$

In order to study the consequences of this theorem, we will introduce a complete orthonormal one-electron set $\boldsymbol{\psi}(1)=\{\psi_k(1)\}$ satisfying the relation $\boldsymbol{\psi}^\dagger\boldsymbol{\psi}=\mathbf{1}$ for describing electron 1, and another complete set $\boldsymbol{\Phi}(2, 3, \cdots p)=\{\Phi_K(2, 3, \cdots p)\}$ for describing the remaining $(p-1)$ electrons. For the sake of simplicity, we will first assume that the expansion theorem is valid so that

$$\Lambda_A(1, 2, 3, \cdots p)=\sum_{kK}\psi_k(1)A_{kK}\Phi_K(2, 3, \cdots p)$$

$$=\boldsymbol{\psi}(1)\mathbf{A}\boldsymbol{\Phi}(2, 3, \cdots p), \tag{10}$$

$$\Lambda_B(1, 2', 3', \cdots p')=\sum_{lL}\psi_l(1)B_{lL}\Phi_L(2', 3', \cdots p')$$

$$=\boldsymbol{\psi}(1)\mathbf{B}\boldsymbol{\Phi}(2', 3', \cdots p'), \tag{11}$$

where $\mathbf{A}=\{A_{kK}\}$ and $\mathbf{B}=\{B_{lL}\}$ are the "rectangular" *matrices* of the expansion coefficients. Substitution into (9) leads to the relation

$$\int\Lambda_A^*(1, 2, 3, \cdots p)\Lambda_B(1, 2', 3', \cdots p')dx_1$$

$$=\boldsymbol{\Phi}^\dagger(2, 3, \cdots p)\mathbf{A}^\dagger[\boldsymbol{\psi}^\dagger(1)\boldsymbol{\psi}(1)]\mathbf{B}\boldsymbol{\Phi}(2', 3', \cdots p')$$

$$=\boldsymbol{\Phi}^\dagger(2, 3, \cdots p)\mathbf{A}^\dagger\mathbf{B}\boldsymbol{\Phi}(2', 3', \cdots p')=0, \tag{12}$$

i.e.,

$$\mathbf{A}^\dagger\mathbf{B}=\mathbf{0}. \tag{13}$$

Instead of the basic set $\{\psi_k\}$ we will now also introduce a basis $\{\phi_k\}$ defined by the relation $\boldsymbol{\phi}=\boldsymbol{\psi}\mathbf{U}$. Substituting $\boldsymbol{\psi}=\boldsymbol{\phi}\mathbf{U}^\dagger$ into (10) and (11), we obtain

$$\Lambda_A(1, 2, 3, \cdots p)=\boldsymbol{\phi}(1)\boldsymbol{\alpha}\boldsymbol{\Phi}(2, 3, \cdots p), \tag{14}$$

$$\Lambda_B(1, 2', 3', \cdots p')=\boldsymbol{\phi}(1)\boldsymbol{\beta}\boldsymbol{\Phi}(2', 3', \cdots p'), \tag{15}$$

or

$$\Lambda_A(1, 2, 3, \cdots p)=\sum_{kK}\phi_k(1)\alpha_{kK}\Phi_K(2, 3, \cdots p), \tag{16}$$

$$\Lambda_B(1, 2', 3', \cdots p')=\sum_{kL}\phi_k(1)\beta_{kL}\Phi_L(2', 3', \cdots p'), \tag{17}$$

where the coefficient matrices $\boldsymbol{\alpha}$ and $\boldsymbol{\beta}$ are given by the relations

$$\boldsymbol{\alpha}=\mathbf{U}^\dagger\mathbf{A}, \qquad \boldsymbol{\beta}=\mathbf{U}^\dagger\mathbf{B}. \tag{18}$$

Instead of (13), we obtain $\boldsymbol{\alpha}^\dagger\boldsymbol{\beta}=\mathbf{0}$ and for the (KL) component,

$$(\boldsymbol{\alpha}^\dagger\boldsymbol{\beta})_{KL}=\sum_k\alpha_{kK}^*\beta_{kL}=0. \tag{19}$$

We will now prove that there exists at least one representation, in which not only the total sum in (19) but also every term separately vanishes, so that $\alpha_{kK}^*\beta_{kL}=0$ for all pairs (K, L).

As in the preceding section, we will consider the Hermitean matrix $\mathbf{C}=\mathbf{A}\mathbf{A}^\dagger$ which is now related to a projection matrix of a more complicated character. For our purpose, it is suficient to note that we may choose our unitary transformation $\mathbf{U}$, so that it brings $\mathbf{C}$ to diagonal form $\mathbf{D}$ so that

$$\mathbf{U}^\dagger\mathbf{C}\mathbf{U}=\mathbf{D}=\text{ diagonal matrix.} \tag{20}$$

Since $\mathbf{D}=\mathbf{U}^\dagger\mathbf{A}\mathbf{A}^\dagger\mathbf{U}=\boldsymbol{\alpha}\boldsymbol{\alpha}^\dagger$ one obtains particularly,

$$D_{kk}=\sum_K\alpha_{kK}\alpha_{Kk}^\dagger=\sum_K|\alpha_{kK}|^2\geq 0, \tag{21}$$

where the last equality sign holds if, and only if, $\alpha_{kK}=0$ for *all* K. By multiplying the relation $\boldsymbol{\alpha}^\dagger\boldsymbol{\beta}=\mathbf{0}$ to the left by $\boldsymbol{\alpha}$, we obtain $\mathbf{D\beta}=\mathbf{0}$ and for the (kL) component,

$$(\mathbf{D\beta})_{kL}=D_{kk}\beta_{kL}=\{\sum_K|\alpha_{kK}|^2\}\beta_{kL}=0, \tag{22}$$

which is a direct generalization of (7). This leads to the separation theorem desired.

Let us consider a fixed index k. Relation (22) implies that, if a single α_{kK} is different from zero, then $D_{kk}\neq 0$ and $\beta_{kL}=0$ for all L. If on the other hand, a single β_{kL} is different from zero, then $D_{kk}=0$ and $\alpha_{kK}=0$ for all K. Hence, *the coefficients* α_{kK} *and* β_{kL} *cannot simultaneously be nonvanishing*. This means that, in the speccial representation chosen here, every term in the sum in (19) vanishes separately. It implies also that, if a particular function $\phi_k(1)$ occurs with a nonvanishing coefficient in one of the expansions (16) and (17), it cannot occur in the other expansion. For every index k, one has hence two functions

$$\sum_K\alpha_{kK}\Phi_K(2,3,\cdots p) \quad\text{and}\quad \sum_L\beta_{kL}\Phi_L(2,3,\cdots p), \tag{23}$$

of which at least one is *vanishing identically* for all values of the coordinates $2, 3, \cdots p$.

This is the generalized form of Arai's separation theorem, and we note that it is easily extended to several groups A, B, C, D, $\cdots$ of electrons. In the proof, we have not changed the functions $\Phi_K(2,3,\cdots p)$ describing the electrons $2, 3, \cdots p$ at all, and one could actually proceed without such an explicit representation. We note further that, if so desired, the groups may contain different numbers of electrons without essentially changing the proof itself.

In concluding this section, we would like to remark on the consequencies of symmetry properties. Let us say that the two functions $\Lambda_A(1,2,3,\cdots p)$ and $\Lambda_B(1,2,3,\cdots q)$ are *antisymmetric* in all their electron coordinates. According to a well-known theorem,[6] they can be expanded in terms of Slater determinants built up from the complete set of one-electron functions $\{\psi_k(x)\}$. From the strong orthogonality (9) with respect to a single electron coordinate it now follows that there exists at least one representation $\{\phi_k(x)\}$ in which the separation theorem is valid. This implies that the set $\{\phi_k(x)\}$ may be divided into two parts (A) and (B) such that all Slater determinants in $\Lambda_A(1,2,3,\cdots p)$ are built up only from functions in (A), whereas all Slater determinants in $\Lambda_B(1,2,3,\cdots q)$ are built up solely from functions in (B). The theorem may be directly extended to several functions Λ_A, Λ_B, Λ_C, $\cdots$. A similar theorem holds for totally symmetric functions in their expansion in terms of permanents instead of determinants.

[6] See e.g., P. O. Löwdin, Phys. Rev. **97**, 1474 (1955), particularly p. 1478.

IV. SPECIAL CASE INVOLVING PAIR FUNCTION

Let us now consider the special case when the group A contains only two electrons. Assuming that the corresponding function $\Lambda_A(1,2)$ is real and either symmetric or antisymmetric, we will now study the simplifications obtained by expressing Λ_A in terms of *natural* orbitals[7] or one-electron functions in general. Choosing $\boldsymbol{\Phi}(2)=\boldsymbol{\psi}^\dagger(2)$, we obtain instead of (10),

$$\Lambda_A(1,2)=\boldsymbol{\psi}(1)\mathbf{A}\boldsymbol{\psi}^\dagger(2)=\sum_{kK}\psi_k(1)A_{kK}\psi_K^*(2). \tag{24}$$

In the symmetric and antisymmetric case, one obtains $\mathbf{A}^\dagger=\mathbf{A}$ and $\mathbf{A}^\dagger=-\mathbf{A}$, respectively, i.e., $\mathbf{A}$ is either Hermitean or anti-Hermitean and, in both cases, it can be brought to diagonal form $\mathbf{a}$ by a unitary transform $\mathbf{V}$ so that

$$\mathbf{V}^\dagger\mathbf{A}\mathbf{V}=\mathbf{a}. \tag{25}$$

In the symmetric case, the diagonal elements a_{kk} are real, whereas, in the antisymmetric case, they are pure imaginary numbers. For the details of the transformation, we would like to refer to the work cited in reference 7. Introducing the natural orbitals χ_k by the relation $\boldsymbol{\chi}=\boldsymbol{\psi}\mathbf{V}$, we obtain

$$\Lambda_A(1,2)=\boldsymbol{\chi}(1)\mathbf{a}\boldsymbol{\chi}^\dagger(2)=\sum_k\chi_k(1)a_{kk}\chi_k^*(2), \tag{26}$$

which is the "natural expansion" of the pair-function Λ_A.

Let us now further assume that Λ_A is orthogonal against a function $\Lambda_B(1,2,3,\cdots p)$ describing a group B containing p electrons in the sense of relation (9),

$$\int\Lambda_A^*(1,2)\Lambda_B(1,2',3',\cdots p')dx_1=0. \tag{27}$$

Starting from the original form of Λ_A, we obtain $\mathbf{C}=\mathbf{A}\mathbf{A}^\dagger$, $\mathbf{U}=\mathbf{V}$, $\mathbf{D}=\mathbf{a}\mathbf{a}^\dagger$, and $\boldsymbol{\phi}=\boldsymbol{\chi}$, i.e., the natural orbitals of Λ_A will occur in the separation theorem. The result implies that if all natural orbitals associated with the group A are actually occupied, i.e., $a_k\neq 0$ for all k, then (16) leads to $\Lambda_B\equiv 0$. If on the other hand, the occupied natural orbitals of A span only a subspace (A) of the total one-electron Hilbert space, then there is a relation of the type (16), if and only if the functions $\phi_k(1)$ occurring with nonvanishing coefficients in the expansion (12) of Λ_B belong to the complementary orthogonal subspace to (A).

In conclusion, we will consider two real pair functions Λ_A and Λ_B, each one having a basic symmetry property, which fulfill relation (9) for $p=2$. Since we can start our discussion with any one of the two functions, we are directly led to the following theorem: the natural orbitals of Λ_A and Λ_B, respectively, which are actually

[7] P. O. Löwdin and H. Shull, Phys. Rev. **101**, 1730 (1956); H. Shull and P. O. Löwdin, J. Chem. Phys. **30**, 617 (1959); H. Shull, *ibid.* **30**, 1405 (1959); J. Am. Chem. Soc. **82**, 1287 (1960).

occupied, span two subspaces (A) and (B) which are mutually orthogonal. The theorem can directly be generalized to several pair functions Λ_A, Λ_B, Λ_C, ····.

V. DISCUSSION

In this little note, we have studied the consequences of the assumption of strong orthogonality of type (9). This assumption is introduced in the theory of molecules based on electron pairs and electron groups[1–4] mainly to render considerable simplifications in the calculations, and whether the assumption is really physically and chemically justified remains to be more thoroughly investigated. It is, of course, particularly important to find out how the assumption could be fitted into a rigorous mathematical theory based on the Schrödinger equation. The results obtained so far make plausible, however, that this type of approach may be quite useful both for practical applications and for studying the connection between the concepts in chemistry and in molecular quantum mechanics.

THE JOURNAL OF CHEMICAL PHYSICS VOLUME 35, NUMBER 1 JULY, 1961

Self-Diffusion and Velocity Correlation

DEAN C. DOUGLASS

Bell Telephone Laboratories, Inc., Murray Hill, New Jersey

(Received December 8, 1960)

Approximate expressions for the self-diffusion coefficients of spherical molecules in solid, liquid, and gas phases are obtained from the relation

$$D=(kT/m)\int_0^\infty \rho(s)ds,$$

where D is the diffusion coefficient and $\rho(s)$ is the velocity correlation function of the spherical molecules. The correlation function is approximated by the function $\cos\alpha\delta s/\cosh\alpha s$ and the parameters α and δ are expressed in terms of molecular properties for liquids and gases. The approximate diffusion coefficient is found to obey an Arrhenius relation in the solid phase and a Sutherland equation for the gas phase. The results of a crude calculation of the self-diffusion coefficient for liquid neopentane are within a factor of two of the experimental diffusion coefficients. The temperature coefficient of the calculated diffusion coefficients is also within a factor of two of the observed temperature coefficient.

INTRODUCTION

THE mechanisms of molecular diffusion in gases and solids can be readily visualized and analyzed in terms of simple physical models. In gases the phenomenon is treated in terms of trajectories and binary collisions of molecules. In solids molecules are viewed as diffusing via a series of jumps through energy barriers into neighboring vacancies. Superficially these models appear to have little in common and attempts to extend either model to the intermediate state of matter, i.e., liquids, usually result in a model of liquid diffusion which must be classified as either solidlike or gaslike, rather than as an appropriate hybrid of the two. The purpose of this paper is to present an approach to the calculation of diffusion coefficients which appears applicable to both solids and gases and does not impose either solidlike or gaslike restrictions on the liquid phase, but instead treats liquids as a state intermediate in its properties between solids and gases.

This approach begins with the quite general relation

$$D=(kT/m)\int_0^\infty \rho(s)ds, \tag{1}$$

where $\rho(s)$ is the momentum correlation function and is defined by the relation

$$\rho(s)=\langle \mathbf{p}(0)\cdot\mathbf{p}(s)\rangle/\langle \mathbf{p}^2\rangle, \tag{2}$$

where the brackets indicate an ensemble average.[1] Obtaining a rigorous $\rho(s)$ is of course an insurmountable task except for exceedingly simple and, for our purposes, unrealistic models of molecular motion; therefore, the immediate concern of this theory is to find an appropriate approximation to $\rho(s)$. A number of qualitative features of $\rho(s)$ are known which certainly should not be ignored and should, if possible, be used. First, $\rho(0)=1$ and $d\rho/ds=0$ at $s=0$. Second, $\rho(s)$ is an even function of s. Third, in an ideal solid (by this we mean an Einstein model lattice in which the center of mass of all molecules oscillate at one frequency), $\rho(s)\cong\cos\omega s$. Fourth, in any real system we shall desire that $\rho(s)\to 0$ for large s and finally for high temperature and large s the correlation function should become characteristic of a Gaussian process, i.e., $\rho(s)\to\exp(-s/\tau)$. It is certainly true that there is a large set of functions

[1] H. C. Longuet-Higgins and J. A. Pople, J. Chem. Phys. **25**, 884 (1956).

which satisfy these requirements. It is also true that because of the nature of the integration process a large part of this set of functions, when integrated and substituted in Eq. (1), gives almost the same diffusion coefficient. Therefore it is the procedure in this paper to adopt a convenient functional form for $\rho(s)$ which contains the required qualitative features. The functional form adopted for this purpose is the two parameter function

$$\rho(s) = \cos\alpha\delta s/\cosh\alpha s. \tag{3}$$

The parameter α determines the rate of decay and δ gives the rate of osillation relative to the time scale determined by α. The diffusion coefficient, in terms of α and δ, is given by substituting Eq. (3) into (1) to obtain

$$D=(\pi kT/\alpha m)\ \mathrm{sech}(\pi\delta/2). \tag{4}$$

It is clear that $|\delta|\gg 1$ corresponds to the solid-state behavior. In order to evaluate α and δ in terms of the mechanical properties of the system, expressions (3) and (2) for the correlation function are expanded in power series in s. Comparison of the first three terms of the two expansions gives α and δ in terms of statistical averages. Demonstration that the chosen $\rho(s)$ is an appropriate approximation and that the expansion procedure is valid rests entirely on the results obtained from the procedure.

The next section of this paper expresses the parameters α and δ in terms of statistical averages. In the third section we derive an expression for a diffusion coefficient calculated by using approximations similar to those used in the jump model for diffusion in solids. It is found that the diffusion coefficient follows an Arrhenius-type relation in agreement with experiment. The fourth section presents an expression for a diffusion coefficient obtained by the procedure outlined above but with approximations similar to those used in the kinetic theory of gases. The results obtained by this method are in agreement with kinetic theory results. Having shown that limiting cases are satisfactory, the fifth section of the paper gives expressions for the self-diffusion coefficient of a simple fluid without approximations characteristic of either a solid or of a gas. The expression obtained in this section may, in a sense, be regarded as an extension of the Kirkwood expression for diffusion in a fluid.[2,3] The last section presents an attempt to apply these results to diffusion in liquid neopentane.

EXPRESSIONS FOR THE PARAMETERS α AND δ

A power series expansion of $\rho(s)$ about $s=0$ has the form

$$\rho(s)=1+a_1s+a_2s^2+a_3s^3+a_4s^4.$$

Since $\rho(s)$ is an even function of s, $a_1=a_3=0$. Using the relation

$$\mathbf{p}(s) = \exp\{[H, \mathbf{p}]s\}\mathbf{p}(0),$$

where $[H, \mathbf{p}]$ is the Poisson bracket operator[4] and $\mathbf{p}(0)$ is the momentum of a particle at zero time, one may expand $\rho(s)$ in Eq. (2) to obtain

$$\rho(s)=1-\langle(\dot{p})^2\rangle s^2/2!\langle p^2\rangle+\langle(\ddot{p})^2\rangle s^4/4!\langle p^2\rangle+\cdots,$$

where dots mean time derivatives. Thus,

$$a_2=-\langle(\dot{p})^2\rangle/2!\langle p^2\rangle$$
$$a_4=\langle(\ddot{p})^2\rangle/4!\langle p^2\rangle. \tag{5}$$

Similarly, expansion of $\rho(s)$ in Eq. (3) gives

$$a_2=-(1+\delta^2)\alpha^2/2!$$
$$a_4=(5+6\delta^2+\delta^4)\alpha^4/4!. \tag{6}$$

Therefore α and δ may be determined from the ensemble averages of Eq.(5). As one might suspect, δ is entirely determined by the ratio

$$C=6a_4/a_2^2=\langle p^2\rangle\langle(\ddot{p})^2\rangle/\langle(\dot{p})^2\rangle^2 \tag{7}$$

so that

$$\delta^2=(5-C)/(C-1). \tag{8}$$

The parameter α is given by

$$\alpha^2=3[C-1]\langle(\dot{p})^2\rangle/12\langle p^2\rangle. \tag{9}$$

The averaging process indicated many be carried out on several levels of accuracy. If the functional form of D is desired it is generally necessary to sacrifice accuracy and use a simple mechanical model of the system under consideration. If no simple model exists, or greater accuracy is desired, one must frequently resort to a procedure which disguises the physics of the problem. The following sections illustrate each situation.

DIFFUSION IN SOLIDS

Molecules in the solid state will be regarded as residing in potential energy wells which are deep compared to kT. The potential energy arises from interaction of neighboring molecules in the crystal lattice. The lattice considered in this discussion will be assumed to contain only one kind of site. In order to approximate a real lattice it is supposed that any molecule finds itself in one of two possible situations, either it has a neighboring vacancy or it does not. For molecules which have neighboring vacancies there is a more or less unique reaction coordinate along which the representative molecule may travel through a potential energy barrier to the available vacancy. Molecules which do not have neighboring vacancies must surmount a relatively large energy barrier in order to diffuse and therefore will be ignored.

[2] D. C. Douglass, D. W. McCall, and E. W. Anderson, J. Chem. Phys. **34**, 152 (1961).
[3] H. L. Frisch and S. Rice, J. Chem. Phys. (to be published); see also S. A. Rice, *ibid.* **33**, 1376 (1960).
[4] H. Goldstein, *Classical Mechanics* (Addison-Wesley Publishing Company, Inc., Reading, Massachusetts, 1951), p. 256.

Assuming that we may write a one-particle Hamiltonian for a representative molecule with a neighboring vacancy as

$$H=(p^2/2m)+f(x), \tag{10}$$

where $f(x)$ is the potential energy along the reaction coordinate we may proceed to evaluate $\langle(\dot{p})^2\rangle$ and $\langle(\ddot{p})^2\rangle$. Since

$$\dot{p}=-\partial H/\partial x=-df(x)/dx=-f'(x)$$

$$\langle(\dot{p})^2\rangle=\langle(f'(x))^2\rangle=\int f'^2\exp(-f/kT)dx \Big/ \int \exp(-f/kT)dx.$$

Integration once by parts gives

$$\langle(\ddot{p})^2\rangle=\{-kTf'\exp(-f/kT)\,|+kT\int f''\exp(-f/kT)dx\} \Big/ \int \exp(-f/kT)dx. \tag{11}$$

It is now presumed that the limits of integration are so chosen that the first term on the right-hand side of Eq. (11) is zero. Then

$$\langle(\dot{p})^2\rangle=kT\int f''\exp(-f/kT)dx \Big/ \int \exp(-f/kT)dx. \tag{12}$$

Using the relation

$$\ddot{p}=[H,\dot{p}]=-(p/m)f''(x),$$

one may obtain a similar expression for $\langle(\ddot{p})^2\rangle$,

$$\langle(\ddot{p})^2\rangle=(kT/m)\langle(f''(x))^2\rangle$$

$$\langle(\ddot{p})^2\rangle=(kT/m)\int f''^2\exp(-f/kT)dx \Big/ \int \exp(-f/kT)dx. \tag{13}$$

For convenience we shall write $f(x)/kT=bu(x)$ where $u(x)$ is chosen so that b is the ratio of the potential energy well depth ΔU to kT. The model assumes that b is a large number so we may use this information in approximating the integrals occurring in Eqs. (12) and (13). Consider first the integral

$$\int f''\exp(-f/kT)dx=bkT\int u''\exp(-bu)dx$$

$$\int f''\exp(-f/kT)dx=bkT\int \exp[h(x)]dx,$$

where

$$h(x)=\ln u''-bu.$$

The major contribution to this integral occurs near the maximum of $h(x)$. Therefore the integral will be approximated by expanding $h(x)$ about the maximum point x_0 and keeping only enough terms to get a nontrivial result. It is further assumed that the potential well is almost symmetrical about x_0, and, worst of all, that the expansion is sufficiently accurate to represent the potential energy function up to the maximum in the barrier. This last point must be kept in mind when we eventually consider particular functional forms for $u(x)$ or $f(x)$. Carrying out the suggested expansion gives

$$\int f''\exp(-f/kT)dx\cong f''(x_0)\exp[-bu(x_0)]\int_{-\infty}^{\infty}\exp\{(\epsilon^2/2)[u''''(x_0)/u''(x_0)-bu(x_0)]\}d\epsilon,$$

and integration gives

$$\int f''\exp(-f/kT)dx\cong 2(2\pi)^{\frac{1}{2}}f''(x_0)\exp[-bu(x_0)][bu''(x_0)-u''''(x_0)/u''(x_0)]^{-\frac{1}{2}}. \tag{14}$$

In an exactly analogous manner

$$\int (f'')^2 \exp(-f/kT)dx \cong (2\pi)^{\frac{1}{2}}[f''(x_0)]^2 \exp[-bu(x_0)][bu''(x_0)-2u''''(x_0)/u''(x_0)]^{-\frac{1}{2}} \tag{15}$$

and

$$\int \exp(-f/kT)dx \cong (2\pi)^{\frac{1}{2}} \exp[-bu(x_0)][u''(x_0)]^{-\frac{1}{2}}. \tag{16}$$

Substituting Eqs. (14)–(16) into Eqs. (12) and (13) we find expressions for $\langle(\dot{p})^2\rangle$ and $\langle(\ddot{p})^2\rangle$. These may in turn be substituted into Eq. (7) to obtain $C=6a_4/a_2^2$;

$$C=\{1-u''''(x_0)/b[u''(x_0)]^2\}/\{1-2u''''(x_0)/b[u''(x_0)]^2\}^{\frac{1}{2}}.$$

In keeping with previous approximations this expression is expanded in a power series in $1/b$ so that

$$C \cong \{1+\{u''''(x_0)/[u''(x_0)]^2\}^2(\tfrac{1}{2}b^2)\}.$$

Use of Eqs. (8) and (9) gives the relatively simple expressions for α and δ,

$$\delta \cong (8)^{\frac{1}{2}}[u''(x_0)]^2 b/u''''(x_0)$$

and

$$\alpha^2 \cong (kT/8bm)[u''''(x_0)]^2/[u''(x_0)]^3.$$

Finally the diffusion coefficient is obtained from Eq. (4) as

$$D=D_0 \exp(-L\Delta U/kT), \tag{17}$$

where

$$D_0=(4C_h\pi/3)(\Delta U/2m)^{\frac{1}{2}}\{[u''(x_0)]^{\frac{3}{2}}/|u''''(x_0)|\}$$

$$L=\pi\sqrt{2}[u''(x_0)]^2/|u''''(x_0)|,$$

and C_h is the fraction of molecules with neighboring vacancies. One feature of the diffusion process which appears in a natural way in this expression is the necessity for appropriate anharmonic terms in the potential energy in order that a molecule may exchange energy with the remainder of the lattice. That is to say, if $u''''(x_0)$ is zero, as in the case of a truly harmonic oscillator, there is no diffusion. The action of the anharmonic terms in the potential energy is equivalent to a number of soft inelastic collisions of a vibrating molecule with its neighbors. Since the parameter δ gives the number of vibrations a molecule makes before the coherence of its oscillations is noticeably destroyed, it gives a measure of the effectiveness of these inelastic collisions in transferring energy to or away from a typical molecule. It is perhaps worth noting in passing that by neglecting 1 compared to δ^2

$$\alpha\delta=[u''(x_0)\Delta U/m]^{\frac{1}{2}}=(f''(x_0)/m)^{\frac{1}{2}}$$

$$\alpha\delta=(\text{force constant}/m)^{\frac{1}{2}}=\omega,$$

as one should anticipate.

There is a limited number of potential functions which will allow the approximations used in this section. However,

$$u(x)=-(\tfrac{1}{2})\cos(2\pi x/a_0)$$

is a potential which meets the requirements. In this case Eq. (17) becomes

$$D=(a_0^2\omega C_h/3\pi\sqrt{2})\exp(-\pi\Delta U/\sqrt{2}kT). \tag{18}$$

The quantity usually called the activation energy appears in this expression as about twice the potential well depth rather than just the well depth as in transition state theory.[5] Analogs of Eq. (18) obtained from similar but different correlation functions and with slight variations of $u(x)$ also contain this discrepancy. The origin of this factor may well lie in the choice of $\rho(s)$ or in other approximations used. While it is true that the models used for this calculation and for transition state theory are very similar, the calculation based on the velocity correlation function has more in common with kinetic theory than it has with transition state theory. In particular, the assumption that energy states near the top of the energy barrier have equilibrium populations does not appear in this approach. The idea of "collisions" with the lattice seems to give a more natural interpretation of the result obtained here. In any event, neither ΔU nor ΔH of transition state theory is well enough defined to be calculated. Furthermore, the two cases are experimentally indistinguishable.

If one does not resort to the model used in this section but instead expressed $\langle(\dot{p})^2\rangle$ and $\langle(\ddot{p})^2\rangle$ in terms of radial distribution functions and an intermolecuoar potential, one can obtain explicit but complicated expressions for the parameters α and δ so that in principle one could compare these results with experimental results. This procedure will, of necessity, be demonstrated in the section on diffusion in liquids. However, such advanced considerations are hardly warranted for the approximate correlation function considered here. If such calculations were of interest one would, at the very least, want to use a Debye distribution of normal modes rather than the single lattice frequency used here. In this case one could use a correlation function appropriate to a distribution of damped normal lattice oscillations. These comments also apply to the treatment of dense fluids.

[5] S. Glasstone, K. J. Laidler, and H. Eyring, *Theory of Rate Processes* (McGraw-Hill Book Company, Inc., New York, 1941).

DIFFUSION IN LOW-DENSITY, HIGH-TEMPERATURE FLUIDS

The high-temperature behavior of the approximate correlation function may be examined in terms of the high-temperature behavior of the parameters α and δ. In order to examine δ, it is convenient to first observe that Eq. (8) gives δ^2 in terms of C where

$$C=\langle p^2\rangle\langle(\dot{p})^2\rangle/\langle(\dot{p})^2\rangle^2.$$

It will be made clear in the next section that $\langle(\dot{p})^2\rangle$ increases with increasing temperature and that $\langle(\dot{p})^2\rangle$ becomes independent of temperature at high temperatures; therefore C increases with increasing temperature. By Eq. (8) δ^2 is negative beyond the temperature and density at which $C=5$ and δ^2 approaches -1 as C becomes very large. The same line of reasoning and the use of Eq. (9) shows that α^2 remains positive and increases somewhat as temperature increases. Therefore, above the temperature at which $C=5$ the correlation function $\rho(s)=\cos\alpha\delta s/\cosh\alpha s$ ceases to oscillate and decays monotonically in time. The asymptotic form of the function is

$$\rho(s)\rightarrow\exp(-2\alpha s/C),$$

as one would desire for gases. Therefore the diffusion coefficient approaches

$$D=(kT/m)(C/2\alpha)=(kT/m)\sqrt{3}a_4^{\frac{1}{2}}/(-a_2)^{\frac{1}{2}} \qquad (19)$$

at high temperature and low density.

In order to calculate a diffusion coefficient for gases based on approximations similar in content to the approximations used in kinetic theory we shall make the following assumptions. Only binary interactions are considered so that a typical molecule, say molecule (1), interacts strongly with at most one other molecule at any given time. As molecule (1) traverses some course in space it experiences periods of interaction, i.e., collisions, with other molecules. It is assumed that the molecular collisions are separated by paths which are long compared to a distance over which a collision occurs. Since the collisions are presumably unrelated we shall choose a single collision and concentrate our attention on it. The Hamiltonian of the pair of molecules under consideration is then

$$H=(p_1^2/2m)+(p_2^2/2m)+f(\mathbf{r}_{12}). \qquad (20)$$

By transforming to a center-of-mass coordinate system it is readily shown that

$$(\dot{p}_1)^2=[df(r_{12})/dr_{12}]^2=(f')^2,$$

and

$$(\ddot{p}_1)^2=(4p_{12}^2/m^2)[d^2f(r_{12})/dr_{12}^2]^2=(4p_{12}^2/m^2)(f'')^2,$$

where

$$\mathbf{p}_{12}=m\dot{\mathbf{r}}_{12}/2.$$

Therefore, from the definitions of a_2 and a_4 [Eq. (5)],

$$a_2=-\langle(f')^2\rangle/6mkT,$$

and

$$a_4=\langle(f'')^2\rangle/36m^2.$$

The diffusion coefficient, in terms of these averages, is

$$D=3\sqrt{2}(kT/m)^{\frac{1}{2}}k^2T^2\langle(f'')^2\rangle^{\frac{1}{2}}/\langle(f')^2\rangle^{\frac{1}{2}}. \qquad (21)$$

First examine the average,

$$\langle(f'')^2\rangle=(4\pi V/N)\int(f'')^2\exp(-f/kT)r_{12}^2dr_{12}\Big/\int\exp(-f/kT)d\mathbf{r}_1d\mathbf{r}_2. \qquad (22)$$

By the assumption that the mean free path is long compared to collision distance, the integral in the denominator of Eq. (22) is approximately $(V/N)^2$ so that

$$\langle(f'')^2\rangle=(4\pi N/V)\int(f'')^2\exp(-f/kT)r_{12}^2dr_{12}. \qquad (23)$$

In an analogous manner it is found that

$$\langle(f')^2\rangle=(4\pi N/V)\int(f')^2\exp(-f/kT)r_{12}^2dr_{12}. \qquad (24)$$

Rather than evaluate these integrals of Eqs. (23) and (24) for a specific potential function, we shall estimate the integrals using approximations reminiscent of the hard-sphere approximation used in kinetic theory. This is done in order to show that the results are equivalent, at very high temperature, to the results of kinetic theory.

Suppose that the potential function f has the form shown in Fig. 1. The parameter κ is taken to be very large compared to kT even though kT itself is large. From a qualitative examination of the integrals in Eqs. (23) and (24) it is clear that the major contribution to the integrals occurs in the region near the minimum in f. It is convenient at this juncture to make some substitutions. Let $r_{12}=\sigma x$, where σ is the molecular diameter, $f=\kappa u(x)$, $\kappa/kT=b$, and $V/N=kT/P$.

Equations (23) and (24) now become

$$\langle(f'')^2\rangle=(\pi\sigma^2P/kT)\,(4\kappa^2/\sigma^3)\int(u'')^2\exp(-bu)x^2dx,$$

$$\langle(f'')^2\rangle=(4\kappa^2/\sigma^3\lambda)\int(u'')^2\exp(-bu)x^2dx \tag{25}$$

and

$$\langle(f')^2\rangle=(\pi\sigma^2P/kT)\,(4\kappa^2/\sigma)\int(u')^2\exp(-bu)x^2dx,$$

$$\langle(f')^2\rangle=(4\kappa^2/\sigma\lambda)\int(u')^2\exp(-bu)x^2dx, \tag{26}$$

where λ is the mean free path of kinetic theory. Equation (26) may be integrated by parts, and using the assumption that b is exceedingly large it becomes

$$\langle(f')^2\rangle\cong(4\kappa^2/\sigma\lambda b)\int u''\exp(-bu)x^2dx.$$

Expanding the integrands about the point x_0, where u'' is maximum, again using the assumption that b is very large, and setting $x^2\approx1$, one obtains that,

$$\langle(f')^2\rangle\cong[4\kappa^2(2\pi)^{\frac{1}{2}}/\sigma\lambda b^{\frac{1}{2}}][u''(x_0)]^{\frac{1}{2}}\exp[-bu(x_0)]$$

and

$$\langle(f'')^2\rangle\cong[4\kappa^2(2\pi)^{\frac{1}{2}}/\sigma^3\lambda b^{\frac{1}{2}}][u''(x_0)]^{\frac{1}{2}}\exp[-bu(x_0)].$$

Substitution of these expressions in Eq. (21) for D gives

$$D\cong3(kT)^{\frac{1}{2}}\exp[bu(x_0)]/4(m)^{\frac{1}{2}}\pi(\pi)^{\frac{1}{2}}\sigma^2P$$

$$D\cong3(kT)^{\frac{1}{2}}\exp[f(\sigma x_0)]/4(m)^{\frac{1}{2}}\pi(\pi)^{\frac{1}{2}}\sigma^2P,$$

where $f(\sigma x_0)$ is the value of the potential at the point where the second derivative of the potential is maximum. This is, in general, just a bit beyond the minimum in the potential well so that $f(\sigma x_0)/kT=-C'/T$ is small at temperatures of interest. Therefore,

$$D\cong3(kT)^{\frac{1}{2}}/4(m)^{\frac{1}{2}}\pi(\pi)^{\frac{1}{2}}\sigma^2P(1+C'/T). \tag{27}$$

For hard spheres $C'=0$ and one obtains an expression very close to the kinetic theory result for hard spheres.[6] If $C'\neq0$ Eq. (27) is of the same form as the Sutherland equation for the diffusion coefficient of a hard-sphere gas with van der Waals attractive forces.[7] If one assumes a Lennard-Jones intermolecular potential $f=4\epsilon(x^{-12}-x^{-6})$, then

$$f(\sigma x_0)\cong4\epsilon \quad\text{and}\quad C'=(\epsilon/2\kappa).$$

Substitution of experimentally determined values of ϵ gives C' in rough agreement with the experimentally determined C parameter of the Sutherland equation.

DIFFUSION IN DENSE FLUIDS

Lacking a well-characterized model of diffusion in liquids to aid in the evaluation of the required statistical

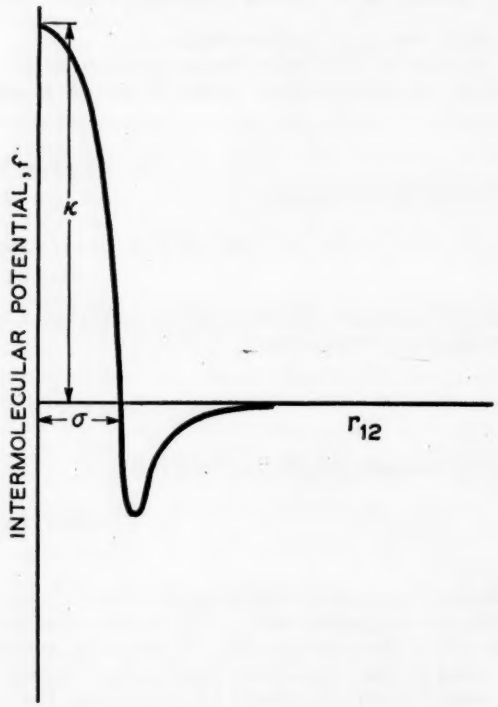

FIG. 1. The form of the intermolecular potential f which is assumed in the calculation of the self-diffusion coefficient of a gas vs intermolecular separation.

[6] J. E. Mayer and M. G. Mayer, *Statistical Mechanics* (John Wiley & Sons, Inc., New York, 1946), p. 29.

[7] E. H. Kennard, *Kinetic Theory of Gases* (McGraw-Hill Book Company, Inc., New York, 1938), p. 199.

averages we shall use a brute force attack on the problem with the hope that the results of this approach may eventually suggest a model. The method is an extension of a previous calculation.[2]

First note that because $\langle \dot{p} \cdot \ddot{p} \rangle = 0$,

$$\langle \dot{p}^2 \rangle = - \langle p \cdot \ddot{p} \rangle .$$

The time derivatives are calculated by using the relation

$$\dot{\mu} = -[H, \mu]. \tag{28}$$

If the p_i and q_i are generalized coordinates and momenta of the system this gives[4]

$$p_i \dot{p}_i = - \sum_j (p_i p_j / m) (\partial^2 V / \partial q_i \partial q_j).$$

Again taking molecule (1) as the typical molecule

$$\langle p_1 \cdot \ddot{p}_1 \rangle = -kT \langle \nabla_1^2 V \rangle .$$

Assuming that only two-body central forces are important in the system

$$V = \sum_{j>i} u_{ij}(r_{ij}).$$

Hence

$$\langle (\dot{p}_1)^2 \rangle = NkT \langle \nabla^2 u_{12} \rangle$$

$$\langle (\dot{p}_1)^2 \rangle = (NkT/V) \int_0^\infty g^{(2)}(r) \nabla^2 u 4\pi r^2 dr,$$

where $g^{(2)}(r)$ is the two-particle radial distribution function. Let $r = \sigma x$, and $u = \epsilon \gamma(x)$ where σ is the molecular diameter and $\gamma(x)$ is the dimensionless reduced potential. It follows that

$$a_2 = - (2\pi\sigma\epsilon\rho/3m) \int_0^\infty g^{(2)}(x) x^2 \nabla^2 \gamma dx,$$

where ρ is the density in molecules per unit volume. The integral on the right will be called ψ_0 so that

$$a_2 = - (2\pi\sigma\epsilon\rho\psi_0/3m). \tag{29}$$

The coefficient a_4 may be obtained in an analogous way but with somewhat more algebraic manipulation. By noting that $\langle p \cdot \ddot{p} \rangle = 0$ it is readily shown that

$$\langle (\ddot{p})^2 \rangle = - \langle \dot{p} \cdot \dddot{p} \rangle .$$

Repeated application of the relation given in Eq. (28) shows that

$$\langle (\ddot{p})^2 \rangle = - \sum_{k=1}^{3N} \sum_{j=1}^{3N} \langle (\partial^3 H / \partial q_i \partial q_j \partial q_k) \partial H / \partial q_i \rangle \langle p_k p_j / m^2 \rangle + \sum_{k=1}^{3N} (1/m) \langle (\partial^2 H / \partial q_i \partial q_k) (\partial H / \partial q_k) \partial H / \partial q_i \rangle .$$

Assuming that the Hamiltonian depends upon the coordinates only through the potential energy and changing notation slightly obtains

$$\langle (\ddot{p}_1)^2 \rangle = (1/m) \sum_{i,j=1}^{3} \sum_{k=1}^{N} \{ kT \langle (\partial^3 V / \partial q_{1i} \partial^2 q_{kj}) \partial V / \partial q_{1j} \rangle - \langle (\partial^2 V / \partial q_{1i} \partial q_{kj}) (\partial V / \partial q_{kj}) \partial V / \partial q_{1i} \rangle \},$$

where the first subscript designates the particle and the second subscript refers to the particle coordinate. Again assuming two-body central forces one obtains after some algebra

$$\langle (\ddot{p}_1)^2 \rangle = -(1/m) \{ NkT \langle \nabla_1 u_{12} \cdot \nabla_1 \nabla_2^2 u_{12} \rangle - (n/2) \langle \nabla_2 u_{12} \cdot \nabla_2 (\nabla_1 u_{12} \cdot \nabla_1 u_{12}) \rangle + NkT \langle \nabla_1 u_{12} \cdot \nabla_1 \nabla_1^2 u_{12} \rangle$$

$$- (N/2) \langle \nabla_1 u_{12} \cdot \nabla_1 (\nabla_1 u_{12} \cdot \nabla_1 u_{12}) \rangle - (N/3)(N-1) \langle \nabla_1 u_{12} \cdot \nabla_1 u_{12} \nabla_1^2 u_{13} \rangle \}.$$

It is more convenient to write the derivatives which appear in this equation in terms of r_{12} and r_{13} than the Cartesian coordinates. These variables give

$$\langle (\ddot{p}_1)^2 \rangle = -(1/m) \{ 2NkT \langle u' (\nabla^2 u)' \rangle - 2N \langle u'' (u')^2 \rangle - (N/3)(N-1) \langle (u_{12}')^2 \nabla^2 u_{13} \rangle \}, \tag{30}$$

where primes indicate differentiation with respect to r_{12}. Again making the substitutions $u = \epsilon\gamma$, $r = \sigma x$, and expressing the averages in terms of radial distribution functions

$$\langle (\ddot{p}_1)^2 \rangle = -(8\pi kT\rho\epsilon^2/m\sigma) \int_0^\infty g^{(2)}(x) \gamma' (\nabla^2 \gamma)' x^2 dx + (8\pi\rho\epsilon^3/m\sigma) \int_0^\infty g^{(2)}(x) \gamma'' (\gamma')^2 x^2 dx$$

$$+ (\sigma^2 \rho^2 \epsilon^3 / 3\pi m) \iint g^{(3)}(\mathbf{r}_{12}, \mathbf{r}_{13}) (\gamma_{12}')^2 \nabla^2 \gamma_{13} d\mathbf{r}_{13} d\mathbf{r}_{12}. \tag{31}$$

In order to simplify notation let

$$\psi_1=\int_0^\infty g^{(2)}(x)\gamma'(\nabla^2\gamma)'x^2dx$$

$$\psi_2=\int_0^\infty g^{(2)}(x)\gamma''(\gamma')^2x^2dx$$

$$\psi_3=\iint g^{(3)}(\mathbf{r}_{12},\mathbf{r}_{13})(\gamma_{12}')^2\nabla^2\gamma_{13}d\mathbf{r}_{13}d\mathbf{r}_{12}/16\pi^2. \tag{32}$$

Using Eqs. (31) and (32) in Eq. (5) gives an expression for the coefficient a_4,

$$a_4=(\pi\rho\epsilon^2/9m^2\sigma)(-\psi_1+(\epsilon/kT)\psi_2+(2\pi\sigma^3\rho\epsilon/kT)\psi_3. \tag{33}$$

This expression, is of course, sufficiently complicated so that any clear physical significance is well disguised. However, one feature of the diffusion process is manifest. Just as in a solid and in a gas, diffusion in a liquid is a result of collisions, i.e., the only large contributions to the integrals of Eq. (32) occur where the derivatives of the intermolecular potentials are large, which is the case only when the molecules are very close together. It is reassuring to see that this is indeed the case but it certainly cannot be counted as a revelation.

The experimental data on the temperature dependence of the self-diffusion coefficients in liquids indicates that the diffusion coefficients follow an Arrhenius law in most cases. If one supposes that this is the case with liquids composed of spherical molecules as well, then the parameter δ^2 must be fairly large. This implies that C is rather small and that δ^2 is quite sensitive to the absolute value of C [see Eq. (8)]. The parameter C may be obtained from Eqs. (29) and (33) as

$$C=[-\psi_1+(\epsilon/kT)\psi_2+4(v_0/v)(\epsilon/kT)\psi_3]/4(v_0/v)\psi_0^2, \tag{34}$$

where $v_0=\pi\sigma^3/6$, the volume of a molecule and $v=V/N$, the volume available in the system per molecule. Qualitative examination of the terms involving ψ_1, ψ_2, and ψ_3 suggests that they do not differ greatly in magnitude, but ψ_2 is probably the largest term, and the integrals themselves should not be very sensitive to changes in density. Therefore, C increases and σ decreases with increasing free volume. Since the activation energy is proportional to δ the activation energy decreases with increasing free volume. Again this feature can hardly be counted as surprising.

A test of the results of this section is a difficult problem in itself. Spherical or quasi-spherical molecules, for which diffusion data is available, are rare. In addition to the diffusion data one apparently requires an intermolecular potential which is valid at small intermolecular separations, and a corresponding radial distribution function. While several potentially useful potential functions are available, the corresponding radial distribution functions are not.

The next section makes an attempt to find out whether one can in practice, obtain reasonable results by using crude approximations to all of these items.

SELF-DIFFUSION IN LIQUID NEOPENTANE

Experimental diffusion coefficients[2] and intermolecular potential functions[8] are available for neopentane but an acceptable radial distribution function is not available. The neopentane molecule is, of course, tetrahedral rather than spherical. However, because of the rotation of the molecule, which persists even in the face-centered cubic solid lattice, we shall presume that it behaves like a spherical molecule.

Hamann and Lambert have used two potential functions, a Lennard-Jones 12-6 and a 28-7 potential to describe the virial coefficients of gaseous neopentane.[8] They conclude that the "hard" 28-7 potential gives a much better fit with the observed virial coefficients and molecular radius than does the "soft" 12-6 potential. In view of this result the neopentane intermolecular potential used here is the 28-7 potential suggested by Hamann and Lambert,

$$u=(E^*/3)(R^*/R)^{28}-4(R^*/R)^7],$$

where R^* is the intermolecular separation at the minimum in u. The hard-core diameter σ will be taken as the intermolecular separation at which $u=0$. Therefore, $\sigma=4^{-\frac{1}{21}}R^*$,

$$u=(4^{4/3}E^*/3)(x^{-28}-x^{-7})$$

$$\gamma=x^{-28}-x^{-7}, \quad \text{and} \quad \epsilon=4^{4/3}E^*/3. \tag{35}$$

Hamann and Lambert find that $E^*/k=581°\text{K}$ and $R^*=6.09$ A so that $\sigma=5.71$ A and $\epsilon=1.70\times10^{-13}$ erg.

In principle the choice of an intermolecular potential determines the radial distribution function. In practice even theoretical two-particle radial distribution functions have not been calculated, except for a rigid-sphere potential[9] and a rigid sphere with a Lennard-Jones 6–12 attractive potential.[10] The presence of the rigid-sphere

[8] S. D. Hamann and J. A. Lambert, Australian J. Chem. **7**, 1 (1954).

[9] J. G. Kirkwood, E. K. Maun, and B. J. Alder, J. Chem. Phys. **18**, 1040 (1950).

[10] J. G. Kirkwood, V. A. Lewinson, and B. J. Alder, J. Chem. Phys. **20**, 929 (1952).

core potential introduces an undesirable behavior into the radial distribution function in the collision region where there are significant contributions to the required integrals. Lacking a good radial distribution function we make the crude assumption that

$$g^{(2)}(r) = \exp[-u(r)/kT], \tag{36}$$

with no attempt at justification of the use of this approximation in the liquid state, except to say that it is qualitatively correct at sufficiently small intermolecular separations. The superposition approximation is used to express the three particle radial distribution function $g^{(3)}(r)$ in terms of $g^{(2)}(r)$ so that

$$g^{(3)}(\mathbf{r}_1, \mathbf{r}_2, \mathbf{r}_3) \approx g^{(2)}(\mathbf{r}_1, \mathbf{r}_2)\, g^{(2)}(\mathbf{r}_2, \mathbf{r}_3)\, g^{(2)}(\mathbf{r}_1, \mathbf{r}_3).^{11} \tag{37}$$

Use of these approximations gives the following expressions for the integrals ψ_i:

$$\psi_0 = \int_0^\infty x^2 \nabla^2\gamma \exp(-b\gamma)\, dx$$

$$\psi_1 = \int_0^\infty x^2 \gamma' (\nabla^2\gamma)' \exp(-b\gamma)\, dx$$

$$\psi_2 = \int_0^\infty x^2 \gamma'' (\gamma')^2 \exp(-b\gamma)\, dx$$

$$\psi_3 = (1/16\pi^2) \int_0^\infty \int_0^\infty x^2 y^2 [\gamma'(x)]^2 \nabla^2\gamma(y) \exp\{-b[\gamma(x)+\gamma(y)]\} \times \int_{\text{angles}} \sin\theta_{12} \sin\theta_{13} \exp[-b\gamma(x^2+y^2-2xy\cos\beta)^{\frac{1}{2}}] \times dx\, dy\, d\phi_{12}\, d\phi_{13}\, d\theta_{12}\, d\theta_{13}, \tag{38}$$

where $b = \epsilon/kT$, $x = r_{12}$, $y = r_{13}$, and β is the angle between $\mathbf{r}_{12}$ and $\mathbf{r}_{13}$. Rotating coordinates so that the angles specifying the orientation of r_{13} are measured relative to r_{12} facilitates integration over all but one of the angles so that ψ_3 becomes

$$\psi_3 = (\tfrac{1}{2}) \int_0^\infty x^2 (\gamma')^2 \exp(-b\gamma)\, dx \int_0^\infty y^2 \nabla^2\gamma \exp(-b\gamma)\, dy \times \int_{-1}^{+1} \exp[-b\gamma(x^2+y^2-2xyz)^{\frac{1}{2}}]\, dz. \tag{39}$$

Since triple integrals are rather unpleasant to deal with numerically, an additional approximation is employed which makes ψ_3 a product of three one-dimensional integrals. In order for the integrand of ψ_3 to be appreciable *both* x and y must be about 1, i.e., all three particles must be interacting simultaneously. Setting both x and y equal to one in the integration over z in Eq. (39), gives

$$\psi_3 = (\psi_0/2) \int_0^\infty x^2 (\gamma')^2 \exp(-b\gamma)\, dx \int_{-1}^{+1} \exp[-b\gamma(2-2z)^{\frac{1}{2}}]\, dz. \tag{40}$$

Comparison of the results of direct calculation of the triple integral of Eq. (39) with ψ_3 obtained from Eq. (40) shows that this simplification introduces only about a 5% error in ψ_3.

Substitution of the algebraic expression for the reduced intermolecular potential γ from Eq. (35) gives explicit expressions for the ψ_i integrals. Numerical evaluation of these integrals has been carried out by Miss M. Grey using a 7090 IBM computer. The results of this calculation, the parameters C, α, and δ, and calculated diffusion coefficients are shown in Table I. In addition to these results, diffusion coefficents calculated from the Kirkwood equation for the friction factor ζ and the relation

$$D = kT/\zeta$$

are included in Table I.[12] The Kirkwood equation for ζ^2 in the notation of this paper, is

$$\zeta^2 = (4\pi/3)\sigma\epsilon m\rho\psi_0.$$

The same crude assumptions regarding the radial distribution function are, of course, also used in this calculation. The relation of the Kirkwood equation to the velocity correlation function has been discussed in a previous paper.[2]

Figure 2 shows a plot of experimental and theoretical diffusion coefficients as a function of temperature. The agreement calculated with experimental diffusion coefficients is clearly not good but, in the author's opinion, is quite satisfactory in light of the qualitative nature of the theory, the character of the integrals ψ_i, and the approximations used in their evaluation. While the calculation of this section is too ambiguous

[11] T. L. Hill, *Statistical Mechanics* (McGraw-Hill Book Company, Inc., New York, 1956), p. 195

[12] J. G. Kirkwood, F. P. Buff, and M. S. Green, J. Chem. Phys. **17**, 988 (1949).

TABLE I.

T°K	263	273	298	308
b	4.676	4.504	4.127	3.993
$10^{-21}\times\rho$ molecules/cm³	5.21	5.12	4.89	4.76[a]
$10^{-2}\times\psi_0$	1.146	1.080	0.952	0.912
$10^{-4}\times\psi_1$	2.473	2.422	2.333	2.310
$10^{-4}\times\psi_2$	1.327	1.341	1.391	1.417
$10^{-3}\times\psi_3$	4.125	3.698	2.949	2.733
C	0.476	0.496	0.554	0.575
δ	1.071	1.015	0.851	0.798
$\alpha\times10^{-13}$ sec	0.973	0.964	0.957	0.955
$10^5\times D$ cm²/sec	1.76	1.93	2.78	3.20
$10^5\times D_{\text{kirk}}$ cm²/sec	2.14	2.30	2.72	2.91
$10^{-12}\nu=(\alpha\delta/2\pi)$ sec^{-1}	1.66	1.56	1.30	1.21

[a] From extrapolation.

to substantiate either the present approach or the Kirkwood equation as the more accurate in calculating diffusion coefficients of spherical molecules, it appears that the temperature dependence of the diffusion coefficient is more accurately represented by the present theory.

Since $C<5$ over the range of temperatures and densities considered, the velocity correlation function oscillates. Table I gives the frequency of oscillation of the correlation function, $\nu=\alpha\delta/2\pi$. Figure 3 shows the approximate correlation function obtained at 0°C. Assuming that the calculated α and δ are correct, the oscillation of the correlation function indicates that even in the liquid state molecules are momentarily trapped in potential wells created by their neighbors. The potential well is rather flat compared to molecular vibration potential functions, the calculated force constant of 0.1×10^5 d/cm is about 50 times smaller than that for a typical molecular vibration force constant. The fact that the calculated diffusion coefficient is low compared to the observed coefficient shows that α, δ or both α and δ are too large so that the real potential well is more flat than these calculations indicate. An oscillating correlation at liquid densities is in agreement with the result of Alder *et al.* who have made modified Monte Carlo calculations of the velocity correlation function of a fluid of rigid spheres.[13]

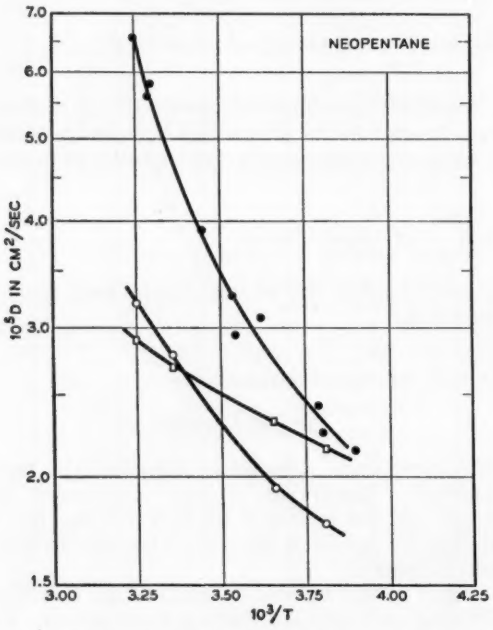

FIG. 2. The logarithm of the self-diffusion coefficient (cm²/sec) of neopentane vs reciprocal temperature (°K^{-1}). Dots indicate experimental data, circles indicate coefficients calculated using the velocity correlation function $\rho(s)=\cos\alpha\delta s/\cosh\alpha s$, and squares indicate coefficients calculated using the Kirkwood equation for the dynamical friction factor.

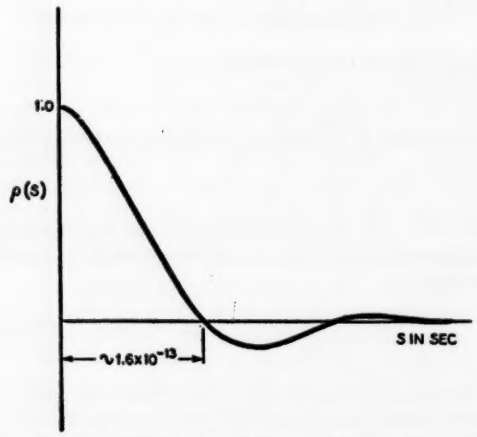

FIG. 3. The approximate velocity autocorrelation function $\rho(s)=\cos\alpha\delta s/\cosh\alpha s$ for $\delta=1.01$ and $\alpha=0.96\times10^{13}$ sec^{-1}. These are the calculated values of α and δ for neopentane at 0°C.

ACKNOWLEDGMENTS

The author is indebted to D. W. McCall for his interest, comments, and aid during the development of the material in this paper. I am also grateful to Miss M. Grey for her generous contribution of time and effort in the evaluation of the integrals in the final section of this paper. Thanks are also due to W. P. Slichter for assistance with the manuscript.

[13] B. J. Alder and T. E. Wainwright, *Proceedings of the I.U.P.A.P. Symposium on Statistical Mechanical Theory of Transport Processes. Brussels* (Interscience Publishers, Inc., New York, 1958).

Some Effects of Temperature and Viscosity on Fluorescence and Energy Transfer in Solutions*

A. WEINREB†

Argonne National Laboratory, Argonne, Illinois

(Received August 15, 1960)

The transfer of excitation energy between molecules of different compounds in solutions is investigated as a function of temperature and viscosity of the solution. In all cases an increase in transfer efficiency with increasing diffusion is observed. The fluorescence of the donor molecules in the absence of acceptor molecules is studied as a function of temperature and the possible influence of the respective changes on the observed transfer efficiencies is discussed.

A. INTRODUCTION

THE distance over which energy can be directly transferred from an excited solvent molecule to an accepting solute molecule in common scintillating solutions has been computed in previous investigations.[1,2] These computations were made in accordance with a theory developed by Förster[3] on the assumption that the energy is transferred by a mechanism of dipole-dipole interaction, the strength of the interaction being determined by the overlap of the absorption and fluorescent spectra of the accepting and donating molecules, respectively. The theoretical transfer distances thus obtained from the spectroscopic data of the molecules involved were shown to be much smaller than those found experimentally. Since Förster's theory assumes that acceptor and donor molecules have fixed positions[4] which do not change during the lifetime of the excited donor molecules, it was assumed[2] that the probability for energy transfer would be increased by the Brownian motion which actually occurs in the usual scintillating solutions. Because of this motion, donor and acceptor molecules could diffuse into the range of interaction during the lifetime of the excited state, even though at the instant the donor became excited they were too far apart to permit energy transfer. Estimates[5] of this effect led to the conclusion that it is too small to remove the apparent discrepancies between the theoretical and experimental values of the reaction distances. Those estimates were based on assumptions regarding the diffusion constants of the molecules involved and thus included one rather arbitrary factor: the molecular radius for diffusion, which can be only very roughly estimated. Instead of relying on such vague assumptions, it seemed preferable to determine the influence of Brownian motion directly by experiment. Preliminary experiments have been mentioned.[2] The present paper is a refinement of these experiments. Their publication now seems more important since other authors[6,7] have claimed that Brownian motion apparently has no significant effect on energy transfer. These authors draw their conclusions from certain similarities between plastic and liquid solutions. It seems that a discussion of their respective procedures[8] might explain the differences between their results and those presented here, namely, that Brownian motion does influence the transfer efficiency—at least in some of the systems investigated in this work. In addition, it will be seen that the interpretation of temperature and viscosity effects on the luminescence of organic solutions might be rather complicated in certain cases.

B. EXPERIMENTAL METHOD

1. Principles

In order to investigate the influence of Brownian motion on the process of energy transfer fron an excited solvent to an accepting solute molecule, the transfer efficiency has to be determined as a function of the rate at which these molecules diffuse towards each other. If

* Work performed under the auspices of the U. S. Atomic Energy Commission.

† On leave from the Hebrew University, Jerusalem, Israel. Requests for reprints should be sent to this address.

[1] F. B. Harrison, thesis, Princeton University (1951).

[2] S. G. Cohen and A. Weinreb, Proc. Phys. Soc. (London) **B69,** 593 (1956).

[3] T. Förster, Ann. Physik **2,** 55 (1948).

[4] Förster's theory applies to highly absorbent and fluorescent dye molecules. In the work cited in reference 3 the author explicitly expresses the view that transfer of energy in a system involving relatively weakly fluorescent molecules (most solvents used in liquid scintillators belong to this class) should be confined to very small distances and therefore should take place mainly by diffusion.

[5] Computations on the influence of diffusion on energy transfer were also carried out by T. P. Belikova and M. D. Galanin, Optika i Spektroskopiia **1,** 168 (1956).

[6] H. Knau, Z. Naturforsch. **12a,** 881 (1957).

[7] R. Hardwick, J. Chem. Phys. **26,** 323 (1957).

[8] In addition, it may be pointed out that we were unable to produce the plastic solution of naphthalene and anthracene in methyl methacrylate at the concentrations that were used in the work described in reference 7. Even when employing considerably higher temperatures over much longer times than given there, the solutions did not polymerize. When as much as 25 cc of solution was used, only the top layer of the solution solidified; but when the volume was reduced to only a few cubic centimeters (so that the whole volume could be considered a top layer) the solution solidified. Since in the work cited in reference 7 the solutions were placed for polymerization in absorption cells which probably had relatively small volume, solidification was observed. However, the homogeneity of such a product seems to be questionable.

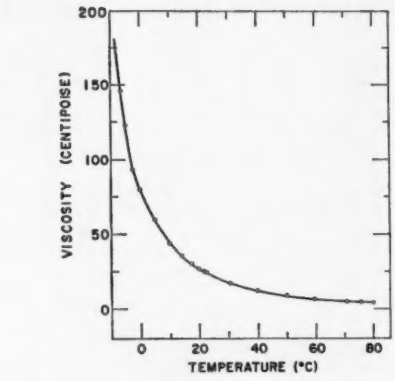

(a)

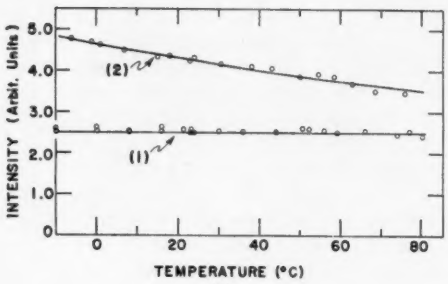

(b)

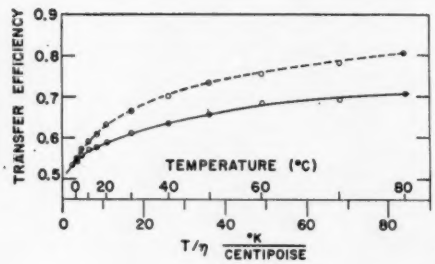

(c)

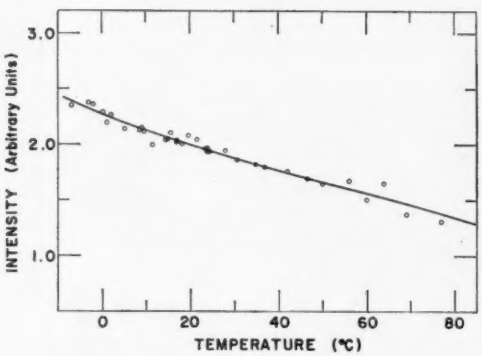

(d)

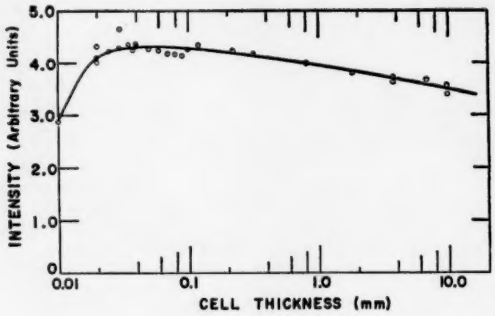

(e)

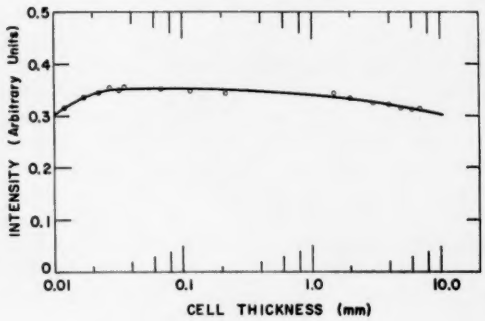

(f)

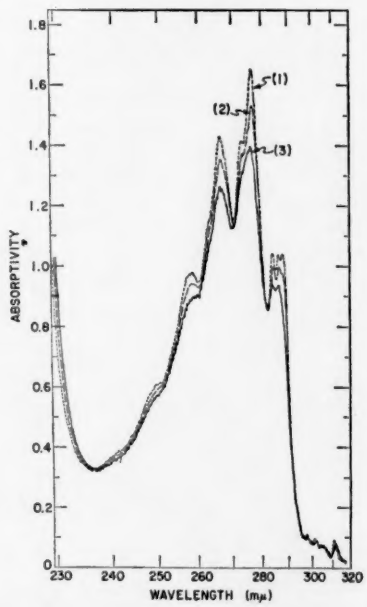

(g)

FIGURE 1 (legend on facing page)

the transfer is dependent on diffusion, a decrease in the viscosity of the system should result in an increase in transfer efficiency. One possible way to investigate this influence of viscosity might be to compare the transfer efficiencies of a solution in the liquid and the crystalline states by freezing the solution. In addition to certain essential technical difficulties involved in this procedure, the possibility was discarded also on the ground that the transfer processes in the two systems might not be identical. The probable anisotropy of the process in a crystal as contrasted to the assumed isotropy in a liquid solution may by itself influence the transfer efficiency. Another possibility which may suggest itself is the comparison between the transfer efficiency in monomeric and polymeric solutions. This cannot be used as a measure of the influence of diffusion on the transfer process, since the chemical change associated with polymerization of the solvent may give rise to entirely different transfer properties. The fact that higher solute concentrations are required in common plastic scintillators than in related liquid scintillators in order to obtain equivalent efficiencies might, however, be interpreted as an indication that diffusion plays an important role in the phenomenon of energy migration in liquids. Incorporation of the common solvent molecules in an inert plastic does not seem feasible.

In this work, the viscosity of the system was changed by changing its temperature. Since only moderate changes in viscosity can be achieved in the aromatic solvents commonly used in energy-transfer experiments, the solution was dissolved in a viscous solvent which is transparent to the exciting and fluorescent radiations. It is thereby possible to obtain much larger changes in viscosity. It has been shown previously[2,9] that dilution of the transferring solvent in an inert solvent (without appreciable change in diffusion constant) does not change the transfer efficiency as long as the concentration of the solute is kept constant. Therefore, any decrease in transfer efficiency in changing from the diluted or undiluted nonviscous system to the diluted viscous one has to be ascribed to the decrease in diffusion constant.

2. Procedure

Several systems were investigated. However, the most extensive information was collected for solutions in paraffin oil, in which the acceptor was anthracene and the donor molecules were naphthalene, toluene, or anisole, respectively. Paraffin oil served as a diluent, the viscosity of which can be varied considerably by changing the temperature. The transfer efficiencies were obtained according to a method described in the work cited in reference 2. The anthracene was directly excited by irradiation with wavelength 3340 A; for excitation via transfer from naphthalene, toluene, or anisole, the exciting wavelength was 2650 A. Most of the experiments were carried out, at least preliminarily, at the Hebrew University in Jerusalem. There the exciting uv was monochromatized by a Bausch & Lomb grating monochromator. Since the dispersion of this monochromator is rather poor and the amount of scattered uv rather high, the scattered radiation at 2537 A (for which anthracene is highly absorbing) had to be removed when the excitation wavelength 2650 A was used. This was accomplished by inserting a solution of 0.02 g/liter anthracene in alcohol between the exit slit of the monochromator and the measured solution, thus using the highly selective absorption of anthracene itself to improve the performance of the monochromator. It was found that exposing the anthracene filter solution to the full strength of the exciting source (a Hanovia mercury lamp furnished with the monochromator) caused a rapid deterioration of the solution by photochemical action, whereas the monochromatized light did not cause any detectable change even after many hours of operation. Because of the low absorption of the monochromatized light and geometric reasons, the anthracene radiation of the filter solution was insignificant in comparison to the radiation of the investigated solutions, and an added filter (Chance No. OX7) rendered it altogether negligible. All the experiments were repeated and extended at Argonne National Laboratory. Here the light was monochromatized by a Beckman DK 2 spectrophotometer using a Corning 9863 filter for additional exclusion of stray light at long wavelengths. For excitation with wavelength 2650 A, an additional chlorine-gas filter was used in order to remove stray radiation in the near uv. The detector system of the spectrophotometer served for the measurement of the fluorescent light. The recorder was detached from the wavelength drive and used to record the intensity over an extended period in order to average fluctuations and in order to make a continuous trace of changes in intensity with changing temperature. The intensity of the exciting light was monitored by measuring the fluorescence of a solution of 1 g/liter aesculin

FIG. 1. (a) Variation of viscosity with temperature of a solution of 20 g/liter naphthalene in paraffin oil. (b) Variation of fluorescent intensity with temperature of a solution of 0.5 g/liter anthracene and 20 g/liter naphthalene in paraffin oil. Curve (1): excitation with wavelength 2650 A (excitation of naphthalene). Curve (2): excitation with wavelength 3340 A (direct excitation of anthracene). (c) Variation of efficiency of energy transfer from naphthalene to anthracene with the diffusion parameter T/η for a solution of 0.5 g/liter anthracene and 20 g/liter naphthalene in paraffin oil. (d) Variation of fluorescent intensity with temperature of 20 g/liter naphthalene in paraffin oil. (e) Variation of measured fluorescent intensity of 20 g/liter naphthalene in paraffin oil with cell thickness. (f) Variation of measured fluorescent intensity of 20 g/liter naphthalene and 0.5 g/liter anthracene in paraffin oil with cell thickness. (g) Absorption spectrum of 5 g/liter naphthalene in paraffin oil (cell thickness 0.05 mm). 1: −5°C; 2: 29°C; 3: 80°C.

[9] V. Bar and A. Weinreb, J. Chem. Phys. **29**, 1412 (1958).

in water. The temperature of the investigated solutions was changed by means of a commercially available thermostatic holder of a Beckman cell, which kept temperatures stable within about 1°C. Before measurements, the solutions were deoxygenated by streaming argon through them. It may be noticed that the quenching effect of oxygen in the viscous solutions is much smaller than in the pure aromatic solvents. This indicates that the quenching process depends on diffusion.

In addition to the fluorescence measurements of the solutions in which energy transfer takes place, the fluorescence of the transferring molecules in the absence of acceptor molecules was measured as a function of temperature. As will be discussed later, these measurements seem indispensable for any understanding of the processes examined. Several other auxiliary intensity and absorption measurements were performed and will be reported in the respective sections.

The viscosity of the solutions as a function of temperature was determined by Cannon-Fenske-Ostwald-type viscometers. For different viscosity ranges, different viscometers were used in order to allow for long enough times of flow. The overlap between the results for different ranges was excellent. The measured viscosities were corrected in the usual way for the changes in density of the solutions with temperature.

Much effort has been invested in the purification of solvents, particularly that of paraffin oil. By running paraffin oil several times through columns of hot silica gel and/or activated alumina, a high degree of purity was reached as concluded from absorption measurements (absorptivity of less than 0.05 at 2650 A for 1 cm of paraffin oil). The most recent experiments showed, however, that purification can be carried further and that 1 cm thickness of paraffin oil is practically transparent down to 2200 A when compared with triple-distilled water.

C. RESULTS AND DISCUSSIONS

1. Solution of 0.5 g/liter Anthracene and 20 g/liter Naphthalene in Paraffin Oil

Results

Figure 1(a) shows the variation of the viscosity of the solution with temperature. Figure 1(b) shows the fluorescence intensity of the solution as a function of temperature when it is excited by uv of wavelength 2650 A (curve 1) and 3340 A (curve 2), respectively. In the first case anthracene is excited via transfer from naphthalene, in the second case it is excited directly. From these curves the transfer efficiency can be computed as a function of T/η (which is proportional to the diffusion coefficient), where T denotes the absolute temperature and η the viscosity. This function is presented in Fig. 1(c). Table I shows the fluorescence intensities and the transfer efficiencies of the solution at room temperature, as compared with the respective magnitudes for a solution of 20 g/liter naphthalene and 0.5 g/liter anthracene in cyclohexane. In addition the table shows the fluorescence intensities of solutions of 20 g/liter naphthalene in paraffin oil and in cyclohexane, respectively. These intensities were determined under somewhat different conditions than those of the solutions containing anthracene and are therefore not to be compared with them. It should be pointed out that the fluorescence of naphthalene is particularly strongly quenched by oxygen. Since this quenching process is diffusion dependent and since cyclohexane is nonviscous and has a relatively high oxygen concentration under normal conditions, thorough deoxygenation of the cyclohexane solution is very important for this comparison of intensities. Figure 1(d) shows the dependence of the fluorescence intensity of 20 g/liter naphthalene in paraffin oil as a function of temperature. The corresponding curve for 1 g/liter naphthalene is identical within the limits of error and therefore is omitted here. The intensity at 25°C was found to be 1.98 as compared with 1.93 for the solution of 20 g/liter. Figure 1(e) shows the dependence of the fluorescence intensity on the thickness of the 20-g/liter solution of naphthalene in paraffin oil. The same function is shown in Fig. 1(f) for a solution of 20 g/liter naphthalene and 0.5 g/liter anthracene in paraffin oil. For these measurements the solution was placed in a micrometer cell. Suitable filters discriminated between the naphthalene and anthracene fluorescence. Figure 1(g) shows the absorption spectrum of 5 g/liter naphthalene in paraffin oil at different temperatures.

Discussion

We consider first the naphthalene solutions in the absence of anthracene. From Table I it is seen that the fluorescence intensities of naphthalene in paraffin oil and in cyclohexane are very similar. This shows that concentration quenching in naphthalene is low. Otherwise, the much greater viscosity of paraffin oil would have caused an increase in intensity because of reduced collision frequency between naphthalene molecules. This is seen also from the similarity between the inten-

TABLE I. Fluorescence of naphthalene and energy transfer from naphthalene to anthracene in cyclohexane and in paraffin oil.

Exciting wavelength	20 g/liter naphthalene and 0.5 g/liter anthracene		20 g/liter naphthalene	
A	in paraffin oil	in cyclohexane	in paraffin oil	in cyclohexane
2650	1.23	1.54	2.25	2.21
3340	2.05	1.75		
Transfer efficiency	0.60	0.88		

sities of the 20 g/liter solution and those of the 1 g/liter solution. This result conforms to the well-known practical use of very high concentrations of naphthalene as secondary solvents in certain scintillator solutions,[10] and with results of Dammers-de Klerk,[11] who found that after an initial decrease the naphthalene fluorescence remains constant with increasing concentration.

By changing temperature one can affect the fluorescent intensity of naphthalene considerably. From Fig. 1(d) it is seen that varying the temperature from −5°C to 80°C causes a decrease in intensity in a ratio of about 1.75:1. A more exact evaluation of the decrease in intensity, however, necessitates a consideration of the self-absorption of naphthalene. Since the experiment was carried out in a cell of 1-cm thickness, a considerable effect of self-absorption and re-emission would tend to increase the change in intensity with temperature. This effect can be estimated from the results shown in Fig. 1(e). After an initial fast rise, the intensity reaches a maximum at a cell thickness corresponding to the minimum thickness required for complete absorption of the exciting light and decreases slowly with increasing thickness of the cell because of self-absorption. These measurements were taken at room temperature and without deoxygenation. In order to estimate what part of the fluorescence observed at the maximum cell thickness of 1 cm is due to re-emission, we have to make certain assumptions. We assume a value of 0.3 for the molecular quantum yield of naphthalene (i.e., the yield in the absence of reabsorption) at the given conditions (room temperature, concentration of 20 g/liter, air saturation of the solution). This seems to be a rather high estimate, since the quantum yield of naphthalene for optimum conditions, as given in the literature, is 0.38.[12] We apply Birk's approximation formula for secondary fluorescence,[13] namely,

$$q_0^n = q_t \equiv q_0 \alpha, \tag{1}$$

where q_0 is the molecular quantum yield, q_t is the apparent quantum yield in the presence of self-absorption and re-emission, α is the ratio of the quantum yields, and n represents the average number of steps of reabsorption. Since the measured intensities I are proportional to the respective quantum yields, the value α is determined by the ratio of the intensities in the presence and absence of self-absorption. From the assumed value of $q_0 = 0.3$ and from the experimental value of $\alpha = 0.8$ [the ratio between the intensity at 1-cm thickness of solution and the intensity obtained at the minimum thickness for complete absorption of the exciting radiation as given in Fig. 1(e)] we obtain $n \approx 1.18$. This value should be considered an upper limit for the effect of re-emission. From Fig 1(g) it can be seen that the absorption spectrum of naphthalene in paraffin oil does not change very much with changing temperature. For practical computations of self-absorption, we may regard it as constant. Then according to Eq. (1), the corrected ratio between the quantum yield at −5°C and that at 80°C (the extreme temperatures of the experiment) is thus given by the expression $(I_{-5}/I_{80})^{1/1.18}$ where I_{-5} and I_{80} are the measured intensities at the respective temperatures. The resulting ratio of 1.60 should be considered a lower limit.

In the work of Dammers-de Klerk it was concluded that at higher concentrations naphthalene forms excited molecular aggregates which for some reason are not subjected to self-quenching. The decrease in fluorescent yield with temperature could then be attributed to a decrease in the formation of these aggregates or to their quicker separation into single molecules which then undergo self-quenching more easily. However, the decrease of quantum yield with temperature for the much lower concentration of 1 g/liter is at least as pronounced as for the concentration of 20 g/liter. We tend thus to conclude tentatively that the decrease in quantum yield of naphthalene is mainly connected with an intramolecular mechanism of temperature quenching.

We now consider the solution of 20 g/liter naphthalene and 0.5 g/liter anthracene in paraffin oil. By means of suitable filters it can be shown that the measured fluorescence of the solution is almost exclusively that of anthracene and that no significant naphthalene radiation is transmitted by anthracene at a 1-cm thickness of solutions. Since for excitation by wavelength 2650 A the direct absorption of the exciting uv by anthracene is negligible as compared with that of naphthalene at the given concentrations, all the observed fluorescence is the result of energy transfer from naphthalene to anthracene. We next establish the fact that this transfer is mainly nonradiative. Indirectly this can be seen from the fact that the transfer efficiency increases with increasing temperature [Fig. 1(c)] whereas the fluorescence of naphthalene decreases. It can also be seen directly from the results given in Fig. 1(f). After an initial increase, the intensity reaches a constant value at a thickness corresponding closely to the minimum thickness for complete absorption of the exciting radiation by naphthalene. If radiative transfer were of any significance, the intensity of anthracene should increase far beyond this thickness since at the given concentration about 15 times as large a thickness is necessary for all the naphthalene radiation to be absorbed by anthracene.

From Fig 1(c) (full line) it is seen that the efficiency of energy transfer from naphthalene to anthracene increases from a value of 0.53 to 0.70 when the temperature is increased from −5°C to 80°C. This corresponds to a variation of the values T/η from 2.2 to 84°K/cp. This increase in transfer efficiency is attributed to the

[10] M. Furst and H. Kallmann, Phys. Rev. **97**, 583 (1955).
[11] A. Dammers-de Klerk, Mol. Phys. **1**, 141 (1958).
[12] E. J. Bowen and A. H. Williams, Trans. Faraday Soc. **35**, 765 (1939).
[13] J. B. Birks, *Scintillation Counters* (Pergamon Press, New York, 1953), p. 98.

increase in Brownian motion which facilitates the closer approach between the molecules of anthracene and naphthalene. Since this increase in Brownian motion has been achieved by increasing the temperature of the solution, the question now arises as to the extent to which the transfer efficiency is affected by the enhancement of radiationless transitions to the ground state which manifests itself in the decrease of the fluorescent intensity of naphthalene with increasing temperature. Several authors have assumed a simple competition between the process of energy transfer, fluorescent emission, and radiationless deactivation processes taking place in the transferring molecule. It seems, however, that only very recently has this relation between these processes been experimentally shown to hold accurately, at least for one system.[14] If we assume this competition between the various processes for our system, the influence of increasing temperature can be determined from the observed variation of fluorescent intensity with temperature [Fig. 1(c)]. In order to find this influence, the additional assumption has to be made that the change with temperature mainly affects either the emission probability or the quenching probability but not both. By quenching we refer here to all radiationless deactivation processes of the excited molecule except transfer of energy to the acceptor molecules. Since the absorption spectrum of naphthalene [Fig. 1(g)] does not change very much with temperature (no attempt to interpret the changes is made here), we infer that the decrease in quantum yield with increasing temperature is mainly due to an enhancement of the quenching process. A determination of the absolute change in transfer efficiency can be made by measurements of decay time. Measurements of the fluorescent intensity (but not of the absolute quantum yield) allow only a relative estimate of the effect of temperature on transfer efficiency. As our point of reference we arbitrarily choose the transfer efficiency at the lowest temperature (−5°C.)

Let I_1 and I_t denote the fluorescent intensities of naphthalene at −5°C and at temperature t [as given in Fig. 1(d)], respectively, η_1 and η_t the respective quantum yields, and Q_1 and Q_t the probabilities for quenching. Let F be the probability for fluorescent emission and T_t the probability for energy transfer at temperature t. Then

$$\eta_1=F/(F+Q_1), \qquad \eta_t=F/(F+Q_t),$$
$$\eta_1/\eta_t=I_1/I_t. \tag{2}$$

The transfer efficiency ϵ_t (at temperature t) is given by

$$\epsilon_t=T_t/(T_t+Q_t+F). \tag{2a}$$

The corrected value ϵ_t', i.e., the transfer efficiency which would be observed if there were no increase in the quenching process with temperature, is given by

$$\epsilon_t'=T_t/(T_t+Q_1+F).$$

The relation between ϵ_t' and ϵ_t is then given by

$$\epsilon_t'=\epsilon_t I_1/[I_t+\epsilon_t(I_1-I_t)]. \tag{2b}$$

The corrected values were thus computed and the results are shown by the dotted line in Fig. 1(c).

The influence of Brownian motion on the transfer efficiency can be seen also from the results of Table I. At room temperature the transfer efficiency in the viscous paraffin oil solutions is considerably lower than in the nonviscous solution in cyclohexane.

In order to obtain the transfer efficiency in the absence of Brownian motion, the results of Fig. 1(c) have to be extrapolated to $T/\eta \to 0$. The value thus obtained is about 0.48. The pronounced curvature of the graph at low values of T/η somewhat reduces the accuracy of the extrapolated value. This result shows that, although the influence of Brownian motion is rather significant, the main mechanism of the transfer process is not one of simple collision. This can, of course, be directly inferred from the occurrence of the transfer process in plastic and glassy solutions, although influences of the media (e.g., probable chain attachment of the solute in plastic solutions and partial crystallization of the solutes in glasses) may not allow a quantitative comparison between the transfer efficiencies in these systems and in solutions.

The extrapolated value of 0.48 for the transfer efficiency in the absence of Brownian motion may now be examined in relation with the "interaction distance" R_0 defined in Förster's theory. When the respective emission and absorption data for naphthalene and anthracene are introduced in Forster's equation for R_0, a value of about 40 A is obtained. This is a much higher value than those obtained for the interaction between anthracene and the solvents usually used in liquid scintillation counters (e.g., toluene). This difference is due to the higher oscillator strength of naphthalene which manifests itself in the greater values of the absorption coefficients. It is also due to the unusually long lifetime of naphthalene (here taken to be 70 mμ sec) which enters in Förster's equation.[15] From the

[14] I. B. Berlman, J. Chem. Phys. **33,** 1124 (1960).

[15] The decay time of naphthalene has been found by Kallmann and Brucker [H. Kallmann and G. J. Brucker, Phys. Rev. **108,** 1122 (1957)] to be 76 mμ sec for crystals and 34 mμ sec for a solution of 10 g/liter in phenylcyclohexane, both under β excitation. After this article was written the decay time of naphthalene was measured (as part of a subsequent study) in this Laboratory by the technique described in the works cited in references 16 and 17. The main decay part of the pulse appeared to be followed by a tail corresponding to a long decay time, which may perhaps result from the particular mode of excitation. The main decay time in deoxygenated solutions of 20/g liter naphthalene in benzene and in cyclohexane at room temperature was found to be less than 70 mμ sec. In paraffin oil, however, it was about 120 mμ sec, increasing with decreasing temperature up to about 240 mμ sec at −6°C. The reason for the longer decay time in paraffin oil is not fully understood; processes connected with the excitation by the solvent might perhaps be involved. The significance of these results for the understanding of the transfer process from naphthalene is somewhat problematic. It could be that the stabilizing mechanism which causes the increase in lifetime stabilizes the molecule also against transfer of energy to anthracene.

value of R_0 we can compute the concentration of anthracene that is necessary for a transfer efficiency of 0.48 according to Förster's theory. The necessary concentration thus obtained is similar to the concentration of 0.5 g/liter used in the present experiment. In this computation, the reduction in Brownian rotation due to the rather high viscosity of the system was neglected. Taking account of this effect would decrease the value of R_0 and hence increase the theoretical value of the necessary concentration. However, in view of the assumed long decay time of naphthalene this effect may not be significant. On the basis of these computations, which have to be regarded as rather crude approximations, it seems thus that the theoretical and experimental values of the transfer efficiency in this system are basically similar.

2. Solutions of Anthracene and Toluene in Paraffin Oil

Results

Figure 2(a) shows the temperature dependence of the viscosity of a solution of 0.5 g/liter anthracene in a mixture of 1 part toluene and 9 parts of paraffin oil. Figure 2(b) shows the temperature dependence of the fluorescent intensity of this solution when it is excited by uv radiation of wavelength 2650 A (curve 1) and 3340 A (curve 2). In the first case almost all the light is absorbed by toluene and the observed anthracene radiation is due to a transfer of energy from toluene. In the second case anthracene is excited directly, toluene being practically transparent to this wavelength. From this figure the transfer efficiencies can be computed. In Fig. 2(c) the transfer efficiency in the solution is shown as a function of temperature and of the diffusion parameter T/η. Figure 2(d) shows the fluorescent intensity of 1 part toluene in 9 parts of paraffin oil as a function of temperature when excited by radiation of 2650 A. In addition the decay time of a solution of 1 part toluene and 9 parts of paraffin oil was measured at various temperatures by use of an apparatus constructed by Swank *et al.*[16,17] For these determinations the solvent was excited by 75-kev electrons. It is assumed that similar results would have been obtained by excitation with uv radiation. Most of the exciting energy is absorbed by the paraffin oil, which then transfers part of the excitation energy to toluene. It is assumed that, because of the high concentration of toluene, this transfer process takes place in a time which is short compared to the decay time of toluene. Below room temperature there is no great change in decay time with temperature. The decay time at the lowest measured temperature (−7°C) was about 32 $m\mu$ sec.

[16] R. K. Swank, H. B. Phillips, W. L. Buck, and L. J. Basile, IRE Trans. on Nuclear Sci. NS-5 **3**, 183 (1958).

[17] R. K. Swank and E. A. Mroz, Rev. Sci. Instr. **30**, 10, 880 (1959).

Discussion

The full line in Fig. 2(c) shows that the transfer efficiency initially increases with temperature and increasing Brownian motion. For the highest temperatures, however, the transfer efficiency decreases again. This decrease can be explained, in analogy with the case of the solution of naphthalene, by an increased temperature quenching and collision quenching of the transferring solvent, toluene. From Fig 2(d) it is seen that the fluorescent intensity of toluene in paraffin oil decreases rapidly with temperature for temperatures higher than 25°C. The transfer efficiency still goes up beyond this temperature, but for the highest temperatures the quenching effect in the solvent outweighs the increase in transfer efficiency due to Brownian motion. If we again assume that the decrease in quantum yield of toluene with increasing temperature is primarily a consequence of increasing deactivation processes, the probability for emission remaining substantially constant, and if we again assume a simple competition between emission, quenching, and transfer of energy to anthracene, then the transfer efficiency can again be corrected according to Eq. (2b). The results of this correction are shown by the broken line in Fig. 2(c). The reference intensity I_1 was chosen at 10°C. Over the whole range between −10°C and 25°C the change in intensity is less than about 5%.

Again we extrapolate the transfer efficiency to $T/\eta \rightarrow 0$ and obtain a value of about 0.28. The highest corrected value is about 0.57. The transfer efficiency in a deoxygenated solution of 0.5 g/liter anthracene in toluene and in toluene diluted by cyclohexane at room temperature has been found previously[9] to be about 0.7. Comparison of these results with those obtained with naphthalene as the transferring agent shows that in the latter system the extrapolated transfer efficiency in the absence of Brownian motion is considerably higher than in the present one. This difference can be qualitatively ascribed to the higher transition moments of naphthalene and its longer lifetime as compared with toluene. The ratio between the transfer probability [T_t in Eq. (2a)] at the highest temperature and that in the absence of Brownian motion (corresponding to the extrapolated value of the transfer efficiency) is about 3 for the solution with toluene and about 4 in the solution with naphthalene. These ratios are the quantitative measures of the influence of Brownian motion on the transfer process. Although the parameter T/η at the highest measured temperature is lower in the naphthalene solution than in the toluene solution (85 against 130°K/cp) the influence of Brownian motion in the naphthalene solution is significantly higher, since the probability for a molecule to enter the "sphere of interaction" by diffusion increases with the "interaction distance" R_0 and with the lifetime of the excited donor molecule.

The theoretical value for the "interaction distance"

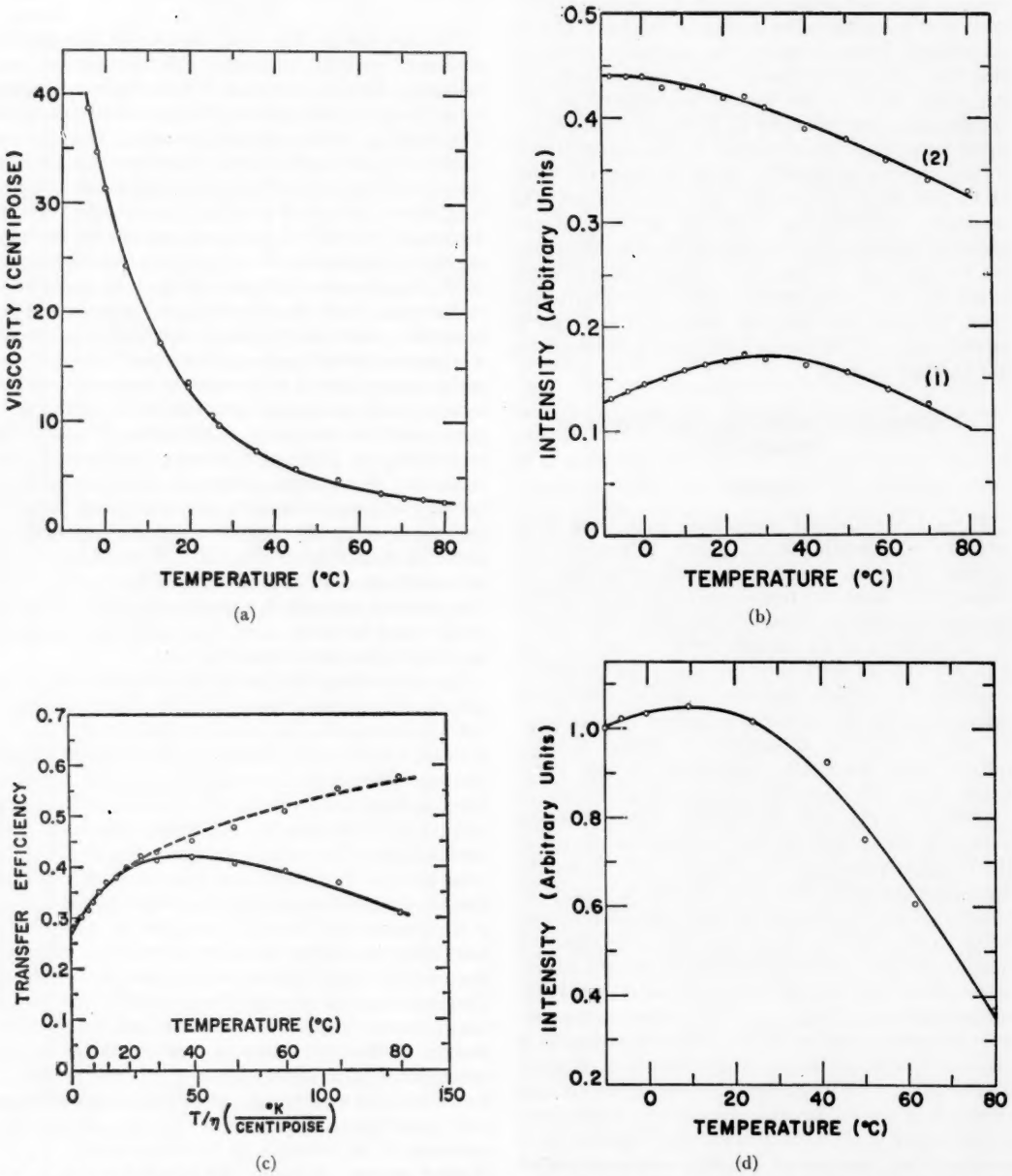

FIG. 2. (a) Variation of viscosity with temperature of a solution of 0.5 g/liter anthracene in a mixture of 1 part toluene and 9 parts paraffin oil. (b) Variation of fluorescent intensity with temperature of a solution of 0.5 g/liter anthracene in a mixture of 1 part toluene and 9 parts paraffin oil. Curve (1): excitation with wavelength 2650 A (excitation of toluene). Curve (2): excitation with wavelength 3340 A (direct excitation of anthracene). (c) Variation of efficiency of energy transfer from toluene to anthracene with temperature and with the diffusion parameter T/η for a solution of 0.5 g/liter anthracene in a mixture of 1 part toluene and 9 parts paraffin oil. (d) Variation of fluorescent intensity with temperature of a mixture of 1 part toluene and 9 parts paraffin oil.

obtained from the absorption and fluorescence spectra of toluene and anthracene according to Förster's theory is about 15 A. Accordingly the concentration which would be necessary in order to obtain the extrapolated transfer efficiency would be about 8 times as great as that actually employed. At present no source of error is seen which would account for this discrepancy, not even considering the great uncertainty in estimating

the overlap integral which appears in Förster's formula. There might be, however, sources of error due to some simplifying assumptions of the theory itself, which may not apply here. Thus it seems that although diffusion is a very important factor in the energy transfer from toluene to anthracene, Förster's theory in its original form is still not quantitatively applicable for this system.[18]

3. Solutions of Anthracene, Diphenyloxazole, and Diphenylhexatriene in Mixtures of Anisole and Paraffin Oil

Results

Figure 3(a) shows the absorption spectrum of anisole dissolved in paraffin oil at a volume ratio of 1:99 at room temperature and at 82°C. Figure 3(b) shows the fluorescence spectrum of deoxygenated samples of pure anisole and of anisole dissolved in paraffin oil at various volume ratios. The thickness of the solution was 1 cm. Similar spectra were obtained for solutions saturated with air. Figure 3(c) shows the fluorescent spectrum of anisole dissolved in paraffin oil at a volume ratio of 1:9 at different temperatures. The solution was brought to a desired temperature in the thermostatically controlled cell holder but for the recording of the spectrum it had to be taken out of this holder. Thus no accurate temperature can be assigned to the respective curves. The higher ordinal number of the curve indicates a higher temperature. The thickness of the solutions for all the recorded spectra was 1 cm. No correction was made for self-absorption or for the variation of the sensitivity of the recording system with wavelength. Figure 3(d) shows the fluorescent intensity of anisole as a function of temperature for pure anisole and for anisole dissolved in paraffin oil at volume ratios of 1:9 and 1:99, respectively. These curves are meant to represent trends rather than accurate magnitudes. Figure 3(e) shows the temperature dependence of the viscosity of solutions of 0.5 g/liter anthracene in anisole and in mixtures of various ratios of anisole in paraffin oil. Figure 3(f) shows the temperature dependence of transfer efficiency in these solutions. For all solutions except that containing 1 part anisole in 99 parts paraffin oil, direct absorption by anthracene is negligible for excitation by wavelength 2650 A. The results for this solution were corrected accordingly. Figure 3(g) shows the dependence of the transfer efficiency on the diffusion parameter T/η for the solutions of 0.5 g/liter anthracene in the various mixtures of anisole and paraffin oil. Figure 3(h) shows the same function for a solution of 2 g/liter anthracene in a mixture of 1 part anisole and 9 parts paraffin oil. The dependence of the viscosity on temperature was assumed to be approximately the same as for the solution containing anthracene at 0.5 g/liter. Figure 3(i) shows the transfer efficiency as a function of T/η for solutions of 0.5 g/liter diphenylhexatriene and for solutions of 0.5 g/liter diphenyloxazole in mixtures of 1 part anisole and 9 parts paraffin oil. The values presented in the figure were obtained by the same method as those for the solutions of anthracene. At low temperatures the viscosity of the solution with diphenylhexatriene has been found to be somewhat higher than that of the corresponding solution with anthracene. However, since they are essentially similar, the curve is not presented. Table II shows preliminary values of the decay time of anisole and anisole in paraffin oil (1:9) as a function of temperature. In addition, the infrared absorption spectra of anisole and of anisole diluted in CCl_4 at various factors of dilution were measured in the region between 2 and 5μ. The dilution produced no appreciable change in the shape of the spectra.

TABLE II. Decay times of pure anisole and of anisole diluted in paraffin oil.

	Decay time in mμ sec			
	Anisole		Anisole-paraffin oil (1:9)	
Temperature	Deoxygenated	Air saturated	Deoxygenated	Air saturated
11°C	14.6	...	...	...
23°C	12.3	...	16.2	14.6
26°C	11.8	8.2	...	...
29°C	11.0	...	...	...
80°C	7.7	6.5	12.5	...

Discussion

From Figs. 3(g), 3(h), and 3(i) it is seen that the transfer efficiency increases with increasing temperature, and that this effect is not confined to a certain concentration or accepting solute. However, from Fig. 3(g) it is also seen that the transfer efficiency is not a univalent function of the diffusion parameter T/η. Up to a value of about 35° K/cp the transfer efficiency is higher at the lower concentrations of the transferring solvent, anisole, at least in the region where there are data for all the concentrations. Beyond this value the transfer efficiency increases with an increase in the concentration of anisole. The fact that the three curves meet at almost the same point may be fortuitous. One would be tempted to explain the many-valued character of the transfer efficiency at the higher values of T/η by a difference between the macroscopic and microscopic viscosities of the systems. Since anthracene is much more soluble in anisole than in paraffin oil, it is possible that anthracene tends to attach itself to anisole molecules. The mutual diffusion between an excited

[18] The discrepancy may probably be reduced by considering the difference between macroscopic and microscopic viscosity (see Sec. 3).

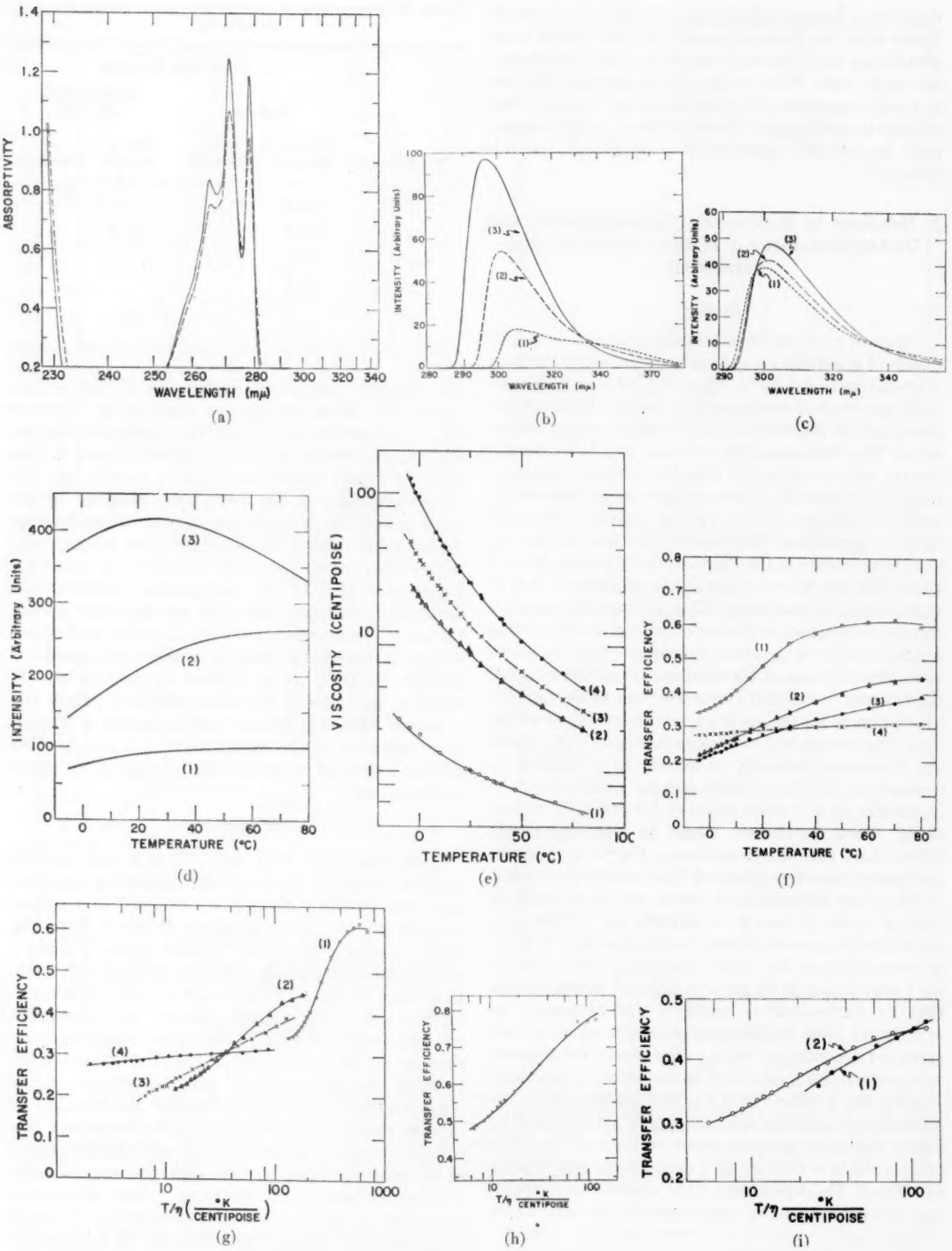

FIGURE 3. (legend on facing page)

anisole and accepting anthracene molecule would thus be greater in solutions containing a greater portion of anisole, in spite of the similarity in the measured viscosity of all the solutions. However, this assumption cannot explain the reversed situation at the lower values of T/η. A partial explanation may be that at the greatest dilution of anisole radiative transfer plays an important role, since in this case the fluorescent yield of anisole is highest. The same explanation may hold for the difference between the two lower dilutions, although these differences are rather small and could perhaps be attributed to some unknown source of error. One can thus make the qualitative statement that with increasing Brownian motion there is a general trend of increase in the efficiency of energy transfer from anisole to anthracene. A crude estimate of the magnitude of this effect according to Fig. 3(g) yields an increase in nonradiative transfer efficiency from about 0.2 at $T/\eta=6$ to about 0.62 at $T/\eta=600$. According to Eq. (2) this corresponds to a change in transfer probability by a factor of 6, all competing processes being assumed to remain constant.

The results presented in Fig. 3(d), however, show that the problem of estimating the change in transfer efficiency with Brownian motion in this system is rather complicated. It is seen that, unlike the case for naphthalene and toluene, the fluorescent yield of pure anisole and of anisole diluted by a factor of 10 in paraffin oil increases with temperature. Also for a solution of 1 part anisole in 99 parts paraffin oil there is an initial rise of the intensity with temperature followed by a decrease at the higher temperatures. We tend to interpret these results by the assumption that anisole has a strong tendency to form dimers or higher molecular complexes. These dimers (and by the term dimer we henceforth will include all possible molecular complexes) may have additional modes of radiationless deactivation and hence a considerably lower fluorescent quantum yield. The decrease of the long-wavelength tail in the fluorescent spectrum upon increasing the temperature [Fig. 3(c)] probably indicates the existence of dimers and the decrease of their concentration with temperature. This also makes plausible the differences in the temperature dependence of the fluorescent intensity of anisole for the various degrees of dilution in paraffin oil. At the highest dilution of anisole the concentration of dimers is relatively low. With increasing temperature the dimers break up and the fluorescent intensity increases. With a further increase of temperature, concentration quenching and/or temperature quenching outweighs the effect of reduced dimer concentration and the intensity decreases again. In the less diluted solution (1:9) the effect of decreasing dimer concentration is stronger than the reducing effect of temperature quenching; thus the intensity increases monotonically with the temperature. The same holds for pure anisole. However, the relative increase of intensity with temperature is smaller in pure anisole than in anisole diluted by a factor of 10. This may probably be due to the greater concentration quenching that results from the much lower viscosity of pure anisole as compared to anisole in paraffin oil. This difference between the quenching actions in the two systems can be seen from the decay times given in Table II. Whereas an increase from room temperature to 80°C causes a decrease in decay time by a factor of 1.6 in pure anisole, a change of 1.3 is observed in diluted anisole for the same change in temperature. The absolute values of the decay time in diluted anisole are also considerably larger than in pure anisole. The change in the relative concentration of dimers with temperature should not in itself affect the decay time if their contribution to the fluorescent yield is low or if their fluorescent decay time is similar to that of the monomer. There might also be a different reason for the greater increase in fluorescent intensity with increasing temperature in the diluted system as compared to pure anisole. The molecules which form the dimer are only loosely bound and may split apart readily at ordinary temperatures. In a viscous medium, however, the two molecules may be trapped by a "cage" effect and their interaction may continue for a longer time. At the highest dilution of anisole, again the concentration of dimers might be so much lower that the change in their concentration does not affect the fluorescence strongly, even with the "cage" effect acting.

It is easily seen that the assumed change in the composition of the transferring solvent with temperature makes it difficult to make a quantitative evaluation of the influence of Brownian motion on the transfer process in this system. Considerable differences may exist between the transfer properties of the monomers and the dimers. This may be the reason for the lower

FIG. 3. (a) Absorption spectrum of anisole dissolved in paraffin oil at a volume ratio of 1:99. Full line: room temperature. Broken line: 82°C. (b) Fluorescence spectrum of anisole in paraffin oil. Curve (1): pure anisole. Curves (2), (3): anisole diluted in paraffin oil by factors of 10 and 100, respectively. (c) Fluorescence spectrum of anisole diluted in paraffin oil by a factor of 10. The curves are numbered in order of increasing temperature. (d) Variation of fluorescent intensity of anisole with temperature. Curve (1): pure anisole. Curves (2) and (3): anisole diluted in paraffin oil by factors of 10 and 100, respectively. (e) Variation of viscosity with temperature of solutions of 0.5 g/liter anthracene in mixtures of anisole and paraffin oil. Curve (1): pure anisole. Curves (2), (3), (4): anisole diluted by factors of 5, 10, and 100, respectively. (f) Variation of transfer efficiency with temperature of solutions of 0.5 g/liter anthracene in mixtures of anisole and paraffin oil. Curve 1: pure anisole. Curves (2), (3), (4): anisole diluted by factors of 5, 10, and 100, respectively. (g) Variation of transfer efficiency with diffusion parameter T/η of solutions of 0.5 g/liter anthracene in mixtures of anisole and paraffin oil. Curve (1): pure anisole. Curves (2), (3), (4): anisole diluted by factors of 5, 10, and 100, respectively. (h) Variation of transfer efficiency with diffusion parameter T/η of a solution of 2 g/liter anthracene in a mixture of 1 part anisole and 9 parts paraffin oil. (i) Variation of transfer efficiency with diffusion parameter T/η of a solution of 0.5 g/liter diphenyloxazole [curve (1)]; and of 0.5 g/liter diphenylhexatriene [curve (2)] in mixtures of 1 part anisole and 9 parts paraffin oil.

transfer efficiency in anisole as compared to toluene. The transfer efficiency in a deoxygenated solution of 0.5 g/liter anthracene in anisole at room temperature is about 0.5 as compared to 0.72 for a similar solution in toluene. At a concentration of 2 g/liter anthracene in anisole-paraffin oil (1:9) the transfer efficiency at −4°C is still about 0.5. From the variation in the fluorescent intensity of anisole in this solution one would assume that more than 50% of the excited anisole molecules are part of dimers at −4°C. This would necessitate a transfer efficiency of more than 1.0 for the remaining monomers, although this is at a temperature at which diffusion is very much reduced. It seems, therefore, that the dimers participate, at least to a certain extent, in the transfer process. On the assumption that the relative contribution of the dimers to the transfer efficiency increases with increasing acceptor concentration, one would expect a deviation from the proportionality between transfer probability and acceptor concentration. It can be shown that only for high concentrations of dimers and only for extreme differences in transfer efficiency between dimers and monomers can any great deviation from linearity be expected. Experiments to clarify this were carried out with diphenyloxazole as solute up to a concentration of 16 g/liter. A slight deviation from linearity was observed which may probably indicate an increase in the relative contribution of dimers to the transfer process with increasing acceptor concentration. More accurate and extensive experiments are necessary to elucidate this question. The present data do not allow a quantitative evaluation of the effect of dimerization on the transfer process.

Some efforts have been made to elucidate the nature of the anisole dimers. Under the assumption that a hydrogen bond might be the reason for dimerization, the infrared absorption spectrum of anisole was investigated as a function of dilution in CCl_4. No significant change in the C—H bond-stretching region could be observed. It is possible that a π-electron complex is formed between anisole molecules. The absorption spectrum of anisole in paraffin oil [Fig. 3(a)] shows a red shift with increasing temperature, and a decrease of the three peaks at 2650, 2710, and 2778 A. By varying the temperature from 25°C to 80°C the peaks change by factors of 1.10, 1.16, and 1.24, respectively. Perhaps monomers and dimers contribute differently to the peaks, and this leads to the differences in the relative changes with temperature. Our equipment did not permit us to investigate the effect of temperature on the absorption peaks of higher anisole concentrations, where one would expect a dimerization effect to be more pronounced.

D. CONCLUSIONS

The results have been interpreted as indications of the influence of Brownian motion on the transfer efficiency. Whether this interpretation is proper, or whether some unknown temperature effects may have caused the results is not fully decided. Formation of dimers or other molecular complexes very probably influenced the transfer efficiency in the systems involving anisole as transferring agent. Similar processes may also be acting in other systems. Taking account of the effect of Brownian motion reduces the discrepancies between the experimental values of the transfer efficiency and the values which would be expected according to Förster's theory, though these discrepancies apparently are not always removed. This does not invalidate the assumption that a dipole-dipole interaction between the transferring solvent and accepting solute is the main transfer mechanism involved. By interaction with the acceptor, transitions of the excited donor molecules, which would otherwise have a low probability, might become more frequent.

A basic improvement of this type of investigation would be to avoid the differences between the macroscopic and microscopic viscosities by using, instead of a viscous inert diluent, a binary system in which the transferring solvent itself has a great range of viscosities. Isopropylbiphenyl, which is very efficient as a transferring solvent, may be a proper material for these studies.

ACKNOWLEDGMENTS

The author wishes to thank J. Brichta for his devoted help in all phases of the work, Dr. J. Ferraro for the measurement and interpretation of the infrared absorption of anisole, and his colleagues L. Basile, I. Berlman, and W. Buck for the use of their equipment and for their help.

Separation of Boron Isotopes. V. The Phenol-BF_3 System*

A. A. PALKO AND J. S. DRURY

Chemistry Division, Oak Ridge National Laboratory, Oak Ridge, Tennessee

AND

W. E. BULL†

Chemistry Department, University of Tennessee, Knoxville, Tennessee

(Received December 2, 1960)

The exchange of boron between BF_3(g) and BF_3·phenol(l) was studied. The single-stage isotopic fractionation factor varied according to the equation, $\log\alpha = (10.315/T) - 0.02423$, over the temperature range -8°C to 37°C. B^{10} is concentrated in the liquid phase. Vapor-pressure measurements of dilute and concentrated solutions of BF_3 in phenol were made at various temperatures from -10°C to 40°C. The freezing point of the BF_3·phenol complex was approximately -15°C; that for the BF_3·2 phenol, -5°C.

INTRODUCTION[1]

PHENOL reacts mildly with BF_3 at room temperature to form two molecular addition compounds; the BF_3·phenol complex, and the BF_3·2 phenol complex.[2–4] In the latter compound the two phenol molecules are associated through hydrogen bonding. The 1:2 complex is considerably more stable than its companion adduct; the saturation pressure of the 1:1 compound is estimated to be 100 times greater than that of the 1:2 complex. The melting point of the 1:2 complex is approximately -5°C; that for the less stable compound, -15°C.

The 1:2 complex[5] is a clear, colorless liquid which is quite stable in the absence of moisture. It reacts with water only slowly. When heated, the complex releases BF_3 smoothly until essentially none remains in solution at the boiling point of phenol.

EXPERIMENTAL

Materials and Methods

The phenol used for these experiments was reagent-grade material purified by fractional distillation. The main contaminant was water which was removed-quite easily by distillation of the phenol-water azeotrope. This azeotrope boils at approximately 100°C and contains 91% water.[6]

The BF_3 was obtained and purified as described previously. (See work cited in reference 1, Part III).

The procedure and apparatus used to determine vapor pressures and separation factors for the phenol-BF_3 system were the same as those described earlier for the anisole-BF_3 and *n*-butyl sulfide-BF_3 systems. (See work cited in reference 1, Parts II and III).

RESULTS AND DISCUSSION

Separation Factor

The single-stage separation factor (α) for the phenol-BF_3 system is the isotopic equilibrium constant for the exchange reaction

$$B^{10}F_3(g) + B^{11}F_3\cdot\text{Phenol}(l) \rightleftharpoons B^{11}F_3(g) + B^{10}F_3\cdot\text{Phenol}(l). \quad (1)$$

If the amount of BF_3 in the liquid phase is large compared to that in the gas phase, then α is satisfactorily approximated by sampling the gas phase before and after contact. Thus,

$$\alpha = \frac{B^{10}/B^{11}(l)}{B^{10}/B^{11}(\text{gas})} \cong \frac{B^{10}/B^{11}(\text{gas}) \text{ before equilibration}}{B^{10}/B^{11}(\text{gas}) \text{ after equilibration}}. \quad (2)$$

In following this simplified sampling procedure, care must be taken that the amount of sample gas removed from the reactor does not appreciably reduce the pressure in the system.

Mass analyses of the BF_3 samples were made with a 6-in., 60° sector, mass spectrometer by scanning the peaks at m/e 48 and 49, and at m/e 10 and 11. The resulting separation factors were generally reproducible to ± 0.002. The results are shown in Table I.

These data may be expressed by the least-squares equation,

$$\log\alpha = 10.315/T - 0.02423. \quad (3)$$

From Eq. (3) estimates have been made of the thermodynamic functions, ΔH, ΔS, and ΔF, for the isotopic

* This paper is based on work performed for the Atomic Energy Commission by Union Carbide Corporation.

† Research participant from the University of Tennessee, Knoxville, Tennessee.

[1] R. M. Healy and A. A. Palko, J. Chem. Phys. **28**, 211 (1958) (Part I); A. A. Palko, R. M. Healy, and L. Landau, *ibid.* **28**, 214 (1958) (Part II); A. A. Palko, *ibid.* **30**, 1187–89 (1959) (Part III); A. A. Palko and J. S. Drury, *ibid.* **33**, 779–81 (1960) (Part IV).

[2] V. Gasselin, Ann. chim. et phys. (7) **3**, 5–83 (1894).

[3] F. J. Sowa, H. D. Hinton, and J. A. Nieuwland, J. Am. Chem. Soc. **55**, 3402–7 (1933).

[4] H. Meerwein and W. Pannwitz, J. prakt. Chem. **141**, 123–48 (1934).

[5] This compound is available in technical grade from Baker and Adamson Products, General Chem. Div., Allied Chemical and Dye Corporation, 40 Rector Street, New York 6, N. Y.

[6] "Azeotropic Data," *Advances in Chemistry Series No.* 6 (American Chemical Society, Washington, D. C., 1952), p. 9.

TABLE I. Single-stage isotopic separation factors for the system $BF_3(g) \rightleftharpoons BF_3 \cdot Phenol(liq)$.

Temp. °C	−8	0	10	11	13	21	30	37
α	1.035	1.034	1.028	1.025	1.029	1.026	1.023	1.022
	1.036	1.033	1.028	1.026		1.027	1.023	
	1.035	1.032	1.028	1.023		1.021	1.023	
	1.036	1.029	1.025			1.026	1.023	
		1.036	1.024				1.024	
			1.030				1.024	
							1.025	
							1.025	
							1.025	
							1.022	
							1.021	
							1.020	
							1.026	
Av. α at 95% C.I.	1.036 ±.001	1.033 ±.003	1.027 ±.002	1.025 ±.004	1.029	1.025 ±.004	1.023 ±.001	1.022

exchange reaction. Values calculated for 30°C are $\alpha = 1.023$, $\Delta H = -47.2$ cal/mole, $\Delta S = -0.074$ cal/deg. mole, $\Delta F = -13.2$ cal/mole. These values are quite similar to those for the Me_2S, Bu_2S, and anisole systems.

Vapor Pressure

The vapor pressures of several different compositions of BF_3 in phenol were measured over a temperature range from −10°C to 40°C. These data are shown in Fig. 1. Least-squares curves of the form $\log P = a - (b/T)$ were fitted to the experimental points. Values of the constants of these curves are given in Table II. As is usually the case for such compounds, the vapor pressure of the 1:2 adduct was much smaller than that for the 1:1 compound. Thus, at 30°C the vapor pressure of the 1:2 complex was 300 mm while the vapor pressure of the 1:1 compound was too great to measure in the glass apparatus which was used. It was estimated to be approximately 30 000 mm.

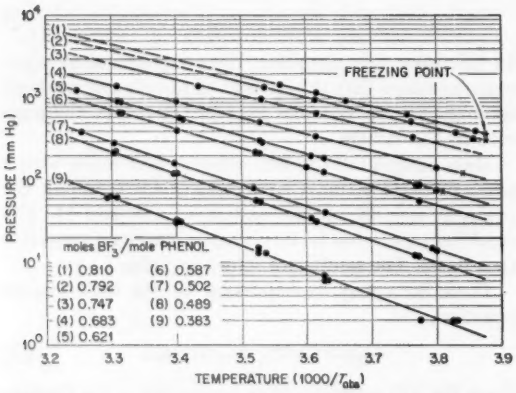

FIG. 1. Vapor pressures of various compositions of the system BF_3+phenol.

The heat change for the exothermic reaction

$$BF_3(g) + 2C_6H_5OH(l) = BF_3 \cdot 2C_6H_5OH(l),$$

was estimated from the vapor-pressure equation, assuming ΔH to be equal to $-2.303\,Rb$. This approximation yielded the value −14 kcal/mole (Table II). A more reliable estimate may be obtained from calorimetric measurements which are to be made with this compound.

Discussion

The phenol-BF_3 exchange reaction may be used as the basis of a system for separating boron isotopes. However, it does not appear as attractive for this

TABLE II. Vapor pressure of phenol-BF_3 solution, from −10°C to +40°C $\log P = a - (b/T)$.

Composition of solution (moles BF_3/mole phenol)	a	b	$2.303\,R\,b$
0.165	10.7	3000	14
0.205	10.8	2970	14
0.286	11.3	3040	14
0.309	11.1	2920	13
0.383	11.7	2990	14
0.489	11.3	2710	12
0.502	11.1	2630	12
0.587	10.4	2300	11
0.622	10.3	2200	10
0.683	9.70	1980	9.1
0.747	9.73	1910	8.8
0.792	9.86	1900	8.7
0.810	9.94	1900	8.7

purpose as some of the exchange reactions previously studied. The separation factor is somewhat smaller than that for the anisole and the Bu_2S reactions. Further, for a given solution composition the vapor pressure of the phenol complex is much greater than that of the other adducts which have been studied. Thus, it would be necessary to operate the phenol system either with less BF_3 in the liquid phase or at considerably greater pressures than, for example, the anisole system.

THE JOURNAL OF CHEMICAL PHYSICS VOLUME 35, NUMBER 1 JULY, 1961

Electronic Structure, Spectra, and Magnetic Properties of Oxycations. III. Ligation Effects on the Infrared Spectrum of the Uranyl Ion*†

S. P. McGLYNN, J. K. SMITH, AND W. C. NEELY

Coates Chemical Laboratories, Louisiana State University, Baton Rouge 3, Louisiana

(Received December 5, 1960)

A series of uranyl complexes $K_xUO_2L_y(NO_3)_2$, where L is the variable ligand (or ligands), has been prepared; it has been shown that a ligand series may be defined using the antisymmetric stretching frequency of the uranyl entity, and this series exhibits a remarkable parallelism with the spectrochemical series defined by Δ in octahedral complexes of transition metals of the 1st and 2nd series. This parallelism has been rationalized using a mixed ligand field theory in which the uranyl ion is considered subject to bonding with ligands which are arranged hexagonally in a plane equatorial to the O—U—O axis. It is shown that the large changes of ν_3 and ν_1 are due primarily to electron population of the ϕ_u and δ_u atomic orbitals of uranium. Such population is physically equivalent to the reductions $AmO_2^{++}\rightarrow AmO_2^{+}$ and $NpO_2^{++}\rightarrow NpO_2^{+}$, which cause a decrease of approximately 100 cm^{-1} in ν_3. It is further shown that $\Delta\bar{\nu}_3 = -\text{electrostatic effect} - \sigma(L\rightarrow M) - \pi(L\rightarrow M) \pm \pi(M\rightarrow L)$, where in the last term the plus sign is the more probable, and the results obtained have been rationalized using this equation.

Some evidence in favor of linearity of the UO_2^{++} has also been induced, and a general criterion for distinguishing the difficulty observable ν_1 has been reestablished. It has also been shown, although not discussed extensively, that the stability of uranyl complexes should increase, roughly as $\bar{\nu}_3$ (or $\bar{\nu}_1$) decreases. The discussion of similar effects in vanadyl, titanyl, chromyl, and other oxycations has been deferred to a later time.

INTRODUCTION

IT may be assumed that the uranyl ion UO_2^{++} is linear. Although such linearity may not be deduced completely unambiguously from any one experiment, there is general accord that a collinear O—U—O structure affords the better interpretation of the Raman,[1] infrared,[2] and electronic[3,4] spectra, and of x-ray diffraction intensities.[5] It is also rather well established[2] that the uranyl ion possesses three characteristic frequencies: the symmetric stretching frequency, ν_1 or σ_g^+, lying in the range 780–900 cm^{-1}; the asymmetric stretching frequency, ν_3 or σ_u^+, lying in the range 800–1000 cm^{-1}; and the bending vibration, ν_2 or π_u, appearing in the neighborhood of 200 cm^{-1}. The rather large frequency intervals quoted for ν_1 and ν_3 are indicative of the fact that appropriate complexation of the uranyl ion by ligand groups presumed to lie in, or nearly in, a plane perpendicular to the axial O—U—O direction, produce extremely large variations in ν_1 and ν_3; this latter is evident from the compilation of Table I. It is also known that similar large variations in the metal-oxygen stretching frequencies of other oxycations are occasioned by change of ligation.[6] Indeed the U—O bond distance of uranyl may vary[5] from 1.60–1.92 A depending on the affixed equatorial ligands. It is with this problem of the effect of ligand on metal-oxygen vibration frequency and on metal-oxygen bond distance that the present article is concerned. This discussion will consider only the uranyl ion; however, any conclusions arrived at may be modified to enable consideration of other oxycations such as neptunyl, vanadyl, zirconyl, titanyl, etc., and such adaptation will form the subject matter of further communications.[7]

It has also been observed[3] that the uranyl stretching frequencies seem to decrease as one proceeds from left to right along the spectrochemical series. This inference was made[3] from consideration of the compounds $RbUO_2(NO_3)_3$, $Cs_2UO_2Cl_4$, $NaUO_2(CH_3COO)_3$, and $K_3UO_2F_5$; since the equatorial coordination number is apparently not identical for these four compounds,

* This research was supported by a Research Corporation Venture Grant and by a National Science Foundation Grant.

† Presented in part at the Symposium on Molecular Electronic Spectroscopy, ACS Meeting, Cleveland, Ohio, April 11, 1960.

[1] S. Minc and Z. Kecki, Roczniki Chem. **32**, 1427 (1958).

[2] L. H. Jones, Spectrochim. Acta **10**, 395 (1958); **11**, 409 (1959).

[3] Paper I in the present series: S. P. McGlynn and J. K. Smith, J. Mol. Spectroscopy **6**, 164 (1961).

[4] Paper II in the present series: S. P. McGlynn and J. K. Smith, J. Mol. Spectroscopy **6**, 188 (1961).

[5] W. H. Zachariasen, Acta Cryst. **8**, 847 (1954).

[6] C. G. Barraclough, J. Lewis, and R. S. Nyholm, J. Chem. Soc. **1959**, 3352.

[7] J. Selbin, W. C. Neely, L. Holmes, W. B. Schomburger, and S. P. McGlynn (to be published).

TABLE I. Vibrational frequencies of some uranyl compounds.

Compound	Serial No.[a]	$\bar{\nu}_3$(cm^{-1})	$\bar{\nu}_1$(cm^{-1})	k_{eff}[b]	rU—O(1)[c]	rU—O(2)[d]
$K_3UO_2F_5$[e–g]	(1)	863	789	6.03	1.76	1.76
$KUO_2(CO_3)_2$	(2)	856	808	6.32	1.74	1.75
$CsUO_2Cl_3$[g]	(6)	920	830	6.67	1.73	1.74
$KUO_2Cl_3 \cdot 2H_2O$	(7)	902.9	831.6	6.69	1.73	1.74
$RbUO_2Cl_3 \cdot 2H_2O$	(8)	903.2	831.8	6.69	1.73	1.74
$CsUO_2Cl_3$	(10)	916.3	836.1	6.76	1.72	1.74
$CsUO_2(CH_3COO)_3$	(11)	920	842.2	6.86	1.72	1.74
$NaUO_2(CH_3COO)_3$[f,g]	(12)	931	850	6.99	1.71	1.74
$RbUO_2(CH_3COO)_3$	(14)	924	852.1	7.02	1.71	1.74
$NaUO_2(CH_3COO)_3$	(15)	927.8	855.1	7.08	1.70	1.73
$Co_2UO_2(SO_4)_2 \cdot 3H_2O$	(16)	923.1	860.5	7.16	1.70	1.73
$UO_2(NO_3)_2 \cdot 6H_2O$	(18)	941	863.9	7.21	1.70	1.73
$KUO_2(NO_3)_3$	(20)	949.5	870.3	7.32	1.69	1.73
$UO_2(NO_3)_2 \cdot 3H_2O$	(22)	948.1	874	7.38	1.69	1.73
$KUO_2(NO_3)_3$	(24)	943.1	875.5	7.40	1.69	1.72
$CsUO_2(NO_3)_3$	(25)	956.2	884.0	7.55	1.68	1.72
$NH_4UO_2(NO_3)$	(26)	967.2	885.7	7.58	1.68	1.72
Impurity in (10)[h]	(10a)	891.2	827.9	...	...	...
Impurity in (10)[h]	(10b)	905.2	827.1	...	...	...
Impurity in (10)[h]	(10c)	904.6	827.7	...	...	...
Impurity in (25)[h]	(25a)	949.8	876.0	...	...	...

[a] The serial number corresponds to that used in Fig. 3.
[b] In millidynes/angstrom.
[c] In A units; evaluated from Eq. (7).
[d] In A units; evaluated from Eq. (6).
[e] All values for this compound are experimental, and were used by Jones to evaluate the constants in Eq. (6).
[f] All values for these compounds are experimental and were used to evaluate the constants in Eq. (7).
[g] These data are from L. H. Jones, Spectrochim. Acta **1959**, 490; all others are from G. H. Dieke and A. B. F. Duncan, *Spectroscopic Properties of Uranium Compounds* (McGraw-Hill Book Company, Inc., 1949), Vol. II. These authors use Eq. (4) in a somewhat different form.
[h] Uranyl ligate impurities, whose exact compositions are unimportant for our present purpose.

since the free metal cation varies, and since some of the vibrational data are for solutions and some for solids, it is obvious that such inference requires further substantiation. This article then has as a concomitant aim the experimental demonstration of whether or not ν_1 (and/or ν_3) decrease regularly as one traverses the spectrochemical series from left to right, and if this is so, to develop a theoretical understanding of such behavior.

EXPERIMENTAL

1. Purification and Preparation of Chemicals

The present effort is concerned with the preparation of a series of uranyl adduct compounds in which both composition and ligand are either varied regularly or maintained constant. It is obvious that such must be the aim of any systematic study, for only in this way may regular variations be detected and classified. The series of compounds chosen for this purpose has the general formula $K_xUO_2L_y(NO_3)_2$, where $X=2$ if the ligand L has a single negative charge, where $X=0$ if L is neutral, and where $Y=2$ or 1 when L is unidentate or bidentate, respectively. The reason for this choice is that methods of preparation and chemical stoichiometries are available for the six compounds:

$UO_2(H_2O)_2(NO_3)_2$,

$UO_2(C_6H_5N)_2(NO_3)_2$,

$UO_2(NH_3)_2(NO_3)_2$,

$UO_2(en)_2(NO_3)_2$,

$K_2UO_2(CN)_2(NO_3)_2$,

and

$K_2UO_2(NO_3)_3$.

Furthermore, there exists an infrared spectral determinant of whether the nitrate group is coordinatively or ionically bound.

(a) $UO_2(NO_3)_2 \cdot 6H_2O$, dioxohexaquouranium (VI) nitrate: The material used was an ACS grade from Fisher Scientific Company, and was recrystallized four times from water before use. The infrared spectrum is recorded in Fig. 1, and agrees with those previously reported for this material.[8,9] This material was used in the preparation of all other compounds.

(b) $UO_2(NO_3)_2 \cdot 2H_2O$, dinitratodioxodiaquouranium (VI): This material was prepared by standard methods,[8,9] and its infrared spectrum (shown in Fig. 1) agrees with those previously reported.[8,9]

(c) $UO_2(C_5H_5N)_2(NO_3)_2$, dinitratodioxodipyridineuranium (VI): Preparation and subsequent purification was carried out in the manner reported by Barr and Horton.[10] These authors determined the composition to be that cited above; the spectrum of the material prepared here and shown in Fig. 2, reproduces that reported by them.

(d) $UO_2(NH_3)_2(NO_3)_2$, dinitratodioxodiammineuranium (VI): Von Unruh[11] reported the formation of a complex of composition $UO_2(NO_3)_2 \cdot 2NH_3$ as a voluminous egg-colored precipitate when ammonia was introduced into an anhydrous diethyl ether solution of $UO_2(NO_3)_2$. The material used in these studies was obtained in a similar manner, and its spectrum is given in Fig. 2.

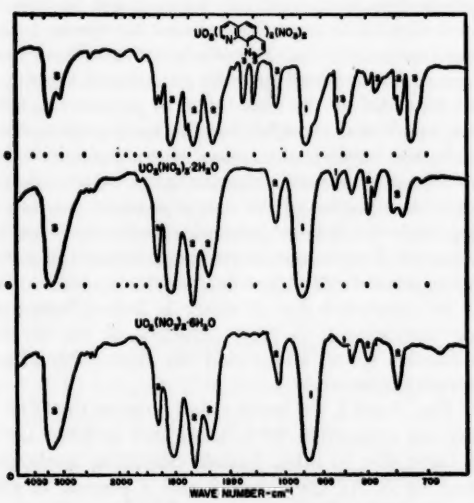

FIG. 1. The vibrational spectra of some uranyl complexes. Uranyl bands are denoted by 1, nitrate bands by 2, and ligand (including H_2O) bands by 3.

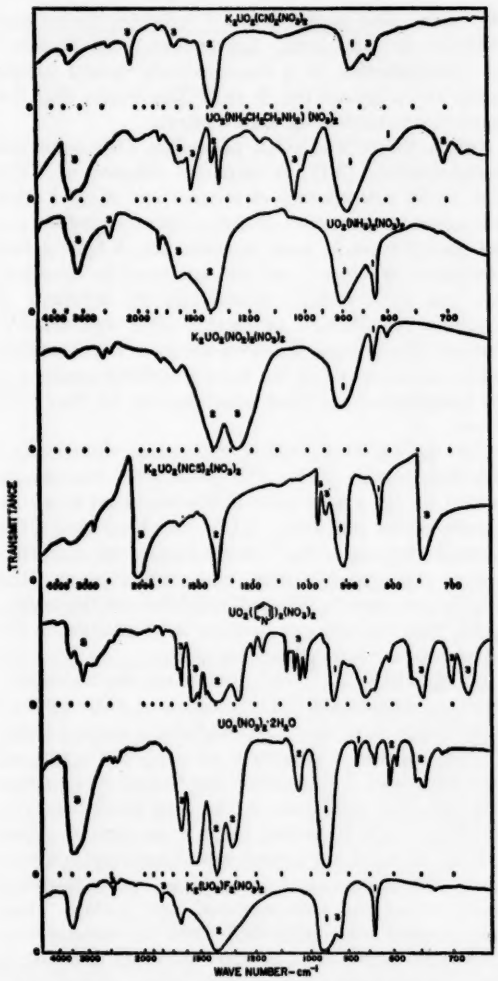

FIG. 2. The vibrational spectra of some uranyl complexes. Uranyl bands are denoted by 1, nitrate bands by 2, and *L* ligand bands by 3.

(e) $UO_2(en)(NO_3)_2$, dinitratothetylenediamineuranium (VI): This material was prepared by the method of Watt and Machel[12] who determined its composition to be that cited above. Its spectrum is given in Fig. 2.

(f) $UO_2(o\text{-phen})_2(NO_3)_2$, dioxo(*bis*-orthophenanthroline)uranium (VI) nitrate: A saturated solution of *o*-phenanthroline in ethanol was added to a solution of uranyl nitrate hexahydrate in ethanol. A yellow crystalline precipitate resulted, which was collected by filtration, washed with diethyl ether and dried in vacuum. The infrared spectrum (Fig. 1) showed the presence of the low ligands (orthophenanthroline and the nitrate group); however, the nitrate seems to

[8] J. G. Allpress and A. N. Hambly, Australian J. Chem. **12**, 9 (1959).

[39] B. M. Gatehouse and A. E. Comyns, J. Chem. Soc. **1958**, 65.

[10] J. T. Barr and C. A. Horton, J. Am. Chem. Soc. **74**, 4430 (1952).

[1] A. Von Unruh, dissertation, Univ. of Rostock, Poland, 1909.

[12] G. W. Watt and A. R. Machel, J. Am. Chem. Soc. **72**, 280 (1950).

exist as an ionic species, if one is to believe the infrared criterion of Gatehouse, Livingstone, and Nyholm[13] for differentiation of a coordinatively bound nitrate group and a nitrate ion. It is for this reason that this material has been designated a nitrate.

(g) $K_2UO_2(CN)_2(NO_3)_2$ potassium dicyanodinitratodioxouranate (VI): A saturated solution of KCN in a 50–50 v/v mixture of ethanol and diethyl ether was added to a solution of uranyl nitrate dihydrate in the same solvent at room temperature. A light yellow precipitate developed, and was gathered by filtration; this was then washed successively by solutions of potasium cyanide and by diethyl ether and dried in vacuum. The infrared spectrum shown in Fig. 2 exhibits bands characteristic of the three absorbing species and the composition has been determined to be that cited above.

(h) $K_2UO_2(NO_2)_2(NO_3)_2$, potassium dinitritodinitratodioxouranate (VI): The preparation was similar to that in (g) except that KNO_2 was used in all instances where previously KCN had been used. The infrared spectrum of Fig. 2 shows frequencies characteristic of the uranyl, nitrito, and nitrato groups. The NO_2^- is presumed to be coordinated through the oxygen rather than the nitrogen because of its position in the determined infrared vibrational series.

(i) $K_2UO_2(NCS)_2(NO_3)_2$, potassium dinitratodioxodithiocyanatouranate (VI): A saturated water solution of potassium thiocyanate was added to a water solution of uranyl nitrate hexahydrate, whereupon a bright red color developed. This solution was heated over a steam bath for 1 hr, and upon cooling, long needlelike crystals formed which seemed to be a mixture of yellow and red forms of the uranyl salt. These crystals were reprecipitated from an alcohol solution upon addition of diethyl ether and now appeared light yellow. These were washed with ether and dried in vacuum over $CaCl_2$ and $CaSO_3$. The infrared spectrum depicted in Fig. 2 shows bands characteristic of the nitrato, thiocyanato, and uranyl groupings.

(j) $K_2(UO_2)F_2(NO_3)_2$, potassium difluorodinitratodioxouranate (VI): A water solution of several grams of uranyl nitrate hexahydrate was added to a saturated aqueous solution of potassium fluoride. The resulting solution was heated at 100°C for 15 min, and upon cooling solidified. This solid was reprecipitated from the previously specified ethyl alcohol-diethyl ether mixture, washed with a saturated solution of KF in the same solvent with diethyl ether, and was finally dried in vacuum over calcium chloride and calcium sulfate. The infrared spectrum of this complex (Fig. 2) contained the characteristic frequencies of the uranyl, nitrato, and metal fluoride groups, and but for the bands due to nitrato and a smaller shift towards lower wave numbers is identical with the spectrum reported[10] for a presumed UO_2F_2 species.

It is to be noted that the stoichiometries of the compounds f, h, i, and j are not known. Compound f is of no great relevance to the present study since in it the nitrate group is apparently ionic. The stoichiometries of the other three were not determined by analysis since this was felt unnecessary in view of the fact that these compounds can be converted by simple mass action effects (*vide infra*) into other complexes the stoichiometries of which are known. Such interconversion experiments leave very little doubt but that the compounds investigated form a series of the general formula $K_xUO_2L_y(NO_3)_2$ quoted above.

2. Instrumental Procedures

All infrared spectra were determined with a Perkin-Elmer 21 recording spectrophotometer. The spectra obtained in KBr pellets are shown in Figs. 1 and 2. It has been noted that anomalies sometimes occur[14] in the infrared spectra of inorganic compounds prepared by the KBr pellet technique, and are apparently associated with exchange of anion between KBr and the compound being investigated, as well as with pressure and orientation effects experienced in or in introduction into the KBr matrix. It is also to be noted that all presented spectra contain the characteristic water band at $\sim$3500 cm^{-1}; this band should occur only in the two compounds $UO_2(NO_3)_2 \cdot 2H_2O$ and $UO_2(NO_3)_2 \cdot 6H_2O$. This latter is rather disturbing since this water might be coordinatively bound to the uranium, and the species being investigated might thus be entirely different from that prepared. It was noted that the intensity of the water band depended on the time taken to prepare the KBr pellet, and it was thought that the hydrophilic nature of KBr was causing absorption of atmospheric water vapor. In order to see if anion exchange, matrix effects, or possible aquation of the uranyl complex was interfering with the results, selected spectra were run in nujol mulls. Despite considerable decrease of the water band no other detectable differences were observed. It may be concluded that if water is indeed bound in these complexes it is most certainly in the second coordination sphere and should not appreciably affect the results obtained here.

In Figs. 1 and 2, the bands ν_1 and ν_3 due to the UO_2^{++} entity are designated by 1, those due to NO_3^- by 2 and those due to other ligands (including nonbound water) by 3. All the bands 2 and 3 present in any spectrum were identified, if possible, by comparison with the spectra of the pure components. However, when a complex is formed it is expected that certain bands may disappear and some new bands may appear. For example, in the pyridine complex seven bands normally found in free pyridine (2.76, 5.02, 5.46, 5.93, 6.33, 9.36, and 10.09 μ) disappear; although no

[13] B. M. Gatehouse, S. E. Livingstone, and R. S. Nyholm, J. Chem. Soc. **1957**, 4222.

[14] V. W. Meloche and H. Kelbui, J. Inorg. Nucl. Chem. **6**, 104 (1955).

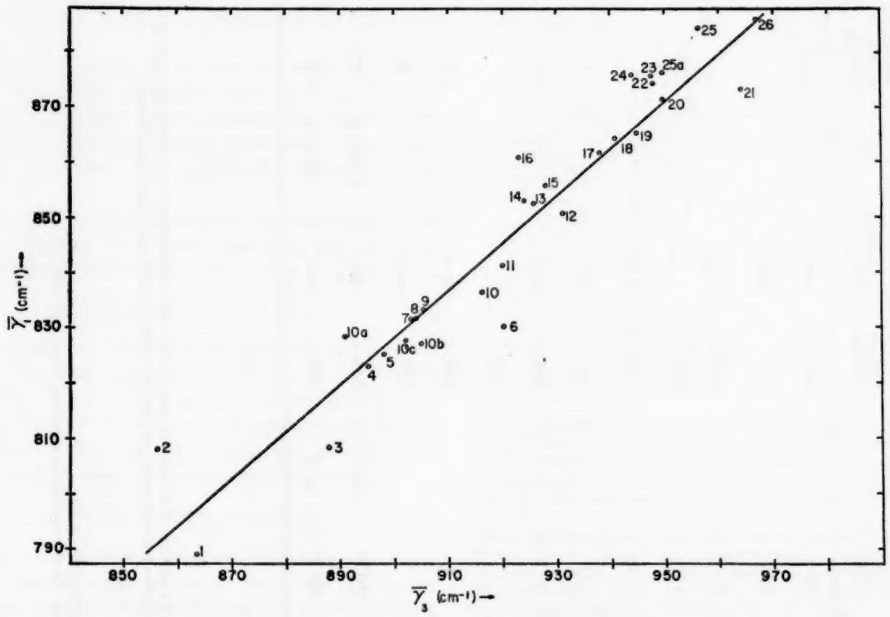

FIG. 3. A plot of $\bar{\nu}_1$ (cm^{-1}) vs $\bar{\nu}_3$ (cm^{-1}). Numbers on the graph correspond to those in Tables I and II.

new bands appear in this complex, the appearance of such in the spectra of pyridine complexes to other metals has been noted.[10] No attempt to regularize the ligand spectra was made, and the bands 2 and 3 were used merely to verify the presence of a given ligand, and by elimination, to yield the bands 1 characteristic of UO_2^{++}.

Since some frequencies forbidden in the free ligands may be allowed when they are complexed some additional confirmation was sought as to the correct identity of the uranyl bands ν_1 and ν_3 (1 in Figs. 1 and 2). If the three vibrations characteristic of the uranyl ion are assumed harmonic, and the assumptions of a valence force field and a linear ion made, the following equations result:

$$\bar{\nu}_1 = (f/M_O)^{\frac{1}{2}}(\tfrac{1}{2}\pi c)\,\text{cm}^{-1} \quad (1)$$

$$\bar{\nu}_2 = (2d(1+2M_O/M_U)/M_O)^{\frac{1}{2}}(\tfrac{1}{2}\pi c)\,\text{cm}^{-1} = \bar{\nu}_3(2d/f)^{\frac{1}{2}} \quad (2)$$

$$\bar{\nu}_3 = [(1+2M_O/M_U)f/M_O]^{\frac{1}{2}}(\tfrac{1}{2}\pi c)\,\text{cm}^{-1} = \bar{\nu}_1(1+2M_O/M_U)^{\frac{1}{2}}, \quad (3)$$

where M_O and M_U are the atomic masses of oxygen and uranium, respectively; f is the elastic force constant in the direction of the U—O bond; and d, that in the direction perpendicular to the U—O bond. If the above relations hold in practice then a plot of $\bar{\nu}_1$ vs $\bar{\nu}_3$ for any series of uranyl complexes should yield a straight line with slope equal to $(1+2M_O/M_U)^{-\frac{1}{2}}$. Such a plot is shown in Fig. 3 and was drawn from the data of Tables I and II. It is obvious that good linearity obtains. The line that is considered the best fit of points was obtained by a least-squares treatment of all points with deviations less than 2.5% from a first least-squares line using all points. This led to neglect of points 2, 11, 12, and 21, which in view of the excellent linearity obtained raises some doubt as to the correct identification of uranyl frequencies for these four compounds. The line obtained obeys the equation

$$\bar{\nu}_1 = 21 + 0.89\bar{\nu}_3, \quad (4)$$

whereas that obtaining for a linear ion with neglect of ligands should be

$$\bar{\nu}_1 = 0 + 0.94\bar{\nu}_3. \quad (5)$$

The frequencies of the complexes prepared in this laboratory are shown in Fig. 3 as points 3, 4, 5, 9, 13, 19, and 23. In all cases except the cyanide and fluoride complexes where the symmetric vibration could not be detected and which are therefore not plotted, all observed vibrational frequencies agree excellently with the determined relationship, leaving little doubt as to the correct identification of the bands, labeled 1 in Figs. 1 and 2, as corresponding to uranyl stretching frequencies.

RESULTS

Before proceeding to what is considered the main result of this work it is appropriate to make the following points:

(a) It is seen from Fig. 3 that ligand masses are not important in determining frequency. This is to be

TABLE II. Properties of the series of compounds $K_xUO_2L_y(NO_3)_2$ as a function of the position of L in the spectrochemical series.

Compound	$RbUO_2(NO_3)_3$	$K_3UO_2(NO_3)_2F_2$		$UO_2(NO_3)_2(H_2O)_2$	$UO_2(o\text{-phen})_x(NO_3)_2$	$UO_2(py)_2(NO_3)_2$	$K_2UO_2(ONO)_2(NO_3)_2$	$K_2UO_2(NCS)_2(NO_3)_2$		$UO_2(NH_3)_2(NO_3)_2$	$UO_2(en)_2(NO_3)_2$		$K_2UO_2(CN)_2(NO_3)_2$
$\bar{\nu}_3$(cm^{-1})	964[a]	960[b]		945	945	926	905	898		895	888		873[b]
$\bar{\nu}_1$(cm^{-1})	873	...		875	865	852	833	825		823	808		...
k_{eff}[c]	7.36	...		7.40	7.23	7.02	6.71	6.59		6.55	6.32		...
rU—O(1)[c]	1.69	...		1.69	1.70	1.71	1.72	1.72		1.73	1.74		...
rU—O(2)[c]	1.73	...		1.72	1.73	1.74	1.74	1.74		1.75	1.75		...
Serial No.[d]	(21)	...		(23)	(19)	(13)	(9)	(5)		(4)	(3)		...
IR Series[e]	$NO_3^->$	$F^->$		$H_2O>$	o-phen>	py>	$ONO^->$	$NCS^->$		$NH_3>$	en>		CN^-
Series A[f]	$NO_3^-<$			$H_2O<$			$ONO^-<$			NH_3			
Series B[g]	$NO_3^-<$			$H_2O<$						$NH_3<$	en<		CN^-
Series C[h]		$F^-<$		$H_2O<$		py<				$NH_3<$	en<		CN^-
Series D[i]	$NO_3^-<$	$F^-<$	$ONO^-<$	$H_2O<$				$NCS^-<$	py<	$NH_3<$	en<	o-phen<	CN^-
Series F[j]		$F^-<$	$ONO^-<$	$H_2O<$				$NCS^-<$	py≤	$NH_3<$	en<	o-phen<	CN^-

[a] This datum from B. M. Gatehouse and A. E. Comyns, J. Chem. Soc. **1958**, 3965.
[b] It was not possible to locate $\bar{\nu}_1$ in these compounds.
[c] Units and meaning are defined in reference to Table I.
[d] The serial number corresponds to that used in Fig. 3.
[e] This series is defined in terms of the most *unambiguous experimental* entity, namely $\bar{\nu}_3$, and is arranged in order of decreasing frequency. If arranged in terms of rU—O(1) or rU—O(2) the inequality signs may be reversed to correspond to those in the various spectrochemical series *A*, *B*, *C*, *D*, or *F*. The following abbreviations are used: o-phen=o-phenanthroline; py=pyridine; ONO^-=nitrite ion; en-ethylenediimine.
[f] R. Tsuchida, Bull. Chem. Soc. Japan **13**, 388 438 (1938).
[g] A. Kiss and D. Czegledy, Z. Anorgan. Chem. **235**, 407 (1937); A. Kiss, *ibid.*, **246**, 28 (1941).
[h] L. E. Orgel, J. Chem. Phys. **23**, 1004 (1955).
[i] T. M. Dunn, *Modern Co-ordination Chemistry*, edited by J. Lewis and R. G. Wilkins (Interscience Publishers, Inc., New York, 1960), p. 229.
[j] C. K. Jörgenson, "Absorption spectra of complexes of heavy metals," Research Rept. to European Research Office, U.S.D.A., Frankfurt-am-Main, Germany, October 25, 1958.

expected, because in Eq. (3) $2M_O/M_U$ is already small compared to 1.

(b) Figure 3 and Eq. (4) may be used to predict the position of the difficulty observable ν_1. The σ_g^+ vibration is forbidden in an isolated $D_{\infty h}$ species, and though present in many uranyl complexes it is generally rather weak in most and completely absent in many others.

(c) In Tables I and II are also tabulated values of k_{eff}, the effective U—O force constant; the modification of Badger's relation for UO_2^{++} due to Jones,[2]

$$r\text{U—O}(2) = 1.08k_{eff}^{-\frac{1}{3}} + 1.17 \qquad (6)$$

has been used to tabulate bond distances in Tables I and II. The predicted value of rU—O(2) for $NaUO_2(CH_3COO)_3$ is 1.73; the experimental value is 1.71 A. This one comparison exhausts at present any further verification of Eq. (6). The distances rU—O(1) of Tables I and II were evaluated using the equation

$$r\text{U—O}(1) = 1.993k_{eff}^{-\frac{1}{3}} + 0.666, \qquad (7)$$

where the two constants were evaluated by solution of the two simultaneous equations based on the known U—O bond lengths of KUO_2F_3 and $NaUO_2(CH_3COO)_3$. It is not intended to imply here that Eq. (7) is better than Eq. (6). There exists no *a priori* reason why either one of these should be preferred to the other, unless one attaches some significance to Badger's initial conclusion that the multiplier of $k_{eff}^{-\frac{1}{3}}$ in all such equations should be about 0.5 A, nor is there sufficient data on U—O bond lengths available to enable *a posteriori* elimination of either Eq. (6) or Eq. (7) on the basis of comparison with experiment. Our intention is merely to point out that irrespective of whichever equation one uses (and this includes Badger's equation[15] using Badger's constants) that a very small change in rU—O conditions a very large change in $\bar{\nu}_1$ and $\bar{\nu}_3$. This has previously been pointed out by Jones[2] using Eq. (6), and the average of rU—O using Eq. (7) is still only twice that found using Eq. (6).

The possibility then arises that one might use the variation in $\bar{\nu}_3$ as a very sensitive probe to measure inductive and conjugative effects of various groups attached to common ligating species as for example $R_2N—CR_2—CR_2—NR_2$ or

$$\begin{array}{ccccc} R—C & — & CH_2 & — & C—R. \\ \| & & & & \| \\ O & & & & O \end{array}$$

This of course implies an understanding of the effects producing the change in $\bar{\nu}_3$ (*vide infra*); this line of reasoning has been suggested by and is being pursued by Dr. Joel Selbin of this department.

(d) Linearity of the data of Fig. 3, and comparison of Eqs. (4) and (5) might be construed as good substantiating evidence of linearity of the uranyl ion.

[15] R. M. Badger, J. Chem. Phys. **3,** 710 (1935).

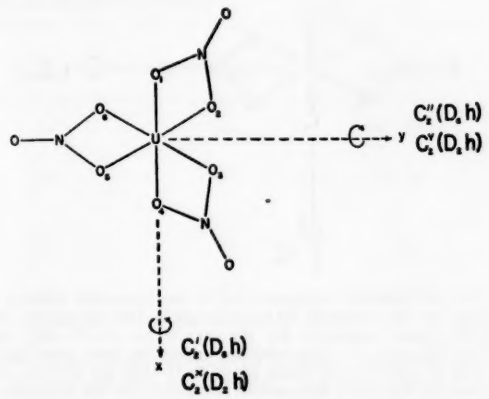

FIG. 4. Schematic representation of the equatorial spacing of atoms in the uranyl-tri-nitrato ion. The two axial oxygens of the UO_2^{++} group are in line with the uranium atom, one directly above, and the other directly below the plane of the paper; their positions have not been indicated in the diagram. The numbered subscripts on the hexagonally disposed ligated oxygens designate position within the hexagon, and correspond to the subscripting used in Tables IV and V. It is presumed in our discussion that the inner ring of six oxygens define a D_{6h} point group. This is only approximately true since the O_6—O_5 distance is actually shorter than either the O_6—O_1 or O_5—O_4 distances, making D_{3h} the more appropriate point group. However, all conclusions arrived at by consideration of a hexagonal disposition of ligating atoms, are also valid for a trigonal distribution. The symbolism to the right of x and y indicate corresponding operations in D_{6h} and D_{2h}.

However such is not warranted without further consideration. Such a study has been carried out and will be reported elsewhere[16]; suffice it to say here that Fig. 3 does indeed lend strong support to a linear O—U—O entity.

(e) It is evident from Table II that $\bar{\nu}_3$ (and $\bar{\nu}_1$) both decrease as one proceeds along the spectrochemical series. The agreement with the series of Tsuchida,[17] Kiss and Czegledy,[18] and Orgel[19] is complete. If, as has been shown above, the compound UO_2 (*o*-phen)$_x(NO_3)_2$ has ionic nitrate, then the relevant structure is most probably UO_2(*o*-phen)$_x(H_2O)_y$, in which case its vibrational frequency by comparison with that of the dihydrate (23) seems reasonable. In any case the *o*-phenanthroline complex should properly not be considered a member of the defined ligation series. Agreement with the series of Dunn[20] and Jørgenson[21] can be obtained if the nitrito and hydrate compounds (9 and 23) are permuted and the pyridine compound displaced to the right in Table II. In any case the

[16] W. Neely and S. P. McGlynn (to be published).
[17] R. Tsuchida, Bull. Chem. Soc. Japan **13,** 288, 438 (1938).
[18] A. Kiss and D. Czegledy, Z. Anorgan. Chem. **235,** 407 (1937); A. Kiss, *ibid.* **246,** 28 (1941).
[19] L. E. Orgel, J. Chem. Phys. **23,** 1004 (1955).
[20] T. M. Dunn, *Modern Coordination Chemistry*, edited by J. Lewis and R. G. Wilkins (Interscience Publishers, Inc., New York, 1960), p. 229.
[21] C. K. Jørgenson, "Absorption spectra of complexes of heavy metals," Research Rept. to European Research Office, U.S.D.A., Frankfurt-am-Main, Germany, October 25, 1958.

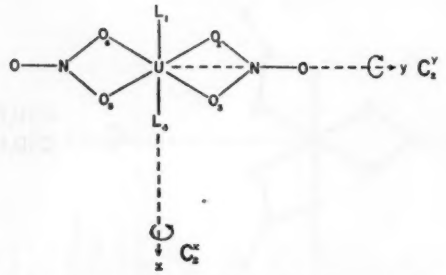

FIG. 5. Schematic representation of the equatorial spacing of atoms in the molecule $UO_2L_2(NO_3)_x^{x(-)}$. This presumed D_{2h} species seems reasonable for the case where $L=F$, H_2O, py, NCS, NH_3, and CN. The subscripting has the same meaning as in Fig. 4. The L's are placed closer to U than are the O's: the reason for this is the supposition (see text) that the strength of the uranium-ligand bond varies inversely as the strength of the uranium-axial oxygen bond.

correlation is alsmost as good as the agreement between the individual spectrochemical series (note the inversion of H_2O and NO_2^- between the series of Judd or Jørgenson and that of Tsuchida).

Such agreement is indeed remarkable and can be attributed only with a very small probability to coincidence. It is the more remarkable when one considers that the various spectrochemical series have been established from considerations of *electronic transitions* of *intra-d-shell type* in ligated elements primarily of the 1st and 2nd transition series. And now there exists a rather excellent inverse correllation of the energies of these intra-*d*-shell transitions with *infrared vibrational transitions* in the uranyl ion, the ligation of which involves primarily the overlap of ligand orbitals with 5*f*-*orbitals* of the uranium. The possibility that this be coincidence cannot be completely ruled out, and further research directed toward the preparation of pure rather than mixed ligand field complexes as reported on here is underway in these laboratories. However, the present data require rationalization of the somewhat surprising results obtained, and it to this end that the following is directed.

DISCUSSION

Although the coordination chemistry of the uranyl ion has received some attention,[22] and the number of known coordination compounds probably runs into several hundred, the structure of none of them is known in detail. It would seem, however, that there is a definite preference for a coordination number of eight, the axial oxygens being considered as ligands, and that all ligands are directly bonded to the uranium atom. The evidence for these presumptions has been summarized elsewhere[3,4]; however, other problems remain. Thus even when the stoichiometry is known there is some doubt as to the way the various ligands might be attached—some could be coordinated directly to the

[22] A. E. Comyns, Chem. Revs. **60**, 115 (1960).

TABLE III. Representations to which atomic orbitals[a] conform in relevant point groups.[b]

Point group	s	$p_x p_y$	p_z	$d_{x^2-y^2}$ d_{xy}	$d_{xz}d_{yz}$	d_z^2	$f_{x(x^2-y^2)}$ $f_{y(x^2-y^2)}$	f_{xyz}	$f_{z(x^2-y^2)}$	f_{xz^2} f_{yz^2}	f_{z^3}
$D_{\infty h}$	σ_g^+	π_u	σ_u^+	δ_g	π_g	σ_g^+	ϕ_u		δ_u	π_u	σ_u^+
D_{4h}	a_{1g}	e_{1u}	a_{2u}	e_{2g}	e_{1g}	a_{1g}	b_{1u}, b_{2u}		e_{2u}	e_{1u}	a_{2u}
D_{2h}	a_g	b_{1u}, b_{2u}	b_{1u}	a_g, b_{1g}	b_{2g}, b_{3g}	a_g	b_{3u}, b_{2u}		b_{1u}, a_u	b_{3u}, b_{2u}	b_{1u}

[a] The atomic orbitals used are those defined by M. G. Shirmazan and M. E. Dyatkina, Doklady Akad. Nauk S.S.S.R. **77**, 75 (1951); **82**, 735 (1953); J. Chem. Phys. (U.S.S.R.) **27**, 491 (1953). These three papers, translated in conjunction with the present work, appear in a report submitted to the Physics Branch, O.N.R., U.S. Navy and to the Chemistry Division, O.S.R., A.R.D.C., U.S. Air Force in December, 1955, by the Florida State University. The orbitals defined by J. C. Eisenstein, J. Chem. Phys. **25**, 142 (1956), and by C. A. Coulson and G. R. Lester, J. Chem. Soc. **1956**, 703, are identical with those used here, but unfortunately present two new notational systems.

[b] The character tables used are from E. B. Wilson, J. C. Decius, and P. Cross, *Molecular Vibrations* (McGraw-Hill Book Company, Inc., New York, 1955). The O—U—O axis is the principal axis of both $D_{\infty h}$ and D_{4h} groups, but is more accurately identified as the C_4^z axis of D_{4h}.

TABLE IV. Ligand group-orbitals of a D_{6h} uranyl ion complex.[a]

Orbital[b]	σ Orbital	$\pi_\perp$ Orbital	$\pi_\parallel$ Orbital[c]	Energy[d]
$(6)^{-\frac{1}{2}}(a_1-a_2+a_3-a_4+a_5-a_6)$	b_{1u}	b_{2g}	a_{2g}	$\alpha-2\beta_m$
$(\frac{1}{2})$ (a_2-a_3 a_5-a_6)	e_{2g}	e_{2u}	e_{1u}	$\alpha-\beta_m$
$(12)^{-\frac{1}{2}}(2a_1-a_2-a_3+2a_4-a_5-a_6)$				
$(\frac{1}{2})$ (a_2+a_3 $-a_5-a_6$)	e_{1u}	e_{1g}	e_{2g}	$\alpha+\beta_m$
$(12)^{-\frac{1}{2}}(2a_1+a_2-a_3-2a_4-a_5+a_6)$				
$(6)^{-\frac{1}{2}}(a_1+a_2+a_3+a_4+a_5+a_6)$	a_{1g}	a_{2u}	b_{2u}	$\alpha+2\beta_m$

[a] Reference should be made to Fig. 4 of text.

[b] The orbitals a, whether they be directed toward the uranium atom and in the equatorial plane (σ orbitals), or whether they be arranged perpendicular to the equatorial plane and thus parallel to the O—U—O axis ($\pi_\perp$ orbitals) are considered normalized. Overlap of type $\int a_i a_j d\tau (j \neq i)$ is neglected in normalizing the group orbitals.

[c] The $\pi_\parallel$ orbitals are p orbitals of the ligand lying in the equatorial plane and perpendicular to the σ orbitals. In order to maintain the same Hückel energy (column 5) for each of the three sets of orbitals (σ, $\pi_\perp$, and $\pi_\parallel$), it becomes necessary for the case of the $\pi_\parallel$ orbitals to define $a_i \equiv (-1)^i p_i(\parallel)$ where $p_i(\parallel)$ is the p orbital on ligand atom i which lies in the equatorial plane. For the σ and $\pi_\perp$ orbitals a_i is defined as $a_i \equiv p_{\sigma i}$ and $a_i \equiv p_i(\perp)$, respectively.

[d] Energy here means a one-electron Hückel molecular orbital energy. The coulomb integral $\alpha = \int a_i H a_i d\tau$ is the same for all three types of orbital. The resonance integral $\beta_m = \int a_i H a_{i\pm 1} d\tau$ varies with orbital type in the manner $|\beta_{\pi\parallel}| > |\beta_\sigma| \geq |\beta_{\pi\perp}|$, and has a negative value.

uranium atom, some could (in solution) be hydrogen bonded, and nitrate ions when coordinated could be unidentate or bidentate. The fact that the coordination number has been shown to be eight in four of the nine complexes studied,

$$UO_2(py)_2(NO_3)_2,^{10}$$

$$UO_2(NO_3)_2(H_2O)_2,^{8,9}$$

$$UO_2(NH_3)_2(NO_3)_2^{11}$$

and

$$UO_2(en)NO_3,^{12}$$

is the basis for presuming the same to be true in all other members of the series $K_xUO_2L_y(NO_3)_2$.

The structure of $RbUO_2(NO_3)_3$ is known to be reasonably close to that depicted in Fig. 4, wherein the nitrato groups are bidentate and are arranged in a plane equatorial to the O—U—O axis. It is presumed then that the relevant spectrosopic entity is the D_{6h} structure of Fig. 4. It may be argued that the complexes studied here are more properly considered to be those of a geometry depicted in Fig. 5 and of species D_{2h}. However, consideration of this point group does not contribute to clarity, and the interested reader will find sufficient information in Tables III, IV, and V to verify that insofar as the discussion in terms of a D_{6h} ligated species has any relevance, it is the same in both point groups.

The transformation properties of the 5*f*, 6*d*, 7*s*, and 7*p* valence orbitals of uranium are given for various point groups in Table III and the uranyl molecular orbitals are schematically arranged energywise on the extreme left of Fig. 6. This diagram has previously been discussed[3] and has been used[3,4] in interpreting the electronic spectra of UO_2^{++}, NpO_2^{+}, and NpO_2^{++}. The effects of a D_{6h} ligand electrostatic field on the

TABLE V. Ligand group-orbitals of a $D_{2h}(V_h)$ uranyl ion complex.[a]

Orbital[b]	σ Orbital	$\pi_\perp$ Orbital	$\pi_\parallel$ Orbital[c]	Energy[d]
$(4+2s^2)^{-\frac{1}{2}}(sL_1-a_2+a_3-sL_4+a_5-a_6)$	b_{3u}	b_{2g}	b_{1g}	$(4\alpha-4\beta_m+2s^2\alpha_L-8s\beta_{Lm})/(4+2s^2)$
$(4+2q^2)^{-\frac{1}{2}}(qL_1-a_2-a_3+qL_4-a_5-a_6)$	a_g	b_{1u}	b_{2u}	$(4\alpha+4\beta_m+2q^2\alpha_L-8q\beta_{Lm})/(4+2q^2)$
$(\frac{1}{2})$ (a_2-a_3 $+a_5-a_6$)	b_{1g}	a_u	b_{3u}	$\alpha-\beta_m$
$(\frac{1}{2})$ (a_2+a_3 $-a_5-a_6$)	b_{2u}	b_{3g}	a_g	$\alpha+\beta_m$
$(4+2r^2)^{-\frac{1}{2}}(rL_1+a_2-a_3-rL_4-a_5+a_6)$	b_{3u}	b_{2g}	b_{1g}	$(4\alpha-4\beta_m+2r^2\alpha_L+8r\beta_{Lm})/(4+2r^2)$
$(4+2p^2)^{-\frac{1}{2}}(pL_1+a_2+a_3+pL_4+a_5+a_6)$	a_g	b_{1u}	b_{2u}	$(4\alpha+4\beta_m+2p^2\alpha_L+8p\beta_{Lm})/(4+2p^2)$

[a] Reference should be made to Fig. 5 in text.

[b] p, q, r, and s are coefficients inter-related by the orthogonality conditions $pq=rs=2$, and whose magnitudes are determinable by energy minimization. L_1 and L_4 are the two new ligand orbitals introduced in proceeding from $K_2UO_2(NO_3)_2$ to $K_xUO_2L_y(NO_3)_2$.

[c] As before $a_i \equiv p_{\sigma i}$, $a_i \equiv p_i(\perp)$, but $a_i \equiv (-1)^i p_i(\parallel)$. Similarly $L_i \equiv p_{\sigma i}{}^L$, $L_i \equiv p_i{}^L(\perp)$, but $L_i \equiv (-1)^i p_i{}^L(\parallel)$.

[d] α and β_m are as previously defined; $\alpha_L \equiv \int L_i H L_i d\tau$; $\beta_{Lm} \equiv \int L_i H a_{i\pm 1} d\tau$. The energy of an MO now depends primarily on relative magnitudes of β_m and β_{Lm}.

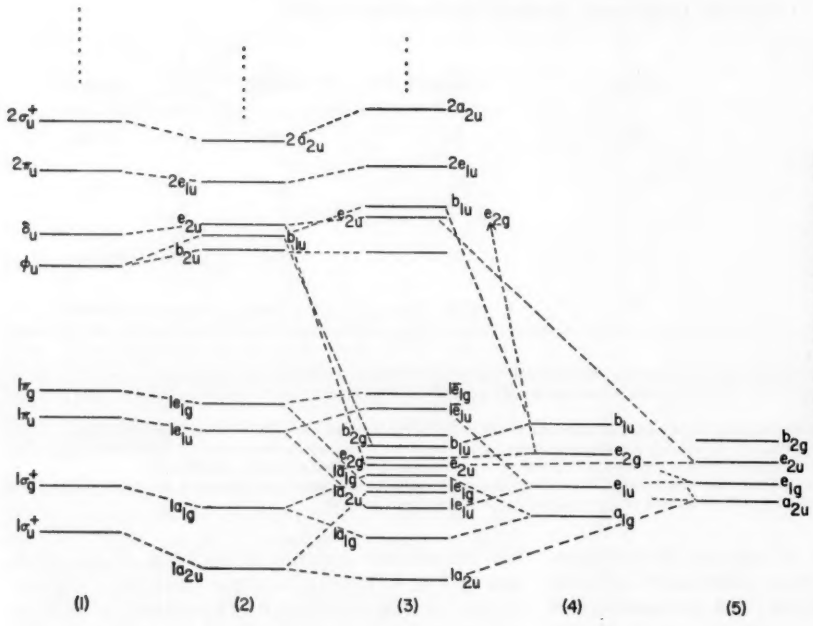

FIG. 6. A composite diagram illustrating the effects of ligation on the molecular orbitals of a linear UO_2^{++} ion. The set of levels (1) are the MO's of an isolated $D_{\infty h}$ uranyl ion; the set (2) are the group orbitals of a linear O—U—O ion subject to an equatorial hexagonally disposed ligand electrostatic field. The group orbitals formed from the σ-AO's of the ligands and from the $\pi\perp$-AO's of the ligands are shown in sets (4) and (5), respectively. Set (3) represents the MO energy levels arising from covalent mixing of the GO's (2), (4), and (5).

uranyl MO's has also been discussed[3,4] and the resultant of these effects is also shown in Fig. 6. On the right of Fig. 6 are shown the orbitals of the ligands, where the $\pi_\perp$ orbitals are those directed perpendicular to the hexagonal plane and the σ orbitals are those which are radially directed toward the uranium atom. The $\pi_{||}$ orbitals have been neglected in drawing Fig. 6 primarily because their effect may be incorporated at least partially into our considerations by increasing the sp^2 hybridization of the σ orbitals. A complete tabulation of σ, $\pi_\perp$, and $\pi_{||}$ oribtals, their wave functions, representation species, and energies are given in Table IV for the D_{6h} complex and in Table V for the D_{2h} species.

The ligand group orbitals and the electrostatically perturbed $D_{\infty h}$ group orbitals of O—U—O are finally mixed to yield the molecular orbitals of the D_{6h} complex depicted in the center of Fig. 6. The extent and manner to which such covalent mixing occurs is difficult to estimate; use was made of the Pauling overlap criterion, using the overlap integrals evaluated by Coulson and Lester[23] for various uranium orbitals with a 1s orbital of hydrogen. However, it was necessary to introduce directional factors for both the ligand orbital and uranium orbital; since there is a great deal of uncertainty associated with all these manipulations, it might seem that even results of a qualitative nature are open to doubt, and perhaps they are. Nonetheless, it is believed that the conclusions arrived at are sufficiently unambiguous and unique group—theoretically to merit consideration. The various types of bond formation in the equatorial plane are individually discussed below:

[23] C. A. Coulson and G. R. Lester, J. Chem. Soc. **1956**, 3650.

σ Bonding

The a_{1g} and e_{1u} orbitals overlap weakly, and since these orbitals on the uranium atom and in the ligand group orbital are filled, the effect should be destabilization of the equatorial complexation. However, there are also empty orbitals, albeit of fairly high energy, of both of these species on the uranium atom and the net effect is most probably a small or negligible stabilization energy accompanied by a small shift of the center of electronic charge density toward the uranium atom. In any case the net effect is small, and is outweighed by the bonding contribution due to the b_{1u} and e_{2g} orbitals of the ligand. The b_{1u} ligand orbital mixes with the empty $f_{z(z^2-y^2)}$ component of the atomic orbital ϕ_u; since both orbitals are directed towards each other the overlap is significant (~ 0.3), with the consequence that a considerable positive contribution to equatorial binding occurs, and a considerable ligand→metal electron density shift results. The same is true of the e_{2g} contribution which mixes with the empty $d_{x^2-y^2}$ and d_{xy} components of the atomic orbital δ_g. However, despite the fact that the overlap is large (~ 0.55), the energy separation between the mixing orbitals is so great[4] ($\sim$ 45 000 cm^{-1}) compared to that between the b_{1u} orbitals[3] ($\sim$20 000 cm^{-1}), that the b_{1u} contribution predominates. It is then concluded that there is a significant $\sigma(L\rightarrow M)$ contribution, in a usual notation, to the equatorial bonding.

TABLE VI. Electron configurations and antisymmetric stretching frequencies of actinyl ions.

Ion	Electron configuration[a]	$\bar{\nu}_3$(cm^{-1})[b]	k(megadynes/cm)[c]
UO_2^{++}	$(1\sigma_u^+)^2(1\sigma_g^+)^2(1\pi_u)^4(1\pi_g)^4$	965±1	0.775±0.02
UO_2^+	$(1\sigma_u^+)^2(1\sigma_g^+)^2(1\pi_u)^4(1\pi_g)^4(\phi_u)^1$	...	...
NpO_2^{++}	$(1\sigma_u^+)^2(1\sigma_g^+)^2(1\pi_u)^4(1\pi_g)^4(\phi_u)^1$	969±1	0.781±0.002
NpO_2^+	$(1\sigma_u^+)^2(1\sigma_g^+)^2(1\pi_u)^4(1\pi_g)^4(\phi_u)^1(\partial_u)^1$	824±4	0.565±0.006
PuO_2^{++}	$(1\sigma_u^+)^2(1\sigma_g^+)^2(1\pi_u)^4(1\pi_g)^4(\phi_u)^1(\partial_u)^1$	962±1	0.771±0.002
PuO_2^+	$(1\sigma_u^+)^2(1\sigma_g^+)^2(1\pi_u)^4(1\pi_g)^4(\phi_u)^1(\partial_u)^1(2\pi_u)^1$	...	...
AmO_2^{++}	$(1\sigma_u^+)^2(1\sigma_g^+)^2(1\pi_u)^4(1\pi_g)^4(\phi_u)^1(\partial_u)^1(2\pi_u)^1$	939±1	0.735±0.002
AmO_2^+	$(1\sigma_u^+)^2(1\sigma_g^+)^2(1\pi_u)^4(1\pi_g)^4(\phi_u)^2(\partial_u)^1(2\pi_u)^1$	832±2	0.577+0.003

[a] Appropriate only for an isolated actinyl ion. This column is from S. P. McGlynn and J. K. Smith, J. Mol. Spectroscopy (to be published).
[b] L. Jones and R. A. Penneman, J. Chem. Phys. **21**, 542 (1953).
[c] Obtained using constants in the Badger equation different to those used in Eqs. (6) or (7).

$\pi_\perp$ Bonding

Of the $\pi_\perp$ bonds between ligand and uranyl, of which there are only three types: a_{2u}, e_{1g}, and e_{2u}, only the latter contributes significantly by mixing with the empty $f_{z(x^2-y^2)}$ and f_{xyz} components of ∂_u. There results a positive contribution to the binding, but since the overlap (~0.15) and the energy separation[4] of the mixing orbitals (~24 000 cm^{-1}) are less favorable than those for b_{1u}, it is considered that the $\pi_\perp(L\rightarrow M)$ contribution to binding and the $\pi_\perp(L\rightarrow M)$ electron density shift are approximately $\frac{1}{6}$ of those for $\sigma(L\rightarrow M)$.

$\pi_{||}$ Bonding

There are three types: e_{1u}, e_{2g}, and b_{2u}; the e_{2g} mixes with the $d_{x^2-y^2}$ and d_{xy} components of the atomic orbital δ_g and b_{2u} mixes with the $f_{y(x^2-y^2)}$ component of ϕ_u. The overlaps are small, and there results a small positive contribution to the binding and a small ligand to metal shift for $\pi_{||}(L\rightarrow M)$.

In ligands such as CN^- and pyridine where there are empty orbitals which are group theoretically and energetically accessible there will of course be a stabilization due to $\pi_\perp(M\rightarrow L)$ bonding. Such bonds will be primarily of species e_{1g} in (an unlikely) equatorially hexacoordinated pyridine compound and of species e_{1g} and e_{1u} in a likely equatorially hexacoordinated cyanide complex.

It may then be concluded, and independently of the model of the complex used, that the stabilization energy (S.E.) of an isolated D_{6h} uranyl complex is given by

$$\text{S.E.}=\text{electrostatic effect}+\sigma(L\rightarrow M)+\pi(L\rightarrow M)\pm\pi(M\rightarrow L)\cdots, \quad (8)$$

where the $\sigma(L\rightarrow M)$ term predominates. Eq. (8) is not thermodynamic, nor to be compared with thermodynamic data, without considering solvation energies and entropies and coordination entropy effects. It is also to be noted that we have not considered 6*f* overlap effects which according to Coulson and Lester[23] should be extremely important in equatorial complexation; their inclusion would indeed increase $\sigma(L\rightarrow M)$ and $\pi(L\rightarrow M)$ considerably if the 5*f*–6*f* energy separation of 0.3 ev of Coulson and Lester were correct, which we doubt.

Equation (8) is to be contrasted with that for the ligand field splitting parameter for octahedral complexes of elements of the 1st and 2nd transition series,

$$\Delta=\text{electrostatic effect}+\sigma(L\rightarrow M)-\pi(L\rightarrow M)+\pi(M\rightarrow L)\cdots. \quad (9)$$

It is to be emphasized that quite apart from the difference in sign in $\pi(L\rightarrow M)$ in Eqs. (8) and (9), Δ and S.E. should be compared only with some caution. For one, the integrals implicit in Eq. (8) involve 6*d* and 5*f* orbitals of uranium, whereas those in Eq. (9) involve *ns*, *np*, and $(n-1)d$ orbitals of the transition metal, where n is 5 or 4; this alone may lead to a considerable difference in the order of importance of terms in Eqs. (8) and (9). Secondly, no significant correlation has been found[20] between Δ and the thermodynamic stabilization energy even within complexes of the 1st and 2nd row transition elements, and it would thus seem impetuous to try and induce such a relationship between a Δ measured for elements near the beginning of the periodic table and a S.E. measured for elements near the end. Thirdly, the measurements have actually consisted of two vibrational frequencies of the uranyl ion, and it is not immediately obvious how $\bar{\nu}_1$ and $\bar{\nu}_3$ are related to S.E.; however, an approach to such a relationship may be made in the following way: The $\sigma(L\rightarrow M)$ and $\pi(L\rightarrow M)$ contributions to S.E. involve transfer of charge into the ϕ_u, δ_u, and ∂_g orbitals of the $D_{\infty h}$ ion (b_{2u}, b_{1u}, e_{2u}, e_{2g} in D_{6h}), and these orbitals are pure atomic uranium orbitals in both point groups, and are not covalently involved in the axial uranium-oxygen bonds. The net result is the piling up of charge on the uranium atom, which then because of increased electrostatic repulsion with the highly negative axial

oxygens causes a loosening of this bond. This effect is perhaps better demonstrated by consideration of Table VI, wherein it is seen that reduction of UO_2^{++} to UO_2^{+} or AmO_2^{++} to AmO_2^{+} is equivalent to putting an extra electron into the ϕ_u orbital, and this results, at least in the latter case, in a decrease of 107 cm^{-1} in $\bar{\nu}_3$. Similarly, the reduction of NpO_2^{++} to NpO_2^{+} is equivalent to putting an extra electron into δ_u, and here a decrease of 145 cm^{-1} in $\bar{\nu}_3$ results. That the decrease upon populating δ_u should be greater than upon populating ϕ_u is expected, because δ_u is more strongly axially directed. The decrease upon populating $2\pi_u$ should be greater still, but no data on the PuO_2^{+} ion can be found to verify or disprove this. In sum then the effect of $\sigma(L\rightarrow M)$ or $\pi(L\rightarrow M)$ bonding is completely equivalent to the reductions specified above, and the range of variation in the frequencies observed (91 cm^{-1} in Table II) upon ligation could be completely explained, disregarding ligand electrostatic effects and $\pi(M\rightarrow L)$ bonding, by transfer of an amount of charge 0.5–1.0e from ligand to metal.

For exactly similar reasons the ligand electrostatic field will cause a decrease in $\bar{\nu}_3$. The $\pi(M\rightarrow L)$ effects are more ambiguous: Since the π uranyl bonding orbitals have a large amplitude on the two axial oxygens, decrease of this amplitude by transfer would undoubtedly lead to increase of $\bar{\nu}_3$ by decreasing the axial electrostatic repulsion. On the other hand both $1e_{1g}$ and $1e_{1u}$ are weakly bonding and depopulation of these bonds would lead to a decrease of $\bar{\nu}_3$. Because of the impossibility of *a priori* decision on this latter it is concluded that

$$\Delta\bar{\nu}_3(\text{or } \bar{\nu}_1) = -\text{electrostatic effect} - \sigma(L\rightarrow M) - \pi(L\rightarrow M) \pm \pi(M\rightarrow L)\cdots, \quad (10)$$

where the choice of sign of the $\pi(M\rightarrow L)$ term is to be determined by comparison with experiment.

It is to be concluded from Eq. (10) that insofar as the contributions of $\pi(L\rightarrow M)$ and possibly $\pi(M\rightarrow L)$ may be considered small that $\bar{\nu}_1$ or $\bar{\nu}_3$ should decrease as Δ increases, and it is thus that the general trends of Table II are rationalized. For those ligands for which the $\pi(L\rightarrow M)$ term is important (halides and OH^-), there should be a considerable displacement to the right in the vibrational series defined by Eq. (10) from their position in the spectrochemical series defined by Δ. In other words they should have "unexpectedly" low frequencies for $\bar{\nu}_2$ and $\bar{\nu}_1$. This has been observed[7] to be the case. On the other hand those ligands for which $\pi(M\rightarrow L)$ is important would be displaced to the left in the series defined by Eq. (10) if this term has a positive sign; this could explain the position of the pyridine ligate in the present work.

It seems obvious that many of the conclusions either deduced or inferred in the present work require substantiation. Because of the present status of *f*-orbital quantum chemistry to do so calculationally at this time would be presumptuous and premature; and the choice of a mixed field series of complexes as in the present work complicates the issue further by making field selection difficult. In order to circumvent the latter, a series of pure uranyl ligates of known compositions has been prepared; to increase the feasibility of the former a study of vanadyl complexes where the relevant integrals are more accessible and a comparison with Δ more reasonable, is underway.[7] Finally it is clear that many other conclusions regarding energies and probabilities of various excited electronic and vibronic states of actinyls may be derived from the present work. These will be discussed separately.[7]

ACKNOWLEDGMENTS

The authors wish to acknowledge their gratitude to the sponsors of this work. They are especially grateful to Dr. Joel Selbin of this Department for much informative discussion, and for his patience with physical chemists who endeavour to do things inorganic.

Electron Spin Resonance of γ-Irradiated Glycylglycine*

MIKIO KATAYAMA† AND WALTER GORDY

Department of Physics, Duke University, Durham, North Carolina

(Received December 7, 1960)

The electron paramagnetic resonance spectra of a gamma-irradiated single crystal of α-glycylglycine have been measured at 9, 24, and 29 kMc/sec for various orientations of the crystal in the external magnetic field. From analysis of the spectroscopic splitting factors and the hyperfine interaction constants, the free radical produced by gamma irradiation is found to be:

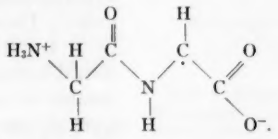

The electron spin density on the —ĊH carbon atom is evaluated as approximately 0.75.

INTRODUCTION

THE present work represents a part of a program of this laboratory directed toward the understanding of radiation damage to proteins. The doublet electron spin resonance found earlier in powdered samples of glycylglycine[1] after X or γ irradiation is similar to that found in many irradiated proteins[2] and like that of other simple peptides such as acetylglycine.[3] The first studies were of an exploratory nature and were made on powdered or polycrystalline samples of a wide variety of amino acids, simple peptides, and proteins. Although useful information was gained from a comparative study of these groups, additional and more specific information can be obtained from detailed study of single crystals of some of these substances, especially those for which structural information is available from x-ray diffraction studies. The ESR of a number of irradiated single crystals, including acetylglycine,[3] has been measured and analyzed in the laboratory. The results on acetylglycine as well as the preliminary findings of the present study on glycylglycine have already been applied in the interpretation of the orientation dependence of the doublet resonance produced by irradiation of certain native proteins.[4] The form of the free radical, XĊHCOX, confirmed in the present single-crystal study, was predicted from an earlier study of powdered samples,[1] and mention was made of this project to test the prediction by measurements on single crystals.

DESCRIPTION OF CRYSTAL

Single crystals of glycylglycine were grown by slow evaporation from aqueous solutions. Thin, platelike crystals, as shown in Fig. 1, were obtained. The crystals of glycylglycine have three modifications, designated as α, β, and γ. The β and γ forms, which crystallize as needles, were never found to grow from the water solutions. Hence, we conclude that the crystals obtained are of the α form. The cell dimension is: $a=7.70$ A, $b=9.57$ A, $c=9.48$ A, and $\beta=124.35°$. The space group is monoclinic, $C_{2h}{}^5-P_{2_1/a}$. The large face on the plates is (001); the b axis bisects the smaller angle, and the a axis bisects the large angle. The three Cartesian axes a, b, and c' were chosen as shown in Fig. 1.

A single crystal of this form has been analyzed by E. W. Hughes.[5] The molecules, except for their terminal NH_3 groups, lie very close to the plane parallel to (100). The longest dimension of the molecule is approximately parallel to c.

EXPERIMENTAL RESULTS

The single crystals were irradiated with γ rays from a kilocurie cobalt 60 source. Dosages of the order of 5 million r were employed. The ESR spectra of the γ irradiated crystals were measured at 9, 24, and 29 kMc/sec at room temperature. The experiment was repeated at 77°K.

The observed g values for various orientations of the crystal in the external magnetic field are shown in Table I. These values are almost isotropic and are close to the g factor of a free electron.

Figure 2 shows the observed curves of the second derivatives of absorption measured at 9 and 24 kMc/sec. The static magnetic field is applied along the a axis and b axis, in which four molecules in an unit cell are

* This research was supported by a contract with the Office of Ordnance Research, Department of the Army.

† On leave from the University of Electro-Communications, Tokyo, Japan.

[1] G. McCormick and W. Gordy, J. Phys. Chem. **62**, 783 (1958).

[2] W. Gordy, W. B. Ard, and H. Shields, Proc. Natl. Acad. Sci. U. S. **41**, 983 (1955); W. Gordy and H. Shields, Radiation Research **9**, 611 (1955).

[3] I. Miyagawa, Y. Kurita, and W. Gordy, J. Chem. Phys. **33**, 1599 (1960).

[4] W. Gordy and H. Shields, Proc. Natl. Acad. Sci. U. S. **46**, 1124 (1960).

[5] E. W. Hughes (private communication).

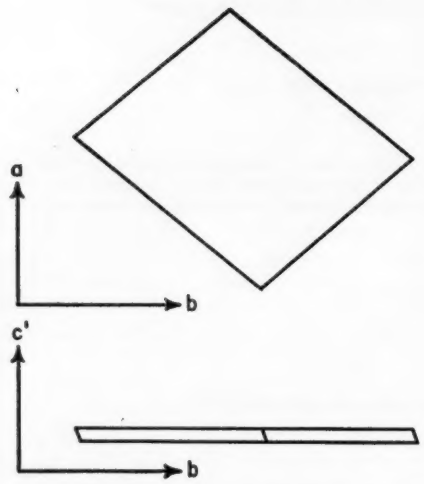

FIG. 1. The crystalline form and the coordinate axes employed, a, b, and c'.

magnetically equivalent. The spectra observed at the different frequencies were almost the same.

Essentially, the same spectra were observed when the experiment was carried out at liquid-nitrogen temperature.

NATURE OF THE FREE RADICAL

Because of the incomplete resolution of the structure, assignment of the free radical was found difficult. However, any reasonable interpretation requires an H atom to be lost from a CH_2 group of the molecule. The difficulty arises in deciding which of the two CH_2 groups loses the H, or whether sometimes one group and sometimes the other does so, thus forming a mixture of the two very similar free radicals I and II;

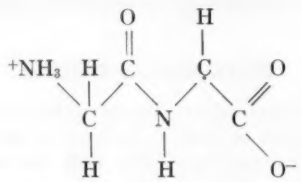

(I)

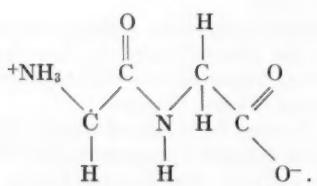

(II)

The result might be explained by either radical I or II alone if we attribute the broadening and the apparent doublet substructure to the interaction between the unpaired electron and the NH group in I or the NH_3 group in II. However, the ESR study of γ-irradiated normal and deuterated glycine[6] shows that the protons of the terminal NH_3 group interacts measurably with an unpaired electron on the adjacent carbon. The NH_3 splitting constant for irradiated glycine is almost 20 gauss[7] and presumably arises from hyperconjugation, as in the case of the $-C-CH_3$ radical. Therefore, if the free radical II were produced by γ irradiation of glycylglycine, the ESR spectra should be very broad and complex. It is therefore reasonable to conclude that the spectra observed from glycylglycine come from structure I. This is the same type of free radical as that found in γ-irradiated acetylglycine.[3]

Substitution of deuterium[8] for the hydrogens bonded to nitrogen after treatment of glycylglycine with D_2O failed to produce any noticeable change in the radiation induced resonance of the powdered samples. This indicates that the apparent substructure in the more widely spaced doublet components must arise from N^{14} nuclear coupling. If completely resolved, the N^{14} for which $I=1$ would of course give a triplet substructure with components of equal intensity. However, the incomplete component separation combined with the distortion caused by the modulation method used for detection prevent the resolution of the triplet. If the separation is about $\frac{2}{3}$ of the linewidth, assuming Gaussian distribution for the line shape, we would observe an apparent doublet instead of a triplet as illustrated in Fig. 3.

The doublet resonance of γ-irradiated single crystals of single crystals of acetylglycine,[3] in which the free radical has been shown to be

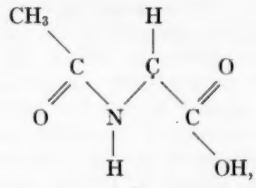

TABLE I. The g factor in different directions.

Direction of magnetic field	g value
a	2.0029
b	2.0032
c'	2.0036

[6] M. Katayama and W. Gordy, Bull. Am. Phys. Soc. **5**, 253 (1960).
[7] D. K. Ghosh and D. H. Whiffen, Mol. Phys. **2**, 285 (1959).
[8] W. Gordy and I. Miyagawa, Bull. Am. Phys. Soc. **5**, 227 (1960).

has no detectable substructure attributable to the NH proton, although evidence for line broadening arising from unresolved N^{14} interaction was observed. For this reason also, we would not expect the NH proton in the similar free radical for glycylglycine to give rise to resolvable splitting. The line broadening attributed to N^{14} in the acetylglycine free radical is comparable to that caused by the unresolved substructure in the glycylglycine free radical.

THEORETICAL ANALYSIS

The spin Hamiltonian for the free radical I above can be expressed with sufficient accuracy for our purposes by

$$\mathcal{H}=\beta H_Z(g_{ZZ}S_Z+g_{ZX}S_X+g_{ZY}S_Y)+(A_{ZZ}{}^{H}I_Z{}^{H}+A_{ZX}{}^{H}I_X{}^{H}+A_{ZY}{}^{H}I_Y{}^{H})S_Z+(A_{ZZ}{}^{N}I_Z{}^{N}+A_{ZX}{}^{N}I_X{}^{N}+A_{ZY}{}^{N}I_Y{}^{N})S_Z,$$

where X, Y, and Z represent space-fixed axes with the applied field H chosen along Z. The g's represent elements of the spectroscopic splitting factor (g tensor),

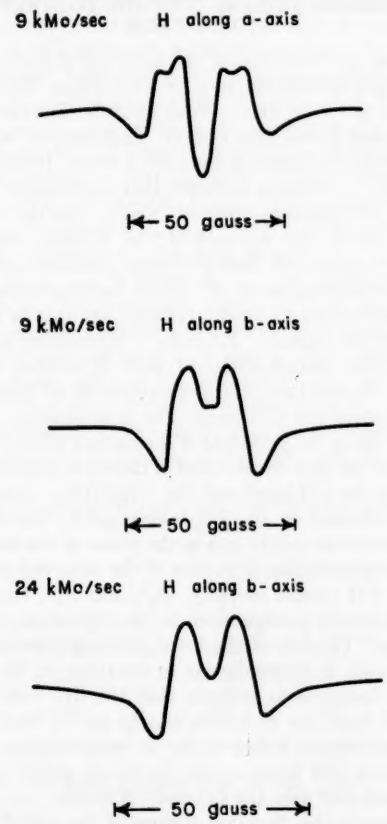

FIG. 2. Electron spin resonance curves (second derivatives of actual resonances) for a γ-irradiated single crystal of glycylglycine at 9 kMc/sec and 24 kMc/sec, with static magnetic field H as indicated.

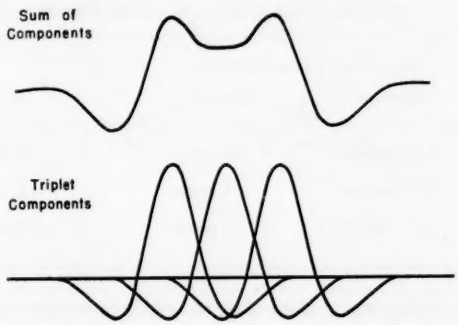

FIG. 3. Illustration of the way second derivative curves of an incompletely resolved triplet resonance can give rise to an apparent doublet. The top curve represents the sum of the three equivalent curves in the lower figure.

the A^H's and I^H's represent the element of the nuclear coupling tensor and the components of the nuclear spin vector of the —CH— hydrogen nucleus, and the A^N's and I^N's represent the corresponding quantities for the N of the NH group. Couplings to other nuclei in the free radical we found to be negligible. The nuclear paramagnetic term $g_I\beta_I I_Z H_Z$ which gives rise to second-order transitions[9] is neglected here since the satellite lines arising from this source were not resolvable because of the large width of the lines. Also, interactions of the electron spin with other nuclei such as N^{14} were not resolvable. Hence their contributions to the spin Hamiltonian are omitted, although they probably broaden the lines appreciably.

To find the resonant field strength for the observation frequency we follow a procedure similar to that of Kurita and Gordy for thioglycolic acid.[10] The above Hamiltonian is expressed as

$$\mathcal{H}=\mathcal{H}^{(0)}+\mathcal{H}^{(1)},$$

where

$$\mathcal{H}^{(0)}=\beta H_Z g_{ZZ}S_Z+A_{ZZ}{}^{H}S_Z I_Z{}^{H}+A_{ZZ}{}^{N}S_Z I_Z{}^{N}$$

and

$$\mathcal{H}^{(1)}=\beta H_Z(g_{ZX}S_X+g_{ZY}S_Y)+(A_{ZX}{}^{H}I_X{}^{H}+A_{ZY}{}^{H}I_Y{}^{H})S_Z+(A_{ZX}{}^{N}I_X{}^{N}+A_{ZY}{}^{N}I_Y{}^{N})S_Z.$$

The eigenvalues of $\mathcal{H}^{(0)}$ are

$$E^{(0)}=g_{ZZ}\beta H_Z M_S+A_{ZZ}{}^{H}M_S M_I{}^{H}+A_{ZZ}{}^{N}M_S M_I{}^{N},$$

where $M_S=\pm\frac{1}{2}$, $M_I{}^{H}=\pm\frac{1}{2}$, and $M_I{}^{N}=+1,\ 0,\ -1$. From second-order perturbation theory the eigenvalues of $\mathcal{H}^{(1)}$ are found to be

$$E^{(1)}=\frac{g_{ZX}{}^2+g_{ZY}{}^2}{2g_{ZZ}}\beta H_Z M_S+\frac{(A_{ZX}{}^{H})^2+(A_{ZY}{}^{H})^2}{2A_{ZZ}{}^{H}}M_I{}^{H}M_S+\frac{(A_{ZX}{}^{N})^2+(A_{ZY}{}^{N})^2}{2A_{ZZ}{}^{N}}M_I{}^{N}M_S.$$

[9] I. Miyagawa and W. Gordy, J. Chem. Phys. **32**, 255 (1960).
[10] Y Kurita and W. Gordy, J. Chem. Phys. **34**, 282 (1961).

TABLE II. Principal values for nuclear hyperfine constants for CH and direction cosine with regard to abc' system.

Magnitude of principal values		Direction cosine			
Observed	Theoretical	a	b	c'	
A_x^H 19 gauss	−20 gauss	±0.84	±0.10	∓0.53	⊥ NCHC plane
A_y^H 28 gauss	−29 gauss	±0.59	±0.03	±0.81	in NCHC plane ⊥ to CH
A_z^H 9 gauss	−7 gauss	±0.03	∓0.99	0.00	along CH bond

The energy eigenvalues of $\mathfrak{H}$ to second order are then

$$E=E^{(0)}+E^{(1)},$$

and the frequencies are

$$h\nu=g_{zz}\beta H+\frac{g_{zx}^2+g_{zY}^2}{2g_{zz}}\beta H+\left[A_{zz}^H+\frac{(A_{zx}^H)^2+(A_{zY}^H)^2}{2A_{zz}^H}\right]M_I^H+\left[A_{zz}^N+\frac{(A_{zx}^N)^2+(A_{zY}^N)^2}{2A_{zz}^N}\right]M_I^N.$$

Since the frequency was held constant and the magnetic field measured, we solved this expression for the observed field, H. We let the fixed $h\nu_0$ correspond to $g_f\beta H_0$ where g_f is the free spin value 2.0023. Hence, $H_0=(h\nu_0)/(g_f\beta)$. Actually, the second term on the right is negligible in comparison with the remaining terms. We omit it and obtain

$$H_0=\frac{g_{zz}}{g_f}H+\frac{1}{g_f\beta}\left[A_{zz}^H+\frac{(A_{zx}^H)^2+(A_{zY}^H)^2}{2A_{zz}^H}\right]M_I^H+\frac{1}{g_f\beta}\left[A_{zz}^N+\frac{(A_{zx}^N)^2+(A_{zY}^N)^2}{2A_{zz}^N}\right]M_I^N,$$

or, to a sufficient approximation,

$$H_0-H=\Delta H=\frac{g_{zz}-g_f}{g_f}H_0+\frac{1}{g_f\beta}\left[A_{zz}^H+\frac{(A_{zx}^H)^2+(A_{zY}^H)^2}{2A_{zz}^H}\right]M_I^H+\frac{1}{g_f\beta}\left[A_{zz}^N+\frac{(A_{zx}^N)^2+(A_{zY}^N)^2}{2A_{zz}^N}\right]M_I^N.$$

By measuring the ΔH's we evaluated the g_{zz}'s and A's for different orientations. We then used these values to solve for the elements of the g and A tensors with the relations

$$g_{zz}=\sum_{i=u,v,w} g_i l_{iz}^2,$$

$$A_{zz}=\sum_{i=x,y,z} A_i l_{iz}^2,$$

and

$$A_{zx}^2+A_{zY}^2=\sum_{i,j=x,y,z} A_i A_j l_{iz} l_{jz}\{\delta_{ij}-l_{iz}l_{jz}\}.$$

Here $\delta_{ij}=1$ when $i=j$, and 0 when $i\neq j$. The l's are direction cosines between Z and the various elements of g and A. The elements of g and A were obtained from these equations and from the observed g_{zz} and A's. The values obtained are listed in Tables II and III.

RELATION OF SPECTROSCOPIC SPLITTING AND HYDROGEN NUCLEAR COUPLING TO STRUCTURE OF CRYSTAL

From the directions of the principal elements of the hydrogen nuclear coupling A^H we can learn the orientation of the —NĊHC— plane and the direction of the ĊH bond in the free radical. Theoretically we could obtain this information from the g tensor. However, the g factor is so nearly isotropic that its direction cosines cannot be reliably evaluated. Neither can the coupling constants of the nitrogen A^N be reliably evaluated. For this reason we shall give most consideration to the proton coupling factor A^H, which has large anisotropy.

From results on other irradiated crystals in which a similar free radical, —R_1ĊHR_2—, is produced and from theoretical consideration of such a radical, we can expect the smallest principal element of A^H (here A_z^H) to lie along the ĊH bond. The intermediate element A_x^H is along the p_x orbital of the carbon which contains most of the spin density and is therefore perpendicular to both the CH bond and the —R_1CHR_2— plane. The largest element of A^H, A_y^H, is expected for the direction perpendicular to CH and in the plane of the molecule. Figure 4 shows the directions of the observed elements of the CH proton coupling, A_y^H, and A_z^H, relative to the molecular configuration in the crystal as given by Hughes.[5] The axis of the third principal element, A_x^H, not shown, is perpendicular to the plane of the figure. These comparisons indicate that the free radicals are formed from the molecules simply by the loss of one CH_2 hydrogen, followed by a reorientation of the remaining CH bond to the C—C—N plane to make angles of 120° with the CC and CN bonds.

Although the direction cosines of the principal elements of g are not as accurately measured, they are in agreement with the orientation of the free radical as indicated by the A tensor. Both from theoretical con-

siderations and from observations of the g tensor for other, similar radicals, the smallest principal element of g, here g_u, is expected to have its axis along that of the p_z orbital of the carbon which contains most of the electron spin density and thus to be directed approximately along b, or perpendicular to the plane of the molecule. This is in agreement with observation. The other two principal elements, g_v and g_w, are approximately equal and are directed approximately in the molecular plane.

It was proposed by McConnell[11] that the Fermi coupling constant of a proton in a π-electron free radical is proportional to the electron spin density on the carbon to which it is bonding, as

$$A_f = \rho_C Q,$$

where ρ_C is the spin density on the adjacent carbon and Q is the proportionality constant, which obviously is the Fermi coupling constant when $\rho_C = 1$. A magnitude of 25 gauss was chosen for Q, as employed for acetylglycine and *l*-alanine. This value is based on measurements of the coupling in the free methyl radical[12] for which ρ_C can be taken as unity. The sign of Q is now known to be negative.[13] A recent evaluation by Katz and Strauss[14] from the cyclo-octatetraenyl radical ion gives Q as -25.67 ± 0.07 gauss.

Since A_x, A_y, and A_z have the same sign, the Fermi term A_f in the CH proton coupling can be obtained from an average of the observed principal elements, $(A_x^H + A_y^H + A_z^H)/3 = 19$ gauss. This quantity is known to be negative in sign.[12] With this value for the isotropic component, the spin density on the CH carbon atom, ρ_C, is found to be 0.75. A theoretical estimate of the anisotropic term has been made by McConnell and Strathdee[15] for the applied static field along the principal axes, x, y, and z. Their calculated values when reduced to correspond with $\rho_C = 0.75$ become $(A_u)_x = -1.2$, $(A_u)_y = -10.4$, and $(A_u)_z = 12.0$ gauss, respectively. The observed isotropic component, $A_f = -19$ gauss, is added to each of these values to give

TABLE III. Principal values of g factor and direction cosine with regard to abc' system.

Principal value		Direction cosine		
		a	b	c'
g_u	2.0028	±0.8	0.0	±0.6
g_v	2.0035	0	±1	0
g_w	2.0033	∓0.6	0.0	±0.8

[11] H. M. McConnell, J. Chem. Phys. **24**, 764 (1956).
[12] W. Gordy and C. G. McCormick, J. Am. Chem. Soc. **78**, 3243 (1956).
[13] H. M. McConnell and D. E. Chesnut, J. Chem. Phys. **28**, 108 (1958); H. M. McConnell, C. Heller, T. Cole, and R. W. Fessenden, J. Am. Chem. Soc. **82**, 766 (1960).
[14] T. J. Katz and H. L. Strauss, J. Chem. Phys. **32**, 1873 (1960).
[15] H. M. McConnell and J. Strathdee, Mol. Phys. **2**, 129 (1959).

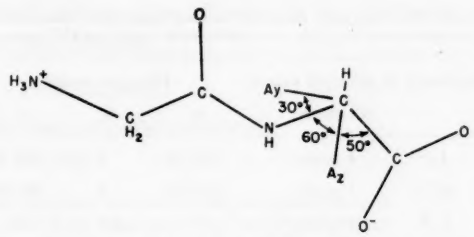

FIG. 4. Diagram of glycylglycine free radical showing the directions of principal elements of nuclear coupling A_z and A_y. The element A_x, not shown, is perpendicular to this plane.

the "theoretical" values of the principal elements of A, which are shown in Table II. The agreement of the semitheoretical values obtained in this way with the observed principal elements is seen to be good.

NITROGEN NUCLEAR COUPLING

The principal elements in the N^{14} nuclear coupling are listed in Table IV. Because of the incomplete resolution of the N^{14} hyperfine structure there is considerable uncertainty in these values. Nevertheless, it seems reasonably certain that the largest principal element, A_z, has its axis approximately along the direction of the minimum element of g and therefore perpendicular to the plane of the —CNHĊH— configuration.

There are probably three sources of interactions of the N^{14} nucleus with the electron spin density which might combine to give rise to the incompletely resolved N^{14} hyperfine structure. The most obvious of these is direct dipole-dipole coupling between the N^{14} nuclear magnetic moment and the electron spin density on the ĊH carbon. This interaction is easily approximated if the simplifying assumption is made that the spin density, ρ_C, is concentrated at the center of the carbon atom. Under these conditions the N^{14} nucleus gives rise to a field H, acting on ρ_C, given for the strong-field case by the equation

$$H_i = (M_I^N / I^N) \mu_I^N \beta_I \langle 1/r^3 \rangle_{Av} (3\cos^2\theta - 1)_{Av}.$$

With our simplifying assumptions and with the numerical value substituted for the nuclear magneton, this gives the splitting constant A^N as

$$A^N(\text{gauss}) \approx \rho_C \frac{10.1 \mu_I^N(\text{nm})}{R_{CN}^3(\text{angstroms})} (3\cos^2\theta - 1).$$

Now $\rho_C = 0.75$, $\mu_I^N = 0.40$ nm, and $R_{CN} = 1.48$ A. The maximum value of A, obtained when the field is along the CN bond, is $+1.8$ gauss, comparable in magnitude to the observed principal values of the N^{14} coupling. At right angles to the bond, this coupling would be -0.9 gauss.

A second source of N^{14} coupling arises from a negative spin density induced on the N^{14} through the large spin density on the ĊH carbon to which the nitrogen is bonded. This negative spin density arises from a spin

TABLE IV. Principal values of nuclear hyperfine constants for nitrogen atom and direction cosine with regard to *abc'* system.

Magnitude of principal values		Direction cosine		
	Observed	*a*	*b*	*c'*
A_x^N	4 gauss	±0.85	0	±0.53
A_y^N	3 gauss	±0.53	0	∓0.85
A_z^N	2 gauss	0	±1	0

polarization of the σ N—C bond through configuration interaction on the carbon. It should be comparable in magnitude to the negative spin density on the ĊH hydrogen which arises from the same mechanism. From the isotropic coupling of the ĊH hydrogen, −19 gauss, and from the known coupling of the hydrogen atom, 504 gauss, the spin density on the hydrogen is found to be: $\rho_H = -19/504 = -0.038$. The sign of this density is negative relative to that on the carbon, i.e., it is polarized in a direction along the field opposite to that of the carbon. We shall assume the induced spin density on the N^{14} to be the same, or $\rho_N = -0.038$.

To use the estimated ρ_N for calculation of the N^{14} coupling we must know the coupling of an electron in the N atomic orbital which joins with a C orbital to form the σ CN bond. This orbital is certainly a hybrid one. We assume it to be an sp_2 hybrid and hence to have $\frac{1}{3}s$ and $\frac{2}{3}p$ character. The coupling of the s and p electrons in nitrogen are not known accurately, but have been calculated by Miyagawa and Gordy[16] with sufficient accuracy for our purpose. With the effective Z taken as 3.90, they obtained the Fermi coupling A_f of a $2s$ electron of N^{14} as 273 gauss and the anisotropic coupling A_μ of a $2p$ electron as 13.7 gauss. The N^{14} interaction due to the negative spin density ρ_N in a nitrogen orbital is

$$A^N = \rho_N a^2 A_f + \rho_N b^2 A_\mu^N (3\cos^2\theta - 1),$$

where $a^2+b^2=1$ and where a^2 represents the s character and b^2 represents the p character of the orbital. For an sp_2 hybrid and with the above constants,

$$A(\text{gauss}) = -3.4 - 0.35(3\cos^2\theta - 1).$$

Thus, along the bond ($\theta=0$) A equals −4.1 gauss, and perpendicular to the bond ($\theta=90°$) A equals −3.0 gauss. The direct dipole-dipole coupling of ρ_C was estimated above as 1.8 gauss along the bond and as −0.9 perpendicular to the bond. A combination of the two coupling mechanisms should therefore lead to a coupling of $-4.1+1.8=-2.3$ gauss along the CN bond and $-3-0.9=-3.9$ gauss, perpendicular to the bond. The last value is in good agreement with the magnitude of the measured principal value $|A_x^N|=4$ gauss, which is perpendicular to the CN bond. On the assumption that these two mechanisms are jointly responsible for the coupling, principal values of −2 and −3.9 should be observed in the molecular plane, along and perpendicular to the CN bond. The observed principal values, $(A_y^N)=3$ gauss and $(A_z^N)=2$ gauss, and their directions (see Table IV) are not sufficiently accurate to provide a critical test of the coupling mechanism nor to justify more exact theoretical calculations.

A third possible source of N^{14} coupling is a positive spin density in the nonbonding N orbital which might arise from small contribution of structure II;

(I) (II)

Because structure II requires a positive charge on the electronegative N atom ($x_N=3.0$ as compared with $x_C=2.5$), it is not expected to be of much significance. If the three σ bonds to the N atom are sp_2 hybrids, as assumed above, the spin density of structure II would be in a p_z orbital perpendicular to the plane of the molecule. The N^{14} coupling from this source would thus be

$$A^N = \rho_N A_\mu^N (3\cos^2\theta - 1).$$

Since ρ_N is positive, this expression gives a positive contribution to A_x and would decrease the magnitude of A_x^N from the value of −3.9 gauss found above, unless its contribution is twice this magnitude. To give a resultant $A_x^N=+4$ gauss, with the component of −3.9 gauss already obtained, requires ρ_N to be +0.30, or a contribution from structure II of about 30%. This appears to be an unreasonably large contribution from the polar structure II. Also it would lead to a negative coupling in the $y-z$ plane larger in magnitude than that which is observed. It seems more reasonable that the first two mechanisms proposed are primarily responsible for the N^{14} coupling and that the contribution from the positive spin density on the N^{14} is small in comparison to them.

If the CNHC configuration is not planar, our assumptions of sp_2 hybrid bonding orbitals would not be justified, nor would the assumption of a pure p orbital for the positive spin density of structure II. A smaller and more reasonable contribution from structure II would then be required to give a value of $A_x^N=4$. However, the incompletely resolved N^{14} coupling does not justify further speculative discussion. The significant feature which seems to be proved is that the spin density on the N^{14} is small, probably less than 5%. The positive spin density not found on the ĊH carbon is probably located primarily on the two oxygens of the CO_2 group.

ACKNOWLEDGMENT

We wish to thank Dr. E. W. Hughes for his kindness in informing us of the results of his x-ray crystal analysis of α-glycylglycine before its publication.

[16] I. Miyagawa and W. Gordy, J. Chem. Phys. **30**, 1590 (1959).

General Relation between Potential Energy and Internuclear Distance for Diatomic Molecules. III. Excited States

E. R. LIPPINCOTT, D. STEELE,* AND P. CALDWELL†

Department of Chemistry, University of Maryland, College Park, Maryland

(Received November 21, 1960)

A previously proposed internuclear potential function has been used to calculate the dissociation energies for the excited states of a large number of diatomic molecules. From these results and the Wigner-Witmer rules the dissociation products are determined, and it is shown that in many cases it is possible to estimate independently, the dissociation energy of the ground state. The three- and five-parameter forms of the proposed function lead to nearly equal values for dissociation energies suggesting an equivalence of the two forms. This leads to a relation between the anharmonicity and the vibrational-rotational coupling constant which is slightly superior to the Pekeris relation. Equations derived from this relation are given relating the parameters a and b of the five-parameter functions to the anharmonicity or vibrational-rotational coupling constant. The parameter b and to a lesser extent a was found nearly constant for the excited states of all diatomic molecules.

INTRODUCTION

In a previous publication (I)[1] a relation between potential energy and internuclear distance was proposed. The relation had the form

$$V=D_e[1-\exp(-n\Delta r^2/2r)]\times[1+af(r)], \quad (1)$$

where D_e=dissociation energy referred to the bottom of the potential curve, $\Delta r=r-r_e$, r_e=equilibrium bond distance, r=bond distance and a=constant. The parameter n is given by

$$n=k_e r_e/D_e, \quad (2)$$

where k_e=force constant referred to zero displacement of the nuclei. When a is chosen zero the potential function Eq. (1) assumes a simple three-parameter form

$$V=D_e[1-\exp(-n\Delta r^2/2r)]. \quad (3)$$

By expansion of V in a power series to the quartic term in Δr, followed by comparison of the corresponding terms with those expected for the solutions of the Schroedinger equation for an anharmonic oscillator, the following relations were obtained

$$D_e(\text{ergs/molecule})=k_e/[64\pi^2 c\mu\omega_e x_e/3h-(1/r_e^2)], \quad (4a)$$

$$\omega_e x_e=3h(n/r_e+1/r_e^2)/64\pi^2 c\mu, \quad (5a)$$

and

$$\alpha_e=0. \quad (6a)$$

Or in terms of Varshnis'[2] notation

$$G=3[nr_e+1]=3[2\Delta+1], \quad (5b)$$

$$F=0, \quad (6b)$$

where

$$F=\alpha_e\omega_e/6B_e^2, \qquad G=8x_e\omega_e/B_e, \qquad \Delta=k_e r_e^2/2D_e;$$

$\omega_e x_e$=anharmonicity constant for zero displacement of the nuclei, α_e=vibration-rotational coupling constant, μ=reduced mass, c=velocity of light, and h=Planck's constant.

By using Eq. (4a) dissociation energies were calculated from bond lengths, force constants, and anharmonicity constants. The calculated values of D_e in general represented a marked improvement over the same D_e values calculated from the Morse function relation $D_e=\omega_e^2/4\omega_e x_e$, the resulting average percent deviations being of the order of 5 and 25%, respectively.[1] Independent empirical methods were given for evaluating the parameter n and with its use anharmonicity constants, as well as dissociation energies, were correlated or calculated more accurately than was previously possible.

The successful application of (3) to the properties of ground states of diatomic molecules suggested other applications. These included potential function models of hydrogen bonds[3,4] and empirical calculations of bond properties for bonds of polyatomic molecules using bond stretching force constants.[3] One disadvantage of (3) is that it predicts $\alpha_e=0$ for all diatomic molecules, corresponding to no interaction between vibrational and rotational motion. Although values of α_e are small for the ground states of diatomic molecules, they are definitely not zero. This suggests that in (1) $a\neq 0$. Some theoretical justifications for this simple potential function are known since it may be derived from a semiempirical quantum-mechanical model of chemical binding.[5]

With $a\neq 0$, the internuclear potential function as-

* Post doctoral research fellow.

† Present address: National Bureau of Standards, Washington, D. C.

[1] E. R. Lippincott, J. Chem. Phys. **21**, 2070 (1953); E. R. Lippincott and R. Schroeder, *ibid.* **23**, 1131 (1955).

[2] Y. P. Varshni, Revs. Modern Phys. **29**, 664 (1957). Varshni has erroneously reported that α_e is negative for the three-parameter function. He also reports an incorrect expression for the value of α_e for the Linnett function (private communication).

[3] E. R. Lippincott and R. Schroeder, J. Chem. Phys. **23**, 1131 (1955); J. Am. Chem. Soc. **78**, 5171 (1956); J. Phys. Chem. **61**, 921 (1957).

[4] C. Reid, J. Chem. Phys. **30**, 182 (1959).

[5] E. R. Lippincott and M. O. Dayhoff, Spectrochim. Acta **16**, 807 (1960); E. R. Lippincott, J. Chem. Phys. **26**, 1678 (1957).

sumed a five-parameter form. The quantity $f(r)$ was a function of r chosen such that $f(r)=\infty$ when $r=0$, and $f(r)=0$ when $r=\infty$. For large values of r the $f(r)$ term was assumed to take the form of a Lennard-Jones 6–12 attractive potential, which is compatible with these conditions.

The general form was then

$$V=D_e[1-\exp(-n\Delta r^2/2r)]\times\{1-a(r_e/r)^6\times[1-\exp(-b^2n\Delta r^2r^{11}/2r_e^{12})]^4+a(r_e/r)^{12}\times[1-\exp(-b^2n\Delta r^2r^{11}/2r_e^{12})]\}, \quad (7a)$$

where $b=$ constant. For large values of r this equation assumes the form,

$$V=D_e[1-\exp(-n\Delta r^2/2r)]\{1+a[-(re/r)^6+(r_e/r)^{12}]\}.$$

Several other forms of V are possible which have the same expansion to the fourth power in Δr and consequently lead to the same relations between ω_e, B_e, α_e, $x_e\omega_e$, and D_e. One of these which appears to reproduce experimental potential curves well, is

$$V=D_e[1-\exp-(n\Delta r^2/2r)]\{1-a(b^2n/2r)^{\frac{1}{2}}\Delta r\times\exp[-(b^2n/2r_e)^{\frac{1}{2}}\Delta r]\}. \quad (7b)$$

This will be discussed in a later section.

The relations which may be derived from the use of (7) as an anharmonic oscillator in the Schröedinger equation are given below. These relations were used to obtain improved correlations and predictions of the five spectroscopic constants r_e, k_e, D_e, ω_ex_e, and α_e. The internuclear potential function (7) has been used by Pliva[6] as the bond stretching part of a physically significant anharmonic potential function describing the motion of polyatomic molecules. With its use, he was able to correlate or predict accurately a number of the constants for the vibrational-rotational motion of triatomic molecules, including anharmonicity and vibrational rotational coupling constants. One important and convenient feature of (6) is that the parameters a and b were approximately constant for the ground states of the diatomic molecules studied, with values of b rarely deviating by more than 3% and values of a by more than 10%.

The purpose of this paper is to illustrate the function's application to the electronically excited states of diatomic molecules using both the three-parameter and five-parameter forms. Its usefulness in correlating and predicting bond properties will be discussed and some new relations given. In addition, the functions will be used to predict the states of separated atoms for diatomic molecules. Such an application can be useful in constructing energy level diagrams for diatomic molecules when the states of the separated atoms are not known from other sources of information.

From a knowledge of the states of the separated atoms and approximate values of the dissociation energies of the excited states it is possible to estimate the dissociation energies of the ground states. In certain cases of considerable interest the derived value allows an unambiguous selection from previously proposed groups of values.

SIMPLE THREE-PARAMETER FUNCTION

The use of the simple function and derived relations for calculating bond properties has been given in I and will not be repeated here. The working equation is (4a), and calculated dissociation energies have been obtained through the use of experimental k_e, r_e and ω_ex_e values. The results for a large number of excited states are given in Tables I, II, and III along with the experimental D_e values for a comparison. Table II contains calculations for salt like compounds, for which the model might be expected to be less reliable, and in Table III are given the dissociation energies for hydrogen containing molecules. The results for the ground states are included for the sake of completeness. The experimental D_e values are based on the assumption that the states for the separated atoms are known. Alternatively the predicted dissociation energy can be used to deduce the states of the separated atoms. The predicted or known separated atom states are given in column 9.

In reference 1 an independent empirical relation was given for the evaluation of n in terms of ionization potentials of the ground states of the separated atoms. From this relation and Eq. (2) it was possible to predict D_e from k_e and r_e values. Because the ionization potential of excited atoms differs from those of the ground state atoms, the values of n calculated for ground-state diatomic molecules are not necessarily valid for excited states of the same molecule and these n values cannot necessarily be used in Eq. (2) without appropriate modifications.

When reliable experimental data are available for comparison, the calculated D_e values agree well with the observed values.

CALCULATIONS WITH THE FIVE-PARAMETER FUNCTIONS

The potential function, Eqs. (7), may be expanded in a power series of $\Delta r/r_e$ giving[1]

$$V=D_e(nr_e/2)(\Delta r^2/r_e^2)\{1-[1+ab(nr_e/2)^{\frac{1}{2}}](\Delta r/r_e)+[1-nr_e/4+3(ab/2)(nr_e/2)^{\frac{1}{2}}+ab(nr_e/2)](\Delta r/r_e)^2+\cdots\cdots\}. \quad (8)$$

Dunham has solved the problem of a nonrigid an-

[6] J. Pliva, Collection Czeckoslov. Chem. Commun. **23**, 777, 1839, 1846, 1852 (1958).

TABLE I. Comparison of dissociation energies calculated from three- and five-parameter potential functions for excited states of diatomic molecules.

Molecule	State	Dissociation energy: Obs[a]	S.F.[b]	5 par. F[b,c]	Atomic excitation energy: Te(ev)	Calc	Theoret	Dissociation products	Ref.
B_2	$X\ ^3\Sigma_g^-$	3.0±0.5	2.87	2.42	0			$2\ ^2P+2\ ^2P$	
	$A\ ^3\Sigma_u^-$	(10.0)	9.44	*c.*	3.790	10.2	10.8	$3\ ^2P+2\ ^2D$	
$^{79}Br^{81}Br$	$X\ ^1\Sigma_g^+$	1.971	2.33	1.75	0			$4\ ^2P+4\ ^2P$	
	$B\ ^3\Pi_{0u}^+$	(0.46)	0.354	*c.*	1.970	0.35	0.46	$4\ ^2P_{\frac{1}{2}}+4\ ^2P_{\frac{1}{2}}$	
C_2	$X\ ^3\Pi_u$	~5.6	5.66	5.44	0			$2\ ^3P+2\ ^3P$	
	$A\ ^3\Pi_g$	(4.5)	4.71	3.50	2.393	1.4	1.26	$2\ ^3P+2\ ^1D$	
	$B\ ^3\Pi_g$	(0.7)	0.73	0.47	4.969	0.1	0.0	$2\ ^3P+2\ ^3P$	
	$a\ ^1\Sigma_g^+$	(5.6)	5.96	5.16	−0.07	0.3	0.0	$2\ ^3P+2\ ^3P$	
	$b\ ^1\Pi_u$	(4.6)	5.20	3.96	0.97	0.6	0.0	$2\ ^3P+2\ ^3P$	
	$c\ ^1\Pi_g$	(5.3)	5.02	4.01	4.18	3.6	3.92	$2\ ^1D+2\ ^1S$	
	$d\ ^1\Sigma_u^+$		5.88	5.88	5.29	5.5	7.45?	$2\ ^3P+3\ ^3P$	?
CN	$X\ ^2\Sigma^+$	8.3	8.00	7.49	0			$2\ ^3P+2\ ^4S$	
	$A\ ^2\Pi_i$	(7.1)	6.25	6.00	1.146	−0.8	0.0	$2\ ^3P+2\ ^4S$	
	$B^2\Sigma^+$		8.00	4.58	3.192	2.9			
CO	$X\ ^1\Sigma^+$	11.2	8.70	8.60	0			$2\ ^3P+2\ ^3P$	9
	$A\ ^3\Pi$	(3.1)	3.39	2.70	8.067	−0.2	0.0	$2\ ^3P+2\ ^3P$	
	$a\ ^3\Pi^+$	(5.2)	5.08	4.83	6.036	0.0	0.0	$2\ ^3P+2\ ^3P$	
	$a'^3\Sigma^+$	(4.3)	3.83	4.33	6.903	−0.3	0.0	$2\ ^3P+2\ ^3P$	
	$d\ ^3\Delta$	(3.4)	4.21	*c.*	7.809	0.8	0.0	$2\ ^3P+2\ ^3P$	
	$c\ ^3\Sigma^-$	(3.1)	3.05	6.23	8.098	0.0	0.0	$2\ ^3P+2\ ^3P$	10
$(CO)^+$	$X\ ^2\Sigma^+$	8.57	7.90	7.28	0				
	$A\ ^2\Pi_i$		4.39	4.35	2.570	−1.6			
	$B\ ^2\Sigma^+$		2.57	2.01	5.687	−0.2			
CP	$X\ ^2\Sigma^+$	6±1	5.45	4.96	0			$2\ ^3P+3\ ^4S$	
	$A\ ^2\Pi_i$	(~5)	4.54	*c.*	8.744 (8.548)	7.8	7.38	$2\ ^3P+3\ ^4P$	
	$B\ ^2\Sigma^+$	(~2.4)	2.87	2.48	3.608	0.5	0.0	$2\ ^3P+3\ ^4S$	
CS	$X\ ^1\Sigma^+$	7.2±1.0	6.25	6.18	0			$2\ ^3P+3\ ^3P$	11
	$A\ ^1\Pi$	(2.4)	2.67	2.84	4.824	0.3	0	$2\ ^3P+3\ ^3P$	
Cl_2	$X\ ^1\Sigma_g^+$	2.51	(1.90)	*c.*	0			$3\ ^2P+3\ ^2P$	
	$A\ ^3\Pi_{0u}^+$	(0.24)	0.25	0.26	2.270	0.01	0	$3\ ^2P+3\ ^2P$	
$(Cl_2)^+$	$X\ ^2\Pi$	4.4	3.46	*c.*	0			$3\ ^3P+3\ ^3P$	
	$A\ ^2\Pi$	(~1.82) (~1.85)	1.45 1.83	*c.*	2.578 2.553	0.0	0	$3\ ^3P+3\ ^3P$	
ClF	$X\ ^1\Sigma$	2.62	1.51	1.02	0			$3\ ^2P+2\ ^2P$	
	$A\ ^3\Pi_0^+$	(0.27)	1.10	*c.*	2.350	~0.8	0	$3\ ^2P+2\ ^2P$	
GeO	$X\ ^1\Sigma^+$	6.8±0.2	5.48	5.81	0			$4\ ^3P+2\ ^3P$	
	$A\ ^1\Sigma^+$		2.41	3.62	4.681	0.2	0(0.07) (0.17) 0.88	$4\ ^3P+2\ ^3P$ $4\ ^1D+2\ ^3P$	
He_2	$X\ ^1\Sigma_g^+$				0				
	$a\ ^3\Sigma_u^+$		1.69	2.10	...				
	$e\ ^3\Pi_g$		4.76	2.08	...				
I_2	$X\ ^1\Sigma^+$	1.556	1.79	1.70	0			$5\ ^2P+5\ ^2P$	12
	$B\ ^3\Pi_{0u}^+$	(0.56)	0.46	0.40	1.939	0.8	0.94	$5\ ^2P_{\frac{1}{2}}+5\ ^2P_{\frac{1}{2}}$	
ICl	$X^1\Sigma^+$	2.178	2.35	2.13	0			$5\ ^2P+3\ ^2P$	
	$A\ ^3\Pi_i$	(0.47)	0.53	0.36	1.704	0.0	0.0	$5\ ^2P+3\ ^2P$	
	$B\ ^3\Pi_0^+$	(0.02)	(0.10)	*c.*	2.149	0.0	0.0	$5\ ^2P+3\ ^2P$	
IO	$X\ ^2\Pi_{\frac{1}{2}}$	1.9	2.59	2.57	0			$5\ ^2P+2\ ^3P$	13
	$A^2\Pi_{\frac{1}{2}}$	(1.19)	1.14	0.84	2.672	1.9	1.96	$5\ ^2P+2\ ^1D$	

TABLE I.—*Continued.*

Molecule	State	Dissociation energy			Atomic excitation energy			Dissociation products	Ref.
		Obs[a]	S.F.[b]	5 par. F[b,c]	Te(ev)	Calc	Theoret		
K_2	$X\ ^1\Sigma_g^+$	0.520	0.60	0.47	0			$4\ ^2S+4\ ^2S$	
	$B\ ^1\Pi_u$	(0.22)	0.35	0.26	1.906	1.7	1.61	$4\ ^2P+4\ ^2S$	
Li_2	$X\ ^1\Sigma_g^+$	1.10±0.05	1.23	1.10	0			$2\ ^2S+2\ ^2S$	
	$A\ ^1\Sigma_u^+$	(1.2)	1.09	1.24	1.744	1.7	1.85	$2\ ^2S+2\ ^2P$	
	$B\ ^1\Pi_u$	(0.4)	0.67	0.59	2.534	2.1	1.85	$2\ ^2S+2\ ^2P$	
N_2	$X\ ^1\Sigma_g^+$	9.92	9.62	8.91	0			$2\ ^4S+2\ ^4S$	14, 15
	$a\ ^1\Pi_g$	(6.1)	5.04	4.82	8.590	3.6	4.74	$2\ ^2D+2\ ^2D$	14
	$q\ ^1\Sigma_u^+$	(2.1)	(1.38)	(1.32)	13.72	(5.2)	5.93	$2\ ^2P+2\ ^2D$	
	$a_\mu'\ (^1\Sigma_u^-)$	(5.9)	4.23	3.47	8.740	3.0	4.74	$2\ ^2D+2\ ^2D$	16
	$x\ ^1\Sigma_g^-$	(5.8)	4.76	5.63	14.351	9.3	10.29	$3\ ^4P+2\ ^4S$	16
	$A\ ^3\Sigma_u^+$	(3.7)	3.71	2.73	6.224	0.0	0.0	$2\ ^4S+2\ ^4S$	
	$B\ ^3\Pi_g$	(4.9)	5.05	4.62	7.392	2.5	2.37	$2\ ^4S+2\ ^2D$	
	$C\ ^3\Pi_u$		5.87	5.11	11.05	7.0			
$(N_2)^+$	$X\ ^2\Pi_g^+$	8.87	7.35	7.47	0			$2\ ^3P+2\ ^4S$	17
	$B\ ^2\Sigma_u^+$	(5.7)	6.08	4.44	3.156	0.3	0.0	$2\ ^3P+2\ ^4S$	
NO	$X\ ^2\Pi_{\frac{1}{2}}$	~6.6	6.32	6.26	0			$2\ ^4S+2\ ^3P$	18
	$A\ ^2\Sigma^+$	(7.7)	8.34	7.91	5.450	7.3	6.54	$2\ ^2D+2\ ^1S$	19
	$B\ ^2\Pi_r$	(3.3)	3.50	3.42	5.692	2.6	2.37	$2\ ^2D+2\ ^3P$	
	$E\ ^2\Sigma^+$	(8.2)	8.67	7.89	7.516	9.7	9.11	$2\ ^4S+3\ ^4S$	
	$D\ ^2\Sigma^+$	(5.5)	5.67	4.40	5.449	4.6	4.33	$2\ ^2D+2\ ^1D$	19
	$B\ ^2\Delta$	(2.7)	2.24	1.73	7.482	3.2	3.56	$2\ ^2P+2\ ^3P$	20
NO^+	$X\ ^1\Sigma^+$	10.6	8.42	9.09				$2\ ^3P+2\ ^2P$ or $2\ ^4S+2\ ^4S$	19
	$A\ ^1\Pi$		2.65	2.04	9.106				19
Na_2	$X\ ^1\Sigma_g^+$	0.75±0.03	0.88	0.72	0			$3\ ^2S+3\ ^2S$	
	$A\ ^1\Sigma_u$	(1.0)	0.95	0.90	1.820	2.0	2.10	$3\ ^2S+3\ ^2P$	
	$B\ ^1\Pi_u$	(0.3)	0.61	0.56	2.519	2.3	2.10	$3\ ^2S+3\ ^2P$	
O_2	$X\ ^3\Sigma_g^-$	5.220	5.04	5.11	0			$2\ ^3P+2\ ^3P$	
	$a\ ^1\Delta_g$	(4.2)	4.29	4.39	0.981	0.0	0.0	$2\ ^3P+2\ ^3P$	
	$b\ ^1\Sigma_g^+$	(3.58)	3.55	3.41	1.636	0.0	0.0	$2\ ^3P+2\ ^3P$	
	$B\ ^3\Sigma_u^-$	(1.0)	1.48	1.18	6.174	2.5	1.96	$2\ ^3P+2\ ^1D$	
	$^1\Sigma_u^-$	(0.68)	0.59	0.45	4.546	0.0	0.0	$2\ ^3P+2\ ^3P$	21
	$^3\Sigma_u^+$		1.03	0.78					22
O_2^+	$X\ ^2\Pi_g$	6.59	5.15	5.05	0			$2\ ^3P+2\ ^4S$	
	$a\ ^4\Pi_u$	(2.6)	2.50	2.81	(3.955)	−0.1	0.0	$2\ ^3P+2\ ^4S$	
	$A\ ^2\Pi_u$	(1.8)	1.45	1.25	4.809	−0.3	0.0	$2\ ^3P+2\ ^4S$	
	$b\ ^4\Sigma_g^+$	(2.5)	2.00	1.84	(6.011)	1.4	1.96	$2\ ^1D+2\ ^4S$	
P_2	$X\ ^1\Sigma_g^+$	5.08	5.24	4.93	0			$(3\ ^3D+3\ ^4D)$	23
	$B\ ^1\Sigma_u^+$		2.07	1.78	5.819	2.8			23
	$A\ ^1\Pi_g$	(2.6)	3.10	2.86	4.278	2.3	1.82	$(3\ ^3P+3\ ^3P)$	23
PN	$X\ ^1\Sigma^+$	6.1±0.8	6.22	5.80	0			$3\ ^4S+2\ ^4S$	
	$A\ ^1\Pi$		4.07	4.39	4.935	2.9	2.37	$3\ ^4S+2\ ^2D$	
							3.56	$3\ ^4S+2\ ^2P$	
							2.31	$3\ ^3P+2\ ^4S$	
PO	$X^2\Pi_r$	5.4	5.65	5.20	0			$3\ ^4S+2\ ^3P$	
	$A\ ^2\Sigma$	(6.0)	6.12	3.97	5.009	5.7	5.57	$3\ ^2D+2\ ^1S$	

TABLE I.—*Continued.*

Molecule	State	Dissociation energy Obs[a]	S.F.[b]	5 par. F[b,c]	Atomic excitation energy Te(ev)	Calc	Theoret	Dissociation products	Ref.
S_2	$X\ ^3\Sigma_g^-$	4.4 or 3.6	4.47	4.58	0			$3\ ^3P+3\ ^3P$	
	$B\ ^3\Sigma_u^-$	(1.6)	1.64	1.72	3.947	1.2	1.14	$3\ ^3P+3\ ^1D$	
SO	$X\ ^3\Sigma^-$	5.22	5.02	5.61	0			$3\ ^3P+2\ ^3P$	
	$B\ ^3\Sigma^-$		(0.68)	(2.28)	4.879	0.0	1.14	$3\ ^3P+2\ ^3P$	
							0.0	$3\ ^1D+2\ ^3P$	
Se_2	$X\ ^1\Sigma_g^+$	2.8±0.1	3.48	2.70	0			$4\ ^3P+4\ ^3P$	
	$B\ (^1\Sigma_u^+)$		0.70	0.47	3.228	1.1			
Si_2	$X\ ^3\Sigma_g^-$	3.2	3.17	3.43				$3\ ^3P+3\ ^3P$	24
	$D\ ^3\Pi_g$		2.99	2.83					
	$H\ ^3\Sigma_u^-$	(0.8)	0.89	0.68	2.984	0.7	0.77	$3\ ^3P+3\ ^1D$	
SiN	$X\ ^2\Sigma^+$	4.5±0.4	4.91	4.63	0			$3\ ^3P+2\ ^4S$	
	$B\ ^2\Sigma^+$	(1.5)	1.50	1.11	3.012	0.0	0.0	$3\ ^3P+2\ ^4S$	
SiO	$X\ ^1\Sigma^+$	8.0±0.3	6.21	5.95	0			$3\ ^3P+2\ ^3P$	
	$A\ ^1\Pi$	(2.7)	2.85	3.35	5.310	0.1	0.0	$3\ ^3P+2\ ^3P$	
SiS	$X\ ^1\Sigma^+$	6.35±0.1	5.34	5.54	0			$3\ ^3P+3\ ^3P$	25
	$D\ ^1\Pi$	(2.2)	2.67	*c.*	4.343	0.6	0.0	$3\ ^3P+3\ ^3P$	

[a] (*G*) = Gaydon (reference 45); (*H*) = Herzberg (reference 8).
[b] Values quoted in brackets are based on uncertain data.
[c] *c* = solution complex.

TABLE II. Comparison of dissociation energies calculated from three- and five-parameter potential functions for excited states of diatomic molecules.

Molecule	State	Dissociation energy Obs[a]	S.F.	5 par. F[b]	Atomic excitation energy Te(ev)	Calc	Theoret	Dissociation products	Ref.
AlBr	$X\ ^1\Sigma^+$	4.3	2.72	5.44	0			$3\ ^2P+4\ ^2P$	
	$A\ ^1\Pi$		0.32	0.21	4.448	0.4	0.0(0.4)	$3\ ^2P+4\ ^2P$	
AlCl	$X\ ^1\Sigma^+$	5.1	2.90	*c.*	0			$3\ ^2P+3\ ^2P$	
	$A\ ^1\Pi$		1.10	*c.*	4.742	0.7	0.0	$3\ ^2P+3\ ^2P$	
AlF	$X\ ^1\Sigma^+$	6.8	3.33	6.01	0			$3\ ^2P+2\ ^2P$	26,27
	$B\ ^1\Sigma^+$		2.41	1.74	6.724	2.3	3.13	$4\ ^2S+2\ ^2P$	
	$A\ ^1\Pi$		2.45	2.25	5.447	0.9	0.0	$3\ ^2P+2\ ^2P$	
	$D\ ^1\Delta$		3.30	2.39	7.587	4.0	4.00	$3\ ^2P+2\ ^2P$	
	$C\ ^1\Sigma$		4.13	4.08	7.158	4.0	4.08	$4\ ^2P+2\ ^2P$	
AlO	$X^2\Sigma^+$	3.80 or 6.00	3.31	3.01	0			$3\ ^2P+2\ ^3P$	28
	$A\ ^2\Sigma^+$		5.3	10.8	2.566	4.1	4.00	$3\ ^2D+2\ ^3P$	
							4.08	$4\ ^2P+2\ ^3P$	
							4.17	$3\ ^2P+2\ ^1S$	
AlS	$X\ ^2\Sigma^+$		2.745	2.33	0				29
	$A\ ^2\Sigma^+$		4.46	7.43	2.904				
BBr	$X\ ^1\Sigma^+$	4.1	3.26	2.94	0			$2\ ^2P+4\ ^2P$	
	$A\ ^1\Pi$		0.54	0.25	4.207	0.4	0.0	$2\ ^2P+4\ ^2P$	

TABLE II.—*Continued.*

Molecule	State	Dissociation energy Obs[a]	S.F.	5 par. F[b]	Atomic excitation energy Te(ev)	Calc	Theoret	Dissociation products	Ref.
BCl	$X\,^1\Sigma$	5.1±0.4	5.09	4.16	0		0.0	$2\,^2P+3\,^2P$	
	$A\,^1\Pi$		1.51	1.06	4.556	0.6	0.0	$2\,^2P+3\,^2P$	
BF	$X\,^1\Sigma^+$	8.5±0.5(*G*) 4.3(*H*)	4.24	3.85	0			$2\,^2P+2\,^2P$	30
	$A\,^1\Pi$		2.62	1.99	6.341	1.2 or 4.6	0.0 or 4.94	$2\,^2P+2\,^2P$ $2\,^2P+3\,^2S$	30
	$a\,^3\Pi$		4.59	*c.*					
	$b\,^3\Sigma$		2.75	1.95					
BN	$X\,^3\Pi$	4.0±0.5	4.57	*c.*	0			$2\,^2P+2\,^4S$	
	$A\,^3\Pi$		2.82	2.14	3.456	~2	2.37	$2\,^2P+2\,^2D$	
BO	$X\,^2\Sigma^+$	9.1(*H*) 7.6±0.4(*G*)	7.45	7.24	0			$2\,^2P+2\,^3P$	
	$A\,^2\Pi_i$		3.48	5.56	2.97				
BaO	$X\,^1\Sigma$	5.6	5.40	5.11	0		(1.15)	$6\,^3D+2\,^3P$	
	$A\,^1\Sigma$		4.12	3.67	2.084	0.4	0.00	$6\,^3D+2\,^3P$	
BeF	$X\,^2\Sigma^+$	4±1	4.35	4.55	0			$2\,^1S+2\,^2P$	
	$A\,^2\Pi_i$		3.87	3.83	4.120	4.0	2.71	$2\,^2P+2\,^2P$	
BeO	$X\,^1\Sigma^+$	5.4	4.59	4.40	0			$2\,^1S+2\,^3P$	
	$A\,^1\Pi$		3.85	4.57	1.166	0.0	0.0	$2\,^1S+2\,^3P$	
	$B\,^1\Sigma^+$		6.11	6.54	2.635	3.5	2.71	$2\,^3P+2\,^3P$	
	$C\,^1\Sigma$		3.16	2.41	4.850	2.5	2.71	$2\,^3P+2\,^3P$	
CuF	$X\,^1\Sigma^+$	3.0	2.37	*c.*	0			$4\,^2S+2\,^2P$	
	$B\,^1\Sigma$		2.57	*c.*	2.444	2.2	1.39(1.64)	$4\,^2D+2\,^2P$	
MgO	$X\,^1\Sigma$	<4.0	2.89	2.58	0			$2\,^1S+2\,^3P$	
	$A\,^1\Pi$		2.76	3.56	4.417	3.2	2.70	$3\,^3P+2\,^3P$	
	$B\,^1\Sigma$		3.48	3.07	2.477	3.0	2.70	$3\,^3P+2\,^3P$	
PbS	$X\,^1\Sigma^+$	3.25±0.3	3.67	*c.*	0			$6\,^3P+3\,^3P$	
	$A\,^1\Sigma^+$		4.77	*c.*	2.337	3.9	3.8	$6\,^1D+3\,^1D$	
SnO	$X\,^1\Sigma^+$	5.7	4.37		0			$5\,^3P+2\,^3P$	
	$D\,^1\Sigma^+$		2.66		3.673	0.6	0.0	$5\,^3P+2\,^3P$	
SrO	$X\,^1\Sigma$	5.0 or 3.6	2.56	1.87	0		(1.80) (1.96)	$5\,^3P+2\,^3P$ $5\,^1P+2\,^1D$	
	$A\,^1\Sigma$		4.80	3.77	1.350	1.1 or 2.5	2.50 0	$5\,^3P+2\,^3P$ $5\,^1P+2\,^1D$	
TiO	$(X)\,^3\Pi_r$	6.9±0.1	5.36	4.49	0			$4\,^3F+2\,^3P$	
	$C\,^3\Pi_r$		3.74	2.86	2.4	−0.8	0	$4\,^3F+2\,^3P$	
VO	$(X\,^3\Delta)$	6.3	5.02	*c.*	0			$^4F+2\,^3P$	
	$A\,(^3\Delta)$		3.29	*c.*	2.170	−0.9	0	$^4F+2\,^3P$	

[a] (*G*)=Gaydon (reference 45); (*H*)=Herzberg (reference 8).
[b] *c*=solution complex.

TABLE III. Comparison of dissociation energies calculated from three- and five-parameter potential functions for excited states of diatomic molecules.

		Dissociation energy			Atomic excitation energy				
Molecule	State	Obs[a]	S.F.	5 par. F	Te(ev)	Calc	Theoret	Dissociation products	Ref.
AgH	$X\,^1\Sigma^+$	2.6	2.28	*c.*	0			$5\,^2S+1\,^2S$	
	$A\,^1\Sigma^+$		0.76	0.54	3.714	1.9	0.0	$5\,^2S+1\,^2S$	
AlH	$X\,^1\Sigma^+$	3.0	2.46	2.76	0			$3\,^2P+1\,^2S$	
	$C\,^1\Sigma^+$		0.47	0.39	5.538	3.0	3.13	$4\,^2S+1\,^2S$	
	$A\,^1\Pi$		1.02	*c.*	2.909	0.9	0.0	$3\,^2P+1\,^2S$	
Al^2H	$X\,^1\Sigma^+$	3.0	2.46	2.70	0			$3\,^2P+1\,^2S$	
	$A\,^1\Pi$		0.28	0.32	2.932	0.2	0.0	$3\,^2P+1\,^2S$	
AuH	$X\,^1\Sigma^+$	3.2	3.06	3.24	0			$6\,^2S+1\,^2S$	
	$A\,^1\Sigma^+$		1.23	1.03	3.430	1.4	0.0	$6\,^2S+1\,^2S$	
Au^2H	$X\,^1\Sigma^+$	3.2	3.06	3.74	0			$6\,^2S+1\,^2S$	
	$A\,^1\Sigma^+$		0.99	0.80	3.427	0.9	0.0	$6\,^2S+1\,^2S$	
	$B\,^1\Sigma^+$		1.67	1.43	4.778	2.9	2.42(2.66)	$2\,^2D+1\,^2S$	
BH	$X\,^1\Sigma^+$	3.1±0.4	2.92	3.05	0			$2\,^2P+1\,^2S$	
	$A\,^1\Pi$		1.03	0.74	2.864	0.8	0.0	$2\,^2P+1\,^2S$	
	$B\,^1\Sigma^+$		2.22	2.78	6.488	5.6	5.91	$2\,^2D+1\,^2S$	
B^2H	$X\,^1\Sigma^+$	3.1±0.4	3.00	3.19	0			$2\,^2P+1\,^2S$	
	$A\,^1\Pi$		1.66	1.39	2.869	1.4	0.0	$2\,^2P+1\,^2S$	
BaH	$X\,^2\Sigma^+$	1.8±0.1	2.169	1.93	0			$6\,^1S+1\,^2S$	
	$B\,^2\Sigma$		2.00	1.93	1.375	1.5	1.41	$6\,^1D+1\,^2S$	
								$6\,^3P+1\,^2S$	
	$E\,^2\Pi$		2.18	2.02	1.866	2.1	2.24	$6\,^1P+1\,^2S$	
			2.18	1.98	1.810				
	$C\,^2\Sigma$		1.92	1.50	2.929	1.8	2.24	$6\,^3P+1\,^2S$	
							1.57		
BeH	$X\,^2\Sigma^+$	2.4±0.3	3.12	3.30	0			$2\,^1S+1\,^2S$	
	$A\,^2\Pi$		2.82	2.90	2.483	2.9	2.71	$2\,^2P+1\,^2S$	
$(Be^1H)^+$	$X\,^1\Sigma^+$	(3.3)	3.21	3.03	0			$2\,^2S+1\,^2S$	
	$A\,^1\Sigma^+$				4.887	5.8	3.95	$2\,^2P+1\,^2S$	
$(Be^2H)^+$	$X\,^1\Sigma^+$	(3.3)	3.22	3.12	0			$2\,^2S+1\,^2S$	
	$A\,^1\Sigma^+$		3.99	5.19	4.886	5.6	3.95	$2\,^2P+1\,^2S$	
BiH	$X(O^+)$	2.6±0.3	2.26	2.33	0			$6\,^4S+1\,^2S$	
	$A(l)$		2.10	1.98	0.6103	0.1	0.0	$6\,^4S+1\,^2S$	
	$B\,O^+$		1.71	1.68	2.636	1.7	1.42(1.91)	$6\,^2D+1\,^2S$	
Bi^2H	$X(O^+)$	2.6±0.3	2.23	2.36	0			$6\,^4S+1\,^2S$	
	$B(O^+)$		1.48	1.18	2.636	1.5	1.42(1.91)	$6\,^2D+1\,^2S$	
CH	$X\,^2\Pi$	3.66	3.23	3.38	0			$2\,^2P+1\,^2S$	
	$A\,^2\Delta$		2.34	2.15	2.870	1.6	1.26	$2\,^1D+1\,^2S$	
	$B\,^2\Sigma^-$		0.407	0.317	3.217	0.0	0.0	$2\,^2P+1\,^2S$	
	$C\,^2\Sigma^+$		1.85	1.62	3.945	2.1	2.67	$2\,^1S+1\,^2S$	
$(C^1H)^+$	$X\,^1\Sigma^+$	3.47			0			$2\,^2P+1\,^2S$	
	$A\,^1\Pi$		0.800	0.795	2.993	0.3	0.0	$2\,^2P+1\,^2S$	
C^2H	$X\,^2\Pi$	3.66	3.23	3.37	0			$2\,^2P+1\,^2S$	
	$A\,^2\Delta$		2.34	2.11	2.874	1.6	1.26	$2\,^1D+1\,^2S$	
	$B\,^2\Sigma^-$		0.38		3.222	0.0	0.0	$2\,^2P+1\,^2S$	
	$C\,^2\Sigma^+$		1.85	1.56	3.946	2.1	2.67	$2\,^1S+1\,^2S$	

TABLE III.—*Continued.*

Molecule	State	Dissociation energy Obs[a]	S.F.	5 par. F[b,c]	Atomic excitation energy Te(ev)	Calc	Theort	Dissociation products	Ref.
CaH	$X\ ^2\Sigma$	≤1.7	2.19	2.04	0			$4\ ^1S+1\ ^2S$	
	$A\ ^2\Pi_r$		2.25	2.14	1.793	2.3	2.52	$3\ ^3D+1\ ^2S$	
							1.88	$4\ ^3P+1\ ^2S$	
	$B\ ^2\Sigma$		2.10	1.72	1.955	2.3	2.52	$3\ ^3D+1\ ^2S$	
							1.88	$4\ ^3P+1\ ^2S$	
	$E\ ^2\Pi$		(1.79)	*c.*	2.527	2.6	2.52	$3\ ^3D+1\ ^2S$	
							1.88	$4\ ^3P+1\ ^2S$	
	$D\ ^2\Sigma$		0.97	0.87	2.802	2.0	2.52	$3\ ^3D+1\ ^2S$	
							1.88	$4\ ^3P+1\ ^2S$	
CdH	$X\ ^2\Sigma^+$	0.774	1.07	0.88	0			$5\ ^1S+1\ ^2S$	
	$A\ ^2\Pi$		1.97	1.85	2.877	3.9	3.8	$5\ ^3P+1\ ^2S$	
$(CdH)^+$	$X^1\Sigma^+$		2.09	1.99	0			$5\ ^2S+1\ ^2S$	
	$A\ ^1\Sigma^+$		5.38	*c.*	5.323	8.6	10.29	$6\ ^2S+1\ ^2S$	
							10.20	$5\ ^2S+2\ ^2P$	
$(Cd^2H)^+$	$X\ ^1\Sigma^+$		2.08	1.97	0			$5\ ^2S+1\ ^2S$	
	$A\ ^1\Sigma^+$		7.26	*c.*	5.322	10.5	10.29	$5\ ^2S+1\ ^2S$	
							10.20	$5\ ^2S+2\ ^2P$	
CsH	$X\ ^1\Sigma^+$	1.8±0.3	1.59	1.37	0			$6\ ^2S+1\ ^2S$	
	$A\ ^1\Sigma^+$		−0.16	*c.*	2.282	0.5	0	$6\ ^2S+1\ ^2S$	
CuH	$X\ ^1\Sigma^+$	2.9	2.57	2.57		2.72	0	$4\ ^2S+1\ ^2S$	
	$A\ ^1\Sigma^+$		1.62	1.55	2.905	1.6	1.39(1.64)	$4\ ^2D+1\ ^2S$	
Cu^2H	$X\ ^1\Sigma^+$	2.9	2.53	2.66	0			$4\ ^2S+1\ ^2S$	
	$A\ ^1\Sigma^+$		1.77	1.73	2.902	1.8	1.39(1.64)	$4\ ^2D+1\ ^2S$	
H_2	$X\ ^1\Sigma^+_g$	4.746	4.59	5.68	0			$1\ ^2S+1\ ^2S$	31
	$B\ ^1\Sigma^+_u$		3.51	*c.*	11.367	10.1	10.15	$2\ ^2P+1\ ^2S$	32
	$C\ ^1\Pi_u$		(2.12)	(3.30)	12.402	10.0	10.15	$2\ ^2P+1\ ^2S$	
	$E\ ^1\Sigma_g^+$		(1.32)	(1.10)	12.405	9.0	10.15	$2\ ^2S+1\ ^2S$	
	$I\ ^1\Pi_g$		1.77	1.72	14.017	11.0	12.04	$3\ ^2P+1\ ^2S$	
	$D\ ^1\Pi_u$		(3.10)	(6.06)	14.119	12.5 ?	12.04	$3\ ^2P+1\ ^2S$	
	$C\ ^3\Pi_u$		2.84	3.62	11.869	10.0	10.15	$2\ ^2P+1\ ^2S$	
	$a\ ^3\Sigma_g^+$		2.81	3.45	11.893	10.0	10.15	$2\ ^2P+1\ ^2S$	
	$e\ ^3\Sigma_u^+$		2.02	2.55	13.361	10.6	10.15	$2\ ^2P+1\ ^2S$	
	$d\ ^3\Pi_u$		2.38	2.97	13.972	11.6	12.04	$3\ ^2P+1\ ^2S$	
	$h\ ^3\Sigma_g^+$		2.53	2.49	13.980	11.7	12.04	$3\ ^2P+1\ ^2S$	
	$n\ ^3\Pi_u$		(2.43)	(2.46)	14.995	13.7		$>5\ ^2P$	
$^1H^3H$	$X\ ^1\Sigma_g^+$	4.746	4.29	4.69	0			$1\ ^2S+1\ ^2S$	
	$a\ ^3\Sigma_g^+$		2.80	3.49			10.15	$2\ ^2S+1\ ^2S$	
	$d\ ^3\Pi_u$		2.43	2.91			12.06	$3\ ^2P+1\ ^2S$	
$^1H^2H$	$X\ ^1\Sigma_g^+$	4.746	4.35	5.63	0			$1\ ^2S+1\ ^2S$	31
	$B\ ^1\Sigma_u^+$		3.13	*c.*	11.369	9.7	10.15	$2\ ^2P+1\ ^2S$	
	$C\ ^1\Pi_u$		1.84	1.68	12.404	9.5	10.15	$2\ ^2P+1\ ^2S$	
	$E\ ^1\Sigma_g^+$		(1.56)	(1.43)	12.411	9.3	10.15	$2\ ^2S+1\ ^2S$	
	$I\ ^1\Pi_g$		(1.80)	(2.16)	14.019	11.0	12.04	$3\ ^2P+1\ ^2S$	
	$a\ ^3\Sigma_g^+$		2.81	3.52	11.893	10.1	10.15	$2\ ^2S+1\ ^2S$	
	$e\ ^3\Sigma_u^+$		1.92	2.25	13.360	10.5	10.15	$2\ ^2P+1\ ^2S$	
	$d\ ^3\Pi_u$		2.38	2.99	13.972	11.6	12.04	$3\ ^2P+1\ ^2S$	

TABLE III.—*Continued.*

Molecule	State	Dissociation energy Obs[a]	S.F.	5 par. F[b,c]	Atomic excitation energy Te(ev)	Calc	Theoret	Dissociation products	Ref.
$^2H_2$	$X\ ^1\Sigma_g^+$	4.746	4.29	4.79	0			$1\ ^2S+1\ ^2S$	31
	$B\ ^1\Sigma_u^+$		2.89	*c.*	11.368	9.6	10.15	$2\ ^2P+1\ ^2S$	
	$C\ ^1\Pi_u$		2.11	2.25	12.408	9.8	10.15	$2\ ^2P+1\ ^2S$	
	$E\ ^1\Sigma_g^+$		(1.76)	(1.73)	12.413	9.6	10.15	$2\ ^2S+1\ ^2S$	
	$I\ ^1\Pi_g$		1.76	1.69	14.015	11.0	12.04	$3\ ^2P+1\ ^2S$	
	$a\ ^3\Sigma_g^+$		2.80	3.65	12.017	10.1	10.15	$2\ ^2S+1\ ^2S$	
	$e\ ^3\Sigma_u^+$		1.92	2.19	13.358	10.5	10.15	$2\ ^2P+1\ ^2S$	
	$d\ ^3\Pi_u$		2.40	3.03	13.972	11.7	12.04	$3\ ^2P+1\ ^2S$	
$^3H_2$	$X\ ^1\Sigma_g^+$	4.746	4.18	4.69	0			$1\ ^2S+1\ ^2S$	
	$a\ ^3\Sigma_g^+$		2.74	3.29			10.15	$2\ ^2S+1\ ^2S$	
	$d\ ^3\Pi_u$		2.39	3.04			12.04	$2\ ^2P+1\ ^2S$	
HF	$X\ ^1\Sigma^+$	5.9	4.92	5.88	0			$1\ ^2S+2\ ^2P$	33
$H^{79}Br$	$X\ ^1\Sigma^+$	3.93	3.89	4.13	0			$1\ ^2S+4\ ^2P$	34
$H^{81}Br$	$X\ ^1\Sigma^+$	3.93	3.89	4.13	0			$1\ ^2S+4\ ^2P$	34
$^2_2H^{79}Br$	$X\ ^1\Sigma^+$	3.93	3.87	4.085	0			$1\ ^2S+4\ ^2P$	34
$H^{81}Br$	$X\ ^1\Sigma^+$	3.93	3.85	4.01	0			$1\ ^2S+4\ ^2P$	34
$(^1HCl)^+$	$X\ ^2\Pi_i$	4.7±0.2	3.34	3.50	0			$1\ ^2S+3\ ^3P$	
	$A\ ^2\Sigma^+$		1.63	*c.*	3.550	0.4	0	$1\ ^2S+3\ ^3P$	
$^2H^{35}Cl$	$X\ ^1\Sigma^+$	4.38	4.30	4.61				$1\ ^2S+3\ ^2P$	34
$^2H^{37}Cl$	$X\ ^1\Sigma^+$	4.38	4.27	4.53				$1\ ^2S+3\ ^2P$	34
Hg^1H	$X\ ^2\Sigma^+$	0.372	0.553	0.399	0			$6\ ^1S+1\ ^2S$	
	$A\ ^2\Pi_{\frac{1}{2}}$		(1.63)	(1.29)	3.047	~4.2	(4.67) (5.46) 4.89	$6\ ^3P+1\ ^2S$	
	$A\ ^2\Pi_{\frac{3}{2}}$		(2.53)	(3.22)	3.503	~5.6	(4.67) (5.46) 4.89	$6\ ^3P+1\ ^2S$	
$(HgH)^+$	$X\ ^1\Sigma^+$	(2.4)	2.20	1.94	0			$6\ ^2S+1\ ^2S$	
	$A^1\ \Sigma^+$		1.50	1.29	5.494	4.7	6.38	$6\ ^2P+1\ ^2S$	
$(Hg^2H)^+$	$X\ ^1\Sigma^+$	(2.4)	2.20	1.94	0			$6\ ^2S+1\ ^2S$	
	$A\ ^1\Sigma^+$		1.49	1.28	5.493	4.6	6.38	$6\ ^2P+1\ ^2S$	
InH	$X\ ^1\Sigma^+$	≤2.58	2.21	2.80	0			$5\ ^2P+1\ ^2S$	
	$A\ ^1\Sigma^+$		0.84	0.37	2.018	0.3	0(0.27)	$5\ ^2P+1\ ^2S$	
	$B\ ^1\Pi$		0.51	0.37	2.097	0.0	0(0.27)	$5\ ^2P+1\ ^2S$	
K^1H	$X\ ^1\Sigma^+$	1.92	1.69	1.46	0			$4\ ^2S+1\ ^2S$	
	$A\ ^1\Sigma^+$		(−0.29)		2.421				
K^2H	$X^1\Sigma^+$	1.92	1.66	1.61	0			$4\ ^2S+1\ ^2S$	
	$A\ ^1\Sigma^+$		−0.33		2.428				
Li^1H	$X\ ^1\Sigma^+$	2.6	2.25	2.45	0			$2\ ^2S+1\ ^2S$	
	$A\ ^1\Sigma^+$		−0.04		3.287	~0.8	1.85	$2\ ^2P+1\ ^2S$	
	$B\ ^1\Pi$		0.026	0.039	4.327	1.8	1.85	$2\ ^2P+1\ ^2S$	38
Li^2H	$X^1\Sigma^+$	2.6	2.22	2.44	0			$2\ ^2S+1\ ^2S$	
	$A\ ^1\Sigma^+$		−0.05		3.287	~0.8	1.85	$2\ ^2P+1\ ^2S$	
	$B\ ^1\Pi$		0.026	0.037	4.323	1.8	1.85	$2\ ^2P+1\ ^2S$	35
Mg^1H	$X\ ^2\Sigma^+$	2.1±0.5	1.77	1.76	0			$3\ ^1S+1\ ^2S$	
	$A\ ^2\Pi_r$		1.57	1.26	2.383	3.0	2.70	$3\ ^3P+1\ ^2S$	
	$C\ ^2\Pi$		1.31	3.61	5.098				

TABLE III.—*Continued.*

Molecule	State	Dissociation energy Obs[a]	S.F.	5 par. F[b,c]	Atomic excitation energy Te(ev)	Calc	Theoret	Dissociation products	Ref.
Mg^2H	$X\ ^2\Sigma^+$	2.1	1.81	1.63	0			$3\ ^1S+1\ ^2S$	
	$A\ ^2\Pi_r$		1.91	1.66	2.383	2.30	2.70	$3\ ^3P+1\ ^2S$	
$(Mg^1H)^+$	$X\ ^1\Sigma^+$	(2.2)	2.40	3.59	0			$3\ ^2S+1\ ^2S$	
	$A\ ^1\Sigma^+$		5.76	*c.*	4.451	~8	8.86	$3\ ^2D+1\ ^2S$	
							8.65	$4\ ^2S+1\ ^2S$	
$(Mg^2H)^+$	$X\ ^1\Sigma^+$	(2.2)	2.32	2.10	0			$3\ ^2S+1\ ^2S$	
	$A\ ^1\Sigma^+$		5.91		4.451	~8	8.86	$3\ ^2D+1\ ^2S$	
							8.65	$4\ ^2S+1\ ^2S$	
MnH	$X\ ^7\Sigma$	<2.4	2.09	1.93	0			$a\ ^6S+1\ ^2S$	36
Mn^2H	$X\ ^7\Sigma$		2.21	1.95	0			$a\ ^6S+1\ ^2S$	36
Na^1H	$X\ ^1\Sigma^+$	2.0	1.79	1.83	0			$3\ ^2S+1\ ^2S$	
	$A\ ^1\Sigma^+$		−0.371		2.816				
O^1H	$X\ ^2\Pi_i$	4.62	4.28	4.81	0			$2\ ^3P+1\ ^2S$	
	$A\ ^2\Sigma^+$		2.66	2.66	4.052	2.0	1.96	$2\ ^1D+1\ ^2S$	
O^2H	$X\ ^2\Pi_i$	4.62	4.25	5.98	0			$2\ ^3P+1\ ^2S$	
	$A\ ^2\Sigma^+$		2.58	2.74	4.447	2.4	1.96	$2\ ^1D+1\ ^2S$	
Pb^1H	$X\ ^2\Pi_i$	1.9±0.2(*G*) ≤1.59(*H*)	2.040	2.47	0			$6\ ^3P+1\ ^2S$	
	$A\ ^2\Sigma$		0.66	0.56	(2.181)	1.0	0(0.97)(1.32)	$6\ ^3P+1\ ^2S$	
	$B\ ^2\Sigma$		0.47	0.38	(2.235)	0.8	0(0.97)(1.32)	$6\ ^3P+1\ ^2S$	
Rb^1H	$X\ ^1\Sigma^+$	1.7±0.2	1.57	1.55	0			$5\ ^2S+1\ ^2S$	
	$A\ ^1\Sigma^+$		−0.30		2.344				
SrH	$X\ ^2\Sigma^+$	1.75±0.1	2.17	2.12	0			$5\ ^1S+1\ ^2S$	
	$D\ ^2\Sigma^+$		1.63	1.22	2.584	2.5	2.69	$5\ ^1P+1\ ^2S$	
							2.50	$5\ ^1D+1\ ^2S$	
	$C\ ^2\Sigma^+$		1.92	3.21	3.252	3.5	3.79	$6\ ^1S+1\ ^2S$	
Zn^1H	$X\ ^2\Sigma^+$	0.95	1.14	0.87	0			$4\ ^1S+1\ ^2S$	
	$A\ ^2\Pi_r$		2.24	2.17	2.885	4.2	4.0	$4\ ^3P+1\ ^2S$	
	$B\ ^2\Sigma^+$		(1.59)	(1.28)	3.420	4.0	4.0	$4\ ^3P+1\ ^2S$	
$(Zn^1H)^+$	$X\ ^1+$	2.9+0.4	2.36	2.35	0			$4\ ^2S+1\ ^2S$	
	$A\ ^1+$		3.37	3.57	5.789	6.2	6.0	$4\ ^2P+1\ ^2S$	
$(Zn^2H)^+$	$X\ ^1+$	2.9	3.36	*c.*	0			$4\ ^2S+1\ ^2S$	
	$A\ ^1+$		0.40	*c.*	5.789	6.2	60	$4\ ^2P+1\ ^2S$	

[a] (*G*)=Gaydon (reference 45); (*H*)=Herzberg (reference 8).
[b] Values quoted in brackets are based on uncertain data.
[c] *c*=Solution complex.

harmonic oscillator using the WBK method and the general potential[7]

$$V=a_0(\Delta r/r_e)^2[1+a_1(\Delta r/r_e)+a_2(\Delta r/r_e)^2+\cdots]\text{hc}. \quad (9)$$

The following values for a_0, a_1, and a_2 in Eq. (9) were obtained from

$$a_0=\omega_e^2/4B_e, \quad (10)$$

$$a_1=-1-\alpha_e\omega_e/6B_e^2=-(1+F), \quad (11)$$

$$a_2=(\tfrac{5}{4})a_1^2-2\omega_e x_e/3B_e=(\tfrac{5}{4})a_1^2-G/12. \quad (12)$$

By comparing Eq. (8) with Eq. (9) and using Eqs.

[7] J. L. Dunham, Phys. Rev. **41**, 713, 721 (1932).

(10), (11), and (12) one obtains the following relations

$$D_e=\omega_e^2/2nr_eB_e, \tag{13}$$

$$\alpha_e=(6abB_e^2/\omega_e)(nr_e/2)^{\frac{1}{2}} \quad \text{or} \quad F=ab\Delta^{\frac{1}{2}}, \tag{14}$$

$$x_e\omega_e=\tfrac{3}{2}B_e\{\tfrac{1}{4}+(nr_e/4)+ab(nr_e/2)^{\frac{1}{2}} +[(5a^2b^2/4)-ab^2](nr_e/2)\}. \tag{15}$$

Equation (13) is equivalent to (2). Equations (14) and (15) may be put in the form

$$2x_e\omega_e/3B_e=\tfrac{1}{4}+(nr_e/4)+(\alpha_e\omega_e/6B_e^2) +\tfrac{5}{4}(\alpha_e\omega_e/6B_e^2)^2-(nr_e/2)^{\frac{1}{2}}b\alpha_e\omega_e/6B_e^2, \tag{16a}$$

or

$$G/12=\tfrac{1}{4}+\Delta/2+F+\tfrac{5}{4}F^2-\Delta^{\frac{1}{2}}bF, \tag{16b}$$

or if one eliminates Δ

$$G=12[(\tfrac{1}{4})+F]+12F^2[(\tfrac{1}{2}a^2b^2)+(\tfrac{5}{4})-(1/a)].$$

Equation (16) has been used to calculate values of D_e from experimental values of k_e, $x_e\omega_e$, α_e, r_e, and b; b was found to be constant within 3%. The value of b used in the calculations was 1.065. The calculated values of D_e are tabulated in Tables I–III and are compared with experimental values and with values for the dissociation energy calculated from the simple three-parameter function. In cases where the experimental values of $x_e\omega_e$ and α_e are well known the calculated values agree well with those calculated from the simple function. The agreement with experimental D_e values is good when these are well known from a knowledge of the excited states of the separated atoms. In most cases where the calculated value of D_e deviates markedly from that given by the simple functions, the experimental value of α_e is not well known or is given with less than three significant figures. A small error in α_e causes a relatively large error in D_e and it would appear that the lack of agreement between the two calculated values of D_e is due in part to the uncertainty in α_e. The experimental data for ω_e, B_e, ω_ex_e, α_e, and T_e have been taken from Herzberg[8] unless other references are quoted in column 10. The additional references[9–39] give more recent and, what has been assumed to be more accurate data. All dissociation energies, apart from that of C_2, have been taken from the second edition of Cottrell's book.[40]

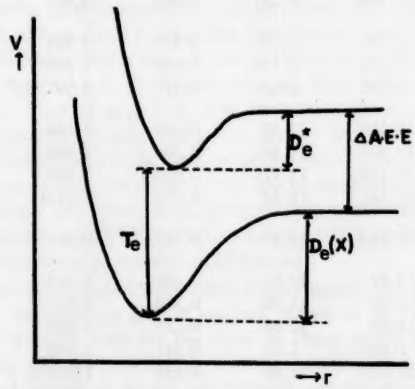

FIG. 1. Relation between dissociation energies of ground and excited states. T_e = electronic energy of the excited state, D_e^* = dissociation energy of the excited state, $D_e(X)$ = dissociation energy of the ground state, and $\Delta A\cdot E\cdot E\cdot$ = difference between the atomic excitation energies in the two states.

The dissociation energies of the excited states are related to those of the ground states as in

$$T_e+D_e^*=D_e(X)+\Delta \text{ A.E.E.}, \tag{17}$$

where T_e is the electronic energy of the excited state, D_e^* is the dissociation energy for the excited state, $D_e(X)$ is the dissociation energy for the ground state, and Δ A.E.E. is the difference between the atomic excitation energies in the two states (see Fig. 1). The electronic energy of the state is usually accurately known, and consequently the change in the atomic excitation energies can be evaluated from the calculated or observed dissociation energies. From the permitted dissociation products, and tables of atomic excitation

[8] G. Herzberg, *Spectra of Diatomic Molecules* (D. Van Nostrand Company, Inc., Princeton, New Jersey, 1950), pp. 502–581.
[9] D. H. Rank, A. H. Guenther, G. D. Saksena, J. N. Shearer, and T. A. Wiggins, J. Opt. Soc. Am. **47**, 686 (1957).
[10] G. Herzberg and T. J. Hugo, Can. J. Phys. **33**, 757 (1955).
[11] A. Lagerqvist, H. Westerlund, L. V. Wright, and R. F. Barrow, Arkiv. Fysik **14**, 387 (1959).
[12] R. D. Verma, J. Chem. Phys. **32**, 738 (1960).
[13] R. A. Durie, F. Legay, and D. A. Ramsey, Can. J. Phys. **38**, 444 (1960).
[14] A. Lofthus, Can. J. Phys. **34**, 780 (1956).
[15] B. P. Stoicheff, Can. J. Phys. **35**, 730 (1957).
[16] A. Lofthus, J. Chem. Phys. **25**, 494 (1956).
[17] P. G. Wilkinson, Can. J. Phys. **34**, 250 (1956).
[18] W. H. Fletcher and G. M. Begun, J. Chem. Phys. **27**, 579 (1957).
[19] E. Miescher, Can. J. Phys. **33**, 355 (1955).
[20] R. F. Barrow and E. Miescher, Proc. Phys. Soc. (London) **70A**, 219 (1957).
[21] G. Herzberg, Can. J. Phys. **31**, 57 (1953).
[22] G. Herzberg, Can. J. Phys. **30**, 185 (1952).
[23] A. E. Douglas and P. T. Rao, Can. J. Phys. **36**, 565 (1958).
[24] A. E. Douglas, Can. J. Phys. **33**, 801 (1955).
[25] G. Nilheden, Arkiv Fysik **10**, 19 (1956).
[26] S. M. Naudé and T. J. Hugo, Can. J. Phys. **31**, 1106 (1953).
[27] S. M. Naudé and T. J. Hugo, Can. J. Phys. **32**, 246 (1954).
[28] A. Lagerqvist, N. E. L. Nilsson, and R. F. Barrow, Arkiv Fysik **12**, 543 (1957).
[29] C. N. McKinney and K. K. Innes, J. Mol. Spectroscopy **3**, 235 (1959).
[30] R. Onaka, J. Chem. Phys. **27**, 374 (1957).
[31] B. P. Stoicheff, Can. J. Phys. **35**, 730 (1957).
[32] Y. Tanaka, Sci. Papers Inst. Phys. Chem. Research (Tokyo) **42**, 49 (1944).
[33] G. A. Kuipers, D. F. Smith, and A. H. Neilson, J. Chem. Phys. **25**, 275 (1956).
[34] H. M. Mould, W. C. Price, and G. R. Wilkinson, Spectrochim. Acta. **16**, 479 (1960).
[35] R. Velasco, Can. J. Phys. **35**, 1204 (1957).
[36] W. Hayes, P. D. McCarvill, and T. E. Neven, Proc. Phys. Soc. (London) **70A**, 904 (1957).
[37] D. F. Smith, M. Tidwell, and D. V. P. Williams, Phys. Rev. **79**, 1007 (1950).
[38] D. T. Smith, M. Tidwell, and D. V. P. Williams, Phys. Rev. **77**, 420 (1950).
[39] R. N. Dixon, Can. J. Phys. **37**, 1171 (1959).
[40] T. L. Cottrell, *The Strengths of Chemical Bonds* (Butterworths Scientific Publications Company, Ltd., London, 1958), 2nd ed.

TABLE IV.

Molecule	State	ω_e	B_e	α_e	$x_e\omega_e$ obs	$x_e\omega_e$ calc	a	b	Ref.
BF	$X\,^1\Sigma^+$	1402.13	1.5107	0.0165	11.84	10.24	0.543	0.987	30
BO	$X\,^2\Sigma^+$	1885.44	1.7803	0.01648	11.769	9.543	0.537	1.055	
	$A^2\Pi_i$	1260.70	1.4132	0.0196	11.157	12.490	0.577	1.130	
$^{79}Br^{81}Br$	$X\,^1\Sigma_g^+$	323.2	0.08091	0.000275	1.07	0.780	0.591	0.925	
	$B\,^3\Pi_{0u}^+$	169.71	0.0595	0.000625	1.913	2.1146	0.690	1.113	
C_2	$X\,^3\Pi_u$	1641.35	1.6326	0.01683	11.67	11.392	0.547	1.051	
	$A\,^3\Pi_J$	1788.22	1.7527	0.01608	16.44	10.744	0.529	0.851	
	$B\,^3\Pi_g$	1106.56	1.1922	0.0242	39.26	19.570	0.638	0.748	
	$a\,^1\Sigma_g^+$	1855.63	1.8205	0.01832	14.08	12.528	0.545	1.001	
	$b\,^1\Pi_u$	1608.33	1.6170	0.01720	12.14	11.584	0.550	1.039	
	$d\,^1\Sigma_u^+$	1829.57	1.8334	0.0204	13.97	13.995	0.559	1.066	
CO	$X\,^1\Sigma^+$	2169.829	1.9312	0.0175	13.295	13.197	0.542	1.061	9
	$A\,^1\Pi$	1515.61	1.6116	0.02229	17.2505	15.27	0.585	1.000	
	$a'\,^3\Sigma^+$	1230.65	1.345	0.0187	11.013	12.37	0.558	1.096	
	$a\,^3\Pi^+$	1739.25	1.6810	0.0193	14.47	14.05	0.570	1.049	
CO^+	$X\,^2\Sigma^+$	2214.24	1.9772	0.01896	15.164	14.44	0.552	1.065	10
	$A\,^2\Pi_i$	1562.06	1.5894	0.0194	13.532	13.48	0.571	1.063	
	$B\,^2\Sigma^+$	1734.18	1.7999	0.0302	27.927	23.44	0.6165	0.9733	
CP	$X\,^2\Sigma^+$	1239.67	0.7986	0.0059	6.86	6.36	0.566	1.03	
	$A\,^2\Pi_i$	1061.99	0.698	0.0077	6.035	9.59	0.622	1.354	
	$B\,^2\Sigma^+$	836.32	0.6829	0.0062	5.917	5.31	0.561	1.006	
CS	$X\,^1\Sigma^+$	1285.1	0.820044	0.005922	6.46	6.42	0.562	1.062	11
I_2	$X\,^1\Sigma_g^+$	214.52	0.03734	0.0001208	0.6127	0.600	0.636	1.054	12
ICl	$X\,^1\Sigma^+$	384.293	0.114154	0.000534	1.465	1.433	0.613	1.053	
	$A\,^3\Pi_i$	209.75	0.08389	0.0003828	1.947	0.664	0.503	0.612	
	$B\,^3\Pi_0^+$	(242)	0.090	0.0029	13	21.6	0.758	1.374	
IO	$X\,^2\Pi_{\frac{3}{2}}$	681.47	0.34026	0.002696	4.29	4.30	0.614	1.066	13
	$A\,^2\Pi_{\frac{1}{2}}$	514.57	0.27635	0.00273	5.52	4.37	0.634	0.945	
K_2	$X\,^1\Sigma_g^+$	92.64	0.05622	0.000219	0.354	0.224	0.459	0.832	
	$B\,^1\Pi_u$	75.00	0.04824	0.000235	0.3876	0.231	0.491	0.807	
Li_2	$X\,^1\Sigma_g^+$	351.435	0.67272	0.00704	2.592	2.287	0.425	0.994	
	$A\,^1\Sigma_u^+$	255.456	0.49749	0.00541	1.574	1.726	0.429	1.366	
	$B\,^1\Pi_u$	269.69	0.55723	0.00804	2.744	2.429	0.479	0.997	
N_2	$X\,^1\Sigma_g^+$	2358.07	1.99874	0.01709	14.188	13.46	0.542	1.036	14,15
	$a\,^1\Pi_g$	1693.70	1.6181	0.0183	13.825	13.46	0.569	1.050	14
	$B\,^3\Pi_g$	1735.42	1.6375	0.01794	15.198	13.71	0.570	1.035	
	$c\,^3\Pi_u$	2047.09	1.8247	0.01868	28.446	15.52	0.572	1.0131	
N_2^+	$X\,^2\Sigma_g^+$	2207.2	1.926	0.01743	16.14	13.45	0.547	0.97	17
NO	$X\,^2\Pi_{\frac{1}{2}}$	1904.03	1.7046	0.0178	13.97	13.91	0.567	1.062	18
	$A\,^2\Sigma^+$	2374.8	1.9972	0.01928	16.46	15.94	0.564	1.047	19
	$B\,^2\Delta$	1216.6	1.330	0.019	15.88	12.68	0.585	0.948	
	$B\,^2\Pi_{\frac{3}{2}}$	1036.96	1.076	0.0116	7.603	7.53	0.547	1.059	
	$E\,^2\Sigma^+$	2373.6	1.9863	0.0182	15.8(5)	14.89	0.556	1.030	
O_2	$X\,^3\Sigma_g^-$	1580.36	1.44566	0.01579	12.0730	12.17	0.570	1.070	
	$b^1\Sigma_g^+$	1432.687	1.400416	0.01817	13.9501	13.67	0.587	1.053	
	$a\,^1\Delta_g$	1509.3	1.4264	0.0171	12.(9)	13.05	0.581	1.071	

TABLE IV.—*Continued.*

Molecule	State	ω_e	B_e	α_e	$x_e\omega_e$ obs	$x_e\omega_e$ calc	a	b	Ref.
O_2^+	$X\ ^2\Pi_g$	1876.4	1.6722	0.01984	16.53	16.37	0.588	1.060	
	$a\ ^4\Pi_u$	1035.69	1.10466	0.01575	10.39	10.88	0.589	1.084	
	$A\ ^2\Pi_u$	900	1.0617	0.01906	13.4	12.61	0.608	1.032	
	$b\ ^4\Sigma_g^-$	1196.77	1.28729	0.02206	17.09	16.36	0.615	1.041	
P_2	$X\ ^1\Sigma_g^+$	780.89	0.30359	0.001477	2.820	2.73	0.579	1.046	23
	$A\ ^1\Sigma_u^+$	475.24	0.24166	0.00165	2.633	2.40	0.589	1.014	
S_2	$X\ ^3\Sigma_g^-$	725.68	0.2956	0.00160	2.852	2.888	0.588	1.107	
	$B\ ^3\Sigma_u^-$	434.0	0.2219	0.0018	2.75	2.112	0.614	1.076	
SO	$X\ ^3\Sigma^-$	1123.7	0.70894	0.005622	6.116	6.40	0.579	1.091	
Si_2	$X\ ^3\Sigma_g^-$	506.72	0.2376	0.00135	1.97	2.04	0.573	1.085	24
	$D\ ^3\Pi_g$	547.94	0.2596	0.00155	2.43	2.35	0.580	1.047	
	$H\ ^3\Sigma_u^-$	271.32	0.1699	0.00135	1.99	1.56	0.581	0.937	
SiN	$X\ ^2\Sigma^+$	1151.68	0.7310	0.00567	6.561	6.35	0.574	1.047	
	$B\ ^2\Sigma^+$	1031.01	0.7235	0.01037	16.743	13.48	0.647	0.954	
SiO	$X\ ^1\Sigma^+$	1241.44	0.72729	0.00508	5.92	6.11	0.566	1.051	
	$A\ ^1\Pi$	852.71	0.63128	0.00695	6.44	7.25	0.596	1.113	

energies, the dissociation products of the excited states can then be deduced. Equation (18) assumes that the potential maxima are negligible. This is not generally true, but is a reasonable first approximation and appears to work very well except for certain hydrides. Where the maximum is not negligible, the effect will be to make Δ A.E.E. too large. The dissociation products have been deduced for the various excited states and are given in column 9 of Tables I–III. In general no ambiguity in the products is possible as a result of the selection rules and widely separated energy states. When $D_e(X)$ is uncertain and the dissociation products are known unambiguously, the calculated D_e^* can be used to deduce $D_e(X)$. Since the dissociation energies of many diatomic molecules are controversial or uncertain, it is important to look critically at this technique. Usually, T_e and Δ A.E.E. will be accurately known. Consequently the uncertainty in $D_e(X)$ will be equal to the uncertainty in D_e^* and in the potential maximum. This means that the uncertainty will be least when D_e^* is smallest. The effect of the potential maximum will be to overestimate $D_e(X)$. This technique will be applied to several cases of considerable interest.

It should be noted that a and b have nearly the same values respectively for all excited states of all molecules, which in turn are the same as those found valid for the ground states of diatomic molecules. The assigned values of a and of b enable one to calculate potential curves using the five-parameter functions and experimental values for k_e, r_e and D_e. If values of D_e are not available predicted values may be obtained from experimental values of $x_e\omega_e$ using Eq. (4a). This method of computing potential curves will be enlarged upon below.

SOME ADDITIONAL RELATIONS

A comparison of $D_e(S)$, dissociation energy calculated from the simple function, with $D_e(C)$, dissociation energy calculated from the five-parameter function as tabulated in Table I shows that these two different internuclear potential functions give essentially the same results for D_e values where reliable data is available. This implies that an additional independent relation between the spectroscopic constants can be obtained by comparing the relations valid for the two functions.

By assuming that

$$D_e(S)=D_e(C),$$

and comparing Eq. (5b) with (16b) one obtains

$$\Delta=[1+(\tfrac{5}{4})F]^2/b^2$$

or

$$D_e=(\tfrac{1}{2})kr_e^2b^2/[1+(\tfrac{5}{4})F]^2 \qquad (18)$$

and by resubstituting Eq. (5b)

$$G/3=1+2[1+(\tfrac{5}{4})F]^2/b^2, \qquad (19)$$

if one uses Eq. (14) with Eq. (16b) and eliminates $nr_e/2=\Delta$, one obtains

$$F=a[1+(\tfrac{5}{4})F]. \qquad (20)$$

Equation (19) can be used to calculate values of $x_e\omega_e$ from experimental values of α_e, ω_e, r_e and b. The known value of b is 1.065 within 3%. A number of these

TABLE V. Calculated values for $x_e\omega_e$ and potential function parameters a and b.

Molecule	State	ω_e	B_e	α_e	$x_e\omega_e$ obs	$x_e\omega_e$ calc	a	b	Ref.
AlH	$X\,^1\Sigma^+$	1682.57	6.3962	0.188	29.145	31.23	0.5192	1.106	
	$C\,^1\Sigma^+$	1575.3	6.664	0.544	125.5	113.56	0.6406	1.012	
AuH	$X\,^1\Sigma^+$	2305.01	7.2401	0.2136	43.12	44.57	0.530	1.084	
	$A\,^1\Sigma^+$	1669.55	6.0069	0.249	55.06	48.18	0.565	0.993	
Au^2H	$X\,^1\Sigma^+$	1634.98	3.6415	0.07614	21.655	22.40	0.529	1.084	
	$A\,^1\Sigma^+$	1195.24	3.036	0.103	34.813	29.86	0.588	0.983	
	$B\,^1\Sigma^+$	1165.4	2.961	0.079	21.85	21.01	0.549	1.043	
BaH	$X\,^2\Sigma^+$	1172	3.3823	0.0655	16	14.13	0.466	0.996	
	$B\,^2\Sigma$	1088	3.267	0.070	15	14.58	0.479	1.049	
	$E\,^2\Pi$	1231	3.486	0.074	17.5	16.43	0.489	1.030	
BeH	$X\,^2\Sigma^+$	2058.6	10.308	0.300	35.5	37.18	0.438	1.093	
	$A\,^2\Pi$	2087.7	10.470	0.329	39.8	40.72	0.454	1.078	
CH	$X\,^2\Pi$	2861.6	14.457	0.534	64.3	66.281	0.484	1.1319	
	$A\,^2\Delta$	2921.0	14.912	0.670	90.4	68.849	0.520	1.029	
	$B\,^2\Sigma^-$	2542.5	12.887	0.485	373.8	70.843	0.487	0.412	
	$C\,^2\Sigma^+$	2824.1	14.629	0.744	105.8	95.199	0.536	1.007	
CsH	$X\,^1\Sigma^+$	890.7	2.709	0.057	12.6	11.69	0.473	1.022	
	$A\,^1\Sigma^+$	204.0	1.126	−0.0185	−5.7	0.53			
HCl	$X\,^1\Sigma^+$	2989.74	10.5943	0.3042	52.05	55.78	0.502	1.052	
$H^{79}Br$	$X\,^1\Sigma^+$	2649.22	8.4671	0.23226	44.077	46.70	0.514	1.085	34
HF	$X\,^1\Sigma^+$	4137.25	20.9456	0.7888	88.726	97.89	0.487	1.124	
LiH	$X\,^1\Sigma^+$	1405.65	7.5131	0.2132	23.200	24.852	0.424	1.1072	
	$B\,^1\Pi$	215.5	3.383	0.986	42.4	54.29	0.636	1.209	35
Li^2H	$X\,^1\Sigma^+$	1055.12	4.2338	0.09198	13.228	14.26	0.424	1.1908	
	$B\,^1\Pi$	177.28	1.908	0.427	29.13	36.59	0.650	1.196	35
MnH	$X\,^7\Sigma$	1548.0	5.6841	0.1570	28.8	22.44	0.490	1.026	36
Mn^2H	$X\,^7\Sigma$	1102.5	2.8956	0.0514	13.9	12.19	0.470	0.991	36
OH	$X\,^2\Pi_i$	3735.21	18.871	0.7138	82.81	88.838	0.487	1.1071	
	$A\,^2\Sigma^+$	3180.56	17.358	0.7868	94.93	92.071	0.522	1.0649	

calculations are reported in Tables IV and V. The calculated values agree well with the experimental $x_e\omega_e$ values, the average percent error being approximately 5% for nonhydrides and 10% for hydrides in general. A particularly likeable feature of the $x_e\omega_e$ calculated from (19) is that the agreement with the observed is better than 1% for the ground states of CS, O_2, O_2^+, CO, IO, and NO for which the data is accurate and well established. This promotes confidence in the validity of the relationship. These results in general are slightly better than one obtains using the Pekeris relation[41] (Morse function), particularly for hydrogen containing molecules.

It is interesting that the relation derived from the Morse function giving α_e as a function of $x_e\omega_e$ works so well, while the relation giving D_e as a function of $x_e\omega_e$ ($D_e=\omega_e^2/4x_e\omega_e$) is so poor, as is the relation giving D_e as a function of α_e. This is well illustrated by Varshni[2] in plots of the experimental quantities G vs Δ and F vs Δ for a number of molecules followed by a comparison with curves expected from various potential functions. The curves for a Morse function deviate greatly from the experimental points, but in such a way that a plot of the G versus F would agree well with the experimental relationship. This illustrates the point that a potential function which relates some spectroscopic quantities well may relate others rather poorly.

Equation (18) can be used to calculate values of D_e from experimental values of ω_e, r_e, and α_e. This would be particularly useful when one has no experimental data from which to obtain $x_e\omega_e$ but does have microwave data giving α_e. Our calculations indicate that Eq. (18) works well on most molecules. However,

[41] C. L. Pekeris, Phys. Rev. **45**, 98 (1934).

TABLE VI. Calculation of D_e and $x_e\omega_e$ from α_e.

Molecule	State	ω_e cm^{-1}	B_e cm^{-1}	α_e cm^{-1}	$x_e\omega_e$ calc cm^{-1}	D_e calc ev	D_e obs ev	Ref.
BrCl	$X\,^1\Sigma^+$	~430	0.152469	0.000745	1.658	2.68	2.31	37
BrF	$X\,^1\Sigma^+$	671	0.357143	0.005214	10.8	0.98	2.19 or 2.60	38
NH	$X\,^3\Sigma^-$	~3125	16.688	0.646	75.8	3.26	~3.8	39
	$A\,^3\Pi_i$	~3034	16.709	0.744	85.9	2.69	~1.4	

the value of D_e calculated for FBr does not agree with the experimental value, although the value of α_e is reported to four significant figures. We have no explanation for this, It is perhaps significant that a evaluated using Eq. (19) is much larger than expected. Dissociation energies and anharmonicities have been evaluated for the ground states of NH and BrCl (Table VI). No anharmonicity values have been determined experimentally for these molecules. The dissociation energies are in accord with those quoted by Cottrell.[40]

Equation (20) can be used to calculate the parameter a. Since values for $\alpha_e\omega_e/6B_e^2 = F$ vary from about 1 to 2.5, a cannot be constant. However it is seen from the calculated values of a given in Table IV, V, and VII that, except for elements in the first row of the periodic table, a has a value near 0.56. These values of a may be compared favorably with the values reported in I, calculated from Eq. (16) and experimental values for α_e, $x_e\omega_e$, D_e and r_e. A more detailed analysis of a shows that it is periodic within the periodic table. This will be discussed in a future publication.[42] The parameter b may be conveniently evaluated from (19). For non-hydrides b is a good constant with a value of 1.065. The deviations from this value are rarely greater than 5% and it is tempting to conclude that where the calculated value deviates considerably from this value the data (in the majority of cases, probably α_e) is in error. The major discrepancies are for the $A\,^3\Pi_g$ and $B\,^3\Pi_g$ states of C_2, $A\,^3\Pi_i$, and $B\,^3\Pi_0^+$ states of ICl and the $X\,^1\Sigma_g^+$ and $B\,^1\Pi_u$ states of K_2. There appears to be no reason why these states should be different from the others for which such calculations have been carried out. The average value for b for the various electronic states of the isotopes of hydrogen is 1.158 with a mean deviation of 0.045. Since b was taken as 1.065 in evaluating $x_e\omega_e$ from Eq. (19) this explains why the calculated anharmonicities for hydrogen are high in general. The anharmonicities have been recalculated for $b = 1.158$ and are reported in column 10 of Table VII.

DISCUSSION

The results in Tables I to VII show that the proposed internuclear potential functions, Eqs. (3) and (7), can be used to correlate and predict spectroscopic quantities for excited states of diatomic molecules as well as for the ground states. Where reliable data are available calculated $D_e(s)$ and $D_e(c)$ values agree rather well. Since small changes in α_e values produce large changes in calculated $D_e(c)$ values, the simple function appears to be more reliable for calculating dissociation energies. This is illustrated by some recent data on the ground state of N_2. Lofthus's[14] data lowers $x_e\omega_e$ from that given by Herzberg[8] by 1.7%, changing $D_e(s)$ from 9.45 to 9.62 ev, whereas α_e changed by about −9% (from 0.0187 to 0.01171) changing $D_e(c)$ from 10.21 to 8.91 ev. The coincidence of $D_e(s)$ and $D_e(c)$ is further illustrated for ground states and excited states by calculations using recent data for CS,[11] CO,[9] O_2, O_2^+, IO,[13] $^{14}N^{16}O$,[18] $^{15}N^{16}O$,[18] which all give D_e agreeing within 2%. Improved data usually gives better correlations or predictions for the functions, and the values for $D_e(s)$ and $D_e(c)$ usually converge. Examples are $P_2(X\,^1\Sigma_g^+)$,[23] $NO(X\,^2\Sigma^+)$,[18] $H_2(^1\Sigma_g^+)$,[31] $N_2(a\,^1\Pi_g)$,[14] $CO(X\,^1\Sigma^+)$[9] and $AlO(X\,^2\Sigma^+)$.

However the $B\,^1\Sigma_u^+$ states of $^1H_2$, $^1H^2H$ and $^2H_2$ give very poor agreement between $x_e\omega_e$ calculated and observed.[8,32] This may be due to the highly ionic character for this state or to an incorrect analysis. It is noted that the relationships hold reasonably well for HF, HCl, HBr, and HI.

The calculated Δ A.E.E. for the $^3\Pi_{0u}^+$ state of Br_2 and I_2 are consistent only with the dissociation products being ^2P ground-state atoms, but with one of the atoms excited to a J value of one-half. This is in agreement with experimental findings and shows the sensitivity of the technique in favorable circumstances.

For many of the hydrides, especially for excited states, the calculated dissociation energies are much higher than is consistent with the known or preferred dissociation products. This suggests that the potential maxima for these cases are large.

One attractive feature of the five-parameter function is the remarkable constancy of b and to a lesser extent of a for all states of all molecules. Values of b and a are even more constant for the range of states of a given molecule. For hydrogen-containing molecules the values for a are usually lower than average. Pliva has shown that values of b and a are transferable to bonds of polyatomic molecules with some excellent results for spectroscopic constants of simple polyatomic molecules.[6]

It is interesting that the criteria that $D_e(s) = D_e(c)$ gives a relation between $x_e\omega_e$ and α_e which is very

[42] D. Steele and E. R. Lippincott (to be published).

TABLE VII. Calculated values for $x_e\omega_e$ and potential function parameters a and b.

Molecule	State	ω_e	B_e	α_e	$x_e\omega_e$ obs	$x_e\omega_e$ calc	$x_e\omega_e$ calc $b=1.158$	a	b	Ref.
H_2	$X\,^1\Sigma_g^+$	4400.39	60.8407	3.0177	120.815	145.66	126.71	0.344	1.192	31
	$B\,^1\Sigma_u^+$	1356.52	19.982	1.1077	22.857	49.55	43.06	0.352	1.762	32
	$C\,^1\Pi_u$	2442.72	31.340	1.626	(67.0)	82.10	71.25	0.365	1.201	
	$I\,^1\Pi_g$	2265.2	29.79	1.515	78.47	75.40	65.50	0.358	1.040	
	$c\,^3\Pi_u$	2465.0	31.07	1.425	61.4	75.15	65.35	0.345	1.203	
	$a\,^3\Sigma_g^+$	2664.83	34.216	1.671	71.65	85.52	74.31	0.355	1.184	
	$e^3\Sigma_u^+$	2195.8	27.30	1.515	65.80	77.47	67.10	0.385	1.171	
	$d\,^3\Pi_u$	2371.58	30.364	1.545	66.27	78.48	68.13	0.363	1.177	
	$K\,^3\Pi_u$	2336	29.40	1.58	(60)	80.44	69.73	0.376	1.268	
	$n\,^3\Pi_u$	2322	29.93	1.3	62.9	68.56	59.72	0.331	1.122	
$^1H^2H$	$X\,^1\Sigma_g^+$	3811.92	45.638	1.9500	90.711	108.86	94.68	0.347	1.066	31
	$C\,^1\Pi_u$	2139.1	23.64	0.938	66.55	56.63	48.25	0.343	0.730	
	$I\,^1\Pi_g$	1962.1	22.36	1.21	58.21	66.90	57.85	0.397	1.192	
	$a\,^3\Sigma_g^+$	2308.44	25.685	1.099	53.77	64.73	56.23	0.357	1.190	
	$e\,^3\Sigma_u^+$	1905.17	20.766	1.010	51.70	58.92	51.03	0.385	1.149	
	$d\,^3\Pi_u$	2054.59	22.810	1.020	49.74	59.57	51.70	0.364	1.186	
$^2H_2$	$X\,^1\Sigma_g^+$	3118.46	30.442	1.0623	64.10	72.69	63.04	0.347	1.16	31
	$C\,^1\Pi_u$	1735.85	15.665	0.5739	39.06	41.17	35.73	0.366	1.098	
	$E\,^1\Sigma_g^+$	1784.5	16.37	0.682	(48.1)	47.14	40.82	0.388	1.053	
	$I\,^1\Pi_g$	1600.1	14.739	0.526	39.42	37.36	32.45	0.358	1.032	
	$d\,^3\Pi_u$	1678.22	15.200	0.5520	32.94	39.56	33.60	0.391	1.268	
	$a\,^3\Sigma_g^+$	1885.84	17.109	0.606	35.96	34.62	37.88	0.360	1.195	
	$e\,^3\Sigma_u^+$	1556.64	13.856	0.541	34.51	38.76	33.58	0.382	1.140	
$^3H_2$	$X\,^1\Sigma_g^+$	2553.8	20.3243	0.59222	43.872	49.38	42.94	0.347	1.143	
	$a\,^3\Sigma_g^+$	1541.57	11.4374	0.3258	24.47	28.79	25.01	0.352	1.173	
	$d\,^3\Pi_u$	1372.11	10.150	0.3050	22.135	26.68	23.15	0.367	1.190	

similar to the Pekeris relation obtainable from the Morse function, but with slightly better results. In addition it offers a rapid method of calculating b and a, the values of which are essentially the same as calculated without this criteria.

DISSOCIATION ENERGIES OF SOME SPECIFIC MOLECULES

$D_e(C_2)$

The dissociation energy of carbon is uncertain. Cottrell lists it as 6.5 ev, but quotes a more recent examination of the evidence which gives 6.16 ev. Calculations from both the simple and five-parameter functions give a value near 5.6 ev. As explained in the introduction the dissociation energies calculated for the excited states can be used to deduce $D_e(X)$. The $A\,^3\Pi_g$ and $B\,^3\Pi_g$ states cannot both arise from the separate atom configurations 2^3P+2^3P. Assuming that $D_e(X)$ lies in the range 4 to 7 ev shows that the $A\,^3\Pi_g$ arises from the $^3P+^1D$ configuration. $D_e{}^*$ for the $B\,^3\Pi_g$ state is calculated to be only 0.7 ev. Allowing a 50% error in this value, this necessitates that $D_e(X)$ is less than 6.0 ev and, assuming no potential maximum for the upper state, more than 5.4 ev (see Table VIII). This is in excellent agreement with the calculated value of 5.6 ev. The dissociation energies of the $A\,^3\Pi_g$ state as evaluated from the three- and five-parameter functions are in poor agreement. This is in accord with the low value of b calculated from Eq. (19). D_e from the simple function is again in good agreement with the assigned value of $D_e(X)$, thus suggesting that the value of α_e for this state is in error.

The splitting of the singlet and triplet states is uncertain. Hicks[43] deduced that the $^1\Sigma_g^+$ state was 0.39 ev above the $X\,^3\Pi_u$ state. According to a private communication from D. A. Ramsey to E. Clementi and K. S. Pitzer,[44] perturbations in the rotational spectrum of the $^3\Sigma_g^-$ state suggest that the $^1\Sigma_g^+$ state lies 0.07 ev below the $^3\Pi_u$ state. The difference between these values is too small compared with the uncertainty in the $D_e{}^*$ of the singlet states for the present calculations to distinguish between them, though Ramsey's value is favored. As shown in Table VIII $D_e(X)=4.9$ ev is definitely too low and $D_e(X)=6.5$ ev is suggested to be too high, in confirmation of the deductions from the triplet states.

[43] W. T. Hicks, Spectroscopy of High Temperature Systems (thesis) UCRL-3696 (Feb. 1957).

[44] E. Clementi and K. S. Pitzer, J. Chem. Phys. **32**, 656 (1960); E. A. Balik and D. A. Ramsey, *ibid.* **31**, 1128 (1959).

TABLE VIII. Correlation of $D_e(X)$ with dissociation products for C_2.

State	Te ev	D_e ev	$\Delta A \cdot E \cdot E$ calc $D_e(X)$ =6.5	=5.6	=4.9	Dissociation products	$\Delta A \cdot E \cdot E$ ·
$X\ ^3\Pi_u$	0	6.5 Cott. 5.6 calc 4.9 old.	0	0	0	$2\ ^3P+2\ ^3P$	0.0
$A\ ^3\Pi_g$	2.39	4.7 (S) 3.5 (C)	0.6 −0.6	1.5 0.3	2.2 1.0	$2\ ^3P+2\ ^1D$	1.26
$B\ ^3\Pi_g$	4.97	0.7	−0.8	0.1	0.7	$2\ ^3P+2\ ^3P$	0.0
$a\ ^1\Sigma_g^+$	−0.07 0.39	6.0	−0.6 −0.1	0.3 0.8	1.0 1.5	$2\ ^3P+2\ ^3P$ $2\ ^3P+2\ ^3P$	0.0
$b\ ^1\Pi_u$	0.97 1.43	5.2	−0.3 0.1	0.6 1.0	1.3 1.7	$2\ ^3P+2\ ^3P$ $2\ ^3P+2\ ^3P$	0.0
$c\ ^1\Pi_g$	4.18 4.64	5.0	2.7 3.1	3.6 4.0	4.3 4.7	$2\ ^1D+2\ ^1S$ $2\ ^3P+2\ ^5S$	3.93 4.16
$d\ ^1\Sigma_u^+$	5.29 5.73	5.9	4.7 5.1	5.6 6.0	6.3 6.7	? ?	

D_e(CO)

The calculated dissociation energy favors the old value near 9 ev. However, the higher value of 11.1 ev now appears to be well established. The dissociation products of the excited states $A\ ^1\Pi$, $a\ ^3\Pi_r$, $a'\ ^3\Sigma^+$, and $C\ ^3\Sigma^-$ are readily identified using $D_e(X)=11.1$ ev as 2^3P+2^3P. The agreement between the calculated and observed Δ A.E.E. is very good indeed. However the data can also be explained, though much less satisfactorily using the low value of D_e. It would be expected that at least some of the excited states that have been studied arise from the 2^3P atoms, thus it would seem that there is little doubt from this analysis that the high value is correct.

D(S_2)

The spectroscopic data for the dissociation energy of S_2 are consistent with any of the values 4.4, 3.6, or 3.3 ev. The individual values are favored by Gaydon, Herzberg and the N.B.S., respectively. Two thermochemical approaches to $D(S_2)$ have been summarized by Cottrell. The first involving the heat of formation of SO favors 3.6 ev for $D(S_2)$ and 5.15 ev for D(SO) (See below). The second approach involving the heat of formation of S-H leads to a preference for the highest value of $D(S_2)$. However the data on which the latter is based does not appear to be too reliable. The calculated dissociation energies using both the simple and five-parameter functions strongly favor the high value, 4.4 ev. This is confirmed by calculations on the $B\ ^3\Sigma_u^-$ state, the calculated dissociation energy indicating that the dissociation products are 3^1D+3^3P and that the ground state dissociation energy is about 4.5 ev.

D_e(SO)

A value of 5.15 ev is favored over 4.0 ev. Thermochemical data also favors the higher value (see Cottrell). Unfortunately the only data for excited states of this molecule, that for the $B\ ^3\Sigma^-$ state, is uncertain and leads to very poor agreement between $D_e(s)$ and $D_e(c)$.

D(BF)

Gaydon[45] gives $D_e=8.5\pm0.5$ ev whereas Herzberg suggests approximately 4.3 ev. The calculated value of $D_e(s)$ is 3.1 ev and of $D_e(c)=2.4$ ev suggesting strongly that the low value quoted by Herzberg is correct. The dissociation energy of the excited state $A\ ^1\Pi$ can be interpreted in terms of either value. The relative electronic energies of the singlet states are unfortunately unknown.

D_e(MnH)

Calculations on MnH and MnD indicate that the value quoted by Cottrell for D_e of 2.4 ev (very uncertain) is of the right order of magnitude. The calculated value is about 2.1 ev.

LIMITING FORMS OF POTENTIAL FUNCTIONS

A further discussion on the limiting forms of the five parameter function used for Eq. (1) is desirable since other information is available as to the form which an inter-nuclear potential function should assume as $r\rightarrow\infty$ and as $r\rightarrow0$.

[45] A. G. Gaydon, *Dissociation Energies* (Chapman and Hall, Ltd., London), 2nd ed.

For example for the $r \rightarrow 0$ limit

$$V = (Z_a Z_b e^2/r) + E_{ab} + \cdots, \tag{21}$$

where Z_a and Z_b are the atomic numbers of atoms A and B, respectively, and E_{ab} is the energy of the state of the united atom formed.

Again, for $r \rightarrow \infty$ and separated atom states without quadrupole moments (S states) one would expect a limiting form

$$V = A/r^n \tag{22}$$

with $n=6$ and A is negative. On the other hand, for separated atomic states with quadrupoles one would expect $n=5$ and A to be negative or positive.[46]

It would be desirable to incorporate some or all of these conditions in the form of $f(r)$ of Eq. (1) provided that the proper relationships between the spectroscopic quantities r_e, ω_e, D_e, α_e and $x_e\omega_e$ are retained. The relationships between these quantities used here can be retained if the form for $f(r)$, on expansion to the second power in Δr, always has the form

$$f(r) = -(b^2 n r_e/2)^{\frac{1}{2}}(\Delta r/r_e) + (b^2 n r_e/2)(\Delta r/r_e)^2 + \cdots . \tag{23}$$

The correlation between the five spectroscopic parameters is extremely sensitive to the form of $f(r)$ and seemly minor but arbitrary changes in its form up to Δr^2, or to Δr^4 in $V(r)$, cause large deviations among the relations for the spectroscopic quantities with the result that they cannot be used to predict unknown spectroscopic quantities from known quantities.

The form of (23) suggests that one form for $f(r)$ would be a potential composed of two parts, one attractive and the other repulsive with the repulsive term the square of the attractive one. The repulsive term would be important for $r < r_e$ but unimportant for $r \gg r_e$, while the attractive term would be important for $r > r_e$ but not for $r \ll r_e$. Consideration of Eq. (1) and separated atom states without quadrupole moments suggests that one limiting form for $f(r)$ would be a Lennard-Jones 6–12 potential. Accordingly $f(r)$ was initially chosen to satisfy this condition. For molecular states which dissociate to atomic states with quadrupoles one could use a (5–10) potential. Since the A/r^5 term would always be attractive, this suggests that for molecular states where the proposed function gives reliable correlation of spectroscopic quantities A must be negative for separated atom states with quadrupoles even though other considerations show that possibly A could be positive.

On the other hand, one can choose $f(r)$ in other forms and still retain the terms given in (23) to Δr^2. One particularly useful form is

$$f(r) = -(b^2 n/2r)^{\frac{1}{2}} \Delta r \times \exp[-(b^2 n/2r_e)^{\frac{1}{2}} \Delta r]. \tag{24}$$

This particular form has the advantage of showing that a repulsive term in $f(r)$ is not essential. It is also particularly easy to manipulate in calculations involving construction of potential curves and also seems to be more accurate than (7) when one makes a comparison with the experimental curves as constructed by the method of Klein-Rydberg-Rees as modified by Vanderslice *et al.*[47]

Although the conditions on $f(r)$ seems to be highly specific, there is such flexibility left for its choice that one cannot choose between various suggested forms without additional considerations, the most important being an expansion to higher powers of Δr followed by correlation and prediction of additional spectroscopic parameters such as the second anharmonicity, $y_e\omega_e$, and the second-order vibration-rotation coupling constant, γ_e. Calculation of these quantities will be reported at a later date.

In conclusion it would seem that the five spectroscopic quantities, D_e, ω_e, $\omega_e x_e$, r_e, and α_e do not give sufficient information concerning the limiting form of a potential function even though they can be adequately related provided that the function expands in a suitable manner up to the forth power of Δr.

CONSTRUCTION OF POTENTIAL CURVES

When experimental data are available for a sufficiently large number of vibrational levels for a given diatomic molecule state the best method for construction of an internuclear potential curve is to use the Klein-Rydberg-Rees[47] method as modified by Vanderslice *et al.*[48] This method has the advantage that the resulting curve is based only on known experimental data for the vibrational levels and not on any assumed form for the potential function. This method has been applied to a number of diatomic molecules for both ground and excited states and for which the appropriate spectral data has been analyzed in detail.[49]

However, if one wished to construct the potential curve beyond the point for which there is information concerning the vibration levels these methods cannot be used and one must still use an empirical function. For this purpose most three-parameter functions are not sufficiently accurate. The Morse function is seriously off for values of $R > R_e$ in that it predicts too much binding energy. The three-parameter function used here works reasonably well for values of $R > R_e$, particularly for large R but gives too much binding energy for $R < R_e$. In constructing empirical potential curves it would seem desirable to use a five-parameter function. One such function which can be readily used is the Hulbert-Hirschfelder function.[50] This function

[46] J. O. Hirschfelder, C. E. Curtiss, and R. B. Bird, *Molecular Theory of Gases and Liquids* (John Wiley & Sons, Inc., New York, 1954).

[47] A. L. G. Rees, Proc. Phys. Soc. (London) **59**, 998 (1947).

[48] J. T. Vanderslice, E. A. Mason, W. G. Maisch, and E. R. Lippincott, J. Mol. Spectroscopy **3**, 17 (1959).

[49] J. T. Vanderslice, E. A. Mason, and E. R. Lippincott, J. Chem. Phys. **30**, 129 (1959); J. T. Vanderslice, E. A. Mason, and W. G. Maisch, *ibid.* **31**, 738 (1959); **32**, 515 (1960).

[50] H. M. Hulbert and J. O. Hirschfelder, J. Chem. Phys. **9**, 61 (1941).

has the convenience that its five parameters can readily be obtained from the five spectroscopic constants D_e, R_e, $x_e\omega_e$ and α_e.

The five-parameter function, Eq. (7a), or the alternative proposed form, Eq. (7b) resulting from the substitution of Eq. (24) into Eq. (1), can be used equally well to construct potential curves from the appropriate spectroscopic constants. The latter form is superior to Eq. (7a) and yields potential curves agreeing well with experimental curves[48,49] over the complete range of r. The proposed function has the additional advantage that the constants b and a are reasonably transferable from molecule to molecule, and thus curves can be constructed from experimental values of k_e, r_e and D_e without other data. An additional advantage is that if an experimental D_e is not available from other information a reasonably accurate one may be computed from k_e, r_e and either $x_e\omega_e$, or α_e and used in the construction of the potential curve.

ACKNOWLEDGMENTS

The authors gratefully acknowledge financial support from the Office of Ordnance Research, U.S. Army, and assistance in the calculations by J. N. Finch.

Internal Rotation of *Cis* 2,3-Epoxybutane from the Microwave Spectrum* †

MARTIN L. SAGE‡

Mallinckrodt Chemical Laboratory, Harvard University, Cambridge 38, Massachusetts

(Received December 1, 1960)

The microwave spectrum of *cis* 2,3-epoxybutane was investigated in the region from 8000 to 29 000 Mc. The spectrum consists of singlets and triplets. The ground torsional state shows a pseudo rigid-rotor spectrum with rotational constants 8057.71, 4461.36, and 3468.60 Mc. The triplets yield a barrier to internal rotation of 1607±150 cal/mole independent of a range of assumptions concerning the coupling of the two methyl groups. The dipole moment was found to be 2.03±0.02*D* with 2.01±0.02*D* in the plane of the ring. A group theoretical discussion of double rotors with one rotor on each side of a plane of symmetry is given.

INTRODUCTION

IT is of interest to study the internal rotation in molecules containing several internal rotors to discover the effect of one rotor on the other. Acetone,[1] dimethyl ether,[2] and dimethyl silane[3] have previously been studied by the microwave frequency method. Since these molecules do not have geometrical isomers or chemically similar one-top molecules, one cannot readily obtain information concerning the interaction of the two tops. A molecule that would yield more information is 2-butene. It exists in two isomers, the *cis* and the *trans*, and is similar in structure to propene, a single rotor. Previous thermodynamic studies[4] have shown the barrier to internal rotation in *trans* 2-butene and propene to be 1950 cal/mole, while in *cis* 2-butene the barrier is only 450 cal/mole. This data is in agreement with a more recent microwave frequency determination of the barrier in propene as 1980 cal/mole.[5] The difference between the *cis* and *trans* isomers has been ascribed to steric interaction.[4]

Unfortunately, because of the small dipole moment of *cis* 2-butene, it is difficult to determine its microwave spectrum. However, the 2,3-epoxybutanes have strong microwave spectra and should show similar steric effects. Also, their one-top analog, epoxypropane, has been studied extensively.[6]

EXPERIMENTAL

Cis 2,3-epoxybutane (see Fig. 1) was prepared from Olin-Mathieson 99% *cis* 2-butene by reaction with *N*-bromoacetamide in aqueous acetic acid to form *threo* 3-bromo-2-butanol which yields the *cis* 2,3-epoxybutane by treatment with aqueous potassium hydroxide.[7] These reactions are stereospecific and the product is greater than 95% *cis*.

The spectrometer used was a 100-kc square-wave Stark modulated Hughes-Wilson type. Oscilloscope and recorder display were used with a phase-sensitive detection system.

TABLE I. Transition frequencies.

Transition	Observed frequency (Mc)[a]	Calculated frequency[b]
b type		
$0_{0,0}$–$1_{1,1}$	11 526.30	11 526.31
$1_{0,1}$–$2_{1,2}$	18 463.52	18 463.52
$2_{1,2}$–$3_{0,3}$	20 327.53	20 328.23
$4_{0,4}$–$4_{1,3}$	10 887.01	10 886.89
$2_{1,1}$–$2_{2,0}$	10 967.72	10 967.71
$3_{1,2}$–$3_{2,1}$	10 281.98	10 281.63
$4_{1,3}$–$4_{2,2}$	10 099.17	10 098.74
$5_{1,4}$–$5_{2,3}$	10 771.40	10 771.06
$4_{2,3}$–$4_{3,2}$	21 011.14	21 011.01
$7_{2,6}$–$7_{3,5}$	24 993.89	24 993.61
$8_{3,5}$–$8_{4,4}$	23 798.49	23 795.48
$10_{3,7}$–$10_{4,6}$	20 556.93	20 552.93
$11_{3,8}$–$11_{4,7}$	20 201.05	20 199.07
c type		
$1_{0,1}$–$2_{1,1}$	21 441.30	21 441.79
$1_{1,1}$–$2_{2,1}$	28 634.49	28 634.49
$3_{1,2}$–$3_{2,2}$	9 423.92	9 423.57
$7_{2,5}$–$7_{3,5}$	11 973.07	11 970.60
$8_{2,6}$–$8_{3,6}$	9 168.84	9 165.35

[a] Estimated uncertainty, ±0.2 Mc.
[b] A=8057.71 Mc, B=4461.36 Mc, C=3468.60 Mc.

* Submitted in partial fulfillment of the requirements for the degree of Doctor of Philosophy in Chemical Physics, February, 1960.

† This research was supported in part by a grant extended to Harvard University by the Office of Naval Research.

‡ Edwin W. Rice, Jr. Fellow. Present Address: Department of Physics, Brandeis University, Waltham, Massachusetts.

[1] J. D. Swalen and C. C. Costain, J. Chem. Phys. **31,** 1562 (1959).

[2] P. H. Kasai and R. J. Myers, J. Chem. Phys. **30,** 1096 (1959).

[3] Louis Pierce, J. Chem. Phys. **31,** 547 (1959).

[4] W. G. Dauben and K. S. Pitzer in *Steric Effects in Organic Chemistry*, edited by M. S. Newman (John Wiley & Sons, Inc., New York, 1956), p. 57.

[5] D. R. Lide, Jr., and D. E. Mann, J. Chem. Phys. **27,** 868 (1957).

[6] J. D. Swalen and D. R. Herschbach, J. Chem. Phys. **27,** 100 (1957); **29,** 761 (1958).

[7] S. Winstein and H. J. Lucas, J. Am. Chem. Soc. **61,** 1576 (1939).

Some frequency measurements were made with multiples of a 5-Mc standard which was monitored by a 100-kc signal from the Cruft Laboratory of Harvard University. This signal is continuously compared with several primary standards including station WWV. Other measurements were made with a Gertsch FM4 oscillator locked to a Gertsch FM6. These two systems for measuring frequency agreed to better than one part in 10^7.

Both *b*- and *c*-type rotational transitions were observed between 8000 and 29 000 Mc. The observed frequencies for those lines with unresolved splittings are listed in Table I together with the calculated frequencies for $A=8057.71$ Mc, $B=4461.36$ Mc, and $C=3468.60$ Mc. The energy levels for the rigid rotor were calculated on the Univac computer at Harvard University using a program written by R. Schwendeman and V. W. Laurie.[8]

TABLE II. Structural parameters.[a]

Assumed		Calculated
C—C(ring)	1.471[b]	∠CCC 124°30′±2°
C—O	1.436[b]	∠CC ⊥[c] 37°4′±2°
C—H(ring)	1.082[b]	
∠CCH	119°17′[b]	
∠CH ⊥[c]	31°52′[b]	
C—C	1.513[d]±0.020 A	
∠HCH	109°28′[e]	
C—H	1.09[e] *A*	
∠H_3CC[f]	0°00′[e]	

	Observed	Calculated
I_a	62.739 amu A²	62.739
I_b	113.313	113.455
I_c	145.745	145.603
I_α[g]		3.194

Angles between the principal axes (a, b, c) and the molecular axes (X, Y, Z)[h]

aX	0 00′	bX	90 00	cX	90 00
aY	90 00	bY	40 29	cY	130 29
aZ	90 00	bZ	49 31	cZ	40 29

Direction cosines of the methyl group axes and principal and molecular axes

	Top 1	Top 2
a	−0.56633	0.56633
b	0.74095	0.74095
c	−0.36093	−0.36093
X	−0.56633	0.56633
Y	0.79790	0.79790
Z	0.20647	0.20647

[a] The conversion factor $h/8\pi^2=5.05531\times10^5$ amu A² Mc was used.
[b] Parameter assumed from epoxyethane.
[c] Acute angle between the bond mentioned and a perpendicular to the ring.
[d] Parameter assumed from epoxypropane.
[e] Methyl-group structure assumed. Methyl-group axis assumed along C—C bond.
[f] Angle between the methyl-group axis and C—C bond.
[g] Moment of inertia of methyl group about its axis.
[h] The X axis is along the C—C bond of the ring, the Y axis is perpendicular to the ring, and the Z axis is the perpendicular bisector of the ring C—C bond in the plane of the ring. The carbon of top 1 has negative X, of top 2 positive X. Both methyl carbons have positive Y and Z. This is shown in Fig. 1.

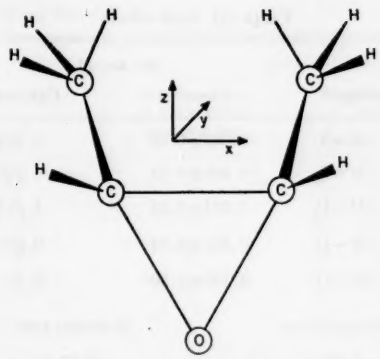

FIG. 1. *Cis* 2,3-epoxybutane.

STRUCTURE

Some structural information may be derived from the observed rotational constants, although 17 parameters are necessary for a complete structural determination. The microwave spectra of epoxyethane and its deuterated species have been measured and its structure determined by Cunningham and co-workers.[9] Using their values of all parameters and fitting a tetrahedral methyl group with C—H distance 1.09 A, Swalen and Herschbach[6] partially determined the structure of epoxyethane. They adjusted the ring-carbon to methyl-carbon distance and the two angles necessary to specify the orientation of this bond. One would expect these angles to change more than any other structural parameters in going to *cis* 2,3-epoxybutane due to the proximity of the two methyl groups. Therefore, it is reasonable to assume all the other structural parameters to be those used by Swalen and Herschbach, and to fit the two angles to the observed rotational constants. The assumed and calculated parameters are listed in Table II. These assumptions will be poorest for the methyl hydrogens since one would expect steric interference to bend the two methyl groups away from each other, and the methyl group axis away from the ring-carbon methyl-carbon bond. However, a small error in the

[8] V. W. Laurie, thesis, Harvard University, 1957, Chap. V.
[9] G. L. Cunningham, Jr., A. W. Boyd, R. J. Myers, W. D. Gwinn, and W. I. Levan, J. Chem. Phys. **17**, 211 (1949); **19**, 576 (1951).

TABLE III. Stark effect.

Transition	$\Delta\nu/\Delta\nu_{OCS}$[a] Observed	Calculated
$0_{0,0}$–$1_{1,1}$ ($M=0$)	6.349±0.06	6.338
$2_{1,1}$–$2_{2,0}$ ($M=2$)	−1.246±0.03	−1.276
$3_{1,2}$–$3_{2,2}$ ($M=3$)	1.894±0.02	1.915
$3_{1,2}$–$3_{2,2}$ ($M=2$)	0.842±0.01	0.850
$3_{1,2}$–$3_{2,2}$ ($M=1$)	0.205±0.005	0.211

Principal axes	Molecular axes
$\mu_a=0.00\ D$	$\mu_X=0.00\ D$
$\mu_b=1.55\pm0.015$	$\mu_Y=0.32\pm0.02$
$\mu_c=1.32\pm0.015$	$\mu_Z=2.01\pm0.02$

$\mu=2.03\pm0.02\ D$

[a] OCS 0–1 transition.

hydrogen position will affect the rotational constants relatively little. In determining the barrier, the direction cosines of the two tops with respect to the principal axes were calculated from the geometry of the molecule. They are listed in Table II.

DIPOLE MOMENT

The Stark effect was measured for those transitions listed in Table III. The apparatus was calibrated with OCS before and after the measurements. Agreement between calibrations was better than 2%. The dipole moment was found to be $2.03\pm0.02D$ and to lie primarily in the plane of the ring. The components with respect to the principal axes and the molecular axes are given in Table III. The dipole moment is in agreement with the expected moment as the dipole of epoxyethane and epoxypropane are 1.88 D[9] and 2.00 D[6], respectively.

TABLE IV. Character tables.

C_3	E	C_3	C_3^2
A	1	1	1
E_0	1	ϵ[a]	ϵ^*
	1	ϵ^*	ϵ

C_{3v}	E	$2C_3$	$3C_2$
A_1	1	1	1
A_2	1	1	−1
E	2	−1	0

[a] $\epsilon=\exp(2\pi i/3)$.

INTERNAL ROTATION. GENERAL THEORY

The kinetic energy for *cis* 2,3-epoxybutane is[10]

$$T/h=AP_a^2+BP_b^2+CP_c^2+F(p_1^2+p_2^2)+2(F+F^*)\mathcal{P}_+^2+2(F-F^*)\mathcal{P}_-^2-2(F+F^*)(p_1+p_2)\mathcal{P}_+-2(F-F^*)(p_1-p_2)\mathcal{P}_-+2F^*p_1p_2, \quad (1)$$

where

$$A=h/8\pi^2I_a, \qquad B=h/8\pi^2I_b, \qquad C=h/8\pi^2I_c,$$

and the I's are the ordinary principal moments of inertia of the whole molecule. Also

$$\mathcal{P}_+=\lambda_b(I_a/I_b)P_b+\lambda_c(I_a/I_c)P_c$$

$$\mathcal{P}_-=\lambda_a(I_a/I_a)P_a$$

$$F=F_{11}=F_{22}; \qquad F^*=F_{12}=F_{21}$$

$$(F^{-1})_{11}=(F^{-1})_{22}=(8\pi^2I_a/h)\left[1-\sum_g\lambda_g^2(I_a/I_g)\right]$$

$$(F^{-1})_{12}=(F^{-1})_{21}=(8\pi^2I_a^2/h)\left[(\lambda_a^2/I_a)-(\lambda_b^2/I_b)-(\lambda_c^2/I_c)\right],$$

TABLE V. Correlation table.

Representations in S	Representation in S'
AA_1	AA
AA_2	AA
AE	AE_0
E_0A_1	E_0A
E_0A_2	E_0A
E_0E	E_1+E_2

with λ_a, λ_b, and λ_c the direction cosines of top 1 with respect to the axes (a, b, c) listed in Table II.

If one ignores six- and higher-fold contributions, the potential can be written

$$V=(V_3^*/2)(2-\cos3\alpha_1-\cos3\alpha_2)+(V_+/2)\left[1-\cos3(\alpha_1+\alpha_2)\right]+(V_-/2)\left[1-\cos3(\alpha_1-\alpha_2)\right]. \quad (2)$$

The group theoretical treatment of this molecule is analogous to that of the more symmetrical acetone-type molecule. This latter class has been treated by Myers and Wilson.[11] The symmetry group under which the Hamiltonian is invariant is generated by the three operations:

$C_3(1)$ which takes $\alpha_1\rightarrow\alpha_1+(2\pi/3)$ and leaves the other variables unchanged, $C_3(2)$ which takes $\alpha_2\rightarrow\alpha_2+(2\pi/3)$ and leaves the other variables unchanged,

[10] B. L. Crawford, Jr., J. Chem. Phys. **8**, 273 (1940).
[11] R. Myers and E. Bright Wilson, Jr., J. Chem. Phys. **33**, 186 (1960).

TABLE VI. Spin weights of torsional states.

Representation	Species of individual top levels	$n=n'$ No. times rep. is contained in torsional fns.	$n=n'$ Weight of each for *H*	*D*	$n\neq n'$ No. times rep. is contained in torsional fns.	$n\neq n'$ Weight of each for *H*	*D*
AA_1	AA	1	16	121	1	16	121
AA_2	AA	0	0	0	1	16	121
AE	EE	1	8	128	2	8	128
E_0A_1	EE	1	8	128	1	8	128
E_0A_2	EE	0	0	0	1	8	128
E_0E	AE	1	32	352	2	32	352

and C_{2x} which takes $\alpha_1\rightarrow-\alpha_2$, $\alpha_2\rightarrow-\alpha_1$, and rotates the molecule about the x axis through an angle π.

If, instead of the variables θ, ϕ, χ, the Eulerian angles, and α_1 and α_2, one uses the variables θ, ϕ, χ, $\alpha_1+\alpha_2$, and $\alpha_1-\alpha_2$, one sees that the subgroup generated by $C_3(1)C_3^2(2)$ acts on $\alpha_1-\alpha_2$ alone, while the subgroup generated by $C_3(1)C_3(2)$ and C_{2x} acts on the other variables. These two groups are C_3 and C_{3v}, respectively. Since they act on independent sets of variables the over-all symmetry group of the molecule is $S=C_2\times C_{3v}$. The symmetry classes of S can be obtained directly from those of C_3 and C_{3v}. The character tables of C_3 and C_{3v} are given in Table IV.

One sees that there are six representations of S: two one-dimensional, AA_1 and AA_2; one two-dimensional, AE; two pseudo two-dimensional (pairs of complex conjugate one-dimensional), E_0A_1 and E_0A_2; one pseudo four-dimensional (pair of complex conjugate two-dimensional), E_0E. The principal difference between this and the results for acetone are the pseudo two- and four-dimensional representations. However, symmetry still requires energy levels to be singly, doubly, or quadruply degenerate.

As in acetone, the dipole moment must be of species AA_2 and thus only the following transitions are allowed: $AA_1\leftrightarrow AA_2$; $AE\leftrightarrow AE$; $E_0A_1\leftrightarrow E_0A_2$; $E_0E\leftrightarrow E_0E$.

INTERNAL ROTATION. WEAKLY COUPLED CASE

In the weakly coupled case, the internal rotational Hamiltonian is to a first approximation

$$H_{0T}=F(p_1^2+p_2^2)+(V_3/2)(2-\cos3\alpha_1-\cos3\alpha_2). \quad (3)$$

There are 18 linearly independent solutions to its Schrödinger equation with the principal quantum numbers n and n' ($n\neq n'$) or nine for $n=n'$. To the approximation that the Hamiltonian is H_{0T}, the torsional wave functions can be written as products

$$U_{n,\sigma}(\alpha_1)U_{n',\sigma'}(\alpha_2); \qquad U_{n',\sigma}(\alpha_1)U_{n,\sigma'}(\alpha_2),$$

where $U_{n,\sigma}(\alpha)$ is the wave function for the Hamiltonian $H=Fp^2+(V_3/2)(1-\cos3\alpha)$ with principal quantum number n and symmetry σ.[12]

In order to find out which irreducible representations occur in the 18 or nine product wave functions with n and n' we need only note that $U_{n,0}(\alpha_i)$ and the pair $U_{n,-1}(\alpha_i)$ and $U_{n,+1}(\alpha_i)$ are A and E_0 representations of $C_3(i)$, respectively. Under the operation C_{2x}, $U_{n,0}$ $(\alpha_i)\rightarrow(-1)^nU_{n,0}(\alpha_j)$ and $U_{n,\pm1}$ $(\alpha_i)\rightarrow U_{n,\mp1}(\alpha_j)$ where $i,j=1,2$ or $2,1$.

Thus we find that the nine functions with $n=n'$ contain the species AA_1, AE, E_0A_1, and E_0E once each. For $n\neq n'$ the 18 functions contain the species AA_1, AA_2, E_0A_1, and E_0A_2 once each and AE and E_0E twice each.

The approximate wave function will consist of the symmetrized product of a torsional and a rotational function. The approximate rotational function will be a solution to the wave equation with the following Hamiltonian:

$$H_{0R}=AP_a^2+BP_b^2+CP_c^2. \quad (4)$$

These are asymmetric rotor functions and are of symmetry AA_1 or AA_2 when K_{-1}, the limiting prolate K, is even or odd, respectively. If the rotational function is of symmetry AA_1, the over-all wave function is of the same symmetry as the torsional function. If the rotational function is of symmetry AA_2, the over-all wave function is of symmetry AA_1, AA_2, AE, E_0A_1, E_0A_2, or E_0E when the torsional function is of symmetry AA_2, AA_1, AE, E_0A_2, E_0A_1, or E_0E, respectively.

INTENSITY IN THE ROTATIONAL SPECTRUM

In order to determine the intensity distribution in the rotational spectra of the various torsional levels, one must consider the subgroup S' of S which interchanges equivalent nuclei. This group is generated by $C_3(1)$ and $C_3(2)$ and is isomorphic with $C_3\times C_3$. Since its elements do not affect ring hydrogens, these nuclei need not be considered in determining nuclear spin weights. The irreducible representations of S' are AA,

[12] D. R. Herschbach, J. Chem. Phys. **27**, 975 (1957).

TABLE VII. Observed triplets.

	ν_{AE}	$\nu_{calc.}$	$\nu_{AA}-\nu_{AE}$	$\nu_{AE}-\nu_{EE}$	S
$8_{1,7}-8_{2,6}$	19 667.05 Mc	19 669.72	0.89	0.90	45.56
$16_{5,11}-16_{6,11}$	26 072.78	26 026.33	a	a	
$17_{5,12}-17_{6,12}$	20 889.68	20 832.81	−0.87	−0.89	45.67
$19_{5,14}-19_{6,14}$	11 205.59	11 142.96	−0.92	−0.88	45.97
$23_{6,17}-23_{7,17}$	9643.07	9539.37	−1.12	−1.18	45.59

$I_a = 3.194$ amu A²

$F/F^* = 0$ (actual+0.002056)

$\lambda_a = \mp 0.56633$

$\lambda_b = 0.74095$

$\lambda_c = -0.36093$

$s = 45.68 \pm 0.30$

$V_3 = 1607 \pm 150$ cal/mole

$|V_e/V_3| < 0.2$

$V_s/V_3 = 0$

[a] Not resolved due to klystron noise; $\Delta\nu$ calculated=0.70.

AE_0, E_0A, E_1, and E_2, where the AA representation is one dimensional and the other representations are pseudo two dimensional. The correlation of the subgroup representations with the group representations is given in Table V.

The six hydrogens of the methyl groups have 64 spin functions. The number of times these functions contain the irreducible representations of S' is

$$\Gamma_{\text{Methyl H}} = 16AA + 4AE_0 + 4E_0A + 8E_1 + 8E_2.$$

If the methyl hydrogens are replaced by deuterium there are 729 spin functions. The number of times these contain the irreducible representations is

$$\Gamma_{\text{Methyl D}} = 121AA + 64AE_0 + 64E_0A + 88E_1 + 88E_2.$$

All the operations of S' interchange an even number of identical nuclei. Hence the over-all wave function must be of symmetry AA. The rotational wave function is of symmetry AA and the torsional functions $AA+AE_0+E_0A+E_1+E_2$ or $2AA+2AE_0+2E_0A+2E_1+2E_2$ if $n=n'$ or $n\neq n'$, respectively. AA is contained in the product $(AA)(AA)$ once and in the products $(AE_0)(AE_0)$, $(E_0A)(E_0A)$, E_1E_1, and E_2E_2 twice each. It is not contained in any other product. Thus for $n=n'$ the weights for AA, AE_0, E_0A, E_1, E_2 are 16, 8, 8, 16, and 16, respectively, for six hydrogens. For six deuteriums they are 121, 128, 128, 176, and 176. For $n\neq n'$ the weights are just doubled.

This is summarized in Table VI in terms of the symmetry of group S and also in terms of A and E levels for each of the tops.

For $n=n'$ we see that the AA, AE, and two types of EE levels would appear in the ratio 2:4:1:1 for hydrogen and 121:352:128:128 for deuterium. For $n\neq n'$ the two types of AA, two types of AE, and four types of EE levels would occur in the ratio 2:2:4:4:1:1:1:1 for hydrogen and 121:121:352:352:128:128:128:128 for deuterium.

INTERNAL ROTATION: APPLICATION TO *CIS* 2,3-EPOXYBUTANE

The observed microwave spectrum consists of singlets (Table I) and triplets (Table VII). The $J_{5,J-5}-J_{6,J-5}$ series were identified by the similarity of the Stark Effect for the $J=16$, 17, and 19 lines. The similarity of the centrifugal distortion for these lines confirmed the assignment. The $23_{6,17}-23_{7,17}$ line was assigned by its internal rotation splitting. No other split intense line occurs within 400 Mc of its predicted frequency. The spectrum can be explained by assuming that the barrier to internal rotation is high with relatively weak coupling between the two tops. Thus the Hamiltonian will be written as

$$H = H_{0R} + H_{0T} + H_{1R} + H_{1T} + H_{1T}'. \tag{5}$$

The first-order Hamiltonian will be taken to be

$$H_{1R} = -2F\mathcal{P}_-(p_1-p_2) - 2F\mathcal{P}_+(p_1+p_2) + 2F\mathcal{P}_-^2 + 2F\mathcal{P}_+^2 \tag{6}$$

$$H_{1T} = V_e(1-\cos 3\alpha_1)(1-\cos 3\alpha_2) \tag{7}$$

$$H_{1T}' = 2F^*[\mathcal{P}_+^2 - \mathcal{P}_-^2 - (p_1+p_2)\mathcal{P}_+ + (p_1-p_2)\mathcal{P}_- + p_1p_2] + V_s \sin 3\alpha_1 \sin 3\alpha_2, \tag{8}$$

where $V_3 = V_3^* + V_+ + V_-$, $V_e = -(V_+ + V_-)/2$, and $V_s = (V_+ - V_-)/2$ in terms of the parameters of Eq.

TABLE VIII. Perturbation sums.

s	72	60	48	40
η_A^{pp}	2.220×10^{-5}	8.454×10^{-5}	3.643×10^{-4}	1.055×10^{-3}
η_E^{pp}	-1.111×10^{-5}	4.227×10^{-5}	1.819×10^{-4}	5.272×10^{-4}
η_{AA}^{ppca}	-4.04×10^{-5}	-1.521×10^{-4}	-6.467×10^{-4}	-1.867×10^{-3}
η_{AE}^{ppca}	-4.04×10^{-5}	-1.521×10^{-4}	-6.466×10^{-4}	-1.866×10^{-3}
η_{EA}^{ppca}	2.05×10^{-5}	7.630×10^{-5}	3.236×10^{-4}	9.533×10^{-4}
η_{EE}^{ppca}	2.05×10^{-5}	7.630×10^{-5}	3.235×10^{-4}	9.528×10^{-4}
$\eta_A^{pp}-\eta_E^{pp}$	3.331×10^{-5}	1.268×10^{-4}	5.462×10^{-4}	1.582×10^{-3}
$2\eta_{AA}^{ppc}-\eta_{AE}^{ppc}-\eta_{EA}^{ppc}$	-6.09×10^{-5}	-2.284×10^{-4}	-9.704×10^{-4}	-2.821×10^{-3}
$\eta_{AE}^{ppc}+\eta_{EA}^{ppc}-2\eta_{EE}^{ppc}$	-6.09×10^{-5}	-2.284×10^{-4}	-9.700×10^{-4}	-2.818×10^{-3}

Value of s required for observed splitting

V_c/V_s	s
0.2	45.41
0.0	45.68
−0.2	45.94

[a] η^{ppc} values for $s=40$ from tables prepared by L. Pierce and M. Hayashi.

(2). For a low barrier a more satisfactory grouping of terms would be to take $V_3=V_3^*$ and have $H_{1T}=-V_c(1-\cos3\alpha_1\cos3\alpha_2)$.

One then approximately diagonalizes the Hamiltonian in the torsional states by means of a Van Vleck transformation.[12] This is a particularly useful method of dealing with Hamiltonians such as the above, since the torsional energy levels of a given symmetry are rather widely spaced compared with the rotation levels. This method will have to be modified and a partial torsional diagonalization used instead for states with $n\neq n'$. In these cases states which are nearly degenerate in their torsional energy interact directly. However, for the ground state the method can be used as with one top molecules. Terms of odd order in H_{1R} are not important since the observed rotational spectrum was fitted using the assumption that the molecule was a rigid rotor with small centrifugal distortion. Terms linear in H_{1R} may become important for high prolate or oblate K. However, due to the large asymmetry ($\kappa=-0.567$) these terms are negligible for transitions listed in Table VII.

In applying the Van Vleck transformation to the Hamiltonian one ignores differences in rotational energy in the perturbation denominators. This will make only slight errors and will only contribute terms of fourth or higher even power in the angular momentum to the Hamiltonian. These terms will influence the centrifugal distortion. Ignoring these differences is equivalent to keeping the corrected Hamiltonian as an operator as far as rotation is concerned. Retaining only those terms which are quadratic in H_{1R}, one obtains a pseudo rigid-rotor Hamiltonian for each torsional state under consideration. It is of the form

$$H_R=H_{0R}+F(W_{\Gamma i}^{+(2)}\mathcal{P}_+^2+W_{\Gamma i}^{-(2)}\mathcal{P}_-^2) \tag{9}$$

with

$$W_{\Gamma i}^{\pm(2)}=\eta_\sigma^{pp}+\eta_{\sigma'}^{pp}+(V_c/V_3)[\eta_{\sigma\sigma'}^{ppc}+\eta_{\sigma'\sigma}^{ppc}\pm\epsilon_{\Gamma i}]$$
$$+\text{ terms in }(V_s/V_3)+\text{ terms in }(F^*/F), \tag{10}$$

where

$$\eta_\sigma^{pp}=1+4F\left[\sum_n{}'\frac{|p_{\sigma n}|^2}{E_0-E_n}\right]_\sigma. \tag{11}$$

A σ subscript on a pair of brackets indicates that all the matrix elements within the brackets are between states of symmetry σ. The quantity η_σ^{pp} has been tabulated by Herschbach.[12]

$$\eta_{\sigma\sigma'}^{ppc}=9sF^2[C_{00}]_{\sigma'}$$
$$\times\left[\sum_{nn'}{}'\frac{p_{0n}p_{nn'}C_{n'0}+p_{0n}C_{nn'}p_{n'0}+C_{0n}p_{nn'}p_{n'0}}{(E_0-E_n)(E_0-E_{n'})}\right.$$
$$\left.-\sum_n{}'\frac{p_{00}p_{0n}C_{n0}+p_{00}C_{0n}p_{n0}+C_{00}p_{0n}p_{n0}}{(E_0-E_n)^2}\right]_\sigma, \tag{12}$$

with $C=(1-\cos3\alpha)$.

The term $\epsilon_{\Gamma i}$ splits the Γ_3 and Γ_4 EE rotational spectra. For a reduced barrier height $s=4V_3/9F=48$ this term is a factor of 10^{-4} the $\eta_{\sigma\sigma'}^{ppc}$ term. For higher barriers it is even smaller.

Terms in H_{1T}' have been ignored. From geometry one can calculate the ratio F/F^*. It is 2×10^{-3}. This small size coupled with the fact that the only appreciable matrix elements of p_1p_2 are off diagonal in both top

quantum numbers, makes the effect of this term negligible. The term in $\sin 3\alpha_1 \sin 3\alpha_2$ is also principally off diagonal in both top quantum numbers and so will have little effect on the rotational spectrum for the ground state.

The perturbation sums are listed in Table VIII.

Since the observed splittings of the rotational constants are small, the value of the barrier can be found directly;

$$\Delta W = W_{AA} - W_{AE} = W_{AE} - W_{EE}$$
$$= (\partial W/\partial A)\Delta A + (\partial W/\partial B)\Delta B + (\partial W/\partial C)\Delta C. \quad (13)$$

For a rigid rotor the energy is

$$W = [(A+C)/2]J(J+1) + [(A-C)/2]E(\kappa), \quad (14)$$

where

$$\kappa = (2B-A-C)/(A-C).$$

Hence

$$\partial W/\partial A = [J(J+1)/2] + [E(\kappa)/2] - [(\kappa+1)/2]E'(\kappa)$$
$$\partial W/\partial B = E'(\kappa)$$
$$\partial W/\partial C = [J(J+1)/2] - [E(\kappa)/2] + [(\kappa-1)/2]E'(\kappa). \quad (15)$$

From Eq. (10) one sees that the effective rotational constants are

$$A' = A + FW_{\Gamma_i}{}^{-(2)}(\lambda_a{}^2 I_a{}^2/I_a{}^2)$$
$$B' = B + FW_{\Gamma_i}{}^{+(2)}(\lambda_b{}^2 I_a{}^2/I_b{}^2)$$
$$C' = C + FW_{\Gamma_i}{}^{+(2)}(\lambda_c{}^2 I_a{}^2/I_c{}^2). \quad (16)$$

The term in $P_b P_c + P_c P_b$ from $\mathcal{P}_+{}^2$ will be ignored.

If one assumes $V_e = 0$, the reduced barrier is 45.68 ± 0.08 and the barrier is 1607 cal/mole. However, one cannot assume $V_e = 0$ since the barrier is about 40% less than that of epoxypropane (2560 cal/mole). For a coupling even as large as $V_e/V_3 = 0.2$ in magnitude, the value of the reduced barrier is changed by only 0.5%. Thus one cannot bring the value of V_3 into agreement with that of epoxypropane with such values of V_e.

From the observed ground-state spectrum one cannot draw any definite conclusions concerning the coupling of the two tops. One would need to study the rotational spectra of higher torsional states. However, with the barrier as low as it is, and with the interaction of nearly degenerate torsional states, one would not expect pseudo rigid-rotor spectra for excited states. No simple multiplet structure which was ascribable to higher torsional states was found.

CONCLUSIONS

The barrier to internal rotation in *cis* 2,3-epoxybutane is 1607 ± 150 cal/mole, independent of a range of assumptions regarding the coupling of the two tops. This is considerably less than the barrier of 2560 ± 75 cal/mole in epoxypropane.[6]

One can explain this as Dauben and Pitzer[4] explained the difference between the 2-butenes and propene. The mutual interaction of the methyl hydrogens is the greatest at the potential minimum. Therefore the minimum is raised more than the maximum and the barrier is lowered. From the structure of *cis* 2,3-epoxybutane one determines the distance of closest approach of the hydrogens on different methyl groups to be 1.89 A. When these two groups are rotated through 60° the distance between the nearest hydrogen is 2.74 A. One would expect the equilibrium configuration to be such that the plane determined by the methyl hydrogen facing the ring, the methyl carbon, and the ring carbon would approximately bisect the adjacent ring-carbon ring-carbon oxygen angle. If this were so the distance between the two nearest hydrogens would be 2.11 A. Thus the greatest interaction would be expected when the two methyl groups were near their expected equilibrium configuration, in agreement with the observed barrier. According to this theory, this effect would be absent in the *trans* isomer and its barrier would be approximately that of epoxypropane.

ACKNOWLEDGMENTS

The author would like to thank Professor E. Bright Wilson, Jr., for his many helpful suggestions concerning this work. He also acknowledges the advice of Dr. Louis Pierce.

ESR Studies on the Bonding in Copper Complexes† *

DANIEL KIVELSON AND ROBERT NEIMAN‡

Department of Chemistry, University of California, Los Angeles 24, California

(Received December 12, 1960)

ESR spectra of copper complexes have been interpreted by means of molecular orbital theory, and the "covalent" character of both σ and π bonds have been discussed for a variety of compounds. Overlap integrals have been considered in a consistent manner in treating σ bonds. Particular attention has been given to Cu phthalocyanine and several of its derivatives. The in-plane π bonding may be as important in determining the properties of a Cu complex as is the in-plane σ bonding.

THEORY

ELECTRON spin resonance studies have been used to investigate the covalent bonding of transition metals in a variety of compounds.[1-4] The work on copper complexes was most highly developed by Maki and McGarvey in their analysis of the ESR spectra of the copper salicylaldehyde imine and acetylacetonate.[4] In the present study the theory is modified slightly and applied to a number of copper complexes.

Van Vleck[5] has shown that an appropriate linear combination of central-ion atomic orbitals and ligand atomic orbitals represents a satisfactory molecular orbital for the complex. The molecular orbital approach has proved most successful in explaining the complex hyperfine structure that is observed in the ESR spectra of covalently bonded metals[1-4,6]; it will, therefore, be used here. The notation of Maki and McGarvey[4] for a square planar complex will be followed and it will be assumed that all complexes considered have approximately square planar symmetry. It will further be assumed that each of the four ligand atoms has available $2s$, $2p_x$, $2p_y$, and $2p_z$ orbitals for the formation of the molecular orbitals with the copper $3d$ orbitals. Since a square planar complex has D_{4h} symmetry, the following antibonding molecular orbitals for the "hole" configuration, labeled according to symmetry species, can be formed from the central atom $3d$ and the ligand $2s$ and $2p$ orbitals. The four ligands are placed on the $\pm x$ and $\pm y$ axes and are labeled by superscripts starting with one on the $+x$ axes and proceeding counter clockwise,

$$B_{1g}=\alpha d_{x^2-y^2}-\alpha'(-\sigma_x^{(1)}+\sigma_y^{(2)}+\sigma_x^{(3)}-\sigma_y^{(4)})/2 \quad (1a)$$

$$B_{2g}=\beta_1 d_{xy}-\beta_1'(p_y^{(1)}+p_x^{(2)}-p_y^{(3)}-p_x^{(4)})/2 \quad (1b)$$

$$A_{1g}=\alpha_1 d_{3z^2-r^2}-\alpha_1'(\sigma_x^{(1)}+\sigma_y^{(2)}-\sigma_x^{(3)}-\sigma_y^{(4)})/2 \quad (1c)$$

$$E_g=\begin{cases}\beta d_{xz}-\beta'(p_x^{(1)}-p_x^{(3)})/2^{\frac{1}{2}} \\ \beta d_{yz}-\beta'(p_z^{(2)}-p_z^{(4)})/2^{\frac{1}{2}},\end{cases} \quad (1d)$$

where

$$\sigma^{(i)}=np^{(i)}\mp(1-n^2)^{\frac{1}{2}}s^{(i)}. \quad (1e)$$

Here $0\leq n\leq 1$; the plus sign applies to the ligand atoms on the positive x and y axes, the minus sign to those on the negative x and y axes.

The overlap between the copper and ligand orbitals has been considered in Eq. (1). Normalization of the B_{1g} orbital yields

$$\alpha^2+\alpha'^2-2\alpha\alpha' S=1, \quad (2)$$

where S is the overlap integral

$$S=\langle d_{x^2-y^2}\,|\,-\sigma_x^{(1)}+\sigma_y^{(2)}+\sigma_x^{(3)}-\sigma_y^{(4)}\rangle/2$$
$$=2\langle d_{x^2-y^2}|\,-\sigma_x^{(1)}\rangle. \quad (3)$$

Similar relations hold between the other coefficients but the other overlap integrals are small and so can be neglected.

The orbitals in Eqs. (1a)-(1e) are given in order of increasing energy although the position of the A_{1g} level is rather uncertain; in any case, the A_{1g} state does not effect the magnetic parameters in second order and so is not relevant to the present discussion. Here B_{1g} represents in-plane σ bonding, B_{2g} represents in-plane π bonding, and E_g represents out-of-plane π bonding. Bonding orbitals could be constructed by replacing the unprimed by the primed and the primed by minus the unprimed coefficients in the antibonding orbitals described above.

Figure 1 gives an approximate representation of the energy levels for σ bonding. The sequence of levels has not been unambiguously assigned but the unpaired electron is almost certainly in the B_{1g} level. Note that there are three A_{1g} levels that interact with each other

* Presented at the American Chemical Society Symposium on Molecular Structure, University of Washington, Seattle, Washington, June, 1960.

† Supported in part by the National Science Foundation and the Research Corporation.

‡ Present address: Central Research and Engineering, Texas Instruments Inc., Dallas, Texas.

[1] K. W. H. Stevens, Proc. Roy. Soc. (London) **A219,** 542 (1953).

[2] J. Owen, Proc. Roy. Soc. (London) **A227,** 183 (1955); Discussions Faraday Soc. **19,** 127 (1955).

[3] M. Tinkham, Proc. Roy. Soc. (London) **A236,** 535, 549 (1956).

[4] A. H. Maki and B. R. McGarvey, J. Chem. Phys. **29,** 31, 35 (1958).

[5] J. H. van Vleck, J. Chem. Phys. **3,** 807 (1935).

[6] For a complete discussion see doctoral thesis by R. Neiman, University of California, Los Angeles (1960).

although one will almost certainly be strongly bonding, one antibonding, and the third will be almost nonbonding. A similar scheme for π bonding is shown in Fig. 2.

For the case of a $3d^9$ copper ion, the appropriate crystal-field Hamiltonian is[7]

$$W'=\lambda(r)\mathbf{L}\cdot\mathbf{S}+\beta_0\mathbf{H}\cdot(\mathbf{L}+2.0023\mathbf{S}) +2\gamma\beta_0\beta_N\{[(\mathbf{L}-\mathbf{S})\cdot\mathbf{I}/r^3]+[3(\mathbf{r}\cdot\mathbf{S})(\mathbf{r}\cdot\mathbf{I})/r^5] -(8\pi/3)\delta(\mathbf{r})\mathbf{S}\cdot\mathbf{I}\}, \quad (4)$$

where $\lambda(r)$ is the spin orbit operator, $\mathbf{L}$ is the orbital angular momentum operator, $\mathbf{S}$ is the spin angular momentum for the electron, β_0 the Bohr magneton, $\mathbf{H}$ the applied magnitic field, γ the gyromagnetic ratio of the nucleus in question, β_N is the nuclear magneton, $\mathbf{I}$ the spin angular momentum operator for the nucleus, r the distance from the central nucleus to the electron, and $\delta(\mathbf{r})$ is the Dirac delta function operator. Quadrupole effects and effects arising from the interaction of the nuclear moment with the external field have been neglected in this expression since they may be expected to be of little importance here.

The wave functions of Eqs. (1a)–(1e) can be used to solve the Hamiltonian given above and to convert it, through second order, to a spin Hamiltonian.[7] The resulting spin Hamiltonian assuming B_{1g} is the ground state, is

$$H=\beta_0[g_{\|}H_zS_z+g_\perp(H_xS_x+H_yS_y)]+AI_zS_z +B(I_xS_x+I_yS_y), \quad (5a)$$

where

$$g_{\|}-2.0023=-8\rho[\alpha\beta_1-\alpha'\beta_1S-\alpha'(1-\beta_1^2)^{\frac{1}{2}}T(n)/2] \quad (5b)$$

$$g_\perp-2.0023=-2\mu[\alpha\beta-\alpha'\beta S-\alpha'(1-\beta^2)^{\frac{1}{2}}T(n)/2^{\frac{1}{2}}] \quad (5c)$$

$$A=P[-\alpha^2(\tfrac{4}{7}+\kappa_0)+(g_{\|}-2)+\tfrac{3}{7}(g_\perp-2) -8\rho\{\alpha'\beta_1S+\alpha'(1-\beta_1^2)^{\frac{1}{2}}T(n)/2\} -\tfrac{6}{7}\mu\{\alpha'\beta S+\alpha'(1-\beta^2)^{\frac{1}{2}}T(n)/2^{\frac{1}{2}}\}] \quad (5d)$$

$$B=P[\alpha^2(\tfrac{2}{7}-\kappa_0)+\tfrac{11}{14}(g_\perp-2) -\tfrac{2}{14}\mu\{\alpha'\beta S+\alpha'(1-\beta^2)^{\frac{1}{2}}T(n)/2^{\frac{1}{2}}\}], \quad (5e)$$

and the following definitions are used

$$\rho=\lambda_0\alpha\beta_1/\Delta E_{xy}; \qquad \mu=\lambda_0\alpha\beta/\Delta E_{zz} \quad (6a,b)$$

$$T(n)=n-(1-n^2)^{\frac{1}{2}}R8(Z_pZ_s)^{5/2}(Z_s-Z_p)/(Z_s+Z_p)^5a_0 \quad (6c)$$

$$P=2\gamma\beta_0\beta_N\langle d_{x^2-y^2}|r^{-3}|d_{x^2-y^2}\rangle. \quad (6d)$$

The λ_0 is the spin-orbit coupling constant for the free Cu(II) ion, i.e., $\langle 3d|\lambda(r)|3d\rangle$; κ_0 is the Fermi-contact term for the free ion; ΔE_{xy} and ΔE_{zz} are, respectively, $E_{xy}-E_{x^2-y^2}$ and $E_{zz}-E_{x^2-y^2}$; R is the metal-ligand distance; hydrogenlike radial functions have been used; Z_s and Z_p represent the effective nuclear charges on the s and p orbitals, respectively; and a_0 is the Bohr radius.

These equations differ from those of Maki and McGarvey in that the contribution of the overlap integral S is included; this term is of the same order of magnitude as the $T(n)$ terms. The equations also differ from those of Roberts and Koski[8] in that these authors treated $\lambda(r)$ as a constant and not as a rapidly decreasing function of r. The Fermi contact interaction would, of course, vanish for $3d$ electrons since these have no density at the Cu nucleus. We have assumed that the required s character is present in the Cu atomic orbitals[9,10] and that the ratio of s to d character is unchanged by the presence of the ligands. Furthermore, it can be shown that the density of ligand orbitals at the Cu nucleus is very small. These arguments allow us to write the Fermi-contact interaction as $\alpha^2\kappa_0$. The parameter κ introduced previously[3,4,8,10] can be equated to the present quantity $\alpha^2\kappa_0$.

Finally it should be mentioned that in the evaluation of the spin Hamiltonian all integrations over the ligand orbitals that involve an inverse dependence upon r were neglected according to the prescription given by Maki and McGarvey.

If the ligand possesses a nuclear spin, the above spin Hamiltonian contains an additional term which gives rise to an extra hyperfine interaction characteristic of the ligand. It is this hyperfine interaction which requires the use of molecular orbitals rather than the crystal-field approach to the problem. The extra hyperfine interaction arises from dipolar interactions between the nuclear and the electronic moments. The anisotropic contribution is small[4] and the isotropic contribution arises from the s character Fermi interaction of

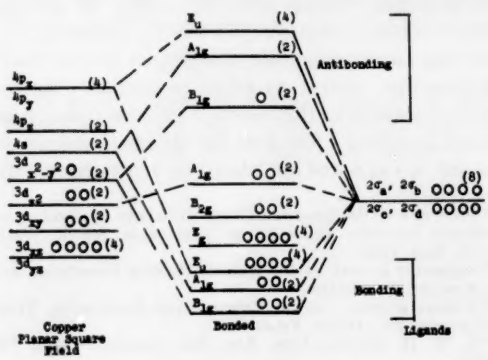

FIG. 1. Energy levels of Cu^{++} complexes with σ bonding.

[7] A. Abragam and M. H. L. Pryce, Proc. Roy. Soc. (London) **A205,** 135 (1951).

[8] E. M. Roberts and W. S. Koski, J. Am. Chem. Soc. **82,** 3006 (1960).

[9] A. Abragam and M. H. L. Pryce, Proc. Roy. Soc. London **A230,** 206 (1951).

[10] A. Abragam, M. H. L. Pryce, and J. Horowitz, Proc. Roy. Soc. (London) **A230,** 169 (1955).

the ligand orbitals. The isotropic interaction energy is

$$W_L = (4\pi/9)\gamma_L\beta_0\beta_N\alpha'^2|\rho_N(0)^2|\mathbf{S}_z\mathbf{I}_z^{(L)}, \quad (7)$$

where L refers to the ligand nucleus, $\rho_N(0)$ is the value of the ligand $2s$ function at the ligand nucleus. It is assumed that the copper orbitals do not make an appreciable contribution to the spin density at the ligand nucleus. Note that if $\alpha'^2=0$, i.e., if the unpaired electron is not even partly on the ligand, the extra hyperfine structure vanishes. Only in the molecular orbital approach is α' nonvanishing.

APPLICATIONS

In order to use the expressions obtained in the last section the overlap integral S must be evaluated. Hydrogenlike functions have been assumed and the following effective charges have been chosen from Hartree[11]:

for nitrogen: $Z_{2s}=4.50$, $Z_{2p}=3.54$

for oxygen: $Z_{2s}=5.25$, $Z_{2p}=4.06$

for copper: $Z_{3d}=11.86$.

Only nitrogen and oxygen ligands will be considered. The ligand-to-metal distance R has been taken as 3.62 a_0; this value differs slightly from compound to compound but is probably about 1.9 A within experimental error. The overlap integrals are then, $S_{\text{nitrogen}}=0.093$, $S_{\text{oxygen}}=0.076$. In obtaining these values n has been chosen as $(\frac{2}{3})^{\frac{1}{2}}$ which implies sp^2 hybridization in the ligands. The corresponding values of $T(n)$ are $T(n)_{\text{nitrogen}}=0.333$, $T(n)_{\text{oxygen}}=0.220$.

The value of λ_0 is chosen to be -828 cm^{-1} while P is 0.036 cm^{-1}.[7,9] The estimated error in these quantities is about 3%. The κ_0 is about 0.43 with an estimated uncertainty of about 5%.[9] The orbital excitation energies ΔE_{xy} and ΔE_{xz} can often be measured from the visible spectrum; however, this is not the case in the phthalocyanine and porphyrin complexes in which the intense π transitions mask the Cu transitions. Generally, ΔE_{xy} is about 15 000 cm^{-1} while ΔE_{xz} is about 25 000 cm^{-1}.

If ΔE_{xy} and ΔE_{xz} as well as $g_{\|}$, $g_{\perp}$, A, and B are known it is, in principle, possible to calculate α, β_1, and β_1'. However, it is usually not possible to obtain a well-defined set of solutions for these equations and for this reason an iterative procedure is preferred. Since α is often of the order of 0.9 and β_1 and β are close to unity, Eq. (5c) can be written in the following approximate form

$$\alpha^2 = -(A/P)+(g_{\|}-2)+(3/7)(g_{\perp}-2)+0.04. \quad (8)$$

Note that $(4/7)+\kappa_0=1.0$. Equation (8) can be used to obtain a first approximation of α^2. If ΔE_{xy} and ΔE_{xz} are known one can then obtain β_1 and β from $g_{\|}$ and $g_{\perp}$; these can then be used to obtain better values for α^2. We have found that the determinations of B are generally not accurate enough to add information to the calculations. Furthermore, in the cases where ΔE_{xy} and ΔE_{xz} are not known they can be estimated because a 20% error in ΔE_{xy} and ΔE_{xz} results in only about a 5% error in β_1 and β, respectively.

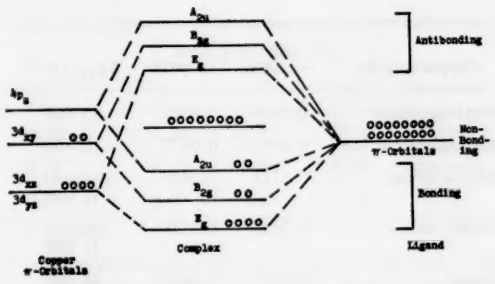

FIG. 2. Energy levels of Cu^{++} complexes with π bonding.

The results of the calculations for α^2 and β_1^2 for several copper complexes are summarized in Table I; the experimental data is taken from several sources. The values of β^2 are probably so close to unity that the uncertainty in the calculations does not allow us to distinguish them from unity. It is quite clear that, except for laccase and ceruloplasmin, α^2 is in the range 0.75 to 0.90 for most copper complexes [α, β, ν, δ tetra phenyl porphin Cu (II) should probably lie within this range; the discrepancy is thought to arise from experimental uncertainties]. This relatively small range of α^2 explains the relative constancy of the values of κ(or $\alpha^2\kappa_0$) as determined by others.[4,8,12] These values of α^2 indicate that the σ bonding is quite covalent in nature since it shows that the bond is delocalized over both the Cu and the ligand orbitals. If $\alpha^2=1$, the bond would be completely ionic. If the overlap integral were vanishingly small and $\alpha^2=0.5$, the bond would be completely covalent. However, because the overlap integral is sizeable we cannot speak strictly of covalent versus ionic bonds, but we can say that the smaller the value of α^2 the greater the covalent nature of the bond. The trend is in the expected direction; salicylaldehydeimines and phthalocyanines are more covalent than oxalates. The two enzymes, laccase and ceruloplasmin, have a very particular behavior; they have been discussed by Vanngard.[13]

By measuring the extra hyperfine splitting α^2 can also be determined. Maki and McGarvey have estimated $|\rho(0)|^2$ to be 33.4×10^{24} cm^{-3}. Then by means of Eq. (7), α'^2 can be determined directly and it can in turn be used to obtain α^2 by means of Eq. (2). Extra hyperfine structure due to nitrogen has been reported in three Cu(II) complexes. Table II gives the com-

[11] D. R. Hartree, *The Calculation of Atomic Spectra* (John Wiley & Sons, New York, 1957).

[12] J. F. Gibson, D. J. E. Ingram, and D. Schonland, Discussions Faraday Soc. **26**, 72 (1958).

[13] B. G. Malmstom and T. Vanngard, J. Mol. Biol. **2**, 118 (1960).

TABLE I.

Copper complex	$g_{\|\|}$ -2.0023	$g_{\perp}$ -2.0023	ΔE_{xy} (cm^{-1})	A (cm^{-1})	α^2	β_1^2	Comments on β_1^2	Reference
Acetyl-acetonate	0.2638	0.0512	15 000	-0.0160	0.75	0.87		4
Salicylaldehydeimine	0.1981	0.0427	16 300	-0.0185	0.76	0.72		4
Phthalocyanine	0.1723	0.0427	assumed 17 000	-0.0202	0.78	0.65	assuming $\Delta E_{xy}=17\,000$ cm^{-1}	this work
Phthalocyanine	0.1627	0.0427	assumed 17 000	-0.0220	0.82	0.59	assuming $\Delta E_{xy}=17\,000$ cm^{-1}	12
Laccase	0.1947	0.0457	16 400	-0.009	0.49	1.0	β_1^2 assumed to be one to get agreement with A, $g_{\|\|}$ and ΔE_{xy}	13
Ceruloplasmin	0.2067	0.0528	16 500	-0.008	0.47	1.0		13
Denatured Laccase	0.2277	0.0527	assumed 16 400	-0.020	0.83	0.76	assuming $\Delta E_{xy}=16\,400$ cm^{-1}	13
Denatured Ceruloplasmin	0.2547	0.0528	assumed 16 500	-0.018	0.80	0.88	assuming $\Delta E_{xy}=16\,500$ cm^{-1}	13
Histidine	0.2277	0.0607	15 600	-0.018	0.78	0.78		13
Imidazole	0.2647	0.0607	16 800	-0.018	0.82	0.89		13
2-2′ Dipyridyl	0.2677	0.0797	14 900	-0.017	0.80	0.84		13
1-10 Phenanthroline	0.2777	0.0857	15 200	-0.015	0.76	0.95		13
Oxalate	0.3137	0.0757	15 400	-0.017	0.84	0.92		13
EDTA	0.3347	0.0877	13 900	-0.016	0.84	0.89		13
Citrate	0.3467	0.0717	13 700	-0.015	0.82	0.93		13
Etioporphyrin II	0.1670	0.0593	assumed 17 000	-0.0188	0.74	0.68	assuming $\Delta E_{xy}=17\,000$ cm^{-1}	8
t-phenylporphin	0.1677	0.0477	assumed 20 000	-0.025	0.90	0.62	assuming $\Delta E_{xy}=20\,000$ cm^{-1}	14

pounds, the observed splittings, the values of α', α'^2, and α^2 calculated from Eq. (5d) and from Eqs. (7) and (2). The agreement between the two different methods of calculating α^2 is quite good and is probably within the uncertainty limits; this lends credence to the assumption of sp^2 bonding for the ligands. The α^2 calculated from Eq. (5d) is smaller than that obtained from the extra hyperfine structure from Eq. (7); this is in accord with previous results.[3] A different hybridization of the σ orbitals on the nitrogen atoms might reduce the discrepancy. If n^2 in Eq. (1e) were about 0.6 instead of 0.667, the α^2 calculated from Eq. (7) would be reduced by about 0.05 while the α^2 calculated from Eq. (5d) would remain almost unchanged. The isotropy of the extra hyerfine splitting in the phthalocyanine is discussed in the next article.

Since the overlap integrals in the B_{2g} function are negligible, β_1^2 is a direct measure of the covalency of the in-plane π bonding. Therefore, the values of β_1^2 listed in Table I also furnish a pronounced trend in in-plane covalent π bonding. The differences in β_1^2 are much more pronounced than are those for α^2. β_1^2 is, therefore, probably a better indication of "covalent character" than is α^2. The marked in-plane π bonding covalent nature of the phthalocyanines may account for their great stability.

PHTHALOCYANINES AND PORPHINS

Copper phthalocyanine is extremely stable; it can be sublimed at 550°C and it can be dissolved only in concentrated H_2SO_4. Its chemistry has been described by Linstead[14] and its structure elucidated by Robertson.[15] Previous ESR studies were carried out by Ingram *et al.*[12,16] who worked on single crystals diluted with diamagnetic Zn phthalocyanine. The present work was carried out on a dilute frozen solution of Cu phthalocyanine in concentrated H_2SO_4, i.e., in a glass. The details are given in the following article but both hyperfine structure and extra hyperfine structure were observed; the results are tabulated in Tables I and II.

The difference between the values of α^2 and β_1^2 for copper phthalocyanine which were calculated from the data of Ingram[12] (but using the present theory) and those values calculated from the experimental data in this work (see the following article) is probably just a reflection of experimental error or a slight differ-

[14] G. J. Byrne, R. P. Linstead, and A. R. Lowe, J. Chem. Soc. **1934,** 1017; C. E. Dent and R. P. Linstead, *ibid.* **1934,** 1027; P. A. Barrett, C. E. Dent, and R. P. Linstead, *ibid.* **1936,** 1719; J. S. Anderson, E. F. Bradbrook, A. H. Cook, and R. P. Linstead, *ibid.* **1938,** 1151.

[15] J. Robertson and R. P. Linstead, J. Chem. Soc. **1936,** 1736.

[16] D. J. E. Ingram, J. E. Bennett, P. George, and J. M. Goldstein, J. Am. Chem. Soc. **78,** 3545 (1956).

TABLE II.

Compound	Splitting (gauss)	from Eq. (7) α'	from Eq. (7) α'^2	from Eq. (7) α^2	from A and Eq. (5c) α'	from A and Eq. (5c) α'^2	from A and Eq. (5c) α^2	Reference
bis-salicylaldehyde-imine	11.1	0.49	0.24	0.84	0.56	0.31	0.76	4
Phthalocyanine	14.6	0.55	0.30	0.79	0.55	0.30	0.78	this work
Etioporphyrin II	14.3	0.55	0.30	0.79	0.59	0.35	0.74	8

ence arising from the fact that the magnetic environment was somewhat different in each case. Ingram,[12] on the other hand, finds no hyperfine (hfs) structure due to nitrogen in his single crystal work; this may be due to two causes: (1) The crystals lack sufficient magnetic dilution so that exchange and dipolar effects wash out the nitrogen hfs and (2) large amplitude modulation of the magnetic field might also wipe out the nitrogen hfs. Reason (1) is more likely since the concentration figures given[12] would imply that the copper phthalocyanine concentration in the single crystal work is about 2 M. A 0.354 M solution of copper phthalocyanine in 96% H_2SO_4 shows no hyperfine structure from the nitrogens; this supports reason (1). Ingram[12] also made an estimate of α^2 based only on first-order theory with neglect of any ligand contributions. In this way ΔE_{xy} was estimated as 31 700 cm^{-1} and ΔE_{xz} as 29 000 cm^{-1} which would of course place the B_{2g} level below the E_g levels. In the present work, ligand contributions were included; ΔE_{xy} was estimated to be about 17 000 cm^{-1} and ΔE_{xz} to be about 26 000 cm^{-1} if $\beta^2 \geq 0.95$ for this compound.

Some comment must also be made about the studies on (α, β, γ, δ-)-tetraphenyl porphin (TTP) and its *p*-chloro derivative (TPPCl).[14] The copper hyperfine splitting constant A was the same for both compounds (0.025 cm^{-1}) which gives a value of α^2 equal to 0.90; this value of α^2 is quite high but is probably within the limits of error quoted for α^2. The most striking result, however, was that the spectrum of TPPCl contained a great number of hyperfine lines (more than those expected just from copper) so that this extra hyperfine splitting was attributed to the chlorine atoms on the periphery of the molecule. These findings are somewhat surprising for several reasons: (1) If the B_{1g} orbital is as covalent as in other compounds, one might expect that the interactions with the nitrogens (which are only about 2 A distant) would be much stronger than the interaction with the chlorines (which are about 9 A distant) and (2) hyperfine splitting due to chlorine has been observed in very few compounds; the most outstanding example is $IrCl_6^{-2}$ in which the chlorine-metal distance is much shorter.[2,17]

With these results in mind, spectra were run of tetra-4-*p*-chloro-copper phthalocyanine (CuPc), tetra-4-nitro-CuPc, and tetra-4-sulfo-CuPc in 96% H_2SO_4. All three compounds gave identical spectra and, since these spectra were also identical to that of the plain CuPc, the assumption can be made that indeed the 3*d* electron of the copper spends a negligible amount of time on the phenyl rings of the phthalocyanine. If this same assumption can be made for the porphins, another explanation must be sought for the observed spectra of these compounds. We feel that the splitting in the case of TPPCl is due to the four nitrogens bound to the copper; failure to observe any further hfs in the unchlorinated TPP is probably again due to lack of magnetic dilution.

[17] J. Owen, Discussions Faraday Soc. **26**, 53 (1958).

FURTHER COMMENTS ON THE THEORY

Thus far the discussion of bonding has been confined to square planar bonding. It is possible, however, for Cu(II) to assume octahedral bonding in some compounds[18]; this of course would invoke the d_{z^2} orbital of the copper ion. Two cases will be discussed: (1) small perturbations along the z axis and (2) complete degeneracy along the x, y, and z axes: a cubic system. For small perturbations along the z axis $g_{||}$, A and B remain unchanged but $g_\perp$ increases slightly.[6]

For the cubic case, the A_{1g} and B_{1g} levels would be degenerate, as would the B_{2g} and E_g levels. Then, $g_{||}$ would still be the same as in the square planar case but $g_\perp$ would be raised since now the $\langle A_{1g}|\mathbf{L}_z|E_g\rangle$ matrix elements contribute; in fact, $g_{||}=g_\perp$ and $A=B$.

No completely cubic compounds are known for Cu(II),[19] presumably because of the Jahn-Teller effect,[19] although the fluorosilicates ($M''SiF_6\cdot 6H_2O$, where M'' is a divalent cation) are trigonal and have $g_{||}\approx g_\perp$ (at certain temperature, this equality disappears and the symmetry is more tetragonal[19]). The Tutton salts $[M_2'M''(SO_4)_2\cdot 6H_2O]$ (where M' is a monovalent cation and M'' a divalent cation) are more nearly tetragonal in their symmetry[19]; in effect, this means that one can consider them to a first approximation, as a square planar complex with perturbations along the z axis. Therefore, one might expect that $g_{||}>g_\perp$; this is borne out by the available ESR data.[19]

The spectra of tetra-4-sulfo copper phthalocyanine (TSCP) in H_2O consists of a single, very broad line

[18] E. Cartnell and G. W. A. Fowles, *Valency and Molecular Structure* (Butterworths Scientific Publications, Ltd., London, 1956).

[19] K. D. Bowers and J. Owen, Repts. Progr. in Phys. **18**, 304 (1955).

($\approx$75 gauss) with no hfs at both room temperature and 77°K. (The spectrum in 96% H_2SO_4 is similar to the plain CuPc in H_2SO_4.) A plausible explanation for this spectrum is that the H_2O approaches the copper along the z axis and the crystal field becomes tetragonal (distorted cubic). The A_{1g} level is now a fairly low-lying excited state and the hydrated TSCP can relax quickly through a spin-orbit mechanism; this gives rise to line broadening and the hyperfine structure is obscured.[20,21] No copper hyperfine structure has been reported in aqueous copper solutions,[21] presumably for the same reason. TSCP in H_2SO_4 gives rise to sharp lines with hyperfine structure; presumably the H_2SO_4 does not interact strongly with the d_{z^2} orbital of the copper.

The interpretation of the results on TSCP in H_2O are supported by the work on copper Tutton salts.[19] Crystals of the Cu Tutton salts give rather broad ESR lines at room temperature but these lines sharpen and the hfs becomes evident at low temperatures.[19] This again is probably due to the fact that the crystal field is that of a distorted cubic field, the d_{z^2} level lies rather close to the $d_{x^2-y^2}$ level, and the spins relax rather rapidly through modulated spin-orbit interactions. This mode of relaxation is reduced at low temperatures.

If the square symmetry does not exist in the plane, instead of $g_\perp$, one must write g_x and g_y where $g_x \neq g_y$ (g_x, g_y, and g_z are the three components of a diagonalized tensor). Furthermore, instead of B, one must write B_x and B_y where $B_x \neq B_y$ (B_x, B_y, and A are the three components of a tensor; this tensor cannot necessarily be diagonalized simultaneously with the diagonalization of the g tensor but the off-diagonal elements are small and have not been detected as yet[22]). Differences between g_x and g_y and between B_x and B_y have been determined[19] but for the cases listed in Table I, no such differences were noted within the experimental error. It is noteworthy that Maki and McGarvey[4] in their work on the salicylaldehyde-imine did not detect such differences since they worked with single crystals and the ligand structure

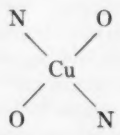

is not obviously square symmetric.

Throughout this discussion, it has been assumed that the B_{1g} level is lowest in energy. It is unlikely that the E_g levels could be the ground state since these orbitals have no appreciable σ character and therefore would probably not give enough electron density at the nitrogen nucleus to account for the nitrogen hyperfine structure. The A_{1g} orbital has some σ character but use of this orbital would predict that $g_{||}$ would be 2, which is not the case. The B_{2g} orbital could be the ground state but again this seems unlikely since the nitrogen hfs is so pronounced and B_{2g} contributes no s character at the nitrogen nucleus. Therefore, the B_{1g} orbital is taken as the ground state since it would be expected to give the largest electron density at the ligands. Further, placing of the unpaired electron in this orbital is in agreement with the modern ligand-field theory.[23] The 4s and 4p can also be ruled out on the basis that the use of these orbitals would predict that $g_{||}=2$. In particular, use of the 4p_z orbital, as in the valence-bond theory, for the ground state would be in error; it is for this reason that the valence-bond theory is not satisfactory for the interpretation of the ESR results. Furthermore, the 4s and 4p states do not in second order contribute to the magnetic parameters.

INTERRELATION OF MAGNETIC PARAMETERS

As the coefficients α and β decrease the bonds become more "covalent," $g_{||}$ and $g_\perp$ decrease and A and B increase. It must also follow that $g_0=(g_{||}+2g_\perp)/3$ decreases and $a=(A+2B)/3$ increases with increasing "covalency." Because $g_{||}-2>g_\perp-2$ and β_1 varies more than β, we expect $\Delta g=g_{||}-g_\perp$ to follow the trend of $g_{||}$. Similarly $b=A-B$ should follow the same trend as A. The most sensitive of these functions appears to be $g_{||}$; consequently, it will be chosen as the best indication of "covalent" character. From Table I it can be seen that compounds considered to be covalent, such as the phthalocyanine and etioporphyrin complexes, have lower values of $g_{||}$ than do the "ionic" oxalate and citrate complexes. A number of the more precisely determined and significant magnetic parameters are plotted against $g_{||}$ in Fig. 3. This figure may be useful in correlating the magnetic properties with the bonding character.

All the magnetic parameters can be obtained from studies on single crystals and often by means of investigations on polycrystalline samples; a and g_0 can be obtained directly from studies of solutions in liquids of low viscosity.[22] The Δg and b can be obtained, in principle, from a careful analysis of the line shapes obtained in low viscosity liquids.[22]

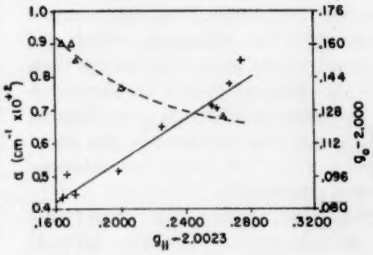

FIG. 3. Plots of a and g_0 vs $g_{||}$; Δ represents a, + represents g_0.

[20] H. M. McConnell, J. Chem. Phys. **25,** 709 (1956).
[21] B. R. McGarvey, J. Phys. Chem. **61,** 1232 (1957).
[22] D. Kivelson, J. Chem. Phys. **33,** 1094 (1960).
[23] J. S. Griffith and L. E. Orgel, Quart. Revs. (London) **11,** 386 (1957).

The compounds *bis*-*N*-methylsalicylaldehydeimine Cu(II), called MSAI, and *bis*-*N*-*t*-butylsalicylaldehydeimine Cu(II), called *t*-BSAI, were studied in benzene solution. Here $g_0=2.116$ and 2.127 for MSAI and *t*-BSAI, respectively, while $a=0.075$ cm^{-1} and 0.042 cm^{-1} for MSAI and *t*-BSAI, respectively. It can be seen from Fig. 3 that the values of these two parameters for MSAI correlate well with a value of about 2.21 for $g_{||}$. The correlation for *t*-BSAI is less satisfactory and, furthermore, the a curve is not yet determined in the region near 0.04 cm^{-1}. The construction of curves similar to those in Fig. 3 should be useful in predicting unmeasured magnetic parameters and relating them to the "covalent" character of the bonds.

ACKNOWLEDGMENTS

We wish to thank Fred Bauer and Dr. William Drinkard for supplying the samples of MSAI and *t*-BSAI. We would also like to express our appreciation to the National Science Foundation and the Research Corporation for their generous financial assistance throughout this work. Thanks are also due to Donald Myers and Dennis Silverman for carrying out some of the computations. We are grateful to Professor B. McGarvey for his useful comments and for pointing out a critical error in our evaluation of $T(n)$, an error which affected all our numerical results.

Note added in proof: Interesting results may be obtained if one investigates the relationship between β^2, $g_\perp$, and ΔE_{xz}. Maki and McGarvey[4] estimate $\Delta E_{xz}\approx 1.5\ \Delta E_{xy}$ to $1.6\ \Delta E_{xy}$ for *bis*-acetylacetonate Cu(II) and *bis*-salicylaldehyde-imine Cu(II). A choice of $\Delta E_{xz}=1.6\ \Delta E_{xy}$ yields $\beta^2=0.98$ for *bis*-salicylaldehyde-imine Cu(II) and $\beta^2=0.93$ for copper phthalocyanine; for all the other compounds in Table I $\Delta E_{yz}=1.6\Delta E_{xy}$ yields $\beta^2>1$, an unrealistic result. In Table III, β^2 has been taken equal to unity, $g_\perp$ has been combined with the values of α, β_1, and ΔE_{xy} given in Table I, and the ratio $\Delta E_{xz}/\Delta E_{yz}$ has been calculated for several compounds. It is interesting to note that for those compounds for which one generally assumes "strong covalent bonds," $\Delta E_{xz}/\Delta E_{yz}$ is large; for those compounds for which one does not assume "strong covalent bonds," $\Delta E_{xz}/\Delta E_{yz}\approx 1$, a condition characteristic of molecules with cubic rather than square planar symmetry. Note that a 20% error in ΔE_{yz} results in a 5% error in β^2. It would be interesting to check these predicted values of ΔE_{xz} by means of optical spectroscopy.

TABLE III. Ratio of Crystal Field Splittings: g, ΔE_{xy}, α, and β_1 are taken from Table I; $\beta^2=1$.

Copper Complex	$\Delta E_{xz}/\Delta E_{xy}$
Acetylacetonate	1.54
Salicylaldehyde-imine	1.67
Phthalocyanine[a]	1.68
Phthalocyanine[b]	1.78
Laccase	0.97
Ceruloplasmin	0.80
Denatured Laccase	1.51
Denatured Ceruloplasmin	1.44
Histidine	1.29
Imidazole	1.27
2–2′ Dipyridyl	1.06
1–10 Phenanthroline	0.89
Oxalate	1.15
EDTA	1.10
Citrate	1.07
Etioporphyrin II	1.14
t-Phenylporphin	1.51

[a] This work.
[b] Reference 4.

ESR Line Shapes in Glasses of Copper Complexes* †

ROBERT NEIMAN‡ AND DANIEL KIVELSON

Department of Chemistry, University of California, Los Angeles 24, California

(Received December 12, 1960)

The study by Sands of ESR line shapes of polycrystalline copper complexes has been extended and various "anomalies" discovered in the line shapes. The spectrum of copper phthalocyanine dissolved in concentrated H_2SO_4 has been studied at 77°K. The $M=-\frac{3}{2}$ hyperfine line has a behavior very different from that discussed by Sands. Isotropic extra hyperfine structure, arising from the presence of the ligand nitrogens, is easily discernible even in the glass.

INTRODUCTION

THE spectra of transition metal complexes in glasses and in magnetically dilute polycrystalline samples have been discussed by Sands[1] and others.[2,3] Although the magnetic parameters are very anisotropic the spectra often exhibit definite hyperfine structure in a glass. We have found that a frozen solution of dilute copper phthalocyanine in concentrated H_2SO_4 exhibits both the copper hyperfine structure and the extra hyperfine structure arising from the interaction of the unpaired electron with the nitrogen nuclei. (See Fig. 1). This spectrum has several anomalies and will be discussed in detail in the following sections.

In the preceding article[4] it was shown that the appropriate spin-Hamiltonian for a square-planar Cu(II) complex is

$$\mathcal{H}=\beta_0[g_{||}H_z\mathbf{S}_z+g_\perp(H_x\mathbf{S}_x+H_y\mathbf{S}_y)]+A\mathbf{S}_z\mathbf{I}_z +B(\mathbf{S}_x\mathbf{I}_x+\mathbf{S}_y\mathbf{I}_y), \quad (1)$$

where β_0 = Bohr magneton; $g_{||}$ and $g_\perp$ are the spectroscopic splitting factors parallel and perpendicular, respectively, to the symmetry axis (the z axis for square-planar complexes) of the molecule; $H_{x,y,z}$ are the components of the magnetic intensity vector; $\mathbf{S}$ and $\mathbf{I}$ are the electron and nuclear spin operators, respectively; and A and B are the hyperfine splitting constants for the copper nucleus. Quadrupole terms and terms arising from the interaction of the applied field with the nuclear spin will be neglected. Hyperfine splittings from the ligands surrounding the copper atom will be considered later.

Bleaney[5] and others[1,6] have shown that the ESR energy $h\nu_0$ corresponding to the Hamiltonian in Eq. (1) (for the case of a perfectly rigid medium) can be written as

$$h\nu_0=g\beta_0H+M_I(A^2g_{||}^2\cos^2\xi+B^2g_\perp^2\sin^2\xi)^{\frac{1}{2}}g^{-1}, \quad (2)$$

where

$$g=(g_{||}^2\cos^2\xi+g_\perp^2\sin^2\xi)^{\frac{1}{2}}, \quad (3)$$

M_I is the nuclear-spin quantum number of the copper atom ($M_I=\pm\frac{1}{2}, \pm\frac{3}{2}$), H is the applied magnetic field, and ξ is the angle between the symmetry axis of the molecule and the applied magnetic field H.

In a magnetically dilute single crystal it is seen that the field H for which resonance occurs at a frequency ν_0 is dependent upon the angle ξ. In polycrystalline or amorphous substances the molecules are randomly oriented and the spectrum is the sum of the resonances of molecules in all orientations; it is this spectrum that will be considered below.

EXPERIMENTAL

An electron-spin-resonance spectrometer operating at about 9 kMc and employing 5000 cps field modulation was used in this work. The spectrometer was equipped with a Varian V-4531 ceramic cavity; this permitted operations at temperatures ranging from 77°–400°K. For some of the work an internally plated Plexiglas cavity was used. Field measurements were made by calibrating the magnetic sweep with diphenyl picryl hydrazyl and a manganese phosphor. The copper phthalocyanine was prepared by the method of Linstead[7] and was sublimed in vacuo.

LINE SHAPE FOR GLASSES

In a polycrystalline sample, all orientations of the crystal field symmetry axis are equally probable; therefore, the number of molecules (dN) whose symmetry axis forms an angle, with respect to the applied magnetic field, between ξ and $\xi+d\xi$ is given by[1]

$$dN=N_0/2\sin\xi d\xi, \quad (4)$$

where N_0 is the total number of molecules.

* Supported in part by the National Science Foundation and the Research Corporation.

† Presented at the American Chemical Society Symposium on Molecular Structure, University of Washington, Seattle, Washington, June 1960.

‡ Present address: Central Research and Engineering, Texas Instruments Inc., Dallas, Texas.

[1] R. H. Sands, Phys. Rev. **99**, 1222 (1955).

[2] B. G. Malmstrom and T. Vanngard, J. Mol. Biol. **2**, 118 (1960).

[3] E. M. Roberts and W. S. Koski, J. Am. Chem. Soc. **82**, 3006 (1960).

[4] D. Kivelson and R. Neiman, J. Chem. Phys. **35**, 149 (1961).

[5] B. Bleaney, Phil. Mag. **42**, 441 (1951).

[6] A. Abragam and M. H. L. Pryce, Proc. Roy. Soc. (London) **A205**, 135 (1951).

[7] P. A. Barrett, C. E. Dent, and R. P. Linstead, J. Chem. Soc. **1936**, 1719.

FIG. 1. Derivative spectrum of 0.05M CuPc in fuming H_2SO_4 at 77°K.

The transition probability is approximately independent of orientation and the absorption intensity arising from the molecules lying between ξ and $\xi+d\xi$ is, therefore, proportional to the number dN lying between these angles. The intensity of the absorption in a range of magnetic field between H and $H+dH$ is proportional to $|dN/dH|$, where

$$|dN/dH| = (dN/d\xi)\,|d\xi/dH|. \tag{5}$$

$dN/d\xi$ is given by Eq. (4); $d\xi/dH$ will be discussed in the following paragraphs.

The case of no nuclear spin will be considered first, i.e., $M_I=0$. The microwave frequency will be assumed to be maintained at a constant frequency ν_0 and the magnetic field will be varied. In this case, Eq. (3) yields

$$H=(h\nu_0/\beta_0)\,(g_{\|}^2\cos^2\xi+g_{\perp}^2\sin^2\xi)^{-\frac{1}{2}}. \tag{6}$$

Note that at $\xi=0$ and $\xi=\pi/2$, H takes on its extreme values $h\nu_0/g_{\|}\beta_0$ and $h\nu_0/g_{\perp}\beta_0$, respectively.

An expression for dN/dH as a function of H may be obtained with the aid of Eq. (2)–(6), together with the elimination of the angle ξ. This expression is

$$dN/dH=(N_0/2)\,(g_0^2H_0^2/H^3)\times\{(g_{\|}^2-g_{\perp}^2)[(g_0H_0/H)^2-g_{\perp}^2]\}^{-\frac{1}{2}}, \tag{7}$$

where

$$H_0=h\nu_0/g_0\beta_0 \tag{8}$$

$$g_0=(g_{\|}+2g_{\perp})/3. \tag{8a}$$

Sands[1] was the first to obtain this relation and to establish its validity. The denominator of Eq. (7) approaches zero as $(g_0H_0/H)^2$ becomes equal to $g_{\perp}^2$; this means that the absorption becomes very large as $\xi\to\pi/2$. Of course, the singularity at $\xi=\pi/2$ is not real because intermolecular dipolar interactions and other line-broadening mechanisms will tend to modify the theoretical curve and bring it into line with the experimental one. The derivative spectrum is proportional to $d(dN/dH)/dH$; this second derivative has a singularity at both extreme values of H corresponding to $\xi=0$ and $\xi=\pi/2$. Therefore one would expect to see a weak "derivative line" at $H=(h\nu_0/g_{\|}\beta_0)\,(\xi=0)$ and a strong one at $H=(h\nu_0/g_{\perp}\beta_0)\,(\xi=\pi/2)$. This will be discussed in some detail later.

One may now turn to the case for which $M_I\neq 0$; H is given by the relation

$$H=g_0H_0/g-M_IK/\beta_0g^2, \tag{9}$$

where

$$K=(g_{\|}^2A^2\cos^2\xi+g_{\perp}^2B^2\sin^2\xi)^{\frac{1}{2}}. \tag{10}$$

The expression for dN/dH is

$$dN/dH=\tfrac{1}{2}N_0\left\{\frac{2\cos\xi}{g^2}\left[\frac{(g_{\|}^2-g_{\perp}^2)g_0H_0}{2g}+\frac{M_I}{\beta_0}\left(\frac{g_{\|}^2A^2-g_{\perp}^2B^2}{2K}-\frac{K(g_{\|}^2-g_{\perp}^2)}{g^2}\right)\right]\right\}^{-1}. \tag{11}$$

In contrast to the expression in Eq. (7), the angle ξ cannot be explicitly eliminated from this expression for dN/dH. One must, therefore, obtain both H and dN/dH as functions of ξ.

The limits of ξ are zero to π; but since H is a function of $\cos^2\xi$ and $|dN/d\xi|$ of $|\cos\xi|$, ξ can be restricted to the range zero to $\pi/2$ provided the right-hand side of Eq. (11) is multiplied by 2, i.e., one is interested in values of ξ ranging from those parallel to the symmetry axis to those perpendicular to the symmetry axis. For those extreme values of ξ

$$H(\xi=0)=(g_0H_0/g_{\|})-(M_IA/\beta_0g_{\|}) \tag{12}$$

$$H(\xi=\pi/2)=(g_0H_0/g_{\perp})-(M_IB/\beta_0g_{\perp}). \tag{12a}$$

$dN/dH\to\infty$ at $\xi=\pi/2$. Note that for $\xi=0$, the onset of absorption is very sudden and also that for $\xi=\pi/2$ the theoretical absorption becomes infinite. This implies that the second derivative $d(dN/dH)/dH$ again has a singularity at both $\xi=0$ and $\xi=\pi/2$, and that the derivative spectrum has a weak line at $H(0)$ and a strong one at $H(\pi/2)$.

Since $M_I=\pm\frac{1}{2}, \pm\frac{3}{2}$ for Cu nuclei, this picture would predict, in the absence of any overlap, four weak "derivative lines" of different intensity separated by a spacing A and four stronger "derivative lines," also of varying intensity separated by a spacing B. This is the model used by Sands[1] and others[2,3,8] and it is illustrated in the article by Sands.[1]

[8] D. E. O'Reilly, J. Chem. Phys. **29**, 1188 (1958).

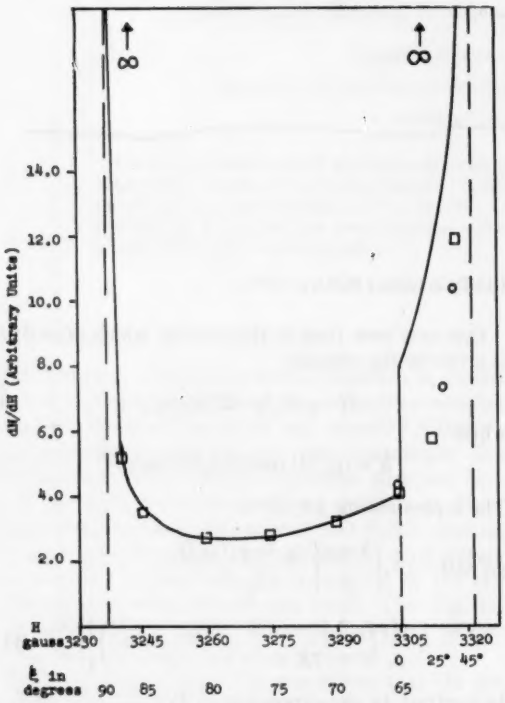

FIG. 2. Theoretical absorption curve for $M=-\frac{3}{2}$ line for CuPc ○ represents H values for 0–45°; □ represents H values for 45°–90°.

However, a careful analysis of Eqs. (10) and (12) shows that for certain interrelationships of the parameters the problem is more complicated; H does not vary monotonically with ξ and dN/dH has an additional singularity for $0<\xi<\pi/2$. Such a condition applies for some of the lines in copper phthalocyanine. The theoretical absorption curve, including only the effects of intramolecular anisotropy, for the $M_I=-\frac{3}{2}$ ESR transition of copper phthalocyanine ($A=0.0202$ cm^{-1}, $B=0.003$ cm^{-1}, $g_{\|}=2.174$, $g_{\perp}=2.045$) is given in Fig. 2. In this figure the intensity (in arbitrary units) is plotted against both H and ξ; it is seen that an absorption maximum occurs at the maximum H corresponding to $\xi\approx\pi/4$ and another occurs at the minimum H ($H=$ 3239 gauss), corresponding to $\xi=\pi/2$. The spacing between the peaks is not given by any simple interrelationship between the magnetic parameters; this will be discussed later. An approximate sketch of the derivative of the absorption is also given in Fig. 3; a third weaker derivative line is observed at an intermediate H ($H=3302$ gauss) which corresponds to $\xi=0$.

NITROGEN HYPERFINE STRUCTURE

The nitrogen ligands attached to the copper in copper phthalocyanine can interact with the unpaired electrons and give rise to extra hyperfine structure. (See the preceding article.[4]) This interaction, as shown below, is relatively isotropic. There are four neighboring nitrogens, each with spin=1; this yields a relative intensity ratio 1:4:10:16:19:16:10:4:1. The predicted spectrum is, therefore, just a superposition of the spectra for each of the nine values of M_I, (-4 to 4).

The experimental derivative spectrum, of copper phthalocyanine in H_2SO_4 is given in Fig. 1. At low field the two "weak" lines corresponding to $M_{Cu}=\frac{3}{2}, \frac{1}{2}$ are observed; these lines are split further by the interactions with the nitrogen nuclei. The weak lines corresponding to $M_{Cu}=-\frac{1}{2}, -\frac{3}{2}$ are obscured by the "stronger" lines that overlap. The nitrogen extra hyperfine structure is readily observed in the higher field part of the spectrum. The cluster of hyperfine lines at the high-field side correspond to the $M_{Cu}=-\frac{3}{2}$ line already discussed; the major peaks in the central region correspond to the $M_{Cu}=-\frac{1}{2}$ "strong" line and possibly the $\xi=\pi/2$ contribution from the $M_{Cu}=-\frac{3}{2}$ line.

Measurements on the extra hyperfine splitting on the low field ($\xi=0$) contributions to the spectrum show that they are approximately equal to the high-field ($\xi=\pi/2$) contributions; this confirms the assumption of isotropy assumed above. The low-field splittings were about 14.3 gauss; the high-field splittings were about 14.6 gauss, this variation is probably within the experimental error (0.5 gauss). The apparent positions of the nitrogen extra hyperfine lines will vary somewhat for each copper hyperfine line because two abundant

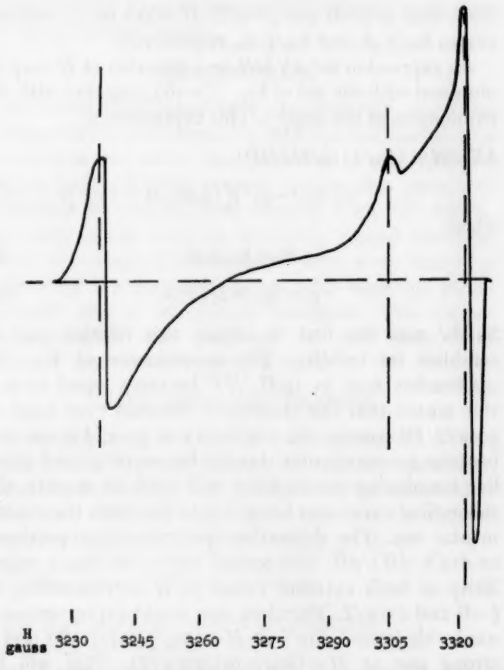

FIG. 3. Theoretical derivative spectrum for $M=-\frac{3}{2}$ line for CuPc (smoothed-out theoretical curve).

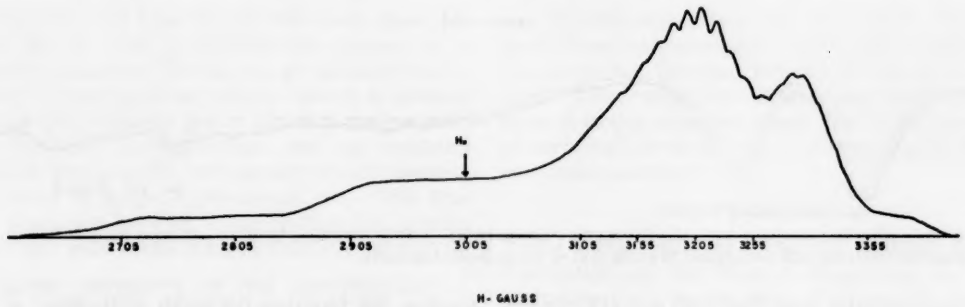

FIG. 4. Intensity (integrated) of 0.05M CuPc in fuming H_2SO_4 at 77°K.

isotopes of copper with slightly different magnetic moments are present, a phenomenon which will tend to broaden the lines and to shift the apparent peaks of the lines arising from both isotopes.

INTEGRATION OF THE DERIVATIVE SPECTRUM AND EVALUATION OF CONSTANTS

The derivative spectrum was detected experimentally since this type of presentation gives a much greater signal to noise ratio; the derivative is also more sensitive to details of hyperfine structure. However, it is easier to compare the absorption spectrum directly with that predicted from Eq. (11). The integrated spectrum of CuPc in H_2SO_4 at 77°K is shown in Fig. 4. It can be seen that the apparent resolution is much less in the absorption spectrum than in the derivative spectrum. The onset of two lines on the low-field side can easily be distinguished. The spacing ΔH_A between these lines is

$$A = |\Delta H_A|\beta_0 g_{||}. \tag{13}$$

We find that $g_{||}=2.174\pm0.004$ and $A=0.0202\pm 0.002$ cm^{-1}. This is in fairly good agreement with the values of Ingram,[9] obtained from a study of a single crystal of Zn Phthalocyanine with Cu Phthalocyanine impurities. The absolute sign of A cannot be determined experimentally; it is expected to be negative on theoretical grounds.[10] The values of $g_\perp$ and B could be determined in a similar way; however, the nature of the spectrum is such that these parameters are difficult to determine.

If one takes Ingrams[9] values for B and $g_\perp$ (0.003 cm^{-1} and 2.045, respectively), several interesting facets of the copper phthalocyanine spectra become evident. For the $M_{Cu}=\frac{3}{2}$ and $\frac{1}{2}$ lines, the low-field end of the absorption curve corresponds to $\xi=0$ and is given by Eq. (12). See Fig. 4. The high-field end for these two lines is given by Eq. (12a). The $M_{Cu}=-\frac{1}{2}$ line has the same low-field ($\xi=0$) behavior but its maximum field strength occurs for ξ slightly less than $\pi/2$, i.e., $\xi\approx 77°$. The intensity has a peak at this point as well as at $\xi=\pi/2$ and therefore one would expect two peaks on the order of Fig. 2; however, the two peaks are so close ($\Delta H\approx 3$ gauss) that they cannot be distinguished and the $M_{Cu}=-\frac{1}{2}$ line behaves similarly to the $M_{Cu}=\frac{3}{2}$ and $\frac{1}{2}$ lines. Note that H_{max} ($\xi=\pi/2$) $-H_{min}$ ($\xi=0$) decreases in the order $M_{Cu}=\frac{3}{2}$, $\frac{1}{2}$, $-\frac{1}{2}$, and that the intensity of the peaks increases in this order.

The $M_{Cu}=-\frac{3}{2}$ line is very anomalous. First of all $H(\xi=\pi/2)<H(\xi=0)$, a reversal from the "normal" order. Secondly, the intermediate peak ($\xi\approx\pi/4$) is easily discerned. This has been discussed above. (See Figs. 2 and 3).

In order to determine $g_\perp$, B, H, and dN/dH, a program was drawn up for the IBM 709 computer and Eqs. (10) and (12) were solved for different values of $g_{||}$, B, and $g_\perp$ as functions of ξ. (A was held constant at 0.0202 cm^{-1}). Unfortunately, this procedure did not yield unambiguous values of $g_\perp$ and B; therefore, the values of Ingram[9] which are $g_\perp=2.045$ and $B=0.003$ cm^{-1} are taken as the most probable values for these quantities. Several points of interest did emerge from the computer results however. Figure 5 depicts the

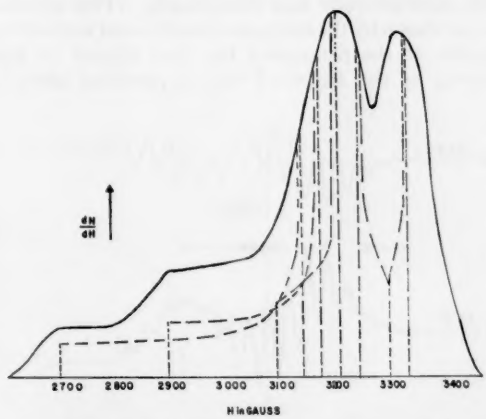

FIG. 5. Theoretical absorption spectrum (neglecting extra-hyperfine structure) for CuPc in H_2SO_4 at 77°K. – – – curves are $M_I=\pm\frac{1}{2}$, $\pm\frac{3}{2}$.

[9] J. F. Gibson, D. J. E. Ingram, and D. Schonland, Discussions Faraday Soc. **26,** 72 (1958).

[10] A. H. Maki and B. R. McGarvey, J. Chem. Phys. **29,** 35 (1958).

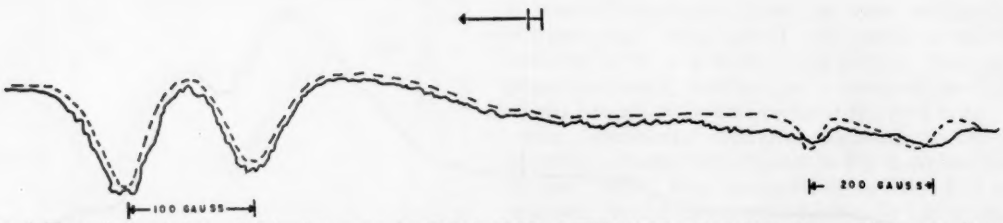

FIG. 6. Theoretical and observed derivative spectra for CuPc in H_2SO_4 at 77°K. (All lines included—nitrogen hfs is omitted); solid line is observed spectrum with modulation 10 gauss, dotted line is theoretical curve.

four curves resulting from Eqs. (10) and (12) for the values of $g_{||}$, $g_\perp$, A and B mentioned above. Note that the most intense absorption (the cut-off point was selected at $\xi=88°$ so that the values of H were within 0.5 gauss of the point where the absorption would theoretically be infinite) seems to occur for $M_{Cu}=-\frac{1}{2}$ and that the $M_{Cu}=-\frac{3}{2}$ curve is rather a lopsided U-shape (see Fig. 2). In fact, for the latter curve, the most intense absorption seems to occur at about $\xi=\pi/4$ and $H=3320$ gauss, which is above the value of H at $\xi=0$. This discontinuity for the $M_{Cu}=-\frac{3}{2}$ line means that $g_\perp$ and B are particularly hard to determine with any accuracy. The four curves of Fig. 5 were then added to give the total absorption; allowance was made for the fact that the lines have a finite width. The recent work of Blinder[11] has shown that the maximum values of the peaked lines, as represented by Eq. (11) and Figs. 2 and 5, may be shifted somewhat when allowance is made for a finite linewidth (Gaussian or Lorentzian). Therefore, in principle, a computer program should be drawn up so that each individual dN/dH [as obtained from Eq. (11) for each value of ξ] would be allowed to have a definite width and shape instead of the infinitely sharp line assumed here. The over-all absorption is in fairly good agreement with that obtained experimentally. See Figs. 4 and 5. Note also that the two intense high-field peaks are separated by about 100 gauss both experimentally and theoretically. (This separation, as shown by the computer results, is not a sensitive function of the parameters but does depend on the behavior of the $M_{Cu}=-\frac{3}{2}$ line as predicted above).

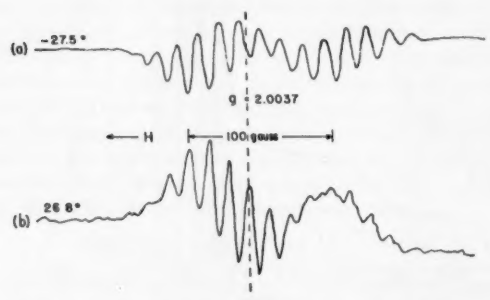

FIG. 7. Derivative spectrum of 0.05M CuPc in H_2SO_4 at (a) −27.5°C; (b) room temperature.

[11] S. Blinder, J. Chem. Phys. **33,** 748 (1960).

Further, the fact that the width (100 gauss) of the peak where the $M_{Cu}=\frac{3}{2}$, $\frac{1}{2}$ and $-\frac{1}{2}$ lines, respectively, overlap and give their most intense contributions ($\xi=\pi/2$) means that $B\approx 0.003$ cm^{-1}, which is also in agreement with the above values.

The theoretical derivative spectrum in which nitrogen extra hyperfine structure is neglected is comparable to the experimental spectrum in which the extra hyperfine structure is obliterated by large amplitude field modulation (compare Fig. 6).

COMPARISON OF THE "GLASS" METHOD WITH THE SINGLE-CRYSTAL METHOD

In order to obtain detailed information on the magnetic parameters of molecules, the paramagnetic molecules must be diluted in a diamagnetic environment. It is easiest to obtain detailed information from single crystals but it is not always easy to grow magnetically dilute single crystals. In order to do this one must find a diamagnetic substance which is isomorphic to the paramagnetic material under investigation, and grow crystals of this paramagnetic material with some sites replaced by the paramagnetic molecules. This is often a difficult task.

A polycrystalline sample or a "glass" can also be analyzed so as to yield almost as much information as a single crystal. This has been done above. It is usually much easier to make a glass dilute in paramagnetic centers than it is to grow suitable crystals. As observed above, a solution of copper phthalocyanine in concentrated H_2SO_4 can be frozen into a glass.

Although one cannot usually extract as much information from liquid solutions, they are easier to obtain. They have been discussed elsewhere.[12,13]

It should be noted that the magnetic parameters depend upon the interaction between the paramagnetic molecule and its neighbors. It is possible that CuPc has slightly different magnetic properties in ZnPc than in H_2SO_4.[4,9] Although ordinary CuPc is water insoluble, the tetra-sulfonated compound (TSCP) is water soluble. The spectrum of a dilute solution of TSCP in H_2O is entirely different from that of TSCP in H_2SO_4; this difference is due to a change in molecular parameters and was discussed in the preceding article.[4]

[12] H. M. McConnell, J. Chem. Phys. **25,** 709 (1956).
[13] D. Kivelson, J. Chem. Phys. **33,** 1094 (1960).

Finally, it should be remembered that a glass may differ slightly from a polycrystalline sample in its magnetic properties. The analysis given above is actually for a polycrystalline sample since it is assumed that all the molecules are in identical environments but that the microcrystalline axes are randomly oriented. In a glass the environment of each molecule, and hence its magnetic parameters, may differ from that of another; however, it appears that this variation is not very great in the substance under consideration.

SOME COMMENTS ON THE TEMPERATURE BEHAVIOR OF THE CuPc SPECTRA

The spectra of CuPc in fuming H_2SO_4 at various temperatures are shown in Fig. 7. Concentrated H_2SO_4 is very viscous: $\eta \approx 0.2$ poise at 20°C.[14] It is seen that, as the temperature increases from 77°K, the resolution of the two groups of high-field lines becomes reversed; the lower set of lines is better resolved at low temperatures and the higher set of lines is better resolved at high temperatures until finally all resolution of the nitrogen hyperfine structure is lost about 80°C. This behavior is probably a reflection of the onset of motion in the system but the exact behavior is difficult to analyze.[4,13] The averaging effect that takes place with the onset of motion is further complicated by the presence of two isotopic species of copper with two slightly different nuclear moments.

[14] J. Perry, *Chemical Engineers Handbook* (McGraw-Hill Book Company, Inc., New York, 1950).

ACKNOWLEDGMENTS

The authors wish to thank the National Science Foundation and the Research Corporation for their continuing financial assistance. They would also like to thank Donald Myers for setting up the computer program.

Note added in Proof. In the time since this manuscript was submitted three interesting articles have appeared on various aspects of the subject of spectra in polycrystalline media.[15–17]

[15] F. K. Kneubühl, J. Chem. Phys. **33,** 1074 (1960).
[16] H. Sternlicht, J. Chem. Phys. **33,** 1128 (1960).
[17] E. L. Cochran, F. J. Adrian, and V. A. Bowers, J. Chem. Phys. **34,** 1161 (1961).

ESR Spectra of Solid Phthalocyanines* †

ROBERT NEIMAN‡ AND DANIEL KIVELSON

Department of Chemistry, University of California, Los Angeles 24, California

(Received December 12, 1960)

Phthalocyanine complexes of paramagnetic metal ions show ESR spectra characteristic of the metals; phthalocyanine complexes of diamagnetic metal ions show strong single ESR lines characteristic of free radicals. The source of this latter resonance is not understood. Intimate molecular mixtures of "paramagnetic" copper and "dimagnetic" zinc phthalocyanines exhibit exchange between the copper unpaired electron and the "free radical" electron in the zinc phthalocyanine. Nickel and zinc phthalocyanine also exhibit a single sharp resonance in dilute solutions of concentrated sulfuric acid.

INTRODUCTION

IN a preceding article,[1] the electron spin resonance of copper phthalocyanine (CuPc) was studied in some detail. We wish to discuss here some results obtained from ESR studies of other metal phthalocyaninces. The central metal may have unpaired electrons (this will be designated as a paramagnetic phthalocyanine) or it may have no unpaired electrons (this will be designated as a diamagnetic phthalocyanine).

EXPERIMENTAL

The phthalocyanines were prepared by the methods of Linstead and co-workers[2]; the two methods employed were: (a) preparation using phthalonitrile and the corresponding metal or metal salt and (b) preparation using phthalic acid, urea, and the appropriate metal or metal salt. The crude phthalocyanines were precipitated from sulfuric acid, extracted with dimethylformamide for 48 hr, and sublimed under high vacuum. The magnetic resonance spectra were taken with a conventional X-band spectrometer using phase-sensitive detection. Concentrated sulfuric acid was used as the solvent for the solution spectra of the phthalocyanines.

RESULTS ON OTHER PHTHALOCYANINES

Paramagnetic Phthalocyanines

Several paramagnetic phthalocyanines, i.e., those whose central metal atom has one or more unpaired electrons, were studies both in sulfuric acid and in the polycrystalline solid. In the polycrystalline state CuPc gave rise to a single, relatively broad ESR line. This line can be explained as the sum of the contributions from all orientations of the molecule (see the preceding article), where the hyperfine structure has been obscured by electron-electron dipolar interactions and exchange; these two latter effects are not observed in the diluted H_2SO_4 solutions discussed previously, because the unpaired electrons are more widely separated in the solutions. Cobalt phthalocyanine CoPc gave only a very broad line in the solid ($\approx$600 gauss); in sulfuric acid, the spectrum was also a very broad line with no evidence of hyperfine splitting, either from the Co nucleus ($I=\frac{7}{2}$) or from the surrounding nitrogens. The fact that a resonance is observed in CoPc at room temperature is unusual since the relaxation through spin-orbit interactions is usually very rapid in Co complexes and the line broadened beyond recognition. The lowered relaxation time in CoPc is probably due to the strong covalent bonding in the compound.[3] Cr(III) phthalocyanine also gave a single line both in the solid and in H_2SO_4 solutions. The line in the solid was rather broad ($\approx$300 gauss); the line in solution was about 100 gauss wide at room temperature but sharpened to about 20 gauss at 77°K. Again no nitrogen hyperfine structure was observed [the nuclear spin of the most abundant (90%) isotope, Cr^{52}, is zero]. The absence of nitrogen hfs in CrPc might indicate that it is less covalently bonded than CuPc. However, no analysis has been made of the bonding in chromium phthalocyanine and it is difficult to tell whether or not one would expect hfs even if it were strongly covalently bonded. Singer[4] has examined the trichelate complex, *tris*-ethylenediamine $Cr(III)(SO_4)_3$, and finds no splitting from the nitrogens. Neither Fe(II) phthalocyanine or Fe(III) phthalocyanine gave a detectable resonance either at room temperature or 77°K. This is probably due to rapid spin-orbit relaxation mechanism.

Diamagnetic Phthalocyanines

ZnPc, NiPc, Al(III)Pc, Sn(II)Pc, Na_2Pc, and the free Pc were also prepared. All of these compounds are "diamagnetic," i.e., their central metal atoms have no unpaired electrons. Most of these were prepared by the phthalonitrile method, although some were prepared

* Presented at the American Chemical Society Symposium on Molecular Structure, University of Washington, Seattle, Washington, June, 1960.

† Supported in part by the National Science Foundation and the Research Corporation.

‡ Present address: Central Research and Engineering, Texas Instruments Inc., Dallas, Texas.

[1] R. Neiman and D. Kivelson, J. Chem. Phys. **35,** 156 (1961) (preceding paper).

[2] P. A. Barrett, C. E. Dent, and R. P. Linstead, J. Chem. Soc. **1936,** 1719.

[3] J. F. Gibson, D. J. E. Ingram, and D. Schonland, Discussions Faraday Soc. **26,** 72 (1958).

[4] L. Singer, J. Chem. Phys. **23,** 379 (1955).

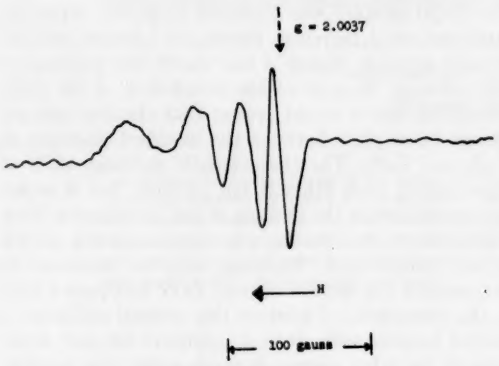

FIG. 1. Derivative spectrum of Sn(II)Pc, sublimed solid.

by the phthalic acid method. All of these compounds in the solid state, however, showed a strong resonance line (about 10 gauss wide) at about the g value of the free electron; no hyperfine structure was observed except for Sn(II)Pc. These results are somewhat surprising since these phthalocyanines should have no paramagnetic character whatsoever. Ingram[5] was the first to notice this behavior; he attributed this "free radical" behavior to a charring which takes place in the preparation of the phthalocyanines.

In all of the "diamagnetic" samples, a single line was observed except in the case of Sn(II) which gave four lines (see Fig. 1). Further the relative integrated intensities differed widely from compound to compound (see Table I); these intensities are not exact since washing the samples with H_2SO_4 would reduce the signal strength; these measurements were done on samples treated alike as far as possible.

If the resonances are due to impurities, charred carbon, or adsorbed oxygen, it would seem that sublimation at 500°C would remove the paramagnetism; however, repeated sublimations under vacuum failed to remove the "free-radical"; in fact, sublimation under O_2, N_2, or vacuum gave the same results. The polycrystalline, and in some cases crystalline, material was, however, exposed to the air during the transfer from the sublimer to the sample holder, and no attempt was made to protect the sample from O_2. However, this exposure to the air, as discussed below, did not seem to effect the "paramagnetic" phthalocyanines and it seems unlikely that adsorbed O_2 on the crystal surfaces would account for such intense lines as that observed in NiPc ($\frac{1}{3}$ free radicals). It was also thought that a charge-transfer complex might be formed with phthalonitrile since Calvin[6] has shown that an ESR spectrum can result from a mixture of tetra-chloro-ortho-semi-quinone and free Pc. Some free Pc was therefore "doped" with phthalonitrile but no change was observed in the ESR of the free phthalocyanine; this result should rule out the charge-transfer concept. Furthermore, sublimation should also destroy any complex present.

TABLE I.

Compound	Intensity (relative to NiPc=1) of solid
DPPH (solid)	3.0
ZnPc	0.06
Free Pc	0.5
Na_2Pc	0.07
AlPc	0.03
NiPc	1.0

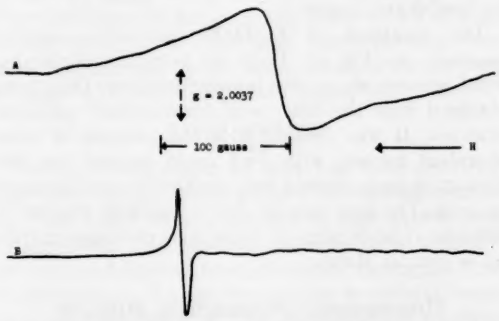

FIG. 2. Cu+Zn phthalocyanine solids: A, CuPc solid (sublimed); B, ZnPc solid (sublimed).

It should be mentioned that Ingram[5] apparently was able to eliminate this paramagnetism but we have been unable to do so; perhaps it is due to an impurity of which one is not aware and which cannot be separated, or perhaps it is due to charred material which is formed and carried over during the sublimation.

The "diamagnetic" phthalocyanines were dissolved in H_2SO_4 and those which were stable (all except SnPc) were studied. No lines were observed except for the Zn and Ni complexes, each of which yielded an intense (the absolute intensities are difficult to measure in H_2SO_4, it is estimated that the fresh solutions of ZnPc and NiPc are about 5 to 10% free radical) single line about 10 gauss wide at a g value of about 2.003; these lines decayed with a half-life of about 12 hr. Although the lack of hfs in the solids could be rationalized by assuming that exchange effects "narrowed" the lines, in dilute solutions one would expect exchange effects to be negligible.[7] The abundant species of both Zn and Ni do not have nuclear spin but one would expect the nitrogens to give rise to hfs. No hfs was observed down

[5] J. E. Bennett, D. J. E. Ingram, and J. G. Tapley, *Defects in Crystalline Solids* (The Physical Society, London, 1955).

[6] D. R. Kearns, G. Tollin, and M. Calvin, J. Chem. Phys. **32**, 1020 (1960).

[7] D. Kivelson, J. Chem. Phys. **33**, 1094 (1960).

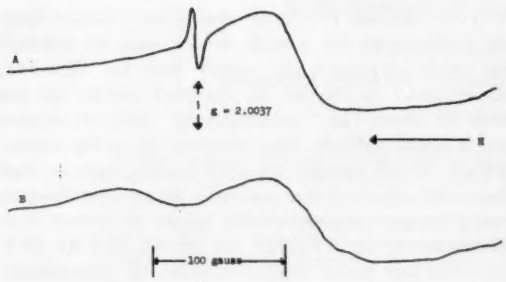

FIG. 3. CuPc—ZnPc mixtures: A, ZnPc—CuPc solid (mechanically mixed); B, ZnPc—CuPc solid (mixed and reprecipitated from H_2SO_4).

to a concentration of about 0.001 M. The origin of these ZnPc and NiPc "radicals" is not understood but may be related to the formation of positive ions studied by Taube[8] and Ingram.[9]

The spectrum of Sn(II)Pc represents another anomaly (see Fig. 1). There are four lines of varying width present; the g value is somewhat lower than those obtained from the other solid "free-radical" phthalocyanines. It was thought that the presence of some abundant nucleus with $I=\frac{3}{2}$ could account for this hfs but no such element was revealed by spectroscopic analysis. The lines may be due to electrons trapped in different crystals sites or perhaps to electrons in triplet or quartet states.

"Diamagnetic"-Paramagnetic Mixtures

The sharp "free-radical" lines were not observed in phthalocyanines containing paramagnetic metal ions. In order to study the effect of the paramagnetic metal ion on the "free-radical" electrons, the CuPc-ZnPc system was studied. Figure 2 shows the solid polycrystalline CuPc spectrum and the solid polycrystalline ZnPc spectrum. Figure 3 shows the spectrum of a mechanically mixed 50-50 ZnPc-CuPc sample; it is clearly a superposition of the two individual spectra. The 50-50 mixture was dissolved in H_2SO_4, reprecipitated and dried; therefore, forming an intimate mixture or solid solution. Figure 3 also shows the spectrum of this solution. Because of the broadening of the ZnPc absorption line it would appear that electron spin exchange takes place between the unpaired electrons on CuPc and ZnPc. The characteristic exchange shift[7] of lines toward each other is not obvious, but it is not easy to determine the position of two overlapping lines. Furthermore, the exchange phenomenon in this sample is very complicated. Exchange may be important in determining the spectra of pure ZnPc and pure CuPc; in the reprecipitated mixture this original exchange is altered because some nearest neighbors are now molecules of the other species. It is, therefore, also possible that the ZnPc line in the reprecipitated mixture is broadened because the exchange effect is decreased over that in pure ZnPc. Finally, if exchange of the unpaired electrons on ZnPc with those on CuPc are important, it should be noted that the ZnPc line lies below the $M=-\frac{3}{2}$ CuPc lines oriented perpendicularly to the applied field and above most of the other CuPc lines[1]; it is, therefore, not easy to predict the exchange-determined shifts in the lines.

The absence of the "free-radical" absorption in the paramagnetic phthalocyanines may arise from exchange of the type described above which would obscure the "free-radical" line. In the dilute H_2SO_4 solution of CuPc no evidence of such exchange exists as witnessed by the presence of detailed hfs. However, it is also true that the "free-radical" paramagnetism seems to vanish in the H_2SO_4 solutions of all the "diamagnetic" phthalocyanines with the exception of NiPc and ZnPc; the "free-radicals" might also vanish in the H_2SO_4 solutions of the "paramagnetic" phthalocyanines.

ACKNOWLEDGMENTS

The authors would like to thank Dr. William Drinkard for his valuable advice on the synthesis of the various phthalocyanines. They also wish to express their appreciation to the National Science Foundation and the Research Corporation for their continued financial assistance.

[8] A. Cahill and H. Taube, J. Am. Chem. Soc. **73,** 2847 (1951).
[9] M. J. Gentiles, P. George, D. J. E. Ingram, and J. E. Bennett, J. Am. Chem. Soc. **79,** 1870 (1957).

Ultraviolet Absorption Spectrum of Ammonia in Solid Argon at 4.2°K*

K. DRESSLER†

National Bureau of Standards, Washington, D. C.

(Received December 12, 1960)

A series of absorption bands in the region 1600 to 1900 A has been observed in thin films of solid argon containing between 0.3% and 3% of ammonia. The bands are attributed to isolated NH_3, and the absence of alternating bands in the observed vibrational progression shows that in the ground state only the $J=0$ level is appreciably populated. Thermal equilibration of NH_3 at 4.2°K involves the interconversion of nuclear spin species. It is suggested that the observed rapid equilibration is due to coupling between the proton spins and the spin of the nitrogen nucleus.

INTRODUCTION

ELECTRONIC absorption spectra of atoms and simple molecular species condensed in inert matrices at low temperatures have come under extensive investigation in recent years by Robinson and McCarty.[1] Such studies often lead to information on the perturbation of electronic, vibrational, and rotational structure of the trapped species by the matrix environment.[2] Dressler and Schnepp have investigated the Schumann-Runge absorption bands of oxygen,[3] condensed in matrices of solid argon and nitrogen at 4.2°K, and have shown that the vibrational structure of O_2 in these solids is very little perturbed except for states which involve exceptionally large amplitudes of molecular vibration.[4] Consequently, it was thought worthwhile to investigate the ultraviolet absorption spectrum of the ammonia molecule in similar solids, with the hope of obtaining information on the rotational degrees of freedom of this light molecule in the matrix cage.

The ultraviolet absorption spectrum of ammonia in pure solid phases shows no band structure and has been described elsewhere.[5] Attempts to observe a matrix spectrum corresponding to the discrete bands of NH_3 below 1700 A have remained unsuccessful. A recent reevaluation of the spectrograms which had been taken at the time in collaboration with Dr. O. Schnepp, revealed that a series of weak and diffuse bands appearing at longer wavelengths can be correlated with the diffuse bands of the longest wavelength absorption system of ammonia in the gas phase.[6] Although the matrix bands show no rotational structure, the observed intensity distribution leads to information on the population of the lowest energy levels of NH_3 at low temperature. Direct evidence for free or nearly free rotation of NH_3 in solid argon, on the other hand, has in the meantime been demonstrated by the observations of Hexter and Milligan in the infrared spectral region.[7]

EXPERIMENTAL

The apparatus employed here has been described elsewhere.[8] Ammonia was purified by vacuum distillation and mixed with argon gas of high purity in a storage flask. The gas was deposited onto a liquid-helium-cooled lithium fluoride window through a tube which was kept at room temperature to prevent freezing of the ammonia in it. Two additional LiF windows were used to separate the vacuum space of the helium cryostat from the light source and from the vacuum spectrograph. Absorption spectra were photographed with a 2-m vacuum spectrograph. A mildly condensed discharge through xenon gas at a pressure of 120 mm Hg served as a light source.[9] The plate density produced by this source was quite uniform in the region 1500 to 1900 A, whereas below 1470 A it was negligible. Since NH_3 is very efficiently photolyzed by light of wavelengths between 1550 and 1100 A,[10] the properties of the xenon continuum, contrary to those of the molecular hydrogen emission, are particularly well suited for an investigation of the absorption bands of NH_3 between 1500 and 1900 A.

RESULTS

Absorption spectra of solid solutions of ammonia in argon at a variety of concentrations are illustrated by densitometer tracings in Fig. 1. The solid obtained

* Part of this work was supported by the Office of Ordnance Research and performed under the National Bureau of Standards Free Radicals Research Program, supported by the Department of the Army.

† Present address: Princeton University Observatory, Princeton, New Jersey.

[1] G. W. Robinson and M. McCarty, Jr., J. Chem. Phys. **28**, 349, 350 (1958); **30**, 999 (1959); M. McCarty, Jr., and G. W. Robinson, J. Am. Chem. Soc. **81**, 4472 (1959); J. chim. phys. **56**, 723 (1959).

[2] M. McCarty, Jr., and G. W. Robinson, Mol. Phys. **2**, 415 (1959).

[3] K. Dressler and O. Schnepp, reported at Symposium on Molecular Structure and Spectroscopy, Columbus, Ohio, June 1959.

[4] K. Dressler and O. Schnepp (to be published).

[5] K. Dressler and O. Schnepp, J. Chem. Phys. **33**, 270 (1960).

[6] A. B. F. Duncan, Phys. Rev. **47**, 822 (1935); **50**, 700 (1936).

[7] R. M. Hexter and D. E. Milligan, reported at 4th International Symposium on Free Radical Stabilization, Washington, D. C., September, 1959.

[8] O. Schnepp and K. Dressler, J. Chem. Phys. **33**, 49 (1960).

[9] P. G. Wilkinson and Y. Tanaka, J. Opt. Soc. Am. **45**, 344 (1955).

[10] O. Schnepp and K. Dressler, J. Chem. Phys. **32**, 1682 (1960).

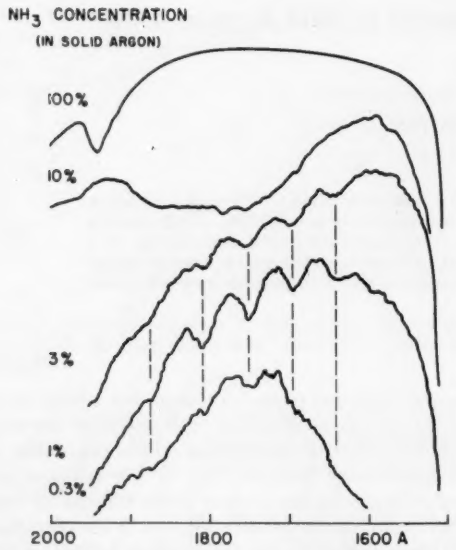

FIG. 1. Absorption spectra of NH_3 at 4.2°K for various molar concentrations of ammonia in solid argon as well as for a deposit of pure ammonia. Densitometer tracings of exposures obtained with a xenon light source are shown.

when pure ammonia vapor is deposited onto a cold surface below 125°K shows a conspicuous absorption band at 1940 A which has been described by Dressler and Schnepp.[5] Except for this absorption band the uppermost tracing of Fig. 1 illustrates closely the background density produced by the light source.

At 10% (molar) of NH_3 in solid argon the spectrum shows no trace of the band at 1940 A, nor do any of the bands of free ammonia appear. The broad absorption observed between approximately 1900 and 1600 A is presumably due to a polymeric form of ammonia. The presence of ammonia polymers in similar deposits has previously been postulated by Becker and Pimentel[11] on the basis of infrared spectral evidence.

At NH_3 concentrations between 3% and 0.3%, a series of diffuse bands appears in the wavelength region 1900 to 1600 A, with absorption maxima at 1867, 1806, 1749, 1692, and 1640 A. The bands are most pronounced in the 1% sample but show less clearly in the 3% sample, indicating that they are due to a species which is isolated more efficiently in deposits of higher dilution. In 0.3% deposits the bands seem to show less contrast than at 1%, but this is believed to be due to the larger thickness of the more dilute deposit necessary to produce comparable ammonia absorption. The increased thickness of the solid argon film gives rise to more serious loss of light due to scattering, and the increased A/NH_3 ratio results in a less favorable scattering-to-absorption ratio.

[11] E. D. Becker and G. C. Pimentel, J. Chem. Phys. **25**, 224 (1956).

Some attempts have been made to obtain similar spectrograms using a hydrogen light source in place of the xenon lamp. These attempts remained almost entirely unsuccessful. It is believed that the ammonia molecules were photodecomposed by the intense hydrogen emission at short wavelengths before enough plate density was accumulated to show the NH_3 absorption spectrum at wavelengths longer than 1700 A where the hydrogen continuum is comparatively weak. The spectrograms obtained with the hydrogen source showed an absorption band at 3380 A which is due to trapped NH radicals in solid argon.[12] This observation has led to a separate investigation of the photolysis of NH_3 in solid solution at low temperatures.[10] The bands shown in Fig. 1 were observed only in samples which had not been previously exposed to the hydrogen arc.

INTERPRETATION

The absorption bands which appear in samples containing 1% of ammonia in solid argon are compared in Fig. 2 with the gas-phase absorption spectrum of NH_3.[13] In the region 2200 to 1600 A the latter spectrum consists of a long progression of diffuse bands which are ascribed to transitions involving the out-of-plane bending vibration of an electronically excited molecule whose equilibrium configuration is planar.[6,14] Inspection of Fig. 2 shows that the matrix-phase spectrum can be closely correlated with the vapor spectrum of NH_3 if it is assumed that alternate bands of the observed vibrational progression are missing in the matrix at 4.2°K. The absence of alternate bands arises

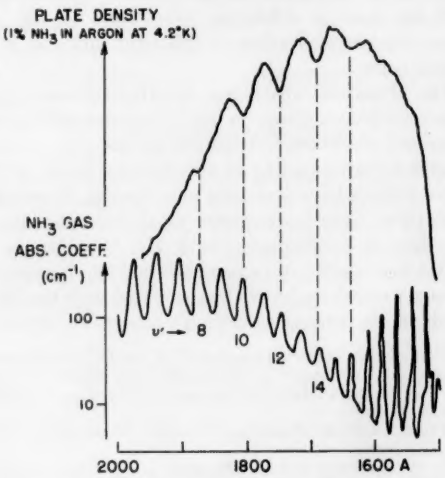

FIG. 2. Absorption bands of NH_3 in the spectral region 1600 to 1900 A at 4.2°K and at room temperature. The plot of gas-phase absorption coefficients has been adopted from the work of Watanabe (see work cited in reference 13).

[12] G. W. Robinson and M. McCarty, Jr., Can. J. Phys. **36**, 1590 (1958).
[13] K. Watanabe, J. Chem. Phys. **22**, 1564 (1954).
[14] W. S. Benedict, Phys. Rev. **47**, 641 (1935).

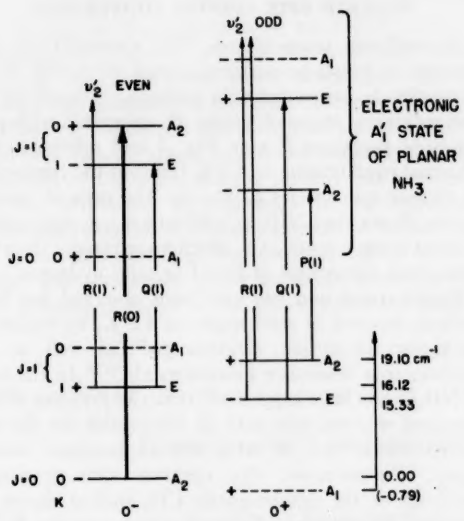

FIG. 3. Energy level diagram (schematic) for parallel transitions of type $(0, v_2', 0, 0) \leftarrow (0, 0^{+,-}, 0, 0)$ between the lowest rotational levels of NH_3 and an excited electronic A_1' state of planar NH_3. For an excited A_2'' state the notations "v_2' even" and "v_2' odd" would have to be interchanged. Ground-state energy values were calculated from the rotational constants given in the work cited in reference 15, but the levels are not drawn to scale.

because (a) in the excited state of NH_3 progressive levels of the out-of-plane bending vibration (which is of species A_2'') alternate in symmetry with respect to inversion, (b) in the ground state at 4.2°K molecules of only one symmetry type with respect to inversion occur, and (c) the selection rules for over-all symmetry with respect to inversion are

$$+\leftrightarrow-,\ +\not\leftrightarrow+,\ -\not\leftrightarrow-. \qquad (1)$$

It appears unjustified at first sight to postulate that condition (b) is fulfilled since the inversion doubling of the ground state amounts to only 0.79 cm^{-1},[15] corresponding to a value of $E/k=1.1$°K. Furthermore, any effect of the matrix environment would be expected to result in a further decrease of this splitting, in accordance with observations in the infrared. The inversion doubling of the ν_2 band of NH_3 in dilute solution in solid argon has been found to be appreciably decreased relative to the gas-phase value.[16]

Inspection of the ground-state energy levels of NH_3 shows that at 4.2°K only the $J=0$ rotational level is expected to be appreciably populated, and that for $J=0$ only one component of the inversion doublet, namely, the antisymmetric one (0^-), can occur with an appropriate nuclear spin function such that the resulting over-all eigenfunction is antisymmetric with respect to an exchange of two H nuclei.[17] A diagram of the lowest energy levels of NH_3 is presented schematically in Fig. 3. The selection rules for dipole transitions of NH_3 are, in addition to (1),

$$A_{\frac{1}{2}} \leftrightarrow A_2,\ E \leftrightarrow E,\ A_{\frac{2}{2}} \not\leftrightarrow E, \qquad (2)$$

where $A_{\frac{1}{2}}$ and E designate over-all species of the rotational levels (apart from nuclear spin), and for parallel-type bands

$$\Delta K=0,\ \Delta J=\pm 1 \qquad \text{if } K=0,$$

$$\Delta K=0,\ \Delta J=0,\ \pm 1 \qquad \text{if } K\neq 0;$$

for perpendicular-type bands

$$\Delta K=\pm 1,\ \Delta J=0,\ \pm 1.$$

The transitions possible from the $J=0$ and $J=1$ levels to states of A_1' and A_2'' vibronic symmetry of planar NH_3 are shown in Fig. 3. The transitions from the *antisymmetric* inversion sublevel (0^-) of the ground state to levels which are vibronically *symmetric* with respect to inversion are consistent with the selection rules (1) and (2) concerning the over-all symmetry properties of the rotational levels. These transitions are also in accordance with the electronic-vibrational selection rules formulated by Herzberg and Teller.[18] The electronic transition moment must be classified according to the species of point group C_{3v}, both electronic states are assumed to be totally symmetric (species A_1), and the electronic transition is allowed. Consequently the vibrational wave functions of the two combining levels must belong to the same symmetry species. This condition is fulfilled for *all* levels of the excited-state progression $(0, v_2', 0, 0)$ because they belong to the totally symmetric vibrational species A_1 of point group C_{3v}. In order to determine in detail whether a given inversion sublevel of the ground state combines with excited-state levels of vibronic symmetry A_1' or A_2'' (corresponding to even or odd values of v_2', respectively, in the case of an excited electronic A_1' state) it is necessary to classify the electronic-vibrational wave functions of both combining states according to the species of point group D_{3h}.[19] The $(0, 0^+, 0, 0)$ and $(0, 0^-, 0, 0)$ *inversion* sublevels of the ground state correlate, respectively, with the *vibrational* levels $(0, 0^{(+)}, 0, 0)$ and $(0, 1^{(-)}, 0, 0)$ of a hypothetical planar NH_3 molecule. The latter levels belong, respectively, to vibronic species A_1' and A_2'' of point group D_{3h}. The inversion sublevels of the ground state can therefore *formally* be treated as levels of vibronic species A_1' and A_2''. Since the selection rules for

[15] W. S. Benedict, E. K. Plyler, and E. G. Tidwell, J. Research Natl. Bur. Standards **61**, 123 (1958).

[16] D. E. Milligan, R. M. Hexter, and K. Dressler, J. Chem. Phys. **34**, 1009 (1961).

[17] G. Herzberg, *Infrared and Raman Spectra of Polyatomic Molecules* (D. Van Nostrand Company, Inc., Princeton, New Jersey, 1945), pp. 406–424.

[18] G. Herzberg and E. Teller, Z. physik. Chem. **B21**, 410 (1933).

[19] Unless this is done, the vibrational selection rule of Herzberg and Teller, cited above, may be misunderstood to mean that the $J=0$ ground level whose vibrational function is of species A_2'', combines with levels of vibrational symmetry A_2'' regardless of whether the excited state is electronically of species A_1' or A_2''.

vibronic symmetry allow transitions of the type $A_1' \leftrightarrow A_2''$ we obtain again the result that the 0^- inversion level of the ground state can combine with vibronic A_1' levels. In the case of an excited electronic state of species A_1' the vibrational structure is *formally* characteristic of a *forbidden* electronic transition as far as symmetry to inversion is concerned, in accordance with the fact that for planar NH_3 electronic transitions of type $A_1' \leftarrow A_1'$ would be forbidden.

The positions of the low-temperature bands coincide with positions of gas-phase bands with even values of v_2'. It follows that the matrix spectrum is consistent with an upper electronic state of species A_1' (or E'') if the wavelength shift of the bands due to the solid matrix is assumed to be small compared to a vibrational quantum. If, however, the matrix shift is exceptionally large for this transition of NH_3 (or if the vibrational numbering of the gas-phase bands is in error), then an upper state of species A_2'' (or E') may be responsible for the bands. Some information on the symmetry of the excited state is available from gas-phase data on ND_3. The corresponding spectrum of this molecule shows discrete rotational structure in some of the bands. This structure has been partially analyzed by Benedict[14] in terms of a parallel transition,[20] i.e., the excited state is expected to be A_1' or A_2''. The same conclusions can be drawn from discussions of electronic orbitals.[21,22]

The transition has been interpreted as being of the Rydberg type.[21,22] The large width of the matrix bands of NH_3 in the ultraviolet is consistent with an electron configuration which due to its large spread in the excited state is strongly perturbed in the solid environment.[23] The failure to observe banded absorption between 1600 and 1500 A may be due to even more severe broadening of the bands belonging to the second transition of ammonia (compare Fig. 2). Similarly, it may be concluded from the absence of banded absorption at wavelengths above 1900 A that the lowest vibrational bands of the first electronic transition have widths that exceed the separations between successive bands. This would indicate that the electronic structure of the excited molecule in or near its planar equilibrium configuration is more strongly perturbed by the environment than the electronic structure in those states which involve large amplitudes of the out-of-plane bending vibration.

NUCLEAR SPIN SPECIES CONVERSION

At ordinary temperatures NH_3 molecules are distributed in equal proportions among rotational states of species A_2, associated with proton spin functions A_1, and rotational states of species E, associated with proton spin functions E (see Fig. 3 and reference 17). Thermal equilibration at 4.2°K involves the conversion of nuclear spin species E into A_1. The present investigation shows that NH_3 in solid argon converts within at most a few minutes, i.e., much more rapidly than the ortho-para conversion of liquid or solid hydrogen.

Rapid conversion has also been observed for NH_2 radicals trapped in solid argon at 4.2°K, by means of electronic absorption spectroscopy[24] as well as by electron spin resonance measurements.[25,26] In the case of NH_2 it has been suggested[24] that the presence of the unpaired electron spin may be responsible for the observed effect, but in NH_3 this explanation cannot apply. Furthermore, the electron spin resonance spectrum of the paramagnetic CH_3 radical shows no evidence in support of rapid interconversion.[27] Although McConnell[26] has pointed out that this observation may be interpreted in terms of severe hindrance to rotation in the argon matrix, it is proposed here that proton spin conversion may be slow in CH_3 and fast in NH_2 and NH_3 due to coupling between the proton spins and the spin of the ^{14}N nucleus. Nuclear spin-spin coupling in molecules is weak, but it is known that electron coupled ^{14}N-proton interaction gives rise to observable hyperfine splittings in the inversion spectrum of ammonia.[28] In the light of this suggestion it would be interesting to investigate further the intensity distributions in the electron spin resonance spectra of such radicals as CH_2 and CH_3, and in the infrared spectra of CH_4, H_2O, etc., at low temperatures. If, for instance, equilibration is inhibited in H_2O on account of the zero spin of ^{16}O the ν_2 band of H_2O should show at all temperatures a strong Q line and R line each originating in the 1_{-1} rotational level, in addition to the $R(0)$ line. It would be interesting to extend to lower temperatures the observations of Catalano and Milligan[29] and Glasel[30] on the infrared spectrum of trapped H_2O in solid argon at 20°K.

Contrary to the observations in the ultraviolet the ν_2 band of NH_3 in solid argon has been reported to show a considerable amount of fine structure.[16] This may indicate that in the infrared experiments the actual

[20] W. S. Benedict (private communication).
[21] R. S. Mulliken, J. Chem. Phys. **3**, 506 (1935).
[22] A. D. Walsh, J. Chem. Soc. (London) **1953**, 2296; A. D. Walsh and P. A. Warsop, in a paper to be published shortly, conclude from a vibrational analysis of "hot" bands in the region 2100 to 2400 A, that the symmetry of the excited state must be A_2." It follows, therefore, that the shift of the observed bands due to the solid argon matrix is approximately equal to either plus or minus 1000 cm^{-1}. I am indebted to Dr. Warsop for communicating the results of Professor Walsh's and his work prior to publication.
[23] I am indebted to Professor R. S. Mulliken for drawing my attention to this fact.
[24] G. W. Robinson and M. McCarty, Jr., J. Chem. Phys. **30**, 999 (1959).
[25] S. N. Foner, E. L. Cochran, V. A. Bowes, and C. K. Jen, Phys. Rev. Letters **1**, 91 (1958).
[26] H. M. McConnell, J. Chem. Phys. **29**, 1422 (1958).
[27] C. K. Jen, S. N. Foner, E. L. Cochran, and V. A. Bowes, Phys. Rev. **112**, 1169 (1958); L. A. Wall, D. W. Brown, and R. E. Florin, J. Phys. Chem. **63**, 1762 (1959).
[28] See for instance G. R. Gunther-Mohr, C. H. Townes, and J. H. Van Vleck, Phys. Rev. **94**, 1191 (1954).
[29] E. Catalano and D. E. Milligan, J. Chem. Phys. **30**, 45 (1956).
[30] J. A. Glasel, J. Chem. Phys. **33**, 252 (1960).

temperature of the sample was appreciably above 4.2°K, since at lower temperature most of the intensity would be expected to fall into the $R(0)$ line on the basis of the observations in the ultraviolet. The fine structure in the infrared has been interpreted in terms of nearly unrestricted rotational motion of the NH_3 molecules in solid argon. Additional evidence for this is provided by the observation of nuclear spin conversion in the ultraviolet. The presence of an appreciable hindering potential of trigonal symmetry would result in a near coincidence of the lowest A and E levels of NH_3. The ultraviolet spectrum shows, however, that the Boltzmann factor of the lowest E level is small at 4.2°K, which at or above this temperature is only possible under conditions of free or nearly free rotation.

ACKNOWLEDGMENTS

Dr. O. Schnepp, Laboratory of Physical Chemistry, Israel Institute of Technology, Haifa, has been associated with this work during the experimental phase. Many stimulating discussions with Dr. O. Schnepp, and with Dr. W. Vedder, Department of Chemistry, Princeton University, are gratefully acknowledged. I wish to thank Dr. H. P. Broida, National Bureau of Standards, for the encouragement and support given to this work.

THE JOURNAL OF CHEMICAL PHYSICS VOLUME 35, NUMBER 1 JULY, 1961

Experimental Townsend Ionization Coefficients for Isopentane

A. E. D. HEYLEN

Electrical Engineering Department, Queen Mary College, London, England

(Received December 21, 1960)

Townsend α and γ values have been measured over the range $60 \leq E/p_0 \leq 3000$ for isopentane using the dc method of measuring the ionization current. The experimental apparatus and procedure are described. It is shown that Townsend's law $\alpha/p_0 = A \exp(-Bp_0/E)$ is obeyed within $80 \leq E/p_0 \leq 500$. Positive ion action at the cathode sets in at $E/p_0 \geq 500$. The results agree with previous breakdown measurements. It was found possible to follow the current growth due to ionization of the gas over a multiplication range exceeding eight orders of magnitude. The influence of space-charge distortion within single avalanches and that due to neighboring ones has been examined. No space-charge reduction of the avalanche multiplication was observed until $e^{\alpha d} \geq 10^7$.

INTRODUCTION

BY comparing the $V_s - pd$ characteristics of a number of hydrocarbon vapors, a correlation has been established between the electric strength, molecular structure, and ultraviolet spectra of molecular gases. Mean scattering cross-section values have been assigned to the molcular bonds or preferably to atomic groups present in the compounds.[1] The results obtained relied for their interpretation on the existence of a particular criterion for breakdown and of a formal dependence of Townsend's α on E/p_0, where E is the field strength in v cm^{-1} and p_0 is the gas pressure at 0°C. Breakdown was assumed to occur when αd reached some critical value

$$\alpha d = \alpha d_s, \tag{1}$$

which for hydrocarbons is known to be large,[2,3] provided $E/p_0 \leq 500$. From conductivity[4] and statistical[5] measurements of Townsend's α, a suitable dependence of α/p_0 over a limited E/p_0 range was found to be

$$\alpha/p_0 = A \exp(-Bp_0/E), \tag{2}$$

and the measurements enabled the constants A and B to be determined for each gas. By combining Eq. (2) with the breakdown criterion of Eq. (1), one obtains

$$\ln(p_0 d) = B \cdot (p_0 d/V_s) + \ln[\alpha d_s/A], \tag{3}$$

and this, in addition, enabled B to be obtained from breakdown measurements. When values of B obtained by these two methods were compared, it was found that although the same stepwise change of B with molecular structure was evident from both methods, a discrepancy of some 20% occurred in their absolute values.[4]

It is the purpose of this paper to examine the reasons for this discrepancy and to show from experiment that both methods lead to the same value of the constants A and B provided the same E/p_0 range is covered in each case. In addition, γ values pertaining to hydrocarbons are presented and it is shown that quite large current densities and gas amplification factors $\exp(\int \alpha dx)$ can be tolerated in these gases

[1] A. E. D. Heylen, J. Chem. Phys. **29**, 813 (1958); **30**, 1106 (1959).
[2] E. Badareu and M. Valeriu, Bull. soc. roumaine phys. **42**, 9 (1941); **43**, 35 (1942).
[3] M. Valeriu-Petrescu, Bull. soc. roumaine phys. **44**, 3 (1943).
[4] A. E. D. Heylen, *Proceedings 4th International Conference on Ionization Phenomena in Gases, Uppsala* (North-Holland Publishing Company, Amsterdam, 1960), Vol. I, p. 150.
[5] H. Schlumbohm, Z. angew. Phys. **11**, 156 (1959).

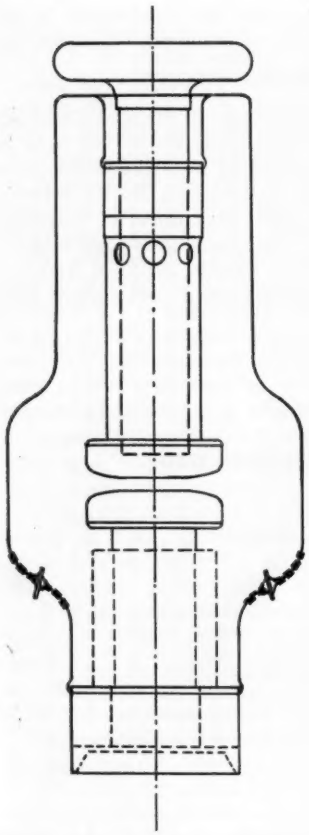

FIG. 1. Simplified drawing of ionization chamber. Not shown are removable cathode guide and micrometer.

without evidence of cathode instability or space-charge distortion occurring.

Besides the measurements reported, few Townsend α values exist for hydrocarbon gases and none have been measured over an extended E/p_0 range. Badareu and Valeriu[2,3] conducted ionization current measurements in benzene, toluene, and cyclohexane in the range $400 \leq E/p_0 \leq 3000$ and reported large α and low γ coefficients in these gases. Hochberg and Sandberg[6] measured Townsend α in n-pentane for $65 \leq E/p_0 \leq 85$ and Geballe and Harrison[7] performed conductivity measurements in isopentane for $75 \leq E/p_0 \leq 140$. These latter measurements agree well with the present results.

APPARATUS

To economize in the use of highly pure hydrocarbon gases, the ionization chamber was made as small as possible consistent with a maximum uniform field gap of 1.5 cm. This allowed ultra-high vacuum techniques to be conveniently applied with provision for bake-out at 450°C. The $\frac{3}{4}$-liter cell, of which a simplified diagram is shown in Fig. 1, was of the type used by Kruithof.[8] The electrodes were contained in a Kodial glass envelope on to which a silver ring was glazed internally and externally to act as a guard. The anode was supported on a hollow bushing which was joined to the glass envelope by a matched seal. The cathode was mounted on a flexible stainless-steel bellows and was guided by a removable holder. The gap could be aligned and adjusted to within 0.004 mm as measured on a micrometer. The insulation resistance between guard ring and cathode was larger than $10^{14}\Omega$. The electrodes were made from 99.99% pure aluminum and had an over-all diameter of 4.5 cm and a central flat portion of 1.5 cm diam. A maximum gap of 1.575 could be set at which the electrodes had the $\psi = 120°$ Rogowski profile.[9] In practice no gap greater than 1.2 cm was used and at this setting, the field along the edge decreases continuously. An optically flat quartz window inside the anode bushing and 121 holes uniformly distributed over a central 1-cm^2 area of the anode allowed the cathode to be illuminated by the parallel light beam from a Hanovia high-pressure mercury arc source. If it is assumed that no diffusion of charge within the gap takes place, then the current density was four times the current measured.

The test cell was evacuated via an outbakeable high-vacuum tap by means of an oil diffusion pump backed by a rotary pump. A second tap served as a needle valve for introducing the gas samples. The complete system was constructed following Alpert's ultra-high vacuum recommendations.[10] The test cell itself was balanced on and supported by a bakeable bellows-type differential pressure manometer[11] which was rigidly fixed to the floor of the bakeout oven. The manometer could detect pressure differences of 10^{-2} mm Hg and at the lowest gas pressure of $\frac{1}{2}$ mm Hg the absolute accuracy of the reading was better than 4%. The other side of the differential pressure manometer was connected to a high-vacuum system incorporating a second set of diffusion and rotary pumps and absolute mercury and oil manometers. Without a bake, vacua of 2×10^{-7} mm Hg could be reached against a leakage rate of $<1\times10^{-6}$ lu/sec. The attainment of ultra-high vacua is not a prerequisite in these experiments, but it is important that the leakage rate be as small as possible. After a bake at 250°C, vacua of $<10^{-9}$ mm Hg were obtained in the complete system against a leakage rate of 3×10^{-9} lu/sec.

In measurements of this kind the lower limit of detection of stable conduction currents is governed by the stability of the high voltage supply. As pressures of up to 1 atm were considered, with a gap setting of 1.2

[6] B. Hochberg and E. Sandberg, Compt. rend. acad. sci. U.R.S.S. **53,** 511 (1946).
[7] L. B. Loeb, *Basic Processes of Gaseous Electronics* (University of California Press, Berkeley, California, 1955), p. 414.
[8] A. A. Kruithof and F. M. Penning, Physica **3,** 515 (1936).
[9] W. Rogowski, Arch. Elektrotech. **12,** 1 (1923); H. Rengier, *ibid.* **16,** 76 (1926).
[10] D. Alpert, J. Appl. Phys. **24,** 860 (1953).
[11] A. E. D. Heylen, J. Sci. Instr. **37,** 251 (1960).

cm, a power pack supplying a positive 50 kv was constructed along the lines outlined by Hopwood, Peacock, and Wilkes.[12] The stability obtained, after allowing for a period of warmup, was 0.01% over a period of hours and 0.001% over periods sufficiently long to allow conduction measurements to be made, (usually 5 sec duration). Voltages could be continuously tapped to better than ½ v and the absolute accuracy of the voltage applied to the test cell was 0.3%. For lower voltage work, the high-voltage pack could be adapted to supply 5 kv across the main resistor chain. To retain the same degree of stability and accuracy, the control by the feedback circuit and the sensitivity of the current detector were correspondingly increased. The ionization current was measured on a Vibron electrometer model 33C with a B33C head unit. A 300-pf capacitor connected across the 10^{10}-Ω resistor used for the current measurement, minimized the effect on the electrometer of fluctuations in the high voltage applied to the test cell; these were less than 10 mv and, with a capacitance of 30 pf due to the electrode arrangement, account for the lower limit of stable current detection which was 10^{-13} A. A neon tube protected the electrometer input against accidental spark over across the gap.

EXPERIMENTAL PROCEDURE AND RESULTS

In the unbaked condition the initial photoelectric current i_0 was stable provided it was kept below 10^{-13} A and the total ionization current was not allowed to exceed 10^{-10} A. The photoelectric current was proportional to the power consumed by the uv lamp and this was controlled to better than 1%. When i_0 was increased to 5×10^{-12} A under vacuum, the value gradually increased until after a few hours it had doubled.[4] When the system had been baked at 250°C, i_0 values of 3.5×10^{-11} A were recorded for the same intensity of excitation and showed no sign of an upward drift after many hours. Under these conditions the dependence of i_0 on gap setting was investigated with an applied field of 100 v/cm across the electrodes. The dependence is shown in Fig. 2. Over the greater part of the gap distance up to the maximum of 1.2 cm, i_0 was constant. When gap distances below 2 mm were employed, a suitable correction to the total current recorded was applied.

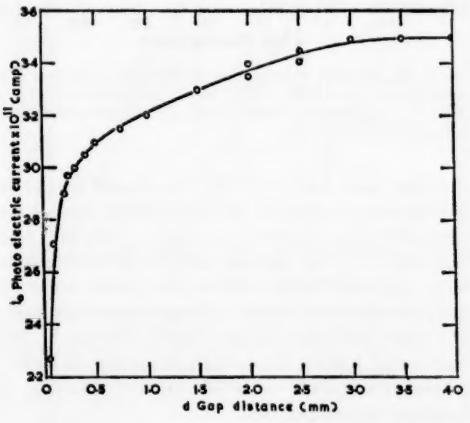

FIG. 2. Initial vacuum photoelectric current i_0 as a function of gap distance d.

No further bakes were carried out as it was estimated that the leakage rate was sufficiently low to prevent contamination of the test sample in the course of a few days. Tests were conducted at pressures ranging from ½ to 400 mm Hg; the gas was 100% pure as certified by the Chemical Research Laboratory. For a given gas filling, the ionization current i was measured at a fixed gap setting for all possible E/p_0 values. The gap was increased in steps of 0.5 mm and the procedure repeated up to the maximum gap setting of 1.2 cm. Plots of ln i vs d enabled α values to be obtained in the usual manner. Values of α obtained over a period of

TABLE I. Summary of α/p_0 vs E/p_0 results for isopentane.

α/p_0 ions cm^{-1} mm^{-1} Hg	E/p_0 v cm^{-1} mm^{-1} Hg
0.0052	60
0.014	65
0.031	70
0.058	75
0.094	80
0.135	85
0.175	90
0.30	100
0.45	110
0.63	120
0.85	130
1.35	150
1.90	170
2.8	200
4.4	250
6.0	300
7.5	350
8.7	400
12.0	500
15.0	600
21.5	800
27.0	1000
33	1200
41	1500
50	2000
59	2500
63	3000

[12] W. Hopwood, N. J. Peacock, and A. Wilkes, Proc. Roy. Soc. (London) **A235**, 334 (1956).

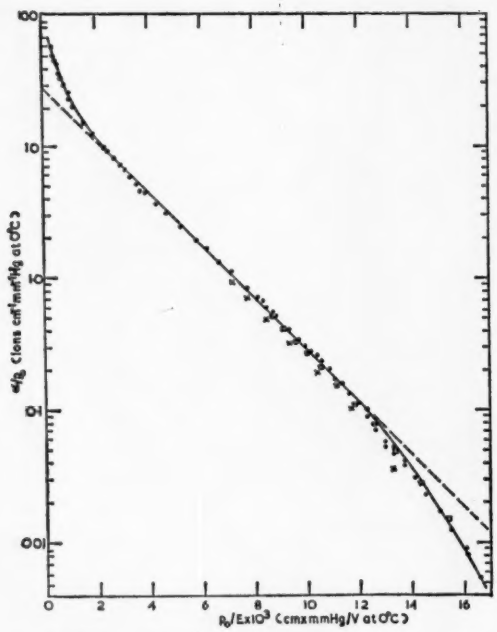

FIG. 3. Townsend's first ionization coefficient α/p_0 as a function of E/p_0. For $80 \leqslant E/p_0 \leqslant 500$, $\alpha/p_0 = 26.5 \exp(-447\ p_0/E)$; ●—present measurements, □—previous measurements[2] and ×—Geballe and Harrison's values.[7]

days agreed within 3%. The initial photoelectric current was observed to remain stable provided the current density did not exceed 7×10^{-8} A/cm². Table I lists the values of α/p_0 vs E/p_0 taken from the smoothed curve of Fig. 3. Measured Townsend secondary coefficient values are shown in Fig. 4 and these were obtained from the upcurving of the ln i vs d plots of which a typical example is shown in Fig. 5. After the passage of a spark, the value of i_0 had altered and was unstable over a period of hours, so that tests were discontinued and the cathode rested.

With the dc method of measuring Townsend's α, it should be possible to investigate two further mechanisms. The first one is the possible deviation from a normal α slope by the interfering action of neighboring

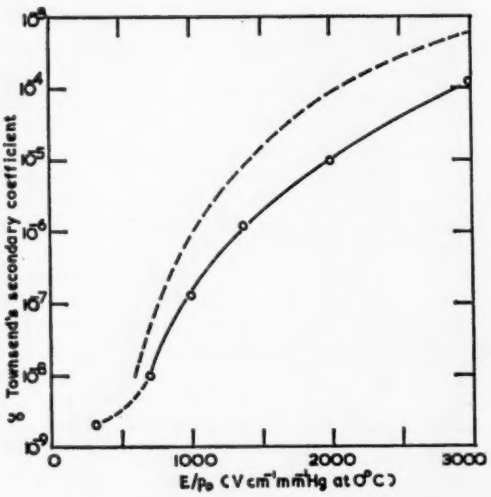

FIG. 4. Townsend's secondary coefficient γ as a function of E/p_0; ○—○ present measurements, ------ cyclohexane Valeriu-Petrescu.[3]

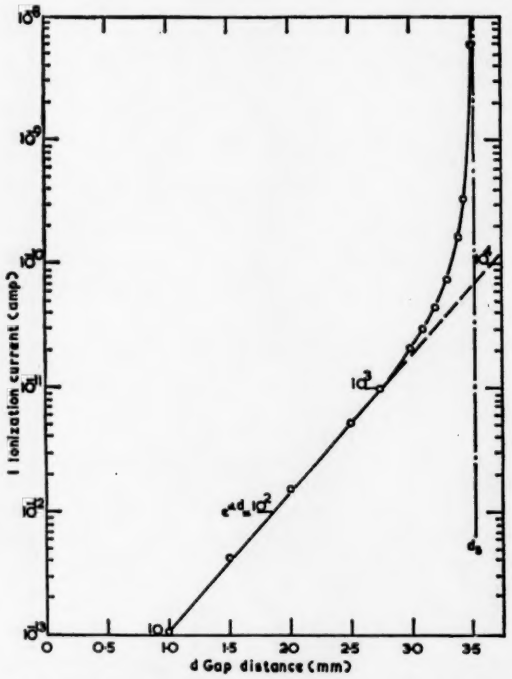

FIG. 5. Typical plot of ionization current i as a function of gap distance d for $E/p = 3000$ v cm^{-1} mm^{-1} Hg, $p = \frac{1}{2}$ mm Hg, $\gamma = 1.3\times10^{-4}$; ——— experimental curve, ○ ○ calculated values from $i = i_0 e^{\alpha d}/1-\gamma(e^{\alpha d}-1)$.

avalanches upon one another. This should be particularly pronounced at large current densities and at large gas amplification factors $\exp(\int \alpha dx)$. This effect was not observed in the present series of measurements possibly because before interaction could occur, the initial photoelectric current i_0 became unstable and no total current densities above 7×10^{-8} A/cm^{-2} could be supported. With an avalanche multiplication of 10^8, this corresponds to 4000 electrons leaving the cathode per second per cm².

The effect of space-charge distortion within single avalanches was examined by measurements of the ionization current as near to breakdown as possible. No deviation from the normal α slope was found as

shown in Fig. 6 for $E/p=300$ and amplifications of 4×10^8 were reached by the successive reduction of i_0. The last slope was obtained with 10 electrons leaving the cathode per second and this type of measurement has often been repeated and confirmed for $E/p_0\leq500$ and for a range of i_0 up to 4000 electrons per second. The time constant of the input circuit to the electrometer was increased from 3 to 10 sec to smooth out the statistical variation in Townsend's α[13] which becomes apparent when so few electrons leave the cathode per second.

DISCUSSION OF RESULTS

It is demonstrated in Fig. 3, that the dependence of α/p_0 on E/p_0 follows accurately the exponential Townsend law $\alpha/p_0=A\exp(-Bp_0/E)$ for the range $80\leq E/p_0\leq500$; the values of the two constants are listed in Table II, first row. For $E/p_0\geq500$, the α/p_0 values exceed those given by the Townsend equation. At these high-field strengths the inelastic collision barrier (mainly determined by the molecular parameter B) is effectively overcome and the number of fast electrons in the tail of the electron energy distribution function is correspondingly high.[14] These electrons are able to ionize an increasing number of ionization levels which for a complex molecule are closely spaced. At $E/p_0\leq80$ the number of electrons in the energy tail is small and becomes increasingly less as losses due to vibration and rotation assume greater importance.[15]

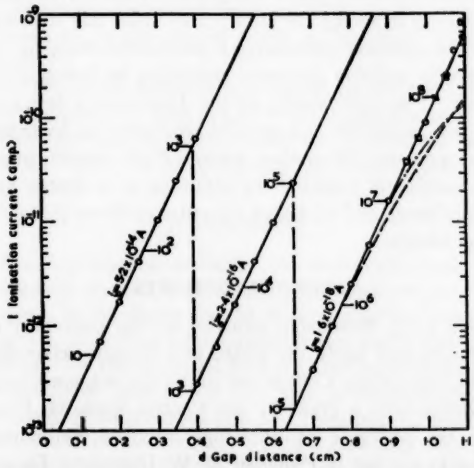

FIG. 6. Ionization current i as a function of gap distance d showing large multiplication possible in isopentane. Spark occurred at $d=1.1$ cm, $E/p=300$ v cm^{-1} mm^{-1} Hg, $p=3$ mm Hg; -○-○- experimental curve, ----- estimated curve, Richter,[16] —•—•— estimated curve, Heylen, and □ □ calculated values from Eqs. (6) and (7).

[13] W. Legler, Z. Physik **140**, 221 (1955).
[14] T. J. Lewis, Proc. Roy. Soc. (London) **A244**, 166 (1958).
[15] A. E. D. Heylen and T. J. Lewis, *Proceedings 4th International Conference on Ionization Phenomena in Gases, Uppsala* (North-Holland Publishing Company, Amsterdam, 1960), Vol. I, p. 156.

TABLE II. Constants obtained for isopentane according to Eqs. (2) and (3).

A ions cm^{-1} mm^{-1} Hg	B v cm^{-1} mm^{-1} Hg	E/p_0 v cm^{-1} mm^{-1} Hg
26.5	447	$80\leq E/p_0\leq500$[a]
24.7 (assuming $\gamma=10^{-8}$)	453	$96.5\leq E/p_0\leq335$[b]
52.7	535	$64.5\leq E/p_0\leq111$[c]
52.0	525	$64.5\leq E/p_0\leq111$[d]

[a] According to Eq. (2), present conductivity.
[b] According to Eq. (3), breakdown[3] (neopentane).
[c] According to Eq. (2), previous conductivity.[4]
[d] According to Eq. (2), present conductivity.

The V_s—pd measurements[1] were carried out over the range $84\leq E/p_0\leq1140$ for neopentane and a linear plot according to Eq. (3) was obtained for $96.5\leq E/p_0\leq335$ which falls within the present range. The constants obtained are shown in Table II, second row. The value of B agrees within $1\frac{1}{2}\%$ with the conductivity value. No explicit value for A was given, but $(\ln\gamma^{-1}/A)=0.86$ was obtained. If a value $\gamma=10^{-8}$ is assumed for breakdown (see further), then $A=24.7$ and this is within 7% of the conductivity value. It is to be noted that neopentane is somewhat stronger electrically than isopentane and agreement would still be better if two identical gases were compared.

The constants obtained from previous conductivity measurements[4] are shown listed in Table II, row three. These values were obtained from results which fell outside the E/p_0 range for which Eq. (2) was found to hold. If the same range of E/p_0 is used and a straight line is fitted to this on Fig. 3, the constants, shown in Table II, row four, agree within 2% with those of row three. Thus it can be concluded that previous conductivity results did not cover a sufficiently large E/p_0 range for them to be compared with the results from breakdown measurements.

The occurrence of a secondary mechanism at high E/p_0 is a true Townsend effect. This is shown in Fig. 5 where the experimental upcurving is compared with the calculated value from the law

$$i=i_0\{e^{\alpha d}/[1-\gamma(e^{\alpha d}-1)]\}, \qquad (4)$$

which fits the experimental results right up to the sparking distance $d_s=0.35$ cm. As the value of E/p_0 increases so the Townsend secondary coefficient increases rapidly at first, then more slowly, as shown in Fig. 4. It is to be noted that electron extraction by positive hydrocarbon-ion impact at the cathode is about three orders of magnitude less than that found for common gases despite the much larger E/p_0 values involved. This is presumably due not so much to the heaviness of the ions as to their tendency to preferentially dissociate upon hitting the cathode. It is at present not clear whether a peak in the curve at $E/p_0\leq500$

due to photoelectric action occurs. At these values, a spark occasionally intervened before the large amplification possible was reached. This random occurrence can be attributed to the statistical nature of the processes involved.[13] The low values of γ make the detection of single avalanches relatively straightforward. Even at the highest E/p_0 values, pulses were detectable on an oscilloscope and due to the secondary effect their number increased as the gap was made larger. The low γ values obtained, offer a guarantee for the freedom of the gas sample from common gas contamination as it is thought that minute amounts of foreign additives would markedly increase the secondary coefficient. The higher values obtained by Valeriu[2,3] for cyclohexane may be due to the presence of small traces of impurities.

The problem of space-charge distortion within a single avalanche has recently received attention.[16,17] Monitoring the pulse shape of the ionic component of the electron avalanche, Richter observed (for ether, a gas exhibiting an extremely low γ coefficient) that the number of carriers n increases less than $e^{\alpha x}$, if n surpasses $N=10^8$. The space-charge field of the positive ions is held responsible for the reduction in ionizing ability of the advancing electrons. It was found that for $n \geq N$, Townsend's α coefficient could be expressed as

$$\alpha_{(n)}=\alpha(1-B \ln n/N), \tag{5}$$

in which $B=0.065$. From this the charge multiplication can be evaluated as[18]

$$n=N \exp\left\{\frac{1-\exp[-\alpha B(x-x_N)]}{B}\right\}, \tag{6}$$

in which $N=e^{\alpha x_N}$. The reduction in the normal α slope according to Eq. (6) is shown in Fig. 6 (dashed line) and it was hoped to confirm this by the dc method of ionization current measurement. As is evident from Fig. 6, no reduction in the normal α slope occurred right up to breakdown. The discrepancy may be explained by the fact that in the dc method, the average amplification of a number of starting electrons is measured and it is possible that a small γ effect takes place, as has been observed in methane[19] and which is sufficient to offset the reduction in α by space charge. This can be taken account of by using the generalized Townsend equation

$$i_x=i_0\frac{\exp\int_0^x \alpha dx}{1-\gamma(\exp\int_0^x \alpha dx-1)}, \tag{7}$$

in which

$$\exp\int_0^x \alpha dx$$

can be found from Fig. 6 (dashed line). An estimate of γ can be obtained by assuming that the experimental curve obeys Eq. (7). Thus for $\gamma=2.2\times10^{-8}$, a normal α slope is obtained up to $d=0.95$; for longer gaps, an upcurving occurs and the Townsend criterion for breakdown is reached at $d=0.985$ cm which is not in agreement with experiment.

From previous work[4] it has been surmized that little space-charge distortion occurs until $n>10^7$ and from Richter's data, an equally good fit to $\alpha_{(n)}$ can be obtained for $B=0.2$. Substitution of these values into Eq. (6) yields the curve as shown in Fig. 6 (dot-dashed line). Combining this with Eq. (7) yields $\gamma=10^{-8}$; the calculated values are shown (Fig. 6, □). It is observed that no deviation from a normal slope occurs to within 5% of the sparking distance at which a faster than usual Townsend-like upcurving takes place.[20]

CONCLUSION

Provided the correct form of Townsend's α dependence on E/p_0 is chosen and tests are carried out under controlled conditions as regards pulse activity,[1] V_s-pd measurements furnish a ready and reasonably accurate means of assessing the influence of molecular structure on the molecular parameter B and consequently on the inelastic collision processes pertaining in hydrocarbon gases. The applicability of the Townsend α law to a typical molecular gas, parallels the trend in hydrogen and perhaps for similar reasons.[21] It should prove interesting to examine the influence of a double and triple bond and of a ring structure on the $\alpha/p_0-E/p_0$ dependence.

ACKNOWLEDGMENTS

An I.C.I. Fellowship awarded by the University of London, and lately the award of a Henley Fellowship by Queen Mary College are gratefully acknowledged, together with a grant by the Central Research Fund for the purchase of ultra-high vacuum equipment. Thanks are due to Professor M. W. Humphrey Davies for facilities provided, to Dr. T. J. Lewis for continued interest, and to The British Aluminium Company, Ltd. for the gift of pure aluminium. Skillful attention by G. A. White and L. W. Borroff materially assisted the construction of apparatus.

[16] K. Richter, Z. Physik **157**, 130 (1958).
[17] K. J. Schmidt-Tiedemann, Z. Naturforsch. **14a**, 989 (1959).
[18] The author is indebted to Dr. P. S. Secker for correcting a mistake in Richter's evaluation.[16]
[19] W. Franke, Z. Physik **158**, 96 (1960).
[20] A. E. D. Heylen, Nature **188**, 734 (1960).
[21] T. Kihara, Phys. Rev. **24**, 45 (1952).

Studies of Fused Salts. III. Heats of Mixing in Silver Nitrate-Alkali Nitrate Mixtures

O. J. KLEPPA, R. B. CLARKE, AND L. S. HERSH

Institute for the Study of Metals, and Department of Chemistry, University of Chicago, Chicago 37, Illinois

(Received January 5, 1961)

The enthalpies of mixing in binary liquid mixtures of silver nitrate with lithium-, sodium-, potassium-, and rubidium nitrate have been measured. It is found that the molar enthalpy of mixing (ΔH^M) changes in a regular fashion from positive values for lithium- and sodium- to negative values for potassium- and rubidium nitrate. Neglecting second-order effects, the mixing enthalpies may be represented by the following semiempirical relation,

$$\Delta H^M \simeq -X(1-X)[140\,\delta^2 - 24(\delta - 0.01)] \text{ kcal/mole.}$$

The parameter δ is $(d_1-d_2)/(d_1+d_2)$, where d_1 and d_2 are the interionic distances characteristic of the two pure components, while X and $(1-X)$ are their mole fractions. In this expression the δ^2 term has been taken from the equivalent expression for the binary alkali nitrates, which presumably are essentially ionic. The value of the numerical factor (140 kcal/mole) is of the order of the lattice energy of these salts. The term which is linear in δ takes into account departures from ionicity in silver nitrate, and is of magnitude comparable to the nonionic contribution to the lattice energy of this compound. It is shown by considering available emf data for the silver halide-alkali halide systems that expressions of this type may be quite useful in predicting the heats of mixing in as yet unexplored systems.

RECENTLY, we have published a detailed report on the heats of mixing in the ten binary liquid systems formed by the alkali nitrates.[1] In the present paper we extend our calorimetric study of fused salt solutions to the mixtures of silver nitrate with lithium-, sodium-, potassium-, and rubidium nitrate. Since silver nitrate undergoes thermal decomposition at the temperature where cesium nitrate melts (414°), no data are reported for this system. In a future communication we shall consider the thallium nitrate-alkali nitrate mixtures.

The new data are compared with our earlier results for the alkali nitrate mixtures and with available emf information on the liquid silver halide-alkali halide systems.[2-5]

For the liquid mixtures of silver nitrate with sodium nitrate recent emf data are reported in the literature.[6] For this system, therefore, we are able to compare our own heat data with corresponding free energy information.

EXPERIMENTAL

The experimental methods and techniques used in the present work were quite similar to those previously adopted in our study of the binary alkali nitrates.[7] However, there were a few modifications: In the present investigation the dc signal produced in the differential thermocouple system of the twin calorimeter was amplified by means of a Leeds and Northrup dc amplifier (No. 9835) and recorded by a Speedomax AZAR recorder.

The magnitude of the heat effect was determined by graphically integrating the area under the emf-time curve through a combined planimetric-analytical procedure. The major part of the area was measured by an Ott precision planimeter. The remainder, i.e., the area under the exponential tail of the curve, was determined analytically by use of the experimentally determined Newton's-law decay constant, k: let $E_t = E_0 \exp(-kt)$ be the observed emf at time t. Then the area under the exponential tail from time t to ∞ is simply

$$\text{Area} = \int_t^\infty E_t dt = E_t/k.$$

In the present series of experiments we observed both *endothermic* and *exothermic* heat effects. Therefore we did not adopt the balanced heat effect method used in our earlier work.[7] This resulted in no significant loss in precision.

The silver nitrate used in this study was of reagent grade purchased from Goldsmith Bros., in the form of a pure white crystalline powder. Prior to its use in the calorimeter this salt was dried at room temperature in a vacuum desiccator, then melted down in a dark room and cast into $\frac{1}{4}$-in. sticks. In the calorimeter these sticks melted to form a clear, slightly yellow liquid.

The alkali nitrates were of the same reagent-grade quality as the salts used in our earlier work. Prior to use, the somewhat hygroscopic lithium nitrate was cast into $\frac{1}{4}$-in. sticks and weighed out in this form.

As in our earlier work, calibration of the calorimeter was achieved by dropping weighed pieces of 2-mm gold wire from room temperature into the apparatus (at 350°). A slight complication arose from the fact that we observed a small deposit of metallic silver on the surface of the gold at the end of each run. Characteristically this deposit amounted to 0.1 to 1 mg of silver on a 1-g gold sample after about 6-hr exposure. Separate experiments were performed in order to estimate the

[1] O. J. Kleppa and L. S. Hersh, J. Chem. Phys. **34**, 351 (1961).
[2] J. H. Hildebrand and E. J. Salstrom, J. Am. Chem. Soc. **54**, 4257 (1932).
[3] M. B. Panish, F. F. Blankenship, W. R. Grimes, and R. F. Newton, J. Phys. Chem. **62**, 1325 (1958).
[4] M. B. Panish, R. F. Newton, W. R. Grimes, and F. F. Blankenship, J. Phys. Chem. **63**, 668 (1959).
[5] K. H. Stern, J. Phys. Chem. **60**, 679 (1956).
[6] R. W. Laity, J. Am. Chem. Soc. **79**, 1849 (1957).
[7] O. J. Kleppa, J. Phys. Chem. **64**, 1937 (1960).

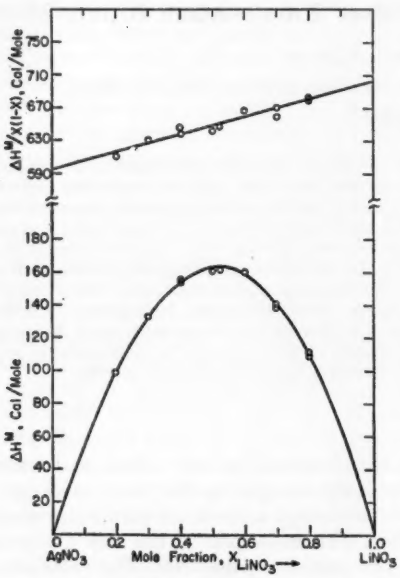

FIG. 1. Molar integral heats of mixing (ΔH^M) in mixtures of lithium nitrate with silver nitrate at 350°.

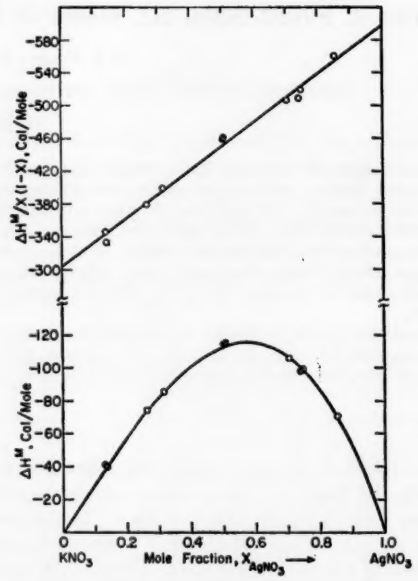

FIG. 3. Molar integral heats of mixing (ΔH^M) in mixtures of potassium nitrate with silver nitrate at 350°.

error introduced into our calibrations by this process. It was found that the heat effect associated with this silver deposition is endothermic, and was of the order of 0.5% or less of the calibration heat. We have made no attempt to correct for this small error.

On the whole the reported heat data are probably correct to within ±1.5%.

RESULTS AND DISCUSSION

The experimental results obtained in the present work are presented graphically in Figs. 1–4. Each figure shows the molar heat of mixing ΔH^M as well as a plot of $\Delta H^M/X(1-X)$, where X is the mole fraction of silver nitrate.

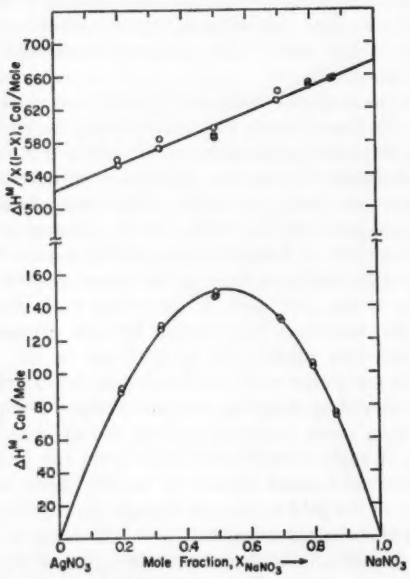

FIG. 2. Molar integral heats of mixing (ΔH^M) in mixtures of sodium nitrate with silver nitrate at 350°.

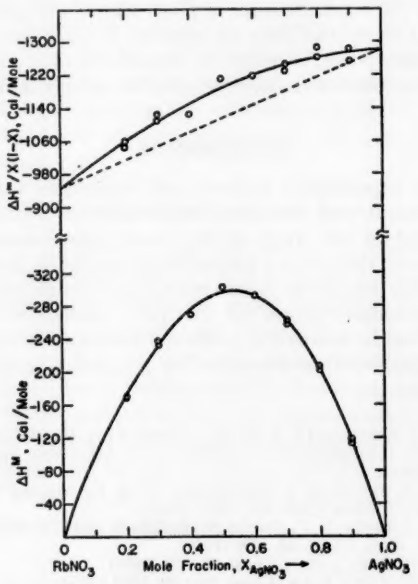

FIG. 4. Molar integral heats of mixing (ΔH^M) in mixtures of rubidium nitrate with silver nitrate at 350°.

These figures demonstrate that the mixtures of silver nitrate with lithium and sodium nitrate are endothermic, while the corresponding potassium and rubidium systems are exothermic. It is of some interest to note that in these systems there is a correlation between exothermic mixing in the liquid state, and the existence of stable double salts (of composition [AgMe] NO_3) in the solid state, i.e., according to available phase-diagram information such double salts are formed in the silver-potassium and silver-rubidium systems,[8,9] but not in the silver-lithium and silver-sodium (nitrate) systems.[9,10]

We note also that for the mixtures involving lithium-, sodium-, and potassium nitrate the quantity $\Delta H^M/X(1-X)$ depends linearly or very nearly linearly on composition, while for the rubidium nitrate mixtures we have a significant curvature. In this respect the latter system is similar to the several alkali nitrate systems which have reasonably large negative enthalpies of mixing.[1]

We have fitted our experimental data (by the least-squares method) with analytical expressions of the form

$$\Delta H^M = X(1-X)[a+bX+cX(1-X)]. \qquad (1)$$

Here X denotes the mole fraction of silver nitrate, while a, b, and c characterize each of the considered binary systems. Among these constants a gives the magnitude of the interaction (in pure alkali nitrate), b represents the energetic asymmetry (i.e., the difference between the heat of solution of the alkali nitrate in pure silver nitrate and of silver nitrate in pure alkali nitrate), while we consider c to be a measure of short-range order (or clustering) among the cations. This particular point is discussed in some detail in our earlier communication.[1] By use of a modified lattice theory we derived there the following approximate relation between a, b, and c:

$$c \cong -2(a+b/2)^2/ZRT.$$

Here Z is the number of next-nearest neighbors in the fused salt mixture (presumably about 10 in the liquid nitrates), while the other symbols have their usual meaning.

We give in Table I a summary of the experimental values of the constants a, b, and c. The variation in a underscores the already mentioned change in interaction from exothermic in rubidium-silver and potassium-silver to endothermic in the sodium-silver and lithium-silver systems. Note, however, the relatively small difference in the values of a for the lithium and sodium systems, and the much larger difference between sodium and potassium, and also between potassium and rubidium.

[8] V. A. Palkin, Doklady Akad. Nauk S.S.S.R. **66**, 71 (1949).
[9] A. P. Palkin, J. Russ. Phys. Chem. Soc. **58**, 1334 (1926).
[10] D. Hissink, Z. physik. Chem. **32**, 537 (1900).

TABLE I. Summary of heat of mixing data (in cal/mole) for silver nitrate-alkali nitrate mixtures at 350°.

($\Delta H^M = X(1-X)[a+bX+cX(1-X)]$;
X is the mole fraction of silver nitrate.)

System	a	b	c (exptl)	c (calc) $-2(a+b/2)^2/10RT$
(Li—Ag)-NO_3	702	−108	~0	−68
(Na—Ag)-NO_3	677	−156	~0	−58
(K—Ag)-NO_3	−303	−294	~0	−33
(Rb—Ag)-NO_3	−944	−337	−297	−200

On the other hand we find that the energetic asymmetry in the considered systems changes in a completely regular fashion from lithium-silver to rubidium-silver, i.e., the interaction between the two species is always more exothermic (or less endothermic) in the mixtures rich in silver nitrate than in the corresponding solutions rich in alkali nitrate. This effect is more pronounced the larger the alkali nitrate ion.

In the last column in Table I we also give the values of c calculated from our modified lattice theory. In view of the very significant uncertainty in the experimental values of c (±50 to 100 cal/mole) we consider the agreement between calculation and experiment to be quite satisfactory.

Here we recall that for the binary alkali nitrates we found the following approximate expression for the enthalpy of mixing,

$$\Delta H^M \cong -140X(1-X)\delta^2 10^3 \text{ cal/mole}. \qquad (2)$$

The symbol δ is used to denote the ratio $(d_1-d_2)/(d_1+d_2)$; d_1 and d_2 are the interionic distances characteristic of each of the two pure salts. This expression neglects second-order effects such as energetic asymmetry and short-range order, but gives the values of ΔH^M near the 50-50 composition to a very good approximation. It is believed that expressions of this type may have application for other purely ionic systems, such as, e.g., the alkali halide mixtures.[1]

Note that this expression predicts negative enthalpies of mixing only. Therefore it clearly does not represent the observed behavior of the silver nitrate-alkali nitrate mixtures. However, it is of considerable interest to explore the deviation of the considered silver nitrate systems from this simple relation. For this purpose we need a value of the characteristic interionic distance in silver nitrate d_{AgNO_3}. As for the alkali nitrates we set

$$d_{AgNO_3} = r_{Ag^+} + r_{NO_3^-}.$$

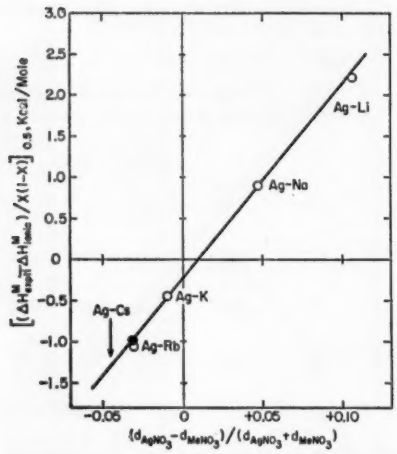

FIG. 5. The deviations of the heats of mixing in silver nitrate-alkali nitrate mixtures from the values calculated for the hypothetical, ionic silver nitrate. Open circles are based on actual experimental values; filled circle (for [Ag-Rb]NO_3) obtained when curvature in $\Delta H^M/X(1-X)$ is neglected. Arrow points toward predicted value for (Ag-Cs)NO_3.

According to Pauling[11] the ionic radius of Ag^+ is 1.26 A, while we have previously calculated a value of $r_{NO_3^-}$ (2.19 A).[1]

In the following we shall, for simplicity, refer to the enthalpies of mixing calculated according to Eq. (2) as $\Delta H_{\text{ionic}}{}^M$. In Fig. 5 we have plotted the deviations from this equation ($\Delta H_{\text{exptl}}{}^M - \Delta H_{\text{ionic}}{}^M$) for the four systems covered in the present study versus the parameter δ. The curve clearly is a straight line, which fails to pass through the origin by only a small amount.[12] The slope of this line is 24 kcal (per mole). Still neglecting second-order terms we accordingly have the following approximate expression for the heats of mixing of all the silver nitrate-alkali nitrate systems

$$\Delta H^M \cong -X(1-X)[140\delta^2 - 24(\delta - 0.01)]10^3 \text{ cal/mole}. \quad (3)$$

Previously we have drawn attention to the fact that the empirical factor which relates the heat of mixing of the alkali nitrates to the parameter δ^2 (140 kcal/mole) is of the order of magnitude of the lattice energy of the salts. It is worth noting that the new empirical factor (24 kcal/mole) which relates departures of the enthalpy of mixing in the silver nitrate systems from the expression valid for the alkali nitrates, is comparable in magnitude to the nonionic contribution to the lattice energy of silver nitrate. According to the very recent work of Ladd and Lee[13] the lattice enthalpy of silver nitrate ($r_{Ag^+}=1.26$ A) is 190 kcal, while the corresponding figures for sodium nitrate ($r_{Na^+}=0.95$) and potassium nitrate ($r_{K^+}=1.33$) are 173 and 157 kcal, respectively.

We believe this should be explored further, by considering additional systems, in which the nonionic contributions to the lattice energy of one of the solution partners differ from that in silver nitrate. We shall return to this point later. For this purpose we are at present also studying the heats of mixing in thallium nitrate-alkali nitrate melts. Undoubtedly thallium nitrate is more nearly ionic than silver nitrate, and we accordingly predict smaller departures from Eq. (2). Preliminary results indicate that such is indeed the case.

While detailed heat and other thermodynamic data are not available for the liquid alkali halide mixtures, there is a considerable amount of information in the literature on the corresponding silver halide (AgY) alkali halide (MeY) systems. In most cases this information has been obtained from study of high-temperature galvanic cells of the type

$$\text{Ag(s)/[AgY+MeY(l)]/Y}_2\text{(g)}.$$

Undoubtedly the most important single piece of work in this field is the now classical investigation by Hildebrand and Salstrom of the liquid bromides.[2] More recently there have been similar studies of the corresponding chloride systems.[3–5] However, to the knowledge of the authors, no equivalent information is as yet available on the iodides or the fluorides.

There is still some doubt about the importance of the entropy of mixing in these mixtures. Hildebrand and Salstrom found ideal or nearly ideal entropies in the bromide systems. However, some of the more recent work on the chlorides points toward positive excess entropies. In all cases the excess entropies have been obtained from the temperature coefficient of the emf only. Until additional independent evidence is available we believe we are justified in assuming that

TABLE II. Characteristic values of $A=\Delta H^M/X(1-X)$ (in kcal/mole) for liquid mixtures of silver nitrate, -bromide, and -chloride with the corresponding alkali salts.

Cation system	Nitrates exptl[a]	Bromides exptl[b]	Bromides calc[c]	Chlorides exptl
Ag—Li	0.65	1.88	1.8	2.0[d]
Ag—Na	0.59	1.05	1.5	0.8[e]
Ag—K	−0.45	−1.48	−0.9$_5$	−0.8[f]
Ag—Rb	−1.19	−2.58	−2.1	...

[a] Evaluated at $X=0.5$.
[b] Reference 2.
[c] Equation (4).
[d] Reference 3 (assuming ideal entropies of mixing).
[e] Reference 4 (assuming ideal entropies of mixing).
[f] Reference 5 (neglecting data at low AgCl concentrations, assuming ideal entropies).

[11] L. Pauling, *Nature of the Chemical Bond* (Cornell University Press, Ithaca, New York, 1948), 2nd ed.
[12] Note that if we had adopted a value of r_{Ag^+} of 1.20 rather than 1.26 A this line would have passed through the origin.
[13] M. F. C. Ladd and W. H. Lee, J. Inorg. & Nuclear Chem. **13**, 218 (1960).

Hildebrand and Salstrom's conclusion may apply also for the chloride systems. Under this assumption we have $\Delta H^M = \Delta F^E$, both for the integral and for the partial molal quantities.

Hildebrand and Salstrom found also that the partial excess free energies in the bromide systems can be represented by expresssions of the type

$$\Delta F_{AgY}{}^E = A(1-X_{AgY})^2 \cong \Delta \bar{H}_{AgY},$$

where A is a characteristic constant for each of the binary systems. Thus we may write for the integral heats of mixing

$$\Delta H^M \cong AX(1-X).$$

In Table II we compare the experimental values of A for the various silver halide-alkali halide systems with the values for the nitrates. Since all the nitrate systems show some energetic asymmetry, we use in this comparison our own values of $\Delta H^M/X(1-X)$ at the 50–50 composition.

This table illustrates in a convincing way the very extensive similarity between the silver nitrate and the silver halide mixtures. We note in particular the fact that the lithium and sodium systems are endothermic throughout, while the potassium and rubidium systems are exothermic. We see also that the numerical values of A are comparable for the bromide and the chloride systems, and in each case two to three times as large as for the nitrates.

In view of this extensive similarity we consider it likely that the observed heats of mixing in the silver nitrate-alkali nitrate mixtures must be accounted for by the same factors which govern the solution properties of the corresponding halide systems.

It was already suggested by Hildebrand and Salstrom that the behavior of the mixed bromide systems arises from the difference in the bonding in silver bromide and in the alkali bromides. This point of view was elaborated further by Thurmond,[14] who studied the molar refractivity of liquid mixtures of silver bromide with lithium and rubidium bromide. Although Thurmond was unable to detect any departure of the molar refractivity from additivity, he suggested that the observed positive and negative deviations from ideality might be accounted for in the following way: in pure liquid AgBr there is resonance between the covalent and ionic bonds which tie the Ag^+ ion to its neighboring Br^- ions. If the Br^- ion has a small cation with a strong field such as Li^+ or Na^+ on its other side, this resonance will be disturbed and a positive enthalpy of mixing results. On the other hand if the second nearest neighbor of the Ag^+ ion is a large cation with a weak field such as K^+ and Rb^+, the covalent bonding will be enhanced, and the mixed system will have a lower energy, i.e., a negative enthalpy of mixing is observed.

[14] C. D. Thurmond, J. Am. Chem. Soc. **75**, 3928 (1953).

An alternative interpretation, advanced by Förland,[15] is based on the observation that silver bromide and silver chloride undergo quite small volume changes on fusion compared to the corresponding alkali salts. Förland suggests that this points toward a difference in structure in the liquid state for the two types of salt. He then goes on to postulate that this structural difference will give rise to a significant positive contribution to the enthalpy of mixing. Only for mixtures involving the larger cations K^+ and Rb^+ is this positive enthalpy contribution overshadowed by a negative contribution which arises in large measure from the changes in the nearest- and next-nearest- neighbor configurations.

We believe that the new heat data for the nitrate mixtures, and their demonstrated similarity with the halides, are more consistent with the Hildebrand-Thurmond interpretation. We recall first that the radius of the bromide ion is 1.95 A, i.e., it is of magnitude comparable to the nitrate ion.[11] Thus we predict that to a first approximation the heats of mixing of the liquid alkali bromides will also be represented by expression (2).

For solid silver bromide the lattice energy is 211 kcal, while the corresponding values for sodium bromide and potassium bromide are 176 and 161.5 kcal, respectively.[16] Since the silver ion is intermediate in size between the sodium and potassium ions, we conclude that the nonionic contribution to the lattice energy of silver bromide must be approximately 45 kcal, or nearly twice as large as for silver nitrate. In analogy with Eq. (3) we accordingly write the following approximate expression for the heats of mixing of the liquid mixtures of silver bromide with alkali bromides,

$$\Delta H^M \cong -X(1-X)[140\delta^2 - 45(\delta - 0.01)]10^3 \text{ cal/mole}. \quad (4)$$

Values of $\Delta H^M/X(1-X)$ calculated from this expression are included in Table II for comparison with Hildebrand and Salstrom's experimental data. In view of the uncertainty associated with our use in Eq. (4) of the numerical "constants" derived for the silver nitrate mixtures, the agreement is remarkably good. This agreement provides additional support for our suggestion that semiempirical expressions such as (2) and (3) may be quite useful in predicting the heats of mixing in as yet unexplored systems.

In concluding the present discussion we finally want to mention the recent emf study by Laity[6] of concentration cells in the binary system silver nitrate-sodium nitrate. Laity found that the entropies of mixing in this system are ideal or very nearly ideal. At about 330° the excess partial free energies of silver nitrate can be

[15] T. Förland, *On the Properties of Some Mixtures of Fused Salts* (N. T. H. Trykk, Trondheim, Norway, 1958).

[16] O. K. Rice, *Electronic Structure and Chemical Binding* (McGraw-Hill Book Company, Inc., New York; 1940), pp. 235–238.

represented by the relation

$$\Delta\bar{F}_{AgNO_3}{}^{E}=840X_{NaNO_3}{}^{2}\ \text{cal/mole}.$$

When we compare this relation with our own heat data, we obtain the following approximate expression for the integral excess entropies of mixing in this system at 330°,

$$\Delta S^{E}=(\Delta H^{M}-\Delta F^{E})/T\cong-0.4X(1-X)\ \text{cal/deg mole}.$$

Thus we are able to confirm that the entropies are nearly ideal. In fact, the excess entropies in the middle of the system should be about -0.1 cal/deg mole.

ACKNOWLEDGMENTS

The authors wish to acknowledge that information regarding the phase diagrams of the silver nitrate-alkali nitrate systems was brought to their attention by Dr. E. Ibserson of the Argonne National Laboratory. This work was supported by the Office of Naval Research at the University of Chicago.

THE JOURNAL OF CHEMICAL PHYSICS VOLUME 35, NUMBER 1 JULY, 1961

Infrared Spectra of NaOH Above and Below the Melting Point

JACOB GREENBERG AND L. J. HALLGREN

Minneapolis-Honeywell Research Center, Hopkins, Minnesota

(Received September 6, 1960)

The absorption spectra of NaOH and mixtures of NaOH in $NaNO_3$, in $NaNO_2$ and in LiCl—KCl eutectic mixture have been observed. The shift in the band position for NaOH as the temperature is varied is explained on the basis of hydrogen bonding in the melt.

ONE of the primary impurities in inorganic alkali metal salts is water. If hydrolysis occurs upon melting, the melt will be contaminated with hydroxides.[1] The presence of these materials is extremely undesirable because of their corrosive action on container materials. In order to be able to analyze for the presence of hydroxide ion and in order to be able to better understand the influence of these ions in various molten salt solvents, the infrared absorption spectra of NaOH above and below the melting point were measured. The data were obtained by supporting NaOH in the interstices of a fine mesh platinum screen which was placed into the light path.[2,3]

Spectra were obtained on samples of assayed reagent (A.R.) grade NaOH (low in carbonate) and by synthesizing NaOH *in situ*. Data were also obtained on systems containing NaOH in $NaNO_3$, $NaNO_2$, and in LiCl-KCl eutectic mixture. The optical cell consisted essentially of a platinum screen fitted into a T-shaped tube which was equipped with NaCl windows. The platinum screen had 32 fibers/cm and was 0.15 mm thick, 2.0 mm long, and about 1.0 cm wide. In order to reduce the amount of thermal emission and in order to keep insulation problems at a minimum only the screen was heated. This was done by passing currents up to 15 amp directly through it. The screen showed no signs of deterioration after repeated use. A Pt-Pt, Rh (13%) thermocouple welded to the center of the screen was used to measure the temperature. The thermocouple was also used as the sensing element of a proportional controller constructed from Brown recorder components. Temperatures were controlled to ± 2°C. The windows were mounted onto the cell simply by placing them into rubber sleeves which were pulled onto each end of the cell. With this arrangement the system could be evacuated to 18 μ Hg pressure with just a rotary pump.

The NaOH samples (containing 0.4% $CO_3^{=}$ by weight) were placed onto the screen which was then fitted onto the optical cell. By simultaneously evacuating and heating, a water-free melt was obtained. This was done by initially observing the absence of the H–O–H peak at 6.1 μ and then continuing treatment for an hour beyond this point. Mixtures of NaOH in LiCl-KCl, $NaNO_3$, and $NaNO_2$ were treated in a similar manner. In order to synthesize NaOH, the platinum screen was dipped into molten NaCl, which was allowed to freeze on the screen, which was then placed into the optical cell. Sodium was then vacuum deposited onto the screen and allowed to react with water vapor. The apparatus is shown in Fig. 1. Two attachments, one containing water and the other containing sodium metal in a Pyrex cup heated by a 1-ohm Nichrome resistance wire, were placed onto the optical cell. After the system had been evacuated, the platinum screen was rotated

[1] D. A. Otterson, J. Chem. Phys. **33**, 227 (1960).
[2] J. Greenberg and L. J. Hallgren, Rev. Sci. Instr. **31**, 444 (1960).
[3] J. Greenberg and L. J. Hallgren, J. Chem. Phys. **33**, 900 (1960).

to face the Pyrex cup by means of the ground glass joint. Sodium metal was then deposited onto the screen. The cup was allowed to cool and at this stage water vapor was introduced and allowed to react and the system was then evacuated.

All measurements were made using the Perkin-Elmer model 21 spectrophotometer equipped with NaCl optics. In order to obtain the 0% to 100% range when the cell was placed into the sample beam, the reference beam had to be attenuated. This was done with the Perkin-Elmer attenuator attachment. The reference beam was masked off by about 75%. The precision of the wavelength measurements was esti-

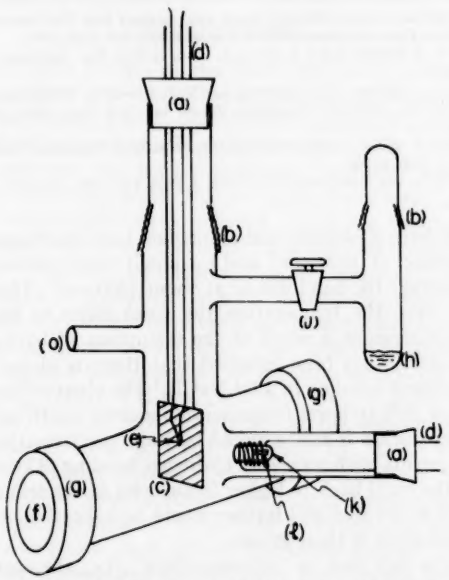

FIG. 1. Optical cell for measuring the infrared absorption of NaOH. (a) Rubber stopper, (b) ground glass joint, (c) platinum screen, (d) heating leads, (e) thermocouple, (f) NaCl window, (g) rubber window holder, (h) water, (j) stopcock, (k) Pyrex boat, (l) sodium, (o) vacuum outlet.

mated to be within 0.5%. The spectra were obtained as a result of subtracting the emission of the sample and cell as observed when the shutter was closed (light being received from the heated salt and cell) from the transmission of the filled cell with the shutter open (light being received from the Nernst glower and the heated sample containing cell). These results are reported as relative transmission.

The infrared absorption spectrum of a sample of molten A.R. grade NaOH placed directly on the screen is shown in Fig. 2. The spectrum from 1 to 15 μ consists primarily of one peak corresponding to the principal O–H stretching frequency. No evidence of a sharp peak was found in the region of the first overtone (~7000 cm^{-1}). It was observed that the position of the band shifted as the temperature was changed. In Table I the

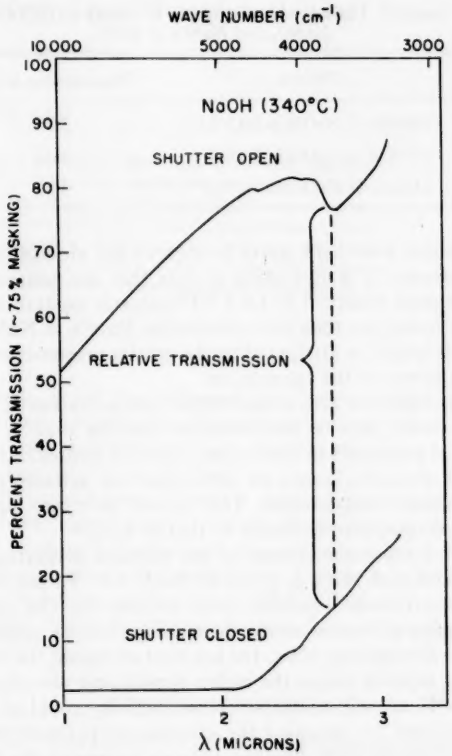

FIG. 2. Spectrum of NaOH at 340°C.

positions of the estimated band centers are given at various temperatures.

Similar results were observed for NaOH synthesized from water and sodium. In Table II the band positions for 15 mole % NaOH in $NaNO_3$, in $NaNO_2$ and in LiCl-KCl eutectic mixture are given.

The bands as observed for the mixtures of NaOH were narrower and less intense than the band observed for the pure material. Since the peaks observed for these dilutions were small, a change in operating conditions were required. In order to maximize the resolution, the platinum screen was removed from the cell and momentarily placed in front of the sample entrance slit. The

TABLE I. Positions of band center of NaOH at various temperatures.

Temperature (°C)	Wave number (cm^{-1})
Room temperature	3610
320	3571
340	3547
360	3547
380	3547
400	3559

TABLE II. Positions of band center of NaOH in LiCl-CCl, $NaNO_3$, and $NaNO_2$ at 100°C.

System	Wave number (cm^{-1})
15 mole % NaOH in LiCl-KCl	355_9
15 mole % NaOH in $NaNO_3$	361_0
15 mole % NaOH in $NaNO_2$[3]	361_0

samples were kept warm to prevent the absorption of moisture. It is interesting to note that the position of the peak observed in LiCl–KCl eutectic mixture is at lower energies than that observed in $NaNO_2$ or $NaNO_3$. This might be attributed to the greater proton-attracting power of the chloride ion.

In order to give a meaningful interpretation of the spectra it may be worthwhile to examine some of the other properties of the system. In alkali hydroxides the OH group is known to have spherical symmetry at elevated temperatures. The crystal structure under these conditions is similar to that of NaCl.[4]

A comparison of some of the physical properties of NaOH and NaCl is given in Table III. Values were selected from available data as close to the same number of degrees above the melting point as possible. The low melting point, the low heat of fusion, the very long liquidus range, the higher density and viscosity of NaOH as well as the lower conductivity could all be explained by assuming the existence of polymer fragments in the melt. Further evidence is given by the fact that the vapor of NaOH consists of dimers.[5] The spectral data can also be interpreted in terms of hydrogen bonding or polymer formation. As the temperature is allowed to rise the band maintains its essential shape and shifts slightly at first to lower then back to higher energies. This shift of band maxima with increasing temperature has been observed in water.[6] However, in this case there is a continuous shift to higher frequencies as the temperature is raised. The O–H stretching frequency for water vapor (no hydrogen bonding) will have a fundamental absorption band in the neighborhood of 3600 cm^{-1} and for liquid water (hydrogen bonding) the band will be at about 3300 cm^{-1}. Thus as we raise the temperature the band shifts to higher frequencies as a result of the disruption of hydrogen bonds. It has been reported that there is almost no hydrogen bonding in solid NaOH.[7] The observed initial band shift to lower frequencies in molten NaOH as the temperature is raised would indicate the formation of fragments with increased hydrogen bonding. The shift of the band back to higher frequencies as the temperature is elevated still further would be indicative of the breakdown of these groups.

The fact that no "dilution effect" (i.e., the appearance of a sharp band at higher frequencies than in the pure sample) was observed in $NaNO_3$, $NaNO_2$, or LiCl-KCl would indicate that there is interaction between the hydroxyl groups and these solvents.

TABLE III. Data on NaOH and NaCl systems.[a]

	NaOH	NaCl
Heat of fusion (kj $mole^{-1}$)	6.356[b]	30.2
Melting point (°C)	322[c]	804.3
Boiling point (°C)	1390[d]	1413[d]
Density (g/ml)	1.98 (350°C)	1.5401 (829.3°C)[e]
Specific conductivity (ohm^{-1} cm^{-1})	2.38 (350°C)	3.660_1 (827.4°C)[e]
Viscosity (cp)	4.0 (350°C)	1.30 °(841°C)

[a] All data unless otherwise noted were obtained from *The International Critical Tables* (McGraw-Hill Book Company, Inc., New York, 1933).

[b] T. B. Douglas and J. L. Dever, J. Research Natl. Bur. Standards, **53,** 81 (1954).

[c] V. A. Khitrov, N. N. Khitrova, and V. F. Khmelkov, *Soviet Research in Fused Salts, 1949–1955* (Consultants Bureau, Inc., New York, 1959), Vol. 1a, p. 3.

[d] N. A. Lange, *Handbook of Chemistry* (Handbook Publishers, Sandusky, Ohio, 1952), 8th ed.

[e] E. R. Van Artsdalen and I. S. Yaffe, J. Phys. Chem. **59,** 118 (1955).

ACKNOWLEDGMENTS

The authors wish to express their appreciation for the assistance given to them by S. A. and Rose Anne.

[4] A. F. Wells, *Structural Inorganic Chemistry* (Oxford University Press, New York, 1959), 2nd ed., Chap. XIII, p. 414.

[5] R. C. Schoonmaker and R. F. Porter, J. Chem. Phys. **28,** 454 (1958).

[6] J. H. Hibben, *The Raman Effect and its Chemical Applications* (Reinhold Publishing Corporation, New York, 1939), Chap. 22, p. 324.

[7] W. R. Busing, J. Chem. Phys. **23,** 933 (1955).

Solid-State Vibrational Spectra of the Methyl and Methyl-d_3 Halides*

MARILYN E. JACOX AND ROBERT M. HEXTER

Mellon Institute, Pittsburgh, Pennsylvania

(Received November 25, 1960)

The vibrational fundamentals of solid CH_3Cl, CH_3Br, and CH_3I and of their fully deuterated counterparts have been examined at 77°K under high resolution. CH_3Cl^{35} has been synthesized and its ν_3 spectrum compared to that of ordinary CH_3Cl, permitting the assignment of the CH_3Cl^{35} and CH_3Cl^{37} contributions in the ν_3 multiplet structure. The relative intensities of absorption in 1:1 CH_3X:CD_3X solid solutions have been measured to test the relationship between splitting, frequency, and absorption intensity predicted by the dipolar correlation model. The test proved to be insensitive. A study of the ν_3 absorption of each component in CH_3Cl:CD_3Cl solid solutions throughout the concentration range has shown that multiplet splitting persists at concentrations as low as 1%.

INTRODUCTION

THE solid methyl halides have often been used for studies of the relationship between crystal structure and solid-state spectra. Solid methyl chloride is among the relatively few simple molecular crystals for which the structure has been determined: Burbank,[1] using x-ray diffraction, found that its space group was C_{2v}^{12}, with four molecules per unit cell. Using this structure together with group theoretical analysis based on the work of Halford and others,[2–4] ν_1, ν_2, and $\nu_3(a_1)$ are predicted to appear in the solid as doublets, while ν_4, ν_5, and $\nu_6(e)$ should have three spectroscopically active components under sufficiently high resolution. Dows[5] has reported measurements on the infrared spectra of CH_3Cl, CH_3Br, CH_3I, CD_3Cl, and CD_3Br at 80°K. Earlier, Hexter[6] had elaborated on the temperature dependence of ν_2 in CH_3I, observed by Mador and Quinn.[7] Hexter concluded that the splitting for this fundamental must be attributed to the correlation field, previously considered to produce splittings too small for observation. Both Hexter and Dows assumed that methyl bromide and methyl iodide have crystal structures isomorphous with that of methyl chloride.

Despite these investigations, many questions concerning the methyl halide spectra and structures remain unanswered. For ν_3 of CH_3Cl and ν_5 of CH_3I the multiplicity observed is greater than that predicted by the theory. A great deal of experimental and theoretical elaboration on the possibility of observable correlation splitting in these molecules has seemed in order. Recently, Hexter[8] has applied the exciton theory of Davydov to dipole-dipole correlation effects in the nondegenerate fundamentals of crystalline methyl chloride. Dows[9] has suggested that hydrogen-hydrogen repulsions in molecular crystals may be more important in causing multiplet structure than are the dipolar correlations favored by Hexter.

The present paper reports a systematic study of the fundamentals of methyl chloride, bromide, and iodide and of their perdeuterated counterparts, using higher resolution than that available to Dows. In addition, solid solutions of the type CH_3X:CD_3X have been studied to gain further information on possible correlation effects.

EXPERIMENTAL DETAILS

The low-temperature cell used for these experiments was a double Dewar constructed of stainless steel, designed for use with liquid nitrogen or liquid helium as coolant in the inner reservoir and with liquid nitrogen in the outer reservoir. The sample was deposited through a glass tube directed at a cesium bromide window, held in good thermal contact with the copper block by a screw-in ring plus a beryllium bronze spring-washer. This copper block was soldered to the bottom of the inner reservoir. The two outer windows of the cryostat were of potassium bromide, held in place by Apiezon W wax. The temperature of the window could be measured using a copper-constantan thermocouple secured directly to the cesium bromide window by Woods metal. The temperature difference between the cesium bromide window and liquid nitrogen in the inner reservoir appeared to be negligible; the window and the copper block gave the same temperature reading when the cell was cooled down.

For all of the measurements we used a Perkin-Elmer 112G spectrometer. This was equipped with a Nernst glower source, a potassium bromide foreprism monochromator, a Bausch & Lomb reflection-type 75-line/mm echelette grating blazed at 12 μ in the first order, a fast thermocouple detector, and a lead telluride detector which is operated at 77°K. The approximate

* This research was supported in part by the United States Air Force through the Air Force Office of Scientific Research of the Air Research and Development Command.

[1] R. D. Burbank, J. Am. Chem. Soc. **75,** 1211 (1953).
[2] R. S. Halford, J. Chem. Phys. **14,** 8 (1946).
[3] H. Winston and R. S. Halford, J. Chem. Phys. **17,** 607 (1949).
[4] D. F. Hornig, J. Chem. Phys. **16,** 1063 (1948).
[5] D. A. Dows, J. Chem. Phys. **29,** 484 (1958); **33,** 1743 (1960).
[6] R. M. Hexter, J. Chem. Phys. **25,** 1286 (1956).
[7] I. L. Mador and R. S. Quinn, J. Chem. Phys. **20,** 1836 (1952).
[8] R. M. Hexter, J. Chem. Phys. **33,** 1833 (1960).
[9] D. A. Dows, J. Chem. Phys. **32,** 1342 (1960).

TABLE I. Spectral resolution of the Perkin-Elmer 112G spectrometer.

ν(cm^{-1})	$\Delta\nu$(cm^{-1})
3961	0.3
2675	0.4
1340	0.2
931	0.6

usable range of this instrument is 600–3900 cm^{-1}. Representative spectral resolutions are given in Table I.

The master calibrations of this instrument, which used frequencies obtained from Downie *et al.*[10] and from Plyler *et al.*,[11] were checked daily against a selected portion of the atmospheric water absorption near 1400 cm^{-1}.

Interference due to atmospheric water in this single beam instrument could be satisfactorily eliminated by sweeping the instrument with compressed air dried in twin columns of Linde 5A molecular sieve. A stream of high-purity nitrogen was necessary to eliminate atmospheric carbon dioxide absorption.

The CH_3Cl and CH_3Br for these experiments were obtained in lecture bottles from the Matheson Company. They were used without further purification, except for freezing with liquid nitrogen and pumping on the frozen sample to remove noncondensable impurities. This procedure was also followed for the other compounds here reported. Mass spectrometric analysis of a typical sample of CH_3Cl indicated 99.4% CH_3Cl, 0.3% CO_2, and 0.3% N_2+O_2. J. T. Baker Company reagent-grade CH_3I was used.

The CH_3Cl^{35} used in several of the experiments was prepared from a sample of 0.125 g Cl^{35} as $NaCl^{35}$ (95.2% of total Cl as Cl^{35}), obtained from the Oak Ridge National Laboratory. Our procedure followed that of Boulin and Simon.[12] To a saturated aqueous solution of $NaCl^{35}$ in vacuum was added an excess of dimethyl sulfate. At 60°–65°C a steady evolution of CH_3Cl^{35} occurred. The yield was good, and reaction was complete in one to two hours. The principal impurity was dimethyl ether, removed by the formation of the oxonium salt when shaken with concentrated sulfuric acid. A mass spectrometric analysis of the product indicated 94.5% CH_3Cl^{35}, 3.8% CH_3Cl^{37}, and approximately 1.7% impurities, chiefly with molecular weights between 88 and 94.

Samples of CD_3I and CD_3Cl were obtained from Merck and Company, Ltd., of Montreal. Gas phase chromatographic analysis (by Dr. M. H. J. Wijnen and Mr. R. T. Steinbeck) of the CD_3I gave its purity as greater than 99%; mass spectrometric analysis (by Professor W. H. Hamill, University of Notre Dame) showed 1% CD_2HI. Mass spectrometric analysis of the CD_3Cl indicated 98.4% CD_3Cl and 1.6% CD_2HCl.

The CD_3Br was prepared from silver acetate-d_3 via the Hunsdiecker reaction, in which bromine vapor was slowly passed through a column very loosely packed

TABLE II. Fundamental frequencies of CH_3Cl and CD_3Cl (cm^{-1}).

CH_3Cl			CD_3Cl	
ν_{gas}	ν_{solid}		ν_{solid}	ν_{gas}
2966.2	2950 ±0.8 2953	ν_1 (a_1)	2146.8±0.6 2148.7	2161
1354.9	1336.0±0.4 1345.5	ν_2 (a_1)	1010.2±0.4 1017.0 1018.2 (*sh*)	1029
732.1	694.5±0.5 698.6 703.9	ν_3 (a_1)	668.2±0.5 672.9 677.8	695
1454.6	1437.6±0.4 1441.8 1445.2	ν_5 (e)	1048.0±0.4 1051.5	1058
1015.0	1021.0±0.4	ν_6 (e)	770.0±0.3	775

[10] A. R. Downie, M. C. Magoon, T. Purcell, and B. Crawford, Jr., J. Opt. Soc. Am. **43,** 941 (1953).
[11] E. K. Plyler, A. Danti, L. R. Blaine, and E. D. Tidwell, J. Research Natl. Bur. Standards **A64,** 29 (1960).

TABLE III. Fundamental frequencies of CH_3Br and CD_3Br (cm^{-1}).

CH_3Br			CD_3Br	
ν_{gas}	ν_{solid}		ν_{solid}	ν_{gas}
2972	2942 ±1	ν_1 (a_1)	2140.5±0.6	2157
1305	1291.4±0.3 1294.2	ν_2 (a_1)	979.8±0.4 982.0	993
611	(doublet)	ν_3 (a_1)	...	578
3056.8	3040 ±2	ν_4 (e)	...	2293
1444	1420.7±0.4 1435.2	ν_5 (e)	1038.0±0.4 1050.0	1056.4
954	957.5±0.3 963.0	ν_6 (e)	715.4±0.3 720.0	712

TABLE IV. Fundamental frequencies of CH_3I and CD_3I (cm^{-1}).

CH_3I			CD_3I	
ν_{gas}	ν_{solid}		ν_{solid}	ν_{gas}
2968.9	2933 ±1	ν_1 (a_1)	...	2130
1251.5	1235.2±0.3 1239.8	ν_2 (a_1)	937.5±0.4 940.0	950.7
1440.3	1395.8±0.4 1401.0 1419.9 1425.2	ν_5 (e)	1028.5±0.4 1038.5	1048.7
880.1	887.0±0.3 895.1	ν_6 (e)	658.2±0.3 665.7	661.5

[12] Ch. Boulin and L-J. Simon, Compt. rend. **170,** 595 (1920).

with the silver acetate mingled with Pyrex wool, then through ascarite. The products were condensed at liquid-nitrogen temperature. Mass spectrometric analysis of the sample used in these measurements indicated 97% CD_3Br, approximately 2% $CO+O_2$, less than 1% CD_3COOCD_3, and less than 0.3% of either CH_3OH or CD_2O.

EXPERIMENTS ON PURE COMPOUNDS

Tables II–IV summarize the results of our experiments. The spectra obtained for the fundamentals of the methyl halides agree well with those reported by Dows.[5] However, the spacing found for the components of ν_1-CH_3Cl is less than that reported by Dows, who observed components at 2951.2 and 2958.2 cm^{-1}. The higher resolution available in our experiments has yielded a doublet also for ν_1-CD_3Cl. Dows reported only a doublet for ν_3-CD_3Cl. However, confirmation

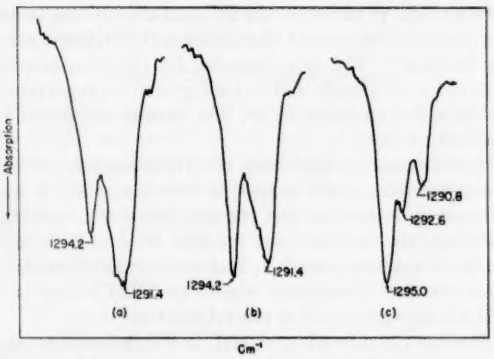

FIG. 1. ν_2-CH_3Br for various deposition rates. (a), (b) Slow deposition; (c) rapid deposition.

of the triplet herein reported has been given by supplementary observations on a Beckman IR-7 spectrometer, which very satisfactorily eliminates interference by atmospheric CO_2 absorption in this region. Components arising from crystal field splittings usually have somewhat more comparable intensities than those assigned by Dows to ν_4-CH_3Br. Possibly the very weak higher frequency component which he reported is a combination with a lattice mode. In this paper only the 3040 cm^{-1} peak is assigned to ν_4-CH_3Br. ν_{gas} values are the observed values reported by King, Mills, and Crawford.[13]

Errors are estimated with respect to the true frequency. The relative positions of peaks in a multiplet band are sufficiently constant to permit a numerically similar estimate for the error in observations of the *splitting* of a multiplet.

ν_3 in CD_3Br, CH_3I, and CD_3I was too low in frequency for study with our instrument. Except in

[13] W. T. King, I. M. Mills, and B. Crawford, Jr., J. Chem. Phys **27**, 455 (1957).

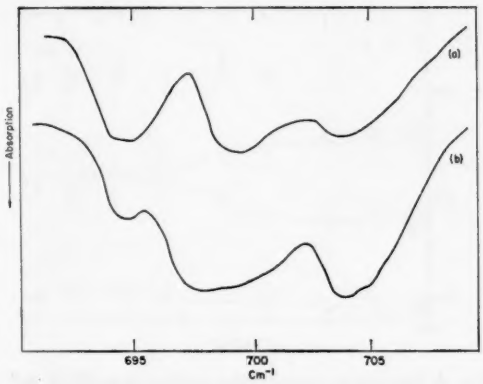

FIG. 2. ν_2-CH_3Cl. (a) Ordinary CH_3Cl (75.4% CH_3Cl^{35}); (b) 94.5% CH_3Cl^{35}.

CH_3Br, ν_4 was not sufficiently intense for convenient study.

Certain of the fundamentals—notably ν_2 in CH_3Cl and CH_3Br and in their deuterated counterparts—are very sensitive to the rate of deposition of the sample. Figure 1 shows three different spectra obtained for ν_2-CH_3Br. Forms (a) and (b) are both obtained with relatively slow deposition rates, while form (c) seems to be associated with more rapid deposition. Once observed, any of these forms seems to be preserved during annealing by warming the sample to a point just short of loss of the sample from the window, then recooling. Annealing CH_3Cl sometimes sharpens individual peaks. Occasionally, the initial CH_3Cl deposit gives a broad singlet whose structure can be resolved after annealing. To detect possible orientation effects in samples showing this anomalous behavior, a Perkin-Elmer six-plate AgCl polarizer was placed in the beam. No observable changes in the spectra were noted, regardless of the polarizer orientation.

Except for ν_3, to be discussed below, these maximum multiplicities are compatible with the observed spectra of CH_3Cl and CD_3Cl. Until recently, it has been assumed that the crystal structures of CH_3Br and CH_3I are isomorphous with that of CH_3Cl. However, Dows'

TABLE V. Predicted and observed absorption intensity ratios in $CH_3X:CD_3X$.

X	Fundamental	$\frac{(\nu_0\Delta\nu)_H}{(\nu_0\Delta\nu)_D}$	$\left(\frac{p_H^2}{p_D^2}\right)_{solid}$	$\left(\frac{p_H^2}{p_D^2}\right)_{gas}$
Cl	ν_1	2.24±0.92	1.35	1.47±0.12
Cl^{35}	ν_3	1.12±0.16	1.33	1.51±0.11
Cl	ν_5	>1.87±0.37	2.25	1.87±0.45
Br	ν_2	1.86±0.38	1.02	1.25±0.10
	ν_5	[1.65]±0.07	2.10	1.72±0.16
	ν_6	[1.45]±0.13	2.66	3.58±0.25
I	ν_2	2.53±0.44	1.61	1.52±0.20
	ν_5	>6.2 ±2.1	1.72	1.78±0.40
	ν_6	[1.26]±0.07	1.48	2.84±0.36

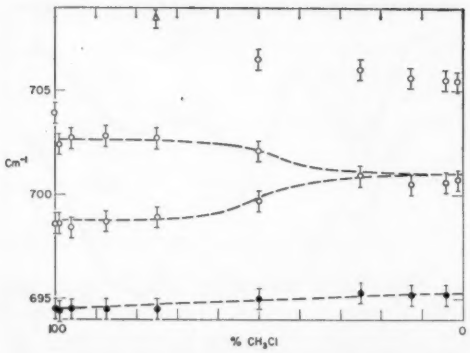

FIG. 3. Frequencies of absorption maxima in ν_3-CH_3Cl region for mixtures of CH_3Cl and CD_3Cl. ● Assigned to CH_3Cl^{37}; ○ attributable to CH_3Cl^{35}; △ shoulder.

observation of a quartet for ν_5-CH_3I is incompatible with this assumption, Hexter[8] has postulated a monoclinic crystal structure for CH_3I which would be compatible with the observed spectrum. The spectrum of solid CH_3Br is sufficiently simple to be compatible with either structure. X-ray determination of at least the space groups of CH_3Br and CH_3I is essential for further analysis of these systems.

The observation of a triplet for ν_3-CH_3Cl and for ν_3-CD_3Cl is incompatible with the group theoretical predictions. Dows[5] has suggested that the central peak may be attributed to $\nu_3-CH_3Cl^{37}$ and the outer peaks to $\nu_3-CH_3Cl^{35}$. It was assumed that the concentration of CH_3Cl^{37} was sufficiently low to prevent observation of a splitting due to correlation between pairs of adjacent like molecules. The sample of 94.5% CH_3Cl^{35} was synthesized to check this assignment. A typical spectrum of $\nu_3-94.5\%$ CH_3Cl^{35}, together with ν_3 for ordinary CH_3Cl, is shown in Fig. 2. Repeated experiments have shown no changes in ν_3 of these samples upon annealing or upon variation of the sample deposition rate. Therefore, it appears clear that a revised assignment attributing $\nu_3-CH_3Cl^{37}$ to the lowest frequency is necessary. In view of the effect of environment on the observed frequencies of solute molecules (ν_3 for 0.5% CH_3Cl^{35} in Ar is a singlet at 722.5 cm^{-1}!), it is easily possible that the correspondences drawn by Dows for 3% CH_3Cl in CH_3I are fortuitous. There were no differences between other frequencies in CH_3Cl^{35} and their counterparts in normal CH_3Cl.

EXPERIMENTS ON MIXTURES OF ISOTOPICALLY RELATED SPECIES

1:1 Mixtures

The validity of the dipolar correlation model can be tested using the relationship

$$(\nu_0\Delta\nu)_H/(\nu_0\Delta\nu)_D=\mathbf{p}_H^2/\mathbf{p}_D^2,$$

derived by Hexter.[8] $\mathbf{p}=(\partial\mu/\partial Q)$ for the molecular normal mode being studied *in the crystal*; ν_0 is the mean frequency of that fundamental in the solid; $\Delta\nu$ is its observed correlation splitting. This relationship is valid for any pair of molecules related by an isotopic substitution which does not alter the molecular symmetry; here it is specialized to the ratios of corresponding quantities in the normal molecule (H) and the perdeuterated molecule (D).

The ratio $\mathbf{p}_H^2/\mathbf{p}_D^2$ is not necessarily the same for molecules in the solid state as for molecules in the gaseous state. An estimate for this ratio in the solid can be obtained by comparing the intensities of the corresponding fundamentals in a 1:1 solid solution of the two isotopically related compounds. In this situation the distribution of various types of molecular interaction, however complicated, should be the same for either species. Moreover, one need not reckon with the problem of estimating the sample thickness.

To obtain areas proportional to the intensities, and hence to the $\mathbf{p}^2$ ratios for the 1:1 mixture, semilog paper was used to plot percent transmission (logarithmic axis) vs frequency. The area bounded by the transmission curves for the sample and its background is proportional to $\int\alpha(\nu)d\nu$ and hence to $\mathbf{p}^2$. The results are given in Table V.

Unfortunately, only half the fundamentals of the methyl halides could be used in this test. Since it was of primary interest to test the possibility of correlation splitting, the unsplit fundamentals were not studied. In all of the compounds ν_4 had too low an absorption intensity for convenient work. ν_2-CD_3Cl and ν_6-CH_3Cl are superposed in the 1:1 mixture.

For ν_5-CH_3Cl and ν_5-CH_3I, in which both site and correlation splitting are observed, it is possible to set a lower limit on the correlation splitting ratio by estimating the half bandwidth as the maximum value of the unresolved correlation splitting in the deuterated compounds. Correlation pairs in these compounds were identified by studying the concentration dependence of the splitting in isotopic mixtures. As CH_3Cl is diluted with CD_3Cl, the 1445.2 cm^{-1} and 1441.8 cm^{-1} peaks merge. Matrix studies on CH_3I have also shown that the 1395.8 cm^{-1} and 1401.0 cm^{-1} peaks merge, as do the 1419.9 cm^{-1} and 1425.2 cm^{-1} peaks.

Brackets are used to indicate intensity ratios where site splitting is likely to be the predominant phenomenon.

The dipole moment derivative ratios for the gas are taken from the work of Dickson, Mills, and Crawford.[14] Corresponding to their measure of error, we have computed the *maximum* likely error in these ratios. The error estimates for our frequency-splitting ratios are based on a normal distribution. Many factors may introduce errors in the area measurements, including the relatively high noise level in many of the spectra,

[14] A. D. Dickson, I. M. Mills, and B. Crawford, Jr., J. Chem. Phys. **27,** 445 (1957).

difficulties in estimating the base line for spectra taken with a single beam grating instrument, and small deviations occurring in spectral replotting and in planimeter tracing. Almost certainly the error in the solid state intensity ratios is greater than that in the gas phase intensity ratios and in the frequency-splitting ratios.

Except possibly for ν_6-CH_3Br and ν_6-CH_3I, these results suggest that the *ratio* of the dipole moment derivatives of the isotopically related methyl halides remains constant in the phase change from gas to solid.

Considering the error involved, agreement of the frequency-splitting ratios with the $\mathbf{p}_H^2/\mathbf{p}_D^2$ values is reasonably good. Nevertheless, the precision of these measurements was not sufficiently great to provide a positive test for correlation splitting. The results for cases of probable *site* splitting are of the same order of magnitude. Indeed, if the site splitting values are substituted into the ratio for ν_5-CH_3I and ν_5-CD_3I the frequency-splitting ratio becomes 4.4, which is in closer agreement with the observed area ratio than is the correlation splitting value, 6.2.

$CH_3Cl:CD_3Cl$ Solid Solutions

The observation of *four* absorption maxima each for ν_3-CH_3Cl and ν_3-CD_3Cl in their 1:1 mixture spurred a series of experiments on $CH_3Cl:CD_3Cl$ mixtures over the entire composition range. Earlier, Hornig and Hiebert[15] had conducted similar experiments on HBr:DBr and HCl:DCl which could be explained in terms of dipolar correlation of chains of like molecules. Among the possibilities which might lead to the ν_3-CH_3Cl quartet is a singlet due to CH_3Cl^{37}, plus a singlet due to isolated CH_3Cl^{35} molecules, plus a correlation doublet due to pairs of CH_3Cl^{35} molecules. The effect of appreciable proportions of longer CH_3Cl^{35} chains would be to broaden this doublet and to increase slightly its separation.

To a good approximation, Hiebert's solutions exhibited chain-type interactions. When interactions in two or three dimensions are important, as for CH_3Cl, correlation splitting might give rise to small shoulders on a predominant "monomer" peak at lower concentrations, down to perhaps 5%. Because ν_3 in the methyl halides is nondegenerate, no site splitting is to be expected, regardless of the crystal structure.

Results of the experiments on $CH_3Cl:CD_3Cl$ solutions are shown in Figs. 3 and 4. Hiebert had found multiplet structure in solutions down to about 20% in the minor component. At such compositions, however, the "monomer" peak predominated, with only small shoulders attributable to pair correlations. In contrast, these experiments showed apparent multiplet structure in the lowest concentrations studied, about 1%, with no evidence for the growth of a well-defined "monomer" peak. Below about 10% of the minor component its ν_3 peaks sharpened, and mixtures of 4% CH_3Cl^{35} in CD_3Cl and of 1% CH_3Cl^{35} in CD_3Cl showed a well-separated doublet (700.6 cm^{-1}, 705.5 cm^{-1}). Using ordinary CH_3Cl, the CH_3Cl^{37} peak at 695.2 cm^{-1} was also observed. The situation was even more complicated in solutions having CD_3Cl as the minor component; the ν_3-CD_3Cl region showed *four* well-defined peaks down to 1% CD_3Cl. By analogy, the lowest of these was assigned to CD_3Cl^{37}.

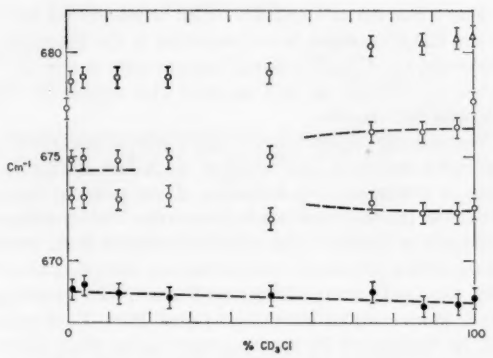

FIG. 4. Frequencies of absorption maxima in ν_3-CD_3Cl region for mixtures of CH_3Cl and CD_3Cl. ● Assigned to CD_3Cl^{37}; ○ attributable to CD_3Cl^{35} or background; △ shoulder.

There was no evidence for splitting of $\nu_3-CH_3Cl^{37}$ in the natural mixture of approximately 25% CH_3Cl^{37}. Because the ν_3 absorption was intense and broad, superposition of a higher frequency $\nu_3-CH_3Cl^{37}$ peak of relatively low intensity on the $\nu_3-CH_3Cl^{35}$ spectrum could conceivably occur. However, the appearance of $\nu_3-CH_3Cl^{35}$ does not support such a possibility.

A simple application of the Teller-Redlich product rule, taking as known the values of $\nu_3-CH_3Cl^{37}$ and $\nu_3-CD_3Cl^{37}$, predicts the unperturbed $\nu_3-CH_3Cl^{35}$ and $\nu_3-CD_3Cl^{35}$ at 701.0 and 674.3 cm^{-1}, respectively. There is good agreement with the 700.6 cm^{-1} peak for dilute solutions of CH_3Cl^{35} in CD_3Cl and with the 674.8 cm^{-1} peak for solutions of CD_3Cl in CH_3Cl. In these calculations, the ν_1 and ν_2 ratios were taken as unity. This approximation should be very good, since each computation compares the corresponding Cl^{35} and Cl^{37} compounds, for which separate Cl^{35} and Cl^{37} contributions have not been resolved.

The broken lines in Figs. 3 and 4 have been drawn to converge in the dilute solution limit to the calculated values for the unperturbed ν_3. At higher concentrations they suggest very approximately the splitting which may result from correlation interactions. Agreement between the observed and the predicted splitting trends is fairly good for the lower frequency peaks of ν_3-CH_3Cl. However, it has not been possible to fit such a curve to the data for CD_3Cl in the intermediate concentration range. This disagreement is particularly disturbing because, except for the frequency decrease arising from its heavier mass, the behavior of a CD_3Cl lattice should be identical to that of a CH_3Cl lattice.

[15] G. L. Hiebert, thesis, Brown University, 1954; D. F. Hornig and G. L. Hiebert, J. Chem. Phys. **27**, 752 (1957).

The spectrum of CD_2HCl, which is present as 1.6% of the CD_3Cl sample, is not recorded in the literature. However, ν_3-CD_2HCl should appear only a few cm^{-1} above ν_3-CD_3Cl. ν_{6a} and ν_{6b} may also appear in the 700–800 cm^{-1} region.

Because the correlation splitting model fails to predict multiplet structure persisting at such low concentrations, a systematic consideration of the possible origin of each of the observed bands is in order. This consideration will be limited to the minor component in the most dilute solid solutions. At concentrations exceeding about 10% the peaks are no longer so distinct, corresponding to the more complex interaction possibilities. Each peak will be designated by its frequency in the most dilute solution.

In Fig. 3, for ν_3-CH_3Cl, the 695.2 cm^{-1} peak has been definitely assigned to $\nu_3-CH_3Cl^{37}$ by comparing the spectra of ordinary CH_3Cl and of CH_3Cl^{35}. The 700.7 cm^{-1} peak certainly is contributed by CH_3Cl^{35}. However, the 705.5 cm^{-1} peak requires further consideration. It is very distinct in the dilute solution of either ordinary CH_3Cl or CH_3Cl^{35} in CD_3Cl. Because it is not present in a thick deposit of CD_3Cl alone, it cannot result either from ν_{6a} of the 1.6% CD_2HCl in the CD_3Cl or from a combination between ν_3-CD_3Cl and a lattice vibration. Its presence in both the ordinary CH_3Cl and the CH_3Cl^{35} minimizes the possibility that it results from an intensely absorbing impurity. The relative intensities of the 700.7 and 705.5 cm^{-1} peaks are approximately the same in 4% and in 1% CH_3Cl^{35}. Only one $\nu_3-CH_3Cl^{35}$ peak, at 722.5 cm^{-1}, appeared in a 200:1 $Ar:CH_3Cl^{35}$ measurement at 4°K, suggesting that the doublet in the $CH_3Cl^{35}:CD_3Cl$ solid solutions arises from a crystalline interaction. It is, however, difficult to explain why the 705.5 cm^{-1} peak disappears as the limit of 100% CH_3Cl is approached.

Figure 4, for ν_3-CD_3Cl in CH_3Cl, is even more difficult to understand. By analogy, the lowest frequency peak, at 668.6 cm^{-1}, has been assigned to $\nu_3-CD_3Cl^{37}$. In the most dilute solutions, the 673.0 cm^{-1} peak is less intense than the 674.8 cm^{-1} peak. If the splitting at low concentrations is real, it might be the second component of CD_3Cl^{37}. However, its intensity appears to approach that of the 674.8 cm^{-1} peak at higher concentrations of CD_3Cl. It seems most likely that both of these peaks are contributed by CD_3Cl^{35}. The 678.6 cm^{-1} peak, which appears only as a shoulder in high concentrations of CD_3Cl, may be contributed by an impurity in the CH_3Cl. When a thick film of CH_3Cl alone is examined, a peak appears just outside the estimated experimental error for coincidence. Two other peaks also appear in the matrix background at somewhat higher frequencies. Unless ν_3-CD_2HCl is extremely strongly absorbing, it probably could not have contributed the 678.6 cm^{-1} peak, which is at least as intense as the 674.8 cm^{-1} absorption. We hope to study the CD_2HCl spectrum, as well as that of CH_2DCl, for report in a later paper.

Explanation of the splitting in dilute solutions remains for the future. Present theory does not favor the possibility that CH_3Cl-CD_3Cl correlations can account for the splitting observed in such dilute solutions. While both dipolar correlation and hydrogen atom repulsion may contribute significantly to the final explanation of the spectra of the solid methyl halides, in the harmonic approximation neither of them would lead to interactions between neighboring molecules of *different* isotopic composition to give a characteristic multiplet splitting. Moreover, the possibility of longer range dipolar interactions accounting for the splitting in dilute solutions seems rather remote. Hexter[8] has compared dipolar correlation effects in a two-dimensional CH_3Cl net considering next-nearest neighbors with effects considering only nearest neighbors. These effects seem to fall off rapidly.

CONCLUSIONS

A review of the spectra of the pure methyl halides under higher resolution has yielded no new features. Neither has the study of the deuterated methyl halides yielded any inconsistencies with the previously postulated crystal structures. A series of experiments on a sample of 94.5% CH_3Cl^{35} has permitted definite assignment of the lowest frequency ν_3-CH_3Cl to peak to CH_3Cl^{37}.

A comparison of the absorption intensities of the corresponding fundamentals in 1:1 $CH_3X:CD_3X$ solid solutions, while beset with high experimental error, has indicated that for these systems the dipolar moment derivative *ratio* remains constant upon condensation. Use of this intensity ratio has not given a sensitive test for the validity of a dipolar correlation splitting mechanism.

A study of $CH_3Cl:CD_3Cl$ solutions over the entire concentration range has indicated that, down to 1% of the minor component, its ν_3 remains a doublet. Existing theory has not provided an adequate explanation for this observation.

ACKNOWLEDGMENTS

We are grateful to G. A. Muccini of the Mellon Institute Radiation Laboratory for the mass spectrometric analyses reported herein and to Dr. D. E. Milligan for suggesting the procedure used in the synthesis of CH_3Cl^{35}, as well as for many helpful discussions.

Thermodynamics of Binary Ion-Exchange Systems*

DAVID H. FREEMAN†

(Received July 22, 1960)

From an algebraic expression for the total excess free energy of a two-component ion-exchange system, separate expressions are derived for the dependence of the logarithm of the activity coefficients of the two components upon the equivalent fraction of counterion in the exchanger. The numerical coefficients required by these expressions and the thermodynamic constant for the ion-exchange reaction are obtained from equilibrium measurements of species activities in the aqueous phase at varying exchanger compositions. This is illustrated with measurements on the distribution of chloride and perchlorate with anion-exchange resin.

A MIXTURE of two ionic species electrostatically bound to the immobile exchange sites of a hydrated ion-exchange material may be treated as a two-component system. The thermodynamic activities of the mixed components may then be obtained from the measured activities of the mixed electrolytes in dilute aqueous solution at varying ratios of the exchangeable ions held in electroneutrality with the exchange sites. This evaluation was first achieved by Kielland[1] in an approximate manner. Later, and independently, Ekedahl, Högfeldt, and Sillèn[2] and Argersinger, Davidson, and Bonner[3] obtained the component activities rigorously using graphical methods. More recently, Gaines and Thomas[4] developed methods for treating water and electrolyte uptakes as additional components. The treatment of a pair of mixed counterions in a water-swollen ion exchanger as a binary system is rigorous, however, if the water content of the exchanger varies linearly with counterion composition, as found for a few systems where this has been studied,[5–7] and if the external electrolyte concentration is sufficiently small such that electrolyte uptake is negligible. Under these conditions the deviations from ideality are simply described by the total excess free energy of the mixed exchanger components. This consideration of ion-exchange equilibria will be used to derive algebraic expressions for the component activity coefficients, an approach which is well known for treating nonelectrolyte mixtures.[8]

We will consider the exchanger as a mixture of two hydrated salts $RA_{1/z_A}\cdot aH_2O$ and $RB_{1/z_B}\cdot bH_2O$, where z_A and z_B are the electrostatic charges of ions A and B. This is equivalent to the following expression for the ion-exchange reaction,

$$1/z_B B + RA_{1/z_A}\cdot aH_2O = 1/z_A A + RB_{1/z_B}\cdot bH_2O + (a-b)H_2O. \quad (1)$$

The activity coefficients for the exchanger salts are divided from the thermodynamic constant K_{th} for this reaction to give the experimentally accessible quantity K_{B-A} as follows,

$$K_{B-A}\equiv\frac{(a_A^w)^{1/z_A}(1-y)^{1/z_B}}{(a_B^w)^{1/z_B}(y)^{1/z_A}}(a_{H_2O})^{a-b}=K_{th}\frac{f_A^{1/z_A}}{f_B^{1/z_B}}. \quad (2)$$

The exchanger salt activities are defined by $a_A = yf_A$ and $a_B=(1-y)f_B$, where y is the equivalent fraction of A in the exchanger. The thermodynamic activities of water and of the aqueous salts are according to the usual conventions. The total excess free energy of the exchanger system G^E is equal to the sum of the excess free energies for the two exchanger salts,

$$G^E = n_A\bar{G}_A^E + n_B\bar{G}_B^E, \quad (3a)$$

where $\bar{G}_A^E = RT\ln f_A$, $\bar{G}_B^E = RT\ln f_B$, and n refers to the number of moles of exchanger salt. Using equivalent fractions and converting the excess quantities per mole into excess quantities per equivalent by the definitions: $\bar{g}_A^E=\bar{G}_A^E/z_A$, $\bar{g}_B^E=\bar{G}_B^E/z_B$ and $\bar{g}^E = G^E/(n_Az_A+n_Bz_B)$ we find

$$\bar{g}^E = y\bar{g}_A^E + (1-y)\bar{g}_B^E. \quad (3b)$$

The logarithm of Eq. (2) includes the quantity $\ln f_A^{1/z_A}/f_B^{1/z_B}$; this term represents the difference between the excess chemical potentials for the two exchanger salts. This quantity is obtained by differentiation of Eq. (3b)

$$(d\bar{g}^E/dy) = \bar{g}_A^E - \bar{g}_B^E, \quad (4)$$

because of the "Gibbs-Duhem" condition for the two components (at constant temperature and pressure)

$$y(d\bar{g}_A^E/dy) + (1-y)(d\bar{g}_B^E/dy) = 0.$$

* Part of Ph.D. thesis by D. H. Freeman, submitted to Chemistry Department, Massachusetts Institute of Technology (1957).

† Present address: Department of Chemistry, Washington State University, Pullman, Washington.

[1] J. Kielland, J. Soc. Chem. Ind. London **52**, 433T (1933).

[2] E. Ekedahl, E. Högfeldt, and L. G. Sillèn, Acta Chem. Scand. **4**, 556 (1950).

[3] W. J. Argersinger, A. W. Davidson, and O. D. Bonner, Trans. Kansas Acad. Sci. **53**, 404 (1950).

[4] G. L. Gaines and H. C. Thomas, J. Chem. Phys. **21**, 714 (1953).

[5] E. Glueckauf and J. F. Duncan, A.E.R.E. C/R: 808.

[6] K. W. Pepper, D. Reichenberg, and K. K. Hale, J. Chem. Soc. **1952**, 3129.

[7] E. W. Baumann and W. J. Argersinger, J. Am. Chem. Soc. **78**, 1130 (1956).

[8] J. H. Hildebrand and R. L. Scott, *The Solubility of Nonelectrolytes* (American Chemical Society Monograph, Reinhold Publishing Co., New York, 1950), 3rd ed.

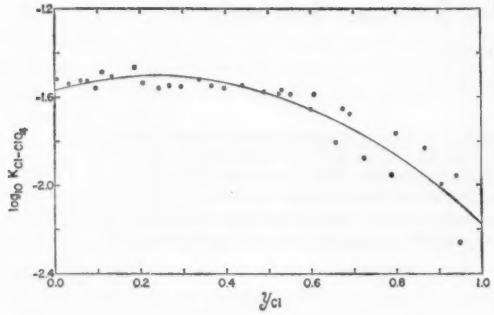

FIG. 1. Measured distributions of chloride and perchlorate with anion-exchange resin at varying fractional chloride composition in the exchanger. The solid line is obtained by least-squares analysis.

Equations (3b) and (4) are readily solved to give the desired excess functions

$$\bar{g}_A{}^E=\bar{g}^E+(1-y)\,(d\bar{g}^E/dy) \tag{5}$$

$$\bar{g}_B{}^E=\bar{g}^E-y(d\bar{g}^E/dy). \tag{6}$$

From the definition of the excess quantities[9] we have the reference states $\bar{g}_A{}^E=0$ at $y=1$ and $\bar{g}_B{}^E=0$ at $y=0$; further, $\bar{g}^E=0$ at both $y=0$ and $y=1$. In the following these boundary conditions must be fulfilled and we will express the equivalental excess free energy using the same expansion as that applied by Guggenheim[10] in the treatment of liquid mixtures which obey Raoult's law

$$\bar{g}^E=y(1-y)\sum_{r=0}^{N}G_r(2y-1)^r. \tag{7}$$

Equations (2), (4), and (7) are combined, using the definitions to give the expression

$$RT\ln K_{B-A}=RT\ln K_{th}+\sum_{r=0}^{N}G_r[-(2y-1)^{r+1}+2ry(1-y)\,(2y-1)^{r-1}]. \tag{8}$$

The experimental values of $\ln K_{B-A}$ are to be fitted parametrically to Eq. (8) using as many terms as the precision requires. From this operation $\ln K_{th}$ and the G_r coefficients are obtained; the latter describe the variation of $\ln f_A$ and $\ln f_B$ with y as derived from Eqs. (5–7),

$$RT\ln f_A=z_A(1-y)^2\sum_{r=0}^{N}G_r[(2y-1)^r+2ry(2y-1)^{r-1}] \tag{9}$$

$$RT\ln f_B=z_By^2\sum_{r=0}^{N}G_r[(2y-1)^r-2r(1-y)\,(2y-1)^{r-1}]. \tag{10}$$

[9] G. Scatchard and C. L. Raymond, J. Am. Chem. Soc. **60,** 1278 (1938).

[10] E. A. Guggenheim, Trans. Faraday Soc. **33,** 151 (1937).

If $\ln K_{B-A}$ is independent of y the system is ideal. If $\ln K_{B-A}$ varies linearly with y only the first term G_0 is necessary, the $\ln f$ values are quadratic in y, and the expressions are identical to those used by Kielland.[1] By expanding these series up to $N=3$ the formation of higher terms becomes apparent:

$$d\bar{g}^E/dy=G_0(1-2y)-G_1[1-6y(1-y)]+G_2[1-8y(1-y)](1-2y)-G_3[1-10y(1-y)](1-2y)^2+\cdots \tag{11}$$

$$\bar{g}_A{}^E/(1-y)^2=G_0-G_1(1-4y)+G_2(1-6y)\,(1-2y)-G_3(1-8y)\,(1-2y)^2+\cdots \tag{12}$$

$$\bar{g}_B{}^E/y^2=G_0-G_1(3-4y)+G_2(5-6y)\,(1-2y)-G_3(7-8y)\,(1-2y)^2+\cdots. \tag{13}$$

As an illustration of the foregoing we will use our equilibrium measurements[11] of the distribution of aqueous KCl and $KClO_4$ with strong base anion exchanger (Dowex 2X8). The total aqueous salt concentration was held at 0.0500 moles/liter and the resulting electrolyte uptake remained less than 0.3% of the total counterion concentration. The number of water molecules in the exchanger corresponded to $RCl\cdot 12H_2O$ and $RClO_4\cdot 4H_2O$ and these numbers did not appear to change with counter-ion loading. The aqueous salts

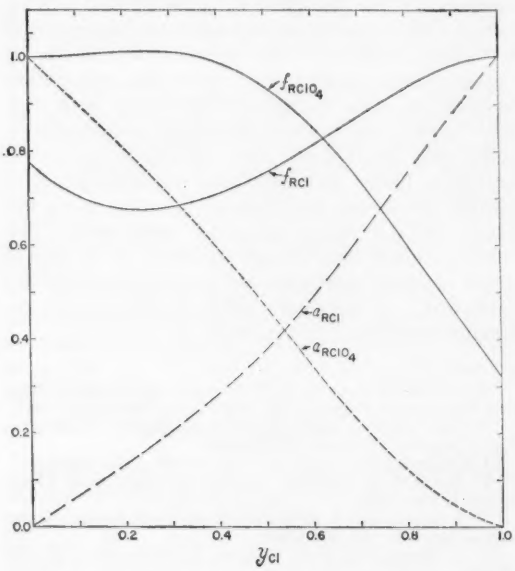

FIG. 2. The activity and activity coefficient functions for each exchanger component RCl and $RClO_4$ follow directly from the least-squares analysis of the measurements in Fig. 1.

[11] Part of Ph.D. thesis by D. H. Freeman, submitted to the Chemistry Department, Massachusetts Institute of Technology (1957).

activity coefficient ratio and the water activity were assumed to be unity in the values of $\log K_{Cl-ClO_4}$ plotted in Fig. 1. The measurements were fitted by least squares to the quadratic $\log K_{Cl-ClO_4} = -1.57 + 0.54y - 1.15y^2$ (± 0.06) where y refers to the equivalent fraction of chloride in the exchanger. From the least-squares coefficients we find $\log K_{th} = -1.68$, $G_0/2.3RT = -0.30$ and $G_1/2.3RT = -0.19$ which gives the activity coefficient expressions: $\log f_{RCl} = (1-y)^2(-0.11-0.76y)$ and $\log f_{RClO_4} = y^2(0.27-0.76y)$. The exchanger salt activities and activity coefficients are shown in Fig. 2.

ACKNOWLEDGMENTS

The author gratefully acknowledges fruitful discussions of this work with Professor Charles D. Coryell, Professor George Scatchard, and Dr. Arthur M. Poskanzer. Financial support was received from the U. S. Atomic Energy Commission.

THE JOURNAL OF CHEMICAL PHYSICS VOLUME 35, NUMBER 1 JULY, 1961

Microwave Spectrum of Methyl Nitrate*

WILLIAM B. DIXON† AND E. BRIGHT WILSON, JR.

Mallinckrodt Chemical Laboratory, Harvard University, Cambridge 38, Massachusetts

(Received December 22, 1960)

The ground-state rotational constants of methyl nitrate show that the five heavy nuclei of the molecule lie in the same plane. The hydrogen atoms of the methyl group are found to be staggered with respect to the nearest oxygen of the NO_2 group. Stark effect measurements yield a dipole moment of 3.10 ± 0.05 D.

Satellites arising from excited states of the torsion of the NO_2 group were observed. Rough relative intensity measurements yield a frequency of 130 ± 20 cm^{-1} for this normal mode and a barrier of 9100 ± 2600 cal/mole. This would seem to indicate a significant amount of double-bond character in the CO—N bond.

The barrier to internal rotation of the methyl group, as determined from torsional satellite splittings, is 2321 cal/mole.

A large discrepancy exists between the experimental and statistical entropies, the reason for which is not clear.

Satellites arising from the combination first excited states of the methyl and NO_2 torsions have an anomalous appearance on the basis of the single internal rotor theory. A qualitative explanation for this is obtained when the theory is extended to include the torsion of the NO_2 group.

INTRODUCTION

METHYL nitrate, CH_3ONO_2, is a molecule whose structure has a bearing on several current controversies. These include the existence of conjugation, the range of validity of Pauling's adjacent-charge rule, the origin of barriers to internal rotation, and the nature of nonbonded interactions. In order to throw light on these questions the microwave rotational spectra of the parent molecule and two isotopic species have been studied from 8000 to 35 000 Mc. While an insufficient number of isotopic species has been studied for a complete structural determination, the data obtained do settle the qualitative structure and the equilibrium conformation.

EXPERIMENTAL

The normal species was prepared by the esterification of cp methanol with cp nitric acid in the presence of concentrated sulfuric acid.[1] Because of its explosive nature, only about 0.01 mole was prepared. It was carefully washed, dried, and purified by bulb-to-bulb vacuum distillation at room temperature, after which the sample showed no signs of decomposition over a two-year interval of storage at room temperature.

The CH_2DONO_2 was prepared in the same way from CH_2DOH. The latter was obtained by the following steps: (a) Partially deuterated malonic acid was prepared by dissolving cp malonic acid in a D_2O–H_2O mixture such that the over-all concentrations of hydrogen and deuterium atoms were in the ratio 3 to 1, respectively. This ratio was calculated to give a favorable statistical yield of CH_2DOH in the final product. The solution was allowed to stand overnight at 60°. (b) The exchanged malonic acid was crystallized out and decarboxylated by heating in a distillation flask, giving partially deuterated acetic acid as the distillate. (c) Silver acetate was formed by neutralizing the acetic acid with ammonium hydroxide and adding a slight excess of a concentrated silver nitrate solution. Re-

* This research was supported in part by the Office of Naval Research and by a grant from the California Research Corporation.

† Present address: Chemical Laboratory, University of Copenhagen, Copenhagen, Denmark. National Science Foundation Predoctoral Fellow, 1957–1960.

[1] *Organic Syntheses*, edited by J. R. Johnson (John Wiley & Sons, Inc., New York, 1939), Vol. XIX, p. 64.

TABLE I. Observed transitions, ground state (Mc).

Transition	Observed ν[a]	Calculated ν[b]
$0_{00}-1_{01}$	8145.90[c]	8145.81
$1_{11}-2_{12}$	15 022.38	[15 022.38]
$1_{01}-2_{02}$	16 135.85	16 135.94
$1_{10}-2_{11}$	17 560.84	[17 560.84]
$2_{12}-3_{13}$	22 441.53	22 441.60
$2_{02}-3_{03}$	23 829.45	23 829.67
$2_{20}-3_{21}$	25 044.80	25 045.18
$2_{11}-3_{12}$	26 237.30	26 237.25
$3_{13}-4_{14}$	29 765.97	29 766.33
$3_{03}-4_{04}$	31 149.42	31 149.63
$3_{22}-4_{23}$	32 461.38	32 461.70
$3_{30}-4_{31}$	32 932.75	32 933.23
$3_{21}-4_{22}$	33 893. [d]	33 984.53
$3_{12}-4_{13}$	34 771.44	34 771.72
$3_{03}-3_{22}$	31 652.05	[31 652.05]
$4_{04}-4_{23}$	32 964.20	32 964.13
$4_{13}-4_{14}$	12 609.40	12 608.73
$6_{24}-6_{25}$	8688.00	8687.61
$9_{36}-9_{37}$	8300.64	8300.83

[a] Estimated uncertainty ±0.1 Mc unless otherwise indicated.
[b] For $A=11\,795.06$ Mc, $B=4707.52$ Mc, $C=3438.29$ Mc.
[c] ±0.2 Mc.
[d] Wavemeter reading (±5 Mc).

moval of all water from the precipitate was necessary in order to ensure the success of the subsequent reaction. (d) Methyl bromide was obtained by decarboxylating the silver acetate with anhydrous bromine[1a] by a method similar to that used by Hauptschein *et al.*[2] for the preparation of perfluoroalkyl bromides. (e) The methyl bromide was finally hydrolyzed with a concentrated sodium hydroxide solution in a sealed tube. The methanol was separated by fractional distillation.

CD_3ONO_2 was made from a commercial sample of CD_3OD kindly made available by Professor M. K. Wilson of Tufts University.

The microwave spectrum was observed on a standard Stark-effect spectrometer[3] with 100-kc square-wave modulation and a phase-sensitive detector. The absorption cell was usually cooled with dry ice. Both oscillographic and recorder display were used. Most of the frequency measurements were made with a frequency standard monitored against the very precise standard of the Cruft Laboratory at Harvard University. Bidirectional sweeps were used.

The observed, assigned frequencies are given in Table I. In addition, there are various weaker lines not assigned and not accurately measured.

Stark effects were quantitatively measured on selected lines, using the 0–1 and 1–2 transitions of OCS for calibration.[4]

Relative intensities of certain satellite lines were obtained from the relative peak heights on recorder traces.

ASSIGNMENTS AND MOMENTS OF INERTIA

The three *a*-type 1–2 pure rotational transitions were identified by their characteristic Stark effects and labelled as ground vibrational state lines by their rough intensities. This led to the assignment of the other lines listed in Table I. All transitions identified were *a*-type but an accurate value of the rotational constant A was obtained from the $3_{03}-3_{22}$ and $4_{04}-4_{23}$ transitions. The rotational constants determined from the bracketed frequencies and rigid-rotor equations are given in Table II. The very satisfactory agreement between observed frequencies and those calculated from the derived values of A, B, and C is displayed in Table I and confirms the assignment.

No fine structure was observed which could be attributed to hyperfine splitting from the nitrogen nuclear quadrupole moment. In the transition which is probably most sensitive to quadrupole effects, the $0_{00}-1_{01}$ transition, there are strong satellite lines so close to the ground-state line that complete resolution was not obtained, thus making it impossible to detect splitting. Otherwise, since splittings as small as about 0.3 Mc were observed in some lines because of internal

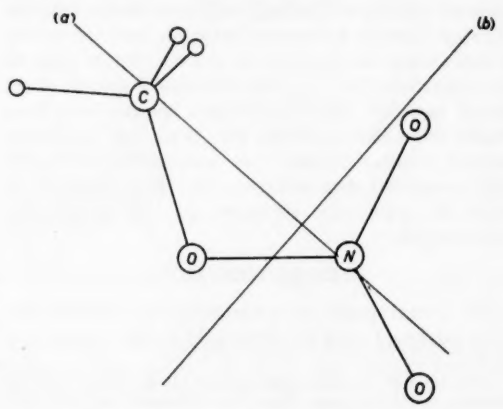

FIG. 1. Conformation of the methyl nitrate molecule.

[1a] A previous attempt had been made at carrying out this reaction in a sealed Pyrex combustion tube at room temperature, as reported by Haszeldine (R. N. Haszeldine, J. Chem. Soc., **1951**, 584). However, one of the runs exploded because of the buildup of carbon dioxide pressure, although no difficulties were mentioned in the literature. In this run 0.025 mole each of silver acetate and bromine were allowed to react in a tube with a volume of about 50 ml.

[2] M. Hauptschein, E. A. Nodiff, and A. V. Grosse, J. Am. Chem. Soc. **74**, 1347 (1952).

[3] K. B. McAfee, R. H. Hughes, and E. B. Wilson, Jr., Rev. Sci. Instr. **20**, 821 (1949).

[4] R. G. Shulman and C. H. Townes, Phys. Rev. **77**, 500 (1950).

rotation effects, an upper limit of about that magnitude can be set on the quadrupole effects.

STRUCTURE

An early electron-diffraction study[5] was not entirely conclusive but favored a configuration with a planar nitrate group and the methyl group out of this plane, the carbon atom lying in a plane of symmetry perpendicular to the plane of the nitrate group. However, it did not completely eliminate a structure with all five heavy atoms lying in the same plane, as shown in Fig. 1.

The observed moments of inertia of Table II are clearly incompatible with the "out-of-plane" structure

TABLE II. Rotational constants and principal moments of inertia.[a]

$A=11\ 795.06$ Mc	$I_a=42.8596$ amu A^2
$B=4707.52$	$I_b=107.388$
$C=3438.29$	$I_c=147.030$

$$I_a+I_b-I_c=3.218 \text{ amu } A^2$$

$$\kappa=-0.696239$$

[a] Conversion factor 5.05531×10^5 Mc amu A^2.

and in good accord with that shown in Fig. 1. Thus, the "planar" structure leads to the relation

$$I_a+I_b-I_c=4m_Hr_H^2=I_\alpha,$$

where m_H and r_H are the mass and distance from the plane of symmetry (a, b plane) of the out-of-plane hydrogen atoms, and I_α is the moment of inertia of the methyl group about its axis. The observed numerical value, 3.218 amu A^2, of $I_a+I_b-I_c$ is very near the expected value for the moment of inertia of a methyl group and, therefore, strongly supports the "planar" structure. The "out-of-plane" structure would have a value of $I_a+I_b-I_c$ estimated to be about seven times larger than the observed value. Evidence against even small deviations from planarity will be given below. In Table III the observed moments are compared with those calculated for the two models discussed by Pauling and Brockway.[5] The agreement with the planar structure, which used the distances C–O 1.43 A, CO–N 1.36 A, N–O 1.26 A and angles CON 105° and ONO 125°16′ is quite good. It would require more isotopic species to obtain accurate interatomic distances from microwave data.[5a]

[5] L. Pauling and L. O. Brockway, J. Am. Chem. Soc. **59**, 13 (1947).

[5a] Recently Millen and Morton[30] have determined the structure of HNO_3, obtaining HO–N 1.405 A, N–O 1.206, ∠HON 105°, ∠HO–NO 116°, ∠HO–NO 114°. If this nitrate group structure is assumed for methyl nitrate together with CH 1.097 A, C–O 1.43 A, CH_3 tetrahedral, ∠CON 105°, the calculated moments deviate considerably more from our experimental values than do those given in Table III.

TABLE III. Comparison of observed and calculated moments o inertia.

	Planar (calc)	Nonplanar (calc)	Observed
I_a	42.5 amu A^2	52.5 amu A^2	42.8596 amu A^2
I_b	106.5	105.7	107.388
I_c	145.8	136.5	147.030

CONFORMATION OF METHYL GROUP

The equilibrium conformation of the methyl group was determined by comparing the experimental rotational constants for CH_2DONO_2 with those calculated from the approximate model. Two possibilities were considered: one in which the methyl hydrogens are staggered with respect to the nearest NO_2 oxygen atom and one in which a methyl hydrogen eclipses the oxygen atom. Either conformation would have both a symmetric and an asymmetric form, the former having the deuterium atom in the plane of symmetry and the latter having it out of the plane. The spectra and rotational constants for the two forms observed are given in Table IV together with the calculated rotational constants for the two conformations. A comparison of rotational constants shows conclusively that the actual conformation is the staggered one, as shown in Fig. 1. Intermediate conformations are ruled out because they would have led to three sets of rotational lines instead of the two observed.

DIPOLE MOMENT

The Stark effect data of Table V leads to the dipole moment components shown here. The calculations were made with the formulas of Golden and Wilson,[6] using the line strengths tabulated by Schwendeman and Laurie.[7] The total dipole moment of 3.10 ± 0.05 D may be compared with the value of 2.85 D from dielectric constant measurements of solutions in benzene.[8]

Without doubt the a component is negatively directed toward the NO_2 group but the direction of the small b component is unknown.

SATELLITE SPECTRUM

Each of the relatively strong ground state transitions is accompanied by a set of weaker satellite lines. A typical set is shown in Fig. 2, with arbitrary labels. The most striking pattern is formed by the lines β, γ, and δ (and sometimes more) quite close to the main line α. These have Stark effects identical with those of the main line. The change of relative intensity with temperature shows that they arise from excited vibrational states, and the mean of the rough values of the

[6] S. Golden and E. Bright Wilson, Jr., J. Chem. Phys. **16**, 699 (1948).

[7] R. Schwendeman and V. W. Laurie, *Line Strengths for Rotational Transitions* (Pergamon Press, New York, 1958)

[8] E. G. Cowley and J. R. Partington, J. Chem. Soc. **1933**, 1252.

TABLE IV. Spectrum of CH_2DONO_2 and comparison of observed and calculated rotational constants.

Transition	Sym	Asym
1_{11}–2_{12}	14 256.37 Mc	14 567.27
1_{01}–2_{02}	15 280.53	15 606.90
1_{10}–2_{11}	16 558.08	16 920.42
2_{02}–3_{03}		23 080.34
3_{03}–4_{04}	29 629.85	30 217.30
A, B, C, obs.	11 657.1 Mc	11 485.2
	4427.23	4524.25
	3276.39	3347.67
A, B, C, calc. Staggered	11 661 Mc	11 491
	4416	4533
	3269	3355
Eclipsed	11 491	11 581
	4608	4436
	3359	3308

relative intensities themselves leads to an estimate of 130 ± 20 cm^{-1} for the separation of the states α to β, β to γ, and γ to δ. Within the limits of error, the separations between these states appear to be equal. Consideration of the vibrational modes and of the infrared[9] and Raman[9a,10] spectra strongly suggest that the only possibilities for a frequency this low are the modes approximately described as the NO_2 group torsion and the methyl group torsion. The latter can be ruled out as follows. None of the lines α, β, γ, or δ is observed to be split into doublets. If they arose from the methyl group torsion with a fundamental frequency near 130 cm^{-1}, the barrier would have to be low enough so that some of the lines would be split by tunnelling through the low barrier. By elimination, these satellites are assigned to rotational transitions of molecules in the first few excited states of the NO_2 group torsional motion. Those whose frequencies have been measured are listed in Table VI, together with the moments of inertia for the first and second excited states.

If it is assumed that the potential barrier hindering the NO_2 torsion is purely sinusoidal with two minima, the frequency 130 ± 20 cm^{-1} gives a barrier height of 9100 ± 2600 cal/mole. This value may be compared with the two NMR determinations of the barrier between the *cis* and *trans* forms of methyl *nitrite* (both of which have approximately the same energy), namely, 9000 ± 2000 cal/mole[11] and $10\,500\pm2000$ cal/mole.[12] Nitric acid has also been reported to have a barrier of similar magnitude.[13,14]

The Stark effects of satellites β and γ were measured in several transitions, and the dipole moments thus obtained for the first and second excited states of the NO_2 torsion were found to be identical with that for the ground state within the experimental error.

The satellite pairs ϵ and ζ have been assigned to methyl group torsionally excited states. The intensity of ϵ relative to α supports this, once β, γ, and δ are accounted for, but the main evidence is the splitting of ϵ and ζ into pairs in a way that can be accounted for only by this assignment.

The satellite η is believed to arise from the next lowest vibrational level which has been observed at 355 cm^{-1} in the Raman[9a,10] and assigned to the bending of the CON bond angle.

The pair θ is believed to arise from a combination of methyl and NO_2 single excitations and is discussed later.

TABLE V. Stark coefficients and dipole moment.

Transition	$\Delta\nu/E^2$[Mc/(v/cm)^2]$\times10^6$ Observed	Calculated
1_{11}–$2_{12}(M=0)$	3.872 ± 0.07	3.932
1_{01}–$2_{02}(M=0)$	-4.400 ± 0.06	−4.460
1_{01}–$2_{02}(M=1)$	3.688 ± 0.05	3.764
1_{10}–$2_{11}(M=0)$	3.462 ± 0.06	3.398

$\mu_a=3.08\pm0.03D$

$\mu_b=0.25\pm0.25$

$\mu=3.10\pm0.05D$

EVIDENCE FOR EXACT PLANARITY

It is not always easy to exclude the possibility of slight deviations from planarity because of the effect of zero-point vibrations on the observed moments of inertia. The value of $I_c-I_a-I_b$ does correspond closely to the geometrical requirements if all the heavy atoms lie in a plane. However, Laurie[15] has pointed out that one expects a small positive contribution to this quantity from the vibrations, the so-called *inertial defect*. In the present case the inertial defect is defined as

$$\Delta=I_c-I_a-I_b+4m_Hr_H^2.$$

[9] (a) J. Lecomte and J. P. Mathieu, J. chim. phys. **39,** 57 (1942); (b) C. D. Brand and T. M. Cawthon, J. Am. Chem. Soc. **77,** 319 (1955); (c) J. F. Brown, Jr., *ibid.* **77,** 6341 (1955).

[10] A. Dadieu, F. Jele, and K. W. F. Kohlrausch, Wien. Ber. **140,** 293 (1931); L. Medard, J. chim. phys. **31,** 281 (1934); J. Chedin, J. phys. radium **10,** 445 (1939); H. Wittek, Z. Physik. Chem. (Leipzig) **B51,** 187 (1942).

[11] L. H. Piette and W. A. Anderson, J. Chem. Phys. **30,** 899 (1959).

[12] P. Gray and L. W. Reeves, J. Chem. Phys. **32,** 1878 (1960).

[13] H. Cohn, C. K. Ingold, and H. Poole, J. Chem. Phys. **24,** 162 (1956); J. Chem. Soc. **1952,** 4272.

[14] A. Palm and M. Kilpatrick, J. Chem. Phys. **23,** 1562 (1955).

[15] V. W. Laurie, J. Chem. Phys. **28,** 704 (1958).

He further showed that it was advantageous to combine data from a deuterated species to obtain both r_H and Δ for the planar atoms, assuming Δ to be unaltered by the substitution. Application of this treatment to the CH_3 and CD_3 species, whose spectrum and moments of inertia are given in Table VII, yields

$$r_H = 0.896\ A$$

$$\Delta = +0.019 \text{ amu A}^2.$$

The value of r_H is quite reasonable, but Δ seems somewhat smaller than expected (+0.04 to +0.30 amu A^2 in representative cases). This value of Δ could be used as an argument that the heavy atoms may deviate very slightly from coplanarity, since any such deviation would make a negative contribution to Δ. However, consideration of the values of $I_c - I_a - I_b$ for the ground

TABLE VI. NO_2 torsional satellites.

Transition	$v=1$	$v=2$	$v=3$	$v=4$
1_{11}–2_{12}	15 031.69 Mc	15 039.95		
1_{01}–2_{02}	16 138.27	16 139.49		
1_{10}–2_{11}	17 555.17	17 548.41		
2_{02}–3_{03}	23 834.15	23 837.43	23 839.80	
2_{11}–3_{12}	26 228.62	26 219.05	26 208.24	26 197.05
3_{13}–4_{14}	29 785.75			
3_{03}–4_{04}	31 157.90	31 165.00		
Moments of inertia				
I_a	43.115 amu A^2		43.356	
I_b	107.463		107.545	
I_c	146.850		146.683	

state (−3.218 amu A^2) and for the first and second excited states of the NO_2 torsion (−3.73 and −4.22 amu A^2, respectively) shows that the argument is invalid. If it is assumed that the value of $4m_H r_H^2$ remains constant, then these large changes in $I_c - I_a - I_b$ will give the changes in Δ between torsional states. From the above value of $\Delta = +0.019$ amu A^2 and from the change in Δ with torsional quantum number, it is possible to arrive at the extrapolated value $\Delta = +0.27$ amu A^2 for the hypothetical case in which the NO_2 group is at rest in its equilibrium position. With the large effects of the NO_2 torsion thus eliminated it is seen that Δ falls well within the range of usual values. Other evidence below strengthens further the case for a planar molecule.

Two forms of nonplanarity are possible. In one, the NO_2 group is twisted out of the CON plane. In the other, it is bent so that both NO_2 oxygens are on one side of the CON plane. The nonplanarity would in either case (or both) be characterized by a potential function with two very close minima separated by a

TABLE VII. Spectrum and moments of inertia of CD_3ONO_2.

Transition	Observed (Mc)	Calculated (Mc)
1_{01}–2_{02}	14 396.45	14 396.61
1_{10}–2_{11}	15 501.59	15 501.59
2_{12}–3_{13}	20 181.61	20 181.61
2_{02}–3_{03}	21 347.74	21 347.74
2_{11}–3_{12}	23 185.23	23 185.35
	$I_a = 45.816$ amu A^2	
	$I_b = 122.516$	
	$I_c = 161.882$	

narrow and probably not very high potential maximum. If this maximum were high enough, the normal molecular species would exist in two mirror image forms, with the same moments of inertia. The asym CH_2D species, however, would show a doubling of its rotational transitions because now it would make a difference whether the deuterium was on the same side of the mirror plane as the farthest oxygen or on the opposite side. Rough calculations show that if the NO_2 group were twisted or bent out of the plane by as little as one degree, the transitions studied for the asym CH_2D species would show splittings of up to 4 Mc. No such doubling is observed, so that the possibility of a fairly high potential maximum is ruled out.

If the barrier were present but so low that rapid tunnelling through it could occur, the effect would be simply to modify the spacing of the harmonic oscillator levels for the given out-of-plane motion. That this

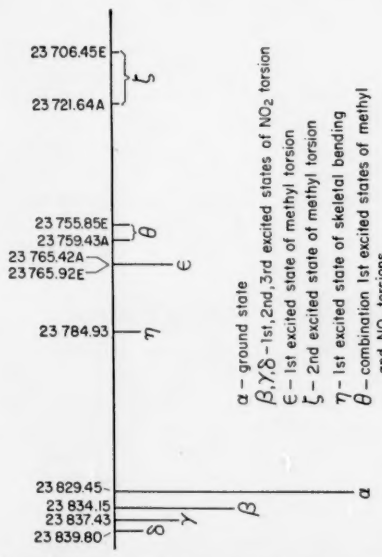
23 706.45E
23 721.64A
23 755.85E
23 759.43A
23 765.42A
23 765.92E
23 784.93
23 829.45
23 834.15
23 837.43
23 839.80
α – ground state
β, γ, δ – 1st, 2nd, 3rd excited states of NO2 torsion
ε – 1st excited state of methyl torsion
ζ – 2nd excited state of methyl torsion
η – 1st excited state of skeletal bending
θ – combination 1st excited states of methyl and NO2 torsions

FIG. 2. Satellites in the $2_{02} \rightarrow 3_{03}$ transition.

TABLE VIII. Barrier to internal rotation of methyl group from second excited torsional state.

Transition	ν obs (Mc)	Contributions to $\Delta\nu$ P_y	P_z	P_y^2, P_z^2	$\Delta\nu$(calc)	$\Delta\nu$(obs)
1_{01}–2_{02}	16 048.11 *E* 16 058.80 *A*	0.59	0.17	10.10	10.86	10.69
1_{10}–2_{11}	17 468.25 *A*					
2_{12}–3_{13}	22 340.04 *A* 22 365.79 *E*	0.19	−34.22	7.59	−26.44	−25.75
2_{02}–3_{03}	23 706.45 *E* 23 721.64 *A*	0.40	0.62	14.55	15.57	15.19
2_{11}–3_{12}	26 041.92 *E* 26 101.23 *A*	−0.01	34.27	23.10	57.36	59.31
3_{13}–4_{14}	29 633.65 *A* 29 637. *E*[a]	0.15	−13.64	9.86	−3.63	−3.35[a]
3_{03}–4_{04}	30 997.1 *E*[b] 31 016.82 *A*	0.10	1.22	18.11	19.43	19.72[b]
3_{12}–4_{13}	34 546.63 *E*					

$\lambda_a = 0.792$ (37.6°)
$\lambda_b = 0.611$ (52.4°)
$s = 64.49$
$V_3 = 2321$ cal/mole
$\nu = 188.5$ cm^{-1}

[a] ±2.0 Mc.
[b] ±0.5 Mc.

effect is not marked with respect to the twisting form of nonplanarity is clear from the regular spacing of the moments of inertia for the NO_2 torsional levels and from the regular intensity decrease of the satellites β, γ, δ shown in Fig. 2. The argument is not so strong with respect to the bending form of nonplanarity because no satellites assignable to this motion have been found, presumably because the lowest excited state is above 500 cm^{-1} (a value of 759 cm^{-1} is claimed[9] from infrared data) and therefore too weakly populated. However, any appreciable potential maximum in the plane would tend to pull together the ground and first excited states of this vibration which should have made a satellite visible. We therefore conclude that it is unlikely that any nonplanarity of the $CONO_2$ group occurs.

METHYL GROUP BARRIER

The tunnelling of the CH_3 group from one to another minimum of the threefold potential barrier hindering internal rotation can cause a splitting of rotational lines into doublets. As has now been discussed many times,[16] these doublet splittings can be used to determine the height of the barrier and also the direction of the axis about which the torsional motion occurs.

None of the ground state transitions observed were resolvable into doublets, showing that the methyl group barrier must be greater than 1800 cal. The satellites ϵ of Fig. 2 were very slightly split into two lines of equal intensity, and the lines ζ form a well-split pair. When the theory[17,18] to second order, was applied to these second excited state transitions, the results shown in Table VIII were obtained after a process of fitting. The *A* components fitted a rigid-rotor formula, but the linear terms in the coupling of internal and overall rotation were important for the *E* components in several of the transitions. Table VIII shows the contributions to the splitting of the first-order terms in the total angular momentum component P_y and P_z, and the second-order terms in P_y^2 and P_z^2, which are simulated by changes in *A* and *B*. Pierce and Krisher[19] have pointed out that the effects of the linear terms in P_y and P_z may often be calculated separately and added, using the simplest representation in each case. This method was applicable here. The effect of one linear term was actually calculated using some power series expansions.

The value 2321 cal depends on the value of I_α used for the second excited torsional state, and the uncer-

[16] E. Bright Wilson, Jr., in *Advances in Chemical Physics*, edited by I. Prigogine (Interscience Publishers, Inc., New York, 1959), Vol. II, p. 367.

[17] R. W. Kilb, Chun Chia Lin, and E. B. Wilson, Jr., J. Chem. Phys. **26**, 1695 (1957).
[18] D. R. Herschbach, J. Chem. Phys. **31**, 91 (1959).
[19] L. Pierce and L. C. Krisher, J. Chem. Phys. **31**, 875 (1959).

tainty in I_a is probably the largest source of uncertainty. Error limits of $\pm 5\%$ are probably conservative. The barrier value also gives agreement within the limits of error for the small splittings observed for the first excited torsional state satellites.

COMBINATION EXCITED STATE

The split pair of satellites θ in Fig. 2 were given considerable attention because they are believed to arise from a combination state with $v=1$ for methyl torsion and $v=1$ for NO_2 torsion. It was originally hoped that they would yield the effect of excitation of the NO_2 torsion on the barrier for the methyl group.[19a] However, it was found that the A component (identified because it fits a rigid-rotor formula whereas the E component does not) occurs at a higher frequency than the E component. The theory based on a rigid methyl group plus a rigid framework predicts the reverse order for a first excited state. In some other transitions the E component was not found at all.

In an attempt to explain these anomalies some calculations were made with a model which allowed torsional motion of the NO_2 group as well as the methyl group. The quantum-mechanical Hamiltonian contains additional coupling terms in the kinetic energy, namely, a coupling of the angular momenta of the two tops and a coupling of the angular momentum of the NO_2 group with the over-all angular momentum, in addition to the coupling of over-all and methyl group angular momenta present in the one-top Hamiltonian. No coupling was assumed in the potential energy. The perturbation treatment employed proved to be too slowly convergent for quantitative results, even to fourth order, but, with excitation of the NO_2 torsion, it did show a shift of the E component to a frequency just below that of the A component, and of the same order of magnitude as the observed shift. For other transitions it predicted a much greater perturbation of the E levels, accounting for their apparent absence in these transitions. Consequently, no further attempt was made to obtain the effect of excitation of the NO_2 motion on the methyl barrier for fear of various nonrigid effects. However, in the ground state of the NO_2 motion the rough two-top treatment does not appear to disagree with the normal one-top treatment lending further support to the validity of treating the framework as rigid, at least for the calculation of barriers.

THERMODYNAMIC DATA

The reported third-law entropy[20,9b] is in very strong disagreement with that calculated statistically on the basis of the microwave structure and barriers to internal rotation and a published analysis[9b,c] of the vibrational spectra. The statistical and third-law entropies are given in Table IX. The huge discrepancy of nearly four entropy units can be eliminated if free rotation is assumed for both the methyl and NO_2 groups, but this model is both *a priori* improbable and in complete disagreement with the microwave spectrum.

TABLE IX. Statistical and third-law entropies for methyl nitrate vapor at 298.2°K.

Translational	38.92
Rotational	24.93
Vibrational (16 modes)[a]	2.74
Hindered rotation (methyl)	2.52
Hindered rotation (NO_2)	3.04
Statistical entropy	72.15 cal/deg
Third law entropy[a]	75.89 cal/deg

[a] See reference 9(b).

The arguments which have been advanced for a planar skeleton are of course arguments against free rotation of the NO_2 group. Furthermore, the satellites β, γ, and δ of Fig. 2 are difficult if not impossible to reconcile with a free rotation model. They cannot be ascribed to excited states of free rotation of the NO_2 group because the intensity falls off too rapidly and in the wrong way. If they are not due to the NO_2 torsion, then there must be another low frequency (~ 130 cm^{-1}) vibration. Such an additional low frequency is hard to understand but in any event, combined with free rotation, the total entropy would now become too high.

One of the reasons for examining the question of accurate planarity in such detail was to see if the entropy discrepancy could be accounted for by a distortion of harmonic oscillator levels, a near pairing of lowest levels, caused by a potential barrier. However, even a complete doubling of all levels would yield only $R \ln 2 = 1.38$ cal/deg, which is not enough.

There is also a discrepancy between the statistical heat capacity and the published heat capacity for the vapor,[21] the latter having been determined from liquid heat capacity measurements[20] plus vapor-pressure data.[22] The experimental values are again too high, but the free rotation model makes matters worse here instead of better.

At present it can only be stated that the entropy discrepancy is very large and disturbing.

DISCUSSION

The experimental results of this study appear to have important consequences with respect to several current questions of theory. One of these has to do with the amount of double-bond character in the N—OC bond. In valence-bond language this is equivalent to

[19a] A preliminary value for this change in barrier which was presented at the Symposium on Molecular Structure and Spectroscopy, Ohio State University, June, 1959, and appeared in the abstracts of the meeting must now be withdrawn.

[20] P. Gray and P. L. Smith, J. Chem. Soc. **1953**, 2380.

[21] P. Gray and M. W. T. Pratt, J. Chem. Soc. **1957**, 2163.

[22] J. S. McKinley-McKee and E. A. Moelwyn-Hughes, Trans. Faraday Soc. **48**, 247 (1952).

asking the importance of structure III below

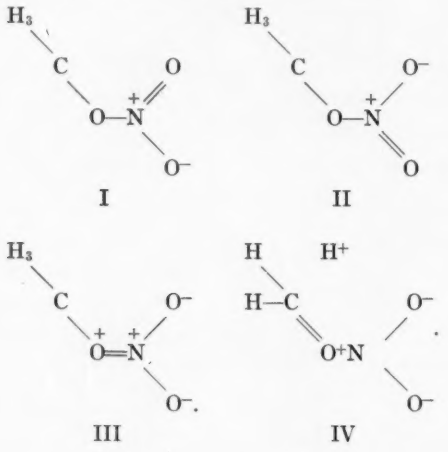

Recently Dewar[23] and others have even challenged the whole concept of conjugation. Further, Pauling has stated a rule, the *adjacent charge rule*,[24] which as originally stated would predict that III would have small importance here. He has, however, modified this concept recently[25] in a way which permits appreciable double bond character in the present instance.

Experimentally, the planar configuration supports a role for III. The high barrier indicated for the NO_2 torsion strengthens the case. An alternative explanation in terms of some kind of attractive force between the CH_3 group and an oxygen would also have to explain the equilibrium conformation of CH_3. In terms of attractive forces between hydrogen and oxygen atoms this conformation would be possible if the force law were such that one hydrogen close to the oxygen had less attraction than two hydrogens somewhat farther away, in other words a force varying rather slowly with distance, such as an inverse-square law.

It is interesting to speculate that there is hydrogen bonding between the hydrogen and the nearby oxygen. However, the high barrier restricting the NO_2 group torsion is higher than can reasonably be accounted for in this way alone.

The rather high barrier for the methyl group rotation is another piece of data to be considered. Methyl alcohol[26] with 1.07, methyl formate[27] 1.19 and dimethyl ether[28] with 2.72 kcal are the other CH_3–O barrier values so far available from microwave data. These do not suggest any simple picture but the comparison with methyl alcohol does suggest that interaction with the nearby oxygen is raising the barrier.

The most obvious explanation of these facts is that there is a steep repulsive interaction, steric hindrance, between the methyl hydrogens and the nearby oxygen. From the structural information available, the hydrogen and oxygen atoms are only about 1.8 A apart at their closest approach. In the equilibrium position of the methyl group the H···O distance is about 2.3 A. Since the sum of the van der Waals radii for hydrogen and oxygen is 2.6 A,[29] it appears that there must be some steric hindrance present as the methyl group rotates. This would raise the barrier and be compatible with the equilibrium conformation of the methyl group. Despite this repulsion, the planar configuration is stabilized by conjugation which gives the CO—N bond enough double-bond character.

If this view is correct, then not only is the idea of conjugation upheld but the importance of the adjacent charge rule is reduced.

The dipole moment is also unusual. The value 3.10 *D* is considerably larger than 2.16 *D* reported for nitric acid.[30] Often the substitution of CH_3 for H attached to oxygen reduces the moment, as in H_2O to CH_3OH to CH_3OCH_3, but there is a similar, although smaller, increase of the dipole moment of methyl formate (1.77 *D*)[27] over that of formic acid (1.35 *D*).[31] In the latter case, the increase may perhaps be explained by the greater polarizability of the methyl group than the hydrogen atom attached to the formate group, but it is uncertain whether such an explanation suffices to explain the much larger increase from nitric acid to methyl nitrate. Perhaps the close approach of the very negative oxygen increases the importance of structures such as IV, which would increase the moment. Such a structure would also be consistent with the idea of internal hydrogen bonding. However, the absence of observable nitrogen nuclear quadrupole splittings puts a limit on the possible importance of IV, since it alone would be expected to contribute quadrupole splitting on simple valence-bond theory.

[23] M. J. S. Dewar and H. N. Schmeising, Tetrahedron **5**, 166 (1959).
[24] L. Pauling, *The Nature of the Chemical Bond* (Cornell University Press, Ithaca, New York, 1960), 3rd ed., p. 270.
[25] L. Pauling, reference 24, p. 284.
[26] E. V. Ivash and D. M. Dennison, J. Chem. Phys. **21**, 1804 (1953).
[27] R. F. Curl, Jr., J. Chem. Phys. **30**, 1529 (1959).
[28] P. H. Kasai and R. J. Meyers, J. Chem. Phys. **30**, 1096 (1959).
[29] L. Pauling, reference 24, p. 260.
[30] D. J. Millen and J. R. Morton, J. Chem. Soc. **1960**, 1523.
[31] G. Erlandsson and H. Selén, Arkiv Fysik **14**, 61 (1958).

Dissociation Energy of Cyanogen and Related Quantities by X-Ray Densitometry of Shock Waves* †

HERBERT T. KNIGHT AND JOHN P. RINK

Los Alamos Scientific Laboratory, Los Alamos, New Mexico

(Received December 16, 1960)

Density ratios across shock waves in a 0.85 Kr+0.15 C_2N_2 mixture at an initial pressure of 50 mm Hg and room temperature, have been determined with an x-ray densitometer as a function of shock velocity. The heat required to dissociate cyanogen into two CN radicals $D(C_2N_2)$ has been determined to be 145±6 kcal/mole by comparing the experimental data with curves of density ratio vs shock velocity calculated as a function of $D(C_2N_2)$. Dissociation energies of 174±3 kcal/mole for CN and 129±3 kcal/mole for HCN forming H and CN, and a heat of formation of 109±3 kcal/mole for CN, were obtained by the application of Hess's law to the appropriate chemical reactions using this value of $D(C_2N_2)$ and the currently accepted values for the dissociation energy of nitrogen (225 kcal/mole) and the heat of sublimation of graphite (170 kcal/mole). The value of D(HCN) was confirmed by analogous density-velocity measurements on shock waves in a 0.85 Kr+0.15 HCN mixture. A rate constant for the recombination of CN to form C_2N_2 at 2900°K was deduced from the variation of density with time behind the shock. The value obtained was of the order of 1×10^9(mole/liter)$^{-2}$ sec^{-1}.

INTRODUCTION

THE heat of formation at 0°K of CN, $H_0°$(CN), the heat required to dissociate cyanogen into two CN radicals $D(C_2N_2)$ and the heat of dissociation of CN, D(CN), are important thermochemical quantities which are still in doubt. They are related by the equations

$$D(C_2N_2)=2H_0°(CN)-H_0°(C_2N_2) \quad (1)$$

$$D(CN)=\tfrac{1}{2}D(N_2)+L(C)-H_0°(CN), \quad (2)$$

where $D(N_2)$ is the heat of dissociation of nitrogen and L(C) is the heat of sublimation of graphite. Since $H_0°(C_2N_2)$, the heat of formation at 0°K of cyanogen, is known,[1,2] and the values[3] 225 kcal/mole for $D(N_2)$[4–8] and 170 for $L(C)$[9–11] have now been established with considerable certainty, a reliable determination of any one of the three remaining quantities in (1) and (2) would fix the other two.

The heat required to dissociate HCN into H and CN, D(HCN), is related to $H_0°$(CN) by the expression

$$D(HCN)=H_0°(CN)+\tfrac{1}{2}D(H_2)-H_0°(HCN). \quad (3)$$

Since $D(H_2)$ and $H_0°$(HCN) are well established[1,12] as 103.2 and 31.3, respectively, a determination of either $H_0°$(CN) or D(HCN) would fix the other.

During the last decade the shock tube has developed into a powerful tool for the study of the gaseous state at high temperatures. This purely thermal technique does not suffer from the uncertainties in the data analysis due to possible excited states or excess kinetic energy of molecular fragments peculiar to other techniques. Thus it is particularly appropriate for the measurement of thermochemical constants, provided only one such constant is uncertain in the chemical system being considered. For example, simultaneous measurement of shock velocity and one state variable behind shock waves in gases have led to reliable values for $D(N_2)$[8] and $L(C)$.[10,11] In the present investigation incident shock velocity U_i and density ratio ρ/ρ_0 across shock waves in Kr–C_2N_2 mixtures were measured simultaneously. A value for $D(C_2N_2)$ was obtained by comparison of the experimental results with curves of density ratio vs shock velocity calculated as a function of that quantity. To provide a check of the method with a different chemical system a Kr–HCN mixture was also studied in a similar fashion.

The most probable first step in the dissociation of a cyanogen molecule is the breaking of the C—C linkage,[13] which will be referred to here as the primary dissociation. Because of the relative magnitudes of bond energies and the effects of cooling and concentration

* This work was done under the auspices of the U. S. Atomic Energy Commission.

† Presented in part at the 136th meeting of the American Chemical Society, Division of Physical Chemistry.

[1] F. D. Rossini, D. D. Wagman, W. H. Evans, S. Levine and I. Jaffe, Natl. Bur. Standards Circ. No. **500,** 140, 12 (1952).

[2] J. W. Knowlton and E. J. Prosen, J. Research Natl. Bur. Standards **46,** 489 (1951) report the heat of formation of cyanogen at 298.16°K to be 73.84 kcal/mole. When converted to 0°K this number becomes 73.37 kcal/mole.

[3] All thermochemical quantities used in subsequent discussions will be given in kcal/mole, and rounded to the nearest kilocalorie, unless otherwise indicated.

[4] G. B. Kistiakowsky, H. T. Knight, and M. E. Malin, J. Chem. Phys. **20,** 876 (1952).

[5] A. E. Douglas, Can. J. Phys. **30,** 302 (1952).

[6] J. M. Hendrie, J. Chem. Phys. **22,** 1503 (1954).

[7] H. D. Hagstrum, J. Chem. Phys. **23,** 1178 (1955).

[8] R. H. Christian, R. E. Duff, and F. L. Yarger, J. Chem. Phys. **23,** 2045 (1955).

[9] W. A. Chupka and M. G. Inghram, J. Phys. Chem. **59,** 100 (1955).

[10] J. P. Toennies and E. F. Greene, J. Chem. Phys. **26,** 655 (1957).

[11] H. T. Knight and J. P. Rink, J. Chem. Phys. **29,** 449 (1958).

[12] Reference 1, p. 110 lists the heat of formation of HCN at 298.16°K as 31.2 kcal/mole, which becomes 31.3 when converted to 0°K using the thermodynamic data of the work cited in reference 22.

[13] H. D. Springall, Trans. Faraday Soc. **43,** 177 (1947).

changes, during the early stages of reaction behind a shock wave it is reasonable to expect primary dissociation to be as much as an order of magnitude faster than subsequent events such as the dissociation of CN radicals and the formation of nitrogen molecules. The precipitation of solid carbon should be even slower. At present the detailed nature of gaseous carbon is far from clear. The presence of polyatomic species larger than C_3 has been established experimentally.[9] Pitzer and Clementi[14] have predicted that large straight-chain molecules should abound in the vapor in equilibrium with graphite, and that species with an odd number of carbon atoms should be the more stable. However, it seemed advisable to attempt to measure $D(C_2N_2)$ under conditions such that the only thermally significant reaction occurring during the time of measurement would be the primary dissociation. The possibility that such conditions might exist was suggested experimentally by the work of Greene[15] who studied shock waves in BrCN and found that emission due to CN appears appreciably earlier than that for C_2. Therefore, in addition to the measurement of density as a function of shock velocity, experiments were performed to determine the relative times of first appearance of CN, C_2, and polyatomic carbon species C_n, by emission and absorption spectroscopy.

CALCULATIONS

All calculations of shock wave parameters were performed on an IBM 704 computer using a code written by R. E. Duff[16] of this Laboratory. The chemical equilibrium equations were solved by the method of Brinkley,[17] as coded by W. Fickett of this Laboratory. A straightforward extension of a previously published procedure[8] was employed for solving the shock wave equations. The thermodynamic data required were enthalpy and free energy as functions of temperature, and the heat of formation at 0°K for each of the species considered, in this case Kr, C_2N_2, CN, HCN, H, and H_2. The CN, H, and H_2 data were obtained from publications by Ohio State University[18] and the National Bureau of Standards.[1,19] For cyanogen, enthalpies and free energies calculated by Peek and Thrap[20] were used. Their data are in good agreement with similar calculations by Rutner, McLain, and Scheller.[21] The HCN data published by Bradley, Haar, and Friedman[22] were used.

EXPERIMENTAL

General

The experimental arrangement, operation, and calibration of the x-ray apparatus, nature of the records obtained, and the method of data analysis have been described in detail elsewhere.[23,24] However, these matters will be summarized here.

The shock tube was of circular cross section with a 4 in. i.d., 4 ft long compression chamber, and a 3 in. i.d., 15 ft long expansion chamber. Both DuPont "Mylar" and soft copper sheet were used as diaphragm materials. Shock velocities above 1.25 mm/μsec were measured with ionization probes developed for detonation work,[25] modified to operate at lower temperatures by the addition of a 0.5-mm step which projected into the flow immediately downstream of the electrodes. The probe signals were amplified, mixed, and displayed on a raster-type oscilloscope.

Although the ionization probes operated reliably down to 1.25 mm/μsec, corresponding to a shock temperature of about 2400°K, occasionally erratic, "late" signals were observed at lower velocities. In order to extend the measurements to velocities appreciably below that value piezoelectric shock detectors[26] were substituted for the ionization probes.

The mole fraction of krypton x_{Kr} used in these experiments was chosen by calculating the change in ρ/ρ_0 produced by a given change in $D(C_2N_2)$ as a function of U_i and x_{Kr} in a mixture of cyanogen and krypton at an initial pressure of 50 mm Hg. The density ratio was most sensitive to $D(C_2N_2)$ for $x_{Kr}=0.85$ and this value was chosen for both the cyanogen and the HCN work.

Commercial cyanogen, obtained from the American Cyanamid Company was used without further purification. Mass spectrometric analysis showed that the only impurities present in greater than trace amounts were 0.5% (mole percent) nitrogen and 0.1% cyanogen chloride. The effect of these impurities on shock density was calculated and found to be negligible. Spectroscopic-grade krypton was used. Commercial HCN was purified by repeated distillation at −78°C, collecting only the middle fraction.

Gas mixtures were prepared manometrically in a brass storage vessel. Each batch was sufficient for about five experiments. The gas nonideality of cyanogen was taken into account by using the van der Waals equation

[14] K. Pitzer and E. Clementi, J. Am. Chem. Soc. **81,** 4477 (1959).
[15] E. F. Greene, J. Am. Chem. Soc. **76,** 2127 (1954).
[16] The code and thermodynamic data, in the form of punched cards, and a set of instructions for the use of the code may be obtained by writing to Dr. R. E. Duff, Los Alamos Scientific Laboratory, P. O. Box 1663, Los Alamos, New Mexico.
[17] S. R. Brinkley, Jr., J. Chem. Phys. **14,** 563 (1946).
[18] H. L. Johnston, L. G. Savedoff and J. Belzer, Nos. 2 and 7 Ohio State Tech. Repts, Series 316; L. Glatt, J. Belzer and H. L. Johnston, *ibid.* No. 9.
[19] *Selected Values of Chemical Thermodynamic Properties,* National Bureau of Standards, Washington, D. C., 1947, Series III and Supplements.
[20] H. Milton Peek and R. G. Thrap, J. Chem. Phys. **26,** 740 (1957).
[21] E. Rutner, W. H. McLain, Jr., and K. Scheller, J. Chem. Phys. **24,** 173 (1956).
[22] J. C. Bradley, L. Haar, and A. S. Friedman, J. Res. Natl. Bur. Standards **56,** 197 (1956).
[23] H. T. Knight and D. Venable, Rev. Sci. Instr. **29,** 92 (1958).
[24] R. E. Duff, H. T. Knight, and J. P. Rink, Phys. Fluids **1,** 393 (1958).
[25] H. T. Knight and R. E. Duff, Rev. Sci. Instr. **26,** 257 (1955).
[26] H. T. Knight, Rev. Sci. Instr. **29,** 174 (1958).

of state in computing mole fractions from observed partial pressures. The data of Giauque and Ruehrwein[27] were used to correct for the association of HCN, which was significant only at reservoir partial pressure. Diffusion and convection over a period of at least 24 hr were relied upon to produce truly homogeneous mixtures. These effects were enhanced by heating the bottom of the vertically oriented cylindrical reservoir. The effectiveness of this technique was clear from gas analyses and the consistency of the measured shock density ratios.

For each experiment the expansion chamber was evacuated to a pressure of less than 10^{-3} mm Hg and filled with 50 mm of experimental mixture. Mixture composition was checked on each experiment by removing a sample for analysis from the tube before the pressure was adjusted to its final value.

Due to the decompositon of cyanogen in the incident and/or reflected shock waves, a small amount of carbon was deposited on the tube walls at the downstream end during each experiment. The velocity probes, x-ray windows, and shock tube were carefully cleaned after each shot.

The tilt and curvature of the shock front were investigated by means of three probes mounted flush with the inner surface of the end plate, one an axis and the other two 90° apart on a circle of a radius 5 mm less than that of the tube. The separation, measured parallel to the tube axis, between the leading and trailing edges of the front was never more than the thickness of the x-ray beam, i.e., 1 mm.

Spectroscopic Experiments

The technique and apparatus used for this phase of the work were basically those described by Bauer, Schott, and Duff.[28] Absorption studies were made of CN and C_2 behind incident shocks in an 0.85 Kr+0.15 C_2N_2 mixture at 50 mm Hg initial pressure. At the higher shock velocities it was possible to study the relative times of first appearance behind the shock of CN, C_2, and C_n by observation of emitted light.

A cyanogen-filled flash lamp served as a source of the CN spectrum. A similar lamp containing butane proved to be rich in light characteristic of C_2. The lamps were operated at the equilibrium vapor-pressure characteristic of each gas at −78°C.

The light from a flash lamp was made parallel by a quartz lens and then passed through collimating slits on either side of the shock tube. The beam thus formed was 1 mm thick by 10 mm high and traversed the shock tube perpendicular to the direction of shock travel through flat quartz windows mounted nearly flush with the inner surface of the tube. A second quartz lens focused the beam on the 20μ wide entrance slit of a JACO grating monochromator. The light from the 500μ wide exit slit was observed by a 931-A photomultiplier tube, the output of which was recorded by a Tektronix 545 oscilloscope. With this slit combination the monochromator passed an 8-A band. Adjustment was made about the band head of interest to give maximum light intensity at the exit slit.

A schlieren effect was used to locate the position of the shock front in time relative to the absorption or emission of light by CN, C_2, or C_n. In absorption experiments the arrival of the shock front at the light beam was indicated on the oscilloscope trace as a sharp spike in the direction of decreasing light intensity, except that at higher temperatures the schlieren spike was obscured by the total absorption produced by the essentially instantaneous appearance of CN.

In the emission experiments interest was centered on wavelengths above 4000 A. Therefore a water-containing flash lamp rich in the violet end of the spectrum was used as a schlieren light source, from which a collimated beam was directed through the shock tube at roughly a 10° angle to the monochromator axis, effectively preventing schlieren light from entering the latter.

Densitometry Experiments

The x-ray beam densitometer, located 14 ft from the diaphragm and midway between the last two velocity probes, utilized a demountable, pulsed, 25–30 kv x-ray tube with an *L* cathode and a tungsten anode. The x-ray beam through the shock tube was defined by 1 mm wide slits covered by a beryllium sheet 0.005 in. thick, mounted flush with the shock-tube bore. The detector consisted of a terphenyl-in-polystyrene scintillator cemented to a photomultiplier tube. The system was calibrated by operating the x-ray tube continuously at low current and observing the photomultiplier output potentiometrically as a function of gas density in the shock tube. During a shock experiment photomultiplier output was fed through a cathode follower to an oscilloscope and the trace photographed. The electronic system responded linearly within 1% over the entire range of photomultiplier signal levels used. Therefore, signal amplitudes, as determined from scope records by an optical comparator, were proportional to transmitted x-ray intensity and were converted to shock density ρ using the calibration data and the initial density ρ_0.

Data analysis required a value of T_0, the x-ray transmission corresponding to the known initial density, which in previous work[23,24] was evaluated just before the sudden decrease in transmission produced by the shock front passing the slits. However, the x-ray tube output was usually not constant during a pulse. This effect introduced an uncertainty in densities measured some distance behind the shock front. In the present experiments this difficulty has been eliminated through the use of a monitor detector-oscilloscope system to

[27] W. F. Giauque and R. A. Ruehrwein, J. Am. Chem. Soc. **61**, 2626 (1939).

[28] S. H. Bauer, G. L. Schott, and R. E. Duff, J. Chem. Phys. **28**, 1089 (1958).

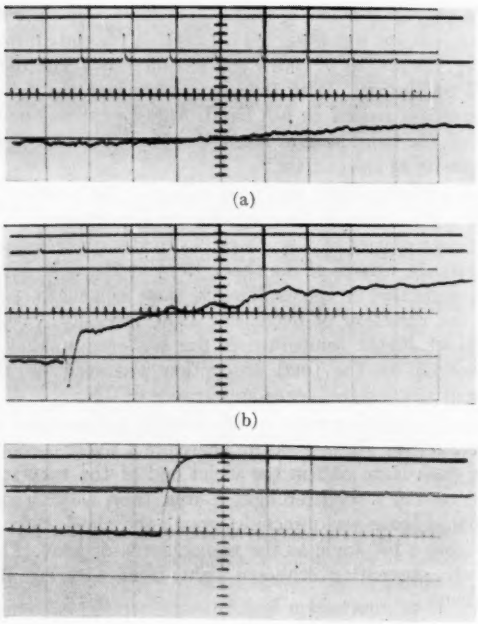

FIG. 1. Oscilloscope records of photomultiplier output indicating light absorption with time behind shock in 0.85 Kr+0.15 C_2N_2 mixture. Monochromator set at 3883 A. Upper trace is zero signal level, middle trace is time calibration, sweep rate was 10 μsec per major scale division. (a) Flash lamp output in absence of shock. (b) Incident shock velocity (U_i) = 1.14 mm/μsec; shock temperature (T_s) = 2000°K; degree of dissociation (α) = 1.17×10^{-4}. Displacement of trace upward indicates absorption. (c) U_i = 1.35 mm/μsec, T_s = 2635, $\alpha = 6.6\times10^{-3}$.

record x-ray tube output during an experiment, from which corresponding variations in T_0 were determined.

EXPERIMENTAL OBSERVATIONS

Spectroscopic Experiments

Light absorption due to the presence of CN was observed as a function of time behind shocks with velocities ranging from 1.1 to 1.5 mm/μsec. Because of the relatively high f number of CN, the shock conditions demanded by good densitometry experiments produced a spectroscopically high concentration of CN at all but the slowest shock velocities studied. Thus, when shock velocity became high enough for the degree of dissociation to become thermally significant, essentially 100% absorption was observed.

Typical oscilloscope records of the absorption as a function of time behind the shock, together with a trace showing the wave form of the flash lamp output in the absence of a shock, are shown in Fig. 1. The temperatures and degrees of dissociation quoted were calculated assuming that only primary dissociation occurred and that $D(C_2N_2) = 145$. The monochromator was set on the (0,0) band head of the $^2\Sigma$—$^2\Sigma$ transition of CN at 3883 A. The starting level of the bottom trace is proportional to the light intensity at the monochromator exit slit. In Fig. 1 (b) we note that at the lower velocity where the degree of dissociation is quite low, absorption occurs relatively slowly reaching a steady level in about 30 μsec.[29] The sharp but momentary decrease in intensity due to the schlieren effect of the wave front starting to cross the light beam is resolved. The subsequent overshoot of intensity occurs when the shock front has almost passed through the beam and extra light is momentarily refracted into the entrance slit of the

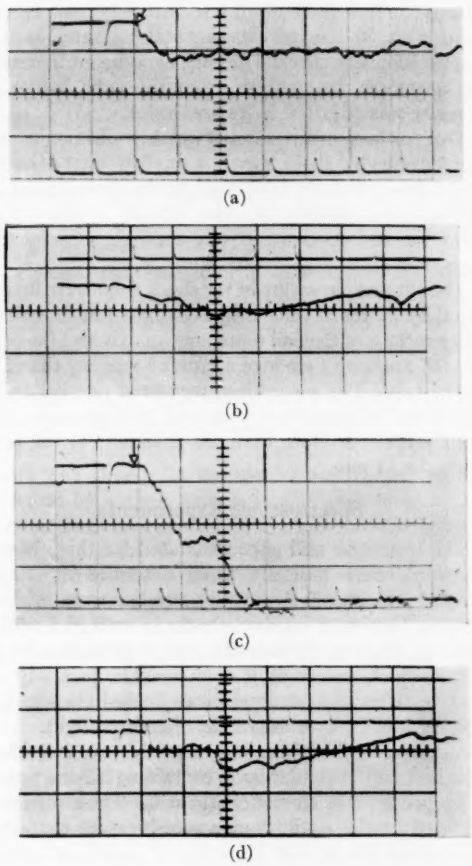

FIG. 2. An example of the determination of the relative times of first appearance of CN and various carbon species with respect to the shock front; U_i = 1.48 mm/μsec, T_s = 3040°K, timing pips at 10 μsec intervals. (a) Emission at 3883 A; first spike on upper trace is time fiducial, common to first spike on bottom trace in (b); the latter shows schlieren signal from shock front; arrow in (a) indicates position of shock front as determined by the time separation of the fiducial and schlieren signals in (b). (c) Emission at 5165 A; arrow indicates position of shock front. (d) Fiducial and schlieren signals for (c).

[29] Here and in subsequent discussions quotations of times behind shocks refer to the experimentally observed or laboratory time. To obtain the corresponding molecule dwell time one must multiply by the appropriate shock density ratio.

monochromator.[30] Figure 1 (c) shows that a velocity of 1.35 mm/μsec the CN concentration rises so rapidly that the schlieren spike is swamped by the absorption signal.

Shock waves where U_i varied between 1.38 and 1.51 mm/μsec were examined for C_2 absorption at 5165 A, the (0,0) band head of the Swan system. No absorption signal of amplitude as great as the statistical fluctuations in flash lamp intensity was ever observed. However, at velocities above 1.40 mm/μsec emission occurred at 5165 A. It was first observed some 30 to 50 μsec behind the shock, but set in more and more promptly as the velocity increased. This emitted radiation was found to be a continuum by several experiments with varying monochromator settings, and from time-integrated shock wave spectrograms obtained on a Kodak 103-F emulsion with a Hilger quartz-prism spectrograph. Presumably this was the well-known continuum characteristic of high-temperature carbon vapor. Emission was first detectable at about 3000 A and increased monotonically to the cutoff point of the film at 6900 A, with CN bands appearing in either emission or absorption depending upon the temperature.

A study was made of the intensity-time history of emission at 3883 and 5165 A from shocks where $1.35 \leq U_i \leq 1.53$ mm/μsec. At the lowest velocities no emission was observed. At 1.40 mm/μsec weak emission due to CN appeared immediately behind the shock front. At 1.45 mm/μsec CN emission again occurred sharply at the shock front while nothing was seen at 5155 A for about 5 μsec. Above 1.5 mm/μsec the delay

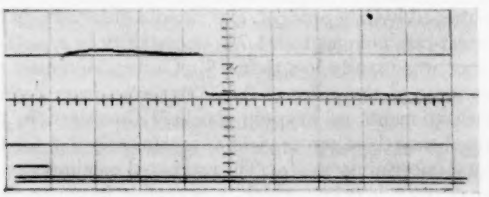

(a)

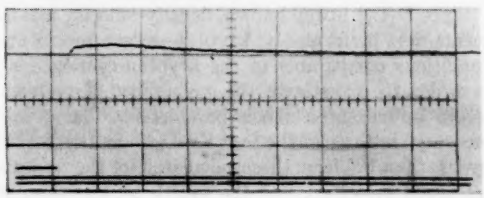

(b)

FIG. 3. (a) An oscilloscope record of the change in x-ray transmission across a shock in a 0.85 Kr+0.15 C_2N_2 mixture, initially at 50 mm Hg and 298°K. U_i=1.24 mm/μsec, timing pips at 100 μsec intervals on bottom trace. (b) X-ray monitor trace for record (a).

[30] The reverse spike is not due to emission as might be at first suspected. Other experiments have shown that shock temperatures must be at least 1000°C higher in order for CN emission to become appreciable.

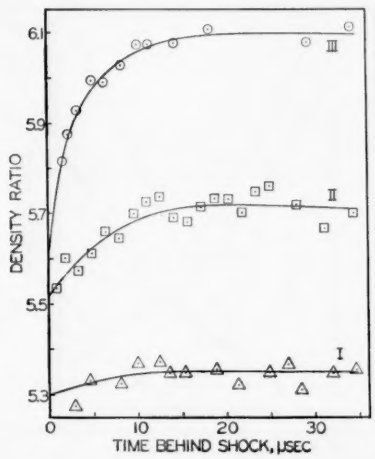

FIG. 4. Plotted points represent observed density ratio as a function of time behind the shock for three experiments. Smooth curves, started at the ρ/ρ_0 calculated for no reaction, represent estimated average of the points. I, U_i=1.24 mm/μsec, see Fig. 3, (a); II, U_i=1.43 mm/μsec; III, U_i=1.54 mm/μsec.

in the appearance of emission due to species other than CN became unresolvable with the present technique. Figure 2 shows the results of two experiments at 1.48 mm/μsec. Records (a) and (b) were obtained simultaneously with the monochromator set at 3883 A. The upper trace in (a) and the bottom trace in (b) show the outputs of the monochromator and the schlieren photomultipliers, respectively. The first spike on each is a fiducial signal from a common source. The second spike on (b) is the schlieren signal from the shock traversing the optical axis of the system. This signal, with the aid of the fiducial signals and the timing traces, permits one to locate the shock front in (a) within ±0.2 μsec. Records (c) and (d) are analogous to the first two, except that the monochromator was set at 5165 A. The small signal which appears in (c) just prior to the shock front is due to scattered and reflected light which finds its way into the monochromator because of imperfections in the collimation system. This effect is nearly obscured in (a) because of a chance coincidence with the oscilloscope graticule and the generally lower level of emission intensity at this wavelength. It is clear that even at 1.48 mm/μsec there is a 2 μsec delay in the appearance of emission at 5165 A due to polyatomic carbon species.

We believe that these experiments have demonstrated that under our experimental conditions a range of shock velocity exists over which there is a delay in the onset of secondary reaction behind the shock front, whereas primary dissociation occurs immediately and to a considerable extent. Therefore for the shock velocities and reaction times delineated by these experiments, the assumption of primary dissociation as the only thermally significant reaction is justified.

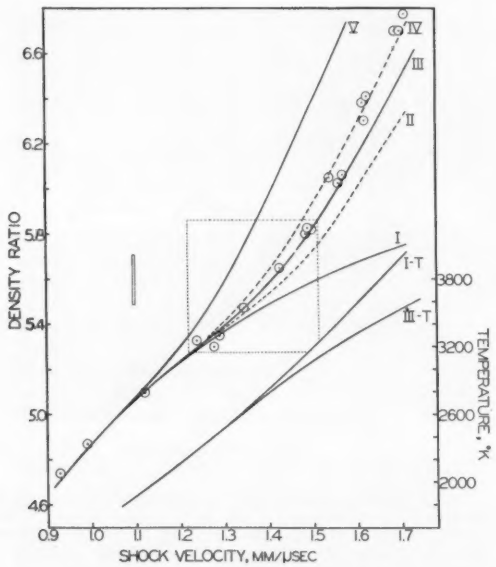

FIG. 5. Comparison of measured shock density-velocity data with curves calculated assuming various values of $D(C_2N_2)$. All curves and points correspond to a 0.85 Kr+0.15 C_2N_2 mixture at 50 mm Hg initial pressure and an initial temperature of 25±3°C. Curve I, vibrational and rotational equilibrium assumed but no chemical reaction; curves II, III, IV, and V primary dissociation and $D(C_2N_2)$ values of 155, 145, 137, and 115 kcal/mole, respectively, were assumed. The two lowest curves show the temperature-velocity relationships corresponding to density-velocity curves I and III. Estimated maximum errors in a single measurement indicated by rectangle at left.

Density Measurements. Kr—C_2N_2 Mixture

A typical oscilloscope record of the change in transmitted x-ray intensity as the shock traversed the beam is shown in Fig. 3(a) together with the corresponding monitor trace (b). To eliminate errors due to drift in the quiescent position of the oscilloscope beam, a zero signal level was established dynamically by triggering the scope a few microseconds sooner than the x-ray tube. A slightly displaced base line and a timing trace were placed on the record just prior to the experiment.

Shock density ratio ρ/ρ_0 was measured at a number of points on such records and plotted as a function of time behind the shock. Data obtained from the records shown in Fig. 3, and from experiments at two other velocities, are plotted in Fig. 4. The scatter in the points is due largely to the statistical fluctuations in x-ray transmission. The basic data analysis problem was to decide the best average value of a quantity always subject to statistical fluctuations and which sometimes varied with time. Comparison of several techniques such as arithmetic averaging and least-squares fitting of a considerable number of data points in the vicinity of the point of interest led to the conclusion that more elaborate techniques held no advantage over the visual averaging of plotted data by experienced individuals. The smooth curves in Fig. 4, starting at zero time with the density ratio calculated for no reaction, represent the latter technique.

The results from 11 experiments on shocks of velocity <1.5 mm/μsec are plotted in Fig. 5, together with curves calculated assuming primary dissociation as the only chemical reaction, and various values for $D(C_2N_2)$. The "no reaction" curve I was calculated assuming rotational and vibrational equilibrium but no dissociation. Curves I–T, and III–T show the temperature-velocity relationships corresponding to the density ratio-velocity curves, I and III. The experimental points up to $U_i=1.5$ mm/μsec represent the maximum average density obtained prior to the appearance of species other than CN, as determined by emission spectroscopy. For velocities up to 1.35 mm/μsec the density profiles were quite flat, as for example, curve I in Fig. 4; and the maximum average densities attained were plotted. For the shots at 1.43 mm/μsec (Fig. 4, curve II) and in the vicinity of 1.49 mm/μsec average densities were measured, respectively, 7 and 2 μsec behind the front.

In another connection considerable data have been obtained at velocities above 1.5 mm/μsec. Although not consistent with the calculational assumption of primary dissociation only, maximum average densities for these experiments are also plotted in Fig. 5 for purposes of comparison.

There are various random errors which contribute to the uncertainty in a single measurement of ρ/ρ_0. Errors in temperature, pressure, and composition may result in an over-all uncertainty in ρ_0 of 0.5%. Film reading errors, based on the maximum spread between results obtained by independent, experienced observers, in the worst case amount to a 1.7% uncertainty in ρ/ρ_0. This error was usually less than 1%. Calibration errors are at most of the order of 0.5% as shown from density measurements on krypton shocks.[24] Combined in the usual way these errors yield approximately 2% for the total uncertainty in ρ/ρ_0. The estimated maximum error in velocity is 0.3%, which is negligible in comparison with density errors.

Since $D(O_2)$ is well known, density-velocity measurements were performed on krypton-oxygen shocks under conditions comparable to the krypton-cyanogen work in order to investigate the possibility of systematic errors in measured shock parameters. The densities measured in three of the four Kr–O_2 shots tried differed by less than 1% from those calculated for the respective measured velocities, and the fourth by less than 2%. These results were considered good evidence that there were no systematic errors in the technique significant at the 1% level. Since the three lowest points in Fig. 5 were obtained under conditions of vanishingly small degree of dissociation, there are no significant thermochemical uncertainties in the calculated curve. Hence the excellent agreement between these data and curve I provides additional proof of the reliability of the density and velocity measurements reported here.

The eight points enclosed by dotted lines in Fig. 5 are considered to be the significant ones in establishing a value for $D(C_2N_2)$. A family of curves, of which II, III, and IV are members, was calculated considering only primary dissociation and assuming a series of values for $D(C_2N_2)$ at 2 kcal/mole intervals. Curve III, calculated for $D(C_2N_2)=145$ was found to yield the best fit of the critical points. Since each point in a sense constitutes a determination of $D(C_2N_2)$, the uncertainty in the value derived from eight points, each with a maximum uncertainty in ρ/ρ_0 of 2%, should be about 0.7% in terms of density ratio. From the relationship between curves III and IV in Fig. 5 in the middle of the critical range of shock velocity we deduce that this corresponds to approximately 6 kcal/mole in $D(C_2N_2)$. Thus we obtain 145 ± 6 as the most probable value of $D(C_2N_2)$. Substituting this result into Eq. (1) leads immediately to 109 ± 3 for $H_0°(CN)$. Equation (2) then yields $D(CN)=174\pm3$.

The order of magnitude of the rates of primary dissociation and recombination may be estimated from a profile of density as a function of time behind a shock under proper conditions. In the experiment at 1.43 mm/μsec a delay of several microseconds was observed in the onset of secondary reaction, while the density change due to primary dissociation should be significant relative to experimental error. Therefore this result was taken as the best available one for purposes of kinetic estimates. Denoting concentration by brackets, let $[c]$ be the formal $[C_2N_2]$ at any time t equal to the sum of the actual $[C_2N_2]$ and $\frac{1}{2}[CN]$. Let the degree of dissociation be $\alpha=[CN]/2[c]$; k_d and k_r the rate coefficients for primary dissociation and recombination, respectively, $[M]$ the total gas concentration; and K_c the equilibrium constant for primary dissociation. For small α the true $[C_2N_2]$ may be approximated by $[c]$. Endothermic processes behind a shock front proceed adiabatically resulting in some change in specific volume and temperature. However, we will consider here only the constant volume rate of change of $[C_2N_2]$ which may be written as

$$-(\partial[C_2N_2]/\partial t)_v=[c](d\alpha/dt)=[c][M](k_d-4k_r[c]\alpha^2). \tag{4}$$

Since $K_c\cong4[c]\alpha_{eq}^2$, where α_{eq} is the degree of dissociation at equilibrium, Eq. (4) becomes

$$d\alpha/dt=[M]k_d\{1-(\alpha/\alpha_{eq})^2\}. \tag{5}$$

Since for small α the temperature change during reaction is small, the temperature dependence of k_d and $[M]$ may be neglected and integration of (5), noting that $t=0$ when $\alpha=0$, leads to

$$k_d=(\alpha_{eq}/[M]t)\tanh^{-1}(\alpha/\alpha_{eq}). \tag{6}$$

From curve II, Fig. 4, we estimate that 10 μsec are required for the density to reach 90% of the equilibrium value. This corresponds to a particle dwell time of 57 μsec. From the calculations which led to curve III, Fig. 5, we obtain for $U_i=1.43$ mm/μsec: $\alpha_{eq}=0.022$; $[M]=0.015$ mole/liter; and $K_c=3.4\times10^{-5}$. Taking $\alpha/\alpha_{eq}=0.9$, substitution of these numbers into (6) yields $k_d=3.8\times10^4$ (mole/liter)$^{-1}$ sec^{-1}. If we assume that under shock conditions $k_r=k_d/K_c$ we find that $k_r=1.1\times10^9$ (mole/liter)$^{-2}$ sec^{-1}. The error in these estimates due to the approximate nature of the reaction-time measurement and neglect of cooling and depletion of C_2N_2 during reaction should be less than an order of magnitude. And indeed, the value of k_r deduced above is quite reasonable in view of the usual experience that rate constants for most recombination reactions lie between 10^8 and 10^{11} (mole/liter)$^{-2}$ sec^{-1}. When equated to an Arrhenius-type expression with an activation energy of 145 kcal/mole and a temperature of 2865°K the experimental value of k_d leads to a pre-exponential factor of 3.3×10^{15}.

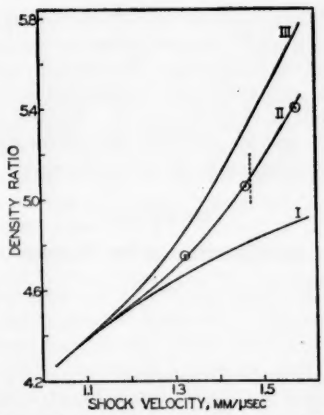

FIG. 6. Observed shock density-velocity data for 0.85 Kr+0.15 HCN mixture at 50 mm Hg initial pressure and 25±3°C initial temperature, compared with curves calculated assuming various values of $D(HCN)$. Curve I, assumptions were vibrational and rotational equilibrium but no chemical reaction; curves II and III, primary dissociation and $D(HCN)$ values of 129 and 115 kcal/mole, respectively, were assumed.

Density Measurements. Kr—HCN Mixture

In the hope of providing a verification of the results of the cyanogen dissociation energy studies, analogous experiments were performed on a different chemical system Kr–HCN. The density-velocity data obtained are plotted in Fig. 6. That velocity corresponding to a shock temperature below which appreciable separation between primary dissociation and subsequent reaction was observed in the Kr–C_2N_2 system, is indicated by a vertical dotted line. The two points to the left of that line represent maximum average densities. The point falling at a somewhat higher velocity corresponds to the density 5 μsec behind the shock front and is 3.5% less than the maximum average density, which was reached in 30 μsec. Curve II, calculated assuming $D(HCN)=129$ and primary dissociation ($HCN\rightleftharpoons H+CN$), fits

the data satisfactorily and is consistent with a value of 145 for $D(C_2N_2)$. These conclusions were not altered by allowing for the formation of H_2 and C_2N_2 in the calculations. Curves I and III were calculated for no reaction and $D(HCN)=115$, respectively. We feel that these experiments provide excellent support for the assumptions and conclusions of the cyanogen work.

DISCUSSION

Interpretation of the Results

The spectroscopic experiments have shown that under our experimental conditons a definite range of shock velocity exists over which CN appears essentially at the shock front, whereas a significant delay occurs in the appearance of emission due to the presence of other species. Unfortunately, due to the strong absorption of CN and the interplay of absorption and emission, it was not possible to establish unequivocally that the CN concentration reached a quasi-steady state before appreciable secondary reaction occurred. However, such was assumed to be the case and the density-velocity measurements were interpreted on this basis.

The experimental density profiles, of which examples are shown in Fig. 4, are consistent with this assumption. Since no evidence for the occurrence of secondary reaction within 30 μsec of the shock front was observed for waves slower than 1.4 mm/μsec, any changes in density with time behind the front should be due to primary dissociation. Although for this velocity range these changes were small, it was found that they occurred relatively close to the shock, and that the density then remained essentially constant for several tens of μsec.

In comparing the observed density-velocity points with the various calculated curves in Fig. 5 it is most significant that the departure of the experimental data from the no reaction curve occurs at a much higher velocity than would be the case if $D(C_2N_2)=115$. For example, the spectroscopic experiments showed no evidence of C_2 or C_n within 150 μsec of the front for $U_i=1.38$ mm/μsec. Hence the assumption of equilibrium with respect to primary dissociation should be excellent for $U_i=1.35$. As shown in Fig. 5, the density observed at this velocity fell well below that expected for $D(C_2N_2)=115$, and in good agreement with $D(C_2N_2)=145$.

It should be noted in Fig. 5 that the maximum average densities observed for velocities above 1.5 mm/μsec fall higher and higher above primary dissociation curve III as the velocity increases. Thus experimentally, the net thermal effect on the system of the occurrence of secondary reactions is endothermic by an amount roughly 25% of that of primary dissociation. It seems clear that the density change across the shock is in fact principally controlled by the endothermicity of the primary dissociation. Therefore, even if it is only approximately true that primary dissociation is the only important reaction under the conditions chosen for the determination of $D(C_2N_2)$, the results obtained should be valid, since they are not very sensitive to deviations from that assumption.

One might be tempted to argue that a much lower value for $D(C_2N_2)$ could be consistent with these experimental observations provided that no quasi-equilibrium with respect to primary dissociation, and correspondingly high density, were ever established due to rapid removal of CN by an exothermic secondary reaction mechanism. However, we recall that between 1.2 and 1.35 mm/μsec no evidence of secondary reaction was ever observed closer than 150 μsec behind the shock front, while CN appeared immediately. Therefore, from a comparison of curves I and V in Fig. 5, one would expect that if $D(C_2N_2)$ were 115 the shock density over this velocity interval would be significantly higher than the no reaction value, especially near the high-velocity end. Because the densities observed at shock velocities above 1.5 mm/μsec fall well below curve V, Fig. 5, between 1.4 and 1.45 mm/μsec where the onset of secondary reaction begins to approach the front one would expect to find a maximum in the observed density profiles if $D(C_2N_2)$ were 115. Since the data showed neither of these effects (see Fig. 4, II and III, and Fig. 5), this argument fails.

We believe that the accuracy and reliability of the technique have been adequately demonstrated by the previously published work on Kr–CO[11] and pure krypton[23] shocks, and by the presently reported calibration experiments on Kr–O_2 and weak Kr–C_2N_2 shocks. We consider that the quasi-equilibrium basis for interpretation of this work has been adequately justified by experimental means. It is therefore concluded that the evidence presented here has definitely established a value for $D(C_2N_2)$ of 145±6 kcal/mole.

Comparison with Other Work

Values for $D(C_2N_2)$ reported in the literature range from 77[31] to 146.[32] However, as Gaydon[33] pointed out in his excellent review of the subject, consideration of spectroscopically admissible values for $D(CN)$, together with the values 225 and 170 for $D(N_2)$ and $L(C)$, respectively, suggests that $D(C_2N_2)$ most probably lies in the range 115–146. Gaydon recommended the lower value, largely because of the work of Brewer, Templeton, and Jenkins.[34] They studied the equilibrium

$$C_{(gr)}+\tfrac{1}{2}N_{2(g)}\rightleftharpoons CN_{(g)}, \qquad (7)$$

in a graphite tube furnace using the emission intensity of the (0,1) band of the $^2\Sigma-{}^2\Sigma$ system of CN as a measure of CN concentration. Applying the van't Hoff

[31] G. B. Kistiakowsky and H. Gershinowitz, J. Chem. Phys. **1**, 432 (1933).
[32] J. U. White, J. Chem. Phys. **8**, 459 (1940).
[33] A. G. Gaydon, *Dissociation Energies* (Chapman and Hall, Ltd., London, 1953), pp. 194–195.
[34] L. Brewer, L. K. Templeton, and F. A. Jenkins, J. Am. Chem. Soc. **73**, 1462 (1951).

isochore to their data they deduced a value of 94±6 for $H_0°(CN)$, corresponding to 115±12 for $D(C_2N_2)$.[35]

White[32] determined the C_2N_2 dissociation equilibrium constant from absorption spectroscopic measurements of the CN concentration produced by heating cyanogen in a furnace. He reported a lower limit of 138 and a most probable value of 146±4 for $D(C_2N_2)$. White's work has never received much favor. It has been suggested[34] that his numbers were high because of lack of equilibrium between C_2N_2 and CN resulting from removal of CN as fast as it was formed through cyanogen polymerization and/or dissociation to form carbon and nitrogen. But this seems unlikely since it is well known that cyanogen doesn't polymerize above 800°C[36,37] and White worked above 1200°C. Furthermore, although White did not mention carbon formation in his furnace, Kistiakowsky and Gershinowitz,[31] who worked under similar conditions, found the amount of carbon deposited during a run to be negligible, indicating that no extensive abstraction of CN by dissociation had occurred.

Schmid, Gero, and Zemplen[38] have studied perturbations in the violet bands caused by the $A^2\pi$ state of CN. They built up a vibrational level scheme for this state, from which they derived a dissociation limit of 173. By Eqs. (1) and (2) this corresponds to values of 147 for $D(C_2N_2)$ and 110 for $H_0°(CN)$. Although Gaydon[33] originally accepted Schmid's work, in his revised edition he instead recommended the result reported by Brewer.[34] Since Brewer has found corrections to his observations which bring his results into agreement with those of Schmid, White, and the present investigation, it seems likely that Gaydon's original appraisal of the situation was correct.

Herron and Dibeler[39] have measured the appearance potentials of singly positive halide ions formed from cyanogen halides in a mass spectrometer. Following an interpretation due to Stevenson[40] they assumed that the CN radical was formed in the $A^2\pi$ state, 26 kcal/mole above the ground state, which led them to report 89 for $H_0°(CN)$. A ground-state assumption would have yielded 115, in fair agreement with the present result. Stevenson worked with the appearance potentials of CN^+ in the mass spectra of HCN and C_2N_2. Although he concluded that for lack of knowledge of the state of the CN radical produced, his results could agree with either those of White,[32] or some lower value, he chose to recommend 107 for $D(C_2N_2)$. McDowell and Warren[41] have pointed out that there is no *a priori* reason to expect dissociation of CNX to lead to an excited CN radical. They measured the appearance potential of CH_3 from CH_3CN, from which they deduced a value of 93 for $H_0°(CN)$, assuming that the CN formed in the process studied was in the ground state. Had they assumed the $A^2\pi$ state as did Stevenson, and Herron and Dibeler, they would have obtained 67.

Investigations leading to $D(C_2N_2)$ values ranging from 115 to 130 have been reported by Long,[42] Robertson and Pease,[36] and Hogness and T'sai.[43] This work has been discussed by Gaydon.[33] Glockler[44] considered a Born-Haber cycle involving potassium and sodium cyanides from which he concluded that $D(C_2N_2)=127$, in agreement with Robertson and Pease, and Hogness and T'sai. But he points out that the electron affinity of CN and the lattice energies of KCN and NaCN are not well known. Hence his arguments cannot definitely rule out a higher value for $D(C_2N_2)$.

CONCLUSION

Simultaneous measurements have been made of shock velocity and density vs time behind shock waves in a mixture of krypton and cyanogen. These experiments establish a value of 145±6 kcal/mole for the energy required to dissociate cyanogen into two CN radicals, assuming the well-known value of 73.4 for the heat of formation of cyanogen at 0°K. These numbers, and the presently accepted values of the heat of dissociation of nitrogen and the heat of sublimation of carbon, 225 and 170, respectively, lead to 109±3 for the heat of formation of CN and 175±3 for the heat of dissociation of CN.

Well-established values for the heat of formation of HCN and dissociation energy of hydrogen, together with the heat of formation of CN determined here, lead to a heat of dissociation of HCN to form H and CN of 129±3. This result was confirmed by separate experiments with a Kr–HCN mixture.

A rate constant of the order of 1×10^9 (mole/liter)$^{-2}$

[35] The authors noted that Brewer *et al.*[34] did not report considering the possibility of self-absorption in their 30 cm long King-type furnace. If this effect had been appreciable it would have made their measured value for $H_0°(CN)$, and therefore $D(C_2N_2)$, too low. A rough calculation of the absorption coefficient at the highest and lowest temperatures used by Brewer indicated that self-absorption should have been appreciable at the high end of his temperature range.

A preliminary account of the present work was sent to Professor Brewer. In a private communication he stated: "There is no conflict between your results and the measurements that I, Templeton, and Jenkins reported, due to self-absorption corrections among other corrections." (see O. H. Krikorian, UCRL 2888 and W. T. Hicks, UCRL 3696). Thus their results are in agreement with those of White[32] and this work on $D(C_2N_2)$, and the results of Schmid, Gero, and Zemplen[38] on $D(CN)$.

[36] N. C. Robertson and R. N. Pease, J. Chem. Phys. **10,** 490 (1942).

[37] L. Troost and P. Hautefeuille, Compt. rend. **66,** 795 (1868).

[38] R. Schmid, L. Gero, and J. Zemplen, Proc. Phys. Soc. (London) **50,** 283 (1938).

[39] J. T. Herron and V. H. Dibeler, J. Am. Chem. Soc. **82,** 1555 (1960).

[40] D. P. Stevenson, J. Chem. Phys. **18,** 1347 (1950).

[41] C. A. McDowell and J. W. Warren, Trans. Faraday Soc. **48,** 1084 (1952).

[42] L. H. Long, Proc. Roy. Soc. (London) **A198,** 62 (1949).

[43] T. R. Hogness and L. T'sai, J. Am. Chem. Soc. **54,** 123 (1932).

[44] G. Glockler, J. Chem. Phys. **16,** 600 (1948).

sec^{-1} has been deduced for the recombination at 2900°K of CN radicals to form cyanogen.

ACKNOWLEDGMENTS

The authors take pleasure in expressing their indebtedness to Dr. Russell E. Duff and Dr. Garry L. Schott for their most helpful suggestions and discussions during the course of this work, to Richard E. Johnston for his assistance in performing the experiments, and to Dr. E. Dan Loughran for performing many mass spectrometric analyses.

THE JOURNAL OF CHEMICAL PHYSICS VOLUME 35, NUMBER 1 JULY, 1961

Paramagnetic Resonance of X-Irradiated Single Crystals of Rochelle Salt* †

GRACE C. MOULTON AND W. G. MOULTON

Department of Physics, University of Alabama, University, Alabama

(Received December 19, 1960)

The electron-spin resonances of single crystals of Rochelle salt and deuterated Rochelle salt irradiated with 40 kv x rays have been studied as a function of orientation of the crystal in the magnetic field. The spectra are time dependent, and by studies of the decay of the spectra it has been found that three kinds of centers are present. In Rochelle salt one of these gives rise to an intense doublet which decays rapidly, another to a doublet which grows and then decays, and the third is an eight-line spectrum which grows and is stable. It is shown that the waters of hydration play an important role in the kinetics of the growth and decay of the centers. The stable spectrum has been analyzed, and it is concluded that two of the lines arise from breaking one of the C—H bonds. This doublet is slightly anisotropic, and arises from hyperconjugation to the proton on the adjacent carbon, and dipolar coupling between it and the large spin density on the carbon. A second pair of lines arises from breaking the other C—H bond, and since the hydrogens are not equivalent, this pair has a different splitting. The other two pairs are shown to be couplings to either OH or water of hydration hydrogens.

INTRODUCTION

IT has been found by Chyneweth[1] that the ferroelectric properties of Rochelle salt and triglycine sulphate are modified when the crystal is irradiated. The purpose of this research was to study the impurity centers produced by x rays in Rochelle-salt single crystals by the method of paramagnetic resonance, in hopes that these studies would eventually lead to an understanding of the mechanisms producing the changes in the ferroelectric properties.

There have been several recent paramagnetic resonance studies in single crystals of fairly complex solids, such as glycine,[2] alanine,[3] succinic acid,[4] malonic acid,[5] and potassium chlorate.[6] In view of the success of these studies, it was felt that the centers produced by x irradiation in Rochelle salt could be determined. This goal has been only partially attained due to several unfortunate circumstances. The spectrum is complex due to the fact that there are several centers produced whose EPR spectra lie on top of one another and are incompletely resolved. We have been able to determine which part of the spectrum is associated with each kind of center with reasonable assurance by studying the time dependence of the spectrum, since the different spectra decay at different rates. Another complicating feature was the fact that there is considerable disagreement in the literature concerning the hydrogen positions in the Rochelle salt crystal.[7–10]

EXPERIMENTAL METHODS

The x-band paramagnetic resonance spectrometer consisted of a V–203B klystron, a rectangular transmission cavity, and a bolometer detector. For studies of the field dependence, a Varian X–13 klystron and a tuneable cylindrical cavity were used. The derivative of the absorption spectrum was displayed on a chart recorder. The x-ray tube was a Machlett AEG–50 with a molybdenum target and a beryllium window. The tube was operated at 40-kv peak and 15 ma. The

* This work supported by U. S. Army Office of Ordnance Research.

† Based in part on a thesis by Grace C. Moulton submitted in partial fulfillment of the requirements for the Ph.D. degree, University of Alabama.

[1] A. G. Chyneweth, Phys. Rev. **713,** 159 (1959).
[2] D. K. Ghosh and D. H. Whiffen, Mol. Phys. **2,** 285 (1959).
[3] I. Miyagawa and W. Gordy, J. Chem. Phys. **32,** 255 (1960).
[4] C. Heller and H. M. McConnell, J. Chem. Phys. **32,** 1535 (1960).
[5] B. H. McConnell, C. Heller, T. Cole, and R. W. Fessenden, J. Am. Chem. Soc. **82,** 766 (1960).
[6] T. E. Hasty, W. B. Ard, and W. G. Moulton, Phys. Rev. **116,** 1459 (1959).
[7] G. Shirane, F. Jona, and R. Pepinsky. Proc. I. R. E. **43,** 1738 (1955).
[8] A. N. Baker and D. S. Webber, J. Chem. Phys. **27,** 689 (1957).
[9] A. Losche, Izvest. Akad. Nauk S.S.S.R. **21,** 1064 (1957).
[10] R. Blinc and A. Prelesnik, J. Chem. Phys. **32,** 387 (1960).

dose rate at the sample was measured by a chemical method to be about 1 Mr/hr.

The Rochelle salt crystals were grown by evaporation from an aqueous solution of Fisher Analyzed Reagent Grade Rochelle salt. Crystals supplied by courtesy of Dr. Hans Jaffe of the Clevite Corporation gave identical spectra. The deuterated sample was kindly loaned to us by Dr. Gerald Burns of the IBM research laboratories.

EXPERIMENTAL RESULTS

X-band paramagnetic resonance data were taken at 10-deg intervals about each of the three crystalline axes. In each case the axis of rotation was perpendicular to H_0. Figure 1 shows x-band paramagnetic resonance spectra of Rochelle salt after irradiation, taken with the ferroelectric a axis perpendicular to H_0. There are at least 12 incompletely resolved lines. There is some orientation dependence, although the total width of the spectrum does not change appreciably. In Fig. 1(a) the outermost lines are split, whereas in Fig. 1(b), which is rotated 130° about the a axis with respect to 1(a), these are not resolved. The other lines also show some orientation dependence. If the c axis is kept perpendicular to H_0 while the crystal is rotated, the outermost lines remain split, as in Fig. 1(a). There is very little orientation dependence about this axis, except for a doublet near the center. There is some orientation dependence when the crystal is rotated about the third crystalline axis.

The strong center line could be observed after 1 min of x irradiation. It was found that the shape of the entire spectrum remained independent of dose up to about 12 hr of irradiation. After longer irradiations the lines broadened. The irradiation times used were usually about 2 or 3 hr.

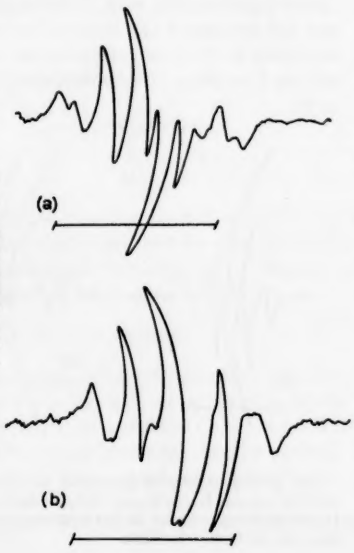

FIG. 1. Derivative of x-band paramagnetic absorption of Rochelle salt. The ferroelectric a axis $\perp H_0$ in both (a) and (b); (a) is rotated 130° about the a axis with respect to (b). The horizontal line in each figure represents 50 gauss.

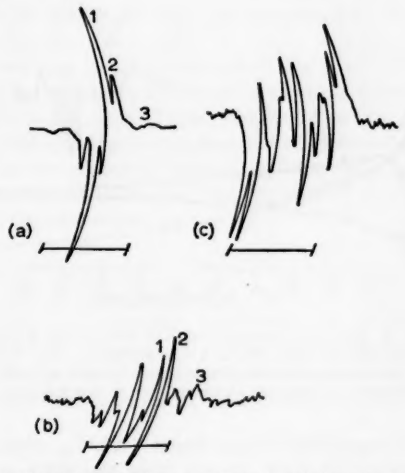

FIG. 2. The effects of aging x-irradiated Rochelle salt. Spectrum (a) was taken 0.3 hr after cessation of x irradiation, (b) after 70 hr, and (c) after two months.

The spectrum is strongly time dependent for approximately 2 weeks after irradiation and then changes relatively slowly. It was the study of this time dependence that led to a separation of the centers.

Figure 2 shows the changes in the spectrum on aging. Figure 2(a) was taken a few minutes after completion of irradiation and Fig. 2(b) after almost 3 days. The orientation of the crystal is identical in these two. The dose was about 2 Mr. The gain of the spectrometer was increased by about a factor of 2 in the second spectrum. Figure 2(c) shows a spectrum of a sample two months old.

Several decay runs were made and in each case the sample was not removed from the cavity or touched during the entire run in order to preserve the exact orientation. For all the decay runs, when the crystal was put in the cavity a very small crystal of naturally paramagnetic $CuSO_4$ was put in the cavity with it, and its orientation was fixed so that its spectrum was considerably down field from the Rochelle-salt spectrum, and its size convenient for comparing amplitudes with the Rochelle salt. The only parameter of the spectrometer that was changed during a run was the gain. The $CuSO_4$ was always run immediately before and after the Rochelle salt. Figure 3 is a plot of the relative line amplitudes as a function of time for one sample. In this run a higher x-ray dose was given than that shown in the previous figure and the data were taken over a longer period (10 days). The amplitude relative to $CuSO_4$ of individual lines in the spectrum is plotted as a function of time. Each curve represents amplitude measurements on a line corresponding to the similarly numbered line in the spectrum. Since there are 3 distinct curves, we conclude that there must be three kinds of centers. The spectrum shown here was taken after about a day and a half.

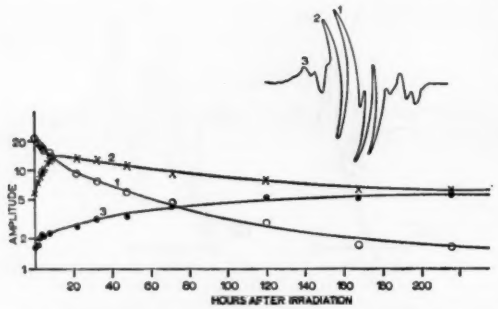

FIG. 3. Amplitude measurements of lines in the Rochelle-salt spectrum relative to $CuSO_4$, as a function of time after irradiation. Each curve represents amplitude measurements on a line corresponding to the similarly numbered line in the spectrum.

The strong line in the center (No. 1), which is an anisotropic doublet, decays from the start and the fastest. The second center (No. 2) is also a doublet which grows initially and then decays. The third center (No. 3) grows from the beginning. It consists of 4 lines which split into 8 lines. Data were taken on other lines in this spectrum and also on other samples and were consistent with these. Data could not be taken on all the lines because of the overlapping. Centers No. 2 and 3 are both holes as determined by their g-value comparison with DPPH. The g value of center No. 1 is slightly less than DPPH, but due to the width of the line and its nearness to DPPH we were unable to determine whether it is an electron or not.

The x-band paramagnetic spectrum of deuterated Rochelle salt after irradiation with x rays was also observed. All hydrogens except the two that are directly attached to the carbons were replaced by deuterium in the deuterated sample. The gross aspects of this spectrum are the same as for the normal Rochelle salt, but there are differences. In Fig. 4 are shown spectra of the deuterated Rochelle salt and the normal Rochelle salt for the same crystalline orientation. These spectra were taken with the c axis $\perp H_0$, $b \perp H_0$, and $a \parallel H_0$. In the deuterated spectrum center No. 1 is no longer a doublet but is now a single line, which must be an unresolved triplet. Center No. 2 is still a doublet with the same splitting. Center No. 3 still consists of 4 lines, but the splitting of each line into two no longer occurs. These small splittings are missing at all orientations of the deuterated samples.

There are some differences exhibited in the decay of the deuterated sample as compared with the normal Rochelle salt. Each center in the deuterated sample has the same qualitative decay characteristics as the normal Rochelle salt, but the relative initial intensities are different. The ratios of initial intensities of center No. 1 to center No. 2 and of center No. 2 to center No. 3 are greater in the deuterated samples. This suggests that either the hydroxyl hydrogens or the waters of hydration play an important role in the kinetics of the radiation damage.

Some effects of dehydrating the Rochelle salt were observed. A crystal of Rochelle salt which had been previously x-rayed and then allowed to decay was placed in a desiccator with dehydrite $[Mg(ClO_4)_2]$ for 2 days. It became opaque and white, and crumbled easily when touched, but its EPR spectrum was not changed, indicating that although it probably had become polycrystalline, the crystals must have remained aligned. However, when a single crystal which had never been irradiated was put into a desiccator with dehydrite for 2 days and then x-rayed, its spectrum was very different. It was only one comparatively broad line which did not decay into other spectra, at least not in the same order of time as the normal Rochelle salt, indicating that the water of hydration must be important to the kinetics of the radiation damage.

The spectrum of normal Rochelle salt was examined at several frequencies ranging from 8.7 to 11.9 kMc. There was no change in the splitting of the outermost lines, indicating that this splitting cannot be a second-order effect.

When a single crystal of Rochelle salt was irradiated in liquid air, the spectrum was not the same as the room-temperature spectrum. It was a comparatively broad, intense line with some structure superimposed on it. The crystal was brownish in color, whereas the room-temperature irradiated crystal is a clear yellow. When the crystal was allowed to warm to room temperature, several rapid color changes were observed, ending in a pale yellow which then slowly became a deeper yellow. After aging at room temperature the EPR spectrum was the same as Rochelle salt irradiated at room temperature, except that the strong doublet at the center was absent (center No. 1). Centers 2 and 3 grew together with with 2 always more intense than 3, and did not decay (at least in the same order of time as it took in the room-temperature irradiated Rochelle salt for 2 to decay to approximately the same intensity as 3).

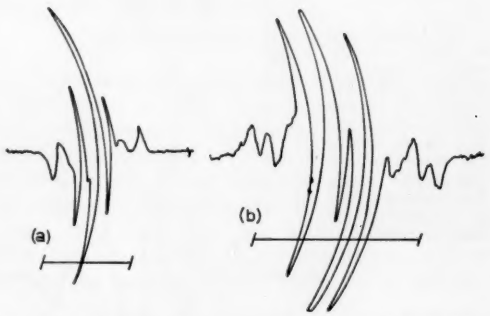

FIG. 4. Comparison of spectra of (a) deuterated Rochelle salt and (b) normal Rochelle salt. In both cases $c \perp H_0$, $b \perp H_0$, $a \parallel H_0$. It should be noted that in the deuterated sample the outermost lines are no longer doublets.

INTERPRETATION OF THE SPECTRUM

A model has been devised for the permanent center, No. 3. The spectrum which must be fitted consists of 8 lines. The outermost lines have a splitting of 52 gauss and are isotropic. The next set are slightly anisotropic, the splitting varying from 52 to 43 gauss, the minimum splitting occurring when $H_0 \approx \perp$ to the crystalline c axis, and the maximum splitting occurring when $H_0 \approx \|$ to the c axis. The maximum splitting of the innermost doublet is 26 gauss. We will refer to these doublets henceforth as A, B, and C, respectively. There is another pair of lines which sometimes overlaps C, but due to the confusion of lines in this region of the spectrum, the variation with orientation could not be determined.

The heavy atoms in the Rochelle salt molecules are biplanar. There is no center of symmetry. The space group is $P2_12_12$ with four molecules per unit cell.

The most likely model, considering other work,[4,5] is one in which one of the C—H bonds is broken. The bonds to the α carbon will then tend to become planar and the unpaired spin on the α carbon will be in a $2p$ orbital with its axis of symmetry perpendicular to the reoriented planar carbon bonds.[4] When the C—H bond is broken, there is coupling by hyperconjugation to the H on the adjacent carbon, which will be isotropic. In the case of Rochelle salt the bond angles of the hydrogens on C_2 and C_3 (using Beevers' and Hughes' notation[11]) are not the same, so that when the C_3—H bond is broken the coupling will be different than when the C_2—H bond is broken, and these will therefore appear as two different radicals:

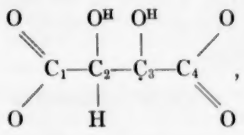

(1)

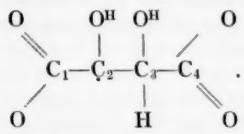

(2)

One would expect the coupling by hyperconjugation to be greater for the first case than for the second case from the semiempirical relationship of Heller and McConnell[4] (hereafter referred to as HM),

$$R(\phi) = K\rho \cos^2\phi.$$

The $R(\phi)$ is the value of the coupling as a function of the angle ϕ between the axis of symmetry of the π orbital of the unpaired spin and the C—H bond, K is a constant, and ρ is the spin density on the carbon. In the first case above where there is coupling to the H on C_2, $\phi \sim 20°$, and in the latter case where the coupling is to the H on C_3, $\phi \sim 49°$.

If one now considers doublet B, the absolute values of the Fermi and dipolar coupling can be obtained from the data. Since the Fermi coupling is much greater than the anisotropic coupling, the approximation that the nuclear magnetic moment of the proton is quantized along H_0 is valid,[2,12] and the angular dependence can be approximated by

$$A = A_f + A_\mu(3\cos^2\theta - 1).$$

The A is the total coupling, A_f the Fermi coupling, A_μ the anisotropic coupling, and θ the angle between the applied field H_0 and the dipolar symmetry axis. For doublet B this axis was found experimentally to be approximately parallel to the crystalline c axis.

$$\text{At } \theta = 0°,\ A_f + 2A_\mu = 52 \text{ gauss},$$

$$\text{at } \theta = 90°,\ A_f - A_\mu = 43 \text{ gauss}.$$

$$\text{Therefore, } A_f = 46 \text{ gauss},$$

$$A_\mu = 3 \text{ gauss}.$$

Because of the inability to follow doublet C as a function of orientation because of the overlapping of lines in this region of the spectrum (centers 1 and 2 apparently never die out completely), a similar determination of A_f and A_μ cannot be made for it in this way. However, the maximum value of A is 26 gauss, and therefore A_f must be less than this value. Doublet B must therefore be due to radical (1) and doublet C, to radical (2).

Using the values of A_f (46 gauss) and ϕ (20°) determined for doublet B, the value of the constant in the expression of HM was determined to be 52 gauss. This is larger than the value used by HM (40 gauss) based on data taken by Gibson *et al.*[13] on the methyl protons in $(CH_3)_2COH$. Miyagawa and Gordy[3], however, reported the value for the coupling in the free methyl radical in various solids to be near 25 gauss. This would give a value of $K = 50$ gauss, since the methyl group is rotating and the 25 gauss represents an average value. McLachlan[14] calculated a value of $+28$ gauss for the coupling to each methyl proton attached to a carbon of a π-electron radical by valence bond theory. This would make $K = 56$ gauss. The value of $K = 52$ gauss determined here therefore seems reasonable.

The anisotropic coupling of doublet B must be due to the dipolar coupling between the large spin density on C_3 and the nuclear moment of the H bonded to C_2. If one assumes that the spin density on C_3 and the H have the same sign,[14] and that there is negligible spin on the other atoms, the spin density on C_3 must be

[11] C. A. Beevers and W. Hughes, Proc. Roy. Soc. (London) **A177,** 251 (1941).

[12] H. Zeldes, G. T. Trammell, R. Livingston, and R. W. Holmberg, J. Chem. Phys. **32,** 618 (1960).

[13] J. F. Gibson, D. J. E. Ingram, M. C. R. Symons, and M. G. Townsend, Trans. Faraday Soc. **53,** 914 (1957).

[14] A. D. McLachlan, Mol. Phys. **1,** 233 (1958).

0.91, since the $A_f=46$ gauss would require a spin density of 0.09 on the hydrogen. A rough measure of $[\langle r^{-3}\rangle]^{-\frac{1}{3}}$, where r is the electron-hydrogen atom distance, was calculated for $A_\mu=3$ gauss and $\rho=0.91$ to be 2.3 A. This is slightly greater than the perpendicular distance from the H to the π-orbital symmetry axis ($\sim$2.0 A), and is therefore a reasonable value. It should be pointed out that in this case the H is not symmetrically placed with respect to the π orbital as has been the situation in other cases reported previously, since the H does not lie in the nodal plane of the carbons. It is on the same side of the nodal plane as one of the π-orbital lobes and is almost symmetrically placed with respect to this one lobe, but is farther away from the other lobe and not at all symmetrically placed with respect to it. Therefore, most of the dipolar coupling must come from the interaction of the H with one lobe of the π orbital.

If one now considers doublet C, an estimate of A_f and A_μ can be made for it. Using HM's expression for hyperconjugation, with the value of K determined here (52 gauss) and the angle ϕ between the C_3—H bond and the axis of the π orbital on C_2 as 49°, A_f was determined to be 22 gauss. A_μ can then be approximated. Since the maximum value of A is 26 gauss, θ will be $\sim$0° for this orientation, and therefore $A_\mu\approx 2$ gauss. The $A_f=22$ gauss requires a spin density of 0.04 on the H bonded to C_3, which will leave a spin density of 0.96 on C_2. The A_μ must be dipolar coupling between the large spin density on C_2 and the nuclear moment of the H bonded to C_3. From the A_μ of 2 gauss and the $\rho=0.96$, a rough estimate of $[\langle r^{-3}\rangle]^{-\frac{1}{3}}$ was found to be 2.4 A. This is a reasonable value since it is slightly greater than the perpendicular distance from the H to the π-orbital symmetry axis.

The above model for doublets B and C fits all the experimental data. Several other models were considered in detail but were rejected, because in each case there was at least one piece of data that would not fit the model. Further evidence that doublets B and C must be due to coupling to the H's on C_2 and C_3 is given by the data taken on the deuterated Rochelle salt, since these two doublets remain in the spectrum of the latter, but doublet A is no longer there. Doublet A must therefore arise from an interaction with an hydrogen in one of the hydroxyl groups or in a water of hydration. The possibility that A and B form a quartet and are due to the same radical was ruled out, and A must be a separate doublet if this is true. Therefore, doublet A should appear in the deuterated sample as a triplet with a smaller total splitting. There is evidence that the lines are there, but due to the overlapping of lines in the expected vicinity of the outer lines of the triplet, their existence cannot be stated conclusively. However, after the deuterated sample has decayed for two months, one can see a line at the center of the expected triplet which is not present in the decayed normal Rochelle salt.

It is concluded that doublet B is due to the breaking of the C_3—H bond, with a spin density of $\sim$0.91 on C_3 and 0.09 on the H bonded to C_2, and doublet C is due to the breaking of the C_2—H bond, with a spin density of $\sim$0.96 on C_2 and 0.04 on the H bonded to C_3. Doublet A is due to coupling to an H of an OH or a water of hydration in another radical.

This work is being continued and the kinetics of the radiation damage is being studied. There are indications, as pointed out previously, that the water of hydration plays an important role in the kinetics. This may lead to an understanding of the anomalous hysteresis effects after irradiation, since the water of hydration is thought to be important to the ferroelectric properties. A study of the centers produced at liquid-air temperature is in progress as well as studies of other tartrates.

ACKNOWLEDGMENTS

We wish to thank Dr. R. A. Mann and Dr. R. A. Kromhout for several helpful discussions.

THE JOURNAL OF CHEMICAL PHYSICS VOLUME 35, NUMBER 1 JULY, 1961

On the Theory of Ion Pairs in Solutions*†

JACQUES C. POIRIER AND JAMES H. DELAP‡

Department of Chemistry, Duke University, Durham, North Carolina

(Received December 27, 1960)

Following the general lines of Fuoss' early analysis, two alternate definitions of ion partners (1) excluding and (2) including partners composed of ions having the same electrical sign are formulated. The resulting sets of coupled integral equations for the ion-partner radial distribution functions $G_{ij}(r)$, differ from Fuoss' by the inclusion of a factor for the probability that the orbital ion does not have a partner closer than the central ion and are valid for electrolytes of any symmetry type or any mixture of electrolytes at any concentration for which the ordinary pair correlation functions $g_{ij}(r)$ for the various types of pairs of ions are known. By the presented iterative numerical method, the set of equations resulting from either definition (1) or (2) may be solved even for a general mixture. Explicit analytical solutions for $G_{ij}(r)$ in terms of an arbitrary (except for an easily relaxed restriction of a hard core) $g_{ij}(r)$ are presented for the following electrolytes: definition (1) symmetrical and unsymmetrical binary; definition (2) symmetrical binary with equal ionic radii. For examples of these electrolytes, graphs of $G_{ij}(r)$ resulting from the use of the Debye-Hückel model and the infinite dilution form of $g_{ij}(r)$ are presented (cations, $10^{-4}M$; $D=20$; $T=25°C$; interionic distance of closest approach, 4.6 A). Numerically obtained $G_{ij}(r)$ are also presented for a 1–1 electrolyte with unequal ionic radii [definition (2); conditions as above except ionic radii of 1.6 A and 3.0 A] and a mixture of two 1–1 electrolytes with a common anion [definition (1); interionic distance of closest approach of the second electrolyte, 7.0 A]. More extensive ion pair formation of the smaller cation shown in the latter case qualitatively explains anomalously low conductance in mixtures. The $G_{ij}(r)$, markedly smaller than the corresponding Fuoss curve at large separation, lead to the same association constant K^{-1} if the same critical distance is used to terminate the ion pair range; a constant critical distance, however, leads to a K^{-1} which is a continuous function of DT in qualitative agreement with some conductance data and is compatible with a "contact ion pair" concept. An equation for the activity coefficient ratio is presented and degrees of association are calculated in a variety of solutions. The formalism presented easily accepts more realistic $g_{ij}(r)$ functions and can be extended to entirely different types of systems. The usefulness of the ion (or particle) pair approach is briefly discussed.

I. INTRODUCTION

THE interpretation of the properties of solutions of electrolytes in sufficiently nonpolar solvents has been extensively discussed for many years. Although the Debye-Hückel model (i.e., a system of rigid, unpolarizable, spherical ions of charge $\pm z\epsilon$ in a homogeneous medium of fixed dielectric constant D) appears to be valid for a great many such solutions, the usual Debye-Hückel theory of the activity coefficient based on the approximation $ze\psi(r) \ll kT$ [where $\psi(r)$ is the electric potential, k is the Boltzmann constant, and T is the absolute temperature] fails because this approximation fails.[1] For these solutions, in order to also explain the negative curvature of the phoreograms[2] near zero concentration and the spectral changes with concentration, it has been postulated[3,4] that there exists a chemical equilibrium between ion pairs (and ion triplets, ··· if necessary) and free ions. The precise definition of an "ion pair," a source of some difficulties, will be considered in detail in Sec. II; suffice it to say here that it consists of two ions, sufficiently close to each other, each ion being sufficiently far removed from other ions. Applying this hypothesis to the Debye-Hückel model, Bjerrum[3] and later Fuoss[5] derived the following expression for the association constant K^{-1} of an electrically neutral ion pair from univalent ions:

$$K^{-1}=4\pi N_0 a^3 b^3 Q(b)/1000, \tag{1}$$

$$Q(b)=\int_2^b e^Y Y^{-4} dY, \tag{2}$$

$$b=\epsilon^2/aDkT, \tag{3}$$

where a is the distance of closest approach between the two ions, N_0 is Avagadro's number, and ϵ is the magnitude of the electronic charge. This equation has been rather successful in interpreting the properties of many solutions.[6] The lack of agreement between Eq. (1) and some experimentally determined association constants has prompted the derivations of several other expressions[7–9] for K^{-1}. Also, a kinetic mechanism[10] for the exchange of ion partners has been used to calculate the properties of the solution. Since, however, (1) different

* Based on a dissertation submitted by James H. DeLap in partial fulfillment of the requirements for the degree of Doctor of Philosophy at Duke University, Durham, North Carolina.

† This work was supported in part by a DuPont Summer Research Grant and by the Alfred P. Sloan Foundation.

‡ DuPont Postgraduate Teaching Assistant, 1959–1960; present address: Chemstrand Research Center, Inc., Durham, North Carolina.

[1] E. A. Guggenheim, Discussions Faraday Soc. **24**, 53 (1957), has shown that the criterion for the approximation to be useful is $|z_+z_-|\epsilon^2/aDkT<2.8$. If a, the sum of the effective radii of the ions, is 6.0 A, then D must be greater than 36 for the approximation to be useful for a 1–1 electrolyte at 25°C.

[2] R. M. Fuoss, J. Chem. Educ. **32**, 527 (1955).

[3] N. Bjerrum, Kgl. Danske Videnskab. Selskab Mat.-fys. Medd. **7**, 1 (1926).

[4] R. M. Fuoss and C. A. Kraus, J. Am. Chem. Soc. **55**, 1019 (1933).

[5] R. M. Fuoss, Trans. Faraday Soc. **30**, 967 (1934).

[6] A number of review articles are available, for example C. A. Kraus, J. Phys. Chem. **60**, 129 (1956).

[7] J. T. Dennison and J. B. Ramsey, J. Am. Chem. Soc. **77**, 2615 (1955).

[8] W. R. Gilkerson, J. Chem. Phys. **25**, 1199 (1956).

[9] R. M. Fuoss, J. Am. Chem. Soc. **80**, 5059 (1958).

[10] H. Reiss, J. Chem. Phys. **25**, 400 (1956).

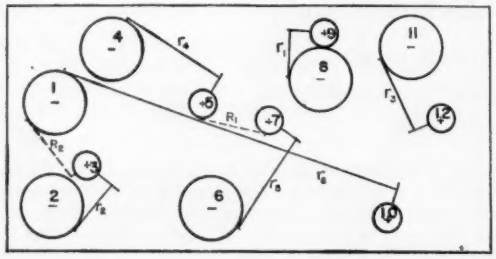

(A)

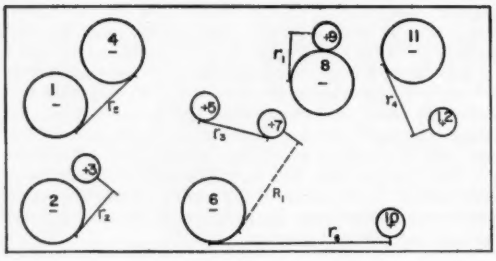

(B)

FIG. 1. Ion partner assignments. A. "Unlike partners-only" definition. Particles 5 and 7 are *not* partners since they are of like charge. Particles 1 and 3 are *not* partners since 3 is the partner of 2($r_2 < R_2$). B. "Like and unlike partners" definition. Particles 6 and 7 are *not* partners since 7 is the partner of 5 ($r_3 < R_1$).

experimental methods seem to yield different values[11] for the association constant, (2) it is not certain that the experimental constant refers to precisely the same process considered in the theory,[12] and (3) the derivations of the recent expressions for K^{-1} are not cogent, it was thought advisable to reexamine in this paper the rather general Fuoss[5] approach with the aim of clarifying the assumptions and procedures and extending the types of systems to which the theory may be applied.

In Sec. II ion partners are defined in *two* alternative ways thus permitting the clarification of the status of ion pairs composed of ions of like charge. In Sec. III, for each of the two alternative definitions, ion-partner radial distribution functions in the form of integral equations are derived and solved, either analytically or numerically, for a variety of systems. From these functions, some thermodynamic properties of the electrolytic solution are determined and discussed in Sec. IV. A comparison of the functions with each other and with previously obtained functions, as well as a discussion of the usefulness of the ion-pair approach and extensions of the present theory comprise Sec. V. The precise significance of experimentally determined association constants will not be considered.

[11] A. I. Popov and R. E. Humphrey, J. Am. Chem. Soc. **81**, 2043 (1959).

[12] S. R. Cohen, J. Phys. Chem. **61**, 1670 (1957).

II. MODEL AND DEFINITIONS

Adopting the Debye-Hückel model of an ionic solution briefly discussed in the preceding section, we shall define "ion partners" in two distinct ways which lead to two different analyses of the same model. These alternate definitions will clarify the role of pairs of particles of the *same* ionic type. Charged ion pairs were briefly considered by Fuoss,[5] dismissed as numerically unimportant, and never considered in the subsequent mathematical treatment. Ion partners will be subsequently subdivided into "ion pairs" and "free ions."

One definition of "ion partners" is: A positive ion and a negative ion are defined as "ion partners separated by a distance r" if the center of one lies in dr at a distance r from the center of the other, provided that neither of these ions has a partner with a *charge of opposite sign* at a distance *less than* r. To clarify the method of assigning ion partners by this definition, which we shall refer to as the "unlike partners only" definition, it is convenient to suppose, as Fuoss[5] did, that the positions of all ions are temporarily fixed within the solution as shown by the simple 1–1 electrolyte example in Fig. 1(A). All distances separating the centers of ions with charges of opposite sign are compared. According to the above definition, the positive ion and negative ion which are closest together (separation r_1) are designated as "ion partners separated by a distance r_1." Mentally removing these two ions from the solution, the next-closest pair of oppositely charged ions (separation r_2) are designated as "ion partners separated by a distance r_2" ($r_2 > r_1$). This process is continued until all of the positive ions *or* all of the negative ions have been assigned partners as shown by the lines r_i in Fig. 1(A). An excess of one type of ion, (e.g., in an unsymmetrical electrolyte) would result in some ions of the type in excess remaining without a partner. We shall call these "solitary ions."[13] In a solution containing a single symmetrical electrolyte, there is only one kind of ion partner; it has no net charge.

A different definition of ion partners is: Two ions, *regardless of their charges*, are defined as "ion partners separated by a distance r" if the center of one ion lies in dr at a distance r from the center of the other ion, provided that neither of these ions has a partner *regardless of its charge* at a distance *less than* r. To assign ion partners by this definition, which we shall refer to as the "like and unlike partners" definition, all distances separating the centers of the ions, regardless of their charges, are compared in the temporarily static solution. The two ions which are closest together (separation r_1), *regardless of their charges*, are said to be "ion partners separated by a distance r_1" and are mentally removed; the next-closest pair of ions (separation r_2) are designated as "ion partners separated by

[13] Although free ions and solitary ions are different species, no distinction between them will be made in considering an equilibrium between paired and unpaired ions in Sec. IV.

a distance r_2" ($r_2>r_1$), etc., until every ion has been assigned a partner with a charge of the same or opposite sign as indicated for the simple example in Fig. 1(B). Employing this "like and unlike partners" definition, a solution of a single symmetrical electrolyte contains three kinds of ion partners, only one of which has no net charge. Any electrically neutral solution contains at most one solitary ion.

The ion pair is defined as ion partners which are separated by a distance less than or equal to a specified value d. Ion partners separated by a distance greater than d are called free ions. Discussion of the methods of selecting d is deferred until Sec. IV.

The two preceding definitions represent the two simplest methods of analyzing the Debye-Hückel model in terms of polyionic entities. By a moderately obvious modification and extension of the foregoing definitions and assignment procedures, one can introduce ion triplets, ion quadruples, etc.; furthermore, one may exclude from the analysis triplets of cations (and triplets of anions) in much the same way as ion partners of like sign are excluded in the first definition above. From the standpoint of self-consistency, each of these analyses is equally valid, although the usefulness of each analysis depends on the particular solvent-solute system and the value of relevant thermodynamic variables.

In the course of the motion of the ions in the solution, the distance separating two ion partners varies, and the two ions comprising a pair may become partners of two other ions. At equilibrium, the solution may be characterized by the ion-partner distribution function $G_{st}(r)$ which is the probability that an s ion has for its partner a t ion a distance r away (within unit distances). These $G_{st}(r)$ functions will be found in the succeeding section.

III. DERIVATIONS OF DISTRIBUTION FUNCTIONS

In this section, from each of the two definitions discussed in the previous section there are derived integral equations for the ion-partner distribution functions $G_{st}(r)$ for any system of mixed electrolytes containing ions of any size and charge. In simple cases, resulting integral equations may be solved analytically; in the general case the coupled integral equations may be solved by the presented numerical method. Several specific systems will be treated in some detail.

Within a solution of volume V containing N_i ions of type i ($i=1, 2, \cdots, s, t, \cdots, n$) with charge $z_i\epsilon$ and radius a_i, $G_{st}(r)dr$ is the probability of finding a t ion in a spherical shell of thickness dr at a distance r from a particular s ion, provided that neither the s ion nor the t ion has a partner within r. The mathematical formulation of the definition is the basic equation for the ion partner distribution function,

$$G_{st}(r)dr = L_t h_{st} r^2 g_{st}(r)\,dr\,P_s(r)\,P_t(r), \tag{4}$$

$$L_t = 4\pi N_t/V. \tag{5}$$

In Eq. (4) $P_i(r)$ is the probability that an i ion does *not* have a partner within r. The symbol h_{st} is the device by which the distinction between the "unlike partners only" definition (for which $h_{st}=1$ if $z_sz_t<0$ and $h_{st}=0$ if $z_sz_t>0$) and the "like and unlike partners" definition (for which $h_{st}=1$) is incorporated into the basic equation. The symbol $g_{st}(r)$ represents the usual pair correlation function for ions of type s and t in a fluid

$$g_{st}(r) = \frac{n_{st}^{(2)}(r)dV_s dV_t}{n_s^{(1)}dV_s n_t^{(1)}dV_t}, \tag{6}$$

where $n_{st}^{(2)}(r)dV_sdV_t$ is the probability of finding simultaneously an s ion in an elemental volume dV_s and a t ion in an elemental volume dV_t a distance r away; and $n_i^{(1)}dV_i$ is the probability of finding an i ion in the elemental volume dV_i regardless of the location of all other ions in the solution. It is assumed in the present analysis that the $g_{ij}(r)$ functions are known for all types of ions i, j in the solution.

In addition to retaining a general $g_{ij}(r)$ rather than a specific function, the basic Eq. (4) differs from the two earlier formulations of this general approach. Bjerrum[3] intentionally excluded the $P_s(r)$ and $P_t(r)$ factors from his distribution function. Fuoss,[5] while considering only pairs of ions with charges of opposite sign, apparently defined the ion pair to include both $P_i(r)$ factors but omitted the $P_t(r)$ factor in the mathematical formulation.

Since $g_{st}(r)=g_{ts}(r)$ from Eq. (6), it is apparent from Eq. (4) that

$$N_sG_{st}(r) = N_tG_{ts}(r). \tag{7}$$

The basic Eq. (4) is an integral equation, for the probability that a particular s ion has a partner of type i within the distance r is

$$\int_{a_{si}}^{r} G_{si}(x)\,dx,$$

where a_{si} is the sum of the effective radii of the s and i ions; therefore,[14] in the basic Eq. (4),

$$P_s(r) = 1 - \sum_{i=1}^{n} \int_{a_{si}}^{r} G_{si}(x)\,dx. \tag{8}$$

Although Eqs. (4) and (8) jointly constitute a set of coupled integral equations for the $G_{ij}(r)$ functions, it proves more expedient to solve them for the $P_i(r)$ functions. The $G_{ij}(r)$ functions are then obtained by a simple substitution into the basic Eq. (4). The following transformation[15] is convenient.

---

[14] More precisely, what is required for $P_s(r)$ is the probability that an s ion does not have for a partner an i ion at a distance less than r, when there is a t ion at r. Both the central s and the orbital t must be excluded as possible partners and hence the factor $(N_i-\delta_i{}^s-\delta_i{}^t)/N_i$ should be included in the summation of Eq. (7). These correction terms omitted in Eq. (7) and therafter are negligible for systems of physical interest in which $N_i \gg 1$.

[15] Other transformations are shown in Appendix I.

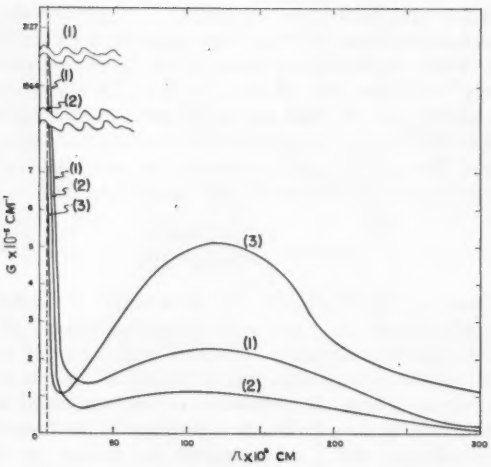

FIG. 2. "Unlike partners only" definition. (1) $G_{it}(r)$ [Eqs. (7) and (25)] and (2) $G_{st}(r)$ [Eq. (25)] in a 1–2 electrolyte solution, and (3) $G_{st}(r)$ [Eq. (17)] in a 1–1 electrolyte solution. Conditions: $a=4.6$ A; $D=20$; $T=25°C$; $c_s=1.00\times10^{-4}M$.

Substitution of the basic Eq. (4) into Eq. (8), differentiation, division by $P_s^2(r)$, and subsequent integration yields

$$P_s(r)=\left[1+\sum_{i=1}^{n}h_{si}L_i\int_{a_{si}}^{r}x^2g_{si}(x)\frac{P_i(x)}{P_s(x)}dx\right]^{-1}. \tag{9}$$

Using in turn both definitions of ion partners we shall solve Eq. (9) for various systems.

"Unlike Partners Only" Definition

Systems containing a single symmetrical binary electrolyte, a single unsymmetrical binary electrolyte, and a mixture of two symmetrical binary electrolytes with a common ion will be explicitly discussed in this section. For all of these, the high dilution limit will be treated in numerical detail.

Single Symmetrical Binary Electrolyte

For this system, Eq. (8) a similar equation for $P_t(r)$ are

$$P_s(r)=P_t(r)=1-\int_a^r G_{st}(x)dx, \tag{10}$$

where $a=a_{st}=a_{ts}$ and from Eq. (7) it is seen that $G_{st}(r)=G_{ts}(r)$. The summation in Eq. (9) reduces to a single term, and

$$P_s(r)=P_t(r)=[1+L\phi_{st}(r)]^{-1}, \tag{11}$$

where $L=L_s=L_t$ is defined by Eq. (5), and

$$\phi_{ij}(r)=\int_{a_{is}}^{r}x^2g_{ij}(x)dx. \tag{12}$$

Substitution of Eq. (11) into the basic Eq. (4) yields

$$G_{st}(r)=Lr^2g_{st}(r)[1+L\phi_{st}(r)]^{-2}. \tag{13}$$

The normalization of the ion-partner distribution function is discussed in Appendix IV.

Limiting case: single 1–1 electrolyte at high dilution. At sufficiently high dilution, the pair correlation function may be taken to be the infinite dilution value $g_{ij}^*(r)$,

$$g_{ij}^*(r)=\exp(-z_iz_jB/r), \quad r\geq a_{ij}$$
$$g_{ij}^*(r)=0, \quad r<a_{ij}, \tag{14}$$

where

$$B=\epsilon^2/DkT. \tag{15}$$

Using Eq. (14) in Eq. (12), one obtains the high dilution limiting form of $\phi_{ij}(r)$,

$$\phi_{ij}^*(r)=\int_{a_{ij}}^{r}x^2g_{ij}^*(x)dx, \tag{16}$$

which appears in all "limiting case" examples of this paper and which may be evaluated as shown in Appendix II. Substituting Eqs. (14) and (16) into Eq. (13), one obtains the desired function,

$$G_{st}(r)=Lr^2\exp(B/r)[1+L\phi_{st}^*(r)]^{-2}. \tag{17}$$

By using methods indicated in Appendix III, the distribution function of Eq. (17) may be shown to have a minimum at

$$r_{\min.}\approx\tfrac{1}{2}B(1+\tfrac{1}{8}LB^3\epsilon^2) \tag{18}$$

provided that $\frac{1}{8}LB^3\epsilon^2\ll1$. A maximum occurs at

$$r_{\max.}\approx(3/2L)^{1/3}[1-\tfrac{1}{3}B(\tfrac{2}{3}L)^{1/3}], \tag{19}$$

while inflection points occur at

$$r_{\text{infl.}}=\{[24\pm9(6)^{\frac{1}{2}}]/10L^{1/3}\} \tag{20}$$

provided that $r_{\max.}$ and $r_{\text{infl.}}$ are large. A graph of the ion-partner distribution function for a 1–1 electrolyte is shown in Fig. 2 [curve (3)] for the following conditions: $c=1.00\times10^{-4}$ M; $a=4.6$ A; $D=20$; $T=25°C$. The critical distances are: $a=4.6$ A; $r_{\min.}=14.23$ A; $r_{\max}=116.3$ A; $r_{\text{infl.}}=63.68$ and 182.6 A.

Single Unsymmetrical Binary Electrolyte in Solution

For this system, the following relationship between $P_s(r)$ and $P_t(r)$ may be derived from the applicable forms of Eqs. (7) and (8),

$$L_s[1-P_s(r)]=L_t[1-P_t(r)], \tag{21}$$

where L_s and L_t are defined by Eq. (5). Substituting for $P_t(r)$ from Eq. (21) into the basic Eq. (4), and further substituting the result into Eq. (8), one obtains an integral equation which may be solved by differentiation, rearrangement,[16] and subsequent integration to

[16] In this step in the derivation, division by L_s-L_t is made and thus the resulting Eq. (21) is not valid for symmetrical electrolytes.

yield

$$P_s(r)=(L_t-L_s)\theta_{st}(r)[L_t-L_s\theta_{st}(r)]^{-1}, \quad (22)$$

where

$$\theta_{st}(r)=\exp[(L_s-L_t)\phi_{st}(r)]. \quad (23)$$

Substituting Eq. (22) and a similar equation for $P_t(r)$ into the basic Eq. (4), one obtains upon rearrangement

$$G_{st}(r)=\frac{L_t(L_t-L_s)^2r^2g_{st}(r)\theta_{st}(r)}{[L_t-L_s\theta_{st}(r)]^2}. \quad (24)$$

The normalization of $G_{st}(r)$ is discussed in Appendix IV.

Limiting case: *single* 1–2 *electrolyte at high dilution.* For this system, $L_s=2L_t$, Eq. (14) is applicable, and Eq. (24) becomes

$$G_{st}(r)=\frac{L_tr^2\exp(2B/r)\exp[L_t\phi_{st}^*(r)]}{\{1-2\exp[L_t\phi_{st}^*(r)]\}^2}; \quad (25)$$

the symbols are defined in Eqs. (5), (15), and (16). When $\frac{3}{2}L_tB^3e^2\ll1$, this ion-partner distribution function has a minimum

$$r_{\min.}=B(1+\tfrac{3}{2}L_tB^3e^2). \quad (26)$$

To a first approximation, a maximum occurs at

$$r_{\max.}\approx(2/L_t)^{1/3}. \quad (27)$$

Graphs of $G_{st}(r)$ [curve (2)] and $G_{ts}(r)$ [curve (1)], related by Eq. (7), are shown in Fig. 2 for the following condition: $a=4.6$ A; $D=20$; $T=25°C$; $c=5.00\times10^{-4}$ M. The critical distances are: $a=4.6$ A; $r_{\min.}=30.87$ A; $r_{\max.}=109.7$ A.

Mixture of Two Symmetrical Binary Electrolytes with a Common Ion

In analyzing a solution containing three or more ionic species, the influence of relative ionic size first becomes apparent. A solution containing two cations and a common anion will be treated.

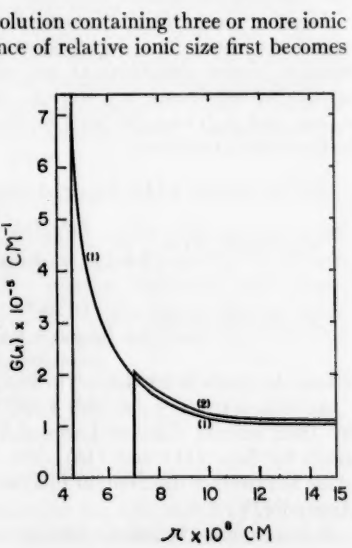

FIG. 3. "Unlike partners only" definition. (1) $G_{st}(r)$ and (2) $G_{qt}(r)$ in an equimolar mixture of two 1–1 electrolytes with a common t ion. Conditions: $a_{st}=4.60$ A; $a_{qt}=7.00$ A, $D=20$; $T=25°C$; $c_s=c_q=1.00\times10^{-4}M$.

Denoting the smaller cation by s, and the larger by q, we shall consider three ranges of separation of ion partners. *Region I*: $0<r<a_{st}$. In this region no ion partners exist, $G_{st}(r)=G_{qt}(r)=0$. *Region II*: $a_{st}<r<a_{qt}$. In this region, only st ion partners form. Since the q and t ions cannot reach this separation distance, $G_{qt}=0$. Since $N_t>N_s$, the system resembles that of an unsymmetrical electrolyte, Eq. (22) and the analogous equation for $P_t(r)$ are valid, and $G_{st}(r)$ may be analytically evaluated. *Region* III: $r\geq a_{qt}$. In this region both st and qt ion partners form. The general Eq. (9) then becomes, for the three ion types,

$$P_s^{-1}(r)=1+L_t\int_{a_{st}}^{r}x^2g_{st}(x)\frac{P_t(x)}{P_s(x)}dx; \quad (28)$$

$$P_q^{-1}(r)=1+L_t\int_{a_{qt}}^{r}x^2g_{qt}(x)\frac{P_t(x)}{P_q(x)}dx; \quad (29)$$

$$P_t^{-1}(r)=1+L_s\int_{a_{st}}^{r}x^2g_{st}(x)\frac{P_s(x)}{P_t(x)}dx + L_q\int_{a_{qt}}^{r}x^2g_{qt}(x)\frac{P_q(x)}{P_t(x)}dx. \quad (30)$$

Although an analytical solution of Eqs. (28)–(30) has not been obtained, a numerical evaluation of $P_s(r)$, $P_q(r)$, and $P_t(r)$ can be obtained if the values of the functions are known at one particular value of r, r_1. This condition is fulfilled for this system since analytical solutions of Eqs. (28)–(30) are obtainable in regions I and II.

Using a small increment Δr where $r_2=r_1+\Delta r$, Eqs. (28)–(30) take the forms

$$P_s^{-1}(r_2)=P_s^{-1}(r_1)+\Delta P_{st}(r); \quad (31)$$

$$P_q^{-1}(r_2)=P_q^{-1}(r_1)+\Delta P_{qt}(r); \quad (32)$$

$$P_t^{-1}(r_2)=P_t^{-1}(r_1)+\Delta P_{ts}(r)+\Delta P_{tq}(r); \quad (33)$$

in which

$$\Delta P_{ij}(r)=L_j\int_{r_1}^{r_2}x^2g_{ij}(x)\frac{P_j(x)}{P_i(x)}dx. \quad (34)$$

The trapezoidal method of numerical integration[17] applied to $\Delta P_{ij}(r)$ yields

$$\Delta P_{ij}(r)=L_j\frac{\Delta r}{2}\left[r_1^2g_{ij}(r_1)\frac{P_j(r_1)}{P_i(r_1)}+r_2^2g_{ij}(r_2)\frac{P_j(r_2)}{P_i(r_2)}\right]. \quad (35)$$

The values of $P_s(r_2)$, $P_q(r_2)$, and $P_t(r_2)$ may be evaluated by an iterative process. The zeroth approximation—which can be $P_s(r_1)$, $P_q(r_1)$, and $P_t(r_1)$—is inserted into the right-hand member of Eq. (35). The approximate $\Delta P_{ij}(r_2)$ thus obtained are substituted

[17] See, for example, W. Kaplan, *Advanced Calculus* (Addison-Wesley Publishing Company, Inc., Reading, Massachusetts, 1953), Chap. 4, p. 171.

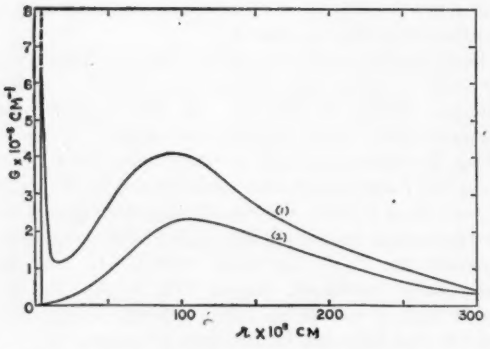

FIG. 4. "Like and unlike partners" definition. (1) $G_{st}(r)$ [Eq. (41)] and (2) $G_{ss}(r)$ [Eq. (42)] in a 1–1 electrolyte solution with ions of equal size. Conditions: $a_{st}=a_{ss}=4.60$ A; $D=20$; $T=25°C$; $c_s=1.00\times10^{-4}M$.

into the right-hand members of Eqs. (31)–(33), thus generating first approximations for the $P_i(r_2)$ which are then recycled into the right-hand member of Eq. (35). From the constant values of $P_i(r_2)$ eventually obtained, $P_i(r_3)$ $(r_3=r_2+\Delta r)$ may be calculated by the same iterative process. This method will be hereafter called the "iterative trapezoidal method."

In the system under discussion, $P_q(a_{qt})$ is unity, and the values of $P_s(a_{qt})$ and $P_t(a_{qt})$ may be evaluated analytically at the upper boundary of region II. Values of the $P_i(r)$ and $G_{ij}(r)$ functions may consequently be determined for any value of r.

Limiting case: equimolar mixture of two 1–1 electrolytes with a common ion at high dilution. Using $L_t=2L_s=2L_q$ and Eq. (14) for the pair correlation function in the formalism developed above, one obtains the following:

$$G_{st}(r)=0, \qquad r<a_{st} \tag{36a}$$

$$G_{st}(r)=\frac{2L_s r^2\exp[(B/r)+L_s\phi_{st}^*(r)]}{\{1-2\exp[L_s\phi_{st}^*(r)]\}^2}, \quad a_{st}\le r\le a_{qt} \tag{36b}$$

$$G_{st}(r)=2L_s r^2\exp(B/r)\,P_s(r)\,P_t(r), \qquad r\ge a_{qt} \tag{36c}$$

$$G_{qt}(r)=0, \qquad r<a_{qt} \tag{37a}$$

$$G_{qt}(r)=2L_q r^2\exp(B/r)\,P_q(r)\,P_t(r), \qquad r\ge a_{qt}. \tag{37b}$$

For a solution ($D=20$) containing an equimolar (1.00×10^{-4} M each) mixture of two 1–1 ($a_{st}=4.6$ A; $a_{qt}=7.0$ A) electrolytes at 25°C the distribution functions were obtained for $r\le a_{qt}$ by the evaluation of Eq. (36b) and for $r\ge a_{qt}$ by solving Eqs. (36c) and (37b) by the iterative trapezoidal method with 0.2-A increments. As a check on the accuracy of the iterative trapezoidal method, it was used to evaluate G_{st} (7.0 A) by proceeding from G_{st} (4.6 A) in 0.2-A increments. Despite the fact that in this interval $G_{st}(r)$ has a relatively large positive curvature conducive to a large cumulative error, the error in G_{st} (7.0 A) was <0.03%. Figure 3 (to be further discussed in Sec. IV and V) shows the resulting small separation range of $G_{st}(r)$ [curve (1)] and $G_{qt}(r)$ [curve (2)].

"Like and Unlike Partners" Definition

For all systems analyzed by this definition, Eqs. (4) and (9) are valid with $h_{st}\equiv1$. The study of the ion-partner distribution of several specific systems and high dilution limiting cases follows.

Single Binary Electrolyte in Solution

By this definition this system contains three species of ion partners, *st*, *ss*, and *tt*, and consideration must be given to four distribution functions $G_{st}(r)$, $G_{ts}(r)$, $G_{ss}(r)$, and $G_{tt}(r)$, of the form given by the basic Eq. (4). Two of them, $G_{st}(r)$ and $G_{ts}(r)$, are trivially related by Eq. (7). The relevant probability functions are to be found from the following expanded forms of Eq. (9),

$$P_s(r)=\left[1+L_t\int_{a_{st}}^{r}x^2g_{st}(x)\frac{P_t(x)}{P_s(x)}dx+L_s\int_{a_{ss}}^{r}x^2g_{ss}(x)\,dx\right]^{-1}; \tag{38}$$

$$P_t(r)=\left[1+L_s\int_{a_{st}}^{r}x^2g_{st}(x)\frac{P_s(x)}{P_t(x)}dx+L_t\int_{a_{tt}}^{r}x^2g_{tt}(x)\,dx\right]^{-1}. \tag{39}$$

Equations (38) and (39) are valid for symmetrical or unsymmetrical electrolytes regardless of ion sizes.

In the case of a symmetrical binary electrolyte, Eqs. (38) and (39) may be solved analytically if the ions are of equal size, but numerical methods must be used if the ions are not of equal size. This is demonstrated in the two following examples.

Limiting case: single symmetrical binary electrolyte with ions of equal size at high dilution. For a single symmetrical binary electrolyte at any concentration, the applicable equations $z_s=-z_t=z$, $L_s=L_t=L$, $a_{ss}=a_{tt}=a$, and $g_{ss}(r)=g_{tt}(r)$ lead to the following physically obvious relations:

$$P_s(r)=P_t(r)=[1+L\phi_{st}(r)+L\phi_{ss}(r)]^{-1}; \tag{40}$$

$$G_{st}(r)=G_{ts}(r)=\frac{Lr^2g_{st}(r)}{[1+L\phi_{st}(r)+L\phi_{ss}(r)]^2}; \tag{41}$$

$$G_{ss}(r)=G_{tt}(r)=\frac{Lr^2g_{ss}(r)}{[1+L\phi_{st}(r)+L\phi_{ss}(r)]^2}, \tag{42}$$

where the symbols are defined in Eqs. (5) and (12).

At high dilution, $g_{ij}(r)$ and $\phi_{ij}(r)$ may be replaced by their infinite dilution forms $g_{ij}^*(r)$ and $\phi_{ij}^*(r)$ given by Eqs. (14) and (16). The normalization of these ion partner distribution functions is discussed in Appendix IV.

It is seen from the infinite dilution forms of Eqs. (41)

TABLE I. Values of $P_s(r)$, $P_t(r)$, $G_{st}(r)$, $G_{ss}(r)$, and $G_{tt}(r)$ at some separations. "Like and unlike partners" definition, solution of a 1–1 electrolyte with ions of different sizes. Conditions: $a_s=1.6$ A; $a_t=3.0$ A; $D=20$; $T=25°C$; $c_s=1.00\times10^{-4}M$.

$r(A)$	$P_s(r)$	$P_t(r)$	$G_{st}(r)$[a]	$G_{ss}(r)$	$G_{tt}(r)$
3.2	1.00000000	1.00000000	0	0.122118	0
4.6	0.99999998	1.00000000	707 756	3.624990	0
6.0	0.9937850	0.9937852	287 093	25.22975	25.22976
7.0	0.9914071	0.9914073	199 578	66.59588	66.59590

[a] $G_{ts}(r)=G_{st}(r)$.

and (42) that

$$G_{st}(r)/G_{ss}(r)=\exp(2z^2B/r). \tag{43}$$

Thus, at small separations, especially, the probability of ion-partner formation between ions of unlike charge is much greater than that between ions of like charge.

The critical and inflection points of $G_{st}(r)$ are

$$r_{\min.}\approx z^2B(2+\tfrac{1}{2}Lz^6B^3\cosh 2), \tag{44}$$

provided $\frac{1}{4}Lz^6B^3\cosh 2\ll 1$;

$$r_{\max.}\approx[3/4L]^{1/3}[1-\tfrac{1}{6}z^2B(\tfrac{4}{3}L)^{1/3}]; \tag{45}$$

$$r_{\text{infl.}}\approx\{[24\pm9(6)^{\frac{1}{2}}]/20L\}^{1/3}. \tag{46}$$

Here $G_{ss}(r)$ has no minimum other than that which accompanies the vanishing of the distribution function at infinity. The maximum of $G_{ss}(r)$ occurs at

$$r_{\max.}\approx[\tfrac{3}{4}L]^{1/3}[1-\tfrac{1}{6}z^2B(\tfrac{4}{3}L)^{1/3}], \tag{47}$$

while the inflection points are given by Eq. (46).

Figure 4 shows $G_{st}(r)$ (curve 1) and $G_{ss}(r)$ (curve 2) for a 1–1 electrolyte under the following conditions: $a=4.6$ A; $D=20$; $T=25°C$; $c=1.00\times10^{-4}$ M. The predominance of partners composed of ions of unlike charge is apparent, particularly at small separations.

Limiting case: a single 1–1 electrolyte with ions of different sizes at high dilution. Four ranges of separation of ion partners will be considered, taking the positive s ion to be smaller than the negative t ion. *Region* I: $0<r<a_{ss}$. The rigid-spheres model prohibits ion-partner formation, hence

$$G_{ss}(r)=G_{st}(r)=G_{tt}(r)=0, \qquad r<a_{ss}. \tag{48}$$

Region II: $a_{ss}\leq r\leq a_{st}$. In this region only charged ss ion partners exist. Analysis of the ss ion-partner formation is similar to that of a solution containing only s ions. Substitution of Eq. (14) and the infinite dilution form of Eq. (38) with $L_t=0$ into the basic Eq. (4) immediately yields the following,

$$G_{ss}(r)=\frac{Lr^2\exp(-B/r)}{[1+L\phi_{ss}^{*}(r)]^2}, \qquad a_{ss}\leq r<a_{st} \tag{49}$$

$$G_{st}(r)=G_{tt}(r)=0,$$

where $L=L_s$ is defined by Eq. (5), and B by Eq. (15). *Region* III: $a_{st}\leq r<a_{tt}$. Only ss and st ion partners can form in this region. The expression for $P_s(r)$ in Eq. (38) is applicable and since $g_{tt}(r)$ is zero in this region, $G_{tt}(r)=0$ and Eq. (39) simplifies to

$$P_t(r)=\left[1+L_s\int_{a_{st}}^{r}x^2\exp(B/x)\frac{P_s(x)}{P_t(x)}dx\right]^{-1}. \tag{50}$$

By solving Eqs. (38) and (50) by the iterative trapezoidal method, values of $P_t(r)$ and $P_s(r)$ can be determined. From these, the nonzero ion-partner distribution functions can be obtained. *Region* IV: $r\geq a_{tt}$. Ion partners of all three types may be formed in this region. The iterative trapezoidal method may be used to evaluate numerically the probability functions in Eqs. (38) and (39).

The above procedure was followed for a sample 1.00×10^{-4} M 1–1 electrolyte solution at 25° C; $D=20$; $a_s=1.6$ A; $a_t=3.0$ A. In the iterative trapezoidal method, increments of 0.2 A were used. The calculated values of the probability and ion-partner distribution functions are shown in Table I. In contrast to the case of a mixture of two symmetrical binary electrolytes with a common ion considered earlier, the effect of the ion size on the ion-partner distribution in this particular system is very small.

It is apparent from the entries in the last two columns that although ss ion partners form at smaller separations than tt ion partners, the ss formation at these small separations is so improbable [compared to $G_{st}(r)$ values in column 4] and diminishes the number of unpaired s ions so slightly that at larger separations $G_{ss}(r)$ is only very slightly smaller than $G_{tt}(r)$, while $P_s(r)$ and $P_t(r)$ are nearly identical.

General Case: Mixture of Electrolytes

The solution of the n equations represented by Eq. (8), from which the ion-partner distribution functions can be obtained by substitution into the basic Eq. (4), is generally possible by employing the iterative trapezoidal method. As shown in the limiting cases above, the problem may be analytically soluble in certain separation ranges (e.g., in which only the smallest ions may form partners) or when two or more ionic species have the same ionic size. Even in unfavorable cases, the iterative trapezoidal method is easily programmed for an electronic computer, while shrewd initial guesses

may greatly reduce the labor of iteration in hand computation.

Comparison of the distribution functions resulting from the two definitions of ion partners with each other and with other existing theories will be deferred until Sec. V.

IV. THERMODYNAMIC FUNCTIONS

The continual rearrangement of the ion pairs, free ions, and solitary ions resulting from the thermal motion of the ions in a solution has been interpreted[3,4] in terms of a dynamic chemical equilibrium. By established methods an expression for the equilibrium constant for such a process can be derived from the law of mass action and a knowledge of the ion-partner distribution function. In this section there are derived expressions for the association constant for the formation of an ion pair from two unpaired ions, as well as expressions for the total degree of association of an ion in the solution. A relation between the activity coefficients of the unpaired ions and that of the ion pair is also deduced. An extension of the earlier method is necessitated by the existence in general of more than one type of ion pair, i.e., the occurrence of several simultaneous associative equilibria.

Association Constants

When the ions of an st ion partner approach within the critical distance d_{st} thereby forming an (st) ion pair,[18] the following chemical reaction may be written,

$$s^{z_s}+t^{z_t}=(st)^{z_s+z_t}. \tag{51}$$

From the law of mass action, the association constant K_{st}^{-1} is

$$K_{st}^{-1}=\frac{[(st)]f_{st}}{[s]f_s[t]f_t}, \tag{52}$$

where the charges on the ions have been omitted for simplicity and where $[i]$ and f_i denote the molar concentration and activity coefficient, respectively, of species i in the solution. The molar concentrations may be found as follows.

The probability that any given s ion has for a partner a t ion at any distance less than d_{st} is the degree of association α_{st} of s ions with t ions,

$$\alpha_{st}=\int_{a_{st}}^{d_{st}}G_{st}(x)\,dx. \tag{53}$$

The number of (st) ion pairs is then $N_s\alpha_{st}/(1+\delta_{t^z})$; the numerator of this expression is the number of s ions in (st) ion pairs and the Kronecker delta is necessary since the number of (ss) ion pairs (the case $t=s$) is only one-half the number of s ions in (ss) ion pairs. Finally, the molar concentration of (st) ion pairs is, using Eq. (53),

$$[(st)]=\frac{1000N_s}{N_0V(1+\delta_{t^z})}\int_{a_{st}}^{d_{st}}G_{st}(x)\,dx, \tag{54}$$

where N_0 is Avogadro's number and V is the total solution volume in milliliters. Introducing the total degree of association of s ions α_s,

$$\alpha_s=\sum_{i=1}^{n}\alpha_{si}=\sum_{i=1}^{n}\int_{a_{si}}^{d_{si}}G_{si}(x)\,dx, \tag{55}$$

one obtains the molar concentration of unpaired s ions

$$[s]=1000N_s(1-\alpha_s)/N_0V. \tag{56}$$

Substitution of Eq. (54) and Eq. (56) into Eq. (52) results in the following form,

$$K_{st}^{-1}=\frac{N_0V}{1000(1-\alpha_s)(1-\alpha_t)(1+\delta_{t^z})}\frac{f_{st}}{f_sf_t}\int_{a_{st}}^{d_{st}}\frac{G_{st}(x)}{N_t}dx. \tag{57}$$

In the limit of infinite dilution, the probability $P_i(r_a)$ approaches unity so that any ion i is *not* paired within any arbitrary finite distance r_a. Since all L_i vanish [Eq. (5)], it is evident from Eq. (4) that all $G_{ij}(r)$ vanish and hence by Eq. (55) all α_i also vanish. In this limit Eq. (4), (5), (14), and (15) show that the integral in Eq. (57) approaches $4\pi h_{st}\phi_{st}^*(d_{st})$. Since the activity coefficients all approach unity, the right-hand member of Eq. (57) takes the following form,

$$K_{st}^{-1}=4\pi N_0h_{st}\phi_{st}^*(d_{st})/1000(1+\delta_{t^z}). \tag{58}$$

Equation (58) is completely general, applicable to ion-pair equilibria in any system of mixed electrolytes regardless of the specific definition of the ion pair and the choice of the cutoff distance d_{st}. If, for the association of a monovalent cation s with a monovalent anion t, one chooses d_{st} to be $\frac{1}{2}B$ (the infinite dilution limiting value of r at which $G_{st}(r)$ has a minimum—*vide infra*), substitutes Eqs. (14) and (16), and makes the change of variable $x=ab/Y$ and $B=ab$ (where $a=a_{st}$) then one obtains Eqs. (1)–(3), the expression derived by the Bjerrum and Fuoss treatments. This result is somewhat surprising since the basic Eq. (4) of this work and all subsequent solutions for $G_{st}(r)$ differ from the earlier treatments. The explanation of this fact, which simultaneously explains the identity of the Fuoss K^{-1} expression with the Bjerrum K^{-1} expression, is that many different expressions for $G_{st}(r)$ in the right-hand member of Eq. (57) reduce at infinite dilution to Eq. (58). Specifically, all that is required is that $P_i(r_a)$ reduce to unity at infinite dilution, and so an incorrect expression for $P_s(r)$ and/or $P_t(r)$ or even their omission from Eq. (4) may still lead to Eq. (58). However, the derived ion-partner distribution functions and some other derivable thermodynamic functions are affected by the detailed structure of Eq. (4). Before treating these "sensitive" thermodynamic

[18] The symbol (st) refers to an ion pair whereas st refers to ion partners.

TABLE II. Association constants for the formation of the tetraisoamylammonium nitrate ion pair in dioxane-water mixtures at 25°C assuming $a=6.4$ A.

D	K_{st}^{-1}(exptl.)[a]	$K_{st}^{-1}(d=q)$ $q(A)$	$K_{st}^{-1}(q)$	$K_{st}^{-1}(d=1.2a)$ $d=7.68$ A	$K_{st}^{-1}(d=2a)$ $d=12.8$ A	$K_{ss}^{-1}(q)$	$K_{ss}^{-1}(2a)$
2.38	5×10^{15}	117	5.77×10^{14}	5.74×10^{14}	5.77×10^{14}	155	3.67×10^{-10}
2.56	1×10^{14}	109	4.72×10^{13}	4.68×10^{13}	4.72×10^{13}	124	1.42×10^{-9}
2.90	1×10^{12}	97	0.99×10^{12}	0.97×10^{12}	0.99×10^{12}	85.4	4.68×10^{-8}
3.48	4.0×10^{9}	80	7.62×10^{9}	7.36×10^{9}	7.62×10^{9}	49.4	...
4.42	3×10^{7}	63	5.14×10^{7}	3.8×10^{7}	5.13×10^{7}	24.1	2.91×10^{-6}
5.84	6.06×10^{5}	48	6.15×10^{5}	4.8×10^{5}	6.04×10^{5}	10.5	3.96×10^{-4}
8.5	1×10^{4}	33	1.16×10^{4}	0.62×10^{4}	0.98×10^{4}	...	...
11.9	1.1×10^{3}	23.5	1.26×10^{3}	0.40×10^{3}	0.67×10^{3}	1.24	1.09×10^{-2}
12.1	1.05×10^{3}	23.2	1.15×10^{3}	0.36×10^{3}	0.56×10^{3}	...	2.98×10^{-1}
35.85	5.2	7.82	4.90	4.44	25.6	...	5.02×10^{-1}
38.0	4.0	7.37	2.98	3.91	21.3	0.021	5.46×10^{-1}
53.28	2.14	$<a$	0	2.12	14.7	...	8.21×10^{-1}
61.68	1.67			1.74	12.0	...	9.43×10^{-1}
70.33	1.38			1.49	10.5	...	1.05
78.48	1.20			1.33	9.1	...	1.14

[a] Experimental values determined by Fuoss and Kraus (see references 4 and 19).

functions, some discussion of the cutoff distance d_{st} to be used in Eq. (58) is appropriate.

Historically d_{st} has been taken as the separation value $r_{\min.}=q=-z_sz_tB/2$ at which the Bjerrum and Fuoss $G_{st}(r)$ show a minimum at infinite dilution. Parenthetically, an examination of Eqs. (18), (26), and (44) shows that the same $r_{\min.}$* is approached by the $G_{st}(r)$ functions of this work in the cases when s and t are of opposite sign. With $d_{st}=q$, the association constant vanishes when, with increasing dielectric constant, α decreases to the hard-sphere cutoff a_{st}. Arguments have been proposed[7] supporting the contention that, in contrast, K_{st}^{-1} should be a continuous function of DT, and expressions for K_{st}^{-1} embodying this feature together with the narrow definition of ion pairs as being "in contact" have appeared.[7,9] While avoiding in this paper a discussion of the precise significance of experimental determinations of K_{st}^{-1}, it should be pointed out that the theory presented in this paper is capable of accomodating the recent "contact" ion-pair idea and of yielding association constants which are continuous functions of DT in qualitative agreement with sample experimental data. This is accomplished by using a constant cutoff distance d for d_{st} in Eq. (58). In Table II is presented (column 2) some experimental[4,19] values of K^{-1} for the formation of tetraisoamylammonium nitrate ion pairs in dioxane-water mixtures together with calculated values of K_{st}^{-1} (column 4) using the conventional d value of q (column 3) which varies with D (column 1). For this choice of d, $K_{st}^{-1}=0$ for $D>43.6$. Values of K_{st}^{-1} in columns 5 and 6 were calculated from Eq. (58) using constant d values of $1.2a$ (7.68 A) and $2a$ (12.8 A), respectively. The sum of the effective radii is taken to be 6.4 A, a value used previously.[20] At low D, the exact choice of d is not critical as nearly all of the ions are paired at very small separation distances. At larger values of D, the influence of the choice of d on the value of K_{st}^{-1} becomes quite marked, and column 5 indicates the good agreement obtained using $d=1.2a$. Ion pairs whose separation range is only one-fifth of their diameter might well be called ion pairs "in contact."

One reason that a claim to quantitative agreement seems premature is that it is precisely in these solutions of high dielectric constant that ion pairs composed of ions of the same sign, *if their existence be recognized*, become numerically significant, and, being current carriers, should be involved in the analysis of conductance data.

The general dependence of K_{ss}^{-1} on D is shown in columns 7 and 8 of Table II for the same conditions ($T=25°$ C; $a=6.4$ A, $z_s=1$) but, for computational simplicity, for the case of cations and anions of equal size. Since there is no minimum in the "like partners" distribution curve $G_{ss}(r)$, and hence no intuitively

[19] R. M. Fuoss and C. A. Kraus, J. Am. Chem. Soc. **79**, 3304 (1957).

[20] In reference 19, an a value of 5.83 A is reported. The exact value of a is of little consequence for the present discussion.

TABLE III. Degrees of association into ion pairs. Conditions: $c_s=c_q=1.00\times10^{-4}M$; $a_{ss}=a_{st}=4.6$ A; $a_{qt}=7.0$ A; $d_{st}=d_{qt}=d_{ss}=14.0$ A; $D=20$; $T=25°$C.

	Unlike partners only			Mixture of	Like and unlike partners
	1–1 elect.	1–2 elect.	2–2 elect.	1–1 elect.	1–1 elect.
α_s	0.0175	0.300	≈1	0.0347	0.0176
α_t	0.0175	0.600	≈1	0.0267	0.0176
α_q	...	...	...	0.0187	...

attractive d_{ss}, values of d_{ss} were chosen to be (in column 7) q, the value of r at the minimum of $G_{st}(r)$ and (in column 8) the constant value of $2a$. The entries in column 7 appear peculiar and unrealistic. As D decreases, the Coulombic repulsion increases, and it is expected on an intuitive physical basis that fewer (ss) ion pairs should exist. Actually, however, the values of K_{ss}^{-1} in column 7 *increase* with decreasing D since the increasingly large q values (column 3) at low D result in counting as (ss) ion pairs those ss ion partners with progressively greater separations. Values of K_{ss}^{-1} in column 8 do decrease with decreasing D, making attractive the choice of a constant d in defining ion pairs composed of ions of like charge.

Degrees of Association

A general expression for the degree of association of s ions is given by Eqs. (53) and (55) with i running over all types of ions with which s is allowed to pair. It is obvious from Eq. (55) that new values of α_s result from the new forms of $G_{st}(r)$ presented in this work. By integrating (numerically if necessary) the appropriate ion-partner distribution functions in a general mixture of electrolytes, the degrees of association of all ions may be calculated.

For example, the degrees of association of s ions, q ions, and t ions were calculated by numerical integration to $d_{st}=d_{qt}=14.0$ A of the distribution functions displayed in Fig. 3 [Eqs. (36) and (37)] which were obtained in part using the iterative trapezoidal method. These degrees of association, tabulated in column 5 of Table III, are discussed later in this subsection. For some systems studied in Sec. III, the degrees of association may be obtained analytically as shown below.

"Unlike Partners Only," Single Symmetrical Electrolyte

Since only one type of ion pair may form, the summations in Eqs. (8) and (55) reduce to a single term, and a comparison of Eqs. (7), (8), (53), and (55) shows that

$$\alpha_s=\alpha_t=1-P_s(d_{st})=1-P_t(d_{st}). \tag{59}$$

Substitution of Eq. (11) into Eq. (59) yields the result,

$$\alpha_s=\alpha_t=\frac{L\phi_{st}(d_{st})}{1+L\phi_{st}(d_{st})}, \tag{60}$$

where $\phi_{st}(d_{st})$ is given by Eq. (12).

"Unlike Partners Only," Single Unsymmetrical Electrolyte

Again the summations in Eqs. (8) and (55) reduce to a single term, and comparison of Eqs. (7), (8), (53), and (55) shows that

$$\alpha_s=1-P_s(d_{st})=N_t\alpha_t/N_s=N_t[1-P_t(d_{st})]/N_s. \tag{61}$$

Substitution of Eq. (22) into Eq. (61) yields, after slight rearrangement,

$$\alpha_s=\frac{N_t\alpha_t}{N_s}=\frac{L_t[1-\theta_{st}(d_{st})]}{L_t-L_s\theta_{st}(d_{st})}, \tag{62}$$

where $\theta_{st}(r)$ is defined by Eq. (23).

"Like and Unlike Ion Partners," Single Symmetrical Binary Electrolyte with Ions of Equal Size

In this case the summations in Eqs. (8) and (55) consist of two terms since s ions may associate with either s or t ions. If $d_{ss}\neq d_{st}$, numerical integration is necessary (although $\alpha_s=\alpha_t$) but if $d_{ss}=d_{st}=d$ then an analytical expression for α_s is obtainable, for comparison of Eqs. (7), (8), (53), and (55) shows that

$$\alpha_s=\alpha_t=1-P_s(d). \tag{63}$$

Substitution of Eq. (40) into Eq. (63) results in the following,

$$\alpha_s=\alpha_t=\frac{\phi_{st}(d)+\phi_{ss}(d)}{L^{-1}+\phi_{st}(d)+\phi_{ss}(d)}. \tag{64}$$

A numerical calculation of α_s requires that the pair correlation functions, which vary with concentration, be known. By making the approximation that $g_{st}(r)$ at high dilution ($\approx10^{-4}$ M) is nearly $g_{st}^*(r)$ at infinite dilution as given by Eq. (14), the entries in Table III were calculated from Eqs. (60), (62), and (64) using $c_s=c_q=1.00\times10^{-4}M$; $a_{st}=a_{ss}=4.6$ A; $a_{qt}=7.0$ A; $d_{st}=d_{ss}=d_{qt}=14.0$ A; $D=20$; $T=25°$ C. The value of 14.0 A is very near to the value of $r_{\min.}$* for the 1–1 electrolyte distribution function, $G_{st}(r)$. A number of trends and general conclusions are apparent from Table III, a few supplementary calculations, and the observation that the ionic charges and D enter into α only as z_iz_jB [Eqs. (14) and (15)] when $g_{ij}^*(r)$ is used. The degree of association of a 2–2 electrolyte in a solution with $D=80$ is thus identical to that of a 1–1 electrolyte

in a solution with $D=20$, all other conditions (including d_{ij}) being the same.

Whenever $G_{st}(r)$ has a low and broad minimum, then α_{st} is relatively insensitive to the choice of d (within limits) provided d is large enough. For example, for the 1–2 electrolyte case [curve (1) of Fig. 2] extending d from 14.0 to 30.9 A (which is $r_{\min.}^*$) increases α_s from 0.300 (column 3, Table III) to only 0.312.

Table III also shows the effect of ionic charge on ionic association. As the charges on the (oppositely charged) ions comprising the ion pair increase, the degree of association increases markedly; a 2–2 electrolyte (column 4) is almost completely associated in a solution of dielectric constant 20, a 1–1 electrolyte (column 2) in the same solvent is less than 2% associated, and a 1–2 electrolyte (column 3) is intermediate. The ratio of the number of ion pairs, $N_s\alpha_s$, composed of ions of opposite charge in a 1–2 electrolyte to $N_s\alpha_s$ in a 1–1 electrolyte in the same solvent is 17.1 for these conditions.

For a 1–1 electrolyte under the conditions in Table III, the explicit recognition of ion pairs composed of ions with charges of the same sign increases the degree of association of either ion from 0.0175 (column 2) to only 0.0176 (column 6). More accurate calculations show that the ratio of the number of s ions in neutral ion pairs to the number of s ions in charged ion pairs in the above solution ($D=20$) is 318. In a solvent with $D=80$, however, this ratio is reduced to 4.5, indicating that in these solutions with high dielectric constant, charged ion pairs should be considered along with uncharged ion pairs. The relative importance of charged ion pairs, however, decreases markedly as the charge on the ion pair increases. The ratio of the number of s ions in neutral ion pairs to the number of s ions in charged ion pairs in 2–2 electrolyte with $a=4.6$ A in the same solvents ($D=20$, $D=80$) is about 10^{12} and 318, respectively, indicating that for 2–2 electrolytes even in aqueous solution charged ion pairs constitute less than 1% of all ion pairs.

As is expected, the degree of association decreases with increasing D, the ratio of the number of ion pairs (unlike partners only) from a 1–1 electrolyte with $a=4.6$ A in a solvent with $D=20$ to that in a solvent with $D=80$ being 18.

The effect of relative ionic size is interesting. Table I shows that $G_{ss}(r)$ and $G_{tt}(r)$, and thus α_s and α_t, are very nearly the same in a 1–1 electrolyte with $a_s=1.6$ A and $a_t=3.0$ A in a solvent with $D=20$. Although the effect of the relative ionic size is small in that particular system containing only one electrolyte, its effect on the degrees of association is appreciable in a mixture of two 1–1 electrolytes ("unlike partners only") as indicated in Fig. 3 and in Table III (column 5). Since the smaller s ion can form Coulombically favored (st) ion pairs at separations impossible for the larger q ions, the ratio of the number of (st) ion pairs to (qt) ion pairs in a solution ($D=20$) containing an equimolar mixture of two 1–1 electrolytes with ions of different sizes ($a_{st}=4.6$ A; $a_{qt}=7.0$ A) is 1.86. From this analysis of a mixture of electrolytes, a qualitative interpretation of some experimental conductance data is now possible. Campbell, Kartzmark, and Sherwood[21] found that the equivalent conductance of concentrated (0.05–6.0 M) equimolar mixtures of certain nitrates in aqueous solutions is lower than the mean of the equivalent conductances of the single-salt solutions at the same ionic strength. In such a mixture many (st) ion pairs might be said to form leaving the larger, less mobile q ions to carry the current. The lower mobility of the excess of unpaired q ions would result in an equivalent conductance lower than a mean value (which would imply an equal number of current carrying unpaired s and q ions). Since the detailed methods of interpreting experimental data may not be in accord with the model or the ion pair analysis, an attempted quantitative comparison would be premature, and any success would be fortuitous.

Activity Coefficients

Combining the expression for the thermodynamic association constant evaluated at infinite dilution, Eq. (58), with the general form of Eq. (57) results in the following expression for the activity coefficient ratio,

$$\frac{f_s f_t}{f_{st}}=\frac{1}{L_t(1-\alpha_s)(1-\alpha_t)\phi_{st}^*(d_{st})}\int_{a_{st}}^{d_{st}} G_{st}(x)\,dx. \quad (65)$$

An integration (numerical if necessary) of the ion-partner distribution functions over the range of ion-pair formation, together with the numerical values of α_i discussed in the preceding subsection, makes possible the evaluation of the activity coefficient ratios even in the general case of a mixture of electrolytes. When $G_{ij}(r)$ are expressible as analytic functions of the $g_{ij}(r)$, then the activity coefficient ratios may also be written explicitly as exemplified below for some systems treated in Sec. III.

"Unlike Partners Only," Single Symmetrical Electrolyte

Since in this case the integral in Eq. (65) is α_s, and $\alpha_s=\alpha_t$, substitution of Eq. (60) into Eq. (65) yields the following,

$$\frac{f_s f_s}{f_{st}}=\frac{\phi_{st}(d_{st})}{\phi_{st}^*(d_{st})}[1+L\phi_{st}(d_{st})], \quad (66)$$

where the symbols are defined by Eqs. (5), (12), and (16).

It should be noted that for a symmetrical electrolyte, the right-hand member of Eq. (66) reduces to the Debye-Hückel limiting law[22] expression for the square of the mean activity coefficient $f_\pm^2$ under the following circumstances. If the pair correlation function resulting

[21] A. N. Campbell, E. M. Kartzmark, and A. G. Sherwood, Can. J. Chem. **36**, 1325 (1958).

[22] P. Debye and E. Hückel, Physik. Z. **24**, 185 (1923).

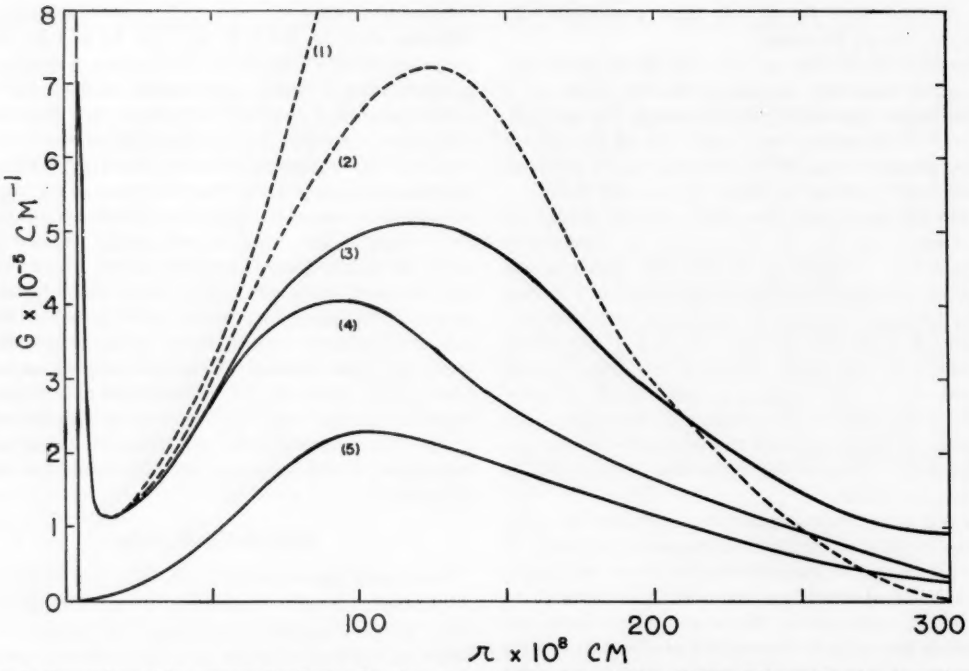

FIG. 5. Comparison of ion-partner distribution functions in a 1–1 electrolyte solution. (1) The Bjerrum function (see reference 3) (2) the Fuoss function (see reference 5); (3) the "unlike partners only" function, Eq. (17); (4) the "like and unlike partners" function Eq. (41); and (5) the "like and unlike partners" function, Eq. (42). Conditions: $a_{st}=a_{ss}=4.6$ A; $D=20$; $T=25°C$; $c_s=1.00\times10^{-4}M$.

from the Debye-Hückel analysis is valid,

$$g_{st}(r)=\exp[z^2Br^{-1}\exp(-\kappa r)], \qquad r\geq a_{st}, \quad (67)$$

where $\kappa^2=8\pi z^2\epsilon^2N_0c/1000DkT$ and $z_s=-z_t=z$, and if the solution is so dilute that terms of order higher than $c^{\frac{1}{2}}$ may be neglected, then the inner exponential in Eq. (67) may be linearized and the following form obtained by comparison with Eq. (12),

$$g_{st}(r)\approx\exp[z^2B(r^{-1}-\kappa)]=g_{st}^*(r)\exp(-z^2B\kappa). \quad (68)$$

Substitution of Eq. (68) into Eq. (12) and comparison of the result with Eq. (16) shows that $\phi_{st}(d_{st})/\phi_{st}^*(d_{st})$ then approaches $\exp(-z^2B\kappa)$. Since $L\phi_{st}(d_{st})$ is of order higher than $c^{\frac{1}{2}}$ and so negligible compared to unity, Eq. (66) takes the following simple form,

$$f_sf_s/f_{st}=\exp(-z^2B\kappa), \quad (69)$$

and the right-hand member is identically the square of the Debye-Hückel expression for the mean activity coefficient. Under the above circumstances, the present theory validates the combination of two common assumptions for dilute solutions: the use of unity for the activity coefficient of a neutral ion pair and the use of the Debye-Hückel limiting law expression for the (product of the) activity coefficients of the unpaired ions. The present theory cannot validate the assumptions individually, however.

"Unlike Partners Only," Single Unsymmetrical Electrolyte

In this case the integral in Eq. (65) is α_s, and substitution of Eq. (62) into Eq. (65) yields

$$\frac{f_sf_t}{f_{st}}=\frac{[1-\theta_{st}(d_{st})][L_t-L_s\theta_{st}(d_{st})]}{[L_t-L_s]^2\theta_{st}(d_{st})\phi_{st}^*(d_{st})}, \quad (70)$$

where $\theta_{st}(d_{st})$ is given by Eq. (23).

V. DISCUSSION

Comparison of Distribution Functions

It has been emphasized in Sec. III that the ion-partner distribution functions there derived are valid at any concentration; one need only use the corresponding pair correlation functions, $g_{ij}(r)$. The lack of a simple and accurate form for $g_{ij}(r)$ at higher concentrations and the explicit use of only the infinite dilution expression, $g_{ij}^*(r)$, in preexisting theories restricts the comparison now presented to solutions of high dilution for which $g_{ij}^*(r)$ may be used. On Fig. 5 are shown ion-partner radial distribution functions from the present work [curves (3)–(5), Eq. (17) and the high dilution forms of Eqs. (41) and (42), respectively] together with the Bjerrum[3] function [curve (1)] and the Fuoss[5] function [curve (2)], for a $1.00\times10^{-4}M$ solution of a 1–1 electrolyte with ions of equal radius (2.3 A) in a solution with $D=20$ at 25°C.

At small separation distances ($a<r<q$) the distribution functions for ion partners composed of ions of unlike charge [curves (1)–(4)] appear very similar, becoming coincident at infinite dilution and thus leading to the same expression for the association constant as shown in Sec. IV. At finite concentrations small differences among the functions (not visible in Fig. 5) would result in somewhat different values of the "sensitive" thermodynamic functions such as the degrees of association and the activity coefficient ratios.

At larger distances the functions vary markedly for different reasons. The Bjerrum function [curve (1)] increases monotonically (and so cannot be normalized) because of the omission of both $P_i(r)$ factors in the definition similar to Eq. (4). While the Fuoss function [curve (2)] is normalized in the same way as the distribution functions of the present work, the omission of the $P_t(r)$ factor (i.e., neglecting the probability that the orbital ion may already have a partner within r) results in a steeper rise in the Fuoss function followed by a more rapid fall. If a constant d (independent of D) is used for d_{st}, then the noticeable difference between curves (2) and (3) (the "unlike partners only" distribution function of this work) should be reflected in noticeable differences in the derived values of the "sensitive" thermodynamic functions for solutions of high dielectric constant. Curve (4), $G_{st}(r)$ using the "like and unlike partners" definition, is everywhere lower than curve (3) because both the central s and orbital t ions may have partners of like charge also. Since $G_{ss}(r)$ and $G_{tt}(r)$ [curve (5)] do not becomes large until moderate separations are reached, it is only at moderate separations that curve (4) becomes noticeably lower than curve (3). No previously published detailed analysis of ion pairs composed of ions of like charge is known to the present writers.

Usefulness of this Ion-Pair Approach

It appears that the characterization of a solution by a set of time average ion partner distribution functions, $G_{ij}(r)$ (possibly augmented by triplet, quadruplet, $\cdots$ distribution functions) can be validly carried out for any stage of the elaboration of the description and at any concentration providing the ordinary ion correlation functions are known. Such a characterization has a number of limitations. As remarked by Griffiths and Symons,[23] this approach appears to ignore certain processes which may be of great interest, e.g., short-range specific ion-ion interactions and the results of relaxation spectrometry in general. This is necessarily so since the ordinary correlation functions which form the starting point obscure these processes, but they are relevant insofar as their existence modifies the form of the ordinary correlation functions.

Having obtained a valid polyionic distribution function description to any given stage of elaboration (say, through the "like and unlike ion partners" description), the usefulness of the description depends on the simplicity and accuracy with which one may make a prediction of properties of the solution considered as one of the "new" species (say, ion pairs of various types and free ions). Additional problems then appear. Since the process of prediction involves an average of the property, weighted by the number of ion partners, over the range of ion-pair formation, the most convenient d_{st} may not be, say, the intuitively attractive minimum in $G_{st}(r)$, and may vary with the property in question. This problem is outside the scope of this paper. The prediction process also involves the interactions among the "new" species; the smaller the interactions, the easier is the prediction and so the more useful is that description of the solution to the given stage of elaboration. Unfortunately, a systematic examination of this question requires that a more elaborate description be obtained and examined. The desirability of considering charged ion pairs along with neutral ion pairs for 1–1 electrolytes in solutions of large D (see Sec. IV) is one result of this approach. If one lacks the more elaborate description then one must make some estimate of the probability that, say, a third ion is sufficiently near an ion pair to materially affect the "properties" of an ion pair.

If one achieves a valid description of a solution of no more elaborateness than that required to ensure only weak or tractable interactions among the "new" species of particles with reference to some property, then this description is most useful; in particular, a (time average) structure may be given for the "new" particles. In contrast, the "sociated pairs" recently introduced by Guggenheim[24] have an obscure structural significance.

Variations on the Model and Definitions

The Debye-Hückel model consisting of rigid, spherical ions demands that the $g_{ij}(r)$ functions be discontinuous at the sum of the effective ionic radii a_{ij}. For this reason the lower limits of the integrals involved in the present analysis have been given as a_{ij}. If the short-range repulsive forces between ions are idealized, not to hard-sphere potentials, but rather to a softer potential resulting in $g_{ij}(r)$ functions decreasing to zero continuously with decreasing r (for small r), the resulting model can easily be analyzed by the methods here developed. It is necessary only to use the improved $g_{ij}(r)$ functions and to extend the lower limits of all integrals to zero. In exactly the same way, any experimentally determined $g_{ij}(r)$ functions could be used.

The discussion in this paper has been concerned with ionic solutions. However, by a simple rewording of the definitions in Sec. II to read "particle partners" instead of "ion partners" the treatment and equations in this paper may be validly applied to any system (whether

[23] T. R. Griffiths and M. C. R. Symons, Mol. Phys. **3**, 90 (1960).

[24] E. A. Guggenheim, Trans. Faraday Soc. **56**, 1159 (1960).

it be an electrolytic solution, an ideal gas, a molten salt, etc.) provided only that the correlation functions for all types of pairs of particles are known. The usefulness of such an alternate description of the system in terms of "particle pairs," depending on the nature of the system and on its thermodynamic parameters, invites investigation.

APPENDIX I

Transformations of Eq. (8)

Differentiation of Eq. (8) yields the following,

$$P_s'(r) = -\sum_{i=1}^{n} G_{si}(r). \tag{A1}$$

Division of Eq. (A1) by any function of $P_s(r)$ and subsequent integration leads to a set of coupled integral equations differing from the original set Eq. (8). For example, substitution of the basic Eq. (4) into Eq. (A1), division of the resulting equation by $P_s(r)$, and integration of the resulting equation yields the following set

$$\ln P_s(r) = -\sum_{i=1}^{n} L_i h_{si} \int_{a_{si}}^{r} x^2 g_{si}(x)\, P_i(x)\, dx. \tag{A2}$$

APPENDIX II

Numerical Evaluation of $\phi_{ij}^*(r)$

The integral

$$\phi_{ij}^*(r) = \int_{a_{ij}}^{r} x^2 \exp(-z_i z_j B/x)\, dx \tag{16}$$

may be numerically evaluated by

$$\phi_{ij}^*(r) = (-z_i z_j B)^3 [Y(b) - Y(-z_i z_j B/r)], \tag{B1}$$

where

$$b = -z_i z_j \epsilon^2 / DkTa_{ij}. \tag{B2}$$

When z_i and z_j are of opposite sign the Y functions in Eq. (B1) may be evaluated by a method described by Fuoss,[5]

$$6Y(x) = Ei(x) - x^{-1}e^x[1 + x^{-1} + 2x^{-2}], \tag{B3}$$

where $Ei(x)$ is the exponential integral,

$$Ei(x) = \int_{-\infty}^{x} e^t t^{-1} dt. \tag{B4}$$

Tables of $Ei(x)$ for $0 < x < 10$ are available.[25] For small positive values of $x(x<10)$, the following series expansion of $Y(x)$ is useful,

$$Y(x) = -\tfrac{1}{3}x^{-3}(1 + \tfrac{3}{2}x + \tfrac{3}{2}x^2) - 0.209352 + \tfrac{1}{6}\ln x + \sum_{n=1}^{\infty} \frac{x^n}{n(n+3)!}. \tag{B5}$$

For large positive values of $x(x>15)$, an asymptotic expansion of $Y(x)$ may be used,

$$Y(x) = e^x x^{-4}(1 + 4x^{-1} + 4\cdot 5x^{-2} + 4\cdot 5\cdot 6x^{-3} + \cdots). \tag{B6}$$

When z_i and z_j in Eq. (16) are of the same sign, the Y functions in Eq. (B1) may be evaluated by

$$6Y(x) = 6Y(-y) = Ei(-y) + y^{-1}e^{-y}(1 - y^{-1} + 2y^{-2}), \tag{B7}$$

where

$$-Ei(-y) = \int_{y}^{\infty} \frac{e^{-t}}{t} dt. \tag{B8}$$

Tables of $-Ei(-y)$ for $0 < y < 10$ are available.[25] For small values of $y(y<10)$, the following series expansion of $Y(-y)$ is useful.

$$Y(-y) = \tfrac{1}{3}y^{-3}(1 - \tfrac{3}{2}y + \tfrac{3}{2}y^2) - 0.401758 - \tfrac{1}{6}\ln y + \sum_{n=1}^{\infty} \frac{(-1)^n y^n}{n(n+3)!}. \tag{B9}$$

For large values of y $(y>15)$, an asymptotic expansion may be used,

$$Y(-y) = y^{-4}e^{-y}(1 - 4y^{-1} + 4\cdot 5y^{-2} - 4\cdot 5\cdot 6y^{-3} + \cdots). \tag{B10}$$

APPENDIX III

Determination of $r_{min.}$, $r_{max.}$, and $r_{infl.}$ of $G_{st}(r)$ in Eq. (17)

Setting the first derivative of $G_{st}(r)$ equal to zero yields

$$0 = G_{st}(r)\left[\frac{2}{r} - \frac{B}{r^2} - \frac{2Lr^2 \exp(B/r)}{1 + L\phi_{st}(r)}\right]. \tag{C1}$$

The function $G_{st}(r)$ and hence its derivative vanish as r becomes large. The value of r at the other minimum may be determined by equating the final factor in Eq. (C1) to zero and using the transformation

$$r_{min.} = \tfrac{1}{2}B(1-k)^{-1}, \tag{C2}$$

thus obtaining

$$(1-k)^3 k e^{2k}\{1 + L\phi_{st}[\tfrac{1}{2}B(1-k)^{-1}]\} = \tfrac{1}{8}LB^3e^2. \tag{C3}$$

If $k \ll 1$, e.g., $r_{min.}$ is only slightly larger than $\frac{1}{2}B$, Eq. (C3) reduces to

$$k = \tfrac{1}{8}LB^3e^2, \tag{C4}$$

since $L\phi_{st} \approx L\phi_{st}^* \approx k$ from Eq. (B1). Therefore, at a dilution sufficient to ensure $\frac{1}{8}LB^3e^2 \ll 1$, substitution of Eq. (C4) into Eq. (C2) yields the result,

$$r_{min.} \approx \tfrac{1}{2}B(1 + \tfrac{1}{8}LB^3e^2). \tag{18}$$

To find the value of r at which $G_{st}(r)$ given by Eq. (17) has a maximum, the final factor in Eq. (C1) may be equated to zero and rearranged to read

$$Lr^3 = [(1-B)/2r][1 + L\phi_{st}(r)] \exp(-B/r). \tag{C5}$$

[25] Mathematical Tables Project, *Tables of Sine, Cosine,* and *Exponential Integrals* (Federal Works Agency, Works Projects Administration for the City of New York, 1940).

If $r_{max.}$ is large, the first and third factors of the right-hand member of Eq. (C5) are nearly unity. In the second factor, the value of $\phi_{st}(r_{max.}) \approx \phi_{st}^*(r_{max.})$ may be obtained from Eqs. (B1) and (B5). In Eq. (B1), $Y(b)$ is small compared to $Y(-z_s z_t B/r)$ when r is large, and to a first approximation $Y(-z_s z_t B/r)$ in Eq. (B5) is equal to $-\frac{1}{3}(-r/z_s z_t B)^3$. Thus

$$\phi_{st}(r_{max.}) \approx \tfrac{1}{3} r^3_{max.}, \tag{C6}$$

and substitution of Eq. (C6) into the large r approximation of Eq. (C5) gives the first approximation,

$$r_{max.} \approx (3/2L)^{1/3}. \tag{C7}$$

A second approximation may be obtained by retaining terms of first order in the small quantity B/r in the right-hand member of Eq. (C5) and substituting therein the first approximation, Eq. (C7), for r_{max}. Since in this approximation $L \approx \frac{3}{2} r^{-3}$, in $\phi_{st}(r) \approx \phi_{st}^*(r)$ the following terms are retained,

$$\phi_{st}(r) \approx (B^3/3)(B/r)^{-3}[1+(3B/2r)], \tag{C8}$$

and after using Eq. (C.7) the following second approximation for $r_{max.}$ results,

$$r_{max.} \approx (3/2L)^{1/3}[1-\tfrac{1}{3}B(\tfrac{2}{3}L)^{1/3}]. \tag{19}$$

The inflection points of $G_{st}(r)$ in Eq. (17) may be determined by setting the second derivative equal to zero,

$$G_{st}''(r) = 0 = 6\left[\frac{Lr^2 \exp(B/r)}{1+L\phi_{st}(r)}\right]^2 + \frac{2}{r^2} - \frac{12Lr\exp(B/r)}{1+L\phi_{st}(r)} - \frac{2B}{r^3} + \frac{B^2}{r^4} + \frac{6LB\exp(B/r)}{1+L\phi_{st}(r)}. \tag{C9}$$

If $r \gg B$, the last three terms in Eq. (C9) are negligible compared to the first three (which typically are of the same order of magnitude). The exponential functions may be approximated by unity and $\phi_{st}(r)$ by Eq. (C6); the resulting equation may be solved by the quadratic formula,

$$r_{infl.} \approx \{[24 \pm 9(6)^{\frac{1}{2}}]/10L\}^{1/3}. \tag{20}$$

The expressions for $r_{min.}$, $r_{max.}$, and $r_{infl.}$ of the other ion-partner distribution functions discussed in this paper were determined in a similar manner.

APPENDIX IV

Normalization of Ion-Partner Distribution Functions

"Unlike Partners Only," Symmetrical Binary Electrolyte

The ion-partner distribution function in Eq. (13) is normalized to unity. Straightforward integration yields the following,

$$\int_{a_{st}}^{\infty} G_{st}(r)\,dr = 1-[1+L\phi_{st}(\infty)]^{-1} \tag{D1}$$

and $\phi_{st}(\infty)$ is infinite, since in Eq. (12), $g_{st}(r)$ must approach unity as $r \to \infty$.

"Unlike Partners Only," Unsymmetrical Binary Electrolyte

The normalization of $G_{st}(r)$ in Eq. (24) can be understood by recalling this first definition of the ion partner. If $N_s < N_t$, each of the s ions is assigned a partner, and the integration of the distribution function from a to infinity should be unity. However, if $N_s > N_t$, only N_t of the s ions have partners, and the result of integrating the distribution function over all space should be N_t/N_s. The remaining $(N_s - N_t)$ s ions are solitary ions.

This behavior is mathematically verified. Integration of the ion-partner distribution function for this system over all space give

$$\int_a^{\infty} G_{st}(r)\,dr = \left.\frac{(N_s-N_t)N_t/N_s}{N_t - N_s\exp[(L_s-L_t)\phi_{st}(r)]}\right|_a^{\infty}. \tag{D2}$$

If $N_s > N_t$, then at the upper limit of integration the exponential in the denominator becomes infinite and the function vanishes, while at $r=a$, the exponential in the denominator becomes unity; the value of the normalization integral N_t/N_s is in agreement with the physical deduction in the preceding paragraph. If $N_s < N_t$, on the other hand, the exponential in the denominator approaches zero as $r \to \infty$, and the value of the function at the upper limit is $(N_s - N_t)/N_s$. Since, as before, the value at the lower limit is N_t/N_s, the value of the normalization integral is unity.

"Like and Unlike Partners," Symmetrical Binary Electrolyte with Ions of Equal Size

The normalization of the functions in Eqs. (41) and (42), the probability that an s ion is assigned either an s ion or a t tion as a partner at any separation distance, is straightforward,

$$\int_a^{\infty} [G_{st}(r) + G_{ss}(r)]\,dr = -[1+L\phi_{st}(r)+L\phi_{ss}(r)]^{-1}\Big|_a^{\infty} = 1, \tag{D3}$$

since the integrals $\phi_{st}(r)$ and $\phi_{ss}(r)$ are both infinite at the upper limit and zero at the lower limit.

Relative Bond Strengths in Trigonal Bipyramid Molecules

F. A. COTTON

Department of Chemistry, Massachusetts Institute of Technology, Cambridge, Massachusetts

(Received September 16, 1960)

Calculations of the relative strengths of the axial and equatorial bonds in PF_5 and PCl_5 have been made using Pauling's criterion of bond strength and using overlap integrals for Slater orbitals as suggested by Mulliken. All calculations were for sp^3d hybridization through the entire range of distribution of s and d character between the axial and equatorial orbitals. The overlap integrals correctly predict that axial bonds are weaker than equatorial ones whereas Pauling's criterion predicts the opposite for all reasonable hybridization conditions.

INTRODUCTION

THE purpose of this note is to discuss the relative strengths of the axial (sometimes called polar) and equatorial sigma bonds in a trigonal bipyramid AB_5 molecule, as calculated by two simple bond strength criteria, namely, the "bond forming power" criterion of Pauling and the overlap integral (OI) criterion of Mulliken.

Both of the aforementioned criteria for estimating the relative strengths of chemical bonds are based upon the assumption that within reasonable limits, and where other factors which might be of importance remain essentially constant, the strength (i.e., energy) of a two-center chemical bond will be proportional to the extent of overlap between the orbitals used by each of the two atoms to form the bond. Pauling and Sherman[1] proposed that relative overlaps could be approximated in a simple way by assigning each of the two atomic orbitals a bond-forming power proportional to (or equal to) the value of the angular part of the wave function along the bond direction. For hybrid orbitals this would be a weighted average of the angular coefficients of the constituent orbitals. The strengths of bonds are then to be assumed proportional to the products of the bond forming powers of the two orbitals involved in each of the bonds. This criterion led immediately to the recognition of some important facts. For example it shows that s-p hybrid orbitals will form stronger bonds than either pure s or pure p orbitals. However, it is far from adequate since it further predicts that the strengths of bonds formed by an atom using s-p hybrid orbitals of varying composition should be in the order $sp^3 > sp^2 > sp$, whereas experimental data leave small doubt that the reverse is actually the case.[2] The most obvious cause of this failure of Pauling's criterion lies in the fact that for hybrid orbitals, computation of the bond-forming power as a weighted average of the values of the constituent hydrogenic orbitals using weighting factors which depend only upon the hybridization coefficients ignores small but presumably critical differences in the radial values of these wave functions.

If small differences in radial dependence between ns and np orbitals can be critical, it is very likely that when d orbitals are involved in the hybridization such radial differences will be very important indeed, even allowing for a certain amount of contraction of the d orbitals for atoms in molecules.[3]

The OI criterion of bond strength is based on the assumption that bond strengths will be porportional to the values of the overlap integrals, usually, in practice, those computed using Slater orbitals. This criterion gives the correct order of energies as a function of p character in s-p hybrids.[2] While more laborious to apply, it is still reasonably handy due to the availability of tables of practically all necessary integrals.[4-9]

CALCULATIONS AND RESULTS

An orthonormal set of trigonal bipyramid hybrid orbitals can be constructed from an sp^3d set of orthonormal atomic orbitals according to the following relations:

$$\left.\begin{aligned}\text{axial}\begin{cases}\psi_1 = (2^{-\frac{1}{2}}\cos\alpha)s + 2^{-\frac{1}{2}}p_z + (2^{-\frac{1}{2}}\sin\alpha)d_{z^2}\\ \psi_2 = (2^{-\frac{1}{2}}\cos\alpha)s - 2^{-\frac{1}{2}}p_z + (2^{-\frac{1}{2}}\sin\alpha)d_{z^2}\end{cases}\\ \text{equatorial}\begin{cases}\psi_3 = (3^{-\frac{1}{2}}\sin\alpha)s + 2^{\frac{1}{2}}3^{-\frac{1}{2}}p_x - (3^{-\frac{1}{2}}\cos\alpha)d_{z^2}\\ \psi_4 = (3^{-\frac{1}{2}}\sin\alpha)s - 6^{-\frac{1}{2}}p_x + 2^{-\frac{1}{2}}p_y - (3^{-\frac{1}{2}}\cos\alpha)d_{z^2}\\ \psi_5 = (3^{-\frac{1}{2}}\sin\alpha)s - 6^{-\frac{1}{2}}p_x + 2^{-\frac{1}{2}}p_y - (3^{-\frac{1}{2}}\cos\alpha)d_{z^2}\end{cases}\end{aligned}\right\} \quad (1)$$

These equations check with those which may be obtained from Duffey's[10] more general equations by setting

[1] L. Pauling and J. Sherman, J. Am. Chem. Soc. **59**, 1450 (1937).

[2] For a detailed discussion see C. A. Coulson, *Valence* (Oxford University Press, New York, 1952), pp. 198-201.

[3] D. P. Craig and E. A. Magnussen, J. Chem. Soc. **1956**, 4895.

[4] R. S. Mulliken, C. A. Riecke, D. Orloff, and H. Orloff, J. Chem. Phys. **16**, 1248 (1949).

[5] H. H. Jaffé, J. Chem. Phys. **21**, 258 (1953).

[6] H. H. Jaffé and G. O. Doak, J. Chem. Phys. **21**, 196, 1111 (1953).

[7] D. P. Craig, A. Maccoll, R. S. Nyholm, L. E. Orgel, and L. E. Sutton, J. Chem. Soc. **1954**, 354.

[8] J. E. Roberts and H. H. Jaffé, J. Chem. Phys. **27**, 883 (1957).

[9] L. Leifer, F. A. Cotton, and J. R. Leto, J. Chem. Phys. **28**, 364, 1253 (1958).

[10] G. H. Duffey, J. Chem. Phys. **17**, 196 (1949).

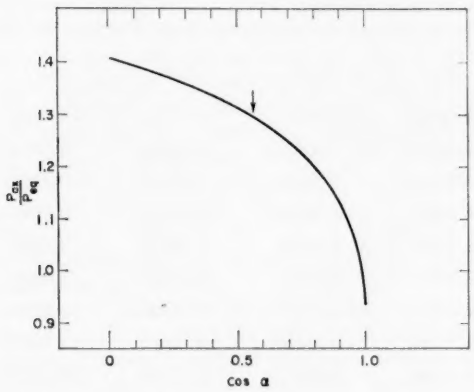

FIG. 1. The ratio of the bond-forming power of axial and equatorial sp^3d hybrid orbitals of phosphorus according to Pauling's criterion as a function of the mixing parameter $\cos\alpha$ in Eqs. (1).

coefficients of d_{xy} and $d_{x^2-y^2}$ equal to zero. Duffey's general expressions cover the entire group theoretically allowed range from sp^3d to spd^3. However, in view of the high energy (8–10 ev) of the $3d$ orbitals relative to the $3s$ and $3p$ orbitals of phosphorus,[11] it seems reasonable that within the limits mentioned, hybrids with minimal d character, i.e., sp^3d hybrids, will be a good approximation.

The results obtained by computing the relative bond-forming powers of axial and equatorial orbitals (P_{ax} and P_{eq}) in sp^3d hybridization as a function of $\cos\alpha$ using the Pauling bond-strength criterion are given in Fig. 1 where the ratio P_{ax}/P_{eq} is plotted versus $\cos\alpha$. At the extreme left, the axial orbitals have no s character and at the extreme right the equatorial orbitals have no s character. It is seen that the axial bonds are calculated to be considerably stronger than the equatorial ones through almost the entire range and only in a very limited range, where the axial orbitals are practically pure sp hybrids, are the equatorial bonds calculated to be slightly stronger than the axial ones.

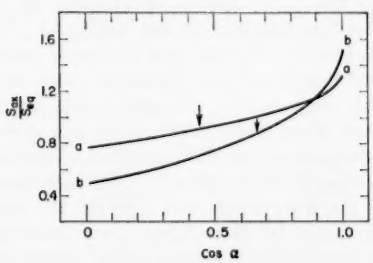

FIG. 2. Ratio of axial to equatorial overlaps in PF_5 assuming (a) use of pure $2s$ orbital by all F's and (b) use of pure $2p$ orbital by all F's.

[11] C. E. Moore, *Atomic Energy Levels* (National Bureau of Standards, U. S. Government Printing Office, Washington, D. C., 1949), Vol I, Circ. No. 467.

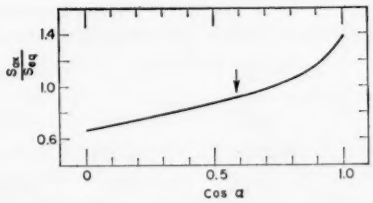

FIG. 3. Ratio of axial to equatorial overlaps in PF_5 when the sp hybridization of each type of F is separately adjusted to give maximum total overlap.

The value of $\cos\alpha$ which maximizes the total bond strength (taken as $3P_{eq}+2P_{ax}$) is indicated by a small arrow on the plot and it is seen that at this point an axial bond is calculated to be ~30% stronger than an equatorial one.

The ratio of the overlap in an axial bond (S_{ax}) to the overlap in an equatorial bond (S_{eq}) was calculated in PF_5 and PCl_5 as a function of the mixing parameter $\cos\alpha$[Eq. (1)] for various assumptions about the nature of the F or Cl bonding orbitals. Throughout these computations μ values of the Slater atomic orbitals were calculated precisely as prescribed by Slater. There does not appear to be any experimental information to justify any particular choice of hybridization of the halogen. Quadrupole coupling constants for Cl in solid PCl_5 are unfortunately of no help since this compound crystallizes as $PCl_4^+PCl_6^-$. However, the same qualitative results are obtained for all reasonable assumptions so that this is not a critical point. In Fig. 2 the ratio S_{ax}/S_{eq} for PF_5 assuming the use of either a pure $2s$ or a pure $2p$ orbital by fluorine is plotted versus $\cos\alpha$. The point of maximum total overlap is indicated. In each case the OI criterion indicates that at this point the axial bonds are 10–20% weaker than the equatorial bonds.

Since the ratio S_{ax}/S_{eq} behaves in the same way whether F is using a pure $2s$ or a pure $2p$ orbital, it will also behave in the same qualitative fashion if the F atoms use an sp hybrid bonding orbital, *providing*

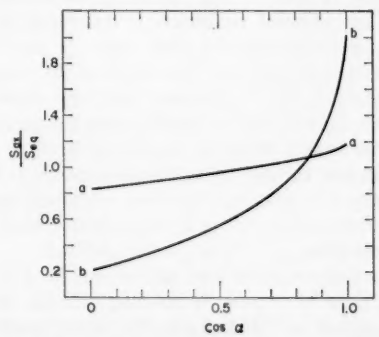

FIG. 4. Ratio of axial to equatorial overlaps in PCl_5 assuming (a) use of pure $3s$ orbital by all Cl's and (b) use of pure $3p$ orbital by all Cl's.

TABLE I. Overlap integrals: $3s$-$3d\sigma$ (Slater orbitals).

p \ t	−0.75	−0.50	−0.25	0	+0.25	+0.50	+0.75
1	−0.00145	−0.01186	−0.01812	+0.00365	+0.03751	+0.03964	+0.01060
2	−0.00441	−0.03280	−0.03880	0.03993	0.14544	0.14454	0.03961
3	−0.00704	−0.04217	−0.02352	0.12013	0.28643	0.27517	0.07992
4	−0.00831	−0.03549	+0.02058	0.20618	0.40037	0.38684	0.12305
5	−0.00840	−0.01964	0.06534	0.25685	0.44900	0.45236	0.16247
6	−0.00754	−0.00492	0.09253	0.25973	0.43211	0.46920	0.19390
7	−0.00645	+0.01023	0.09822	0.22671	0.37109	0.46440	0.21552
8	−0.00472	0.01798	0.08860	0.17736	0.29230	0.38985	0.22812
9	−0.00328	0.02110	0.07168	0.12748	0.21517	0.32743	0.23198
10	...	...	0.04283	0.08250	0.13940	0.22685	0.16982

the degree of sp hybridization is the same for axial and equatorial fluorine atoms. However, if it is vastly different for the different kinds of fluorines (or chlorines) this no longer follows. Since it is found that the fluorine or chlorine ns ($n=2$ or 3) orbitals overlap better with the phosphorus orbitals than do the fluorine or chlorine np($n=2, 3$) orbitals by a factor of 1.5 to 2.0 (a result not to be expected by the Pauling criterion it may be noted) it is clear that one could find a combination of axial fluorine hybridization and equatorial hybridization such that the axial overlap would be best even where total overlap was greatest. However, the question is not whether it is possible to make such poor assumptions that the criterion is found to give an incorrect result, but whether, with *reasonable* choices, one can obtain the correct result

A reasonable assumption would be that for any value of the mixing parameter in the phosphorus hybridization, the degree of sp hybridization of the axial and equatorial halogen atoms be adjusted separately to get the best overlap in each bond. In other words the bonding orbital of an axial halogen is taken as $N(s+cp)$ and that of an equatorial halogen $N'(s+c'p)$ where N and N' are normalization factors and c and c' are adjusted separately to maximize the axial and equatorial overlap for each value of $\cos\alpha$ in the phosphorus hybridization. The result of this computation is shown in Fig. 3. It is seen that even under these conditions, the OI criterion predicts that the axial bonds will be the weaker when the total bond strength is at a maximum and through a considerable range. It is also noteworthy that the best overlaps, obtained using sp hybridization of F, are 2 to $2\frac{1}{2}$ times better than those for fluorine using pure $2s$ or pure $2p$ orbitals.

Similar computations were carried out for PCl_5 with Cl using pure $3s$ or pure $3p$ bonding orbitals, and the results graphed in Fig. 4. Again the correct qualitative result is obtained, namely that the axial-bonds are weaker. The computation for PCl_5 in which the Cl sp hybridization was adjusted for maximum overlap was not carried through since it seemed so likely from the results in Fig. 4 and the work on PF_5 that again the axial overlap will be found smaller than the equatorial as in PF_5.

DISCUSSION

We shall now compare the results of the computations described above with some experimental data bearing on the relative bond strengths and states of hybridization in PF_5 and PCl_5. The Pauling bond-strength criterion leads us to expect that at the hybridization which provides the orbitals capable of forming the strongest bonds, the axial bonds will be considerably stronger than the equatorial ones. Only at the extreme in which there is virtually no s character in the equatorial hybrids does the Pauling criterion predict the opposite ratio of bond strengths. On the contrary, the OI criterion predicts that through large ranges of the hybridization parameter, and particularly at values corresponding to the greatest total overlap, the axial bonds should be weaker than the equatorial bonds.

Experimental data on PCl_5 indicate that the relative strengths of axial and equatorial bonds are in the latter relation. The bond lengths determined by electron diffraction[12] are 2.19 for the axial bonds and 2.04 for the equatorial bonds. Since it is an extremely general rule that bond length and bond strength are inversely related, this suggests that the axial bonds are actually the weaker. More recently, the results of a study of the vibrational spectrum of PCl_5 have been used to calculate the stretching force constants.[13] These were found to be 1.80 for the axial bonds and 2.89 for the equatorial bonds in units of 10^5 d/cm. These results leave no doubt that the axial bonds are appreciably weaker than the equatorial bonds.

For PF_5 there are no bond length or bond force constant data available. However, some data on the

[12] M. Rouault, Ann. phys. **14**, 78 (1940).
[13] J. K. Wilmshurst and H. J. Bernstein, J. Chem. Phys. **27**, 661 (1957).

electron-coupled P–F nuclear spin-spin interactions have recently become available, and provide some evidence that the Pauling bond-strength treatment cannot be salvaged by assuming the extreme distribution of the s and d orbitals wherein $\cos\alpha \approx 1$. In CF_3PF_4 it is found that $J_{P-F}(\text{axial}) = J_{P-F}(\text{equatorial}) = 1103$ cps within experimental error,[14] and in several $(C_6H_5)_nPF_{5-n}$ compounds $J_{P-F}(\text{axial})$ has been found to be 700–800 cps while $J_{P-F}(\text{equatorial})$ has been found to be 1000–1100 cps.[15] If we assume that the Fermi contact term will be predominant in fixing the magnitudes of the J_{P-F}'s,[16] the fact that those for axial and equatorial F's are of comparable magnitude means that the amounts of s character in the axial and equatorial hybrid orbitals of phosphorus cannot differ greatly.

Thus, in conclusion, it appears that in trigonal bipyramid molecules the ratio of axial to equatorial bond strengths cannot be correctly predicted using the Pauling bond-strength criterion, while overlap integrals computed using Slater orbitals do give a qualitatively correct answer.

[14] W. Mahler and E. L. Meutterties, J. Chem. Phys. **33,** 636 (1960).

[15] J. E. Lancaster, American Cyanamid Research Laboratories, Stamford, Connecticut (private communication).

[16] J. A. Pople, W. G. Schneider, and H. J. Bernstein, *High-Resolution Nuclear Magnetic Resonance* (McGraw-Hill Book Company, Inc., New York, 1959), Chap. 8.

ACKNOWLEDGMENT

This work was carried out with financial support from the U. S. Atomic Energy Commission.

APPENDIX

The $3s$–$3d\sigma$ overlap integrals required here do not appear to have been tabulated previously. They were therefore calculated by the standard procedures. The master formula used was[17]

$$S(3s, 3d\sigma) = 2880^{-1}(5)^{\frac{1}{2}}(1-\ell^2)^{7/2}\rho^7\{B_0(3A_4-A_6) + 6B_1(A_3-A_5) - 3B_2(3A_4-A_6) - 6B_3(A_1-A_5) - 3B_4(A_0-3A_2) + 6B_5(A_1-A_3) + B_6(A_0-3A_2)\}.$$

The numerical values of the $3s-3d$ overlaps are presented in Table I.

[17] It was observed that the master formula in the work cited in reference 7 for the $3p_z-3d_{z^2}$ overlap has a number of errors in it. The correct formula is

$$S(3p, 3d) = 192^{-1}15^{\frac{1}{2}}(1-\ell^2)^{7/2}\rho^7[-A_0(3B_3-B_5) + A_1(-3B_2+2B_4+B_6) + A_2(3B_1+B_3+2B_5) + A_3(3B_0-B_2+B_4-3B_6) - A_4(2B_1+B_3+3B_5) + A_5(-B_0-2B_2+3B_4) - A_6(B_1-3B_3)].$$

Spot checks indicated that the numerical values given in the table are correct however.

On the Theory of Condensation*

NOBUHIKO SAITÔ†

Department of Chemistry, University of Oregon, Eugene, Oregon

(Received December 14, 1959)

A calculation based on the Bragg-Williams approximation in lattice gases is presented, which shows a connection between the Yang-Lee and Mayer theories of condensation through an analogy with image charges in a two-dimensional electrostatic problem. The main features of this calculation are presumed to be retained in an exact treatment of lattice gases and real gases. A determination of the singularities of Mayer's series is made by making use of the results of recent investigations of cluster integrals by the approximation of the diagram method. It is concluded to be very probable that Mayer's theory cannot locate the condensation point but determines instead the supersaturation limit. Further, there is no *Derby hat* region near the critical point.

I. INTRODUCTION

THE theory of condensation has been developed in two ways. One is the virial expansion theory due to Mayer,[1,2] Born and Fuchs,[3] and Kahn and Uhlenbeck,[4] and the other is Yang and Lee's theory[5] based on the zeros of the grand partition function. The latter theory leaves no room for doubt about the validity of the formal conclusions reached, which is in contrast to Mayer's theory which has been criticized (see the following). Thus the question remains whether the condensation point predicted by Mayer and others is the same point assigned by Yang and Lee.

According to statistical mechanics, the pressure of a gas is expressed as the value of a certain power series in the limit $V\to\infty$ [see Eqs. (2.1) and (2.17)]. The coefficients of this series are functions of the volume of the total system. In Mayer's theory one assumes that the limit of an infinitely large volume may be taken in every term of the infinite series, and one replaces the volume-dependent coefficients by their limiting volume-independent ones. This procedure cannot always be justified.[4] In fact Katsura and Fujita[6] gave a few examples which yielded wrong results by the above-mentioned procedure and which throw doubt on the validity of Mayer's conclusions concerning the condensation. Further Katsura[7] and Temperley[8] showed that, in the Husimi-Temperley model, the condensation point predicted by Mayer is not the true condensation point but the supersaturation end point. Their theories, being based essentially on the Bragg-Williams approximation in the theory of lattice gases, are weak in that the Bragg-Williams approximation in the canonical ensemble implicitly assumes that the system has a uniform density everywhere. Consequently the two theories cannot exclude the possibility of yielding metastable states such as supersaturation, whereas a rigorous treatment of the canonical-ensemble partition function should give just the equilibrium equation of state,[9] although, as was shown by Hill[10] and Katsura,[7] the calculation based on the grand partition function in the Bragg-Williams approximation gives a horizontal line in the gas-liquid transition region of the $p-v$ diagram. On the other hand, Ikeda[11] supported Mayer's conclusions by giving the conditions for Mayer's theory needed to yield the same correct result as that of a treatment which takes proper account of the volume-dependent cluster integrals. However, Ikeda's conclusion also is not definite, in spite of his elaborate mathematical treatment, because of lack of knowledge about cluster integrals for large numbers of molecules.

Besides the above, there are some critiques to be made on Mayer's theory of the critical region. It has not yet been made clear, either experimentally or theoretically, whether we must introduce two temperatures T_c and T_m to describe the critical region.[12]

In the present paper we will first give further calculations on the Bragg-Williams approximation for lattice gases, and show a connection between the distribution of zeros of the grand partition function and the singularities of Mayer's series in terms of electrostatic analogies to the functions expressing the pressure and the density. Second, a discussion will be given dealing with the slope of the tangent to the $p-\rho$ dia-

* This work was supported in part by a research grant from the National Science Foundation.

† Present address: Department of Applied Physics, Waseda University, Tokyo, Japan.

[1] J. E. Mayer and M. G. Mayer, *Statistical Mechanics* (John Wiley & Sons, Inc., New York, 1940), Chap. 14; J. E. Mayer, *Handbuch der Physik*, edited by S. Flügge (Springer-Verlag, Berlin, 1958), Vol. 12, p. 73.

[2] J. E. Mayer and S. F. Harrison, J. Chem. Phys. **6,** 87 (1938).

[3] M. Born and K. Fuchs, Proc. Roy. Soc. (London) **A166,** 391 (1938).

[4] B. Kahn and G. E. Uhlenbeck, Physica **5,** 399 (1938).

[5] C. N. Yang and T. D. Lee, Phys. Rev. **87,** 404, 410 (1952).

[6] S. Katsura and H. Fujita, J. Chem. Phys. **19,** 795 (1951); Progr. Theoret. Phys. (Kyoto) **6,** 498 (1951); S. Katsura, *ibid.* **11,** 476 (1954).

[7] S. Katsura, J. Chem. Phys. **22,** 1277 (1954); Progr. Theoret. Phys. (Kyoto) **13,** 571 (1955).

[8] H. N. V. Temperley, Proc. Phys. Soc. (London) **A67,** 233 (1954).

[9] L. Van Hove, Physica **15,** 951 (1949).

[10] T. L. Hill, J. Phys. Chem. **57,** 324 (1953).

[11] K. Ikeda, Progr. Theoret. Phys. (Kyoto) **16,** 341 (1956).

[12] H. N. V. Temperley, *Changes of States* (Cleaver-Hume Press, Ltd., London, 1956), pp. 77–89; B. H. Zimm, J. Chem. Phys. **19,** 1019 (1951); J. E. Mayer, *ibid.* **19,** 1024 (1951).

gram at the condensation point. It is shown by use of reasonable assumptions on the distribution of zeros of the grand partition function near the positive real axis that the slope is not horizontal except at the critical point. The aforementioned properties are presumed to be retained in the exact treatments of lattice gases and real gases as well, by comparing the singularities of $\rho(z)$ in the Bragg-Williams approximation with those in real gases. In the latter case, we make use of the asymptotic evaluation of b_l, which is shown to be valid from the conjectural discussion based on the recent investigations of the cluster integrals by the approximations of the diagram method.

II. INTUITIVE DISCUSSION OF THE SINGULARITIES OF MAYER'S SERIES

First of all, we will summarize the results of the theories of imperfect gases based on the Ursell-Mayer expansion and on the zeros of the grand partition function. The pressure p and the density ρ are given as functions of the fugacity z, respectively, by

$$p/kT=\lim_{V\to\infty}(1/V)\ln\Xi, \tag{2.1}$$

$$\rho=z(\partial/\partial z)(p/kT), \tag{2.2}$$

$$\Xi=\sum_{N=0}^{M(V)}Q_N z^N, \tag{2.3}$$

$$Q_N=\sum_{\{lm_l=N\}}\prod_l\frac{\{Vb_l(V)\}^{m_l}}{m_l!}, \tag{2.4}$$

where $M(V)$ is the maximum number of particles which can be accommodated in a finite volume V, when we assume that each molecule has a hard core of finite dimensions, and $b_l(V)$ is the cluster integral. We define the volume-independent cluster integral by

$$b_l=b_l(\infty)=\lim_{V\to\infty}b_l(V). \tag{2.5}$$

Substituting Ξ from Eqs. (2.3) and (2.4) into Eq. (2.1), we have an infinite series for $\ln\Xi$ and we take the limit $V\to\infty$. If the infinite series is uniformly convergent for $V\to\infty$, i.e., in the gaseous state, the limit $V\to\infty$ is allowed to be taken in each term of the series. Thus the $b_l(V)$ in Eq. (2.4) can be replaced by b_l and in Eq. (2.3) we can put $M(V)=\infty$. Consequently we have[13]

$$\Xi_0=\exp(V\sum_{l=1}^{\infty}b_l z^l), \tag{2.6}$$

$$p_0/kT=\sum_l b_l z^l, \tag{2.7}$$

$$\rho_0=\sum_l l b_l z^l. \tag{2.8}$$

[13] In the following, the suffix 0 is used to denote thermodynamical or statistical mechanical quantities defined in terms of $b_l(\infty)$'s.

The inverse of Eq. (2.8) is given by

$$z=\rho_0\exp[-\partial G(\rho_0)/\partial\rho_0], \tag{2.9}$$

$$G(\rho_0)=\sum_k B_k\rho_0^k, \tag{2.10}$$

where the B_k's are irreducible cluster integrals, and the pressure can also be expressed by

$$\begin{aligned}p_0/kT&=\rho_0-\sum(k-1)B_k\rho_0^k \\ &=\rho_0+G(\rho_0)-\rho_0\partial G/\partial\rho_0.\end{aligned} \tag{2.11}$$

On the other hand, Yang and Lee[5] showed that Ξ, p, and ρ are given, respectively, by

$$\Xi=\prod_{j=1}^{M(V)}\left(1-\frac{z}{z_j}\right), \tag{2.12}$$

$$p/kT=\lim_{V\to\infty}V^{-1}\sum_{j=1}^{M(V)}\ln[1-(z/z_j)], \tag{2.13}$$

$$\rho(z)=\lim_{V\to\infty}V^{-1}\sum_j[z/(z-z_j)], \tag{2.14}$$

$$=z[(\partial/\partial\alpha_z)-i(\partial/\partial\beta_z)]\lim_{V\to\infty}V^{-1}\sum_j\ln r_j, \tag{2.15}$$

where the z_j's are the zeros of the grand partition function for a system of finite volume V, and we put

$$\begin{aligned}&z=\alpha_z+i\beta_z, \qquad z_j=\alpha_j+i\beta_j, \\ &r_j^2=(\alpha_z-\alpha_j)^2+(\beta_z-\beta_j)^2;\end{aligned} \tag{2.16}$$

$\sum_j\ln r_j$ can be interpreted as the electrostatic potential in two-dimensional problems due to unit charges at the z_j's. In a system of finite volume V and hence of finite $M(V)$, the z_j's are never real. In the limit of an infinitely large system, some of the zeros will lie concontinuously on lines which will intersect the real positive axis. The points of intersection give the points of phase change, among which the one z_c nearest to the origin gives the condensation point. In a region of small $|z|$ which contains no zero of the grand partition function, i.e., in the gaseous state, Ξ_0, p_0, and ρ_0 are equal to Ξ, p, and ρ, respectively. However, this is not always true at the condensation point, which is supposed to be given by a singular point of $\lim(1/V)\ln\Xi$. Thus the condensation point will not be determined by the singularity of Ξ_0, p_0, or ρ_0. This is intuitively recognized in the following way. In case of a finite volume, Ξ is a polynomial in z, but $\ln\Xi$ is an infinite series, which may be written formally as

$$(1/V)\ln\Xi=\sum_l b_l^{\dagger}(V)z^l, \tag{2.17}$$

where the $b_l^{\dagger}(V)$'s for $l\leq M(V)$ are equal to the $b_l(V)$'s, but the $b_l^{\dagger}(V)$'s for $l>M(V)$ are expressed by the $b_l(V)$'s for $l\leq M(V)$. Hence, when we let V become very large, the $b_l^{\dagger}(V)$'s for $l\leq M(V)$ are nearly equal to the $b_l(\infty)$'s, respectively, but the $b_l^{\dagger}(V)$'s for $l>M(V)$ are quite different from the $b_l(\infty)$'s. We can always take sufficiently large $l>M(V)$ for an arbitrarily

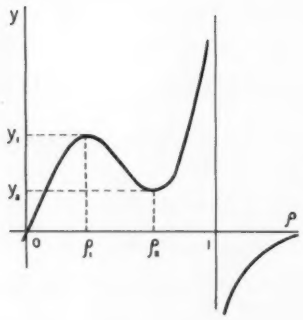

FIG. 1. y as a function of ρ for $0<s<1$.

large V, and in case the contribution of these terms for $l>M(V)$ is important in the series (2.17), i.e., at the singularity of this series, the behavior of Eq. (2.17) may be quite different from that given by the right-hand side of Eq. (2.7).[14] This simple consideration suggests that the singularity of p_0 given by Eq. (2.7) does not coincide with the singularity of Eq. (2.1) or Eqs. (2.12)–(2.15). We denote by z_s the singularity nearest to the origin of the series (2.7) or its analytic continuation. Since we have $\rho_0=\rho$ for $z<z_c$, it is evident that

$$z_s \geq z_c. \tag{2.18}$$

The relation $z_s>z_c$ may be expected from the electrostatic analog of Eq. (2.15). If the distribution of zeros on a line is interpreted as a continuous charge distribution on the line, we will be able to find image charges on the other side of this charged line.[15] This means that the analytic continuation of $\rho(z)$ can be extended beyond the line of the distribution of zeros. The position of the image charge on the positive real axis nearest to the charged line gives the first singularity on the real axis of the analytic continuation of the function $\rho(z)$. If we are in the gaseous region, i.e., $z<z_c$, the position of the image charge nearest to the origin on the other side of the charged line is the singular point z_s in Mayer's series (2.7) and (2.8) since, in this region, Mayer's series should coincide with Eqs. (2.1) and (2.2) or Eqs. (2.13) and (2.14). If z_s is not on the charged line, as is usually to be expected,[16] z_s is not the point of condensation, but gives the supersaturation limit, because at $z=z_s$ the pressure p_0 as a function ρ_0 has a horizontal tangent as will be seen later. This was pointed out by Katsura in the case of lattice gases. The same reasoning can be applied to the liquid phase (i.e., $z>z_c$) and the superdilatation (or super cooling at constant volume) of the liquid phase.

In the following sections more detailed calculations on image charges will be given to obtain a relation between z_c and z_s.

III. BRAGG-WILLIAMS APPROXIMATION IN LATTICE GASES

For the sake of concreteness, a calculation based on the Bragg-Williams approximation in lattice gases will be given in this section. Although this approximation has a weakness pointed out in Sec. I, it reveals an important connection between the theories of Mayer and Yang-Lee.

According to the Bragg-Williams approximation,[17] the fugacity z is expressed as a function of the density ρ, by the equation

$$z=[\rho/(1-\rho)]\exp[-(4/s)\rho], \quad s=-(4kT/c\epsilon), \tag{3.1}$$

where ϵ is the interaction energy between two neighboring molecules in the lattice, c is the coordination number of the lattice, and $s>0$ for molecules with attractive forces. This is the case of present interest. Now define y by

$$y=z\exp(2/s). \tag{3.2}$$

Then (3.1) becomes

$$y=[\rho/(1-\rho)]\exp(2/s)(1-2\rho) \tag{3.2}$$

We investigate two cases $0<s<1$ and $s>1$.

(*a*) $0<s<1$. For sufficiently low temperature, $0<s<1$, y has a maximum at $\rho=\rho_1$, and a minimum at $\rho=\rho_2$, as shown in Fig. 1; ρ_1 and ρ_2 are given by the solutions of the following equation:

$$\rho^2-\rho+(s/4)=0, \tag{3.3}$$

$$\left.\begin{matrix}\rho_1\\ \rho_2\end{matrix}\right\}=\tfrac{1}{2}[1\mp(1-s)^{\frac{1}{2}}]. \tag{3.4}$$

Let y_1 and y_2 be the values of y corresponding to $\rho=\rho_1$ and $\rho=\rho_2$, respectively; ρ as a function of y thus has branch points at $y=y_1$, and $y=y_2$.

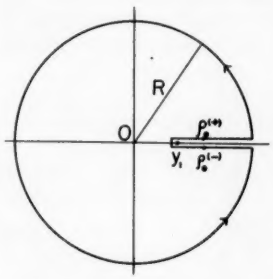

FIG. 2. The path of the integration of Eq. (3.5).

[14] The author is indebted for this observation to a discussion with Professor T. Yamamoto.

[15] The distribution of image charges is not unique. However, we can expect that some of them, which correspond to isolated singularities or branch points, are uniquely determined. In later discussion we will see that z_s is a branch point and thus the corresponding image is uniquely determined. The idea of image charges was introduced first in the theory of irreversibility by the present author. See the discussion in N. Saitô, Phys. Rev. **117**, 1163 (1960).

[16] The case when the image charge falls on the original charged line is the critical temperature.

[17] See, for example, T. L. Hill, *Statistical Mechanics* (McGraw-Hill Book Company, Inc., New York, 1956), p. 345, or reference 7.

First we will investigate the behavior of ρ in a Riemannian surface having a branch cut on a positive real axis from y_1 to ∞. This corresponds to ρ_0 in the gaseous state and its analytic continuation. In this region $\rho_0(y)$ is expressed by a contour integral.

$$\rho_0(y)=(2\pi i)^{-1}\oint\frac{\rho(y')}{y'-y}dy', \tag{3.5}$$

where the integration is carried out along the line shown in Fig. 2. Thus Eq. (3.5) can be rewritten as

$$\rho_0(y)=\lim_{R\to\infty}\left[\int_{y_1}^{R}\frac{f(y')}{y'-y}dy'+(2\pi i)^{-1}\oint_{|y'|=R}\frac{\rho(y')}{y'-y}dy'\right], \tag{3.6}$$

$$f(y')=(2\pi i)^{-1}[\rho_0{}^{(+)}(y')-\rho_0{}^{(-)}(y')], \tag{3.7}$$

where $\rho_0{}^{(+)}(y')$ and $\rho_0{}^{(-)}(y')$ are the values of ρ_0 at y' immediately above and below the branch cut, respectively. The determination of the function $f(y)$ is given in Appendix A. The form of $f(y)$ is shown schematically in Fig. 3.

Putting $y=0$ in Eq. (3.6), substracting it from Eq. (3.6), and taking into account $\rho_0(0)=0$ and

$$\lim_{R\to\infty}(2\pi i)^{-1}\oint_{|y'|=R}\frac{y\rho(y')}{(y'-y)y'}dy'=0$$

(because $|\rho(y')|\sim\ln R$ for $|y'|=R\to\infty$), we have

$$\rho_0(y)=\lim_{R\to\infty}\int_{y_1}^{R}\frac{y}{y-y'}\left(-\frac{f(y')}{y'}\right)dy'$$

$$=\lim_{R\to\infty}y\left(\frac{\partial}{\partial\alpha}-i\frac{\partial}{\partial\beta}\right)\int_{y_1}^{R}\left[-\frac{f(y')}{y'}\right]\ln r(y')dy', \tag{3.8}$$

where we put

$$y=\alpha+i\beta,$$

$$r(y')^2=(\alpha-y')^2+\beta^2.$$

The integral in Eq. (3.8) is interpreted as the two-dimensional electrostatic potential due to the charge distribution $-f(y')/y'$ along the real axis from y_1 to ∞. The total charge is infinite for $R\to\infty$. However, we can add a constant (infinitely large) charge

$$e=1+\int_{y_1}^{\infty}[f(y')/y']dy', \tag{3.9}$$

at infinity to make the total charge equal to unity without changing the value of ρ_0. Thus Eq. (3.8) can again be rewritten as

$$\rho_0(y)=\lim_{R\to\infty}y\left(\frac{\partial}{\partial\alpha}-i\frac{\partial}{\partial\beta}\right)\left[\int_{y_1}^{R}\left(-\frac{f(y')}{y'}\right)\ln r(y')dy'\right.$$

$$\left.+\left(1+\int_{y_1}^{R}[f(y')/y']dy'\right)\ln R\right]. \tag{3.10}$$

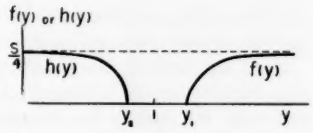

FIG. 3. Functions $f(y)$ and $h(y)$ $(s<1)$.

Now, as an interpretation of Eq. (3.8) or (3.10), we consider the unit circle around the origin as a conductor and we denote by $G(\theta)$ the $(-)$ induced charge distribution on the circle due to the charge distribution referred to above. A simple electrostatic calculation yields, on letting $R\to\infty$,

$$G(\theta)=2\pi^{-1}+2\pi^{-1}\int_{y_1}^{\infty}\frac{f(y)}{y}dy \tag{3.11}$$

$$+2\pi^{-1}\int_{y_1}^{\infty}\frac{y^2-1}{1+y^2-2y\cos\theta}\left[-\frac{f(y)}{y}\right]dy$$

$$=2\pi^{-1}+(2/2\pi)\int_{y_1}^{\infty}\frac{(1-y\cos\theta)}{1+y^2-2y\cos\theta}\frac{f(y)}{y}dy. \tag{3.12}$$

The first two terms in Eq. (3.11) come from the charge (3.9) at infinity and the last term corresponds to the charge induced by the charge distribution $-f(y)/y$ for $y_1<y<\infty$. Thus in a region $|y|<1$, $\rho_0(y)$ is equivalent to

$$\rho_0(y)=y\left(\frac{\partial}{\partial\alpha}-i\frac{\partial}{\partial\beta}\right)\int_{-\pi}^{\pi}G(\theta)\ln r(\theta)d\theta,$$

$$r(\theta)^2=(\alpha-\cos\theta)^2+(\beta-\sin\theta)^2. \tag{3.13}$$

Yang and Lee[5] showed that in lattice gases the zeros of the grand partition function are distributed on a circle of radius $\exp(-2/s)$ around the origin in the z plane or on the unit circle in the y plane. This is true of the Bragg-Williams grand partition function as well.[7] Thus we can write

$$\rho(y)=\lim_{V\to\infty}V^{-1}\sum_j\frac{y}{y-e^{i\theta_j}}=\int_{-\pi}^{\pi}\frac{y}{y-e^{i\theta}}g(\theta)d\theta \tag{3.14}$$

$$=y\left(\frac{\partial}{\partial\alpha}-i\frac{\partial}{\partial\beta}\right)\int_{-\pi}^{\pi}g(\theta)\ln r(\theta)d\theta, \tag{3.14'}$$

where $g(\theta)$ is the distribution function of zeros of the grand partition function with the properties

$$g(\theta)>0,$$

$$\int_{-\pi}^{\pi}g(\theta)d\theta=1. \tag{3.15}$$

From Eq. (3.12) it can be shown that

$$G(\theta)>0 \quad\text{and}\quad \int_{-\pi}^{\pi}G(\theta)d\theta=1. \tag{3.16}$$

Thus we can identify $G(\theta)$ with $g(\theta)$ in the Bragg-Williams approximation. Further $G(\theta)$ has a minimum

at $\theta=0$ and is monotonically increasing in $0\leq\theta\leq\pi$, in agreement with the consideration of Yang-Lee.

Next we consider the behavior of ρ in the Riemannian surface having a branch cut from 0 to y_2 on the real axis. We denote this branch of ρ by ρ_L; $\rho_L(y)$ is expressed in the same way as in Eq. (3.6),

$$\rho_L(y)=2\pi i^{-1}\int_0^{y_2}\frac{\rho_L^{(+)}(y')-\rho_L^{(-)}(y')}{y'-y}dy' +2\pi i^{-1}\oint_{|y'|=R\to\infty}\frac{\rho(y')}{y'-y}dy'. \quad (3.17)$$

In a way analogous to that of Eq. (3.8), we have, from the condition $\rho_L(y)=1$ for $y\to\infty$,

$$\rho_L(y)=1-\int_0^{y_2}\frac{h(y')}{y-y'}dy', \quad (3.18)$$

where

$$h(y')=2\pi i^{-1}[\rho_L^{(+)}(y')-\rho_L^{(-)}(y')]. \quad (3.19)$$

The determination of $h(y)$ is given in Appendix A and the form of $h(y)$ is drawn schematically in Fig. 3. Equation (3.18) can be rewritten as

$$\rho_L(y)=e'-\int_0^{y_2}\frac{y}{y-y'}\frac{h(y')}{y'}dy' \quad (3.20)$$

$$=\int_0^{y_2}\frac{y}{y-y'}\left[-\frac{h(y')}{y'}+e'\delta(y')\right]dy'$$

$$=y\left(\frac{\partial}{\partial\alpha}-i\frac{\partial}{\partial\beta}\right)\int_0^{y_2}\left[-\frac{h(y')}{y'}+e'\delta(y')\right]\ln r(y')dy',$$

where (3.21)

$$e'=1+\int_0^{y_2}\frac{h(y')}{y'}dy', \quad (3.22)$$

$$\begin{cases}\delta(y)=0, & y\neq 0,\\ \int_0^{y_2}\delta(y)dy=1,\end{cases}$$

and

$$r(y')^2=(\alpha-y')^2+\beta^2.$$

The integral of Eq. (3.21) is interpreted as the electrostatic potential due to an infinitely large charge e' at the origin and a negative charge distribution $-h(y')/y'$ along the real axis from 0 to y_2. As is proved in Appendix A, we have

$$f(y)=h(1/y), \quad (3.23)$$

and from $y_1y_2=1$ we see that e given by Eq. (3.9) is equal to e',

$$e=e'. \quad (3.24)$$

Equations (3.22) and (3.23) show that the charge distribution $-f(y)/y$ for $y_1<y<\infty$ and e at infinity (outside the unit circle) and the charge distribution $-h(y)/y$ for $0<y<y_2$ and e' at the origin (inside the unit circle) are images of each other with respect to the unit circle. The $(-)$ induced charge distribution on the unit circle due to the charges inside the circle is just $g(\theta)$ or $G(\theta)$ given by Eq. (3.12).

The above results can also be put in the following way. If the system is in the gaseous region, i.e., inside the unit circle $|y|<1$, the charge distribution outside the circle, $-f(y)/y$ for $y_1<y<\infty$ and e at infinity, is the image of the charge distribution $g(\theta)$ on the unit circle. We can say almost the same thing about the charge distribution $-h(y)/y$ for $0<y<y_2$ and e' at the origin, if the system is in the liquid state $|y|>1$. This is just what is said in Sec. II. The singularity of $\rho_0(y)$, which is equivalent to Mayer's series Eq. (2.8) in the Bragg-Williams approximation, lies at $y=y_1>1$ or $z=z_s=y_1e^{-2/s}$; z_s is different from the true condensation point $z_c=e^{-2/s}$, and is the supersaturation limit since we can make an analytic continuation up to this point and we have

$$\partial p_0/\partial\rho_0=(kT/y)(\partial y/\partial\rho_0), \quad (3.25)$$

which is equal to zero at $y=y_1$ (i.e., $z=z_s$).

Equations (3.8), (3.18), and (3.23) yield the following relation

$$\rho_0(y)+\rho_L(1/y)=1. \quad (3.26)$$

This is the relation which holds generally in lattice gases.[18]

The $g(\theta)$ given by Eq. (3.12) for $s<1$ can be expanded near $\theta=0$ as follows:

$$g(\theta)=g(0)+(\theta^2/\pi)\int_{y_1}^{\infty}\frac{y+1}{(y-1)^3}f(y)dy+\cdots, \quad (3.27)$$

$$g(0)=\pi^{-1}\left[\tfrac{1}{2}-\int_{y_1}^{\infty}\frac{f(y)}{(y-1)y}dy\right]. \quad (3.28)$$

In view of Eqs. (3.8) and (3.26), we see that

$$g(0)=\pi^{-1}[\tfrac{1}{2}-\rho_0(1)]=\pi^{-1}[\rho_L(1)-\tfrac{1}{2}]. \quad (3.29)$$

At the critical temperature, we have $\rho_0(1)=\rho_L(1)=\frac{1}{2}$, $y_1=1$, and $f(y)\propto(y-1)$ near $y=1$ [see Eq. (A.5) of Appendix A]. Then it is found that

$$g(0)=0, \quad (3.30)$$

and the integral of the coefficient of θ^2 diverges. This means that $g(\theta)$ cannot be expanded about $\theta=0$. As we will see in Appendix A, $g(\theta)$ has the form

$$g(\theta)\propto|\theta|^{1/3}+\cdots \quad (3.31)$$

at the critical temperature [see Eq. (A.14)].

(b) $s>1$. Above the critical temperature, $s>1$, the branch points of $\rho(y)$, which are determined by Eqs.

[18] T. L. Hill, *Statistical Mechanics* (McGraw-Hill Book Company, Inc., New York, 1956), p. 304.

(3.3) and (3.4), lie at

$$\left.\begin{matrix} y_1 \\ y_2 \end{matrix}\right\} = \frac{1 \pm it}{1 \mp it} \exp[\mp i(2/s)t] = \exp(\pm i\Theta), \tag{3.32}$$

where $t=(s-1)^{\frac{1}{2}}$ and

$$\Theta_1 = 2\tan^{-1}t - (2/s)t > 0. \tag{3.33}$$

The corresponding ρ_1 and ρ_2 are

$$\left.\begin{matrix} \rho_1 \\ \rho_2 \end{matrix}\right\} = \tfrac{1}{2}(1 \pm it). \tag{3.34}$$

Thus we make a branch cut on the unit circle around the origin in the y plane from argument Θ_1 to $2\pi-\Theta_1$, and we can write

$$\rho(y) = 2\pi i^{-1} \oint \frac{\rho(y')}{y'-y} dy', \tag{3.35}$$

where the integration is carried out around the cut and along a large circle at infinity. In a way analogous to to that of Eq. (3.8), we have, from the condition $\rho=0$ when $y=0$

$$\begin{aligned} \rho(y) &= \int_{\Theta_1}^{2\pi-\Theta_1} \frac{yk(\theta)}{e^{i\theta}-y} d\theta \\ &= y\left(\frac{\partial}{\partial\alpha} - i\frac{\partial}{\partial\beta}\right) \int_{\Theta_1}^{2\pi-\Theta_1} [-k(\theta)] \ln r(\theta) d\theta, \end{aligned} \tag{3.36}$$

where

$$\begin{aligned} y &= \alpha + i\beta, \\ k(\theta) &= 2\pi^{-1}\{\rho^{(i)}(\theta) - \rho^{(0)}(\theta)\}, \\ r(\theta)^2 &= (\alpha-\cos\theta)^2 + (\beta-\sin\theta)^2, \end{aligned} \tag{3.37}$$

and $\rho^{(i)}(\theta)$ and $\rho^{(0)}(\theta)$ mean the values of ρ at $y=e^{i\theta}$ just inside and outside of the unit circle, respectively. Equation (3.36) is given the same electrostatic interpretation as Eq. (3.8). The determination of $k(\theta)$ is given in Appendix A. We can show

$$k(\theta) > 0$$

and

$$\int_{\Theta_1}^{2\pi-\Theta_1} k(\theta) d\theta = 1.$$

Therefore we can identify $k(\theta)$ with the distribution function $g(\theta)$ of zeros of the grand partition function.

An alternative determination of $g(\theta)$ in the present model was given by Katsura.[7]

In closing this section, we notice that $\rho(y)$ has a continuous distribution of poles on the unit circle in the y plane for $0<s<1$, as is seen in Eq. (3.14), but this unit circle is not the natural boundary of the function $\rho_0(y)$ defined in $|y|<1$. $\rho_0(y)$ can be continued analytically beyond this circle up to $y=y_1$. The same is true of $\rho_L(y)$ for $|y|>1$, which can be continued analytically inside the unit circle up to $y=y_2$.

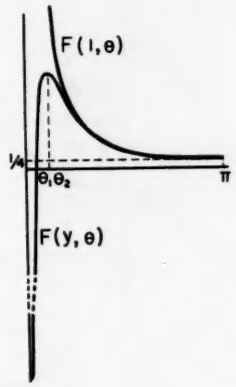

FIG. 4. $F(y, \theta)$ vs θ for $y \approx 1$.

IV. BEHAVIOR OF $\rho(y)$ NEAR THE CONDENSATION POINT IN LATTICE GASES

Equation (3.14) can be written, when y is real, as

$$\rho(y) = 2y\int_0^\pi \frac{y-\cos\theta}{y^2-2y\cos\theta+1} g(\theta) d\theta. \tag{4.1}$$

Differentiation with respect to y yields

$$\partial\rho/\partial y = 2\int_0^\pi F(y,\theta) g(\theta) d\theta, \tag{4.2}$$

$$F(y,\theta) = \frac{-(y^2+1)\cos\theta + 2y}{(y^2-2y\cos\theta+1)^2}. \tag{4.3}$$

Now the problem is whether

$$\partial\rho/\partial y = \text{infinite}$$

or

$$\partial\rho/\partial y = \text{finite} \tag{4.4}$$

at the condensation point $y\to 1$. (4.4) means, from the thermodynamical relation (3.25), that the tangent of the $p-\rho$ diagram is continuous (horizontal) or not at the condensation point. Onsager[19] and Yang[20] obtained an exact expression for the coexistence curve in the $p-v$ diagram of two-dimensional lattice gases. However, the problem just mentioned still remains unsolved even in the two-dimensional case. In this section a discussion will be given on the plausible behavior of ρ near the condensation point.

To do this, we first notice the following property of $F(y, \theta)$:

$$\int_0^\pi F(y,\theta) d\theta = 0, \qquad y \neq 1. \tag{4.5}$$

Equations (4.1), (4.2), and (4.5) hold for $y<1$ as well as for $y>1$. However, $F(1, \theta) = \frac{1}{2}(1-\cos\theta)^{-1}$ does not

[19] L. Onsager and B. Kaufman, Nuovo cimento Suppl. 2 **6**, 261 (1949), reported in the discussion.
[20] C. N. Yang, Phys. Rev. **85**, 808 (1952).

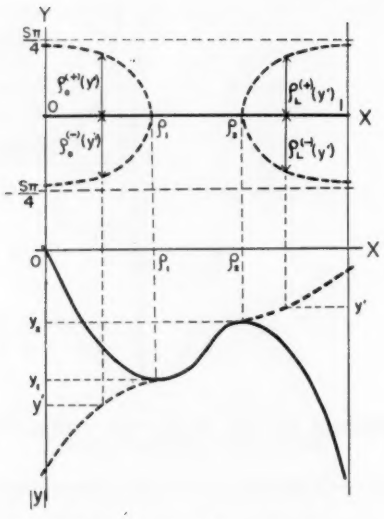

FIG. 5. Determination of Y as a function of y.

have the property (4.5),

$$\int_0^\pi F(1,\theta)d\theta=\text{infinite}.$$

$F(y,\theta)$ for $y\approx 1$ is drawn schematically in Fig. 4. $F(y,\theta)$ is zero at $\theta=\theta_1$ and has a maximum at $\theta=\theta_2$, where θ_1 and θ_2 are determined, respectively, by

$$\cos\theta_1=2y/(y^2+1),$$
$$\cos\theta_2=(-y^4+6y^2-1)/2y(y^2+1). \tag{4.6}$$

Put

$$y=1\pm\delta, \qquad \delta>0.$$

Then we have for small δ,

$$\theta_1\approx\delta, \qquad \theta_2\approx\sqrt{3}\delta,$$
$$F(y,0)=-\delta^{-2}, \qquad F(y,\theta_2)=\tfrac{1}{8}\delta^{-2}.$$
$$F(y,\theta)\approx-(\delta^2-\theta^2)/(\delta^2+\theta^2)^2, \quad \text{for } \theta\leq\delta. \tag{4.7}$$

The $g(\theta)$ is an even function of θ. It has been shown in Sec. III that in the Bragg-Williams approximation (i) $g(\theta)$ has a minimum at $\theta=0$ and is monotonically increasing in $0\leq\theta\leq\pi$, (ii) below the critical temperature we can write

$$g(\theta)=g(0)+g_1(\theta),$$
$$g_1(\theta)=\alpha\theta^2+\cdots, \qquad \alpha>0, \tag{4.8}$$

and (iii) at the critical temperature we have $g(0)=0$ and

$$g_1(\theta)=\beta|\theta|^{1/3}+\cdots, \qquad \beta>0, \tag{4.9}$$

or more generally

$$g_1(\theta)=\beta|\theta|^n+\cdots, \qquad \beta>0, \qquad 0<n<1. \tag{4.10}$$

We assume that the rigorous treatment of lattice gases retains these properties. Thus below the critical temperature, we write Eq. (4.2) as

$$\partial\rho/\partial y=2\int_0^\pi F(y,\theta)[g(0)+g_1(\theta)]d\theta$$
$$=2\int_0^\pi F(y,\theta)g_1(\theta)d\theta$$
$$=2\int_0^{\theta_1}F(y,\theta)g_1(\theta)d\theta+2\int_{\theta_1}^\pi F(y,\theta)g_1(\theta)d\theta. \tag{4.11}$$

where $g_1(\theta)$ has an expansion of the form (4.8). The first integral of Eq. (4.11) goes to zero for $y\to 1$ in view of the properties (4.7) for small δ, and the second integral is positive and finite since the integrand remains finite for $\delta\to\infty$. Therefore, in this case, $\partial\rho/\partial y$ is positive and finite at the condensation point. On the other hand, at the critical temperature, $g_1(\theta)$ is of the form (4.10) and it is an increasing function of θ for $0\leq\theta\leq\pi$. Therefore Eq. (4.11) can be written as

$$\partial\rho/\partial y\geq 2\int_0^{\theta_1}F(y,\theta)g_1(\theta)d\theta+2g_1(\theta_1)\int_{\theta_1}^\pi F(y,\theta)d\theta$$
$$=-2\int_0^{\theta_1}[-F(y,\theta)]g_1(\theta)d\theta$$
$$+2g_1(\theta_1)\int_0^{\theta_1}[-F(y,\theta)]d\theta, \tag{4.12}$$

by virtue of the property (4.5) for $y=1\pm\delta$, $\delta>0$. For small δ, these integrals can be evaluated as

$$\int_0^{\theta_1}F(y,\theta)g_1(\theta)d\theta\approx-\int_0^\delta\frac{\delta^2-\theta^2}{(\delta^2+\theta^2)^2}\beta\theta^n d\theta$$
$$=-\beta\delta^{n-1}[\tfrac{1}{2}-\alpha], \tag{4.13}$$

and

$$g_1(\theta_1)\int_0^{\theta_1}[-F(y,\theta)]d\theta\approx\tfrac{1}{2}\beta\delta^{n-1},$$

where

$$\alpha=(n/4)\left[\psi\left(\frac{n+3}{4}\right)-\psi\left(\frac{n+1}{4}\right)\right],$$
$$\psi(q)=\Gamma'(q)/\Gamma(q), \tag{4.14}$$

and $\Gamma(q)$ is the gamma function. Since $\psi(q)$ is an increasing function for $0<q<1$, α is a positive quantity. Thus we finally have

$$\partial\rho/\partial y\geq-\beta\delta^{n-1}[\tfrac{1}{2}-\alpha]+\tfrac{1}{2}\beta\delta^{n-1}=\alpha\beta\delta^{n-1}\to\infty$$

for $\delta\to 0$ since $0<n<1$. The above conclusions are at variance with the conjecture of Lee and Yang.[5]

Mayer has shown that there is a region just below the critical temperature where the slope to the $p-v$ diagram at the condensation point is horizontal. This region should be found also in lattice gases. The

behavior of $g(\theta)$ given by (4.8) and (4.10) seems very plausible. If this proves to be the case, it will be sufficient to disprove Mayer's theory.

V. SINGULARITIES OF MAYER'S SERIES

According to the virial expansion theory of condensation, the condensation point is determined by the smaller ρ_s satisfying either of the following conditions:

$$\rho\partial^2 G(\rho)/\partial\rho^2=\sum_k k(k-1)B_k\rho^{k-1} \text{ is singular} \quad (5.1)$$

or

$$\rho\partial^2 G/\partial\rho^2=1. \quad (5.2)$$

The condition (5.2) yields

$$\partial z/\partial\rho=0 \quad (5.3)$$

and

$$\partial p/\partial\rho=0. \quad (5.4)$$

This condition is supposed to be realized at a temperature slightly lower than the critical temperature, while (5.1) is supposed to be effective at lower temperatures. Both conditions locate the singularities of the functions (2.7) and (2.8). Generally speaking, it is a difficult task to find the singularities of the functions (2.7), (2.8), and (2.10). To do this, we have to know the behavior of b_k or B_k at large k. Now we have some information on b or B values for small k,[21] and there have been some efforts to get b or B values at higher k,[22] in particular the contribution to B_k from some special diagrams.[23] Although there is some doubt about the validity of the approximate evaluation of the sum in the right-hand side of Eq. (5.1) by means of the diagram method for treating the condensation problem, this method seems to give the maximum information for the cluster integral available at the present stage. It is well known that the ring approximation for the cluster integral is equivalent to the method of the linearized Born-Green integral equation, and the condition (5.2) is satisfied with smaller ρ than that of the condition (5.2). The latter property is shown by Ikeda[24] to be the case in the approximations higher than the ring approximation, such as the netted-ring approximation of Hiroike or the watermelon approximation of Abe. Thus we may make a conjecture that (5.2) is satisfied with smaller ρ than that of the condition (5.1) in the exact treatment of the cluster integral, then we can determine the singularities of the functions defined by Eqs. (2.7) and (2.8).

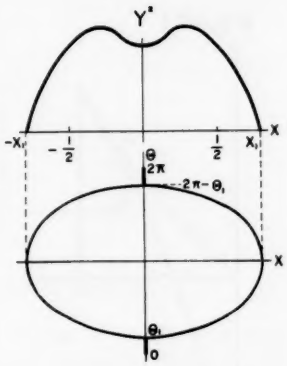

FIG. 6. Determination of χ as a function of Θ.

Before doing this, we notice that p_0 is maximum at $\rho=\rho_s$, where we denote by ρ_s the smallest ρ satisfying Eq. (5.2). It is obvious that $\rho\partial^2 G/\partial\rho^2<1$ for small ρ. On increasing ρ, $\rho\partial^2 G/\partial\rho^2$ reaches 1 for the first time at $\rho=\rho_s$. Differentiation of Eq. (2.11) gives

$$kT^{-1}(\partial p_0/\partial\rho)=1-\rho(\partial^2 G/\partial\rho^2); \quad (5.5)$$

therefore, $\partial p_0/\partial\rho$ is positive for $\rho<\rho_s$ and becomes negative for $\rho>\rho_s$. This means that p_0 is maximum at $\rho=\rho_s$. [The case where $\partial p_0/\partial\rho$ is maximum and does not change sign at $\rho=\rho_s$ is at the critical temperature.]

The cluster integral b_l is expressed by a contour integral in terms of the irreducible cluster integrals B_k as follows:

$$l!b_l=2\pi i^{-1}\oint\frac{\exp[l\sum kB_k\zeta^{k-1}]}{\zeta^l}d\zeta, \quad (5.6)$$

where the B_k's are functions of the temperature, but not of the volume. For large l, this contour integral is evaluated under certain conditions by the method of steepest descent to be[3]

$$l!b_l\cong\left[\frac{\rho\exp\{l(\partial G/\partial\rho-\ln\rho)\}}{\{2\pi\rho(\partial/\partial\rho)[\rho(\partial^2 G/\partial\rho^2)]\}^{\frac{1}{2}}l^{\frac{1}{2}}}\right]_{\rho=\rho_s} \quad (5.7)$$

where ρ_s is given by the smallest ζ satisfying

$$\zeta\partial^2 G(\zeta)/\partial\zeta^2=1. \quad (5.8)$$

In this derivation use is made of the facts that, as is conjectured in the above discussion, no singular point of $\sum kB_k\zeta^{k-1}$ or $\sum B_k\zeta^k$ lies between 0 and ρ_s, and that $(\partial/\partial\rho)[\rho(\partial^2 G/\partial\rho^2)]$ is positive at $\rho=\rho_s$, since we have from Eq. (2.11)

$$kT^{-1}(\partial^2 p_0/\partial\rho_s)=-(\partial/\partial\rho)[\rho(\partial^2 G/\partial\rho^2)] \quad (5.9)$$

and p_0 is maximum at $\rho=\rho_s$. At the critical temperature, $(1/kT)\partial^2 p_0/\partial\rho^2$ becomes zero and C defined by

[21] T. Kihara, Revs. Modern Phys. **25,** 831 (1953); J. O. Hirschfelder, C. F. Curtiss, R. B. Bird, *Molecular Theory of Gases and Liquids* (John Wiley & Sons, Inc., New York, 1954); T. Kihara and S. Kaneko, J. Phys. Soc. Japan **12,** 994 (1957); H. N. V. Temperley, Proc. Phys. Soc. (London) **B70,** 536 (1957); S. Katsura, Progr. Theoret. Phys. (Kyoto) **20,** 192 (1958); S. Katsura, Phys. Rev. **115,** 1417 (1959); R. Bergeon, J. recherches centre natl. sci. Lab. Bellevue (Paris) **44,** 171 (1958).

[22] R. J. Ridell and G. E. Uhlenbeck, J. Chem. Phys. **21,** 2056 (1953); H. N. V. Temperley, Proc. Phys. Soc. (London) **72,** 1141 (1958).

[23] E. W. Montroll and J. E. Mayer, J. Chem. Phys. **9,** 626 (1941); G. S. Rushbrooke and H. I. Scoins, Proc. Roy. Soc. (London) **A216,** 203 (1953); K. Hiroike, J. Phys. Soc. Japan **13,** 1497 (1958); R. Abe, *ibid.* **14,** 10 (1959); T. Morita, Progr. Theoret. Phys. (Kyoto) **20,** 920 (1958); E. Meeron, Phys. Fluids **1,** 139 (1958).

[24] K. Ikeda, lecture at the Nagoya meeting of the Physical Society of Japan (October, 1960).

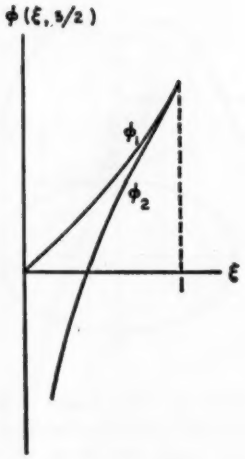

FIG. 7. $\phi(\xi, 5/2)$.

(5.11) becomes infinite, and the evaluation (5.7) does not hold. We denote by $\bar{b}_l$ the asymptotic b_l evaluated by Eq. (5.7),

$$\bar{b}_l = Ca^l/l^{5/2}, \tag{5.10}$$

where

$$C = \left[\rho\left\{2\pi\rho\frac{\partial}{\partial\rho}\left(\frac{\partial^2 G}{\partial\rho^2}\right)\right\}^{-\frac{1}{2}}\right]_{\rho=\rho_s} \tag{5.11}$$

$$a = [\rho^{-1}\exp(\partial G/\partial\rho)]_{\rho=\rho_s}. \tag{5.12}$$

Both C and a are independent of l. Now we define a function $\phi(\xi, \sigma)$ by

$$\phi(\xi, \sigma) = \sum_{n=1}^{\infty} \xi^n/n^\sigma. \tag{5.13}$$

The properties of this function have been studied by many investigators, especially in connection with Bose-Einstein condensation. We summarize the properties of $\phi(\xi, \frac{5}{2})$ and $\phi(\xi, \frac{3}{2})$ in Appendix B. Both functions have a branch point at $\xi = 1$.

If we define a function $\bar{\rho}$ in terms of $\bar{b}_l$,

$$\bar{\rho} = \sum l\bar{b}_l z^l = C\phi(az, \tfrac{3}{2}),$$

then $\partial\bar{\rho}/\partial z$ is infinite at

$$z = z_s = a^{-1} = \rho_s \exp[-\sum_k kB_k\rho_s^{k-1}], \tag{5.14}$$

and we see, referring to Eq. (2.9), that z_s is the fugacity at the density $\rho = \rho_s$. On the other hand we have $\partial\rho/\partial z = \infty$ at $z = z_s$, and both ρ and $\bar{\rho}$ are analytic for $0 < z < a^{-1}$. Therefore the function $\varphi(z) = \rho(z) - \bar{\rho}(z)$ is analytic at least in a region $0 < z < a^{-1}$.

According to Eq. (B3) in Appendix B, we have

$$\rho(z) = \varphi(z) + C\phi(za, \tfrac{3}{2})$$
$$= \varphi(z) + \frac{C}{\Gamma(\frac{3}{2})}\int_{a^{-1}}^{\infty} \frac{z}{z-\zeta}\left[-\frac{(\ln\zeta a)^{\frac{1}{2}}}{\zeta}\right]d\zeta. \tag{5.15}$$

Comparing this with Eq. (3.8), we note the electrostatic interpretation that there is a charge distribution

$$-\frac{C}{\Gamma(\frac{3}{2})}\left[\frac{(\ln\zeta a)^{\frac{1}{2}}}{\zeta}\right] \tag{5.16}$$

along the positive real axis from a^{-1} to ∞. Further we can see that $(\ln\zeta a)^{\frac{1}{2}}$ is of the same form as $f(y)$ given in Fig. 3 in its general trend. Besides this charge distribution we have another one arising from the function $\varphi(z)$. The first branch of $\bar{\rho}(z)$ is monotonic increasing up to $z = z_s = a^{-1}$. The addition of $\varphi(z)$ analytic in $0 < z < a^{-1}$ to $\rho(z)$ does not alter this property, since, if there occurred a maximum or minimum somewhere between 0 and a^{-1}, we would have $\partial\rho/\partial z = 0$ or $\partial z/\partial\rho = \infty$ at this point, which is in contradiction to the fact that there is no singularity of G between 0 and a^{-1}.

In Sec. VI we have shown that it is very probable that $\partial\rho/\partial y$ or $\partial\rho/\partial z$ has a positive and finite value at the condensation point. If we take this point of view, the true condensation point is not given by Eq. (5.14) which yields $\partial\rho/\partial z = 0$. In effect the condensation point is determined by $y = 1$, or $z = z_c = \exp(-2/s)$ in lattice gases; z_s would never happen to be equal to z_c except at the critical temperature. Consequently we can expect in general, below the critical temperature,

$$z_c < z_s. \tag{5.17}$$

The "charge" distribution (5.16) and, besides this, the charge distribution arising from $\varphi(z)$ can be interpreted as the image charge of the charge distribution $g(\theta)$ on the unit circle in the y plane in the case of lattice gases, or, a similar charge distribution on a certain line in the case of general real gases. This is what we have said in Sec. II, and z_s is the limit of supersaturation.

Mayer and Harrison[2] assumed that (5.2) is satisfied with smaller ρ than (5.1) in a region immediately below the critical temperature, and they conjectured the presence of the *Derby hat* region near the critical point. However, the above discussion throws some doubt on their conclusion.

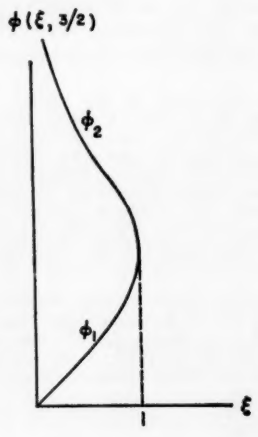

FIG. 8. $\phi(\xi, 3/2)$.

ACKNOWLEDGMENTS

The author wishes to express his deep appreciation to Professor T. L. Hill and Professor T. Yamamoto for stimulating discussions and reading the manuscript. Thanks are also due to Dr. H. N. V. Temperley for his valuable communications. The author is also grateful for the hospitality of the staff of the Departments of Chemistry and Physics, University of Oregon.

APPENDIX A. SINGULARITIES OF $\rho(y)$ IN BRAGG-WILLIAMS APPROXIMATION

Consider the equation

$$y=[\rho/(1-\rho)]\exp(2/s)(1-2\rho), \quad s>0. \tag{A1}$$

Put $\rho=X+iY$ and $y=|y|e^{i\Theta}$ in Eq. (A1), and we have

$$|y|=[\exp(2/s)(1-2X)]\frac{(X^2+Y^2)^{\frac{1}{2}}}{[(1-X)^2+Y^2]^{\frac{1}{2}}}, \tag{A2}$$

and

$$\Theta=\tan^{-1}\frac{Y}{X-X^2-Y^2}-\frac{4Y}{s}$$

$$=\tan^{-1}\frac{Y}{X}+\tan^{-1}\frac{Y}{1-X}-\frac{4Y}{s}. \tag{A3}$$

Now we investigate two cases, $0<s<1$ and $s>1$.

(a) $0<s<1$; $\rho(y)$ has branch points at

$$\left.\begin{matrix}y_1\\ y_2\end{matrix}\right\}=\frac{1\mp(1-s)^{\frac{1}{2}}}{1\pm(1-s)^{\frac{1}{2}}}\exp[\pm(2/s)(1-s)^{\frac{1}{2}}],$$

and branch cuts from y_1 to ∞ and 0 to y_2. We can put $\Theta=0$ for y on the positive real axis and (A3) determines Y as a function of X. The branches of Y as functions of X are given in the upper part of Fig. 5. The full line curve in the lower part of Fig. 5 represents $|y|$ vs X for $Y=0$ and $-\infty<X<\infty$ and the dashed line curve represents $|y|$ vs X for the $Y-X$ relation expressed by the dashed-line curves of the upper part of Fig. 5. Both are determined by making use of Eq. (A2). As is seen from Fig. 5 the left-hand dashed line curve corresponds to the Y values for $y_1<y<\infty$, and the right-hand dashed line curve to the Y values for $0<y<y_2$. These Y values determine $\rho^{(+)}$ and $\rho^{(-)}$ (the values of y immediately above and below the branch cut) as functions of y, as indicated in Fig. 5. Thus $f(y)$ and $h(y)$, defined, respectively, by Eqs. (3.7) and (3.19), are found to have the forms given in Fig. 3 in the text. Further we can see from Eq. (A2) that $|y|$ for $X<\rho_1$ is just the inverse of $|y|$ for $X'>\rho_2$, $X'+X=1$, hence we have

$$f(y)=h(1/y). \tag{A4}$$

At the critical temperature, $s=1$, $f(y)$ and $h(y)$ are not of the form in Fig. 3. Simple calculation shows that

$$f(y)=h(1/y)=(\sqrt{3}/4\pi)(y-1)+\cdots, \quad y\geq 1 \tag{A5}$$

near $y=1$.

(b) $s>1$. Put $|y|=1$ and $X=\frac{1}{2}+\chi$ in Eq. (A2) and we have

$$\exp(8\chi/s)=\frac{(\frac{1}{2}+\chi)^2+Y^2}{(\frac{1}{2}-\chi)^2+Y^2}. \tag{A6}$$

This equation has two branches; one is given by

$$\chi=0, \qquad Y=\text{arbitrary} \tag{A7}$$

and the other is given by

$$Y^2=\frac{(\frac{1}{2}+\chi)^2}{\exp(8\chi/s)-1}+\frac{(\frac{1}{2}-\chi)^2}{\exp(-8\chi/s)-1}. \tag{A8}$$

The Y being real, $|\chi|$ is less than $\chi_1>\frac{1}{2}$ determined by

$$\frac{\chi_1-(\frac{1}{2})}{\chi_1+(\frac{1}{2})}=\exp(-4\chi_1/s). \tag{A9}$$

The curve Y^2 vs χ is given schematically in the upper part of Fig. 6. The Θ is determined by Eq. (A3) and Eqs. (A7) or (A8). The former gives $-\Theta_1<\Theta<\Theta_1$ and $\chi=0$ as a first branch and the latter gives the oval shape curve shown in the lower part of Fig. 6. Thus $k(\theta)$ defined by Eq. (3.37) is given by $\chi(\theta)/\pi$, the real part of $[\rho(\theta)-\frac{1}{2}]/\pi$, on putting $\Theta=\theta$,

$$k(\theta)=\chi/\pi=[\Re\rho(\theta)-\tfrac{1}{2}]/\pi. \tag{A10}$$

The integral of $\rho(\theta)$ around the unit circle is calcu-

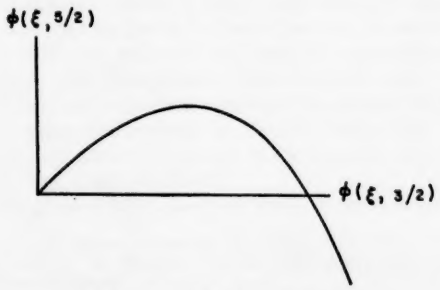

FIG. 9. $\phi(\xi, 5/2)$ vs $\phi(\xi, 3/2)$.

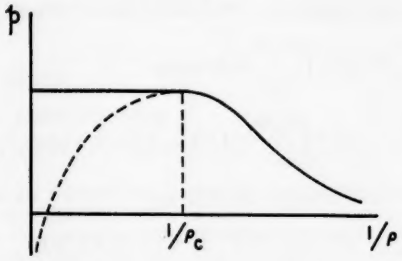

FIG. 10. p vs $1/\rho$ in ideal Bose gases.

lated as follows,

$$\int_{\Theta_1}^{2\pi-\Theta_1}\rho(\theta)d\theta=\int_{\frac{1}{2}(1+it)}^{\frac{1}{2}(1-it)}\rho(d\theta/d\rho)d\rho$$

$$=i^{-1}\int_{\frac{1}{2}(1+it)}^{\frac{1}{2}(1-it)}\{[1/(1-\rho)]-(4/s)\rho\}d\rho, \quad \text{(A11)}$$

where use is made of the relation

$$i\theta=\ln\rho-\ln(1-\rho)+(2/s)(1-2\rho)$$

and the path of the integration of (A11) is clockwise around the point $\rho=1$. Therefore (A11) is shown to be equal to $2\pi-\Theta_1$ Thus we have

$$\int_{\Theta_1}^{2\pi-\Theta_1}k(\theta)d\theta=1. \quad \text{(A12)}$$

Above the critical temperature $s>1$, we can express $k(\theta)$ near $\theta=\Theta_1$ by

$$k(\theta)\propto[\,|\theta|-\Theta_1]^{\frac{1}{2}}+\cdots, \quad \text{for} \quad \pi>|\theta|\geq\Theta_1,$$

$$k(\theta)=0, \quad \text{for} \quad |\theta|<\Theta_1. \quad \text{(A13)}$$

However at the critical temperature $s=1$, this expansion cannot be allowed, since the coefficient of $(|\theta|-\Theta_1)^{\frac{1}{2}}$ becomes infinite. Simple calculation yields near $\theta=0$,

$$k(\theta)=(3/4\pi)(12)^{-1/6}|\theta|^{1/3}+\cdots. \quad \text{(A14)}$$

APPENDIX B. ON THE ANALYTIC CONTINUATION OF $\phi(\xi,\sigma)$

The function $\phi(\xi,\sigma)$ defined by

$$\phi(\xi,\sigma)=\sum_n\xi^n/n^\sigma \quad \text{(B1)}$$

is expressed by an integral for $|\xi|<1$ and $\Re\sigma>0$ as follows,[25]

$$\phi(\xi,\sigma)=\Gamma(\sigma)^{-1}\int_0^\infty\frac{\xi p^{\sigma-1}}{e^p-\xi}dp \quad \text{(B2)}$$

$$=\Gamma(\sigma)^{-1}\left[\int_1^\infty[(\zeta-\xi)^{-1}-(1/\zeta)](\ln\zeta)^{\sigma-1}d\zeta\right], \quad \text{(B3)}$$

where $\Gamma(\sigma)$ is the gamma function. Therefore the analytic continuation of this function to $\xi>1$ has a branch cut from $\xi=1$ to $+\infty$ on the real axis. If we denote the first branch of $\phi(\xi,\sigma)$ by $\phi_1(\xi,\sigma)$ and the second branch obtained by going counterclockwise around $\xi=1$ by $\phi_2(\xi,\sigma)$, we have from Eq. (B3)[26]

$$\phi_2(\xi,\sigma)=\phi_1(\xi,\sigma)-[2\pi i/\Gamma(\sigma)](\ln\xi)^{\sigma-1}. \quad \text{(B4)}$$

Thus $\phi_2(\xi,\sigma)$ has a singularity at $\xi=0$. Especially, we have for $\xi<1$,

$$\phi_2(\xi,\tfrac{5}{2})=\phi_1(\xi,\tfrac{5}{2})-[2\pi/\Gamma(\tfrac{5}{2})][\ln(1/\xi)],^{\frac{3}{2}} \quad \text{(B5)}$$

$$\phi_2(\xi,\tfrac{3}{2})=\phi_1(\xi,\tfrac{3}{2})+[2\pi/\Gamma(\tfrac{3}{2})][\ln(1/\xi)]^{\frac{1}{2}}. \quad \text{(B6)}$$

Both functions $\phi_1(\xi,\frac{5}{2})$ and $\phi_1(\xi,\frac{3}{2})$ are finite at $\xi=1$, and the derivative of $\phi_1(\xi,\frac{5}{2})$ at $\xi=1$ is finite, while that of $\phi_1(\xi,\frac{3}{2})$ at $\xi=1$ is infinite. The behaviors of $\phi(\xi,\frac{5}{2})$ and $\phi(\xi,\frac{3}{2})$ against ξ are shown schematically in Figs. 7 and 8.[27] By eliminating ξ from $\phi(\xi,\frac{5}{2})$ and $\phi(\xi,\frac{3}{2})$ we have $\phi(\xi,\frac{3}{2})$ as a function of $\phi(\xi,\frac{3}{2})$, which is drawn schematically in Fig. 9. There is no singularity of $\phi(\xi,\frac{5}{2})$ on the positive real axis of $\phi(\xi,\frac{3}{2})$ except at infinity.[28]

The physical meanings of $\phi(\xi,\frac{5}{2})$ and $\phi(\xi,\frac{3}{2})$ are the pressure and the density (except factors depending on temperature) of an ideal Bose gas and the value ϕ_c of $\phi(\xi,\frac{3}{2})$ which gives the maximum of $\phi(\xi,\frac{5}{2})$ corresponds to the density at the condensation point. Thus if we plot p against $v=1/\rho$ in an ideal Bose gas, the isotherm will be given schematically by the full curve in Fig. 10 and the dashed curve is the analytic continuation of the equation of state in the gaseous region. The analytic continuation of the isotherm of the gaseous phase tends to $-\infty$ as $v=1/\rho$ approaches zero; ρ_c gives the point of condensation,[29] contrary to the case of real gases discussed in the text.

---

[25] E. T. Whittaker and G. N. Watson, *A Course of Modern Analysis* (Cambridge University Press, New York, 1927), p. 280; C. Truesdell, Ann. Math. **46,** 144 (1945).

[26] H. S. Shapiro, Phys. Rev. **99,** 1673 (1955).

[27] See also J. E. Robinson, Phys. Rev. **83,** 678 (1951); J. Clunie, Proc. Phys. Soc. (London) **A67,** 632 (1954).

[28] See works cited in reference 25 and B. Widom, Phys. Rev. **76,** 16 (1954).

[29] In this connection see S. Katsura, Progr. Theoret. Phys. (Kyoto) **16,** 589 (1956).

Infrared Spectra of Acetylene and Acetylene Derivatives Adsorbed on Alumina and Silica

D. J. C. YATES* AND P. J. LUCCHESI

Esso Research and Engineering Company, Linden, New Jersey

(Received December 9, 1960)

An infrared study of adsorbed acetylenes has revealed several features of the nature and orientation of the adsorbed species. Acetylene, deuteroacetylene, methyl acetylene, and dimethyl acetylene are strongly chemisorbed at room temperature on alumina. Weak chemisorption also occurs with acetylene, deuteroacetylene, and methyl acetylene. The strongly held acetylene is held normal to the surface, while the weakly held acetylene is held parallel to the surface. Similar effects occur with methyl acetylene, all of the strongly held molecules being attached to the surface by the acetylenic end. Both the strongly and weakly adsorbed dimethyl acetylene is adsorbed parallel to the surface. The sites responsible for the strong chemisorption of dimethyl acetylene are different from those active in the strong chemisorption of acetylene. With silica, no strong chemisorption occurred at room temperature for either acetylene or dimethyl acetylene. For both adsorbents, the interaction between the OD (and OH) groups of the surface and the adsorbates has been studied. Exchange takes place between the highest frequency OH groups on alumina and the strongly adsorbed C_2D_2. An OD group at the expected frequency was observed after the exchange had taken place. The remaining two types of OH groups on alumina did not appear to interact with the strongly held species, but only with the weakly held species. With dimethyl acetylene, the silica OD groups interacted to much the same degree as did the two lower frequency alumina OD groups.

1. INTRODUCTION

ALTHOUGH alumina and alumina-based catalysts are very widely used, most adsorption studies on these solids have been restricted to organic adsorbates of high molecular weight. In particular, as far as we can determine, no detailed data have been published on the chemisorption of acetylene on alumina by either classical adsorption techniques or by more recent methods. However, detailed information on the chemisorption of such hydrocarbons would be of obvious value in understanding the catalytic properties of aluminas.

Infrared spectra of adsorbed molecules give direct information about the nature and orientation of the surface species, which cannot readily be obtained with other methods. In this paper, the infrared method has been used to investigate the interaction between eta alumina and acetylene and its derivatives. It has been found that both acetylene and methyl acetylene are strongly chemisorbed, and are oriented normal ("end-on") to the surface. A much weaker interaction using the same adsorbates has also been found at higher pressures, which can best be classified as weak chemisorption. Such molecules are probably adsorbed parallel to the surface. Dimethyl acetylene is strongly chemisorbed to sites on the surface which are not the same as those which are active in the "end-on" adsorption of acetylene. The dimethyl acetylene is not held "end-on," and seems to be adsorbed parallel to the surface. All the above molecules interact in varying ways with the residual OH (and OD) groups of the alumina, and this interaction is also discussed.

Some studies have also been made of the adsorption of acetylene and dimethyl acetylene on silica; no strong chemisorption could be detected in either case.

2. EXPERIMENTAL

Materials

The alumina used was donated by the Morton Chemical Company, Woodstock, Illinois, and was designated "super-pure alumina." No details of its method of manufacture are known. X-ray analyses carried out in this laboratory showed it to be beta trihydrate[1] as supplied. After heating in air at 600°C for four hours, it gave an x-ray pattern characteristic of eta alumina. Its surface area (B.E.T. method) after heating was 190 m^2/g. Some experiments were conducted with silica (Cabosil HS5) supplied by the Cabot Company, Boston, of surface area 340 m^2/g.

To put the alumina in a form suitable for infrared examination, small quantities of the material, as received, were pressed in a 1-in. die at 16 000 lb/in.^{2}. The "thickness" of the resulting disks was about 0.02 g/cm^2. The piece which was used for the experiments described in this paper was 0.019 g/cm^2 thick, weighed 0.022 g and was 1.9×0.6 cm in size. The silica was pressed at 2000 lb/in.^{2}, and was 0.016 g/cm^2 thick.

Acetylene and methyl acetylene were supplied by the Matheson Company, and purified by distillation. The infrared spectra of the acetylene, in a 10-cm cell at a pressure of 9 cm, showed no impurities. The main impurity in the methyl acetylene was acetylene. The purification was continued until no sign of the strong ν_5 band (for notation, see reference 2) of acetylene could be detected at a pressure of 52 cm, in a 10-cm cell.

* School of Mines, Columbia University, New York 27, New York. Now at the National Physical Laboratory, Teddington, Middlesex, England.

[1] A. S. Russel, *Alumina Properties* (The Aluminum Company of America, Pittsburgh, Pennsylvania, 1956).

[2] G. Herzberg, *Infrared and Raman Spectra of Polyatomic Molecules* (D. Van Nostrand Company, Inc., New York, 1945).

TABLE I. Slit widths and resolution as a function of frequency in wavenumbers.

Frequency (cm^{-1})	Slit width (mm)	Resolution[a] (cm^{-1})
3300	0.44	2.9
3200	0.49	3.0
3100	0.55	3.1
3000	0.61	3.2
2900	0.81	3.8
2850	0.97	4.3
2780	0.62	3.9
2700	0.58	3.5
2600	0.60	3.3
2400	0.64	2.9
2150	0.68	2.4
2000	0.44	2.2
1900	0.39	1.8
1700	0.43	1.5
1600	0.46	1.4
1500	0.55	1.4
1400	0.63	1.4
1300	0.82	1.4
1200	1.25	1.8

[a] Calculated from data given in maker's handbook.

Dimethyl acetylene as supplied by the Air Reduction Company, contained slightly more methyl than dimethyl acetylene. The impure gas was frozen at 195°K with a solid carbon dioxide and successively distilled into a trap at 77°K until the remaining material showed no ν_1 band of methyl acetylene, using a pressure of 48 cm in a 10-cm cell. Despite this, small amounts of methyl acetylene were detected in the adsorbed phase after adsorbing dimethyl acetylene. A gas chromatogram of the purified material showed that there was one part of methyl acetylene in 2×10^4 parts of dimethyl acetylene. Deuterium was supplied by the General Dynamics Corporation, of San Carlos, California, and was stated to be greater than 99.5% pure. Before use, it was dried by passage through a trap at 77°K. Deuteroacetylene (C_2D_2) was supplied by the New England Nuclear Corporation, Boston, with a purity greater than 99%, and was used as received.

Apparatus

The cell was a dual cell, one end being made of barium fluoride windows (2 cm apart) attached to a Pyrex tube. The other end of the cell was made of fused silica and joined by a silica-to-Pyrex seal. The cell could be rotated on a greased cone joint to slide the sample from the silica end, for evacuation at elevated temperatures, to the window end. The thin sample was held parallel to the flat windows by flattening the main tube of the cell and extending it down into the wider tube between the windows. Before the wide tube was sealed on, a slot 5 mm wide was cut in the end of the main tube to permit infrared radiation to pass through the cell. The volume of the cell, to stopcocks, was 32.3 cm^3, and the volume of the manometer and connecting tubing, 106.6 cm^3.

The vacuum system consisted of a mechanical backing pump, a metal oil diffusion pump, and a trap cooled with solid carbon dioxide. Dynamic vacua of about 10^{-7} mm were recorded on the Veeco (Alpert type) ionization gauge.

A Beckman IR 7 double-beam grating spectrometer was used, with two mirror systems providing two external foci. The cell was placed at one of these, and wire gauges were put in the other beam to balance the energy in the two beams. Wider slits than normal had to be used to compensate for these losses. The alumina transmitted about 30% of the incident radiation from 1000–2000 cm^{-1}, decreasing at higher wavenumbers quite markedly. At 4000 cm^{-1}, about 2% was transmitted. The slit widths (in mm) and resolution (in cm^{-1}) used in the main regions of interest are given in Table I.

Procedure

After inserting the samples in the cell, they were evacuated and heated slowly to 600°C. Evacuation for one hour gave vacua in the region of 5×10^{-6} mm. The spectrum of the sample was then run from 4000–1100 cm^{-1}. The sample was then reheated to 600°C while pumping, and treated with deuterium at 600°C. Pressures in the region of 50–40 cm were used, and deuteration was continued until all the surface OH groups were replaced with OD groups. This required one to two hours. The deuterium was evacuated for 15 min to a final vacuum of about 5×10^{-6} mm. After cooling down in vacuo, the adsorbate was admitted, and the spectrum run as before. Spectra on desorption were recorded in a similar fashion.

3. RESULTS

Figure 1 shows the spectra obtained with acetylene in the CH stretching region. The band at 3300 cm^{-1} [a in Fig. 1(a)] which appears after the first dose is adsorbed is caused by the strongly held acetylene. The 3220 cm^{-1} band, due to the weakly adsorbed acetylene, appears only at pressures above 0.5 cm, and continues to grow over the entire pressure range used. At the two highest pressures, both the 3300 and 3220 cm^{-1} bands are overlapped by the ν_3 band of the gas phase acetylene. The spectra in Fig. 1(a) have not been corrected for this effect, but this introduces a perceptible error in intensities only at the highest pressure used. Before evacuating, the pressure was reduced by expanding the gas in the cell into the manometer, and

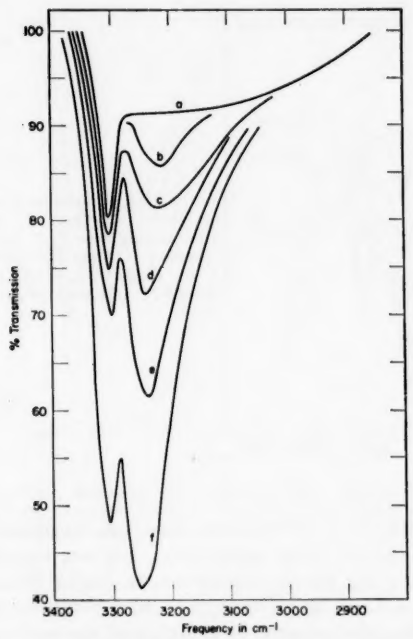

FIG. 1(a). Adsorption of acetylene. Pressures in cm Hg; a, 0.20; b, 0.59; c, 1.31; d, 3.11; e, 6.45; and f, 14.80.

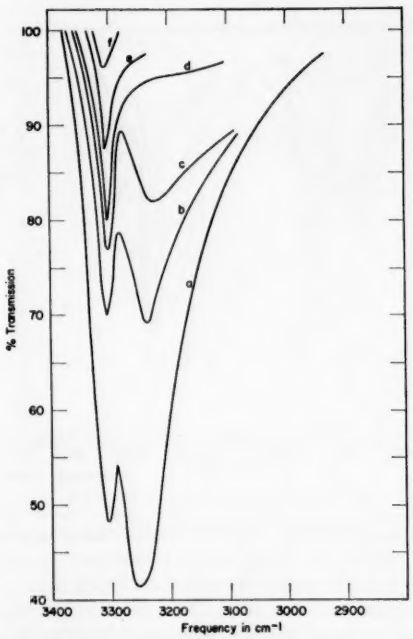

FIG. 1(b). Evacuation of acetylene. Pressure in cm Hg; a, 14.80; b, 3.94; c, 1.08. Evacuation for: d, 5 sec at room temperature; e, 10 min at 100°C; and f, 10 min at 200°C.

spectra run [b and c in Fig. 1(b)]. In one case [c, Fig. 1(b)], the pressure was quite close to one used on adsorption, and there is quite a close agreement between the spectra, showing the reversible nature of the adsorption. Evacuation for 5 sec (d) removed all of the

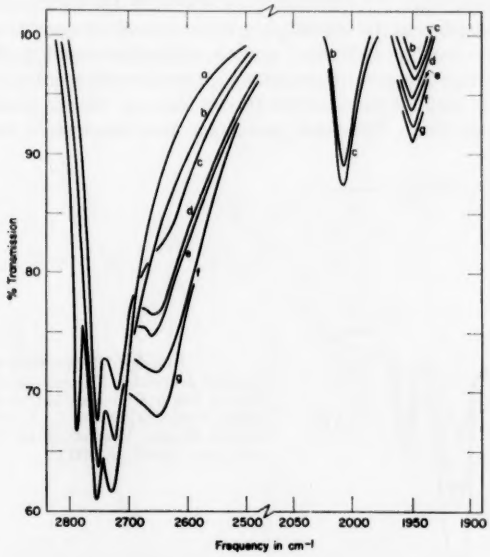

FIG. 2(a). Adsorption of acetylene. Spectra: a, after deuterium treatment at 600°C. Pressures after adsorption in cm Hg: b, 0.20; c, 0.59; d, 1.31; e, 3.11; f, 6.45; and g, 14.80.

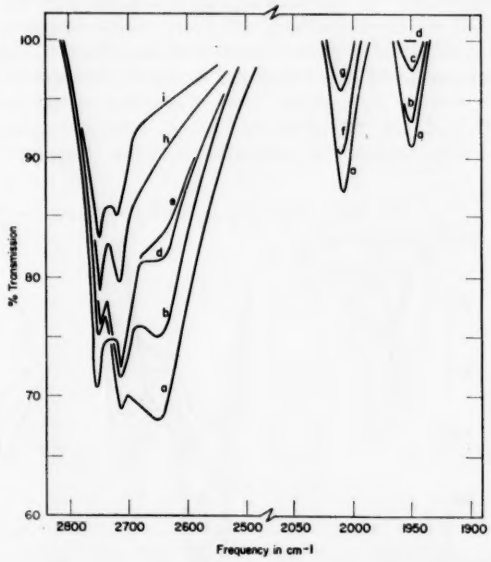

FIG. 2(b). Evacuation of acetylene: Pressure in cm Hg: a, 14.8; b, 3.94; c, 1.08. Evacuation at room temperature for d, 5 sec, and e, 5 min. Evacuation for 10 min at: f, 100°; g, 200°; h, 300°; and i, 600°C.

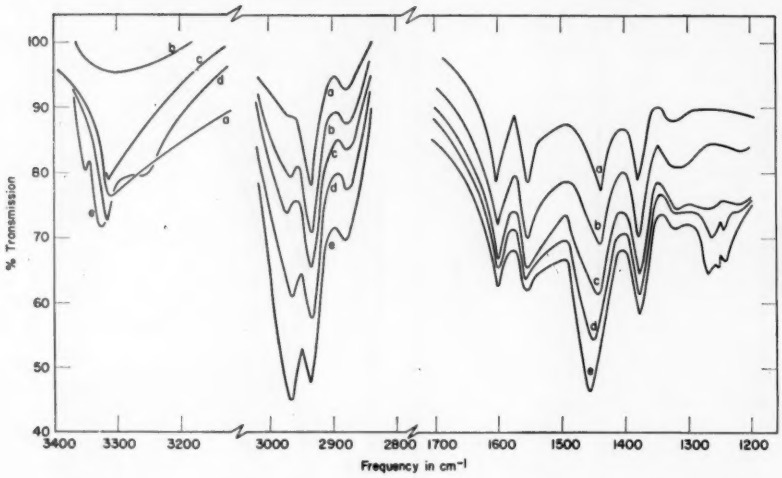

FIG. 3(a). Adsorption of methyl acetylene. Spectrum a, shortly after adding dose 1; b, next day (pressure 0.16 cm Hg). Doses 2, 3, and 4, spectra c, d, and e, pressures 0.53, 1.51 and 3.00 cm.

molecules giving the 3220 cm^{-1} band. After evacuation for 10 min at 300°C, no band at 3300 cm^{-1} remained.

Figure 2 shows the OD and C≡C stretching regions of the spectrum. On adding the first dose, the high-frequency OD band was removed, and the other two OD bands weakened. This weakening continued on adding more acetylene, but spectra have been omitted at pressures above 1 cm to avoid overlapping on the figure. The 2007 cm^{-1} ν_2 band did not change in position or intensity at pressures above 1 cm, but the 1950 cm^{-1} ν_2 band increased in intensity over the whole pressure range used. On evacuation [Fig. 2(b)], the 2650 cm^{-1} band was removed (b, d, and e) at room temperature. The 2755 and 2720 cm^{-1} bands were unaffected by this, but weakened on evacuation at higher temperatures (h and i). The spectra after evacuation at 100° and 200°C, in the 2800–2600 cm^{-1} region, were quite similar to that obtained by evacuation at room temperature (e). The ν_2 band at 2007 cm^{-1} was unaffected by evacuation at room temperature, but was completely removed by 10-min evacuation at 300°C. The 1950 cm^{-1} ν_2 band, in contrast, was markedly affected by reducing the pressure (b and c), and was entirely removed (d) by 5-sec evacuation at room temperature. Very similar effects in the ≡C—H and C≡C regions were found on adding acetylene to a surface having only OH groups.

For methyl acetylene, on adding the first dose, marked changes with time were found in the 3300 cm^{-1} region of the spectrum [a and b, Fig. 3(a)]. Although adsorption was continuing, as shown by the increase in intensity of the bands in the remainder of the spectrum, the band at 3300 cm^{-1} became weaker on standing. At higher pressures (spectrum e), considerable overlap of the band of the adsorbed species and ν_1 in the gas phase took place. The peak percentage transmissions of the

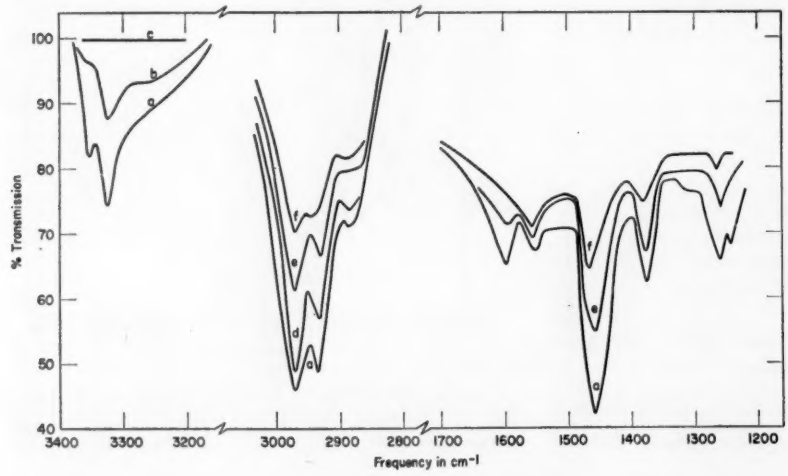

FIG. 3(b). Evacuation of methyl acetylene. Pressure in cm Hg: a, 3.0; b, 0.93. Evacuation at room temperature for c, 5 sec, and d, 30 min. Evacuation for 10 min at: e, 100°C; f, 200°C.

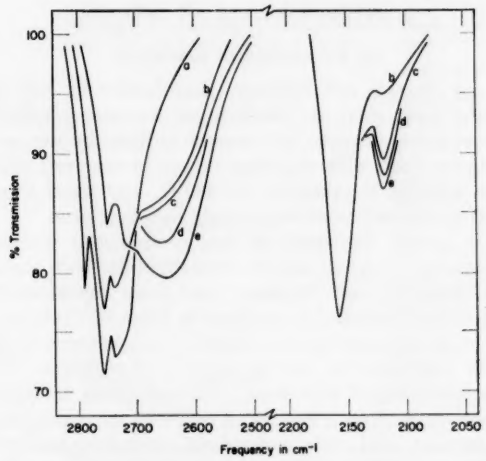

FIG. 4(a). Adsorption of methyl acetylene. Spectra: a, after deuterium treatment at 600°C. Pressures after adsorption in cm Hg: b, 0.16; c, 0.53; d, 1.51; and e, 3.00.

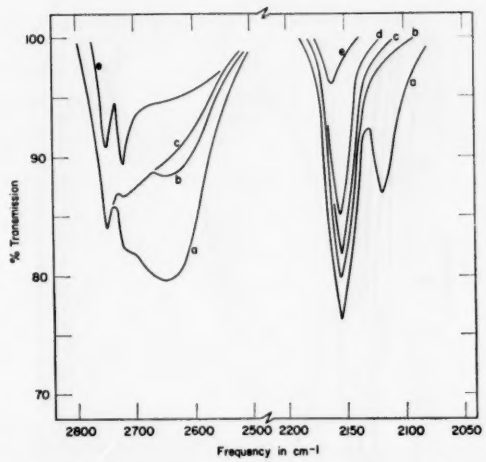

FIG. 4(b). Evacuation of methyl acetylene. Pressure in cm Hg: a, 3.00. Evacuation at room temperature for b, 5 sec and c, 30 min. Evacuation for 10 min at: d, 100°; and e, 200°C.

P and R branches of ν_1 in the gas phase were about 82% at 3.00 cm. The 3300 cm^{-1} band is produced by weakly held molecules, as a small reduction in pressure [Fig. 3(b), b] weakens the band considerably and a short evacuation (c) removes it entirely. This treatment weakened the bands a little in the 3000–2800 and 1700–1200 cm^{-1} regions, but these spectra have been omitted to avoid overlapping. Evacuations at 100° and 200°C removed quite large amounts of the methyl acetylene, and it was nearly all removed by evacuation for 10 min at 300°C.

Figure 4 shows the OD and C≡C stretching regions. Generally similar effects occur in the OD region on adsorbing methyl acetylene as occur with acetylene. The spectra for the second and third dose (c) and (d) are intermediate in the 2800–2690 cm^{-1} region between those of the first and fourth doses (b) and (e) and have been omitted for clarity. The ν_3 band at 2155 cm^{-1} did not change in position or intensity when the second and subsequent doses were adsorbed, but a pressure dependent band at 2120 cm^{-1} appeared. On evacuation at room temperature, the 2650 cm^{-1} band was removed. Evacuation at 100°C gave a spectrum in the 2800–2500 cm^{-1} region which was similar to (c) and has been omitted to avoid overlap. All the modified OD groups were removed by evacuation at 300°C. The ν_3 band at 2120 cm^{-1} was all removed by the first evacua-

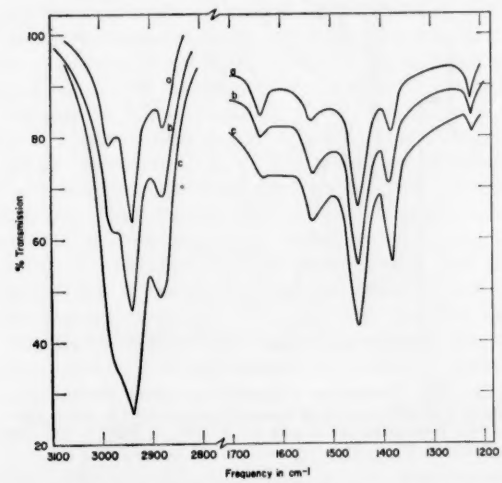

FIG. 5(a). Adsorption of dimethyl acetylene. Pressure in cm Hg: a, 0.08; b, 0.56; and c, 1.48.

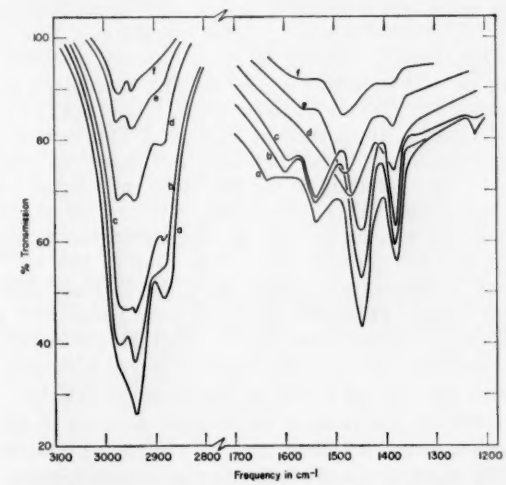

FIG. 5(b). Evacuation of dimethyl acetylene. Pressure in cm Hg: a, 1.48. Evacuation at room temperature for b, 5 sec, and c, 26 min. Evacuation for 10 min at: d, 200°; e, 300°; and f, 400°C.

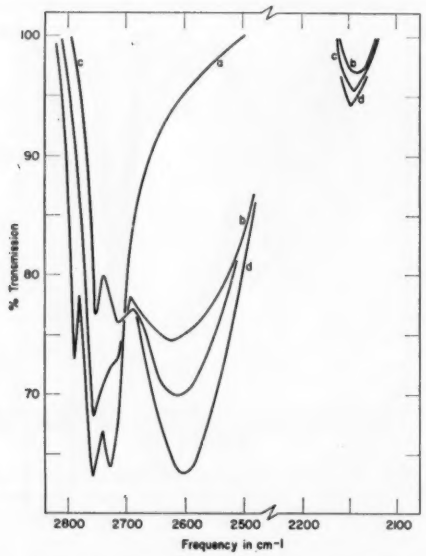

FIG. 6(a). Adsorption of dimethyl acetylene. Spectra: a, after deuterium treatment at 600°C. Pressures after adsorption in cm Hg: b, 0.08; c, 0.56; and d, 1.48.

tion (b), and the 2155 cm^{-1} band was gradually removed at higher temperatures until at 300°C it was gone.

On adsorbing dimethyl acetylene [Fig. 5(a)] the bands did not change in position as the pressure was increased. On evacuation above room temperature [Fig. 5(b), d, e, and f], the bands at 1600 and 1540 cm^{-1} disappeared, and the band at 1450 cm^{-1} moved to 1480 cm^{-1} (f). This change has not been investigated in detail, but is probably due to some decomposition of the adsorbed species at higher temperatures. Evacuation at 600°C removed all of the dimethyl acetylene. In the OD stretching region, the first dose added removed the 2790 cm^{-1} band entirely [b, Fig. 6(a)], but also gave a strong band at 2620 cm^{-1}. This increased in intensity at higher pressures and moved to 2600 cm^{-1}. The spectrum in the 2800–2680 cm^{-1} region for the last dose (d) is quite similar to that of the second dose (c). Evacuation at room temperature for 26 min [c, Fig. 6(b)] removed all of the band at 2600 cm^{-1} and at temperatures above 200°C the 2755 and 2720 cm^{-1} bands weakened. At 600°C, these bands were a little weaker than those shown at (g). It is of interest to note that the 2720 cm^{-1} band is removed more easily than the 2755 cm^{-1} band. A weak band at 2145 cm^{-1}, caused by the ν_3 vibration of small amounts of adsorbed methyl acetylene, grew with increasing pressure [Fig. 6(a), b, c, and d]. Evacuation at room temperature [Fig. 6(b)] did not affect this band, and it was only slightly weakened by evacuation at 100°C (d). Evacuation at 200°C (e) removed it completely.

4. INTERPRETATION OF SPECTRA

(a) Adsorption of Acetylene

(i) *Strongly held acetylene.* Examination of Figs. 1 and 2 shows there are two forms of acetylene adsorbed on alumina. One can be removed entirely by evacuation for 5 sec, while the other cannot be removed until the alumina is evacuated at 300°C. The latter form will be referred to as the strongly held acetylene.

A general discussion of the infrared and Raman spectra of acetylene and its derivatives has been given by Sheppard and Simpson,[3] and some fundamental vibrational frequencies are given in Table II. Combination and overtone bands are usually weak in comparison with fundamentals, but in the case of acetylene and monosubstituted acetylenes, they are often intense.[2] Strongly held acetylene has a ≡C—H stretching frequency at 3300 cm^{-1}, and a C≡C stretching band at 2007 cm^{-1} (Table II), but has no band which can be ascribed to the combination band ($\nu_4+\nu_5$) in the region scanned (4000–1100 cm^{-1}). The lack of a band in the adsorbed phase due to $\nu_4+\nu_5$ is surprising, as this band is a strong one in the infrared spectra of the gas[3] at 1328.1 cm^{-1} and is also present at 1407 cm^{-1} in crystalline acetylene.[4] Its absence is in agreement with the idea that the acetylene is held "end-on" to the alumina, as discussed below.

The triple-bond stretching vibration ν_2 is forbidden in the infrared spectra of gaseous acetylene by the sym-

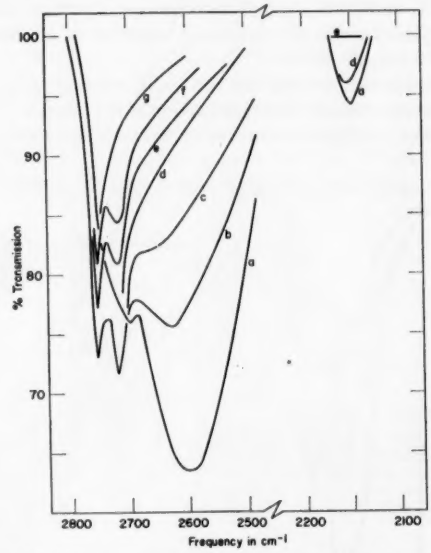

FIG. 6(b). Evacuation of dimethyl acetylene. Pressure in cm Hg: a, 1.48. Evacuation at room temperature for b, 5 sec, and c, 26 min. Evacuation for 10 min at: d, 100°; e, 200°; f, 300°; and g, 400°C.

[3] N. Sheppard and D. M. Simpson, Quart. Revs. **6**, 1 (1952).
[4] E. Krikorian, Ph.D. thesis, Columbia University, 1957.

TABLE II. Frequencies in wavenumbers of bands in gaseous, liquid, and adsorbed acetylene and deuteroacetylene.

Molecule	Phase	≡C—H (or ≡C—D) stretching frequency in cm^{-1}	Activity ref.	C≡C stretching frequency in cm^{-1}	Activity ref.
C_2H_2	Gas	3287	ν_3, I,[a]		
	Gas	3373.7	ν_1, R,[b]	1973.8	ν_2, R,[b]
	Liquid	3341	ν_1, R,[c]	1961	ν_2, R,[c]
	Anisotropic single crystal	3263	ν_3, I,[d]		
	Adsorbed strongly held	3300	ν_3(?), I	2007	ν_2, I
	Weakly held	3220	ν_3, I	1950	ν_2, I
C_2HD	Gas	3334.8 (CH)	ν_1, I, R,[b]	1851.2	ν_2, I, R,[b]
	Gas	2584 (CD)	ν_3, I,[a]		
C_2D_2	Gas	2700.5	ν_1, R,[b]	1762.4	ν_2, R,[b]
	Gas	2427	ν_3, I,[a]		
	Adsorbed strongly held	2570	ν_3(?), I	1890	ν_2, I
	Weakly held	2410	ν_3, I	1740	ν_2, I

[a] G. Herzberg, *Infrared and Raman Spectra of Polyatomic Molecules* (D. Van Nostrand Company, New York, 1945).
[b] G. Glocker and C. E. Morrell, J. Chem. Phys. **4**, 15 (1936).
[c] G. Glocker and M. M. Renfrew, J. Chem. Phys. **6**, 340 (1938).
[d] E. Krikorian, Ph.D. thesis, Columbia University, 1957.

metry of the molecule. The change in selection rules implied by ν_2 being infrared active in the adsorbed phase is capable of several interpretations, and cannot in itself be used to deduce information about the orientation of the adsorbed molecules. Similar changes in selection rules have been observed[5] even when methane and hydrogen are physically adsorbed. They are probably due to the asymmetrical electrical fields present at many solid surfaces.

However, the positions of the C≡C and ≡C—H stretching bands in the adsorbed acetylene gives information about the mode of attachment of the acetylene. Table II shows that the ≡C—H stretching band occurs in the adsorbed phase at 3300 cm^{-1}. This value is intermediate between ν_3 in gaseous acetylene (3287 cm^{-1}) and the corresponding ≡C—H vibration (ν_1) in methyl acetylene[6] and monodeuteroacetylene.[2] Both the above monosubstituted acetylenes have very similar ν_1 frequencies (3334 and 3334.8 cm^{-1}), as do other monosubstituted acetylenes.[3,7,8] Resonance between two identical CH oscillators in C_2H_2 (and C_2D_2) produces a symmetrical (ν_1, R) CH stretching vibration and an asymmetric (ν_3, I) CH stretching vibration. When this resonance is removed[2] by monosubstitution, only one infrared active ≡C—H stretching vibration remains (ν_1). On liquefying methyl acetylene, ν_1 decreases to 3305 cm^{-1}. This frequency is very close indeed to that of the relatively narrow ≡C—H band of the adsorbed acetylene. Therefore, the observed frequency and width of the band of the strongly chemisorbed species points to an essentially free CH group, and implies that the species contains a C≡C—H group oriented normal to the surface.

If the contrary assumption is made, i.e., that the strongly held acetylene is held parallel to the surface, both hydrogens would be affected by van der Waal's forces, and ν_3 would be expected to be a few tens of wavenumbers lower than in the gas phase. Similar effects are expected on liquefying acetylene, and occur in the Raman spectrum for ν_1 (Table II). No value for ν_3 in liquid acetylene seems available, but in crystalline acetylene,[4] it is at 3263 cm^{-1}.

The change in C≡C stretching frequency on adsorption also provides information on the orientation of adsorbed acetylene. If the hydrogen in acetylene is successively replaced by deuterium,[2] the C≡C frequency decreases first by 122.6 cm^{-1}, and on disubstitution, by 211.4 cm^{-1}. These decreases are to be expected, as the mass of the end groups is increased with very little change in any of the force constants. However, if the mass of the end groups is increased by 15 by replacing the hydrogens by methyl groups, the C≡C frequency increases by 168.4 and 259.2 cm^{-1} for methyl acetylene[6] and dimethyl acetylene,[9] respectively. This increase cannot be attributed solely to changes in the C≡C force constants, as it has been shown[10] that they are quite close to those of acetylene. Further increase of mass of the end groups above 15 seems to have little effect, as the C≡C frequency in monosubstituted[3,11] acetylenes occurs in the region 2140–2100 cm^{-1}, and in disubstituted acetylenes[3,11] in the region 2260–2190 cm^{-1}. Furthermore, it is the same in CD_3CCH [8] as in CH_3CCH. It is well known that it is

[5] N. Sheppard and D. J. C. Yates. Proc. Roy. Soc. (London) **A238**, 69 (1956).
[6] D. R. J. Boyd and H. W. Thompson, Trans. Faraday Soc. **48**, 493 (1952).
[7] N. Sheppard, J. Chem. Phys. **17**, 74 (1949).
[8] M. T. Christensen and H. W. Thompson, Trans. Faraday Soc. **52**, 1439 (1956).
[9] I. M. Mills and H. W. Thompson, Proc. Roy. Soc. (London) **A226**, 306 (1954).
[10] B. L. Crawford and S. R. Brinkley, J. Chem. Phys. **9**, 69 (1941).
[11] L. J. Bellamy, *The Infrared Spectra of Complex Molecules* (Methuen and Company, Ltd., London, 1958), 2nd ed.

an approximation to consider ≡C—H and C≡C stretching vibrations in a molecule such as acetylene as separate entities, ignoring the effects of the vibrations of the molecule as a whole. In most molecules similar assumptions are often unobjectionable, but in acetylene and deuteroacetylenes this is not the case, as quite a strong interaction occurs between C—H and C≡C vibrations (see reference 2, p. 196). This forces the C≡C frequency in acetylene down from its true "diatomic" value.[3] The C≡C frequency in C_2HD is 1851.2 cm^{-1}, and in methyl acetylene is 2142.1 cm^{-1}. Hence, the C≡C frequency in the adsorbed phase (2007 cm^{-1}) is consistent with the lower end of the molecule having an "effective" mass between 2 and 15. The adsorbed species may consist of an undissociated acetylene molecule with the lower hydrogen strongly interacting with a surface atom (Su), H—C≡C—H———Su, or be of the type H—C≡C⁻ or H—C≡C—Su. (See later discussion.)

No bands corresponding to the Su———H or H—C≡ vibrations in the Su———H—C≡ complex were detected (Su represents a surface atom). As most alumina surfaces are energetically heterogeneous, the Su———H bonds probably have a range of energies. This would give a range of Su—H stretching frequencies, and a broad absorption band. Little is known about the frequency of such bands, but they are expected to be below 1000 cm^{-1}. The sample used here becomes opaque at about this frequency. These effects on the Su—H bond would also be expected to affect the CH bond in the Su———H—C≡ complex, giving a range of CH stretching frequencies, and hence, a broad absorption band.

On adding C_2D_2 to the same sample of alumina, the strongly held molecules absorbed at 2570 and 1890 cm^{-1}.

No C≡C or ≡C—H bands due to strongly held acetylene were observed on silica. Pressures of up to 15 cm were used, and the 4000–1700 cm^{-1} region was scanned. This observation agrees with earlier work[5] on thicker silica samples, where only physical adsorption of acetylene was observed.

(ii) *Weakly held acetylene.* As the pressure of acetylene is increased, bands appear at 3220 and 1950 cm^{-1} and then increase in intensity [Figs. 1(a) and 2(a)]. No band with intensity similar to that of ν_3 was detected which would correspond to the combination band $\nu_4+\nu_5$ in the adsorbed phase. Although there was quite a strong overlap in the 1380–1280 cm^{-1} region from the gas phase acetylene at the highest pressure used, a band of greater than 10% absorption would have been detected. The band at 3220 cm^{-1} is very broad, indicating that the ν_3 vibration in the molecules producing this band is perturbed to varying degrees by the adsorption forces. This is consistent with such data as are available on the surface heterogeneity of aluminas. The 1950 cm^{-1} ν_2 band is similar in width to the 2007 cm^{-1} band of the strongly held acetylene. The molecules producing both bands at 3220 and 1950 cm^{-1} can be entirely removed from the surface by evacuation for 5 sec. Such a very weak interaction with the surface indicates that physical adsorption might be present. This seems rather unlikely, however, as the vapor pressure of acetylene at room temperature is 40 atm. The highest relative pressure used here is 4.8×10^{-3}. Another indication of the weak attachment is shown in Fig. 2(b), where the ν_2 band is shown as the pressure is reduced from 14.8 to 3.9 cm, and then to 1.1 cm. Similar changes take place in ν_3 [Fig. 1(b)]. Such complete reversibility is more often associated with physical adsorption than with strong chemisorption, indicating that this is probably an instance of weak chemisorption.

Both ν_2 and ν_3 have frequencies below the corresponding vibrations in gaseous acetylene. The C≡C stretching frequency falls from 1973.8 to 1762.4 cm^{-1} on going from C_2H_2 to C_2D_2 and is at 1950 cm^{-1} in the adsorbed phase. Similar effects occur with the CH stretching frequency. This has an average value of 3330.3 cm^{-1} in C_2H_2 and an average value of 2563.7 cm^{-1} in C_2D_2 and is at 3220 cm^{-1} in adsorbed acetylene. These changes are about twice as large as those occurring on liquefaction. In this case, ν_2 decreases by 12.8 cm^{-1} relative to the gas, and ν_1 by 32.7 cm^{-1}. No data for ν_3 of the liquid seem to be available, but in the crystalline state[4] it is at 3263 cm^{-1}, a decrease of 24 cm^{-1}.

The weakly held acetylene molecules have been perturbed considerably more by adsorption than they are by liquefaction, but the magnitude of the forces involved is probably similar in both cases. It is considered likely that this form of adsorbed acetylene is held flat on the surface.

For silica, a very small amount of acetylene was weakly adsorbed, with ν_3 at about 3265 cm^{-1}. This band could only be detected at a pressure of 15 cm by the following method. The gas plus adsorbed phase showed the *P* branch of the resolved ν_3 band to be stronger than the *R* branch. After moving the sample out of the beam, the gas phase only was scanned, using the same slit width (0.26 mm at 3300 cm^{-1}) as before. The *P* branch (at 3265 cm^{-1}) was then weaker than the *R* branch (at 3315 cm^{-1}). This indicates that a weak band at about 3265 cm^{-1} is present in the adsorbed phase. Some broadening of the OH and OD groups present on the silica occurred at this acetylene pressure (15 cm), but this effect, and the band at 3265 cm^{-1}, were entirely removed by evacuation for 5 sec. No bands in the region 2200–1700 cm^{-1}, where a band due to the ν_2 vibration might occur, were detected at any pressure. On a thick (2.8 mm) sample of porous glass, a weak ν_3 band at 3255 cm^{-1} was detected[5] on adding acetylene at room temperature. This agrees with the observations made here on a thinner sample of Cabosil and may indicate that silica shows relatively little variation in its strength of adsorption of acetylene at room temperature.

(b) Adsorption of Methyl Acetylene

(i) *Strongly held methyl acetylene.* As observed with acetylene, two forms of adsorbed methyl acetylene occur. The strongly held methyl acetylene cannot be removed until the alumina is evacuated at 300°C. Table III shows the relevant fundamental and overtone bands of methyl acetylene using Herzberg's notation.[2] Methyl acetylene is asymmetrical along the C≡C axis and the C≡C stretching vibration (ν_3) is infrared active in this molecule.

By analogy with acetylene, it was expected that the strongly held methyl acetylene would be attached normal to the surface by its acetylenic end. Figure 3(a) [spectrum (a)] shows that on adding the first dose of gas, a broad asymmetric band is found at 3300 cm^{-1}, in the region of the observed ν_3 band of adsorbed acetylene. On standing overnight, this band was reduced in absorption to about 5% [spectrum (b)]. This indicates that, on attaining equilibrium, the ≡C—H bonds of almost all of the molecules adsorbed from the first dose are strongly interacting with the surface. Confirmation of this can be obtained from the CH stretching frequencies of the methyl groups in the adsorbed molecules. For the first dose, bands at 2880 and 2930 cm^{-1} were present, together with a broad band at about 2980 cm^{-1}. These values are close to those found in the Raman spectra of the liquid[12] for $2\nu_7$, ν_2, and ν_6. This indicates that the methyl groups are only perturbed to a relatively small extent.

The evacuation experiments offer further evidence for the end-on attachment. In Fig. 3(b), the band at 3300 cm^{-1} was entirely removed by evacuation for 5 sec, while leaving quite a strong band due to methyl groups. The ν_1 band of methyl acetylene is entirely absent in the strongly held molecules, and yet the coverage is sufficient to give quite strong bands due to methyl groups. The spectra of gaseous methyl acetylene, taken with the same slit width as that used for studying the adsorbed phase, shows that the integrated intensity of the ν_1 band is greater than that of the combined bands due to ν_6, ν_2, and $2\nu_7$. The entire absence of ν_1 in the strongly held methyl acetylene when ν_6, ν_2, and $2\nu_7$ are strong, proves conclusively that such molecules interact with the surface very strongly through their acetylenic ends.

The ν_3 frequency of the strongly held methyl acetylene agrees with this assignment. While ν_3 in the weakly held methyl acetylene is at 2120 cm^{-1}, 22 cm^{-1} lower than in the gas phase, in the strongly held methyl acetylene it is at 2155 cm^{-1}, 13 cm^{-1} higher than the gas phase. On increasing the mass of the acetylenic hydrogen to 2, ν_3 decreases to 2060 cm^{-1} in CH_3CCD.[13] Further increase of mass to 15 on going to dimethyl acetylene increases the triple bond stretching frequency[9] to 2233 cm^{-1}. Hence, the C≡C frequency in strongly adsorbed methyl acetylene is again consistent with the lower end of the molecule having an effective mass greater than 2, but less than 15.

[12] G. Glocker and H. M. Davis, J. Chem. Phys. **2**, 881 (1934).
[13] R. J. Grisenthwaite and H. W. Thompson, Trans. Faraday Soc. **50**, 213 (1954).

TABLE III. Frequencies in wavenumbers of bands in gaseous, liquid, and adsorbed methyl acetylene

Band	Activity			*I*, Adsorbed	
	I, gas,[a]	*R*, gas,[b]	*R*, liquid,[c]	Strongly held	Weakly held
ν_1	3334.0		3305.0		3300
ν_2	2941.0	2941	2926.2	2940	2935
ν_3	2142.2	2142	2123.5	2155	2120
ν_4	...	...	1382.2	1375	1375
ν_6	3008.3	...	2971.0	2970	2970
ν_7	1452.0	...	1448.0	1460	1460
$2\nu_7$	2881.0	...	2867.0	2880	2880
$2\nu_9$	1255.0	...	...	1260	1260
?	...	...	...	1600	...
?	...	...	...	1555	...

[a] D. R. J. Boyd and H. W. Thompson, Trans. Faraday Soc. **48**, 493 (1952).
[b] G. Glocker and F. T. Wall, Phys. Rev. **51**, 529 (1937).
[c] G. Glocker and H. M. Davis, J. Chem. Phys. **2**, 881 (1934).

Figure 3 shows that there are two quite strong bands at 1600 and 1555 cm^{-1} on adding the first dose of methyl acetylene. These bands do not seem to increase in intensity on adding more methyl acetylene, although they might appear to do so from a cursory examination of Fig. 3(a). There is quite a large general lowering of transmission in the region 1700–1200 cm^{-1} with increasing methyl acetylene pressure. The 1600 and 1555 cm^{-1} bands are not removed by evacuation at room temperature, but are both removed at 100°C and replaced by one band at 1560 cm^{-1} [Fig. 3(b)]. This latter band persists even on evacuation to 600°C. The infrared and Raman spectra of methyl acetylene in this region have no bands which can be plausibly assigned to the 1600 and 1555 cm^{-1} bands in the adsorbed phase. Apart from a medium intensity combination band[2] at 1515 cm^{-1}, no bands at all are reported in the 1700 to 1500 cm^{-1} region,[2,6,12] and it is possible that these bands are due to some dissociation fragment of methyl acetylene.

On silica, no experiments were carried out with methyl acetylene.

(ii) *Weakly held methyl acetylene.* Little can be deduced from the methyl stretching or bending frequencies about the orientation of the weakly held methyl acetylene, since the bands overlap with those of the strongly held methyl acetylene. Slight differences can be detected in ν_2, but no difference could be observed in the ν_4, ν_6, ν_7, $2\nu_7$, and $2\nu_9$ bands.

A band at 3300 cm^{-1} is seen on adding dose 2 [Fig. 3(a)], which moves to 3320 cm^{-1} at higher pressures. For the highest pressure used, the position of this band

TABLE IV. Frequencies in wavenumbers of bands in gaseous, liquid, and adsorbed dimethyl acetylene.

Band	Activity	Gaseous[a]	Liquid[a]	Adsorbed
ν_1	R	...	2916	...
ν_2	R	...	2233	...
ν_3	R	...	1380	?
ν_6	I	2938	...	2940
ν_7	I	1382	...	1380
ν_9	I	2973	...	2970
ν_{10}	I	1456	...	1450
ν_{13}	R	...	2966	...
ν_{14}	R	...	1448	?
$\nu_{10}+\nu_{14}$	I	2875	...	2880
$\nu_{12}+\nu_{15}(b)$	I	1215	...	1220
?	I	...	...	1600
?	I	...	...	1640
?	I	...	...	1540
?	I	...	...	1320

[a] I. M. Mills and H. W. Thompson, Proc. Roy. Soc. (London) **A226**, 306 (1954).
[b] G. Herzberg, *Infrared and Raman Spectra of Polyatomic Molecules* (D. Van Nostrand Co., New York, 1945).

is uncertain due to overlap by ν_1 of the gas phase molecules. The band at 3300 cm^{-1} is produced by the ν_1 vibration of the adsorbed molecules, and is 5 wavenumbers lower than the same band in the Raman spectra of the liquid. These shifts on adsorption are quite close to those of ν_3 in weakly held acetylene, and indicate the presence of perturbations similar to those occurring on liquefaction.

The triple bond stretching vibration (ν_3) of this species is at 2120 cm^{-1} in the adsorbed phase. This can be seen by its growth on increasing the pressure [Fig. 4(a)] and its removal on evacuation for 5 sec [Fig. 4(b)]. This frequency is 21 cm^{-1} lower than that in the gas phase, and 3.5 cm^{-1} lower than in the liquid phase. These shifts are very similar to those found with ν_2 of weakly held acetylene.

It is considered that the weakly held methyl acetylene is held sideways on the surface. The forces of adsorption are greater, but of the same magnitude, as those present in liquids.

The data for ν_3 of the methyl acetylene in Fig. 4(a) for dose 1 [spectrum (b)] are those calculated from the spectra recorded after the system had been standing overnight. Immediately after admitting dose 1, ν_3 at 2155 cm^{-1} had 80.0% transmission, and ν_3 at 2120 cm^{-1} had 90.6% transmission. This confirms the idea that during the attainment of equilibrium of the first dose of methyl acetylene, some of the molecules which had been weakly held desorb, and re-adsorb in the end-on configuration. This explains the increase in the 2155 cm^{-1} band and the decrease in the 2120 cm^{-1} band on standing.

(c) Adsorption of Dimethyl Acetylene

From the results with acetylene and methyl acetylene, it seemed that the C≡C bond in these molecules did not interact strongly with the alumina. The molecules, held flat to the surface, which would be expected to have triple bonds interacting most strongly with the surface, could all be removed by a brief evacuation at room temperature.

As dimethyl acetylene has no acetylenic hydrogen, the sites on the alumina which interact with the strongly held acetylene would not be expected to interact with this gas. If the triple bond in dimethyl acetylene interacted with the surface in the same fashion as does the triple bond in acetylene, the sideways held dimethyl acetylene would be easily desorbed. This was not found to occur. Dimethyl acetylene was strongly adsorbed, and to some extent weakly adsorbed. In contrast with acetylene and methyl acetylene, there is no band in the spectrum which is characteristic of strongly held species. The only way in which weakly held dimethyl acetylene can be detected is by the decrease in absorption of all the bands that takes place on evacuation.

Figure 5(a) shows that CH stretching bands occur at 2875, 2940, and 2985 cm^{-1} on adding the initial dose, and remain at similar frequencies on adding more gas. These bands are at frequencies close to those of $\nu_{10}+\nu_{14}$, ν_6, and ν_9 in the gas phase.[9] For the bending modes, bands at 1450 and 1380 cm^{-1} were found, at frequencies quite close to ν_{10} and ν_7. It is possible that ν_{14} and ν_3 (normally only Raman active) are infrared active in the adsorbed phase. If so, they would not be expected to be distinguishable from the bands due to the ν_{10} and ν_7 vibrations.

Although the bands of the adsorbed molecules are close to the values found for gaseous dimethyl acetylene (Table IV), the adsorbed species could not be removed until temperatures of 400°C were used [Fig. 5(b)]. No band due to a triple bond stretching frequency[9] (ν_2, at 2233 cm^{-1}) was found over the pressure range used here. This could be understood if the adsorbed molecules were lying sideways on the surface and any interaction with the triple bond was symmetrical. Such a configuration would not necessarily change the selection rules, and ν_2 could remain Raman active only.

The appearance of ν_3 of methyl acetylene in the adsorbed phase (Fig. 6) provides evidence that the sites which hold dimethyl acetylene strongly are not those with which acetylenic hydrogens interact. Despite purification of the dimethyl acetylene to the point where the dimethyl:methyl ratio was 2×10^4:1, a band of 3% absorption was found at 2150 cm^{-1} on adding the first dose. This strengthened on further addition, giving a band with 6% absorption at the highest pressure

used [Fig. 6(a)]. No other bands due to methyl acetylene were observed. However, apart from ν_1 at about 3300 cm^{-1}, they would be masked by the much more intense bands of the dimethyl acetylene. For strongly held methyl acetylene, ν_1 is absent from the region 3400–3100 cm^{-1}.

To further determine the nature of the sites responsible for adsorbing the strongly held dimethyl acetylene, acetylene was pre-adsorbed on a deuterated alumina sample. Sufficient acetylene was added to saturate the sites responsible for the strongly held acetylene, and some weakly held acetylene was also present. The latter was removed completely by evacuation for three minutes, and then dimethyl acetylene adsorbed. The doses used were nearly the same as those used in Figs. 5 and 6 and the bands found were similar in frequency and intensity to those found before, with the exception that no band at 2150 cm^{-1} was observed. Evidently, occupying the sites which have a strong affinity for acetylenic hydrogen does not affect the subsequent adsorption of dimethyl acetylene. The only effects on the pre-adsorbed acetylene were that the 2007 cm^{-1} ν_2 band became weaker and shifted to 2005 cm^{-1} after the dimethyl acetylene was adsorbed.

When dimethyl acetylene was added to silica, weak bands at 2870 and 2935 cm^{-1} were observed. The gas phase dimethyl acetylene overlapped so strongly from 2950 to 3050 cm^{-1} that it is uncertain whether a band at 2980 cm^{-1} (ν_9) was present. No band at 1450 cm^{-1} was detected; the region scanned was 4000–1400 cm^{-1}. Despite the small amount of dimethyl acetylene adsorbed, strong interaction with the OH and OD groups of the silica took place. Well-defined peaks were found at 3500 and 2600 cm^{-1}, the corresponding unperturbed OH and OD bands being at 3750 and 2765 cm^{-1}. The 2600 cm^{-1} band is at a similar frequency to that found on alumina (Fig. 6). In addition, a very weak band was found at 2232 cm^{-1}, probably corresponding to ν_2. At the highest pressure used (2.83 cm) the 2232 cm^{-1} band had a peak absorption of 3%. The presence of ν_2 when dimethyl acetylene is adsorbed on silica is surprising, as no band was found under the same conditions on alumina. Since the dimethyl acetylene is quite strongly chemisorbed on the alumina used here, this observation indicates that it is not the strength of adsorption *per se* which determines whether ν_2 is permitted in the infrared, but rather the detailed topography of the particular surface (or OH groups) concerned, and the detailed way in which the adsorbed molecules are oriented on the surface.

(d) Interaction of Adsorbed Molecules with OD Groups

Figures 2, 4, and 6 show that, after deuterium treatment, the alumina used in this work has three distinct OD stretching frequencies (2790, 2755, and 2735 cm^{-1}). Bands at generally similar frequencies have been found on alumina gel by Peri.[14] This is in contrast to silica, where most specimens examined seem to have one OH peak[15] at about 3750 cm^{-1}, and a corresponding OD peak at 2765 cm^{-1}. The significance of three OD (and OH) frequencies on alumina is not yet clear, and this point will not be discussed here.

The first dose of acetylene added [Fig. 2(a)] interacts so strongly with the groups producing the 2790 cm^{-1} band that this band is removed from the spectrum. If a strong hydrogen bond is formed between the 2790 cm^{-1} OD groups and the acetylene, a broad band at lower frequencies would result. A general lowering of transmission between 2680 and 2500 cm^{-1} was observed after adding dose 1, which may be due to this hydrogen bonding. However, the 2755 and 2735 cm^{-1} OD bands are also weakened on adding the first dose, and hydrogen bonding with these groups may also contribute to the band in the 2680 to 2500 cm^{-1} region. At higher pressures, a definite band at 2650 cm^{-1} is seen. This is due to hydrogen bonding between the weakly held acetylene and the two lower frequency OD groups, as shown by Fig. 2. Evacuation for 5 sec removes a considerable fraction of the band at 2650 cm^{-1}, while increasing the intensity of the 2755 cm^{-1} band. The 2715 cm^{-1} band decreases in intensity, but this is probably due to the removal of the overlap with the 2650 cm^{-1} band which was present before evacuation. The 2790 cm^{-1} OD band does not reappear, however, even when the sample is evacuated at 600°C. Above 200°C, the 2755 and 2715 cm^{-1} bands decrease in intensity. This removal of the OD groups is probably due to their exchange into OH groups, as the OD groups are quite stable, in vacuum, at 600°C. The hydrogen used in this exchange may have come from the residual strongly held acetylene.

It seems likely that the OD groups producing the 2790 cm^{-1} band interact mainly with the strongly held acetylene. Their continued absence even after evacuation at 600°C may indicate that they exchanged with the hydrogen in the strongly held acetylene, giving an OH group at about 3780 cm^{-1}. However, no detailed spectra were taken in the OH stretching region after adding the acetylene. To investigate this, in one of the C_2D_2 experiments the surface was treated with hydrogen before adding the deuteroacetylene, leaving no OD groups on the alumina. This gave OH bands at 3785, 3745, and 3710 cm^{-1}. On adding the first dose of C_2D_2, which was nearly all strongly adsorbed, an OD band at 2785 cm^{-1} grew, and the OH band at 3785 cm^{-1} became much weaker. Thus within 15 min a considerable number of the 3785 cm^{-1} OH groups had exchanged with deuterium from the C_2D_2. No ≡C—H stretching bands at 3300 cm^{-1} were seen after this change had taken place, while a ≡C—D band at 2570

[14] J. B. Peri, paper presented at the Second International Congress on Catalysis, Paris, July 4–9, 1960.
[15] R. S. McDonald, J. Phys. Chem. **62**, 1168 (1958).

cm^{-1} was detected. This indicates that the following surface exchange has taken place.

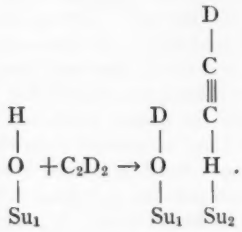

The adsorbed C_2HD may be held on an adjacent site. Su_2 different from that holding the OD group, as shown, or the C_2HD may be attached to the same site. As the ν_2 frequency in gaseous C_2HD is 89 cm^{-1} higher than that in gaseous C_2D_2, it might be expected that ν_2 for adsorbed C_2HD (held by the H end) would be different from ν_2 in adsorbed C_2D_2. This is not necessarily correct, since C_2HD where the H has an "effective" mass above 2 (but less than 15) would probably have a ν_2 band at a frequency close to that of C_2D_2 with one D having an effective mass above 2.

To eliminate the possibility that the strong ν_2 band at 1890 cm^{-1} found on adsorbing C_2D_2 might all be due to the formation of C_2HD by exchange, C_2D_2 was added to a surface treated with deuterium until only OD groups were present. The strongly adsorbed C_2D_2 still gave a band at 1890 cm^{-1}. If the C_2HD formed by exchange was held by the D end, a $\equiv$C—H band at 3300 cm^{-1} would be present, and ν_2 would be expected to occur close to 2007 cm^{-1}. No bands at 3300 and 2007 cm^{-1} were observed at any time on adding C_2D_2 to the alumina.

Similar effects were found with the OD groups on adding methyl acetylene (Fig. 4). In the methyl acetylene, as with acetylene, the 2650 cm^{-1} band is due to an interaction between the triple bond of the weakly adsorbed molecules and the two lower frequency OD groups.

Removing all the OD groups from the alumina by evacuation at 900°C for 20 min did not seem to affect the strength of attachment of the strongly held acetylene. After adding the same amount of acetylene as previously used, the ν_2 and ν_3 bands were at the same frequency as before, but were a little weaker. This latter effect may have been due to sintering of the alumina during its evacuation at 900°C. At higher pressures, ν_3 of the weakly held acetylene was at the same frequency as before, and of similar intensity at any given acetylene pressure. The 1950 cm^{-1} ν_2 band was markedly decreased in intensity. Thus, the appearance of ν_2 for the weakly held acetylene is connected with the presence of OD (or OH) groups on the alumina surface. The ν_2 vibration of the strongly held acetylene is permitted, to some considerable extent, by its orientation normal to the surface, and it is not surprising that this band is unaffected by the removal of the OD groups.

The silica used contained about equal numbers of OH and OD groups, giving bands at 3750 and 2765 cm^{-1}. Adding acetylene to this surface gave no definite band corresponding to that at 2650 cm^{-1} found with alumina at a pressure of 14.8 cm [Fig. 2(a), (g)]. At the maximum pressure used with the silica (15.1 cm) weak shoulders extending from 2720 to 2620 cm^{-1} and from 3720 to 3500 cm^{-1} were seen. These were entirely removed on evacuating the sample for 5 sec.

Much more interaction with the OD groups on alumina occurred on adsorbing dimethyl acetylene [Fig. 6(a)]. As before, the 2790 cm^{-1} band was entirely removed, but a strong band due to hydrogen bonding at 2620 cm^{-1} was found after adding the first dose. This became stronger on adding more dimethyl acetylene, and moved to 2600 cm^{-1}. Compared with methyl acetylene, the 2620 cm^{-1} band was more difficult to remove at room temperature, but the spectra taken after evacuation at higher temperatures were quite similar. These effects may be due to the higher boiling point of dimethyl acetylene as compared to methyl acetylene. Quite a significant amount of physical adsorption is expected to occur at the pressures used with dimethyl acetylene.

With silica, on adding the first dose of dimethyl acetylene, strong bands due to hydrogen bonding were observed at 3550 and 2615 cm^{-1}. At the highest pressure used (2.83 cm) these bands moved to 3510 and 2600 cm^{-1}. The bands were considerably weakened on evacuation for 5 sec and were entirely removed by evacuation for 3 min. Evidently the strength of the hydrogen bonding between the weakly held dimethyl acetylene and OD groups is to a large extent independent of the substrate to which the OD groups are attached.

In summary, the surface OH (or OD) groups interact with all adsorbed species and some are capable of chemical exchange with the hydrogen of the acetylenes. They do not, however, seem to be essential for the strong interaction with acetylenes. Their presence seems very important for the weak interaction between the surface and acetylene.

5. CONCLUSIONS

On alumina it has been determined that:

1. Acetylene, methyl acetylene, and dimethyl acetylene are chemisorbed at room temperature.

2. For all adsorbates, both strong and weak adsorbent-adsorbate interactions occur.

3. The strongly chemisorbed species from acetylene are held normal to the surface, while the weakly chemisorbed acetylene molecules are held flat on the surface. Deuteroacetylene has similar adsorption characteristics.

4. The strongly chemisorbed species from methyl

acetylene are also held normal to the surface. The weakly chemisorbed methyl acetylene molecules are held parallel to the surface.

5. Both the strongly chemisorbed and weakly held dimethyl acetylene are adsorbed parallel to the surface.

6. All the adsorbates interact strongly with the OD groups having the highest stretching frequency (2790 cm^{-1}). Both of the lower frequency OD groups interact to a smaller extent with the weakly held adsorbates. On adding C_2D_2, exchange took place with the OH groups having the highest frequency, forming 2790 cm^{-1} OD groups.

On silica it has been found that:

1. Neither acetylene or dimethyl acetylene is strongly adsorbed at room temperature.

2. On adding acetylene, little interaction with the OH and OD groups occurred. A very small amount of weakly held acetylene was found.

3. Hydrogen bonding between the OH and OD groups of the silica and weakly held dimethyl acetylene was observed. The shifts in frequency were similar to those found under the same conditions on alumina.

The adsorption of organic molecules on surfaces such as oxides has been discussed from several points of view. For example, concepts of surface "acidity" and adsorbate "basicity" have been used in which the precise nature of the acidity and basicity is not elucidated but can be of the form reminescent of ordinary solution chemistry. In these approaches, the oxide or solid can be considered an acid in the Bronsted sense (proton donor) or the Lewis sense (acceptor of an electron pair). The adsorbate then behaves as a base by accepting a proton to form "carbonium" and other ions or by donating an electron pair to form a coordinate covalent bond. In addition to this essentially chemical language describing the adsorption process, one recognizes the more physical descriptions involving electronic effects, defects of various types, etc. In the case of the systems discussed in this paper, it seems more instructive to discuss the adsorption in the chemical language.

Acetylene ranks among the hydrocarbons as relatively acidic, being capable in some reactions of losing one of its acidic protons. At the carbon-carbon triple bond, however, the system of pi electrons can be considered "basic" in the sense of being essentially nucleophilic. The introduction of two methyl groups into the acetylene molecule would, of course, eliminate the site of proton acidity and, by "inductive" effects, render the C≡C site more nucleophilic. With regard to the adsorbent, one can consider the aluminum sites in alumina as acidic since they seek an electron pair and the oxygen sites as basic since they can donate an electron pair. If this is correct, the "acidic" acetylene would be expected to interact with the basic oxygen sites. The surface hydroxyl groups may be proton donors ($Su-OH \rightarrow SuO^- + H^+$) or proton acceptors ($Su-OH + H^+ \rightarrow Su-OH_2^+$), depending upon the adsorbate and other factors (Su is a surface atom). In any case, their interaction with adsorbents having chemically acidic or basic properties is straightforward, at least in principle.

In this language, the strong chemisorption of acetylene can involve an acid-base reaction,

$$HC{\equiv}CH + :\ddot{O}\text{-}Su \longrightarrow HC{\equiv}C^{\ominus}\overset{\oplus}{H} :O\text{-}Su$$

although it remains an open question whether any $HC{\equiv}C^{\ominus}$ species formed then remain attached to the same site as the proton, or attain greater stability by moving to some other electron-deficient site.

The weak interaction between acetylene and silica must then be interpreted in terms of a decreased electron-donating ability of the oxygen sites in silica relative to alumina. Similarly, the substitution of methyl for hydrogen, forming dimethyl acetylene, is observed to give stronger lateral chemisorption and no end-on chemisorption. This could be rationalized from the increased nucleophilic character of the triple bond which should give stronger interaction with acidic surface sites of the proton type

$$(Su-OH) \text{ or Lewis type } (Su-\ddot{\underset{\ddot{}}{Al}}).$$

No end-on interaction was detected between the surface and dimethyl acetylene, a fact which seems reasonable in the light of the removal, by methyl substitution, of acidic acetylenic hydrogens.

Although the essentially chemical description given is undoubtedly an over-simplification, it accounts in a qualitative way for the observations and it is the best one can do in the light of what is currently known about these processes. The catalytic effect of acidic oxides in promoting ionic organic reactions is well known and has been discussed with some success in terms of acid-base interactions and ionic intermediates. From this point of view, the adsorption of unsaturated hydrocarbons on oxides can at least be qualitatively understood.

ACKNOWLEDGMENTS

We wish to thank Mr. D. L. Baeder, Esso Research and Engineering Company, for helpful discussions and encouragement. Thanks are also due to Professor R. S. Halford of Columbia University, for advice on some spectroscopic aspects of this work.

Shock Wave Studies by Mass Spectrometry. I. Thermal Decomposition of Nitrous Oxide

J. N. BRADLEY* AND G. B. KISTIAKOWSKY

Gibbs Chemical Laboratory, Harvard University, Cambridge, Massachusetts

(Received August 13, 1959)

An apparatus is described in which the reacting gas behind a reflected shock wave is sampled continuously and analyzed at intervals of 50 or 100 μsec by a time-of-flight mass spectrometer. The thermal decomposition of N_2O in the temperature range 1780–2000°K has been used as a test case to demonstrate that the experimental technique is valid. It has also been shown that the mechanism and rate constants of this reaction at high temperatures are consistent with earlier measurements at much lower temperature.

THE rapid, homogeneous temperature rise through a shock front has proved invaluable in studying the kinetics of fast reactions, but up to the present, the very short times available have seriously limited the choice of analytical techniques. In the majority of previous experiments, a spectroscopic method has been used, and it has been necessary to study species having high extinction coefficients.[1,2]

The time-of-flight mass spectrometer has already been shown to combine short resolution times (50 μsec) with the ability to follow the concentrations of several species simultaneously.[3] In the present experiments, it has been used to follow reactions behind reflected shock waves by allowing the reacting gas to flow directly into the instrument. It has been possible to identify reaction intermediates and to measure rate constants of elementary steps at high temperatures.

APPARATUS

The operating principles of the Bendix-type time-of-flight mass spectrometer have been described previously.[4] They may be summarized as follows: Ions are formed in a bunch by a pulsed electron beam; and the ions are then accelerated by a pulsed grid into a field-free drift tube. Because the ion velocities depend on the charge to mass ratios, the bunch separates into groups of different e/m as it moves down the tube. The time between the accelerating pulse and the arrival of each of the mass resolved groups at the ion-multiplier detector is proportional to $M^{\frac{1}{2}}$ for ions of the same charge. The detector output is displayed on an oscilloscope which is triggered by the accelerating pulses. Successive oscilloscope sweeps display complete mass spectra of the sample at repetition rates of 10 or 20 kc/sec. The sweeps are photographed individually by a rotating-drum camera and thus the concentrations of various ions measured as functions of time. The instrument used in the present research is described in the work cited in reference 3. It has been modified slightly to increase its sensitivity and mass resolution. The oscilloscope and rotating-drum camera have been improved to provide more legible photographic records, but this remains one of the major sources of random experimental error. The reaction cell which was used in the earlier experiments has been replaced by the downstream end of the shock tube. The end wall of the shock tube, which is also the ground electrode of the mass spectrometer, supports the sample leak. This is a piece of 0.001 in. thick gold foil with a 0.005-in. diam hole in its center. The sample gas flows directly from the shock tube, where the pressure is approximately 0.4 atm after shock wave reflection, into the mass spectrometer ion source, where the pressure is maintained at approximately 10^{-6} atm. The gas is ionized after it has traveled a distance of 1 mm from the leak. A block diagram of the apparatus is shown in Fig. 1.

The experimental section of the shock tube consists of a 1 m length of ½ in. i.d. Pyrex tubing and a 1 m length of ½ in. i.d. stainless-steel tubing, both with a tolerance of 0.002 in. on the inside diameter. The latter tubing is fitted with six Pyrex inserts which support platinum-film resistance gauges used for shock velocity measurements.[5] The platinum strips, 2 cm long and 0.5 mm wide, have a resistance of 500 ohms and, when operated at 25 ma, they give signals of about 0.5 mv. These are amplified to about 36 v and their display on a single sweep of a raster oscilloscope is photographed. Owing to the location of the raster scope in another part of the building, it was necessary to make mass spectrometric analyses and velocity measurements in separate experiments.

The two sections of the experimental part of the shock tube are separated by a rotary valve with three settings: the first to permit replacement of the diaphragm without admitting air to the spectrometer; the second to enable the tube to be evacuated and filled with reactant gases; and the third to prevent side inlets from interfering with the shock wave.

The driver section of the shock tube consists of a

* Present address: The University of Liverpool, Department of Inorganic and Physical Chemistry, 8 Vine Street, Liverpool 7, England.

[1] G. Schott and N. Davidson, J. Am. Chem. Soc. **80**, 1841 (1958).

[2] H. B. Palmer and D. F. Hornig, J. Chem. Phys. **26**, 98 (1957).

[3] G. B. Kistiakowsky and P. H. Kydd, J. Am. Chem. Soc. **79**, 4825 (1957).

[4] W. C. Wiley and J. H. McLaren, Rev. Sci. Instr. **26**, 1150 (1955).

[5] V. H. Blackman, J. Fluid Mech. **1**, 61 (1956).

21.3 ft length of ½ in. i.d. seamless hydraulic steel tubing, 20 ft of which (because of space limitation) is coiled to a diameter of 3.3 ft. This extreme length is required to delay the arrival of the reflected expansion wave at the reflected shock region. The whole of the shock tube assembly is connected to a conventional mercury-pumped vacuum system and is evacuated to a pressure of 10^{-5} mm before each run.

One-thousandth inch cellophane diaphragms held between the driver and experimental sections by two Teflon gaskets are used and a small strip of aluminum foil adhering to the diaphragm surface is arranged to ground the input of a gating circuit when the diaphragm is pierced by a spring-actuated needle. The mass-spectrometer oscilloscope trace is kept off the screen by a potential bias on the input and the gating circuit is designed to remove the bias and return the trace to the screen for a period slightly less than one revolution of the drum camera.

EXPERIMENTAL PROCEDURE

To perform an experiment, the driver section is filled with hydrogen at a pressure of 400 to 700 mm and a previously prepared reaction mixture admitted to the experimental section at 2 to 10 mm pressure. A ballast flask is connected to this section until a few seconds before each run to keep the experimental pressure constant despite leakage through the pinhole. After focusing and alignment of the instrument, the trace is biased off the screen and, as soon as the drum camera reaches maximum rpm, the shock is initiated. Separate static experiments permit calibration of the mass peaks against the doubly charged argon peak, since argon is used as a diluent throughout.

In each series of runs the pressure difference across the diaphragm is held constant to better than 1% to obtain maximum reproducibility of the rupture. Separate velocity measurements are then made to determine the shock strengths for given diaphragm pressure ratios.

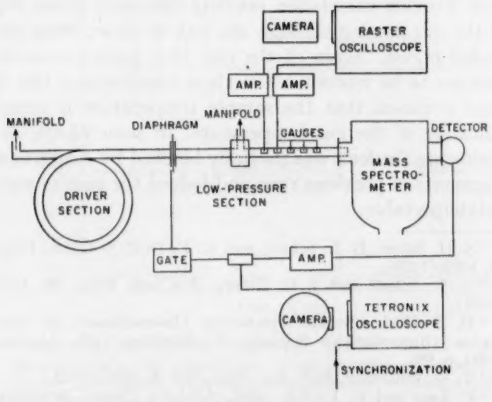

FIG. 1. Diagram of apparatus.

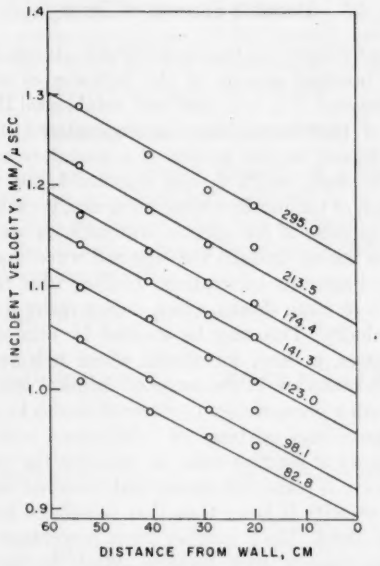

FIG. 2. A plot of logarithm of shock velocity against distance from end wall. Figures above the lines are diaphragm pressure ratios.

RESULTS

Calculation of the Shock Parameters

A knowledge of the shock velocity is required to determine the temperature and density of the gas behind the reflected wave prior to reaction. In the small-bore tubes used by necessity here, it was essential to make a correction for the attenuation of the wave as it travelled down the tube. The attenuation is described by $-du/dx = Au$ where u is the shock velocity, A is a constant, and x is the distance along the tube.[6] Thus, a plot of the logarithm of the velocity against distance should give a straight line. A series of such measurements is shown in Fig. 2, where the distance corresponding to each velocity is taken at the midpoint of two gauges. Although the scatter is quite high, reasonably reliable plots may be obtained since all such lines should be parallel, and, in general, errors due to inaccurate measurements of the time intervals should cause the points to alternate above and below the straight line. The velocity at the reflecting wall is then found by extrapolation. A plot of this velocity against bursting pressure ratio shows the maximum deviation from a smooth curve to be about 0.007 mm/μsec, corresponding to a deviation of 25°K in a typical reflected shock temperature. This is reassuring, since this plot depends on the intercepts at zero distance axis of Fig. 2 and none of the smoothing procedures above involved any foreknowledge of their values.

[6] R. N. Hollyer, Jr., J. Appl. Phys. **27**, 254 (1956).

Possible Sources of Error

Recently there has been considerable attention given to the nonideal aspects of the behavior of reflected shock waves.[7–10] It is by now well established that two types of phenomena may be encountered, both of which depend on the growth of a boundary layer on the tube wall, which is also responsible for the attenuation of the incident wave.[6] The first is that strong shocks in gases of low specific heat ratio do not reflect as plane waves. Instead the reflected wave undergoes what is known as bifurcation, dividing near the wall into two or more shocks, which do not move with uniform velocity. This may be avoided by dilution with noble gases, at least for shocks whose reflected temperature ratios are in the range of chemical interest.

The other phenomenon is observed in shocks in pure noble gases and mixtures of noble gases with small percentages of reactive ones. In this case the reflected shock wave is plane and moves with constant velocity, but its velocity is lower than that calculated from the incident shock Mach number by a percentage which increases linearly with incident Mach number[8] and depends on the tube parameters in the same way as the attenuation of the incident shock.[6,7] Combining the results of the works cited in references 7 and 8 on this phenomenon with the dimensions of our tube and a typical initial pressure and Mach number, one calculates that the reflected shock velocity should be some 25% less than that calculated from the extrapolated incident velocity.

Although the deficit in shock velocity is unquestionably a real effect, arising from interaction with the boundary layer behind the incident shock, its consequences on the estimation of reflected shock temperature are obscure.

Skinner has measured pressure ratios in argon shocks and finds reflected pressures near the end wall which are initially slightly below calculated ones, but which increase to or above the calculated value. In this laboratory W. Gardiner has measured reflected shock densities in xenon at temperatures of 6–8000°K and finds that they agree with those calculated initially, but rise gradually as the gas behind the reflected shock cools. If both results are correct, the temperature must be less than that calculated, although Skinner uses his results to argue that it will not be much less. It should be pointed out that the center of the end wall of the tube is certainly more likely to experience the expected reflected shock temperature as it is farthest from the boundary layer on the walls and the gas is definitely at rest at this point. This assertion is supported by previous investigations of chemical reactions behind reflected shock waves[8,11,12] in which the calculated temperatures allowed a sensible interpretation of the results. Where a chemically reacting system has been allowed to come to equilibrium behind the reflected shock wave, the final composition has always agreed with calculations based on the ideal reflected temperature.[13] In addition, spectroscopic measurements of the reflected temperature have confirmed calculations based on the incident velocity over a very wide range of conditions.[14]

As the reflected wave moves into gas which is meeting it at an increasing static pressure, due to the attenuation of the initial shock, the temperature may change, and as sampling proceeds this condition will confuse the issue still further.

Since these effects are difficult if not impossible to treat as a whole theoretically, the measured rate of a test reaction can serve as the best check on the validity of temperatures calculated on the basis of the one-dimensional theory, using extrapolated incident Mach numbers.

A related question is whether the gas sample flowing into the mass spectrometer is truly representative of the bulk composition behind the reflected shock. Two possible sources of error enter here.

The first of these is that the gas flowing through the leak may be at a lower than average temperature because of the heat conduction from the hot gas to the shock tube walls. The diameter of the leak is approximately 100 times the mean free path in the doubly shocked gas, which ensures hydrodynamic rather than effusive flow. This should induce a flow in the shocked gas and eliminate the boundary layer growing from the end wall of the shock tube near the leak. This view of the situation is made more probable by the fact that convection will be slow compared to the over-all duration of an experiment ($\frac{1}{2}$ msec at 2000°K) and that the presence of a cold surface stabilizes laminar flow.[15] Temperature profiles calculated on this basis for argon at 1800°C indicate that in this time appreciable cooling of the gas only takes place within 1 mm of the wall. Further calculation predicts that only about 3% of the gas passing through the leak is drawn from the cooled region. Again, if the rate of a known reaction appears to be reproduced in these experiments, this is good evidence that the sample temperature is representative of the gas temperature. In some of the experiments the leak was partially blocked by diaphragm fragments of previous runs and indeed the results were uninterpretable.

[7] J. P. Toennies and E. F. Greene, J. Chem. Phys. **26,** 655 (1957).
[8] R. A. Strehlow and A. Cohen, J. Chem. Phys. **30,** 257 (1959).
[9] G. Skinner, J. Chem. Phys. **31,** 268 (1959).
[10] H. Mark, J. Aeronaut. Sci. **24,** 304 (1957).
[11] S. H. Bauer, G. L. Schott, and R. E. Duff, J. Chem. Phys. **28,** 1089 (1958).
[12] G. L. Schott and J. L. Kinsey, J. Chem. Phys. **29,** 1177 (1958).
[13] H. S. Glick, *Seventh Symposium (International) on Combustion* (Butterworth's Scientific Publications, Ltd., London, 1959), p. 98.
[14] T. D. Wilkerson, Bull. Am. Phys. Soc. **5,** 362 (1960).
[15] L. Lees and C. C. Lin, Natl. Advisory Comm. Aeronaut. Tech. Mem. **1115** (1946).

The other possible difficulty is that the sample gas may suffer a number of collisions with the internal parts of the mass spectrometer before being ionized. This would spoil the time resolution of the measurements and make it impossible to observe very reactive species. Hydrodynamic flow through the leak assures that only a small fraction of the sample will collide with this surface. The mass spectrometer was specifically designed to minimize internal collisions and a rough calculation indicates that approximately half of the sample molecules leave the vicinity of the ionizing region without colliding with any internal parts. Of those which do suffer collisions only about 10% return to the ionizing region, and again 50% are removed permanently. Thus the probability of a molecule being ionized decreases rapidly with the number of collisions which it undergoes and it is unlikely that more than 10% of the ions arise from molecules which have struck the walls. Again the experimental evidence is the best proof that the data are reliable. The fact that it is possible to observe reactive intermediates and follow the progress of extremely fast reactions argues that the bulk of the sample is coming directly from the leak.

It is obvious from the above considerations that we need an appropriate test reaction to demonstrate that the apparatus functions properly despite the possible difficulties. The requirements on this reaction are that its mechanism and reaction rate at low temperatures be known, that it have a sufficient temperature coefficient to indicate the temperature of the gas sampled from behind the reflected shock wave, and that its mechanism include a free radical or atom. All three of these requirements are met by the thermal decomposition of N_2O, which has the additional advantage that all species involved are easily identifiable.

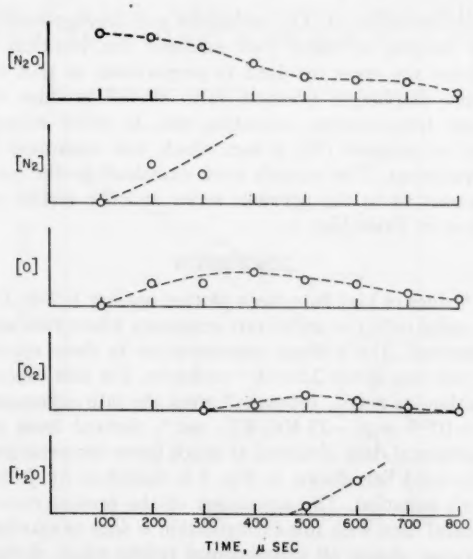

FIG. 3. A plot of peak heights (in arbitrary units) vs time. Each species is determined from its parent peak after correction for the contribution from other molecules, but without a correction for the relative sensitivity. The temperature in this experiment was 1872°K.

Thermal Decomposition of N_2O

This reaction is a classic example of a quasi-unimolecular decomposition and although it is possible that the high pressure limiting rate has never been attained, the literature data is voluminous and reasonably self-consistent.[16-20]

The mechanism is believed to be

$$N_2O \xrightarrow{k_1} N_2+O \qquad \Delta H_0^0=+38.3 \text{ kcal}, \quad (1)$$

followed by

$$O+N_2O \xrightarrow{k_2} N_2+O_2 \qquad \Delta H_0^0=-78.9 \text{ kcal}, \quad (2)$$

or

$$\xrightarrow{k_2'} 2\,NO \qquad \Delta H_0^0=-35.9 \text{ kcal}, \quad (2')$$

and later still by

$$NO+N_2O \xrightarrow{k_3} N_2+NO_2 \qquad \Delta H_0^0=-32.5 \text{ kcal} \quad (3)$$

$$NO_2+N_2O \xrightarrow{k_4} N_2+O_2+NO \qquad \Delta H_0^0=-7.5 \text{ kcal} \quad (4)$$

$$O+NO+M \xrightarrow{k_5} NO_2+M \qquad \Delta H_0^0=-71.4 \text{ kcal} \quad (5)$$

$$O+O+M \xrightarrow{k_6} O_2+M \qquad \Delta H_0^0=-117 \text{ kcal}. \quad (6)$$

Reactions (5) and (6) are not likely to be of importance in the present experiments because of the very short time available. Similarly no wall reactions are possible.

Johnston gives $k_1=4.4\times10^9 \exp(-57\,400/RT)$ sec^{-1} at an N_2O concentration of 2.5×10^{-6} mole/cc so that the activation energy provides a suitable test of the temperature of the gas sample. Oxygen atoms are an important intermediate in the mechanism. They are known to recombine fairly readily on metal surfaces,[21] the fraction of collisions which result in reaction being 5×10^{-3} for gold and 3×10^{-2} for iron and nickel, the materials of which the leak and the internal parts of the mass spectrometer, respectively, were made.

[16] N. Nagasako and M. Volmer, Z. physik. Chem. **B10,** 414 (1930).
[17] F. F. Musgrave and C. N. Hinshelwood, Proc. Roy. Soc. (London) **A135,** 23 (1932).
[18] H. S. Johnston, J. Chem. Phys. **19,** 663 (1951).
[19] F. Kaufman, N. J. Gerri, and R. E. Bowman, J. Chem. Phys. **25,** 106 (1956).
[20] C. P. Fenimore and G. W. Jones, J. Phys. Chem. **62,** 178 (1958).
[21] J. C. Greaves and J. W. Linnett, Trans. Faraday Soc. **54,** 1323 (1958); **55,** 1338 (1959).

TABLE I. Experimental results in nitrous oxide and argon.

Initial pressure (mm)	Incident velocity (mm/μsec)	Reflected temperature (°K)	Total reflected density (molecules/cc×10^{-18})	Initial rate constant (sec^{-1}×10^{-3})	Maximum rate constant
5.95	0.928	1565	2.29	1.51	
4.25	0.991	1783	1.76	1.64	
4.07	0.999	1806	1.70	1.94	7.97
3.67	1.018	1872	1.55	1.45	4.49
3.04	1.053	1997	1.33	10.0	

Experiments with Nitrous Oxide-Argon Mixtures

The gases used in the experiments were Matheson NO (99.0%) and N_2O (98.0%) purified by repeated condensation in liquid N_2 and distillation of the middle fraction. Argon (99.998%) and Matheson prepurified N_2 (99.996%) were also used. Pressures for determining mixture composition and initial shock tube pressure were read on a simple Todd gauge.

The first runs were made with a mixture of 24% N_2O and 76% argon, using a 10 kc/sec spectrometer cycling rate. The records obtained are similar in appearance to those illustrated previously.[8] A plot of peak heights vs time is shown in Fig. 3, the zero time being uncertain by 100 μsec, i.e., the time between successive spectra. All such runs show the same general features: a fall in the nitrous oxide peak, a corresponding increase in the nitrogen molecule and oxygen atom peaks, followed a short time later by a rise in the oxygen molecule concentration. At some later time, which increases as the initial temperature is reduced, there is a sharp rise in the heights of the 17 and 18 mass peaks indicating the formation of water. Since this is associated with a corresponding decrease in the oxygen atom and molecule peaks, it can be attributed to interface burning with the hydrogen driver gas. This has the advantage of showing when contact surface mixing begins to interfere with the experiment. There appears to be a rise in the NO concentration, but, since there is a large contribution to the NO peak by N_2O and the increase of the adjacent 28 peak due to nitrogen formation depresses the base line of the scope trace, reliable estimates of the NO concentration are difficult. As the instrument has not been calibrated against atomic species, the magnitude of the 16 peak indicates only that the maximum oxygen concentration is comparable with the initial concentration of N_2O.

The natural logarithm of the N_2O concentration (in arbitrary units) plotted against time shows two types of curves. At the intermediate temperatures, the rate constant of decomposition consistently increases with time (as shown for one run in Fig. 4) but, at low temperatures, the effect is obscured by scatter of the data, and at the highest temperatures, the time interval between successive spectra is too long to permit an increase in the rate constant of decomposition to be detected. For reasons which will be explained later both an initial rate constant and a maximum rate constant have been taken where possible. The results are summarized in Table I, the shock parameters quoted having been calculated on the basis of the one-dimensional theory. The specific heat ratio of this mixture in the reflected shock is 1.38.

Experiments with Nitrous Oxide-Nitric Oxide-Argon and Nitrous Oxide-Nitrogen-Argon Mixtures

NO is known to be a product of the reaction, and previous work[17,18] has shown that it catalyzes the N_2O decomposition, but inhibits its own formation.[19] Two mixtures with the following compositions

$$N_2O-12.1\%, \quad NO-12.4\%, \quad Ar-75.5\% \quad (a)$$

$$N_2O-12.1\%, \quad N_2-12.3\%, \quad Ar-75.6\% \quad (b)$$

were investigated. The enthalpies and average molecular weights of these two mixtures are identical to within the error involved in preparation so that the same diaphragm pressure ratio should produce the same temperatures, velocities, etc., in either mixture (a) or mixture (b), a fact which was confirmed by experiment. The records were examined in the same manner as in the previous series and the results are given in Table II.

DISCUSSION

Values of $\log k$ have been plotted against $1/T$ in Fig. 5, using only the initial rate constants where two were observed. The average concentration in these experiments was about 2.5×10^{-6} moles/cc. For this concentration, as noted, Johnston[18] gives the rate expression: $k_1=10^{9.64}\exp(-27\,400/RT)$ sec^{-1}, derived from experimental data obtained at much lower temperatures. The solid line drawn in Fig. 5 is described by Johnston's equation. The agreement of the present experimental data with this extrapolation is seen as excellent because almost all experimental points which deviate from the line by more than a factor of two were obtained in experiments where it was not possible to separate the initial from the maximal rate constant. If a suitable correction could be applied to these

points, the average deviation from the line (exclusive of the run at 1565°) would be found probably to be not larger than a factor of two, i.e., well within the combined errors of the experiments and the extrapolation over a range of about 1000° by a simple equation.

Since the oxygen atom and nitrogen molecule concentrations show a similar initial time dependence, it is clear that the initial decomposition rate constant corresponds to the reaction

$$N_2O \longrightarrow N_2+O. \quad (1)$$

The three-body collision rate is insufficient to account for removal of oxygen atoms by

$$O+O+Ar \longrightarrow O_2+Ar, \quad (6)$$

so that the most probable second steps are

$$O+N_2O \xrightarrow{k_2} N_2+O_2 \quad (2)$$

and

$$O+N_2O \xrightarrow{k_2'} 2\,NO. \quad (2')$$

To obtain a value of the sum of k_2+k_2', the point at which the reaction shifts from initial to maximum rate in Fig. 4 can be compared with graphical integration for (N_2O) of the rate expression,

$$d(N_2O)/dt = k_1(N_2O)+(k_2+k_2')(N_2O)(O)$$

$$d(O)/dt = k_1(N_2O)-(k_2+k_2')(N_2O)(O),$$

which are shown as dotted lines in Fig. 4 for several values of (k_2+k_2'). Values of k_2+k_2' between 2×10^9 and 5×10^9 cc mole^{-1} sec^{-1} at 1806°K are seen to give

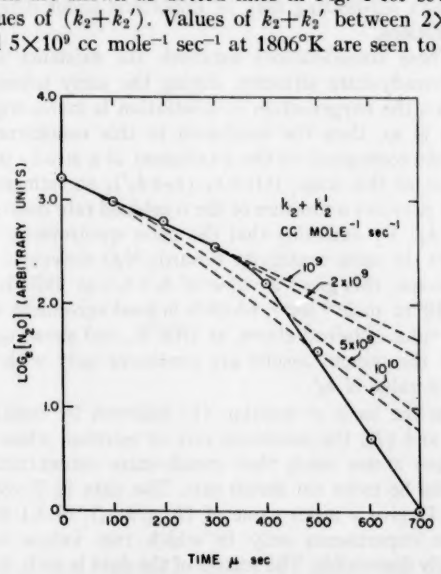

FIG. 4. The solid line is a plot of log$_e$ concentration of N_2O vs time. This run was made at a temperature of 1806°K and is typical of runs at this and higher temperatures. The dotted lines are graphical integrations of the over-all rate expression for the values of k_2 and k_2' given.

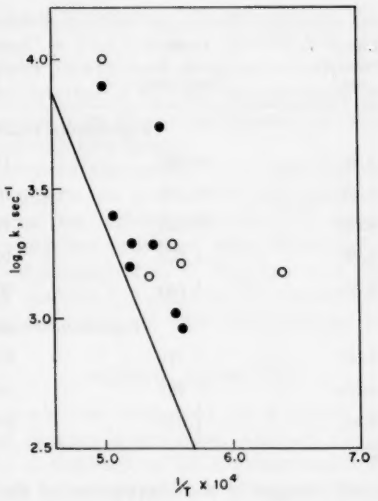

FIG. 5. Log$_{10}$ of initial (or average) first-order rate constants for N_2O decomposition vs $1/T$; ○: N_2O+Ar experiments; ●: N_2O+NO+Ar and N_2O+N_2+Ar experiments; solid line: Johnston extrapolation from low-temperature data.

the optimum fit to the experimental curve, although the maximum rates of all integrated curves are less than that observed in the run shown in Fig. 4.

This result for k_2+k_2' is in agreement with an extrapolation of Kaufman's rate constants which gives

$$k_2 = 3\times10^{10}\exp(-14\,500/RT) = 5\times10^8 \text{ cc mole}^{-1}\text{ sec}^{-1}$$

$$k_2' = 10^{11}\exp(-15\,500/RT) = 1.3\times10^9 \text{ cc mole}^{-1}\text{ sec}^{-1}$$

$$k_2+k_2' = 1.8\times10^9 \text{ cc mole}^{-1}\text{ sec}^{-1}.$$

This would indicate that the products of the reaction should be in the ratio 43% N_2, 9% O_2, and 48% NO after the maximum rate has been attained, and the amount of O_2 observed in these experiments is in qualitative agreement with this prediction. If further reactions of NO take place, they would tend to increase N_2 and O_2 with respect to NO.

Fenimore and Jones[22] have recently confirmed their earlier measurement of a higher value of E_2' at temperatures comparable to those in the present work. Their best value for k_2' is

$$2\times10^{14}\exp(-28\,000/RT) \text{ cc mole}^{-1}\text{ sec}^{-1}.$$

This gives a rate of 8×10^{10} cc mole^{-1} sec^{-1} at 1806° which is 40 times the rate estimated from these experiments and is incompatible with the estimated oxygen atom concentration observed here.

The measurements of k_1, consistent with Johnston's extrapolation, provide convincing evidence for the validity of the calculated reflected shock temperatures.

[22] C. P. Fenimore and G. W. Jones (private communication).

TABLE II.

Initial Pressure (mm)	Incident velocity (mm/μsec)	Reflected temperature (°K)	Total reflected density (molecules/cc×10^{-18})	Initial rate constant (sec^{-1}×10^{-3})		Maximum rate constant
Experimental results in nitrous oxide, nitric oxide, and argon						
5.05	0.982	1798	1.72	1.05		1.80
4.68	0.996	1840	1.61		5.47	
4.06	1.021	1924	1.43	1.60		7.56
3.69	1.034	1968	1.32	2.51		7.92
3.50	1.044	2003	1.26		7.91	
Experimental results in nitrous oxide, nitrogen, and argon						
5.20	0.976	1780	1.76		0.91	
4.58	0.999	1852	1.62	1.93		4.22
3.81	1.030	1954	1.36		1.95	

Subsequent changes in the temperature of the system depend on the nature of the reactions which occur. On the basis of the scheme above, the initial stage of the reaction will be the approach to a steady state concentration in O atoms. Because reaction (1) is endothermic and k_1 possesses a large temperature coefficient while reactions (2) and (2′) are exothermic and k_2 and k_2' have lower temperature coefficients, the approach to a steady state will take place under essentially isothermal conditions. When the steady state has been established, the temperature will either increase rapidly or remain steady depending on whether reaction (2) or reaction (2′) predominates. Because of the high temperature coefficient of reaction (1) the steady-state concentration of O atoms provides a sensitive indication of the temperature changes in the system.

The increasing O-atom concentration observed in these experiments could be due to an approach to a steady state under semi-isothermal conditions or to an increasing temperature under steady-state conditions. One method of determining what is actually taking place is to integrate the various kinetic expressions, with assumed values of the rate constants, and then compare the reaction profiles with the experimental results. This is rather unsatisfactory because of the uncertainty in the zero time in these runs and because the critical ratio of k_2 to k_2' is not accurately known.

Sufficient evidence on which a decision may be based is provided, however, by the nature of the experiments themselves. To begin with, if the temperature changes are significant, the mixtures containing N_2 and NO as diluents should show a much lower change in O-atom concentration whereas actually, to within the experimental error, these runs display identical behavior.

Second, the temperature should show an exponential rise to a "thermal explosion" if self-heating is important. This conflicts with the leveling of the O-atom concentration which occurs precisely when the decomposition rate constant of the N_2O begins to increase.

The most important observation is provided by the temperature-indicating effect of the O-atom concentration under steady-state conditions. If Fenimore's rate constant for k_2' were correct, which implies that the steady state is established virtually instantaneously, then a change in (O) over a factor of ten, as observed here, would correspond to a temperature increase of 1000° and an increase in the rate of decomposition of N_2O by a factor of one hundred. This behavior is definitely excluded by the present experiments, although self-heating may be important under different conditions.

These considerations establish the existence of a nonsteady-state situation during the early period in which the oxygen-atom concentration is increasing. If this is so, then the maximum in this concentration should correspond to the attainment of a steady state. Since, at this stage, $(O)=k_1/(k_2+k_2')$, an estimate of (O) provides a measure of the combined rate constants k_2+k_2'. By assuming that the mass spectrometer displays the same sensitivity towards N_2O molecules and O atoms, this gives a value of k_2+k_2', at 1870°K, of 5×10^9 cc $mole^{-1}$ sec^{-1}, which is in good agreement with the value obtained above, at 1806°K, and shows again that the present results are consistent only with the lower value of k_2'.

On the basis of reaction (1) followed by reactions (2) and (2′) the maximum rate of reaction, when the oxygen atoms reach their steady-state concentration, should be twice the initial rate. The data in Tables I and II give a mean value of (k_{max}/k_{init}), of 3.1 from those experiments only in which two values were clearly discernible. The scatter of the data is such, however, that not much numerical significance can be attached to this figure and the magnitude of the observed increase is regarded as in reasonable agreement with the proposed mechanism.

Reuben and Linnett[23] have proposed a mechanism for the secondary processes which involves the reaction of translationally hot oxygen atoms. In this mechanism the reaction of O^* with N_2O is expected to take place within the first few collisions before the energy of excitation (12 kcal) is lost. The present result that O atoms build up relatively slowly to a large steady-state concentration before secondary reaction proceeds at a significant rate, demonstrates that the excited-atom mechanism cannot be an important factor under these conditions.

In Fig. 5 all measurements of the initial decomposition rate constants were included and it is seen that the addition of NO or N_2 has no significant effect on the observed rate. Despite earlier evidence for autocatalysis by

$$NO+N_2O\rightarrow N_2+NO_2 \qquad (3)$$

at lower temperatures, it is obvious that, under the present conditions, this reaction must be appreciably slower than the over-all rate. A recent value of the rate constant of reaction (3), obtained by Kaufman and Kelso,[24] is $2.5\times10^{14}\exp-(50\,000/RT)$ cc mole^{-1} sec^{-1}. If the present work is taken to indicate that k_3 is not greater than $\frac{1}{5}$ k_1, then the maximum value of k_3 obtainable from these experiments is in very close agreement with this figure.

To summarize the results, it has been demonstrated that at temperatures up to 2000°K the present method of sampling from behind reflected shock waves gives results which are consistent with theoretical predictions. The decomposition of N_2O has been shown to occur by reaction (1) followed by reactions (2) and (2′) and rate constants have been obtained for both steps.

ACKNOWLEDGMENTS

This work was supported by a grant from the National Science Foundation. One of the authors (J.N.B.) is indebted to the Commonwealth Fund of New York for the award of a fellowship. The authors wish to express their appreciation to Dr. P. H. Kydd for valuable help in the interpretation of the data and the preparation of the manuscript.

[23] B. G. Reuben and J. W. Linnett, Trans. Faraday Soc. **55,** 1543 (1959).

[24] F. Kaufman and J. R. Kelso, J. Chem. Phys. **23,** 602 (1955).

Shock Wave Studies by Mass Spectrometry. II. Polymerization and Oxidation of Acetylene

J. N. BRADLEY* AND G. B. KISTIAKOWSKY

Gibbs Chemical Laboratory, Harvard University, Cambridge, Massachusetts

(Received August 13, 1959)

The polymerization and oxidation of acetylene have been investigated at temperatures from 1800°–2700°K and 950°–1100°K, respectively, by the technique of time-of-flight mass spectrometry in reflected shock waves. In the absence of oxygen, a simple bimolecular reaction produces a dimer, probably vinylacetylene, and higher polymers, which appear to reach "equilibrium" with the acetylene. A sharp drop in the concentration of these polymers is observed at a later time, which is correlated with the formation of carbon after an induction period. In the presence of oxygen, a dimer, probably diacetylene, is formed simultaneously with the formation of CO and H_2O, after an induction period. This suggests that it is a product of the branching chain reaction, a specific mechanism for which is proposed.

THE effect of heat on acetylene has been the subject of numerous investigations, but much of the data which has been obtained is very confusing. This difficulty, as will be seen later, appears to stem from the previous lack of distinction between processes leading to carbon formation, and those leading to polymerization.

In general, the low temperature products are polymers, whereas high temperatures lead to the formation of "acetylenic" carbon, hydrogen, and methane.[1] Diacetylene and more complex hydrocarbons, including aromatics, have been found as products of the low temperature reaction.[2,3] The two simple decompositions into free radicals

$$C_2H_2 \rightarrow 2CH \quad (1)$$

$$C_2H_2 \rightarrow C_2H + H \quad (2)$$

are both very endothermic, about 230 and 121 kcal, respectively,[4] so that they seem unlikely in a reaction which appears to be of second order in acetylene concentration and to possess an activation energy of about 40 kcal.[5] Several workers find the reaction to be inhibited by the addition of nitric oxide.[6–9]

Porter[10] is able to show from flash photolysis experiments that *aromatic* polymers and C_2 intermediates are not present during the reaction, but he does not eliminate the possibility of short-chain aliphatic molecules. In a review of possible mechanisms,[11] he concludes that the most probable process is a simultaneous condensation and dehydrogenation of acetylene, i.e., the C_2H_2 adds to the growing carbon chain as C_2, but this species never exists as a free intermediate.

Several shock tube investigations have been carried out. Hooker[12] finds, for visible emission from the reaction, an activation energy of 39 kcal/mole, in agreement with the previous work. He also finds that the formation of carbon, as measured by radiation from the solid particles, has an appreciable induction period. Aten and Greene[13] are able to relate formation of polymer products, in this case mainly diacetylene and vinylacetylene, to the change in turbidity of the gas. The possibility that in their experiments these products are formed during the cooling process cannot be entirely eliminated. It must be stressed that the appearance of polymers in the reaction is not *direct* evidence of their function as intermediates.

The use of the time-of-flight mass spectrometer to study reactions behind reflected shock waves has been described previously.[14] Its value in the present study lies in its ability to identify the polymer products during their formation and to follow their concentrations as functions of time.

EXPERIMENTAL DETAILS AND RESULTS

"Prest-O-Lite" acetylene was purified by passing successively through a trap cooled by a dry ice-trichloroethylene bath, concentrated sulphuric acid, Ascarite, and Drierite, and was then collected in a liquid nitrogen

* Present address: The University of Liverpool, Department of Inorganic and Physical Chemistry, Liverpool 7, England.

[1] Reviewed in E. W. R. Steacie, *Atomic and Free Radical Reactions* (Reinhold Publishing Corporation, New York, 1954), 2nd ed.

[2] R. N. Pease, J. Am. Chem. Soc. **51,** 3470 (1929).

[3] N. D. Zelinski, Ber. **57,** 264 (1924).

[4] T. L. Cottrell, *Strengths of Chemical Bonds* (Butterworths Scientific Publications, Ltd., London, 1958).

[5] H. A. Taylor and A. van Hook, J. Phys. Chem. **39,** 811 (1935).

[6] H. D. Burnham and R. N. Pease, J. Am. Chem. Soc. **64,** 1404 (1942).

[7] D. A. Frank-Kamenetsky, J. Phys. Chem. U.S.S.R. **18,** 329 (1944).

[8] C. G. Silcocks, Proc. Roy. Soc. (London) **A242,** 411 (1957).

[9] G. J. Minkoff, D. M. Newitt and P. Rutledge, J. Appl. Chem. **7,** 406 (1957).

[10] G. Porter, Proc. Roy. Soc. (London) **A200,** 284 (1950).

[11] G. Porter, The Mechanism of Carbon Formation, AGARD Memorandum, AG13/M9 (1954).

[12] W. J. Hooker, *Seventh Symposium (International) on Combustion* (Butterworth's Scientific Publications, Ltd., London, 1959), p. 949.

[13] C. F. Aten and E. F. Greene (to be published).

[14] J. N. Bradley and G. B. Kistiakowsky, J. Chem. Phys. **35,** 256 (1961).

TABLE I. Polymerization experiments.

Initial pressure mm	Driver gas	Velocity mm/μsec	Temperature °K	Density ratio	Initial rate constant (1 mole^{-1} sec^{-1}) $\times 10^{-7}$	Induction Period μsec
3.08	H_2	1.01	1870	9.66	0.37	1250±50
2.70	H_2	1.04	1944	9.91	0.97	300±100
2.34	H_2	1.06	2032	10.15	1.43	...
1.77	H_2	1.11	2192	10.58	2.51	200±100
1.75	He	1.09	2124	10.39	1.87	400±100
1.56	H_2	1.14	2287	10.84	2.02	600±100
1.50	H_2	1.15	2321	10.91	3.94	175±50
1.49	He	1.12	2238	10.71	...	100±100
1.36	He	1.14	2307	10.88	3.13	600±100
0.97	H_2	1.25	2700	11.67	...	100±100

trap. The oxygen, Airco 99.5%, was not purified further. Spectroscopic grade argon was used as a diluent. The two mixtures studied were:

Polymerization: C_2H_2—11.2%; Ar—88.8%

Oxidation: C_2H_2—10.8%: O_2— 8.4%: Ar—80.8%.

The shock parameters were computed from the shock velocity as described before.[14] The enthalpy for acetylene was calculated from the fundamental frequencies,[15] using the simple harmonic oscillator approximation, and that for oxygen was obtained from standard tables.[16] The experiments were conducted as before,[14] using 1–3 mm pressure of reactant gas in the low-pressure section with 500 mm of hydrogen or 750 mm of helium as driver in the polymerization runs and 4–10 mm of reactant gas with 400–600 mm of helium as driver in the oxidation runs.

POLYMERIZATION OF ACETYLENE

The polymerization experiments showed the formation of three hydrocarbon polymers. The concentration of each of these rapidly reached a steady value and, after a short time, fell rapidly to about $\frac{1}{3}$ of its maximum value. The plot obtained from a typical run is shown in Fig. 1 and the results are given in Table I. The hydrocarbons are designated "A", "B", and "C" in order of ascending mass number.

Characterization of Polymers

Since the times of flight of the ions are proportional to the square roots of their masses, the position of the mass peaks on the spectrum permits an estimation of their mass numbers. Most of the spectra include three known mass peaks, i.e., Ar^{++}, Ar^+, and either C_2H^+ or $C_2H_2^+$, so that two independent estimates of an unknown mass are possible from each run. This method has been checked by determining known masses and is found to be accurate to one mass unit, in the range 40–60, and to show no significant systematic errors such as might be caused by end effects in the flight path of the ions. Taking the mean of estimates from all possible runs (15 for the "A" peak, 8 for the "B" peak and 4 for the "C" peak) the following masses are found:

"A"—51.1±0.4

"B"—75.4±0.9

"C"—97.3±4.0.

(The limits listed here correspond to probable errors.) This suggests that the "A" peak is due to the $C_4H_3^+$ ion and, since the C_4H_3 radical is unlikely to be very stable, the most obvious molecule to produce this ion would be C_4H_4, vinylacetylene. The mass spectrum of this compound[17] shows an approximately equal distribution on mass peaks 50, 51, and 52, so that, due to the limited resolution of the mass spectrometer and the low quality photographs, a peak centering near mass 51 might be expected for this compound. The molecule which fits the "B" peak most closely is C_6H_4, vinyl diacetylene. However, the mass uncertainty of this peak is higher than that of the "A" peak and since the ion mass may be expected to be lower than the mass of the parent molecule, as above, the "B" peak may well correspond to the trimer C_6H_6. The only deduction which can be made from the mass of the "C" species is that it corresponds to a C_8 hydrocarbon.

[15] G. Herzberg, *Molecular Spectra and Molecular Structure. II. Infra-red and Raman Spectra of Polyatomic Molecules* (D. Van Nostrand Company, Inc., Princeton, New Jersey, 1945), p. 290.

[16] E. Justi, *Spezifische Warme, Enthalpie, Entropie, and Dissoziation Technischer Gase* (Springer Verlag, Berlin, Germany, 1938).

[17] Mass Spectral Data, American Petroleum Institute, Research Project 44 (1958).

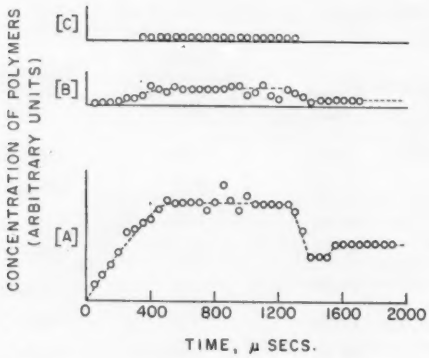

FIG. 1. Concentrations as a function of time from the polymerization experiments. An experiment at a fairly low temperature (1870°K) has been illustrated to show clearly the main features of these plots.

Kinetics of Polymer Formation

The polymer peaks reach a stationary intensity long before all the acetylene is consumed, so that after 1 msec or less, the following equilibrium appears to be attained:

$$C_2H_2 \rightleftharpoons \text{“A”} \rightleftharpoons \text{“B”} \rightleftharpoons \text{“C”}. \qquad (3)$$

The over-all consumption of acetylene was determined both from the extent of polymer formation, assuming reasonable values for the sensitivity of the mass spectrometer to these species, and from *separate* experiments in which the heights of the 26 m/e peak could be measured. In neither case did the concentration of acetylene fall below 70% of the original. The time at which the acetylene concentration ceased to decrease appeared to coincide with the attainment of stationary concentrations of polymers, although the experimental evidence does not eliminate the possibility of a very slow disappearance (less than 10% of the original rate) of acetylene after this point. These experiments suggest that the reactions reach equilibrium, rather than a steady state in which the polymers are consumed to form some other unobserved products as fast as they are formed. Had acetylene been consumed at the rate (see below) which is indicated by the initial rate of formation of the polymers, virtually all would have disappeared by the end of this “steady state” period. It might be noted here that Aten and Greene[13] also find consumption of acetylene not exceeding 30% under comparable conditions. It is very interesting to note that the ratios $(B)/(A)$ and $(C)/(B)$ remain constant, within the error of measurement, from the beginning of the reaction, long before the $(A)/(C_2H_2)$ ratio has attained its equilibrium value. It is concluded, therefore, that the time for equilibration of reaction (4) below, is much longer than that of reactions producing higher polymers. These reactions might be written as

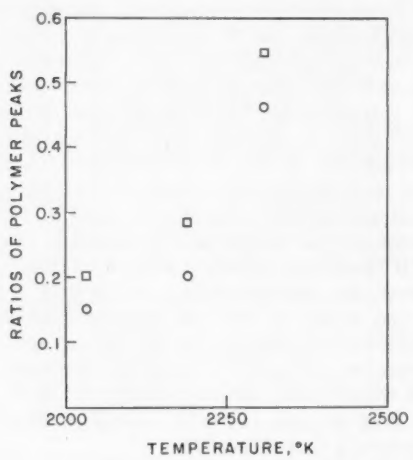

FIG. 2. Ratio of polymer peak heights at equilibrium vs temperature. Only runs where all peaks could be measured simultaneously are included. □=“C”/“B”; ○=“B”/“A”.

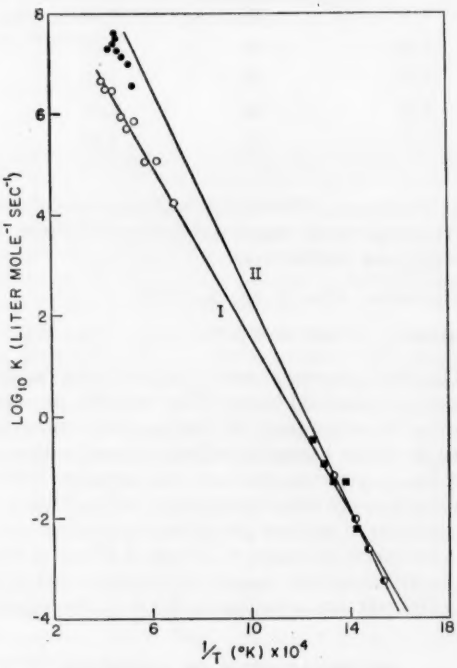

FIG. 3. Plot of $\log_{10}k$ for C_2H_2 disappearance vs $1/T$. Line I is the plot obtained by Greene using combined low and high temperature data. Line II is the extrapolation from Silcocks' results. ●=present results; ○=Greene (reference 13); ◐=Silcocks (reference 8); and ■=Minkoff, Newitt, and Rutledge (reference 9).

$$C_2H_2 + C_2H_2 \rightleftharpoons C_4H_4 \quad \text{(rate determining)} \qquad (4)$$

$$C_4H_4 + C_2H_2 \rightleftharpoons C_6H_6 \qquad (5)$$

$$C_6H_6 + C_2H_2 \rightleftharpoons C_8H_8. \qquad (6)$$

It is not likely that the reactions involve the formation of molecular hydrogen because, in view of the concentrations and collision frequencies involved, the equilibria are established too quickly to involve reverse reactions of the type

$$H_2+C_6H_4\rightarrow C_4H_4+C_2H_2. \qquad (7)$$

A plot of the ratios $(C)/(B)$ and $(B)/(A)$ against temperature, in Fig. 2, shows that the equilibria are shifted in the direction of higher molecular weights with increasing temperature. Semi-empirical calculations[18] on polymeric carbon molecules have shown that higher molecular weight species increase in abundance with increasing temperature.

It is interesting that the six carbon polymer is not present in abnormally large amounts and that no C_{10} polymer is found. This seems to demonstrate that the aromatic hydrocarbons are not preferentially formed from acetylene at these temperatures in the gas phase.

Although the Ar^+ and the $C_2H_2^+$ peaks are too large to be recorded on the spectrum, it has been possible to estimate the polymer concentrations approximately by assuming them to have unit sensitivity, relative to argon, and comparing them with the C_2H^+ and the Ar^{++} peaks. This measurement was possible in three experiments and the equilibrium concentration of "A", as a percentage of the initial acetylene concentration, was found to be 9.1 at 2030°K, 9.5 at 2165°K, and 6.2 at 2190°K. Taking the mean value of these results, and using the ratios of Fig. 2, it has been possible to estimate the approximate initial rates of consumption of acetylene from plots of the type shown in Fig. 1.

Due to the approximations involved, accurate rates are not to be anticipated. However, a plot of the logarithm of the rate constant vs $1/T$ is shown in Fig. 3 together with some of the more recent data from the literature. A line drawn through the present values and the low-temperature data would lie between the extrapolated rates[8,9] and those obtained by Greene,[13] also from a combination of high and low-temperature results. Although the present results are probably less accurate than the other determinations, it should be noted that Greene assumes that there is no reaction reforming acetylene, which appears to be contradicted by these results, and so the correct rates should properly lie above his data. The rate constant obtained from the plot through the present values is $k=3.6\times10^{14}\exp(-44\,100/RT)$ cc mole^{-1} sec^{-1}.

The absence of an induction period, and the fact that an equilibrium is established, provide good evidence that a chain mechanism is not responsible for the formation of polymers in these experiments. An alternative explanation is the formation of an excited acetylene molecule, which then reacts with acetylene to form the dimer, as proposed by Frank-Kamenetsky[7] and Greene.[13] This excited state may be the triplet state of acetylene, as Laidler has set an upper limit to the energy of this species at 27.3 kcal,[19] which is well below the observed activation energy of the reaction.

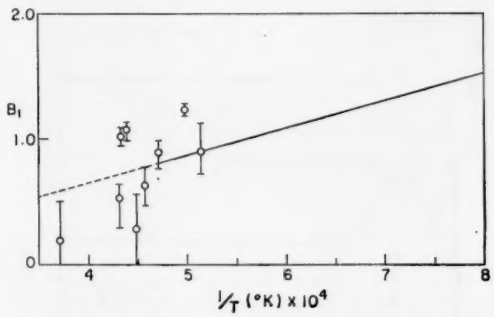

FIG. 4. Plot of $B_1=\log_{10}[(pC_2H_2)\Delta\tau]$ vs $1/T$. The solid line is taken from Hooker's data, the broken line indicating the extrapolation to the temperature range covered in the present experiments.

Kinetics of Polymer Decay

The sudden disappearance of two-thirds of the polymer concentrations is most probably due to a reaction to form another species which is undetectable by the mass spectrometer. The Ar^{++} peak height is constant during this process, ruling out the possibility of a sudden density change, and the rate of this disappearance is faster than the rate of formation of polymers by approximately a factor of 3. It is, therefore, unlikely that a sudden drop in temperature leads to the reformation of acetylene and the establishment of a new equilibrium, or that acetylene has reacted to form an undetectable species with the same result.

Hooker[12] showed that the formation of carbon occurs at the end of an induction period. In Fig. 4 the function $B_1=\log_{10}(P_{C_2H_2})\Delta\tau$ (where $\Delta\tau$ is the induction time until polymer decay) is plotted against $1/T$ for the present results and compared with Hooker's curve for the induction period for carbon formation. This comparison shows that the sharp drop in the polymer concentration occurs at about the same time that measurable amounts of carbon particles appear.

Since the rapidity of the observed drop in polymer concentration eliminates the possibility that it is due to reaction of acetylene to form carbon, followed by the attainment of a new equilibrium and since it is unlikely that the polymers are physically adsorbed on the growing particles at temperatures near 2000°K, the most reasonable explanation seems to be that the polymers react directly to form solid carbon after an induction time due to nucleation. This is especially so if the slight rise in polymer concentration following the sudden decrease is a real effect. This could be interpreted as

[18] K. S. Pitzer and E. Clementi, J. Am. Chem. Soc. **81**, 4477 (1959).

[19] K. J. Laidler, *The Chemical Kinetics of Excited States* (Oxford University Press, New York, 1955), p. 93.

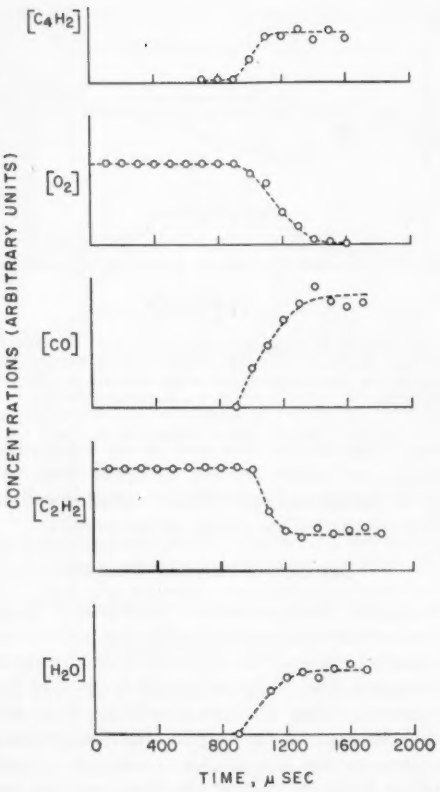

FIG. 5. Concentration as a function of time from the oxidation experiments. To a first approximation the peaks for H_2O, O_2, and C_4H_2 correspond to their relative concentrations and the C_2H_2 and CO peak heights should be multiplied by factor of about 10. The temperature of the run shown here was 997°K.

the establishment of a new steady state with the remaining acetylene after a large fraction of the polymers had condensed, but is difficult to account for on any other basis.

OXIDATION OF ACETYLENE

The oxidation runs at lower temperatures show an appreciable induction period, followed by the rapid formation of carbon monoxide, water, and a hydrocarbon with a mass number of about 50. (Hydrogen is not detectable in the present spectrometer.) A plot of concentrations vs time obtained in a typical experiment is shown in Fig. 5 and the results are listed in Table II. Several experiments were required to follow all the peaks due to different gain settings being necessary and the relative peak heights do not correspond to relative concentrations for the different species. As most of the runs used a spectrometer cycling rate of 20 kc/sec, there is an error of up to ± 50 μsec in the measurement of the induction period. In the earlier experiments an additional error was introduced due to loss of gas through the sampling orifice between the time the pressure was measured and the initiation of the shock. This time lapse was reduced in later runs to the point where its effect was negligible.

As indicated in the previous paper,[14] contact surface mixing will eventually vitiate the result of the analyses. In these low temperature experiments, the length of time during which reliable results could be obtained was approximately 2 msec.

The important distinction between these experiments and those discussed above is that the dimer is formed at a higher rate and at lower temperatures, but only after an induction period. Since, even after the combustion reaction is over, the temperature is at most 1700°K, the bimolecular polymerization reactions are too slow to be important. The only explanation is a branching-chain reaction, completely different from the mechanism of polymer formation in the polymerization runs.

Analysis of the mass number of the dimer peak, using the method described above, leads to a value of 50.1 with a probable error of ± 0.3. This indicates that the dimer is not the same as that observed previously, and is probably diacetylene, whose main peak lies at mass number 50.[17] No peaks at higher mass numbers were observed. Unfortunately, information on the CH and C_2H radicals is unobtainable because of ionization fragmentation of the acetylene present.

Reaction Mechanism

Richards[20] and Gardiner[21] have shown that induction times in the acetylene-oxygen reaction at high temperatures are the same as those of the hydrogen-oxygen

TABLE II. Oxidation experiments.

Initial pressure mm	Velocity mm/μsec	Temperature °K	Density ratio	Induction period mean value from all peaks) μsec
10.0	0.68	954	5.97	2000
9.9	0.68	957	5.99	1700
9.7	0.69	964	6.04	1100
9.5	0.69	964	6.04	2400
9.3	0.69	967	6.07	1050
9.0	0.71	1023	6.40	300
8.5	0.74	1086	6.79	100
8.3	0.70	992	6.20	400
8.3	0.70	995	6.23	750
8.2	0.70	997	6.25	850
7.7	0.73	1065	6.66	100
7.3	0.71	1020	6.39	350
5.7	0.74	1090	6.80	300

[20] L. W. Richards, Thesis, Harvard University, 1960.
[21] W. C. Gardiner, Thesis, Harvard University, 1960.

reaction,[22] both in their dependence on temperature and oxygen concentration.

The results obtained in the present work at the lower temperatures agree very well with this finding as shown in Fig. 6, but the higher temperature results fall below an extrapolation of Gardiner's data, which were taken at still higher temperatures. Since the time at which the shock wave reflected is uncertain by ± 50 μsec, it is difficult to measure short induction times accurately by the present method. In addition, there may have been some peculiar ignition phenomenon behind the reflected shock at the higher temperatures which would not affect the earlier work in incident shocks. Consequently, it is felt that Richard's and Gardiner's data represent the true situation.

This indicates that possible elementary steps are

$$H+O_2 \rightarrow OH+O \qquad \Delta H_0^0 = 17 \text{ kcal} \quad (8)$$

$$O+C_2H_2 \rightarrow C_2H+OH \qquad \Delta H_0^0 \leq 20 \text{ kcal}^4 \quad (9)$$

$$OH+C_2H_2 \rightarrow C_2H+H_2O \qquad \Delta H_0^0 \leq 1 \text{ kcal}^4 \quad (10)$$

by analogy with

$$H+O_2 \rightarrow OH+O \qquad \Delta H = 17 \text{ kcal} \quad (8)$$

$$O+H_2 \rightarrow H+OH \qquad \Delta H = 3 \text{ kcal} \quad (11)$$

$$OH+H_2 \rightarrow H+H_2O \qquad \Delta H = -16 \text{ kcal}, \quad (12)$$

with reaction (8) being the rate limiting step in both cases. This seems even more likely on the basis of the recent finding that the rate of consumption of O_2 in acetylene-oxygen flames is given by the measured H atom concentration and the rate constant of reaction 8.[23]

For this to be a chain reaction H atoms must be regenerated, which can take place by

$$C_2H+C_2H_2 \rightarrow C_4H_2+H; \quad \Delta H = -23 \text{ kcal}. \quad (13)$$

This would account for the rapid formation of relatively large amounts of diacetylene which have been observed in the present experiments. Following the chain reaction the diacetylene is presumably oxidized by H_2O and CO_2 so that it does not appear in large amounts in the final products of combustion. This gives as the branching-chain reaction

$$H+O_2+6C_2H_2 \rightarrow 3C_4H_2+2H_2O+3H; \quad \Delta H = -20 \text{ kcal}. \quad (14)$$

This branching-chain mechanism for the acetylene-oxygen reaction is formally similar to the mechanism operating in the hydrogen-oxygen reaction. In particular, reaction (8) must be the rate determining step, even though reactions (9) and (10) are probably more endothermic than (11) and (12), respectively. However, if reaction (9) were rate determining, reactions (8), (10), and (13) would constitute a straight chain and the branching coefficient would then be determined by reaction (9). This would suggest a strong dependence of induction periods on acetylene concentration. Richards,[20] however, found that induction periods depend mainly on oxygen concentration, as in the hydrogen-oxygen reaction. We conclude, therefore, that reaction (9) is not rate determining.

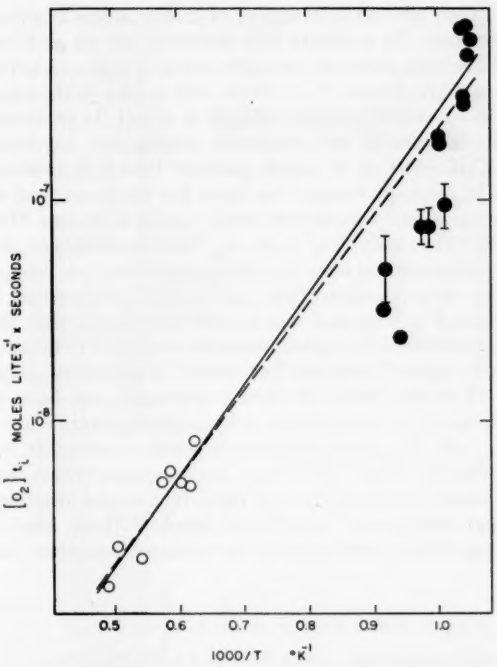

FIG. 6. Induction times for the C_2H_2-O_2 reaction. ●=present results; ○=Gardiner's results. Solid line-least squares fit to Gardiner's data for C_2H_2-O_2. Dashed line-least squares fit to Schott's data for H_2-O_2.

As in the hydrogen-oxygen reaction the chain is practically thermoneutral; however, it is obvious that there are other important reactions in the acetylene case which do not occur with hydrogen. These reactions produce CO and all of the heat of combustion.[21] They proceed at a very high rate which is comparable with that of the chain.

These experiments give no direct evidence for the mechanism which produces CO. It is produced from the end of the induction period at a rate comparable to that of the chain reaction. This indicates that the reaction forming it must involve one of the parent molecules O_2 or C_2H_2, and since the initial consumption of O_2 can be explained by the reaction with H, the most likely step is one involving C_2H_2. The bonds of C_2H_2 are very strong so that the other partner is likely to be one of the free radicals produced by the chain reaction, e.g., O or OH as otherwise the reaction would involve too high an activation energy. Such a reaction must have a hydro-

[22] G. L. Schott and J. L. Kinsey, J. Chem. Phys. **29**, 1177 (1958).

[23] C. P. Fenimore and G. W. Jones, J. Phys. Chem. **63**, 1834 (1959).

carbon with an odd number of carbon atoms as a final product. No products with masses in the range 12–16 have been observed, but since argon in large excess was used as a diluent, C_3 products with masses in the range 36–44 would have been difficult to detect. In particular it is possible to construct mechanisms involving $2C_2H_2+OH$ or O which produce $CO+C_3H_4$(allene). The mass spectrum of the latter has its parent peak at mass 40 and successively smaller peaks at masses 39 to 36. The individual steps in these mechanisms are exothermic and obey the spin conservation rule rendering them plausible. That some such C_3 intermediate is formed is suggested also by the observation that the concentration of carbon monoxide continues to increase after that of acetylene has reached a stationary value.

The chief result of these experiments has been to demonstrate the presence of hydrocarbon intermediates in both the pyrolysis and oxidation of acetylene. In the pyrolysis there are three intermediates which are formed from acetylene by rapid bimolecular reactions and which reach equilibrium concentrations. After a time which correlates with the measured induction time for carbon precipitation their concentrations drop sharply to a new steady state value. There is some evidence that the carbon is formed directly from the polymers. In the oxidation reaction there is an induction period after which there is a rapid branching chain reaction consuming acetylene and oxygen and producing diacetylene. By combining this with earlier results a plausible mechanism for the chain may be written. There are also reactions which produce carbon monoxide at a rate comparable to that of the chain reaction. It is felt that these reactions must involve a second hydrocarbon intermediate which was unobservable in the present experiments.

ACKNOWLEDGMENTS

This work was supported by a grant from the National Science Foundation. One of the authors (J. N. B.) is indebted to the Commonwealth Fund of New York for the award of a Fellowship. The authors wish to express their appreciation to Dr. P. H. Kydd for valuable assistance in the interpretation of the data and the preparation of the manuscript.

THE JOURNAL OF CHEMICAL PHYSICS VOLUME 35, NUMBER 1 JULY, 1961

Effect of Chemisorbed Hydrogen on the Magnetization of Nickel

R. E. DIETZ* AND P. W. SELWOOD

Department of Chemistry, Northwestern University, Evanston, Illinois

(Received October 20, 1960)

The effect of chemisorbed hydrogen on the saturation magnetization of nickel was investigated on fine particles of nickel. For certain preparations the saturation moment of the nickel was within 1 or 2% of that of massive nickel; this is considered evidence that the surfaces of the nickel in these samples were substantially free from chemisorbed impurities, and that the electronic state of the nickel was identical to that of massive nickel. For these preparations, hydrogen decreases the saturation moment of the nickel by about 0.7 Bohr magneton per average atom of hydrogen adsorbed. This effect appears independent of temperature up to 300°K (the highest temperature investigated) and of surface coverage over nearly the entire range.

1. INTRODUCTION

THE effect of chemisorbed hydrogen on the magnetization of fine nickel particles has been investigated by Selwood and co-workers[1,2], and by Broeder, van Reijen, and Korswagen.[3] Measurements at high magnetic fields and at temperatures as low as 20°K indicated that the magnetization of nickel suffers a decrease, but measurements at still lower temperatures were necessary for a quantitative determination of the effect on the saturation. Measurements of the effect of hydrogen were also carried out in alternating magnetic fields of low intensity; at 300°K a decrease in the magnetization was observed while at 20°K an increase was observed in some samples.

The present work extends these measurements to 4.2°K, and to dc magnetic fields of 10 000 oe, conditions which enable the saturation magnetization of nickel particles in certain nickel-silica catalysts to be measured precisely; this investigation occupies the first four sections of this paper. In the fifth and remaining sections are discussed the magnetic properties of these systems measured under less strenuous conditions of temperature and magnetic field intensity; these non-saturation investigations not only further characterize the hydrogen-nickel surface interaction, but also

* Present address: Bell Telephone Laboratories, Murray Hill, New Jersey.

[1] P. W. Selwood, S. Adler, and T. R. Phillips, J. Am. Chem. Soc. **76**, 2281 (1954).

[2] P. W. Selwood, S. Adler, and T. R. Phillips, J. Am. Chem. Soc. **77**, 1462 (1955), and later papers.

[3] J. J. Broeder, L. L. van Reijen, and A. R. Korswagen, J. chim. Phys. **54**, 37 (1957).

establish a basis for comparing the present saturation experiments to the results of those investigations performed under less rigorous conditions, which have been previously reported in the literature.

2. EXPERIMENTAL TECHNIQUE

Procedure

In a typical experiment the following sequence of steps was carried out. A pellet containing fine particles of nickel was reduced for about 12 hr in flowing hydrogen at 350°C. To remove the residual hydrogen, the sample was evacuated at 350°C for several hours until a pressure of 10^{-6} mm Hg was attained. The sample was then cooled, and magnetization measurements as a function of magnetic field intensity were made at temperatures ranging from 4.2° to 300°K. The sample was warmed to room temperature, and a measured volume of hydrogen was admitted. The magnetization measurements were then repeated. In all cases, about 0.1 ml of helium gas was introduced to induce thermal equilibrium.

Since the maximum changes in magnetization for these systems are about 10% or less, the saturation must be measurable to $\pm 0.1\%$ to provide a precision in the relative change in saturation magnetization of 1%. Since actual measurement of the saturation magnetization is impossible, the magnetization must be extrapolated to infinite field intensity. This improves precision by almost another order of magnitude under the most favorable circumstances. Thus, magnetization measurements and the corresponding measurements of the magnetic field intensity are sufficiently precise if made with an average error of 1% or less over a linear portion of the magnetization curve comprising about 10 experimental points.

Construction of the Apparatus

The apparatus developed for the magnetic measurements, shown in Fig. 1, was adapted from a method of Weiss and Forrer.[4] Magnetization was measured by moving the sample from one set of sensing coils to another set having the same number of turns, but wound in opposition; the current induced in the coils by the change in flux was integrated by a Leeds and Northrup model 2290 ballistic galvanometer used as a fluxmeter. The bucking sets of coils balanced out currents induced by transient changes in the applied magnetic field. Thermal emf's were balanced out by superimposing a small reverse emf.

The sample, consisting of a single cylindrical pellet, 0.63 cm in diameter and about the same length, fitted snugly in the bottom of a Pyrex tube, the upper end of which was attached to a glass-encased iron slug. A movable solenoid then raised or lowered the assembly in the vacuum envelope. The sample tube was fitted with a hook at its upper end which permitted the sample to be suspended about 15 cm above the sensing coils. This was necessary during reduction and evacuation at elevated temperatures to avoid overheating the sensing coils by the electrical resistance sleeve furnace used to obtain these temperatures.

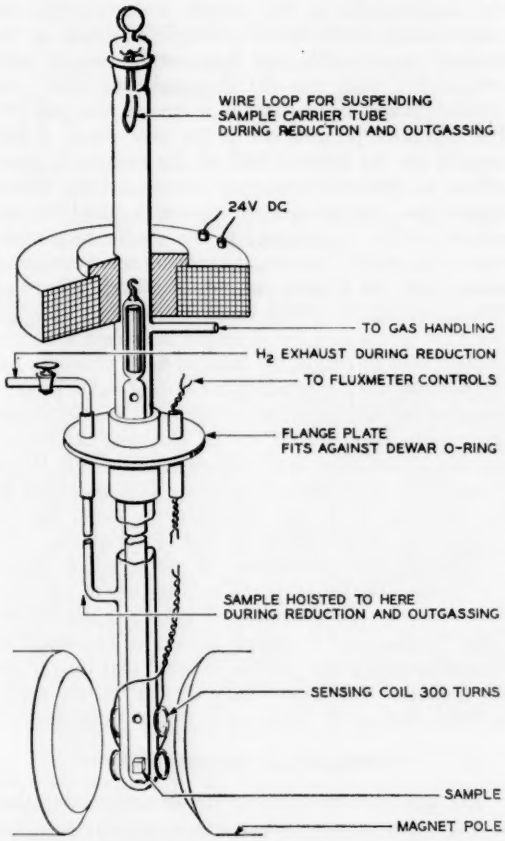

FIG. 1. Apparatus designed for *in situ* measurements of magnetization after various surface treatments.

A homogeneous magnetic field of intensities to 10 000 oe was provided by a 4-in. electromagnet of the Weiss design. The field in the region of the sensing coils was uniform within the sensitivity of a Rawson model 720 rotating coil gaussmeter used to monitor the field while the magnetization was being measured.

The lower portion of the vacuum envelope around the sample tube was cooled by immersion in a double Dewar containing a refrigerant. Boiling helium was used for the saturation experiments. Measurements could also be made at elevated temperature by using a small sleeve-type resistance furnace.

Analysis of the Method

The question now arises as to whether the current integrated by the fluxmeter actually was a measure of

[4] P. Weiss and R. Forrer, Ann. Phys. **5**, 153 (1926).

the magnetization of the sample. Unfortunately two complicating effects render a complete analysis of the method impracticable, but these can be treated semi-empirically. They are (a) demagnetizing fields and inhomogeneous magnetization of the samples, and (b) the effects of polarization of the pole pieces of the magnet by the induced field of the sample. If these effects are ignored, elementary electromagnetic theory shows that the integrated current induced in the sensing coils is proportional to the specific magnetization of the sample. Because the samples never contained more than 10 volume percent of nickel, effects of demagnetizing fields were small. Corrections were applied by subtracting the demagnetizing field from the applied field to obtain the internal field; since the demagnetizing field approaches a constant value proportional to the magnetization at high fields, it affects only slightly the slope of a M vs $1/H$ plot near saturation, and has no influence on the saturation intercept. When corrections for demagnetizing fields were necessary at low magnetic fields, the demagnetizing factor for the samples was approximated by that of the sphere.

Although the contributions to the apparent, measured magnetization from the polarization of the pole pieces by the sample (commonly known as the "image effect") amounted to several percent of the observed magnetization, it was possible to show[5] that corrections for the effect were unnecessary for the relative measurement techniques employed in this investigation.

Calibration of the Apparatus

The apparatus was calibrated to obtain the saturation of the various samples relative to pure, polycrystalline nickel, for which the saturation megnetization is precisely known.[6] Very pure, powdered nickel, obtained from the International Nickel Company, was mixed with graphite and silica gel and was pressed into pellets of the same shapes, sizes, and density of nickel as those employed in experiment. To insure complete reduction of the nickel, the pellets were heated in hydrogen for 12 hr at 350°C prior to measurement. The saturation per gram of nickel, of the various calibration samples, showed a standard deviation of 0.6%. The extrapolations to infinite field were made from M vs $1/H^2$ plots[7]. The approaches to saturation on these plots were quite linear above 2000 oe.

Preparation of Samples

Since a large surface to volume ratio is necessary to observe appreciable changes in the saturation magnetization due to absorbed molecules, the selection of samples was restricted to those containing nickel particles of diameters less than 100 A. Such systems are most stable and reproducible when the nickel particles are suspended in a matrix of silica, and several different preparations of this type were used. These samples were generally prepared either by impregnating an existing silica matrix, such as kesselguhr or Davison gel, with a concentrated solution of nickel nitrate, drying, compressing into pellets, and finally reducing *in situ* in a stream of flowing hydrogen at 350°C for about 12 hr; or by coprecipitating nickel hydroxide and silica by mixing boiling solutions of nickel nitrate and basic sodium silicate according to the method described by van Eijk van Voorthuysen and Franzen.[8]

The impregnation-type samples were commercial nickel-silica hydrogenation catalysts prepared by the Universal Oil Products Company. For some saturation experiments, these catalysts were sintered at elevated temperatures in hydrogen. Graphite was used as a binder and lubricant during the pellet forming process for all but the coprecipitate samples. All samples were evacuated after reduction with a mercury diffusion pump for four hours at 350°C. This lowered the pressure, during pumping, to 10^{-6} mm Hg.

Electrolytic tank hydrogen, used both for reducing the nickel samples and subsequent chemisorption, was purified by catalytically combining any free oxygen with the hydrogen in a "Deoxo" unit. The resulting water was then frozen out of the gas stream in a silica gel trap at 200°K. The helium used to attain thermal equilibrium was purified by passage over finely divided, hydrogen-reduced copper at 600°C, and then through a dry-iced silica gel trap. A mercury micro gas buret was used to measure aliquots of hydrogen to the sample, and the pressure was measured by a McLeod gauge.

Each sample was quantitatively analyzed for nickel by solution in hydrofluoric acid and electrodeposition of the nickel on weighed platinum electrodes. The samples were also examined spectrochemically for impurities. Calcium and sodium present to 1% were the chief impurities in the impregnation-type samples. These were believed present in the preexisting silica matrix. Other impurities, such as the transition metals, constituted less than 0.3% by weight of the sample. The coprecipitate samples contained less than 0.1% impurities.

3. SATURATION MAGNETIZATION OF FINE NICKEL PARTICLES

Since the saturation magnetization of massive polycrystalline nickel has been thoroughly investigated, a comparison of the saturation of the experimental systems of fine particles and the massive nickel calibration samples was first attempted. Any differences found should arise chiefly from the differences in specific surface area. The polycrystalline nickel had a negligible surface area; the particles used for adsorption studies, on the other hand, had approximately

[5] R. E. Dietz, doctoral dissertation, Northwestern University, 1960.
[6] H. Danon, Compt. rend. **246,** 73 (1958).
[7] C. P. Bean and I. S. Jacobs, J. Appl. Phys. **31,** 1228 (1960).
[8] J. J. B. Van Eijk van Voorthuysen and P. Franzen, Rec. trav. chim. **70,** 793 (1951).

20 to 30% of their atoms on the surface. Thus any factors which significantly alter the saturation properties of these surface atoms would produce large differences in the relative saturation.

We now must consider the problem of how to determine the saturation from the magnetization data: Should extrapolations to infinite field intensity be made from a plot of M vs $1/H$, or M vs $1/H^2$, or perhaps some other function of H? The answer must lie in the equation of state for the magnetization of the particular sample, and it is obvious that different types of samples probably follow different laws of approach. The question of the proper inverse power of H for extrapolation to saturation is a critical one, since serious errors may result in the determination of saturation from improper extrapolation technique.[7]

It is not surprising that the samples containing the smallest particles are also the most difficult to saturate. These particles approach molecular dimensions and are quite disordered by thermal energy, even at liquid helium temperatures (in the absence of a magnetic field). In Sec. 5 we shall show that such particles follow a $1/H$ law of approach to saturation if measurements are carried out under certain conditions. For some samples, however, the particles are so small that our maximum field intensities were inadequate to bring all of the particles into the $1/H$ law region. Figures 2 and 3 depict the approach to saturation for two types of samples, measured at different temperatures, as a function of $1/H$. Inspection of these curves shows that for disperse systems of small particles the curves are concave upward, and linear for larger particles. Although these samples contain approximately the same volume fraction of nickel as the calibration samples of polydomain nickel, they show no indication of the $1/H^2$ approach law. This behavior is due, apparently, to the large effect of thermal disordering of the particle moments which obscures the effects of the magneto-

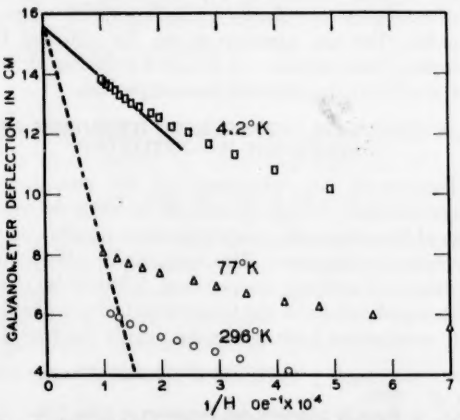

FIG. 2. Approach to saturation magnetization of a sample of coprecipitated nickel in silica at 4.2°, 77°, and 296°K. The dashed line is used to estimate the mean particle volume by Eq. (14).

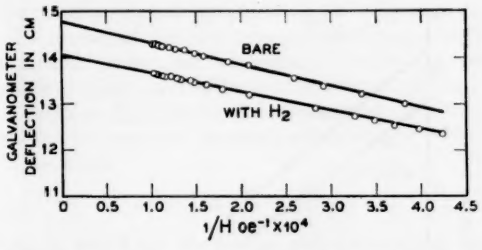

FIG. 3. Approach to saturation magnetization of a sample of sintered UOP catalyst with and without chemisorbed hydrogen, at 4.2°K.

crystalline anisotropy. If the $1/H$ approach law converts to a $1/H^2$ law at very high magnetic fields, then the saturation as extrapolated from the portion of the curve going by a $1/H$ law will be higher than the true saturation. However, if the difference between the magnetization represented by the last experimental point and the saturation magnetization is already a small fraction of the saturation magnetization, as shown in Fig. 3, then the error induced in performing the $1/H$ extrapolation will be at least as small, and probably smaller. At any rate, the ratio of particular interest is the saturation after adsorption of hydrogen to the saturation before adsorption. Since the law of approach does not seem to change greatly after adsorption, the error here will also be very small.

The measurements showed that the saturation of the samples prepared by the impregnation process was very close to that of massive nickel. If these samples are sintered slightly at 800°C in helium, the approaches to saturation become long linear curves for M vs $1/H$ plots, affording accurate extrapolations to infinite field. Five experiments with the sintered UOP nickel-silica catalyst produced an average saturation of $98.4\pm1.0\%$ that of massive nickel. The preparations made by the coprecipitation procedure showed consistently high saturations, about 130% that of massive nickel. These samples consisted of extremely fine particles, and the approach to saturation was quite steep. Consequently the extrapolations are somewhat uncertain for these samples, but we do not feel that this uncertainty can account entirely for the observed discrepancy with the saturation of massive nickel.

There are several reasons why the saturation magnetization of these systems might be *less* than that observed for massive nickel. A common apprehension regarding adsorption on powders concerns the difficulty of obtaining and characterizing "clean" surfaces under the moderately high vacuum conditions of this investigation. Such criticism may not apply to this investigation, however, for two reasons: (a) The surface area of nickel in each pellet is of order of 10 m², while the external area of the pellet is about one square centimeter. Thus the rate at which the internal surface area of the pellet is covered is limited by the rate at

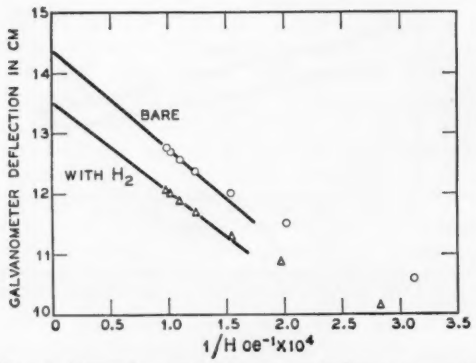

FIG. 4. Approach to saturation magnetization of a sample of coprecipitated nickel in silica with and without chemisorbed hydrogen, at 4.2°K.

which the gas molecules impinge on the external surface of the pellet. The rate at which the internal surface of the pellet is covered with gas, in this case at 10^{-6} mm Hg, is comparable to the rate of coverage for a plane surface at 10^{-11} mm Hg. (b) Since the individual particles are insulated from one another by the silica matrix, the gas molecules crossing the surface of the pellet must penetrate inward by a gaseous diffusion mechanism. As the interstices between the particles are of the same order of size as the particles (less than 100 A), the diffusion mechanism is of the Knudsen type and is, therefore, relatively slow.

The factors discussed above determine that provided the surface were initially clean, it would remain relatively clean for the duration of an experiment. The point that the surfaces were initially clean remains to be established. To this effect, we may use the data of Roberts and Sykes[9] who measured adsorption isotherms for hydrogen on coarse nickel powders at low pressures and to about 430°C. They found that very little hydrogen is adsorbed at 305°C and pressures less than 10^{-3} mm Hg, relative to the amount adsorbed at higher pressure and lower temperatures. From the isotherms published by Roberts and Sykes, we estimate that the equilibrium adsorption at 305°C and 10^{-3} mm Hg represents no more than 4% of the coverage at −183°C and 0.1 mm Hg. Another reason for considering that the surfaces of the nickel as prepared under the conditions described above are essentially clean is that the saturation moment of the nickel particles in the sintered samples coincides with that of massive nickel within 1 or 2%, depending on the run. Since the admission of hydrogen to atmospheric pressure results in a decrease in the saturation of about 10%, we can safely say that at the onset of an experiment, the surface is 80–90% free of hydrogen atoms. The saturation is also reduced by 30–40% when the sample is exposed to air; although such oxidation probably proceeds to a depth of several monolayers, it nevertheless serves to support the view that reduction is virtually complete.

Although there has been a report[10] that supported nickel suffers an appreciable decrease in magnetization because of electronic interaction between the support (generally alumina or alumina doped with semiconducting oxides) and the metallic phase, no such behavior was observed for the silica supports.

The saturation data also suggest that samples showing good agreement with the saturation of massive nickel are in a similar electronic state with respect to ferromagnetic ordering and number of unpaired spins. Considerable conjecture and evidence have been presented in the past few years that the exchange energy is a function of the particle size (or in the case of films, the film thickness) and that below certain critical dimensions this energy rather abruptly becomes very small compared to thermal energy, and a transition from a ferromagnetic, ordered state to a paramagnetic, disordered state ensues. However, other investigations, chiefly measurements of the saturation magnetization of fine ferromagnetic particles precipitated from copper alloys or from mercury amalgams, have demonstrated that the saturation magnetization at 300°K and below is not significantly different from that of the bulk substance.[11] Neugebauer[12] has also shown that the spontaneous magnetization of thin nickel films prepared under ultrahigh vacuum conditions exhibit a temperature dependent spontaneous magnetization similar to that of massive nickel.

In conclusion, these saturation results demonstrate that, with the exception of the coprecipitated samples, the adsorption occurs on a nickel substrate that is electronically similar to massive nickel, insofar as the saturation moment is sensitive to these electronic properties. Since we may, therefore, use the saturation magneton number for massive nickel to describe the saturation of these experimental systems, we are justified in relating the fractional change in saturation of the samples to a change in the saturation magneton number. For the experiments on the sintered UOP samples, there appears to be good evidence that the surface is substantially free from impurities.

4. EFFECT OF CHEMISORBED HYDROGEN ON SATURATION MAGNETIZATION

Because of the complexity of the nonsaturation magnetization of these systems, an accurate determination of the saturation magnetization is possible only at very low temperatures. This necessitates adsorption of hydrogen at ambient temperature, followed by cooling with liquid helium to the temperature of measurement. The unadsorbed hydrogen remaining in the free space

[9] M. W. Roberts and K. W. Sykes, Trans. Faraday Soc. **54,** 548 (1958).

[10] G. M. Schwab, J. Block, and D. Schultze, Z. angew. Chem. **71,** 101 (1959).

[11] C. P. Bean, in *Structure and Properties of Thin Films,* edited by C. A. Neugebauer *et al.* (John Wiley & Sons, New York, 1959), p. 331.

[12] C. A. Neugebauer, Phys. Rev. **116,** 1441 (1959).

was maintained at such low pressures that any subsequent adsorption on the sample during cooling would represent a small fraction of the total amount of gas initially adsorbed.

Figures 3 and 4 represent typical experiments of this type, performed on two different nickel substrates. It is apparent that some difficulty was encountered in making precise extrapolations to saturation magnetization for samples containing very fine particles.

We note that these results are in fair agreement with Moore and Selwood[13] on sintered samples, but that they do not confirm that the fractional change in magnetization diminishes as saturation is approached for unsintered samples. The new results also differ from the work of Lee, Sabatka, and Selwood[14] who observed that the low-field magnetization of similar nickel preparation increased with chemisorption of hydrogen. The reasons for our differences with Moore and Selwood are doubtless based on the increased precision of the present work. The observations of Lee *et al.* are now understood and will be discussed in the next section.

We must express the relative change in saturation $\Delta M_s/M_s$ in terms of the fundamental electronic interaction. The appropriate unit for this purpose is the Bohr magneton β. Since saturation magnetization at absolute zero corresponds to the state with maximum multiplicity for the particle and for the assembly of particles, we can write

$$\Delta M_0/M_0=\Delta(N_{\mathrm{Ni}}\mu_{\mathrm{Ni}})/N_{\mathrm{Ni}}\mu_{\mathrm{Ni}}, \tag{1}$$

where N_{Ni} is the total number of nickel atoms, and μ_{Ni} is the saturation magnetic moment of a metallic nickel atom defined by

$$N_{\mathrm{Ni}}\mu_{\mathrm{Ni}}/V_s=M_0, \tag{2}$$

V_s being the volume of the sample. μ_{Ni} is well known to be about 0.60 β; N_{Ni} may be obtained by analysis of the sample. $\Delta(N_{\mathrm{Ni}}\mu_{\mathrm{Ni}})$ must be related to the effect of the chemisorbed hydrogen. We assume an average attrition ϵ of the magnetic moment of the nickel for each hydrogen atom chemisorbed so that

$$N_{\mathrm{H}}\epsilon=\Delta(N_{\mathrm{Ni}}\mu_{\mathrm{Ni}}), \tag{3}$$

where N_{H} represents the total number of hydrogen atoms chemisorbed. By combining Eqs. (1) and (3),

$$\epsilon=(\Delta M_0/M_0)\,(\mu_{\mathrm{Ni}}N_{\mathrm{Ni}})/N_{\mathrm{H}}. \tag{4}$$

The parameter ϵ is not a completely experimental quantity since it depends on an assumed value of μ_{Ni}; however, if we restrict our consideration to samples which show good agreement with the saturation magnetization of massive nickel, then we may consider the direct calculation of ϵ justified.

To express ϵ more graphically, we may relate it to the number of electron spins cancelled by pairing in the *d* band. In fact, we occasionally identify ϵ as "the number of spins cancelled per hydrogen atom adsorbed." To validate this interpretation, however, we must consider the sources of magnetic moment μ_{Ni}.

If we define

$$\mu=\beta\langle\mathbf{L}+2\mathbf{S}\rangle=g\beta\langle\mathbf{S}\rangle, \tag{5}$$

where $\mathbf{L}$ and $\mathbf{S}$ are the orbital and spin angular momentum respectively, g is the "spectroscopic splitting factor." We can then write $g=2+\xi$, where ξ is a measure of orbital contribution to the magnetic moment. Bagguley,[15] using electron spin resonance on fine particles of nickel gives $g=2.22$. Standley and Reich[16] obtained $g=2.19$, and Meyer[17] obtained $g=2.193$. Argyres and Kittel[18] have pointed out that the number of effective electron spins n_s contributing to the saturation magnetization is just $\mu_{\mathrm{Ni}}(2/g)$; thus $n_s=0.54$.

If the change in magnetic moment arises solely from a cancelling of electron spins, then ϵ calculated by Eq. (4) represents the actual number of spins canceled. If the change in magnetic moment arises from a simultaneous quenching of the orbital magnetic moment with the spin moment so as to keep g constant, then the number of electron spin moments canceled per hydrogen atom adsorbed will be $\epsilon\times(0.54/0.60)=0.90\epsilon$. Values for ϵ have been determined for the various preparations of nickel previously described. For the unsintered samples (this does not include the coprecipitated preparations which exhibit high saturation moments), $\epsilon=0.56\pm0.09$. For the sintered UOP samples, $\epsilon=0.71\pm0.04$. Because of the uncertainty in the extrapolations for preparations containing very small particles, we do not believe that definite conclusions can be reached from these data alone as to whether ϵ varies with particle size, and we shall therefore use the value 0.7 in the following discussions to characterize the interaction of hydrogen and nickel surface.

The fact that only a fractional number of spin moments are canceled when a hydrogen atom chemisorbs on nickel may be rationalized as follows: One can consider that the protons create a set of levels, either continuous or discrete, which the electrons may fill with the restriction that only states below the Fermi energy may be occupied; the remainder of the electrons will occupy holes in the *d* and *s* bands of the nickel.

A second possibility pertains to the similarity between ϵ and μ_{Ni}, suggesting that for each hydrogen atom chemisorbed the moment of a nickel atom is lost to the crystal. One may argue that this atom no longer

[13] L. E. Moore and P. W. Selwood, J. Am. Chem. Soc. **78,** 697 (1956).
[14] E. L. Lee, J. A. Sabatka, and P. W. Selwood, J. Am. Chem. Soc. **79,** 5391 (1957).
[15] D. M. S. Bagguley, Proc. Roy. Soc. (London) **A228,** 549 (1955).
[16] K. J. Standley and K. H. Reich, Proc. Phys. Soc. (London) **B68,** 713 (1955).
[17] A. J. P. Meyer, Compt. rend. **246,** 1517 (1953).
[18] P. Argyres and C. Kittel, Acta Met. **1,** 241 (1953).

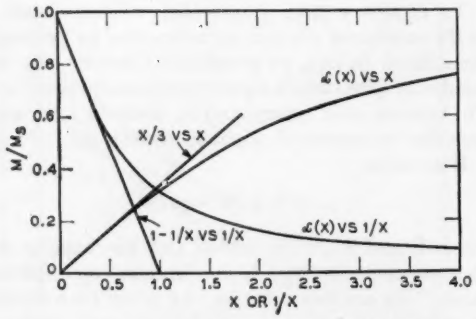

FIG. 5. The Langevin function and its approximations ($x=\mu H/kT$).

contributes to the moment of the particle, and that the hydrogen-nickel interaction does not affect the moment of neighboring atoms.

The first mechanism has an analogy in the magnetic properties of the transition metal alloys, such as the copper-nickel series. Recent experiments[19,20] have shown that the saturation magnetization of copper-nickel alloys decreases linearly with added copper, reaching zero at 53 at.% copper, corresponding to an ϵ for this system of about 0.46 for each copper atom added. (This is just the number of 4*s* electrons a metallic copper atom possesses in excess of metallic nickel atom). It is generally considered that the copper atoms in Cu—Ni retain all ten of their *d* electrons, the remaining electron being divided between the *s* and *d* bands of the alloy. A fraction of this electron must occupy the 4*s* state of the copper atom as dictated by the Fermi level, and the remainder may then occupy states in the *d* band of the alloy, thus accounting for the fractional value of ϵ for Cu—Ni.[21,22] This case may be analogous to that for hydrogen chemisorbed on a nickel surface, and if so, the value of $\epsilon=0.7$ suggests that the electron of the chemisorbed hydrogen atom may likewise have an appreciable density about the hydrogen nucleus.

5. NONSATURATION PROPERTIES

Several questions, important for this investigation, cannot be answered by data derived from our saturation measurements. These concern the dependence of the spin-pairing effect of chemisorbed hydrogen on temperature and of surface coverage over a wide range of coverages. The effect of temperature cannot be obtained from saturation measurements because saturation can only be approached at low temperatures with the highest available magnetic fields. The effect of surface coverage is difficult because of lack of sensitivity in the method, as described. But both factors influence the nonsaturation magnetization strongly, and if we can relate the nonsaturation magnetization to the spontaneous magnetization of the particles, we can separate out the effects.

Fortunately, a theoretical model exists which has been very successful in describing the magnetization curve of fine-particle ferromagnetic systems. Bean and Livingston[23] review the magnetic properties of fine single domain particles.

Bulk ferromagnetic materials consist of regions, called "domains," in which the magnetization is essentially constant and arises spontaneously because of the ferromagnetic exchange energy. The upper limit for the volume of a single domain particle depends on the shape of the particle, but an approximate figure corresponding to a sphere is 150 A in radius. Although a polydomain particle may magnetize by both domain boundary motion and then rotation of the atomic moments, the single domain particle is constrained to magnetize solely by rotation processes. Particles not too eccentric in shape probably magnetize by a coherent rotation of all of the atomic moments in the particle. If such rotation is uniformly facile over all directions, then the particle may be thought of as a paramagnetic atom of very large quantum number, and provided the particles do not interact with one another, their magnetization obeys the classical Langevin equation of state:

$$M/M_s=\coth(\mu H/kT)-(kT/\mu H), \qquad (6)$$

where M is the magnetization under the conditions of field intensity H and temperature T, μ is the magnetic moment of the particles, and M_s is the saturation magnetization corresponding to perfect alignment of the particle moments with the field. Since $\mu=n\mu_{Ni}$, where n is the number of atoms in a particle, approximately 10^2 to 10^5, and μ_{Ni} is the moment per ferromagnetic nickel atom ($=0.6\beta$) the particle acts as an atom with a very large atomic moment: hence the appellation, "superparamagnetism." This equation is derived by applying the Boltzmann distribution law to the assembly of isotropic, noninteracting dipoles, and therefore requires that the assembly be in thermal equilibrium.

Real particles never exhibit such isotropic behavior, however, and magnetization in certain directions always requires more energy than in others. The sources of this anisotropy may lie in the dependence of the magnetostatic energy on the shape of the particle, in differences in energy for magnetizing along the different crystal lattice directions, or from magnetizing energy differences resulting from applications of stress. If the anisotropy is of cubic or randomly oriented uniaxial symmetry, the above equation can be shown to hold at

[19] S. A. Ahern, M. J. Martin, and W. Sucksmith, Proc. Roy. Soc. (London) **A248**, 145 (1958).
[20] A. J. P. Meyer and C. Wolff, Compt. rend. **246**, 576 (1958).
[21] Lomer and W. Marshall, Phil. Mag. **3**, 185 (1958).
[22] Absorbed hydrogen has also been observed to decrease the susceptibility of palladium metal to zero at a H:Pd ratio of about 0.7. Although ϵ is generally taken to be unity for this system [see J. Wucher, Ann. phys. **7**, 317 (1952)], there is no reliable, independent measurement of the moment of palladium to substantiate this assumption.
[23] C. P. Bean, J. D. Livingston, J. Appl. Phys. **30**, 120S (1959).

very low fields where the approximation

$$M/M_s=\mu H/3kT \tag{7}$$

is valid, and also for very high fields where the approximation

$$M/M_s=1-(kT/\mu H) \tag{8}$$

is valid. Figure 5 shows Eqs. (6)–(8) plotted vs $x=\mu H/kT$, and $1/x$. However, if the anisotropy energy is very great, the particle moments may not be in thermal equilibrium, and the Langevin function would not apply. Since the total anisotropy energy is proportional to the volume of the particle, larger particles will be found often to deviate considerably from superparamagnetic behavior, while very small particles should obey the Langevin function more closely. Néel[24] has shown that the approach to equilibrium for an assembly of initially aligned uniaxial particles proceeds as a decay in the remanent magnetization, characterized by a relaxation time τ, where

$$1/\tau=f_0\exp(-Kv/kT), \tag{9}$$

f_0 is a frequency factor of the order of 10^9 sec^{-1}, K is the anisotropy energy per unit volume, and v is the volume of the particle. Thus there will be some critical particle volume for which τ will become very long with respect to experiment, while smaller particles will approach equilibrium almost instantaneously. If particles larger than the critical volume are present, appreciable remanence will be measurable, and this effect is in itself indicative of nonsuperparamagnetic behavior.

Throughout the above discussion we have assumed that μ was independent of the variables of state T and H. This is not strictly true, for the spontaneous magnetization of nickel is a function of both variables, but to a negligible extent for the conditions of this investigation.

Consideration of Eq. (6), and the approximations, shows the magnetization to be a function only of the combined state variable H/T. Thus magnetization

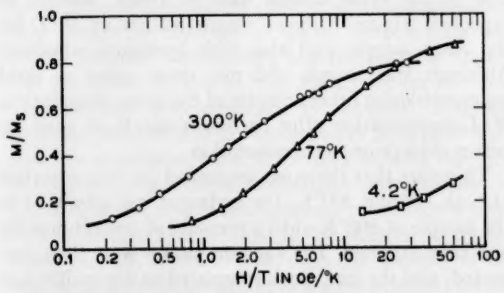

FIG. 6. Test of H/T superposition for a sample of sintered UOP catalyst.

[24] L. Néel, Compt. rend. **228,** 664 (1949); see also W. F. Brown, Jr., J. Appl. Phys. **30,** 130S (1959).

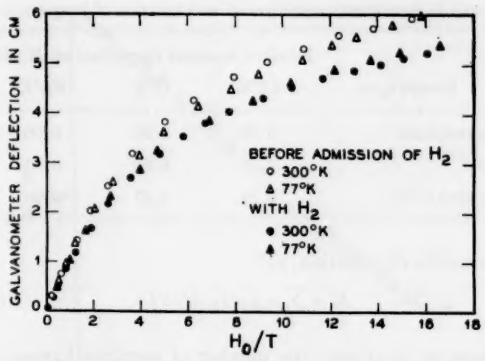

FIG. 7. Test of H/T superposition with and without chemisorbed hydrogen for a sample of coprecipitated nickel on silica. Small corrections were made to correct H for demagnetizing fields as described in the text.

measurements for a variety of field intensities and temperatures should fall on the same curve when M is plotted versus H/T. Such behavior has been observed by Bean and Jacobs[25] with fine particles of iron suspended in mercury, Becker[26] with cobalt particles precipitated from a homogeneous copper-cobalt (copper rich) alloy, and others. The data of Heukelom *et al.*,[27] who were the first to apply the Néel theory to catalyst systems, may also be made to show H/T superposition for nickel-silica catalysts.

We have also made such a study as an adjunct to the chemisorption experiments. Figures 6 and 7 describe tests of H/T superposition for two types of samples. Of our preparations the coprecipitated samples alone exhibit good H/T superposition below 300°K and can, therefore, be classified as superparamagnetic in that region. The behavior of the other samples is apparently complicated by effects of anisotropy, particle interaction, or perhaps other phenomena to cause varying degrees of deviation from the H/T superposition criterion.

Since a consequence of the short relaxation time criterion for superparamagnetic behavior requires that no remanence should be observed, the appearance of remanent magnetization is also a quick indication of nonsuperparamagnetic behavior. The coprecipitated samples, for instance, fail to exhibit measurable remanence at 77°K and above. They do possess remanence at 4.2°K amounting to about 0.10 M_s. Measurements of the remanent magnetization are summarized in Table I for a number of samples.

In such preparations, the particles of metal always have a distribution of sizes. The expression for the magnetization must, therefore, be modified to account

[25] C. P. Bean and I. S. Jacobs, J. Appl. Phys. **27,** 1448 (1956).
[26] J. J. Becker, Trans. Am. Inst. Mining, Met. Petrol. Engrs. **209,** 59 (1957).
[27] W. Heukelom, J. J. Broeder, and L. L. van Reijen, J. chim. phys. **51,** 474 (1954).

TABLE I. Remanent magnetization as a function of temperature.

Sample type	Relative remanent magnetization M_r/M_s 4.2°K	77°K	300°K
Coprecipitate	0.10	0.00	0.00
UOP	0.18	0.02	0.00
Sintered UOP	0.26	0.07	0.00

for such a distribution, as[28]

$$M=\sum_i n_i\mu_i\mathfrak{L}(\mu_iH/kT), \tag{10}$$

where n_i represents the number of particles having a volume v_i and $\mathfrak{L}$ is the Langevin function. By substituting $\mu_i=v_iI_s$, we obtain for the low-field approximation

$$M=(I_s^2H/3kT)\sum_i n_iv_i^2 \tag{11}$$

from which an average particle volume $\langle v^2\rangle_{Av}/\bar{v}$ may be derived:

$$\langle v^2\rangle_{Av}/\bar{v}=(3kT/I_sH)(M/M_s). \tag{12}$$

The high-field approximation (note, this equation predicts a $1/H$ law for the approach to saturation, as is experimentally observed for our samples)

$$M=I_s\sum_i n_iv_i\left(1-\frac{kT}{v_iI_sH}\right) \tag{13}$$

yields an expression for the mean volume $\bar{v}$:

$$\bar{v}=\frac{kT}{I_sH}\left[\frac{1}{1-(M/M_s)}\right]. \tag{14}$$

Because of the deviation due to anisotropy from superparamagnetic behavior at the high field intensities and low temperatures needed to effect saturation, the use of Eq. (7) is generally prohibited, and the low-field volume average must be relied upon. This average $\langle v^2\rangle_{Av}/\bar{v}$, of course, is always larger than the mean volume $\bar{v}$ by a factor characteristic of the volume distribution. As shown in Fig. 2, use of the 77°K data for a coprecipitated sample, which exhibits H/T superposition, would lead to a very low value for the saturation and would not reflect the true slope of the approach to saturation at that temperature. If we suppose that the 4.2°K data reflect true saturation, then the dashed line represents the maximum possible slope. Measurement at higher fields would certainly reveal an even steeper slope for the actual magnetization curve. The dashed line, however, when used to calculate the high field average particle volume gives $\bar{v}=4.5\times10^{-21}$ cm³, corresponding to a spherical particle radius of 10 A. This value, although an upper limit for $\bar{v}$, is considerably smaller than the value $\langle v^2\rangle_{Av}/\bar{v}$ calculated from the initial slope of the magnetization curve for the same sample: $\langle v^2\rangle_{Av}/\bar{v}=63\times10^{-21}$ cm³, corresponding to a spherical particle radius of 25 A. The low-field average volume, therefore, must be used with the understanding that $\bar{v}$ may be appreciably smaller. If we use the value 10 A to calculate the surface area per gram of nickel, we obtain a value of 31 m². The volume of hydrogen adsorbed at complete coverage for similar samples has been estimated by Dr. P. G. Fox in this Laboratory to be about 24 cc/g of nickel. This figure may be related to the surface area by multiplying the number of hydrogen atoms adsorbed by 6.4 A², the area of a single adsorption site.[8] Thus the adsorption measurements indicate an approximate surface area of 43 m²/g of nickel.[29] This figure is in agreement with the magnetic measurement in the sense that the figure 10 A represents an upper limit for $\bar{v}$ and therefore a lower limit for the surface area.

Average particle volumes were also determined for two other preparations using the low field calculations. The corresponding sphere radius for the unsintered UOP preparation was 42 A, and for the sintered UOP 64 A. But as these two preparations did not exhibit H/T superposition at 77° and 300°K, these determinations must be regarded as uncertain.

6. EFFECT OF HYDROGEN ON LOW FIELD MAGNETIZATION

The simplest description for the nonsaturation magnetization is from a viewpoint of superparamagnetism: that is, we consider the effects on systems of particles which show good H/T superposition and zero remanence. The effects of adsorption on nonsuperparamagnetic systems are then approached by considering how these systems deviate from ideal superparamagnetic behavior.

In Sec. 5 we showed that the spontaneous magnetization of samples which exhibit H/T superposition, such as the coprecipitated samples, does not change appreciably over the range of temperature measurements. A similar experiment *after* hydrogen was adsorbed shows the magnetization curve depressed below that of the same sample with a "clean" surface as expected. Figure 7 shows magnetization vs H/T for the clean sample and also with hydrogen adsorbed. Although this sample did not show quite as good superposition as other samples of the same preparation, H/T superposition after chemisorption is as good, or better than prior to chemisorption.

To ensure that the same amount of gas was adsorbed at both 77° and 300°K, the hydrogen was admitted to the sample at 300°K until a pressure of several mm Hg had been attained. The vacuum pumps were then connected, and the free space evacuated to an equilibrium

[28] J. W. Cahn, Trans. Am. Inst. Mining, Met. Petrol. Engrs. **209**, 1309 (1957).

[29] Measurements on similar preparations by adsorption of carbon monoxide have produced nickel surfaces between 31 and 75 m²/g (see reference 2). The total BET surface area on these preparations is about 200 m²/g, but a large fraction of this is, of course, due to the silica support.

pressure of about 0.01 mm Hg. The magnetization was then measured as a function of field intensity at 300°, at 77°, and finally again at 300°K. There was no hysteresis between the two sets of measurements at 300°K.

Although the H/T superposition of this particular sample was poorer than desired, it probably permits the following conclusions. Since H/T superposition implies constancy of the spontaneous magnetization with temperature, we must conclude that the degree of spin-pairing by the chemisorbed hydrogen does not change appreciably over the range between 77° and 300°K. Thus if two different kinds of chemisorbed species are present in equilibrium at some temperature T then either (a) the equilibrium constant does not vary appreciably over the range $77<T<300$, or (b) the two (or more) species have the same spin-pairing effect. In order for (a) to be correct, ΔH for conversion of one type of adsorbed species into another would have to be very small. However, if the conversion is from an atomically adsorbed state to a molecular species as often postulated to account for changes in heats of adsorption and surface potentials with coverage, ΔH would be rather large, making (a) implausible; also (b) would be equally implausible for such a system. On the other hand, if the distribution of bond types is governed by some temperature invariant surface heterogeneity, as the nature of the lattice site, then the distribution of bond types need not necessarily be an equilibrium distribution characteristic of any particular temperature at very high coverages.

A better defined consequence of H/T superposition of the sample with chemisorbed hydrogen is that the spontaneous magnetization has decreased by approximately the amount expected from the spin-pairing mechanism only. These results provide no evidence that the exchange interaction is altered to produce large decreases in the Curie temperature of the particles, as was previously suspected. But the possibility that this may occur at higher temperatures is not yet excluded.

Because of the unsuitability of saturation measurements for investigating the effect of adsorbed gases over wide ranges of coverage at room temperatures and above, Selwood[30] developed a low frequency ac induction apparatus capable of high sensitivity for low field magnetization measurements at elevated temperatures and pressures. Many studies have been performed with this apparatus, most of the results being reported as magnetization-volume isotherms similar to that in Fig. 8. The relative magnetizations so measured have been considered proportional to the relative saturation magnetization. *If this is true*, then the linearity of the magnetization-volume isotherm is good evidence for the independence of the number of electrons paired per gas atom chemisorbed over a wide range of coverage. Also,

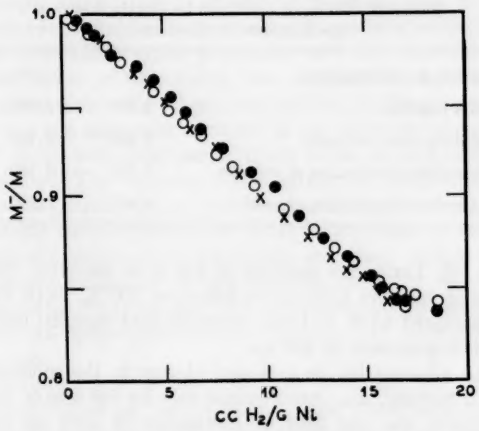

FIG. 8. Three successive magnetization-volume isotherms for hydrogen adsorbed on a sample of unsintered UOP nickel-silica catalyst (after Lee, Sabatka, and Selwood). The ordinate is the ratio of magnetization after some degree of coverage to the initial magnetization. The measurements were performed in a low field (about 100 rms oe) ac induction apparatus at 300°K, and are described in detail in reference 14.

the slope of the isotherm is proportional to the number of spins paired per atom adsorbed ϵ and if this slope could be related to a similar experiment for hydrogen, then the number of d electrons involved in the chemisorption bond with any other molecule could be determined.

As discussed in Sec. 5, the magnetization of an assembly of fine nickel particles is evidently not always linearly related to their saturation magnetization; thus changes in nonsaturation magnetization may not be proportional to the change in saturation. Therefore, we must determine under what conditions these changes are proportional to the corresponding changes in saturation, to validate analysis of the data described in the previous paragraph.

Since we would not expect linear relations between the low field magnetization and saturation magnetization in samples which exhibit remanence or other non-equilibrium behavior, the following discussion will be limited to superparamagnetic systems. This is not a severe practical limitation since the coprecipitated preparations show good superparamagnetic behavior, and in addition have large surface areas. Moreover, other preparations such as nickel-impregnated Davison Gel also exhibit ideal superparamagnetism, and possess superior adsorption properties.[31]

In constructing a theory for the change in magnetization resulting from the adsorption of a given volume of gas, considerable mathematical simplification is attained by limiting consideration to the region $\mu H/kT<0.5$, where we may use the low field approximation of the Langevin function with a maximum error

[30] P. W. Selwood, J. Am. Chem. Soc. **78**, 3893 (1956).

[31] G. C. A. Schuit and L. L. van Reijen, Advances in Catalysis **10**, 242 (1958).

TABLE II. Values of α and α/δ for certain arbitrary particle size distributions.

Particle size distribution	α	α/δ
Delta function	2.000	2.000
Infinitely wide rectangle	1.600	2.400
Maxwellian distribution of volumes	3.734	2.100
Maxwellian distribution of radii	1.471	2.500

of 2%. For nickel particles of 100 A in diameter, this region includes fields up to 100 oe at 300°K. Both the unsintered UOP and the coprecipitated samples meet this requirement at 300°K.

By allowing for an arbitrary change in the moment of a particle, $\Delta\mu_i$ characterized only by the size of the particle, the low field magnetization of such an assembly of superparamagnetic particles is

$$M'=(H/3kT)\sum_i n_i(\mu_i-\Delta\mu_i)^2. \quad (15)$$

The relative change in the magnetization $\Delta M/M$ is then

$$(\Delta M/M)=\frac{\sum n_i(\Delta\mu_i)^2-2\sum n_i\mu_i\Delta\mu_i}{\sum n_i\mu_i^2}. \quad (16)$$

Notice that Eq. (16) is independent of H and T. If we assume spherical particles,

$$\Delta\mu_i=4\pi r_i^2\eta\theta\epsilon, \quad (17)$$

where r_i is the particle radius, η is the number of molecules adsorbed per unit area of surface at complete coverage, and θ is the fraction of the surface covered. We notice that

$$(\eta\theta\epsilon)\,A/I_sV_0=\Delta M_s/M_s, \quad (18)$$

where A is the total surface area of the particles, and V_0 is the total volume of ferromagnetic metal. Upon solving Eq. (18) for $\eta\theta\epsilon$ and substituting into Eq. (17), and converting the radius to the sphere volume, we obtain

$$\Delta\mu_i=(\Delta M_s/M_s)\,(I_sV_0/A)\,4\pi(3v_i/4\pi)^{2/3}. \quad (19)$$

It is convenient to transform n_i into a continuous volume distribution function[26]:

$$n_i\longrightarrow f(v)dv/v, \quad (20)$$

where

$$\int_0^\infty f(v)dv=V_0. \quad (21)$$

Expressing A in terms of the continuous distribution function:

$$A=\int_0^\infty 4\pi r^2[f(v)dv/v]=4\pi(3/4\pi)^{\frac{1}{3}}\int_0^\infty[f(v)dv/v^{\frac{1}{3}}]. \quad (22)$$

Substitution of Eq. (22) in Eq. (16) gives

$$\Delta M/M=-\alpha(\Delta M_s/M_s)+\delta(\Delta M_s/M_s)^2, \quad (23)$$

where α and δ are parameters related to the particle size distribution:

$$\alpha=2\frac{\int_0^\infty v^{\frac{1}{3}}f(v)dv\int_0^\infty f(v)dv}{\int_0^\infty v^{-\frac{1}{3}}f(v)dv\int_0^\infty vf(v)dv}$$

$$\alpha/\delta=2\frac{\int_0^\infty v^{\frac{1}{3}}f(v)dv\int_0^\infty v^{-\frac{1}{3}}f(v)dv}{\int_0^\infty f(v)dv\int_0^\infty v^{\frac{1}{3}}f(v)dv}.$$

From the symmetry of the ratio of integrals, we expect that α/δ and α both are approximately equal to the number 2. Calculations applying these functions to arbitrary volume distributions, summarized in Table II, indicate this expectation to be substantially correct. Furthermore, experimental values for α are: For unsintered UOP, $\alpha\sim2.5$; for coprecipitate, $\alpha\sim3.3$, in approximate agreement with the theoretical values in Table II.

Provided α/δ is of the order of 2 or larger, the second term of Eq. (23) may be neglected, and $\Delta M/M$ is proportional to $\Delta M_s/M_s$. By Eq. (18), $\Delta M_s/M_s$ is linear with θ *provided* ϵ *is independent of* θ. Since linear magnetization-gas volume isotherms are obtained experimentally, as shown in Fig. 8, we conclude that ϵ is independent of surface coverage from $\theta=0$ to that coverage corresponding to a hydrogen pressure over the nickel of nearly an atmosphere.

So far we have not discussed in detail the behavior of particles which do not exhibit superparamagnetic behavior. It is now obvious that the anomalous effects observed by Lee *et al.*,[14] namely, that the effect of chemisorbed hydrogen *increased* the magnetization of a nickel-silica catalyst when measured at 20°K but *decreased* the magnetization at 300°K probably arose

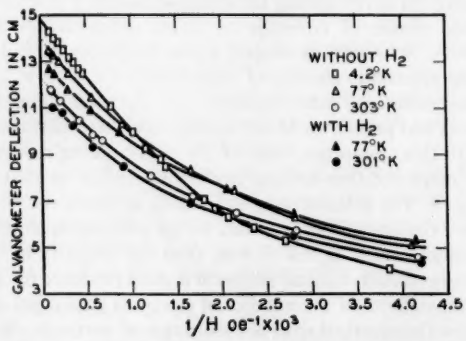

FIG. 9. Approach to saturation of a sample of sintered UOP nickel-silica catalyst, with and without chemisorbed hydrogen.

because the nickel particles were not behaving superparamagnetically at such a low temperature. Taking a cue from Leak's observation[32] that larger particles appear to give the increases in magnetization at higher temperatures than smaller particles, we determined the magnetization curves of a sample of sintered UOP, shown in Fig. 9. Adsorption of hydrogen decreases the magnetization at 300°K, as Lee observed. However, the corresponding data at 77°K show a decrease at high fields, but an increase at low fields. One observes the same sort of effect by merely lowering the temperature of the sample, as evidenced by the curve at 4.2°K. Thus the increase in magnetization at 77°K observed at low fields after adsorbing hydrogen does not result from an increase in the spontaneous moment, but rather from an alteration in the process by which the particle moments rotate to align themselves with the applied magnetic field. It seems possible that the magnetic anisotropy is decreased by the hydrogen, thereby decreasing the relaxation time for the particles; however, as we observed earlier, the remanence of a sample at low temperatures did not appear to be altered appreciably by adsorbed hydrogen. In any event the effects previously thought to be evidence for a change in bond type with, perhaps, formation of a negative hydride ion are seen to be a consequence of deviations from superparamagnetic behavior.

7. CONCLUSIONS

The effect of chemisorbed hydrogen on the saturation magnetization of nickel was investigated on fine particles of nickel. For certain preparations the saturation moment of the nickel was within 1 or 2% of that of massive nickel; this is considered evidence that the surfaces of the nickel in these samples were substantially free from chemisorbed impurities, and that the electronic state of the nickel was identical to that of massive nickel. For these preparations, hydrogen decreases the saturation moment of the nickel by about 0.7 Bohr magneton per average atom of hydrogen adsorbed. The decrease in the saturation magnetization was attributed, as previously suspected,[2] to spin moment cancellation of the nickel 3*d* electrons by the hydrogen electrons. A comparison was made with the magnetic properties of homogeneous alloys. If valid, this comparison indicates that the interacting electrons have an appreciable density around the hydrogen nucleus.

Investigations of the effect of hydrogen on the magnetization of these systems under conditions far from superparamagnetic saturation indicate that: (1) The effect of chemisorbed hydrogen on the saturation magnetization of nickel appears independent of temperature up to 300°K (the highest temperature investigated) and the surface coverage over nearly the entire range; (2) the effect of hydrogen on the saturation magnetization can be simply related to the effect on the low field magnetization of superparamagnetic nickel particle systems; and (3) anomalous effects observed by other investigators probably arose because of deviations from superparamagnetic behavior.

ACKNOWLEDGMENTS

The authors would like to express their gratitude to Professor J. A. Marcus for his advice and assistance in supplying liquid helium, and to C. R. Abeledo for informative discussions. This work was performed under contract with the Office of Naval Research.

[32] R. J. Leak and P. W. Selwood, J. Phys. Chem. **64**, 1114 (1960).

Intermolecular Coupling of Vibrations in Molecular Crystals. II. Intermolecular Forces in CH_3Cl and CD_3Cl†

DAVID A. DOWS

Department of Chemistry, University of Southern California, Los Angeles 7, California

(Received July 28, 1960)

The effect of isotope substitution on band splittings caused by dipole coupling between molecules is examined. For methyl chloride and methyl bromide, the results support the contention that the theory of dipole coupling in its present form is not sufficient to explain the splittings in most bands.

The theory of atom-atom interactions presented in part I of this series is applied to various possible potentials coupling the motions of normal and deuterated methyl chloride molecules. A repulsive potential acting between hydrogen atoms of neighboring molecules accounts for the splittings of several bands. Certain types of coupling potentials seem ruled out by the results of these calculations, while others are left as possible factors in band shifts which occur when a gas is condensed.

IN a recent paper[1] we have presented the infrared spectra of crystalline methyl chloride-d_3 and methyl bromide-d_3. It is the purpose of this article further to investigate the mechanisms of intermolecular coupling which cause the splitting of bands in these spectra and in those of the normal methyl halides. The theoretical approach to be used is presented in part I of this series.[2] Previous application of the theory in I has been made to methyl chloride in a section of the previous paper.[2]

This paper consists of two parts. The first concerns the effect of isotopic substitution on intermolecular dipole interactions. The second applies various "atom-atom" [2] interaction potentials to normal and deuterated methyl chloride to calculate band splittings and shifts.

DIPOLE COUPLING

In I dipole coupling was tested as a mechanism for band splitting. It was concluded that this mechanism predicts splittings which are too small by roughly an order of magnitude in the case of CH_3Cl (one band, corresponding to the C—Cl stretching frequency, is an exception; its splitting is probably largely attributable to dipole coupling). Several approximations in the calculations make desirable further testing of these conclusions. We shall now calculate the ratios of band splittings for isotopically related molecules on the dipole hypothesis for comparison with observation.

The fundamental equation for dipole coupling is[2,3]

$$f_{ij}=\sum(\Phi_{ij}/R_{ij}^3)(\partial\mu/\partial Q)^2, \tag{1}$$

where f_{ij} is the intermolecular coupling constant between molecules i and j, $(\partial\mu/\partial Q)$ is the dipole derivative with normal coordinate for the vibration in question, and the other factors depend only on the geometry. The summation extends over molecules j' which are equivalent to j under translation in the crystal.

The band splitting is obtained from

$$8\pi^2c^2\nu\Delta\nu=\sum\alpha_j f_{ij}, \tag{2}$$

where the α_j are obtained from the coefficients of the unit-cell symmetry coordinates based on molecular normal coordinates and from the unit-cell secular equation. In the above formulas only the frequencies and dipole derivatives are isotope dependent. Thus combining (1) and (2) and taking ratios we obtain[4]

$$\frac{\Delta\nu_H}{\Delta\nu_D}=\frac{\nu_D}{\nu_H}\frac{(\partial\mu/\partial Q)_H^2}{(\partial\mu/\partial Q)_D^2}, \tag{3}$$

where H and D can more generally represent any two isotopic species. This equation does not depend on geometrical factors or on assumptions such as the direction or origin of the transition dipole (except to assume constancy of these factors under isotopic substitution).

For the methyl halides the dipole derivatives in (3) have been determined experimentally in the gas phase.[5] We may thus test the data on the band splittings[1,6] against the predictions of (3) on the assumption that the derivatives do not change on condensation. Table I presents the data and the test. Columns two and three give the observed band splittings, while four and five give, respectively, the observed and calculated ratios of splittings for each fundamental frequency. The solid-phase frequencies themselves are to be found in Table II. For ν_3 of CH_3Cl we take the 698.3 and 702.6 cm^{-1} lines as determining the splitting[1]; for CD_3Cl we assume that the 4-cm^{-1} linewidth indicates a splitting of about 3 cm^{-1}.

Of the 12 pairs in Table I five fail the test, three pass, and four are no test. Of those passing, two are the carbon-halogen stretching bands, which have the largest

† This work was supported by the Office of Ordnance Research, U. S. Army.

[1] D. A. Dows, J. Chem. Phys. **33,** 1743 (1960).

[2] D. A. Dows, J. Chem. Phys. **32,** 1342 (1960) (hereafter referred to as I).

[3] J. C. Decius, J. Chem. Phys. **22,** 1941 (1954).

[4] This result has also been obtained by R. M. Hexter (private communication).

[5] A. D. Dickson, I. M. Mills, and B. Crawford, Jr., J. Chem. Phys. **27,** 445 (1957).

[6] D. A. Dows, J. Chem. Phys. **29,** 484 (1958).

TABLE I. Observed factor group splittings in CH_3Cl, CD_3Cl, CH_3Br, and CD_3Br, and calculated and observed isotopic frequency splitting ratios [Eq. (3)]. Column 1 indicates the vibration and columns two and three give observed splittings in wave number units. An unsplit band is indicated as "<the linewidth."

ν	$\Delta\nu(CH_3X)$[a]	$\Delta\nu(CD_3X)$[a]	$(\Delta\nu_H/\Delta\nu_D)I_{obs}$	$(\Delta\nu_H/\Delta\nu_D)_{calc}$	Result
(X=Cl)					
1	7.0	<4	>1.7	1.07	fail
2	10.4	7.0	1.49	0.48	fail
3	4.3	~3	~1.4	1.46	pass
4	4.9	b	b	1.43	no test
5	7.5	3.2	2.4	1.31	fail
6	<4	<5	...	2.76	no test
(X=Br)					
1	<5	<3	...	1.25	no test
2	3.1	1.9	1.63	0.96	fail
3	6	5.1	1.18	1.21	pass
4	<3	<3	...	1.61	no test
5	11.5	11.9	1.21	1.25	pass
6	5.0	5.7	0.88	2.67	fail

[a] Experimental accuracy is indicated by the number of significant figures as either a few tenths or about one wave number. Data are from works cited in references 1 and 6.
[b] Not observed.

dipole derivatives and smallest motion of atoms other than halogens. These were previously[2,6] considered to be examples of dipole coupling. It is our feeling that the remaining passed case is a coincidence, since the band splitting in question is explained by another coupling interaction in CH_3Cl (below). Thus our conclusion is that dipole coupling is not the major cause of band splitting in these crystals. It remains to be shown, however, that the dipole derivatives (or at least their ratios) remain more or less constant on passage from gas to solid. There are no data on these compounds to substantiate this assumption. We mention below another approach to electrostatic coupling which may prove useful.

COUPLING VIA ATOM-ATOM POTENTIALS

An intermolecular potential involving repulsion between hydrogen atoms (on adjacent molecules) separated by a distance of 2.86 A has been used in I with some success to calculate band splittings for CH_3Cl. A mistake in the calculations[7] has been corrected which changes the result therein in a quantitative sense, though leaving them qualitatively correct. This section of this paper deals with calculations of band splitting force constants for CH_3Cl and CD_3Cl on the assumption of several potentials which can be described as atom-atom potentials in the sense of I. The purpose is to attempt to predict splittings in this molecular crystal and if possible to discover general rules relating two potentials which might be thought of as coupling vibrations in similar crystals. With these aims in mind, the crystal structure of methyl chloride[8] was examined, and the following potentials were selected for trial. The potentials are designated by number, followed by the atoms interacting and the interatomic distance in the crystal. Burbank's preferred hydrogen position is assumed, with H_1 being the hydrogen at zero on the c axis and H_2 being either of the pair above and below the H_1-C-Cl plane of a molecule. The numerals in parentheses indicate the molecule to which an atom belongs, using Burbank's numbering. The potentials are

V_1,	$H_2(I)$–$H_1(II)$,	2.86 A
V_2,	$H_2(I)$–$Cl(IV)$,	3.00 A
V_3,	$H_1(I)$–$Cl(I_{0\bar{1}0})$,	3.01 A
V_4,	$C(I)$–$Cl(II)$,	3.47 A
V_5,	$C(I)$–$Cl(IV)$,	4.08 A
V_6,	$C(I)$–$Cl(I_{010})$,	4.05 A
V_7,	$Cl(I)$–$Cl(II_{0\bar{1}0})$,	4.05 A
V_8,	$Cl(I)$–$Cl(III)$,	4.14 A.

[7] In our calculation of the V_{ij} of Table II of this paper, and of the corresponding numbers of I, the motions of atoms are resolved into Cartesian vector displacements. In subsequent multiplication by the interatomic vector *one* component was consistently given the wrong sign. The erroneous results are not simply related to the correct ones, but the magnitudes of the results were not changed enough to affect the conclusion of I that hydrogen repulsions were important.

[8] D. R. Burbank, J. Am. Chem. Soc. **75**, 1211 (1953).

TABLE II. Calculated factors v_i and w_i for the interactions V_1–V_4 in methyl chloride. The observed solid-state frequencies are included (mean frequency for multiplets).

			V_1		V_2		V_3		V_4	
	Observed frequency	Vibration	v_1	w_1	v_2	w_2	v_3	w_3	v_4	w_4
CH_3Cl	2954.7 cm^{-1}	ν_1	−0.0475	0.0952	−0.00040	0.326	−0.00045	0.323	0.00000	0.00368
	1340.9	ν_2	0.357	0.729	−0.00029	0.0010	−0.00046	0.0022	−0.00001	0.0130
	700.4	ν_3	0.0227	0.0476	−0.00414	0.0117	−0.0052	0.0152	0.00013	0.0489
	3033.7	ν_{4a}	0.0350	0.189	0.00015	0.144	0.00060	0.567	0.00000	0.00001
	1441.3	ν_{5a}	−0.156	0.362	0.00001	0.0001	−0.00005	0.00044	−0.00001	0.00002
	1021.5	ν_{6a}	−0.0568	0.252	−0.00099	0.0139	−0.0040	0.0555	0.00007	0.00038
		ν_{4b}	−0.0042	0.0253	−0.00007	0.438	0	0	0	0
		ν_{5b}	−0.0952	0.205	0.00089	0.0106	0	0	0	0
		ν_{6b}	−0.0222	0.296	0.00311	0.0370	0	0	0	0
CD_3Cl	2147 cm^{-1}	ν_1	−0.0218	0.0481	−0.00055	0.156	−0.00060	0.155	0.00000	0.0083
	1010.5	ν_2	0.155	0.325	0.00015	0.00038	0.00014	0.00032	−0.00002	0.0296
	675.5	ν_3	0.0192	0.0399	−0.00410	0.0108	−0.0045	0.0118	0.00011	0.0338
		ν_{4a}	0.0175	0.0860	0.00014	0.0590	0.00063	0.252	0.00001	0.00002
	1048.5	ν_{5a}	−0.0723	0.165	0.00002	0.00057	0.00005	0.00058	−0.00001	0.00002
	767.0	ν_{6a}	−0.0403	0.118	−0.00120	0.0111	−0.0049	0.0459	0.00010	0.00069
		ν_{4b}	−0.0003	0.0083	−0.00027	0.194	0	0	0	0
		ν_{5b}	−0.0062	0.0279	−0.00006	0.00073	0	0	0	0
		ν_{6b}	−0.0135	0.138	0.00390	0.0321	0	0	0	0

The potentials chosen have the following significance in this crystal: V_1 is a nearest-neighbor hydrogen interaction, already found to be of importance but requiring recalculation; V_2 and V_3 are direct molecular contacts, as is V_4; the other four were taken to represent possible attractive dispersion interactions at minimum distances. It should be noted that potentials V_3, V_6, and V_8 cannot cause factor group ("correlation field") splitting of bands since they act between translationally equivalent molecules in different primitive cells, but can cause site splitting and general shifting.[2]

The theory is exactly as in I. Necessary data include the crystal structure[8] (assumed identical for CH_3Cl and CD_3Cl), the unit-cell analysis [see work cited in reference 2, Eq. (II-3)], and the **L**, **U**, and $\mathbf{D}^{-1}$ matrices for CH_3Cl and CD_3Cl. The matrices are: **L**:—transformation from normal to symmetry coordinates obtained by inversion of $\mathbf{L}^{-1}$ taken from King, *et al.*[9] **U**: transformation from symmetry to internal coordinates.[9] $\mathbf{D}^{-1}$: transformation from internal to Cartesian coordinates, including conditions on center of gravity and angular momenta.[2]

The intermolecular force constants are calculated from equations taken from I,

$$f_n=(\partial^2V/\partial Q_n{}^2)=\gamma\sum\sum(\partial^2V/\partial r_{ij}{}^2)\times[(\partial r_{ij}/\partial r_i)\cdot(\partial r_i/\partial Q_n)]^2 \quad \text{(I-7a)}$$

$$f_{nm}=(\partial^2V/\partial Q_n\partial Q_m)=\gamma\sum\sum(\partial^2V/\partial r_{ij}{}^2)\times[(\partial r_{ij}/\partial r_i)\cdot(\partial r_i/\partial Q_n)][(\partial r_{ij}/\partial r_j)\cdot(\partial r_j/\partial Q_m)], \quad \text{(I-7b)}$$

where $\partial^2V/\partial r_{ij}{}^2$ is the parameter β, the coefficients $\partial r_{ij}/\partial r_i$ are geometrical factors from the crystal structure (r_{ij} is the interatomic vector), and the coefficients $\partial r_i/\partial Q_n$ are the elements of the product matrix $\mathbf{C}=\mathbf{D}^{-1}\mathbf{UL}$, since $\mathbf{r}=\mathbf{CU}$; γ is the number of interactions between one molecule and its neighbors.

It is to be noted that the only way in which the actual form of the potential connecting two atoms enters this calculation is through the second derivative (β) of the potential.[10]

Equations (I-7) can be rewritten in the form

$$f_{nm}=N_a\beta_i\gamma_iv_{nm}, \qquad f_n=N_a\beta_i\gamma_iw_n. \quad (4)$$

[8] W. T. King, J. A. Mills, and B. Crawford, Jr., J. Chem. Phys. **27**, 455 (1957).

[10] In a complete treatment, the first derivative of the potential enters in another factor. Reasons for neglecting this second factor are given in I.

TABLE III. Correlation coupling force constants, observed and calculated.[a]

Band	CH_3Cl $\pm f_{nm}$ (obs)	V_1	V_2	CD_3Cl $\pm f_{nm}$ (obs)	V_1	V_2
1	1220	−53	−39	<380[b]	−25	−53
2	820	400	−28	355	174	15
3	175	26	−400	~120[b]	22	−390
4	865	39	15	c	20	14
5	645	−175	1	185	−80	2
6	<120[b]	−64	−95	<90[b]	−45	−115

[a] All entries in units of $(10^{28}\ \text{sec}^{-2}/N_a) = (1.66\times10^{4}\ \text{sec}^{-2})$.
[b] Not split. Linewidth quoted.
[c] Not observed.

Here N_a is Avogadro's number, γ is defined above, and β_i is $(\partial^2 V_i/\partial r_{ij}^2)_{r=r_e}$. The terms v_{nm} and w_n come from the **U** and **D** matrices in Eqs. (I-7) and are evaluated on a computer. These values are summarized in Table II, in which have been included for convenient reference the solid-state observed frequencies[1,6] (mean frequencies if multiplets occur). In this table only the results for potentials V_1–V_4 are included, as it was discovered that V_5–V_8 are without doubt of little significance in the present problem. Potentials V_5–V_8 were fully calculated, using potentials of the Lennard-Jones 6–12 type estimated in various ways, including assuming that C and Cl were, respectively, similar to Ne and A. No reasonable potentials give intermolecular force constants of any importance, except perhaps in the case of ν_3, where the largest values obtained are in order of magnitude smaller than the values given by V_1.

To compare the results in Table II with experiment we must first assume potentials connecting motions of the relevant pairs of atoms. The potentials needed are: V_1, H···H; V_2 and V_3, H···Cl; V_4, C···Cl. From the assumed potentials we then may obtain the factors β_i needed for use in (4). The following potentials have been assumed,

$$V_{H\ldots H}=1.20\times10^{-10}\exp(-3.54r)-3.42\times10^{-12}r^{-6}$$

$$V_{F\ldots Cl}=9.20\times10^{-8}r^{-12}-57.1\times10^{-12}r^{-6}$$

$$V_{H\ldots Cl}=10.9\times10^{-12}[624\exp(-1.77r)-1]r^{-6}, \qquad (5)$$

where V is in ergs and r in angstrom units. The attractive parts (dispersion forces) of these potentials were obtained as discussed by Pitzer and Catalano.[11] Actually the C···C and Cl···Cl potentials were obtained this way, and the C···Cl potential was obtained in the Lennard-Jones 6–12 form by taking the usual arithmetic and geometric means, respectively, of the distance and energy parameters in the first two potentials.[12] The repulsive term in the H···H potential is that calculated by deBoer.[13] The repulsive part of the H···Cl potential was obtained as the geometric mean of the H···H and Cl···Cl potentials, and is apparently rather unsatisfactory, as will appear below. From these potentials, the second derivatives are $\beta_1=280$, $\beta_2=\beta_3=24\,000$, and $\beta_4=2830$ erg cm^{-2} at the appropriate interatomic distances.

To indicate the magnitudes of the calculated results in comparison with experiment, we first obtain from the splittings given in Table I the phenomenological force constants f_{nm}. These are given by

$$2f_{nm}=8\pi^2c^2\nu\Delta\nu$$

(assuming the observed splittings are all of the correlation coupling type). This relation is just the conversion from frequency (ν) to the frequency parameter ($\lambda=4\pi^2c^2\nu^2$), the factor 2 coming from the unit-cell secular equation as shown in I. These f_{nm} are tabulated in Table III along with the calculated values using the β_i's given above and in Eq. (4). Since V_3, by symmetry does not contribute to correlation coupling, no entries are given; V_4, connecting C(I) and Cl(II) does not contribute to this table because the motions of these atoms are almost identically perpendicular for all vibrations, resulting in practically zero values for f_{nm} (calculated).

From Table III we see several things. First, except for ν_3, potential V_2 seems of little importance; we shall see below that the factor β_2 is probably too large, so that V_2 is even less important in splittings of this type. Second, V_1 seems promising in the cases of ν_2 and ν_5 for both compounds, though it seems of little importance in the case of ν_1 or ν_3. The splittings predicted for ν_6 are less than the observed linewidths; V_1 will be con-

[11] K. S. Pitzer and E. Catalano, J. Am. Chem. Soc. **78**, 4844 (1956).

[12] J. O. Hirschfelder, C. F. Curtiss and R. B. Bird, *Molecular Theory of Gases and Liquids* (John Wiley & Sons, Inc., New York).

[13] J. deBoer, Physica **9**, 363 (1942); also the work cited in reference 11, p. 1085. We have used *only one* pairwise term from deBoer's results, as discussed in I.

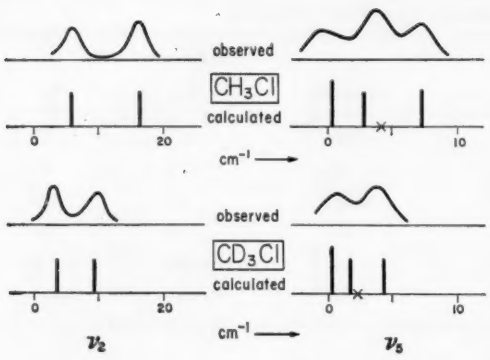

FIG. 1. Calculated and observed spectra in the ν_2 and ν_5 regions of CH_3Cl and CD_3Cl. Based on a hydrogen-hydrogen interaction potential. Intensities and linewidths are indicated.

sidered further below. Third, an interesting though not particularly relevant fact emerges in comparing the V_2 results for CH_3Cl with those for CD_3Cl; it is seen that some of the contributions to the splitting *may increase* even though the band frequency *decreases* on isotopic substitution. Examples are ν_1 and ν_6. This effect is not dependent on the exact form of the potential assumed. This effect was found to be of quite general occurrence in the potentials V_5–V_8, which are also of little importance in the crystals at hand.

HYDROGEN INTERACTIONS

In view of the probable importance of the hydrogen-hydrogen interactions (V_1) for ν_2 and ν_5, we have calculated the crystal spectrum for these bands from the present theory, using this potential. The formulas for the band component positions relative to the unperturbed frequency are given as in Eq. (II-3) in I. Since potential V_1 acts only between molecules I and II, we may drop other force constants and the line frequencies are thus obtained from

$$\begin{aligned}
\lambda_{A_1}-\lambda^0&=f_a+f_{12} \qquad (c \text{ axis})\\
\lambda_{B_2}-\lambda^0&=f_a-f_{12} \qquad (b \text{ axis})\\
\lambda_{A_2}-\lambda^0&=f_b-f_{12} \qquad (\text{inactive})\\
\lambda_{B_1}-\lambda^0&=f_b+f_{12} \qquad (a \text{ axis}).
\end{aligned} \tag{6}$$

It is to be noted that ν_5 alone contributes A_2 and B_1 bands in the solid,[6] and that the formulas (6) involving these frequencies use force constants derived from out-of-plane motions in the crystal. The b–c crystallographic plane is here referred to, and such constants in Table II have subscripts "b." The in-plane constants have subscripts "a" or no subscript, and contribute to A_1 and B_2 frequencies, Since there are four equivalent interactions between molecule I and its neighbors ($\gamma_1=4$), we combine Eqs. (6) and (4) with the data of Table II in the following way to get the line positions,

$$\begin{aligned}
\lambda_{A_1}-\lambda^0&=4\beta_1 N_a[w_{1_a}+v_{1_a}]\\
\lambda_{B_2}-\lambda^0&=4\beta_1 N_a[w_{1_a}-v_{1_a}]\\
\lambda_{A_2}-\lambda^0&=4\beta_1 N_a[w_{1_b}-v_{1_b}]\\
\lambda_{B_1}-\lambda^0&=4\beta_1 N_a[w_{1_b}+v_{1_b}].
\end{aligned} \tag{7}$$

Table IV gives the results before application of a specific value of β_1.

To compare these results with experiment we shall assume a value of $\beta_1=600$ erg cm^{-2}, which is given by the deBoer repulsive potential between two hydrogen atoms.[13] This is higher by a factor of two than the β_1 given by our H···H potential above. Our purpose here is to demonstrate a pattern of the multiplets, and this value of β_1 adjusts the scale to agree with the experimental ν_2 splitting. If the neglect of the attractive part of the potential is taken askance, the equivalent result can be obtained by increasing the repulsive potential by about 50%, more or less in line with our earlier conclusion.[2] The calculated spectrum is shown in Fig. 1, which also includes the observed spectrum. Line intensities are shown roughly by line heights. To compare observed and calculated multiplets, the centers of gravity of the observed lines have been adjusted for each band to match these of the allowed calculated bands. Zero on the scale gives the position of the unperturbed line and the small x's show the position of the inactive A_2 component of ν_5.

The only disagreement of any note between observed and calculated spectra is in the case of ν_5 of CD_3Cl, where the central predicted component does not show up. In view of the breadth of the observed lines it is quite probable that this component is unresolved from one of the other two. The discrepancies in intensities are not to be regarded seriously in view of our present lack of knowledge of intensities in crystals and of the results on component intensities summarized in our previous paper.[6] We note that the centers of gravity of all the bands are predicted to be higher than the gas frequency, as a result of the net repulsive interaction; it is felt that another factor—the normal red shift of lines due to refractive index of the crystal—is probably enough to counteract this effect and give the observed result, namely, that the frequencies in question are lower in the solid than in the gas.

TABLE IV. Calculated line positions for a hydrogen-hydrogen interaction.

	CH_3Cl		CD_3Cl	
	ν_2	ν_5	ν_2	ν_5
$(\lambda_{A_1}-\lambda^0)/4\beta N_a$	1.086	0.206	0.480	0.093
$(\lambda_{B_2}-\lambda^0)/4\beta N_a$	0.372	0.518	0.170	0.237
$(\lambda_{A_2}-\lambda^0)/4\beta N_a$	...	0.300	...	0.110
$(\lambda_{B_1}-\lambda^0)/4\beta N_a$	...	0.034	...	0.022

The results pictured in Fig. 1 are strong indications that the hydrogen repulsion interaction is the major source of line splitting in these cases. The near agreement with a potential with the appropriate attractive term and a repulsive term about 1.5 times the deBoer value is quite satisfactory.

Another term in the H···H interaction potential should be investigated which may be considered an alternate approach to the dipole coupling hypothesis we reject in the first part of this paper. If the hydrogen atoms are considered to carry positive charges ($q$esu) then a repulsion between hydrogens will occur, given by $V=q^2/r$. This potential term contributes to the β factors previously applied to the hydrogen-hydrogen interaction, and the further contribution to the force constants is simply additive. For this potential, $\beta=2q^2/r^3$; if the CH dipole moment is taken to be 0.3 debye units β is 60 erg cm^{-2}. Thus the additional contribution due to electrostatic effects is about 10% of that necessary to fit the observed splitting.

Of course, due to the slow falloff of electrostatic potential with distance, our neglect of other interactions than the H···H one is very crude. It is clear that this type of approach could be carried out for any assumed arrangement of charges on atoms, using the general theory of I. However, since the charges on atoms in molecules are not well known, and since they may well change during vibration, and since the usual problems of convergence of such potentials would arise, we suggest that this approach is tenuous at best. Another modification of dipole coupling theory would consider bond dipoles as units instead of molecular dipoles. Again, any improvements might be indicative, but could not be clear-cut.

SITE SHIFTS

A feature of general interest which can be derived from the data in Table II is the site shift of various frequencies due to various potentials. These shifts are traceable both to the w_i factors and to those v_i factors connecting molecules which are *equivalent* under simple translations in the crystal. In general the magnitudes of the site shifts predicted by the potential functions assumed in this paper are from zero to four wave numbers, though the adjustment of the hydrogen-hydrogen potential made above to fit the ν_2 and ν_5 band multiplets would raise some predicted shifts as high as 6–7 wave numbers. The potentials (V_5–V_8) which are not important in splitting also are not important in shifting bands. Of interest is V_4, which does not cause correlation splitting because of approximate symmetry in the crystal but which will cause site shifts in the bands derived from ν_1 through ν_3 which are comparable with those caused by V_1. This is because these vibrations involve serious repulsion between C(I) and Cl(II).

As has been intimated before, the potential assumed for H···Cl interaction is not realistic. The very high value of $\beta_2=\beta_3$ would not give large correlation splittings, but would give site shifts of over 100 wave numbers in several bands. This seems entirely unacceptable, and probably the repulsion steepness is overestimated. If the β factor is reduced about tenfold to a more reasonable value, no significant correlation coupling is produced, though site shifts of up to ten wave numbers still remain, mainly in the hydrogen motions.

CONCLUSION

It seems well demonstrated that the correlation splittings of ν_2 and ν_5 are due to hydrogen repulsion, which, with a reasonable potential function predict the spectrum quite well, and independently of any assumed potential function predict the ratios of splittings on isotopic substitution. It is probable that ν_3 is coupled by dipole interactions. There is no real evidence in the case of ν_6, since the line is not split. Either dipole or hydrogen repulsion coupling is in agreement with this observation, and the repulsion assumption yields larger calculated force constants. The splitting of the C—H stretching frequencies is not well explained by either of these mechansims, both of which are too low in their predictions. As pointed out in I, dipole coupling is strong enough to cause about 25% of the splitting at best, and the first line of Table I of this paper weighs against this mechanism.

We have previously concluded that the crystal structure of methyl bromide is the same as that of methyl chloride. We feel now that the mechanisms which cause the splittings of bands in the former compound (and its deuterated analog) are probably analogous to those in the latter. If the bromide crystal structure were well known it might be possible to find the cause of the coupling between ν_6 vibrations, since they are split in the bromide.

ACKNOWLEDGMENT

During the course of this work the author has been greatly aided by numerous discussions, especially with Dr. R. M. Hexter and Professor W. B. Person.

Maximum Overlap Atomic and Molecular Orbitals* †

PETER G. LYKOS AND HOWARD N. SCHMEISING

Department of Chemistry, Illinois Institute of Technology, Chicago 16, Illinois

(Received December 14, 1960)

The eigenvectors of the overlap matrix are shown to be maximum overlap orbitals (MO–O's). Naive MO methods, such as that due to Hückel, are shown often to reduce to the MO–O problem. The potential usefulness of MO–O's in the determination of atomic hybrid orbitals and as starting orbitals for SCF calculations is considered.

INTRODUCTION

LÖWDIN[1] has pointed out in a recent review paper that in the application of LCAO-AO and -MO theory to atomic and molecular problems, one often uses nonorthogonal basis sets which are assumed to be linearly independent. For linear dependence to obtain, the overlap matrix must have a nonzero determinent.[2] In fact, as Löwdin observes, the magnitude of the smallest eigenvalue of the overlap matrix is a measure of the near linear dependence of the basis set. Löwdin's observation may be interpreted geometrically as follows.[3]

The n nonorthogonal orbitals comprising the basis set may be considered as n vectors in a function space. The $n\times n$ matrix of n eigenvectors of the overlap matrix, when applied to the basis set, transforms the latter into a new set of n orthogonal vectors with the following properties. The eigenvector belonging to the largest eigenvector value of the overlap matrix transforms the basis set to give a new vector, such that *the sum of the projections of the basis set on the new vector is a maximum*; the second new vector is similarly chosen with the added constraint that it be orthogonal to the first; and so on. Linear dependence will arise if any two or more of the new vectors are not unique.

The criterion of maximum overlap has long been advocated as a measure of the strength of the chemical bond.[4] Looking at Lowdin's argument from the opposite point of view, the largest eigenvalue of the overlap matrix ought to be a measure of maximum overlap. The foregoing geometrical argument certainly indicates this. In the next section, we give an analytical proof of the proposition that the MO–O coefficients are indeed the eigenvectors corresponding to the eigenvalues of the overlap matrix. Following sections deal with applications of the method.

MAXIMUM OVERLAP ORBITALS

Suppose we have a set of orbitals χ_i that we wish to use as a basis for a description of some atom or molecule. The approximate wave function ϕ for the atom or molecule we will take to be a linear combination of the orbitals comprising the basis set, i.e.,

$$\phi=\sum_i c_i\chi_i. \tag{1}$$

If we interpret the χ_i as vectors in a function space then ϕ is some new vector and the projection of χ_p, say, on ϕ is given by the integral

$$\int \chi_p{}^*\phi dv.$$

The magnitude of the projection is most conveniently measured in terms of the real quantity

$$\left|\int \chi_p{}^*\phi dv\right|^2,$$

and the sum of those real quantities over the original basis set we designate as ω, i.e.,

$$\omega=\sum_i\left|\int \chi_i{}^*\phi dv\right|^2. \tag{2}$$

Substitution of (1) into (2) gives

$$\omega=\sum_i\sum_j\sum_k c_j S_{ij}c_k{}^* S_{ki}$$

$$\omega=\sum_k\sum_j c_k{}^*\Big(\sum_i S_{ki}S_{ij}\Big)c_j$$

$$\omega=\mathbf{c}^\dagger\mathbf{S}^2\mathbf{c}, \tag{3}$$

where

$$S_{ij}\equiv\int \chi_i{}^*\chi_j dv$$

is the ijth element of the square matrix $\mathbf{S}$, and $\mathbf{c}$ is a column matrix with elements $c_1, c_2, \cdots, c_n$. The extremum of (3), subject to the constraint that

$$\int \phi^*\phi dv=1=\mathbf{c}^\dagger\mathbf{S}\mathbf{c},$$

* We wish to thank Illinois Institute of Technology for a generous contribution of UNIVAC 1105 computing time.

† This work was supported in part by a grant from the National Science Foundation to Illinois Institute of Technology for which grateful acknowledgment is given.

[1] P. O. Löwdin, Ann. Rev. Phys. Chem. **11**, 107 (1960).

[2] Since the determinant of a matrix is equal to the product of its eigenvalues, the latter must also be nonzero in this case.

[3] T. L. Gilbert, Solid Science Division, Argonne National Laboratory, whom one of us (P.G.L.) thanks for several helpful discussions, and C. Lanczos, *Applied Analysis* (Prentice-Hall Inc., Englewood Cliffs, New Jersey, 1956), pp. 81–95.

[4] L. Pauling, *The Nature of Chemical Bond* (Cornell University Press, Ithaca, New York, 1960), 3rd ed.

TABLE I. AO coefficients for naphthalene calculated by various methods.

		Overlap neglected			Overlap included	
MO	AO	Hückel nearest neighbors only	MO—O	SCF[a]	MO—O	SCF[b]
ϕ_1	+1; +4; +5; +8	0.303	0.303	0.290	0.231	0.237
	+2; +3; +6; +7	0.231	0.255	0.256	0.194	0.217
	+9; +10	0.461	0.432	0.448	0.329	0.288
ϕ_2	+1; +4; −5; −8	0.263	0.272	0.280	0.226	0.255
	+2; +3; −6; −7	0.425	0.419	0.414	0.348	0.327
	+9; +10	0.0	0.0	0.0	0.0	0.0
ϕ_3	+1; −4; −5; +8	0.400	0.404	0.389	0.356	0.344
	+2; −3; −6; +7	0.174	0.186	0.225	0.163	0.235
	+9; −10	0.347	0.322	0.311	0.284	0.216
ϕ_4	+1; +4; +5; +8	0.0	−0.015	0.055	−0.014	0.054
	+2; +3; +6; +7	0.408	0.391	0.361	0.360	0.298
	−9; −10	0.408	0.440	0.483	0.405	0.500
ϕ_5	+1; −4; +5; −8	0.425	0.419	0.408	0.400	0.376
	+2; −3; +6; −7	0.263	0.272	0.288	0.260	0.295
	+9; +10	0.0	0.0	0.0	0.0	0.0
ϕ_6	+1; +4; −5; −8	0.425	0.419	0.414	0.474	0.460
	−2; −3; +6; +7	0.263	0.272	0.280	0.308	0.329
	+9; +10	0.0	0.0	0.0	0.0	0.0
ϕ_7	+1; −4; −5; +8	0.0	0.014	0.020	0.016	0.001
	−2; +3; +6; −7	0.408	0.398	0.331	0.471	0.385
	+9; −10	0.408	0.427	0.529	0.505	0.638
ϕ_8	+1; +4; +5; +8	0.400	0.397	0.404	0.487	
	−2; −3; −6; −7	0.174	0.179	0.233	0.220	
	−9; −10	0.347	0.346	0.256	0.424	
ϕ_9	+1; −4; +5; −8	0.263	0.272	0.288	0.353	
	−2; +3; −6; +7	0.425	0.419	0.408	0.544	
	+9; +10	0.0	0.0	0.0	0.0	
ϕ_{10}	+1; −4; −5; +8	0.303	0.294	0.308	0.417	
	−2; +3; +6; −7	0.231	0.238	0.294	0.338	
	−9; +10	0.461	0.463	0.371	0.657	

[a] C. M. Moser, J. chim. phys. **52**, 24 (1955).

[b] S. Kolboe and A. Pullman, *Calcule des Fonctions d'Onde Moleculaire* (Editions du Centre National de la Recherche Scientifique, Paris, 1958), p. 213. It seems that in Table I (p. 215), ϕ_4 and ϕ_5, have been reversed; similarly with ϕ_6 and ϕ_7.

defines the condition for maximum overlap and leads to the eigenvalue problem

$$\mathbf{S}^2\mathbf{C}=\mathbf{SCA}, \tag{4}$$

or, equivalently, (if $\mathbf{S}^{-1}$ exists),

$$\mathbf{SC}=\mathbf{CA}, \tag{5}$$

where $\mathbf{\Lambda}$ is the diagonal matrix of eigenvalues λ_i and $\mathbf{C}$ is a square matrix made up of the c_i belonging to the λ_i.

The extremum of ω is therefore given by that ϕ_r (or, equivalently, those c_r) which belongs to the largest eigenvalue (λ_r) of $\mathbf{S}$, proving our proposition.

The argument has an immediate extension. A ϕ_s exists such that maximum overlap is attained with the additional constraint that

$$\int \phi_r^* \phi_s d\tau = 0.$$

Such a ϕ_s is given by that c_s which belongs to the second highest eigenvalue (λ_s) of $\mathbf{S}$. Thus, a set of ordered orthogonal ϕ_i can be constructed from the basis set with the c_i which belong to the ordered set of λ_i.

It follows that the eigenvectors of the overlap matrix arising from a LCAO-AO or -MO problem, ordered according to the eigenvalues to which they belong, represent a set of orthogonal AO's or MO's satisfying the criterion of maximum overlap.

STATUS OF HÜCKEL THEORY

The usual Hückel procedure for treating homonuclear pi-electron systems involves the assumption that the diagonal matrix elements of an H_{eff} are all equal to α; that the off-diagonal matrix elements are equal to β for nearest neighbors, and zero otherwise. It is further assumed that β_{ij} is proportional to S_{ij} in the event the various nearest-neighbor pairs are not all equidistant. Then the problem $\mathbf{HC}'=\mathbf{C}'\mathbf{E}'$ is solved for the eigenvalues E_i'. If the substitution $\beta=kS$ is made where k is a constant, and if the matrix equation is divided through by k,

$$[\mathbf{S}+(\alpha k^{-1}-1)\mathbf{I}]\mathbf{C}'=\mathbf{C}'\mathbf{E}'k^{-1}. \tag{6}$$

TABLE II. LCAO-AO coefficients for ground state beryllium.

		Roothaan *et al.* SCF		MO-AO's (this paper)		
ζ	n	$1S$	$2S$	1st eigenvector	2nd eigenvector	eigenvalues
6.50	0	0.442306	−0.106320	0.225961	−0.246009	6.8565019
	1	0.196025	−0.036690	0.303434	−0.257808	3.0757703
	2	0.069198	−0.006877	0.339354	−0.207757	1.4274026
	3	0.029984	−0.001767	0.344673	−0.127165	0.4683782
3.40	0	−0.000000	0.000171	0.336168	−0.224973	0.1293558
	1	0.494810	−0.303578	0.367019	−0.099831	0.0366284
	2	−0.161936	0.058670	0.338228	0.054697	0.0045809
	3	0.026115	−0.061146	0.289478	0.186126	0.0011311
0.90	0	0.006644	0.496479	0.325306	0.260498	0.0001706
	1	−0.007953	0.694577	0.211476	0.457469	0.0000664
	2	0.004735	−0.050554	0.135054	0.490612	0.0000142
	3	−0.001211	0.044122	0.090641	0.444555	0.0000005
						sum = 12.0000009

Since $\mathbf{I}$ multiplied by a scalar commutes with any matrix, (6) becomes

$$\mathbf{SC}'=\mathbf{C}'[k^{-1}(\mathbf{E}'-\alpha\mathbf{I})+\mathbf{I}]. \tag{7}$$

Comparison with (5) shows that, up to normalizing factors,

$$\mathbf{C}=\mathbf{C}'. \tag{8}$$

Also

$$k^{-1}(\mathbf{E}'-\alpha\mathbf{I})+\mathbf{I}=\mathbf{\Lambda}$$

or

$$\mathbf{E}'=k(\mathbf{\Lambda}-\mathbf{I})+\alpha\mathbf{I}. \tag{9}$$

Equation (8) states that the Hückel MO's neglecting overlap are identical with the MO–O's if the MO–O's are normalized such that $\mathbf{C}^{\dagger}\mathbf{C}=\mathbf{I}$. Furthermore, (9) states that the Hückel orbital energies are simply related to the MO–O eigenvalues as follows:

$$E_i'=\alpha+(\lambda_i-1)k. \tag{10}$$

If overlap is *included* in the Hückel treatment, then we have to solve the problem $\mathbf{HC}''=\mathbf{SC}''\mathbf{E}''$. After substituting for $\mathbf{H}$, we have

$$k\mathbf{SC}''+(\alpha-k)\mathbf{C}''=\mathbf{SC}''\mathbf{E}''$$

or

$$\mathbf{SC}''=\mathbf{C}''(k-\alpha)(k\mathbf{I}-\mathbf{E}'')^{-1}.$$

Comparison with (5) shows that

$$\mathbf{\Lambda}=(k-\alpha)(k\mathbf{I}-\mathbf{E}'')^{-1}$$

or

$$\mathbf{E}''=(\alpha-k)\mathbf{\Lambda}^{-1}+k\mathbf{I} \tag{11}$$

or

$$\mathbf{E}''=\mathbf{\Lambda}^{-1}\mathbf{E}' \tag{12}$$

and

$$\mathbf{C}''=\mathbf{C}. \tag{13}$$

We note that the Hückel orbitals found here are normalized in the sense that $(\mathbf{C}'')^{\dagger}\mathbf{SC}''=\mathbf{I}$. If we consider that our secular equation solver produces solutions normalized such that $(\mathbf{C}')^{\dagger}\mathbf{C}'=\mathbf{I}$, i.e., neglecting overlap (as is usually the case), then we may transform that set of solutions to a set normalized such that $(\mathbf{C}'')^{\dagger}\mathbf{SC}''=\mathbf{I}$, i.e., including overlap, by taking $\mathbf{C}''=\mathbf{S}^{-\frac{1}{2}}\mathbf{C}'$ or, equivalently, $\mathbf{C}''=\mathbf{C}'\mathbf{\Lambda}^{-\frac{1}{2}}$. A particular member of (12) is $E_i''=E_i'/\lambda_i$. This shows explicitly that the orbital energies including overlap are equal to the corresponding orbital energies neglecting overlap divided by the corresponding eigenvalue of the overlap matrix. Furthermore, the normalized eigenvector (LCAO–AO or –MO) including overlap is equal to the corresponding normalized eigenvector (LCAO–AO or –MO) neglecting overlap divided by the square root of the corresponding eigenvalue of the overlap matrix, i.e.,

$$C_j''=\lambda_j^{-\frac{1}{2}}C_j'.$$

Equations (9) and (11) show that all previous Hückel type calculations carried out for homonuclear systems in terms of α and β—with or without overlap—are tantamount to solving the eigenproblem of an overlap matrix in association with a suitable scale factor k; and a disposable parameter α. The sole effect of the latter is to shift the spectrum of energy levels. Equations (8) and (13) show that the results obtained with neglect of overlap are readily transformed to those obtainable if it were included.

Since the matrix $\mathbf{S}$ reflects the geometry of the molecule, in the case of homonuclear systems *the Hückel method merely constrains the solution of the problem to conform to the molecular geometry, subject to the criterion of maximum overlap.* In other words, such Hückel MO's are MO–O's.

The correspondence between maximum overlap and Hückel MO's breaks down when nonequivalent atoms are involved. For an asymmetrically substituted ethylene within the pi-electron approximation, for example, the maximum overlap orbitals will be just the sum and difference of the two atomic orbitals as for ethylene itself. The source of the trouble is most easily seen by examining the term $(\alpha k^{-1}-1)\mathbf{I}$ in (6). This has now to be replaced by a diagonal matrix $\mathbf{\Delta}$, at least one

of whose elements is unique. We now have to deal with the matrix equation

$$(\mathbf{S}+\mathbf{\Delta})\mathbf{C}'=\mathbf{C}'\mathbf{E}'k^{-1}.$$

But we *cannot* deduce from this

$$\mathbf{SC}'=\mathbf{C}'(\mathbf{E}k^{-1}-\mathbf{\Delta}),$$

because $\mathbf{\Delta C}'$ is not necessarily equal to $\mathbf{C}'\mathbf{\Delta}$. However, the MO–O's may be used as the basis of a perturbation calculation as with atom-atom, atom-bond, and bond-bond polarizabilities;[5] or, more generally, as internally programmed starting orbitals in an SCF calculation.[6]

MO-O'S AND SCF LCAO-AO AND -MO CALCULATIONS

Hückel orbitals have long been used as a starting set for SCF LCAO–MO calculations. In fact, Pople[7] has presented a pi-electron theory which is formally cast into an SCF LCAO–MO framework but which in fact uses Hückel MO's. In the last section we demonstrated that such a starting set can be readily obtained by solving the problem $\mathbf{SC}=\mathbf{C\Lambda}$ with $\mathbf{C}^{\dagger}\mathbf{C}=\mathbf{I}$ whence the starting set is either $\mathbf{C}$ or $\mathbf{CA}^{-1}$ according as overlap is to be neglected or not. The Hückel orbitals used in the past have usually (if not always) been those calculated for first neighbor interactions only. As an illustration of the usefulness and general advantages of MO–O's over Hückel MO's, we have collected the results of several calculations within the pi-electron approximation for naphthalene in Table I.

As we might expect from the results of the previous section, the middle three columns of Table I are in substantial agreement. We note that the agreement between the MO–O's and SCF MO's without overlap is rather better than that between the Hückel MO's and the SCF MO's. This is because the former pair of results were computed including *all* neighbors. The agreement between the last two columns is also very satisfactory. However, this need not necessarily have been the case because in actual fact, the SCF energy operator $\mathbf{F}$ and $\mathbf{S}$ do not necessarily commute.[8] Accordingly, we *expect* nonperfect agreement between the MO–O's and the SCF LCAO–MO's whether overlap is included or not. However, a close agreement implies that $\mathbf{F}$ and $\mathbf{S}$ *nearly* commute.

An important point to notice is that $\mathbf{F}$, like $\mathbf{S}$ also reflects the molecular geometry. Bearing in mind our remarks about the breakdown in the correspondence between MO–O's and Hückel MO's for heterosystems, an important factor in determining the commutability of $\mathbf{F}$ and $\mathbf{S}$ is that the *diagonal* elements of $\mathbf{F}$ should not differ greatly.

[5] C. A. Coulson and H. C. Longuet-Higgins, Proc. Roy. Soc. (London) **A191,** 39, (1947); **A192,** 16 (1947).

[6] O. W. Adams of this laboratory is in fact using this technique in an open and closed shell SCF LCAO-MO general pi-electron computer program.

[7] J. A. Pople, Trans. Faraday Soc. **49,** 1375 (1953).

[8] A necessary and sufficient condition that two matrices shall commute is that they have simultaneous eigenvectors.

TABLE III. Maximum overlap molecular orbitals for ClF_3.

Eigenvalues[a]		The chlorine symmetry hybrid orbitals χ_i (normalized to ½ or to 1 according as the fluorine orbitals occur in the MO or not)								The fluorine molecular orbitals: (normalized to ½)		
		S	X	Y	Z	Z^2	(X^2-Y^2)	XY	XZ	YZ	ϕ_1'	ϕ_2'	ϕ_3'
1.3619	ϕ_1	0.1556	0	0	−0.1556	−0.4752	0.4752	0	0	0	−0.3251	0.4440	0.4440
1.2811	ϕ_2	0.3869	0	0	0.3869	0.3167	0.3167	0	0	0	0.6280	0.2298	0.2298
1.2449	ϕ_3	0	0.7071	0	0	0	0	0	0	0	0	0.5000	−0.5000
1.0000	ϕ_4	−0.2797	0	0	0.8069	−0.1442	−0.5000	0	0	0	0	0	0
1.0000	ϕ_5	−0.7576	0	0	0.0334	0.5719	0.3129	0	0	0	0	0	0
1.0000	ϕ_6	0	0	0	0	0	0	1	0	0	0	0	0
1.0000	ϕ_7	0	0	0	0	0	0	0	1	0	0	0	0
1.0000	ϕ_8	0	0	1	0	0	0	0	0	1	0	0	0
1.0000	ϕ_9	0	0.7071	0	0	0	0	0	0	0	0	−0.5000	0.5000
0.7550	ϕ_{10}	0.3869	0	0	0.3869	0.3167	0.3167	0	0	0	−0.6280	−0.2298	−0.2298
0.7189	ϕ_{11}	0.1556	0	0	−0.1556	0.4752	0.4752	0	0	0	0.3251	−0.4440	−0.4440
0.6381	ϕ_{12}												
Sum = 12.0000													
No. of orbitals													

[a] The eigenvalues reported here are the actual eigenvalues divided by ten so as to correspond to an overlap matrix with unity on the principal diagonal. This in no way affects the corresponding eigenvectors.

SCF calculations are carried out for atoms as well as molecules, and so we solved the eigenproblem of the overlap matrix which arises from a recent analysis of the ground state of beryllium.[9] The basis set of twelve STO's (Slater-type orbitals) taken by Roothaan *et al.* (see reference 9) gives unnormalized matrix elements of the form

$$S_{(ij,kl)}=\int \exp[-(\zeta_i+\zeta_k)r]r^{(j+l+2)}dr$$

$$=\frac{(j+l+2)!}{(\zeta_i+\zeta_k)^{(j+l+2)}}, \qquad (14)$$

where ζ_i, ζ_k are the orbital exponents, and j, l are the principal quantum number analogs belonging to i, k. In the present case, $\zeta=6.5$, 3.4, and 0.9; $i, j=0$, 1, 2, 3. The eigenvalues and the vectors belonging to the two largest eigenvalues are presented in Table II, together with the LCAO–AO coefficients obtained by Roothaan *et al.* (see reference 9).

We may make two observations: (1) The correspondence between the SCF and MO–AO's is poor; and (2) the eigenvalues of the overlap matrix rapidly became very small. Since the diagonal elements of the energy operator will be quite different in magnitude, near commutability of the energy and overlap matrices will not obtain, and hence our first observation was to be expected. Löwdin[1] specifically points out that near linear dependence is liable to arise if STO's are used as a basis set—the smallest eigenvalue of the overlap matrix being a measure of such near dependence. Our second observation suggests that near linear dependence obtains in this basis set for beryllium.

MAXIMUM OVERLAP VALENCE BOND HYBRIDS

Murrell has recently invoked the criterion of maximum overlap in a valence bond framework.[10] The problem which he considered as an example involved the molecule ClF_3 which is approximately T-shaped as shown:

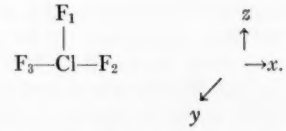

He considered explicitly the chlorine $3s$, $3p$, and $3d$ orbitals and some unspecified orbital, ϕ', at each fluorine. If we recognize that his overlap integrals are not over normalized orbitals and if we neglect the overlaps between different fluorine orbitals, the overlap matrix assumes an interesting form as shown:

	S	X	Y	Z	Z^2	(X^2-Y^2)	XY	XZ	YZ	ϕ_1'	ϕ_2'	ϕ_3'
S	10									1	1	1
X		10								0	$3^{\frac{1}{2}}$	$-3^{\frac{1}{2}}$
Y			10				0			0	0	0
Z				10						$3^{\frac{1}{2}}$	0	0
Z^2					10					$5^{\frac{1}{2}}$	$-\frac{1}{2}(5)^{\frac{1}{2}}$	$-\frac{1}{2}(5)^{\frac{1}{2}}$
(X^2-Y^2)			0			10				0	$\frac{1}{2}(15)^{\frac{1}{2}}$	$\frac{1}{2}(15)^{\frac{1}{2}}$
XY							10			0	0	0
XZ								10		0	0	0
YZ									10	0	0	0
ϕ_1'	1	0	0	$3^{\frac{1}{2}}$	$5^{\frac{1}{2}}$	0	0	0	0	10		
										0		
ϕ_2'	1	$3^{\frac{1}{2}}$	0	0	$-\frac{1}{2}(5)^{\frac{1}{2}}$	$\frac{1}{2}(15)^{\frac{1}{2}}$	0	0	0		10	
										0		
ϕ_3'	1	$-3^{\frac{1}{2}}$	0	0	$-\frac{1}{2}(5)^{\frac{1}{2}}$	$\frac{1}{2}(15)^{\frac{1}{2}}$	0	0	0			10

[9] C. C. J. Roothaan, L. M. Sachs, and A. W. Weiss, Revs. Modern Phys. **32,** 186 (1960).
[10] J. M. Murrell, J. Chem. Phys. **32,** 767 (1960).

The chlorine orbitals are mutually orthogonal and the fluorine orbitals are assumed to be mutually orthogonal. Thus there is neither chlorine orbital intra-atomic overlap nor any fluorine interatomic overlap. The only overlap is between the several chlorine orbitals and the several fluorine orbitals (except where it is zero by symmetry). Hence in this case the maximum overlap molecular orbitals ϕ_i contain the maximum overlap chlorine *symmetry hybrid orbitals* χ_i, i.e., that part of ϕ_i which contains chlorine atomic orbitals only, plus the several linear combinations of the fluorine orbitals as shown in Table III. The chlorine *symmetry hybrid orbitals* obtained here, of course, reflect the symmetry of the molecule. The first three may be transformed to an equivalent set of *directed hybrid orbitals*, ψ_1, ψ_2, and ψ_3 as follows. If the symmetry of the molecule is invoked and if the ψ_i are required to be orthonormal then one readily obtains the following:

$$\psi_1 = a\chi_1 + (1-a^2)^{\frac{1}{2}}\chi_2$$

$$\sqrt{2}\psi_2 = (1-a^2)^{\frac{1}{2}}\chi_1 - a\chi_2 + \chi_3$$

$$\sqrt{2}\psi_3 = (1-a^2)^{\frac{1}{2}}\chi_1 - a\chi_2 - \chi_3,$$

where ψ_1, ψ_2, and ψ_3 "point" more or less at F_1, F_2, and F_3, respectively, depending on the value of a and where ψ_2 and ψ_3 are equivalent orbitals. A reasonable way to take up the remaining degree of freedom, namely, the value of a, would be to require that the overlap between ψ_1 and ϕ_1', or that between ψ_2 and ϕ_2', or some weighted average of those overlaps, be at a maximum. The fact that the odd Cl—F bond is shorter than the other two[11] suggests that the overlap between ψ_1 and ϕ_1' should be favored. Explicitly the distinct pair of overlap integrals is

$$\int \psi_1 \phi_1' dv \equiv X_{11} = -1.6637a + 2.4964(1-a^2)^{\frac{1}{2}}$$

and

$$\int \psi_2 \phi_2' dv \equiv X_{22} = -0.6461a + 1.6070(1-a^2)^{\frac{1}{2}} + 1.2247$$

$$\left(\int \psi_3 \phi_3' dv \equiv X_{33} = X_{22}\right).$$

We calculated the value of a such that $X_{11}+X_{22}+X_{33}$ or, equivalently, such that $X_{11}+2X_{22}$ should be a maximum and found as expected that the corresponding hybrid orbitals are the same as Murrell's. We also calculated a for extremum values of X_{11} and X_{22} separately. These values of a and the corresponding values of X_{11} and X_{22} are as follows:

	X_{11} max	X_{22} max	$(X_{11}+2X_{22})$ max
a	−0.5546	−0.3730	−0.4597
X_{11}	3.0000	2.9368	2.9818
X_{22}	2.9203	2.9568	2.9489

For the two lone pairs which are yet to be accommodated, we observe that the next six *symmetry hybrid orbitals*, χ_4 through χ_9, are degenerate. We may classify these according as they are symmetric (+) or antisymmetric (−) to reflection in the planes xz and yz, respectively, as follows: $\chi_4(+,+)$, $\chi_5(+,+)$, $\chi_6(-,-)$, $\chi_7(+,-)$, $\chi_8(-,+)$, and $\chi_9(-,+)$. We require that the two equivalent orbitals ψ_4 and ψ_5 go into each other on reflection in xz and into themselves on reflection in yz. This eliminates χ_6 and χ_7 from each and indicates that χ_4 and χ_5 enter in the same way in both while the combination of χ_8 and χ_9 enters with opposite sign. Explicitly the orthonormal pair of equivalent hybrids is

$$\sqrt{2}\psi_4 = [a\chi_4 + (1-a^2)^{\frac{1}{2}}\chi_5] + [b\chi_8 + (1-b^2)^{\frac{1}{2}}\chi_9]$$

and

$$\sqrt{2}\psi_5 = [a\chi_4 + (1-a^2)^{\frac{1}{2}}\chi_5] - [b\chi_8 + (1-b^2)^{\frac{1}{2}}\chi_9].$$

Two additional conditions would have to be specified in order to uniquely determine ψ_4 and ψ_5.

CONCLUSION

It has been shown that the eigenvectors corresponding to the eigenvalues of the overlap matrix of some set of orbitals are, in fact, maximum overlap orbitals. Since commuting matrices have simultaneous eigenvectors, the maximum overlap eigenvectors will resemble the minimum energy eigenvectors whenever the energy matrix and the overlap matrix nearly commute. Hückel pi-electron theory for homonuclear systems reduces to the maximum overlap problem, if the assumption is made that the β_{ij} are proportional to the corresponding S_{ij}. When rather different basis orbitals are used as in the analytical representation of Hartree-Fock atomic orbitals, the diagonal elements of the energy matrix are dissimilar; hence the correspondence to maximum overlap orbitals breaks down. There appears to be merit in the use of maximum overlap orbitals within a valence bond framework in the determination of hybrid orbitals.

Master tables and relatively simple formulas for overlap integrals have been collected together in a paper by Mulliken, *et al.*[12] Most computer centers have ready-made programs for solving eigenvalue problems. Thus maximum overlap orbitals are quite accessible and may be used directly as such when more desirable orbitals are not immediately available.

[11] D. F. Smith, J. Chem. Phys. **21**, 609 (1953).

[12] R. S. Mulliken, C. A. Rieke, D. Orloff, and H. Orloff, J. Chem. Phys. **17**, 1248 (1960).

On the Approximation of Zero Differential Overlap*

C. A. COULSON

Mathematical Institute, Oxford, England

AND

L. J. SCHAAD

Department of Chemistry, Indiana University, Bloomington, Indiana

(Received November 28, 1960)

The approximation of zero differential overlap is shown unreliable when applied to nonempirical calculations on HF and H_2.

I. INTRODUCTION

ALTHOUGH the approximation of zero differential overlap has been found to give good results in semiempirical calculations,[1,2] still one might feel on safer ground if it were shown good in nonempirical calculations as well.

Stewart[3] has examined the electron-repulsion energy of H_2 and of the π electrons in ethylene. He concludes that the zero differential overlap approximation is appropriate to already approximate calculations on π systems, but that it is probably dangerous in $1s\sigma$ systems. He further feels that the approximation should not be used in any variational computation.

We report here LCAO-SCF calculations, with varying orbital exponents, on the HF molecule and LCAO calculations on H_2 in which we have neglected differential overlap. We agree with Stewart; the approximation is dangerous.

II. HYDROGEN FLUORIDE

A. Method

The wave function used was the single Slater determinent

$$\Psi = (10!)^{-\frac{1}{2}} \det|\phi_1(1)\alpha(1)\phi_1(2)\beta(2)\cdots\phi_5(10)\beta(10)| \tag{1}$$

with

$$\phi_1 = (a^3/\pi)^{\frac{1}{2}} \exp(-ar_F),$$

$$\phi_2 = (\mu_1^5/\pi)^{\frac{1}{2}} y_F \exp(-\mu_1 r_F),$$

$$\phi_3 = (\mu_1^5/\pi)^{\frac{1}{2}} x_F \exp(-\mu_1 r_F),$$

$$\phi_4 = (1+k^2+\lambda^2)^{-\frac{1}{2}}[(\mu_1^5/\pi)^{\frac{1}{2}} z_F \exp(-\mu_1 r_F) + kS + \lambda(b^3/\pi)^{\frac{1}{2}} \exp(-br_H)],$$

$$\phi_5 = (1+k^2)^{-\frac{1}{2}}[k(\mu_1^5/\pi)^{\frac{1}{2}} z_F \exp(-\mu_1 r_F) - S], \tag{2}$$

where

$$S = (1-K^2)^{-\frac{1}{2}}[(\mu_2^5/3\pi)^{\frac{1}{2}} r_F \exp(-\mu_2 r_F) - K(a^3/\pi)^{\frac{1}{2}} \exp(-ar_F)],$$

$$K = 8(3a^3\mu_2^5)^{\frac{1}{2}}(a+\mu_2)^{-4}.$$

In Eq. (1), ϕ_1, ϕ_2, and ϕ_3 are fluorine $1s$, $2p\pi_y$, and $2p\pi_x$ atomic orbitals, not used in bonding; ϕ_4 is the molecular orbital to describe the bond, and ϕ_5 is the remaining lone-pair orbital, chosen to have no hydrogen $1s$ orbital in it. All five ϕ functions (see later) form an orthonormal set. The coefficients of ϕ_4 and ϕ_5 are related because of the zero differential overlap approximation.

We have investigated two ways of applying the zero differential overlap approximation. Method I, abbreviated to (I), consists of replacing by zero any one-electron integral, $\int \Theta(1)\Omega(1)d\tau_1$, or two-electron integral, $\int \Theta(1,2)\Omega_1(1)\Omega_2(2)d\tau_{12}$, containing a two-center charge distribution Ω. [Here $\Theta(1)$ and $\Theta(1,2)$ are one- and two-electron operators; Ω's are charge distributions.] Method II, abbreviated to (II), is the same for two-electron integrals, but the only one-electron integrals dropped are the two-center overlaps [$\Omega(1)$ a two-center distribution and $\Theta(1)=1$]. The second method is the usual one,[1-3] but the first also seems to deserve consideration. It is perhaps the more consistent of the two, and it gives the better total energy for the ground state of both HF and H_2, (though perhaps only through accidental canceling of neglected integrals). With either of the two approximations, the functions $\phi_1\cdots\phi_5$ form an orthonormal set.

Using Eq. (1), the energy of the HF ground state was minimized with respect to the parameters λ, k, a, μ_1, and μ_2 at an internuclear distance of 1.7328 a.u.[4] As far as the total energy, the total wave function, and the orbital energies of ϕ_1 to ϕ_3 are concerned, this is equivalent to an LCAO-SCF calculation without $(1s)_F$ mixing and with neglect of differential overlap. The orbitals ϕ_4 and ϕ_5 are not themselves LCAO-SCF orbitals, but linear combinations of them. However, in view of the determinantal character of Eq. (1),

* Supported by the National Institutes of Health and by the National Science Foundation.

[1] R. Pariser and R. G. Parr, J. Chem. Phys. **21**, 466, 767 (1953).
[2] J. A. Pople, Trans. Faraday Soc. **49**, 1375 (1953).
[3] E. T. Stewart, J. Chem. Soc. **1959**, 1856.

[4] We use atomic units throughout. See D. R. Hartree, *The Calculation of Atomic Structures* (John Wiley & Sons, Inc., New York, 1957), p. 5.

there is no need to determine the correct mixing to obtain these LCAO-SCF orbitals.

B. Computational Details[5]

The energy of Eq. (1) is given by

$$E=2\sum_{i=1}^{5}H_i+\sum_{i,j=1}^{5}(2J_{ij}-K_{ij}), \qquad (3)$$

where the symbols have their usual meaning.[6] Having neglected differential overlap, the integrals remaining in Eq. (3) can all be written in closed form. This was done, and the results were checked against Roothaan's formulas.[7] As a further check, the integrals evaluated at $R=1.7328$ a.u. with Slater exponents ($a=8.70$, $b=1.00$, $\mu_1=\mu_2=2.60$) were compared with the values of Karo and Allen[8] and were found to agree to the fifth decimal.

A steepest descent method was used to minimize the energy of Eq. (3). With a set of starting parameters, k_0, λ_0, b_0, μ_{10}, μ_{20}, the energy and derivatives of the energy with respect to these parameters were computed. Each parameter was then varied by an amount proportional to its derivative.

$$k_1=k_0-\alpha(\partial E/\partial k)_{k=k_0},$$
$$b_1=b_0-\alpha(\partial E/\partial b)_{b=b_0},$$
$$\cdots \quad \cdots \quad \cdots. \qquad (4)$$

At parameter values corresponding to the minimum on a plot of α vs E, the energy derivatives were recomputed and a second iteration made. This was continued until the total molecular energy was constant to the fifth decimal.

In all calculations, a, the orbital exponent of $(1s)_F$, was fixed at 8.70. Slater values of the other orbital exponents were used as starting points in the steepest descent minimization. Starting values of 0.9 for λ and 0.0 for k were obtained from Karo and Allen's[8] two highest filled orbitals by a unitary transformation causing the coefficient of $(1s)_H$ to vanish in one resulting orbital.

In a calculation neglecting differential overlap by (I) and in which both orbital exponents and linear coefficients were varied, the method of steepest descents was found unsatisfactory. After 10 cycles, all parameters but λ were oscillating; λ had changed from 0.9 to 1.5 and was still increasing slowly. At this point, the other parameters were held fixed and λ alone was varied. This single variation gave an energy minimum at $\lambda=2.4$. After some trial, the most rapid convergence was found to be given by a λ variation followed by two or three steepest descent cycles; the whole process being repeated to the desired accuracy. At convergence, λ had become infinite (effectively $1/\lambda=0$), while the other parameters were fairly near their starting values. Had steepest descents been used alone, and the process stopped upon the energy being constant to the fifth decimal from one cycle to the next, we should never have reached convergence.

TABLE I. LCAO SCF energies of HF at $R=1.7328$ a.u. (Slater exponents).

Calculation	Total energy (a.u.)
Method I	−99.4601
Method II	−107.8571
Method II—no $(1s)_F$ mixing	−107.7282
Exact, using Karo and Allen's integrals[a]	−99.4844
Karo and Allen's integrals—no $(1s)_F$ mixing	−99.5452
Experimental[b]	−100.528

[a] See reference 8.
[b] Quoted by R. A. Ballinger, Mol. Phys. **2**, 139 (1959).

As a partial check that we did in fact reach convergence, integrals computed with the best set of orbital exponents were put into an LCAO-SCF program[9] to obtain the best linear coefficients. These, after a unitary transformation as above, were found to agree with the k and λ from the steepest descents procedure. Total energies also were in agreement. The LCAO-SCF program itself was checked by putting in Karo and Allen's HF integrals.[8] The resulting electronic energy agreed to 6 figures with that computed by Karo and Allen. Molecular orbitals and orbital energies were also in agreement.

C. Results

With all exponents fixed at their Slater values, the energy was minimized with respect to k and λ to compare (I) and (II). In applying (I) we have neglected $(1s)_F$ mixing as well as differential overlap. Method II was applied with and without $(1s)_F$ mixing. These results and those of exact calculations with and without $(1s)_F$ mixing are shown in Table I.

Strictly, the exact calculation without $(1s)_F$ mixing involves nonorthogonal molecular orbitals. This gives a problem at least as difficult as one would have allowing mixing. So what is usually done in neglecting inner shell-outer shell mixing is to start with inner-shell orbitals orthogonal to outer-shell orbitals on the same atom and to neglect overlap between this inner shell and all orbitals on other atoms.[10,11] This is what we have done here. Making this approximation, the variation theorem no longer holds and the otherwise exact

[5] The computations were begun at Oxford with a desk calculator and finished at Bloomington on Indiana University's IBM 650 computer.
[6] C. C. J. Roothaan, Revs. Modern Phys. **23**, 69 (1951).
[7] C. C. J. Roothaan, J. Chem. Phys. **19**, 1445 (1951).
[8] A. M. Karo and L. C. Allen, J. Am. Chem. Soc. **80**, 4496 (1958).
[9] Written by Dr. Darrell Ebbing for an IBM 650 computer with magnetic tapes.
[10] F. O. Ellison and H. Shull, J. Chem. Phys. **23**, 2348 (1955).
[11] A. B. F. Duncan, J. Am. Chem. Soc. **77**, 2107 (1955).

TABLE II. HF results neglecting differential overlap by method I.

	Slater orbital exponents	Best orbital exponents
k	0.0085	0.0136
λ	2.32	$>10^8$
μ_1	2.60	2.72
μ_2	2.60	2.63
b	1.00	0.95
Total energy (a.u.)	−99.4601	−99.4740

calculation without $(1s)_F$ mixing may, and is in fact found to, give a lower energy than the one with mixing. On the other hand, having already made the approximation of zero differential overlap as in (II), neglecting $(1s)_F$ mixing can then be done without additional approximations. Therefore (II) without mixing must give a higher energy than with mixing.

However, the effect of $(1s)_F$ mixing is in any case small, and Table I shows that neglecting differential overlap by (I) gives a considerably better energy than by (II). Further calculations in which orbital exponents were varied were done only with (I). These results are given in Table II. The most obvious fault in the results with varying exponents is that λ has become infinite: the orbital ϕ_4 has become pure $(1s)_H$ and the HF molecule is described as H^-F^+.

III. HYDROGEN MOLECULE

Starting with a $(1s)=(\pi)^{-\frac{1}{2}}\exp(-r)$ function on each hydrogen nucleus, one can form the two symmetry adapted functions

$$\phi=[2(1+S)]^{-\frac{1}{2}}(1s_A+1s_B),$$

$$\chi=[2(1-S)]^{-\frac{1}{2}}(1s_A-1s_B), \qquad (5)$$

where

$$S=\int 1s_A 1s_B d\tau.$$

From these one can construct four molecular states[12]

$$\psi_1=\phi(1)\phi(2) \qquad {}^1\Sigma_g,$$

$$\psi_2=\phi(1)\chi(2)-\chi(1)\phi(2) \qquad {}^3\Sigma_u,$$

$$\psi_3=\phi(1)\chi(2)+\chi(1)\phi(2) \qquad {}^1\Sigma_u,$$

$$\psi_4=\chi(1)\chi(2) \qquad {}^1\Sigma_g.$$

The energies of these four states at an internuclear distance of 1.40 a.u., computed exactly and by (I) and (II), are shown in Fig. 1.[13]

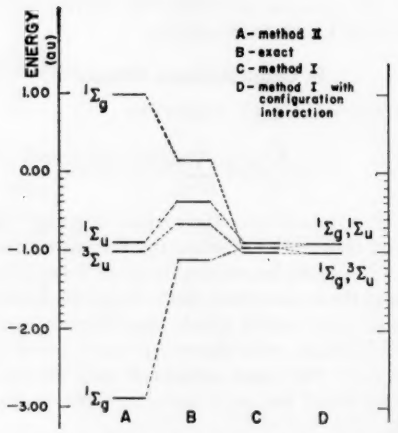

FIG. 1. Energy of four states of H_2 by various approximations.

The value obtained for the energy of the lowest ${}^1\Sigma_g$ state by (I) is nearer the exact than that calculated by (II). But the order of the states by (I) does not agree with the exact calculation, where ψ_1 with a doubly-filled bonding orbital is the lowest and ψ_4 with a doubly-filled antibonding orbital is the highest. By (I) both these states are of the same energy. In the Appendix it is shown that this is a general result, since bonding and antibonding orbitals of homonuclear diatomics are not distinguished by (I).

Method II gives all the states in the same order as the exact calculation, but the energies are spread over much too wide a range.

Since ψ_1 and ψ_4 are of the same symmetry, they will mix. This configuration interaction has small effect in the exact and (II) calculations, but by (I) the degenerate ${}^1\Sigma_g$ level is split, giving $(\psi_1-\psi_4)$ with the same energy as the ${}^1\Sigma_u$ state and $(\psi_1+\psi_4)$ degenerate with ${}^3\Sigma_u$.

IV. CONCLUSIONS

Although neglecting differential overlap by method I gives fairly good ground state energies for HF and H_2—much better than by method II—still the resulting charge density in the case of HF and the order of the states in the case of H_2 indicate that neither method is to be trusted in a nonempirical calculation.

ACKNOWLEDGMENT

L. S. thanks Professor Harrison Shull for his support during the latter part of this work and especially for his urging that the problem be programmed for the IBM 650 computer.

[12] C. A. Coulson and I. Fischer, Phil. Mag. **40**, 386 (1949).

[13] The integrals used in these H_2 calculations were supplied by Dr. Ebbing and are thought accurate to 6 figures.

APPENDIX

Suppose the diatomic molecule A−B is described by the wave function

$$\Psi = (N!)^{-\frac{1}{2}} \det|\phi_1(1)\phi_2(2)\cdots\phi_N(N)|, \quad \text{(A1)}$$

with

$$\phi_i = \eta_i[\sum_r a_{ri}\chi_r^a + \lambda_i \sum_s b_{si}\chi_s^b], \quad \text{(A2)}$$

$$\int \phi_i^* \phi_j d\tau = \delta_{ij}, \quad \text{(A3)}$$

where χ_r^a is an atomic orbital on atom A, χ_s^b is an atomic orbital on atom B, λ_i is either 1 or -1, and η_i is a spin function, either α or β. Then

$$E = \sum_i H_i + \tfrac{1}{2}\sum_{i,j}(J_{ij} - K_{ij}), \quad \text{(A4)}$$

where

$$H_i = \int \phi_i^*(1) H(1) \phi_i(1) d\tau_1$$

$$= \int [\sum_r a_{ri}\chi_r^a(1)]^* H(1) [\sum_r a_{ri}\chi_r^a(1)] d\tau_1$$

$$+ \lambda_i^2 \int [\sum_s b_{si}\chi_s^b(1)]^* H(1) [\sum_s b_{si}\chi_s^b(1)] d\tau_1, \quad \text{(A5)}$$

$$J_{ij} = \int \phi_i^*(1)\phi_i(1)(1/r_{12})\phi_j^*(2)\phi_j(2) d\tau_{12}$$

$$= \int [|\sum_r a_{ri}\chi_r^a(1)|^2 + \lambda_i^2 |\sum_s b_{si}\chi_s^b(1)|^2](1/r_{12})$$

$$\times [|\sum_r a_{rj}\chi_r^a(2)|^2 + \lambda_j^2 |\sum_s b_{sj}\chi_s^b(2)|^2] d\tau_{12}, \quad \text{(A6)}$$

$$K_{ij} = \int \phi_i^*(1)\phi_j(1)(1/r_{12})\phi_j^*(2)\phi_i(2) d\tau_{12}$$

$$= \int [(\sum_r a_{ri}\chi_r^a(1))^* (\sum_r a_{rj}\chi_r^a(1))$$

$$+ \lambda_i\lambda_j (\sum_s b_{si}\chi_s^b(1))^* (\sum_s b_{sj}\chi_s^b(1))]$$

$$\times (1/r_{12}) [(\sum_r a_{rj}\chi_r^a(2))^* (\sum_r a_{ri}\chi_r^a(2))$$

$$+ \lambda_i\lambda_j (\sum_s b_{sj}\chi_s^b(2))^* (\sum_s b_{si}\chi_s^b(2))] d\tau_{12}. \quad \text{(A7)}$$

The cross terms, which are linear in λ, have been dropped because of the zero differential overlap approximation (I). Note that the integrals in Eq. (A4) are over spin orbitals, while those in Eq. (3) are over the space parts only.

Since all terms in these integrals have an even number of λ factors, if one constructs Ψ' which is identical with Ψ except that $\lambda_i' = -\lambda_i$ for all i, then Ψ' and Ψ will have the same energy. The functions ψ_1 and ψ_4 for H_2 are an example.

This result generalizes at once to polyatomic molecules.

Electrical Resistivity of Cubic Sodium Tungsten Bronze*

L. D. ELLERBECK,† H. R. SHANKS, P. H. SIDLES, AND G. C. DANIELSON

Institute for Atomic Research and Department of Physics, Iowa State University, Ames, Iowa

(Received November 21, 1960)

The electrical resistivities of the nonstoichiometric compounds Na_xWO_3 have been measured as a function of sodium concentration from $x=0.48$ to $x=0.88$, and as a function of temperature from $T=4°K$ to $T=873°K$. The minimum in electrical resistivity near $x=0.75$, which had been reported by earlier investigators, was absent in single crystals which were selected to be electrically homogeneous. Above room temperature, the electrical conductivity increased approximately linearly with sodium concentration; at liquid-helium temperatures, the electrical conductivity increased approximately as the fourth power of sodium concentration.

INTRODUCTION

THE sodium tungsten bronzes are the nonstoichiometric compounds Na_xWO_3 which are cubic when x is between 0.45 and 0.90. Although one would expect the electrical properties of these compounds to change monotonically with increasing sodium concentration, Brown and Banks[1] and Gardner and Danielson[2] reported a minimum in the curve of electrical resistivity versus sodium concentration at x values of about 0.70 and 0.75, respectively. Brown and Banks[1] interpreted the minimum in terms of an equilibrium between undissociated sodium atoms and sodium ions plus free electrons; while Gardner and Danielson[2] suggested the ordering of sodium atoms as a possible explanation. Subsequent investigations at this Laboratory into the cause of this minimum indicated that sample homogeneity, particularly large macroscopic growth defects, might be an important factor. The present investigation was undertaken to determine the electrical resistivity of these compounds both as a function of sodium concentration and as a function of temperature when only samples carefully selected to be electrically homogeneous were used.

PREPARATION AND SELECTION OF SAMPLES

The samples of Na_xWO_3 for this investigation were prepared by electrolysis of a fused mixture of reagent-grade sodium tungstate and tungsten trioxide in glazed ceramic crucibles. The electrolysis was carried out at approximately 700°C with nichrome cathodes and graphite anodes. Crystal growth occurred on the cathode; and current densities of about 20 ma/cm² yielded the best single crystals. If a single-crystal seed was placed initially over the end of the cathode, large single crystals were obtained. Without seeding, many small crystals formed initially, but most of these crystals were subsequently overgrown and only a few large crystals developed in the later stages of growth. From each of these larger crystals it was possible to obtain several single-crystal samples for resistivity measurements. When the cathodes, together with the adhering crystals, were removed from the molten solution, the crystals were coated with a layer of the growth mixture which protected them from the atmosphere while they cooled to room temperature. This coating was then removed by means of boiling water.

Previous investigators[3–5] have shown that the sodium concentration of cubic Na_xWO_3 is quite accurately related to the lattice parameter by the relation $a_0=0.0820x+3.7845$, where a_0 is the lattice constant in angstroms and x is the sodium concentration. In this investigation, as in the previous works of Brown and Banks[1] and of Gardner and Danielson,[2] this method was used to determine the sodium concentration. Precise determinations of a_0 were obtained from Debye-Scherrer powder photographs. If this relation between the lattice constant and sodium concentration is valid, the sodium concentrations for the samples measured in this investigation are correct to within ± 0.002.

Rectangular samples about 2.5 mm² in cross section and from 3 to 5 mm long were cut from the large crystals with a diamond saw. Final shaping was accomplished with No. 500 emery paper. Forty-five specimens, several at each available x value, were prepared. Electrical resistivity determinations, at 25°C, were used to test for sample homogeneity. A total of 24 independent measurements, distributed from end to end and around the periphery, were carried out on each specimen. From these measurements, an average resistivity and an average deviation from the average resistivity were computed for each specimen. If the ratio of the average deviation to the average resistivity was less than 5%, the specimen was considered to be electrically homogeneous. With this criterion for electrical homogeneity, only 15 of the original 45 samples were homogeneous.

* Contribution No. 966. Work was performed in the Ames Laboratory of the U. S. Atomic Energy Commission.

† Present address: University of Omaha, Omaha, Nebraska.

[1] B. W. Brown and E. Banks, Phys. Rev. **84,** 609 (1951).

[2] W. R. Gardner and G. C. Danielson, Phys. Rev. **93,** 46 (1954).

[3] M. E. Straumanis, J. Am. Chem. Soc. **71,** 679 (1949).

[4] E. W. Brimm, J. C. Brantley, J. H. Lorenz, and M. H. Jellinek, J. Am. Chem. Soc. **73,** 5427 (1951).

[5] E. Banks, Polytechnic Institute of Brooklyn, Third Interim Rept., Lattice Contract DA 36-039 Sc-193 (1951).

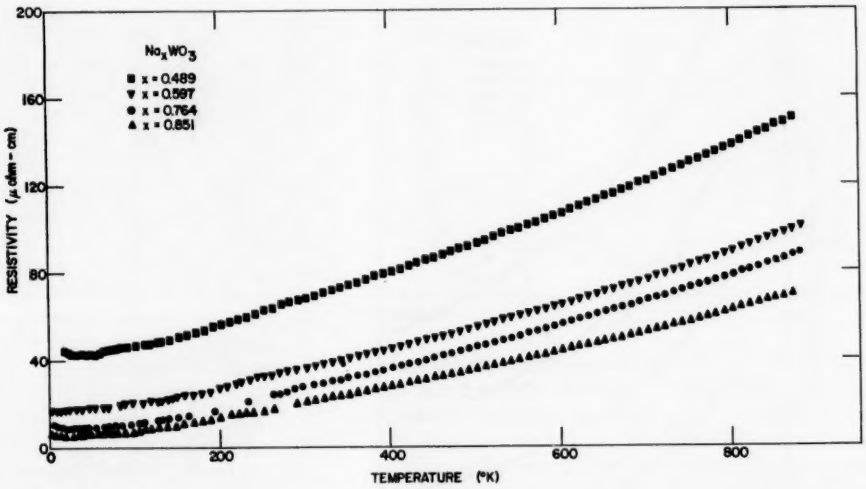

FIG. 1. Resistivity vs temperature for four bronze compositions.

Some preliminary measurements of the electrical resistivity at elevated temperatures had suggested that the stability of the electrical properties of our samples might be improved by prolonged heating. Consequently, 35 of the original 45 specimens (including all of the 15 crystals which satisfied the criterion for electrical homogeneity even without heat treatment) were placed in a vacuum furnace, which was heated to 675°C at a rate of 125°C/hr, and maintained at 675°C for 24 hr. The crystals were then rechecked for homogeneity at room temperature and the specimen with the smallest resistivity deviation for each available x value was selected for the measurement of resistivity as a function of temperature.

While the effects of heat treatment were not studied extensively, some general observations can be made. The average resistivity (ρ) and the fractional average deviation (δ) (defined as the ratio of the average deviation to the average resistivity) of nonhomogeneous samples were usually reduced appreciably by heat treatment. For example, sample 138A2 with $x=0.64$ had ρ decreased from 35.5 to 29.3 μohm cm and δ from 9.9 to 1.0%; sample 142A5 with $x=0.84$ had ρ decreased from 29.5 to 20.9 μohm cm and δ from 28 to 14%. Homogeneous samples were affected very little by the heat treatment; a typical example might be sample 125A2 with $x=0.87$, which had a decrease in ρ from 18.1 to 17.9 μohm cm and a decrease in δ from 2.3 to 2.0%. Samples

TABLE I. Coefficients for the equation $\rho=a_0+a_1T+a_2T^2$.

x value	a_0	a_1	a_2
0.489	6.64×10^{-5}	11.21×10^{-8}	5.46×10^{-11}
0.539	5.48	10.76	3.09
0.596	3.69	8.24	5.04
0.597	3.80	7.99	5.93
0.662	2.87	7.71	4.83
0.694	3.28	8.14	4.44
0.718	2.31	7.16	3.92
0.764	2.40	8.39	3.28
0.776	2.16	7.22	4.59
0.793	2.19	7.47	3.92
0.851	1.90	6.76	3.25
0.878	1.45	5.47	3.79

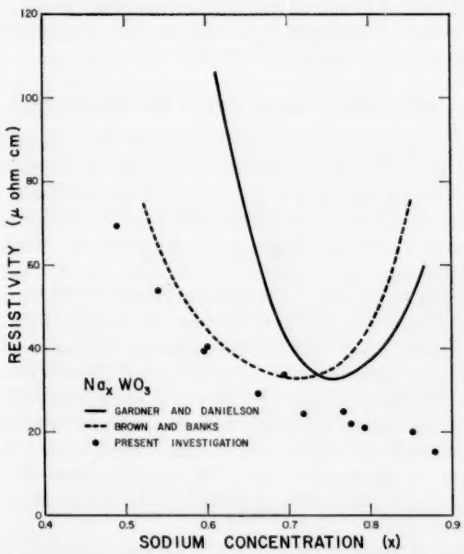

FIG. 2. Room temperature resistivity vs sodium concentration.

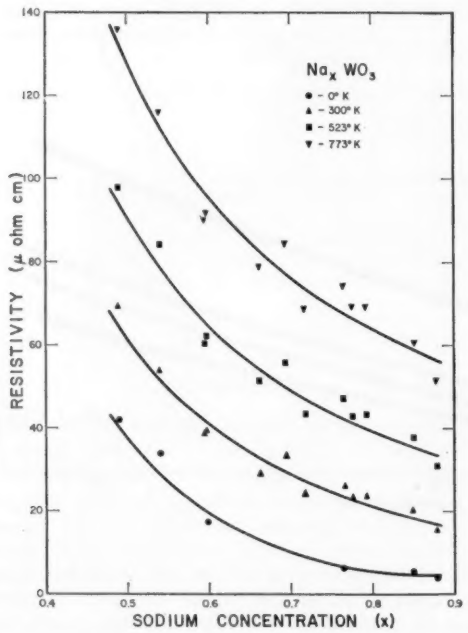

FIG. 3. Resistivity vs sodium concentration at several temperatures.

which had large fractional average deviations before heat treatment still did not satisfy the 5% homogeneity requirement after heat treatment; but, with only one exception, all samples which had δ less than 10% before heat treatment had δ less than 5% after heat treatment. We concluded that heat treatment is beneficial, but not adequate for very inhomogeneous crystals, in obtaining electrical homogeneity (δ less than 5%). Further details have been given by Ellerbeck.[6]

ELECTRICAL RESISTIVITY MEASUREMENTS

Electrical resistivity measurements were made from 4° to 873°K by means of a standard potential-drop technique. Sharpened tungsten wires served as potential probes. Separate equipment was used for the measurements above and below room temperature. Since the high-temperature measurements were done in vacuum, measurements were not extended above 873°K in order to avoid any appreciable loss of sodium from the samples. Small pits for the potential probes were cut into the samples so that identical probe placement could be obtained throughout the entire temperature range. Measurements were made at regular temperature intervals while the sample temperature was changed at the rate of about 60°K/hr. The over-all error of each resistivity measurement is believed to be less than 2%.

[6] L. D. Ellerbeck, M. S. thesis, Iowa State University, Ames, Iowa, 1959 (unpublished).

The electrical resistivity (ρ) as a function of temperature (T) for four representative x values is shown in Fig. 1. These resistivities can be represented as a function of temperature in the range above room temperature by the quadratic equation $\rho = a_0 - a_1 T - a_2 T^2$. The coefficients a_0, a_1, and a_2 for these four samples, as well as for the other eight samples which were measured, are tabulated in Table I. In order to compare these results with those of Brown and Banks[1] and with those of Gardner and Danielson,[2] the room-temperature resistivities as a function of sodium concentration are shown in Fig. 2. It is seen that the results of this investigation are in fair agreement with those of Brown and Banks at low x values. However, a substantial difference is observed at the higher x values. The absence of a minimum in resistivity near $x=0.70$ for electrically homogeneous specimens is in striking contrast to the deep minimum reported by both previous investigators. For our samples, the resistivity decreased monotonically with increasing sodium concentration from $x=0.48$ to $x=0.88$. In Fig. 3, similar plots are shown for three additional temperatures, 0°, 523°, and 773°K. The points shown for 0°K were obtained by extrapolation of data from about 20°K. Very slight increases in resistivity (probably caused by chemical impurities) were observed between 20° and 4°K, but this effect was disregarded in the extrapolation from 20° to 0°K. From Fig. 3 it is apparent that there is no suggestion of a minimum in resistivity at any temperature, not even in the residual resistivity at absolute zero.

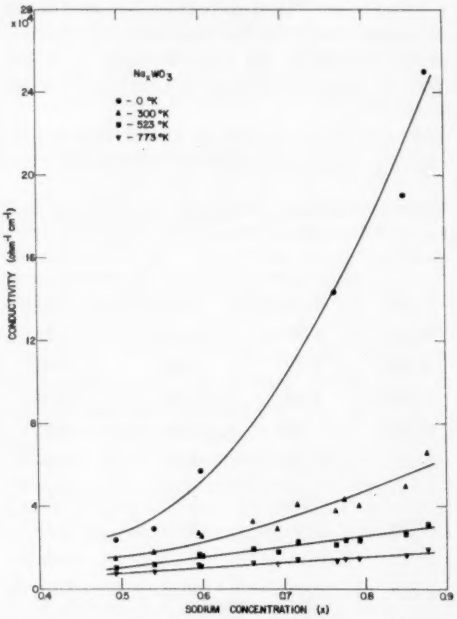

FIG. 4. Conductivity vs sodium concentration at several temperatures.

DISCUSSION

A. Resistivity Minimum

From this investigation, it appears almost certain that no minimum exists in the curve of resistivity (ρ) vs sodium concentration (x), if the crystals are grown by the electrolytic method, and if the crystals are selected to be electrically homogeneous. If electrical homogeneity is ignored, exceptionally large errors in electrical resistivity may result. For example, our sample 122A2 with $x=0.64$ had a resistivity of 106 μohm cm which was over three times the resistivity of homogeneous samples having the same x value. The fractional average deviation (δ), however, was 40% for this sample.

In looking for the cause of these deviations in electrical resistivity with probe positions, we have polished the surfaces of several crystals and looked at these surfaces with a microscope. A white crystalline impurity, with somewhat the appearance of the $Na_2WO_4-WO_3$ mixture, was found to be present in macroscopic quantities. These impurities were probably inclusions of the molten material in which the crystal was grown. As the crystals grew in layers, macroscopic amounts of such highly insulating material could be trapped in the manner suggested by Sheftal[7] who observed similar inclusions in other crystalline materials. Such macroscopic inclusions could drastically reduce the effective cross section of the Na_xWO_3 sample, and hence greatly increase the resistivity. The Hall coefficients observed by Gardner and Danielson,[2] however, might be affected to a much smaller extent; a large inclusion with its small dimension normal to the current would increase the resistivity substantially, but have little effect on the Hall coefficient. The number and size of these inclusions seemed to be smallest near $x=0.75$, where Atoji and Rundle[8] have found ordering of the sodium atoms.

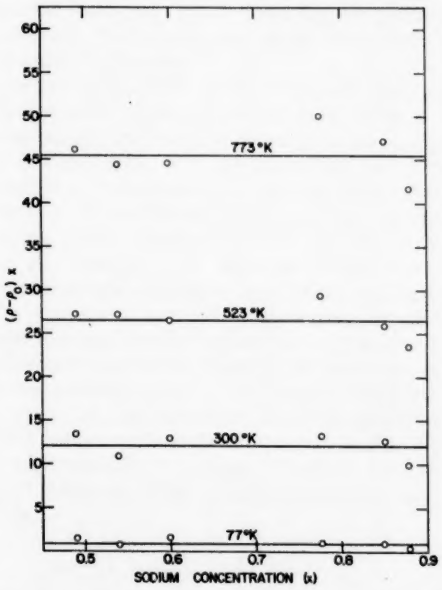

FIG. 5. Thermal resistivity normalized to a constant number of carriers vs sodium concentration.

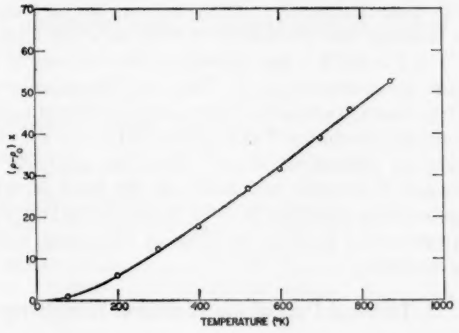

FIG. 6. Thermal resistivity normalized to a constant number of carriers vs temperature.

In order to keep the number of inclusions constant, we attempted to prepare a high x-value crystal by diffusion of sodium into a low x-value crystal in the manner suggested by Brown and Banks.[1] A 0.05-g crystal with $x=0.64$, $\rho=31.3\mu$ohm cm, and $\delta=4.5\%$ was heated 110 hr at 750°C in a bomb containing 23 g of $Na_{0.89}WO_3$. After this treatment the outside layer (about 0.25 mm thick) had its average x value increased to $x=0.70$, and ρ increased (rather than decreased 25% to 39.0 μohm cm. The inside of the crystal still had $x=0.64$, however, showing incomplete diffusion, a result one might expect from the high activation energy for sodium diffusion (over 50 kcal/mole) reported by Smith and Danielson.[9] Presumably, the increase in resistivity must be caused by lattice distortion arising from the variation in sodium concentration with distance from the crystal surface. In any case, increasing x values by diffusion is a very unreliable method for obtaining high x-value homogeneous crystals.

B. Residual Resistivity

As shown in Fig. 3, sodium tungsten bronze differs from a pure metal in having a large residual resistivity at 0°K. The conductivity of Na_xWO_3 as a function of sodium concentration (x) is shown in Fig. 4. The conductivity at 0°K increases extremely rapidly with increasing values of x. From $x=0.48$ to $x=0.88$, this residual conductivity at 0°K increases approximately

[7] N. N. Sheftal, *Growth of Crystals* (Academy of Sciences, U.S.S.R. Press, Moscow, March, 1956) (English translation by Consultants Bureau Inc., New York, p. 5).

[8] M. Atoji and R. E. Rundle, J. Chem. Phys. **32,** 627 (1960).

[9] J. F. Smith and G. C. Danielson, J. Chem. Phys. **22,** 266 (1954).

as x^4. Since, the number of free electrons has been shown by Gardner and Danielson[2] to vary as x (at least for $77°K<T>369°K$), the mobility of the electrons at 0°K varies approximately as x^3. This rapid dependence cannot be understood in terms of a simple alloy of sodium atoms and vacancies. The formula $\sigma=1/x(1-x)$, which holds for gold-silver alloys,[10] does not apply to the bronzes. A detailed calculation of the band structure appears to be necessary in order to understand the rapid dependence of electron mobility at 0°K upon sodium concentration.

C. Thermal Part of the Electrical Resistivity

The dependence of conductivity (σ) upon sodium concentration (x) at high temperatures is approximately linear, as shown in Fig. 4. At high temperatures, thermal scattering is dominant and the linear dependence of σ upon x would indicate that for thermal scattering the conductivity is proportional to the number of free electrons, and the mobility of the electrons (μ) is independent of the sodium concentration.

In order to verify this conclusion, we subtracted the residual resistivity (ρ_0) from the total resistivity (ρ) and multiplied by x to get the expression $(\rho-\rho_0)x$ which is proportional to $1/\mu$. A graph of $(\rho-\rho_0)x$ vs x is shown in Fig. 5 for temperatures of 77°, 300°, 523°, and 773°K. For each temperature we obtained a horizontal line indicating that the mobility due to thermal scattering was indeed independent of sodium concentration from $x=0.48$ to $x=0.88$. The mobility of the electrons, therefore, must also be independent of the electron concentration (which equals the sodium concentration), and hence independent of the Fermi energy.

The result is consistent with the slow increase in density of states obtained by Vest, Griffel, and Smith[11] for $x=0.56$ to $x=0.70$. However, the anomalous rapid increase in density of states at $x=0.81$ $x=0.89$, reported by Vest *et al.*,[8] is not evident in our resistivity measurements, nor in magnetic susceptibility measurements by Greiner, Shanks, and Wallace.[12]

The thermal part of the electrical resistivity (or ideal resistivity) for all sodium concentrations in the range $0.48<x>0.88$ and for all temperatures in the range $0°K<T>873°K$ can be represented by the single curve of $(\rho-\rho_0)x$ vs T as shown in Fig. 6.

ACKNOWLEDGMENTS

We wish to thank Dr. J. M. Keller for helpful discussions and Ned Sissel for assistance in making the homogeneity measurements.

[10] A. H. Wilson, *Theory of Metals* (Cambridge University Press, New York, 1954), p. 274.

[11] R. W. Vest, M. Griffel, and J. F. Smith, J. Chem. Phys. **28**, 293 (1958).

[12] J. Greiner, H. R. Shanks, and D. C. Wallace (private communication).

Effect of Intermolecular Forces on Macromolecular Configurational Changes and on Other Isomeric Equilibria*

TERRELL L. HILL†

Department of Theoretical Chemistry, Cambridge University, Cambridge, England

(Received December 9, 1960)

The effect of intermolecular forces on isomeric equilibria (configurational changes in macromolecules are a special case) is investigated. The term corresponding to the second virial coefficient is derived but the method can easily be extended to higher terms. A significant and measurable effect is predicted for (a) isomeric equilibria involving atoms or small molecules or (b) configurational changes in macromolecules at a first-order phase transition or critical point. A negligible effect is predicted for configurational changes in macromolecules otherwise. These conclusions apply to "proper" thermodynamic variables only; the end-to-end length r of a random coil is excluded.

OUR primary object in this paper is to investigate, quasi-thermodynamically, the effect that intermolecular forces might have on "phase transitions" occurring in macromolecules in solution. Examples are: the helix-random coil transition in proteins, nucleic acids, polypeptides, and polynucleotides; swelling of bovine serum albumin in the *p*H range 2–4; the $\alpha-\beta$ transition in fibrous proteins, etc. But the equations we write down at the outset will also be applicable to much simpler gas-phase isomeric equilibria such as those involving (a) an atom in different electronic states, (b) structural isomers of simple hydrocarbons, etc. We include only first-order effects of concentration or intermolecular forces, i.e., effects involving the second virial coefficient. The method can easily be extended to higher virial coefficients.

Consider first a *very dilute system* of N molecules (or atoms) in a volume V. The molecules are all "isomers" of one another, in the broadest sense (e.g., including different configurations of a macromolecule and are in equilibrium at temperature T. This is a one component system, thermodynamically, but on the molecular level we group together from the totality (i.e., including all "isomers") of quantum states available to one molecule all those states which will have essentially the same intermolecular forces. In this way, namely, using identity or near identity in intermolecular interactions as the criterion, we divide up the single thermodynamic species into subspecies (isomers) $i=1, 2, \cdots$. Let the canonical ensemble partition function for a single molecule of subspecies i be Vq_i/Λ^3, where $\Lambda=h/(2\pi mkT)^{\frac{1}{2}}$. Of course, V and Λ are the same for all subspecies. The chemical potential of subspecies i is

$$\mu_i=kT\ln(\Lambda^3/q_i)+kT\ln\rho_i, \tag{1}$$

where $\rho_i=N_i/V$. At equilibrium, $\mu_i=$constant (all i) and hence

$$\rho_i=\rho q_i/q, \tag{2}$$

where

$$\rho=N/V, \qquad N=\sum_i N_i, \qquad q=\sum_i q_i.$$

Here q is the complete partition function for one molecule (it includes all isomers or subspecies). This is a standard result (the "Boltzmann distribution"). If we denote ρ_i/ρ, the fraction of all molecules which belong to subspecies i by P_i, then we have found that in the limit $\rho\to 0$, $P_i\to P_i^0$, where $P_i^0=q_i/q$. We shall investigate how P_i depends on ρ when $\rho>0$.

For an atom distributed between two electronic states (the "subspecies") we would have simply $q_1=\omega_1\exp(-\epsilon_1/kT)$ and $q_2=\omega_2\exp(-\epsilon_2/kT)$, in obvious notation. For ordinary molecular isomers in their ground electronic states, q_1, q_2, $\cdots$ would each involve a sum over the appropriate vibrational and rotational levels. But macromolecules, although not differing in principle, require special comment. In the first place, when a solvent is present, q_i includes a factor which takes care of the interaction between solute i and solvent.[1] Second a typical macromolecule is itself practically a macroscopic system. If n is the number of monomers in the macromolecule, n may be of order 10^3, 10^4, or more. This being the case, it is natural to introduce some convenient *extensive*[2] size or shape (configura-

* Supported in part by a research grant from the Heart Institute, Public Health Service.

† Public Health Service Special Research Fellow, 1960–61, and Alfred P. Sloan Foundation Fellow. Permanent address: Department of Chemistry, University of Oregon, Eugene, Oregon.

[1] See, for example, T. L. Hill, *Introduction to Statistical Thermodynamics* (Addison-Wesley Publishing Company, Inc., Reading, Massachusetts, 1960), pp. 343–344.

[2] It is essential that x be a "proper" thermodynamic variable. Thus x must be proportional to n (f, T constant) and fx must be of order nkT. For example,[3] for a random coil, the end-to-end length l with ends on a given line is "proper" but the end-to-end length r with free ends is not ($r\propto n^{\frac{1}{2}}$). The length l of a random coil is, however, a "degenerate" case in that $l=0$ when $f=0$. We are primarily interested in macromolecular phase transitions (at $f=0$) in this paper. When one phase is a random coil with $l=0$, the situation is somewhat analogous to the ideal Bose-Einstein condensation where the condensed phase has zero volume. In summary: although random coils represent a degenerate case here and we do not have them primarily in mind, it is not necessary to exclude them from the discussion.

tional) parameter denoted by x such as length, volume, etc., on which the potential of (mean) intermolecular force depends. We then use $q(x)$ (instead of q_i) to represent the canonical ensemble partition function (excluding translation) of a macromolecule with length, or volume, etc., x. For a single macromolecule, the familiar independent variables N, V, T of statistical mechanics are thus replaced by n, x, T, of which n is a constant here. The (mean value of the) intensive variable f conjugate to x is determined in the canonical ensemble by

$$\bar{f}=-kT(\partial \ln q/\partial x)_{n,T}. \tag{3}$$

However, a macromolecule in a very dilute solution is under no external force so that we are in fact primarily concerned with the case $f=$constant$=0$. Thus the independent variables n, f, T are more appropriate, with $n=$constant and $f=0$. The corresponding partition function is[3]

$$\Delta(n, f, T)=\sum_x q(n, x, T)\exp(fx/kT). \tag{4}$$

The probability of observing the value x, when n, f, and T are given and fixed, is proportional to $q(n, x, T)\exp(fx/kT)$. When $f=0$, this reduces to $q(n, x, T)$, in agreement with Eq. (2). Except at a phase transition or critical point, $q(x)$ for a given T will have a very sharp maximum[2] at the mean $\bar{x}^0$ given by

$$\bar{x}^0=kT(\partial \ln\Delta/\partial f)_{n,T}, \tag{5}$$

evaluated at $f=0$. The superscript zero refers to the fact that we are considering the limit $\rho\to 0$. Equation (5) at $f=0$ is equivalent to

$$\bar{x}^0=\sum_x xq(x)/q=\sum_x xP^0(x)=\int xP^0(x)\,dx,$$

where

$$q=\sum_x q(x), \qquad \sum_x P^0(x)=1, \qquad \int P^0(x)\,dx=1.$$

Summation or integration is used as convenient. The dispersion about the mean is

$$\sigma^2\equiv\langle x^2\rangle_N{}^0-(\bar{x}^0)^2=kT(\partial\bar{x}^0/\partial f)_{n,T}, \tag{6}$$

again evaluated at $f=0$. The macromolecular case differs in a qualitative way from the isomeric atomic or small molecule case in that $P^0(x)$ for a macromolecule (except at a phase transition or critical point) is concentrated near $\bar{x}^0$ with very small fluctuations[2] about $\bar{x}^0$ while P_i^0 for small molecules has a broad spread with large fluctuations about any mean value of interest.

It should be noted that the above discussion has been put in statistical-mechanical rather than thermodynamic language so that it is valid whether or not the system (molecule) is macroscopic in size.

[3] See Chap. 13 of reference 1.

Having considered q_i and $q(x)$, we now turn to the case of actual interest: the total concentration ρ is large enough so that the second virial coefficient B in the expansion of the pressure (osmotic pressure, if a solvent is present) in powers of ρ needs to be taken into account. For the system regarded as a one-component system (the strict thermodynamic point of view),

$$p/kT=\rho+B(T)\rho^2+\cdots \tag{7}$$

$$z=\rho+2B(T)\rho^2+\cdots, \tag{8}$$

where the activity z is defined by

$$z=\lambda q/\Lambda^3, \qquad \lambda=\exp(\mu/kT). \tag{9}$$

For the same system regarded as a multicomponent (subspecies $i=1, 2, \cdots$) imperfect gas,

$$p/kT=\sum_i\rho_i+\sum_{i,j\geq 1}B_{ij}(T)\rho_i\rho_j+\cdots \tag{10}$$

$$\rho_i=z_i-2z_i\sum_{j\geq i}B_{ij}z_j+\cdots \qquad i=1, 2, \cdots, \tag{11}$$

where

$$z_i=\lambda_i q_i/\Lambda^3, \qquad \lambda_i=\exp(\mu_i/kT), \tag{12}$$

and B_{ij} $(=B_{ji})$ is a second virial coefficient determined by the potential of (mean) intermolecular force between one molecule of subspecies i and one of subspecies j. The one component and multicomponent points of view are interrelated by

$$F=N\mu \text{ (one component)}$$
$$=\sum_i N_i\mu_i \text{ (multicomponent)}.$$

Since the system is at equilibrium, all subspecies must have the same chemical potential. Hence

$$N\mu=\mu_i\sum_i N_i=\mu_i N,$$

or

$$\mu_i=\mu, \qquad \lambda_i=\lambda \qquad i=1, 2, \cdots. \tag{13}$$

Therefore we put

$$z_i=\lambda_i q_i/\Lambda^3=\lambda q_i/\Lambda^3=zq_i/q=zP_i^0 \qquad i=1, 2, \cdots, \tag{14}$$

in Eq. (11) and find

$$\rho_i=zP_i^0-2z^2P_i^0\sum_{j\geq 1}B_{ij}P_j^0+\cdots \qquad i=1, 2, \cdots. \tag{15}$$

To obtain $P_i=\rho_i/\rho$ in powers of ρ, we replace z by ρ in Eq. (15), using Eq. (8):

$$P_i=P_i^0[1+2\rho(B-\sum_{j\geq 1}B_{ij}P_j^0)+\cdots] \quad i=1, 2, \cdots. \tag{16}$$

This is the desired result. It shows how the equilibrium distribution of subspecies or isomers is altered from P_i^0 at $\rho=0$ (no intermolecular forces) to P_i for $\rho>0$ (intermolecular forces effective via the B's). If, in Eq. (10), we put $\sum_i\rho_i=\rho$ and substitute $\rho_i=\rho P_i^0$ in

the quadratic terms, comparison with Eq. (7) shows that

$$B=\sum_{i,j\geq 1}B_{ij}P_i^0P_j^0. \tag{17}$$

This relation is also required by Eq. (16) since $\sum_i P_i = \sum_i P_i^0 = 1$.

The application of Eq. (16) to isomeric equilibria of atoms and small molecules requires no special comment. We turn, then, directly to the macromolecular case. By some method such as light scattering we can observe or deduce $\bar{x}$ as a function of T (this corresponds, for an ordinary fluid, to measuring V as a function of T at constant p). The question is: How does $\bar{x}$ depend on ρ for small ρ (T constant)? There is no corresponding question for an "ordinary fluid." From the ensemble point of view in statistical mechanics, we have an ensemble ("constant pressure") of systems (one macromolecule = one system) which interact with each other with more than the usual "weak" interaction (to maintain equilibrium); we are interested in how these "intersystem" interactions change the probability distribution $P^0(x)$ and in particular the mean value $\bar{x}^0$.

If we multiply Eq. (16) by x and integrate over x, we find

$$\bar{x}=\bar{x}^0-2\rho\int B(x,x')(x-\bar{x}^0)P^0(x)P^0(x')dxdx'+\cdots. \tag{18}$$

Similarly,

$$\langle x^2\rangle_{Nv}-\bar{x}^2=\langle x^2\rangle_{Nv}^0-(\bar{x}^0)^2-2\rho\int B(x,x')\{(x-\bar{x}^0)^2 -[\langle x^2\rangle_{Nv}^0-(\bar{x}^0)^2]\}P^0(x)P^0(x')dxdx'+\cdots. \tag{19}$$

Except for a phase transition or critical region, $P^0(x)$ is Gaussian in form[4] for a large macromolecule,

$$P^0(x)=(2\pi)^{-\frac{1}{2}}\sigma^{-1}\exp[-(x-\bar{x}^0)^2/2\sigma^2]. \tag{20}$$

Since $P^0(x)$ is sharply peaked about $\bar{x}^0$, we expand $B(x,x')$ about $x=x'=\bar{x}^0$,

$$B(x,x')=B(\bar{x}^0,\bar{x}^0)+(\partial B/\partial x)_{x=x'=\bar{x}^0}[(x-\bar{x}^0)+(x'-\bar{x}^0)]+\cdots. \tag{21}$$

Then Eq. (18) gives

$$\bar{x}=\bar{x}^0[1-2\rho(\partial B/\partial x)_{\bar{x}^0}(\sigma^2/\bar{x}^0)+\cdots], \tag{22}$$

to the linear term in ρ and σ^2. To the same order we find from Eq. (19)

$$\langle x^2\rangle_{Nv}-\bar{x}^2=\langle x^2\rangle_{Nv}^0-(\bar{x}^0)^2=\sigma^2. \tag{23}$$

Thus, to this order, $\bar{x}^0$ appears to be shifted when $\rho>0$, but not the dispersion. But if we examine the magnitude of the correction term in Eq. (22) we see that it is of order $\rho B\sigma^2/(\bar{x}^0)^2$ or, in view of Eq. (6), of order $\rho B/n$ or $1/n$. Since n is usually of order 10^3 or more, we conclude that at concentrations ρ such that the second virial coefficient is necessary and adequate for the osmotic pressure, the effect of intermolecular forces on the mean size or shape (configuration) parameter $\bar{x}^0$ is negligible. This negative result is a direct consequence of the small fluctuations about $\bar{x}^0$ for a macromolecule[2]: $\sigma^2/(\bar{x}^0)^2$ is of order n^{-1}.

There is, however, an appreciable effect of intermolecular forces when $\sigma^2/(\bar{x}^0)^2$ is of order unity. This situation obtains (a) for small molecules [see Eq. (16)] and (b) for macromolecules at a first-order phase transition or critical point. In the case of a first-order transition, to a first approximation we will have[4]

$$P^0(x)=\alpha\delta(x-x_1)+(1-\alpha)\delta(x-x_2)$$
$$\alpha=(x_2-\bar{x}^0)/(x_2-x_1), \tag{24}$$

where x_1 and x_2 are the values of $\bar{x}^0$ at the two ends of the transition at temperature T. For a finite but large system, such as a macromolecule: (a) $P^0(x)$ will actually consist of two Gaussian functions centered about x_1 and x_2, but the δ functions suffice to give first-order effects; and (b) the curve of $\bar{x}^0$ against T will not be quite vertical at the transition (as it would be for an infinite system). On substituting Eq. (24) in Eq. (18), we obtain

$$\bar{x}=\bar{x}^0+2\rho\alpha(1-\alpha)(x_2-x_1)\times\{\alpha[B(x_1,x_1)-B(x_1,x_2)]-(1-\alpha)[B(x_2,x_2)-B(x_1,x_2)]\}+\cdots. \tag{25}$$

For example, if $\alpha=\frac{1}{2}$, that is, if $\bar{x}^0=(x_1+x_2)/2$ (the midpoint in the transition), then

$$\bar{x}=\bar{x}^0\{1+[\rho(x_2-x_1)/4\bar{x}^0][B(x_1,x_1)-B(x_2,x_2)]+\cdots\}. \tag{26}$$

The correction in Eqs. (25) and (26) is of the same order as in the osmotic pressure (ρB relative to unity), and hence is measurable and not negligible. It is easy to see that at a critical point, where $P^0(x)$ presumably has an essentially flat top[4] over a finite range in x, we also obtain a nonnegligible result of the same magnitude.

The effect of concentration on macromolecular transitions has not been studied experimentally so far as the author is aware. It would appear that an observed effect of ρ on $\bar{x}$ of the same magnitude as on the osmotic pressure could be used as a qualitative test for a first-order transition when there is doubt about the nature of the transition. Indeed, this kind of uncertainty will be usual with systems which are not quite macroscopic and hence behave ambiguously (nonvertical slope of $\bar{x}$ against T, for example) on this account alone.

We might draw one general statistical mechanical conclusion: interactions between macroscopic systems in a statistical mechanical ensemble will have a negligible effect on the average thermodynamic[2] properties of the systems of the ensemble, except in a two-phase or critical region.

[4] See, for example, T. L. Hill, *Statistical Mechanics* (McGraw-Hill Book Company, Inc., New York, 1956), Appendix 9.

THE JOURNAL OF CHEMICAL PHYSICS VOLUME 35, NUMBER 1 JULY, 1961

Variation of the Intensity of the Methyl Symmetrical Bending Vibration in Paraffins

MICHAEL R. BASILA AND GEORGE F. CRABLE

Gulf Research & Development Company, Pittsburgh, Pennsylvania

(Received December 7, 1960)

The integrated infrared absorption coefficients of the methyl C—H symmetrical bending vibration of a number of normal and branched paraffins have been studied. Several approaches to the correlation of intensity variations with structure are discussed and evaluated in terms of the experimental data. The conclusions are (a) the intensities of the branched and normal paraffins must be treated as two distinct classes, and (b) the branched paraffin group intensities must be further broken down into three types: (1) methyl groups adjacent to a tertiary or quaternary carbon atom having no other methyl groups directly adjacent, (2) methyl groups adjacent to tertiary or quaternary carbon atoms having other adjacent methyl groups directly attached, and (3) methyl groups at the ends of branches or chains of two or more carbon atoms in length. Integrated absorption coefficients are given for each type of group and approximate C—H bond moments are calculated from these values.

THE intensities of the methyl 1380 cm^{-1} symmetrical bending vibration in normal and branched paraffins have been the subject of many investigations in recent years.[1–6] The most recent studies have shown that the integrated absorption coefficient per methyl group varies depending on the arrangement of the methyl groups in the molecule. Alternate interpretations have been profferred to explain these observations. Hughes and Martin[6] have suggested the existence of individual group integrated absorption coefficients for methyl, ethyl, propyl, etc., with methyl the largest. The difference diminishes with increasing carbon number and reaches constancy with the propyl or butyl group. Luther and Czerwony[5] have studied normal and branched paraffins and have shown the branched to have greater integrated extinction coefficients than would be predicted from the data on the normal compound. This greater intensity is also accompanied by a slight increase in the half-bandwidth. These observations were thought to indicate the presence of a tertiary C–H bending vibration occurring in the same wavelength region but masked by the methyl bending absorption. The results of this investigation indicate that a masked tertiary C–H vibration does not contribute significantly to the integrated absorption coefficient and is therefore probably not present. The proposal of Hughes and Martin is not completely eliminated but is necessarily modified such that all the methyl groups in a branched molecule have the same integrated absorption coefficient except the pendant[7] methyl groups which have a larger value. The normal paraffins are considered as an independent class and are treated separately.

EXPERIMENTAL

The intensities were measured on a Perkin-Elmer model 21 spectrophotometer. The wavelength scale was expanded from the normal 5 to 80 cm/μ to provide a larger area for measurement. The computed spectral slit width at 1380 cm^{-1} was approximately 2.5 cm^{-1}. The majority of the hydrocarbons were American Petroleum Institute high purity materials.[8] A few of the lower molecular weight compounds were Phillips Pure Grade materials. All were used without further purification. Fisher Certified Reagent grade carbon tetrachloride was used as the solvent. The intensities were measured at four different concentrations in the same cell. The individual sets of measurements showed no trends within themselves so that the average of the four results was used rather than a Wilson-Wells extrapolation[9] to zero concentration.

Integrated absorption coefficients are conventionally expressed in wave number units. Since the instrument is calibrated linearily in wavelength, it is necessary to replot the data in linear wave numbers. The replotting was done for several measurements, and the results compared with those obtained from an integration of the linear wavelength curve and subsequent numerical conversion to wave number units according to the equation

$$A = (cL\lambda_0^2)^{-1}\int_{\lambda_1}^{\lambda_2} \ln(I_0/I)d\lambda,$$

where A is the integrated absorption coefficient, c the concentration in mole liter,$^{-1}$ L the cell path length in centimeters, and λ_0 the wavelength of the band center in centimeters. Because of the relatively small interval

[1] S. A. Francis, J. Chem. Phys. **18,** 861 (1950).
[2] S. A. Francis, Anal. Chem. **25,** 1466 (1953).
[3] R. Silas, paper Q-6 presented at Symposium on Molecular Structure and Spectroscopy, Columbus, Ohio, June 11–18, 1956.
[4] S. H. Hastings, A. T. Watson, R. B. Williams, and J. A. Anderson, Anal. Chem. **24,** 612 (1952).
[5] H. L. Luther and G. Czerwony, Z. Physik. Chem. **6,** 286 (1956).
[6] R. H. Hughes and R. J. Martin, Symposium on Composition of Petroleum Oils, Special Publication No. 224, ASTM.
[7] A pendant methyl is a methyl group adjacent to a tertiary or quaternary carbon atom.
[8] The authors are indebted to Dr. J. A. Dixon and the American Petroleum Institute, Research Project 42, for supplying several of the hydrocarbons used in this work.
[9] E. B. Wilson and A. J. Wells, J. Chem. Phys. **14,** 578 (1946).

TABLE I. Intensities of 1380 cm^{-1} band of paraffins.

	A $\times 10^{-5}$ (cm mole^{-1})	$A_{CH_3}{}^T$ $\times 10^{-5}$ (cm mole^{-1})	A_{CH_3} $\times 10^{-5}$ (cm mole^{-1})	A_p $\times 10^{-5}$ (cm mole^{-1})	A_s $\times 10^{-5}$ (cm mole^{-1})	$(A_{CH_3}{}^T)_{calc}$ $\times 10^{-5}$ (cm mole^{-1})	Δ	A_p' $\times 10^{-5}$ (cm mole^{-1})
n-Pentane	9.94	7.46	3.73			7.40	0.06	
n-Heptane	11.51	7.37	3.69			7.40	0.03	
n-Decane	13.84	7.23	3.62			7.40	0.17	
n-Tridecane	16.56	7.47	3.74			7.40	0.07	
n-Hexadecane	19.03	7.47	3.74			7.40	0.07	
			3.70±0.04					
3-Methylpentane	18.43	16.78	5.59	6.74		16.56	0.22	6.74
3-Methylhexane	18.62	16.14	5.38	6.10		16.56	0.42	6.10
4-Methylheptane	19.63	16.33	5.44	6.29		16.56	0.23	6.29
7-Methyltridecane	25.22	16.96	5.65	6.92		16.56	0.40	9.56
3-Methyleicosane	30.98	16.94	5.65	6.90		16.56	0.38	8.22
10-Methyleicosane	30.24	16.22	5.41	6.18		16.56	0.34	8.82
			5.52±0.11					
4,9-di-*n*-Propyldodecane	30.24	20.33	5.08			20.08	0.25	
3-Ethylhexane	18.32	15.02	5.01			15.06	0.04	
5-*n*-Butylnonane	22.08	14.65	4.88			15.06	0.41	
3,3-Diethylpentane	23.81	20.51	5.13			20.08	0.43	
			5.02±0.08					
2-Methyldecane	24.69	18.91	6.30		6.95	19.56	0.65	
2-Methylpentadecane	30.61	20.70	6.91		7.34	19.56	1.14	
2,2-Dimethlhexane	29.39	26.91	6.73		7.30	26.83	0.08	
2,2-Dimethylpentane	29.27	27.62	6.91		7.53	26.83	0.79	
3,3-Dimethylhexane	26.95	24.47	6.12		7.22	24.58	0.11	
			6.59±0.31					
3-Methyl-3-ethylpentane	25.56	23.08	5.77			21.58	1.50	

defined by λ_1 to λ_2, the values of A determined by the two methods agreed to within approximately 1%. Therefore, to avoid tedious replotting, all the integrations were performed on linear wavelength curves and converted to wave number units by the above equation. The integration was performed on an automatic table top integrator which has previously been described.[6] The integration limits were 1355 to 1415 cm^{-1}. No wing corrections to the band area were applied.

RESULTS

The integrated absorption coefficients obtained are tabulated in Table I. Luther and Czerwony[5] have shown the intensities of the 1380 cm^{-1} band to be a combination of CH_2 and CH_3 group absorptions with the CH_3 absorption the more intense. The CH_2 absorption is quite appreciable in the higher molecular weight materials as is shown by a pronounced asymmetry in the band shape of compounds such as *n*-hexadecane. The integrated absorption coefficient was considered to be a linear combination of noninteracting methyl and methylene absorptions, i.e.,

$$A = n_{CH_3}A_{CH_3} + n_{CH_2}A_{CH_2}, \quad (1)$$

where n_{CH_3} and n_{CH_2} are the numbers and A_{CH_3} and A_{CH_2} the apparent integrated absorption coefficients of methyl and methylene groups, respectively. By rearranging terms, the equation for a straight line is obtained.

$$A/n_{CH_3} = A_{CH_2}(n_{CH_2}/n_{CH_3}) + A_{CH_3}. \quad (2)$$

Figure 1 is a plot of A/n_{CH_3} vs n_{CH_2}/n_{CH_3} for the normal

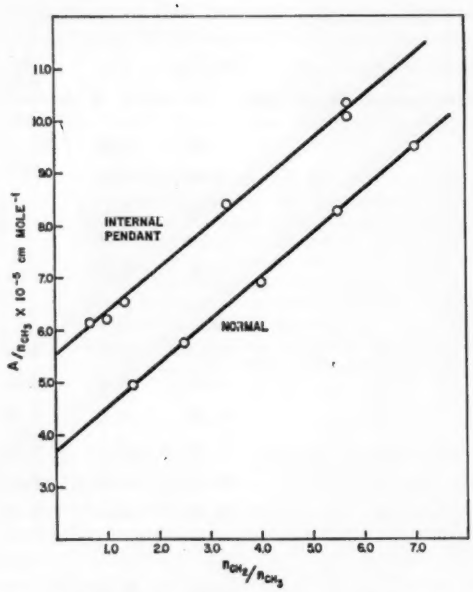

FIG. 1. Apparent integrated absorption coefficient for 1380 cm^{-1} methyl bending vibration.

paraffins. The resulting intercept and slope give

$$A = 3.69\times10^5 n_{CH_3} + 0.829\times10^5 n_{CH_2} \text{ cm mole}^{-1}. \quad (3)$$

A similar plot can be constructed for the branched hydrocarbons containing a single internal pendant methyl[10] branch from the data of Table I. This plot is also shown in Fig. 1. The resulting slope and intercept are $A_{CH_2}=0.823\times10^5$ and $A_{CH_3}=5.54\times10^5$ cm mole^{-1}, respectively. From these two plots, an average value of $A_{CH_2}=0.826\times10^5$ cm mole^{-1} is obtained. This value was assumed constant for all aliphatic paraffins and was used to correct the observed integrated absorption coefficients for methylene absorption. The resulting total methyl integrated absorption coefficients $A_{CH_3}{}^T$ are listed in Table I.

Equation (3) is in reasonable agreement with the corresponding Eq. (12) of Luther and Czerwony,[5] i.e.,

$$A = 4.26\times10^5 n_{CH_3} + 1.08\times10^5 n_{CH_2} (\text{cm mole}^{-1}).$$

DISCUSSION

Before an explanation of the observed variation in the methyl absorption can be obtained, it is necessary to determine a good empirical fit to the data. The third column of Table I is a tabulation of the apparent methyl group integrated absorption coefficients, A_{CH_3}. It is clear that these values are numerically clustered and grouped according to the nature of the branching in the molecule.

In interpreting the data, it is convenient to consider the normal, the branched with gem polymethyl substitution, and the branched group separately. The justification for separating the normal paraffins will be apparent later. The compounds with gem polymethyl substitution are separated because the absorption band is split into two peaks and would thereby introduce an additional unknown into the considerations. The apparent methyl group integrated absorption coefficients of the remaining compounds fall into either of two ranges which are separated by more than the sum of the average deviations of each group. This separation is in accord with the ideas of Martin and Hughes.[6] However, there is no observed distinction between ethyl, propyl, or butyl groups. An additional comparison within this group provides evidence for the elimination of the suggestion of Luther and Czerwony[5] concerning the occurrence of a tertiary C–H bending absorption in the measured interval; the methyl group integrated absorption coefficient for 3,3-diethylpentane would be expected to be much smaller than the others in its subdivision if a tertiary C–H bending absorption was important. This conclusion will be further substantiated when the gem polymethyl class is discussed.

The integrated absorption coefficient A_0 for methyl groups in ethyl, propyl, butyl, or longer branches adjacent to tertiary or quaternary carbon atoms is taken as the average of the observed values,

$$A_o = (5.02\pm0.08)\times10^5 \text{ cm mole}^{-1}.$$

This value was subsequently used to correct the $A_{CH_3}{}^T$ values of the remaining compounds which contain an internal pendant methyl group in order to determine an integrated absorption coefficient A_p for internal pendant methyls. The values are shown in column 4 of Table I. The average value is

$$A_p = (6.52\pm0.40)\times10^5 \text{ cm mole}^{-1}.$$

The value of A_o was also used to derive values of the integrated absorption coefficient A_s for pendant methyl groups adjacent to a quaternary carbon atom, or a tertiary having an additional pendant methyl group attached. These values are given in column 5 of Table I, the average being

$$A_s = (7.27\pm0.13)\times10^5 \text{ cm mole}^{-1}.$$

The absence of a significant decrease between the A_s values of the 2,2- or 3,3-disubstituted as compared with those for the 2-monosubstituted compounds is in accord with the evidence already given. Thus, the occurrence of a tertiary CH bending vibration in the wavelength interval of interest cannot account for the

[10] The term internal pendant methyl denotes a methyl group attached to a tertiary or quaternary carbon which has no other methyl group attached; an example is the branched methyl in 7-methyltridecane. It is also convenient to use the term gem di- or trimethyl to indicate two or three pendant methyl groups attached to the same carbon atom. Thus, 2-methylpentane and 2,2-dimethylpentane contain gem dimethyl and gem trimethyl structures, respectively. When both gem di- and trimethyl substitution are indicated, the term gem polymethyl is used.

observed variation in the methyl integrated absorption coefficient.

The value of the integrated absorption coefficient for methyl groups in normal paraffins is obtained directly from column 3 as

$$A_t = (3.70 \pm 0.04) \times 10^5 \text{ cm mole}^{-1}.$$

This completes the scheme devised to account for the fluctuating intensity of the methyl symmetrical bending vibration. It is now possible to test the internal consistency by calculating the expected experimental values of $A_{CH_3}{}^T$. These values and the deviation from the experimental value, Δ, are given in Table I, columns 6 and 7. The average deviation, excluding the normal compounds, is 2.1%. The average deviation, excluding the normal compounds, of the calculated as compared to the observed total intensities, A, is 1.6%. If the normal compounds are included, these values fall to 1.9 and 1.4%, respectively.

This is but one of several schemes which were tried. The most obvious one is to carry over the A_t value and solve for the integrated absorption coefficients for internal pendant methyl, and methyl in ethyl, propyl, and butyl branches. This is accomplished by solving a set of simultaneous equations for the nongem dimethyl or trimethyl substituted branched compounds having the form,

$$A_{CH_3}{}^T = n_t A_t' + n_p A_p' + n_e A_e' + n_z A_z' + n_b A_b', \quad (4)$$

where the subscripts t, p, e, z, b refer to methyls in terminal, internal pendant, ethyl, propyl, and butyl positions or branches. The terminal methyl is a methyl at the end of a chain or branch longer than a butyl branch, and it is assumed that $A_t' = A_t$. In this scheme as in the last, an examination of the data on the third group of molecules (which have no terminal methyl groups) shows that $A_e' = A_z' = A_b'$. The values calculated for A_p' are given in column 8 of Table I. The average value is

$$A_p' = (7.62 \pm 1.25) \times 10^5 \text{ cm mole}^{-1}.$$

The large average deviation for this value seems unreal compared to that observed upon treating the branched and normal compounds separately. Furthermore, this scheme requires the internal pendant methyl group to have twice the integrated absorption coefficient as a terminal methyl group in the same molecule. On the other hand, the internal pendant methyl group in the first scheme is of the order of $\frac{1}{3}$ more intense than a terminal methyl in the same molecule, a situation which might possibly result from an inductive effect of the tertiary carbon atom. Also, the constancy of the integrated absorption coefficient for methyl groups in ethyl, propyl, and butyl branches required by the second scheme seems unreal since the value must eventually decrease to that of the terminal group (A_t'). This, of course, is not a requirement of the first scheme. For these reasons, therefore, it is felt that the first scheme is more desirable than the second. However, no explanation for the difference between A_t and A_o is available. It is also difficult to imagine the difference in A_o and A_p to be entirely due to an inductive effect of the tertiary carbon atom. Further experimentation with other substituents adjacent to the tertiary carbon should help decide the nature of the interaction.

TABLE II. CH bond moments calculated for the different methyl types.

Methyl type	μ/r_e (debye/A)[a]	μ This work (debye)[b]	μ Other work (debye)
o	±0.34	±0.38	...
p	±0.39	±0.43	...
s	±0.41	±0.46	...
t	±0.29	±0.32	±(0.3±0.06)[c]; ±0.31[d]; ±0.26, and ±0.21[e]; ±0.33[f]; ±0.47, and ±0.39[g]

[a] Calculated using Eq. (7).
[b] Calculated using $r_e = 1.116$ A from B. A. Bonham, L. S. Bartell, and D. A. Kohl, J. Am. Chem. Soc. **81**, 4765 (1959).
[c] Ethane; I. M. Nyquist, I. M. Mills W. B. Person, and B. L. Crawford, J. Chem. Phys. **26**, 552 (1957).
[d] Methane; R. Rollefson and R. Havens, Phys. Rev. **57**, 710 (1940).
[e] Ethylene; R. C. Golike, I. M. Mills, W. B. Person and B. L. Crawford, J. Chem. Phys. **25**, 1266 (1956).
[f] Deuterated methanes; R. E. Hiller, Jr., and J. W. Straley, J. Mol. Spectroscopy **5**, 24 (1960).
[g] Reference 1, these values are expected to be high since no correction was made for the CH_2 background.

The foregoing discussion is based on the hypothesis that methyl groups can be treated as individual structural units, the vibrations of which are independent of those of the rest of the molecule. The narrow frequency range in which the absorption band due to the methyl symmetrical bending vibration of a great many molecules is observed lends support to this hypothesis. In paraffins the frequency is essentially constant except when split by a specific interaction.[11] Additional support is provided by the remarkable constancy of the $A_{CH_3}{}^T$ values within classes having the same number and arrangement of methyl groups, particularly the normal and branched with a single internal pendant methyl. It is felt that the self-consistency of the empirical scheme justifies further considerations of the group integrated absorption coefficient with respect to the bond moments of the different methyl types. Francis[1] has given an equation which relates the change in dipole moment in the ith normal coordinate $\partial\mu/\partial Q_i$ to the corresponding group integrated absorption coefficient.

$$A_i = \frac{\pi(\epsilon+2)^2}{27 c_m \epsilon} [\partial\mu/\partial Q_i]^2 \text{ cm}^2 \text{ molecule}^{-1} \text{ sec}^{-1}, \quad (5)$$

[11] L. J. Bellamy, *The Infrared Spectra of Complex Molecules* (John Wiley & Sons, Inc., New York, 1958), p. 21.

where ϵ is the dielectric constant of the solvent, and c_m the velocity of light in the medium. If the Maxwell relationship $n^2=\epsilon$ is valid for the system, Eq. (5) amounts to the assumption that the Polo-Wilson equation[12] relating the gaseous and pure liquid intensities A_G and A_L, respectively, i.e.,

$$A_L=(1/n)[(n^2+2)/3]^2 A_G,$$

where

$$A_G=(\pi/3c)[\partial\mu/\partial Q_i]^2$$

is applicable to a dilute carbon tetrachloride solution of the liquid.[13] Francis[1] has also derived an equation relating the effective bond moment μ/r_e to the integrated absorption coefficient of the methyl symmetrical bending vibration.

$$A_i=[2.167(\mu/r_e)^2-0.060(\mu/r_e)(\partial\mu/\partial r)]\times 10^{13}\ \text{cm}^2\ \text{molecule}^{-1}\ \text{sec}^{-1}. \quad (6)$$

This equation was derived by considering the methyl group as an individual unit independent of the rest of the molecule and is, therefore, directly applicable to the results reported here. The approximation

$$\mu/r_e=[(A_i/2.167)\times 10^{-13}]^{\frac{1}{2}} \quad (7)$$

was used because of the lack of bond moment derivative data for these molecules. The values calculated are given in Table II. The omission of the second term in Eq. (6) results in a difference of 3 to 4% in the value of μ/r_e, a small difference considering the approximations already made.

The value of the bond moment for the *s* methyl groups which was calculated by the same equation as was used for the others is uncertain because of the unknown factors involved in the coupling of vibrations which cause the band to split. The values of μ reported by other workers are listed for comparative purposes in Table II. It is not clear whether this comparison should be restricted to the bond moment value derived for the *t*-type groups or whether the value for *o*-type groups should also be considered. Obviously, the value calculated for *t*-type groups is in good agreement with the values derived for saturated hydrocarbons by other workers. It is felt that further comparison or discussion of the bond moment calculated for the different methyl types, other than to say that the differences between those for the *t*-, *o*-, and *p*-type groups do not seem unreasonably large, is to be avoided at this time in view of the assumptions already made.

While the foregoing discussion provides a scheme whereby the apparent fluctuations of the methyl group integrated absorption coefficient for the symmetrical bending vibration can be accounted for, it seems worthwhile to briefly consider the experimental data from another standpoint. It is necessary for this discussion to accept the A_{CH_3} value previously derived. The remarkable constancy of the values of $A_{CH_3}{}^T$ for a series of compounds which have the same number and arrangement of methyl groups, particularly the normal and branched with a single internal pendant methyl series, suggest an alternate interpretation of the data. That is, it might be inferred that it is not possible to break down the total integrated absorption coefficient into individual group absorption coefficients. If this is the case, then the fundamental absorbing unit would be the total number of methyl groups in the molecule coupled in such a way as to give a total integrated absorption coefficient which is unique for each particular number and arrangement of groups. This possibility cannot be completely ruled out, although the data of Table I do tend to favor the alternate scheme originally presented. The evidence for this is drawn from the branched compounds containing no internal pendant or gem di- or trimethyl substitution. The three methyl configurations represented by these four compounds yield essentially a constant A_{CH_3} value. Also, one might expect the $A_{CH_3}{}^T$ values for the 3-ethylhexane and 5-*n*-butylnonane to be the same as those for the internal pendant methyl series. Obviously, more complete data are needed in order to determine the correct hypothesis. While the authors favor the scheme originally presented, they are cognizant that additional data, when they become available, might completely reverse the interpretation.

ACKNOWLEDGMENTS

The authors are grateful to Dr. N. D. Coggeshall for his interest and advice in this work. We also thank Mr. S. J. Staruch for his assistance in obtaining the data.

[12] S. R. Polo and M. K. Wilson, J. Chem. Phys. **23**, 2376 (1955).

[13] The values of $\partial\mu/\partial Q_i$ obtained using the Polo-Wilson equation are essentially the same as those obtained with the equations of the following authors which were derived specifically for use with solution intensities: W. B. Person, J. Chem. Phys. **28**, 319 (1958); W. C. Mallard and J. W. Straley, J. Chem. Phys. **27**, 877 (1957); E. Hirota, Bull. Chem. Soc. Japan **27**, 295 (1954). The equations of Person, and Mallard and Straley gave results which agreed within 2%, while the equation of Hirota agreed within 18%.

SCF LCAO Study of Linear and Bent Acetylene*

LOUIS BURNELLE†

Solid State and Molecular Theory Group, Massachusetts Institute of Technology, Cambridge 39, Massachusetts

(Received December 5, 1960)

The self-consistent field molecular orbital method has been applied to linear acetylene, and to the *cis*- and *trans*-bent molecule, for various values of the bending angle. All 14 electrons have been taken into account, and free inner-shell outer-shell mixing has been allowed. As for the multicenter integrals, they have been evaluated by the Mulliken approximation. Reasonable values are obtained for the first ionization potential and for the excitation energy corresponding to the first $\pi \rightarrow \pi^*$ transition. The variation of the orbital energies induced by the distortion brings a confirmation of the qualitative predictions made by Walsh on the basis of the simple molecular orbital theory, but the treatment fails to predict the correct shape of the molecule in its first excited state, very likely because of the approximation of the three- and four-center integrals. The difference in energy between the *cis*- and the *trans*-configurations is predicted correctly, and there is a rough agreement between the calculated force constants and the experimental values. The results of an electron population analysis agree with experimental evidence and with the current views on hybridization, and they are confirmed by an examination of the equivalent orbital representation.

I. INTRODUCTION

AN adequate understanding of the properties of the simpler hydrocarbons is still one of the major problems of organic chemistry. As a step in this direction, the calculation of good wave functions for those molecules is not without a certain interest. One may hope that such calculations will eventually lead to fruitful syntheses from which the significance of new concepts introduced recently, such as the amount of promotion from the 2*s* orbital of carbon, will emerge in a clearer way. This point has already been stressed by Mulliken.[1]

It is with this purpose in mind that we have undertaken the study of acetylene. Interest in this molecule was particularly increased some years ago, when it was established experimentally by Ingold and King[2] and by Innes[3] that it is characterized by an important change of shape in its first excited state. Walsh,[4] in a general study of the shape of polyatomic molecules, has brought forward arguments explaining this type of phenomenon. His discussion is based on the correlation between the orbital energies in the various possible geometrical configurations which can be adopted by a given type of molecule. On the other hand, King[5] has used a simple model to study the excited states of the molecule. As a step toward a more accurate treatment, we have taken into account the two hydrogen atoms and all electrons and have calculated the wave functions not only for linear acetylene but also for the molecule distorted in various *cis*- and *trans*-bent configurations, which would provide a means for testing Walsh's correlation diagrams.[4] This line of approach in fact was suggested by Mulliken.[6]

The Roothaan SCF procedure[7] has been used, and by considering the bent configurations we have investigated the extent to which the SCF wave functions can be used to obtain information on the vibrational properties of a polyatomic molecule. In this particular problem, it was of some interest to see if it was possible to predict the observed difference between the vibration frequencies corresponding to *cis*- and *trans*-distortions (π_u and π_g vibrations, respectively), and to predict at least the sign of the coupling constant which correlates the bending of the two CH bonds.

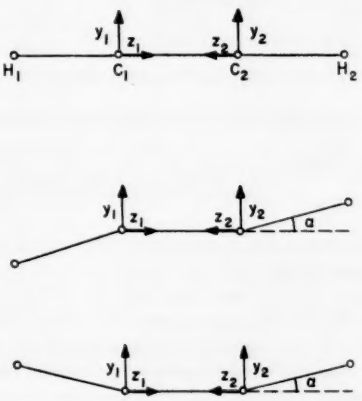

FIG. 1. Systems of axes used.

* This work was done in part at the M.I.T. Computation Center.

† Present address: Institut d'Astrophysique, Université de Liège, Cointe-Sclessin, Belgium. Appointment at M.I.T. supported by the International Cooperation Administration under the Visiting Research Scientists Program administered by the National Academy of Sciences of the U.S.A. This work was also supported in part by a grant from the National Science Foundation and the Office of Naval Research.

[1] R. S. Mulliken, J. Chem. Phys. **23,** 1833 (1955).
[2] C. K. Ingold and G. W. King, J. Chem. Soc. **1953,** 2702.
[3] K. K. Innes, J. Chem. Phys. **22,** 863 (1954).
[4] A. D. Walsh, J. Chem. Soc. **1953,** 2288.
[5] G. W. King, Can. J. Chem. **37,** 700 (1959).
[6] R. S. Mulliken, Can. J. Chem. **36,** 10 (1958).
[7] C. C. J. Roothaan, Revs. Modern Phys. **23,** 69 (1951).

TABLE I. Symmetry orbitals for acetylene.

	Trans (C_{2h})	*Cis* (C_{2v})	Linear ($D_{\infty h}$)
h_+			
c_+	A_g	A_1	Σ_g^+
s_+			
z_+			
h_-			
c_-	B_u	B_2	Σ_u^+
s_-			
z_-			
y_+	B_u	A_1	Π_u
x_+	A_u	B_1	Π_u
y_-	A_u	B_2	Π_g
x_-	B_g	A_2	Π_g

In a preliminary note,[8] we have given the expression of the MO's and the results of the electronic population analysis for the linear molecule. McLean[9] has made a similar but independent study of linear acetylene, calculating the multicenter integrals in a different way. A comparison of the two sets of results has been made by McLean, Ransil, and Mulliken.[10]

II. BASIS FUNCTIONS AND MODE OF APPROACH

The basis functions consist of the 1*s* orbitals of the hydrogens, and of the *K* and *L* shell orbitals of the carbons. These are Slater-type orbitals, with fixed orbital exponents, and their expressions are as follows:

$$h=1s_H=(1/\pi)^{\frac{1}{2}}\exp(-r_H)$$

$$c=1s_C=(k_1^3/\pi)^{\frac{1}{2}}\exp(-k_1r_C)$$

$$s=2s_C=(k_2^5/3\pi)^{\frac{1}{2}}r_C\exp(-k_2r_C)$$

$$z=2pz_C=(k_2^5/\pi)^{\frac{1}{2}}r_C\exp(-k_2r_C)\cos\theta_C$$

$$\begin{Bmatrix}y\\x\end{Bmatrix}=\begin{Bmatrix}2py_c\\2px_c\end{Bmatrix}=(k_2^5/\pi)^{\frac{1}{2}}r_C\exp(-k_2r_C)\sin\theta_C\begin{Bmatrix}\cos\phi\\\sin\phi\end{Bmatrix}.$$

The constants k_1 and k_2 have been taken equal to 5.7 and 1.59, respectively.

The axes chosen and the labeling of the atoms are given in Fig. 1. The calculations have been carried out for values of the bending angle equal to 5°, 10°, 30°, and 60°. For the bond lengths we have used the following values:

$$r_{CC}=1.2080\text{ A}$$

$$r_{CH}=1.0578\text{ A},^{11}$$

which have been kept constant throughout the whole calculation.

Because this simplifies the calculation of the integrals, we have not used an orthogonal 2*s* orbital for carbon, as is generally done, but the problem of orthogonality has been taken into account by allowing free mixing with the 1*s* orbitals of the carbons. Configuration interaction has been neglected, and in view of the formidable task which the exact calculation of all the integrals for the considered geometrical configurations would represent, the multicenter integrals have been approximated. First, all the three- and four-center integrals involving the 1*s* orbitals of the carbons have been neglected.[12] Secondly, we have calculated all the other multicenter integrals by using the Mulliken approximation.[13] This procedure, though justified by the simplifications which it introduces, undoubtedly influences to some extent the accuracy of the final results. Since in his treatment McLean[9] has calculated all the three- and four-center integrals exactly, it is possible, by comparison, to judge the influence of the Mulliken approximation on the SCF MO's (see further).

In order to factorize the secular determinant, we have made use of the symmetry properties of the molecule to build from the atomic wave functions normalized symmetry orbitals, which belong to the irreducible representations of the appropriate point group ($D_{\infty h}$ for the linear molecule, C_{2v} and C_{2h} for the *cis*- and *trans*-forms, respectively). The symmetry orbitals with the corresponding irreducible representations are given in Table I. The notations are self-explanatory. For instance, with S_h representing the overlap integral between the 1*s* orbitals of the hydrogens,

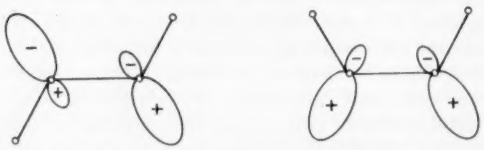

FIG. 2. Hybrids forming the MO originating, in the bent molecule, from the π_u orbital.

$$h_+=(h_1+h_2)/(2+2S_h)^{\frac{1}{2}},$$

and

$$h_-=(h_1-h_2)/(2-2S_h)^{\frac{1}{2}}.$$

The notations used for the irreducible representations are those adopted by Walsh.[4] Ingold and King[2] use a

[8] L. Burnelle, J. Chem. Phys. **32,** 1872 (1960).
[9] A. D. McLean, J. Chem. Phys. **32,** 1595 (1960).
[10] A. D. McLean, B. J. Ransil, and R. S. Mulliken, J. Chem. Phys. **32,** 1873 (1960).
[11] These are the distances at zero-point energy obtained by B. D. Saksena, J. Chem. Phys. **20,** 95 (1952).

[12] The largest of these integrals will be the so-called "Coulomb-type" $(AA:BC)$ integrals. We list hereafter the values in atomic units of a few integrals of this category, estimated by the Mulliken approximation for the linear molecule:

$(h_1c_1:s_2s_2)=0.0264$ $\quad$ $(h_1z_1:z_2c_2)=-0.00422$
$(h_1s_1:s_2c_2)=0.04159$ $\quad$ $(h_1c_1:h_2h_2)=0.01558$
$(h_1c_1:s_2c_2)=0.01424$ $\quad$ $(h_1h_2:c_1c_1)=0.01347$
$(h_1z_1:s_2c_2)=-0.03713$ $\quad$ $(h_1h_2:c_1s_1)=0.00285.$
$(h_1s_1:z_2c_2)=0.00422$

If, moreover, one takes into account the fact that, for instance, $(h_1s_1:s_2s_2)=0.18596$ and $(h_1z_1:s_2s_2)=-0.15813$, it appears that the simplification we have made is largely justified.

[13] R. S. Mulliken, J. chim. phys. **46,** 500 (1949).

TABLE II. LCAO SCF MO's for the linear and *cis*-bent molecule.

MO	SO	$\alpha=0°$	$\alpha=5°$	$\alpha=10°$	$\alpha=30°$	$\alpha=60°$
	h_+	0.0026	0.0026	0.0026	0.0014	−0.0021
$1a_1$	c_+	0.9961	0.9961	0.9961	0.9961	0.9959
	s_+	0.0138	0.0138	0.0138	0.0148	0.0173
$(1\sigma_g)$	z_+	0.0039	0.0039	0.0039	0.0033	0.0025
	y_+	0	-0.4×10^{-4}	−0.0004	0.6×10^{-4}	0.0016
	h_-	0.0008	0.0005	0.0005	−0.0002	−0.0024
$1b_2$	c_-	0.9968	0.9968	0.9968	0.9967	0.9965
	s_-	0.0180	0.0180	0.0182	0.0189	0.0217
$(1\sigma_u)$	z_-	0.0063	0.0061	0.0063	0.0065	0.0078
	y_-	0	0.6×10^{-4}	−0.0003	0.0006	0.0023
	h_+	0.4259	0.4258	0.4255	0.4248	0.4758
$2a_1$	c_+	−0.1942	−0.1943	−0.1947	−0.1917	−0.1914
	s_+	0.7128	0.7125	0.7116	0.6991	0.6072
$(2\sigma_g)$	z_+	−0.1770	−0.1751	−0.1695	−0.1189	−0.0125
	y_+	0	0.0192	0.0391	0.1075	0.1605
	h_-	0.4750	0.4751	0.4749	0.4712	0.4439
$2b_2$	c_-	−0.1578	−0.1577	−0.1577	−0.1584	−0.1658
	s_-	0.3619	0.3624	0.3637	0.3852	0.4964
$(2\sigma_u)$	z_-	−0.2733	−0.2725	−0.2705	−0.2448	−0.1374
	y_-	0	0.0182	0.0368	0.1080	0.2012
	h_+	0.2810	0.2816	0.2831	0.2962	0.3232
$3a_1$	c_+	0.1410	0.1407	0.1398	0.1326	0.1241
	s_+	−0.3522	−0.3510	−0.3475	−0.3213	−0.2939
$(3\sigma_g)$	z_+	−0.7850	−0.7854	−0.7865	−0.7907	−0.7957
	y_+	0	0.0203	0.0390	0.1350	0.2464
	h_+	0	−0.0047	−0.0091	−0.0280	−0.0159
$4a_1$	c_+	0	0.0037	0.0082	0.0221	0.0510
	s_+	0	−0.0339	−0.0692	−0.2043	−0.4335
(π_u)	z_+	0	0.0460	0.0907	0.2802	0.5172
	y_+	1	0.9989	0.9958	0.9597	0.8378
	h_-	0	0.0165	0.0320	0.0845	0.1154
$3b_2$	c_-	0	0.0106	0.0210	0.0561	0.0708
	s_-	0	−0.0392	−0.0729	−0.1890	−0.0540
(π_g)	z_-	0	0.0225	0.0492	0.1484	0.4935
	y_-	1	0.9982	0.9928	0.9436	0.8320

slightly different convention, inverting the notations for B_1 and B_2. The notations used here are actually those recommended by the Joint Commission for Spectroscopy of the International Astronomical Union and the International Union of Pure and Applied Physics [see R. S. Mulliken, J. Chem. Phys. **23,** 1997 (1955)].

For the linear molecule, the secular equation reduces to two 4×4 and two 1×1 determinants, due to the space degeneracy between the $2px$ and the $2py$ orbitals. For the bent molecule, the degeneracy is not maintained, and the $2py$ orbitals mix with the other functions located in the molecular plane; in this case one has to solve two 5×5 and two 1×1 determinants. The electronic configuration for the ground state of acetylene may be written as follows[14]:

$$(1\sigma_g)^2(1\sigma_u)^2(2\sigma_g)^2(2\sigma_u)^2(3\sigma_g)^2(\pi_u)^2(\bar{\pi}_u)^2, \qquad {}^1\Sigma_g{}^+$$

The MO's $1\sigma_g$ and $1\sigma_u$ are formed mainly by the $1s$ orbitals of the carbons, $2\sigma_g$, $2\sigma_u$, and $3\sigma_g$ are associated with the two CH bonds and the CCσ bond. Suppose π_u is formed by the in-phase overlap of the $2py$ orbitals, and $\bar{\pi}_u$ is built similarly from the $2px$'s.

For the ground state of the bent molecule, we have assumed the following configurations,

Cis-C_2H_2:

$$(1a_1)^2(1b_2)^2(2a_1)^2(2b_2)^2(3a_1)^2(4a_1)^2(b_1)^2, \quad {}^1A_1$$

Trans-C_2H_2:

$$(1a_g)^2(1b_u)^2(2a_g)^2(2b_u)^2(3a_g)^2(3b_u)^2(a_u)^2, \quad {}^1A_g;$$

b_1 and a_u are formed from the $2px$ orbitals perpendicular to the molecular plane. They thus correlate with $\bar{\pi}_u$, which may be expected to be little affected by the bending. Here $4a_1$, to which $3b_u$ corresponds in the *trans*-bent model, correlates with π_u which, contrary to $\bar{\pi}_u$, must be transformed considerably through the distortion. It must take on more and more s character as the bending increases and, when α equals 60°, it may be thought of as consisting of the in-phase overlap of two sp^2 hybrids (see Fig. 2).

It should be noted that the configurations indicated above, though the most likely for small values of the bending angle, might no longer be valid for large dis-

[14] R. S. Mulliken, J. Chem. Phys. **3,** 517 (1935).

TABLE III. LCAO SCF MO's for the *trans*-bent molecule.

MO	SO	$\alpha=5°$	$\alpha=10°$	$\alpha=30°$	$\alpha=60°$
	h_+	0.0026	0.0026	0.0015	−0.0015
	c_+	0.9961	0.9961	0.9961	0.9959
$1a_g$	s_+	0.0138	0.0138	0.0147	0.0170
	z_+	0.0039	0.0039	0.0033	0.0027
	y_-	-0.1×10^{-4}	0.0004	−0.0003	−0.0012
	h_-	0.0005	0.0005	−0.0002	−0.0017
	c_-	0.9968	0.9968	0.9968	0.9964
$1b_u$	s_-	0.0180	0.0182	0.0188	0.0224
	z_-	0.0061	0.0064	0.0064	0.0090
	y_+	-0.9×10^{-4}	0.0002	−0.0007	−0.0016
	h_+	0.4256	0.4248	0.4166	0.4113
	c_+	−0.1944	−0.1950	−0.2004	−0.2071
$2a_g$	s_+	0.7128	0.7132	0.7141	0.6779
	z_+	−0.1752	−0.1695	−0.1170	0.0166
	y_-	−0.0128	−0.0260	−0.0688	−0.1129
	h_-	0.4753	0.4755	0.4755	0.4744
	c_-	−0.1576	−0.1574	−0.1549	−0.1471
$2b_u$	s_-	0.3622	0.3630	0.3742	0.4508
	z_-	−0.2722	−0.2693	−0.2355	−0.0722
	y_+	−0.0266	−0.0537	−0.1606	−0.3262
	h_+	0.2816	0.2836	0.3013	0.3324
	c_+	0.1406	0.1395	0.1285	0.0947
$3a_g$	s_+	−0.3507	−0.3460	−0.3032	−0.1396
	z_+	−0.7855	−0.7871	−0.7997	−0.8896
	y_-	−0.0190	−0.0361	−0.1168	−0.1081
	h_-	−0.0003	−0.0001	0.0006	0.0098
	c_-	−0.0105	−0.0211	−0.0612	−0.1027
$3b_u$	s_-	0.0370	0.0719	0.2098	0.1895
	z_-	−0.0162	−0.0343	−0.1036	−0.4308
	y_+	0.9987	0.9950	0.9557	0.8097
	h_+	−0.0107	−0.0219	−0.0576	−0.1039
	c_+	−0.0035	−0.0078	−0.0211	−0.0589
$4a_g$	s_+	0.0428	0.0866	0.2450	0.4437
	z_+	−0.0542	−0.1064	−0.3020	−0.3532
	y_-	0.9983	0.9934	0.9457	0.8775

tortions, such as those considered in the present work. It might well happen that the changes in the orbital energies caused by the bending would have as a consequence a modification in the order of the energy levels,

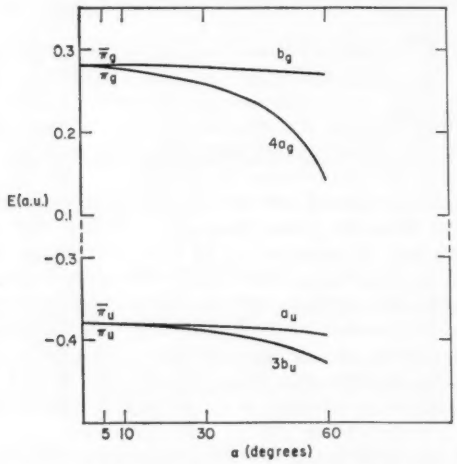

FIG. 3. Variation of the π orbital energies with the distortion in the *trans*-bent model.

and hence a change of the ground-state electronic configuration.

For the linear molecule, we have calculated the SCF wave functions by using a general program written for an IBM 650 with additional features by Dr. D. Ebbing at Indiana University. For the calculations concerned with the bent molecule, we have written a SCF program appropriate to this particular problem. This program has been written in the FORTRAN language, and can be used therefore on the IBM 704 and 709 computers, and on any other computer for which a FORTRAN compiler is available.[15]

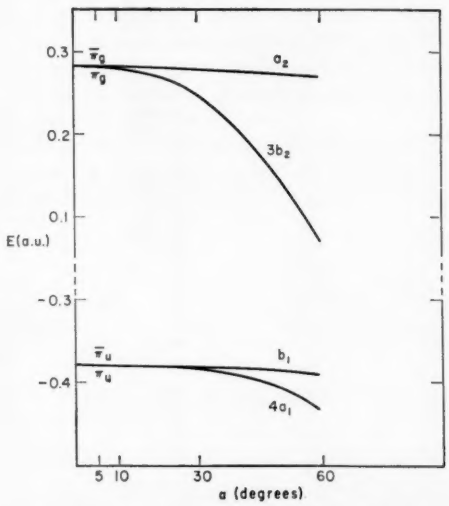

FIG. 4. Variation of the π orbital energies with the distortion in the *cis*-bent model.

III. RESULTS AND DISCUSSION

1. Expressions of the SCF MO's and Orbital Energies

The LCAO coefficients obtained are listed in Tables II and III, and the orbital energies in Table IV, for all the occupied orbitals and the first two excited ones. In Table V, we compare our orbital energies with those of McLean. The two sets of results agree as far as the order of the MO's in the energy scale is concerned,[16] but significant differences are observed. The same remark applies to the LCAO coefficients. It is noticed that except for the π_u orbital, the orbital energies resulting from the more accurate calculation are always higher than ours. It may be of some interest to note that the disagreement in the orbital energies is of

[15] We gratefully acknowledge help from Professor M. P. Barnett of M.I.T., in the writing of the SCF program. We are also very indebted to Dr. Ebbing, who has kindly put his program at our disposal.

[16] This order of the MO's also agrees with the predictions made earlier on a simple MO basis by Mulliken, see reference 14.

TABLE IV. LCAO SCF orbital energies (a.u.).

	Trans-bent molecule				Linear molecule			*Cis*-bent molecule		
MO	$\alpha=60°$	$\alpha=30°$	$\alpha=10°$	$\alpha=5°$	$\alpha=0°$	$\alpha=5°$	$\alpha=10°$	$\alpha=30°$	$\alpha=60°$	MO
$1a_g$	−11.577	−11.592	−11.592	−11.592	−11.592 ($1\sigma_g$)	−11.592	−11.591	−11.586	−11.588	$1a_1$
$1b_u$	−11.573	−11.588	−11.588	−11.588	−11.588 ($1\sigma_u$)	−11.588	−11.587	−11.582	−11.581	$1b_2$
$2a_g$	−1.156	−1.082	−1.066	−1.065	−1.064 ($2\sigma_g$)	−1.065	−1.066	−1.084	−1.188	$2a_1$
$2b_u$	−1.006	−1.000	−1.002	−1.001	−1.001 ($2\sigma_u$)	−1.001	−1.000	−0.987	−0.935	$2b_2$
$3a_g$	−0.729	−0.837	−0.859	−0.861	−0.862 ($3\sigma_g$)	−0.861	−0.858	−0.834	−0.756	$3a_1$
$3b_u$	−0.427	−0.390	−0.381	−0.380	−0.380 (π_u)	−0.380	−0.380	−0.381	−0.433	$4a_1$
a_u	−0.393	−0.383	−0.381	−0.380	−0.380 ($\bar{\pi}_u$)	−0.380	−0.380	−0.380	−0.393	b_1
$4a_g$	0.145	0.257	0.279	0.282	0.283 (π_g)	0.282	0.278	0.248	0.074	$3b_2$
b_g	0.270	0.279	0.282	0.283	0.283 ($\bar{\pi}_g$)	0.283	0.283	0.283	0.269	a_2

the same order as that caused in ammonia by a difference in the choice of the basis functions.[17,18]

If one assumes the validity of Koopmans' theorem,[19] the first ionization potential is found to be 0.380 a.u., or 10.34 ev, which compares reasonably well with the experimental value of 11.41 ev.[20]

Figures 3 and 4 show the change, as a function of the distortion, of the π orbital energies, which are evidently most affected by the bending. As it was to be reasonably expected, the orbitals formed from the $2px$ orbitals, i.e., $\bar{\pi}_u$ and $\bar{\pi}_g$, are practically not affected by the bending. As to π_u, originally formed by the in-phase overlap of the $2py$ orbitals in the linear molecule, it becomes more bonding, which is a little surprising since, as it appears from Fig. 2, the overlap between the hybrids which form it must decrease as the molecule bends. The MO which undergoes the most drastic change is π_g (out-of-phase overlap of the $2py$'s, originally), whose energy curve goes down steeply, in both *cis*- and *trans*-models, as α increases. This is in agreement with the predictions of Walsh,[4] and strongly supports his view that the *trans*-shape of the molecule in its first excited state is due to the stabilizing of the π_g orbital induced by the bending. However, if one calculates the energy of this electronic state by using the MO's obtained from the ground-state calculations, one finds that the minimum of the energy curve still corresponds to the linear configuration. The main reason that our treatment fails to predict the correct shape of the excited molecule, although it provides a good picture of the circumstances underlying the observed distortion, is very likely that the multicenter integrals are approximated. It is very probable that the other simplifications introduced, namely, the neglect of the rearrangement of the electronic charge subsequent to the excitation, the use of a constant CC bond length, and the neglect of configuration interaction, are of lesser importance.

In agreement with Ingold and King's conclusions,[2] and with Kings' calculations,[5] we find that the first singlet excited state of the molecule is ^1A_u. The excitation energy, which evidently corresponds to a transition to a linear configuration in our calculation, is found to be 6.24 ev. This compares fairly well with the experimental value of 5.23 ev.[2] It may be mentioned that the agreement is better than that obtained in earlier treat-

TABLE V. Effect of the Mulliken approximaton on the orbital energies.

	Orbital energies	
MOs	McLean	Burnelle
$1\sigma_g$	−11.400	−11.592
$1\sigma_u$	−11.397	−11.588
$2\sigma_g$	−1.041	−1.064
$2\sigma_u$	−0.776	−1.001
$3\sigma_g$	−0.683	−0.862
π_u	−0.441	−0.380
π_g	0.251	0.283

TABLE VI. Total molecular energy.

α	*Cis*	*Trans*
0°	−77.9482	
5°	−77.9468	−77.9472
10°	−77.9417	−77.9437
30°	−77.8781	−77.8954
60°	−77.7401	−77.7623

[17] H. Kaplan, J. Chem. Phys. **26,** 1704 (1957).
[18] A. B. F. Duncan, J. Chem. Phys. **27,** 423 (1957).
[19] T. Koopmans, Physica **1,** 104 (1933).
[20] K. Watanabe, J. Chem. Phys. **26,** 542 (1957).

TABLE VII. Overlap population.

	$1\sigma_g$	$1\sigma_u$	$2\sigma_g$	$2\sigma_u$	$3\sigma_g$	$\pi_u+\bar{\pi}_u$	Total
$n(i; C_1H_1)$	0.0004	0.0001	0.3373	0.4398	0.0963	0	0.87
$n(i; C_1C_2)$	0.0050	−0.0115	0.1738	−0.0233	0.6804	1.0308	1.86

ments, which neglected the hydrogens and the inner-shell electrons.[5,21,22]

2. Total Energy

The values found for the total energy, for all the geometrical configurations considered, are given in Table VI. It is noticed that, in all cases, the energy of the *cis*-bent model is higher than that of the corresponding *trans*-bent model, indicating a positive coupling constant, in agreement with experiment.[23] If one assumes an harmonic vibration potential function and uses the energies of the *cis*- and *trans*-bent molecule, for $\alpha=5°$, one obtains 0.539×10^5 d/cm for the bending force constant, and 0.089 for the coupling. The experimental values are 0.188 and 0.069, respectively.[23]

It is to be noted, however, that the calculated energy is lower than the experimental value, which is −77.39 a.u. for the linear molecule. This is undoubtedly a consequence of the approximation of the multicenter integrals. Although it seems impossible at present to draw general conclusions on the effect of the Mulliken approximation on the total energy, it is of some interest to mention that in the case of Be_4 it has also been found that the Mulliken approximation causes an appreciable lowering of the energy.[24] These results clearly emphasize the great importance of the exact calculation of multicenter integrals. Under such conditions, it is really gratifying that we succeed in calculating the variations of the total energy with a reasonable accuracy; this seems to indicate that, although our integrals are inaccurate, their changes are given satisfactorily by the Mulliken approximation.

3. Electron Population Analysis and Equivalent Orbital Representation

An electron distribution analysis has been carried out, according to Mulliken's definitions.[1] Table VII gives the contributions of the various MO's to the overlap populations between a carbon and the adjacent hydrogen, and between the two carbons.

A SCF study of ethylene has been done recently,[25] following a line of approach similar to ours. It is found that in that molecule the overlap populations of each CH bond is equal to 0.68 and that of the CC σ bond 0.575. The fact that in acetylene the corresponding values are larger, 0.87 and 0.82, respectively, is in agreement with the idea that the strength of a bond increases with the percentage of *s* character of the hybrids involved in the bond.[26] For the overlap population between a carbon and the nonadjacent hydrogen, we find a negative value (−0.55), as is usually found for nonbonded atoms. We also find small negative values for the overlap population between the 1*s* orbital of a carbon and the orbitals centered on the other atoms,

$$n(h_1, c_1) = -0.018; \qquad n(c_1, s_2) = -0.011;$$
$$n(c_1, z_2) = -0.027.$$

This antibonding effect, which is a consequence of forced hybridization, has already been observed in other molecules.[1]

We list in Table VIII the gross atomic populations with their various components. One notices that a charge of 0.92 *e* has been promoted from the 2*s* orbital of carbon, which indicates a state of hybridization close to *sp*. It may be seen on the other hand, that a charge of 0.105 *e* has been transferred from each hydrogen to the adjacent carbon, giving rise to a polarity C^-H^+, in agreement with the acidic character of acetylene. It is to be noted that McLean[10] finds a gross atomic charge of +0.21 *e* on the hydrogens, and that Berthod[25] reports the same value of +0.21 *e* for ethylene. This latter point is a little disturbing, in view of the large difference in acidic character between acetylene and ethylene. This merely shows the sensitivity of the results of the population analysis to the MO's and emphasizes the need for accurate wave functions.

It appears from Table VII that the main contributions to the overlap population of the CH bonds comes from the MO's $2\sigma_g$ and $2\sigma_u$, whereas that of the CC bond is essentially due to $3\sigma_g$. Since this suggests a certain localization of the bonds,[27] we have investigated the possibility of transforming the MO's into localized orbitals. A convenient way to do this is to use the equivalent orbital representation.[28] If one looks for a unitary transformation which leads to three EO's, of which one represents the CC σ bond and the two others represent the two CH bonds, one has one degree of

[21] I. G. Ross, Trans. Faraday Soc. **48,** 973 (1952).
[22] J. Serre and A. Pullman, J. chim. phys. **50,** 447 (1953).
[23] G. Herzberg, *Infrared and Raman Spectra of Polyatomic Molecules* (D. Van Nostrand Company, Inc., Princeton, New Jersey, 1945).
[24] R. D. Cloney and J. S. Dooling, J. Chem. Phys. **29,** 425 (1958).
[25] H. Berthod, Compt. rend. **249,** 1354 (1959).
[26] C. A. Coulson, *Valence* (Oxford University Press, New York, 1952).
[27] The same remark applies to McLean's molecular orbitals, with the difference that $2\sigma_g$ contributes mainly to the CC σ bond and the $2\sigma_u$ and $3\sigma_g$ to the CH bonds.
[28] J. E. Lennard-Jones, Proc. Roy. Soc. (London) **A198,** 1, 14 (1949).

TABLE VIII. Gross atomic populations.

	$1\sigma_g$	$1\sigma_u$	$2\sigma_g$	$2\sigma_u$	$3\sigma_g$	$\pi_u+\bar{\pi}_u$	Total
$N(i;\mathrm{C})$	0.9997	0.9999	0.6269	0.5652	0.9129	2.0000	6.105
$N(i;\mathrm{H})$	0.0003	0.0001	0.3731	0.4348	0.0871	0	0.895
		$1s$	$2s$	$2pz$	$2py+2px$		
$N(\chi_C)$		1.998	1.083	1.024	2.000		

freedom in carrying the transformation, and we have imposed on the EO's the condition that the CC bond should contain no contribution from the hydrogens.

Under these conditions, the expressions found for the equivalent orbitals are as follows,

$$\sigma(\mathrm{CC})$$
$$=0.3846(s_1'+s_2')+0.3481(z_1+z_2)-0.0750(c_1+c_2)$$
$$\sigma(\mathrm{C_1H_1})$$
$$=0.4926h_1+0.4144s'_1-0.4174z_1-0.0309c_1$$
$$+0.0082h_2-0.0968s_2'-0.0946z_2+0.0156c_2,$$

where s_1' and s_2' are orthogonal $2s$ orbitals based on carbons 1 and 2, respectively.

It may be seen that in $\sigma(\mathrm{CC})$, the coefficients of the $2s$ and $2pz$ orbitals are very close to each other, which indicates an sp hybridization. The same remark applies to the hybrids engaged in the CH bonds. On the other hand, the expression of the orbitals associated with the CH bonds indicates a fair degree of localization. The conclusions drawn from the electron distribution analysis are thus fully confirmed by the results of the unitary transformation. If one attempts to do the same transformation on the MO's of the bent molecule, it is legitimate to consider the $4a_1(3b_u)$ orbital as a member of the new set, since this orbital retains in all the bent configurations a fairly pronounced localized character. This may be seen from Tables II and III. The other localized orbitals will then still be associated with the two CH bonds and the CC σ bond, respectively.

The following are the expressions found in those conditions for the localized orbitals in the two bent cases with $\alpha=60°$. One would expect to find here a hybridization close to sp^2.

Trans (60°):

$$\sigma(\mathrm{C_1H_1})=0.5016h_1+0.4924s_1'-0.2837z_1-0.2369y_1$$
$$-0.0171c_1+0.0103h_2-0.1443s_2'$$
$$-0.1985z_2-0.0441y_2-0.0086c_2$$
$$\sigma(\mathrm{CC})=0.2995(s_1'+s_2')+0.4384(z_1+z_2)$$
$$+0.0115(y_1-y_2)-0.0789(c_1+c_2)$$
$$\pi'(\mathrm{CC})=0.0072(h_1-h_2)+0.1893(s_1'-s_2')$$
$$-0.3598(z_1-z_2)+0.4933(y_1+y_2)$$
$$-0.0314(c_1-c_2).$$

Cis (60°):

$$\sigma(\mathrm{C_1H_1})=0.5092h_1+0.4841s_1'-0.2830z_1+0.2413y_1$$
$$-0.0217c_1+0.0255h_2-0.2170s_2$$
$$-0.1207z_2-0.0077y_2-0.0086c_2$$
$$\sigma(\mathrm{CC})=0.3273(s_1'+s_2')+0.4065(z_1+z_2)$$
$$-0.0693(y_1+y_2)-0.0774(c_1+c_2)$$
$$\pi'(\mathrm{CC})=0.0105(h_1+h_2)+0.2428(s_1'+s_2')$$
$$-0.3228(z_1+z_2)-0.5104(y_1+y_2)$$
$$+0.0169(c_1+c_2).$$

The symbol $\pi'(\mathrm{CC})$ has been used to designate the "transformed" π orbital, which was originally π_u.

Note that the orbital labeled $\sigma(\mathrm{CC})$ is no longer of pure σ type, since it contains a small contribution from $2py$ AO's. Yet from the ratio of the coefficients of the $2s$ and $2pz$ orbitals, it may be considered as formed by hybrids of practically sp^2 character, in both *cis*- and *trans*-models. However, the same cannot be said about the other orbitals; $\pi'(\mathrm{CC})$ appears to have less, and $\sigma(\mathrm{C_1H_1})$ more s character than that involved in a sp^2 state. Moreover, it may be seen that the carbon hybrids used to form the CH bonds are not oriented along the CH line. A similar situation has been found in water[29] and ammonia,[18] and it is very probable, that, as has been found in those two molecules,[30] the transverse component of the bond dipole moment gives a large contribution to the infrared intensity of the absorption band corresponding to the active bending mode.

IV. CONCLUSIONS

It can be seen that the procedure described in this paper leads to a consistent model of the ground state of acetylene. For the linear molecule, the values obtained for the orbital energies are reasonable and compare fairly well with the results of a more exact calculation. The same may be said of the charge distribution and hybridization. The predicted behavior of the molecule, as a function of bending, also seems reasonable. However, the fact that we calculate a too low total energy and fail to predict the right shape of the molecule in its first excited state emphasizes the importance of the

[29] F. O. Ellison and H. Shull, J. Chem. Phys. **23**, 2348 (1955).
[30] L. Burnelle and C. A. Coulson, Trans. Faraday Soc. **53**, 403 (1957).

role of multicenter integrals and stresses the need for their exact calculations. It is obvious from our results that before bringing any improvement to our treatment, such as an extension of the basis or the introduction of configuration interaction, the very first step must be the exact calculation of all the integrals.

It is with this point in mind that we have been working on a general program which calculates three-center integrals for any arbitrary position of the nuclei, by means of the zeta function method.[31] It is our intention to repeat the calculation at a later juncture, using this program.

[31] M. P. Barnett and C. A. Coulson, Phil. Trans. Roy. Soc. (London) **A243,** 221 (1951).

ACKNOWLEDGMENTS

The author wishes to acknowledge the hospitality he has enjoyed both at the Quantum Chemistry Group of Indiana University and at the Solid State and Molecular Theory Group of M.I.T. He is also grateful to Professor J. Duchesne, of the University of Liege, Belgium, for his continuing interest in the general program of research, of which the work described in this paper forms a part.

THE JOURNAL OF CHEMICAL PHYSICS VOLUME 35, NUMBER 1 JULY, 1961

Molecular Association in Sodium Cyanide Vapor*

RICHARD F. PORTER†

Department of Chemistry, Cornell University, Ithaca, New York

(Received October 17, 1960)

Mass spectra of vapors from samples of NaCN indicate that the compound evaporates as NaCN(g) and $Na_2(CN)_2$(g) molecules at temperature around 1000°K. The mass spectrum resembles that obtained for sodium halide and hydroxide vapors. A comparison of relative ion currents produced by electron bombardment of NaCN vapors effusing from single- and double-oven-type Knudsen cells, yielded information related to the processes of ion formation. For the reaction

$$Na_2(CN)_2(g) = 2NaCN(g),$$

we obtain $\Delta H_{1000}° = 41.0 \pm 3.0$ kcal/mole dimer. This indicates a dimer stability comparable to that for Na_2I_2(g).

INTRODUCTION

IN some respects, the alkali cyanides show properties that indicate a similarity to the alkali halides. It is of interest to examine whether analogous behavior may be anticipated with respect to the vaporization processes for the two classes of compounds. The halides are known to vaporize to some degree as dimeric and polymeric molecules, which are assumed to be stabilized through the highly ionic character of these substances. Data related to the stoichiometry of the vaporization process for NaCN indicate a complicated behavior. Ingold[1] observed the vapor pressure of NaCN at temperatures between 800°C and about 1360°C. He interpreted his measurements in terms of a volatile gaseous NaCN species. On the other hand, there is also evidence[2] that a decomposition reaction plays an important role in the vaporization process. It seemed of value, therefore, to investigate by mass spectrometric means, the nature of the vaporization process for NaCN in the Knudsen range of pressure. A rather extensive amount of mass[3] spectrometric and molecular beam work[4] has been reported for the alkali halides in this pressure range.

EXPERIMENTAL

The mass spectrometer and high-temperature furnace assembly has been described earlier.[5] Condensable gases leaving a Knudsen cell are ionized by electron bombardment and mass analyzed in a 12-in., 60° direction-focusing mass spectrometer. A movable shutter located between the ion source and the effusion cell may be used to intercept the gases flowing from the cell. By this means corrections may be made for background ion currents that arise at masses coinciding with ions formed from effusing gases.

For the present experiments a double-oven effusion cell similar to that indicated in Fig. 1 was used. This cell was constructed of pure silver and could be heated

* Work supported by the Advanced Research Projects Agency.
† Alfred P. Sloan Fellow.
[1] C. K. Ingold, J. Chem. Soc. **123,** 885 (1923).
[2] E. W. Guernsey and M. S. Sherman, J. Am. Chem. Soc. **48,** 695 (1926).
[3] L. Friedman, J. Chem. Phys. **23,** 477 (1955); J. Berkowitz and W. A. Chupka, *ibid.* **29,** 653 (1958); R. C. Schoonmaker and R. F. Porter, *ibid.* **29,** 1070 (1958); T. A. Milne, H. Klein, and D. Cubicciotti, *ibid.* **28,** 718 (1958).
[4] R. C. Miller and P. Kusch, J. Chem. Phys. **25,** 860 (1956); **27,** 981 (1957).
[5] R. F. Porter and R. C. Schoonmaker, J. Phys. Chem. **62,** 234 (1958).

to over 800°C without noticeable effect of chemical reaction with NaCN. The use of this type cell for high-temperature mass spectrometric work has been discussed by Milne.[6] Akishin and co-workers[7] have employed double-oven techniques in mass spectrometric studies of gaseous alkali halides. The construction of this cell enables one to load the upper and lower chambers with NaCN or to load only the lower chamber with NaCN and the upper chamber with a substance for a sensitivity calibration of the mass spectrometer. In these experiments, vapor effusing from the upper portion of the cell is examined mass spectrometrically and thus the temperature of the upper oven only is needed explicitly for thermochemical computations. As shown in Fig. 1, a small deflection plate was located over the entrance channel to the upper chamber. This was to ensure that molecules entering the upper chamber would undergo a number of wall collisions before leaving the upper orifice. In general, the temperature of the lower oven was cooler than the upper oven since its temperature was determined primarily by heat conduction from the upper portion of the cell. Under normal operating conditions with a NaCN sample in the lower oven only, the vapor in the upper chamber would then be below saturation pressure corresponding to condensed-vapor equilibrium at the temperature of the upper oven.

Unlike the alkali halides, NaCN is readily hydrolyzed under ordinary conditions and thus problems of handling the compound are apparent. During early stages of outgassing high ion currents of HCN^+, CO_2^+ and $(N_2^+ + CO^+)$ were observed. The HCN^+ which is attributed to HCN(g) formed by partial hydrolysis was removed by pumping through liquid-nitrogen traps and diminished with time while N_2^+ due to N_2(g) remained quite high even after the sample had been heated for several hours. During the course of the experiments, it became obvious that N_2(g) was being evolved from the sample either directly or by reaction of the sublimed material on the hot radiation shields. The fraction of sample that decomposed in the oven during the experiments, however, was probably not large since permanent gases leaving the effusion cell enter the ion source in a much higher flux than do condensable gases passing from the orifice through highly collimated source slits. Noncondensable gases like N_2 thus behave as ordinary background gases and do not show shutter effects. Deposits of cyanide were found on the cooler portions of the furnace and shutter plate at the termination of an experiment. The CO_2^+ presumably results from CO_2(g) formed by decomposition of carbonate impurity in the sample. A small background ion current of $C_2N_2^+$ was also observed.

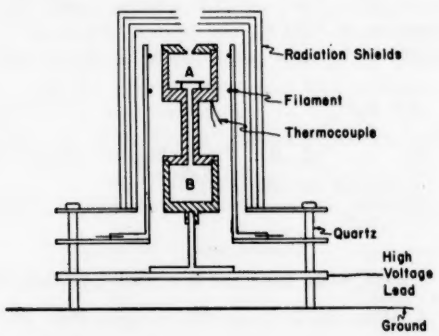

FIG. 1. Double-oven furnace assembly; sections A and B refer to upper and lower chambers, respectively.

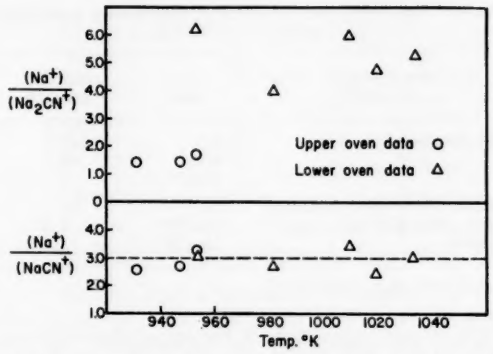

FIG. 2. Ion-current ratios observed as a continuous function of upper-oven temperature with NaCN sample loaded in upper and lower chambers of the effusion cell. Lower-oven data were taken after sample from upper chamber had evaporated. Ionizing electron energy = 100 v.

RESULTS

Ions with well-defined shutter effects observed on electron impact of sodium cyanide vapors were Na^+, $NaCN^+$, and Na_2CN^+. The mass spectrum resembles that of the sodium halides where the principal ions are Na^+, NaX^+, and Na_2X^+. At an electron acceleration energy of 10 v the Na^+ ion current was undetectable. This implied that Na^+ was not originating primarily by simple ionization of Na atoms since this process requires a threshold of about 5 v. Further considerations of the insensitivity of $Na^+/NaCN^+$ to experimental conditions indicated that Na^+ originated mainly by dissociative ionization. Reduction of NaCN by the silver container was therefore not a major factor in the vaporization process. The problem of reduction may be more severe when other metallic materials are used. Guernsey and Sherman,[2] for example, obtained evidence of reduction of NaCN by iron. A problem that is apparent in these studies is the extent of ion-fragmentation processes occurring in the ion source. To aid in elucidating fragmentation effects, mass spectra were obtained in a series of experiments with samples of NaCN loaded in upper and lower chambers of the effusion cell. Mass spectra

[6] T. A. Milne, J. Chem. Phys. **28,** 717 (1958).
[7] P. A. Akishin, L. N. Gorokhov, and L. N. Sidorov, Zhur. Fiz. Khim. **33,** 2822 (1959).

TABLE I. Ion-current data observed in double-oven experiment (T, upper oven = 973°K).

Experimental conditions	Ion[a]	Relative intensity
KBr in upper oven	K^+	100
	KBr^+	62
	K_2Br^+	51
NaCN in lower oven (observations after KBr had evaporated)	Na^+	13
	$NaCN^+$	5.3
	Na_2CN^+	1.1

[a] Ionizing electron energy = 100 v.

of the vapors originating in the upper chamber were obtained as a function of temperature. Eventually, as the temperature was increased, ion currents decreased markedly. This indicates that the sample in the upper oven had been removed by evaporation. Subsequent observations were then made as the upper chamber was raised to still higher temperatures. Under these conditions, the gas pressure in the upper oven is determined by the rate of flow of gases from the cooler, lower oven. A comparison of ion-current ratios obtained from the two sets of experimental conditions is illustrated in Fig. 2. The $Na^+/NaCN^+$ ratio was found to be nearly independent of experimental conditions while the Na_2CN^+/Na^+ ratio decreased quite considerably in changing from one set of conditions to another. At the point where the break in sample pressure occurred the absolute intensities of Na^+ and $NaCN^+$ dropped slightly over a factor of three while the Na_2CN^+ intensity decreased by a factor of about 15, or nearly as the square of the Na^+ change. These observations are consistent with the following proposed ionization processes:

$$NaCN(g)+\bar{e}\rightarrow Na^++CN+2e$$

$$NaCN(g)+\bar{e}\rightarrow NaCN^++2e$$

$$Na_2(CN)_2(g)+\bar{e}\rightarrow Na_2CN^++CN+2e.$$

Further checks indicated that for a fixed cell temperature the quantity $(Na^++NaCN^+)^2/(Na_2CN^+)$, as observed from lower or upper ovens, was independent of the degree of vapor saturation within the limit of experimental reproducibility.

In a second series of experiments, NaCN was loaded into the lower oven and KBr, which was to be used for a sensitivity calibration, was loaded into the upper oven. With this experimental arrangement, it was possible to observe the KBr system and evaporate the entire sample before appreciable mixing of the two samples could occur. Mass spectra of vapors from mixtures are expected to be complicated by the presence of mixed dimers (i.e., Na_2BrCN, etc.). A mass spectrum of NaCN vapor originating from the sample in the lower oven was then obtained and a comparison with data for the KBr system could be made. One set of data is given in Table I. The similarity in the behavior of the two systems is obvious.

HEAT OF DIMERIZATION OF NaCN(g)

From third-law procedures $\Delta H°$ for the reaction

$$Na_2(CN)_2(g)=2NaCN(g) \qquad (1)$$

was calculated by combining free-energy and entropy increments. The entropy change was estimated by assuming a linear structure for NaCN(g) and that the dimer has a structure similar to that for Na_2Cl_2 with CN^- replacing Cl^-. Theoretical[8–10] and experimental[10] values for $\Delta S°$ of dimerization for NaCl are between about 28 and 31 entropy units for a temperature of about 1000°K. For the Na—CN stretching frequency in the monomer we take a value obtained by increasing the Na—Cl frequency[11] (i.e., 366 cm^{-1}) by 10%. This factor was obtained by comparison of the H—Cl and H—CN frequencies. This is also the approximate change in going from Cl—Cl to Cl—CN. A value of r_{NaC} of 2.13 A was estimated. This was obtained by shortening the NaCl distance by the factor corresponding to the shortening of the H—CN from the H—Cl distance.[12] The C—N distance was assumed to be that in HCN or approximately 1.16 A. For the NaCN dimer we assume the planar structure shown in Fig. 3 with the CN^- ions polarized toward the carbon atom. A C—Na—C bond angle of 105° was used and Na—C bond distances were increased by 10% of the monomer distance. Berkowitz[13] has recently estimated the six normal vibration frequencies in Na_2Cl_2. For the six corresponding frequencies in $Na_2(CN)_2$ where CN acts as a mass point we have used the Berkowitz values increased by 10% to correct for the mass effect. In addition there are four frequencies which are associated with bending or oscillatory motion of CN. Since there will presumably be low frequency motions similar to the doubly degenerate bending motions in the monomer, we assume that the entropy contributions from these cancels in the dimerization reaction. Similarly the high-frequency C—N frequencies should contribute negligible entropy. We thus obtain $\Delta S°_{trans}+\Delta S°_{vib}+\Delta S°_{rot}=25.9$ entropy units for a temperature of 1000°K. The uncertainty in $\Delta S°_{vib}$ is estimated to be ±2.0 eu while $\Delta S°_{rot}$ is only about

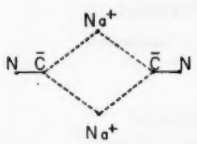

FIG. 3. Proposed structure for NaCN dimer.

[8] S. H. Bauer, R. M. Diner, and R. F. Porter, J. Chem. Phys. **29,** 991 (1958).
[9] T. A. Milne and D. Cubicciotti, J. Chem. Phys. **29,** 846 (1958).
[10] S. Datz, ORNL 2933 (1960).
[11] S. A. Rice and W. Klemperer, J. Chem. Phys. **27,** 643 (1957).
[12] Bond distance in NaCl was taken from A. Honig, M. Mandel, M. L. Stitch, and C. H. Townes, Phys. Rev. **96,** 629 (1954). Other distances were taken from Cottrell's *The Strength of Chemical Bonds* (Academic Press, Inc., New York, 1954).
[13] J. Berkowitz, J. Chem. Phys. **32,** 1519 (1960).

TABLE II. Thermochemical data for $Na_2(CN)_2=2$ NaCN from sensitivity calibration with NaCN.

Experimental conditions	Temp. °K	I_M (relative units)	I_M/I_D	P_{NaCN} (atm)	$\Delta F°$ (kcal/mole dimer)	$\Delta H°$ (kcal/mole dimer)
NaCN sample in upper oven	903	23.8	1.6	1.6×10^{-5}	18.3	41.7
	931	58.5	2.1	3.9×10^{-5}	16.6	40.7
	953	82.5	2.2	5.5×10^{-5}	16.3	42.0
NaCN sample in lower oven (observations after sample in upper oven evaporated)	1009	43.3	7.8	2.9×10^{-5}	16.0	42.1
	1033	100.0	7.1	6.7×10^{-5}	14.8	41.6

±0.5 eu since the latter is relatively insensitive to the assumed orientation of the CN^- groups.

For reaction (1) values for $\Delta F°$ were obtained from pressure measurements determined with the aid of sensitivity calibrations of the mass spectrometer. Two methods of calibration were used. In the first method the vapor pressure of NaCN was used directly. The constant temperature relationship

$$P_D=C(I_D/I_M)P_M, \qquad (2)$$

was combined with total vapor-pressure data obtained by extrapolation of Ingold's vapor-pressure equation to calculate P_M and P_D. In the above equation $I_M=I_{Na^+}+I_{NaCN^+}$, $I_D=I_{Na_2CN^+}$ and C is a temperature-insensitive constant which includes ionization cross section and detection efficiency terms. This constant is estimated to be about 0.7 for the dimer-monomer relationship. Values for P_M and P_D were computed for a temperature of 903°K and a sensitivity calibration, I_M/P_M was obtained from mass spectrometric observations from an NaCN sample in the upper chamber of the effusion cell. These data are indicated in the first row of Table II. Subsequent pressure data in Table II were then calculated with the aid of this calibration point and Eq. (2). The points at 1009°K and 1033°K refer to observations taken after the sample used for calibration had evaporated. These points then correspond to the condition of undersaturation as described earlier. In the second method of calibration a KBr sample in the upper chamber of the effusion cell was evaporated prior to observations of NaCN vapor originating from the lower chamber. The vapor-pressure data of Zimm and Mayer[14] were used to compute I_M/P_M for KBr. As indicated in Table II the presence of dimer in KBr vapor requires that a correction be applied to the effusion data of Zimm and Mayer to compute the KBr monomer pressure. In our calculations we initially assume 20% dimer in KBr vapor for our experimental conditions. With this we calculate the monomer pressure of KBr and a sensitivity constant $(I_{K^+}+I_{KBr^+})/P_{KBr}$. The pressure of NaCN was then obtained from this constant and the assumption of equal ionization cross sections for KBr(g) and NaCN(g). The pressure of NaCN dimer was then obtained from Eq. (2). The calculations are quite insensitive to the fraction of KBr dimer and to ion fragmentation effects in KBr vapor so long as we maintain equal dimer cross sections and equal monomer cross sections for the two systems. The change in $\Delta F°$ from assuming K^+ and KBr^+ are formed entirely from KBr(g) to assuming they are formed entirely from K_2Br_2 amounts to less than 0.5 kcal. These calculations are summarized in Table III. All of the data refer to the condition of undersaturation where fragmentation effects to form Na^+ and $NaCN^+$ from $Na_2(CN)_2$ are negligible compared with Na^++NaCN^+ produced from the monomer.

The temperature dependence of

$$(I_{Na^+}+I_{NaCN^+})^2/(I_{Na_2CN^+}),$$

was obtained from experiments in which samples of NaCN were loaded into both chambers of the effusion cell. Experimental results were then obtained by the same procedure as that employed with reference to the data in Fig. 2. With this procedure the experimental temperature range could be extended slightly. A second law treatment of these data is given in Fig. 4. The highest temperature points refer to the situation where the vapor is undersaturated and the low temperature

TABLE III. Thermochemical data for $Na_2(CN)_2=2$ NaCN from sensitivity calibration with KBr.

Temp. °K	I_M (relative units)	I_M/I_D	P_M (atm)	$\Delta F°$ (kcal/mole)	$\Delta H°$ (kcal/mole)
987	28.6	11.0	3.5×10^{-5}	14.6	40.2
995	39.0	10.0	4.8×10^{-5}	14.3	40.1
1025	70.0	9.0	8.9×10^{-5}	13.7	40.3
1049	100.0	6.4	1.3×10^{-4}	13.9	41.1

[14] B. H. Zimm and J. E. Mayer, J. Chem. Phys. **12,** 362 (1944).

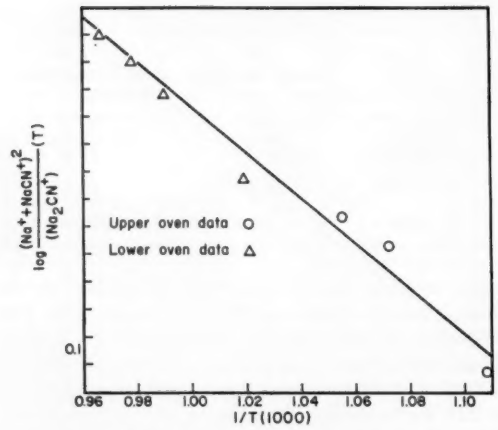

FIG. 4. Second-law data for evaluation of $\Delta H°$ for reaction $Na_2(CN)_2(g) = 2\ NaCN(g)$.

points refer to the condition of vapor saturation. From the slope of this curve we obtain $\Delta H_{1000}° = 38$ kcal/mole dimer with an estimated uncertainty of ± 4 kcal. A small contribution to Na^+ and $NaCN^+$ due to fragmentation from $Na_2(CN)_2$ might tend to lower the points on the curve obtained from upper-oven data and thus raise the slope of the curve slightly. Effects of ion fragmentation on the lower-oven data can be neglected.

DISCUSSION

Results of this work indicate that the vapors in equilibrium with condensed NaCN contain an appreciable fraction of dimeric molecules. The behavior of NaCN, in this respect, is similar to that of the alkali halides and hydroxides.

From the data in Tables II and III we deduce a third-law heat of dimerization of NaCN(g) of -41.0 kcal/mole dimer with a probable uncertainty of ± 3.0 kcal. Errors in $\Delta H°$ result mainly from uncertainties in $\Delta S_{vib}°$ and in the pressure calibrations. Variations in $\Delta F°$ for the two methods of calibration amount to about 1 kcal, although the over-all uncertainty in this quantity is estimated to be $\pm$ 2 kcal. As indicated in Table II no discernible difference can be seen in the values of $\Delta H°$ obtained from calculations with upper- and lower-oven data. An appreciable amount of ion fragmentation of $Na_2(CN)_2$ to form Na^+ and $NaCN^+$ should show a trend toward higher values in $\Delta H°$ in going from upper-oven to lower-oven data. A few percent fragmentation, however, would hardly be noticeable in these third-law calculations. Errors of this type would be more fully reflected in the second-law procedure, although the agreement between the methods is satisfactory. We are thus inclined to place slightly more weight in the third-law value.

Calculations based on our value for $\Delta H°$ (dimerization) indicate that in the saturated vapor the pressure ratio of dimer to monomer is between about 1.0 and 0.5 at 1100°K, while at the boiling point (i.e., about 1770°K) the ratio is less than 0.1. This variation in P_D/P_M probably accounts for the curvature in the vapor-pressure curve obtained by Ingold. It is interesting to note that from Ingold's vapor-pressure equation one calculates a hypothetical $\Delta H°$ of vaporization of 40 kcal/mole at 1100°K, which is presumably quite close to the true values for either species. Within our experimental error, the heat of dimerization of NaCN(g) is comparable to that of NaI(g) for which a value of $\Delta H°$ of approximately 41 kcal/mole dimer has been obtained.[4,8,15] The presently available thermochemical data indicate that for dimers with a common alkali metal, the stability of the dimer (i.e., absolute value of the dimerization energy) increases as the mean dimensions of the dimer decrease. If we use a simple ionic model for the dimer, we may then express this correlation in terms of the relative size of the anion with decreasing dimer stability in the sequence Na_2F_2 to Na_2I_2 and with $Na_2(OH)_2$ lying between Na_2F_2 and Na_2Cl_2. Extending this simple picture to NaCN we would predict, on the basis of the "ionic radius"[16] of CN^- that $Na_2(CN)_2$ would be between Na_2Cl_2 and Na_2I_2 in stability. As in the case of the alkali halide dimers, the energy of the NaCN dimer as computed from an ionic model[9,17] must also involve some polarization factors. Polarization effects presumably play an important role in determining the orientation of the CN groups in the dimer. A thorough examination of these factors may lead to a refined structure which departs from perfect planarity.

ACKNOWLEDGMENT

I wish to thank E. Zeller for his assistance with part of the experimental work.

---

[15] S. Datz and W. T. Smith, Jr., J. Phys. Chem. **63,** 938 (1959).
[16] From crystal data $r_{CN^-} = 1.92$ A for a spherical CN^- ion. See, for example, Verweel and Bijovet, Z. Krist. **100,** 201 (1938).
[17] J. Berkowitz, J. Chem. Phys. **29,** 1386 (1959).

Interpretation of the Absorption Spectra of $K_3Fe(CN)_6$†

C. S. NAIMAN

Solid State and Molecular Theory Group, Massachusetts Institute of Technology, Cambridge, Massachusetts

(Received December 19, 1960)

By interpreting the absorption spectra of $K_3Fe(CN)_6$ in solution, we are able to explain the results of the pressure dependence of the solid spectra, obtained by Parsons and Drickamer.

The intense absorptions at 24 000 and 32 900 cm^{-1}, are identified as charge-transfer spectra from the ligand to the T_{2g} level of the metal ion, while the one at 38 460 cm^{-1} is identified as the same type of transition, but into the E_g level. Fitting of the weaker spectra yields the values of 3500, 720, and 3285 cm^{-1} for the crystalline field parameters Dq, B, and C, respectively.

One of the results of Parsons and Drickamer shows evidence of a charge-transfer transition that is symmetry restricted, and made allowed by vibrational-electronic perturbations. A perturbation treatment is carried out that follows the method developed by Liehr and Ballhausen for the $d^n \rightarrow d^n$ crystal-field transitions, that are also symmetry forbidden.

Finally, two types of experiments that would test the proposed explanations are described.

INTRODUCTION

AN interpretation of the absorption spectra of $K_3Fe(CN)_6$ is presented here, which fully explains results found by Parsons and Drickamer[1] in their study of the pressure dependence of the absorption spectra of certain transition metal complexes. This is done by the close inspection of the intensities and energies of the solution spectra, within the framework of a one electron model for a "strong crystal field." [2]

In Secs. I and II we summarize the experimental data for the pressure-dependent solid, and solution spectra, respectively. We next identify the intense charge-transfer peaks in Sec. III. In Sec. IV, by fitting the weaker absorptions, we were able to obtain values for the parameters Dq, B, and C.

An unexplained result of the work by Parsons and Drickamer[1] is an irregular but definite decrease of intensity with increasing pressure. We have found an explanation of this by considering the possibility of a symmetry restricted charge-transfer transition, that is made allowed by vibrational-electronic perturbations. In Sec. V we carry out a perturbation treatment, mixing the ligand and/or d orbitals, with higher orbitals of opposite parity of the system. We conclude that the interplay of the relevant parameters *does* allow for a decrease in intensity. (We believe this to be the first such calculation for *charge-transfer* spectra.)

In the last section (Sec. VI) we describe pressure and temperature experiments that would test the proposed explanations.

Use of the crystal field theory to explain charge transfer, and crystal field spectra, in the following manner, appears quite fruitful, and we are applying it to a number of other "strong field" metal ion complexes.

I. ABSORPTION SPECTRA OF $K_3Fe(CN)_6$ UNDER PRESSURE

Parsons and Drickamer[1] have studied the pressure dependence of the absorption spectra of a number of crystals containing octahedrally coordinated iron-group ions (either single crystals or dilute pellets in a NaCl matrix). One of the complexes they studied was $K_3Fe(CN)_6$, which is known to have the "strong crystal field" [2] ground state corresponding to a spin of $\frac{1}{2}$, to determine if its behavior was of a different character than the "weak crystal field" complexes. The results for the band whose maximum is about 400 mμ (25 000 cm^{-1}) may be summarized as follows:

(1) The estimated absorption coefficient is of the order of 100 times larger than those of the "weak crystal field" complexes studied, as is evidenced by the necessity of using a very dilute sample.

(2) The maximum absorption exhibits a definite shift to lower energies, about 2100 cm^{-1} in 118 000 atm, which is too great to be ascribed to the "background" (such as the discharge lamp).

(3) The shape of the band changes considerably, exhibiting a doublet appearance. The higher energy maximum of the doublet appears mostly as a broad "shoulder" on the decreasing, lower energy maximum.

(4) As the pressure is increased, one can see [their diagram, Fig. 16 of work cited in reference 1, only goes up to 28 500 cm^{-1}] the beginning of an intense absorption band which is decreasing in energy with increasing pressure. By 118 000 atm, the intensity of this absorption has almost swamped the shoulder of the lower energy doublet.

(5) The intensity of the 25 000 cm^{-1} band decreases irregularly with pressure. Parsons and Drickamer did not make any theoretical interpretation of these results.

† This work was supported in part by the Navy Department (Office of Naval Research) of the U. S. Government.

[1] R. W. Parsons and H. G. Drickamer, J. Chem. Phys. **29**, 930 (1958).

[2] For a general discussion of crystalline (or ligand) field theory, and an explanation of the various terms used here, see the review article by D. S. McClure, Solid State Phys. **9**, 400 (1959).

TABLE I. Absorption spectra of $K_3Fe(CN)_6$ from Kiss *et al.*[a]

Wave number (in cm^{-1})	log ϵ
18 180	−0.542
24 100	3.022
31 250[b]	3.078
32 900	3.202
35 710[b]	3.000
38 460	3.100
≈44 000[b]	≈3.4

[a] See work cited in reference 3.

[b] The two bands at 31 250 and 35 710 cm^{-1} are shoulders of the maximum at 32 900 cm^{-1}. The ≈44 000 cm^{-1} is a shoulder on a more intense band >50 000 cm^{-1}.

II. ABSORPTION SPECTRA OF $K_3Fe(CN)_6$ IN SOLUTION

Kiss *et al.*[3] have studied the absorption spectra of $K_3Fe(CN)_6$ in solution at room temperature. They report a broad weak band at 18 180 cm^{-1} and three high bands at 24 100 cm^{-1}, 32 900 cm^{-1}, and 38 460 cm^{-1}. In addition the band at 32 900 cm^{-1} has two nearby less intense maxima at 31 250 cm^{-1} and 35 710 cm^{-1}. One can also see from their absorption curve the beginning of a broad, intense, absorption band, whose maximum occurs at some point >50 000 cm^{-1} and which has a shoulder at about 44 000 cm^{-1}. The data are summarized in Table I.

III. IDENTIFICATION OF THE INTENSE MAXIMA

A. Absorption at 24 100 cm^{-1}

From the data in Sec. II we see that Parsons and Drickamer were observing the maximum corresponding to the 24 100 cm^{-1} peak in the solution. It is well established fact that the intensities of crystal field spectra are weak, rarely higher than log$\epsilon \approx 1$ and usually lower.[4]

In addition, upon inspection of the Orgel diagram for d^5 in the strong crystal field limit,[4] (some of which is reproduced here in Fig. 1), one finds that all absorption bands should *increase* in energy as Dq (and the pressure) increases. Therefore the result that the 24 100 cm^{-1} band decreases, coupled with the fact that it is so intense, leads us to identify it as a charge-transfer transition from ligand to metal ion. A reasonable explanation for the *decrease* in energy with the increase of pressure presents itself when one considers the acceptor d level involved. Utilizing a single electron model in the strong crystal field limit, we may think of the d level as being split into a lower triply degenerate T_{2g} level, and a much higher doubly degenerate E_g level. For five d electrons, all will go into the lower T_{2g} level, not quite filling it up. Therefore, both the lower T_{2g} level and the higher E_g level may act as acceptor levels. In general the lowest charge transfer band will be into the T_{2g} level. (This same reasoning explains why, for strong crystalline fields, the first charge-transfer absorption in d^5 ions is consistently lower than the corresponding one in d^6 ions.[5] In the d^6 ions, the T_{2g} level is completely filled, and so only the considerably higher E_g level can act as an acceptor.) As the pressure is increased the difference in energy $10Dq = E_g - T_{2g}$ increases, but the difference in energy $T_{2g} - L_1$ (L_1 = Donor ligand level) may increase *or* decrease. In fact Stephens and Drickamer[6] found just the same effect to be true of the charge transfer absorption of Re^{+4} (which has the d^3 configuration), whose energy decreased ≈700 cm^{-1} in 45 000 atm. On the other hand, they found that for Co^{+2} (which has the d^7 configuration, and so the T_{2g} level is completely filled) the charge-transfer maximum increased by ≈1000 cm^{-1} in 70 000 atm.

B. Absorption at 38 460 cm^{-1}

We now proceed to estimate at what energy the charge-transfer transition $L_1 \rightarrow E_g$ should occur and to see if it corresponds to any of the observed peaks. We do this in two ways.

Consider the two final, iron ion, d configurations of the $L_1 \rightarrow T_{2g}$ and $L_1 \rightarrow E_g$ transitions. They are t^6 and t^5e, respectively. A good approximation of the difference of the charge-transfer energies would be, then, the lowest crystal field transition energy $t^6 \rightarrow t^5e$ of $[Fe(CN)_6]^{-4}$.

Unfortunately, the author has not been able to locate any crystal field absorption data for this complex. We therefore try to estimate it.

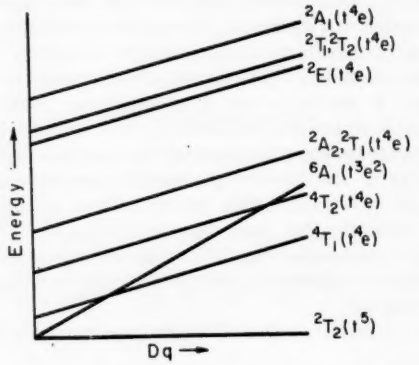

FIG. 1. Orgel diagram for d^5 in a strong crystal field (see works cited in references 2 and 4). Note: The diagram is adjusted so that $^2T_2 = 0$. For an explanation of the parameters, notation, etc., see work cited in reference 2. The diagram is not drawn to scale.

[3] A. V. Kiss, J. Abraham, and I. Hegedüs, Z. anorg. u. allgem. Chem. **244**, 98, (1940).

[4] Y. Tanabe, and S. Sugano, J. Phys. Soc. (Japan) **9**, 766, (1954).

[5] See e.g., p. 506 of work cited in reference 2.

[6] D. R. Stephens and H. G. Drickamer, J. Chem. Phys. **30**, 1518 (1959).

In the strong field limit, if we set the ground level $^1A_1$, which has the t^6 configuration, zero for all values of Dq and measure all energies from it, the expression for the first t^5e configuration level is $^3T_1(t^5e)=10Dq-3C$. It will be shown in Sec. IV that for $[Fe(CN)_6]^{-3}$, $10Dq\approx 36\,000$ cm^{-1}. In going from Fe^{+3} to Fe^{+2}, with the same ligands, we may expect Dq to decrease by about $\frac{1}{3}$.[2,4] We may therefore place $10Dq(Fe^{+2})\approx 24\,000$ cm^{-1}. Now it is found that $\gamma=C/B$, is about constant in going from free ion to the ion in the crystal field, so we use the value $\gamma=4.406$ from Tanabe and Sugano.[4] The B value will be decreased from its free ion value of 917 cm^{-1}, but not by as large a fraction as the decrease of the B value of the Fe^{+3} ion, which we will see in Sec. III is $\approx 70\%$ (since the crystal field is not as strong). We therefore choose a value $(B)_{crystal}\approx 0.8(B)_{free\ ion}$ which gives $^3T_1-{}^1A_1=10Dq-3C\approx 24\,000-(14.2)(734)=13\,600$ cm^{-1} which implies that this is the 38 460 cm^{-1} line.

There is another method of approximation which we may employ. Since we are dealing with the strong field limit we may approximate the $L_1\rightarrow E_g(t^5e)$ transition, by the $L_1\rightarrow E_g(t^6e)$ transition of Fe^{+2} and neglect the effect of the single hole in the t shell. The first charge transfer of $K_4Fe(CN)_6$ does indeed occur at 38 000 cm^{-1}.[5,7]

We may expect this band to display some multiplet structure since the $^3T_1$ level considered above is only the lowest level having the t^5e configuration.[8] The next two levels are $^3T_2=10Dq+8B-3C$ and $^1T_1=10Dq-C$ in our strong field approximation. We see therefore that the next t^5e configuration occurs at $8B\approx 5870$ cm^{-1} higher in energy, or at about 43 530 cm^{-1}. This then may be the shoulder observed at $\approx 44\,000$ cm^{-1}. We will see later that there is possible another identification of this shoulder.

TABLE II. Energy levels for d^5 in a strong crystal field.[a]

Level[b] (Bethe notation)	Level[b] (Mulliken notation)	Configuration	Variation with Dq, B, C.
$^2\Gamma_1$	$^2A_1$	t^4e	$10Dq+17B-C$
$^2\Gamma_4$, $^2\Gamma_5$	$^2T_1$, $^2T_2$	t^4e	$10Dq+12B-C$
$^2\Gamma_3$	^2E	t^4e	$10Dq+7B-C$
$^2\Gamma_2$, $^2\Gamma_4$	$^2A_2$, $^2T_1$	t^4e	$10Dq-2B-C$
$^6\Gamma_1$	$^6A_1$	t^3e^2	$20Dq-15B-10C$
$^4\Gamma_5$	$^4T_2$	t^4e	$10Dq+3B-4C$
$^4\Gamma_4$	$^4T_1$	t^4e	$10Dq-5B-4C$
$^2\Gamma_5$	$^2T_2$	t^5	0

[a] See works cited in references 2 and 4.

[b] The levels are adjusted so that $^2T_2\equiv 0$. For an explanation of parameters, notation, etc., see work cited in reference 2.

[7] G. Kortüm, Z. physik. Chem. **B33,** 243 (1936).

[8] The writer is grateful to Professor Koster for pointing this out.

TABLE III. Energy differences of the doublet levels in terms of B.

$$^2A_1-{}^2A_2,\ (^2T_1)=19B$$
$$^2A_1-{}^2E=10B$$
$$^2A_1-{}^2T_2,\ (^2T_1)=5B$$
$$^2T_1,\ (^2T_2)-{}^2A_2(^2T_1)=14B$$
$$^2T_1(^2T_2-{}^2E=5B$$
$$^2E-{}^2A_2,\ (^2T_1)=9B$$

C. Absorption at 32 900 cm^{-1}

Since this is the strongest of the three sharp maxima, we identify this too as a charge-transfer transition. Its position of being between the $L_1\rightarrow T_{2g}$ and $L_1\rightarrow E_g$ transitions implies that it is from another ligand orbital level $L_2<L_1$ to the T_{2g} level of the metal ion. This implies that the maximum of this absorption might also decrease with pressure, and we believe that evidence of this is found in result (4) of Sec. I, where we noted the beginning of an intense band decreasing in energy with pressure.

This also implies that, as with the L_1 level, we found an $L_1\rightarrow E_g$ absorption $=L_1\rightarrow T_{2g}+14\,400$ cm^{-1}, the same should be true of L_2 or, i.e., there should be an absorption $L_2\rightarrow E_g=32\,900+14\,400=47\,300$ cm^{-1} which gives us another interpretation of the shoulder at 44 000 cm^{-1}.

IV. IDENTIFICATION OF THE WEAKER MAXIMA

There remain three more maxima of our data to be determined. They are the broad weak band at 18 180 cm^{-1}, and the sidebands of the 32 900 cm^{-1} maximum, occurring at 31 250 and 35 710 cm^{-1}. Their lower intensity clues them to be crystal field transitions, and we proceed to deduce from them values for Dq and B. We refer the reader to Fig. 1 and Table II.

Let us first note that the intensity of the $^2T_2(t^5)\rightarrow {}^6A_1(t^3e^2)$ transition would hardly be measurable since it corresponds to the highly forbidden transition of a double electron excitation ($\Delta S=+2$). We therefore disregard it in our calculations.

Let us now note that the two shoulders, spaced apart by 4460 cm^{-1}, are of about the same intensity. This implies that they are both transitions from the ground state to levels of the same multiplicity. By inspecting the Orgel diagram[4] we see that this rules out the possibility of $^2T_2\rightarrow {}^4T_2=31\,250$ cm^{-1}, since all higher bands in the range of 35 710 cm^{-1} would have multiplicity $2S+1=2$ and so would be much more intense. If anything, the reverse is true.

We rule out the pair $^2T_2\rightarrow {}^4T_1$, $^2T_2\rightarrow {}^4T_2$ since then we have no assignment left for the 18 180 cm^{-1} band. We therefore assign the first observable band of 18 180 cm^{-1} to the $^2T_2\rightarrow {}^4T_1$ transition and the two upper levels to two levels of multiplicity 2. This checks with the fact that these are expected to be the most easily visible crystal field spectra.

TABLE IV. Crystal field energy levels (fitted).[a]

Level (Mulliken notation)	Computed (cm^{-1})[b]	Observed (cm^{-1})
$^2T_2$	0	...
$^4T_1$	18 206	18 180
$^4T_2$	23 966	see text
$^6A_1$	26 240	not observed
$^2A_2$, ($^2T_1$)	30 224	30 250
^2E	37 704	36 710
$^2T_1$, ($^2T_2$)	41 304	not observed
$^2A_1$	44 904	44 000(?)

[a] *Note added in proof*: The diagram given by Jørgensen in Acta Chem. Scand. **10**, 518 (1956) shows a shoulder at 40 000 cm^{-1}.

[b] The computed levels are for $Dq=3495$ cm^{-1}, $B=720$ cm^{-1}, $C=3286$ cm^{-1}. The observed levels are from Kiss *et al.*[3]

We give in Table III all the possible differences of these levels in terms of B. This difference should correspond to 4460 cm^{-1}, except that we may expect that the strong charge transfer peak at 32 900 cm^{-1} would draw them both in closer. From the diagram of Kiss[3] *et al.* we estimate that each are drawn in about 1000 cm^{-1} closer and so the difference is ≈ 6500 cm^{-1}.

The free ion value[4] of $B=1015$ cm^{-1} and is expected to be reduced in the strong field of the cyanide ligands by as much as 70%.[4,2] We may therefore expect a B value ≈ 700 cm^{-1} in the crystal. We see therefore that we may rule out all but two possible pairs, $^2A_1-{}^2E$ and $^2E-{}^2A_2$, ($^2T_1$).

We now make use of our $^2T_2\rightarrow{}^4T_1$ transition to determine which it is. In a crystalline field, whereas the values of B and C are considerably decreased, $\gamma_{\text{crystal}}\approx\gamma_{\text{free ion}}=4.7$ for Fe^{+3}.[4] Therefore, $10Dq-5B-4C\approx 10Dq-(23.8)B=18\,180$ cm^{-1}. For $B\approx 650$ cm^{-1} this gives $10Dq\approx 33\,700$ cm^{-1}. This then places the $^2A_1$ and ^2E levels at 41 700 and 37 450 cm^{-1}, respectively, in poor agreement with 36 700 cm^{-1} and 30 000 cm^{-1}. On the other hand, the $^2A_2$, ($^2T_1$) level is predicted to fall at $\approx 29\,350$ cm^{-1} and so we are led to the assignments,

$$^2T_2\rightarrow{}^4T_1=18\,180\ cm^{-1}$$
$$\rightarrow{}^2A_2,\ (^2T_1)\approx 30\,250\ cm^{-1}$$
$$\rightarrow{}^2E\approx 36\,710\ cm^{-1}.$$

A least-square fit of these levels yields the value $Dq=3495$ cm^{-1}, $B=720$ cm^{-1}, $C=3286$ cm^{-1}, $\gamma=4.564$. In Table IV we give the values for all the levels of the Orgel diagram, Fig. 1, computed with the above values. Concerning the $^4T_1$ level predicted to occur at 23 966 cm^{-1}, we see that this transition would be swamped by the charge transfer band at 24 100 cm^{-1} and would not be observable, under ordinary conditions.

However, if Dq would be increased, as when one applies hydrostatic pressure, this peak which goes as $10Dq$, would increase, while the charge transfer peak decreases (see Sec. III.A). As they separate they would therefore exhibit a doublet appearance, with the higher energy half being less intense. We believe that this explains effect (3) found by Parsons and Drickamer.

The $^2A_1$ level falls at $\approx 45\,000$ cm^{-1} and may also be adding to the 44 000 cm^{-1} shoulder.

V. INTENSITY OF THE CHARGE TRANSFER TRANSITIONS

A. Introduction

We are left with one major effect, the decrease of intensity of the $L_1\rightarrow T_{2g}$ transition. In the previously mentioned work of Stephens and Drickamer,[6] for all cases they found an *increase* in intensity. We give here a possible explanation that treats the $L_1\rightarrow T_{2g}$ transition as symmetry forbidden, but made allowed by vibronic (vibrational-electronic) perturbations.

The perturbation treatment follows the method developed by Liehr and Ballhausen[9] for the $d^n\rightarrow d^n$ vibronic transitions, which are also symmetry forbidden ($g\nrightarrow g$). The approximations are made along the lines of Tanabe and Sugano,[4] for the same type of $d^n\rightarrow d^n$ transitions. Use is made of the present understanding of the charge transfer process, in light of the molecular orbital ligand field theory, which is described by McClure.[2,10]

The discussion of the possible increase or decrease of various terms follows, in part, an explanation presented by Keating and Drickamer[11] for the increase and decrease of crystalline field absorption spectra, with pressure.

B. Charge Transfer Vibronic Transitions

In the absence of symmetry-destroying vibronic perturbations, electric dipole transitions from the ligand to the various d^n molecular orbitals of an octahedrally coordinated complex, can only occur from a u (odd) ligand orbital, since the d orbitals are g (even). Therefore if we wish to consider transitions from a g-type ligand orbital to a d orbital, we have to consider the mixing of the ligand and/or d orbitals with higher orbitals of opposite parity, brought about by odd vibrations. These higher orbitals are not limited to excited states of the central ion (such as $4p$ orbitals) but include those of the complex as a whole.

We consider the case where we have an initial configuration of n_1 electrons in the L_1 molecular orbital of the ligand (all other ligand levels being completely filled at all times, and thus neglected) and n_2 d electrons. We denote this configuration, in the usual way, by

[9] A. D. Liehr and C. J. Ballhausen, Phys. Rev. **106**, 1161 (1957).
[10] See p. 445 of work cited in reference 2.
[11] K. B. Keating and H. G. Drickamer, **34**, 140 (1961).

$\ell^{n_1}d^{n_2}$. Our final state is $l^{n_1-1}d^{n_2+1}$, where we have transferred one electron from the ligand to the metal ion.

The integrated intensity is proportional to the oscillator strength f, of the absorption. The f number of our interaction will be given by[9]

$$f(\ell^{n_1}d^{n_2}\rightarrow\ell^{n_1-1}d^{n_2+1})=\sum_k\sum_{v_k}f(\ell^{n_1}d^{n_2},\quad v_k\rightarrow\ell^{n_1-1}d^{n_2+1},\quad v_k\pm1).$$

Here the v_k are the harmonics of the normal mode Q_k that has a frequency ν_k. The individual f numbers are given by[9]

$$f(\ell^{n_1}d^{n_2},\quad v_k\rightarrow\ell^{n_1-1}d^{n_2+1},\quad v_k\pm1)$$
$$=CN_{v_k}[\langle\Phi(\ell^{n_1}d^{n_2},v_k)\,|\mathbf{m}|\,\Phi(\ell^{n_1-1}d^{n_2+1},v_k\pm1)\rangle]^2\Delta E,$$

where N_{v_k} is the molar fraction of the population in the ground state $\Phi(\ell^{n_1}d^{n_2})$ of the (v_k+1)th harmonic of the Q_k mode, ΔE is the energy difference of the charge transfer absorption, C is a constant, $\mathbf{m}$ is the electric dipole moment of the system, and the two Φ's are the total wave functions of the configurations, including the nuclear wave functions. Integration is over the electronic and nuclear coordinates.

The Born-Oppenheimer approximation allows us to separate the total wave function into a product of electronic wave functions, denoted by Ψ, containing the nuclear coordinates as parameters, and nuclear wave functions which we take as harmonic oscillator wave functions. The integration over the nuclear wave function, after squaring, yields a term proportional to $(v_k+\frac{1}{2})$. For a Boltzmann distribution

$$N_{v_k}=(\exp[-v_kX_k])(1-\exp[-X_k])$$

where $X_k\equiv(h\nu_k)/(kT)$. We now have,

$$f(\ell^{n_1}d^{n_2}\rightarrow\ell^{n_1-1}d^{n_2+1})$$
$$=\sum_k\sum_{v_k}f(\ell^{n_1}d^{n_2},\,v_k\rightarrow\ell^{n_1-1}d^{n_2+1},\,v_k\pm1)$$
$$=C\sum_k\coth(X_k/2)\Delta E$$
$$\times[\langle\Psi(\ell^{n_1}d^{n_2}),0\,|\mathbf{m}\,|\Psi(\ell^{n_1-1}d^{n_2+1}),1\rangle]^2,$$

where the $\coth(X_k/2)$ has come about from the $\sum_0^\infty(v_k)$. We have anticipated the result, that, when the electronic functions are expanded to first order in the nuclear coordinates, the above matrix element only depends on the difference $|v_k-(v_k\pm1)|=1$, and so may be factored out of the $\sum(v_k)$.

(The $\coth[h\nu_k/2(kT)]$ dependence on temperature for $d^n\rightarrow d^n$ transitions, was derived by Liehr and Ballhausen[9] and has been confirmed experimentally by Pratt and Coelho.[12])

In order to evaluate the expectation of the dipole moment, we consider the mixing of the zeroth-order wave functions $\Psi_g^0(\ell^{n_1}d^{n_2})$ and $\Psi_g^0(\ell^{n_1-1}d^{n_2+1})$, with excited ungerade states, such as $\Psi_u^0(\ell^{n_1}d^{n_2-1}p)$ and $\Psi_u^0(\ell^{n_1-1}d^{n_2}p)$. According to the perturbation theory the perturbed wave functions will be given by

$$\Psi(\ell^{n_1}d^{n_2})=\Psi_g^0(\ell^{n_1}d^{n_2})+\sum_{k,j}Q_k\gamma_i^k(j)\Psi_u^0(j)$$
$$\Psi(\ell^{n_1-1}d^{n_2+1})=\Psi_g^0(\ell^{n_1-1}d^{n_2+1})+\sum_{k,j}Q_k\gamma_f^k(j)\Psi_u^0(j),$$

where the summations are carried out over all normal coordinates Q_k, and all excited, ungerade, states, denoted by the index j. The mixing coefficients $\gamma_i^k(j)$ and $\gamma_f^k(j)$ (the subscripts denoting initial and final), are obtained in the following fashion.

Expand the crystalline field $V(Q,\tau)$ in a power series in the Q_k;

$$V(Q,\tau)=V_0(\tau)+\sum_k V'(Q_k,\tau)Q_k+\cdots.$$

Here τ denotes the electron coordinates, $V_0(\tau)$ is the equilibrium value of the crystalline field$\approx(10Dq)$ and $V'(Q_k,\tau)$ is the linear term of the series. We then get

$$\gamma_i^k(j)=-[E(j)-E(\ell^{n_1}d^{n_2})]^{-1}\int\Psi_u^0(j)V'(Q_k,\tau)\times\Psi_g^0(\ell^{n_1}d^{n_2})d\tau$$

$$\gamma_f^k(j)=[E(j)-E(\ell^{n_1-1}d^{n_2+1})]^{-1}\int\Psi_u^0(j)V'(Q_k,\tau)\times\Psi_g^0(\ell^{n_1-1}d^{n_2+1})d\tau.$$

We now introduce a number of approximations so that we may see if the intensity could decrease with pressure. The final analysis does not depend on the approximations, but is certainly simplified by the reduction of the number of terms.

We note that the perturbing ungerade, levels are closer to the d levels than the ligand levels by about 24 000 cm^{-1}. The nearest such level is a $4p-t_{1u}$ level,[10] and we will ignore perturbations from any higher ones. We therefore have to consider two types of excited states, $\ell^{n_1}d^{n_2-1}p$ and $\ell^{n_1-1}d^{n_2}p$. From energy considerations, we see that the former will probably be more important for $\ell^{n_1}d^{n_2}$ and the latter for $\ell^{n_1-1}d^{n_2+1}$. We further approximate

$$E(\ell^{n_1}d^{n_2-1}p)-E(\ell^{n_1}d^{n_2})\approx E(\ell^{n_1-1}d^{n_2}p)-E(\ell^{n_1-1}d^{n_2+1})$$
$$\approx E(4P)-E(3T_{2g})\equiv\Delta E'.$$

Since $QV'(Q,\tau)$ is the perturbation term, we may approximate it as do Tanabe and Sugano,[4]

$$Q\langle\ell^{n_1}d^{n_2-1}p\,|\,V'\,|\,\ell^{n_1}d^{n_2}\rangle\approx Q\langle\ell^{n_1-1}d^{n_2}p\,|\,V'\,|\,\ell^{n_1-1}d^{n_2+1}\rangle$$
$$\approx Q\langle p\,|\,V'\,|\,d\rangle\approx V_0[\delta R/\langle r\rangle],$$

where V_0 is the equilibrium value $\approx 10Dq$, $\langle r\rangle\equiv\langle d\,|\,r\,|\,d\rangle$, and $\delta R(<M^{-\frac{1}{2}}Q)$ is the zero-point amplitude of the vibrations, where M is the central ion's mass.

[12] G. W. Pratt, Jr., and R. Coelho, Phys. Rev. **116**, 280 (1959).

In addition Liehr and Ballhausen[9] have shown, that for a complex of octahedral symmetry, of the six normal modes of vibration, the only allowed, ungerade ones are the T_{1u} and T_{2u} modes, and the most effective one is the T_{1u} mode. (Essentially this is the mode that produces the most unsymmetrical potential at the central ion.) We therefore neglect all other modes and drop the index k. This yields for our wave functions

$$\Psi(\ell^{n_1}d^{n_2})=\Psi_g{}^0(\ell^{n_1}d^{n_2})$$
$$-[QM^{-\frac{1}{2}}(10Dq)/(\langle r\rangle\Delta E')]\Psi_u{}^0(\ell^{n_1}d^{n_2-1}p)$$
$$\Psi(\ell^{n_1-1}d^{n_2+1})=\Psi_g{}^0(\ell^{n_1-1}d^{n_2+1})$$
$$-[QM^{-\frac{1}{2}}(10Dq)/(\langle r\rangle\Delta E')]\Psi_u{}^0(\ell^{n_1-1}d^{n_2}p).$$

Substituting this into our expression for the dipole moment we get

$$[\langle\Psi(\ell^{n_1}d^{n_2}),\, v_k\,|\mathbf{m}|\Psi(\ell^{n_1-1}d^{n_2}),\, v_k+1\rangle]^2$$
$$=[\langle 0\,|Q|\,1\rangle M^{-\frac{1}{2}}(10Dq)/(\langle r\rangle\Delta E')]^2$$
$$\times[\langle\Psi_u{}^0(\ell^{n_1}d^{n_2-1}p)\,|\mathbf{m}|\Psi_g{}^0(\ell^{n_1-1}d^{n_2+1})\rangle$$
$$+\langle\Psi_g{}^0(\ell^{n_1}d^{n_2})\,|\mathbf{m}|\Psi_u{}^0(\ell^{n_1-1}d^{n_2}p)\rangle]^2.$$

All other terms vanish because of symmetry.

Without a detailed knowledge of the wave functions it is hard to say too much about how the dipole moment elements will vary with pressure, except that we may expect them to increase as the wave functions get more compressed and overlap more. The $\langle 0\,|Q|\,1\rangle\, M^{-\frac{1}{2}}$ we may approximate by $<\delta R$, the zero-point amplitude of the vibrations.

We find then that the integrated intensity f is proportional to

$$[(\delta R)(10Dq)/(\Delta E'\langle r\rangle)]^2[\langle\,|\mathbf{m}|\,\rangle]^2\Delta E.$$

Of these terms $10Dq$ will increase with pressure, $\langle r\rangle$ will stay about constant, δR will decrease (since there is less "room" for the central atom to vibrate), ΔE we know decreases, and $\Delta E'$ may increase, decrease, or remain constant. However, since the T_{2g} d level decreases with pressure, as is evidenced above in Sec. III, an increase in $\Delta E'=E(4P)-E(3T_{2g})$, is not unreasonable. We see, therefore, that the interplay of the above parameters, certainly does allow for a decrease in intensity.

On the other hand the intensity of a $u\rightarrow g$ transition should *only* decrease with pressure, since the dipole moment $\langle\Psi_u{}^0(\ell^{n_1}d^{n_2})\,|\mathbf{m}|\Psi_g{}^0(\ell^{n_1-1}d^{n_2+1})\rangle$ increases as ligand and metal ion wave functions overlap more as the pressure is increased. (The integrated intensity will have a decreasing factor of ΔE but for the charge-transfer spectra the effect due to just this term is expected to be negligible.)

It is also reasonable that the intensity of the $g\rightarrow g$ transition will be greater in solution where vibrations are more probable, than in a solid solvent where it is more tightly bound.

According to our result the higher ligand level L_1, will be a g level, and the next one, L_2, a u level. This corroborates McClure's level diagram[10] which gives first a higher t_{1g} ligand orbital and next a lower t_{2u} orbital.

VI. PROPOSED TEST OF THE THEORY

A. Charge Transfer Spectra

Two types of experiments may test the above explanations:

(1) Variation of the integrated *intensities* with temperature should produce a $\coth[h\nu_k/(2kT)]$ temperature dependence for $g\rightarrow g$ transitions, with relatively no temperature dependence for $u\rightarrow g$ transitions. (The latter can couple with *even* vibrations, but it is expected that this will be a higher order effect.)

(2) High-pressure experiments in the 25 000–50 000 cm^{-1} region should show an increase in *energy* with increasing pressure for the transitions ending on the E_g level.

In addition the transitions originating from the $L_2(u)$ level should uniformly increase in *intensity*, with increasing pressure.

B. Crystal Field Spectra

The same types of experiments should yield the following results:

(1) The temperature variation for the integrated *intensity* of all such field spectra is expected to be $\coth[h\nu_k/(2kT)]$ since they are all $g\rightarrow g$ transitions.

(2) With increase of pressure, all crystal field spectra should uniformly increase in *energy*.

ACKNOWLEDGMENTS

The author expresses his thanks to Professor G. F. Koster and Dr. A. J. Freeman for valuable criticism and comment. He also thanks Professor H. G. Drickamer for a preprint of his paper (reference 11), and fruitful discussions.

Thermal Conductivity and Equilibrium Constant of the System $N_2O_4 \rightleftharpoons 2NO_2$

B. N. SRIVASTAVA AND A. K. BARUA

Indian Association for the Cultivation of Science, Calcutta, India

(Received September 19, 1960)

An all-glass apparatus has been used to measure the thermal conductivity of the system $N_2O_4 \rightleftharpoons 2NO_2$ by the thick-wire variant of the hot-wire method in a temperature range of 32°–90°C and up to a pressure of about 50 cm Hg. The apparatus is capable of measuring the equilibrium constant and the thermal conductivity of the system simultaneously. The experimental data have been discussed in the light of theories based on the assumption of local chemical equilibrium. The discrepancy between the experimental and the calculated values of the heat conductivity which is particularly large at the lower pressures shows the necessity of applying nonequilibrium heat transfer theory to interpret the data.

I. INTRODUCTION

THE problem of heat transfer in dissociating gases apart from its fundamental interest has recently, considerably increased in importance as these gases exist in the exhaust nozzles of jet engines and within the boundary layers on supersonic aircrafts. In reacting gases, concentration gradients exist due to the variation of composition with temperatures. Large amount of heat may be carried as chemical enthalpy of molecules which diffuse because of concentration gradients and as a result, heat conductivity in reacting gases may be considerably higher than in nonreacting mixtures.

Heat transfer in dissociating gases was first treated theoretically by Nernst[1] and later by several other workers.[2–5] Recently Hirschfelder[6] has obtained an expression for the thermal conductivity of a reacting gas mixture on the assumption of local chemical equilibrium and has considered a few special cases. Subsequently, Butler and Brokaw[7] have obtained a general expression for the thermal conductivity of chemically reacting gas mixtures on the local chemical equilibrium assumption. For reactions of the type $A \rightleftharpoons nB$, all workers arrive at expressions which are equivalent.

It should be noted, however, that usually the chemical reaction rates are not fast enough to maintain the condition of local chemical equilibrium and that the most realistic treatment will be that of taking into consideration the relaxation of the chemical energy. The first attempt in this direction has been made by Franck and Spalthoff.[8] A more elaborate and rigorous theory is being developed by Secrest and Hirschfelder.[9]

The earliest measurements of the thermal conductivity of the system $N_2O_4 \rightleftharpoons 2NO_2$ were performed by Magnanini and Zunino[10] and Feliciani[11] and are not very reliable due to the simple methods employed in the measurements. Recently, Coffin and O'Neal[12] have measured the thermal conductivity of the system $N_2O_4 \rightleftharpoons 2NO_2$ over wide ranges of temperatures and pressures and have compared their data with the theoretical values. Their measurements, however, suffer from the following drawbacks, viz. (a) a calibration method, has been used in which the temperature rise of the wire in the conductivity cell is assumed to depend uniquely on the conductivity of the gas[13] which in this case is chemically reacting; (b) pressure has been measured by manometers using mercury which is attacked by N_2O_4 so that their results are likely to be vitiated by chemical reactions; (c) the diameter of the conductivity cell used by them is possibly too large to avoid convection particularly at the higher pressures. More recently, Coffin,[14] by employing his previous method, has measured the thermal conductivity of the system $N_2O_4 \rightleftharpoons 2NO_2$ diluted by inert gases. In view of the above mentioned sources of error in the measurements of Coffin and O'Neal and also due to the great interest in the system $N_2O_4 \rightleftharpoons 2NO_2$, it was thought desirable to study the system by a more refined method. In the present investigation, the following improvements have been made over the apparatus used by Coffin and O'Neal, viz. (a) The absolute method[15,16] has been used to measure the thermal conductivity so that the accuracy of measurements is expected to be higher; (b) an all-glass apparatus has been used to avoid all chemical reactions; (c) the diameter of the conductivity cell has been kept quite small and ob-

[1] W. Nernst, Festschr. Ludwig Boltzmann Gewidmet, 904 (1904).
[2] P. A. M. Dirac, Proc. Cambridge Phil. Soc. **22,** 132 (1924).
[3] J. Meixner, Z. Naturforsch. **7a,** 553 (1952).
[4] R. Hasse, Z. Naturforsch. **8a,** 729 (1953).
[5] I. Prigogine and R. Buess, Acad. roy. Belg. **38,** Ser. 5, 711, 851 (1952); F. Waelbroeck, S. Lafleur and I. Prigogine, Physica **21,** 667 (1955).
[6] J. O. Hirschfelder, J. Chem. Phys. **26,** 274, 282 (1957).
[7] J. N. Butler and R. S. Brokaw, J. Chem. Phys. **26,** 1636 (1957).
[8] E. U. Franck and W. Spalthoff, Z. Elektrochem. **58,** 374 (1958).
[9] D. Secrest and J. O. Hirschfelder, University of Wisconsin, WIS-AF-14A, June 20 (1960).
[10] G. Magnanini and V. Zunino, Gazz. Chim. ital. **30,** 405 (1900).
[11] C. Feliciani, Physik. Z. **6,** 20 (1905).
[12] K. P. Coffin and C. O'Neal, Natl. Advisory Comm. Aeronaut., Tech. Notes, 4209 (1958).
[13] H. A. Daynes, *Gas Analysis by Measurement of Thermal Conductivity* (Cambridge University Press, New York, 1933).
[14] K. P. Coffin, J. Chem. Phys. **31,** 1290 (1959).
[15] W. G. Kannuluik and L. H. Martin, Proc. Roy. Soc. (London) **A141,** 144 (1933); **A144,** 496 (1934).
[16] W. G. Kannuluik and E. H. Carman, Proc. Phys. Soc. (London) **B65,** 701 (1952).

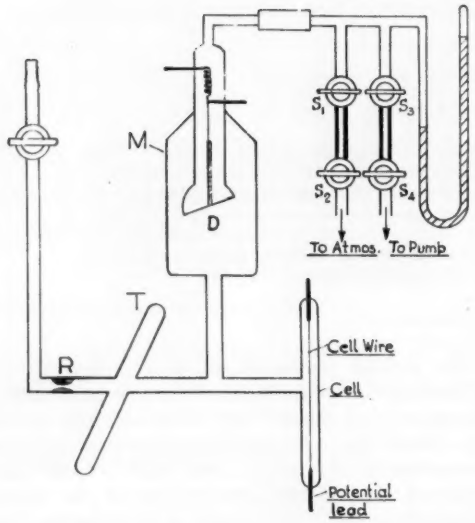

FIG. 1. Apparatus for the measurement of the thermal conductivity and the equilibrium constant of the system $N_2O_4 \rightleftharpoons 2NO_2$.

servations have been taken only below a pressure of about 50 cm Hg in order to minimize convection effects; (d) the apparatus is capable of measuring the thermal conductivity and the equilibrium constant of the system to be studied which is a great advantage.

In the present paper the thermal conductivity of the system $N_2O_4 \rightleftharpoons 2NO_2$ in the temperature range 32°–90°C and up to a pressure of about 50 cm Hg have been reported. Attempts have been made to interpret the data in terms of the theories based on the assumption of local chemical equilibrium. In a subsequent paper the experimental results will be discussed in the light of nonequilibrium heat transfer theory. The equilibrium constant of the system $N_2O_4 \rightleftharpoons 2NO_2$ in the above mentioned temperature and pressure ranges has also been reported.

II. APPARATUS AND THEORY

The method employed for the thermal conductivity measurements is the thick-wire variant of the hot-wire method, the theory of which has been worked out[15,16] completely. The apparatus used is shown in Fig. 1. It consists of the conductivity cell C made of thick-walled glass capillary tube. A thin platinum wire is welded at the ends to two thicker platinum potential leads and sealed axially along the capillary tube. The glass diaphragm manometer M is similar to that described by Daniels.[17] The pressure regulation unit $S_1S_2S_3S_4$ is self-explanatory. The electrical circuit for measuring the resistance of the cell wire is similar to that employed previously.[18]

[17] F. Daniels, J. Am. Chem. Soc. **50,** 115 (1928).
[18] B. N. Srivastava and S. C. Saxena, Proc. Phys. Soc. (London) **B70,** 369 (1957).

As shown by Kannuluik and Martin,[14] the solution of the differential equation for heat flow can be written in the form

$$f(\beta l) = [1/(\beta l)^2][1-\tanh\beta l/(\beta l)] = 2\pi r_1^2 \lambda J(R-R_0)/R_0^2 I^2 \alpha l, \quad (1)$$

with

$$\beta^2 = (2h/r_1\lambda) - (I^2 R_0 \alpha / 2\pi r_1^2 J l \lambda),$$

$$h = K_u/[r_1 \ln(r_2/r_1)], \quad (2)$$

where R is the resistance of the wire when a current of I amp is flowing through it, R_0 is the resistance of the cell wire at bath temperature for $I=0$; λ and K_u are the thermal conductivity of the wire and the gas, respectively.

When the hot-wire cell is highly evacuated, the conduction loss through the gas is replaced by the radiation loss h_r which will in general be small so that β will also be small. Under such conditions Eq. (1) can be expanded to yield

$$\lambda = \frac{1}{6}\left[\frac{RR_0^2 I^2 \alpha l}{\pi r_1^2 J(R-R_0)}\right]\left[1+\frac{1}{30}\left(\frac{RI^2\alpha l}{\pi r_1^2 \lambda J}\right)\right]\left[1-\left(\frac{4h_r l^2}{5\, r_1 \lambda}\right)\right]. \quad (3)$$

Equation (3) can be utilized for determining λ by the method of successive approximation.

III. PREPARATION OF N_2O_4

Pure N_2O_4 was prepared by heating crystals of $Pb(NO_3)_2$ according to the reaction

$$2\ Pb(NO_3)_2 = 2\ PbO + 2N_2O_4 + O_2.$$

By constructing a suitable glass apparatus, N_2O_4 was first liquefied by a freezing mixture and collected in a U tube. The liquid N_2O_4 was then solidified by placing the U tube in an alcohol-liquid oxygen bath and all O_2 in the system was pumped out by a high vacuum pump. The resulting pure N_2O_4 was then distilled into ampoules which were sealed off and weighed. The ends of the ampoules were made so thin that they could be easily broken by mere tilting.

IV. EXPERIMENTAL PROCEDURE

The constants of the conductivity cell at the temperatures 32°, 45°, 60°, 75°, and 90°C were determined by the procedure already described in detail by various workers[15,17] and are given in Table I. The glass diaphragm manometer was calibrated in the range of 10–76 cm Hg. The asymmetry in the construction of the cell was determined through the factor $(1-C)$ expressed as

$$K = K'(1-C), \quad (4)$$

where K is the true conductivity and K' is the value obtained experimentally after all corrections due to radiation loss, wall effect, etc., have been applied. In order to determine $(1-C)$ the thermal conductivity of He as given by Kannuluik and Carman[15] was taken as standard. The effect of pressure change on the thermal

TABLE I. Constants of the conductivity cell at different temperatures.

Constants	Temperature in °C 32	45	60	75	90
Thermal conductivity λ of the cell wire in cal/cm^{-1}/sec^{-1}/°C^{-1}	0.167	0.168	0.169	0.170	0.172
Temperature coefficient of resistance α of the platinum wire in °C^{-1}	0.00310	0.00296	0.00279	0.00273	0.00263
Resistance of the cell wire (R_0) in ohms	1.5561	1.6178	1.6884	1.7594	1.8304
Cell constant C	−0.0014	−0.0064	−0.0035	−0.0040	+0.0084
Length of the cell wire ($2l$)		...	11.311 cm		
Radius of the cell wire (r_1)		...	0.005001 cm		
i.d. of the tube ($2r_2$)		...	0.2879 cm		
o.d. of the tube ($2r_3$)		...	0.5243 cm		

conductivity of He was assumed to be negligible in the pressure range of 10–76 cm Hg.

A weighed ampoule of N_2O_4 was introduced through the side tube T and the apparatus was evacuated and sealed off at R. The ampoule of N_2O_4 was broken by tilting the apparatus and the entire apparatus consisting of the cell and the manometer was immersed in the thermostat which was then raised to the desired temperature. Sufficient time was allowed for the system to attain a steady temperature and the resulting pressure was measured by the diaphragm manometer M. Next a certain current was passed through the cell wire and the thermal conductivity of the gas was determined by the usual procedure.[15,18,19] The tube T was opened and the ampoule of N_2O_4 taken out, and the volume of the apparatus was determined by dropping water from a burette.

The entire procedure described above was repeated with every ampoule.

V. EXPERIMENTAL RESULTS

A. Equilibrium Constant

Using the perfect gas theory, the equilibrium constant K_p of the system $N_2O_4 \rightleftarrows 2NO_2$ is given by

$$K_p = 4\alpha^2 P/(1-\alpha^2), \tag{5}$$

where α is the degree of dissociation and P is the pressure of the system in atmospheres. Here α can be expressed as

$$\alpha = (P-p^0)/p^0, \tag{6}$$

where p^0 is the pressure of the system if there had been no dissociation of N_2O_4 into NO_2; p^0 is given by

$$p^0 = (g/M_1)(RT/V), \tag{7}$$

where g is the weight of N_2O_4, M_1 is its molecular weight and, R, T, and V have their usual significance.

[19] B. N. Srivastava and A. K. Barua, J. Chem. Phys. **32**, 427 (1960).

However, it is possible to take into consideration the corrections due to gas imperfections by introducing fugacities.[20] Then we can express the equation of state of mixture of two real gases in the form

$$p = [(n_1+n_2)RT/V] + (RT/V^2)(B_{11}n_1^2 + 2B_{12}n_1n_2 + B_{22}n_2^2), \tag{8}$$

where n_1 and n_2 are the mole numbers of N_2O_4 and NO_2, respectively, and B_{11} and B_{22} are the corresponding second virial coefficients. The method of calculation of B_{11}, B_{12}, and B_{22} has been given in detail by Hirschfelder, Curtiss, and Bird.[21] From the law of conservation of mass,

$$n_1M_1 + n_2M_2 = g, \tag{9}$$

where M_1 and M_2 are the molecular weights of N_2O_4 and NO_2, respectively; B_{11}, B_{12}, and B_{22} were calculated on the L-J (6:12) potential by taking the force constants of N_2O_4 and NO_2 as determined by Brokaw.[22] Hence from Eqs. (8) and (9), n_1 and n_2 can be determined by solving for the two unknowns.

The fugacities p_1^* and p_2^* of N_2O_4 and NO_2, respectively, are given by

$$\ln p_1^* = \ln(n_1RT/V) + 2[(B_{11}n_1 + B_{12}n_2)/V], \tag{10}$$

$$\ln p_2^* = \ln(n_2RT/V) + 2[(B_{22}n_2 + B_{12}n_1)/V], \tag{11}$$

and

$$(K_p)_f = p_2^{*2}/p_1^*. \tag{12}$$

We have calculated α and K_p from our experimental data both from the perfect and imperfect gas equations given above. The results are given in Table II, along with the values of K_p calculated by Giauque and

[20] I. Prigogine and R. Defay, *Chemical Thermodynamics* (Longman's Green and Company, Inc., New York, 1954).

[21] J. O. Hirschfelder, C. F. Curtiss, and R. B. Bird, *Molecular Theory of Gases and Liquids* (John Wiley & Sons, Inc., New York, 1954).

[22] R. S. Brokaw, Natl. Advisory Comm. Aeronaut., RME57K19, March 5, 1958.

TABLE II. Equilibrium constant of the system $N_2O_4 \rightleftarrows 2NO_2$.

T°C	P in cm Hg	V in cc	g in gm	Equilibrium constant: α From Eqs. (5)–(7)	α From Eqs. (8)–(9)	From Eq. (5) K_p	From Eqs. (10)–(12) $(K_p)_f$	From work cited in footnote 23
	14.51	162.6	0.0769	0.485	0.484	0.235	0.261	
	24.33	171.4	0.1436	0.404	0.408	0.250	0.260	
32	27.12	164.7	0.1562	0.383	0.385	0.245	0.257	0.253
	52.50	163.6	0.3250	0.278	0.285	0.232	0.256	
	10.22	150.4	0.0406	0.756	0.756	0.718	0.724	
	17.03	162.6	0.0769	0.670	0.673	0.730	0.737	
45	28.06	171.4	0.1436	0.553	0.567	0.651	0.678	0.636
	31.18	164.7	0.1562	0.525	0.531	0.624	0.649	
	11.37	150.4	0.0406	0.865	0.868	1.784	1.854	
	19.22	162.6	0.0769	0.799	0.812	1.789	1.861	
60	32.38	171.4	0.1436	0.711	0.716	1.746	1.796	1.852
	36.20	164.7	0.1562	0.691	0.696	1.744	1.728	
	12.17	150.4	0.0406	0.911?	0.920	...	...	
	21.08	162.6	0.0769	0.888	0.892	4.13	4.32	
75	36.08	171.4	0.1436	0.824	0.825	4.03	4.29	4.286
	40.62	164.7	0.1562	0.815	0.818	4.22	4.48	
	12.89	150.4	0.0406	0.940?	0.972	...	...	
	23.23	162.6	0.0769	0.996?	0.956	...	...	
90	39.07	171.4	0.1436	0.895	0.897	8.25	8.41	8.933
	44.08	164.7	0.1562	0.889	0.890	8.80	8.49	

TABLE III. Observations taken for the thermal conductivity K of $N_2O_4 \rightleftarrows 2NO_2$ at 32°C expressed in cal/cm^{-1}/sec^{-1}/°C^{-1}.

P in cm, Hg	I in mA	$R-R_0$ in mΩ	$K_u \times 10^5$	$K_u' \times 10^5$	$K' \times 10^5$	$K \times 10^5$
14.51	255.32	15.8	34.33	34.23	34.09	34.14
24.33	218.59	9.8	36.74	36.63	36.27	36.35
27.12	220.81	10.7	37.73	37.21	37.03	37.04
52.50	191.18	9.5	31.88	31.49	31.08	31.10

TABLE IV. Thermal conductivity of the system $N_2O_4 \rightleftarrows 2NO_2$ expressed in cal/cm^{-1}/sec^{-1}/°C^{-1}.

T°C	P in cm Hg	$(K_f) \times 10^5$ (calc.)	$(K_r) \times 10^5$ (calc.)	$K = (K_f + K_r) \times 10^5$	$K_{expt.} \times 10^5$	$K_{expt.} \times 10^5$ from work cited in footnote 12
	14.51	3.73	34.59	38.32	34.14	33.2
	24.33	3.64	33.63	37.27	36.35	36.1
32	27.12	3.62	33.06	36.68	37.04	37.2
	52.50	3.54	27.84	31.38	31.10	31.4
	10.22	4.17	26.55	30.72	26.59	25.7
	17.03	4.09	31.66	35.75	32.88	31.8
45	28.06	3.99	33.18	37.17	37.21	35.2
	31.18	3.98	33.31	37.29	37.36	36.5
	11.37	4.54	16.49	21.03	17.95	18.0
	19.22	4.47	22.17	26.64	25.77	22.9
60	32.38	4.39	27.41	31.80	31.73	28.4
	36.20	4.37	28.39	32.76	32.75	30.8
	12.17	4.85	8.06	12.91	12.07	12.9
	21.08	4.81	12.69	17.50	16.53	15.3
75	36.06	4.76	18.12	22.88	21.58	20.5
	40.62	4.74	19.42	24.16	23.21	21.3
	12.89	5.14	4.12	9.26	10.78	...
	23.23	5.12	6.93	12.05	12.11	...
90	39.07	5.08	10.61	15.69	14.71	...
	44.08	5.06	11.66	16.72	16.65	...

Kemp[23] from the data of Bodenstein and Böes[24] after correcting for gas imperfections.

It may be seen from Table II that at any particular temperature K_p is not strictly independent of pressure. At least a part of this variation of K_p with pressure must be ascribed to gas imperfections. To test this, the equilibrium constant $(K_p)_f$ was calculated from fugacities and a small noticeable improvement was observed. The lack of constancy still persisting may be due to experimental errors. Values of K_p have not been presented for a few observations at high temperature and low pressures as the second dissociation of N_2O_4 is likely to be present under these conditions, and further when α exceeds 0.9 a small error in α produces a very large error in K_p.

B. Thermal Conductivity

In Table III, the observations taken at 32°C are recorded and may be taken as typical of the whole set. In Table III, K_u is the apparent conductivity calculated from Eqs. (1) and (2), K_u' is the conductivity reduced to the bath temperature and K' is that obtained after correcting for nonradial flow, temperature-jump effect, radiation loss, and wall effect. In order to obtain K_u' from K_u, the temperature coefficient of thermal conductivity of $N_2O_4 \rightleftarrows 2NO_2$ was obtained at the required temperature and pressure from the calculated values of the conductivity.[12] K is the conductivity obtained after correction has been applied for asymmetry in the cell construction.

In Table IV the thermal conductivity of the system $N_2O_4 \rightleftarrows 2NO_2$ at different temperatures and pressures as obtained in the present investigations are recorded in column 6.

VI. COMPARISON WITH THEORY

As has already been mentioned, all the treatments of the heat transfer in a system $A \rightleftarrows nB$ lead to expressions which are equivalent. The thermal conductivity of the system $N_2O_4 \rightleftarrows 2NO_2$ may be written as

$$K = K_f + K_r = K_f + \frac{D_{12}P}{RT} \cdot \frac{\Delta H^2}{RT^2} \cdot \frac{x_1 x_2}{(1+x_1)^2}, \qquad (13)$$

where K_f is the "frozen" (no chemical reaction) conductivity of the mixture and may be calculated from the following expression obtained by Hirschfelder,[25]

$$K_f = K_{\text{mix(mon)}} + [K_1 - K_{1\text{ mon}}][1 + (x_2/x_1)(D_{11}/D_{12})]^{-1} + [K_2 - K_{2\text{ mon}}][1 + (x_1/x_2)(D_{22}/D_{12})]^{-1}. \qquad (14)$$

In Eqs. (13) and (14) the subscripts 1 and 2 refer to N_2O_4 and NO_2, respectively; $K_{\text{mix(mon)}}$ is the thermal conductivity of the N_2O_4—NO_2 mixture when they are treated as monatomic and may be calculated on the Chapman-Enskog theory. Here K_1 and K_2 are the thermal conductivities, x_1 and x_2 the mole fractions, D_{11} and D_{22} are the self-diffusion coefficients of the components 1 and 2, and D_{12} is the coefficient of interdiffusion. The $K_{1\text{ mon}}$ and $K_{2\text{ mon}}$ are the thermal conductivities of 1 and 2 when they are treated as monatomic; K_1 and K_2 may be calculated from the equation derived by Hirschfelder.[6]

In order to calculate K_f and K_r in Eq. (13), we require the values of ΔH, x_1, and x_2. In principle it is possible to obtain ΔH, the heat of reaction for the system $N_2O_4 \rightleftarrows 2NO_2$ at different temperatures from the K_p values given in Table II, but the accuracy obtained thereby is not sufficient. Similarly the values of x_1 and x_2 can be obtained from the values of α recorded in Table II, but in order to eliminate the possibility of experimental errors in the first experiment affecting the calculations of conductivity, and further for making the results more easily comparable with those of Coffin and O'Neal we have preferred to use the same data for ΔH, x_1 and x_2 as used by them and have in fact read the calculated conductivity values from the tables given by them. The values of K_f and K_r thus calculated are given in columns 3 and 4 of Table IV. The experimental values obtained by Coffin and O'Neal[12] were interpolated from the graphs given by them and are, therefore, subject to some uncertainty.

VII. DISCUSSION OF RESULTS

It may be seen from columns 5 and 6 of Table IV that the agreement between theory and experiment is only fair. However, it is seen, as predicted by the theory, that the thermal conductivity of a reacting gas mixture is actually an order of magnitude higher than the corresponding nonreacting mixture. The discrepancy between theory and experiment is quite considerable at the lower pressures. It is interesting to note that Coffin and O'Neal[12] did not take into account their heat conductivity data below a pressure of $\frac{1}{3}$ atm since they considered accommodation effects to be quite large at the lower pressures. In our experiments we have observed the same trend in the heat conductivity below $\frac{1}{3}$ atm as was obtained by Coffin and O'Neal, but it is unlikely that at such pressures the wall accommodation coefficients should play any significant role.

A part of the discrepancy between theory and experiment might be attributed to the choice of force constants and gas imperfections, but these sources of error cannot be responsible for such a large discrepancy. It is seen that the experimental values are almost always lower than the calculated values and this may be ascribed to the effect of relaxation of chemical energy as a result of which the condition of local chemical equilibrium is not satisfied. This relaxation will be more marked at lower pressures due to fewer

[23] W. F. Giauque and J. D. Kemp, J. Chem. Phys. **6**, 40 (1938).
[24] M. Bodenstein and F. Böes, Zeit. f. physik. Chemie **100**, 75 (1922).
[25] J. O. Hirschfelder, *Sixth Symposium (International) on Combustion* (Reinhold Publishing Corporation, New York, 1957), p. 351.

collisions. This aspect of the problem has been discussed by Coffin[14] on the basis of the treatment of Franck and Spalthoff.[8] The results obtained by Coffin are hardly satisfactory on account of several simplifying assumptions. Recently Hirschfelder[9] has been trying to develop a theory for the heat transfer in a non-equilibrium reacting gas mixture. In a subsequent paper we propose to examine the problem from the standpoint of relaxation of chemical energy.

ACKNOWLEDGMENTS

One of the authors (A.K.B.) is indebted to the C.S.I.R., New Delhi, for the award of a Senior Research Fellowship.

THE JOURNAL OF CHEMICAL PHYSICS VOLUME 35, NUMBER 1 JULY, 1961

Spin-Orbit Interactions in f^n Electron Configurations*

B. G. WYBOURNE

The Johns Hopkins University, Baltimore, Maryland

(Received October 27, 1960)

Simple relationships can be shown to exist between the spin-orbit matrix elements of different f^n electron configurations. These relationships allow a great reduction in the labor of calculating the spin-orbit interaction matrices for f^n electron configurations. Several examples are given.

INTRODUCTION

THE theoretical analysis of the energy levels of the rare earth ions requires the calculation of the spin-orbit interaction matrices for the different f^n electron configurations. These matrices have been calculated for all the states of the f^2, f^3, and f^4 electron configurations.[1–3] The spin-orbit matrices for the two highest multiplicities of the f^5 and f^6 have also been calculated.[4]

The successful analysis of the spectra of the rare earth ions requires that the spin-orbit interactions be calculated for at least the three highest multiplicities, as it can be shown that the interactions of the states of second highest multiplicity with those states of third highest multiplicity are by no means negligible.[4] As the number of f electrons, or f-electron holes increases up to seven, the size of the matrices increases up to order 50 for the $J=7/2$ matrix for the f^7 configuration. It is the purpose of this paper to show that simple relationships frequently exist between the spin-orbit interaction matrix elements of one f^n configuration and those of another f^n configuration containing a different number of f electrons.

* This work was carried out with the partial support of the Air Force Office of Scientific Research.

[1] F. H. Spedding, Phys. Rev. **58**, 255 (1940).

[2] B. R. Judd and R. Loudon, Proc. Roy. Soc. (London) **A251**, 127 (1959).

[3] W. A. Runciman and M. H. Crozier (to be published).

[4] B. G. Wybourne, Ph.D thesis, University of Canterbury (1960).

THE SPIN-ORBIT MATRIX FACTORS

Racah[5] has shown that all the states of the f^n electron configurations may be labeled with distinct sets of quantum numbers by introducing two groups which provide two additional sets of quantum numbers W and U. The first is a set of three integral numbers $W\equiv(w_1, w_2, w_3)$ with $w_1\geq w_2\geq w_3\geq 0$ and all $w\leq 2$, while the second is a set of two integers $U\equiv(u_1, u_2)$. In addition to the $WUSL$ quantum numbers it is useful for the purposes of this paper to make use of Racah's "seniority number" v which is essentially equivalent to W.

Using Tables I and II of Racah's[5] paper, all the states of the different f^n electron configurations may be labeled in the $vWUSL$ notation with the exception of some of the states labeled with $U\equiv(31)$ and $U\equiv(40)$ where the same LS label occurs twice. These states can only be separated in an arbitrary manner. Using this system of classification, Elliott, Judd, and Runciman[6] have labeled all the states of the f^2, f^3, and f^4 configurations together with the states of the two highest multiplicities of the f^5, f^6, and f^7 configurations. The states for all the multiplicities of these latter configurations are given in Table I of this paper.

The fundamental formula for calculating the matrix elements of the spin-orbit interaction has been given by

[5] G. Racah, Phys. Rev. **76**, 1352 (1949).

[6] J. P. Elliott, B. R. Judd, and W. A. Runciman, Proc. Roy. Soc. (London) **A240**, 509 (1957).

Elliott *et al.* In the $6-j$ notation[7] it is

$$(f^n\alpha vWUSLJJ_z|\zeta\sum_{i=1}^{n}(s_i\cdot l_i)|f^n\alpha'v'W'U'S'L'J'J_z')$$
$$=\delta(J,J')\delta(J_z,J_z')3n\zeta$$
$$\times[14(2L+1)(2L'+1)(2S+1)(2S'+1)]^{\frac{1}{2}}$$
$$\times(-1)^{J+S+S'-\frac{1}{2}}\begin{Bmatrix}L & L' & 1\\ S' & S & J\end{Bmatrix}\sum_{\bar\psi}(\psi\{|\bar\psi)(\psi'\{|\bar\psi)(-1)^{\bar S+\bar L}$$
$$\times\begin{Bmatrix}S & S' & 1\\ \frac{1}{2} & \frac{1}{2} & \bar S\end{Bmatrix}\begin{Bmatrix}L & L' & 1\\ 3 & 3 & \bar L\end{Bmatrix}, \quad (1)$$

where ψ stands for the set of quantum numbers $\alpha vWUSL$ and $\bar\psi$ the sets of quantum numbers $\bar\alpha\bar v\bar W\bar U\bar S\bar L$ designating the parent states. For the special case of $S=S'$ Eq. (1) simplifies to

$$(f^n\alpha vWUSLJ|\zeta\sum_{i=1}^{n}(s_i\cdot l_i)|f^n\alpha'v'W'U'SL'J)$$
$$=(\zeta/4S)\delta(\psi,\psi')[J(J+1)-L(L+1)-S(S+1)]$$
$$+n\zeta[21(2L+1)(2L'+1)(2S+1)^3/S(S+1)]^{\frac{1}{2}}$$
$$\times\begin{Bmatrix}L & L' & 1\\ S & S & J\end{Bmatrix}(-1)^{J+S+1}\sum_{\bar\psi}{}'(\psi\{|\bar\psi)(\psi'\{|\bar\psi)$$
$$\times\begin{Bmatrix}L & L' & 1\\ 3 & 3 & \bar L\end{Bmatrix}(-1)^{\bar L}, \quad (2)$$

where the summation $\sum'$ is restricted to those parent states with $\bar S=S+\frac{1}{2}$. It will be noted that Eq. (2) is the sum of two parts, the first part being diagonal in the $\alpha vWUSL$ scheme. For the purposes of this paper the properties of the nondiagonal part of Eq. (2) will be first discussed and then the results generalized.

By removing the J dependent factor,

$$(-1)^J\begin{Bmatrix}L & L' & 1\\ S' & S & J\end{Bmatrix}$$

for even n and

$$(1)^{J-\frac{1}{2}}\begin{Bmatrix}L & L' & 1\\ S' & S & J\end{Bmatrix}$$

for odd n, the remaining part, the spin-orbit factor Λ, of Eqs. (1) and (2) depends only on the $\alpha vUWSL$ quantum numbers and it is from a study of the calculation of these factors for different f^n configurations that many simple relationships have been found. For odd n the spin-orbit factor Λ may be written as

$$(f^n\alpha vWUSL|\Lambda|f^n\alpha'v'W'U'S'L')$$
$$=3n[14(2L+1)(2L'+1)(2S+1)(2S'+1)]^{\frac{1}{2}}(-1)^{S+S'}$$
$$\times\sum_{\bar\psi}(\psi|\bar\psi)(\psi'\{|\bar\psi)(-1)^{\bar L+\bar S}\begin{Bmatrix}S & S' & 1\\ \frac{1}{2} & \frac{1}{2} & \bar S\end{Bmatrix}\begin{Bmatrix}L & L' & 1\\ 3 & 3 & \bar L\end{Bmatrix} \quad (3a)$$

for $S\neq S'$; and $S=S'$ as

$$(f^n\alpha vWUSL|\Lambda|f^n\alpha'v'W'U'SL')$$
$$=n[21(2L+1)(2L'+1)(2S+1)^3/S(S+1)]^{\frac{1}{2}}(-1)^{S-\frac{1}{2}}$$
$$\times\sum_{\bar\psi}{}'(\psi\{|\bar\psi)(\psi'\{|\bar\psi)(-1)^{\bar L}\begin{Bmatrix}L & L' & 1\\ 3 & 3 & \bar L\end{Bmatrix}. \quad (3b)$$

For n even the formulas are identical apart from the change in the phase factors.

For practical calculation of the spin-orbit matrix elements, the spin-orbit factors Λ may be calculated using Eq. (3) and then the actual matrix elements obtained from these by multiplication by the appropriate J dependent factor with the addition of the factor $J(J+1)-L(L+1)-S(S+1)/4S$ to the result for those elements which are diagonal in the $\alpha vWUSL$ scheme. The factor $J(J+1)-L(L+1)-S(S+1)/4S$ is tabulated in Table II for the most significant cases.

The calculation of the spin-orbit factors involves summations over the several parent states of the f^n configuration. In practice Eq. (3a) is used whenever $S=S'+1$, and Eq. (3b) whenever $S=S'$. The summation in (3a) is thus usually restricted to parents of spin $\bar S=S'+\frac{1}{2}$ and hence in all practical cases the summation need only be made over parents of a single multiplicity. Furthermore, the summation is restricted to those parents where $\bar v=v\pm1$ and hence whenever the seniority numbers of the interacting states differ by two, or whenever one of the interacting states has maximum or minimum seniority the summation is restricted to parents of a single multiplicity and seniority number.

In all these special cases the spin-dependent factor and the seniority factors occurring in the coefficients of fractional parentage may be taken outside of the summations of Eqs. (3a) and (3b). Many relationships between the spin-orbit factors may be found by noting all instances where the summation is over parents of the same W classification. This is best shown by a typical example. The calculation of the spin-orbit factors of $(f_5^5(110)U^6L|\Lambda|f_5^5(211)U'^4L')$ requires use of Eq. (3a) with a summation over the parent states $f_4^4(111)\bar U^5\bar L$, while the calculation of the spin-orbit factors of $(f_2^4(110)U^3L|\Lambda|f_4^4(211)U'^3L')$ requires use of (3b) and a summation over the parent states $f_3^3(111)\bar U^4\bar L$. The calculation of these two sets of spin-orbit factors are over parent states of the same WUL

[7] R. Bivens, N. Metropolis, M. Rotenberg, and J. K. Wooten, *The 3-j and 6-j Symbols* (M.I.T., Cambridge, Massachusetts, 1959).

TABLE I. Classification of the states of the f^n configurations ($n>4$).

n	v	W	U	SL	n	v	W	U	SL
5	5	(110)	(10)	^6F	6	6	(100)	(10)	^7F
			(11)	^6PH		6	(210)	(11)	^5PH
	5	(211)	(10)	^4F				(20)	^5DGI
			(11)	^4PH				(21)	^5DFGHKL
			(20)	^4DGI		4	(111)	(00)	^5S
			(21)	^4DFGHKL				(10)	^5F
			(30)	$^4PFGHIKM$				(20)	^5DGI
	3	(111)	(00)	^4S		6	(221)	(10)	^3F
			(10)	^4F				(11)	^3PH
			(20)	^4DGI				(20)	^3DGI
	5	(221)	(10)	^2F				(21)	^3DFGHKL
			(11)	^2PH				(30)	$^3PFGHIKM$
			(20)	^2DGI				(31)	$^3PDFFGHHIIKKLMNO$
			(21)	^2DFGHKL		4	(211)	(10)	^3F
			(30)	$^2PFGHIKM$				(11)	^3PH
			(31)	$^2PDFFGHHIIKKLMNO$				(20)	^3DGI
	3	(210)	(11)	^2PH				(21)	^3DFGHKL
			(20)	^2DGI				(30)	$^3PFGHIKM$
			(21)	^2DFGHKL		2	(110)	(10)	^3F
	1	(100)	(10)	^2F				(11)	^3PH
						6	(222)	(00)	^1S
								(10)	^1F
								(20)	^1DGI
								(30)	$^1PFGHIKM$
								(40)	$^1SDFGGHIIKLLMNQ$
						4	(220)	(20)	^1DGI
								(21)	^1DFGHKL
								(22)	$^1SDGHILN$
						2	(200)	(20)	^1DGI
						0	(000)	(00)	^1S
					7	7	(000)	(00)	^8S
						7	(200)	(20)	^6DGI
						5	(110)	(10)	^6F
								(11)	^6PH
						7	(220)	(20)	^4DGI
								(21)	^4DFGHKL
								(22)	$^4SDGHILN$
						5	(211)	(10)	^4F
								(11)	^4PH
								(20)	^4DGI
								(21)	^4DFGHKL
								(30)	$^4PFGHIKM$
						3	(111)	(00)	^4S
								(10)	^4F
								(20)	^4DGI
						7	(222)	(00)	^2S
								(10)	^2F
								(20)	^2DGI
								(30)	$^2PFGHIKM$
								(40)	$^2SDFGGHIIKLLMNQ$
						5	(221)	(10)	^2F
								(11)	^2PH
								(20)	^2DGI
								(21)	^2DFGHKL
								(30)	$^2PDFGHIKM$
								(31)	$^2PDFFGHHIIKKLMNO$
						3	(210)	(11)	^2PH
								(20)	^2DGI
								(21)	^2DFGHKL
						1	(100)	(10)	^2F

classification. The two summations will be identical apart from the seniority and spin-dependent factors which may be taken outside the summation. Thus the spin-orbit factors will be simply proportional one to the other. The proportionality constant will be simply the ratio of the factors outside the summation sign which may be readily evaluated to give

$$(f_5^5(110)U^6L|\Lambda|f_5^5(211)U'^4L') = [(10)^{\frac{1}{2}}/2](f_2^4(110)U^3L|\Lambda|f_4^4(211)U'^3L'). \quad (4)$$

Thus, the 36 spin-orbit factors pertaining to the f^5 configuration may be found very simply from those of

TABLE II.

(a) $[J(J+1)-L(L+1)-S(S+1)]/4S$ for n odd

Quartets $S=3/2$

J	S	P	D	F	G	H	I	K	L	M
1/2		−5/6	−3/2							
3/2	0	−1/3	−1	−2						
5/2		1/2	−1/6	−7/6	−5/2					
7/2			1	0	−4/3	−3				
9/2				3/2	1/6	−3/2	−7/2			
11/2					2	1/3	−5/3	−4		
13/2						5/2	1/2	−11/6	−9/2	
15/2							3	2/3	−2	−5
17/2								7/2	5/6	−13/6
19/2									4	1
21/2										9/2

Doublets, $S=1/2$

J	P	D	F	G	H	I	K	L	M	N	O
1/2	−1										
3/2	1/2	−3/2									
5/2		1	−2								
7/2			3/2	−5/2							
9/2				2	−3						
11/2					5/2	−7/2					
13/2						3	−4				
15/2							7/2	−9/2			
17/2								4	−5		
19/2									9/2	−11/2	
21/2										5	−6
23/2											11/2

(b) $[J(J+1)-L(L+1)-S(S+1)]/4S$ for n even

Quintets, $S=2$

J	S	P	D	F	G	H	I	K	L
0		−1	−3/2						
1		−3/4	−5/4	−2					
2	0	−1/4	−3/4	−3/2	−5/2				
3		1/2	0	−3/4	−7/4	−3			
4			1	1/4	−3/4	−2	−7/2		
5				3/2	1/2	−3/4	−9/4	−4	
6					2	3/4	−3/4	−5/2	−9/2
7						5/2	1	−3/4	−11/4
8							3	5/4	−3/4
9								7/2	3/2
10									4
11									
12									

Triplets, $S=1$

J	P	D	F	G	H	I	K	L	M	N	O
0	−1										
1	−1/2	−3/2									
2	1/2	−1/2	−2								
3		1	−1/2	−5/2							
4			3/2	−1/2	−3						
5				2	−1/2	−7/2					
6					5/2	−1/2	−4				
7						3	−1/2	−9/2			
8							7/2	−1/2	−5		
9								4	−1/2	−11/2	
10									9/2	−1/2	−6
11										5	−1/2
12											11/2

TABLE III.

(a) Spin-orbit factor relationships for the f^5 configuration

$$(f_0^5(110)\,U^6L \mid \Lambda \mid f_0^5(211)\,U'^4L') = [(10)^{\frac{1}{2}}/2]\,(f_2^4(110)\,U^2L \mid \Lambda \mid f_4^4(211)\,U'^2L')$$
$$(f_0^5(110)\,U^6L \mid \Lambda \mid f_0^5(111)\,U'^4L') = [(6)^{\frac{1}{2}}/2]\,(f_2^4(110)\,U^2L/\mid \Lambda \mid f_4^4(110)\,U'^6L')$$
$$(f_0^5(211)\,U^4L \mid \Lambda \mid f_0^5(211)\,U'^4L') = -[(10^{\frac{1}{2}}/3]\,(f_4^4(211)\,U^2L \mid \Lambda \mid f_4^4(211)\,U'^2L')$$
$$(f_0^5(211)\,U^4L \mid \Lambda \mid f_3^5(111)\,U'^4L') = [-(6)^{\frac{1}{2}}/3]\,(f_4^4(211)\,U^2L \mid \Lambda \mid f_4^4(111)\,U'^6L')$$
$$(f_3^5(111)\,U^4L \mid \Lambda \mid f_3^5(111)\,U'^4L') = \tfrac{1}{2}(f_3^3(111)\,U^4L \mid \Lambda \mid f_3^3(111)\,U'^4L')$$
$$(f_3^5(111)\,U^4L \mid \Lambda \mid f_3^5(210)\,U'^2L') = \tfrac{1}{2}(f_3^3(111)\,U^4L \mid \Lambda \mid f_3^3(210)\,U'^2L')$$
$$(f_3^5(111)\,U^4L \mid \Lambda \mid f_1^5(100)\,(10)^2F) = [2(10)^{\frac{1}{2}}/5]\,(f_3^3(111)\,U^4L \mid \Lambda \mid f_1^3(100)\,(10)^2F)$$
$$(f_3^5(210)\,U^2L \mid \Lambda \mid f_3^5(210)\,U'^2L') = \tfrac{1}{2}(f_3^3(210)\,U^2L \mid \Lambda \mid f_3^3(210)\,U'^2L')$$
$$(f_3^5(210)\,U^2L \mid \Lambda \mid f_1^5(100)\,(10)^2F) = [2(10)^{\frac{1}{2}}/5]\,(f_3^3(210)\,U^2L \mid \Lambda \mid f_1^3(100)\,(10)^2F)$$

(b) Spin-orbit factors relationships for the f^6 configuration

$$(f_0^6(100)\,(10)^7F \mid \Lambda \mid f_0^6(210)\,U^5L) = [-(14)^{\frac{1}{2}}/2]\,(f_1^3(100)\,(10)^2F \mid \Lambda \mid f_3^3(210)\,U^2L)$$
$$(f_0^6(100)\,(10)^7F \mid \Lambda \mid f_4^6(111)\,U^5L) = [(14)^{\frac{1}{2}}/2]\,(f_1^3(100)\,(10)^2F \mid \Lambda \mid f_3^3(111)\,U^4L)$$
$$(f_0^6(210)\,U^5L \mid \Lambda \mid f_0^6(210)\,U'^5L') = [-(5)^{\frac{1}{2}}/2]\,(f_3^3(210)\,U^2L \mid \Lambda \mid f_3^3(210)\,U'^2L')$$
$$(f_4^6(111)\,U^5L \mid \Lambda \mid f_4^6(111)\,U'^5L') = \tfrac{1}{3}(f_4^4(111)\,U^5L \mid \Lambda \mid f_4^4(111)\,U'^5L')$$
$$(f_0^6(210)\,U^5L \mid \Lambda \mid f_4^6(111)\,U'^5L') = (5)^{\frac{1}{2}}/2]\,(f_3^3(210)\,U^2L \mid \Lambda \mid f_3^3(111)\,U'^4L')$$
$$(f_0^6(221)\,U^3L \mid \Lambda \mid f_0^6(221)\,U'^3L') = -(f_0^5(221)\,U^2L \mid \Lambda \mid f_0^5(221)\,U'^2L')$$
$$(f_4^6(211)\,U^3L \mid \Lambda \mid f_4^6(211)\,U'^3L') = \tfrac{1}{3}(f_4^4(211)\,U^3L \mid \Lambda \mid f_4^4(211)\,U'^3L')$$
$$(f_2^6(110)\,U^3L \mid \Lambda \mid f_2^6(110)\,U^3L) = (1/5)\,(f_2^2(110)\,U^3L \mid \Lambda \mid f_2^2(110)\,U^3L)$$
$$(f_0^6(210)\,U^5L \mid \Lambda \mid f_0^6(221)\,U'^3L') = [-(15)^{\frac{1}{2}}/3]\,(f_3^5(210)\,U^2L \mid \Lambda \mid f_3^5(221)\,U'^2L')$$
$$(f_0^6(210)\,U^5L \mid \Lambda \mid f_4^6(211)\,U'^3L') = [(15)^{\frac{1}{2}}/3]\,(f_3^5(210)\,U^2L \mid \Lambda \mid f_3^5(211)\,U'^4L')$$
$$(f_4^6(111)\,U^5L \mid \Lambda \mid f_0^6(221)\,U'^3L') = [(15)^{\frac{1}{2}}/3]\,(f_3^5(111)\,U^4L \mid \Lambda \mid f_3^5(221)\,U'^2L')$$
$$(f_4^6(111)\,U^5L \mid \Lambda \mid f_4^6(211)\,U'^3L') = \tfrac{1}{3}(f_4^4(111)\,U^5L \mid \Lambda \mid f_4^4(211)\,U'^3L')$$
$$(f_4^6(111)\,U^5L \mid \Lambda \mid f_2^6(110)\,U'^3L') = [(6)^{\frac{1}{2}}/2]\,(f_4^4(111)\,U^5L \mid \Lambda \mid f_2^4(110)\,U'^3L')$$
$$(f_0^6(221)\,U^3L \mid \Lambda \mid f_4^6(211)\,U'^3L') = -(f_0^5(221)\,U^2L \mid \Lambda \mid f_0^5(211)\,U'^4L')$$
$$(f_4^6(211)\,U^3L \mid \Lambda \mid f_2^6(110)\,U'^3L') = [(6)^{\frac{1}{2}}/2]\,(f_4^4(211)\,U^2L \mid \Lambda \mid f_2^4(110)\,U'^2L')$$

(c) Spin-orbit factor relationships for the f^7 configuration

$$(f_7^7(000)\,(00)^8S \mid \Lambda \mid f_0^7(110)\,(11)^6P) = -4(21)^{\frac{1}{2}}$$
$$(f_7^7(200)\,(20)^6L \mid \Lambda \mid f_0^7(110)\,U^6L') = [-(70)^{\frac{1}{2}}/5]\,(f_2^2(200)\,(20)^1L \mid \Lambda \mid f_2^2(110)\,U^3L')$$
$$(f_7^7(200)\,(20)^6L \mid \Lambda \mid f_0^7(211)\,U^4L') = -(5)^{\frac{1}{2}}(f_2^4(200)\,(20)^1L \mid \Lambda \mid f_4^4(211)\,U^2L')$$
$$(f_7^7(220)\,U^4L \mid \Lambda \mid f_0^7(110)\,U'^6L') = -(5)^{\frac{1}{2}}(f_4^4(220)\,U^1L \mid \Lambda \mid f_2^4(110)\,U'^2L')$$
$$(f_7^7(220)\,U^4L \mid \Lambda \mid f_0^7(211)\,U'^4L') = [2(5)^{\frac{1}{2}}/3]\,(f_4^4(220)\,U^1L \mid \Lambda \mid f_4^4(211)\,U'^2L')$$
$$(f_3^7(111)\,U^4L \mid \Lambda \mid f_0^7(110)\,U'^6L') = (2)^{\frac{1}{2}}(f_4^4(111)\,U^5L \mid \Lambda \mid f_2^4(110)\,U'^2L')$$
$$(f_3^7(111)\,U^4L \mid \Lambda \mid f_0^7(211)\,U'^4L') = -[2(2)/3]^{\frac{1}{2}}(f_4^4(111)\,U^5L \mid \Lambda \mid f_4^4(211)\,U'^2L')$$

the f^4 configuration without repeating the summation. The fact of the simple proportionality of Eq. (4) is hardly surprising, since the identity representation occurs but once[8] in the reduction $(110)\times(110)\times(211)$ and only once in the reduction $U\times(11)\times U'$. However, the explicit value of the proportionality constant is not immediately evident from purely group-theoretical considerations.

For those cases where $v=v'+2$ with $v<n$ Racah[9] has shown that for every symmetric operator F the simple relationship

$$(l^n\alpha vSL\,|\,F\,|\,l^n\alpha' v-2S'L') = \tfrac{1}{2}[(n+2-v)(4l+4-n-v)/(2l+2-v)]^{\frac{1}{2}} \times[l^v\alpha vSL\,|\,F\,|\,l^v\alpha' v-2S'L'] \quad (5)$$

holds. Equation (5) readily gives the proportionality constants for these cases.

The only remaining cases to be considered are those where $v=v'<n$. Here the summations of Eqs. (3) are over the parent states of two different seniority numbers, $\bar{v}=v\pm1$. It will be noted that the spin-orbit factor Λ defined in this paper corresponds directly to Racah's[9] double tensor v^{11}. Racah[9] has also shown that for any irreducible double tensor T^{sk} with $s+k$ even, the simple relation

$$(l^n\alpha vSL\,||\,T^{sk}\,||\,l^n\alpha' vS'L') = [(2l+1-n)/(2l+1-v)] \times(l^v\alpha vSL\,||\,T^{sk}\,||\,l^v\alpha' vS'L') \quad (6)$$

holds. Thus even for these cases the proportionality constant may be simply found.

Using the results of the preceding discussions many simple relationships between the spin-orbit factors of the different f^n configurations have been established and are listed in Table III for the three highest multiplicities of the f^5, f^6, and f^7 configurations.

Again the use of this table is best illustrated by an example. To calculate the spin-orbit matrix element

$$(f_5^5(211)\,(21)^4D_{\frac{1}{2}}\,|\,\zeta\sum_{i=1}^{5}(s_i\cdot l_i)\,|\,f_5^5(211)\,(21)^4D_{\frac{1}{2}}),$$

the relationship

$$(f_5^5(211)\,U^4L\,|\,\Lambda\,|\,f_5^5(211)\,U'^4L') = -[(10)^{\frac{1}{2}}/3](f_4^4(211)\,U^3L\,|\,\Lambda\,|\,f_4^4(211)\,U'^3L') \quad (7)$$

is used. To find the spin-orbit factor for

$$(f_4^4(211)\,(21)^3D\,|\,\Lambda\,|\,f_4^4(211)\,(21)^3D)$$

we note that the spin-orbit matrix element for this interaction is equal to $5/14$ for $J=1$. The factor $[J(J+1)-L(L+1)-S(S+1)/4S$ is found from Table II and subtracted from the spin-orbit matrix element. The result is divided by

$$-\begin{Bmatrix}2 & 2 & 1\\ 1 & 1 & 1\end{Bmatrix}$$

to give the spin-orbit factor $\Lambda=-(26/7)(5)^{\frac{1}{2}}$. Applying Eq. (7) the spin-orbit factor

$$(f_5^5(211)\,(21)^4D\,|\,\Lambda\,|\,f_5^5(211)\,(21)^4D)$$

is found to be equal to $-(130/21)(5)^{\frac{1}{2}}$. Finally the spin-orbit matrix element is found by multiplication of this spin-orbit factor by

$$\begin{Bmatrix}2 & 2 & 1\\ \frac{3}{2} & \frac{3}{2} & \frac{1}{2}\end{Bmatrix}$$

and addition of the

$$[J(J+1)-L(L+1)-S(S+1)]/4S$$

factor to give the result

$$(f_5^5(211)\,(21)^4D_{\frac{1}{2}}\,|\,\zeta\sum_{i=1}^{5}(s_i\cdot l_i)\,|\,f_5^5(211)\,(21)^4D_{\frac{1}{2}}) = 5\zeta/14.$$

For the matrix elements which are not diagonal in the $vWUSL$ scheme the calculation will be even simpler. Using the results of Table III the complete spin-orbit matrices of the three highest multiplicities of the f^7 configuration may be readily written down with only the aid of the spin-orbit matrices of the f^2 and f^4 configurations[1,3] and tables of $6-j$ symbols.[7] This represents a remarkable saving in labor. Likewise all the interactions of the two highest multiplicities of the f^5 configuration may be readily found from the results for the f^3 and f^4 configuration.[2,3] Again, all the interactions of the two highest multiplicities of the f^6 configuration may be found from those of the f^3 configuration,[2] while all the interactions of the states of the third highest multiplicity can be derived from the spin-orbit matrices of the f^5 configuration. (The spin-orbit matrices of the f^5 configuration are the subject of a forthcoming report.)

The results expressed in Table III should be of assistance in the analysis of rare earth and actinide spectra.

[8] A. G. McLellan, Proc. Phys. Soc. (London) **76**, 419 (1960).
[9] G. Racah, Phys. Rev. **63**, 367 (1943).

Electrostatic Energy Matrices of the f^5 and f^6 Configurations

B. G. WYBOURNE*

Physics Department, University of Canterbury, Christchurch, New Zealand

(Received June 8, 1960)

The electrostatic energy matrices of f^5 and f^6 electron configurations are calculated by the Racah methods. Checking rules are used for all the diagonal matrix elements and certain of the nondiagonal matrix elements.

A GROUP theoretical method for the classification of the terms of any f^n electron configuration and the calculation of their electrostatic energies has been devised by Racah.[1] Using the methods of Racah, all the energy matrices for the f^5 and f^6 electron configurations have been calculated and are given in Tables I and II, respectively. The terms of the energy matrices are labeled as follows: The multiplicity $(2S+$

TABLE I. The electrostatic energy matrices of the f^5 configuration.

	$^5P_{11}$		$^5F_{10}$		$^5H_{11}$
$^5P_{11}$	$33E^3$	$^5F_{10}$	0	$^5H_{11}$	$-9E^3$

	$^3S_{00}$		$^5L_{21}$		$^5M_{30}$
$^3S_{00}$	$9E^1$	$^5L_{21}$	$5E^1+85E^2-23E^3$	$^5M_{30}$	$5E^1-50E^2-23E^3$

	$^5P_{11}$	$^5P_{30}$
$^5P_{11}$	$5E^1+44E^3/3$	$5(11)^{\frac{1}{2}}(78E^2-E^3)/3$
$^5P_{30}$	$5(11)^{\frac{1}{2}}(78E^2-E^3)/3$	$5E^1+104E^2-14E^3/3$

	$^5K_{21}$	$^5K_{30}$
$^5K_{21}$	$5E^1-219E^2-13E^3/3$	$8(17)^{\frac{1}{2}}(3E^2+E^3)/3$
$^5K_{30}$	$8(17)^{\frac{1}{2}}(3E^2+E^3)/3$	$5E^1+188E^2+16E^3/3$

	$^5D_{20}$	$^5D_{21}$	$^3D_{20}$
$^5D_{20}$	$5E^1+22(52E^2+E^3)/7$	$2(66)^{\frac{1}{2}}(78E^2+5E^3)/7$	$-33(7)^{\frac{1}{2}}E^3/7$
$^5D_{21}$	$2(66)^{\frac{1}{2}}(78E^2+5E^3)/7$	$5E^1-(1781E^2-202E^3)/7$	$6(462)^{\frac{1}{2}}E^3/7$
$^3D_{20}$	$-33(7)^{\frac{1}{2}}E^3/7$	$6(462)^{\frac{1}{2}}E^3/7$	$9E^1$

	$^5H_{11}$	$^5H_{21}$	$^5H_{30}$
$^5H_{11}$	$5E^1-4E^3$	$-10(182)^{\frac{1}{2}}E^2$	$-5(39)^{\frac{1}{2}}(6E^2+E^3)/3$
$^5H_{21}$	$-10(182)^{\frac{1}{2}}E^2$	$5E^1+197E^2+26E^3$	$-2(42)^{\frac{1}{2}}(33E^2-2E^3)/3$
$^5H_{30}$	$-5(39)^{\frac{1}{2}}(6E^2+E^3)/3$	$-2(42)^{\frac{1}{2}}(33E^2-2E^3)/3$	$5E^1-176E^2+14E^3$

* Present address: Physics Department, Johns Hopkins University, Baltimore, Maryland.

[1] G. Racah, Phys. Rev. **76**, 1352 (1949).

TABLE I.—*Continued.*

	$_5{}^4I_{20}$	$_5{}^4I_{30}$	$_3{}^4I_{20}$
$_5{}^4I_{20}$	$5E^1+40E^2-2E^3$	$-2(3)^{\frac{1}{2}}(60E^2-E^3)$	$3(7)^{\frac{1}{2}}E^3$
$_5{}^4I_{30}$	$-2(3)^{\frac{1}{2}}(60E^2-E^3)$	$5E^1-50E^2-11E^3$	$-6(21)^{\frac{1}{2}}E^3$
$_3{}^4I_{20}$	$3(7)^{\frac{1}{2}}E^3$	$-6(21)^{\frac{1}{2}}E^3$	$9E^1$

	$_5{}^4F_{10}$	$_5{}^4F_{21}$	$_5{}^4F_{30}$	$_3{}^4F_{10}$
$_5{}^4F_{10}$	$5E^1$	$-(165)^{\frac{1}{2}}E^3/3$	$20(143)^{\frac{1}{2}}E^2$	0
$_5{}^4F_{21}$	$-(165)^{\frac{1}{2}}E^3/3$	$5E^1-65E^2+3E^3$	$-2(195)^{\frac{1}{2}}(36E^2+E^3)/3$	$9(11)^{\frac{1}{2}}E^3$
$_5{}^4F_{30}$	$20(143)^{\frac{1}{2}}E^2$	$-2(195)^{\frac{1}{2}}(36E^2+E^3)/3$	$5E^1-76E^2+42E^3$	0
$_3{}^4F_{10}$	0	$9(11)^{\frac{1}{2}}E^3$	0	$9E^1$

	$_5{}^4G_{20}$	$_5{}^4G_{21}$	$_5{}^4G_{30}$	$_3{}^4G_{20}$
$_5{}^4G_{20}$	$5E^1-8(130E^2-E^3)/7$	$-(2145)^{\frac{1}{2}}(48E^2-5E^3)/21$	$4(15)^{\frac{1}{2}}(39E^2+E^3)/3$	$-12(7)^{\frac{1}{2}}E^3/7$
$_5{}^4G_{21}$	$-(2145)^{\frac{1}{2}}(48E^2-5E^3)/21$	$5E^1+11(297E^2+E^3)/21$	$-2(143)^{\frac{1}{2}}(24E^2-E^3)/3$	$(15015)^{\frac{1}{2}}E^3/7$
$_5{}^4G_{30}$	$4(15)^{\frac{1}{2}}(39E^2+E^3)/3$	$-2(143)^{\frac{1}{2}}(24E^2-E^3)/3$	$5E^1+2(156E^2+11E^3)/3$	$-4(105)^{\frac{1}{2}}E^3$
$_3{}^4G_{20}$	$-12(7)^{\frac{1}{2}}E^3/7$	$(15015)^{\frac{1}{2}}E^3/7$	$-4(105)^{\frac{1}{2}}E^3$	$9E^1$

	$_5{}^2N_{31}$	$_5{}^2O_{31}$
$_5{}^2N_{31}$	$8E^1+76E^2-37E^3$	
$_5{}^2O_{31}$		$8E^1+10E^2-26E^3$

	$_5{}^2M_{30}$	$_5{}^2M_{31}$
$_5{}^2M_{30}$	$8E^1-(25E^2+43E^3)/2$	$-3(35)^{\frac{1}{2}}(21E^2+E^3)/2$
$_5{}^2M_{31}$	$-3(35)^{\frac{1}{2}}(21E^2+E^3)/2$	$8E^1-(43E^2-11E^3)/2$

	$_5{}^2L_{21}$	$_5{}^2L_{31}$	$_3{}^2L_{21}$
$_5{}^2L_{31}$	$8E^1-5(257E^2+23E^3)/11$	$-3(95)^{\frac{1}{2}}(48E^2+E^3)/11$	$18(11)^{\frac{1}{2}}E^3/11$
$_5{}^2L_{31}$	$-3(95)^{\frac{1}{2}}(48E^2+E^3)/11$	$8E^1-4(589E^2+40E^3)/11$	$-9(1045)^{\frac{1}{2}}E^3/11$
$_3{}^2L_{21}$	$18(11)^{\frac{1}{2}}E^3/11$	$-9(1045)^{\frac{1}{2}}E^3/11$	$12E^1+105E^2-21E^3$

	$_5{}^2P_{11}$	$_5{}^2P_{30}$	$_5{}^2P_{31}$	$_3{}^2P_{11}$
$_5{}^2P_{11}$	$8E^1+121E^3/6$	$-(110)^{\frac{1}{2}}(312E^2+5E^3)/12$	$(1430)^{\frac{1}{2}}(24E^2-E^3)/4$	$-33(2)^{\frac{1}{2}}E^3/2$
$_5{}^2P_{30}$	$-(110)^{\frac{1}{2}}(312E^2+5E^3)/12$	$8E^1+26E^2+193E^3/12$	$(13)^{\frac{1}{2}}(456E^2+17E^3)/4$	$3(55)^{\frac{1}{2}}E^3/2$
$_5{}^2P_{31}$	$(1430)^{\frac{1}{2}}(24E^2-E^3)/4$	$(13)^{\frac{1}{2}}(456E^2+17E^3)/4$	$8E^1-302E^2+143E^3/4$	$-3(715)^{\frac{1}{2}}E^3/2$
$_3{}^2P_{11}$	$-33(2)^{\frac{1}{2}}E^3/2$	$3(55)^{\frac{1}{2}}E^3/2$	$-3(715)^{\frac{1}{2}}E^3/2$	$12E^1+22E^3$

TABLE I.

	${}^5{}^2D_{20}$	${}^5{}^2D_{21}$
${}^5{}^2D_{20}$	$8E^1+22(13E^2-2E^3)/7$	$2(3)^{\frac{1}{2}}(390E^2-11E^3)/7$
${}^5{}^2D_{21}$	$2(3)^{\frac{1}{2}}(390E^2-11E^3)/7$	$8E^1-(3055E^2-911E^3)/77$
${}^5{}^2D_{31}$	$-216(182)^{\frac{1}{2}}E^2/7$	$-3(546)^{\frac{1}{2}}(60E^2-E^3)/77$
${}^3{}^2D_{20}$	$-33E^3/7$	$-132(3)^{\frac{1}{2}}E^3/7$
${}^3{}^2D_{21}$	$-18(33)^{\frac{1}{2}}E^3/7$	$-171(11)^{\frac{1}{2}}E^3/77$

	${}^5{}^2I_{20}$	${}^5{}^2I_{30}$
${}^5{}^2I_{20}$	$8E^1+10E^2+4E^3$	$2(3)^{\frac{1}{2}}(15E^2+2E^3)$
${}^5{}^2I_{30}$	$2(3)^{\frac{1}{2}}(15E^2+2E^3)$	$8E^1-(25E^2+E^3)/2$
${}^5{}^2I_{31}$	$270E^2$	$-3(3)^{\frac{1}{2}}(57E^2-5E^3)/2$
${}^5{}^2I'_{31}$	0	$27(102)^{\frac{1}{2}}E^2$
${}^3{}^2I_{20}$	$3E^3$	$-12(3)^{\frac{1}{2}}E^3$

	${}^5{}^2K_{21}$	${}^5{}^2K_{30}$
${}^5{}^2K_{21}$	$8E^1+(6273E^2-281E^3)/33$	$-(374)^{\frac{1}{2}}(60E^2+29E^3)/33$
${}^5{}^2K_{30}$	$-(374)^{\frac{1}{2}}(60E^2+29E^3)/33$	$8E^1+47E^2-5E^3/3$
${}^5{}^2K_{31}$	$-(14858)^{\frac{1}{2}}(156E^2+7E^3)/253$	$-(4807)^{\frac{1}{2}}(741E^2-23E^3)/253$
${}^5{}^2K'_{31}$	$-21(759)^{\frac{1}{2}}(96E^2-E^3)/253$	$219(2346)^{\frac{1}{2}}E^2/46$
${}^3{}^2K_{21}$	$-6(11)^{\frac{1}{2}}E^3/11$	$3(34)^{\frac{1}{2}}E^3$

	${}^5{}^2G_{20}$	${}^5{}^2G_{20}$	${}^5{}^2G_{30}$
${}^5{}^2G_{20}$	$8E^1-4(65E^2+4E^3)/7$	$-(390)^{\frac{1}{2}}(240E^2+11E^3)/42$	$-(15)^{\frac{1}{2}}(39E^2-8E^3)/3$
${}^5{}^2G_{21}$	$-(390)^{\frac{1}{2}}(240E^2+11E^3)/42$	$8E^1+(2943E^2+356E^3)/21$	$(26)^{\frac{1}{2}}(480E^2-29E^3)/12$
${}^5{}^2G_{30}$	$-(15)^{\frac{1}{2}}(39E^2-8E^3)/3$	$(26)^{\frac{1}{2}}(480E^2-29E^3)/12$	$8E^1+26E^2+37E^3/3$
${}^5{}^2G_{31}$	$45(1365)^{\frac{1}{2}}E^2/7$	$(14)^{\frac{1}{2}}(2208E^2+7E^3)/28$	$(91)^{\frac{1}{2}}(30E^2+E^3)$
${}^3{}^2G_{20}$	$-12E^3/7$	$-11(390)^{\frac{1}{2}}E^3/7$	$-8(15)^{\frac{1}{2}}E^3$
${}^3{}^2G_{21}$	$-3(4290)^{\frac{1}{2}}E^3/14$	$15(11)^{\frac{1}{2}}E^3/7$	$3(286)^{\frac{1}{2}}E^3/4$

	${}^5{}^2F_{10}$	${}^5{}^2F_{21}$	${}^5{}^2F_{30}$
${}^5{}^2F_{10}$	$8E^1$	$54(30)^{\frac{1}{2}}E^3/30$	$5(143)^{\frac{1}{2}}E^3$
${}^5{}^2F_{21}$	$43(30)^{\frac{1}{2}}E^3/30$	$8E^1-5(299E^2-48E^3)/11$	$(4290)^{\frac{1}{2}}(720E^2+29E^3)/132$
${}^5{}^2F_{30}$	$5(143)^{\frac{1}{2}}E^2$	$(4290)^{\frac{1}{2}}(720E^2+29E^3)/132$	$8E^1-19E^2+24E^3$
${}^5{}^2F_{31}$	$4(3)^{\frac{1}{2}}E^3$	$-9(10)^{\frac{1}{2}}(104E^2+E^3)/11$	$-4(429)^{\frac{1}{2}}(18E^2+E^3)/11$
${}^5{}^2F'_{31}$	$-15(429)^{\frac{1}{2}}E^2$	$3(1430)^{\frac{1}{2}}(48E^2-E^3)/44$	$-3(3)^{\frac{1}{2}}(49E^2-2E^3)$
${}^3{}^2F_{21}$	$3(330)^{\frac{1}{2}}E^3/10$	$27(11)^{\frac{1}{2}}E^3/11$	$-3(390)^{\frac{1}{2}}E^3/4$
${}^1{}^2F_{10}$	0	$36(5)^{\frac{1}{2}}E^3/5$	0

—Continued.

$^5{}^2D_{31}$	$^3{}^2D_{20}$	$^3{}^2D_{21}$
$-216(182)^{\frac{1}{2}}E^2/7$	$-33E^3/7$	$-18(33)^{\frac{1}{2}}E^3/7$
$-3(546)^{\frac{1}{2}}(60E^2-E^3)/77$	$-132(3)^{\frac{1}{2}}E^3/7$	$-171(11)^{\frac{1}{2}}E^3/77$
$8E^1+(2396E^2+269E^3)/11$	0	$9(6006)^{\frac{1}{2}}E^3/11$
0	$12E^1-2(429E^2-66E^3)/7$	$-12(33)^{\frac{1}{2}}(39E^2+E^3)/7$
$9(6006)^{\frac{1}{2}}E^3/11$	$-12(33)^{\frac{1}{2}}(39E^2+E^3)/7$	$12E^1+(1131E^2+183E^3)/7$

$^5{}^2I_{31}$	$^5{}^2I'_{31}$	$^3{}^2I_{20}$
$270E^2$	0	$3E^3$
$-3(3)^{\frac{1}{2}}(57E^2-5E^3)/2$	$27(102)^{\frac{1}{2}}E^2$	$-12(3)^{\frac{1}{2}}E^3$
$8E^1-(1151E^2+11E^3)/10$	$-3(34)^{\frac{1}{2}}(51E^2-4E^3)/5$	0
$-3(34)^{\frac{1}{2}}(51E^2-4E^4)/5$	$8E^1+(788E^2+53E^3)/5$	0
0	0	$12E^1-30E^2-12E^3$

$^5{}^2K_{31}$	$^5{}^2K'_{31}$	$^3{}^2K_{21}$
$-(14858)^{\frac{1}{2}}(156E^2+7E^3)253$	$-21(759)^{\frac{1}{2}}(96E^2-E^3)/253$	$-6(11)^{\frac{1}{2}}E^3/11$
$-(4807)^{\frac{1}{2}}(741E^2-23E^3)/253$	$216(2346)^{\frac{1}{2}}E^2/46$	$3(34)^{\frac{1}{2}}E^3$
$8E^1+(61753E^2+2675E^3)/253$	$24(21318)^{\frac{1}{2}}(3E^2+E^3)/253$	$-21(16348)^{\frac{1}{2}}E^3/253$
$24(21318)^{\frac{1}{2}}(3E^2+E^4)/253$	$8E^1-4(967E^2+8E^3)/23$	$63(69)^{\frac{1}{2}}E^3/23$
$-21(16348)^{\frac{1}{2}}E^3/253$	$63(69)^{\frac{1}{2}}E^3/23$	$12E^1-135E^2-5E^3$

$^5{}^2G_{31}$	$^3{}^2G_{20}$	$^3{}^2G_{21}$
$45(1365)^{\frac{1}{2}}E^2/7$	$-12E^3/7$	$-3(4290)^{\frac{1}{2}}E^3/14$
$(14)^{\frac{1}{2}}(2208E^2+7E^3)/28$	$-11(390)^{\frac{1}{2}}E^3/7$	$15(11)^{\frac{1}{2}}E^3/7$
$(91)^{\frac{1}{2}}(30E^2+E^3)$	$-8(15)^{\frac{1}{2}}E^3$	$3(286)^{\frac{1}{2}}E^3/4$
$8E^1-122E^2+41E^3$	0	$3(154)^{\frac{1}{2}}E^3/4$
0	$12E^1+4(195E^2+12E^3)/7$	$(4290)^{\frac{1}{2}}(24E^2-E^3)/7$
$3(154)^{\frac{1}{2}}E^3/4$	$(4290)^{\frac{1}{2}}(24E^2-E^3)/7$	$12E^1-11(153E^2-2E^3)/7$

$^5{}^2F_{31}$	$^5{}^2F'_{31}$	$^3{}^2F_{21}$	$^1{}^2F_{10}$
$4(3)^{\frac{1}{2}}E^3$	$-15(429)^{\frac{1}{2}}E^2$	$3(330)^{\frac{1}{2}}E^3/10$	0
$-9(10)^{\frac{1}{2}}(104E^2+E^3)/11$	$3(1430)^{\frac{1}{2}}(48E^2-E^3)/44$	$27(11)^{\frac{1}{2}}E^3/11$	$36(5)^{\frac{1}{2}}E^3/5$
$-4(429)^{\frac{1}{2}}(18E^2+E^3)/11$	$-3(3)^{\frac{1}{2}}(49E^2-2E^3)$	$-3(390)^{\frac{1}{2}}E^3/4$	0
$8E^1+2(1105E^2+221E^3)/11$	$4(143)^{\frac{1}{2}}(42E^2-5E^3)\frac{1}{2}11$	$-27(110)^{\frac{1}{2}}E^3/11$	$-36(2)^{\frac{1}{2}}E^3$
$4(143)^{\frac{1}{2}}(42E^2-5E^3)/11$	$8E^1-41E^2+12E^3$	$-9(130)^{\frac{1}{2}}E^3/4$	0
$-27(110)^{\frac{1}{2}}E^3/11$	$-9(130)^{\frac{1}{2}}E^3/4$	$12E^1+195E^2+6E^3$	$-12(55)^{\frac{1}{2}}E^3/5$
$-36(2)^{\frac{1}{2}}E^3$	0	$-12(55)^{\frac{1}{2}}E^3/5$	$18E^1$

TABLE I.

	5^2H_{11}	5^2H_{21}	5^2H_{30}
5^2H_{11}	$8E^1-11E^3/2$	$14(10010)^{\frac{1}{2}}E^2/11$	$(390)^{\frac{1}{2}}(24E^1-5E^3)/12$
5^2H_{21}	$14(10010)^{\frac{1}{2}}E^2/11$	$8E^1(977E^2+59E^3)/11$	$(231)^{\frac{1}{2}}(330E^2-29E^3)/33$
5^2H_{30}	$(390)^{\frac{1}{2}}(24E^2-5E^3)/12$	$(231)^{\frac{1}{2}}(330E^2-29E^3)/33$	$8E^1-44E^2+41E^3/4$
5^2H_{31}	$(3315)^{\frac{1}{2}}(24E^2-E^3)/12$	$(7854)^{\frac{1}{2}}(186E^2-E^3)/66$	$-(34)^{\frac{1}{2}}(240E^2-E^3)/8$
$5^2H'_{31}$	$-(3003)^{\frac{1}{2}}(600E^2+11E^3)/132$	$(30)^{\frac{1}{2}}(618E^2-37E^3)/66$	$-(770)^{\frac{1}{2}}(528E^2-31E^3)/88$
3^2H_{11}	$9(2)^{\frac{1}{2}}E^3/2$	0	$3(195)^{\frac{1}{2}}E^3/2$
3^2H_{21}	0	$-45(11)^{\frac{1}{2}}E^3/11$	$3(21)^{\frac{1}{2}}E^3$

1) of the term is the left superscript, the seniority number v is the left subscript, and the quantum numbers U, introduced by Racah, are given as the right subscript. These quantum numbers are sufficient to distinguish all the terms apart from some of those which have $U\equiv(31)$ and (40) where terms with the same v USL classification may occur twice. In these few cases, the different terms are distinguished by a dash after the manner of Racah.

The matrix elements are expressed in terms of the parameters E^0, E^1, E^2 and E^3, which have been defined by Racah[1] in terms of the Slater radial F_k integrals as follows

$$\begin{aligned} E^0&=F_0-10F_2-33F_4-286F_6\\ E^1&=(70F_2+231F_4+2002F_6)/9\\ E^2&=(F_2-3F_4+7F_6)/9\\ E^3&=(5F_2+6F_4-91F_6)/3. \end{aligned} \tag{1}$$

The energy contribution involving the parameter E^0 is a constant for all the terms of a given f^n configuration and has been omitted from Tables I and II. The coefficient e_0 associated with E^0 for a given f^n configuration is given by the general expression

$$e_0=n(n-1)/2. \tag{2}$$

The coefficients e_2 and e_3 associated with the parameters E^2 and E^3, respectively, have been checked in the case of the diagonal matrix elements by the application of the relations

$$\sum_L(2L+1)e_2=0 \quad \text{and} \quad \sum_L(2L+1)e_3=0, \tag{3}$$

where the summation extends over all the terms having the same v, S, and U quantum numbers. These relationships follow from the Eq. (88) and (89) of Racah[1] and have been given previously, without the restriction on U, by Jørgensen.[2]

The complete checking of the off-diagonal matrix elements, which involve only the coefficients e_2 of E^2 and e_3 of E^3, is not so easily attained. However, partial checking procedures can be developed for most of these matrix elements.

The coefficient e_2 of E^2 were calculated separately for the f^5 and f^6 configurations and checked, for the three highest multiplicities, by use of the equation

$$(f^nWUSL\,|e_2|\,f^nWU'SL) = -(f^{n\pm1}WUS'L\,|e_2|\,f^{n\pm1}WU'S'L), \tag{4}$$

which follows directly from Racah's[1] Eq. (73) and an inspection of his Table I.

For the singlet states of the f^6 configuration (i.e., those states of the fourth highest multiplicity), checks of the coefficient e_2 were possible for all the interactions except those involving states with $U\equiv(40)$. These checks were performed by making use of Eq. (4) and the electrostatic energy matrices of several other f^n configurations, namely those of the f^2 and f^3 configurations calculated by Racah,[1,3] those of the f^4 configuration calculated by Reilly,[4] and those for the three highest multiplicities of the f^7 configuration calculated by Runciman,[5] together with those for the f^5 configuration given in Table I of this paper.

Further checks of the coefficients were obtained from considerations of Racah's Eq. (74),

$$(WUL\,|e_2|\,WU'L)=\sum_\gamma\chi_\gamma(W,UU')\,(U\,|\chi_\gamma(L)\,|U'), \tag{5}$$

where χ_γ is independent of L and $\chi_\gamma(L)$ is independent of W; the maximal number of independent $(U|\chi_\gamma(L)|U')$ is $c\,[UU'(40)]$, which is given in Racah's[1] Table V.

Racah[1] has shown that the linear combinations in Eq. (5) are proportional to one another, and it is, therefore, possible, except for $UU'\equiv(21)(21)$, to express the results by means of one $\chi_\gamma(L)$ for every

[2] C. K. Jørgensen, *Energy Levels of Complexes and Gaseous Ions* (Jul. Gjellerups, Copenhagen, 1957)

[3] G Racah, Phys. Rev. **62,** 438 (1942).

[4] E. F. Reilly, Phys. Rev. **91,** 876 (1953).

[5] W. A. Runciman J. Chem. Phys. (to be published).

—*Continued.*

${}_5{}^2H_{31}$	${}_5{}^2H'_{31}$	${}_3{}^2H_{11}$	${}_3{}^2H_{21}$
$(3315)^{\frac{1}{2}}(24E^2-E^3)/12$	$-(3003)^{\frac{1}{2}}(600E^2-11E^3)/132$	$9(2)^{\frac{1}{2}}E^3/2$	0
$(7854)^{\frac{1}{2}}(186E^2-E^3)/66$	$(30)^{\frac{1}{2}}(618E^2-37E^3)/66$	0	$-45(11)^{\frac{1}{2}}E^3/11$
$-(34)^{\frac{1}{2}}(240E^2-E^3)/8$	$-(770)^{\frac{1}{2}}(528E^2-31E^3)/88$	$3(195)^{\frac{1}{2}}E^3/2$	$3(21)^{\frac{1}{2}}E^3$
$8E^1-92E^2+13E^3/8$	$-(6545)^{\frac{1}{2}}(192E^2+5E^3)/88$	$-(6630)^{\frac{1}{2}}E^3/4$	$-(714)^{\frac{1}{2}}E^3/2$
$-(6545)^{\frac{1}{2}}(192E^2+5E^3)/88$	$8E^1+(10720E^2+2199E^3)/88$	$-(6006)^{\frac{1}{2}}E^3/4$	$-37(330)^{\frac{1}{2}}E^3/22$
$-(6630)^{\frac{1}{2}}E^3/4$	$-(6006)^{\frac{1}{2}}E^3/4$	$12E^1-6E^3$	0
$-(714)^{\frac{1}{2}}E^3/2$	$-37(330)^{\frac{1}{2}}E^3/22$	0	$12E^1+21E^2+21E^3$

TABLE II. The electrostatic energy matrices of the f^6 configuration.

${}_6{}^7F_{10}$

${}_6{}^7F_{10}$	0

${}_4{}^5S_{00}$

${}_4{}^5S_{00}$	$9E^1$

${}_6{}^5P_{11}$

${}_6{}^5P_{11}$	$6E^1+11E^3$

${}_6{}^5K_{21}$

${}_6{}^5K_{21}$	$6E^1+135E^2-7E^3$

${}_6{}^5L_{21}$

${}_6{}^5L_{21}$	$6E^1-105E^2-15E^3$

	${}_6{}^5F_{21}$	${}_4{}^5F_{10}$
${}_6{}^5F_{21}$	$6E^1-195E^2+15E^3$	$-6(11)^{\frac{1}{2}}E^3$
${}_4{}^5F_{10}$	$-6(11)^{\frac{1}{2}}E^3$	$9E^1$

	${}_6{}^5H_{11}$	${}_6{}^5H_{21}$
${}_6{}^5H_{11}$	$6E^1-3E^3$	$-12(455)^{\frac{1}{2}}E^2$
${}_6{}^5H_{21}$	$-12(455)^{\frac{1}{2}}E^2$	$6E^1-21E^2+6E^3$

${}_6{}^5I_{20}$

${}_6{}^5I_{20}$	$6E^1+30E^2-7E^3$
${}_4{}^5I_{20}$	$-2(14)^{\frac{1}{2}}E^3$

${}_4{}^5I_{20}$

${}_4{}^5I_{20}$	$-2(14)^{\frac{1}{2}}E^3$
	$9E^1+7E^3$

	${}_6{}^5D_{20}$	${}_6{}^5D_{21}$	${}_4{}^5D_{20}$
${}_6{}^5D_{20}$	$6E^1+11(78E^2+7E^3)/7$	$468(33)^{\frac{1}{2}}E^2/7$	$22(14)^{\frac{1}{2}}E^3/7$
${}_6{}^5D_{21}$	$468(33)^{\frac{1}{2}}E^2/7$	$6E^1-3(377E^2-42E^3)/7$	$12(462)^{\frac{1}{2}}E^3/7$
${}_4{}^5D_{20}$	$22(14)^{\frac{1}{2}}E^3/7$	$12(462)^{\frac{1}{2}}E^3/7$	$9E^1-11E^3$

	${}_6{}^5G_{20}$	${}_6{}^5G_{21}$	${}_4{}^5G_{20}$
${}_6{}^5G_{20}$	$6E^1-4(195E^2-7E^3)/7$	$-24(4290)^{\frac{1}{2}}E^2/7$	$8(14)^{\frac{1}{2}}E^3/7$
${}_6{}^5G_{21}$	$-24(4290)^{\frac{1}{2}}E^2/7$	$6E^1+11(153E^2+7E^3)/7$	$2(15015)^{\frac{1}{2}}E^3/7$
${}_4{}^5G_{20}$	$8(14)^{\frac{1}{2}}E^3/7$	$2(15015)^{\frac{1}{2}}E^3/7$	$9E^1-4E^3$

${}_6{}^3O_{31}$

${}_6{}^3O_{31}$	$10E^1-10E^2-34E^3$

${}_6{}^3N_{31}$

${}_6{}^3N_{31}$	$10E^1-76E^2-23E^3$

	${}_6{}^3L_{21}$	${}_6{}^3L_{31}$	${}_4{}^3L_{21}$
${}_6{}^3L_{21}$	$10E^1+5(257E^2-33E^3)/11$	$72(380)^{\frac{1}{2}}E^2/11$	$-32(11)^{\frac{1}{2}}E^3/11$
${}_6{}^3L_{31}$	$72(380)^{\frac{1}{2}}E^2/11$	$10E^1+4(589E^2-11E^3)/11$	$-6(1045)^{\frac{1}{2}}E^3/11$
${}_4{}^3L_{21}$	$-32(11)^{\frac{1}{2}}E^3/11$	$-6(1045)^{\frac{1}{2}}E^3/11$	$13E^1-85E^2-11E^3$

	${}_6{}^3M_{30}$	${}_6{}^3M_{31}$	${}_4{}^3M_{30}$
${}_6{}^3M_{30}$	$10E^1+(25E^2-42E^3)/2$	$63(35)^{\frac{1}{2}}E^2/2$	$(2)^{\frac{1}{2}}E^3$
${}_6{}^3M_{31}$	$63(35)^{\frac{1}{2}}E^2/2$	$10E^1+(43E^2-26E^3)/2$	$3(70)^{\frac{1}{2}}E^3$
${}_4{}^3M_{30}$	$(2)^{\frac{1}{2}}E^3$	$3(70)^{\frac{1}{2}}E^3$	$13E^1+50E^2-23E^3$

TABLE II.

	$^6D_{20}$	$^6D_{21}$
$^6D_{20}$	$10E^1-11(26E^2-7E^3)/7$	$-780(3)^{\frac{1}{2}}E^2/7$
$^6D_{21}$	$-780(3)^{\frac{1}{2}}E^2/7$	$10E^1+3055E^2/77+18E^3$
$^6D_{31}$	$72(1638)^{\frac{1}{2}}E^2/7$	$180(546)^{\frac{1}{2}}E^2/77$
$^4D_{20}$	$66(2)^{\frac{1}{2}}E^3/7$	$-44(6)^{\frac{1}{2}}E^3/7$
$^4D_{21}$	$12(1617)^{\frac{1}{2}}E^3/147$	$304(11)^{\frac{1}{2}}E^3/77$

	$^6P_{11}$	$^6P_{30}$	$^6P_{31}$
$^6P_{11}$	$10E^1+11E^3$	$26(110)^{\frac{1}{2}}E^2$	$-6(1430)^{\frac{1}{2}}E^2$
$^6P_{30}$	$26(110)^{\frac{1}{2}}E^2$	$10E^1-26E^2+23E^3$	$-114(13)^{\frac{1}{2}}E^2$
$^6P_{31}$	$-6(1430)^{\frac{1}{2}}E^2$	$-114(13)^{\frac{1}{2}}E^2$	$10E^1+302E^2+31E^3$
$^4P_{11}$	$-121(5)^{\frac{1}{2}}E^3/15$	$-19(22)^{\frac{1}{2}}E^3/6$	$(286)^{\frac{1}{2}}E^3/2$
$^4P_{30}$	$-(55)^{\frac{1}{2}}E^3/3$	$83(2)^{\frac{1}{2}}E^3/6$	$17(26)^{\frac{1}{2}}E^3/2$
$^2P_{11}$	$-11(30)^{\frac{1}{2}}E^3/5$	$(33)^{\frac{1}{2}}E^3$	$3(429)^{\frac{1}{2}}E^3$

	$^6I_{20}$	$^6I_{30}$	$^6I_{31}$
$^6I_{20}$	$10E^1-10E^2-7E^3$	$-30(3)^{\frac{1}{2}}E^2$	$-270E^2$
$^6I_{30}$	$-30(3)^{\frac{1}{2}}E^2$	$10E^1+(25E^2+6E^3)/2$	$171(3)^{\frac{1}{2}}E^2/2$
$^6I_{31}$	$-270E^2$	$171(3)^{\frac{1}{2}}E^2/2$	$10E^1+(1151E^2+110E^3)/10$
$^6I'_{31}$	0	$-27(102)^{\frac{1}{2}}E^2$	$153(34)^{\frac{1}{2}}E^2/5$
$^4I_{20}$	$-6(2)^{\frac{1}{2}}E^3$	$8(6)^{\frac{1}{2}}E^3$	0
$^4I_{30}$	$4(6)^{\frac{1}{2}}E^3$	$7(2)^{\frac{1}{2}}E^3$	$-15(6)^{\frac{1}{2}}E^3$

	$^6K_{21}$	$^6K_{30}$	$^6K_{31}$
$^6K_{21}$	$10E^1-(2091E^2+77E^3)/11$	$20(374)^{\frac{1}{2}}E^2/11$	$156(14858)^{\frac{1}{2}}E^2/253$
$^6K_{30}$	$20(374)^{\frac{1}{2}}E^2/11$	$10E^1-47E^2-4E^3$	$741(4807)^{\frac{1}{2}}E^2/253$
$^6K_{31}$	$156(14858)^{\frac{1}{2}}E^2/253$	$741(4807)^{\frac{1}{2}}E^2/253$	$10E^1-(61753E^2-1012E^3)/253$
$^6K'_{31}$	$1008(3036)^{\frac{1}{2}}E^2/253$	$-219(2346)^{\frac{1}{2}}E^2/46$	$-72(21318)^{\frac{1}{2}}E^2/253$
$^4K_{21}$	$32(11)^{\frac{1}{2}}E^3/33$	$-10(34)^{\frac{1}{2}}E^3/3$	$-14(163438)^{\frac{1}{2}}E^3/253$
$^4K_{30}$	$-16(187)^{\frac{1}{2}}E^3/33$	$-14(2)^{\frac{1}{2}}E^3/3$	$-2(9614)^{\frac{1}{2}}E^3/11$

	$^6G_{20}$	$^6G_{21}$	$^6G_{30}$
$^6G_{20}$	$10E^1+260E^2/7+4E^3$	$40(390)^{\frac{1}{2}}E^2/7$	$13(15)^{\frac{1}{2}}E^2$
$^6G_{21}$	$40(390)^{\frac{1}{2}}E^2/7$	$10E^1-981E^2/7+11E^3$	$-40(26)^{\frac{1}{2}}E^2$
$^6G_{30}$	$13(15)^{\frac{1}{2}}E^2$	$-40(26)^{\frac{1}{2}}E^2$	$10E^1-26E^2+14E^3$
$^6G_{31}$	$-45(1365)^{\frac{1}{2}}E^2/7$	$-552(14)^{\frac{1}{2}}E^3/7$	$-30(91)^{\frac{1}{2}}E^2$
$^4G_{20}$	$24(2)^{\frac{1}{2}}E^3/7$	$-22(195)^{\frac{1}{2}}E^3/21$	$16(30)^{\frac{1}{2}}E^3/3$
$^4G_{21}$	$(4290)^{\frac{1}{2}}E^3/21$	$-80(11)^{\frac{1}{2}}E^3/21$	$-5(286)^{\frac{1}{2}}E^3/6$
$^4G_{30}$	$8(30)^{\frac{1}{2}}E^3/3$	$-4(13)^{\frac{1}{2}}E^3/3$	$10(2)^{\frac{1}{2}}E^3/3$

— Continued.

$^{6}{}^{3}D_{31}$

$72(1638)^{\frac{1}{2}}E^{2}/7$
$180(546)^{\frac{1}{2}}E^{2}/77$
$10E^{1}-2396E^{2}/11+29E^{3}$
0
$6(6006)^{\frac{1}{2}}E^{3}/11$

$^{4}{}^{3}D_{20}$

$66(2)^{\frac{1}{2}}E^{3}/7$
$-44(6)^{\frac{1}{2}}E^{3}/7$
0
$13E^{1}-11(104E^{2}+13E^{3})/7$
$-4(66)^{\frac{1}{2}}(39E^{2}-4E^{3})/7$

$^{4}{}^{3}D_{21}$

$12(1617)^{\frac{1}{2}}E^{3}/147$
$304(11)^{\frac{1}{2}}E^{3}/77$
$6(6006)^{\frac{1}{2}}E^{3}/11$
$-4(66)^{\frac{1}{2}}(39E^{2}-4E^{3})/7$
$13E^{1}+(1781E^{2}+88E^{3})/7$

$^{4}{}^{3}P_{11}$

$-121(5)^{\frac{1}{2}}E^{3}/15$
$-19(22)^{\frac{1}{2}}E^{3}/6$
$(286)^{\frac{1}{2}}E^{3}/2$
$13E^{1}+484E^{3}/15$
$-(11)^{\frac{1}{2}}(390E^{2}-E^{3})/3$
$-11(6)^{\frac{1}{2}}E^{3}/5$

$^{4}{}^{3}P_{30}$

$-(55)^{\frac{1}{2}}E^{3}/3$
$83(2)^{\frac{1}{2}}E^{3}/6$
$-17(26)^{\frac{1}{2}}E^{3}/2$
$-(11)^{\frac{1}{2}}(390E^{2}-E^{3})/3$
$13E^{1}-104E^{2}-14E^{3}/3$
$(66)^{\frac{1}{2}}E^{3}$

$^{2}{}^{3}P_{11}$

$-11(30)^{\frac{1}{2}}E^{3}/5$
$(33)^{\frac{1}{2}}E^{3}$
$3(429)^{\frac{1}{2}}E^{3}$
$-11(6)^{\frac{1}{2}}E^{3}/5$
$(66)^{\frac{1}{2}}E^{3}$
$18E^{1}-132E^{3}/5$

$^{6}{}^{3}I'_{31}$

0
$-27(102)^{\frac{1}{2}}E^{2}$
$153(34)^{\frac{1}{2}}E^{2}/5$
$10E^{1}-(788E^{2}-55E^{3})/5$
0
0

$^{4}{}^{3}I_{20}$

$-6(2)^{\frac{1}{2}}E^{3}$
$8(6)^{\frac{1}{2}}E^{3}$
0
0
$13E^{1}-40E^{2}-13E^{3}$
$-4(3)^{\frac{1}{2}}(30E^{2}+E^{3})$

$^{4}{}^{3}I_{30}$

$4(6)^{\frac{1}{2}}E^{3}$
$7(2)^{\frac{1}{2}}E^{3}$
$-15(6)^{\frac{1}{2}}E^{3}$
0
$-4(3)^{\frac{1}{2}}(30E^{2}+E^{3})$
$13E^{1}+50E^{2}-11E^{3}$

$^{6}{}^{3}K'_{31}$

$1008(3036)^{\frac{1}{2}}E^{2}/253$
$-219(2346)^{\frac{1}{2}}E^{2}/46$
$-72(21318)^{\frac{1}{2}}E^{2}/253$
$10E^{1}+(3868E^{2}+92E^{3})/23$
$42(69)^{\frac{1}{2}}E^{3}/23$
0

$^{4}{}^{3}K_{21}$

$32(11)^{\frac{1}{2}}E^{3}/33$
$-10(34)^{\frac{1}{2}}E^{3}/3$
$-14(163438)^{\frac{1}{2}}E^{3}/253$
$42(69)^{\frac{1}{2}}E^{3}/23$
$13E^{1}+219E^{2}-25E^{3}/3$
$-8(17)^{\frac{1}{2}}(3E^{2}+2E^{3})/3$

$^{4}{}^{3}K_{30}$

$-16(187)^{\frac{1}{2}}E^{3}/33$
$-14(2)^{\frac{1}{2}}E^{3}/3$
$-2(9614)^{\frac{1}{2}}E^{3}/11$
0
$-8(17)^{\frac{1}{2}}(3E^{2}+2E^{3})/3$
$13E^{1}-188E^{2}+16E^{3}/3$

$^{6}{}^{3}G_{31}$

$-45(1365)^{\frac{1}{2}}E^{2}/7$
$-552(14)^{\frac{1}{2}}E^{2}/7$
$-30(91)^{\frac{1}{2}}E^{2}$
$10E^{1}+122E^{2}+22E^{3}$
0
$(154)^{\frac{1}{2}}E^{3}/2$
$-2(182)^{\frac{1}{2}}E^{3}$

$^{4}{}^{3}G_{20}$

$24(2)^{\frac{1}{2}}E^{3}/7$
$-22(195)^{\frac{1}{2}}E^{3}/21$
$16(30)^{\frac{1}{2}}E^{3}/3$
0
$13E^{1}+4(260E^{2}+13E^{3})/7$
$8(2145)^{\frac{1}{2}}(6E^{2}+E^{3})/21$
$-4(15)^{\frac{1}{2}}(39E^{2}+2E^{3})/3$

$^{4}{}^{3}G_{21}$

$(4290)^{\frac{1}{2}}E^{3}/21$
$-80(11)^{\frac{1}{2}}E^{3}/21$
$-5(286)^{\frac{1}{2}}E^{3}/6$
$(154)^{\frac{1}{2}}E^{3}/2$
$8(2145)^{\frac{1}{2}}(6E^{2}+E^{3})/21$
$13E^{1}-11(297E^{2}-31E^{3})/21$
$4(143)^{\frac{1}{2}}(12E^{2}-E^{3})/3$

$^{4}{}^{3}G_{30}$

$8(30)^{\frac{1}{2}}E^{3}/3$
$-4(13)^{\frac{1}{2}}E^{3}/3$
$10(2)^{\frac{1}{2}}E^{3}/3$
$-2(182)^{\frac{1}{2}}E^{3}$
$-4(15)^{\frac{1}{2}}(39E^{2}+2E^{3})/3$
$4(143)^{\frac{1}{2}}(12E^{2}-E^{3})/3$
$13E^{1}-104E^{2}+22E^{3}/3$

TABLE II.

	$^6F_{10}$	$^6F_{21}$	$^6F_{30}$	$^6F_{31}$	$^6F'_{31}$
$^6F_{10}$	$10E^1$	0	$-5(143)^{\frac{1}{2}}E^2$	0	$15(429)^{\frac{1}{2}}E^2$
$^6F_{21}$	0	$10E^1+5(2093E^2+231E^3)/77$	$-60(4290)^{\frac{1}{2}}E^2/11$	$936(10)^{\frac{1}{2}}E^2/11$	$-36(1430)^{\frac{1}{2}}E^2/11$
$^6F_{30}$	$-5(143)^{\frac{1}{2}}E^2$	$-60(4290)^{\frac{1}{2}}E^2/11$	$10E^1+19E^2+18E^3$	$72(429)^{\frac{1}{2}}E^2/11$	$147(3)^{\frac{1}{2}}E^2$
$^6F_{31}$	0	$936(10)^{\frac{1}{2}}E^2/11$	$72(429)^{\frac{1}{2}}E^2/11$	$10E^1-2210E^2/11+26E^3$	$-168(143)^{\frac{1}{2}}E^2/11$
$^6F'_{31}$	$15(429)^{\frac{1}{2}}E^2$	$-36(1430)^{\frac{1}{2}}E^2/11$	$147(3)^{\frac{1}{2}}E^2$	$-168(143)^{\frac{1}{2}}E^2/11$	$10E^1+41E^2+26E^3$
$^4F_{10}$	0	$46(15)^{\frac{1}{2}}E^3/11$	0	$-8(6)^{\frac{1}{2}}E^3$	0
$^4F_{21}$	$-(330)^{\frac{1}{2}}E^3/3$	$-48(11)^{\frac{1}{2}}E^3/11$	$5(390)^{\frac{1}{2}}E^3/6$	$-18(110)^{\frac{1}{2}}E^3/11$	$-3(130)^{\frac{1}{2}}E^3/2$
$^4F_{30}$	0	$4(2145)^{\frac{1}{2}}E^3/33$	$-12(2)^{\frac{1}{2}}E^3$	$8(858)^{\frac{1}{2}}E^3/11$	$-12(6)^{\frac{1}{2}}E^3$
$^2F_{10}$	0	$-48(10)^{\frac{1}{2}}E^3/5$	0	$-36E^3$	0

	$^6H_{11}$	$^6H_{21}$	$^6H_{30}$	$^6H_{31}$	$^6H'_{31}$
$^{93}H_{11}$	$10E^1-3E^3$	$14(10010)^{\frac{1}{2}}E^2/11$	$-2(390)^{\frac{1}{2}}E^2$	$-2(3315)^{\frac{1}{2}}E^2$	$50(3003)^{\frac{1}{2}}E^2/11$
$^6H_{21}$	$-14(10010)^{\frac{1}{2}}E^2/11$	$10E^1+977E^2/11+6E^3$	$-10(231)^{\frac{1}{2}}E^2$	$-31(7854)^{\frac{1}{2}}E^2/11$	$-103(30)^{\frac{1}{2}}E^2/11$
$^6H_{30}$	$-2(390)^{\frac{1}{2}}E^2$	$-11(231)^{\frac{1}{2}}E^2$	$10E^1+44E^2+9E^3$	$30(34)^{\frac{1}{2}}E^2$	$6(770)^{\frac{1}{2}}E^2$
$^6H_{31}$	$-2(3315)^{\frac{1}{2}}E^2$	$-31(7854)^{\frac{1}{2}}E^2/11$	$30(34)^{\frac{1}{2}}E^2$	$10E^1+92E^2+17E^3$	$24(6545)^{\frac{1}{2}}E^2/11$
$^6H'_{31}$	$50(3003)^{\frac{1}{2}}E^2/11$	$-103(30)^{\frac{1}{2}}E^2/11$	$6(770)^{\frac{1}{2}}E^2$	$24(6545)^{\frac{1}{2}}E^2/11$	$10E^1-1340E^2/11+17E^3$
$^4H_{11}$	$11(5)^{\frac{1}{2}}E^3/5$	0	$-19(78)^{\frac{1}{2}}E^3/6$	$(2652)^{\frac{1}{2}}E^3/12$	$(60060)^{\frac{1}{2}}E^2/60$
$^4H_{21}$	0	$80(11)^{\frac{1}{2}}E^3/11$	$-10(21)^{\frac{1}{2}}E^3/3$	$-(714)^{\frac{1}{2}}E^3/3$	$-37(330)^{\frac{1}{2}}E^3/33$
$^4H_{30}$	$-(195)^{\frac{1}{2}}E^3/3$	$-8(462)^{\frac{1}{2}}E^3/33$	$-5(2)^{\frac{1}{2}}E^3/2$	$-(17)^{\frac{1}{2}}E^3/2$	$-31(385)^{\frac{1}{2}}E^3/22$
$^2H_{11}$	$3(30)^{\frac{1}{2}}E^3/5$	0	$3(13)^{\frac{1}{2}}E^3$	$3(442)^{\frac{1}{2}}E^3/2$	$3(10010)E^3/10$

	$^6P_{30}$
$^6P_{30}$	$12E^1+156E^2+23E^3$

	$^6M_{30}$	$^6M_{40}$
$^6M_{30}$	$12E^1-75E^2-21E^3$	$-9(165)^{\frac{1}{2}}E^2$
$^6M_{40}$	$-9(165)^{\frac{1}{2}}E^2$	$12E^1-291E^2-9E^3$

	$^6K_{30}$	$^6K_{40}$	$^4K_{21}$
$^6K_{30}$	$12E^1+282E^2-4E^3$	$-84(3)^{\frac{1}{2}}E^2$	$4(51)^{\frac{1}{2}}E^3$
$^6K_{40}$	$-84(3)^{\frac{1}{2}}E^2$	$12E^1-36E^2+8E^3$	$-2(17)^{\frac{1}{2}}E^3$
$^4K_{21}$	$4(51)^{\frac{1}{2}}E^3$	$-2(17)^{\frac{1}{2}}E^3$	$15E^1-129E^2-3E^3$

	$^6F_{10}$	$^6F_{30}$	$^6F_{40}$	$^4F_{21}$
$^6F_{10}$	$12E^1$	$3(1430)^{\frac{1}{2}}E^2$	$9(1430)^{\frac{1}{2}}E^2$	$3(22)^{\frac{1}{2}}E^3$
$^6F_{30}$	$-3(1430)^{\frac{1}{2}}E^2$	$12E^1-114E^2+18E^3$	$90E^2$	$-3(65)^{\frac{1}{2}}E^3$
$^6F_{40}$	$9(1430)^{\frac{1}{2}}E^2$	$90E^2$	$12E^1+294E^2+30E^3$	$3(65)^{\frac{1}{2}}E^3$
$^4F_{21}$	$3(22)^{\frac{1}{2}}E^3$	$-3(65)^{\frac{1}{2}}E^3$	$3(65)^{\frac{1}{2}}E^3$	$15E^1-195E^2-3E^3$

—Continued.

	$_4{}^3F_{10}$	$_4{}^3F_{21}$	$_4{}^3F_{30}$	$_2{}^3F_{10}$
	0	$-(330)^{\frac{1}{2}}E^3/3$	0	0
	$46(15)^{\frac{1}{2}}E^3/15$	$-48(11)^{\frac{1}{2}}E^3/11$	$4(2145)^{\frac{1}{2}}E^3/33$	$-48(10)^{\frac{1}{2}}E^3/5$
	0	$5(390)^{\frac{1}{2}}E^3/6$	$-12(2)^{\frac{1}{2}}E^3$	0
	$-8(6)^{\frac{1}{2}}E^3$	$-18(110)^{\frac{1}{2}}E^3/11$	$8(858)^{\frac{1}{2}}E^3/11$	$-36E^3$
	0	$-3(130)^{\frac{1}{2}}E^3/2$	$-12(6)^{\frac{1}{2}}E^3$	0
	$13E^1$	$-8(165)^{\frac{1}{2}}E^3/15$	$-20(143)^{\frac{1}{2}}E^2$	0
	$-8(165)^{\frac{1}{2}}E^3/15$	$13E^1+65E^2+21E^3$	$4(195)^{\frac{1}{2}}(18E^2+E^3)/3$	$-6(110)^{\frac{1}{2}}E^3/5$
	$-20(143)^{\frac{1}{2}}E^2$	$4(195)^{\frac{1}{2}}(18E^2+E^3)/3$	$13E^1+76E^2+42E^3$	0
	0	$-6(110)^{\frac{1}{2}}E^3/5$	0	$18E^1$
	$_4{}^3H_{11}$	$_4{}^3H_{21}$	$_4{}^3H_{30}$	$_2{}^3H_{11}$
	$11(5)^{\frac{1}{2}}E^3/5$	0	$-(195)^{\frac{1}{2}}E^3/3$	$3(30)^{\frac{1}{2}}E^3/5$
	0	$80(11)^{\frac{1}{2}}E^3/11$	$-8(462)^{\frac{1}{2}}E^3/33$	0
	$-19(78)^{\frac{1}{2}}E^3/6$	$-10(21)^{\frac{1}{2}}E^3/3$	$-5(2)^{\frac{1}{2}}E^3/2$	$3(13)^{\frac{1}{2}}E^3$
	$(2652)^{\frac{1}{2}}E^3/12$	$-(714)^{\frac{1}{2}}E^3/3$	$-(17)^{\frac{1}{2}}E^3/2$	$3(442)^{\frac{1}{2}}E^3/2$
	$(60060)^{\frac{1}{2}}E^3/60$	$-37(330)^{\frac{1}{2}}E^3/33$	$-31(385)^{\frac{1}{2}}E^3/22$	$3(10010)^{\frac{1}{2}}E^3/10$
	$13E^1-44E^3/5$	$10(182)^{\frac{1}{2}}E^2$	$(39)^{\frac{1}{2}}(30E^2+E^3)/3$	$3(6)^{\frac{1}{2}}E^3/5$
	$10(182)^{\frac{1}{2}}E^2$	$13E^1-197E^2-4E^3$	$2(42)^{\frac{1}{2}}(33E^2-4E^3)/3$	0
	$(39)^{\frac{1}{2}}(30E^2+E^3)/3$	$2(42)^{\frac{1}{2}}(33E^2-4E^3)/3$	$13E^1+176E^2+14E^3$	$3(26)^{\frac{1}{2}}E^3$
	$3(6)^{\frac{1}{2}}E^3/5$	0	$3(26)^{\frac{1}{2}}E^3$	$18E^1+36E^3/5$

$_6{}^1Q_{40}$

$12E^1+6E^2-42E^3$

	$_6{}^1N_{40}$	$_4{}^1N_{22}$
$_6{}^1N_{40}$	$12E^1+144E^2-19E^3$	$-2(230)^{\frac{1}{2}}E^3$
$_4{}^1N_{22}$	$-2(230)^{\frac{1}{2}}E^3$	$15E^1+60E^2-39E^3$

	$_6{}^1S_{00}$	$_6{}^1S_{40}$	$_4{}^1S_{22}$	$_0{}^1S_{00}$
$_6{}^1S_{00}$	$12E^1$	$-30(143)^{\frac{1}{2}}E^2$	$-4(165)^{\frac{1}{2}}E^3/5$	0
$_6{}^1S_{40}$	$-30(143)^{\frac{1}{2}}E^2$	$12E^1-384E^2+36E^3$	$4(195)^{\frac{1}{2}}E^3$	0
$_4{}^1S_{22}$	$-4(165)^{\frac{1}{2}}E^3/5$	$4(195)^{\frac{1}{2}}E^3$	$15E^1+390E^2-6E^3$	$-36(110)^{\frac{1}{2}}E^3/5$
$_0{}^1S_{00}$	0	0	$-36(110)^{\frac{1}{2}}E^3/5$	$27E^1$

	$_6{}^1H_{30}$	$_6{}^1H_{40}$	$_4{}^1H_{21}$	$_4{}^1H_{22}$
$_6{}^1H_{30}$	$12E^1-264E^2+9E^3$	$-72(42)^{\frac{1}{2}}E^3$	$6(14)^{\frac{1}{2}}E^3$	0
$_6{}^1H_{40}$	$-72(42)^{\frac{1}{2}}E^3$	$12E^1-192E^2+21E^3$	$-12(3)^{\frac{1}{2}}E^3$	$6(26)^{\frac{1}{2}}E^3$
$_4{}^1H_{21}$	$6(14)^{\frac{1}{2}}E^3$	$-12(3)^{\frac{1}{2}}E^3$	$15E^1+183E^2+36E^3$	$-36(78)^{\frac{1}{2}}E^2$
$_4{}^1H_{22}$	0	$6(26)^{\frac{1}{2}}E^3$	$-36(78)^{\frac{1}{2}}E^2$	$15E^1+156E^2-3E^3$

TABLE II.

	${}^6{}^1L_{40}$	${}^6{}^1L'_{40}$
${}^6{}^1L_{40}$	$12E^1-1164E^2/31$	$252(1995)^{\frac{1}{2}}E^2/31$
${}^6{}^1L'_{40}$	$252(1995)^{\frac{1}{2}}E^2/31$	$12E^1+3210E^2/31$
${}^4{}^1L_{21}$	$22(465)^{\frac{1}{2}}E^3/31$	$-12(4123)^{\frac{1}{2}}E^3/31$
${}^4{}^1L_{22}$	$8(1767)^{\frac{1}{2}}E^3/31$	$24(1085)^{\frac{1}{2}}E^3/31$

	${}^6{}^1D_{20}$	${}^6{}^1D_{40}$	${}^4{}^1D_{20}$
${}^6{}^1D_{20}$	$12E^1+78E^2+11E^3$	$-72(26)^{\frac{1}{2}}E^2$	$61(770)^{\frac{1}{2}}E^3/70$
${}^6{}^1D_{40}$	$-72(26)^{\frac{1}{2}}E^2$	$12E^1-12E^2+33E^3$	$-6(5005)^{\frac{1}{2}}E^3/35$
${}^4{}^1D_{20}$	$61(770)^{\frac{1}{2}}E^3/70$	$-6(5005)^{\frac{1}{2}}E^3/35$	$15E^1+(4290E^2+3971E^3)/140$
${}^4{}^1D_{21}$	$12(7)^{\frac{1}{2}}E^3/7$	$-6(182)^{\frac{1}{2}}E^3/7$	$-3(110)^{\frac{1}{2}}(195E^2+16E^3)/35$
${}^4{}^1D_{22}$	$-3(78)^{\frac{1}{2}}E^3/2$	$18(3)^{\frac{1}{2}}E^3$	$-3(15015)^{\frac{1}{2}}(30E^2-7E^3)/140$
${}^2{}^1D_{20}$	$-6(55)^{\frac{1}{2}}E^3/5$	$6(1430)^{\frac{1}{2}}E^3/5$	$-33(350)^{\frac{1}{2}}E^3/350$

	${}^6{}^1I_{20}$	${}^6{}^1I_{30}$	${}^6{}^1I_{40}$
${}^6{}^1I_{20}$	$12E^1+7(30E^2-11E^3)/11$	$-90(462)^{\frac{1}{2}}E^3/11$	$306(64790)^{\frac{1}{2}}E^2/341$
${}^6{}^1I_{30}$	$-90(462)^{\frac{1}{2}}E^2/11$	$12E^1-75E^2+3E^3$	$-9(61845)^{\frac{1}{2}}E^2/31$
${}^6{}^1I_{40}$	$306(64790)^{\frac{1}{2}}E^2/341$	$-9(61845)^{\frac{1}{2}}E^2/31$	$12E^1-669E^2/31+15E^3$
${}^6{}^1I'_{40}$	$-108(110670)^{\frac{1}{2}}E^2/341$	$756(28985)^{\frac{1}{2}}E^2/341$	$180(74613)^{\frac{1}{2}}E^2/341$
${}^4{}^1I_{20}$	$-61(770)^{\frac{1}{2}}E^3/110$	$24(15)^{\frac{1}{2}}E^3/5$	$-6(4123)^{\frac{1}{2}}E^3/31$
${}^4{}^1I_{22}$	$-3(1870)^{\frac{1}{2}}E^3/22$	0	$6(10013)^{\frac{1}{2}}E^3/31$
${}^2{}^1I_{20}$	$42(55)^{\frac{1}{2}}E^3/55$	$6(210)^{\frac{1}{2}}E^3/5$	$42(1178)^{\frac{1}{2}}E^3/31$

	${}^6{}^1G_{20}$	${}^6{}^1G_{30}$	${}^6{}^1G_{40}$	${}^6{}^1G'_{40}$
${}^6{}^1G_{20}$	$12E^1-780E^2/11+4E^3$	$39(2310)^{\frac{1}{2}}E^2/11$	$53(38610)^{\frac{1}{2}}E^2/33$	$7(835380)^{\frac{1}{2}}E^2/33$
${}^6{}^1G_{30}$	$39(2310)^{\frac{1}{2}}E^2/11$	$12E^1+156E^2+14E^3$	$-16(91)^{\frac{1}{2}}E^2$	$64(4862)^{\frac{1}{2}}E^2/11$
${}^6{}^1G_{40}$	$53(38610)^{\frac{1}{2}}E^2/33$	$-16(91)^{\frac{1}{2}}E^2$	$12E^2-1520E^2/3+26E^3$	$-34(2618)^{\frac{1}{2}}E^2/33$
${}^6{}^1G'_{40}$	$7(83580)^{\frac{1}{2}}E^2/33$	$64(4862)^{\frac{1}{2}}E^2/11$	$-34(2618)^{\frac{1}{2}}E^2/33$	$12E^1+10942E^2/33+26E^3$
${}^4{}^1G_{20}$	$122(770)^{\frac{1}{2}}E^3/385$	$16(3)^{\frac{1}{2}}E^3$	$8(2457)^{\frac{1}{2}}E^3/63$	$-2(14586)^{\frac{1}{2}}E^3/33$
${}^4{}^1G_{21}$	$(910)^{\frac{1}{2}}E^3/7$	$(429)^{\frac{1}{2}}E^3$	$-131(2079)^{\frac{1}{2}}E^3/189$	$17(102)^{\frac{1}{2}}E^3/9$
${}^4{}^1G_{22}$	$-2(1430)^{\frac{1}{2}}E^3/11$	0	$-8(3)^{\frac{1}{2}}E^3/9$	$-34(7854)^{\frac{1}{2}}E^3/99$
${}^2{}^1G_{20}$	$-24(55)^{\frac{1}{2}}E^3/55$	$4(42)^{\frac{1}{2}}E^3$	$-8(702)^{\frac{1}{2}}E^3/9$	$4(51051)^{\frac{1}{2}}E^3/33$

—Continued.

$_4{}^1L_{21}$	$_4{}^1L_{22}$
$22(465)^{\frac{1}{2}}E^3/31$	$8(1767)^{\frac{1}{2}}E^3/31$
$-12(4123)^{\frac{1}{2}}E^3/31$	$24(1085)^{\frac{1}{2}}E^3/31$
$15E^1+15E^2-27E^3$	$-24(95)^{\frac{1}{2}}E^2$
$-24(95)^{\frac{1}{2}}E^2$	$15E^1-54E^2+18E^3$

$_4{}^1D_{21}$	$_4{}^1D_{22}$	$_2{}^1D_{20}$
$12(7)^{\frac{1}{2}}E^3/7$	$-3(78)^{\frac{1}{2}}E^3/2$	$-6(55)^{\frac{1}{2}}E^3/5$
$-6(182)^{\frac{1}{2}}E^3/7$	$18(3)^{\frac{1}{2}}E^3$	$6(1430)^{\frac{1}{2}}E^3/5$
$-3(110)^{\frac{1}{2}}(195E^2+16E^3)/35$	$-3(15015)^{\frac{1}{2}}(30E^2-7E^3)/140$	$-33(350)^{\frac{1}{2}}E^3/350$
$15E^1-5(507E^2-48E^3)/7$	$135(546)^{\frac{1}{2}}E^2/7$	$-24(385)^{\frac{1}{2}}E^3/35$
$135(546)^{\frac{1}{2}}E^2/7$	$15E^1-(150E^2-39E^3)/4$	$-3(4290)^{\frac{1}{2}}E^3/10$
$-24(385)^{\frac{1}{2}}E^3/35$	$-3(4290)^{\frac{1}{2}}E^3/10$	$20E^1+286E^2+143E^3/5$

$_6{}^1I'_{40}$	$_4{}^1I_{20}$	$_4{}^1I_{22}$	$_2{}^1I_{20}$
$-108(110670)^{\frac{1}{2}}E^2/341$	$-61(770)^{\frac{1}{2}}E^3/110$	$-3(1870)^{\frac{1}{2}}E^3/22$	$42(55)^{\frac{1}{2}}E^3/55$
$756(28985)^{\frac{1}{2}}E^2/341$	$24(15)^{\frac{1}{2}}E^3/5$	0	$6(210)^{\frac{1}{2}}E^3/5$
$180(74613)^{\frac{1}{2}}E^2/341$	$-6(4123)^{\frac{1}{2}}E^3/31$	$6(10013)^{\frac{1}{2}}E^3/31$	$42(1178)^{\frac{1}{2}}E^3/31$
$12E^1+108264E^2/341+15E^3$	$-18(17391)^{\frac{1}{2}}E^3/341$	$150(7161)^{\frac{1}{2}}E^3/341$	$18(243474)^{\frac{1}{2}}E^3/341$
$-18(17381)^{\frac{1}{2}}E^3/341$	$15E^1+(150E^2-361E^3)/20$	$-3(119)^{\frac{1}{2}}(30E^2-E^3)/4$	$3(14)^{\frac{1}{2}}E^3/10$
$150(7161)^{\frac{1}{2}}E^3/341$	$-3(119)^{\frac{1}{2}}(30E^2-E^3)/4$	$15E^1-3(362E^2+E^3)/4$	$-3(34)^{\frac{1}{2}}E^3/2$
$18(243474)^{\frac{1}{2}}E^3/341$	$3(14)^{\frac{1}{2}}E^3/10$	$3(34)^{\frac{1}{2}}E^3/2$	$20E^1+70E^2-91E^3/5$

$_4{}^1G_{20}$	$_4{}^1G_{21}$	$_4{}^1G_{22}$	$_2{}^1G_{20}$
$122(770)^{\frac{1}{2}}E^3/385$	$(910)^{\frac{1}{2}}E^3/7$	$-2(1430)^{\frac{1}{2}}E^3/11$	$-24(55)^{\frac{1}{2}}E^3/55$
$16(3)^{\frac{1}{2}}E^3$	$(429)^{\frac{1}{2}}E^3$	0	$4(42)^{\frac{1}{2}}E^3$
$8(2457)^{\frac{1}{2}}E^3/63$	$-131(2079)^{\frac{1}{2}}E^3/189$	$-8(3)^{\frac{1}{2}}E^3/9$	$-8(702)^{\frac{1}{2}}E^3/9$
$-2(14586)^{\frac{1}{2}}E^3/33$	$17(102)^{\frac{1}{2}}E^3/9$	$-34(7854)^{\frac{1}{2}}E^3/99$	$4(51051)^{\frac{1}{2}}E^3/33$
$15E^1-(975E^2-361E^3)/35$	$4(143)^{\frac{1}{2}}(15E^2-2E^3)/7$	$(91)^{\frac{1}{2}}(285E^2+7E^3)/7$	$-6(14)^{\frac{1}{2}}E^3/35$
$4(143)^{\frac{1}{2}}(15E^2-2E^3)/7$	$15E^1+11(201E^2-3E^3)/7$	$36(77)^{\frac{1}{2}}E^2/7$	$-2(2002)^{\frac{1}{2}}E^3/7$
$(91)^{\frac{1}{2}}(285E^2+7E^3)/7$	$36(77)^{\frac{1}{2}}E^2/7$	$15E^1+141E^2+57E^3$	$-2(26)^{\frac{1}{2}}E^3$
$-6(14)^{\frac{1}{2}}E^3/135$	$-2(2002)^{\frac{1}{2}}E^3/7$	$-2(26)^{\frac{1}{2}}E^3$	$20E^1-260E^2+52E^3/5$

couple UU'. This property allows us to write

$$\frac{(WUL|e_2|WU'L)}{(W''UL|e_2|W''U'L)}=\frac{\sum_\gamma \chi_\gamma(W, UU')}{\sum_\gamma \chi_\gamma(W'', UU')}$$

$$=\frac{\chi(W, UU')}{\chi(W'', UU')}, \quad (6)$$

where the $\chi(W, UU')$ may be found from Racah's[1] Tables VII–XI. Equation (6) allows many recurrence equations to be written down which are useful for checking the matrix elements of e_2. For example,

$$(f^5(211)(21)^4L|e_2|f^5(211)(30)^4L)=-[(22)^{\frac{1}{2}}/5]$$

$$\times(f^5(221)(21)^2L|e_2|f^5(221)(31)^2L)$$

$$(\text{for } L=FGHK). \quad (7)$$

Except for $UU'\equiv(21)(21)$, Eq. (6) holds for both the diagonal and nondiagonal matrix elements of e_2 if $c[UU'(40)]\geq 1$.

Checks for the matrix elements of e_3 can be found by considering the tensorial properties of e_3. Racah[1] has noted that e_3 has the same tensorial properties as the operator Ω, defined by his Eq. (76) as

$$\Omega=-(462)^{\frac{1}{2}}\sum_k(2k+1)^{\frac{1}{2}}U^{(k)2}((110)(11)k$$

$$+(110)(11)k|(110)(22)S), \quad (8)$$

where Ω is diagonal in the vUL scheme. From Racah's[1] Eq. (87) we have, when $c[UU'(22)]\geq 1$,

$$(f^nvUSL|e_3+\Omega|f^nv'U'SL)=y(f^n, vSU, v'SU')$$

$$\times(U|\phi(L)|U'). \quad (9)$$

The values of $y(f^n, vSU, v'SU')$ can be found from Racah's[1] Tables XV–XXIV. Noting that the quantities $(U|\phi(L)|U')$ depend only on $UU'L$, we may write

$$\frac{(f^nvUSL|e_3+\Omega|f^nv'U'SL)}{(f^{n''}v''US''L|e_3+\Omega|f^{n''}v'''U'S''L)}$$

$$=\frac{y(f^n, vSU, v'SU')}{y(f^{n''}v''S''U, v'''S''U')}, \quad (10)$$

without exception. Since Ω is diagonal in the vUL scheme, we may obtain many recurrence equations to check the nondiagonal matrix elements of e_3. For example,

$$(f^6{}_6{}^3L_{31}|e_3|f^6{}_4{}^3L_{30})=-2(2)^{\frac{1}{2}}(f^5{}_5{}^2L_{31}L|e_3|f^5{}_5{}^2L_{30})$$

$$(\text{for } L=PFF'GHH'II'KK'M). \quad (11)$$

The electrostatic energy matrices of the f^5 and f^6 configurations will be useful for the analysis of the spectra of several of the rare earth and actinide ions.

ACKNOWLEDGMENTS

The author wishes to express his thanks to W. A. Runciman for suggesting the problem, and to Professor A. G. McLellan for several interesting discussions.

Part of this work was done during the tenure of a New Zealand University Research Fund Fellowship.

Use of Mass Spectral Data in Radiation Chemistry

JEAN H. FUTRELL

Aeronautical Research Laboratory, Wright-Patterson Air Force Base, Ohio

(Received December 9, 1960)

The quasi-equilibrium theory of mass spectra of Wahrhaftig *et al.* is applied to the propane molecule ion to calculate the extent of unimolecular dissociation at 10^{-10} sec. This approximates the collision time for propane at moderate pressures and is therefore the ion distribution appropriate to irradiation studies. Two formulations of the theory are used, and it is concluded that the analytical mass spectrum of paraffin hydrocarbons is a good first approximation of the ion distribution in irradiated systems.

A NUMBER of authors[1] have recently proposed mechanisms for the formation of products in vapor-phase radiolysis in which ion-molecule reactions play a dominant role. In general it has been assumed that the distribution of ionic species produced by the incident radiation is properly represented by the mass spectrum of the compound under study. Actually the situation may be quite different, as the mass spectrum represents the extent of unimolecular dissociation of an isolated molecule ion in a microsecond. Ion-molecule reactions are thought to occur at every collision[2]; and decomposition reactions, if they are to compete, must have specific rate constants of the order of 10^{10} sec^{-1}. Stated in another fashion, the "mass spectrum" which should be used in radiation chemistry calculations is one determined by an instrument with a resolving time of the order of the reciprocal of the collision frequency in an atmospheric gas (i.e., approx 10^{-10} sec). Such an instrument is purely hypothetical and likely to remain so, and calculation methods must be used to derive such a mass spectrum.

This problem has been treated by Stevenson,[3] who posed the question whether decomposition of the molecule ion could compete with these very fast bimolecular reactions. He used the quasi-equilibrium theory of mass spectra[4] in a one-parameter form to estimate the fraction of molecule ions of a number of hydrocarbons remaining at 10^{-10} sec after ionization. He concluded, "For the more complex alkanes, and presumably alkenes, the rates of dissociation of the molecule ions are comparable with the rates that have been found for bimolecular reactions of ions with molecules, and reactions of fragment ions must be considered along with reactions of the molecule ions." Complex molecules in this context include propane and heavier hydrocarbons.

This result is encouraging evidence that the usual mass spectrum may be a reasonable first approximation to the required distribution, but it seemed desirable to investigate this problem in detail. A recent theoretical paper by Kropf, Eyring, Wahrhaftig, and Eyring treated the mass spectrum of propane and 2,2-dideutero propane,[5] and the accuracy with which they reproduced experimental spectra prompted us to use their parameters to calculate a 10^{-10} sec spectrum. A still more recent report by Eyring and Wahrhaftig[6] shows that substantial revision of the characteristic parameters is necessary to fit additional data they have obtained, and we have recalculated an ion distribution using this information. This paper presents the results and certain implications of these calculations.

CALCULATION METHOD

A. Simplified Theory

The quasi-equilibrium theory of mass spectra of Rosenstock *et al.*[4] presumes that fragment ions formed by electron impact arise from unimolecular decomposition of excited molecule ions. The specific rate constant is given by the expression

$$K(E)=h^{-1}\int_0^{E-\epsilon_0}[\rho^{\ddagger}(E,\epsilon_0,\epsilon_t)/\rho(E)]\delta\epsilon_t, \qquad (1)$$

which reduces to

$$K_i(E)=Z_i[1-(\epsilon_i/E)]^{p_i}(E-\epsilon_i)^{q_i}, \qquad (2)$$

where

$$p_i=N-(L/2)-1; \qquad q_i=(L-L^{\ddagger})/2.$$

Here N and L denote the total internal degrees of freedom and the number of rotational degrees of freedom, respectively; the detailed reasoning in assignment of frequency factors Z_i and activation energies ϵ_i is given in the original reference.[5]

Numerical calculations were performed on a Univac 1105 scientific digital computer, which calculated

[1] (a) G. G. Meisels, W. H. Hamill, and R. R. Williams, Jr., J. Phys. Chem. **61,** 1456 (1957); (b) J. H. Futrell, J. Am. Chem. Soc. **81,** 5921 (1959); (c) K. Yang, J. Chem. Phys. **32,** 1892 (1960); (d) J. H. Futrell, J. Phys. Chem. **64,** 1634 (1960); (e) L. M. Dorfman and M. C. Sauer, Jr., J. Chem. Phys. **32,** 1886 (1960).

[2] D. P. Stevenson, J. Phys. Chem. **61,** 1453 (1957).

[3] D. P. Stevenson, Radiation Research **10,** 610 (1959).

[4] H. M. Rosenstock, M. B. Wallenstein, A. L. Wahrhaftig, and H. Eyring, Proc. Natl. Acad. Sci. U.S. **38,** 667 (1952).

[5] A. Kropf, E. M. Eyring, A. L. Wahrhaftig, and H. Eyring, J. Chem. Phys. **32,** 149 (1960).

[6] E. M. Eyring and A. L. Wahrhaftig, J. Chem. Phys. **34,** 23 (1961).

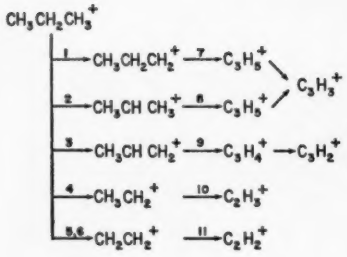

FIG. 1. Unimolecular decomposition reactions for the propane molecule ion.

$K_i(E)$ from Eq. (2) for the decomposition reactions of Fig. 1, using values of the characteristic parameters from the work cited in reference 5. Parent ions with energies such that $\sum k_i < 10^{10}$ sec^{-1} are counted as the molecule ion, and those with greater energy yield the indicated product ions in the ratios of

$$K_i(E)/\sum_1^6 K_i(E).$$

At some critical energy E_i^c for molecule ions decomposing by path i the primary ion will contain sufficient excitation energy to decompose further. This critical energy is calculated in the following manner: For reactions 7–11 of Fig. 1 the energy at which $k_i = 10^{10}$ sec^{-1} is determined. Assuming equipartition of energy in internal degrees of freedom of products, and assigning reasonable activation energies for the respective forward and reverse reactions, the excess energy requirement of each primary decomposition is estimated.[4,5] The resulting values of E_i^c are given in the first column of Table I, and all primary ions with precursors of $E > E_i^c$ are assumed to decompose into the corresponding secondary ion.

The final computation consists of introducing a probability function weighting parent-ion energy. The function used in the first calculation was unit probability from zero to 12×10^{-12} ergs/molecule, 0.4 from 12 to 20×10^{-12} ergs/molecule, and zero for higher energies. The numerical integration

$$S_i = \int_a^b [P(E)K_i(E)/\sum_i K_i(E)]dE \qquad (3)$$

is performed over the appropriate intervals for the primary and secondary products, the parent-ion abundance is calculated as $\sum P(E)$ over the interval where $\sum k_i < 10^{10}$ sec^{-1}, and the sums are normalized to a total ionization of 100. The results are given in Table II.

B. Semiempirical Theory

A number of authors have pointed out difficulties encountered in applying the simplified theory,[7] particularly at low voltages. Eyring and Wahrhaftig have made a detailed critical analysis of this problem in a recent study.[6] They have demonstrated that the approach described, which reproduces 70-v spectra very well, is inadequate to describe mass spectra as a function of bombarding electron energy.

By treating p_i, Z_i, and ϵ_i of Eq. (2) as variable parameters and devising a modified probability function they achieved a reasonably quantitative fit of the data which retained the structure of Eq. (2). The resulting values of Z, ϵ, and p describe some kind of average nuclear motion but have lost the attractively simple significance of the earlier version. Most unfortunately for our purpose there seems no way to deduce these parameters for other systems except by a repetition of the techniques applied to propane[6] for each molecule of interest.

The assignment of values of E_i^c, the critical energy at which secondary decompositions occur, is entirely empirical in this formulation. Attempting to retain the systematics of Eyring and Wahrhaftig's treatment, we require one value of E_i^c for reactions 1 and 2, another value for reaction 3, and a third value for reactions 4, 5 and 6. The increase in E_i^c is assigned by comparing the values of this quantity computed in Part A [corresponding to $K_i(E) = 10^{10}$ sec^{-1} for reactions 7 through 11 of Fig. 1] to those of Kropf *et al.*[5] [$K_i(E) = 10^6$ sec^{-1} for these reactions]. The same increments were then applied to the values of Eyring and Wahrhaftig[6] to estimate E_i^c for calculating our 10^{-10}-sec mass spectrum. The resulting values are given in Table I.

The calculations were repeated using the final parameters deduced by these workers[6] and a probability function in Eq. (3) of unity from 0.2 to 8×10^{-12} erg/molecule and from 11.2 to 16×10^{-12} erg/molecule, zero elsewhere. Numerical integrations were performed over the appropriate intervals for the primary and secondary ions as before. The molecule ion concentration is computed as the product of the probability function times the energy interval over which $\sum k_i(E) < 10^{10}$ sec^{-1}, and the normalized results are reported in Table II.

TABLE I. Critical energies E_i^c at which secondary decompositions occur. (a) Simplified theory, (b) semiempirical approach.

Reaction	Ergs/molecule$\times10^{12}$ (a)	(b)
1	12.95	12.6
2	12.60	12.6
3	10.77	10.1
4	15.30	13.0
5	12.65	13.0
6		13.0

[7] (a) W. A. Chupka, J. Chem. Phys. **30,** 191 (1959); (b) L. Friedman, F. A. Long, and M. Wolfsberg, *ibid.* **30,** 1605 (1959); (c) F. W. Lampe and F. H. Field, J. Am. Chem. Soc. **81,** 3238 (1959); F. H. Field and F. W. Lampe, *ibid.* **80,** 5587 (1958).

DISCUSSION

In Table II are tabulated the experimental values for the distribution of ions (mass spectrum) produced by electron impact and subsequent unimolecular dissociation in a time interval of the order of a microsecond. For comparison are given the computed distributions using both versions of the quasi-equilibrium theory for a time interval of 10^{-10} sec. Calculated values for a microsecond are not reported, but the results[5,6] agree very well with the experimental values.

The semiempirical quasi-equilibrium treatment is quite promising for our purposes because of the restrictions placed on the p, Z, E, and P parameters by experiment.[6] So long as the structure of Eq. (2) is retained only rather small changes in these parameters are tolerated without worsening the fit of the authors' theoretical curves to their experimental points. It is possible that an alternative theoretical expression with an equivalent number of experimentally determined constants could also fit the data. However, quite apart from considerations of the validity of the quasi-equilibrium theory we may deduce that this formulation with optimized parameters is the best method now available for extrapolating mass spectra to a 10^{-10} sec time scale. Hence the results of this computation are the proper yardstick for comparison with alternative approaches and with radiolysis data.

We may now ask whether the mass spectrum is a reasonable measure of the extent of fragmentation at 10^{-10} sec and whether the simple quasi-equilibrium theory gives a better approximation. From Table II we conclude that the mass spectrum is a remarkably good approximation, and that the simple theory, if anything, gives poorer values. With the exception of the propane, propyl, and ethylene ions, mass spectrum and theory values essentially coincide. The discrepancy in propyl ion arises primarily from an abnormally low frequency factor-low activation energy process for reaction 2 of Fig. 1 such that the specific rate constant does not reach high enough values to compete with collision, although it does contribute to the microsecond spectrum.[8] The theory also predicts that the propane ion is present in significantly larger amount at 10^{-10} sec. This is most reasonable, as the excited propane ion is the "reservoir" for subsequent unimolecular decomposition if the system remains undisturbed.

Let us consider briefly the effect on calculation of radiolysis yields of the lower concentrations of these ions. It seems likely that the so-called hydride-ion transfer reaction

$$R^+ + C_3H_8 \rightarrow RH + C_3H_7^+, \qquad (4)$$

will be the predominant ion-molecule reaction for this system.[1b,c,d,9] Hence the ethylene ions are converted to ethyl radicals, which will react by disproportionation and combination with themselves and with other free radicals to form a number of products. Propyl is the prominent free radical formed in this system, and the ethyl radical concentration affects chiefly the products of ethyl-propyl combination and disproportionation. Uncertainties in the relative rate constants for mixed radical disproportionations and experimental errors in measuring the various products of ethyl-propyl reactions make it difficult to assess the results of a change in ethylene ion concentration of the magnitude indicated by this calculation. An additional complication exists in that studies of propane radiolysis have been conducted at such conversions that scavenging reactions of unsaturated products may have perturbed initial yields.[10]

The propyl ion is one of the products of the hydride transfer reaction (4), so that any perturbation in the initial concentration from unimolecular dissociation is completely washed out by ion-molecule reactions. The enhanced propane ion concentration will affect as yet unknown ion-molecule reactions of this entity or will be manifested in products of neutralization of the molecule ion. Thus it appears unlikely that the small changes in ion distribution indicated by this calculation will be confirmed by product analysis of irradiated propane. Studies of the radiation chemistry of propane are now in progress in this laboratory, and a detailed analysis of the results will be published at a later date.

It is unfortunately not possible to extend the semiempirical theory approach to other molecules at this time. An extended mass spectrometer study of each

TABLE II. Relative abundances.

Ion	Reaction	MS[b]	Simplified theory	Semiempirical theory
$C_3H_8^+$	Parent	12.7	17.2	30.6
$C_3H_7^+$	1,2	10.6	12.4	1.3
$C_3H_6^+$	3	1.5	4.1	1.3
$C_3H_5^+$ [a]	7,8	9.5	0.6	9.2
$C_3H_4^+$ [a]	9	1.9	6.0	1.3
$C_2H_5^+$	4	31.1	33.0	33.7
$C_2H_4^+$	5,6	19.2	16.9	8.7
$C_2H_3^+$	10	10.5	8.0	11.8
$C_2H_2^+$	11	1.9	1.8	2.1

[a] Values include tertiary decomposition products indicated in Fig. 1.
[b] D. O. Schissler, S. O. Thompson, and J. Turkevitch, Disc. Faraday Soc. **10**, 46 (1951).

[8] This reaction has a frequency factor of 5.0×10^9 sec^{-1} compared to values from 10^{14} sec^{-1} to 10^{21} sec^{-1} (ergs/molecule)$^{-q}$ for the other processes. See work cited in reference 6.

[9] F. H. Field and F. W. Lampe, J. Am. Chem. Soc. **80,** 5587 (1958).
[10] (a) R. A. Back, J. Phys. Chem. **64,** 124 (1959). (b) J. H. Futrell, *ibid.* **65,** 565 (1961).

molecule in parallel with arduous curve-fitting procedures is required to deduce the necessary parameters. It seems likely, however, that the general features of this computation may apply to other systems, at least to paraffin hydrocarbons. We may anticipate that the parent ion will be present in somewhat higher abundance than the mass spectrum indicates and that fragment ions are produced in approximately the same abundance. This is consistent with Stevenson's calculations and observations which discussed only parent ions.[3] Finally, the simple quasi-equilibrium theory gives results which are suspect, and it is doubtful that it can be used to derive a meaningful ion distribution for radiation chemistry purposes.

ACKNOWLEDGMENTS

The author gratefully acknowledges helpful discussions of this paper with Dr. E. M. Eyring and Dr. A. Wahrhaftig of the University of Utah and is indebted to them for access to their data prior to its publication.

THE JOURNAL OF CHEMICAL PHYSICS VOLUME 35, NUMBER 1 JULY, 1961

Effect of Pressure on the Charge Transfer Spectra of Heavy Transition Metal Hexahalide Complexes*

A. S. BALCHAN AND H. G. DRICKAMER

Department of Chemistry and Chemical Engineering, University of Illinois, Urbana, Illinois

(Received December 21, 1960)

The effect of pressure has been measured on the charge transfer bands of seven hexahalide salts of heavy transition metal ions (with 4*d* and 5*d* configurations). The lowest energy peaks always exhibited a large red shift with increasing pressure. Higher energy peaks always showed less shift, and in one case actually shifted to the blue. While there are undoubtedly several factors involved, the data are consistent with the assumption of increased spin-orbit coupling at high pressure. The marked broadening of the bands can be discussed in terms of the effect of decreased lattice spacing on the molecular charge transfer.

RECENTLY Jørgensen[1] has published an extensive study of the charge transfer bands in the hexahalide crystals of heavy transition metals. The effect of pressure on these peaks has been studied for seven of these compounds. The hexahalides were obtained from A. D. Mackay and used without further purification. The crystals were diluted with NaCl to about 0.5–1.0% concentration. The high-pressure techniques have been described elsewhere.[2] The shifts are shown in Figs. 1–7.

The bands in the solid are shifted slightly red from the corresponding bands in solution[1] and somewhat broadened. At one atmosphere the transition is presumably largely isolated within the $MX_6^{=}$ ion which exists either in the solid or solution. The halide ligands are exposed to a different environment in the crystal than in solution. This could modify the ligand levels and cause the shift. It is also possible that the ligand-metal distance is slightly smaller in the solid than in solution, which could give a red shift. The initial broadening on going from solution to solid is, in part at least, due to the wider slit necessitated by the poorer optics in the high pressure system.

The identification of the solid state bands studied with those found in solution is given in Table I. In some cases, the splittings observed in the liquid were masked in the solid by the broadening. For this reason a particular peak in the solid often corresponded to two or three small bands in the liquid. In some cases the doublet structure could be seen in the solid, but the resolution did not allow this splitting to be observed accurately. In cases such as this, the shift was referred to the absorption maximum at all pressures. It is for this reason that the data on bands formed by the overlap of several smaller peaks cannot be regarded as absolute, as relative shifts and intensity changes within the band could easily account for part of the apparent shift. Wherever possible, however, an effort was made to remove all extraneous absorption by subtraction, and the shifts given are the most accurate that could be obtained from the data.

In every case the initial shift of the peak was to lower energies. For any given compound the higher energy peaks always showed smaller red shifts than the lower energy ones. In the case of $IrCl_6^{=}$ at 50 kbars there was actually a reversal in the direction of the shift of the higher energy transition. The net result was, then, an increased splitting among the peaks with increase of pressure.

Jørgensen[1] identifies the low energy transition studied in the Os (IV) and Ir (IV) complexes as $\pi \rightarrow t_{2g}$ transi-

* This work was supported in part by the U. S. Atomic Energy Commission.

[1] C. K. Jørgensen, J. Mol. Phys. **2**, 309 (1959).

[2] R. A. Fitch, T. E. Slykhouse, and H. G. Drickamer, J. Opt. Soc. Am. **47**, 1015 (1957).

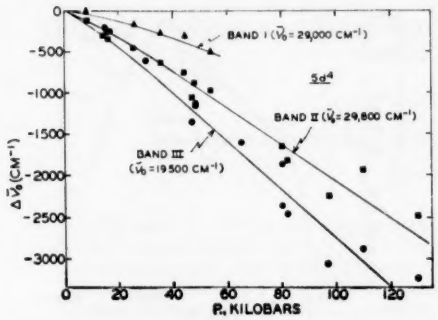

FIG. 1. Shift of charge transfer bands with pressure—K_2OsCl_6.

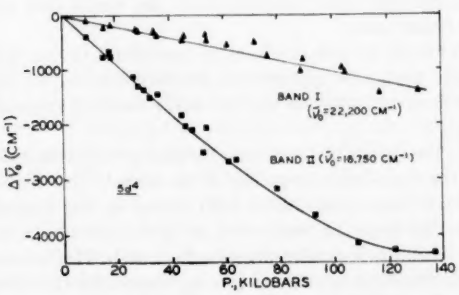

FIG. 2. Shift of charge transfer bands with pressure—K_2OsBr_6.

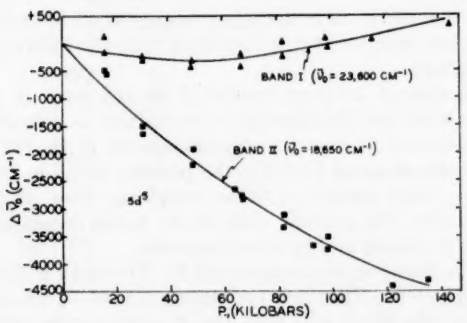

FIG. 3. Shift of charge transfer bands with pressure—Na_2IrCl_6.

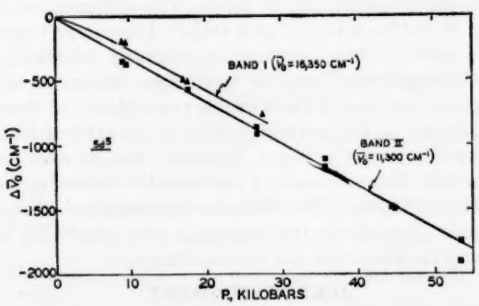

FIG. 4. Shift of charge transfer bands with pressure—K_2IrBr_6.

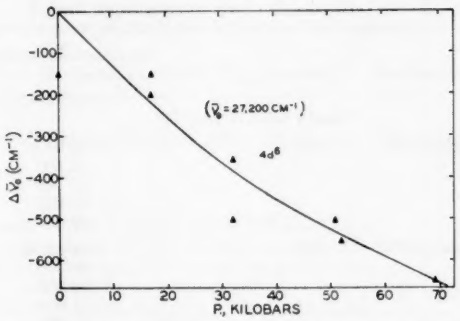

FIG. 5. Shift of charge transfer band with pressure—K_2PbCl_6.

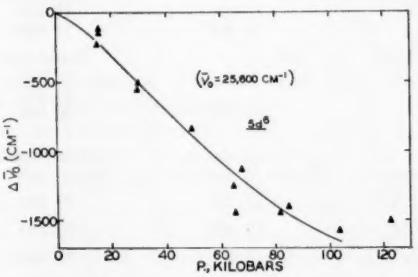

FIG. 6. Shift of charge transfer band with pressure—K_2PtBr_6.

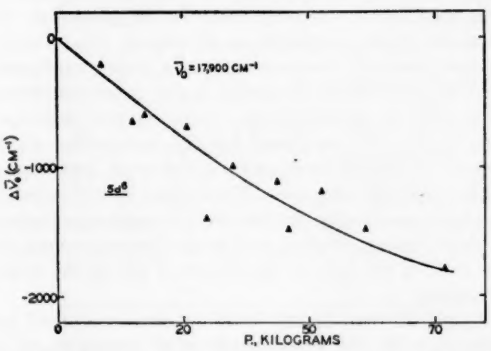

FIG. 7. Shift of charge transfer band with pressure—K_2PtI_6.

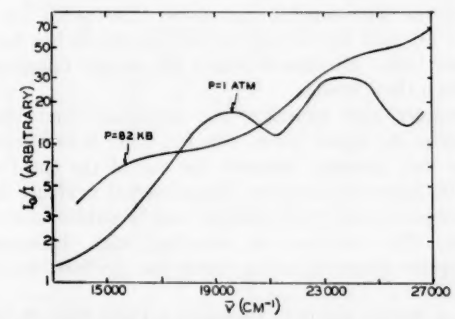

FIG. 8. Pressure broadening of charge transfer bands—Na_2IrCl_6.

TABLE I. Hexahalide charge-transfer bands studied.

Compound	Maxima in solid (cm^{-1}) band I	band II	band III	Corresponding band(s) in liquid (cm^{-1}) (1)
$K_2OSBr_6(5d^4)$	22 000			Triplet at 22 600 23 700 25 050
		16 750		20 450
$K_2OSCl_6(5d^4)$	29 000			Doublet at 29 300 30 000
		25 800		27 000
			19 500	23 900 17 150
$K_2IrBr_6(5d^5)$	16 350			Doublet at 14 300
		11 300		14 900
$Na_2IrCl_6(5d^5)$	23 600			Doublet at 23 050 24 400
		18 650		20 500

Compound	Maxima in solid (cm^{-1})	Corresponding band in liquid (cm^{-1}) (1)
$K_2PdCl_6(4d^6)$	27 200	29 400
$K_2PtI_6(5d^6)$	17 900	20 250
$K_2PtBr_6(5d^6)$	25 600	27 000

tions. Three strong band groups would be expected for this transition in d^5 compounds. In the spectra of the aqueous chloro-complexes of d^5 metals, this division is clear, but in the bromo complexes a more complicated splitting is observed. Similarly, in the chloro complexes of Ir (IV) in the solid state, a more definite identification can be made and band I in the case studied represented the highest band group of the $\pi \rightarrow t_{2g}$ transitions, as identified by Jørgensen. The highest band studied in the corresponding bromo compound strongly overlapped a higher energy doublet, and hence the uncertainty on the shift of this band is the largest of any of the measurements.

Using the two energy level schemes presented by Jørgensen for the $\pi \rightarrow t_{2g}$ bands in d^5 complexes, it is possible to obtain qualitative agreement with the data.

There are a number of ways in which pressure can affect the ligand-metal interaction. The metal ion d levels are split by the field of the ligands. It has been shown[3,4] that pressure increases the energy difference between these levels.

Pressure also increases the covalency[4] and thus perturbs the ligand levels. Finally, there is the possibility that pressure increases the size of the splitting due to spin-orbit coupling. Experimental evidence for this effect in $CoX_4^=$ (X = halide) will be published elsewhere. The increase in coupling with increased covalency seems plausible since the electron would undergo spin-orbit coupling with the metal and with the halide nuclei.

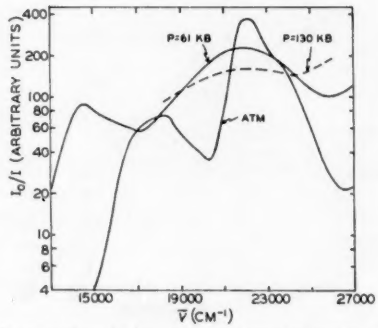

FIG. 9. Pressure broadening of charge-transfer bands—K_2OsBr_6.

While all factors doubtlessly contribute to the shifts of the peaks, an explanation consistent with the data can be given based on the spin-orbit coupling argument only.

In the theory of Jørgensen, for pure $\pi \rightarrow t_{2g}$ transitions, as the spin-orbit coupling is increased, the highest allowed transition should shift either in the opposite direction from the two lowest, or in the same direction, but with much smaller magnitude of shift. He indicates that, while this appears to give agreement for the chloro complexes, it is necessary to include configurational mixing with the σ hole states to explain the data on bromo and iodo compounds. In all cases, however, the fact that in our study the highest energy band shows the smallest pressure shift is consistent with the theory of Jørgensen.

Because of the large number of excited states in d^4 complexes, an identification of transitions is difficult. Nonetheless, just as the aqueous spectra of Os (IV) resemble those of Ir (IV), the pressure shifts in the $\pi \rightarrow t_{2g}$ band groups of these complexes show great similarity, the pressure shift of the bands decreasing with increasing energy of the transition.

The lowest energy bands in the Pt (IV) and Pd (IV) complexes are identified by Jørgensen as $\pi \rightarrow e_g$ transitions. The metal ions have the d^6 configuration. The peaks shifted red with no unusual features.

Of interest in the charge-transfer work is the large pressure broadening of the bands. This is illustrated in Figs. 8 and 9 for $OsBr_6^=$ and $IrCl_6^=$. The charge transfer process in these complexes is relatively localized at one atmosphere. Thus, the solid state spectra of the complex ions bear a considerable resemblance to those in solution, as the perturbing effect of the surroundings is small. As the pressure increases, the decrease in interionic distance causes a considerable delocalization of the excitation. The ultimate in delocalized charge transfer gives rise to the absorption edge observable in crystalline insulators and semiconductors.

ACKNOWLEDGMENT

A. S. Balchan would like to acknowledge financial assistance from an Autoclave Engineers Fellowship.

[3] R. L. Parsons, and H. G. Drickamer, J. Chem. Phys. **29,** 930 (1958).
[4] D. R. Stephens, and H. G. Drickamer, J. Chem. Phys. **34,** 937 (1961).

Effect of Pressure and Temperature on the Absorption Spectra of Four Alkali Halide Phosphors*

A. S. BALCHAN AND H. G. DRICKAMER

Department of Chemistry and Chemical Engineering, University of Illinois, Urbana, Illinois

(Received December 21, 1960)

The effect of pressure and temperature has been measured on the "A" bands in KI:Tl and in three alkali halides containing Pb^{++} impurity. The effect of temperature is to impose a red shift on the observed room-temperature pressure shift. The most remarkable result is the appearance of a new band in the high-pressure phase of KCl:Pb and KBr:Pb upon heating under pressure. The band remains after cooling, but disappears upon lowering the pressure into or through the region of the transformation back to the fcc phase. Repressuring and reheating reintroduces the band. It seems most probably that the band is associated with the ionic configuration near the Pb^{++} ion; especially with the location of the accompanying K^+ vacancy.

THE "A" band in one thallium-activated and three lead-activated alkali halides were investigated as a function of temperature and pressure. In all cases, the investigations were carried out in the CsCl phase (30-120 kbar) and data were taken along an "isobar." Because of the unusual results obtained, spectra were also taken after heating and subsequent cooling from each temperature. The experimental procedures have been described previously.[1,2] Spectra at room temperature have been published by Eppler and Drickamer.[3]

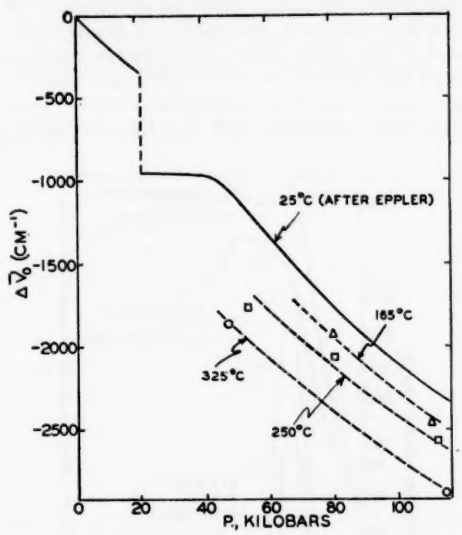

FIG. 1. Shift of band maximum with pressure and temperature "A" peak in KI:Tl.

The crystals used in this work were from the same stock as those used by Eppler.

The effect of temperature on the "A" band in KI:Tl is shown in Fig. 1 for pressures in the range 40–110 kbar. The solid line represents Eppler's[3] data. The points and dotted lines represent data obtained in these experiments. The shift with temperature at all pressures occurred toward lower energy and the apparent slope of the pressure shift of the band was independent of temperature. The shift was accompanied in all cases by a slight broadening of the band, but this appeared in some cases to be due to the movement toward lower energy of adjoining bands.

The effect of temperature to 325°C on the "A" band in KCl:Pb was measured at pressures from 35–125 kbar (Fig. 2). At a reproducible temperature (which was a function of pressure, Table I) a new band suddenly appeared at about 2000 cm^{-1} higher energy than the first. The induced band was stable when brought to room temperature. In Fig. 3 is illustrated a typical run in which the peak was introduced by heating to 325°C

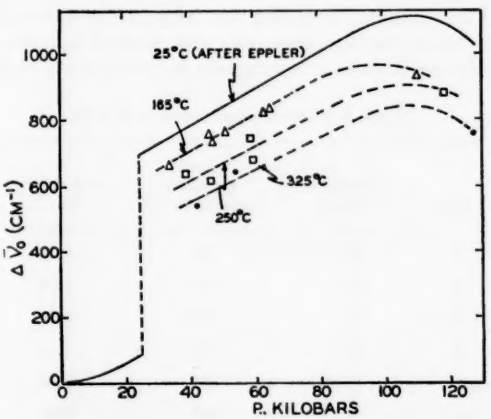

FIG. 2. Shift of band maximum with pressure and temperature "A" peak in KCl:Pb.

* This work was supported in part by U. S. Atomic Energy Commission.

[1] R. A. Fitch, T. E. Slykhouse, and H. G. Drickamer, J. Opt. Soc. Am. **47**, 1015 (1957).

[2] A. S. Balchan, and H. G. Drickamer, Rev. Sci. Instr. **31**, 511 (1960).

[3] R. A. Eppler, and H. G. Drickamer, J. Phys. Chem. Solids **15**, 112 (1960).

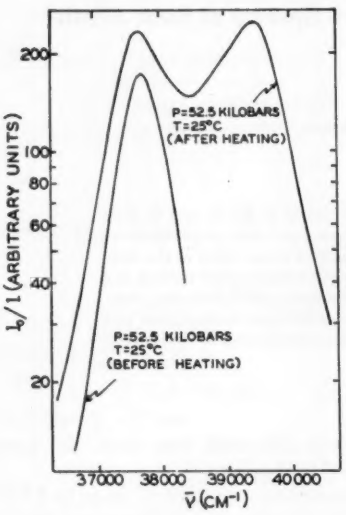

FIG. 3. Temperature induced peak in KCl:Pb at 52.5 kbars.

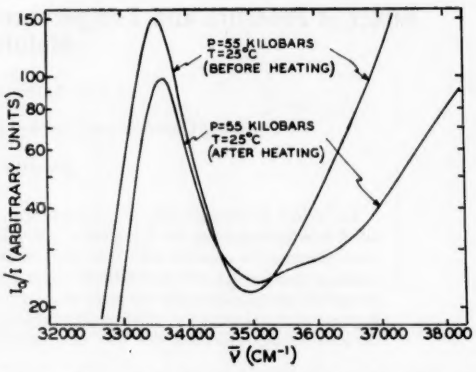

FIG. 4. Effect of heating on "A" bord in KBr:Pb in CsCl structure.

at 52.5 kbar. The spectra at 325°C and thereafter at room temperature showed the second band. Various experiments were run and several interesting observations made; these can be summarized as follows:

(1) The temperature at which the second band was first noticed was apparently a function of the pressure of the isobar. Because no continuous method was available of observing the "transition" as the temperature was raised, the temperature of transformation could not be obtained accurately. Nonetheless, it is seen in Table I that the observed lowest temperature at which the second peak was noticed definitely increased with pressure. At 111 kbar it was found impossible to introduce the peak at 325°C.

(2) The relative intensities of the two bands proved independent of all variables tested. Two identical runs, for example, could conceivably show the relative intensity of the second peak varying by a factor of ten. It was possible, by heating to a temperature above that at which the transition was first noticed, to produce *either* an increase or a reduction in the intensity of the second band. One consistent result was the observation that the second band never appeared without a reduction in intensity of the first. (The integrated area, however, was always greater than the initial "A" area.)

(3) It was found possible to cause a complete disappearance of the high-energy band, after it had been introduced, by decreasing the pressure at room temperature until the bulk crystal transformed to the NaCl phase. The peak then would not be present in either phase, although it could be reintroduced at approximately the same temperature if the pressure was raised to the initial value. This process could be repeated with identical results. It was found that the new band disappeared if the pressure was lowered until the CsCl→NaCl transition had just initiated, and then

TABLE I. Transition parameters in KCl:Pb.

Run	Pressure (kbar)	Apparent transition temperature (°C)	Peak splitting (cm^{-1})
1	30	222	1550
2	40	250	1575
3	44	250	...
4	48	325	...
5	52.5	325	1800
6	54	325	1850
7	111	no transition	

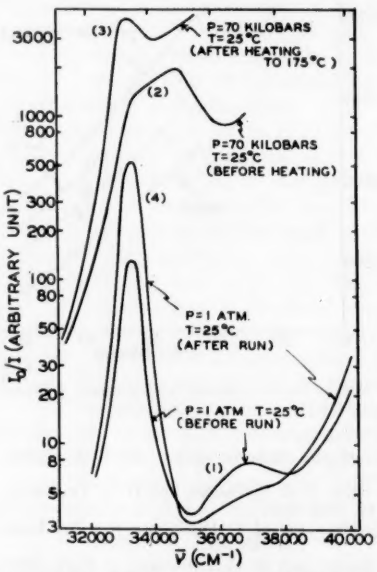

FIG. 5. Effect of heating on bands in RbBr:Pb.

raised again to the initial value. The initiation of the phase transition can be observed optically by the partial cutoff of light, whether one starts from below or above the transition. The mechanism and kinetics of the transition are discussed by Wiederhorn and Drickamer.[4]

(4) An attempt was made to measure the splitting of the bands as a function of pressure. Because of the large overlap the results are necessarily inaccurate, but, as Table I indicates, the splitting shows a definite increase with pressure.

The temperature effect on the "A" band in KBr:Pb and RbBr:Pb was also measured. In the CsCl phase of both phosphors, however, the overlap between the "A" and higher bands is larger, and it is difficult to observe structure on the high-energy side of the "A" peak. Figures 4 and 5 show typical spectra for the two phosphors after heating to at least 250°C. It is seen that in KBr:Pb it is probable that a peak at about 2000 cm^{-1} higher energy is present. It is dangerous to draw conclusions from changes in intensity of the "A" band, as optical scatter is large in this region; small changes in this scatter could easily alter the apparent intensity of a band. The curves numbered 1, 2, 3, and 4 in Fig. 5 represent the same crystal in four stages; before applying pressure, after compressing, after heating and cooling at 70 kbar, and after reducing the pressure to atmospheric.

The results of the experiments on KCl:Pb (particularly the destruction of the higher energy band during the lattice transition) indicate that the induced peak is due to a change in configuration around the Pb^{++} impurity. The fact that the "transition" occurs at reasonably well-defined temperature, and that the relative intensities of the "A" and "induced" bands can be varied at will, by repetitive heating, indicate that the process causing the second band is strongly dependent on the thermal energy of the lattice. This would be true for any diffusion mechanism.

The induced bands in KCl:Pb and KBr:Pb appear in positions similar to that of the second band in RbBr:Pb (Fig. 5), although the latter exists in both NaCl and CsCl phases at room temperature.

An attempt was made to introduce the higher energy band in KCl:Pb at 1 atm. A spectrum was taken at about 450°C and after subsequent cooling to room temperature; neither showed the appearance of the second peak.

The proposal which appears to be consistent with the greatest amount of experimental information is that the "induced" band is due to the K^+ vacancy which accompanies the Pb^{++} center, probably in its association with the impurity center. Some of the bands occurring in Ag^+ doped alkali halides have been ascribed to centers which include an associated vacancy.[5,6]

ACKNOWLEDGMENT

Mr. A. S. Balchan would like to express appreciation for a Consolidated Coal Fellowship and an Autoclave Engineer Fellowship.

[4] S. Wiederhorn, and H. G. Drickamer, J. Appl. Phys. **31,** 1666 (1960).

[5] R. A. Eppler, and H. G. Drickamer, J. Chem. Phys. **32,** 1734 (1960).

[6] H. W. Etzel, and J. H. Schulman, J. Chem. Phys. **22,** 1549 (1954).

Electron Spin Resonance of an Irradiated Single Crystal of Urea Oxalate*

D. V. G. L. NARASIMHA RAO† AND WALTER GORDY

Department of Physics, Duke University, Durham, North Carolina

(Received December 27, 1960)

Free radicals produced in a single crystal of urea oxalate by gamma-irradiation have been investigated with the method of electron spin resonance. Only one species of free radical was observed at room temperature. Analysis of the resonance leads to the conclusion that the free radical has the form RĊHOH and is probably

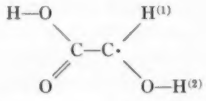

with the electron spin density concentrated mostly on the CH carbon. The radical was found to be very stable: Its ESR pattern was observed, essentially undiminished, for more than a year after the irradiation. The g factor was found to be only slightly anisotropic, with principal values: $g_u=2.0024$, $g_v=2.0048$, and $g_w=2.0047$. Couplings with two H nuclei are believed to be those indicated by $H^{(1)}$ and $H^{(2)}$, with principal elements of coupling, in gauss, of 15.7, 26.5, and 8.1 for $H^{(1)}$, and of 6.2, −0.3, and 8.3 for $H^{(2)}$. With irradiation and observation at 77°K, a different free radical was observed, one with hyperfine structure from only one H, similar to $H^{(2)}$.

INTRODUCTION

A STUDY of the electron spin resonance spectra is now an established method of investigating the free radicals produced by x or gamma irradiation. A large number of organic chemicals have been investigated in this laboratory in the powder form at room temperature as well as at low temperatures. Though the free radicals induced by the radiation can sometimes be identified, there is always an uncertainty in the conclusions drawn when anisotropy in the g factor or the nuclear hyperfine coupling constants occurs. On the other hand, if it is possible to make an analysis of the spectra obtained with the sample in the form of a single crystal, more information about the anisotropies in the g value and the hyperfine splittings can be obtained, and conclusions can be drawn with more assurance. Investigations on the anisotropic proton hyperfine splittings in ESR spectra of single crystals, though often difficult and involved, yield valuable information on the electronic structure. A number of irradiated single crystals have already been investigated by ESR. Miyagawa and Gordy have made an analysis of the N^{14} nuclear coupling in an irradiated single crystal of dimethylglyoxime[1] and of the anisotropic proton hyperfine splittings of an irradiated single crystal of alanine,[2] taking into consideration second-order transisitions also. Kurita and Gordy have made similar studies of irradiated single crystals of cystine dihydrochloride[3] and thiodiglycolic acid,[4] in which considerable electron spin density was found on the sulfur. Whiffen and his collaborators have obtained results for single crystals of glycine[5] and glycolic acid.[6] McConnell *et al.* have successfully analyzed the spectra of single crystals of malonic[7] and succinic acids.[8]

The present article describes a study of a single crystal of urea oxalate. While working on some of the substitution products of urea in the powder form, we found that urea oxalate when irradiated with gamma rays gave a spectrum with four hyperfine components which are almost symmetric. The radical is very stable at room temperature. We undertook the present investigation of the single crystal of the compound in the hope of finding the chemical form and structure of the free radical produced by the gamma irradiation.

EXPERIMENTAL DETAILS

Single crystals of urea oxalate were grown by slow evaporation of water from an aqueous solution of the compound. Crystals as large as 6×3×2 mm could be obtained. They are monoclinic prisms (space group C_{2h}^5-P21/c) flat on $\{010\}$. There is a perfect cleavage parallel to $\{20\bar{1}\}$. The crystallographic data given by Loschmidt[9] are $a:b:c=0.5642:1:0.4106$, $\beta_2=97°50'$; the dimensions of the unit cell are $a=7.02$, $b=12.42$, $c=5.08$ a.u. There are two molecules in the unit cell with the formula $2\,CO(NH_2)_2\cdot C_2H_2O_4$. The crystal is known to possess a layer structure with the molecules lying parallel to $\{20\bar{1}\}$ and linked together by means of hydrogen bonds.

The crystals were irradiated at room temperature with a kilocurie cobalt 60 gamma-ray source (24–48 hr). Experiments carried out at room temperature on an evacuated powdered sample have shown no oxygen

* This research was sponsored by the U. S. Air Force Office of Scientific Research.

† On leave from the Department of Physics, Andhra University, Waltair, India.

[1] I. Miyagawa and W. Gordy, J. Chem. Phys. **30,** 1590 (1959).
[2] I. Miyagawa and W. Gordy, J. Chem. Phys. **32,** 255 (1960).
[3] Y. Kurita and W. Gordy, J. Chem. Phys. **34,** 282 (1961).
[4] Y. Kurita and W. Gordy, J. Chem. Phys. **34,** 1285 (1961).
[5] D. K. Ghosh and D. H. Whiffen, Mol. Phys. **2,** 285 (1959).
[6] N. M. Atherton and D. H. Whiffen, Mol. Phys. **3,** 1 (1960).
[7] H. M. McConnell, C. Heller, T. Cole, and R. W. Fessenden, J. Am. Chem. Soc. **82,** 766 (1960).
[8] C. Heller and H. M. McConnell, J. Chem. Phys. **32,** 1535 (1960).
[9] Loschmidt, Sitzber. Akad. Wiss. Wien. **51,** 9 (1865).

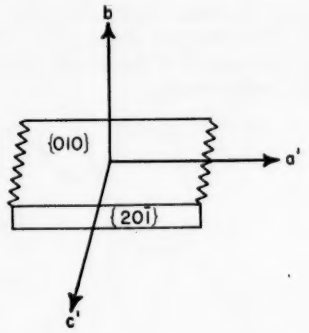

FIG. 1. The crystal form of urea oxalate and coordinate system employed.

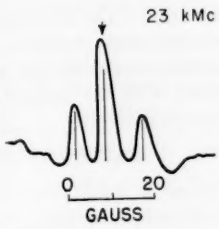

FIG. 3. Electron spin resonance spectrum of a γ-irradiated single crystal of urea oxalate with the static magnetic field parallel to b axis (23 kMc/sec).

effect on the spectra even weeks after the irradiation. Measurements have been made on a number of crystals at both 9 and 23 kMc/sec, and essentially the same spectra were obtained for corresponding orientations. The radical formed is found to be very stable, and samples gave the same spectra even after a lapse of a year after irradiation, with almost the same intensity.

The measuring apparatus consisted of a low-frequency (140 cps), magnetic modulation type spectrometer with a phase lock-in detector and amplifier tuned to the second harmonic of the modulation frequency synchronized with a gradual variation of the magnetic field through the resonance. The spectra, recorded on a Texas Instruments chart recorder with linear coordinate paper, are the second derivatives of the actual absorption curves.

The spectra were measured at regular intervals of 15° by a rotation of the crystal along three mutually perpendicular directions. The mount for holding the crystal in the microwave cavity was made of Teflon to which it was glued with silicone grease. At 9 kMc/sec the mount could be rotated around two perpendicular axes and graduated at every 5° around one and at every 15° around the other. The mount used at K band could be rotated around one axis only and graduated at every 5°. The accuracy of measurement of the angle is $\pm 2°$ at X band at $\pm 3°$ at K band. The calibration of the magnetic field was done with both Mn and DPPH samples which were placed close to the crystal on the mount.

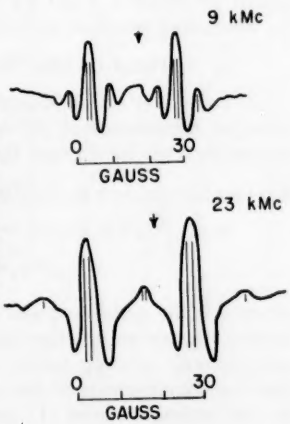

FIG. 2. Electron spin resonance spectra of a γ-irradiated single crystal of urea oxalate with the static magnetic field parallel to a' axis. The bars show the theoretical patterns. The arrows pointing downward indicate the position of DPPH line ($g=2.0036$). Upper pattern is for 9 kMc/sec and lower pattern is for 23 kMc/sec.

DESCRIPTION OF OBSERVED SPECTRA

For convenience of interpretation of the observed spectra in terms of the crystal structure, the coordinate system is chosen as shown in Fig. 1. The b axis is the same as the crystalline b axis and the a', c', axes lie in $\{010\}$, mutually perpendicular to each other. As the crystal is monoclinic, the two molecules in the unit cell are magnetically equivalent when the external magnetic field H is in $\{010\}$. The spectrum when H is in $\{010\}$ and parallel to the a' axis (Fig. 3) consists of two strong hyperfine lines separated by 26.5 gauss. This splitting was found to be the same within experimental error at both 9.04 and 23.05 kMc/sec. Each of the two strong lines has a pair of satellites symmetrically located on opposite sides of the main lines. The intensity of the satellite components relative to the main components decreases and their separation from the main components increases with increase in the observation frequency. The disposition of the satellites at 23 kMc/sec is also shown in Fig. 2; their intensity is only about 1/30 to 1/40 of that of the main hyperfine component and their separation from the main line is about 13 gauss.

Although the pattern at 23 kMc/sec consists of only one strong doublet for H parallel to the a' axis, upon a small rotation of 15° each line is again split into two close, equally intense components. At X band, as far as 45° from the a' axis, the lines are not split, perhaps because of the difference in second-order effects at the two frequencies. When H is parallel to the b axis the spectrum consists (Fig. 3) of three equally spaced lines with an intensity ratio of 1:2:1 and a separation of 8.2 gauss. The two protons giving rise to the hyperfine splitting seem to be equivalent for this orientation. For any other general orientation in this plane (rota-

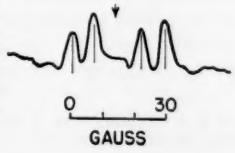

FIG. 4. Electron spin resonance spectrum of γ-irradiated single crystal of urea oxalate with the static magnetic field in bc' plane and at 60° with b axis (measured in the direction of c') (23 kMc/sec).

tion around the a' axis), the pattern consists of two nonequivalent doublets (Fig. 4). The spectra are generally complex for different orientations of the crystal with the applied field in the $a'b$ plane, i.e., for rotation about c'.

NATURE OF THE FREE RADICAL

From a qualitative examination of the observed patterns it is evident that the free radical has two proton spin moments which interact significantly with the electron spin moment. The coupling of both protons is anisotropic. With different orientations of the crystal in the magnetic field the splitting of one proton varies from 8–26 gauss, the other form <2–8 gauss.

In the undamaged crystal, molecules of urea and of oxalic acid are arranged in hydrogen-bonded layers

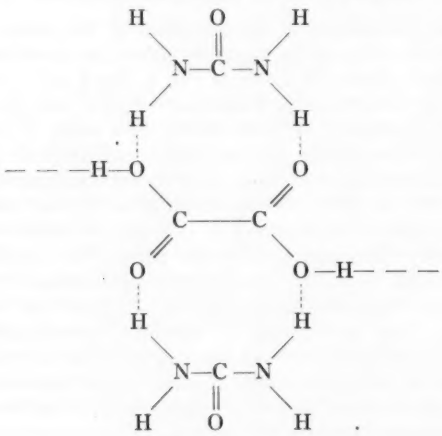

Unless there is chemical rearrangement, it is difficult to understand how from these molecules a free radical could be formed which could give the observed ESR patterns. There can be no significant electron spin density on the N atoms since no N^{14} coupling was detected. Hydrogens bonded to nitrogen could not give the observed anisotropic splittings without significant electron spin density on the N. Such spin density on the N^{14} would, in turn, lead to observable N^{14} splitting, which was not detected. Thus it seems clear that the spin density which gives rise to the anisotropic proton coupling must be concentrated either on a carbon or an oxygen atom.

One possible free radical which could give two protons with unequal anisotropic couplings is the hydrogen-bonded O–H free radical. This free radical could be formed simply by a breakage of a C—OH bond. However, both the anisotropy in g and the range of variation in the proton coupling are significantly less than those recently found for the OH free radical in irradiated ice by McMillan, Matheson, and Smaller.[10] Furthermore, it seems improbable that the OH free radical would be trapped in the preferred orientation required by the analysis of the present data. A positively charged free radical such as

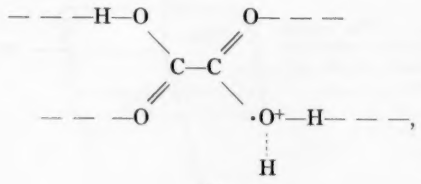

(I)

in which the spin density is concentrated on the O^+ atom, might conceivably give the observed proton splitting, but such a free radical would not likely have the long life required to account for this resonance which has been found to remain stable for at least a year.

As will be shown in the analysis given below, the principal elements of the coupling A for one of the protons and the g tensor is that expected for an electron spin density concentrated mainly on the carbon of a

fragment. It will be shown that the free radical

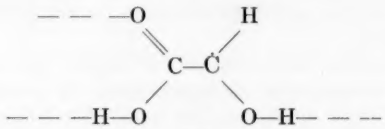

(II)

is entirely consistent with the observed results, although it is not readily apparent how this free radical might be formed by irradiation of the crystal.

It may be mentioned that the spectra obtained for the present free radical are very similar to those obtained by Whiffen *et al.*[6] for irradiated glycolic acid for which they proposed the radical HOĊHCOOH.

FIRST-ORDER TREATMENT

For many, but not all, orientations of the crystal the principal components of the resonance are accounted for satisfactorily by the spin Hamiltonian:

$$\mathcal{H}=(g_{ZZ}S_Z+g_{ZX}S_X+g_{ZY}S_Y)\beta H_Z+(A_{ZZ}^{(1)}I_Z^{(1)}+A_{ZX}^{(1)}I_X^{(1)}+A_{ZY}^{(1)}I_Y^{(1)})S_Z+(A_{ZZ}^{(2)}I_Z^{(2)}+A_{ZX}^{(2)}I_X^{(2)}+A_{ZY}^{(2)}I_Y^{(2)})S_Z, \quad (1)$$

where Z is the space-fixed axis along which the field is applied, the g's are the significant components of the spectroscopic splitting factor, and the A's are the significant components of the nuclear coupling tensor for the hydrogen nuclei (1) and (2). Terms such as

[10] J. A. McMillan, M. S. Matheson, and B. Smaller, J. Chem. Phys. **33**, 609 (1960).

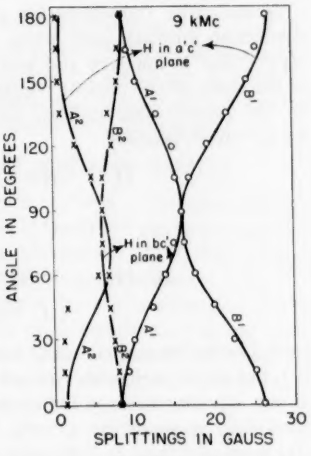

FIG. 5. Calculated (solid lines) and observed (⊙ or ×) splittings of the electron spin resonance spectra of irradiated urea oxalate single crystal at 9 kMc/sec. The curves marked A′ and B′ give the splittings of proton H^1 when the static magnetic field is in the bc' and $a'c'$ planes, respectively. The angle is measured from a' axis in the direction away from c' axis in bc' plane. The curves marked A^2 and B^2 give the splittings of proton H^2 for the corresponding orientations.

$A_{XX}M_XS_Y$ are not important for the strong fields employed in our experiments where, to a good approximation, S is quantized along the field direction Z. In the present treatment of the first-order transitions the nuclear paramagnetic terms $\beta_I g_I{}^{(1)}\mathbf{I}^{(1)}\cdot\mathbf{H}$ and $\beta_I g_I{}^{(2)}\mathbf{I}^{(2)}\cdot\mathbf{H}$ are not included in the spin Hamiltonian, although in the next section it is shown how one of these terms gives rise to observable second-order transitions for some orientations of the crystal in the applied field.

In the finding of the eigenvalues of $\mathfrak{H}$ it is convenient to treat the nuclear interaction as a perturbation upon the terms in g,

$$\mathfrak{H}=\mathfrak{H}^{(0)}+\mathfrak{H}'. \tag{2}$$

The eigenvalues of $\mathfrak{H}^{(0)}=(g_{ZZ}S_Z+g_{ZX}S_X+g_{ZY}S_Y)\beta H_Z$ are readily found to be

$$E^{(0)}=g\beta HM_S, \tag{3}$$

where

$$M_S=\pm\tfrac{1}{2}$$

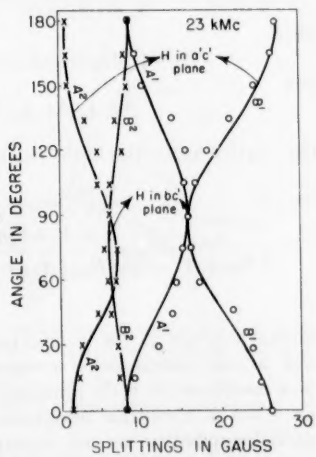

FIG. 6. Calculated and observed splittings as described for Fig. 5 but at 23 kMc/sec.

TABLE I. Principal elements and direction cosines for the hyperfine splittings of $H^{(1)}$.

Splitting tensor in $c'a'b$ axes system			Principal elements		Direction cosines with respect to $c'a'b$ axes system		
15.8	0.8	0	$A_x{}^{(1)}$	15.7	0.997	0.075	0.009
0.8	26.5	1.0	$A_y{}^{(1)}$	26.5	−0.074	0.996	0.060
0	1.0	8.2	$A_z{}^{(1)}$	8.1	0.006	0.998	0.055

and

$$g=(l^2g_u{}^2+m^2g_v{}^2+n^2g_w{}^2)^{\frac{1}{2}}, \tag{4}$$

where g_u, g_v, and g_w are the principal elements of the g tensor and where l, m, and n are the direction cosines which the respective elements make with the applied field H_Z.

Because of the small anisotropy in g, in comparison with that of the nuclear couplings, we can neglect the anisotropy in g when computing the eigenvalues of $\mathfrak{H}'$ and can employ $M_S=\pm\frac{1}{2}$ for the eigenvalues of S_Z. We then can express $\mathfrak{H}'$ as

$$\mathfrak{H}'=\pm\tfrac{1}{2}(A_{ZZ}{}^{(1)}I_Z{}^{(1)}+A_{ZX}{}^{(1)}I_X{}^{(1)}+A_{ZY}{}^{(1)}I_Y{}^{(1)})$$
$$\pm\tfrac{1}{2}(A_{ZZ}{}^{(2)}I_Z{}^{(2)}+A_{ZX}{}^{(2)}I_X{}^{(2)}+A_{ZY}{}^{(2)}I_Y{}^{(2)}). \tag{5}$$

The eigenvalues of $\mathfrak{H}'$ are then

$$E'=\pm(\tfrac{1}{2})A^{(1)}M_I\pm\tfrac{1}{2}A^{(2)}M_I{}^{(2)}, \tag{6}$$

where the positive sign corresponds to the upper ($M_S=\frac{1}{2}$) and the negative to the lower ($M_S=-\frac{1}{2}$) spin-state, and where for either nucleus A has the form

$$A=(A_{ZZ}{}^2+A_{ZX}{}^2+A_{ZY}{}^2)^{\frac{1}{2}}$$
$$=(l_{Z_z}{}^2A_z{}^2+l_{Z_x}{}^2A_x+l_{Z_y}{}^2A_y{}^2)^{\frac{1}{2}}, \tag{7}$$

in which A_z, A_x, and A_y are the principal elements of the nuclear coupling tensor of either nucleus (1) or (2) and where l_{Zz}, l_{Zy}, and l_{Zz} are the direction cosines of the respective elements with the space-fixed axis Z (direction of the applied field). By combining E^0 and E' and applying the selection rules $M_S=-\frac{1}{2}\rightarrow\frac{1}{2}$, one obtains

$$h\nu=g\beta H+A^{(1)}M_I{}^{(1)}+A^{(2)}M_I{}^{(2)}. \tag{8}$$

In the actual measurements the observation frequency was held constant and the magnetic field was varied

TABLE II. Principal elements and direction cosines for the hyperfine splittings of $H^{(2)}$

Splitting tensor in $c'a'b$ axes system			Principal elements		Direction cosines with respect to $c'a'b$ axes system		
6.0	−1.2	0	$A_x{}^{(2)}$	6.2	0.986	0.164	−0.117
−1.2	0	−0.7	$A_y{}^{(2)}$	−0.3	−0.186	0.975	−0.122
0	−0.7	8.2	$A_z{}^{(2)}$	8.3	0.047	0.091	0.995

TABLE III. Principal elements and direction cosines for g values.

	Principal elements	Direction cosines with respect to $c'a'b$ axes system		
g_u	2.0024	1	0	0
g_v	2.0048	0	1	0
g_w	2.0047	0	0	1

through the resonance. The g factor was measured relative to that for DPPH, for which $g_0=2.0036$. The relative field strength was then $H_0=(h\nu_0)/(g_0\beta)$. The separations of the hyperfine components were measured by comparison with known Mn^{++} hyperfine components of Mn^{++} impurity in ZnS.

Figures 5 and 6 show the measured positions of the principal hyperfine components of the resonance at different orientations of the crystal in the magnetic field. The principal elements of g and the A's are given in Tables I, II, and III. They were obtained by a process of adjustment of the coupling parameters for the best over-all agreement with the observations. The solid lines are the theoretical curves calculated from the principal elements shown in the tables.

SECOND-ORDER TRANSACTIONS

Second-order transitions corresponding to the simultaneous flipping of the electron and the nuclear spin were detected for the hydrogen nucleus having the weaker coupling, $H^{(2)}$. The theory for such second-order transitions has been worked out by Miyagawa and Gordy[2] for a coupling proton which has a significant first-order interaction (appreciable splitting for $\Delta M=0$), including an isotropic Fermi contact term, A_f. Trammell, Zeldes, and Livingston[11] have developed the corresponding theory for a hydrogen atom free radical where a nearby H nucleus, with which the free radical atom interacts only weakly through dipole-dipole coupling, flips simultaneously with the electron spin. The present second-order transitions for $H^{(2)}$, which has only a small Fermi contact term, represents an intermediate case. Although the proton $H^{(2)}$ is believed to be bonded to the free radical and although for some orientations it gives a first-order splitting ($\Delta M_I=0$) as large as 8 gauss, the first-order splitting by $H^{(2)}$ is too small to be resolved for the orientation of the magnetic field along the a' axis. For this orientation (see Fig. 2) satellites appear on opposite sides of each component of the strong doublet caused by $H^{(1)}$. This phenomenon is completely analagous to the flipping of a proton near a free H atom, treated by Trammell, Zeldes, and Livingston.[11] For the H along c', however, there are no detectable satellites, although $H^{(2)}$ gives rise to an additional doublet splitting of each component of the $H^{(1)}$ doublet. These features are accounted for by the theory of Miyagawa and Gordy.[2]

[11] G. T. Trammell, H. Zeldes, and R. Livingston, Phys. Rev. **110**, 630 (1958).

Second-order transitions for a given nucleus are of significant strength only when its off-diagonal term $A_{ZX}^2+A_{ZY}^2$ is not zero and when, in addition, A_{ZZ} is of the order of the nuclear paramagnetic term, $g_I\beta_I H_Z$. In the present free radical, believed to be of form $RCH^{(1)}OH^{(2)}$, possibly

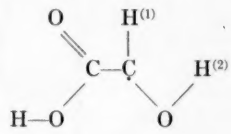

(III)

second-order transitions occur for nuclei both (1) and (2), but are of noticeable strength under the conditions of our experiments only for nucleus (2) when the applied field is along the a' axis. For this orientation, A_{ZZ} is smaller than $2g_I\beta_I H_Z$, also smaller than $(A_{ZX}^2+A_{ZY}^2)^{\frac{1}{2}}$. To simplify the discussion of this interesting case, we shall neglect the less pronounced second-order effects for nucleus (1). The appropriate spin Hamiltonian is obtained by the addition of the nuclear paramagnetic term, $g_I\beta_I I_Z^{(2)}H_Z$ to Eq. (1). Since the nuclear spin coordinates of (1) and (2) are independent, we can solve the secular equation for nucleus (2) separately and can then add the results of the first-order splitting already obtained for nucleus (1). This secular equation has already been solved by Miyagawa and Gordy,[2] and the relative intensities of the first- and second-order transitions have been calculated. We shall employ their solutions.

When there are second-order transitions, a single hydrogen nucleus gives rise to a pair of doublets rather than to a single doublet, although both doublets may not be of resolvable separation nor of detectable intensity. The separations of the two doublets, in magnetic field units, are

$$d_+=(A_++A_-)/2 \tag{9}$$

and

$$d_-=(A_+-A_-)/2, \tag{10}$$

where

$$A_\pm=\{(A_{ZZ}\pm 2g_I\beta_I H_Z)^2+c^2\}^{\frac{1}{2}} \tag{11}$$

and

$$c^2=A_{ZX}^2+A_{ZY}^2. \tag{12}$$

The relative intensities of the two doublets are given by

$$I_{d-}/I_{d+}=\frac{c^2(A_+-A_-+4g_I\beta_I H_Z)^2}{\{(A_{ZZ}+A_--2g_I\beta_I H_Z)(A_{ZZ}+A_++2g_I\beta_I H_Z)+c^2\}^2}. \tag{13}$$

For nucleus (2) at the a' orientation, $A_{ZZ}\ll 2g_I\beta_I H_Z$, even at the lowest field strength employed. Under these conditions, d_- is the principal, or stronger, doublet but is not of resolvable separation. Since $2g_I\beta_I H_Z$ is a calculable quantity, we can, nevertheless, use d_+ and a

comparison of the intensity of the resolved d_+ and the unresolved d_- with these equations to calculate approximate values of the coupling constants for Z along a'. Figure 2 shows a comparison of the observed spectra with the patterns calculated with this theory.

STRUCTURE OF THE FREE RADICAL

The principal elements of the spectroscopic splitting factor of the coupling of $H^{(1)}$ and $H^{(2)}$ are those expected for the planar free radical shown in Fig. 7. The orientation of the free radical in the figure is chosen so that its parts which are common to the undamaged oxalic acid molecule have the same positions as in the unirradiated crystal. The newly formed $CH^{(1)}$ group is oriented along A_z, the principal axis of minimum coupling for $H^{(1)}$, as would be expected from theoretical considerations. The $CH^{(1)}$ bond then makes angles of about 120° with the CC and C—O bonds, as would be expected for planar sp_2 hybrid orbitals. The orientation of the $OH^{(2)}$ group, not necessarily the same as that in the undamaged molecule, is chosen in the plane of the molecule with the reasonable COH angle of 100°. Of the two possible orientations, *cis* and *trans*, which have this COH angle, we have chosen the one suggested by the $H^{(2)}$ coupling elements on the assumption that this coupling arises primarily from the dipole-dipole interaction with the spin density on the $CH^{(1)}$ carbon.

The $H^{(1)}$ coupling has an isotropic component A_f the magnitude of which is $(A_x+A_y+A_z)/3=17$ gauss. From this we can estimate the spin density on the $CH^{(1)}$ carbon from the relation[7] $\rho_C=A_f/Q$, in which the magnitude Q can be taken as 25 gauss. Thus for the present case $\rho_C=17/25=0.7$. Both Q and A_f are known to be negative in sign.[7]

McConnell and Strathdee[12] have calculated the pure dipole-dipole coupling of a CH hydrogen nucleus with an electron entirely in a p orbital ($\rho_C=1$) on the carbon. They obtain the values: +15.6 gauss along the CH bond, −1.7 gauss along the p orbital, and −13.9 gauss for the direction perpendicular to both the CH bond and the p orbital. For agreement with $\rho_C=0.7$ we must reduce these values by 30%, and for comparison with the observed principal elements $A^{(1)}$ we must add to them the Fermi component, $A_f=-17$ gauss. The resulting semitheoretical values,

$$A_x=17.3, \qquad A_y=25.7, \qquad A_z=5.4, \quad \text{in gauss,}$$

are found to be in good agreement with the observed principal coupling element for $H^{(1)}$ listed in Table I. This agreement seems to justify our assumption of a free radical with the CH group. Furthermore, the direction of the CH bond as determined by the axis of the minimum coupling element A_z conforms to a reasonable structure for the free radical. See Fig. 7.

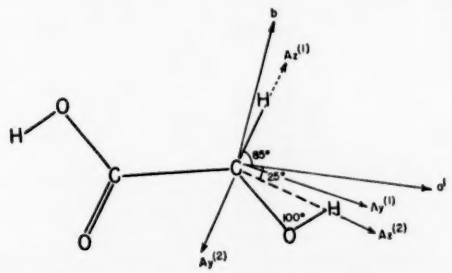

FIG. 7. Proposed structure for the free radical showing directions of the principal axes $A_z^{(1)}$ and $A_z^{(2)}$ relative to the crystalline axes. The structure is assumed to be planar. The $A_y^{(1)}$ and $A_y^{(2)}$ axes lie in the plane of the figure and normal to $A_z^{(1)}$ and $A_z^{(2)}$, respectively, while $A_x^{(1)}$ and $A_x^{(2)}$, not shown, are normal to the plane of the figure.

[12] H. M. McConnell and J. Strathdee, Mol. Phys. **2**, 129 (1959).

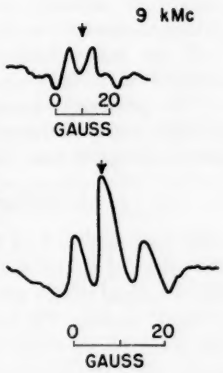

FIG. 8. Electron spin resonance spectra of an irradiated single crystal of urea oxalate at 77°K when the static magnetic field is parallel to the b axis (9 kMc/sec). Upper curve is at 77°K. Lower curve is obtained for the same orientation after warming to room temperature for 24 hr.

The coupling elements of $H^{(2)}$ are smaller than those of $H^{(1)}$ and their origin is less certain. If the assumed model is the correct one, the $H^{(2)}$ coupling would probably arise from a combination of the dipole-dipole interaction of the spin densities on the $CH^{(1)}$ carbon and the $OH^{(2)}$ oxygen combined with a Fermi constant interaction caused by a very small spin density on the $H^{(2)}$ hydrogen. Although the spin density on the oxygen would certainly be very much smaller than that on the C, its effects may not be negligible because of the small OH distance, 0.97 A.

If it is assumed that the coupling of $H^{(2)}$ arises entirely from dipole-dipole interaction with ρ_C, one can estimate the relative intensity of the satellites for the a' orientation with the dipole-dipole theory of Trammell, Zeldes, and Livingston.[11]

$$\text{Rel. int.}=(\tfrac{9}{8})\rho_C(g\beta/H)(\sin^2\theta\cos^2\theta)/r^6. \qquad (14)$$

In our example, r can be taken approximately as the C—$H^{(2)}$ distance (1.74 A) and $\theta=25°$ as the angle between C—$H^{(2)}$ and the crystalline axis a' in the model of Fig. 7. With these assumptions the intensity of the satellites is estimated to be about 20% that of the principal components at 9 kMc/sec and about 3% of the principal components at 23 kMc/sec. These values are in reasonable agreement with the observation (compare with Fig. 2). However, as will be described below, we must assume a small Fermi constant com-

ponent to account satisfactorily for the observed principal elements in the coupling.

If the pure dipole-dipole interaction between ρ_C and $H^{(2)}$ is the only significant interaction of $H^{(2)}$, one of the principal elements should be directly along $C—H^{(2)}$ and would have the approximate value +7.4 gauss estimated from the formula[13]

$$A_\mu = (28\rho_C/r^3)(3\cos^2\theta+1)^{\frac{1}{2}}, \qquad (15)$$

with $\theta=0$ and $r=1.74$ A. At right angles to $C—H^{(2)}$ the principal values would be equal, −3.7 gauss, with this simplified theory which assumes the ρ_C concentrated at the C nucleus. The values are not in agreement with the observed principal values +0.3, −8.3, and −6.2 gauss, but can be brought into fair agreement by the addition of an isotropic Fermi component, $A_f=-4.7$. The possible origin of a negative Fermi component suggests a significant positive spin density on the $OH^{(2)}$ oxygen. This would lead also to an additional dipole-dipole interaction with $H^{(2)}$ and a shift in the direction of the principal axis from that caused by ρ_C. Probably, therefore, the small $H^{(2)}$ coupling arises from at least two or three different interactions, all of comparable magnitude.

[13] H. Zeldes, G. T. Trammell, R. Livingston, and R. W. Holmberg, J. Chem. Phys. **32,** 618 (1960).

OBSERVATIONS AT 77°K

When irradiated and observed at the temperature of liquid nitrogen, 77°K, urea oxalate was found to give an ESR pattern (Fig. 8) of only one coupling proton, one which causes a splitting similar to that of $H^{(2)}$ in the free radical II produced at room temperature. This suggests that the free radical observed at 77°K may be the negatively charged one,

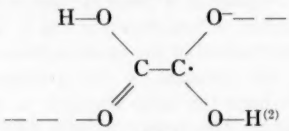

(IV)

in which the $H^{(2)}$ should have a coupling similar to that of $H^{(2)}$ in the free radical II. If so, radical IV is probably the precursor of the free radical observed at room temperature. Because of the atomic rearrangement required to form radical II it would certainly not be expected to occur at a temperature of 77°K.

ACKNOWLEDGMENTS

We wish to thank Dr. Mikio Katayama for valuable discussions. One of the authors (D.V.G.L.N.R.) is grateful to the United States Educational Foundation in India for awarding him a Fulbright travel grant.

Letters to the Editor

THE Letters to the Editor section is subdivided into three parts entitled Communications, Comments and Errata, and Notes. These three sections are all subject to the same limitations on length. The textual material of each Letter is limited to a number of words equal to 950 minus the following: (a) 200 words for each average-sized figure; (b) 50 words for each displayed equation; (c) 7 words for each line of table including headings and horizontal rulings. No proof will be sent to the authors of "Communications" and "Comments and Errata." Proof will be sent to the authors of "Notes." The publication charge for Letters is $30 per page, with a minimum of $30 per Letter. If honored, the Institution will be entitled to 100 reprints without covers. See issues of May–September, 1957, for descriptions of categories.

Communications

Normal Vibrations and Raman Spectrum of Polyoxymethylene

HIROYUKI TADOKORO, AKIRA KOBAYASHI, YÔICHI KAWAGUCHI, SHIGENOBU SOBAJIMA, AND SHUNSUKE MURAHASHI

Department of Polymer Science, Faculty of Science, Osaka University, Nakanoshima, Osaka, Japan

AND

YOSHIKI MATSUI

Research Laboratory, Shionogi and Company, Ltd., Imafuku, Amagasaki, Japan

(Received May 1, 1961)

IN the previous papers the method of calculation of the normal vibrations of helical polymer molecules, the skeletal vibrations of polyoxymethylene (POM),[1] and a simple method of factoring of the secular equations for helical molecules under the factor group $D(2m\pi/n)$[2] have been reported. Therefore we have studied the normal vibrations of POM by use of these methods, and have obtained fairly good results.

The fiber identity period of POM (17.3 A) contains nine chemical units —CH_2O— and five turns.[3] For simplicity we assumed whole bond angles $=109°28'$ and the internal rotation angles $=78°$. The C—O and C—H bond lengths were taken as 1.43 and 1.09 A, respectively. The Urey-Bradley field[4] was used and torsional coordinates were omitted. The values of force constants $K_{CH}=4.07$, $K_{CO}=3.25$, $H_{HCH}=0.4$, $H_{COC}=0.5$, $H_{OCO}=0.3$, $H_{OCH}=0.25$, $F_{CC}=0.43$, $F_{OO}=0.8$, $F_{OH}=0.6$, $F_{HH}=0.1$ md/A, $F'=-0.1$ F, and $\kappa=0.05$ md·A, have been determined[5] so as to explain the observed infrared[6] bands (the A_2 and E_1 species). Then the vibrations of the Raman active A_1 species were calculated by using these values. The results are given in Table I, which shows fairly good agreement between the observed and calculated frequencies. The maximum and average deviations are 6.5 and 2.0%, respectively. The table also gives the potential energy distributions among the symmetry coordinates.[7] The signs denote the phase relations of the coupling.

The dichroism and intensity of the bands can be interpreted well by the present assignments. The 1235-cm^{-1} band was found to be strongly crystallization sensitive from the spectra measured at various temperatures. This fact may be interpreted by the complicated coupling assigned to this band, which is probably characteristic of the helical structure of POM and should disappear above the melting point. The

TABLE I.

Species	Observed frequency (cm^{-1}) Infrared[6,7]	Raman	Calculated frequency (cm^{-1})	Assignments[a] (Potential energy distribution %)
			2935	$\nu_s(CH_2)$
		1493 w	1481	$\delta(CH_2)$
A_1	Inactive	1344 vw	1297	$t(CH_2)\,(95)-\nu_s(COC)\,(4)$
		919 m	916	$\nu_s(COC)\,(85)-\delta(OCO)\,(8)$
			549	$\delta(COC)\,(59)-\delta(OCO)\,(40)$
	2978(π) s		2967	$\nu_a(CH_2)$
	1381(π) m		1430	$w(CH_2)$
A_2	1097(π) vvs	Inactive	1136	$\nu_a(COC)\,(84)+r(CH_2)\,(16)$
	903(π) vvs		944	$r(CH_2)\,(81)-\nu_a(COC)\,(19)$
	2979(σ) s		2967	$\nu_a(CH_2)$
	2919(σ) s		2935	$\nu_s(CH_2)$
	1471(σ) m		1478	$\delta(CH_2)$
	1434(σ) w		1428	$w(CH_2)\,(89)+\nu_s(COC)\,(10)$
	1286(σ) vw		1282	$t(CH_2)\,(91)+\nu_a(COC)\,(8)$
E_1	1235(σ) vs	1229 vvw	1155	$r(CH_2)\,(50)-\delta(COC)\,(25)+\nu_s(COC)\,(24)$
	1091(σ) vvs	1091 vvw	1060	$\nu_a(COC)\,(81)-\delta(OCO)\,(11)$
	932(σ) vvs	929 sh	926	$\nu_s(COC)\,(73)-r(CH_2)\,(25)$
	630(σ) s		615	$\delta(OCO)\,(90)+\nu_a(COC)\,(8)$
	455(σ) m		467	$\delta(COC)\,(76)+r(CH_2)\,(23)$

[a] π, parallel band; σ, perpendicular band; ν_s, symmetric stretching; ν_a, antisymmetric stretching; δ, bending; w, wagging; t, twisting; r, rocking.

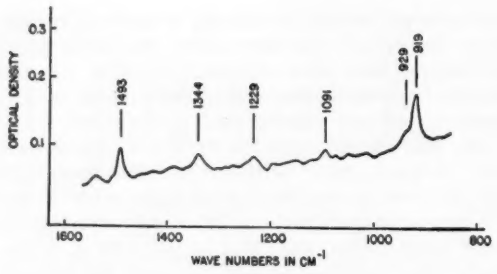

FIG. 1.

630- and 455-cm^{-1} bands were found to exhibit a small and a large shifts (to 618 and 363 cm^{-1}), respectively, in the deuterated spectrum.[8] The calculated values for the deuterated polymer with the same force constants are 597 [δ(OCO)(87%)+ν_a(COC)(8)] and 363 cm^{-1} [δ(COC)(64)+r(CD_2)(36)], respectively. Thus the feature of these shifts can be satisfactorily explained.

In Fig. 1 is reproduced the Raman spectrum (microphotometer curve) of POM (powder sample of paraformaldehyde) taken by using the Hg$-e$ line and $NaNO_2$ aqueous solution filter.[9]

The detailed report will be published soon.

[1] H. Tadokoro, J. Chem. Phys. **33,** 1558 (1960).
[2] H. Tadokoro, J. Chem. Phys. (to be published).
[3] H. Tadokoro, T. Yasumoto, S. Murahashi, and I. Nrtta, J. Polymer Sci. **44,** 266 (1960).
[4] T. Simanouti, J. Chem. Phys. **17,** 245 (1949).
[5] These values are in good agreements with those determined independently by Y. Kanazawa for dimethyl ether (K_{CH}=4.3, K_{CO}=3.2, H_{HCH}=0.45, H_{COC}=0.49, H_{OCH}=0.22, F_{CC}=0.18, F_{OH}=0.9, F_{HH}=0 md/A, and κ=−0.04 md·A). Bull. Chem. Soc. Japan (to be published).
[6] H. Tadokoro, T. Yasumoto, G. Morimoto, and S. Murahashi, Chem. High Polymers (Tokyo) **17,** 95 (1960).
[7] Novak and Whally, Trans. Faraday Soc. **55,** 1484 (1959).
[8] Y. Morino and K. Kuchitsu, J. Chem. Phys. **20,** 1809 (1953).
[9] Commercial samples (Delrin-acetal resin) have given only poor spectra probably because of the fluorescence.

Electron Spin Resonance Spectra of Free-Radical Intermediates Formed by Reaction of Polystyrene with Atoms of Hydrogen and Deuterium*

R. B. INGALLS

Atomics International, Canoga Park, California

AND

LEO A. WALL

National Bureau of Standards, Washington 25, D. C.

(Received March 30, 1961)

KNOWLEDGE of the concentrations and identities of free-radical and atom intermediates during reaction between gaseous atoms and organic liquids or polymers is important for the elucidations of the mechanisms of radiolytic and photolytic reactions in such materials. Although electron spin resonance is quite sensitive and the obvious spectrometric means for the study of free radical intermediates, methods for obtaining sufficient concentrations of reactive intermediates in the microwave cavity are needed. In this note a method for investigating the reaction of hydrogen atoms and deuterium atoms with polystyrene will be described and the spectra obtained discussed. The method hinges on the fact that, by freeze-drying[1] benzene solutions of polystyrene and many other polymers, extremely finely divided fibrous fluffs can be formed. These fluffs can be placed in a tube passing through the cavity of an ESR spectrometer and will remain in place. By connecting the tube to an electric discharge tube for the production of hydrogen atoms a stream of atoms mixed with hydrogen molecules can be swept through the fluff at low pressures.

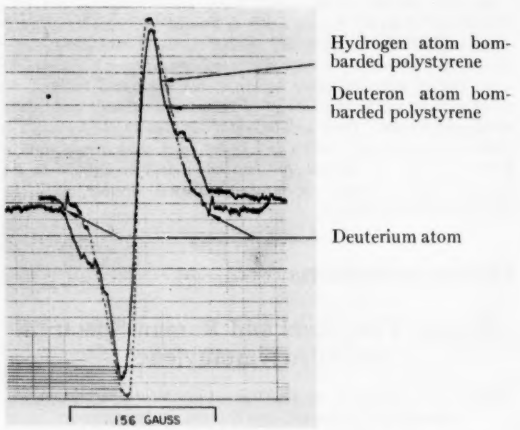

FIG. 1. ESR spectra produced by bombarding polystyrene with hydrogen and with deuterium atoms.

The spectra obtained (see Fig. 1) would be quite difficult to obtain under ordinary circumstances because the half-depth of hydrogen atom penetration[2] into an aromatic liquid or solid at room temperature is probably about 10^{-5} cm. Thus, a poor filling factor in the expression for the intensity of an ESR signal would result from the use of bulk material. In the technique described sufficient accessibility of the polymer molecules to the atoms is created so as to obtain an observable number of free-radical intermediates. This fluff is like a frozen gas in that the polymer molecules are suspended in space, and the material may be so finely divided that the atom reaction is not diffusion controlled in any way. The reaction differs from a gas phase reaction in that the radicals are not pumped out of the cavity but allowed to accumulate until a detectable number is obtained. The technique permits the direct observation of free-radical intermediates during a reaction and should therefore prove quite useful in the

study of certain elementary reactions in many heterogenous systems.

The spectrum (see Fig. 1) obtained with hydrogen atoms differs considerably from that obtained with deuterium atoms. With hydrogen atoms the spectrum is very much the same as that found in gamma-irradiated polystyrene[3] under conditions of partial power saturation. At lower power, however, the shoulders in the spectrum were more distinct.[3] The spectrum found with deuterium atoms is considerably sharper than the other and shows no signs of structure. The two outermost lines of the spectrum of deuterium atoms alone are shown. Similar lines of the hydrogen-atom spectrum are at spacings outside the span of Fig. 1.

The differences between the two spectra give striking evidence that the observed polymer radicals are not produced by abstraction reactions alone. At first sight the results appear to imply that the hydrogen or deuterium atoms are incorporated into the radicals that are formed. This supports the hypothesis that the radicals are formed by addition of the atoms to the aromatic rings. An alternative view that appears possible is that both abstractions and additions are occurring. An isotope effect may then shift the relative rates of these reactions and hence significantly change the relative concentrations of the possible radicals, or sufficient deuterium is incorporated into the polymer so as to alter the spectrum prior to detection of the spectrum. The kinetics of the formation and reactions of these radical intermediates are also being studied and will be reported later.

* Based in part on work supported by the Atomic Energy Commission.

[1] F. M. Lewis and F. R. Mayo, Ind. Eng. Chem. Anal. Ed. **17,** 134 (1945).

[2] R. B. Ingalls and J. R. Hardy, Can. J. Chem. **38,** 1734 (1960).

[3] R. E. Florin, L. A. Wall, and D. W. Brown, Trans. Faraday Soc. **56,** 1304 (1960).

Comments and Errata

Energy and Free Energy of Cohesion*

BRUNO LINDER

Department of Chemistry, The Florida State University, Tallahassee, Florida

(Received April 17, 1961)

IN various problems dealing with bulk properties of matter there is a need for knowing the total interaction potential of the system. The latter can, in principle, be determined from pair-interaction potentials and molecular distribution functions, but quite often the total potential is calculated from some macroscopic property of the system. Thus, the interaction potential is often equated to the negative of the energy of vaporization, the assumption being made that the molecular rotations, vibrations, and translation are the same in the liquid as in the gas phase. One can object to this procedure on the basis of these assumptions alone, but even if these conditions were satisfied there is still no assurance that the energy of vaporization would correctly give the interaction potential. For the potential has clearly the nature of a *free energy function*,[1] whereas the energy of vaporization is an *energy function* in the thermodynamic sense and ought to be related to the energy of cohesion. In order to make the distinction clear we shall call the interaction potential the free energy of cohesion. The difference between energy and free energy of cohesion is well recognized in problems dealing with noncentral forces,[2] but is generally ignored when only central forces are being considered. Yet, as was pointed out by Rushbrooke several years ago,[1] the problem will arise whenever the energy levels of an assembly are temperature dependent or can be so considered. Temperature-dependent energy levels come about as a result of preliminary averaging over states. The total interaction potential of a condensed phase has this property.

TABLE I. Energy and free energy of cohesion at 25°C in kcal/mole.

Substance	Free energy of cohesion F_c	Energy of cohesion E_c	Experimental energy of vaporization ΔE^{vap}
benzene	5.32	6.61	7.39
cyclohexane	4.36	5.45	7.30
carbon tetrachloride	5.65	6.92	7.23
stannic tetrachloride	6.47	7.86	8.95

In a previous article,[3] an expression was derived which relates the interaction potential of liquid to the dielectric constant and other molecular prameters. The quantity so obtained (which was termed total potential energy and denoted by the symbol U_l) is clearly a free energy function, for it was derived from the work done in bringing a molecule (treated as a harmonic oscillator) from empty space inside a dielectric. It has the form

$$U_l = -\tfrac{1}{8} N\gamma \langle m_0^2 \rangle_{Av} g \qquad (1)$$

where N is Avogadro's number, $g = 2\epsilon - 2/(2\epsilon+1)a^3$ with ϵ and a being, respectively, the dielectric constant and cavity radius; $\langle m_0^2 \rangle_{Av}$ is the average square of the instantaneous dipole moment; and γ a numerical factor. For the classical oscillator $\langle m_0^2 \rangle_{Av} = 3kT\alpha$ and $\gamma = \frac{1}{2}$; for the quantum oscillator $\gamma = \frac{1}{4}$ and $\langle m_0^2 \rangle_{Av}$ may be approximated by $\langle m_0^2 \rangle_{Av} \approx \frac{3}{2} I\alpha$, where I is the ionization potential and α the polarizability. Values for U_l computed for several liquids on the basis of the quantum-mechanical values for $\langle m_0^2 \rangle_{Av}$ are listed in Table II of reference 3 along with the experimental energies of vaporization ΔE^{vap}.

In the present note, we shall compute the cohesion

energy, which is the relevant quantity to be compared with the energy of vaporization, by making use of the Gibbs-Helmholtz equation $\partial(F_c/T)/\partial(1/T)=E_c$. (The cohesive free energy obtained from Eq. (1) is strictly the Helmholtz free energy but pv is so small for ordinary liquids that F_c may be used indiscriminantly for Gibbs and Helmholtz free energies.)

Table I lists the cohesive energies and free energies of some nonpolar liquids. The calculations are based on refractive indices for the Na$-D$ line measured at the temperatures 25°, 35°, and 45°C.[4] The $\langle m_0^2\rangle_{Av}$ values were obtained from ionization potentials ($\langle m_0^2\rangle_{Av}\approx\frac{3}{2}I\alpha$) and the a^3's were calculated from the molar volumes $[V=(4\pi/3)Na^3]$ at 25°C and assumed to be constant. The a^3 values so obtained are very close to the values that would be obtained from the Böttcher[5] equation $(\epsilon-1)(2\epsilon+1)V/g\epsilon=(4\pi/3)N\alpha/1-\alpha g$ by the use of gaseous molar refractions for the determination of α and the measured refractive indices to obtain ϵ. It is seen that the energy of cohesion and free energy of cohesion differ considerably.

In the present scheme we have calculated energies of cohesion from given $\langle m_0^2\rangle_{Av}$ values and the temperature variation of n^2. The converse procedure provides a means for obtaining effective $\langle m_0^2\rangle_{Av}$ values, which could then be used in other connections.

* Supported by a grant from The Petroleum Research Fund administered by the American Chemical Society.

[1] G. S. Rushbrooke, Trans. Faraday Soc. **36,** 1055 (1940).
[2] J. S. Rowlinson, Mol. Phys. **1,** 414 (1958).
[3] B. Linder, J. Chem. Phys. **33,** 668 (1960).
[4] P. J. Karabatsos and B. Linder (to be published).
[5] C. J. F. Böttcher, *Theory of Electric Polarization* (Elsevier Publishing Company, New York, 1952), pp. 205–212.

Notes

Infrared Spectroscopic Study of the Photolysis of Chlorine Azide in Solid Argon at 4.2°K*

DOLPHUS E. MILLIGAN

Mellon Institute,
Pittsburgh, Pennsylvania

(Received March 15, 1961)

THE photolysis of chlorine azide (ClN_3) in solid argon has been studied using infrared spectroscopic detection. These experiments were undertaken in hope of producing the chloroimino radical (ClN) under conditions suitable for infrared spectroscopic study.

Chlorine azide was prepared according to the method of Raschig.[1] After several rather violent explosions all attempts to purify samples of ClN_3 were abandoned. The gaseous material was dried with anhydrous magnesium perchlorate and mixed with sufficient argon to give mixtures of the desired mole ratio.

The low-temperature cell used in these experiments is similar in design to one which has been described previously.[2] Spectral measurements were made on Perkin-Elmer model 13 and 112G spectrometers. A medium-pressure mercury lamp (GE AH-4) without the Pyrex envelope was used for sample irradiations. The radiation was condensed by means of a fused quartz lens and focused on the solid deposits through a KBr window. The gaseous mixtures of ClN_3 and argon were deposited on a CsBr window (equipped with a copper-constantan thermocouple) maintained at 4.2°K. Experiments were carried out at mole ratios of argon to chlorine azide of 200, 300, 400, and 500. The mole ratios given here should be considered as lower limits in view of our uncertainty as to the purity of the samples. However, these estimates are considered to be fairly reliable in that infrared spectra of the deposits indicate no significant amount of impurities other than a small amount of HN_3. In each experiment the volume of gaseous mixture deposited was adjusted to give on the order of 40 μmole of ClN_3.

Four strong bands (655, 723, 1143, and 2062 cm^{-1}) are found in the spectrum of ClN_3 in solid argon. A weak band is observed at 2137 cm^{-1}. The bands at 2062, 1143, and 655 cm^{-1} are associated with vibrations of the N_3 group. The 723-cm^{-1} band is most likely associated with the N–Cl stretching vibration.

On irradiation the strong bands are observed to decrease in intensity whereas the 2137-cm^{-1} band remains unchanged. The behavior of the 2137-cm^{-1} band indicates that it is due to an impurity, most likely HN_3. New bands are observed to develop at 818±0.5 and 824±0.5 cm^{-1}. These bands grow continuously during irradiation, that is, until all of the ClN_3 is decomposed. Observation of the irradiated deposits after the ultraviolet light is extinguished indicate a greenish-blue phosphorescence emanating from the sample and surrounding copper block. The phosphoresence persists for several minutes after the lamp has been turned off.

In each of the experiments spectral scans were made during slow warmup of the irradiated deposits from 4.2 to 45°K. The bands at 818 and 824 cm^{-1} begin to decrease in peak intensity at a temperature near 20°K and eventually disappear near 40°K. The greenish-blue phosphoresence reappears on warmup near 20°K and persists until the temperature of the deposit reaches approximately 40°K. Spectra recorded after slow warming of the deposits to approximately 45°K and recooling to 4.2°K indicate the absence of the 818- and 824-cm^{-1} bands. No new bands are observed after diffusion.

In one experiment, spectra of ClN_3 and the ClN_3 photolysis product were examined under high spectral resolution in order to obtain accurate frequency and peak-intensity measurements. Under higher resolution a shoulder is observed on the low-frequency side of the 818-cm^{-1} band. The ratio of the peak intensities of the 824- and 818-cm^{-1} bands without correction for absorption due to the shoulder is found to be of the order of 2.

On subtracting the estimated contribution of the shoulder from the peak intensity of the 818-cm^{-1} band the ratio is found to range between 2.5 and 2.7. It should be remarked here that the shoulder appears to be more pronounced in experiments where diffusion is suspected, which suggests that it is due to absorption by a secondary product.

The behavior of the 818- and 824-cm^{-1} bands on diffusion indicates that they are associated with reactive or unstable species. The frequency separation between the bands agrees to within a wave number with the frequency separation calculated for $N^{14}Cl^{37}$, assuming one of the bands is due to NCl. The intensity ratio of the $N^{14}Cl^{35}$ and $N^{14}Cl^{37}$ bands should be of the order of three whereas the peak intensity ratio is found to range between 2.5 and 2.7, using the most conservative estimates of the contribution of the shoulder to the peak intensity of the 818-cm^{-1} band. The several pieces of information appear to argue strongly for the assignment of these bands to $N^{14}Cl^{35}$ and $N^{14}Cl^{37}$.

Failure to observe new spectral features after the irradiated deposits are allowed to diffuse could be due to a low concentration of product species or possibly to instability of these species. Under the conditions employed here dimerization of NCl to dichlorodiazine (N_2Cl_2) is expected to be the principal reaction. The greenish-blue phosphoresence observed immediately after irradiation and during diffusion is quite reminiscent of the greenish-blue emission observed during deposition and warmup of discharged nitrogen condensed at 4.2°K. It is quite possible that the emission observed here is associated with the formation or decomposition of N_2Cl_2.

* This research was supported in part by the U.S. Air Force through the Air Force Office of Scientific Research of the Air Research and Development Command.

[1] F. Raschig, Ber. deut. chem. Ges. **41**, 4194 (1908).
[2] E. D. Becker and G. C. Pimentel, J. Chem. Phys. **25**, 224 (1956).

Infrared Spectrum and Molecular Configuration of Glutaronitrile

IKUO MATSUBARA

Central Research Laboratories, Toyo Rayon Company, Ltd. Otsu, Shiga-ken, Japan

(Received February 13, 1961)

THE infrared spectrum in the 1500~400 cm^{-1} region of glutaronitrile, NC-$(CH_2)_3$-CN, in both the liquid and crystalline solid states has been studied. A low-temperature transmission cell of the type described by Nukada[1] has been used to obtain the spectrum in the solid state.

The liquid-state spectrum of glutaronitrile shows a complex feature which may be ascribed to the existence of a number of rotational isomers [Fig. 1(a)]. There are four possible spectroscopically distinguishable rotational isomers, *TT*, *TG*, *GG*, and *GG'*.[2] However, the *GG'* isomer (symmetry C_s) will not be considered here, because it must be very unstable for steric reasons. Only one of these isomeric forms is expected to exist in the crystalline solid state. It is interesting to note, however, that this compound forms two different crystalline solid phases, depending on the mode of crystallization. The first, metastable form is obtained by cooling the liquid rapidly down to −60°C. The marked simplification of the spectrum which results from the crystallization of the liquid is clearly shown in Fig. 1(b). When the solid is warmed up to about −40°C a considerable modification of the spectrum is observed, which remains unchanged after the specimen is recooled down to −60°C, showing that an irreversible transition to a second, more stable crystalline form has taken place [Fig. 1(c)].

The possibility that glutaronitrile takes the *TT* form in either of the two solid phases can be excluded from the following reasons:

(1) The relatively strong band observed at 737 cm^{-1} in the liquid-state spectrum, which certainly corresponds to the CH_2 rocking vibration of the methylene chain of the planar all-*trans* configuration,[3] has disappeared in both cases.

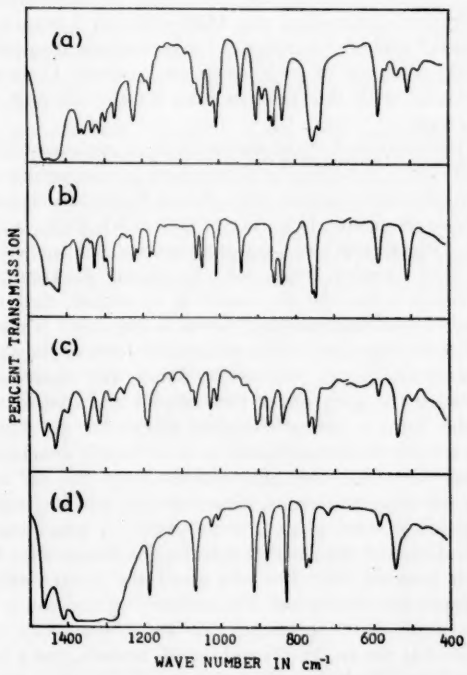

FIG. 1. Infrared spectra of glutaronitrile in various states. (a) liquid; (b) solid (metastable form); (c) solid (stable form); (d) copper(I) complex (in Nujol).

TABLE I. Assignments of the infrared bands of glutaronitrile in the 1500~400 cm^{-1} region.

	Complex[a]	*GG*[b]	*TG*[b]	*TT*[c]
CH_2 bending		1460	1451	
	1414	1433	1420	
CH_2 wagging		1350	1364	
		1316	1328	
		1250	1289/82	
CH_2 twisting	1271	1287/79	1300	
	1188	1190	1224/14	
	1130	1125	1181/74	
CH_2 rocking	913	903	943	
	830	837	839/35	
	778/67	768/54	757/51	737
C—C stretching	1066	1065	1060	1056
	1027	1026	1045	998
	1009	1010	1009	
	880	873	859	888
C—C—C bending	586	588	586	565
	544	537	511	481

[a] In Nujol.
[b] Crystalline solid state.
[c] Liquid state (values obtained by subtracting the bands which correspond to the *GG* and the *TG* isomers).

(2) The vibrational selection rules predict that the *TT* form (symmetry C_{2v}) has only 10 fundamental vibrations allowed in the 1400~700 cm^{-1} frequency region,[3] while the number of the prominent absorption peaks observed in each spectrum is about 13 in accordance with the selection rules for the *TG* and the *GG* form.

The isomeric form of glutaronitrile in each crystalline solid phase can then be determined by comparing the two solid-state spectra with that of *bis*(glutaronitrilo)-copper(I) nitrate, $[Cu\{NC-(CH_2)_3-CN\}_2]NO_3$. It has been found from the x-ray analysis that in the crystals of this complex compound the ligand glutaronitrile molecule takes the *GG* form.[4] It is evident that the spectrum of this complex shown in Fig. 1(d) is much different from that of the metastable form of the solid glutaronitrile. On the other hand, the agreement between the spectrum of the complex and that of the stable form is almost complete except for the region covered by the nitrate bands. It is necessarily concluded from these facts that glutaronitrile takes the *TG* and the *GG* configurations in the metastable and the stable crystalline solid phases, respectively. A preliminary calculation of the skeletal deformation frequencies for each isomeric form has also given the results which support this conclusion. The majority of the bands in the liquid-state spectrum can be satisfactorily explained as due to the *TG* and the *GG* isomers, and a few remaining bands including the one at 737 cm^{-1} mentioned above must be attributed to the *TT* isomer. In Table I are included the proposed assignments of the absorption bands to the vibrations of each isomer.

The author wishes to thank Dr. T. Yoshino of Toyo Rayon Company, Ltd., for helpful discussions.

[1] K. Nukada, J. Chem. Soc. Japan (Pure Chem. Sect.) **80,** 218 (1959).
[2] For the nomenclature of the isomers see S. Mizushima, *Structure of Molecules and Internal Rotation* (Academic Press Inc., New York, 1954), Part I, Chap. V.
[3] J. K. Brown, N. Sheppard, and D. M. Simpson, Phil. Trans. Roy. Soc. (London) **A247,** 35 (1954).
[4] Y. Kinoshita, I. Matsubara, and Y. Saito, Bull. Chem. Soc. Japan **32,** 1216 (1959).

Multiple Vibrational Relaxation in Gaseous Dibromomethane

P. G. DICKENS AND D. SCHOFIELD*

Inorganic Chemistry Laboratory, Oxford University, Oxford, England

(Received March 8, 1961)

A recent ultrasonic experiment by Meyer[1] was interpreted as evidence for the presence of three nearly independent vibrational relaxation processes in CH_2Br_2 characterized by the following relaxation times τ_i (sec), and associated specific heat contributions C_i (units of R): $\tau_1 > 1.80\times10^{-6}$, $C_1 = 0.784$; $\tau_2 = 3.02\times10^{-8}$, $C_2 = 1.294$; $\tau_3 = 1.46\times10^{-9}$, $C_3 = 0.493$. Seven vibrational modes make significant contributions to the total specific heat at the experimental temperature (296°K): these are (units of R), $C_1' = 0.9417$, $\nu_1 = 174$ cm^{-1}; $C_2' = 0.5405$, $\nu_2 = 576$ cm^{-1}; $C_3' = 0.4742$, $\nu_3 = 637$ cm^{-1}; $C_4' = 0.3133$, $\nu_4 = 810$ cm^{-1}; $C_5' = 0.1416$, $\nu_5 = 1091$ cm^{-1}; $C_6' = 0.1064$, $\nu_6 = 1183$ cm^{-1}; $C_7' = 0.0534$, $\nu_7 = 1388$ cm^{-1}.

Meyer's assignment of the modes contributing to the separate dispersion regions is 2+5+6 (with τ_1), 1+4+7 (with τ_2), and 3 (with τ_3). Current theoretical interpretation of multiple vibrational relaxation in gases[2,3] appears not to support this empirical assignment. The pattern of vibrational frequencies in CH_2Br_2 reveals an unusually large frequency separation between the fundamentals of the two lowest modes (402 cm^{-1}), and there is no accidental coincidence of overtone levels. Theoretically a large difference between the rates of vibrational deactivation of the two lowest modes is to be expected. Consequently two dispersion regions at least should occur, with virtually the whole of the specific heat contribution of the mode 1 being associated with the higher frequency process (more rapid deactivation). Further dispersion regions are not to be expected, since the frequency spacing of all higher modes is such that the maximum frequency gap between different modes is much less than the corresponding gap between the lowest pair of modes. Consequently all the higher modes would be expected to relax together, with an over-all relaxation time closely related to the deactivation rate of mode 2. This series process would lead to a single lower frequency

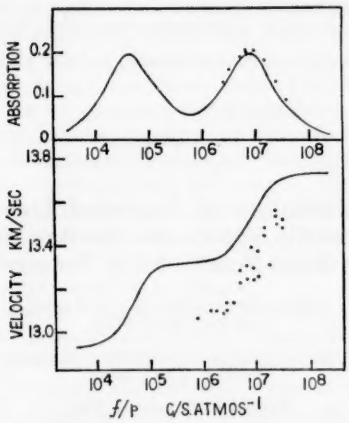

FIG. 1. Calculated ultrasonic absorption (Nepers/wavelength) and velocity for CH_2Br_2. Experimental points from reference 1.

dispersion region involving the specific heat contributions of all modes except the lowest. In particular, since modes 2 and 3 differ in frequency by only 61 cm^{-1}, it is very unlikely that they should be associated with different relaxation times (contrast Meyer's assignment).

A calculation of the predicted relaxation behavior for this molecule has been carried out by the method described by Tanczos,[2] extended in an obvious way to take account of transitions involving up to four vibrational quanta. Lennard-Jones intermolecular force parameters for CH_2Br_2 were not available, and estimated values of $\epsilon/k=450°K$, $r_0=5.06$ A were used; these are consistent with the viscosity coefficient used by Meyer. The *shape* of the dispersion curve was found to be relatively insensitive to the actual values of ϵ and r_0 chosen. The sound velocity a and the amplitude absorption coefficient α were calculated through the expressions

$$(a/a_0)^2=1+\sum_i \frac{D_i(\omega\tau_i)^2}{1+(\omega\tau_i)^2}$$

$$(\alpha/\omega)(a/a_0)^2=2a^{-1}\sum_i \frac{D_i\omega\tau_i}{1+(\omega\tau_i)^2},$$

where ω is the angular frequency, and τ_i and D_i are the effective relaxation times and associated constants as defined by Tanczos.[2] Values of these were found to be $\tau_1=3.5\times10^{-6}$ sec, $D_1=0.0632$ (corresponding to specific heat $C_1=1.630R$); $\tau_2=1.9\times10^{-8}$ sec, $D_2=0.0662$ ($C_2=0.942R$). The remaining relaxation times were associated with negligible D's.

The plot of calculated absorption (Fig. 1) agrees well with the experimental points of reference 1. The dispersion curve differs from the experimental points in two main respects: (i) there is no dispersion predicted at $f/p>50$ Mc/atm; (ii) the shorter relaxation time is associated with the specific heat of mode 1 alone, the contributions of other modes having dropped out at lower frequencies. There is thus a fundamental disagreement between theory and experiment for this molecule, which further experimental work covering wider frequency range might resolve.

* Present address: Department of Chemistry, Cornell University, Ithaca, New York.

[1] N. J. Meyer, J. Chem. Phys. **33,** 487 (1960).
[2] F. I. Tanczos, J. Chem. Phys. **25,** 439 (1956).
[3] P. G. Dickens and J. W. Linnett, Proc. Roy. Soc. (London) **A243,** 94 (1957).

Effect of Pressure on the Electronic Absorption Spectra of Ferrocene and Ferricinium Ion*

J. C. ZAHNER AND H. G. DRICKAMER

Department of Chemistry and Chemical Engineering, University of Illinois Urbana, Illinois

(Received March 30, 1961)

THE effect of pressure has been measured on the electronic absorption peak near 24 000 cm^{-1} of ferrocene $[(C_5H_5)_2Fe]$, and of two derivatives of ferrocene $[C_5H_4CH_3)_2Fe]$ and $[(C_5H_4SO_3Na)_2Fe]$. The peak of the ferricinium ion in ferricinium fluosilicate near 16 000 cm^{-1} has also been studied. The samples were studied as crystallites distributed in NaCl. The high-pressure optical techniques have been described previously.[1,2]

Figure 1 shows the shift of the peak maximum for ferrocene and its derivatives. There is a blue shift of the peak which is quite independent of the compound involved. According to Yamazaki[3] the most probable assignment for this transition is $A_1'\rightarrow A_2''$ for D_{5h} symmetry (or $A_{1g}\rightarrow A_{2u}$ for D_{5d} symmetry). The shift would then be from a $3d$ level (or $3d$–$4s$ hybrid) to the $4p_z$

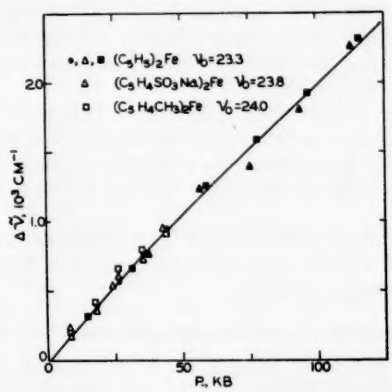

FIG. 1. Shift of peaks vs pressure, ferrocene and derivatives.

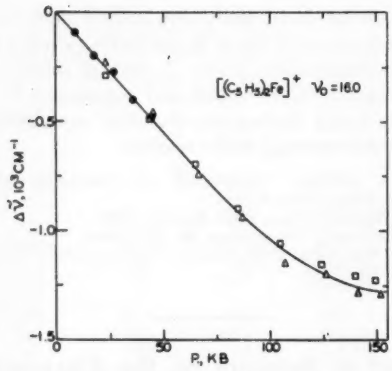

FIG. 2. Shift of peak vs pressure, ferricinium fluosilicate.

state. This assignment is not inconsistent with the discussions of ferrocene energy levels by Moffitt,[4] Dunitz and Orgel,[5] or Liehr and Ballhausen.[6]

It would also seem reasonable that the energy of the p_z state would be increased with increasing compression due to repulsion interaction with the cyclopentadiene electrons.

Figure 2 shows the shift of the 16 000-cm^{-1} peak in ferricinium ion. The peak shifts to the red (to lower energies) with increasing pressure, with a distinct degree of leveling of the shift at high pressure.

As yet, there have been, to our knowledge, no quantitative treatments of the energy levels of the ferricinium ion. Dunitz and Orgel[4] point out that the metallic levels must be somewhat stabilized vis-a-vis the cyclopentadiene levels. Second, they point out that the positive charge is probably distributed over the cyclopentadiene rings. In this case the excited state could then still be a metallic $4p_z$ level. At least at low pressures the energy of this level would be lowered by compression because of increasing interaction with the positively charged rings. The leveling could be due to ultimate overlap with the ring electrons. The situation would, in a qualitative way, be analogous to the situation in solid nickel dimethylglyoxime and related chelates, where a red shift followed by a leveling (and ultimate reversal) has been assigned to a $3d \rightarrow 4p_z$ transition.[7]

In the absence of a quantitative treatment these assignments must be regarded as tentative, but not unreasonable. In particular, the possibility of charge transfer, in the case of ferricinium ion, has not been eliminated.

The authors wish to thank K. L. Rinehart for the ferrocene and ferrocene derivatives, and T. S. Piper for the ferricinium fluosilicate.

* This work was supported in part by the U.S. Atomic Energy Commission.

[1] R. A. Fitch, T. E. Slykhouse, and H. G. Drickamer, J. Opt. Soc. Am. **47,** 1015 (1957).
[2] H. G. Drickamer, Rev. Sci. Instr. **32,** 212 (1961).
[3] M. Yamazaki, J. Chem. Phys. **24,** 1260 (1956).
[4] W. Moffitt, J. Am. Chem. Soc. **76,** 3386 (1954).
[5] J. D. Dunitz and L. E. Orgel, J. Chem. Phys. **23,** 954 (1955).
[6] A. D. Liehr and C. J. Ballhausen, Acta. Chem. Scand. **11,** 207 (1957).
[7] J. C. Zahner, and H. G. Drickamer, J. Chem. Phys. **33,** 1625 (1960).

Depolarization of Scattered Light by *n*-Paraffin Vapors and the Additivity of Bond Polarizability Tensors*

JOSEPH POWERS,† DANIEL A. KEEDY, AND RICHARD S. STEIN

Department of Chemistry, University of Massachusetts, Amherst, Massachusetts

(Received February 22, 1961)

THE principle of additivity of bond polarizability tensors is controversial.[1–5] The difference between values of the C—C bond anisotropy obtained from vapor-phase and crystal measurements and on comparing birefringence values of polyethylene and polypropylene films have been ascribed to deviations from additivity resulting from internal field effects.[4] In order to evaluate these effects more critically, a careful measurement of the depolarization of the scattering of a series of *n*-paraffins up to heptane was undertaken.[6]

Measurements were conducted[6] by enclosing the vapors in a Teflon-lined brass Rayleigh cross of about 3-in. diam cross section provided with optical thermal glass windows and surrounded with an oil jacket for thermostatting. Parallel incident light (0.35° divergence) originating from an Osram HB0109 100-w dc mercury arc was used. Parallel scattered light was po-

TABLE I. Depolarizations and anisotropies.

Substance	ρ (meas) $\times 10^2$	ρ (lit) $\times 10^2$	γ (A)^3	C (theory)	Γ_{CC}(exptl) (A)^3
CO_2	8.47±0.03	9.8[a]	...	...	...
		7.24–9.72[b]			
Ar	0.17±0.02	0.42–0.56[b]	...	...	...
		0.5[a]			
N_2	2.48±0.06	3.6[a]	...	...	...
ethane	0.77±0.02	0.5[b]	1.09	1.00	1.09
		1.6[a]			
n-propane	0.94±0.02	0.7[b]	1.73	1.15	1.50
		1.6[a]			
n-butane	1.02±0.02	0.9[b]	2.28	1.63	1.42
		1.7[a]			
n-pentane	1.23±0.02	1.3[a]	3.17	1.93	1.64
		1.2[c]			
n-hexane	1.64±0.01	1.5[a]	4.28	2.33	1.84
		1.56[c]			
n-heptane	2.00±0.06	1.6[a]	5.24	2.59	2.09
		1.4[c]			

[a] J. Cabannes, *La Diffusion Moleculaire de la Lumiere* (University Press of France, Paris 1929), p. 88.
[b] S. Bhagavantam, *Scattering of Light and the Raman Effect* (Chemical Publishing Company, Brooklyn, New York, 1942), p. 54.
[c] H. A. Stuart, *Die Physik der Hochpolymeren* (Springer-Verlag, Berlin, 1952), Chap. 6, Vol. I.

larized by a rotatable Ahrens prism, collected with a lens and pinhole collimating system and measured with a 1P21 photomultiplier tube refrigerated with a dry-ice ligroin bath to suppress thermal noise. The photomultiplier output was measured with a type 1230A General Radio electrommeter amplifier and recorded with a recording milliammeter. Precautions were exercised to exclude dust from the cross and samples. Stray light was corrected for by subtracting readings with the evacuated cross from those with the sample present. In all cases the stray light represented a very small fraction of the light scattered by the gas.

Depolarization values were obtained by making separate measurements of intensity with horizontal and vertical orientation of the Ahrens prism and taking ratios of intensities. Depolarization values ρ for polarized incident light obtained for gases and vapors at 1 atm pressure are listed in Table I. In most cases, the depolarization values are within the range reported in the literature. The lower value found for argon is gratifying in that it is closer to the theoretically expected value of zero than values reported previously.

The molecular anisotropy may be described in terms of a parameter γ defined by

$$\gamma^2=\tfrac{1}{2}[(\alpha_1-\alpha_2)^2+(\alpha_2-\alpha_3)^2+(\alpha_1-\alpha_3)^2], \quad (1)$$

where α_1, α_2, and α_3 are the principal molecular polarizabilities. Smith and Mortensen point out[1] that this anisotropy of polarizability of the *n*-paraffins may be given by an equation of the type

$$\gamma=C[(b_1-b_2)_{CC}-2(b_1-b_2)_{CH}]$$
$$=C\Gamma_{CC}, \quad (2)$$

where C is a constant dependent upon the particular molecule and b_1 and b_2 are the longitudinal and transverse polarizabilities, respectively, of the C—C and C—H bonds. The γ may be related to the depolarization by the pair of equations[7]

$$\rho=6\delta/5+7\delta \quad (3)$$

$$\delta=\gamma^2/(3\bar{P})^2, \quad (4)$$

where $\bar{P}$ is the average molecular polarizability.

The C may be calculated theoretically from considerations of the geometry of the molecule. Values of the constant were calculated for the temperature of measurement assuming that the molecule consists of a mixture of *gauche* and *trans* rotational isomers with the *trans* having an energy 800 cal/mole lower than the two symmetrical *gauche* energy minima. Values of this constant are included in Table I.

The values of Γ_{CC} obtained by dividing the experimental γ by C are also listed in Table I. There appears to be a definite trend for Γ_{CC} to increase with chain length. Two possible causes for this, (which are interrelated), are the decreasing influence of the terminal methyl group (which probably contributes to a lower anisotropy), and an increasing distortion of the external field by the internal field as the chain length is increased.

It is of interest to attempt to extend this series of measurements to higher *n*-paraffins in order to see whether Γ_{CC} asymptotically approaches a limiting value characteristic of C—C bond in the center of an infinite chain.

* Supported in part by a grant from the Petroleum Research Fund, and in part by a contract with the Office of Naval Research.

† Taken in part from a M.S. thesis in Chemistry, University of Massachusetts, 1959.

[1] R. P. Smith and E. M. Mortensen, J. Chem. Phys. **32,** 502 (1960).
[2] K. S. Pitzer in *Advances in Chemical Physics* (Interscience Publishers, Inc., New York, 1959), Vol. II, p. 79.
[3] I. Tinoco, J. Chem. Phys. **33,** 1332 (1960).
[4] D. A. Keedy, J. Powers, and R. S. Stein, J. Appl. Phys. **31,** 1911 (1960).
[5] R. S. Stein, J. Chem. Phys. **21,** 1193 (1953).
[6] J. Powers, M.S. thesis, University of Massachusetts, Amherst, Massachusetts, 1959.
[7] R. Gans, Ann. Physik **37,** 881 (1912).

Further Notes on the Magnetic Centers in Neutron-Irradiated Calcite*

JAMES C. KEMP†
Department of Physics, University of California
Berkeley, California

(Received March 8, 1961)

FOLLOWING previous work[1] on the low-temperature ($T\lesssim 77°K$) electron spin resonance (ESR) spectrum in neutron-irradiated calcite, we report the spectrum seen at higher temperatures, which shows additional complexities, including the emergence of lines with much longer T_1 and T_2 than were noted in the lines studied at 77°K.[1] Certain lines visible most readily at $T>77°K$ prove to have phenomenally long relaxation times at 300°K ($T_2\simeq 4$ μsec and $T_1\geq 50$ μsec, in one measurement), making this material a most convenient solid for the observation of transient paramagnetic phenomena such as electron spin echoes. Using pulsed klystron techniques,[2] we have observed microwave spin echoes, both normal and stimulated types,[3] at 300°K. As previously,[1] present ESR work was carried out at a frequency of about 8700 Mc.

The previously reported spectrum, dominated by a threefold set of lines, the A lines, is actually seen only at low (roughly $<100°K$) temperatures and in samples with not too high spin density[4] ($<10^{19}$ spins/cc). The high-temperature spectrum appears different in two ways: (1) At 300°K the A lines appear replaced by a single line, denoted A', at about the center of gravity of the A lines. This is seen easiest in very dilute samples, in which other lines are much weaker. As one warms from 77°K, the A lines broaden in the interval 150°–250°K, and are replaced by the single A′ line, which then narrows with T to about 0.5 gauss (with $\lesssim 10^{16}$ spins/cc) at 300°K. (2) An entire new complex

of very narrow, easily saturable lines, denoted the α lines, shows up at temperatures above some 200°K (depending on concentration). Though details have not been worked out, the α spectrum seems dominated by a set of six equally strong lines, centered at about the A' position in the spectrum. With the field H_0 normal to the c axis, for certain azimuthal angles ϕ the six lines coincide in pairs at about the A line positions. The symmetry seems closely related to that of the A lines but with an additional twofold splitting (in maximum magnitude comparable to the threefold splitting, some 5 gauss).

Besides the main A-A′ and α lines, at all temperatures and concentrations we see many other lines, exemplified by the sets *BCDX* of reference 1 and lying, mostly, in the spectral region covered by the *BCDX* lines. We refer to these as "lesser" lines since they are always weaker than the main lines, although the intensity pattern is complex, and in some spectrograms certain of them appear almost as strong as the main lines. (We usually see such a relatively strong line at about the line X position of reference 1, for H_0 anywhere in the plane normal to the c axis). Most of the lesser lines apparently have linewidths and relaxation times comparable to those of either the A-A′ system or the sixfold α set, as if they arose from splittings within the spin systems responsible for the main lines.

Electron spin echo experiments gave the following relaxation times for the α lines at 300°K. A sample with 10^{18} spins/cc was studied, in which the α linewidths were (0.3 ± 0.1) gauss, or T_2^* (inverse linewidth) $\simeq 0.3$ μsec. We found $T_2=(4\pm1)$ μsec. The linewidth was mostly inhomogeneous, as with the low temperature A lines.[1] Stimulated echo storage time, dependent on spin-spin effects as well as T_1, was (50 ± 2) μsec. For the (direct) spin-lattice relaxation time T_1, a very safe conclusion is $T_1 \geq 50$ μsec. Concentration dependences of these times remain to be examined.

The speculation[1] that electrons trapped about CO_2 molecules play a part in the spectrum has been lent weight by infrared absorption studies.[5] An absorption peak at about the ν_3 CO_2 stretching vibration frequancy, with intensity increasing with irradiation dosage and ESR intensities, has been observed. A CO_2 model might conveniently explain the replacement of the three A lines by the A' line at high temperatures. Though the actual arrangement might be somewhat different, for simplicity suppose CO_2 molecules to lie normal to the c axis at CO_2 positions. At low T each CO_2 would be frozen into one of three directions about the c axis, giving rhombic symmetry for the potential seen by a locally trapped electron, but with a threefold distribution of rhombic axis directions. At high T suppose the molecules rotate rapidly, compared to the electron Zeeman frequency, effectively removing the dissimilarity in magnetic behavior between electrons trapped at different CO_2 sites. Any models for the centers must account for the various other lines, besides the A-A' lines. One source of multiplicity to be considered is charge compensation effects, possible with singly charged centers in divalent crystals. We have no convenient explanation for the emergence of the α complex of lines.

What appears to be the A-A' complex of lines has shown up in certain nonirradiated natural calcite samples, in weak concentration ($\sim 10^{15}$ spins/cc). These samples are not visibly colored. As in irradiated samples, a CO_2-like infrared absorption (very weak) was detected.[5] The A lines at 77°K and the A' line at 300°K were a factor of ten stronger than other lines in these specimens.

We wish to thank Professor Erwin Hahn for suggestions regarding relaxation time and spin echo studies; and J. Wakabayashi for some observations on the spectrum.

* Research supported by the Office of Naval Research.

† Present address: Department of Physics, University of Oregon, Eugene, Oregon.

[1] J. C. Kemp, J. Chem. Phys. **33,** 1269 (1960).

[2] J. P. Gordon and G. D. Bowers, Phys. Rev. Letters **1,** 368 (1958).

[3] E. L. Hahn, Phys. Rev. **80,** 580 (1950). In stimulated echo sequences we used a value $\tau=0.9$ μsec (see p. 588 of this reference).

[4] Spin densities here are a rough estimate for the whole complex of lines seen in a particular sample at 77°K, and are about five times the densities per single A line in medium-density samples.

[5] G. R. Wilkinson, King's College, London (private communication). The IR and optical spectra will be reported in detail separately.

Effect of Chemisorbed Hydrogen on the Ferromagnetic Resonance of Finely Divided Nickel*

DONALD P. HOLLIS

Instrument Division, Varian Associates, Palo Alto, California

AND

P. W. SELWOOD

Department of Chemistry, Northwestern University, Evanston, Illinois

(Received December 12, 1960)

IT is well known that the magnetization of typical nickel-silica hydrogenation catalysts is decreased when hydrogen is chemisorbed on the nickel surface.[1] Studies by both static and low-frequency magnetic measurements have been used to derive information about the chemisorption bond formed between the adsorbed hydrogen and the surface nickel atoms.[2,3] In brief, the interpretation accorded this effect is that the chemisorption of hydrogen by nickel consists in the formation of a bond, which is at least partially covalent, between the surface nickel atoms and the hydrogen atoms. This bond involves the pairing of a nickel d

electron with the *s* electron of the hydrogen. Since the unpaired *d* electrons are responsible for the ferromagnetism of nickel, the formation of the chemisorption bond results in a decrease in the magnetic moment of the nickel. Since chemisorption is a surface phenomenon, it is necessary that an appreciable fraction of the nickel atoms reside on the surface if an effect is to be observed. The nickel particles found in typical nickel-silica catalysts have diameters in the range of 10-150 A and hence meet the requirement of large surface to mass ratio. Particles in this diameter range exhibit superparamagnetic behavior.[4] An excellent review of the chemical and physical properties, as well as methods for the preparation of such catalysts, has been given by Schuit and van Reijen.[5]

We wish to report the use of the magnetic resonance technique for the detection of the effect of chemisorbed hydrogen on the magnetization of nickel in these catalyst systems. Several preparations have been studied, varying in nickel content from about 1% to 50%, as well as in nickel particle size. A typical experiment consisted in first reducing a small amount of catalyst in flowing hydrogen at 350°C for a suitable time, usually several hours, then pumping off the excess hydrogen at 350°C, and finally obtaining the magnetic resonance spectrum before, and again, after admission of sufficient purified hydrogen to saturate the nickel surface. The spectra were obtained on a Varian V4500 EPR spectrometer with 100-kc field modulation. Figure 1 shows the results obtained on a catalyst containing 10% nickel and prepared by impregnating Davison silica gel with nickel nitrate solution, drying, igniting, and reducing. It is seen that the linewidth remained constant within experimental error when hydrogen was admitted while the signal amplitude decreased. On sweeping back and forth through the resonance it was found that the linewidth was reproducible within about 10%, but the average width before and after chemisorption was the same. The measured linewidth is found to be 470±30 gauss. In several runs the fractional decrease in signal height varied from 15% to 25% for this particular sample, with an average decrease of about 18%. The line shape appears not to change when hydrogen is adsorbed as can be seen by inspection of Fig. 1.

The *g* value of 2.22 of the nickel also remains constant on admission of hydrogen. Similar results have been obtained on other nickel catalysts, but the fractional decrease in signal amplitude varies with the nickel particle size. For example, a commercial nickel-kieselguhr catalyst[3] manufactured by Universal Oil Products Company and having an average particle radius of 40 A, gives a decrease in signal amplitude of only 6% as compared to the 18% decrease obtained for the 10% nickel catalyst[6] mentioned above, the average particle radius of which is only 15 A. From experiments in which the hydrogen was admitted in increments, it appears that the signal amplitude decreases linearly with the quantity of hydrogen adsorbed. These intensity changes are about half the changes of magnetization observed by classical low-field measurements.[2] This is expected because the low-field method gives a change $\Delta M/M$ approximately twice $\Delta M_0/M_0$ where M_0 is the saturation magnetization.[7]

That the observed resonance is due to nickel metal is confirmed by the facts that the resonance is observed only on reduced catalyst and that the measured *g* value

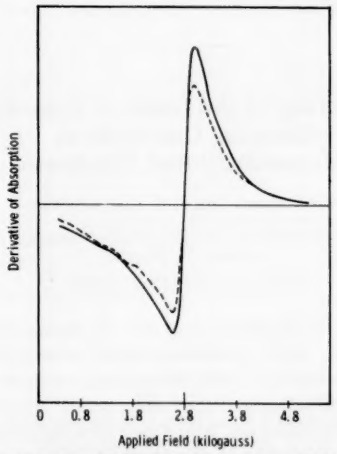

FIG. 1. EPR signal from Ni–SiO_2 catalyst (10% Ni) reduced in hydrogen at 350°C; —— evacuated ---- hydrogen saturated. Instrument settings are identical for the two traces. The peak-to-peak linewidth is 470±30 gauss.

of 2.22 agrees with that obtained for nickel by other workers.[8,9]

The principal advantage of the resonance method of studying the effects of chemisorption on the magnetization of nickel catalysts over the static or low-frequency methods lies in the far greater sensitivity of the former. By using a very dilute nickel dispersion, it might be possible to prepare and study very small nickel particles most or all of whose atoms reside on the surface, and whose magnetization could be completely quenched by hydrogen chemisorption. The resonance method should detect a minimum of about 10^{15} nickel atoms.

This sensitivity makes it possible to study magnetic changes produced by adsorbed gases simultaneously with the absorption spectra of the adsorbate. The change of signal amplitude independent of any change in *g* value makes it probable that the amplitude diminishes directly with the number of nickel atoms suffering *d*-electron involvement, as is the case for static or low-frequency measurements.

* This research was supported in whole or in part by the U.S. Air Force, monitored by the Materials Laboratory, Wright Air Development Center, Wright-Patterson Air Force Base, Ohio.

[1] P. W. Selwood, S. Adler, and T. R. Phillips, J. Am. Chem. Soc. **76,** 1462 (1954).

[2] P. W. Selwood, J. Am. Chem. Soc. **78,** 3893 (1956).

[3] R. E. Dietz and P. W. Selwood, J. Appl. Phys. **30,** 101S (1959).
[4] C. P. Bean and J. D. Livingston, J. Appl. Phys. **30,** 120S (1959).
[5] G. C. A. Schuit and L. L. van Reijen, *Advances in Catalysis*, edited by D. D. Eley and P. B. Weisz (Academic Press, Inc., New York, 1958), Vol. X, p. 242.
[6] C. Abeledo, Northwestern University (private communication).
[7] P. W. Selwood, Second International Congress on Catalysis, Paris, 1960 (Preprint No. 88).
[8] D. M. S. Bagguley, Proc. Roy. Soc. (London) **A228,** 289 (1954).
[9] A. J. P. Meyer, Compt. rend. **235,** 1382 (1952).

Constancy of the Sums of Spin-Spin Coupling Constants in Monosubstituted Ethylenes

G. S. Reddy and J. H. Goldstein

Department of Chemistry, Emory University, Atlanta 22, Georgia

(Received March 23, 1961)

THE NMR coupling constants in monosubstituted ethylenes have previously been correlated with molecular geometry,[1] with substituent electronegativities,[2] and with chemical shift differences.[3] As far as we can ascertain, however, it has not previously been observed that the sums of the three coupling constants, for a wide variety of substituents, fall into two reasonably well-defined groups. Some selected data have been assembled in Table I to illustrate this point.

For the first group listed (A) the sum turns out to fall in the range 19–21 cps, with the exception of vinyl fluoride, and for the second group (B) the sum is in the range 29–31 cps. For all the compounds in the first group the gem coupling constant is negative and the ratio J_{trans}/J_{cis} is approximately 2.0 (except for vinyl fluoride); for the second group J_{gem} is positive and J_{trans}/J_{cis} has a value near 1.7.

Table I. Coupling constants for some monosubstituted ethylenes (cps).

	Substituent	*trans*	*cis*	gem	Sum
A.	F[a]	12.8	4.7	−3.2	14.3
	Cl	14.7	7.5	−1.3	19.9
	Br	15.0	7.2	−1.6	20.6
	OCH_3	14.1	7.0	−2.0	19.1
	$OCH{=}CH_2$[a]	14.4	6.4	−1.8	19.0
B.	CH_3[b]	16.8	10.0	2.0	28.8
	CN	18.2	11.4	1.0	30.6
	C_6H_5[c]	17.2	10.6	1.2	29.0
	C_2H_5[c]	17.4	10.4	1.9	29.7
	$t\,C_4H_9$[c]	17.5	10.8	1.4	29.7

[a] Values reported in reference 2.
[b] A. A. Bothner-By (private communication). All other values were obtained in this Laboratory.
[c] Values listed in J. A. Pople, W. G. Schneider, and J. H. Bernstein, *High Resolution Nuclear Magnetic Resonance Spectroscopy* (McGraw-Hill Book Company, Inc., New York, 1959).

Perhaps the most obvious difference between the two groups of substituents is the fact that only those in the first set (A) possess lone-pair electrons which can interact with the π-electron system of ethylene, while this is not possible in group B. In most other respects, the latter substituents are strikingly dissimilar.

There are also indications that some metallic substituents (Hg, Sn, Al) may comprise another group for which the sum of the couplings is ~40 cps and the value of J_{gem} increases somewhat.[4] An analysis of some vinyl silanes nearing completion in these laboratories indicates that silicon may fall in this group.

In addition to the utility of such generalizations in spectral analysis, the regularities noted should have a bearing on the valence picture and the theory of spin-coupling in vinylic systems.

Further work on this problem is currently in progress.

[1] H. S. Gutowsky, M. Karplus, and D. M. Grant, J. Chem. Phys. **31,** 1278 (1959).
[2] C. N. Banwell and N. Sheppard, Mol. Phys. **3,** 352 (1960).
[3] W. Brugel, T. Ankel, and F. Kruckeberg, Z. Elektrochem. **64,** 1121 (1960).
[4] D. W. Moore and J. A. Happe, J. Phys. Chem. **65,** 224 (1961).

Recombination of Ions in Flames. Effect of Temperature*

I. R. King

Exploratory Research Laboratory, Texaco Experiment Inc. Richmond, Virginia

(Received March 16, 1961)

IN previous articles[1,2] a technique for measuring recombination rates in flames has been described, and several values, obtained in different flames, have been reported. It is the purpose of this letter to report some results obtained recently in which the recombination coefficient of natural flame ions has been determined as a function of flame temperature. Since little if any such information is available today, results should be of interest to the theoretician as well as to the engineer interested in ion propulsion.

Measurements were conducted with an alternate probe technique in a propane-air flame burning on a Meker-type burner 5.5 cm in diam. Two probes of different length, mounted at right angles to each other on a common shaft (the two probes being in a plane perpendicular to the shaft), entered the flame from the side, parallel to the flame front. By measuring current first with one probe, then with the other, and subtracting the two readings, it was possible to determine the ion concentration in the center of the flame. Previous studies[1] in which ion profiles through the flame zone were obtained showed ions were formed to an abnormal extent in the reaction zone and then recombined as they moved downstream until recombination equilibrium was ob-

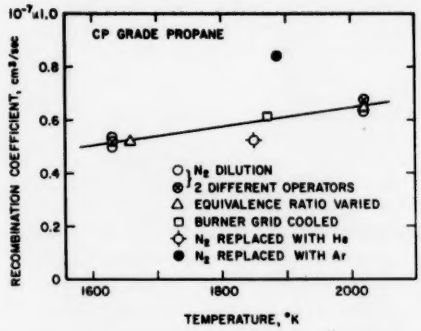

FIG. 1. Effect of temperature on recombination in propane-air flame at 1 atm.

tained. By measuring ion concentration as a function of distance downstream of the reaction zone (or time after formation), the recombination rate may be obtained. Flame temperatures were varied by four different methods: (1) by varying the fuel-air ratio, (2) by diluting the flame with nitrogen, (3) by using a water-cooled burner grid to extract heat from the flame, and (4) by replacing the nitrogen in the air with argon. Good agreement was obtained between the various methods with the exception of method 4. Here, mass spectrometric data obtained elsewhere have shown that different types of ions are formed when nitrogen is replaced with argon, and so one would suspect perhaps that temperature may have a different effect on the recombination rate.

Results of the study to date are shown in Fig. 1. Although the temperature range covered is fairly small (400°K) and a certain amount of scatter in the results is unavoidable, the results show a definite trend: the recombination rate increases slightly with increasing temperature. The order of magnitude of the recombination coefficient (10^{-7} cm³/sec indicates that either third-body or dissociative recombination must be the predominant process in these flames.

It is interesting to compare the results obtained here with results predicted by present-day theories on recombination of gaseous ions. The two most widely accepted theories are the Thomson theory and the Langevin theory. The Thomson theory, which stresses the importance of thermal energy and which requires a third-body collision to absorb some of the excess energy of the combining ions, predicts a decrease in the recombination rate with increasing temperature while the Langevin theory, which stresses the importance of electrostatic attraction between ions, predicts an increase in recombination rate with increasing temperature. It is generally accepted that the Thomson theory is applicable at pressures below 1.0 atm and that the Langevin theory applies at pressures above about 1.5 atm. A somewhat more recent theory, based on dissociative recombination, has been suggested by Bates.[3] According to this theory, the recombination coefficient should vary as $T^{-\frac{1}{2}}$, where T is the absolute temperature. Data reported here tend to follow the Langevin prediction even though they were obtained at pressures of 1.0 atm and below. The reported temperature effect becomes even more pronounced as the pressure is decreased below 1.0 atm.

In the light of recent experiments[4,5] in which the identification of the ions in a flame was attempted with a mass spectrometer, it seems unlikely that a simple recombination process could be occurring in flames. Certainly if there are anywhere near as many different types of ions in hydrocarbon flames as these investigations indicate, the recombination process must truly be complex.

* This research was supported by the Air Force Office of Scientific Research of the Air Research and Development Command.

[1] H. F. Calcote and I. R. King, *Fifth Symposium (International) on Combustion* (Reinhold Publishing Corporation, New York, 1955), p. 423.
[2] I. R. King, J. Chem. Phys. **27,** 817 (1957).
[3] D. R. Bates, Phys. Rev. **78,** 492 (1950).
[4] P. E. Knewstubb and T. M. Sugden, *Seventh Symposium (International) on Combustion* (Butterworth Scientific Publications, Ltd., London, 1959), p. 247.
[5] J. Deckers and A. Van Tiggelen, *Seventh Symposium (International) on Combustion* (Butterworth Scientific Publications, Ltd., London, 1959), p. 254.

B^{11} Quadrupole Coupling Constants in Trimethoxyboroxine and *N*-Trimethylborazole*

M. A. RING AND W. S. KOSKI

Department of Chemistry, The Johns Hopkins University Baltimore 18, Maryland

(Received March 6, 1961)

A VARIAN V-4200B NMR spectrometer was used to obtain broad band spectra of trimethoxyboroxine and *N*-trimethylborazole from which the B^{11} nuclear electrical quadrupole interaction was measured. The Townes and Dailey[1] method of analysis is used to estimate the electron configuration of these molecules. The quadrupole coupling constant eQq/h of B^{11} for one excess p electron is taken as 5.39 Mc/sec.[1,2] In both compounds, the quadrupole interaction split the central transition, $m=\frac{1}{2}\rightarrow-\frac{1}{2}$. A relationship between the derivative maxima eQq/h and the asymmetry parameter η, is given by Silver and Bray[3] where the distance between the maxima is equal to

$$[(eQq/h)^2/192\,\nu_0][25+13.7\,\eta+0.56\,\eta^2].$$

The compounds were prepared by the Callery Chemical Company. Spectra were obtained from precooled samples as they warmed to just below their melting points where resolution was best. Table I lists $\Delta(p-p)$, the distance between the derivative maxima and ν_0.

Due to the symmetry of trimethoxyboroxine in the XY plane, η is zero. In this case, $eQq/h=2.14\pm0.05$

Mc/sec. However, in *N*-trimethylborazole η is not zero and it cannot be evaluated. If η is zero, then eQq/h is 1.71 ± 0.05 Mc/sec. It is thought that η is fairly small since the boron atom has sp^2 hybridization in the only structure that contributes to the coupling constant. Even if $\eta=0.5$, then $eQq/h=1.53$ Mc/sec which represents a 10% change from the case where η is zero. In our further discussion, we will consider eQq/h for *N*-trimethylborazole to be 1.71 Mc/sec.

The two compounds in question can each be described by two structures as given below.

$[BO(OMe)]_3$

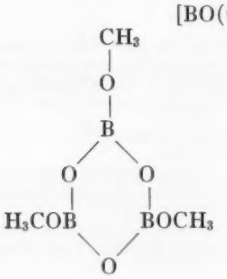

I

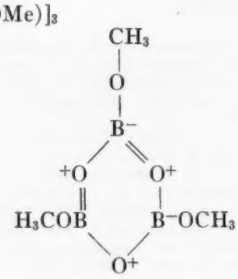

II

$B_3H_3N_3Me_3$

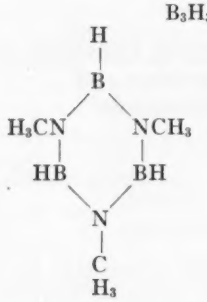

III

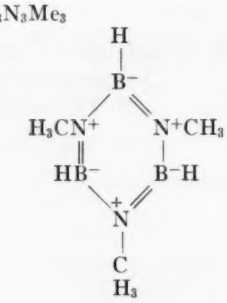

IV

For structures I and III, $eQq/h=5.39$ Mc/sec, and for II and IV, eQq/h is zero. Therefore, the ratio of the measured coupling constants and 5.39 Mc/sec yields the percentage of structures I and III in the respective molecules. Thus, our data indicates that trimethoxyboroxine can be represented as 60% structure II and *N*-trimethylborazole as 68% structure IV. These results are consistent with those for similar molecules and are in agreement with the conclusions made by other methods. Trimethoxyboroxine resembles boric oxide with a methoxy group which should increase the acidity of the boron and thus the double-bond character of trimethoxyboroxine over that found in boric oxide. This is in accord with the data obtained by Silver and Bray,[3] who reported a B^{11} quadrupole coupling constant of 2.76 Mc/sec in boric oxide. From this value a double-bond character of 50% is obtained for boric oxide compared to our 60% for trimethoxyboroxine. It should be noted that any π bonding in the boron oxygen (methoxy) bond would decrease the ring double-bond character from 60%. The percentage of structure IV in *N*-trimethylborazole was found to be 64% by Rector, Schaeffer, and Platt[4] from uv spectra and 67% by Coffin and Bauer[5] from bond-length data compared to our 68%. These results are in harmony with those for borazole. The methyl groups are expected to increase the basicity of the nitrogen and therefore the double-bond character in *N*-trimethylborazole is increased over that of borazole. Again this concurs with other work which reports borazole to have about 47% double-bond character.[4,6] Nuclear quadrupole data also exists for *B*-trichloroborazole, which should have more double-bond character than borazole due to a greater acidity on the boron atoms. This is in agreement with the data of Silver and Bray,[7] who report a lower limit of 85% for the double-bond character of boron. From a Cl^{35} quadrupole resonance frequency of 20.05 Mc/sec,[8] an estimate of 6% can be made for the π character of the boron chlorine bond, which leaves a lower limit of 79% for the double-bond character of the ring in *B*-trichloroborazole.

TABLE I.

Compound	$\Delta(p-p)$ Mc/sec	ν_0 Mc/sec
Trimethoxyboroxine	0.0434	13.70
N-trimethylborazole	0.0278	13.70

* This research was supported by the United States Air Force through the Air Force Office of Scientific Research of the Air Research and Development Command.

[1] C. H. Townes and A. L. Schawlow, *Microwave Spectroscopy* (McGraw-Hill Book Company, Inc., New York, 1955).
[2] G. Wessel, Phys. Rev. **92,** 158 (1953).
[3] A. H. Silver and P. J. Bray, J. Chem. Phys. **29,** 984 (1958).
[4] C. W. Rector, G. W. Schaeffer, and J. R. Platt, J. Chem. Phys. **17,** 460 (1949).
[5] K. P. Coffin and S. H. Bauer, J. Phys. Chem. **59,** 193 (1955).
[6] H. Watanabe, K. Ito, and M. Kubo, J. Am. Chem. Soc. **82,** 3294 (1960).
[7] A. H. Silver and P. J. Bray, J. Chem. Phys. **32,** 288 (1960).
[8] R. P. Hamlen, Ph.D. thesis, The Johns Hopkins University (1956).